

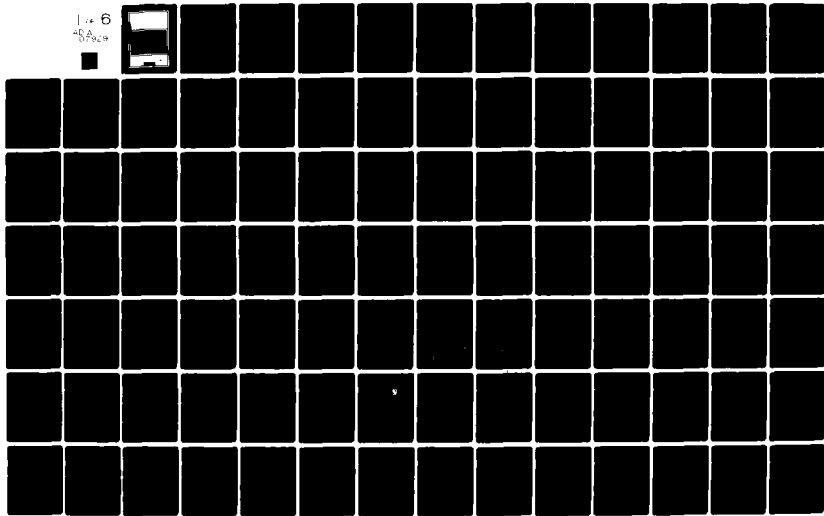
AD-A079 292 ADVISORY GROUP FOR AEROSPACE RESEARCH & DEV. NEUILLY-SUR-SEINE FR F/G 3/
AERODYNAMIC CHARACTERISTICS OF CONTROLS CONFERENCE PROCEEDINGS
SEP 79

UNCLASSIFIED

AGARD-CP-262

N/L

1 of 6
8/2/79



AGARD

ADVISORY GROUP FOR AEROSPACE RESEARCH & DEVELOPMENT

7 RUE ANCELLE 92200 NEUILLY SUR SEINE FRANCE

ADA 079292

AGARD CONFERENCE PROCEEDINGS No. 262

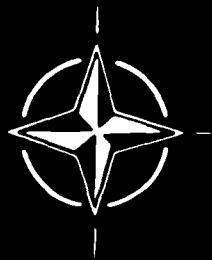
Aerodynamic Characteristics of Controls

DISTRIBUTION STATEMENT A

Approved for public release;
Distribution Unlimited

NORTH ATLANTIC TREATY ORGANIZATION

REPRODUCED BY
NATIONAL TECHNICAL
INFORMATION SERVICE
U.S. DEPARTMENT OF COMMERCE
SPRINGFIELD, VA. 22161



NOTICE

THIS DOCUMENT HAS BEEN REPRODUCED FROM THE BEST COPY FURNISHED US BY THE SPONSORING AGENCY. ALTHOUGH IT IS RECOGNIZED THAT CERTAIN PORTIONS ARE ILLEGIBLE, IT IS BEING RELEASED IN THE INTEREST OF MAKING AVAILABLE AS MUCH INFORMATION AS POSSIBLE.

REPORT DOCUMENTATION PAGE

1. Recipient's Reference	2. Originator's Reference	3. Further Reference	4. Security Classification of Document						
	AGARD-CP-262	ISBN 92-835-0252-3	UNCLASSIFIED						
5. Originator	Advisory Group for Aerospace Research and Development North Atlantic Treaty Organization 7 rue Ancelle, 92200 Neuilly sur Seine, France								
6. Title	AERODYNAMIC CHARACTERISTICS OF CONTROLS								
7. Presented at	the Fluid Dynamics Panel Symposium held at the Italian Air Force Academy, Pozzuoli, Italy, 14-17 May, 1979.								
8. Author(s)/Editor(s)	Various		9. Date September 1979						
10. Author's/Editor's Address	Various		11. Pages 528						
12. Distribution Statement	This document is distributed in accordance with AGARD policies and regulations, which are outlined on the Outside Back Cover of all AGARD publications.								
13. Keywords/Descriptors	<table> <tr> <td>Active control</td> <td>Aircraft</td> </tr> <tr> <td>Flight control</td> <td>Wind tunnel tests</td> </tr> <tr> <td>Aerodynamic characteristics</td> <td>Flight tests</td> </tr> </table>			Active control	Aircraft	Flight control	Wind tunnel tests	Aerodynamic characteristics	Flight tests
Active control	Aircraft								
Flight control	Wind tunnel tests								
Aerodynamic characteristics	Flight tests								
14. Abstract	<p>✓ The aim of the Symposium was to determine the current "State of the Art" in aerodynamic controls with respect to the rapidly expanding flight envelopes of aircraft, applications of active control technology (ACT), and development of control-configured vehicles (CCV). A further goal was to direct attention to the major problem areas for future research.</p> <p>Twenty-nine papers were presented in five categories: (1) General Aspects, (2) Novel Controls, (3) Direct Force Controls, (4) Dynamic Effects, and (5) Interference Effects. Several of the papers were invited to survey conventional and novel methods of control, prediction methods, experimental data from wind tunnel and flight, and flight experience with ACT and CCV. A final session, transcribed for the Proceedings, took the form of a roundtable discussion involving the authors of the survey papers and Symposium attendees.</p> <p>AGARD will also publish a Technical Evaluation Report on the Symposium as Advisory Report (AR) 157, at a later date. The Symposium was held 14-17 May 1979 at the Italian Air Force Academy, Pozzuoli.</p>								

NORTH ATLANTIC TREATY ORGANIZATION
ADVISORY GROUP FOR AEROSPACE RESEARCH AND DEVELOPMENT
(ORGANISATION DU TRAITE DE L'ATLANTIQUE NORD)

AGARD/Conference Proceedings No. 262

**AERODYNAMIC CHARACTERISTICS
OF CONTROLS**

THE MISSION OF AGARD

The mission of AGARD is to bring together the leading personalities of the NATO nations in the fields of science and technology relating to aerospace for the following purposes:

- Exchanging of scientific and technical information;
- Continuously stimulating advances in the aerospace sciences relevant to strengthening the common defence posture;
- Improving the co-operation among member nations in aerospace research and development;
- Providing scientific and technical advice and assistance to the North Atlantic Military Committee in the field of aerospace research and development;
- Rendering scientific and technical assistance, as requested, to other NATO bodies and to member nations in connection with research and development problems in the aerospace field;
- Providing assistance to member nations for the purpose of increasing their scientific and technical potential;
- Recommending effective ways for the member nations to use their research and development capabilities for the common benefit of the NATO community.

The highest authority within AGARD is the National Delegates Board consisting of officially appointed senior representatives from each member nation. The mission of AGARD is carried out through the Panels which are composed of experts appointed by the National Delegates, the Consultant and Exchange Programme and the Aerospace Applications Studies Programme. The results of AGARD work are reported to the member nations and the NATO Authorities through the AGARD series of publications of which this is one.

Participation in AGARD activities is by invitation only and is normally limited to citizens of the NATO nations.

The content of this publication has been reproduced directly from material supplied by AGARD or the authors.

Published September 1979

Copyright © AGARD 1979
All Rights Reserved

ISBN 92-835-0252-3



Printed by *Technical Editing and Reproduction Ltd*
Harford House, 7-9 Charlotte St, London, W1P 1HD

EXECUTIVE SUMMARY

The rapidly expanding flight envelopes of aircraft, the growing applications of active control technology (ACT) and the associated development of control configured vehicles (CCV) have revealed a need to improve our knowledge and understanding of controls and to explore new modes of control. The aim of the Symposium was to determine the current 'state of the art' and to direct attention to the major problem areas for future research.

The Symposium was divided into six Sessions with topic headings: General Aspects, Novel Controls (2 Sessions), Direct Force Controls, Dynamic Effects and Interference Effects. In addition to the papers submitted and accepted for presentation there were a number of invited key papers surveying conventional and novel methods of control, prediction methods, experimental data derived from wind tunnel and flight measurements, and flight experience of ACT and CCV. A final session took the form of a Round Table Discussion involving the authors of the invited papers.

The Symposium showed that we are still very much dependent on ad hoc wind tunnel model tests as a basis for the design and development of the controls of specific aircraft and our basic understanding is deficient, even of such factors as the effects of control gaps. Numerical calculation methods which are proving increasingly effective for the prediction of overall aerodynamic characteristics of aircraft with attached flow are finding application to control problems, but so far with very limited success because of the dominance of viscous effects which are generally not predicted with adequate accuracy, and the theories are not yet able to account for the effects of flow separation. Dynamic effects are important in connection with some applications of ACT and for highly manoeuvrable aircraft, but they are also inadequately understood.

Interesting examples were presented of novel methods of control, these included flaperons, tailerons, wingerons, canards (horizontal and vertical), leading edge slats, pylon split flaps, blowing, vortex generators, digitally controlled segmented flaps and spoilers. These were mainly developed with particular applications in mind, but their potential for further development and applications was evident.

The Symposium did not reveal as much as was hoped on direct force controls although the importance of the subject was well emphasised in the course of the discussions. There was also a lack of papers on the use of propulsion sources for control as well as on the buffeting characteristics of controls. A future symposium may help to remedy these deficiencies.

Important problem areas for future research revealed by the Symposium were:

- (1) The need for a better data base. To this end improved correlation between wind tunnel and flight data was strongly urged. At present agreement between theory and experiment and between flight and wind tunnel tests is sometimes good and sometimes bad and reasons for this variability of agreement are generally not known. Ad hoc data tend not to lend themselves easily to correlation and systematic tests should be planned to supplement the ad hoc work.
- (2) Dynamic effects on control characteristics. One paper for example presented results showing marked reduction of spoiler effectiveness with increase of the frequency parameter.
- (3) Reliable theoretical methods must be developed to account for viscous effects and the effects of flow separation both structured and unstructured.
- (4) Interference and cross-coupling effects. It was evident that these effects could be very important and in some applications can be used to advantage if properly understood e.g. horizontal canards can produce appreciable side-forces.
- (5) The important control derivatives needed for ACT. We should determine these and plan systematic work on them.
- (6) Mission requirements of future aircraft. These need to be more clearly defined so that attention can be focused on the appropriate control problems.

Finally, a strong plea was made that since the subject of ACT properly concerns a number of disciplines a Symposium should be organised on it but on an inter-disciplinary basis, involving some or all of the relevant Panels e.g. FDP, FMP, SMP, GCP and AVP.

A.D. YOUNG
Symposium Chairman
June 1979

AGARD FLUID DYNAMICS PANEL

Chairman: Mr J.L.Jones, MS 200-10
Special Assistant for Planning and Analysis
NASA Ames Research Center
Moffett Field
California 94035, USA

Deputy Chairman: Dr. K.J.Orlik-Rückemann
National Aeronautical Establishment
National Research Council
Montreal Road
Ottawa, Ontario K1A OR6

PROGRAM COMMITTEE MEMBERS

Professor A.D.Young (Chairman)
Queen Mary College
Department of Aeronautical Engineering
Mile End Road
London E1 4NS, UK

Mr J.P.Hartzuiker
Chief, Compressible Aerodynamics Department
NLR, PO Box 90502
1059 BM Amsterdam, Netherlands

Professor Dr Ing. B.Laschka
Institut für Strömungsmechanik
der Techn. Univers.
Bienroder Weg 3
D-3300 Braunschweig, Germany

M. l'Ing. en Chef B.Monnerie
Chef de la Division d'Aérodynamique
Appliquée
ONERA
29 Avenue de la Division Leclerc
92320 Chatillon, France

Professor Dr. L.G.Napolitano
Chair of Aerodynamics
Faculty of Engineering
P. le Tecchio 80
80125 Naples, Italy

Dr H.Yoshihara
The Boeing Aerospace Company
Mail Stop 41-18
PO Box 3999
Seattle, WA 98124, USA

PANEL EXECUTIVE

Robert H.Rollins II

CONTENTS

	Page
EXECUTIVE SUMMARY	iii
PROGRAM AND MEETING OFFICIALS	iv
	Reference
<u>SESSION I – GENERAL ASPECTS</u>	
THEORETICAL AERODYNAMIC METHODS FOR ACTIVE CONTROL DEVICES by H.Körner	1
A SURVEY OF EXPERIMENTAL DATA ON THE AERODYNAMICS OF CONTROLS, IN THE LIGHT OF FUTURE NEEDS by A.J.Ross and H.H.B.M.Thomas	2
CORRELATION OF F-15 FLIGHT AND WIND TUNNEL TEST CONTROL EFFECTIVENESS by J.W.Agnew and J.F.Mello	3
SOME WIND TUNNEL MEASUREMENTS OF THE EFFECTIVENESS AT LOW SPEEDS OF COMBINED LIFT AND ROLL CONTROLS by D.S.Woodward, R.F.A.Keating and C.S.Barnes	4
<u>SESSION II – NOVEL CONTROLS I</u>	
FLIGHT CONTROL AND CONFIGURATION DESIGN CONSIDERATIONS FOR HIGHLY MANEUVERABLE AIRCRAFT by W.T.Kehrer	5
WIND TUNNEL MEASUREMENTS AND ANALYSIS OF SOME UNUSUAL CONTROL SURFACES ON TWO SWEEP WING FIGHTER CONFIGURATIONS by D.Welte and S.Ehekircher	6
ROLL CONTROL BY DIGITALLY CONTROLLED SEGMENT SPOILERS by K.Jonas, H.Wünnenberg and K-H.Horstmann	7
THE YC-14 UPPER SURFACE BLOWN FLAP: A UNIQUE CONTROL SURFACE by A.H.Lee	8
FLAPERON CONTROL – THE VERSATILE SURFACE FOR FIGHTER AIRCRAFT by J.F.Moynes and W.E.Nelson, Jr	9
<u>SESSION III – NOVEL CONTROLS II</u>	
AFFDL EXPERIENCE IN ACTIVE CONTROL TECHNOLOGY by R.P.Johannes and R.A.Whitmoyer	10
CONTROL CONSIDERATIONS FOR CCV FIGHTERS AT HIGH ANGLES OF ATTACK by L.T.Nguyen, W.P.Gilbert and S.B.Grafton	11
FIN DESIGN WITH A.C.T. IN THE PRESENCE OF STRAKES by D.J.Walker	12
<u>SESSION IV – DIRECT FORCE CONTROLS</u>	
CONTROL INTEGRATION TECHNOLOGY IMPACT by C.A.Scolatti	13

✓

	Reference
DIRECT SIDE FORCE AND DRAG CONTROL WITH THE AID OF PYLON SPLIT FLAPS by P.Esch and H.Wünnenberg	14
CONTROL OF FOREBODY THREE-DIMENSIONAL FLOW SEPARATIONS by D.J.Peake and F.K.Owen	15
IN-FLIGHT MEASURED CHARACTERISTICS OF COMBINED FLAP-SPOILER DIRECT LIFT CONTROLS by O.Rix and D.Hanke	16
WIND TUNNEL INVESTIGATION OF CONTROLS FOR DF ON A FIGHTER-TYPE CONFIGURATION AT HIGHER ANGLES OF ATTACK by W.Sonnleitner	17
<u>SESSION V – DYNAMIC EFFECTS</u>	
PROBLEMES D'AERODYNAMIQUE INSTATIONNAIRE POSES PAR L'UTILISATION DES GOUVERNES DANS LE CONTROLE ACTIF par R.Destuynder	18
EFFETS INSTATIONNAIRES D'UNE GOVERNE EN ECOULEMENT BIDIMENSIONNEL SUBSONIQUE ET TRANSSONIQUE par R.Grenon, A.Desopper et J.Sides	19
AERODYNAMIC CHARACTERISTICS OF MOVING TRAILING-EDGE CONTROLS AT SUBSONIC AND TRANSONIC SPEEDS by D.G.Mabey, D.M.McOwat and B.L.Welsh	20
UNSTEADY AERODYNAMICS OF TWO DIMENSIONAL SPOILERS AT LOW SPEEDS by S.R.Siddalingappa and G.J.Hancock	21
Paper 22 cancelled	
TRAJECTORY BEHAVIOUR OF A CONTROL CONFIGURED AIRCRAFT SUBJECTED TO RANDOM DISTURBANCES by A.Danesi, S.Smolka and F.Borrini	23
FOREBODY VORTEX BLOWING – A NOVEL CONTROL CONCEPT TO ENHANCE DEPARTURE/SPIN RECOVERY CHARACTERISTICS OF FIGHTER AND TRAINER AIRCRAFT by A.M.Skow, W.A.Moore and D.J.Lorincz	24
<u>SESSION VI – INTERFERENCE EFFECTS</u>	
NONLINEAR AERODYNAMICS OF ALL-MOVABLE CONTROLS by C.A.Smith and J.N.Nielsen	25
ON THE EFFECT OF WING WAKE ON TAIL CHARACTERISTICS by K.Gersten and D.Glück	26
INTERACTION AERODYNAMIQUE ENTRE UN CANARD PROCHE ET UNE VOILURE par Y.Brocard et V.Schmitt	27
ON THE EFFECTS OF GAPS ON CONTROL SURFACE CHARACTERISTICS by C.Michael and G.J.Hancock	28
ETUDE AERODYNAMIQUE DES GOUVERNES DE MISSILE par J.Perinelle et L.Mifsud	29
SOME INVESTIGATIONS CONCERNING THE EFFECTS OF GAPS AND VORTEX GENERATORS ON ELEVATOR EFFICIENCY AND OF LANDING FLAP SWEEP ON AERODYNAMIC CHARACTERISTICS by H.Neppert and R.Sanderson	30
ROUND TABLE DISCUSSION	RTD

1-1

THEORETICAL AERODYNAMIC METHODS FOR ACTIVE CONTROL DEVICES

Horst Körner *)
 Institut für Entwurfsaerodynamik der DFVLR, Braunschweig, Germany

SUMMARY

A brief survey of the theoretical aerodynamic aspects of active control devices is given. Various calculation methods for subsonic, transonic and supersonic attached flow are reviewed. This is followed by comments on separated flow. After a presentation of typical correlations between theoretical and experimental results for steady and unsteady characteristics of controls, this survey concludes with a resume of the shortcomings of the theoretical approaches and some recommendations for future efforts.

CONTENT

1. Introduction
2. Subsonic attached flow
3. Transonic attached flow
4. Supersonic attached flow
5. Leading edge vortex flow
6. Separated flow without primary structures
7. Conclusions

NOTATIONS

x, y, z	coordinate system	f	frequency
t	time	ϕ, φ	potential functions
τ, \hat{t}	dimensionless time	φ	phase shift of the unsteady values
c	chordlength	a	spanwise loading function
\bar{c}	mean aerodynamic chord	h	chordwise loading function
s	halfspan or location of the spoiler	c_p	pressure coefficient
h	height of the spoiler	Δc_p	load coefficient
l	characteristic length ($l = c/2$ for airfoil) ($l = s$ or \bar{c} for wings)	c_p', c_p''	real resp. imaginary part of the unsteady pressure distribution (eqn. 4)
α	angle of attack	$c_L, c_{L\delta}, c_{L\delta}'$	lift coefficient resp. derivative due to flap deflection
δ	flap resp. spoiler deflection	c_D	drag coefficient
U	undisturbed flow speed	$c_m, c_{m\delta}, c_{m\delta}'$	pitching moment resp. derivative due to flap deflection
a	speed of sound	$c_h, c_{h\delta}, c_{h\delta}'$	hinge moment resp. derivative due to flap deflection
$M = \frac{U}{a}$	Mach number		
M^*	critical Mach number		
$Re = \frac{U \cdot \bar{c}}{\nu}$	Reynolds number		
$k = \frac{\omega \cdot l}{U}$	reduced frequency		
$\omega = 2\pi f$	circular frequency		

*) Dr.-Ing.
 Head (acting) of Institute for Design Aerodynamics, DFVLR

SUBSCRIPTS

S	steady
K	kink
m	medium
i	amplitude
FF	far field

1. INTRODUCTION

For the improvement of the performance of airborne vehicles several new technologies have been proposed within the last decade. The most promising among these are

- supercritical wings
- composite materials in primary structures
- advanced high bypass engines
- active control devices
- integrated digital guidance and control.

Technology programs are in progress to demonstrate the superiority of these new techniques. Some of these techniques have already been brought to such a standard that the application in production aircrafts is justified. Others are still in the process of being elucidated and developed.

One of the most promising new technologies is the active control technique [1], [2], [3], [4]. This technology implies the instantaneous fast deflection of control devices to react on disturbances at the moment when they occur. This new technology which can only be developed as an interdisciplinary technique, requiring flight mechanics, guidance and control, structures and materials and not at least aerodynamics has an impact on

- performance
- safety
- ride quality

of the aircraft and on the

- abatement of noise in the environment of airports.

Active control technique on an aircraft may be used for

- relaxed static stability
- load control for manoeuvre and gust load alleviation
- flutter mode control
- direct force control.

As active control devices, conventional or new controls may be used. Figure 1 shows control devices on an airplane, some of them typical for a fighter type aircraft, others for a subsonic transport aircraft. There is a subdivision between longitudinal and lateral controls. This is not at all stringent since longitudinal devices may also be used for lateral control as spoilers and differential tail for roll control and vice versa.

As can be seen the main aerodynamic problems that have to be treated are

- wings with control devices and
- mutual interference of wings.

The problem of the aerodynamicist is, to give good prediction for the effectiveness of control devices for steady and unsteady deflection. This is a task which can be solved by theoretical and experimental means.

The most straight-forward way providing data for control-surfaces, is the theoretical approach. Figure 2 gives a classification of the methods available or in development. First there has to be done a subdivision into

- attached flow and
- separated flow.

For attached steady and unsteady flow powerful methods have been developed on the basis of the potential theory with some allowance for viscous effects by boundary layer which give reasonable results for subsonic and supersonic flow. In the transonic case there are still severe deficiencies which are connected with the strong nonlinearity of the governing equations. Since most of the control devices used, work in the attached flow regime, there is a good chance to get a realistic theoretical prediction for the effectiveness.

For separated flow a distinction must be made between those flow types where there exists a well-formed primary structure, e.g. the shedding of a free vortex sheet rolling up, and those where no primary structure can be observed, e.g. the flow behind bluff bodies. For the separated flow with certain primary structures, singularity models of the separated region may be constructed, in order to achieve an approximate solution. This leads to good results. When there is obviously no primary structure the singularity models are somewhat doubtful and the full solution of the Navier-Stokes-equations would be appropriate. This way is indeed the most comprehensive but also the most laborious one, and only a few solutions for practical purposes have been given up to now.

Another subdivision of methods resp. problems, which may be used, is the classification between steady and unsteady deflection of the control devices. The following states may be distinguished:

- Fixed control device.
This is the case of steady flow. There exist special classes of methods.
- Slowly oscillating movement of the device ($k \leq 0.05$).
For this case the steady methods can be used for a quasi-steady evaluation, since the aerodynamic forces and moments are in phase with the movement.
- Fast oscillating movement of the device ($k \geq 0.05$).
Methods for attached flow have been developed for this case. The aerodynamic forces and moments are no longer in phase with the movement.
- Suddenly deflected control device.
This case can be treated by the oscillatory methods by a Fourier analysis of the step-function. For some cases exact solutions exist which can be used for inspection of approximate methods.

General literature on theoretical methods is available. [5] and [6] among others give the basis, [7] and [8] concentrate on practical prediction methods and applications for the steady case, whereas [9], [10] and [11] deal with the unsteady case. [12], [13] and [14] give short resumes of prediction-methods for the unsteady case. The recent development of prediction-methods is given in [15], [16] and [17].

2. SUBSONIC ATTACHED FLOW

2.1 Basic equations

The basic equation of linearized subsonic potential flow is

$$(1 - M) \phi_{xx} + \phi_{yy} + \phi_{zz} = 0 \tag{1}$$

where M is the free stream Mach number and ϕ is the velocity potential. This equation can be transferred by Goethert rule to the Laplace-equation

$$\phi_{xx} + \phi_{yy} + \phi_{zz} = 0 \tag{2}$$

or

$$\nabla^2 \phi = 0 .$$

The linearized potential equation for the unsteady case is

$$\nabla^2 \phi - \frac{1}{a^2} \left[\frac{\partial}{\partial t} + U \frac{\partial}{\partial x} \right]^2 \phi = 0 \tag{3}$$

where a is the speed of sound and U the flight speed.

2.2 Outline of the methods

Since the solution procedure for steady and unsteady flow is similar, a unique treatment of both cases will be given. Two main classes of methods have to be distinguished (figure 3), the

- conformal mapping methods
- singularity methods.

The conformal mapping technique has been worked out by THEODORSON [18] to a comprehensive theory for steady and unsteady twodimensional flow. Nevertheless the singularity-methods have become much more important since these methods could be extended without major difficulties to the 3D case.

Due to the linearity of the subsonic potential equation the principle of superposition of solutions can be applied. So basic solutions of the equations as sources, vortices and doublets may be combined in an arbitrary way to find the flow field required. This singularity technique has been used for the development of a large number of subsonic theories and will be described subsequently for the 3D case, which includes the 2D one. For the development of these methods both the velocity and the acceleration potential have been used successfully.

1-4 The subsonic singularity method can be divided into two classes:

- loading function methods
- discrete loading methods.

The loading function method, also called lifting surface method, is a thin wing resp. thin airfoil theory. The basic steady approach has been developed by MÜLTHOPP [19] and TRUCKENBRODT [20], the extension to the unsteady case has been given by LASCHKA [21], [22] and DAVIES [23].

Thin wing theory means that thickness effects are neglected because they are of minor importance compared with the lift effects. Since lift effect can be simulated by vortices and doublets, these singularities are the basis of thin wing theory. The problem to be solved may then be formulated as an integral-equation for the downwash of the wing. This equation can also be derived by Green's theorem.

The solution of this integral equation is found by introducing loading functions with unknown scale factors in chordwise and spanwise direction to approximate the load of the wing. Figure 4 shows typical loading functions for the subsonic lifting surface theory. The choice of the loading functions must be consistent with the singular behaviour of the leading edge of the wing (h_0, h_1, h_2, h_K), the hinge line (h_K) and the wing tip (a_0, a_1). The load must also satisfy the Kutta condition at the trailing edge. After introduction of these loading functions the integral-equation is reduced to a system of linear equations where the scale factors of the loading-functions have to be evaluated. This can be done after having introduced a number of control-points on the wing where flow tangency has to be satisfied.

The other type of methods which will be discussed here are discrete loading methods. Here it is useful to subdivide in

- vortex/doublet lattice methods and
- panel methods.

While vortex/doublet lattice methods only treat the thin wing, panel methods enable a general solution of thick lifting bodies.

The vortex-lattice method for steady flow has been developed by FALKNER [24] and RUBBERTI [25], extensions of this method have been given among others in [26] and [27]. The unsteady case has been treated by HEDMAN [28] and ABANO and RODDEN [29].

Basis of this method again is the downwash-equation of lifting surface theory. The idea of this method is, to discretize the load of the wing in small elements. Thus the wing has to be subdivided in a large number of small trapezoidal elementary wings - called panels - arranged in strips parallel to the free stream and with leading edge, trailing edge and hinge-line coinciding with edges of the panels (see figure 5). It has been shown that the lift of a panel can be concentrated on the quarter chord line of the panel with trailing vortices at the tips. This horseshoe-vortex whose strength has to be determined represents the steady effect of the panel. By a line of doublets on the quarter chord line the oscillatory effect can be taken into account. The downwash boundary condition then is satisfied at a pivot-point which is located at 3/4 chord along the center line of each panel. The basic integral equation of lifting surface theory is thus reduced to a set of linear equations, which has to be solved for the unknown load.

The advantage of this method is its rather simple handling in comparison to the lifting surface method since it can be used without difficulties for complex nonplanar lifting systems [30], [31]. When using the loading function method complications arise since the characteristic singular behaviour of the solution must be known a priori and must be incorporated in the method in form of appropriate loading functions. This is not the case with the vortex/doublet-lattice method where singular behaviour is a result of the computation.

In order to get good accuracy for the vortex/doublet-lattice method, 100 panels are necessary to get an appropriate load distribution in span- and chordwise direction. A still higher number is needed for a wing with control devices. Even with this high number of panels the accuracy of this method is not as high as of the loading function method. Since it seems not worthwhile to achieve a higher accuracy than +3% because thickness and viscous effects have not been taken into account, also the vortex/doublet-lattice method can be seen as a powerful method.

A somewhat different approach to the thin wing discrete methods has recently been given by ROOS [32] and GEISSLER [33]. Instead of a doublet-line Geißler uses a doublet-field on the panel.

The most recent and most comprehensive approach to subsonic lifting bodies is the panel method. For steady flow the basics of this method are derived by HESS and SMITH [34] and RUBBERTI and SAARIS [35]. Amplifications of this method have been given in [36] to [40]. The unsteady approach has been treated in [41], [42], [43] and [44]. A survey on panel methods as well as vortex-lattice methods is given in [45].

The basic idea of the panel method is similar to the vortex-lattice method. The surface of the body is subdivided into a large number of trapezoidal panels as shown in figure 6. The solution of the governing Laplace equation for steady flow is constructed by arranging a distribution of basic singularities on body and wake surface. The effect of these discrete singularity distributions on each panel produces disturbance velocities at other points of the surface. At these pivot-points - each panel has one on its centre - the velocities are evaluated as an integral, employing Green's theorem. This integral expresses the induced velocity at a body pivot-point in terms of the known body geometry and the unknown perturbation singularity strength. Satisfying the condition of flow tangency at the pivot-points yields determining the singularity strength. This procedure is quite similar to the vortex-lattice method.

The version most widely used in practice for steady flow has source singularities on the surface to get the thickness effect and vortex singularities in the body mean surface and the wake for representation

of the lift effect. Unsteady effects can be treated by placing doublets on the mean surface or on the surface itself. For steady flow this powerful method is already extensively used. For unsteady flow first results have been achieved. 1-5

2.3 Discussion of results

To prove the validity of the methods described, some typical theoretical results will be presented, which have been verified experimentally by wind-tunnel investigations. In order to have a consistent nomenclature within this paper, a few denominations of the original contributions have been changed. Unchanged remain different presentations of unsteady pressure and derivatives, which can be given either divided in real and imaginary part or in magnitude and phase shift.

$$c_{\text{unsteady}} = c' + ic'' = |c| \cdot e^{i\varphi} . \quad (4)$$

Both nomenclatures have been used here.

Figure 7 shows results for a twodimensional airfoil with oscillating flap [46]. The real and imaginary part of the pressure distribution are given for a reduced frequency between 0 and 1. The singular behaviour of the flap-kink can be seen quite clearly. It can also be seen that the flap-singularity acts in phase with the movement of the flap. The figure shows furthermore that good agreement between theory and experiment can be achieved. It must however be noted that with rising frequency the discrepancies in c_p'' are growing.

The data at least important for control effectiveness are the derivatives. Fig. 8 shows results for a 16% thick airfoil with a trailing edge flap [47]. Results are given for lift, pitching moment and hinge moment over the reduced frequency for two Mach numbers (0.3 and 0.76). The theory used is the conformal mapping technique for a thin plate with flap [18].

At $M = 0.3$ a good agreement can be seen for the phase shift, while the magnitude of the coefficients deviates between 15% and 50% from the experimental values. The highest deviations result for the hinge moment. This is due to thickness, camber and before all viscous effects which have been neglected.

At $M = 0.76$ the discrepancies are even higher and for the pitching moment the tendency is not predicted in the right way. Here subsonic theory fails, since the flow on the airfoil is supercritical.

Let us now have a look on the 3D case. Figure 9 shows results for an untapered swept wing with two flaps acting in antiphase. Theoretical results achieved with the discrete loading method by GEISSLER [35] are compared with wind-tunnel results [48]. Results are given for two sections. The agreement between theory and experiment is quite good. Some small discrepancies can be observed at the leading edge of the control surface. This is obviously due to a small gap in the experimental case.

Results for a swept wing with oscillating flap at a high subsonic Mach number are given in figure 10. The results achieved with a loading function method after [49] compare quite well with the experimental data.

All results presented up to now have been achieved with thin airfoil resp. thin wing theories. One major deficiency of these theories is the neglect of thickness effects. This can be overcome by the use of panel-methods. Figure 11 compares results from thin wing theory [35] and panel-method [44] for the wing discussed in figure 9. The thickness effect alters the pressure distribution significantly. Compared with the experiment, it is difficult to decide, whether the incorporation of the thickness effect brings an improvement or not. Obviously thickness effects and viscous effects are partially cancelling each other as known from the steady case. This may explain the rather good agreement which is usually found when comparing pressure distributions received from inviscid thin-wing theories and experiments.

Now the straightforward way is, to combine potential theory, especially the panel-method with viscous calculations (boundary layer). For steady flow this technique will be discussed in chapter 6 including separation-effects. For the unsteady case pilot calculations have been done by GEISSLER [44], which show encouraging results.

The second main problem of control aerodynamics is the interference between main wing and tail or canard. Figure 12 shows theoretical results from loading function method [22] for a wing with variable sweep followed by a tail-unit. Results are given for the unsteady pressure distribution in a specified section of the tailplane due to wing pitch oscillation compared with experiments [50]. For the moderate sweep cases the agreement between theory and experiment is quite good. In the case of 70° sweep larger discrepancies occur since now the tailplane is strongly influenced by the boundary layer of the wing, the deformation of the vortex-sheet and before all by the tip-vortex. All these viscous effects are not covered by theory.

Figure 13 shows results for the reverse problem: interference of a pitching tail on the main wing. As can be seen this influence is rather small. The theoretical prediction agrees fairly well with the experimental data.

3. TRANSONIC ATTACHED FLOW

3.1 Basic equations

In the transonic flow regime the nonlinearities are no longer of second order and must therefore be taken into account. Basic equations for the steady case are

1-6

$$(a^2 - \phi_x^2)\phi_{xx} + (a^2 - \phi_y^2)\phi_{yy} + (a^2 - \phi_z^2)\phi_{zz} - 2\phi_x\phi_y\phi_{xy} - 2\phi_x\phi_z\phi_{xz} - 2\phi_y\phi_z\phi_{yz} = 0 \quad (5)$$

$$a_0^2 - a^2 = \frac{\kappa-1}{2} [\phi_x^2 + \phi_y^2 + \phi_z^2] \quad (6)$$

For the unsteady case the basic equations are

$$(a^2 - \phi_x^2)\phi_{xx} + (a^2 - \phi_y^2)\phi_{yy} + (a^2 - \phi_z^2)\phi_{zz} - 2\phi_x\phi_y\phi_{xy} - 2\phi_x\phi_z\phi_{xz} - 2\phi_y\phi_z\phi_{yz} + 2\phi_x\phi_{xt} + 2\phi_y\phi_{yt} + 2\phi_z\phi_{zt} - \phi_{tt} = 0 \quad (7)$$

$$a_0^2 - a^2 = (\kappa-1) \left[\frac{1}{2}(\phi_x^2 + \phi_y^2 + \phi_z^2) - \phi_t \right] \quad (8)$$

In contrast to the subsonic case these equations are nonlinear and the well-known techniques used in subsonic flow as superposition of solutions cannot be used.

Another difficulty that arises in the transonic flow regime is due to the occurrence of subsonic and supersonic flow fields around the wing at the same time. This means for the steady case, that the governing equation changes its type from elliptic (subsonic) to hyperbolic (supersonic) within the flow field. This difficulty has been overcome by the introduction of different regions of influence for the subsonic and the supersonic case [51]. In the unsteady case this brings no difficulties since these equations are uniformly hyperbolic. Therefore time-dependent methods also have been used to find the steady state solution ($t \rightarrow \infty$).

Another difficulty arises from the occurrence of shock-waves, which does not allow a priori the assumption of isentropic flow. Since the existence of potential flow suggests isentropy, this is a crucial point. It has been shown that for weak shocks, potential theory is still appropriate, but if exact solutions are wanted, the Euler- or Navier-Stokes-equations must be used.

On the other hand the treatment of the full potential equation or moreover the Euler equations is so difficult, that there have been several attempts to reduce these equations to a form which can be handled easier, as e.g. the transonic-small-perturbation equation (TSP), the parabolic equation, the integral equation and the hodograph equation. Each of these equations forms the basis of powerful evaluation techniques for at least steady flow.

3.2 Outline of the methods

Figure 14 gives a survey over theoretical methods available for transonic flow. The great number of different approaches shows the large effort devoted to this complicated problem.

Hodograph method: Basis of this method is the linear hodograph equation which has to be evaluated in the hodograph-plane. This method has its special merits for twodimensional airfoil design [52], [53], [54].

Local linearization: Due to the relative simplicity of the parabolic equation used for this approach, this method has been exploited to a large extent. Nevertheless the method of local linearization did not achieve major importance since it has several shortcomings which restrict its applicability. So this method is only applicable to M-numbers near 1. Furthermore shock-waves, and round leading edges cannot be treated. Results of this method are known for the steady and unsteady case [55], [56], [57], [58], [59].

Integral equation: Basis of this method is an integral equation which can be derived from the potential equation using Green's theorem. The method due to Oswatitsch allows substantial savings in computation efforts since it provides a reduction of dimensions by one when an appropriate assumption for the decay of the velocity transverse to the streamwise direction is made. The integral equation gives good results for subcritical flow but exhibits some critical features, when the flow becomes supercritical. Nevertheless also these difficulties can be overcome. Steady methods of this type have been developed by [60] and [61], unsteady methods by [62] and [63].

Finite difference: This type of method has been pushed forward in the last years to such an extent, that effective prediction methods for steady and with some restrictions for unsteady flow are available. Two different types of methods have to be distinguished

- relaxation methods
- time progressing methods.

The relaxation technique is at the moment the most widely used prediction method for steady and unsteady flow. Therefore this technique will be described a bit more in detail for the steady 3D case [64], [65], [66].

Basic equations for this technique may be the widely used TSP equation together with equation 6. These equations are transferred into finite difference equations for which the solution has to be evaluated throughout the flow field near the wing-body-configuration (see **figure 15**). At a certain distance from the configuration the far field solution is connected with the finite difference solution. For the finite difference procedure within the network different types of operators are used

- centered finite difference molecules for subsonic (elliptic) points
- backward oriented finite difference molecules for supersonic (hyperbolic) points and
- a mixture of both for points aft of the boundary supersonic-subsonic flow.

1-7

The boundary condition on the configuration is satisfied by yielding flow tangency at mesh-points, which border on the body.

The solution for the potential within the finite difference network is found by successive line relaxation following the direction of the flow. This so called sweeping through the flow field has to be repeated until a converged solution has been achieved. Since the number of field points for a 3D wing is approximately 50 000 to 200 000, and up to 400 iterations are needed, the computer time is rather high. It takes up to 3 h on an IBM 370/158.

The method described here is with certain modifications, e.g.

- use of full potential equation [67]
- use of mapping technique to get a more appropriate computation field [67], [68]
- different application of boundary conditions [66]
- conservative or non-conservative formulation [67]
- different far field approaches [68]

the at this time standard method for 3D transonic flow computations with shocks. These methods can be used without difficulties for flap deflections as far as no separation effects occur.

For the relaxation methods a rather simple extension to the unsteady oscillatory flow is possible, when only small deflections are assumed [69], [72], [74]. The other promising type of finite difference method is the time progressing method which first has been developed for the steady case using the solution $t \rightarrow \infty$ as the steady solution. This method which has been developed on the basis of the Euler equations by YOSHIHARA [75], [76] and others [77], [78], [79], is especially appropriate for the suddenly deflected control device. Results for oscillatory flow achieved with this most accurate method may also be used as reference for the much faster relaxation methods which only give approximate result. An alternative approach to this method is the Alternating-Direction Implicit (ADI) method proposed by BALLHAUS [70], [71], [73] which uses an implicit discretization of the governing equations. Due to this technique the computation time needed can be speeded up considerably.

Finite element: A further alternative approach to the transonic problem is the finite element method. This method which is widely used in the calculation of static structures, has not been adopted in fluid mechanics to a large extent. Methods for 2D and 3D steady flow have been developed by [80], [81] and [82], unsteady approaches have been given by [83] and [84]. As in the relaxation technique, special care has to be taken for the supercritical case.

Finite volume: The perhaps most effective approach to the steady and unsteady flow-problem in transonic flow is the finite-volume approach. The development of this method shows that a not too complicated conservative formulation of the problem is feasible. Furthermore the treatment of boundary conditions at the contour can be satisfied easier than with other discrete methods, except finite element. Basic work in this field has been done by [85], [86] and [87].

Although a number of methods for transonic flow are given here - these are only a selection of much more publications on this topic - a comprehensive method for 3D wings with oscillating flaps has not been presented up to now. A survey of unsteady 2D-methods is given in [88].

3.3 Discussion of results

For the transonic case some selected results will be presented which show the special features and the state of the art of methods in transonic flow. These results are compared with experiments from wind-tunnel.

Figure 16 shows experimental results for a 6% thick airfoil with oscillating flap over the Mach number [88]. These results are compared with subsonic thin airfoil theory and demonstrate quite clearly the limits of validity of subsonic theory. Up to the critical Mach number, which lies slightly below $M = 0.85$, magnitude and phase shift of the coefficients are well in agreement, except for the magnitude of the hinge-moment but here the rather low level of the value must be taken into account. At higher subsonic Mach numbers ($M > 0.85$) the magnitude and phase shift of the coefficients diverge. This behaviour is due to strong nonlinear effects.

Figure 17 shows the calculated unsteady upper surface pressure distribution for the same airfoil for different flap positions. The theoretical evaluation with the ADI method after BALLHAUS et al. [73] shows quite clearly the change of pressure distribution due to flap oscillation, especially the movement of the shock and the change in shock-strength.

In figure 18 the calculated movement of the shock on the airfoil is compared with experiments. The method used is the time-marching method by YOSHIHARA [76]; experiments are taken from TIJDEMAN [88]. Although the

most comprehensive method has been used without and with consideration of viscous effects, no acceptable agreement between theory and experiment can be achieved. It must however be beared in mind that the shock location is a very sensitive criterion for the quality of methods.

Let us have a look on the load and pressure distributions. Figure 19 shows a comparison of theory and experiment for a subcritical and a supercritical case. The theories used are the subsonic thin airfoil theory and the transonic relaxation method after EHLERS [69]. For the subsonic case the magnitude of Δc_l is given very badly by the transonic theory; on the other hand at $M = 0.85$ the specific feature of the moving shock is predicted qualitatively quite well, but the absolute value is overestimated. Also in phase shift there are remarkable discrepancies. Figure 20, which gives results from the relaxation-method by FRITZ [74] shows the same tendency.

All these discrepancies may have several reasons as

- inadequacy of the small perturbation-approach
- inadequacy of the shock-treatment in the theory
- separation-effects at the foot of the shock or at the trailing edge
- Reynolds number influence.

These deficiencies are only partially typical unsteady effect. In fact the steady case already exhibits most of the difficulties cited. This can be seen in figure 21 where the hinge-moment over the flap deflection for the NACA 64A006 airfoil at $M = 0.95$ is given for the steady case. Due to different shock-arrangements on upper and lower surface, the lift-slope exhibits highly nonlinear characteristics.

Unsteady flap deflection creates an unsteady movement of the shock on the airfoil. Tijeman has observed three different types of shock movement [88]:

type A: sinusoidal shock-wave motion. In this case the shocks on the upper and lower surface move in sinusoidal mode in antiphase.

type B: interrupted shock-wave motion. The motion is characterized by the disappearance of the shock during a part of its backward motion. Figure 18 shows the location for this type as observed in experiment. The calculation shows type A.

type C: upstream propagated shock wave motion. This type is especially observed, when the flow is just supercritical. The shock moves upstream first increasing in strength, then weakening and finally leaving the airfoil from the leading edge.

This phenomenology may show what difficulties arise in transonic unsteady flow. These effects may lead to highly nonlinear behaviour of the coefficients and derivatives.

Another nonlinear effect is given in figure 22, where c_L over the medium flap deflection angle is shown [89]. Linear theory would suggest that there is no dependence. The figure demonstrates however that there is an influence already at low speed ($M = 0.5$), an effect which increases at high subsonic Mach numbers. This effect must be attributed to viscous interaction which has not been investigated up to now in detail.

That there is a strong viscous effect, especially in the transonic flow regime shows figure 23, where experimental results for a small aspect ratio tapered wing with trailing edge flap compared with theory are given. The figure shows the $c_{L\delta}$ and $c_{L\delta}$ over Mach number with Reynolds number as parameter [90]. These results demonstrate quite clearly the important influence of the Reynolds number. It can be concluded that low Reynolds number experiments may be misleading for the estimation of flight performance. It must be mentioned that all experimental results presented here have been achieved in the Reynolds number range up to $5 \cdot 10^6$. Since this is a very critical range discrepancies between theory and experiment should not always be attributed to inaccuracies of the theory.

4. SUPERSONIC ATTACHED FLOW

4.1 Basic equations

As in the subsonic case the pure supersonic flow can be treated by linearized theory. This allows all the simplifications implicated with a linearized treatment as discussed for subsonic flow. The basic equation for steady flow is

$$(M^2 - 1)\phi_{xx} - \phi_{yy} - \phi_{zz} = 0 \quad (9)$$

The linearized potential equation for the unsteady case is identical to subsonic case

$$\nabla^2 \phi - \frac{1}{a^2} \left[\frac{\partial}{\partial t} + U \frac{\partial}{\partial x} \right]^2 \phi = 0. \quad (10)$$

When the Mach number comes near 1 or exceeds 3 nonlinear terms of the full potential equation have to be taken into account. Linear theory also fails in areas, where shock-waves impinge with the surface.

4.2 Outline of the methods

According to the type of equation to be solved two different types of methods must be distinguished (figure 24)

- singularity-methods for the solution of the linear potential equation
- field-methods for the solution of the potential-equation with nonlinear terms or the Euler equations.

1-9

Singularity-methods: As in subsonic flow, the potential-equation can be transferred into an integral-equation which is the basis of all supersonic theories. Special features of supersonic theory are

- range of dependence: only the area of the Mach-cone in front of the pivot-point has an influence on the flow condition in the pivot point
- subdivision between sub- and supersonic edges: subsonic edges have a singular behaviour different from the supersonic case. When there is a supersonic edge, there is no mutual dependence of upper and lower side of the wing around this edge.

There exist several different formulations to treat the supersonic problem. Among others the most important are

- integration of the downwash |91|, |92|
- integration of the velocity potential |93|, |94|
- acceleration potential |95|.

All three formulation have their special merits. There are also several ways integrating the range of influence. The most important are given in figure 25, covering

- square boxes |96|
- Mach boxes |93|, |95|, |97|
- characteristic boxes |91|, |92|
- boxes adjusted to wing geometry |98|, |99|.

No best choice can be given, since this depends often from geometry and range of Mach number. All these techniques give appropriate results if the evaluation for each box is done in a proper way.

Field-methods: For a more refined analysis of the supersonic flow of complex configurations methods must be used which base on a potential equation with the most important nonlinear terms, the full potential equation or even the Euler equations abandoning the concept of isentropic flow. Such methods - at this time in the status of development - are finite difference |100| and finite volume techniques |101|. Up to now none of these methods has been used for the prediction of control effectiveness.

4.3 Discussion of results

For steady flow figure 26 shows results evaluated with the flexstab-program |102|, a program-set developed by BOEING and NASA, which contains elements of the theories described in |35| and |99| for subsonic and supersonic flow. The results show quite good agreement in the subsonic part, except at the hinge-line where some deviations occur. The supersonic case exhibits good accuracy on the main wing but rather large discrepancies for the load on the flap, although the tendency is given in the right manner.

An unsteady result is given in figure 27 for a swept wing with an oscillating flap at a low supersonic Mach number |103|. Here results of theory and experiment are compared in four spanwise sections. The theories used are lifting surface theory after SADLER and ALLEN |93| (BAC method) and an extension of STARK's theory |92| (MBB method). As can be seen the calculated load distribution on the rear part of the wing agrees quite well with the measurements.

For the same wing figure 28 shows the lift coefficient and the hinge moment due to flap oscillation over the reduced frequency. Although the discrepancies in the real part of the coefficients go up 25%, fair agreement between the two theories, which give nearly identical results, and experiment is obvious.

A general comparison of methods for unsteady subsonic and supersonic flow has been given by WOODCOCK |104|.

5. LEADING EDGE VORTEX FLOW

Among separated flows leading edge vortex flow as it occurs on

- slender delta wings and on
- strakes

is a phenomenon that can be used in flight since this flow exhibits favorable nonlinear lift effects. Comprehensive information on this type of flow is given in |105|.

Methods based on potential theory have been established to solve the vortex flow field above slender wings. Three different approaches have been developed (figure 29)

- leading edge suction analogy [106], [107]
- vortex-lattice method [108], [109], [110]
- free vortex sheet method [111].

The first method only gives overall forces and moments, the vortex-lattice some information on the load distribution of the wing, while the free vortex sheet method, which is a higher order panel method gives detailed results of the pressure distribution.

Figure 30 shows the discretization after the vortex-lattice method for a rectangular wing of small aspect ratio. As in plain flow case the wing itself is subdivided into a number panels with appropriate horseshoe-vortices and pivot-points. While the trailing vortices in general leave the wing at the trailing edge, those vortices which originate from the wing tip, roll up. The figure shows quite clearly this rolling-up process of the different trailing vortices originating from the tip.

Steady results for a highly swept wing with trailing edge flap achieved with the vortex-sheet method are given in figure 31 [112]. The comparison with experimental data shown for two sections exhibits fair agreement between theory and experiment. Nevertheless it can be seen that there remain discrepancies especially due to secondary separations, which are not taken into account in theory.

Since the rolling-up is an iteration-procedure, this process can be interpreted to be an unsteady effect. This has been done by [113] and [114]. Figure 32 shows the development of the lift coefficient with time for a sudden setting in motion. This example is given for a rectangular wing of small aspect ratio at high angle of attack. The two theories after REIBACH (lower and higher order) [113] are compared with theoretical results after BELOTSERKOWSKI [115]. Experimental results are not available for this case.

6. SEPARATED FLOW WITHOUT PRIMARY STRUCTURES

Attached flow can be tackled with potential theory as has been shown in the chapters 2 to 4. Even separated flow with free vortex shedding can be treated by potential theory using appropriate models for the vortex shedding. In contrast to this the generally separated flow exhibits more difficulties since the solution of the full Navier-Stokes-equations has to be executed, if a comprehensive solution is required.

Now fully separated flow in flight should in general be avoided - except post-stall operations of fighters. Nevertheless there is urgent need in the knowledge of occurrence of separation and its development after its beginning, since this effects the loss of control effectiveness. Therefore these solutions are of special importance, but unfortunately only few methods with restricted applicability have been developed so far. The theoretical methods can be subdivided into two classes (figure 33)

- hybrid methods using potential- and boundary-layer theory
- methods solving Navier-Stokes equations.

Whereas the first class of methods still use potential theory combined with boundary-layer calculations and some empirical modelling of the dead air region, the second approach is the most comprehensive but also the most laborious one with respect to computer time.

Hybrid methods: Some methods - up to now only steady approaches - have been developed to evaluate the maximum lift of single airfoils and airfoils with flap [116] - [120]. Figure 34 shows the theoretical model for the flow past an airfoil with flap after JACOB [121]. In this theory a vortex distribution is located along the contour of the airfoil and the flaps to simulate the potential flow. This potential flow calculation is followed by a boundary layer calculation for each part of the airfoil. If the boundary-layer calculation indicates separation, beginning from the point of separation, a dead air model on the rest of the surface is constructed by a source distribution located on the separated part of the contour. Claiming the same pressure value for S, T and U gives a boundary condition for the rate of outflow. The separation point depends on the pressure distribution. Since this pressure distribution itself is not known a priori but has to be evaluated, an iteration-process has to be started which has a good chance to converge as JACOB has shown [116]. Figure 34 shows results of this theory compared with experiments after [122]. As can be seen quite good agreement is achieved not only for the slope of the lift curve but also for the lift maximum.

A different approach for an airfoil with a spoiler based on the conformal-mapping technique has been given by PARKINSON [123]. In figure 35 results of this theory are compared with experimental results. The agreement is quite good except in front of the spoiler, where obviously a second separation area occurs which cannot be treated with this theory.

Figure 36 shows the normalized lift and pitching moment coefficient after a sudden erection of the spoiler [124]. Figure 37 gives information on the stability derivatives $C_{h\delta}$ and $C_{h\delta}$ in dependence of the reduced frequency k . In the range of practical interest $0.1 < k < 1$ both derivatives have regular stable behaviour. Experimental results to back up this theoretical work have not been provided.

Using the 2D characteristics of an airfoil respectively airfoil plus flaps the high lift performance of a 3D wing of moderate and large aspect ratio can be evaluated after the method of WELTE [125].

Solution of the Navier-Stokes equations: At least the solution of the Navier-Stokes equation provides results for partly and fully separated flow. A survey of solutions of the Navier-Stokes equations is given in [126]. But this is no well established technique for general cases. There arise difficulties in the solution especially of those cases relevant for practical application. The following statements can be given: 1-11

- most of the solutions provided up to now deal with laminar flow
- the calculation in the turbulent flow regime requires models for turbulence. Only some very crude models are available up to now
- the computer time for the solution of the Navier-Stokes equations for practical cases is extremely high.

Therefore calculations of practical interest as on airfoils at high Reynolds numbers are scarce. One practical method has been given by DEIWERT [127] who calculated the transonic separated flow past an airfoil. Figure 38 shows a comparison between this theory and experiment for a NACA 0012 airfoil which shows considerable discrepancies. STEGER and BAILEY [128] have developed an alternative approach to deal with the unsteady flap deflection and give pilot results for transonic aileron buzz which compare fairly well with experiments.

7. CONCLUSIONS

For the prediction of control-effectiveness theoretical methods are available for the all speed ranges. The applicability of these methods is generally restricted to attached flow. Separated flow can only be treated in some specific cases. As to the different speed ranges and flow conditions conclusions as follow can be drawn:

Subsonic attached flow:

For the steady case powerful singularity methods are available. Thin wing theory gives good results for the static lift-dependent coefficients of control devices. Panel methods combined with boundary layer calculations offer the possibility of detailed inspection of the flow and the provision of drag dependent data. For the 2D case efficient approaches on this basis are in use. The 3D application of this approach is still in the status of development since general 3D boundary-layer methods with accurate prediction of transition and separation are not yet available.

For the unsteady case again lift dependent data from thin wing theory are in good agreement with experience within the bandwidth which can be accepted for technical applications. For the evaluation of drag-dependent data unsteady panel and boundary layer methods have to be developed. A difficult problem which has to be solved within this context, is the replacement of the Kutta-condition for the unsteady case.

Transonic attached flow:

In contrast to subsonic flow the theoretical prediction of this type of flow exhibits much more difficulties. This is due to the nonlinearity of the basic equations, the change of flow type within the flow field and the occurrence of shocks. For the solution of the inviscid flow problem a number of different techniques have been proposed and investigated. Although the finite difference methods seem to be the at this time most powerful methods for steady and unsteady flow, the question what will be the standard technique for the future is still open.

Furthermore unsolved problems are posed by viscous effects. On those parts of the wing where shock-waves impinge with the surface and at the trailing edge, boundary layer assumptions are no longer valid. New approaches have to be developed here. Nevertheless for steady flow fairly good theoretical results have been achieved as far as shocks remain weak. For the unsteady case only 2D results have been provided up to now.

Another difficulty that arises in transonics is the relative inaccuracy of experimental results from wind-tunnel. Reynolds numbers of wind-tunnel investigations differ from flight and wall-interference brings falsification of the results, so that differences between theory and experiment cannot be attributed totally to deficiencies of the theoretical approach.

Supersonic attached flow:

As in subsonic flow linear singularity methods give useful results for technical application purposes as far as lift dependent coefficients are concerned. More accurate field methods are in the status of being developed, but the computational amount for this type of approach is much higher. Viscous correction have only been used to a small extent.

Leading edge vortex flow:

Theoretical results for this type of flow, which is of special importance for fighter type aircraft, is available only for simple configurations. First results for wings with control-surfaces are given. Generally it has to be mentioned that methods for this type of flow are still in development and theoretical results have to be taken with great care. So secondary vortices are up to now not taken into account.

Separated flow without primary structures:

The general problem of separated flow on a 3D wing, which is of great importance for the determination of loss of control efficiency, is up to now unsolved. Up to now only methods for detail-problems as airfoils

at stall and multi-component airfoils at high-lift condition are available on the basis of potential theory plus boundary layer plus modelling of the separated areas. These methods have up to now not been extended to 3D flow.

The most comprehensive but also most laborious approach is the solution of Navier-Stokes equations, which is a long-term aim.

Both approaches especially the second one need detailed theoretical and experimental investigation with respect to the quasisteady and unsteady structure of separated regions.

8. LITERATURE

- [1] - Advanced Control Technology and its Potential for Future Transport Aircraft. NASA TM X-3409 (1976).
- [2] - Impact of Active Control Technology on Airplane Design. AGARD-CP-157 (1974).
- [3] BURNS, B.R.A. Control configured vehicles - the way ahead? Flight International, 13 June 1974, p. 777 to 782.
- [4] KURZHALS, P.R. Active Controls in Aircraft Design. AGARDograph No. 234 (1978).
- [5] LAMB, H. Hydrodynamics. Cambridge University Press, New York, 1963.
- [6] MILNE-THOMPSON, M.L. Theoretical Hydrodynamics. McMillan Comp., London, 1955.
- [7] SCHLICHTING, H. TRUCKENBRODT, E. Aerodynamik des Flugzeuges, Band I und II. Springer-Verlag Berlin/Heidelberg/New York, 1967/1969.
- [8] THWAITES, B., ed. Incompressible Aerodynamics. Oxford University Press, 1960.
- [9] MAZET, R., ed. AGARD Manual of Aeroelasticity, Vol. II. London 1961.
- [10] BISPLINGHOFF, R.L. ASHLEY, H. HALFMAN, R.L. Aeroelasticity. Addison-Wesley Publ. Comp. Inc., Reading, Mass. 1957.
- [11] FÖRSCHING, H.W. Grundlagen der Aeroelastik. Springer Verlag, Berlin/Heidelberg/New York, 1974.
- [12] LASCHKA, B. Unsteady aerodynamic prediction methods applied to aeroelasticity in "Unsteady Aerodynamics". AGARD-R-645, p. 1-1 to 1-31 (1975).
- [13] ASHLEY, J. Unsteady subsonic and supersonic inviscid flow. AGARD-CP-227, p. 1-1 to 1-32 (1977).
- [14] FÖRSCHING, H.W. Prediction of unsteady airloads on oscillating lifting systems and bodies for aeroelastic analyses. Prog. Aerosp. Sci. 1978, Vol. 18, p. 211 to 269, Pergamon Press, Oxford.
- [15] - Prediction of Aerodynamic Loading. AGARD-CP-204 (1976).
- [16] - Unsteady Airloads in Separated and Transonic Flow. AGARD-CP-226 (1977).
- [17] - Unsteady Aerodynamics. AGARD-CP-227 (1977).
- [18] THEOLOFSEN, T. General theory of aerodynamic instability and the mechanism of flutter. NACA Rep. 496 (1935).
- [19] MÜLTHOFF, H. Methods for calculating the lift distribution of wings. ARC R+M 2884 (1955).
- [20] TRUCKENBRODT, E. Tragflächentheorie bei inkompressibler Strömung. Jb. 1953 WGL, p. 40 to 65 (1953).
- [21] LASCHKA, B. Zur Theorie der harmonisch schwingenden tragenden Fläche bei Unterschallanströmung. Z. Flugwiss. Vol. 11 (1963), p. 265 to 292.
- [22] LASCHKA, B. Interfering lifting surfaces in subsonic flow, Z. Flugwiss. 18 (1970), p. 359 to 368.
- [23] DAVIES, D.E. Calculation of unsteady generalized airforces on a wing oscillating harmonically in subsonic flow. ARC R+M 3409 (1965).
- [24] FALKNER, V.M. The calculation of aerodynamic loading on surfaces of any shape. ARC R+M 1910 (1943).
- [25] RUBBERT, P.E. Theoretical characteristics of arbitrary wings by a non-planar-vortex lattice method. BOEING Comp. Rep. D6-9244 (1962).
- [26] GIESING, J.P. Lifting surface theory for wing-fuselage combinations. McDonnell-Douglas Rep. DAC 67212, Vol. I (1968).
- [27] KÖFNER, H. Berechnung der potentialtheoretischen Strömung um Flügel-Rumpf-Kombinationen und Vergleich mit Messungen. Z. Flugwiss. Vol. 20 (1972), p. 351 to 368.
- [28] HALFMAN, S.G. Vortex lattice method for calculation of quasisteady state loadings on thin elastic wings. FFA Rep. 105 (1965).
- [29] ABANO, E. RODDEN, W.P. A doublet-lattice method for calculating lift distribution on oscillating surfaces in subsonic flow. AIAA Vol. 7, p. 279 to 285 (1969).
- [30] KALMAN, T.P. RODDEN, W.P. GIESING, J.P. Application of the doublet-lattice method to nonplanar configurations in subsonic flow. J. Aircraft Vol. 8, p. 406 to 413 (1971).
- [31] RODDEN, W.P. A comparison of methods used in interfering lifting surface theory. AGARD Rep. 643 (1976).

- 1-13
- [32] ROCS, R. The use of panel methods for stability derivatives. AGARD-CP-235, p. 21-1 to 21-11 (1978).
- [33] GEISSLER, W. Calculation of the unsteady airloads on oscillating three-dimensional wings and bodies. AGARD-CP-227, p. 5-1 to 5-13 (1977).
- [34] HESS, J.L.
SMITH, A.M.O. Calculation of potential flow about arbitrary bodies. In: D. Küchemann et al: Progress in Aeronautical Sciences, Vol. 8, Pergamon Press, Oxford, 1967, p. 1 to 138.
- [35] RUBBERT, P.E.
SAARIS, G.R. A general three-dimensional potential flow method applied to V/STOL aerodynamics. SAE Air Transportation Meeting, New York 1968.
- [36] LABRUJERE, Th.E.
LOEVE, W.
SLOOFF, J.W. An approximate method for the calculation of the pressure distribution on wing-body combinations at subcritical speeds. AGARD-CP-71, p. 11-1 to 11-19 (1971).
- [37] KRAUS, W.
SACHER, P. Das MBB-Unterschall-Panelverfahren. MBB-Rep. UFE 672-70 (1970).
- [38] AHMED, S.R. Calculation of the inviscid flow field around three-dimensional lifting wings, fuselages and wing-fuselage combinations using panel method. ESA TT-210 (1975). In German: DLR-FB 73-102 (1973).
- [39] ROBERTS, A.
RUNDLE, K. Computation of incompressible flow about bodies and thick wings using the spline mode system. BAC Aero Ma 19 (1972).
- [40] JOHNSON, F.T.
EHLERS, F.E.
RUBBERT, P.E. A higher order panel method for general analysis and design applications in subsonic flow. Lecture Notes in Physics, Vol. 59, p. 247 to 253 (1976).
- [41] GIESING, J.P. Nonlinear two-dimensional unsteady potential flow with lift. J. Aircraft 5 (1968), p. 155 to 145.
- [42] HESS, J.L. The problem of three-dimensional lifting surface potential flow and its solution by means of surface singularity distribution. Computer Methods in Applied Mechanics and Engineering 4 (1974), p. 283 to 319.
- [43] MORINO, L.
TSENG, K. Steady, oscillatory and unsteady, subsonic and supersonic aerodynamics (SOUSSA) for complex aircraft configurations. AGARD-CP-227, p. 3-1 to 3-14 (1977).
- [44] GEISSLER, W. Nonlinear unsteady potential flow calculations for three-dimensional oscillating wings. AIAA Journ. 16, p. 1168 to 1174.
- [45] KÖRNER, H.
HIRSCHEL, E.H. The calculation of flow fields by panel methods: a report on Euromech 75. J. Fluid Mech. (1977), Vol. 79, part 1, p. 181 to 189.
- [46] BERGH, H.
HJEDEMAN, H. Binary flutter calculations with theoretical and empirical aerodynamic derivatives for a wing-control surface in two-dimensional incompressible flow. NLR-TR 68096U (1968).
- [47] GRENON, R.
TIERS, J. Étude d'un profile supercritique avec gouverne oscillante en écoulement subsonique et transsonique. AGARD-CP-227, p. 8-1 to 8-10 (1977).
- [48] FÖRSCHING, H.
TRIEBSTEIN, H.
WAGENER, J. Pressure measurements of a harmonically oscillating swept wing with two control surfaces in incompressible flow. DLR-IB 70-47 (1970).
- [49] MÜLLER, A.
SCHMID, H.
KINDLER, M. Berechnung der instationären Luftkräfte an Flügeln mit Rudern in Unterschallströmung. VFW-Fokker Rep. ZTL 4.05, Teil 2/1970.
- [50] BECKER, J. Interfering lifting surfaces in unsteady subsonic flow - comparison between theory and experiment. AGARD Rep. 614 (1974).
- [51] MURMAN, E.M.
COLE, J.D. Calculation of plane steady transonic flow. AIAA Journal 9, p. 114 to 121 (1971).
- [52] BAUER, F.
GARABEDIAN, P.
KORN, D. Supercritical wing sections. Lect. Notes in Economics and Math. Systems, Vol. 66, Springer Verlag Berlin/Heidelberg/New York, 1972.
- [53] BOLKSTOEL, J.W. Review of the application of hodograph theory to transonic airfoil design and theoretical and experimental analysis of shock-free aerofoils. Symposium Transsonicum II. Springer Verlag Berlin/Heidelberg/New York, 1976, p. 109 to 133.
- [54] SOBIECZKY, H. The application of generalized potentials on plane transonic flow. Symposium Transsonicum II. Springer Verlag Berlin/Heidelberg/New York, 1976, p. 306 to 313.
- [55] SPREITER, J.R.
ALKSNE, A.Y. Thin airfoil theory based on approximate solution of the transonic flow equation. NACA TR 1359, 1958.
- [56] ZIEREP, J. Schallnahe Strömungen - Beiträge zur parabolischen Methode. ZAMM Vol. 43, p. 1182 to 1187 (1963).
- [57] STAHARA, S.
SPREITER, J.R. Development of a nonlinear unsteady transonic flow theory. NASA-CR 2258 (1973).
- [58] ISOGAI, K. A method for predicting unsteady aerodynamic forces on oscillating wings with thickness in transonic flow near Mach number 1. NAL Rep. TR-368T (1974).
- [59] PARK, P.H. Calculation of aerodynamic derivatives in unsteady two-dimensional flow using Dowells's linearization method. Princeton University, AMS Rep. 1238-T (1975).
- [60] NÖRSTRUD, H. The transonic airfoil problem with embedded shocks. The Aero. Quart. 24, 2 (1973), p. 129 to 138.

- [61] NIXON, D. HANCOCK, G.J. Integral equation methods - a reappraisal. Symposium Transsonicum II, Springer-Verlag Berlin/Heidelberg/New York, 1976, p. 174 to 182.
- [62] NIXON, D. A twodimensional airfoil with a control surface oscillating at low frequency in high subsonic flow. The Aero. Quart. 25, 3 (1974), p. 186 to 198.
- [63] ISOGAI, K. Approximate method for calculating aerodynamic loadings on an airfoil oscillating in high subsonic flow. NAL Rep. TR-455T (1976).
- [64] BALLHAUS, W.F. BAILEY, F.R. Numerical calculation of transonic flow about swept wings. AIAA paper 72-677 (1972).
- [65] KLUNKER, E.B. NEWMAN, P.A. Computation of transonic flow about lifting wing-cylinder combinations. J. Aircraft 11, (1974), p. 254 to 256.
- [66] SCHMIDT, W. ROHLFS, S. VANINO, R. Some results using relaxation methods for two- and three-dimensional transonic flows. Lecture Notes in Physics 35, Springer Verlag Berlin/Heidelberg/New York, p. 364 to 372, (1975).
- [67] JAMESON, A. Iterative solution of transonic flow over airfoils and wings, including flows at Mach 1. Comm. Pure Appl. Math. 27 (1974), p. 283 to 309.
- [68] ALBONE, C.M. HALL, M.G. JOYCE, G. Numerical solutions for transonic flows past wing-body combinations. Symposium Transsonicum II. Springer Verlag Berlin/Heidelberg/New York 1976, p. 541 to 548.
- [69] EHLERS, F.E. A finite difference method for the solution of the transonic flow around harmonically oscillating wings. NASA CR 2257 (1973).
- [70] BALLHAUS, W.F. LOMAX, H. The numerical simulation of low frequency unsteady transonic flow fields. Lecture Notes in Physics Vol. 35, Springer-Verlag Berlin/Heidelberg/New York, 1975, p. 57 to 63.
- [71] COUSTON, M. ANGELINI, J.J. Solution of nonsteady two-dimensional transonic small disturbance potential flow equation. ONERA TP 1978-69.
- [72] WEATHERILL, W.H. SEBASTIAN, J.D. EHLERS, F.E. Application of a finite difference method to the analysis of transonic flow over oscillating airfoils and wings. AGARD-CP-226, p. 17-1 to 17-13 (1977).
- [73] BALLHAUS, W. COORJIAN, P. YOSHIHARA, H. Unsteady force and moment alleviation in transonic flow. AGARD-CP-227, p. 14-1 to 14-10, 1977.
- [74] FRITZ, W. Transsonische Strömung um harmonisch schwingende Profile. Dornier Rep. 78/16B (1978).
- [75] MAGNUS, R.J. YOSHIHARA, H. Inviscid transonic flow over airfoils. AIAA paper No. 70-47 (1970).
- [76] MAGNUS, R.J. YOSHIHARA, H. The transonic oscillating flap. AGARD-CP-226, p. 13-1 to 13-3 (1977).
- [77] BEAM, R.M. WARMING, R.F. Numerical calculations of two-dimensional unsteady transonic flow with circulation. NASA TN-D 7605 (1974).
- [78] LAVAL, P. Calcul de l'écoulement instationnaire transsonique autour d'un profil oscillant par une methode à pas fractionnaires. ONERA TP No. 1975-115 (1975).
- [79] LERAT, A. SIDES, J. Calcul numerique d'écoulement transsonique instationnaire. AGARD-CP-226, p.15-1 to 15-10 (1977).
- [80] BERNUT, P. Bedeutung der Variationsrechnung in der Strömungsmechanik und ihre Anwendung bei kompressiblen Potentialströmungen. Dr.-Ing. Thesis, TU Munich, 1973.
- [81] PERIAUX, J. Calcul tridimensionnel de fluides compressibles par la méthode des éléments finis. 10eme Colloque d'Aérodynamique Appliquée, Nov. 1973.
- [82] EBERLE, A. Transonic potential flow computations by finite elements: airfoil and wing analysis, airfoil optimization. MBB-Rep. UF 1428 (1978).
- [83] CHAN, S.T.K. BRASHEAR, M.R. Finite element analysis of unsteady transonic flow. AIAA Paper 75-875 (1975).
- [84] EBERLE, A. Computerprogrammtests des Finite-Element-Verfahrens zur Berechnung instationärer Profilströmungen. MBB-UFE122-AERO-MT-396 (1979).
- [85] EVANS, M.W. HARLOW, F.H. The particle-in-cell method for hydrodynamic calculations. Rep. LA-2139, 1957, Los Alamos Scientific Lab., Los Alamos, N.Mex.
- [86] JAMESON, A. CAUGHEY, D.A. A finite-volume scheme for transonic potential flow calculations. AIAA-paper 77-635 (1977).
- [87] RIZZI, A. BAILEY, H. Finite-volume solution of the Euler equations for steady three-dimensional transonic flow. Lecture Notes in Physics, Vol. 59 (1976), p. 347 to 352.
- [88] TIJDEMAN, H. Investigations of the transonic flow around oscillating airfoils. NLR TR 77090U (1977).
- [89] GRENON, R. DESOPPER, A. Effets instationnaires des gouvernes. 15^e Colloque d'Aérodynamique Appliquée, Marseille, Nov. 1978.
- [90] GRAY, R. DAVIES, D.E. Comparison of experimentally and theoretically determined values of oscillatory aerodynamic control surface hinge moment coefficients. RAE TR 72023 (1972).
- [91] ETKIN, B. Numerical integration method for supersonic wings in steady and oscillating motion. UTIA Rep. 36 (1955).

- [92] STARK, V.J.E. Calculation of aerodynamic forces on two oscillating finite wings at low supersonic Mach numbers. SAAB TN 53, 1964.
- [93] ALLEN, D.J.
SADLER, D.S. Oscillatory aerodynamic forces in linearized supersonic flow for arbitrary frequencies, planforms and Mach numbers. ARC R+M 3415, 1963.
- [94] WOODCOCK, D.L.
YORK, E.J. A supersonic box collocation method for the calculation of unsteady airforces of tandem surfaces. AGARD Symposium on Unsteady Aerodynamics for Aeroelastic Analyses of Interfering Surfaces, Tonsberg, Norway, 1970.
- [95] MÜLLER, A. Berechnung der Druckverteilung an schwingenden Tragflügeln in Überschallströmung mittels eines Kollokationsverfahrens für die Küssnersche Integralgleichung. Dr.-Ing. Thesis, TU Munich, 1973.
- [96] PINES, S.
DUGUNDJI, J.
NEURINGER, J. Aerodynamic flutter derivatives for an oscillating finite thin wing in supersonic flow. JAS 23, p. 693, 1955.
- [97] TA LI Aerodynamic influence coefficients for an oscillating finite thin wing in supersonic flow. JAS 23, p. 613 to 622, 1955.
- [98] WOODWARD, F.A.
LARSON, J.W. A method of optimising camber surfaces for wing-body combinations at supersonic speeds. BOEING Rep. 106-10741 (1965).
- [99] WOODWARD, F.A. Analysis and design of wing-body combinations at subsonic and supersonic speeds. J. Aircraft 5 (1968), p. 528 to 534.
- [100] WEILAND, C.
THIESS, H.J. Analysen berechneter dreidimensionaler reibungsfreier Strömungsfelder mit eingebetteten Verdichtungsstößen, Teil I. DFVLR-FB 78-09 (1978).
- [101] RIZZI, A.W.
KLAVINS, A.
McCORMACK, R.W. A generalized hyperbolic marching technique for three dimensional supersonic flow with shocks. Lecture Notes in Physics Vol. 35, Springer-Verlag Berlin/Heidelberg/New York, 1975, p. 341 to 346.
- [102] MANRO, M.E.
BOBBITT, P.J.
RODGERS, J.T. Comparison of theoretical and experimental pressure distributions on an arrow-wing configuration at subsonic, transonic and supersonic speeds. AGARD-CP-204, p. 11-1 to 11-14 (1976).
- [103] LODGE, C.G.
SCHMID, H. Unsteady pressures due to control surface rotation at low supersonic speeds. AGARD Rep. 647 (1976).
- [104] WOODCOCK, D.L. A comparison of methods used in lifting surface theory. AGARD Rep. 585 (1971).
- [105] - High Angle of Attack Aerodynamics. AGARD-CP-247 (1978).
- [106] POLHAMUS, E.C. A concept of the vortex lift of sharp-edge delta wings based on a leading-edge-suction analogy. NASA TN D-3767 (1966).
- [107] LAMAR, J.E. Extension of leading-edge-suction analogy to wings with separated flow around the side edges at subsonic speeds. NASA TR R-428 (1974).
- [108] BELOTSERKOVSKII, S.M. Calculation of the flow about wings of arbitrary planform at a wide range of angles of attack. RAE Lib. Transl. No. 1433 (1970).
- [109] REHBACH, C. Numerical investigation of vortex sheets issued along a separation line near the leading edge of wings. EUROMECH 41 Colloquium, Norwich (G.B.) (1973).
- [110] SCHRÖDER, W. Berechnung der nichtlinearen Beiwerte von Flügeln mit kleinem und mittlerem Seitenverhältnis nach dem Wirbelleiterverfahren in inkompressibler Strömung. DFVLR-FB 78-26 (1978).
- [111] BRUNE, G.W.
WEBER, J.A.
JOHNSON, F.T.
LU, P.
RUBBERT, P.E. A three-dimensional solution of flows over wings with leading-edge vortex separation. NASA-CR 2709 (1975).
- [112] TINICO, E.N.
YOSHIMURA, H. Subcritical drag minimization for highly swept wings with leading edge vortices. AGARD CP-247, p. 26-1 to 26-9 (1978).
- [113] REHBACH, C. Calcul instationnaires de nappes tourbillonnaires émises par des surfaces portantes fortement inclinées. AGARD-CP-247, p. 14-1 to 14-9 (1978).
- [114] KANDIL, O.A.
ATTA, E.H.
NAYFEH, A.H. Three dimensional steady and unsteady asymmetric flow past wings of arbitrary planforms. AGARD-CP-227, p. 2-1 to 2-19 (1977).
- [115] BELOTSERKOVSKII, S.M. Non stationary non linear theory of a thin wing of arbitrary planform. Izv. Akad. Nauk SSSR, Mekh. Zhidk Gaza 4: 100-8, Fluid Dyn. 9 (4); p. 583 to 589 (1974).
- [116] JACOB, K. Berechnung der abgelösten inkompressiblen Strömung um Tragflügelprofile und Bestimmung des maximalen Auftriebs. Z. Flugwiss. 17, July 1969.
- [117] STEVENS, W.A.
GORADIA, S.H.
BRADEN, J.A. Mathematical model for twodimensional multicomponent airfoils in viscous flow. NASA CR-1843 (1971).
- [118] GRASHOF, J. Berechnung der Druck- und Schubspannungsverteilung auf Körpern mit Totwasser in ebener inkompressibler Parallelströmung. Dr.-Ing. Thesis, TU Karlsruhe (1973).
- [119] DVORAK, F.A.
WOODWARD, F.A. A viscous/potential flow interaction analysis method for multi-element infinite swept wings. NASA CR-2476 (1974).
- [120] BRUNE, G.W.
MANKE, J.W. Upgraded viscous flow analysis of multi-element airfoils. AIAA Paper 78-1224 (1978).

- [121] JACOB, K.
STEINBACH, D. A method for prediction of lift for multi-element airfoil systems with separation. AGARD-CP-143, p. 12-1 to 12-16.
- [122] FORSTER, D.N.
IRWIN, H.P.A.H.
WILLIAMS, B.R. The two-dimensional flow around a slotted flap. RAE TR 70164 (1970).
- [123] PARKINSON, G.V.
BROWN, G.P.
JANDAKI, T. The aerodynamics of two-dimensional airfoils with spoilers. AGARD-CP-143, p. 14-1 to 14-10 (1974).
- [124] BERNIER, R.
PARKINSON, G.V. Oscillatory aerodynamics and stability derivatives for airfoil spoiler motion. AGARD-CP-235, p. 25-1 to 25-7 (1978).
- [125] PROKSCH, H.J.
WELTE, D. Theoretische Ermittlung des Überziehverhaltens und des Maximalauftriebs von Pfeilflügeln. ZTL Do 4.01/5 (1972).
- [126] WIRZ, H.J.
SMOLDEREN, J.J. Numerical integration of Navier-Stokes-equations. AGARD-LS-64, p. 3-1 to 3-13 (1973).
- [127] DEIWERT, G.S. Recent computations of viscous effects in transonic flow. Lecture Notes in Physics, Vol. 59, p. 159 to 164 (1976).
- [128] STEGER, J.L.
BAILEY, H.E. Calculation of transonic aileron buzz. AIAA Paper 79-0134 (1979).

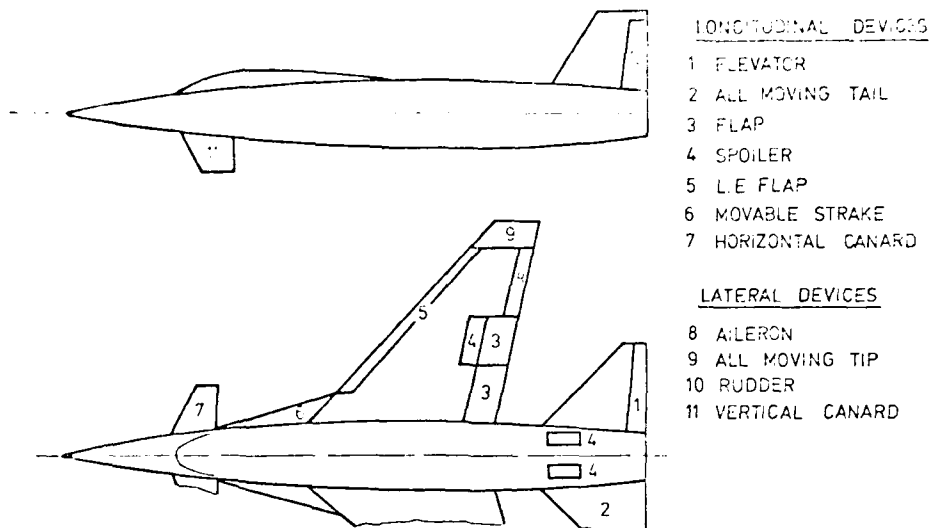


Fig. 1: Control surfaces

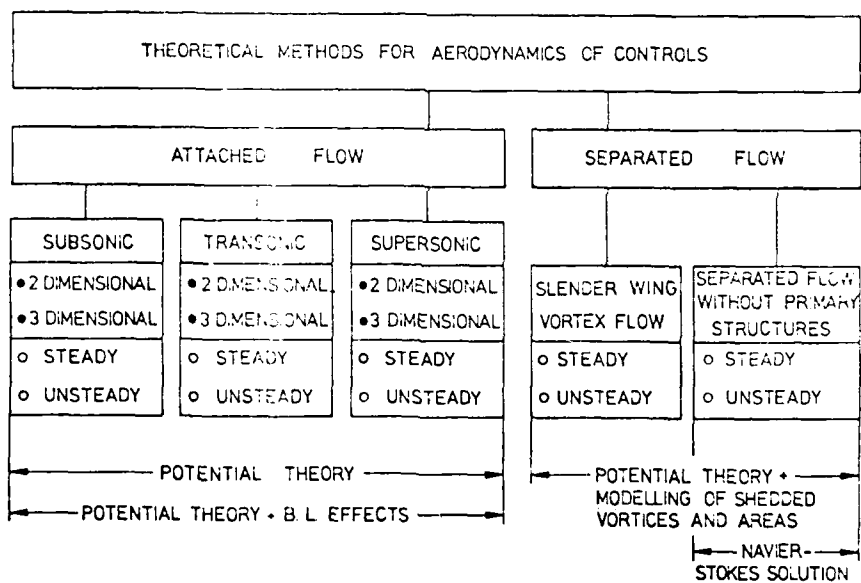


Fig. 2: Survey of theoretical methods

TYPE OF METHOD	STEADY		UNSTEADY	
	2D	3D	2D	3D
— CONFORMAL MAPPING	●		●	
— SINGULARITY METHODS				
-- LOADING FUNCTION	●	●	●	●
-- DISCRETE LOADING				
--- VORTEX / DOUBLET LATTICE	●	●	●	●
--- PANEL	●	●	●	●

● AVAILABLE ○ UNDER DEVELOPMENT

Fig. 3: Methods for subsonic flow

1-18

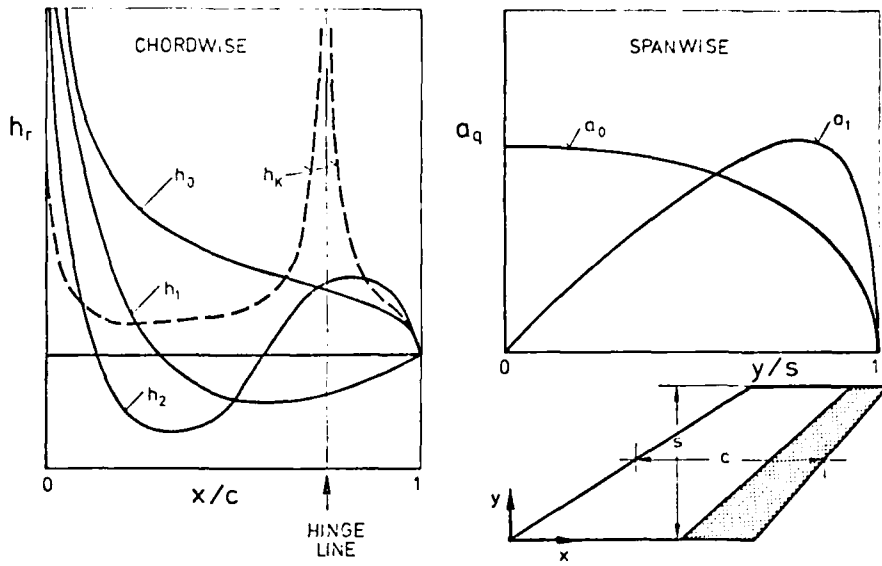


Fig. 4: Loading functions

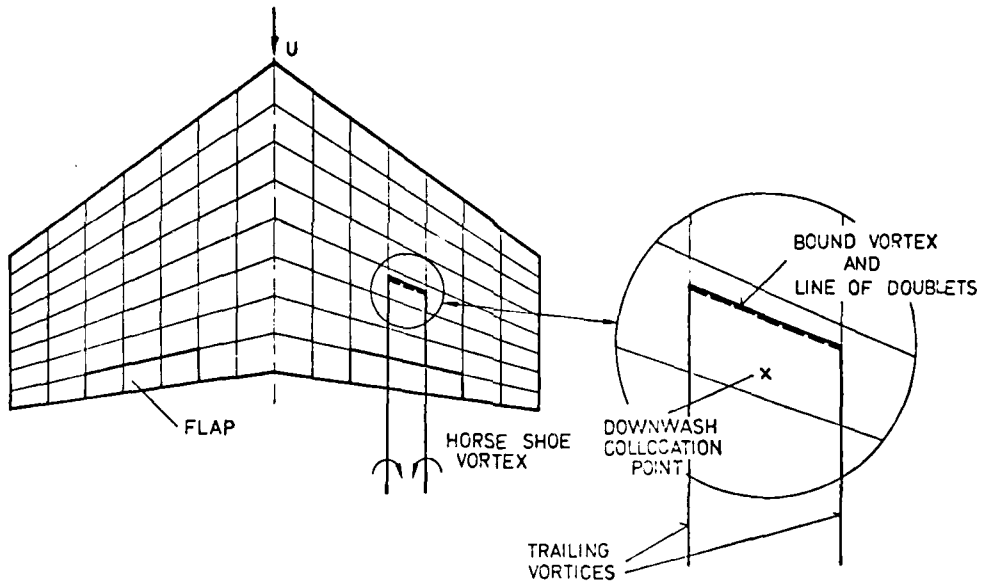
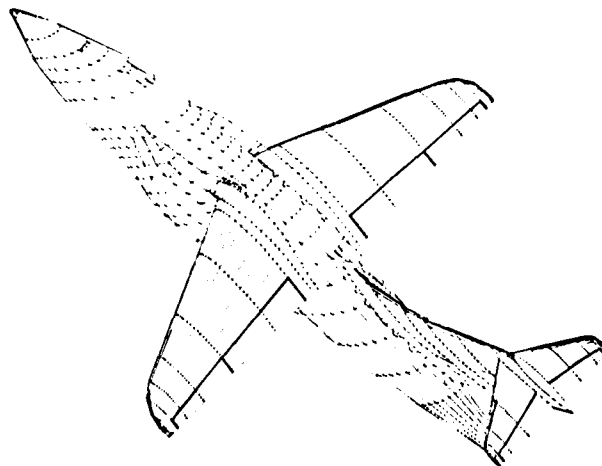


Fig. 5: Discretization of the wing for the vortex/doublet-lattice method

Fig. 6: Discretization of a fighter type aircraft for the panel method



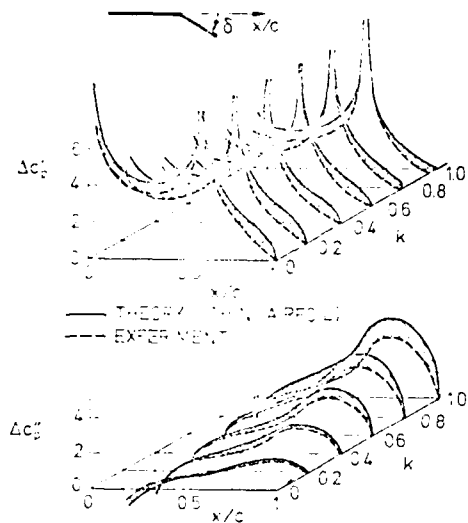


Fig. 7: Comparison theory - experiment for a two-dimensional airfoil with oscillating flap at various frequencies (adapted from [46])

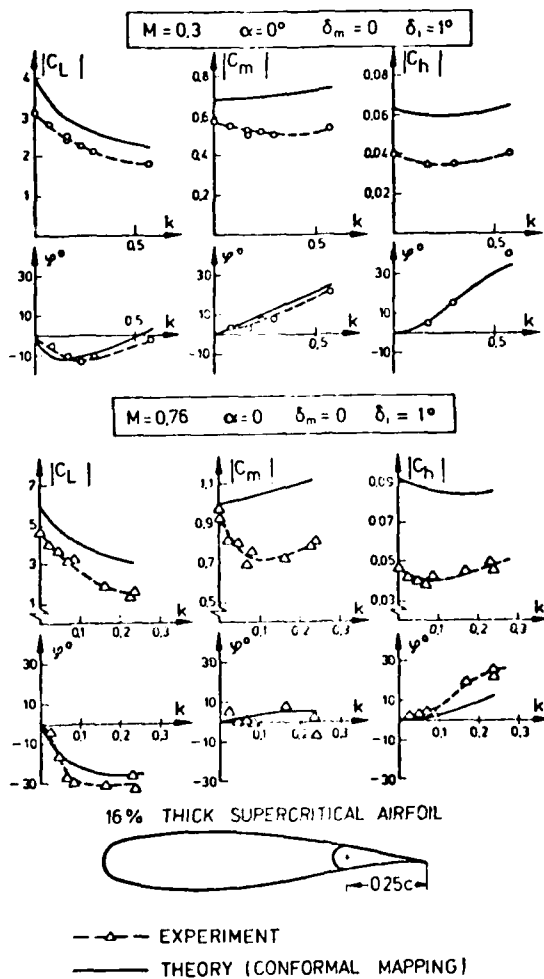
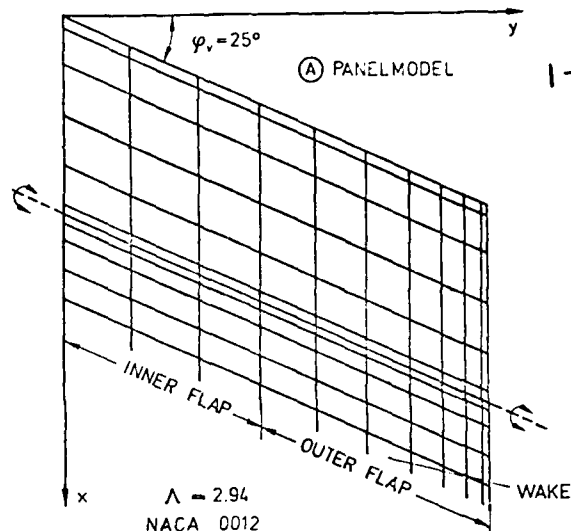


Fig. 8: Comparison theory - experiment for an airfoil with oscillating flap at different Mach numbers (adapted from [47])



(B) COMPARISON THEORY-EXPERIM. FLAPS IN ANTIPHASE

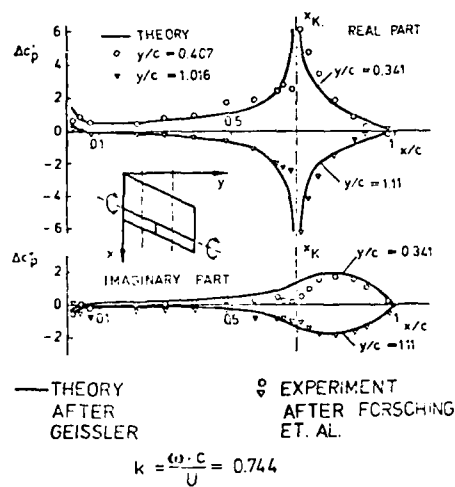


Fig. 9: Comparison theory - experiment for a swept wing with oscillating flap in incompressible flow (adapted from [33])

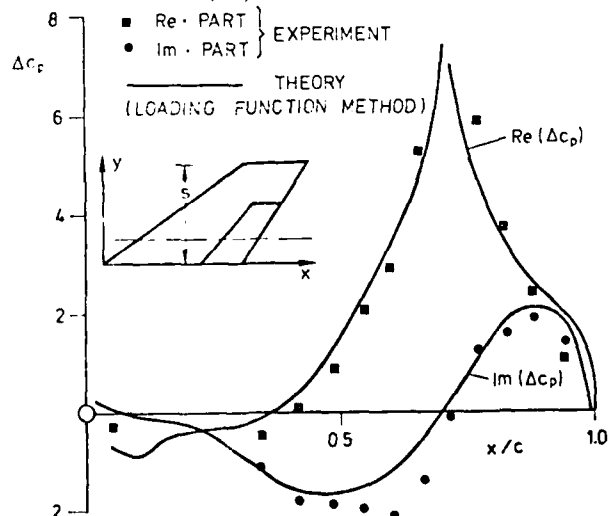


Fig. 10: Comparison theory - experiment for a swept tapered wing with oscillating flap at subsonic speed ($M = 0.85$, $k = 0.85$, $y/s = 0.25$; adapted from [12])

1-20

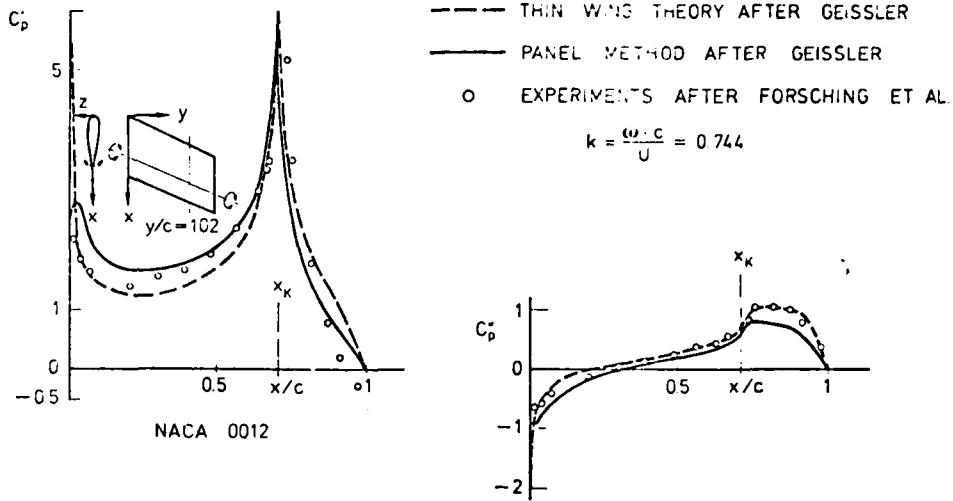


Fig. 11: Comparison theory - experiment for a swept wing with oscillating flap in incompressible flow (adapted from [44])

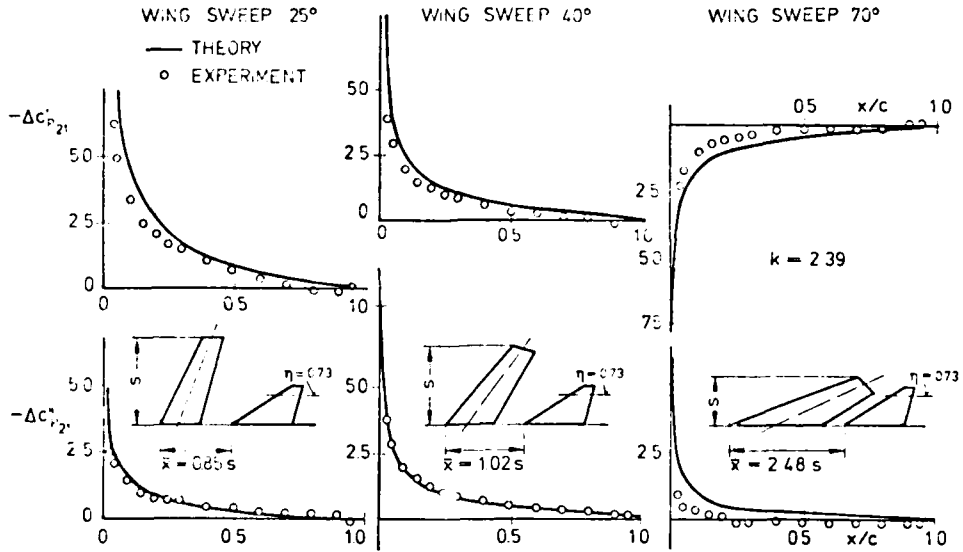


Fig. 12: Comparison theory - experiment for the pressure distribution on the tail due to wing pitch oscillation (adapted from [50])

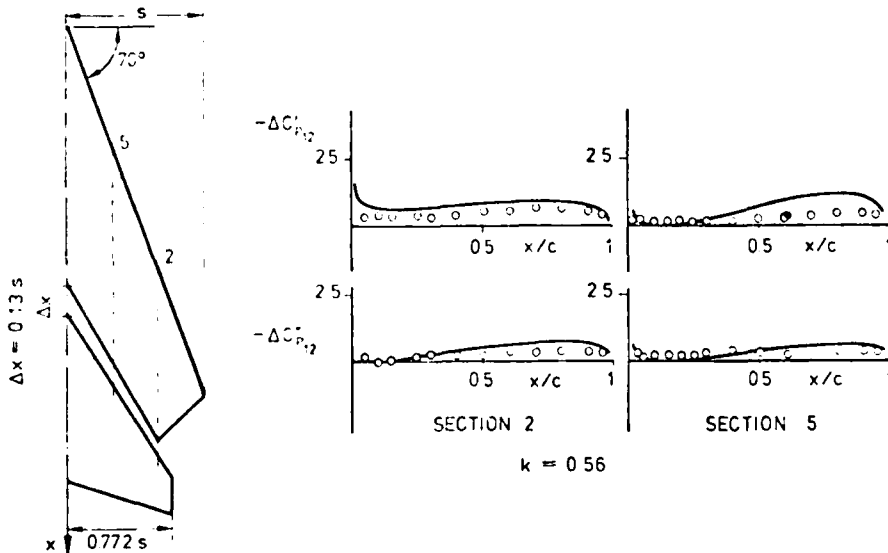


Fig. 13: Comparison theory - experiment for the pressure distribution on the swept wing due to tail pitch oscillation (adapted from [50])

	STEADY		UNSTEADY	
	2D	3D	2D	3D
— HODOGRAPH	●			
— LOCAL LINEARIZATION	●	●	●	○
— INTEGRAL EQUATION	●	●	●	
— FINITE DIFFERENCE				
— — RELAXATION	●	●	●	○
— — TIME MARCHING	●		●	○
— FINITE ELEMENT	●		●	
— FINITE VOLUME	●	●	●	○

● AVAILABLE ○ UNDER DEVELOPMENT

Fig. 14: Methods for transonic flow

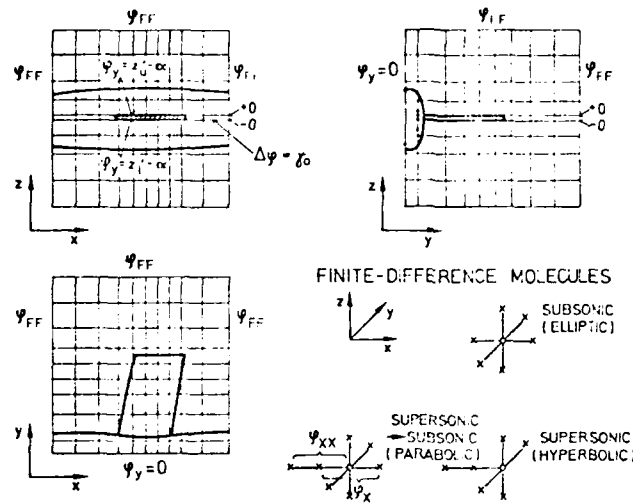


Fig. 15: 3D-finite-difference mesh for the solution of the transonic-small-perturbation equation

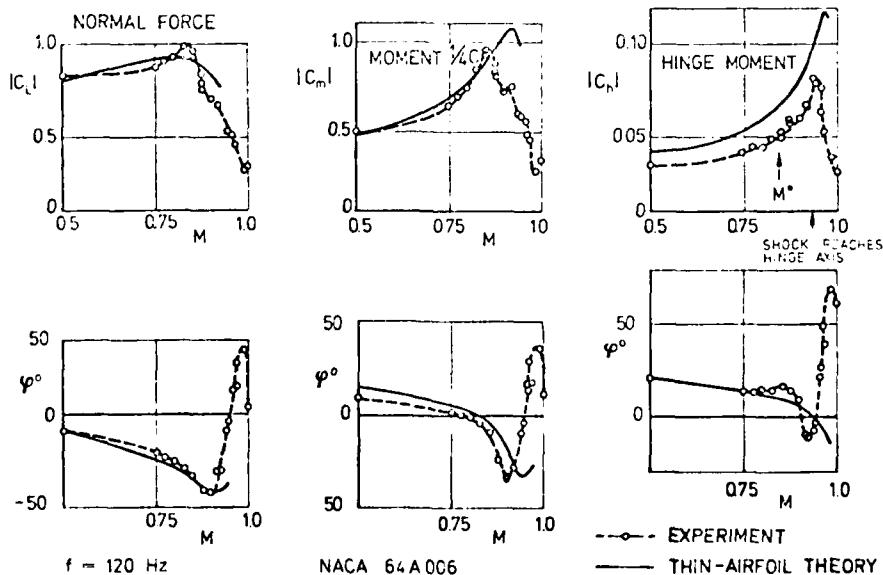
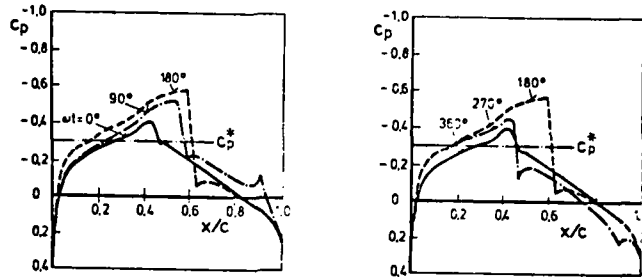
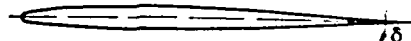


Fig. 16: Comparison theory - experiment for a thin airfoil with oscillating flap at subsonic and transonic speed (adapted from [88])

1-22



NACA 64A006



$k = 0,2$
 $M = 0,85$

$\delta = \sin(\omega t)$
 $\delta_{max,min} = \pm 2^\circ$

THEORY: FINITE DIFFERENCE METHOD

Fig. 17: Unsteady upper surface pressure distribution of an airfoil with oscillating flap at transonic speed (adapted from [73])

NACA 64 A 006
WITH TRAILING EDGE FLAP
 $M = 0.875$
 $f = 120 \text{ Hz}$

— EXPERIMENT
- - - INVISCID THEORY
- - - VISCOUS THEORY

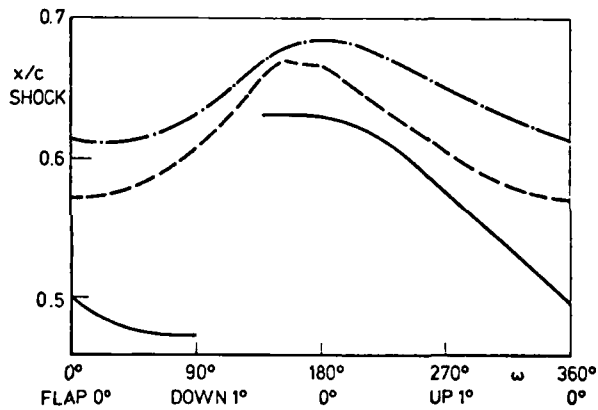
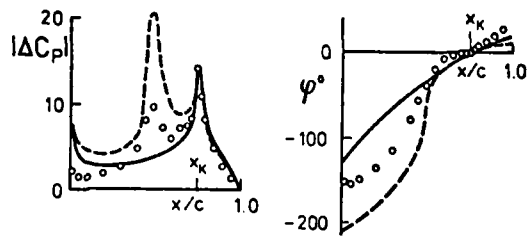


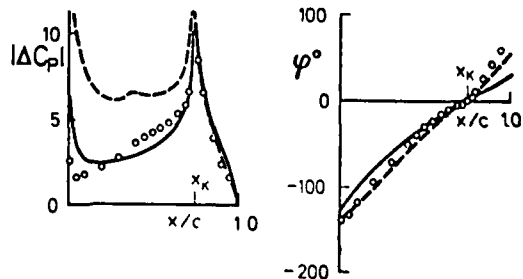
Fig. 18: Shock positioning on an airfoil due to an oscillating flap (adapted from [76])

$M = 0.85$
 $k = 0.253$



$M = 0.8$
 $k = 0.179$

— THEORY, THIN AIRFOIL
- - - THEORY, EHLERS
o EXPERIMENT



NACA 64 A 006

Fig. 19: Comparison theory - experiment for an airfoil with oscillating flap at transonic speed (adapted from [88])

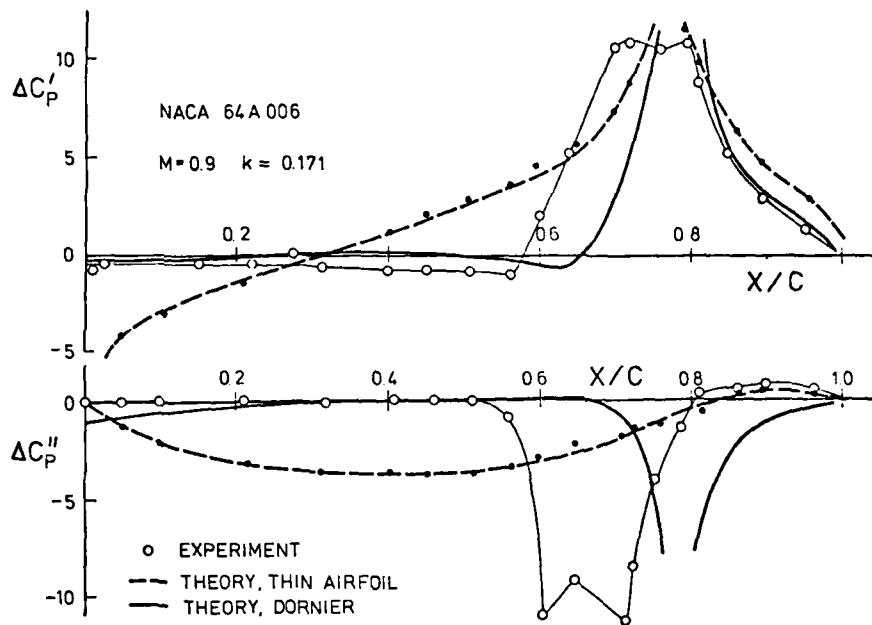


Fig. 20: Comparison theory - experiment for an airfoil with oscillating flap at transonic speed (adapted from [74])

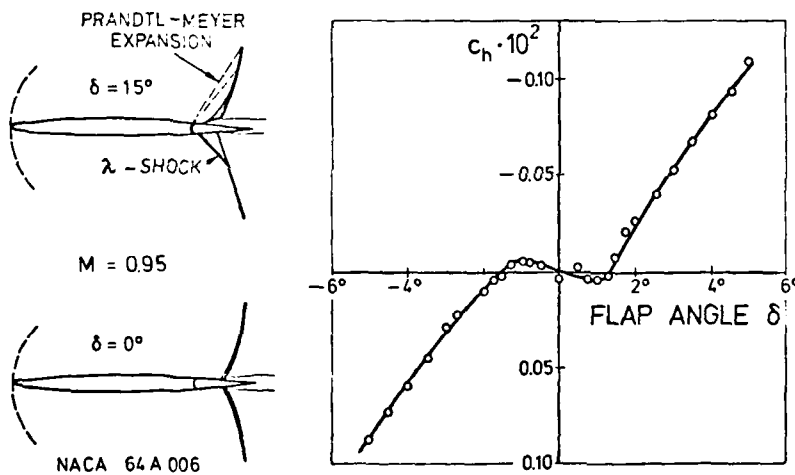


Fig. 21: Special flow condition for an airfoil, showing a strongly nonlinear behaviour (adapted from [88])

16% THICK SUPERCRITICAL AIRFOIL

$\alpha = 0 \quad \delta_m = 1^\circ$
 $k = 0.167$

○ $M = 0.3$
 △ $M = 0.73$

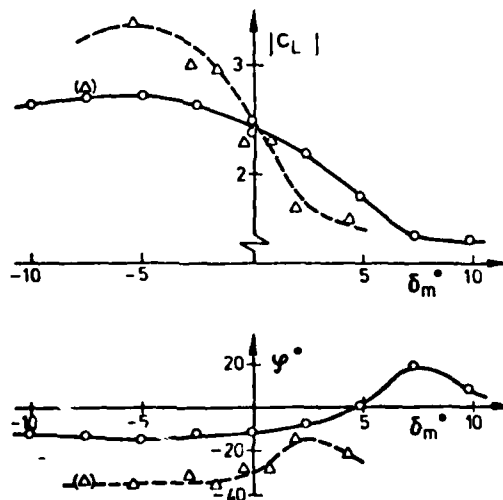


Fig. 22: Influence of the mean flap deflection on the unsteady lift coefficient due to flap oscillation (adapted from [89])

1-24

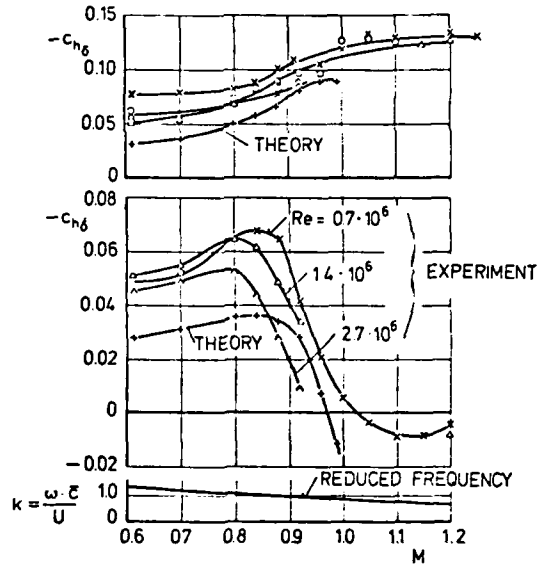
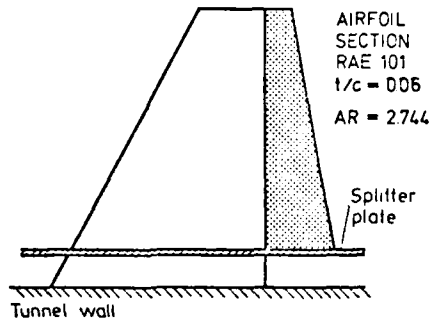


Fig. 23: Comparison theory - experiment for a tapered wing in transonic flow, Influence of the Reynolds number (adapted from [90])

TYPE OF METHOD	STEADY		UNSTEADY	
	2D	3D	2D	3D
— SINGULARITY METHODS				
-- LOADING FUNCTION	●	●	●	●
-- DISCRETE LOADING	●	●	○	○
— FIELD-METHODS	○	○	○	○

Fig. 24: Methods for supersonic flow

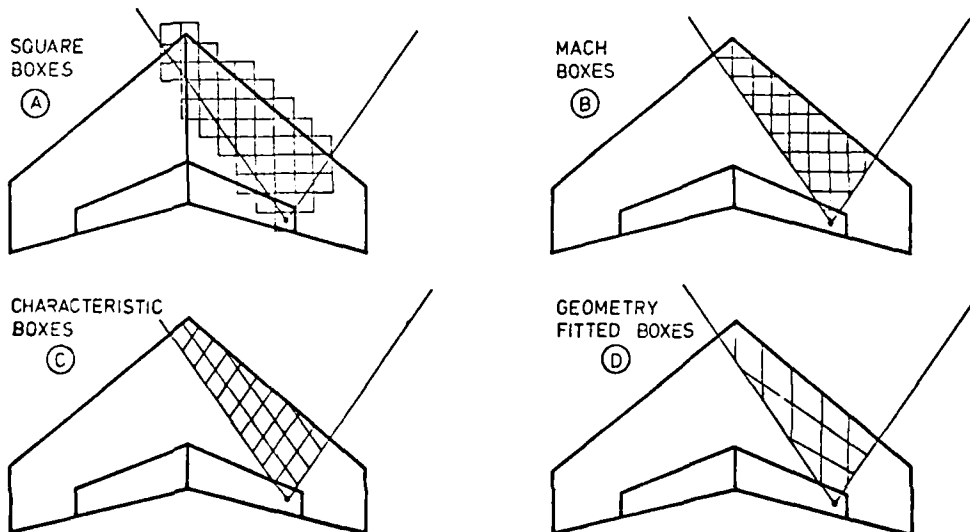
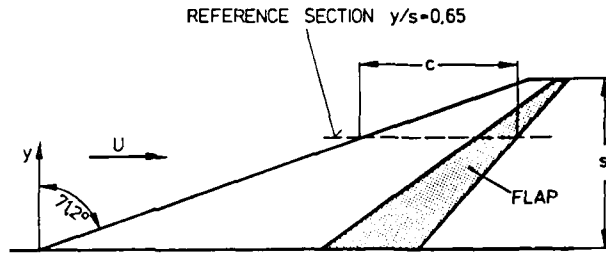


Fig. 25: Subdivision of the wing area inside the Mach-cone for different evaluation techniques

$\delta = 83^\circ$
 $\alpha = 0^\circ$
 $y/s = 0.65$



1-25

○ UPPER SIDE EXPERIMENT
 ▽ LOWER SIDE EXPERIMENT
 — FLEXSTAB (THEORY)

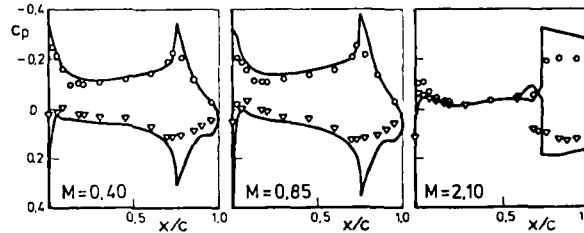


Fig. 26: Comparison theory - experiment for an arrow-wing with flap deflection (adapted from [102])

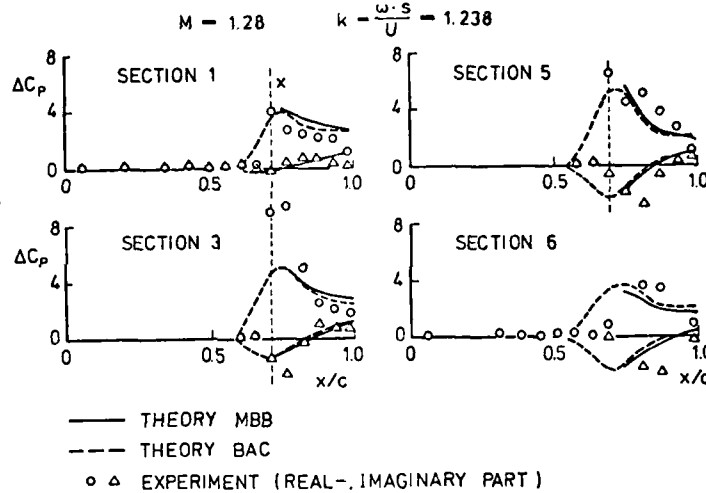
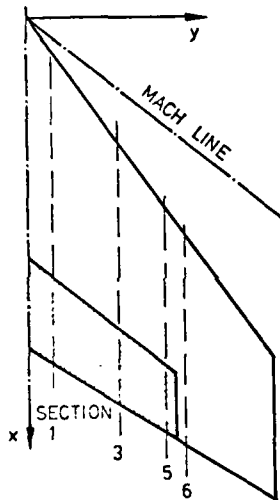


Fig. 27: Comparison theory - experiment for a swept wing with oscillating flap in supersonic flow (adapted from [103])

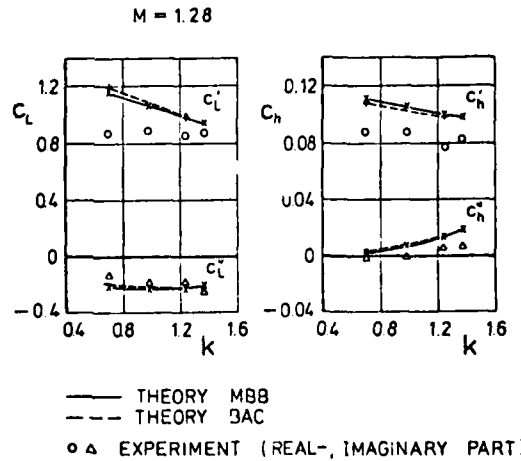
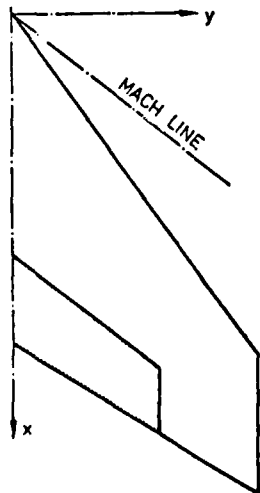


Fig. 28: Comparison theory - experiment for a swept wing with oscillating flap in supersonic flow (adapted from [103])

1-26

	STEADY	UNSTEADY
— LEADING EDGE SUCTION ANALOGY	●	
— VORTEX LATTICE	●	○
— VORTEX SHEET	●	

Fig. 29: Methods for slender-wing vortex flow

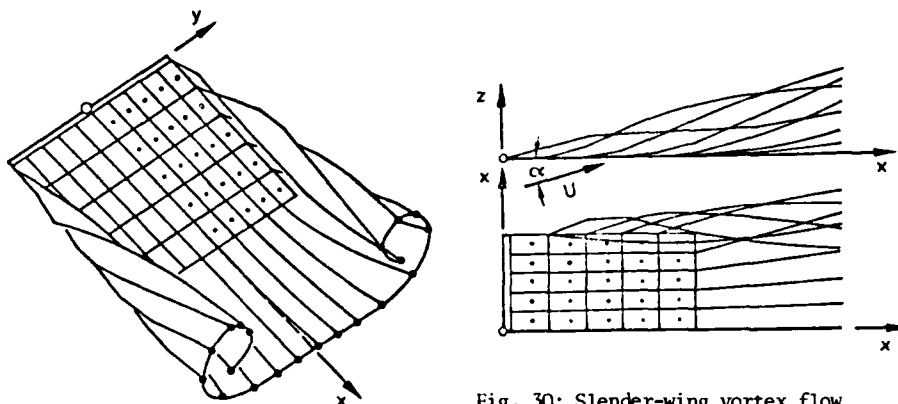


Fig. 30: Slender-wing vortex flow

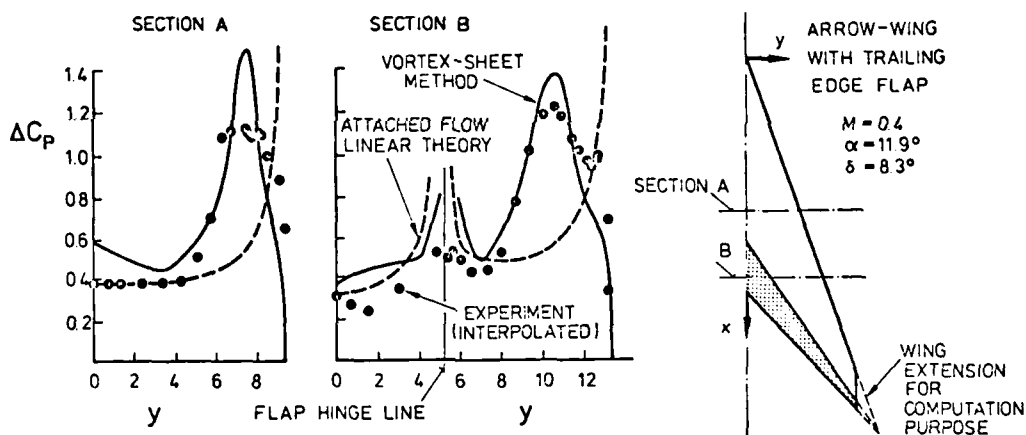


Fig. 31: Comparison theory - experiment for an arrow-wing with flap deflection (adapted from [112])

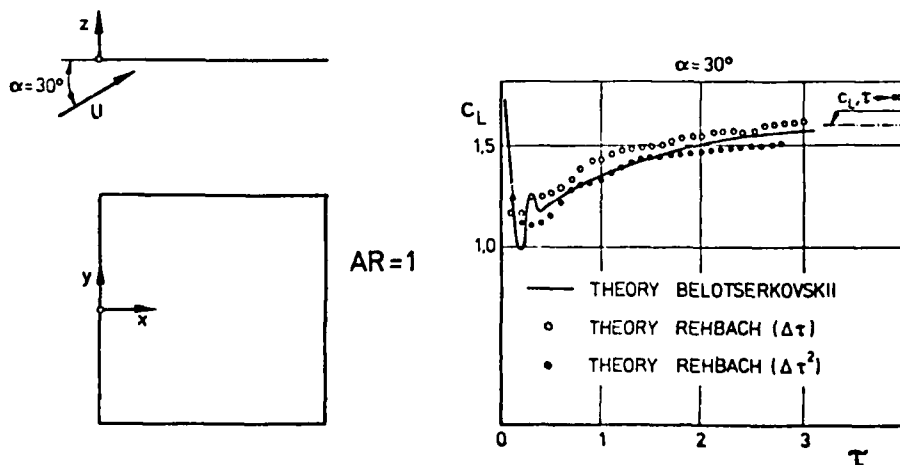


Fig. 32: Time dependent lift of a small aspect ratio wing after a sudden set in motion (adapted from [113])

	STEADY		UNSTEADY	
	2D	3D	2D	3D
— HYBRID METHODS	●	●		
— SOLUTION NAVIER-STOKES EQUATIONS	○	○	○	○

Fig. 33: Methods for separated flow without primary structures

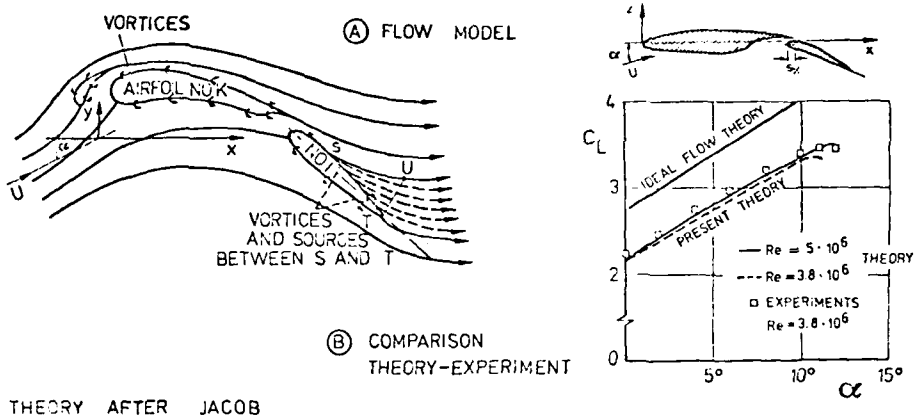


Fig. 34: Comparison theory - experiment for the maximum lift of a multi-element airfoil (adapted from [121])

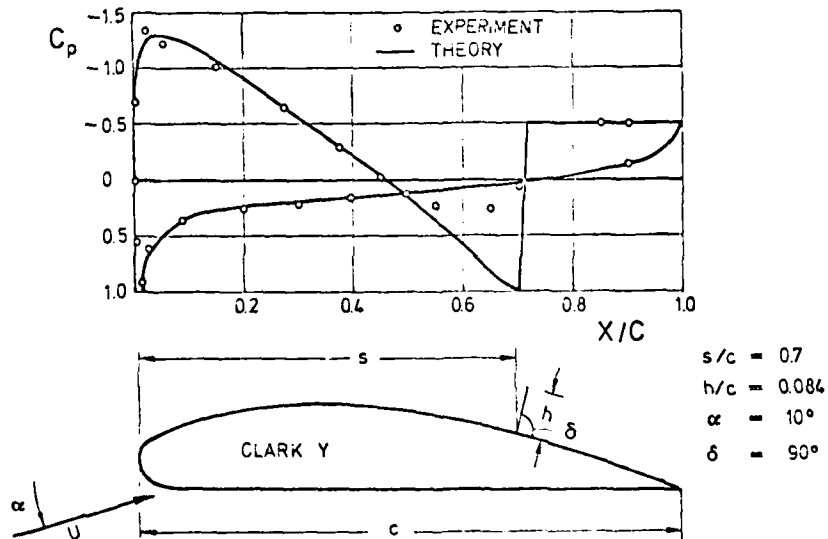


Fig. 35: Comparison theory - experiment for an airfoil with a normal spoiler (adapted from [123])

1-28

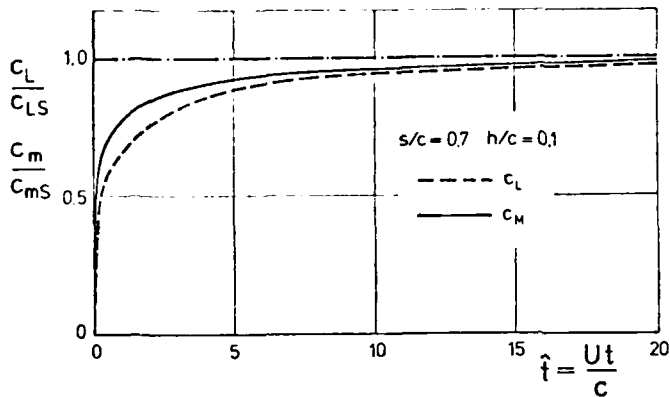


Fig. 36: Calculated lift and pitching moment of an airfoil after a sudden erection of the spoiler (adapted from [124])

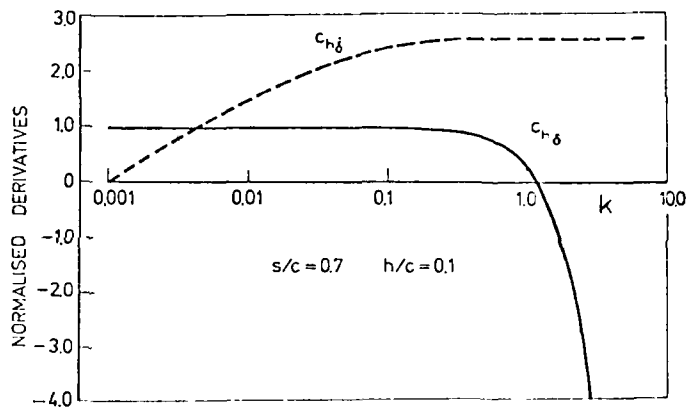
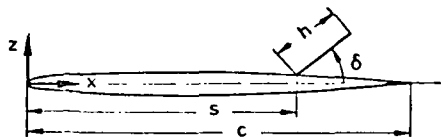
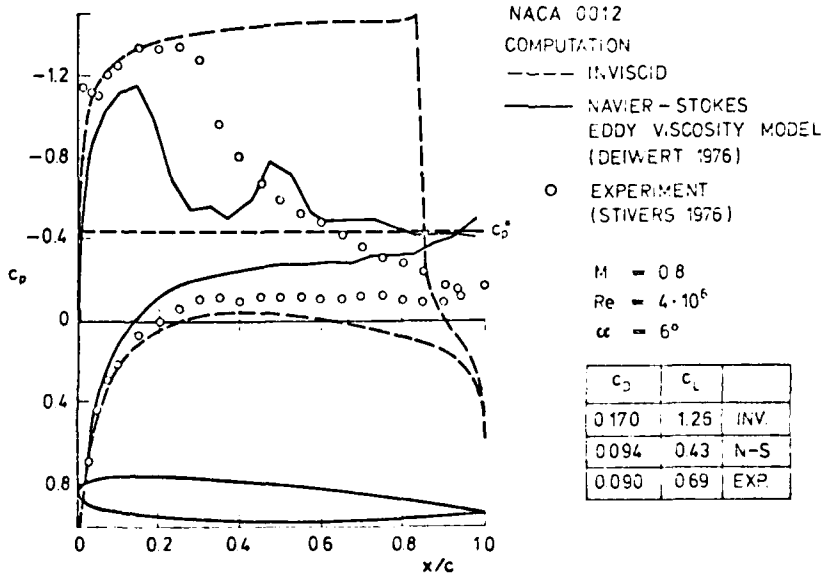
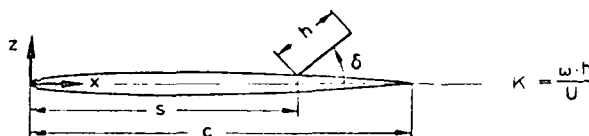


Fig. 37: Calculated derivatives for an oscillating spoiler (adapted from [124])



NACA 0012
COMPUTATION
----- INVISCID
———— NAVIER-STOKES
EDDY VISCOSITY MODEL
(DEIWERT 1976)
○ EXPERIMENT
(STIVERS 1976)

$M = 0.8$
 $Re = 4 \cdot 10^6$
 $\alpha = 6^\circ$

C_D	C_L	
0.170	1.25	INV.
0.094	0.43	N-S
0.090	0.69	EXP.

Fig. 38: Comparison theory - experiment for an airfoil with a large area of separated flow (adapted from [127])

A SURVEY OF EXPERIMENTAL DATA ON THE AERODYNAMICS OF CONTROLS,
IN THE LIGHT OF FUTURE NEEDS

A. Jean Ross and H.H.B.M. Thomas
Royal Aircraft Establishment
Farnborough, Hampshire, GU14 6TD, UK

2-1

SUMMARY

The advent of Active Control Technology means that the aircraft designer needs as much, if not more, knowledge of control characteristics, with more emphasis on maximum control power and actuating force or moment than for the previous generation of aircraft. Much of the systematic testing of conventional control surfaces was done over twenty years ago, and on this work rests the current design methods. A bibliography of control data has been compiled, and data from this source and for current aircraft are used to provide material for discussion, principally to describe trends and to highlight gaps in knowledge. Both direct and indirect effects for a range of conventional and unconventional motivators are included. Maximum control power at the extremes of the flight envelope is particularly emphasised, since that available at high angle of attack and high subsonic speed is likely to be the critical design case. The indirect and coupling effects are also more marked at high angle of attack and/or high control deflection, and are of importance in the control system design. Hinge moment characteristics are described, although experimental data published recently are sparse. Some thought is given to the means of generating required control powers for the new aircraft configurations made possible by ACT, and to the integration of the motivators in the control system.

1 INTRODUCTION

When one views the evolutionary path of the aeroplane one is immediately struck by the fact that at any stage in the process the attributes of controllability and stability are of paramount importance to the vehicle's handling qualities. The interwoven relationship of these two properties of the aircraft system only emphasises this and makes clear the important role the control surfaces or motivators played throughout.

This point is made more graphically in Fig 1, which illustrates the structuring of the control system of the aircraft at three stages in its evolution. Firstly, for the simple unaugmented aeroplane with its direct mechanical link between pilot and motivator, the control surfaces or motivators* are important in allowing the pilot to impose his will on the path the aircraft follows by means of its response to application of one or more motivators. Additionally the motivators can influence the stability with the controls freed, but the other aerodynamic parameters are of at least equal significance. The pilot had to co-ordinate his control inputs to produce the desired response within the prescribed levels of stability.

Next comes the aircraft in which the usual motivators are used to augment or modify the stability and controllability. At this stage the augmentation amounted in effect to adding damping to the longitudinal and lateral oscillatory modes of motion and shaping the response to the motivators as, for instance, in the so-called manoeuvre-demand systems. Successful design now shows increased dependence on the characteristics of the motivators and hence on the knowledge needed to achieve the desired characteristics. It was the adoption of power operation of the motivators coupled with feasibility of introducing servo-systems that made this step possible.

Thirdly, we come to the aircraft of current interest, in which the flying qualities are enhanced in many directions (relaxed stability, de-coupling of degrees of freedom, load alleviation and or limitation etc) by utilizing not only the usual motivators used for flying, but also additional, and perhaps more specialized, motivators to the full. This step required the abandoning of the mechanical link (that is, the system becomes a 'fly-by-wire' system) and the emergence of the on-board computer. The resulting aircraft has been referred to as a 'control-configured vehicle' or 'an active control technology aircraft', this latter term in reference to the nature of the technology on which it rests. Neither term is entirely satisfactory but we do not propose to explore that question here. The dependence of the design on motivator characteristics has increased even further and may even dominate particularly in the design of an aircraft control system which aims to be adaptive.

Three aspects of the characteristics of motivators are reviewed here, (i) the direct force and moment produced by activation of the motivator, expressed both as effectiveness (force or moment per unit deflection) and as maximum power (maximum force or moment produced), and classified in section 2 according to the desired aircraft response, (ii) the indirect forces and moments also produced, which are discussed in section 3, and (iii) the actuating force or moment (usually hinge moment), in section 4. It is judged that all these characteristics need to be known for the design and assessment of control systems, but the relative degree of accuracy needed is not considered in this paper.

Maximum control power at the extremes of the flight envelope comes in for special scrutiny, since that available at combined high angle of attack and high subsonic Mach numbers is likely to prove the critical design case. Comparisons of the behaviour of different types of motivator, as either of these two flight parameters is changed, are made. Of equal importance in the design of an active control system are the

* The term 'motivator' is used to describe all types of surfaces, jets, etc used to control an aircraft.

2-2

indirect effects, eg the yawing moment due to aileron, or pitching moment due to spoiler. These tend to become more marked at high angles of attack for most motivators, as do also the coupling effects between two control actions (eg moments due to combined symmetrical (elevator) tailplane deflection and differential tail deflection) and between a motion parameter and a control deflection (eg moments due to combined side-slip and symmetrical tailplane deflection).

With an increase in the number of motivators in use plus the fact that some active control functions will demand high rates of actuation, an increased emphasis needs to be put on the measurement of (and possibly the reduction of) the hinge moments (or actuating force) and hence the power needed to operate the motivators.

Much of the systematic testing of the conventional control surfaces, aileron, elevator or tailplane and rudder, was done over twenty years ago and on this work rests the design methods given in the ESDU Data Items and in DATCOM. More recently data have been acquired on an *ad hoc* basis for particular configurations. In order to define a starting point for this review of 'recent experimental data', it has been assumed that the DATCOM (1970)¹ and ESDU² methods incorporate empirical factors from data up to 1960, so that papers published before 1960 have not been studied. An extensive Bibliography³ which includes earlier reports has been compiled at the RAE, and is to be published separately.

Examples of typical results are taken from the papers listed in the Bibliography (1960-1978), or from unpublished data on current aircraft designs, to illustrate general characteristics. Results for both combat and transport aircraft are included, with more emphasis on the former, up to Mach numbers of 2.0. The control characteristics of the many STOL configurations are considered to be too dependent on the particular design to merit discussion in this general review, and so motivators for specific V/STOL operations are omitted. Comparisons of the experimental data with estimated values have not been made, but it was observed that the estimation methods of Refs 1 and 2 often introduce empirical factors based on experimental data for aircraft and control configurations which are very different from those being considered currently, to which they are, therefore, not necessarily applicable. The resulting gaps in knowledge are noted in section 2, but no attempt has been made to correlate the more recent data presented here.

Although some results from full-scale flight experiments are included in this review, most of the experimental data on control characteristics are obtained from wind-tunnel tests, and this is necessarily so at the design stage of an aircraft. Thus the implications in wind-tunnel testing have to be considered, and are discussed in section 5 under the headings, Reynolds number, aeroelasticity, unsteady flows and dynamic effects, and interference and coupling effects. In section 6, some thought is given to the implications in the design of active control systems. An overall assessment is made of the status of the experimental data on control characteristics, and of the possible methods of increasing control effectiveness. It is suggested that control studies need to be made to see how far existing motivators fulfil the needs of the separate functions of active control systems, and that further aerodynamic research is required to open up new possibilities.

2 DIRECT EFFECTIVENESS

In view of the changing emphasis brought about by the use of active control systems, it was decided to arrange the description of the experimental data according to the resulting aircraft response, rather than according to the type of control surface. The pitching, rolling and yawing moments are considered first, as conventional aircraft are controlled by applying moments via the basic motivators, elevator, aileron and rudder respectively. Other motivators have been developed to increase effectiveness, and they are included in the appropriate section. However, it is unclear at present whether horizontal canards will be used primarily to generate pitching moment or direct lift, and so the experimental results for canard deflections are reviewed in both sections 2.1 and 2.4. The generation and use of direct lift and direct sideforce are comparatively new concepts, and new types of motivators are required, particularly moving canards. The characteristics of flaps are also described in section 2.4, and the discussion of direct lift has been broadened to include the important topic of maximum usable lift. This defines the manoeuvring capability of combat aircraft, and the maximum benefit of aerodynamic and control system features is achieved only if the design takes due account of all these factors, which are, therefore, also relevant to our discussion.

The data have been collected from various sources, and as presented in the original reports use various notations. In order to avoid ambiguity, it was decided to present the data here using British notation, viz a symbol for motivator deflection according to the resulting response, but a suffix is added to denote the type of surface. Thus, η is used for the deflection of motivators producing mainly pitching moment, ξ for rolling moment, ζ for yawing moment, and δ for lift*, so that, eg η_T is used for tailplane deflection, and ξ_S for spoiler deflection if the spoiler is used to generate rolling moment. A full list is given in Table 1, for the motivators considered in this report, together with the equivalent American notation. For added clarity the control derivatives are written in full, eg $\partial C_m / \partial \eta_T$ is the pitching moment due to tailplane derivative, and the motivator deflections are expressed in radians rather than degrees.

2.1 Pitching moment

Pitching moments need to be applied to an aircraft for two reasons, namely, to trim the aircraft and to enable it to be manoeuvred away from a given trimmed state.

For much of its history the aeroplane has been equipped with an aft tail for this purpose, which provides the pitching moments by generating lift at an appreciable distance from the aircraft's centre of gravity, by deflection of part or the whole of the tail chord. For the aft-tail arrangement the presence of the wing exerts a powerful influence on the efficiency of the pitch motivator (elevator or all-moving tail) according to the tailplane's position relative to the wing wake. The latter alters in character and

* No particular symbol has been suggested for sideforce motivators, and it was not found necessary to introduce one in this report.

position with the angle of attack of the wing. There is a direct effect through the kinetic pressure of the local flow around the tail and the indirect effect through the downwash, which determines the effective angle of attack of the tailplane. 2-3

In contrast the canard operates in virtually free-stream conditions (no reduction in kinetic pressure), but there can still be significant interference effects between wing and canard when the latter is deflected. The effective angle of attack of a foreplane or canard is the sum of the angle of attack of the aeroplane and the upwash caused by the flow field of the wing. Hence the lift generated by the trailing-edge down or positive deflection of the canard is limited by stalling of the aerofoil surface.

It is, of course, possible to dispense with the use of the tail surface of either kind. In this case the trim and control functions of the pitch motivator have to be incorporated into wing-mounted devices. The most common of these is the elevon.

The lift and drag associated with provision of the pitching moments needed to trim the aircraft can penalize, or otherwise, the maximum lift coefficient and the maximum lift to drag ratio for trimmed flight. The extent to which the aircraft's performance is affected in this way depends upon the degree of static stability it inherently possesses. This in its turn depends upon the speed regime.

Hitherto, the aircraft designer has in the main opted to choose a compromise solution in this matter of trim, control and stability. There has been the occasional exception such as the solution adopted for the Concorde aircraft, in which the aircraft's centre of gravity is adjusted in flight by pumping fuel from one set of tanks to another. The concept of relaxed static stability, that is, removing, to a greater or lesser degree, the insistence on having inherent static stability, introduces a new dimension into the design process. At the same time it imposes new demands on the pitch motivators as the level of stability must be restored using an active control system. New design aims emerge and these will differ in the emphasis they will place on lift, lift-drag ratio and manoeuvring power of the pitch motivator according to the type of aircraft. At this stage in our knowledge, this new development does not favour any of the basic types of pitch motivators discussed. Since it is important to bear in mind the interference of both canard and aft-tail with the wing-body flow field, it is proposed to discuss the illustrative examples under the headings of tailed aircraft, tailless and canard aircraft.

2.1.1 Tailed aircraft

The primary pitch control surface has been the elevator, evolving to all-moving tailplanes with or without elevator, as the requirement for trim and control power at supersonic speeds became important, and as the tail arm of combat aircraft decreased. The elevator has been used extensively in pitch damper systems, and more recently in manoeuvre demand systems, so is already proved in some active control applications. Estimation of the pitch control derivative in the linear range is comparatively straightforward, being based on lift curve slope of the control surface and the moment arm, with empirical corrections for body effects, but high angle of attack characteristics cannot usually be calculated with any degree of confidence.

The classic characteristics are well demonstrated by results from a tunnel model of a current fighter concept⁴, which has a cambered sweptback wing and cambered fuselage designed for optimum cruise and manoeuvre performance at $M = 1.4$. For the given reference centre of moments, the configuration is just stable for $M < 1$ (Fig 2), with pitch down tendency at high C_L , and is, of course, more stable for $M > 1$. The control derivative, $\partial C_m / \partial \eta_T$, shown in Fig 2b, is a maximum in the transonic region, but reduces rapidly as speed increases further, so that its value at $M = 2$ is half that at $M = 0.5$. For this low tail position, $\partial C_m / \partial \eta_T$ is not much affected by increase of C_L (or α) up to $C_L = 0.8$, throughout the Mach number range. These results indicate that the tail does not become immersed in the wing wake with attendant loss of kinetic pressure nor are there any adverse effects of angle of attack. There are indications, at subsonic and transonic speeds, that the tailplane effectiveness falls off at large negative deflections ($\eta_T < -15^\circ$). At a Mach number of 1.8, however, the pitching moment due to tailplane deflection remains linear in the range $-15^\circ < \eta_T < 5^\circ$. Non-linearity is also present at a Mach number of 0.9 for quite small positive tail angles in combination with large angle of attack. These results are fairly representative of those for a layout employing a low, close-coupled tail, typical of the combat aircraft.

In contrast, the pitching moments for a high tailplane are much affected by adverse wake effects at high angles of attack, as is well known from the superstall problem. A number of transport aircraft designs with high tails have been tested and the results⁵ chosen for illustration include both tail and elevator deflections. At zero angle of attack the pitching moment due to tailplane deflection begins to fall off as the angle reaches the stall angle for the tail surface, see Fig 3. Deflection of the elevator in the same sense increases the pitching moment and extends the linear range, but is followed by a more marked fall-off. As is to be expected at 10° angle of attack the maximum nose-down pitching moment occurs at a smaller tailplane angle ($\eta_T \sim 10^\circ$). Even though the original results show that wing stalls at an angle of attack of 16° and the pitching moment characteristics with angle of attack are affected beyond this angle of attack, the pitching moment due to the tail and elevator at an angle of attack of 20° shows little effect around zero tail angle, but the maximum nose-down pitching moment is now reached even earlier ($\eta_T \sim 7.5^\circ$). At an angle of attack of 30° , it is clear from the results shown (Fig 3) that the tailplane has become immersed in the wake thereby operating at much reduced kinetic pressure. This causes a large reduction in the effectiveness of both tailplane and elevator. However, the large downwash over the tail unstalls it, resulting in more linear characteristics (see Fig 3).

There are a number of reports giving motivator effectiveness in derivative form, being the results of analysis of dynamic manoeuvres performed in flight. It is interesting and instructive to compare these results with their counterparts from wind-tunnel tests. Fig 4 gives data for the F-4E aircraft⁶ obtained from a well-instrumented aircraft and the use of a sophisticated computer program for the analysis. The two flight records analysed cover the angle-of-attack range $5^\circ < \alpha < 20^\circ$ and $20^\circ < \alpha < 40^\circ$ respectively. A variation of the motivator effectiveness is indicated for the lower angles of attack, whilst the results at high angle of attack show little or no variation. Also shown on the same figure are results from two tunnel tests. One set shows a trend with angle of attack not dissimilar to that indicated by the flight

2-4

results. The other indicates a sharper and continued drop in effectiveness at high angle of attack. At low angles of attack this latter set agrees reasonably well with the flight test results. However, at angles of attack in excess of 30° both sets of wind-tunnel test results lie numerically well below the flight test result.

Although a somewhat simpler computer program was used to analyse flight data⁷ for the Kestrel (an experimental fore-runner of the Harrier), it was decided to include these, Fig 5, as they show dependence upon another parameter, θ_j , the deflection angle of the vectored thrust. The tailplane effectiveness falls off as the normal force coefficient (C_N) is increased, for the largest deflection angle of $\theta_j = 30^\circ$, but is not significantly affected at the lower deflection angles. It is worth noting that the results show a consistent and plausible trend with C_N . It was also stated in Ref 7 that the levels of tailplane effectiveness are consistent with the results obtained for incremental normal acceleration per tailplane deflection from parallel flight tests. However, tunnel tests⁸ do not show such a large effect of deflection angles, and the results are compared in Fig 5 for the flight condition $M = 0.43$, $\alpha \approx 8^\circ$ and with thrust coefficient of approximately 0.2. The discrepancy cannot be explained without further data becoming available, but could be partly due to the simulation of the jet engines in the tunnel.

2.1.2 Tailless aircraft

One of the penalties of using a tailplane on a supersonic aircraft is the large trim drag, and a more efficient design results from discarding the tail. Trailing edge elevators (or elevons) have then to be used for trim and control, and are usually found to have well-behaved characteristics. Variation of effectiveness with Mach number is similar to that for tailplane effectiveness; for example Fig 6 shows values of C_m/η_E for a supersonic cruise fighter concept⁹ (designed for optimum performance at $M = 1.8$), which has outboard trailing edge elevons. The value of C_m/η_E is greatest in the transonic region, and shows characteristic reduction as Mach number approaches 2.

For slender wing aircraft, trailing edge controls remain effective to moderately high angles of attack, as shown by the tunnel and flight results¹⁰ for the HP 115 aircraft in Fig 7, where the slight trend is for an increase of effectiveness as angle of attack increases from 6° to 20°. If angle of attack is increased until vortex bursting occurs near the wing, then some reduction in elevator effectiveness can be expected.

2.1.3 Canard aircraft

As already mentioned the canard surface operates in near-freestream conditions. For present-day close-coupled configurations this advantage can be offset by the fact that when the canard is developing lift some cancellation of the lift due to the wing occurs, which is exaggerated by decrease in wing aspect ratio. This redistribution of lift causes the pitching moment due to the canard to depart from that estimated on the basis of the canard's lift. If the trimming function is performed by the canard, the deflection of the canard is in the trailing-edge down (or positive) sense for all practical designs. Manoeuvring in the pull-up sense (increase of angle of attack) results in larger positive angle. Since the canard is operating at an effective angle of attack close to the sum of the angle of attack and the canard deflection the surface can stall at moderate angles of attack. In the trimmed state there is the question of the possible penalty of increased drag, but in this section we are mainly concerned with the pitching moment a canard can produce. Only a few reports giving the pitching moments due to deflected canards are available, but such as there are show the expected trends. Reports which show how undeflected canards influence the behaviour of other motivators are included in the discussion and Bibliography.

A number of closely-coupled canard configurations has been tested by NASA covering various aspects of the influence of a canard surface on pitching moments.

For the simple swept canard and trapezoidal swept wing configuration¹¹ of Fig 8, the pitching moment due to a 10° deflection of the canard drops off as angle of attack or C_L is increased, becoming zero at $C_L \approx 0.8$. The very small effect that spanwise blowing over the wing has on this trend clearly shows that it is a consequence of the canard surface stalling. In contrast, spanwise blowing over the canard results in it retaining its effectiveness up to the highest lift coefficient tested, 1.3. The results shown in Fig 9, which refer to a wing-canard combination¹² of somewhat larger sweep, show the same trends with lift coefficient (or angle of attack). The same wing has been fitted with trailing-edge flaps and tested in combination with a flapped canard of increased size. In these tests the canard flap was set at 30° and the canard deflection and that of the wing trailing-edge flap varied, with the results shown in Fig 10. The curves for a +5° deflection of the canard indicate a pitch-up tendency at about $C_L = 1.0$, whilst with a -5° deflection the same tendency is delayed to $C_L \approx 1.8$. In both conditions the canard is developing upload and as we have already seen is more likely to stall than to produce lift at an increased rate, cf Fig 8. It thus seems probable that the cause of the pitch-up is an adverse interference effect on the wing, in which case it would be present in results for the configuration with zero canard setting. Unfortunately these are not available, but the fact that the quoted angles of attack for pitch-up onset, 15° (canard deflection +5°) and 24° (canard deflection -5°), are separated by almost exactly the change in canard deflection supports the conjecture. This result emphasises again the importance of the canard-wing interference effects and the need for more detailed study. It is interesting to note that the pitching moments generated by wing trailing-edge flaps are almost invariant with the lift coefficient (or angle of attack). They are only affected to a small extent by canard deflection.

In the light of previously discussed results, it is interesting to examine test results in which pitch control is by use of trailing-edge flaps on the wing alone, keeping the canard fixed. Fig 11 shows results¹³ for an outboard trailing-edge flap and an inboard flap incorporating a two-dimensional nozzle tested at low speed on three configurations, a wing-body, a wing-body with canard and a wing-body with canard fitted with a strake. Tests were made at three values of the thrust coefficient zero, 0.2 and 0.3. The results for zero thrust coefficient in Fig 11a indicate that the addition of a canard at zero setting produces an appreciable increase in the effectiveness of the wing trailing-edge flap accompanied by an increase in the maximum lift coefficient. Improvement in the control effectiveness extends to the increased maximum lift conditions. The addition of a strake to the canard surface has only a slight effect.

Near the limiting lift condition the wing-body configuration displays a nose-down tendency in pitch. With the canard added this tendency (somewhat exaggerated by canard stall) only persists in the zero-flap case. At all other flap deflections there is a pitch-up tendency. This trend is present at all flap settings for the canard with strakes. Without further detailed tests it is difficult to analyse the precise nature of this adverse interference between canard and wing at high angles of attack. 2-5

The objective of the test of Ref 13 was to see to what extent deflected thrust over the inboard flap would alleviate the pitch-up revealed by earlier tests¹⁴ on the same model. It is seen that with a thrust coefficient of 0.3 the pitching moments due to flap deflection shown in Fig 11b are increased by about 50% for all three configurations. Some alleviation of the pitch-up tendencies occurs, but the improvement is probably not sufficient in the case of the canard with strake to remove anxiety on this account. Some tests at $C_T = 0.2$ indicate that most of the benefit obtained at $C_T = 0.3$ would be achieved at the lower value of C_T . This suggests that no augmentation above the boundary-layer-control values occurs. Interesting and illuminating though these tests results are they leave some questions unresolved. In contrast to the data given in Fig 10, the wing trailing-edge flap is affected by canard-wing interference at high angle of attack. The reasons may be sought along the same lines, but the matter is far from clear.

The data on canard behaviour described thus far refers to low Mach number conditions. An example¹² is now considered in which a comparison is made of the effectiveness of a surface used as either a canard or an aft-tail control. Both controls maintain effectiveness through the transonic speed regime with the expected fall-off as the Mach number increases supersonically, as shown in Fig 12. The slightly larger numerical value of $\delta C_m/\delta \alpha$ for the aft-tail is accounted for by the 10% longer tail arm, but the large difference in the numerical values transonically (aft-tail 65% more effective at $M = 0.9$) indicate appreciable adverse interference effects with the canard.

The two American experimental CCV aircraft¹⁵⁻¹⁷ have had canards installed to allow direct lift and direct sideforce modes to be used, the YF-16 having twin canted vertical canards, and the F-4 having separate horizontal and vertical canards. The manoeuvring capabilities of the CCV versions are better than those of the basic aircraft, so that the drag penalty of the extra surfaces has been compensated by the improved lift achieved. The added freedoms that such a configuration, with both tail and canards, gives with regard to the choice of motivators may prove to be important, but more design studies need to be made before decisions can be taken.

2.2 Rolling moment

Because conventional ailerons exhibit a loss of effectiveness as the angle of attack is increased and also at supersonic speeds, it has become necessary to introduce other forms of roll motivators either to replace the conventional ailerons or to supplement them. This is particularly so for combat aircraft. The data discussed in this section cover the various devices currently in use and are arranged according to type.

2.2.1 Ailerons

Experimental subsonic sectional data can be incorporated into the methods of estimation of aileron effectiveness given in DATCOM¹ and ESDU² series. Application is restricted, however, to the linear range.

If the angle of attack of a wing is increased sufficiently the flow separates over some part of its span. On sweptback wings this first occurs over the outer span portions, where ailerons have conventionally been located to take advantage of the moment arm. Deflection of the aileron surface in the same sense as the angle of attack, that is, positively, aggravates the situation. To offset these adverse effects, the ailerons on some combat aircraft have been relocated at mid-semi-span, although there exists a possibility of adverse interference with the tail through the use of this arrangement. That such a layout is only partially successful is best illustrated by data drawn from unpublished data for a configuration having ailerons located in this manner. The rolling moment due to deflection of a pair of ailerons over the angle of attack range, -10° to $+30^\circ$ and aileron deflections of $\pm 7\frac{1}{2}^\circ$ to $\pm 30^\circ$ are shown in Fig 13 for four Mach numbers, 0.3, 0.8, 1.2 and 1.7. At all Mach numbers the aileron effectiveness does not drop off markedly with aileron deflection even up to the largest tested when the angle of attack is small. However, for the two subsonic Mach numbers, the results show a loss of effectiveness at large angles of attack combined with decreasing effectiveness at the larger aileron deflections. Flow separation seems to be more abrupt at a Mach number of 0.8 than it is at a Mach number of 0.3.

The usual drop in the level of effectiveness is present in the results for Mach numbers 1.2 and 1.7, but, perhaps not unexpectedly, the rolling moments are more linear with respect to the aileron deflection. Furthermore the aileron effectiveness is maintained to a greater extent as angle of attack is increased, that at a Mach number of 1.7 being virtually unaffected by angle-of-attack variation.

The losses in rolling effectiveness at high angles of attack/high subsonic speeds can be alleviated by the leading-edge devices used to improve lifting performance (to be discussed further in section 2.4), due to their beneficial effect on the flow over the wing. The effect of slats on incremental rolling moment due to 30° aileron on the F-4¹⁸, shown in Fig 14a, is typical of the improvements possible. At $M = 0.6$, a loss in rolling moment occurring abruptly at $\alpha = 12^\circ$ on the unslatted wing indicates a breakdown in the flow over the aileron position of the wing. The main effect of the slat is to delay the onset of this flow breakdown, but the results show that beyond an angle of attack of around 20° the slat has little effect. This is an indication that flow breakdown has once more taken place. At a Mach number of 0.9 an abrupt loss in effectiveness again occurs, at an angle of attack of about 12° . However, the more significant recovery of effectiveness which occurs at around 16° indicates a more complex flow pattern. Shock-induced separation is certainly present and may be the main factor affecting the variation with angle of attack. Nevertheless, the presence of the slat has a beneficial effect in that it eliminates the dip in the curve of the rolling moment against angle of attack, so that the aileron remains effective up to an angle of attack of 20° albeit with a 40% reduction in effectiveness. A similar increase in angle of attack range due to the slats is observed for the rolling moment due to aileron and spoiler (Fig 14b), and the results are discussed under Spoilers.

The other important factor for aileron effectiveness which needs to be considered is the deformation of the outer wing under load, which significantly reduces the rolling moment. Results for wing tip ailerons on Concorde¹⁹ are a good example of the magnitude of this reduction, and some results are shown in Fig 15a. Estimated values of $\partial C_l / \partial \epsilon_A$ for the aeroelastic aircraft are close to the flight results throughout the speed range, whereas the estimates for a rigid aircraft are at least twice as large. The tips of swept wings can also experience comparable deformations, and so wind-tunnel results must be corrected using static aeroelastic factors obtained theoretically, or elastic models have to be used in the tunnel tests. (This topic is discussed further in section 5.) Both techniques have been applied successfully to the Vigen²⁰, and yield the interesting results shown in Fig 15b. The calculated aeroelastic factor on $\partial C_l / \partial \epsilon_A$, i.e. the ratio of aeroelastic to rigid estimates, agrees well with the experimental values obtained from elastic and rigid models tested in a transonic tunnel, although it is not possible to calculate the factor accurately at $M = 1.0$. The tunnel results for the rigid model have also been corrected for aeroelastic distortion calculated for the full-scale aircraft, and the resulting $\partial C_l / \partial \epsilon_A$ compares well with the values obtained in flight, as shown in the lower figure.

2.2.2 Spoilers

There does not seem to have been much development in spoiler technology since the 1950s, although various aircraft configurations have been tested more recently which have spoiler roll control. The summary of data on spoiler effectiveness given in DATCOM¹ has not been invalidated by recent data, and so excerpts are quoted here:- "At subsonic and transonic speeds, spoilers do not, in general, provide linear variation of effectiveness with spoiler projection, particularly at small deflections. This deficiency can be corrected by use of a slot or slot-deflector behind the spoiler. For thin wings at high angles of attack plain spoilers are ineffective. This ineffectiveness can be partially overcome by the use of a slot behind the spoiler, and by the use of leading-edge devices. In order to achieve maximum effectiveness, spoilers should be located towards the rear portion of the wing, for the following reasons (i) the ineffectiveness of spoilers at small deflections increases with distance from the trailing edge (ii) the lag time at low speeds becomes excessively long for forward-mounted spoilers. The optimum spanwise extent and position of spoilers are determined primarily by wing sweep. The higher the sweep angle, the farther inboard the spoilers should be placed".

The charts given in DATCOM¹ refer to the low angle-of-attack range, and give no indication of onset of loss in effectiveness, which usually has to be determined experimentally. A typical example of results for a fighter-type wing²¹ is shown in Fig 16, where the effect of opening the slot-deflector increases the rolling moment by approximately 40%, the factor suggested in DATCOM. There is the usual marked reduction in rolling moment due to spoiler alone, which begins at $\alpha = 7^\circ$ at both $M = 0.6$ and 0.9 , and the rolling moment is near zero at $\alpha = 20^\circ$, $M = 0.6$. Such behaviour is to be expected, since the spoiler can only be effective if the flow ahead of it is attached to the wing. The loss is delayed to slightly higher angles of attack by opening the slot-deflector, and some rolling power is still available at the highest angles of attack tested.

For the plain spoiler tested with the aileron on the F-4¹⁸ (Fig 14b) the effectiveness is maintained to higher angles of attack by deflection of the leading-edge slats, but the contribution of the spoiler is near zero for $\alpha > 18^\circ$ at $M = 0.6$. The variation of the rolling moment with angle of attack at $M = 0.9$ is markedly different if the spoiler is deflected, with a 50% reduction between $\alpha = 5^\circ$ and 10° for the unslatted wing, and a similar reduction between $\alpha = 7^\circ$ and 12° for the wing with slats although some effectiveness is recovered for $\alpha > 12^\circ$.

It can be expected that leading-edge devices which improve flow separation characteristics will also have a beneficial effect on spoiler efficiency at the higher angles of attack. For future applications, spoilers are likely to continue to be used in conjunction with other roll motivators to enhance roll power, but are not efficient enough to be the main roll control.

2.2.3 Differential tails or canards

The published results on rolling moment due to differential deflection of the tailplane surfaces are very sparse, although a number of combat aircraft currently use tail to augment rolling moment. The contribution is limited by the necessarily small moment arm, but interference effects on the fin can increase the effectiveness. Their attraction is that the loss in rolling moment at high angle of attack is usually small, typically 20% reduction at $\alpha = 20^\circ$, unlike aileron and spoiler characteristics. Wind-tunnel results for YF-16^{22,23} indicate that combined inboard aileron and differential tail give almost constant rolling moment up to an angle of attack of 20° (Fig 17). Beyond this angle of attack the rolling moment produced decreased gradually to reach roughly half the value at zero angle of attack around an angle of attack of 35° . This drop in effectiveness is confined to the contribution of the aileron as indicated by the separately shown contribution from the differentially deflected tailplane surfaces. This good behaviour of the differential tail control at high angles of attack is likely to favour its use in future active control systems.

In isolation, differentially deflected canard surfaces would be expected to produce a rolling moment, but tests have shown that this is almost completely cancelled by the induced rolling moments (at least for the configurations tested). Such an arrangement does, however, produce sizeable sideforce. It is more appropriate, therefore, to regard this as the direct effect (see section 2.5) and the remnant of rolling moment as an indirect effect (see section 3.2).

2.2.4 Other methods

All moving wing-tip ailerons have been tested particularly on low aspect ratio delta wings. They do not seem to have found favour and there may be a number of reasons for this. On thin wings there are difficulties in accommodating the pivot mechanism, aeroelastic losses are on the high side, and their use inhibits the tip-mounting of missiles.

Devices which produce an asymmetric arrangement of unflapped wings yield rolling moments which only become appreciable at large angles of attack. Two such schemes are illustrated in Fig 18, namely, an asymmetric strake and one-sided spanwise blowing with the rolling moments each produces. Extension of the wing span on one side produces rather similar rolling moment variation with angle of attack, in this case it is practically proportional to the lift coefficient. The use of differential sweep on variable-sweep wings may be limited by the difficulty in deflecting the panels rapidly enough.

2-7

2.3 Yawing moment

2.3.1 Aft motivators

The traditional rudder provides sufficient yawing moment control for most aircraft, and it is only recently that all-moving fins have been considered. The yawing moment due to rudder deflection is usually near constant with angle of attack, up to and even beyond the wing stall, and with varying subsonic Mach number, but is reduced as M is increased supersonically. Estimates of effectiveness based on the force due to control deflection (for an equivalent isolated fin surface) and fin moment arm give satisfactory first approximations for design purposes, for aircraft configurations which are not close-coupled, but there may be interference factors due to the presence of the fuselage and tailplane. As an example of characteristics at low speed, high angle of attack and large rudder angles, the results of Ref 24 are typical, and also show the effect of using jet-flap augmentation. The transport aircraft design has external-flow jet flaps on the high wing, and a high tail. With no blow, and rudder deflection of 20° (Fig 19a), the yawing moment is maintained well beyond wing stall (which occurs at about 10° angle of attack) and is still appreciable at $\alpha = 35^\circ$. In sharp contrast the yawing moment due to 40° rudder deflection suffers a sharp drop beyond an angle of attack of 20° and even reverses between 26° and 35° . When these results are compared with those on the right-hand side (for $C_{NR} = 0.038$) with blowing applied over the rudder, it is interesting to note that, although the rudder effectiveness at angles of attack less than 15° is materially increased for both rudder deflections, blowing does little to improve high angle-of-attack behaviour. Indeed, in contrast to the no-blow case, a sharp drop in effectiveness occurs around an angle of attack of 25° . These results seem to indicate that the adverse effects come more from the interference from the other aircraft components than from flow separation induced by rudder deflection. With this in mind it is instructive to examine the effect of deflecting the engine jet over the inboard wing-flap has on rudder effectiveness, Fig 19b. To indicate the extent to which the wing flow is affected by the jet momentum coefficient of 3.74, it is worth noting that the maximum lift coefficient of the aircraft for a 60° flap setting is increased from 2.5 (at $\alpha = 10^\circ$) to 8.5 (at $\alpha = 25^\circ$). In spite of such a powerful effect on the wing this deflected jet thrust only marginally affects the yawing moments produced by either 20° or 40° of rudder at low angles of attack. What is striking is the way in which the rudder maintains effectiveness at both settings as the angle of attack is increased. This effect is particularly noticeable when blowing over the rudder as well. Presumably the flow changes induced over the rear of the aircraft by the jet-flap improves the flow environment within which the rudder operates.

The straightforward effect of engine thrust is likely to be significant as the evidence that follows shows. In Fig 20 are shown the rates of change of yawing moment by unit rudder deflection for a model of the B1 aircraft²⁵, as measured on an unpowered model mounted on a sting, and on a strut-mounted model with simulated thrust effects. Both sets of results show maximum control power at transonic speeds, and reduction as M increases supersonically, as is to be expected. The difference between the two sets derives from two sources, α : the thrust and interference from aft fuselage shape. The boat-tail shape of the fuselage, which can be accurately represented on the model mounted on the strut, and the jet plumes of the fuselage-mounted engines have a beneficial effect on the flow over the rudder. From the results quoted it is impossible to assess these effects separately.

It would be expected that the effect of engine thrust would be smaller in the case of combat aircraft, for which the engine or engines are usually embedded within the fuselage and exhaust at the fuselage base. Even so some significant effect of thrust might be expected. Whether the following example provides evidence of this is open to question. A comparison has been made²⁶ between the results obtained from 3/8-scale, unpowered free-flight model of the F-15 and from flight tests of the full-scale aircraft at three rates of engine mass flow. The latter do not show any consistent trends with engine mass flow, and so it was concluded that C_{n_r}/C_R is independent of power, and the mean curve through the individual results shows the variation with angle of attack in Fig 21. However, the results from the unpowered model, also shown, indicate that its rudder effectiveness is about 20% lower than full-scale. It is suggested in Ref 26 that the difference may be due to scale effects, since any other explanation is made unacceptable by the fact that good agreement was achieved for the other yawing moment derivatives, n_v and n_r . These results also show that rudder power is maintained to moderate negative angles of attack, to $\alpha = -15^\circ$. Unfortunately, tunnel results are not available for comparison.

Reduction of rudder control power due to fin (and fuselage) bending can be appreciable, and results for Concorde¹⁹ and Viggen²⁰ are again used for illustration. For Concorde¹⁹, the estimated value of C_{n_r}/C_R for the rigid aircraft is reduced by up to 50% when theoretical aeroelastic effects are included (as shown in Fig 22a) but results from flight tests do not indicate such a large loss. The aeroelastic correction to the tunnel results from a rigid model of Viggen²⁰ is of the same magnitude at low altitudes (Fig 22b), transonic speeds, but is much less throughout the speed range at high altitudes, due to the reduction in air density. The agreement between flight results and the corrected tunnel results is excellent at both heights.

The use of active control systems has at least two possible repercussions on rudder design. Relaxed directional stability is being considered, so that fin area can be reduced, resulting in lower aircraft weight and lower profile drag. However, large yawing moments are required for control, and so all-moving fins, or slotted rudders²⁷ may be needed to increase rudder effectiveness for given fin area. Secondly, if a direct side force mode is used, in order to sidestep without banking, the effectiveness of rudders at large sideslip angles is likely to become more important than in the past. Wind-tunnel results are not readily available, but it can be expected that rudder effectiveness would be reduced, due to flow separation on the fin/rudder and the immersion of the fin in a wing wake of low kinetic pressure at high angles of attack.

2.3.2 Canard surfaces

2-8

It is possible to generate yawing moments either by deflection of vertical canard surfaces, or by differential deflection of horizontal canards. The former method is more akin to using a rudder, as the effectiveness is due to a sideforce generated at a moment arm, but experimental results obtained so far tend to show that interference effects are adverse. The control derivative due to the deflection of the twin vertical canards has been measured in flight¹⁶ and in the tunnel for the CCV VF-16, and the variation with angle of attack at $M = 0.6$ is shown in Fig 23. The two available flight results agree well with the tunnel values, and show reduced effectiveness as angle of attack increases, unlike the rudder²³ which remains effective up to beyond $\alpha = 30^\circ$ (also shown in Fig 23). It is also stated that C_n is nonlinear with canard deflection within the required range, so that the vertical canards are not very attractive as yaw motivators.

Although differential deflection of horizontal canards is more likely to be used to generate direct side force (as discussed in section 2.5) it is worth noting here that their yawing moment characteristics¹⁴ are more linear with deflection angle, and do not vary significantly with angle of attack.

2.4 Lift

2.4.1 Low speed

The need for means of augmenting the lift experienced by an aircraft during the take-off and landing phases of flight has existed for a long time. It has been progressively met by developments in the trailing-edge flap arrangements. To these lift augmentation requirements are now added those arising from the use of lift generating devices to improve the lift capability in manoeuvring conditions, and as part of flight systems which aim to alleviate gust loads or improve ride quality, according to which of these two objectives is the more appropriate.

The last set of requirements are pertinent to the entire flight envelope of the aircraft, whereas the first set are specifically low speeds. In this section the emphasis is on the low speed.

Experimental data on flapped aerofoil sections and wings published prior to 1970 have been incorporated into the analysis resulting in the estimation methods of Ref 1 (DATCOM). The methods of estimation for C_L/α and C_{Lmax} cover a variety of trailing-edge flap configurations - slotted, split, plain, etc, and also include the effects of leading-edge flaps.

The charts, which use the incremental sectional lift due to flap deflection as part of the estimation process, include explicit empirical factors. As these may be subject to change for geometries lying well outside those included in the analysis, it is pertinent to make an assessment of the trends in aircraft geometry. Flap chord ratios and flap deflections currently being used fall within the coverage of the data analysed in Ref 1. The other primary parameter affecting the two dimensional (or sectional) derivative C_L/α and C_{Lmax} is the thickness-chord ratio of the aerofoil. Again the coverage is reasonably representative of current trends, but it must be remarked that data for thin aerofoil-sections ($t/c < 6\%$) are confined to simple section shapes. In other respects the changes that have taken place in the shape of combat aircraft over the last two decades imply that data from the 142 reports used in formulating the estimation method for C_{Lmax} are not particularly relevant to the estimation of the effectiveness of trailing-edge flaps on wings. To illustrate the point Fig 24 has been prepared. Here the aspect ratios and sweepback angles of the wings with flaps used in section 6.1.4.3 of Ref 1 are compared with those of the combat aircraft being included in the Advisory Report of an AGARD Flight Mechanics Panel Working Group²⁸. The overlap of these two sets of data is practically non-existent.

Data for trailing-edge flaps on more recent combat aircraft must exist, but clearly have not yet been included in the correlation of data.

Before proceeding to discuss some recent test results two general remarks are in order. In application of trailing-edge flaps to date the emphasis has been entirely on the production of an upward or positive lift force. However, in the context of active control systems equal importance attaches to the reduction of lift or the production of a negative lift force. Many of the flap assemblies are ill-suited to deflection in the upward sense and, because of the nature of the past use, the effectiveness for deflection in this sense is almost never obtained.

In addition, to use any lift-adjusting device actively in a control system calls for quick-acting response. This may prove difficult to achieve by deflection of large flaps and schemes whereby the lift produced at a given deflection may be varied could prove more promising.

In this latter context results obtained for a flap in combination with slot spoilers fitted to a 9% thick aerofoil²⁹ are of interest. Fig 25 shows the variation of the lift coefficient with slot width. The results are encouraging in as much as the lift-curve slope (C_L/α) is unchanged, in contrast to the behaviour with fence or flap type spoilers (Fig 25b) and the change of lift with slot width is progressive.

The Bibliography³ contains some of the references on flap data, and a few results for the types of aircraft configurations currently being considered have been chosen to illustrate general characteristics.

The tunnel tests on the Buccaneer³⁰ wing/body give results for lift due to plain trailing-edge flaps, with added interest of the augmentation achieved by using blowing at the leading edges of the flap and of the wing. The aileron surface is also deflected in a symmetrical sense to increase lifting capability, and so the results chosen for illustration in Fig 26 are mainly for the configuration with both flap and aileron deflected 30° on the half-model. For the unblown flap, the incremental C_L decreases with increasing angle of attack, until wing stall occurs at $\alpha \approx 17^\circ$, and marginally smaller C_L 's result from increasing the deflection of the inboard flap from 30° to 45° , due to flap stall. The effectiveness of the flap is doubled by relatively low levels of blowing momentum coefficient, C_{μ} , and the incremental C_L

remains near constant with increasing angle of attack at the highest C_{μ} tested (0.065), until the wing stalls. Further improvement at high angle of attack results from blowing at a nozzle near the leading edge of the wing ($1\frac{1}{2}$ chord), as this delays flow separation and the wing stalls at $\alpha = 20^{\circ}$.

2-9

Most of the results for blown flaps with higher C_{μ} 's, and for other implementations of the jet flap principle have been obtained on STOL configurations, and so further discussion of this topic is deferred until section 6.2, which is part of a general assessment of design implications.

For canard configurations, the research model¹³ described in section 2.1 (Fig 11), which has been tested with various additional surfaces, yields some interesting results on lift generation, as well as the pitching moments discussed previously. The addition to the basic wing of both foreplane or canard and the strake improve the maximum lift coefficient, but, as the results with zero thrust coefficient, ($C_T = 0$) show, the flap effectiveness remains reduced in the neighbourhood of the stall angle of attack, see Fig 27. The deflected thrust (see results for $C_T = 0.3$), causes the lift increments due to flap deflection to remain appreciable at high angle of attack by delaying flow separation, and also reduces the loss in flap effectiveness at large angles ($\delta_F > 20^{\circ}$). It should be noted that the lift coefficients quoted in Fig 27 include the direct thrust contribution, $C_T \sin(\alpha + \delta_N)$ and so the results for $C_L - C_T \sin(\alpha + \delta_N)$ are also shown in Fig 27c.

Although the addition of a canard, either with or without a strake, does not affect C_L / C_F significantly (see Fig 27), the addition of tail surfaces near flaps will do so for closely-coupled aircraft configurations as a result of the induced downwash. This effect is illustrated by the low-speed wind-tunnel test results for a large-scale model of an advanced fixed-wing fighter³¹ shown in Fig 28. It is seen that the presence of the tailplane, at zero setting, reduces the trailing edge flap effectiveness by 40% at near zero angles of attack (Fig 28a) and by 30% at an angle of attack of 13° (Fig 28b). When the tailplane is deflected nose-down to 20° , the incremental lift due to the highlift system (trailing edge flap 30° , and segmented leading edge flap 50° inboard, 35° outboard) is found to increase back to the tail-off value as shown in the right-hand graphs in Fig 28, although total (untrimmed) lift is reduced both by adding the tail and deflecting it nose down.

The improvements in the lifting capacity, and hence manoeuvrability, of low-aspect ratio, low sweep wings due to spanwise blowing near their leading edges are well summarised in Ref 11. In particular, this reference includes a comparison, at zero flap deflection, of the lift coefficient of the wing-canard-strake model of Fig 27 and that of the wing-canard model with spanwise blowing. It is also shown that blowing in combination with leading and trailing-edge flaps yield encouraging results, but the data are not reproduced here.

In contrast to the appreciable adverse interference effect of the aft-tail and trailing-edge flap noted previously for the aircraft of closely-coupled geometry, this effect becomes near negligible for transport aircraft of conventional geometry. The results from Ref 32 for a model of a transport aircraft fitted with a supercritical wing illustrates the point in Fig 29. Lift increments due to various inboard/outboard flap deflections are almost independent of the presence or otherwise of the tailplane regardless of its deflection or its location (high and low); see Fig 29. (It should be noted that the results quoted for the high tail configuration had a leading edge slot, whereas the low tail configuration had Kruger flaps, so the 'tail off' values are slightly different.)

2.4.2 Transonic speeds

It seems probable that the direct lift needed in the high subsonic and transonic speed regime, in order to implement active control systems for such functions as improved ride quality and load alleviation or limitation, can be provided by current devices. Thus the manoeuvre flaps of the combat aircraft or the usual trailing-edge flaps of transport aircraft may be used for the purpose although segmented flaps may need to be used to obtain spanwise variation of deflection. In this context three gaps in our knowledge may be noted. The first, concerning the lack of data for negative (up) flap deflections, has already been remarked upon in the discussion of the low-speed data. The second refers to the limitation of the estimation methods of Ref 1 arising from the apparent absence of data at high Mach numbers from the analysis and the restrictive sub-critical correction factors applied to the sectional lift coefficient derivative, C_L / C_F . The third is the lack of data on segmented flaps, particularly for combat aircraft.

Active control systems are already being used on current aircraft to optimise lift and drag during combat manoeuvres, by varying the camber of the wing, particularly at the leading edge. The advantages of using leading edge manoeuvre slats or flaps at fixed deflection, determined as the best mean setting, have been exploited for some time, and aircraft performance is now improved further by actively scheduling the deflection with angle of attack and Mach number, as is discussed in Ref 33. Several examples are described there, and some of the tunnel results on which the F-18 system is based are shown in Fig 30. Both leading edge and trailing edge flaps are used to achieve the optimum camber, i.e. minimum drag for maximum lift. The experimental results for $C_{L_{trim}} - v - (C_D - C_{D_0})_{trim}$ at a number of flap deflections define a minimum drag envelope at each Mach number, and so it is possible to define separate schedules for deflections of the leading and trailing edge flaps with angle of attack and Mach number, which will yield minimum drag throughout the transonic flight envelope.

2.4.3 Maximum usable lift

Before leaving the question of lift generation, it is necessary to examine another aspect, the continuing search for means of attaining and sustaining increased g-levels. Although it does not relate directly to active control systems, it is important in defining the aerodynamic environment in which the control system is required to operate. A variety of manoeuvre flaps, slats, etc have been devised, the object being not so much to generate incremental lift as to render the basic wing more efficient. The distinction has to be drawn between the maximum C_L measured under static conditions in the tunnel, and the maximum C_L at which the pilot can use the aircraft^{28,34} since dynamic phenomena such as buffet, pitch-up, nose slice, wing drop, wing rock, etc define a manoeuvre boundary below wing stall. Many of these dynamic phenomena are associated with the type and development of flow separation on the wings, and so the

leading edge devices developed to maintain lift also usually delay their onset. Some of the leading edge devices are fixed, for example notches, vortex generators, fences, and strakes, and their presence can also influence control characteristics significantly. Both tunnel and flight results have been published for slat development on the F-4E aircraft^{35,36}. The two sets of data are also available for the performance of vortex generators and fences on the Harrier³⁷. Much emphasis has been placed of late on the need to design for good inherent handling characteristics at high angle of attack. This has resulted in the definition of the necessary wind-tunnel testing and the production of the relevant data for the current generation of American fighters, for example, the YF-16. It is particularly at these flight conditions of high angle of attack, high subsonic Mach number, that the aerodynamicist and control system engineer need to cooperate, in order to achieve a solution.

The development of the YF-16 has been documented sufficiently for this cooperation to be discerned, and so it is thought worthwhile to describe briefly both the contributions from the aerodynamics and the control system, and the dynamic phenomena which had to be considered, in achieving maximum usable lift. Ref 38 describes the 'Aerodynamic design evolution of the YF-16', and particularly emphasises the improvements due to the strake and the scheduled leading edge flap deflection. First, the trimmed lift-v-drag is shown in Fig 31, where the variable leading-edge flap deflection has been determined in the same way as the F-18 schedules described above. The basic variations of C_L and C_m with angle of attack are also shown in Fig 31, and it may be seen that the increased lift is obtained with reduced pitching moment at high C_L 's, which leads to the improvements in both trimmed C_L and C_D . The active control system is required to schedule the leading-edge flap deflection, and also to overcome the near-neutral static stability, but there could still be dynamic phenomena preventing this lift being achieved in flight. The first concern is the buffet characteristics, which are given in Ref 38. Unfortunately, the effects of strake and leading-edge flap deflection are shown at different Mach numbers, so that direct comparisons of each contribution cannot be made, but the improvements in buffet intensity are striking enough to warrant reproduction here, in Fig 32. Next,²³ several of the possible adverse flying qualities are associated with loss of directional stability, expressed as either n_y or dynamic $n_y = n_y - i_z \dot{v} \sin \alpha / i_x$ ($C_{n\beta}$ or $C_{n\beta \text{dynamic}}$). The presence of the strake and leading-edge flap deflection each improve sideslip characteristics at high angles of attack, $i_e n_y$ more positive and i_v more negative, and the resulting dynamic n_y at $M = 0.9$ remains well positive up to $\alpha = 40^\circ$, shown in Fig 33. Adverse aileron yaw is another source of poor handling characteristics³⁹, and can lead to departure from controlled flight. Negative values of the Lateral Control Departure Parameter, $LCDP = n_y - n_z \dot{v} / i_x$, indicate problem areas, and an aileron-rudder-interconnect is incorporated in the YF-16 to improve roll control. The variation of LCDP with angle of attack and Mach number is shown in Fig 33; it may be seen that although the gain has been scheduled with angle of attack and Mach number, it has not been possible to achieve $LCDP > 0$ for $\alpha > 34^\circ$ at $M = 0.2$. Departure is actually prevented by using a control law to limit the maximum angle of attack which the pilot can demand, below which flying qualities are good. Of course, the control system of the YF-16 also includes other features, but those described above are also directly relevant to the manoeuvre enhancement and direct lift modes of the CCV YF-16.

Some of the wind-tunnel tests for CCV YF-16 with both horizontal and vertical canards are described in Ref 15. Addition of the canards (and removal of the strake) obviously affects C_L , C_D and C_m , and the substantial additional trimmed lift possible at $M = 0.9$ is shown in Fig 34. The tunnel results show that deflections of canards, flaperons and tail could be used to generate the direct lift, which is an additional control mode on the CCV YF-16. The untrimmed lift due to canard deflection is augmented by the positive tail contribution to trim. Such large increments have not been obtained in flight, as the configuration flow¹⁶ retains the strake instead of the horizontal canards, and so the direct lift is generated by the wing trailing-edge flaps and tail. The buffet characteristics are changed adversely¹⁶, at given angle of attack, by the deflection of the trailing-edge flaps, and it may be seen in Fig 35 that moderate buffet levels are reached at low angles of attack if the flap is deflected 20° at $M = 0.68$. The DLC command had to be limited to flap deflections of 15° to avoid this moderate buffet, and to prevent penetration to strong buffet at the higher angles of attack. The directional stability is also affected¹⁶ by the presence and deflection of the canards. The flight results show that n_y is halved at low angles of attack when the vertical canards are added, at zero deflection, but that directional stability is increased as angle of attack increases to 20° . The dihedral of the canted vertical canards also increases the magnitude of i_v , so that 'dynamic n_y ' has better characteristics at high angles of attack if the canards are on (Fig 35). The horizontal canards were tested in the tunnel at various deflections¹⁵, and the directional stability was found to be very sensitive at the high angles of attack $\alpha > 15^\circ$ due to changing interference effects. Thus the departure parameter, dynamic n_y can be affected significantly by the addition and use of canard surfaces. Data on roll control power are not available, to evaluate LCDP, but it is stated in Ref 16 that canard interference reduced the rolling effectiveness of the differential tail, and also had a smaller reducing effect on the ailerons.

This brief description of part of the YF-16 development history shows that wind-tunnel tests need to cover buffet, rolling and yawing moments due to sideslip and due to aileron, as well as lift, drag and pitching moment, over the range of motivator deflections, so that adequate data are available for pre-flight assessment of manoeuvring capability at transonic speeds.

2.5 Sideforce

The use of direct sideforce as a means of controlling an aircraft has only recently⁴⁰ come to the fore. Accordingly the experimental data available are particularly sparse and no attempt has been made to develop methods of estimation. Research models^{14,19} have been tested in wind tunnels, but the results¹⁵ presented here for illustration are those obtained in the flight and wind-tunnel programme for the CCV YF-16.

Two types of motivators were tested in the wind tunnel, namely, twin 'vertical' canards mounted on the fuselage in the manner indicated by Fig 23 and differentially deflected horizontal canards. In addition to the sideforce each of these motivators generates a yawing moment, which needs to be trimmed by rudder deflection. This in its turn produces some additional sideforce.

As can be seen (Fig 36a) the particular vertical canards tested give rise to a sideforce which is highly dependent on the angle of attack, so that by an angle of attack of 12° the sideforce is only half

its value of at zero angle of attack. A motivator with such characteristics is likely to prove an unattractive proposition.

In contrast to this, the differentially deflected horizontal canards (Fig 36b) yield a sideforce, which even increases somewhat with angle of attack increase. In the trimmed condition the sideforce is substantially augmented by the rudder sideforce and the increase with increase in angle of attack is more pronounced. It was also found that the incremental force is more or less linear with respect to the total angle of deflection, see Fig 36c, for a given angle of attack. Furthermore, there is little variation in effectiveness over the Mach number range 0.2 to 1.2 (Fig 36d). These findings are somewhat unexpected when it is remembered that the sideforce arises from an interference effect upon the adjoining parts of the aircraft. Similar results have been obtained on the CCV F-4¹⁷ and on research models at NASA¹⁴ and ONERA¹⁹. Thus, differentially deflected horizontal canards constitute a suitable sideforce motivator. However, it must be borne in mind that any application which requires differential deflection about different mean positions can have repercussions on other characteristics, due to interference, and the yawing moment due to sideslip was found¹⁵ to be particularly sensitive at high angles of attack.

2-11

Split flaps have been installed on the four pylons of the CCV Alpha Jet⁴¹, and yield more trimmed sideforce than the vertical canard on the YF-16, but less than the differential horizontal canard. Other forms of motivator mounted on the wings have been tested, particularly twin fins, but the area of surface needed appears to be too large for use on combat aircraft. Such a motivator needs only small rudder deflection to trim the yawing moment, and so loses the augmentation of sideforce shown in Fig 36b for the forward-mounted canard.

Differential spanwise blowing¹¹ is another possible sideforce motivator, and can be designed to require little trimming up to moderate angles of attack. The sideforce seems to increase rather faster than linearly with jet coefficient, C_{jv} (Fig 37) but is almost independent of angle of attack up to $\alpha = 16^\circ$, and even increases in magnitude for $\alpha > 16^\circ$. The differential strake projection tested on the same configuration gives only small sideforce at moderate angles of attack, but is slightly more effective than blowing at $C_{jv} = 0.03$ for $\alpha > 12^\circ$. This strong variation with angle of attack makes it unpromising as a sideforce generator, besides being difficult to engineer.

2.6 Drag or thrust

Variation of forward speed is in the main a matter of controlling engine thrust and active control systems based on energy management will play an increasing role in this. Discussion of the engine controls and data pertinent to this problem lies outside the scope of the present paper.

Equally the increase of drag during dives by means of dive or air brakes is not in the present sense a motivator and the properties of these devices are not discussed here. Even the combat manoeuvres of the decelerating type now being introduced are unlikely to involve active control directly. Two such manoeuvres are the result of using vectored thrust and manoeuvring to very high angle of attack to achieve the required deceleration. In both these cases the use of active control systems may be required to obtain satisfactory flying qualities during these manoeuvres.

The aircraft performance requirements are always uppermost in the designer's mind and active control systems aimed at optimizing C_{Lmax} and L/D have found application^{15,33}. As discussed in section 2.4 the optimization is achieved by the appropriate choice of the pitch motivator to use for the trimming task with other devices such as flaps, thrust vectoring and leading-edge slats to augment lift. At present the development of such systems has to rely heavily on wind-tunnel testing with the aircraft model being progressively tailored in order to achieve the optimum lift and drag.

3 INDIRECT EFFECTS

The forces and moments discussed in section 2 are those which the motivators are intended to generate (hence the designation, direct effects), but the pressure distribution which gives rise to these direct effects can result in other forces and moments, either because of its nature or its induced effect on some other part of the airframe. This second class of forces and moments are here termed the indirect effects and are largely undesired.

The pilot of an unaugmented aircraft has to learn to compensate for these indirect effects, but control systems in augmented aircraft can be designed to relieve him of this task, for example an aileron-rudder interconnect has often been used in combat aircraft to overcome adverse aileron-yaw. For this relatively simple control law, the designer needs to know the relative yawing moments due to aileron and rudder in order to determine the gearing between the two control surfaces. In practice this gearing usually has to be scheduled to account for the variation of aileron-yaw with angle of attack. A knowledge of the indirect forces and moments is also required for the design of active control systems, and so the characteristics of various motivators are discussed in this section from this point of view. The examples chosen for illustration do not cover all the indirect effects likely to be encountered, but it is hoped that the more important features are included.

3.1 Indirect pitching moment

3.1.1 Trailing edge flaps

Pitching moment due to flap deflection has always had to be considered, both in obtaining values for trimmed C_L in high-lift conditions, and in retaining longitudinal stability since deflected flaps tend to reduce $\partial C_m / \partial \alpha$. The requirement of ACT for additional lift without change in angle of attack necessitates a control law to negate the associated pitching moment, which of course is highly dependent on configuration. The data given in Ref 1 for estimating $\partial C_m / \partial \delta_F$ throughout the subsonic and supersonic speed ranges are based on experimental results over the ranges of angle of attack and flap deflection for which $\partial C_m / \partial \delta_F$ is linear, corresponding to the data used for estimating $\partial C_L / \partial \delta_F$. Some additional data on the effect of flap span and position on the pitching moment characteristics at high angle of attack are also

described in Ref 1, but refer to a particular wing, and so serve only as a reminder of the importance of flap size as a parameter.

The pitching moment due to flap at high angle of attack is even more sensitive to configuration than the lift discussed in section 2.4, and to illustrate this point some particular results are selected. The height of the tailplane does not affect the lift characteristics of the transport aircraft layout³² with supercritical wing, as shown in Fig 29 but the pitching moments due to angle of attack and flap deflection are quite different for the two tails tested, see Fig 38. Deflection of the flaps gives rise to a pitching moment, which is in part due to the pressure distribution change on the wings and in part due to a change in the tailplane contribution. Whilst the former must be essentially the same for both layouts, it is evident that for the flapped-wing, the tail interference is very different. For the high tail configuration the characteristic pitch up tendency is present in the pitching moments for all flap settings and for the two tailplane settings (0° and -10°), but the net contribution to the nose-down pitching moment due to flap deflection is nearly independent of these two variables and falls off gradually with increase of angle of attack. Over the range of angles tested the value of the pitching moment derivative, $\partial C_m / \partial \delta_F$, is only reduced by about 30%. In contrast, for the low tail layout the pitching moment contribution due to flap deflections (at all settings) reduces rapidly in magnitude with increase in angle of attack and reverses sign to become a nose-up contribution (at $\alpha = 15^\circ$ for $\eta_T = 0^\circ$, and at $\alpha = 20^\circ$ for $\eta_T = -10^\circ$). The cause of differences in the pitching moment characteristics of the two layouts may be sought in flow environment of the tail in the two cases. As is well known the high tail (or T-tail) enters the wing wake at the large angles of attack. Under these conditions it is possible for downwash to be high and the kinetic pressure low. The consequent low effectiveness of the tail is reflected both in its pitching moments due to angle of attack and due to tailplane deflection. The flow over the wing has broken down and is probably not materially affected by flap deflection. At low angles of attack the tailplane is well clear of the wing or wing-flap wake and so there is little interference. This adds up to all curves exhibiting the pitch-up trend, which is a consequence of a gradually decreasing tail effectiveness as the tail enters the wing wake. The increment in pitching moment due to 10° up deflection of the tailplane shows an increasing drop in magnitude beyond an angle of attack of 20° and this drop is almost the same for all flap settings. This trend accords with the explanation of the results given above.

If the same quantity, ΔC_m for $\Delta \eta_T = -10^\circ$, is examined in the case of the low-tail layout, it is seen that, whilst it is practically independent of angle of attack for zero flap setting, it exhibits a pronounced loss of tail effectiveness between the angles of attack of 12° and 22° . At its worst condition the tail retains a little over half of its effectiveness at low angles of attack. These results imply that the low tailplane is clear of the wake and in a region of low downwash for all angles of attack for the unflapped wing. Deflection of the flaps intensifies and broadens the wake and the tail comes sufficiently within this wake, for the previously mentioned range of the angle of attack, to lose a great deal of its basic effectiveness through adverse downwash and kinetic pressure changes.

Interference effects of the same general character, but in this case for upward deflection of wing mounted flaps, were encountered¹⁶ on the CCV YF-16. The direct lift control mode requires deflection of the flap in either sense. It was found during flight tests that large down-tailplane deflections were needed to trim out the pitching moments due to -15° of flap (Fig 39a). Wind-tunnel test results, see Fig 39b, reveal that the tailplane effectiveness decreases with increase of the angle of attack and its level is much reduced by upward deflection of the wing flap. These results indicate that the wing-flap-tail interference affects the pitching moment due to flap deflection and the power of the tail to trim this moment. The recovery pitching moment is inadequate to prevent departure for $\alpha > 18^\circ$, with DLC operative, and so a restriction had to be placed on the utilization of the DLC mode at high angle of attack.

As mentioned in section 2, the control surfaces on wing-canard configurations can be used for various primary tasks. Data was presented in section 2.1 for both canard and trailing edge flap as pitch motivator but in section 2.4 the trailing edge flap was viewed as the lift motivator. Thus the indirect effects have to be interpreted in relation to the concept of the overall design.

3.1.2 Leading edge devices

The effect of leading edge flaps or slats on pitching moment is usually to reduce static stability ($\partial C_m / \partial \alpha$), although the increment in C_m at a given angle of attack is smaller than that due to trailing edge flaps, so that lift and drag penalties from trim are smaller, and in fact L/D is often improved. An example of this type of behaviour is shown in Fig 31 for the leading edge flaps on the YF-16, and the many slat or flap deflections tested¹⁸ on the F-4 also exhibited reduced $\partial C_m / \partial \alpha$, over the low to moderate angle of attack range as shown in Fig 40. The pitching moment characteristics at high angle of attack are highly dependent on configuration, but it can be expected that pitch-up tendencies are alleviated by the presence of leading edge devices, which delay the flow separation on the wings.

3.1.3 Spoilers

The pitching moments associated with antisymmetric deflection of spoiler for roll control can be very significant, especially for the current relative positions of spoiler surfaces (towards the rear of the chord) and of the centre of gravity (near quarter mean chord). The results for the pitching moment due to large spoiler on a wing²¹ (shown in Fig 16) illustrate the magnitudes which can be expected, see Fig 41. The moment arm may be reduced for aircraft with relaxed static stability, but it is likely that pitching moments due to spoiler would remain sufficiently large to require compensation via the control system.

3.1.4 Canards

The attraction of using canards to generate direct lift is that the elevator deflection required for trimming the associated pitching moment contributes positively to the lift, as described in section 2.4. For example, the results shown in Fig 9, where the canard is assumed to be primarily a pitch motivator, could also be interpreted as indirect pitching moment on the lifting canard.

Differential antisymmetric deflection of horizontal canards¹⁵ did not produce significant pitching moments on the CCV versions of the YF-16 and F-4, but it would seem that this characteristic depends on relative height of and longitudinal position of the wing/canard/tail especially when the aircraft is at high angle of attack. Some evidence for the need for caution in this respect is forthcoming from results for a research model¹⁴ with a high canard just ahead of the wing but no tail, as sketched in Fig 42. 2-13

By virtue of the symmetry of the aircraft about its median longitudinal plane the pitching moments due to deflection of either a port or a starboard panel of the canard would be expected to be equal. Thus within the ranges of angles for which linear characteristics might be expected, equal and opposite pitching moments would be expected from a deflection of $+10^\circ$ or -10° regardless of whether the port or starboard panel was being deflected. This expectation is confirmed by the results shown in Fig 42 for both Mach numbers. By the same token it would be anticipated that deflecting the canards antisymmetrically through $\pm 10^\circ$ would give rise to the same pitching moment characteristics as for zero deflection of the canard surfaces. This is very nearly so for lift coefficients less than 0.4 for both Mach numbers (0.4 and 0.9). The non-linear behaviour at the larger lift coefficients, more evident at Mach number 0.4, is probably accountable for in terms of flow breakdown over the canard surfaces and canard-wing interference. However, it is not clear what portion of the pitching moments derives from interference effects.

3.2 Indirect rolling moment

The main source of indirect rolling moment on conventional aircraft is the rudder, but the effects on aircraft response are usually not very significant. The ratio of rolling to yawing moment obviously depends on the height and sweepback of the fin (and on fin arm), and is usually less than 0.3. Variation of $\partial C_L / \partial C_R$ (if measured in geometric body areas) with angle of attack and with Mach number is small, as shown in Fig 43. The ratio of rolling moment to yawing moment for the rudder of the B-1 aircraft²⁵ is seen to be near 0.2 throughout the Mach number range, and corresponding results for the F-111E⁴² (with $\Lambda_{LE} = 50^\circ$) are near-constant up to $\alpha = 16^\circ$ at transonic speeds. The ratio can be greater than 0.3 if the tailplane is mounted at a high position, so that it acts as a reflection plate for the fin and rudder, and the resulting centre of pressure is relatively higher. For example, the results for the model of Fig 19, with its high tailplane and large aspect ratio fin, give a ratio of $\partial C_L / \partial C_R$ to $\partial C_N / \partial C_R$ of nearly 0.5.

At high angles of attack, rudder is sometimes used to augment rolling moment, as roll motivators alone cannot always achieve the required roll rate for combat aircraft. For future designs, with possibly smaller fin arms and a more powerful yaw motivator (all-moving fins etc), the rolling moment due to rudder may increase relative to its yawing moment, as compared to present levels, and so could become more important.

It might be expected that differential deflection of canard surfaces might also induce rolling moments, but it is important to appreciate the extent to which the interference effects on the wing can affect the nett contribution to rolling moment. Asymmetric deflection of canard surfaces can induce an asymmetric downwash field at the wing location, which gives rise to a rolling moment opposing that due to the forces on the canard, within the linearized regime of flow. At larger angles of attack the matter becomes very complex as two effects enter, firstly the effective angle of attack of a panel can exceed its stalling angle and secondly at some stage the variation of downwash may become non-linear.

With these thoughts in mind it is interesting to examine some wind-tunnel test results for the configuration of Fig 42. By virtue of the aircraft symmetry the rolling moments at zero angle of attack should be equal for equal and opposite deflections of the individual canard panels, provided the magnitude of the deflection is such that downwash is still linear with respect to it. It is seen (Fig 44) that at 10° deflection this is not strictly the case, although the very small nett rolling moment is, at any rate, of the same sign. Away from zero angle of attack the effective angle of attack of a panel is made up of (a) its geometric angle of attack (b) its deflection relative to neutral and (c) the small upwash induced by the wing. This last effect is small and is, in any case, modified by the secondary pressure distribution on the wing arising from the flow field of the canard. If this upwash may be ignored, it follows that a combination of $+10^\circ$ deflection of the panel on the port side and a given angle of attack is equivalent to a -10° deflection of the starboard panel at an angle of attack 10° larger. It is, of course, necessary that all effective angles of attack lie within the range leading to linear characteristics. Unfortunately no results are quoted for negative angles of attack in the case of port panel alone deflected. However, the near zero values of rolling moment coefficient, for an angle of attack of about 8° for the case of deflection of the starboard panel alone and for an angle of attack about -2° for the case of deflection of the port panel alone, would be expected on the basis of this argument. On the basis of the quoted results it seems that this line of reasoning fails to account for the opposite signs in the rolling moments due to an upward deflection of a starboard panel at an angle of attack of 10° , and that due to a downward deflection of a port panel at zero angle of attack, notwithstanding the fact that the effective angles of attack on each panel would be approximately equal (0° starboard and 10° port side). Whether flow conditions have already been reached for which the effect of the upstream flow field of the wing may not be neglected, or that non-linear effects are confusing the issue is difficult to say. The latter does not necessarily invalidate the basic argument and in this connection it is of interest to note that superposition of the sum of the rolling moments for individual panel deflection on the curve for the antisymmetric deflection ($\pm 10^\circ$) shows good agreement throughout. To put the rolling moments generated into perspective it should be noted that the sideforce coefficient produced by the antisymmetric deflection is between 0.02 and 0.03, that is, about ten times the size of the rolling moment coefficient.

The horizontal canards¹⁵ tested in the YF-16 and F-4, CCV programmes also generated insignificant rolling moments, when being used to produce sideforce. Corresponding results for the deflection of vertical canards do not seem to be available, but rolling moments did not feature in Ref 16, which describes the aerodynamic interactions on the CCV YF-16, so are presumably also insignificant.

The other motivators currently in use do not cause indirect rolling moments. However, if the differential spanwise blowing¹¹ (or differential strake projection) described in section 2.3 is used to generate sideforce (see Fig 37) as the direct effect then the associated rolling moments (see Fig 18) at the high angles of attack represent important indirect effects, which need to be taken into account in the

design of the control system. The differential strake arrangement could result in even larger rolling moments at supersonic speeds.

3.3 Indirect yawing moment

3.3.1 Roll motivators

The adverse yawing moments, which result from differential deflection of the aileron, have long been a source of difficulty in the lateral control of aircraft at moderate to high angles of attack. A number of parameters have been used to assess their influence on aircraft handling qualities, such as ω_c^2/ω_d^2 and the so-called Lateral Control Departure Parameter. These are various manifestations of the behaviour of the quantity $(n_v - n_{\xi} v / \xi)$, which, for instance, needs to be greater than zero for stability of pilot-in-the-loop modes. If $\partial C_n / \partial \xi$ and $\partial C_y / \partial \xi$ (hence n_{ξ} and ξ_{ξ}) are of opposite sign the above quantity can change sign at some angle of attack, because of the behaviour of n_v and ξ_v at moderate to large angle of attack*.

At the relevant angles of attack the yawing moment arises from changes in the lift-dependent drag caused by motivator deflection, and so is difficult to estimate. The increments in yawing moment produced by a total aileron deflection of 30° on a model of the F-4 aircraft¹⁸, at Mach numbers of 0.6 and 0.9, are shown in Fig 45a, with leading-edge slats on and off. The presence of a slat has an effect on the small yawing moments present for angles of attack below 10° , but leaves the characteristics at high angles of attack virtually unaffected. In the present instance the aileron deflection is in the sense which produces a positive rolling moment. Deflection of a spoiler so as to augment this rolling moment results in the yawing moments due to the combined effects of the aileron and spoiler becoming positive up to a moderate angle of attack (14° at $M = 0.6$, 12° at $M = 0.9$, see Fig 45b). Beyond this angle of attack the moments become negative once more and are not much affected by the spoiler, either with or without the slats. This trend is in accord with results for plain spoilers²¹, for which the yawing moment has the same sign as the rolling moment and both moments tend to zero as the stalling angle of attack for the wing is approached. Results for a flap-type spoiler on the wing of Fig 16 exhibit these characteristics as shown in Fig 46. The spoiler-slat-deflector arrangement shows similar trends, but with larger yawing moments for a given spoiler deflection, as might be expected. There is in the results for the lower Mach number ($M = 0.6$) just a suggestion that the moments do not become zero, but possibly reach a minimum and increase again as the angle of attack exceeds the value corresponding to that minimum.

Although the yawing moment due to differential tail deflection shows similar characteristics to that due to aileron, the adverse effects are usually less severe, occurring at higher angles of attack, and being of smaller magnitude. The other possible motivators suggested for supplementing roll power at high angles of attack, i.e. differential strake projection and blowing along the span¹¹, also produce adverse yawing moments. The magnitudes are appreciable, see Fig 47, and the strake induces rolling and yawing moments of approximately equal magnitudes at $\alpha = 20^\circ$. The asymmetric blowing along the span is, however, more efficient in generating rolling moment than yawing moment, the ratio $\Delta C_n / \Delta C_{\ell}$ being approximately -0.5 for $\alpha < 16^\circ$.

3.3.2 Sideforce motivators

When horizontal or vertical canard surfaces are used to produce sideforce changes yawing moments are induced, which in this context must be regarded as unwanted. Use of the rudder to trim out the yawing moments results in an augmented sideforce contribution, as discussed in section 2.5. The results¹⁵ for vertical canards on the CCV YF-16 are shown in Figs 23 and 36, from which it is seen that increase in the angle of attack reduces the effectiveness of motivators in generating sideforce, but at the same conditions a reduction occurs in the induced yawing moment.

The yawing moments generated by the differential deflection of the horizontal canards on the CCV YF-16 are not published in detail, but some results for the research model of a close-coupled canard¹⁴ layout are of interest. Deflection of one canard negatively was found to generate greater sideforce and yawing moment than an equal positive deflection, shown by the results in Fig 48 for $\delta C_s = -10^\circ$ and $\delta C_p = +10^\circ$ respectively, but the results for differential deflection of $\pm 10^\circ$ are essentially given by the sum of the two increments. It is also noticeable that yawing moment is not linear with differential deflection, with small increase in C_n due to increasing δ from $\pm 5^\circ$ to $\pm 10^\circ$, although the corresponding sideforce (not shown) is linear. The reason why this is so even at zero angle of attack is difficult to understand. It may be remarked, however, that there are four possible contributions to these yawing moments. These are (1) that arising directly from the load distribution on the canard, (2) that arising from the asymmetric loading induced on the wing, (3) that arising from the pressure distribution induced on the fuselage and (4) that arising from the action of the flow field at the fins. The quoted results do not permit a breakdown into these individual contributions. If, for the condition of zero angle of attack and $\delta C_s = -10^\circ$, $\delta C_p = 0^\circ$, each of the above yawing moment increments is represented in magnitude by $(\Delta C_{n_c})_0$; $(\Delta C_{n_b})_0$; $(\Delta C_{n_w})_0$ and $(\Delta C_{n_f})_0$ respectively, then for the case of $\delta C_s = 0^\circ$, $\delta C_p = +10^\circ$, $\alpha = 0^\circ$ the magnitudes of these different contributions would be expected to be the same, but for some the signs differ. Thus, the following relationships exist,

* Care needs to be exercised when comparing wind-tunnel test results from different sources as the derivatives may refer to different axis systems, usually either aerodynamic body axes (stability axes) or geometric body axes. If the plain symbols are used for the former type of derivative and those with a suffix b for the latter, the following relationship exists;

$$(n_v - n_{\xi} v / \xi) = \left(\frac{\xi_{\xi}}{n_{\xi b}} \right) (n_{v_b} - n_{\xi_b} v_b / \xi_b)$$

$$C_n(\delta_{C_p} = 0, \delta_{C_s} = -10^\circ, \alpha = 0^\circ) = (\Delta C_{n_C})_0 - (\Delta C_{n_B})_0 + (\Delta C_{n_W})_0 + (\Delta C_{n_F})_0$$

and

$$C_n(\delta_{C_p} = +10^\circ, \delta_{C_s} = 0^\circ, \alpha = 0^\circ) = -(\Delta C_{n_C})_0 - (\Delta C_{n_B})_0 - (\Delta C_{n_W})_0 + (\Delta C_{n_F})_0$$

2-15

The former yawing moment exceeds the latter by $2\left\{(\Delta C_{n_C})_0 + (\Delta C_{n_W})_0\right\}$, which offers a possible explanation of the difference noted in the single panel deflection results. For the combination $\delta_{C_p} = 0, \delta_{C_s} = -10^\circ, \alpha = 10^\circ$ the contributions from the canard, fuselage and fin are again of magnitude $(\Delta C_{n_C})_0, (\Delta C_{n_B})_0$ and $(\Delta C_{n_F})_0$, but the wing on the starboard side has an angle of attack of 10° whilst that on the port side has an angle of attack of 10° less the downwash due to the canard, giving rise to a yawing moment contribution of $(\Delta C_{n_W})_1$, say. Thus the difference in overall yawing moment for $\delta_{C_p} = 0, \delta_{C_s} = -10^\circ$ at 10° angle of attack and at 0° angle of attack is $\left\{(\Delta C_{n_C})_0 - (\Delta C_{n_B})_0 - 2(\Delta C_{n_C})_1\right\}$, which could possibly explain why the two yawing moments differ so little.

In spite of the non-linearity exhibited by the $\pm 10^\circ$ deflection results in comparison with the $\pm 5^\circ$ deflection results, the results for individual panel deflection may be superimposed to give total yawing moments very close to those for the antisymmetric deflection of $\pm 10^\circ$. This holds for both Mach numbers.

3.4 Indirect lift

3.4.1 Longitudinal motivators

The main emphasis in design considerations of indirect effects of motivators on lift is on performance, and it is obviously beneficial if the control surface deflection required for trim contributes positive lift - hence the interest in relaxed static stability and canard layouts. Comparisons of performance parameters are not discussed further here, although many of the reports on longitudinal control surfaces listed in Bibliography are primarily concerned with $C_{L_{trim}}$, L/D and effect of static margin^{4,9,12,13,38}. It is usually found that the lift associated with the level of pitching moment required by other applications of active control does not have a significant effect on aircraft response. More attention may have to be paid to the lift for very closely coupled configurations, *eg* when the trailing-edge flap on the wing-canard and wing alone configurations is considered principally as a pitch motivator in section 2.1 (Fig 11), notwithstanding the fact that the lift is large enough to have been included in the data discussed in section 2.4.

3.4.2 Lateral motivators

The only lateral motivators to induce lift are spoilers used for roll control, and the lift loss can be appreciable. For example, the large spoiler ($h_g/c = 0.08$) shown in Fig 16 causes an incremental lift of -0.2 at low angle of attack (see Fig 49), which becomes near zero as the wing stalls at higher angles of attack. The spoiler-slot-deflector is more efficient as a roll motivator than the plain spoiler, and the lift loss is correspondingly greater, and is still appreciable at the highest angle of attack tested, $\alpha = 20^\circ$, as also shown in Fig 49.

3.5 Indirect sideforce

The sideforce induced by conventional controls is small, that due to the rudder being the most significant. For current aircraft designs, $\partial C_Y / \partial \tau_R$ does not affect the response sufficiently to need correction, but with the trend towards shorter fin arms, the magnitude of sideforce relative to yawing moment becomes larger, and may need to be considered.

3.6 Indirect drag

All motivators cause increased profile drag when in operation, and many motivators also cause increased overall lift-dependent drag, the main exception being ailerons and differential tails. The design aim is obviously to achieve the required level of control power at minimum overall 'cost', to which drag is a major contributor, but a comparison of drag levels is not attempted in this review. As mentioned in section 2, the reports on experimental data for flaps and other lift-augmentation devices include drag measurements, and most discuss performance parameters. Measurements of drag due to lateral motivators are not always recorded in the published literature, as in the past the drag increments have not been important for design considerations.

4 HINGE MOMENTS

Deflection of most of the motivators described in the preceding sections requires a significant effort, which, since the deflection usually takes the form of a rotation about a hinge line, is a moment about that hinge. In the early years of the aircraft, this effort had to be supplied by the pilot, via a mechanical system linking the motivator (usually a flap-type control surface) to the pilot's cockpit control. Physiological limitations and fatigue set absolute limits on the hinge moments, whilst the ease and rapidity with which control could be applied caused the aircraft designer to aim for values considerably below the above limits. As the speed range of aircraft increased and the range of size became larger the designer was forced to ever smaller hinge moment coefficients. The hinge moments themselves, of course, increased at least as the square of speed (often more as compressibility became more important) and as the cube of the linear dimensions. These trends made for exceedingly fine aerodynamic balance ($\partial C_H / \partial \delta$ etc close to zero) and hence very small tolerances on manufacture. This, of itself, did not put an end to the quest for aerodynamic balance of the hinge moments, but taken together with the fact that the conventional forms of balance failed to give the required relief through the speed range, which was rapidly extending into the supersonic regime, meant that designers saw power-operation of the control surfaces as a

2-16
means of escape from the recurring tedium of making adjustments in lengthy flight tests. Hinge moment characteristics assumed less importance in aircraft design and, perhaps not surprisingly, the research and wind-tunnel testing also decreased, apart from tests aimed at supplying data on oscillating control surfaces for flutter investigations, of which more is said later.

This somewhat relaxed attitude towards hinge moment characteristics was perhaps accompanied by more uncertainty about their estimation, since development of the methods given in the ESDU² and DATCOM¹ series failed to take place. Indeed it is probable that in many instances there was no advantage taken of the advances made in the theoretical side of the calculation of flows around lifting surfaces. Be that as it may, it is a matter of record⁴³ that problems were encountered with undesirable behaviour of a flight control system, because the actuator hinge moment limit was reached. In this instance, it is only fair to remark that the discrepancy between estimated or design data and those realized in flight test was confined to the hinge moment at zero tail lift (or, in fact, to the b_0 effect). The aircraft in question was the USAF/Rockwell B-1 and the problem was aggravated by a discrepancy in the pitching moment coefficient at zero lift, tail off. Difficulty was first encountered on a flight manoeuvre initiated by a rudder doublet input and during which the yaw autostabilization was made inactive. The resulting aircraft response is illustrated in Fig 50. As the port and starboard tail panels, each in its turn, reach a down angle of $+5.8^\circ$ the flight record shows flats. Close examination of the hinge moments in these conditions revealed that a limit for the actuator had been reached. The consequence of this was the uncommanded (and potentially dangerous) response in pitch as indicated by the normal load factor in Fig 50.

An explanation of the events just described may be sought on the following lines. In the absence of augmented yaw damping the Dutch-roll mode is lightly damped, so larger than usual roll and yaw oscillations would ensue in the manoeuvre described above. The roll channel of the flight control system responds by providing differential tail deflection according to the roll rate. For a downward-going panel it becomes possible to reach the actuator's hinge moment limit. When this happens, as, for example, for the second time in the flight of the B-1 aircraft, the starboard tail panel is prevented from deflecting further whereas the deflection of the port panel is not restrained. A more negative rolling moment than intended is produced, and is accompanied by an uncommanded nose-up pitching moment. The latter causes the uncommanded response in the load factor. As soon as the roll rate drops sufficiently, there is no danger of limiting in this way and the control system behaves normally.

Since, at aft centre-of-gravity locations, the effect on the hinge moment of the increasing angle of attack in a pull-up can more than counterbalance the effect of the negative tail deflection, it is also possible for difficulties, arising from the same cause, to occur.

As previously remarked the output of experimental data on controls (motivators) which reached flood proportions in the 1950s dropped to a mere trickle in the next two decades. The impression may be misleading in that it is not possible to account for the results of unpublished *ad hoc* work. For this reason it has been decided to describe the readily available data under the two headings of (a) quasi-static hinge moments (b) hinge moments for oscillating motivators, rather than according to type.

4.1 Quasi-static hinge moments

Figs 51 and 52 show some of the results⁴⁴ available from an investigation made of the load and hinge moment characteristics of a sweptback high tail (T-tail) fitted to a model of a transport aircraft (actually a seaplane). Tailplane pressure distribution, normal force and hinge moments were obtained for the Mach number range 0.60 to 1.075 and a wing angle-of-attack range of -4° to $+14^\circ$. A thin ($t/c = 0.05$) tail of delta planform and area equal to that of the original tail was also tested. For an all-moving surface it is convenient to plot the hinge moment coefficient against the tail normal force coefficient and the latter against angle of attack, as in Fig 51. Some slight non-linearity of characteristics is present at the most negative and positive angles of attack tested. The effect of tail setting on the variation of the hinge moment coefficient with the normal force coefficient of the tail was found to be small and it is thus instructive to examine the trends with Mach number of the derivative $(\partial C_H / \partial C_N)_{\text{tail}}$, or the aerodynamic centre location. For the original tail the aerodynamic centre moves aft as Mach number increases from 0.9 upwards, see Fig 52, with an overall shift of about 20% chord between $M = 0.8$ and $M = 1.08$. The delta tail exhibits about the same overall shift, but it is confined in this case to the range $1.0 < M < 1.08$. An important difference is noted in the hinge moment coefficients for zero normal force (b_0) for the delta and swept tails, see Fig 52. Devices that alter the level of the b_0 effect may be employed to change the level of hinge-moment, without any change in the slope of the curve of hinge-moment coefficient against tail normal force coefficient. What is desirable depends upon whether the trim of the aircraft is achieved with download or upload on the tail.

Data from the next series of wind-tunnel tests²¹ have featured already in the earlier sections of this review. They refer to two spoiler arrangements fitted to a half-model of a 45° sweptback wing and fuselage combination. One is a flap-type spoiler and the other is a spoiler-slot-deflector arrangement. A Mach number range of 0.6 to 0.95 was covered in the tests and an angle-of-attack range of -4° to $+20^\circ$ for the lower Mach numbers, but a more restricted range in angle of attack for Mach numbers between 0.85 and 0.95.

For the flap-type spoiler positioned as shown in Fig 16 the hinge moment coefficients varied with spoiler deflection and Mach number as shown in Fig 53a for zero angle of attack. Whereas the variation of the hinge moment coefficient is approximately linear with spoiler deflection, it exhibits a departure from linearity with respect to angle of attack, which becomes more pronounced as either the spoiler deflection or the angle of attack is increased, see Fig 53a. The hinge moments for a given spoiler projection decrease in magnitude as the angle of attack becomes large.

Hinge moment data are given for simultaneous deflection of the lower surface deflector for a range of spoiler projection and deflector projection. As explained in the section on rolling moments, there is a progressive improvement in rolling power with increase of deflector to spoiler gearing up to 0.75 at the lower Mach numbers and up to about 0.5 at the higher Mach numbers tested. The hinge moment to be provided by the actuator can be reduced by suitably linking the spoiler and deflector since their hinge moments

are, over much of the range, of opposite sign. If the individual hinge moment coefficients are based on $S_s c_s$ and $S_d c_d$ where S_s = area of spoiler surface and c_s = spoiler chord and S_d = area of deflector surface and c_d = deflector chord, then the nett hinge moment coefficient based upon the total area and either chord of identical surfaces is given by

$$C_{H_{\text{nett}}} = \frac{1}{2} \left(C_{H_s} + \frac{dh_d}{dh_s} C_{H_d} \right) \quad 2-7$$

From the data given in Ref 21 this quantity can be evaluated for any specified gearing. To illustrate how the hinge moment required can be reduced the coefficients (Fig 54a) have been calculated at $M = 0.6$ and $\alpha = 0^\circ$ for $h_d/h_s = 0.25$ and 0.50 for a range of h_s . The data for $\alpha = 8^\circ$, $M = 0.6$ were analysed in a similar way for $h_d/h_s = 0.25$ and 0.50 for $0 \leq h_s/c \leq 0.08$ but only for $h_s/c = 0.01, 0.02$ for $h_d/h_s = 0.75$, see Fig 54b. These results, in their turn, can be used to estimate an idealized gearing resulting in zero hinge moments. This linkage gearing is also shown in Fig 54b. Since the data for other Mach numbers and angles of attack show similar trends it would seem possible to achieve very low hinge moment requirements throughout, possibly at the expense of a gearing scheduled with Mach number, angle of attack and deflection.

Not many flight measurements of hinge moment characteristics are to be found in the literature, but test results have been reported for the Fairey Delta 2 aircraft⁴⁵ and the XB-70 aircraft⁴⁶. The aileron and elevator hinge moment derivatives for the former aircraft were extracted from flight records of hinge moments, aircraft response and the control input pulses. Where possible the results were compared with wind-tunnel test results. These comparisons are reproduced herein, Figs 55 to 57 and show that $\partial C_{H_A} / \partial \delta$, $\partial C_{H_E} / \partial \eta$ and $\partial C_{H_E} / \partial \alpha$ for the elevators were in good agreement, but differences do exist between the two sets of $\partial C_{H_A} / \partial \alpha$ for the ailerons. It is also concluded that the induced effects $\partial C_{H_A} / \partial \eta$ and $\partial C_{H_E} / \partial \delta$ are important, at any rate at transonic speeds, see Fig 57. The hinge moment coefficient for zero angle of attack of each motivator proved difficult to obtain. It was necessary to apply aero-elastic corrections. On the basis of the simple procedures followed these were significant for the elevator, but small for the aileron. The agreement of results at 10000 ft and 40000 ft altitude suggest that the corrections for the elevator distortion were of the right order of magnitude. For the aileron there is an unexplained discrepancy.

The data for the XB-70 aircraft are essentially a flight-tunnel comparison, so that in Fig 58 can be seen the agreement between the results of flight tests, rigid wind-tunnel test results and the latter corrected for elastic effects. The tip portions of the wing are folded downwards in supersonic flight and the two outboard elevon segments on each tip are locked in a neutral position. To obtain the elevon hinge-moment data in coefficient form, the sum of the hinge moments of the segments in use on the wing panel, for which measurements were taken, was divided by the product of free stream kinetic pressure, the total area of these segments and the mean elevon chord for this area. In forming the derivative b_2 the average deflection of the above-mentioned segments was used.

Trailing-edge flaps at various spanwise locations on a supercritical wing⁴⁷ (shown in Fig 29) were the subject of the tests the results of which are presented in Fig 59. The non-linear character of the hinge moment coefficient ($M = 0.90$, $\alpha = 2^\circ$) for positive flap deflection is noteworthy, as is also the fact that for the most inboard of the three flap motivators the non-linearity extends into the negative deflection range. At the lower Mach number, $M = 0.6$, the curve of hinge moment coefficient against flap deflection is more nearly linear. Calculated hinge moments agree well with measurements in this instance.

4.2 Oscillatory hinge moments

In the context of active use of motivators for gust load alleviation or to delay the onset of flutter, knowledge of the hinge moment characteristics of oscillating flaps is essential. At the high frequencies involved, these characteristics depend upon the value of the frequency parameters, particularly at transonic speeds. A number of the papers published on the topic of oscillatory hinge moments are concerned with the development of test techniques (see Bibliography), but as the various techniques yield data of comparable accuracy this aspect is not of immediate interest, except to remark that in the usual analysis the moments are effectively linearized.

The data displayed in Figs 60 and 61 show the influence of large trailing-edge thickness on the stiffness and damping derivatives for a trailing-edge, flap-type control fitted to a half-wing model⁴⁸ (effective aspect ratio 1.8, taper ratio 0.74). The damping derivative results indicate instability at transonic speeds for the basic aerofoil section. For the controls with thickened trailing edges the aerodynamic damping is stable, but only for a limited amplitude of oscillation. However, the amplitude over which the damping is stable increases with increasing trailing-edge thickness. The stiffness derivative, like its quasi-steady counterpart, is increased in magnitude at subsonic speeds as the trailing-edge thickness is increased, but its variation with Mach number at transonic speeds is decreased, see Fig 61. Similar unstable characteristics were noted in tests⁴⁹ of a swept fin with full-span rudder mounted on a half body and attached to the wind-tunnel wall (Fig 62). In this case the instability is confined to Mach numbers in excess of 0.975. For the basic tests the rudder was unbalanced and it was found that the addition of forward balance (setback hinge) had a stabilizing influence on the damping derivative, although, not surprisingly, the stiffness derivative changes sign at subsonic speeds (Fig 62). The addition of small spoilers, mounted on the control surface just aft of the hinge line, had an even greater beneficial effect on the unstable damping characteristic, whilst reducing the hinge moment due to deflection at Mach numbers in excess of 0.9. These improvements are obtained at the expense of about 40% reduction in control effectiveness.

The influence of aerofoil and control section shape is also the subject of the investigation⁵⁰ of a rectangular wing of aspect ratio 3 with stores of different weight attached to the wing tip. Four thickness-chord ratios, 0.04, 0.06, 0.08 and 0.10, were tested with controls having a fixed trailing-edge angle of 13.33° (the true contour trailing-edge angle of the 65A010 aerofoil section) and Fig 63 shows typical results for the aerodynamic damping derivative. Control surfaces with trailing-edge angles of 5.25° , 13.33° and 19.75° were fitted to the 10% thick wing. Fig 64 shows that increasing the trailing-edge angle, with a fixed thickness-chord ratio, has a stabilizing effect on the unstable damping present for the control with a trailing-edge angle of 5.25° for Mach numbers between 0.9 and 1.02, the maximum of these tests.

The test results for the stiffness derivative (not reproduced here) show that changes in the aerofoil thickness-chord ratio, while holding the control trailing-edge angle constant, has little effect on either the static hinge moment derivative with respect to control angle or the stiffness derivative of the oscillatory tests. The largest trailing-edge angle leads to slight overbalance up to a Mach number of unity, (Fig 65).

Other modifications to the control surface more akin to those of Ref 49 were also tested and demonstrate the same trends.

Some tests of a half-wing model, of effective aspect ratio 2.744, and fitted with 26% full-span flap are described in Ref 51. The trends shown by the stiffness and damping derivatives quoted follow those shown by the results described previously, that is, the magnitude of the stiffness derivative increases as Mach number is increased whilst the damping, after exhibiting an increase at subsonic speeds, drops in magnitude near a Mach number of unity and thereafter shows a tendency to reverse in sign. This paper⁵¹ makes special mention of the effect of Reynolds number as indicated by these particular tests. The scale effect seems to be a more definite trend in the case of the damping derivative. In contrast, the authors of Ref 49 state that for the range of Reynolds number used in their tests (1.4×10^6 to 4.95×10^6) scale effects are small. Work on the topic has continued in the UK, see Bibliography and in particular Ref 52, which refers specifically to active control.

5 IMPLICATIONS IN WIND-TUNNEL TESTING

Mention has already been made of some of the topics discussed in this section, but such remarks have been of a superficial nature. It is thought worthwhile to discuss in somewhat greater depth certain aspects of wind-tunnel testing which have repercussions upon the ease of acquisition or the accuracy of experimental data.

5.1 Scale effects - Reynolds number

The need to operate combat aircraft at flight conditions for which flow separation occurs has been the spur to much of the recent aerodynamic and flight dynamic research. Ironically scale effects are at their most significant in conditions of flow separation, in which control characteristics depart from linearity and have to be measured rather than estimated. This state of affairs is likely to continue to challenge the aerodynamicist for some time, both in achieving satisfactory characteristics and in extrapolating from model to full-scale.

A few tunnels are coming into operation which are capable of achieving high Reynolds numbers and would seem to offer a straightforward way out of our troubles with scale effects. However, it is likely to prove difficult, and certainly expensive, to make large models with operative control surfaces strong enough to withstand the high loads resulting from testing at high angles of attack and high speed. An alternative attack on the problem lies in the techniques which aim to simulate full-scale boundary-layer conditions on wind-tunnel models. The final justification of the efficacy of these techniques rests on comparison with tests at full-scale Reynolds number.

More data on control characteristics are now becoming available from flight tests and these provide a useful comparison with wind-tunnel derived data. However, any differences may be attributed, in part at least, to a variety of causes, including Reynolds number, aeroelastic and dynamic effects. It may be impossible to isolate the pure scale effects. Another possible source of data at high Reynolds number is the testing of large-scale models, in free or remotely-piloted flight. To achieve high subsonic speeds in such tests would prove expensive.

It is fortunate that flow separation is usually delayed to a higher angle of attack by a large increase in Reynolds number, thus rendering wind-tunnel results conservative. A difficulty arises when the design of the control system relevant to a particular task is dictated by the control characteristics beyond the onset of flow separation. In this case final adjustments must await the outcome of flight trials.

As regards the data used in the illustrative examples of the text, which are in the main drawn from wind-tunnel test results, possible scale effects have been indicated by quoting the Reynolds number for each test. The extent to which transition strips or other means of modifying the boundary layers of the various aircraft components have been used is not noted and reference must be made to the original papers for these details.

5.2 Aeroelasticity

Attention has already been drawn to the fact that ailerons and rudders are particularly sensitive to aeroelastic effects, but it is not possible to cater for these effects by constructing models having the correct aeroelastic scaling. Two techniques have been developed to circumvent this difficulty. The more common technique is to apply theoretical static aeroelastic corrections to data obtained from a rigid model. The alternative is to test the control surface on distorted shapes calculated for the various flight conditions. Both techniques assume pseudo-steady conditions, that is, the aircraft shape is determined by the steady load at the mean flight condition, and dynamic or time-dependent effects are neglected. This assumption is justified away from flutter speeds, but, of course, must not be made in deriving data to be used in the design of a control system which delays the onset of flutter and increases the pre-flutter damping.

It is also necessary to take due account of aeroelastic effects in the design of variable camber systems intended to optimize lift and drag. The desired shape is that of the loaded wing for the design flight condition, from which the geometry of the unloaded wing and variable camber system has to be deduced.

An active control system which is designed to alleviate loads must be based to an increasing extent upon a fully-representative mathematical model of the aircraft embracing both aerodynamic and structural aspects. One difficulty here is how to reconcile in a meaningful manner data from semi-empirical or empirical sources on the one hand with data only available from theoretical sources.

5.3 Unsteady flows and dynamic effects

The two aspects of time-dependent aerodynamics which have to be considered for control surfaces are the effect of high-frequency oscillations due to structural response (in flutter postponement systems) and the transient changes due to rate of deflection (in gust load or response alleviation systems). Wind-tunnel test techniques for measuring the characteristics of oscillating control surfaces have been developed, and some new results will be described later in this Symposium. The transient changes in pressure distribution due to rate of deflection of control surfaces have largely been ignored until recently, but the higher rates of control application demanded by some types of active control systems mean that some knowledge is needed. Theoretical methods are being developed, and experimental data are becoming available, for plain flaps, but there is a gap in our knowledge of aerodynamic characteristics and of the effects on control system design.

5.4 Interference and coupling effects

In the context of this review the term interference is taken to imply an aerodynamic interaction, often mutual, between two components of an aircraft. It also manifests itself in effects due to test set-up in wind-tunnel testing, *viz* tunnel wall interference and model-sting interference, mention of which is made in section 2.3. Here we prefer to lay stress upon the increasing importance of the interference, often mutual, between surfaces, both fixed and movable, which is a feature of the closely-coupled aircraft configurations. Examples of such effects on control powers have been given in sections 2 and 3. Under the same heading comes the influence that leading-edge devices, introduced to improve aircraft performance, have on such things as control power and flying-quality parameters.

Coupling is taken to signify the effect whereby the forces and/or moments relating to one axis (of a body axis-system) are affected by the presence of a parameter related basically to another axis, for example, yawing moment due to aileron deflection, pitching moment due to rate of yaw. Here we are concerned particularly with the coupling effect wherein the aerodynamic forces and/or moments generated by one parameter are altered significantly by the presence of another parameter. Where the two parameters are motivator deflections the coupling is, in effect, a form of interference. It may be noted in passing that the inclusion of such terms in the aerodynamics renders the mathematical model of the aircraft non-linear and usually couples the longitudinal and lateral motions. In the context of the linearized mathematical model it has been customary to include contributions to the sideslip derivatives due to the flap deflection, as such contributions to the rolling and yawing moments due to sideslip are often important. However, in these circumstances the flap deflection was invariant. We are now concerned with the case where the flap deflection (or some other parameter) and the sideslip are varying simultaneously. Such coupling effects have not been previously discussed, but are probably of considerable importance in the design of a system using a direct sideforce motivator. Published experimental data are sparse, and it does not seem possible to draw firm conclusions as to which effects are likely to be significant for particular configurations. Some initial guidance has to be intuitive, and it seems logical to assume that forces and moments highly dependent on angle of attack and sideslip for zero control deflections will also vary with sideslip when control surfaces are deflected. For example, pitching moment due to sideslip is small for the research slender aircraft, HP 115, (Fig 66) and so is the incremental pitching moment due to trailing edge elevons. In contrast, the corresponding unpublished results for a tailed aircraft in Fig 66 show that pitching moment is highly dependent on sideslip throughout the angle of attack range, and that the increment in pitching moment due to trailing edge flap deflection is halved at sideslip angles of 10° for small angles of attack. Control surfaces generating primarily lift and/or pitching moment also generate rolling and yawing moments at non-zero sideslip. The trailing edge elevon on the HP 115 exhibits such characteristics as shown in Fig 67a. The rolling moment induced by 20° down elevator is near-linear with sideslip, almost independent of angle of attack, and is equivalent to about $2\frac{1}{2}^\circ$ of aileron at 6° of sideslip. The yawing moment is also near-linear with sideslip, but is dependent on angle of attack (as is rudder power), and 6° of sideslip generates the same yawing moment as 7° of rudder.

A combat configuration with tail and twin fins shows similar levels of rolling and yawing moments due to deflection of the high lift system at $\alpha = 13^\circ$, as shown in Fig 67b. This model was also tested with roll motivators deflected at various sideslip angles, and the results in Fig 67c show that the increasing sideslip reduces control effectiveness for both aileron and spoiler. The loss at 5° of sideslip is about 20%, which should not have serious repercussions on aircraft response, but is large enough to warrant consideration. For this configuration, the incremental yawing moment due to aileron or spoiler is not affected by sideslip, up to $\beta = -7^\circ$. A further indication of the growing importance attached to these interference and coupling effects is provided by the results quoted in Ref 54. There the effect of ignoring in turn each of a number of such contributions to the forces and moments on the motion during post-stall excursions and spin entry was examined. In some cases neglect of the term had a dramatic effect on the calculated motion.

The complex nature of interference and coupling effects is such that obtaining reasonably reliable estimates remains a long-term prospect, especially when flow separation is present. If this is accepted as a true statement of the position the implications in wind-tunnel testing could be far-reaching, costly and time consuming, for it implies that models should be fitted with a full set of motivators and that measurements be taken for various combinations of motivators. Furthermore, these tests need repeating over a range of each of the three variables, angle of attack, angle of sideslip and Mach number. Such a complicated model can only be envisaged as being tested during a late stage in the design.

It is not possible, at present, to say whether this will prove wholly acceptable and there is a need for studies to establish to what extent the inclusion of such effects render control system design difficult. If it should prove so then some generalized wind-tunnel testing may be needed to establish orders of magnitude and major design factors.

2-20 6.1 Status of experimental data

This review of experimental data has sought to gather information on the aerodynamic derivatives and maximum power of a variety of motivators, and on their actuation forces and moments. These characteristics are of importance, to a greater or lesser extent, in the design of each of the active control systems currently being considered, and the degrees of importance are suggested in Fig 68. This illustrates the emerging importance of maximum control power available, which has only been a major consideration in the past for high lift systems, although some attention has had to be paid to flight conditions in which effectiveness is reduced, *eg* aileron power at high angle of attack, and elevator power at supersonic Mach numbers. (These latter problems arose from the conflicting requirements for control power at the extremes of the flight envelope, in that aileron deflection needed at high angle of attack could allow the pilot to reach roll rates leading to inertia cross-coupling at lower angles of attack, and the size of elevator needed for supersonic manoeuvring is too powerful at low speeds for easy control.) Such conflicts can be resolved by using active control systems.

Information on maximum control powers is particularly needed in the design of relaxed stability systems and departure/spin prevention systems, as the limiting flight conditions, particularly maximum angle of attack, are defined by the power available. This has to be determined experimentally, since the forces and moments generated by the motivators are much affected by such phenomena as flow separation and interference between surfaces, which cannot be predicted with any degree of confidence. The results available show that the maximum power is highly dependent on the configuration, and can be influenced by, for example, leading edge devices or engine power. Thus it is not possible to correlate the results for maximum power of motivators on complete configurations, although the recent data on maximum lift due to flaps on isolated surfaces could possibly be used to extend the DATCOM methods¹. In order to apply the results of such correlations to an actual aircraft design, a knowledge of the local flowfield is needed, to define local angles of attack and sideslip, and local kinetic pressure.

The substantial body of data on control derivatives has been assessed from several points of view. Firstly, the geometric features of aircraft designs are changing radically, so that the empirical factors used in DATCOM¹ and ES DU² to correct theoretical values may not be applicable to, for example, the thinner wings, lower aspect ratio/lower sweepback wings, shorter and wider bodies and closely-coupled wing-tail or wing-canard layouts of future combat aircraft. The influence of strakes and leading edge devices, which lead to controlled flow separation, has also to be considered, as the efficiency of the control surfaces is determined by the flow field in which they are operating. Secondly, derivatives which were previously unimportant can become significant. It is not possible to be categorical about the relative importance of each derivative, but some speculations for the general trends are summarised in Fig 69, which also shows the present standard of knowledge for the usual controls on conventional aircraft. The use of active control systems is judged to increase the importance of most of the control derivatives. Derivatives due to elevators and rudders are thought to be well-documented and correlated, but derivatives due to other motivator deflections are not so well known. Thirdly, the use of active control systems introduces both new control surfaces and new usage of conventional motivators. The latter necessitates a wide range of tunnel testing, to cover, for example, up deflection of trailing edge flaps, and asymmetric control surface deflection (in contrast to symmetric or antisymmetric), besides the various combinations of motivator deflections which may cause mutual interference. Some applications of active control technology also require fast actuation of the motivators, and so testing of oscillating surfaces is required if dynamic effects are thought to be appreciable. No results for oscillatory control derivatives (apart from hinge moments) are quoted in this review, as data are very sparse. Fourthly, it may well be necessary to use segmented control surfaces, either to obtain the range of levels of control power required, or to adjust aerodynamic loads along the span. The listing of these four topics highlights the gaps in knowledge of control derivatives.

Hinge moments, particularly at extreme deflections, present even greater difficulties. To achieve the necessary accuracy in the determination of the hinge moments at all flight conditions, it is necessary to test the motivators in as representative a wind-tunnel test as possible. Accuracy of the data, rather than possible reduction of the magnitude of the actuating moments, is likely to be paramount. However, in the struggle for the optimum design, the possibilities of reduction of these moments, with attendant reduction of weight etc, should not be lost sight of.

It is unlikely that systematic testing of a complete series of models can be undertaken to fill the gaps in knowledge, as this seems to be prohibitive in time and money. More may be gained, perhaps, by restricting attention to a few particular basic layouts, and exploring variations on these basic themes. To be effective, this approach to research demands closer links between industry and the research establishments.

6.2 Methods of increasing effectiveness

It is apparent from the descriptions of possible future active control systems that large control powers are likely to be required throughout the flight envelope, particularly for combat aircraft. The discussion of the results in section 2 has revealed the strong dependence of control effectiveness on most motivators on angle of attack, and that significant losses occur when the flow separates from the surfaces. Some methods of maintaining the level of control power have been described, in particular, leading edge devices which cause controlled flow separation via vortex generation. However, these devices must fail to be effective at some flight conditions, and they cannot affect the additional losses at high motivator deflection angles, when the flow separates from the control surface itself. Since the maximum control power increases with increase in either control derivative, or control surface area, or maximum effective deflection angle, the aircraft designer has a choice of either increasing the relative area of control surface to main surface (until the ultimate of all-moving tail, fin or wing is reached), or seeking other means of maintaining effectiveness. Examples of using some of the engine power to augment flap effectiveness have been given in section 2, and this seems to be the most attractive source of increased control power. Various ways of applying the concept have been used, from pure jet flap with no control surface,

to blown flaps with jet efflux at the leading edge of the control surface, and now to 'two-dimensional' nozzles deflected as a flap. The added engineering complexity is offset by the very high control powers available, with no degradation in aircraft performance. The augmentation achieved by some jet flap installations described in section 2 include the blown trailing edge flap (Fig 26), jet-augmented rudder (Fig 19), and the nozzle flap (Figs 11,27). It would seem that such techniques will continue to be developed for application to combat aircraft, apart from their obvious use for STOL aircraft. An added attraction is that two control variables are associated with each surface, the flap deflection for faster response control, and jet momentum coefficient for slower, larger changes in control levels. 2-21

The characteristics for direct jet controls have not been discussed in this review, but should be mentioned as another source of control power. Small jets at the extremities of the aircraft, *ie* wing tips and fore-and-aft fuselage, may be used to generate forces and moments. In this case the maximum power is limited, of course, by the engine bleed available. The main problem is in providing fast response via changes in thrust level, as lag times are appreciable; one solution is to provide variable deflection of the jets, which then have to be interconnected to maintain trimmed flight conditions. Interference effects on control surfaces may be significant due to changes in local induced flow, and so it is unlikely that the control powers would be additive. Tunnel tests would be needed to provide an adequate data base.

6.3 Integration of the motivators in active control systems

In the past, each motivator had one primary task, for which it was optimised with regard to the control power required for manoeuvring, while maintaining the required aircraft performance throughout the flight envelope. It is in this context that the direct effectiveness of the various motivators were discussed in section 2, in which the information was arranged according to the major contribution of the motivator to force or moment. For the actively controlled aircraft, the number of tasks has increased, since the motivators are required to provide forces and moments for some or all of the control systems listed in Fig 68. Thus the one-to-one correspondence of motivator and task is unlikely to continue, and each motivator will be required to respond to the demands of a number of control laws. In addition, there may be greater freedom in the design of the control laws if more than one surface contributes to the total required force or moment, so that optimum performance can then be achieved in each control mode. It would also be easier to make such multi-surface systems fail-safe. The present state of evolution is that the concept of more than one type of motivator being used for a particular task (*eg* aileron and spoiler for generation of rolling moment) has been extended to the use of several individual surfaces in actively-controlled combination (segmented trailing edge flaps and ailerons for modifying loads, combined vertical canard and rudder for direct sideforce etc). Such concepts need an extensive aerodynamic data base so that the best choice of motivators can be made. It is helpful in this context to consider the closed-loop and open-loop (*ie* pilot action required to activate the system) aspects of control systems separately. The latter require large forces and moments, while the former require fast actuation rates, and these requirements may not be compatible for some types of motivators.

Two of the systems listed in Fig 68 emphasise the open-loop aspect, *viz* manoeuvre demand and decoupled response, and it can be expected that conventional flap-type control surfaces (including canards) will provide most of the direct forces and moments. However, the indirect effects generated by such control surfaces have also to be considered in the design of the control laws. Examples, such as aileron yaw and the incremental lift or sideforce obtained by trimming the moments induced by canards, have been described earlier in sections 2 and 3, to illustrate the importance of knowing all the aerodynamic characteristics of motivators. The designer has then to devise the simplest control laws compatible with performance requirements throughout the flight envelope, for the ranges of height, Mach number and normal acceleration.

The choice of motivators from the closed-loop aspect is not so obvious. The actuation rates required for stability augmentation systems are comparable to those needed for the open-loop aspects of the systems, but slightly higher rates may be necessary for the development of departure and spin prevention systems, and for relaxed stability systems. Until now, the motivators used for these three systems are those commanded by the pilot, with no extra surfaces added solely for the closed-loop system, but it may be advantageous to consider this possibility for aircraft designs which are intended to be control-configured from their inception. Gust, load and flutter alleviation systems require high actuation rates, and some modifications to existing motivators have had to be made in the experimental aircraft demonstrating such systems. It is here that there is probably the most need for new developments and novel ideas.

The concepts of adaptive and insensitive control systems can be used for both closed- and open-loop systems, and are in early stages of development. At first sight, it seems that the design process does not depend so much on a detailed knowledge of the aerodynamic characteristics, but knowledge at the same level is probably still needed for new aircraft designs. Decisions have to be made as to the types and numbers of motivators, particularly considering the matching of maximum control power required and that available, *ie* the designer still needs to know the response characteristics which have to be controlled at the extremes of the flight envelope, and the capability of the motivators, in order to be able to achieve a safe system.

This discussion of the integration of the motivators in the active control system would not be complete without mention of other aspects which are basic to aircraft design, particularly performance and safety. Some of the advantages of using active controls to achieve optimum manoeuvring performance have been described in section 2.4, expressed there as maximum usable lift with minimum drag. These performance advantages can be expressed alternatively in terms of maximum turn rate, specific excess energy or sustained normal acceleration. The motivators currently being used are leading-edge and trailing-edge flaps, with the additional variable of wing sweep on the F-14, and these are scheduled with angle of attack and Mach number. Such motivators are likely to continue to be used in future applications (with possible addition of canards), in conjunction with relaxed-stability systems for enhanced improvements. Other performance requirements, such as take-off and landing, also influence the choice of motivators. For example, tail size is likely to be determined by considerations of nose-wheel-lift, and rudder size by cross-wind landing requirements, and these sizes cannot be reduced by incorporating additional active control systems. Thus the complete aircraft layout has to be considered, and the critical requirements determined for such a layout, before the motivators can be chosen.

2-22
From the safety viewpoint, the need to know maximum demanded and available control powers has been emphasised already, particularly for aircraft with relaxed-stability and/or departure and spin-prevention systems. Saturation of the actuator system is another potential hazard (section 4), for which hinge-moment data is critical. A different class of safety problem is that associated with structural integrity, and the extent to which gust, load and flutter alleviation systems can be utilized has yet to be defined. The discussion of failure states is beyond the scope of this paper, but they appear to have important repercussions on the possible advantages to be gained by incorporating such systems.

7 CONCLUDING REMARKS

Because of the implications of other factors such as drag, stores installation etc, the shapes of future aircraft are likely to be such that the data available and reviewed is not likely to be immediately applicable. Therefore the task of estimating the control characteristics of any new design is likely to prove difficult, unless tunnel tests on similar configurations have already been made. It is usually possible to estimate the control derivatives for attached flow conditions with reasonable confidence. However, due to the effects of flow separation, the maximum control powers, which are often crucial for the design of the active control systems, have to be determined experimentally. The results from wind-tunnel tests demonstrate the highly nonlinear behaviour of the control characteristics at high angles of attack, usually resulting in significant losses in direct effectiveness, and increased indirect (and undesirable) effects. Interference between surface is also significant, especially for the closely-coupled configuration typical of those for combat aircraft. Some of the results are unexpected, and as such, need further experimental investigation in order to understand them, let alone develop empirical or theoretical methods of estimation. Notwithstanding such unexplained phenomena, there is still a need to check, and if necessary extend, the estimation methods of DATCOM¹ and ESDU², by correlation of the recently published experimental data for current configurations. The gaps in knowledge have been discussed in sections 5 and 6 but it is not clear how these can be filled at reasonable cost and effort. However, it is clear that more experiments will be required, which cover a wide range and large number of variables, in order to provide answers to future questions. At present, the research on active control technology is mainly directed towards adapting existing aerodynamic technology (on the motivator side), related to limited use of active controls, to the needs of more advanced control systems. In future, the more intensive use of active controls could imply a need for aerodynamic improvement. We are now approaching the stage when the main question will be "What motivators can be designed to achieve the total demand of the active control systems?", that is, the motivators become the central feature of the aircraft design, by the aid of which performance, weight, handling qualities and aircraft safety are optimised. The work already done has shown that close cooperation between the design teams in aerodynamics, controls, structures and possibly engines is required to achieve a successful aircraft, and the need for such cooperation is likely to increase further. The demand for experimental data on control characteristics will be basic for all active control studies.

REFERENCES

- 1 Stability and Control Handbook of the United States Air Force.
- 2 Aerodynamics Sub-series, Engineering Sciences Data. Engineering Sciences Data Unit, London
- 3 Joy C. Donaldson, Bibliography of Control Characteristics of Aircraft. RAE to be published
- 4 S.M. Dollyhigh, Subsonic and supersonic longitudinal stability and control characteristics of an aft-tail fighter configuration with cambered and uncambered wings and cambered fuselage. NASA TN D-8472, September (1977)
- 5 K. Aoyagi and W.H. Tolhurst, Large-scale wind tunnel tests of a subsonic transport with aft engine nacelles and high tail. NASA TN D-3797, January (1967)
- 6 B.J. Eulrich and E.G. Rynaski, Identification of nonlinear aerodynamic stability and control parameters at high angle of attack. Paper 2 of AGARD CP 172 (1974)
- 7 W.T. Suit and J.L. Williams, Longitudinal aerodynamic parameters of the Kestrel aircraft (XV-6A) extracted from flight data. NASA TN D-7296 (1973)
- 8 R.J. Margason, R.D. Vogler and M.M. Winston, Wind-tunnel investigation at low speeds of a model of the Kestrel (XV-6A) vectored thrust V/STOL airplane. NASA TN D-6826 (1972)
- 9 B.L. ShROUT, Aerodynamic characteristics at Mach numbers from 0.6 to 2.16 of a supersonic cruise fighter configuration with a design Mach number of 1.8. NASA TM X-3559 (1977)
- 10 A. Jean Ross, Determination of aerodynamic derivatives from transient responses in manoeuvring flight. Paper 14 of AGARD CP 172 (1974)
- 11 G.E. Erickson and J.F. Campbell, Improvement of maneuver aerodynamics by spanwise blowing. NASA TP 1065 (1977)
- 12 R.B. Eberle, R.T. Stancil and W.C. Fowler, A critical review of canard relative to aft horizontal tail based on low- and high-speed tunnel tests of a fighter/attack configuration. AIAA 71-8 (1971)
- 13 L.P. Yip and J.W. Paulson, Effects of deflected thrust on the longitudinal aerodynamic characteristics of a close-coupled wing-canard configuration. NASA TP 1090 (1977)
- 14 R.J. Re and F.J. Capone, An investigation of a close-coupled canard as a direct side-force generator on a fighter model at Mach numbers from 0.4 to 0.9. NASA TN D-8510 (1977)

- 15 S.C. Stumpfl and R.A. Whitmoyer, Horizontal canards for two-axis CCV fighter control. Paper 6 of AGARD CP 157 (1974)
- 16 R.A. Whitmoyer, Aerodynamic interactions on the fighter CCV test aircraft. Paper 16 of AGARD CP 235 (1978)
- 17 D.H. Bennett, F4/CCV - Flight tests of advanced technology. SAE 740861 (1974)
- 18 E.J. Ray and E.G. Hollingsworth, Subsonic characteristics of a twin-jet swept-wing fighter model with maneuvering devices. NASA TN D-6921 (1973)
- 19 Ph. Poisson-Quinton, Slender wings for civil and military aircraft. Israel Annual Conference on Aviation and Astronautics (1978)
- 20 J. Kloos and L. Elmeland, Static aeroelastic effects on the aerodynamics of the SAAB 37 Viggen aircraft, a comparison between calculations, windtunnel tests and flight tests. ICAS 74-55 (1974)
- 21 A.D. Hammond, Aerodynamic characteristics of a spoiler-slot-deflector control on a 45° sweptback-wing-fuselage model at high subsonic speeds. NASA TN D-2037 (1963)
- 22 W.P. Gilbert, L.T. Nguyen and R.W. van Gunst, Simulator study of the effectiveness of an automatic control system designed to improve the high-angle-of-attack characteristics of a fighter airplane. NASA TN D-8176 (1976)
- 23 J.P. Lamers, Design for departure prevention in the YF-16. AIAA 74-794 (1974)
- 24 L.P. Parlett, H.D. Greer and R.L. Henderson, Wind-tunnel investigation of an external-flow jet-flap transport configuration having full-span triple-slotted flaps. NASA TN D-6391 (1971)
- 25 H. August, B-1 airplane model support and jet plume effects on aerodynamic characteristics. AIAA 73-153 (1973)
- 26 K. Iliffe, Estimation of aerodynamic characteristics from dynamic flight test data. Paper 15 of AGARD CP 235 (1978)
- 27 R.F. Osborn, Investigation of a double slotted rudder for application on advanced tactical support aircraft. AFFDL-TR-75-94 (1975)
- 28 Manoeuvre limitations of combat aircraft. AGARD AR to be published
- 29 J.W. Stickle and R.C. Henry, Wind-tunnel study to explore the use of slot spoilers to modulate the flap-induced lift of a wing. NASA TN D-4664 (1968)
- 30 S.F.J. Butler, Low-speed wind-tunnel tests on a sweptback wing model (Buccaneer Mark 1) with blowing at the wing leading edge and over the flaps and drooped ailerons. ARC R & M 3655 (1967)
- 31 D.J. Giulianetto and R.L. Maki, Low speed aerodynamic characteristics of a large-scale model with a thin, highly swept, 2.67 aspect ratio wing having a cranked leading edge. NASA TN D-6919 (1972)
- 32 P. Fournier, Low-speed aerodynamic characteristics of a transport model having 42.33° swept low wing with supercritical airfoil, double-slotted flaps, and T-tail or low tail. NASA TM X-3276 (1975)
- 33 R.F. Stewart and R.E. Whitehead, Analysis of advanced variable camber concepts. Paper 14 of AGARD CP 241 (1977)
- 34 The effects of buffeting and other transonic phenomena on maneuvering combat aircraft. AGARD AR 82 (1975)
- 35 E.J. Ray, L.W. McKinney and J.G. Carmichael, Maneuver and buffet characteristics of fighter aircraft. Paper 24 of AGARD CP 102 (1972)
- 36 W.R. Burns and J.T. Lawrence, Aerodynamic design and flight test of US Navy aircraft at high angles of attack. Paper 25 of AGARD CP 102 (1972)
- 37 C.L. Bore, Post/stall aerodynamics of the Harrier GR1. Paper 19 of AGARD CP 102 (1972)
- 38 J.K. Buckner, P.W. Hill and D. Benepe, Aerodynamic design evolution of the YF-16. AIAA 74-935 (1974)
- 39 J.P. Lamers, YF-16 high angle of attack flight test experience. Paper 25 of AGARD CP 199 (1975)
- 40 E.F. Carlson, Direct sideforce control for improved weapon delivery accuracy. AIAA 74-70 (1974)
- 41 H. Wunnenberg and W.J. Kubbat, Advanced control concepts for future fighter aircraft. Paper 8 of AGARD CP 241 (1977)
- 42 P.W. Kirsten, A comparison and evaluation of two methods of extracting stability derivatives from flight data. Paper 18 of AGARD CP 172 (1974)
- 43 J.N. Ball, Rolling tail design and behaviour as affected by actuator hinge moment limits. AIAA 78-1500 (1978)

2-24

- 44 J.M. Hallissy and R.J. Ward, Transonic wind tunnel investigation of pressures and hinge moments on sweptback T-mounted horizontal aircraft tail. NASA TM X-61 (1959)
- 45 O.P. Nicholas, R. Rose and G. Vorley, Flight measurements of the elevator and aileron hinge-moment derivatives of the Fairey Delta 2 aircraft up to a Mach number of 1.6 and comparisons with wind-tunnel results. RAE TR 65143 (1965), (ARC R & M 3485)
- 46 V.M. de Argelis, E.L. Friend, J.M. Jenkins and R.C. Monaghan, Flight measurements of canard loads, canard buffeting and elevon and wing tip hinge moments on the XB-70 aircraft including comparisons with predictions. NASA TN D-5359 (1969)
- 47 B. Perry, Control surface hinge moment calculations for a high aspect ratio supercritical wing. NASA TM 78664 (1978)
- 48 W.C. Moseley and R.F. Thompson, Effect of control trailing edge thickness on aspect ratio on the oscillating hinge-moment and flutter characteristics of a flap type control at transonic speeds. NACA RM L58B25 (1958)
- 49 F.W. Gibson, R.W. Herr and R.S. Osborne, Some effects of flow spoilers and of aerodynamic balance on the oscillating hinge moments for a swept fin-rudder combination in a transonic wind tunnel. NACA RM L58C28 (1958)
- 50 T.G. Gainer and W.C. Moseley Jr., Some effects of control profile and control trailing-edge angle on the oscillating hinge-moment and flutter characteristics of flap-type controls at transonic speeds. NASA TM X-170 (1960)
- 51 D.R. Gaukroger, D.A. Drane and R. Gray, A technique for measuring oscillatory aerodynamic control surface hinge moments from forced response characteristics. RAE TR 71211 (1971), (ARC CP 1253)
- 52 D. Mabey, D.M. McOwat and B.L. Welsh, Aerodynamic characteristics of moving trailing edge controls at subsonic and transonic speeds. Paper 20 of AGARD Symposium "Aerodynamic Characteristics of Controls" May (1979)
- 53 P.B.E. Engler and G.F. Moss, Low-speed wind tunnel tests on a $\frac{1}{4}$ th scale model of the Handley-Page HP 115. RAE TR 65180 (1965), (ARC R & M 3486)
- 54 H.H.B.M. Thomas and G.F. Edwards, Mathematical models of aircraft dynamics for extreme flight conditions (theory and experiment). Paper 27 of AGARD CP 235 (1978)

Copyright ©, Controller HMSO, London 1979

Table 1

NOTATION USED FOR MOTIVATOR DEFLECTIONS

(a) Symbols for motivators generating mainly:-

Pitching moment	η
Rolling moment	ξ
Yawing moment	ζ
Lift	δ

(c) Equivalence to other notations

This report	American	Other
-------------	----------	-------

(b) Suffices for motivator type:-

Aileron	A
Canard	C
Horizontal canard	HC
Vertical canard	VC
Elevator	e
Elevon	E
Flap	F
Leading edge flap	LEF
Trailing edge flap	TEF
Nozzle flap	N
Rudder	R
Spoiler	S
Tail	T

η_e	δ_e	
η_E	δ_E	
η_T	δ_e	i_T
ξ_A	δ_a	
ξ_S	δ_{sp}	
ξ_T	δ_D	η_D
ζ_R	δ_r	
ζ_{VC}	δ_{VC}	
δ_C	δ_C	i_C

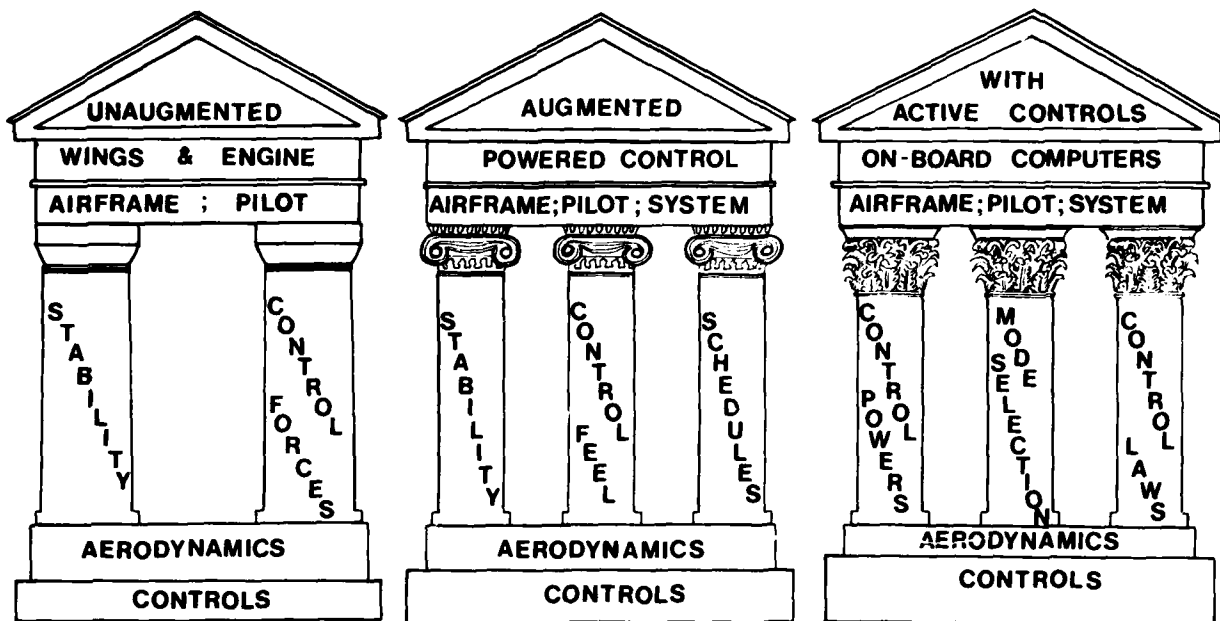


Fig 1 Dependence of aircraft design on aerodynamic and control data

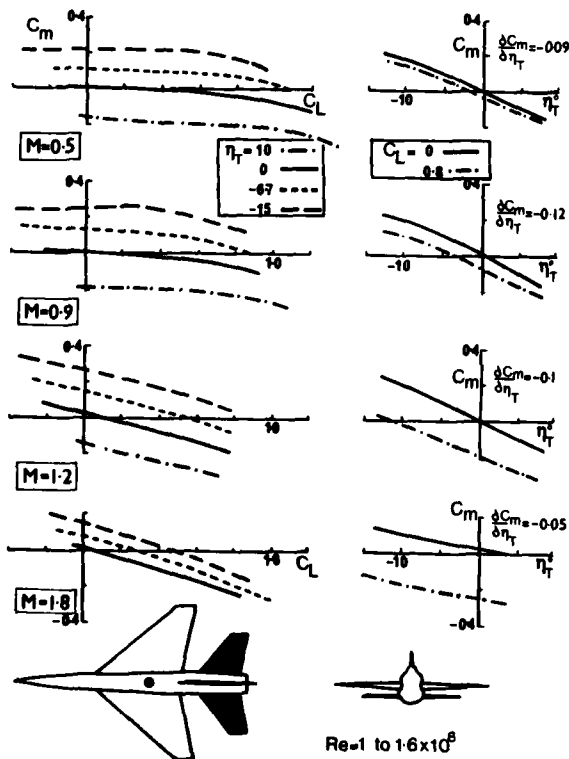


Fig 2 Effect of Mach number on pitching moment due to tailplane deflection and angle of attack; subsonic fighter concept

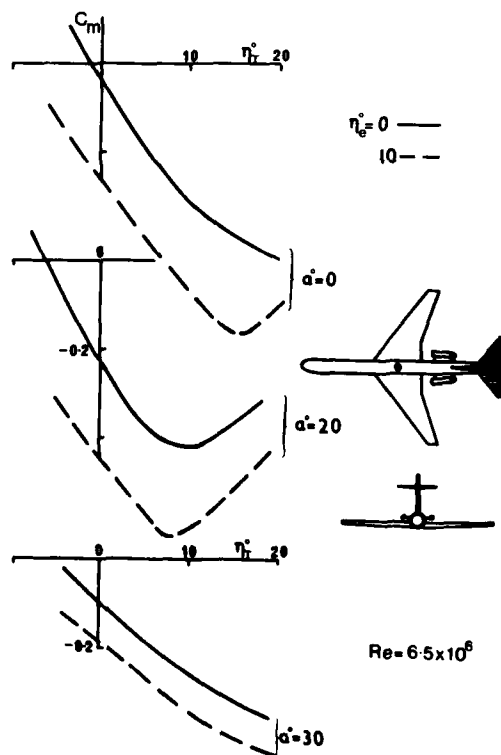


Fig 3 Effect of angle of attack on pitching moment due to tailplane deflection and elevator setting; high-tailed transport concept

2-26

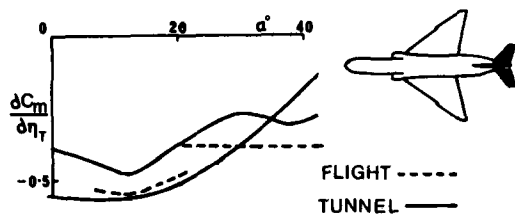


Fig 4 Variation of pitching moment derivative due to tailplane with angle of attack; F-4E

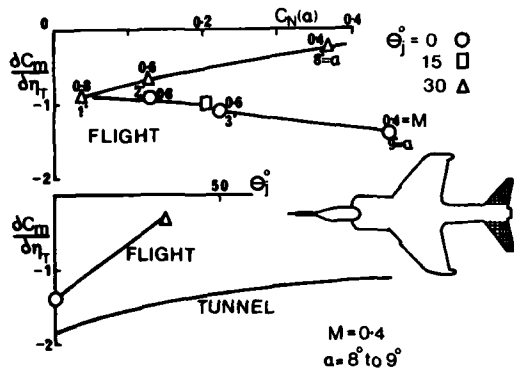


Fig 5 Variation of pitching moment derivative due to tailplane with normal force coefficient and with thrust deflection; Kestrel

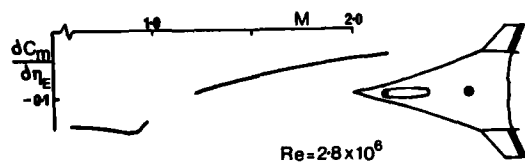


Fig 6 Variation of pitching moment derivative due to elevons with Mach number; supersonic fighter concept

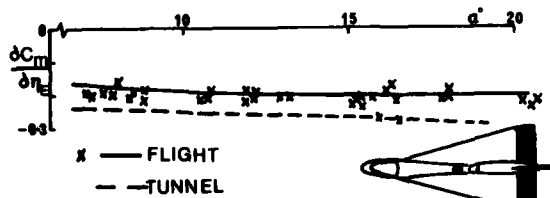


Fig 7 Variation of pitching moment derivative due to elevons with angle of attack; HP 115

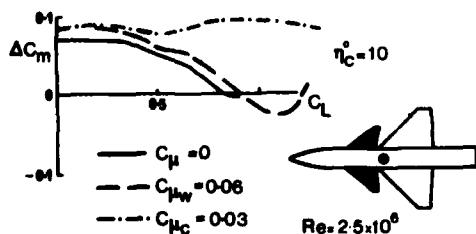


Fig 8 Effect of spanwise blowing on incremental pitching moment due to canard deflection and angle of attack; research canard model

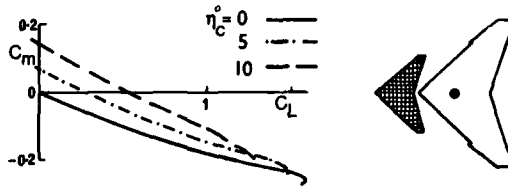


Fig 9 Pitching moment due to deflected canard and angle of attack; swept-wing canard configuration

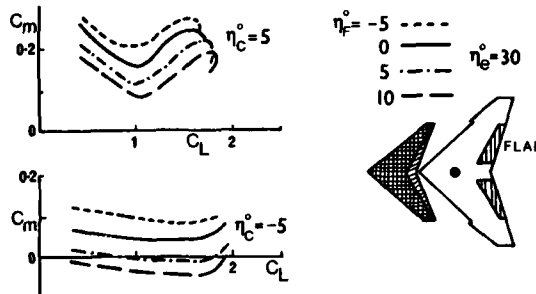


Fig 10 Effect of canard setting on pitching moment due to trailing edge flap and angle of attack; swept-wing canard configuration

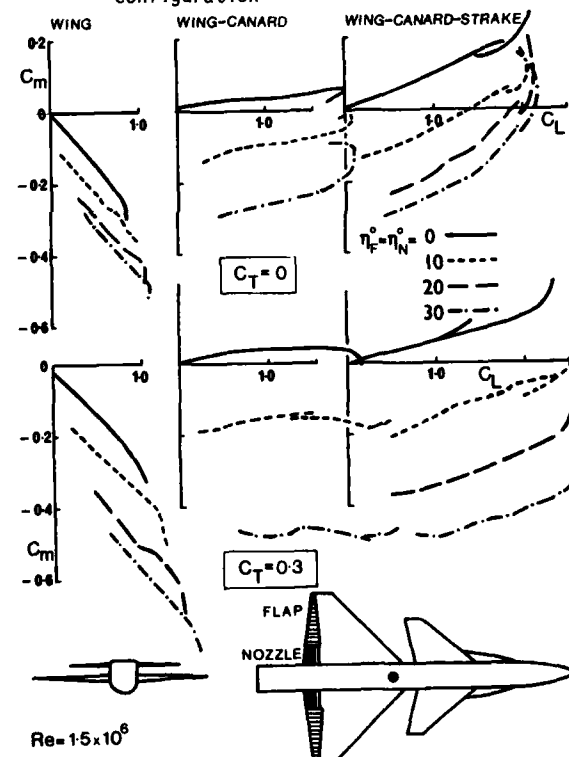


Fig 11 Effect of thrust on pitching moment due to trailing edge and nozzle flaps, and angle of attack; wing-canard-strake configurations

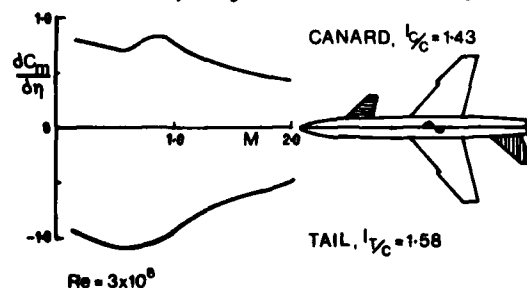


Fig 12 Variation of pitching moment derivative due to canard or tailplane with Mach number; research configuration

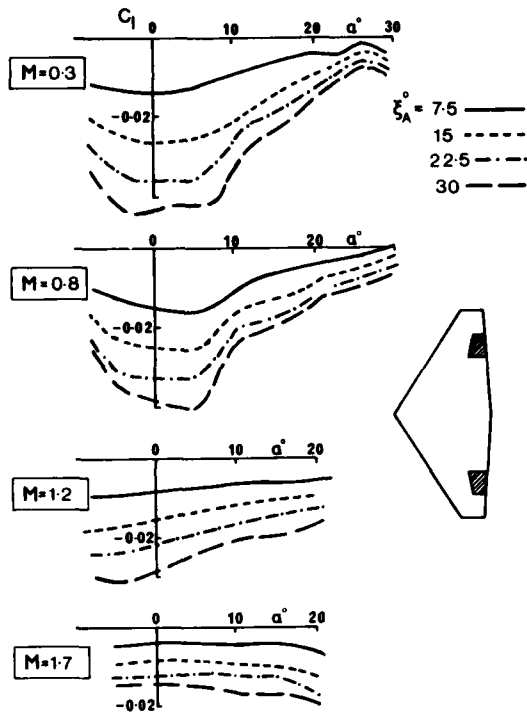


Fig 13 Effect of Mach number on rolling moment due to midspan ailerons at angle of attack; combat aircraft

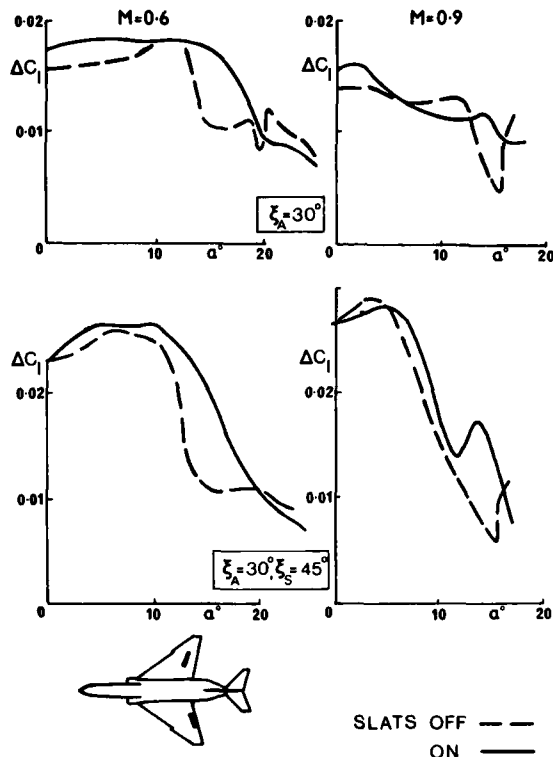


Fig 14 Effect of leading edge slats on the rolling moment due to aileron and spoiler at angle of attack; F-4

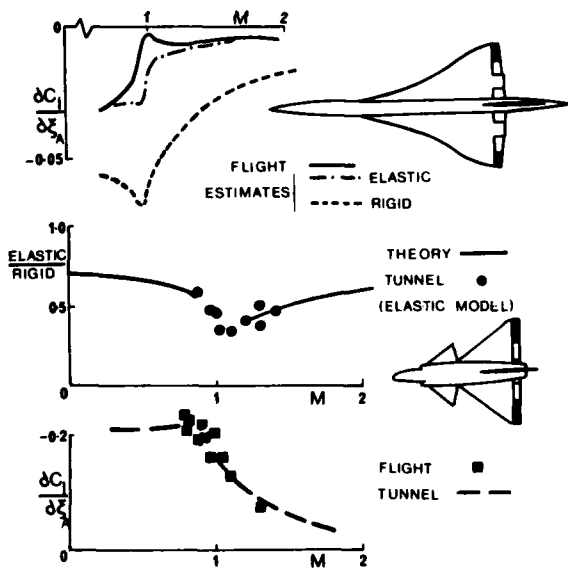


Fig 15 Effect of aeroelasticity on variation of rolling moment derivative due to aileron with Mach number (a) Concorde (b) Viggen

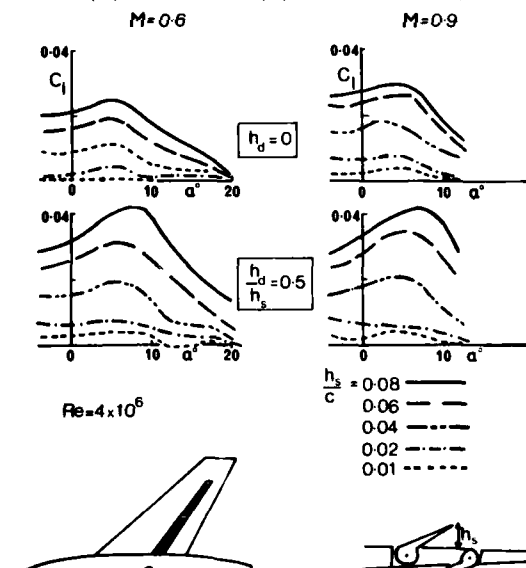


Fig 16 Effect of Mach number on rolling moment due to spoiler and spoiler-slat-deflector at angle of attack; research wing (a) spoiler (b) spoiler-slat-deflector

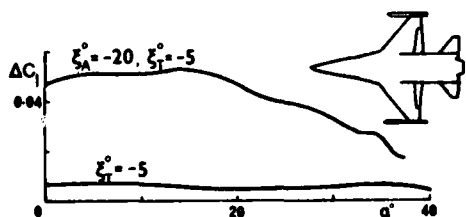


Fig 17 Variation of rolling moment due to aileron and differential tail with angle of attack; YF-16

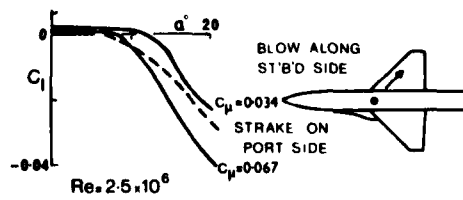


Fig 18 Variation of rolling moment due to differential strake projection or differential spanwise blowing with angle of attack; research canard model

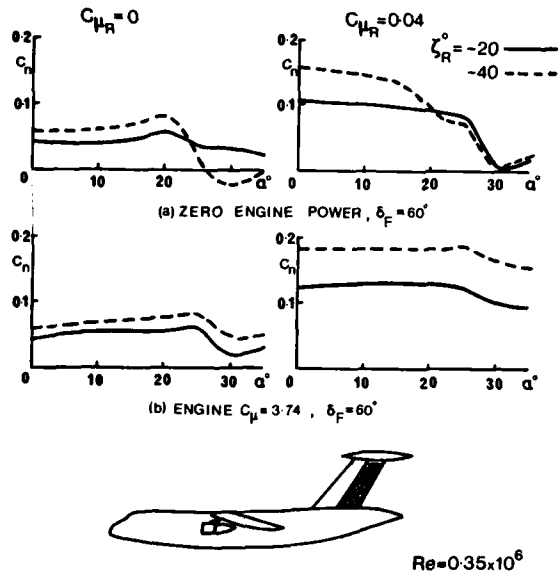


Fig 19 Effects of jet momentum coefficients on yawing moment due to jet-flap rudder at angle of attack; jet flap transport concept

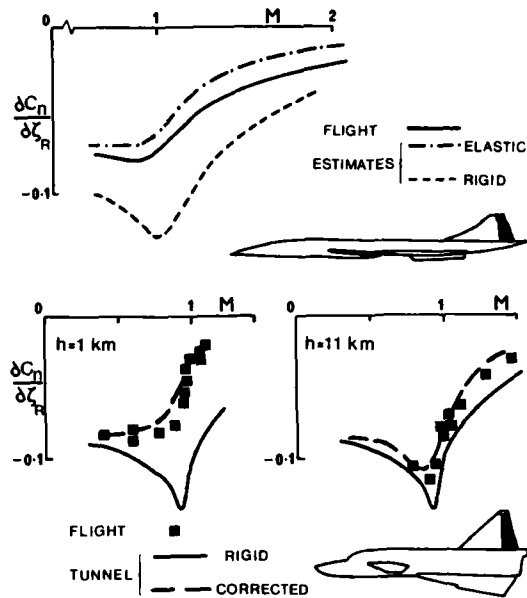


Fig 22 Effect of aeroelasticity on variation of yawing moment derivative due to rudder with Mach number
(a) Concorde
(b) Viggen

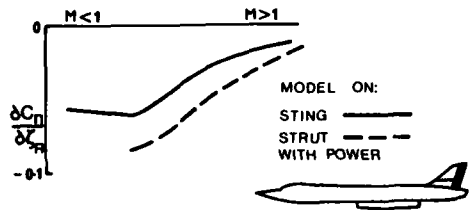


Fig 20 Interference effects on variation of yawing moment derivative due to rudder with Mach number, tunnel tests; B-1

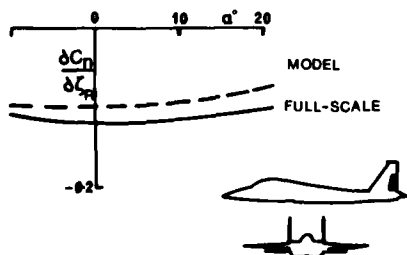


Fig 21 Scale effects on variation of yawing moment derivative due to rudder with angle of attack, flight tests; F-15

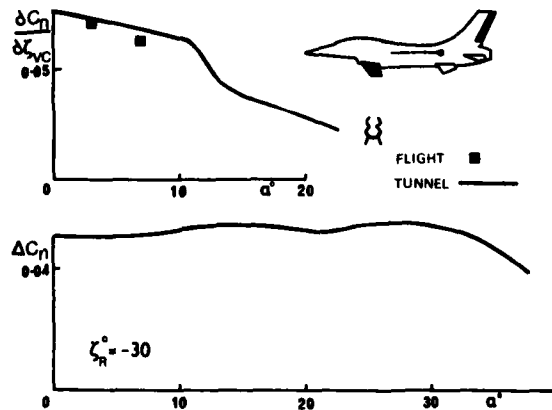


Fig 23 Variation of yawing moment derivative due to vertical canard and incremental yawing moment due to rudder with angle of attack; CCV YF-16

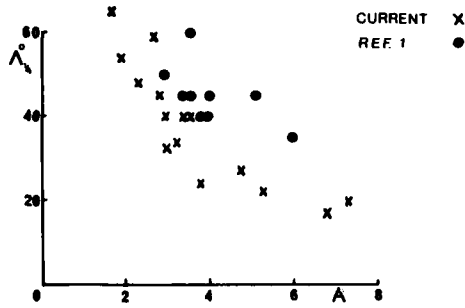


Fig 24 Sweepback and aspect ratio of current aircraft and configurations used in Ref 1, section 6.1.4.3

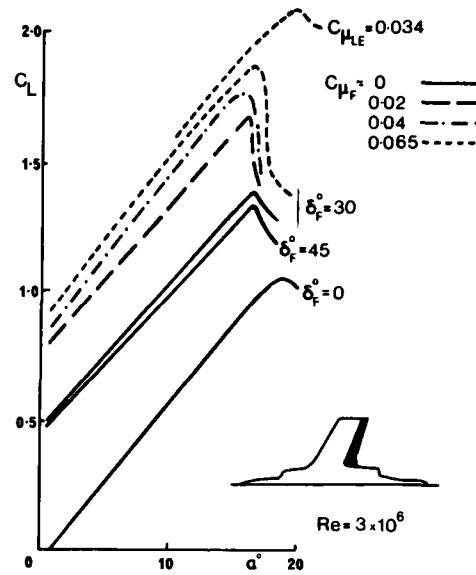


Fig 26 Effects of blowing on the lift due to trailing edge flap and angle of attack; Buccaneer

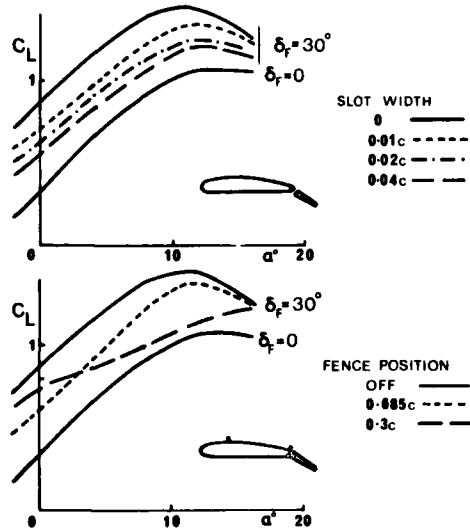


Fig 25 Effects of slot width and fence position on lift due to trailing edge flap and angle of attack; 9% aerofoil

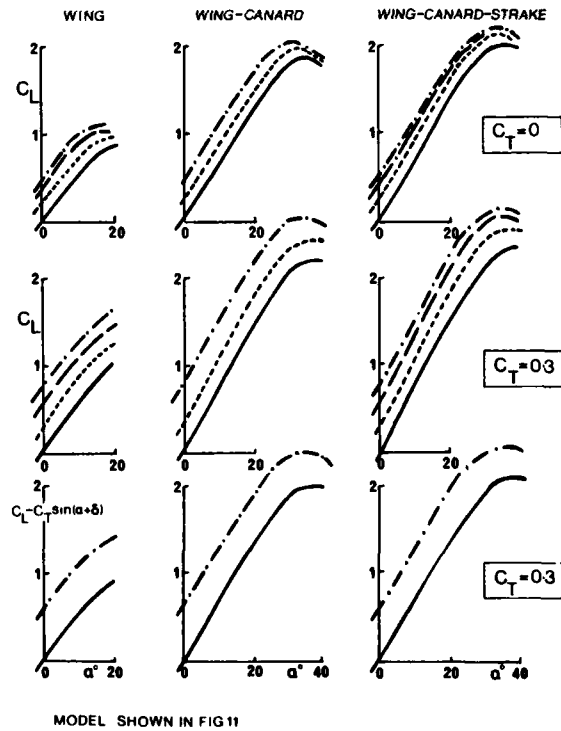


Fig 27 Effect of thrust coefficient on lift due to trailing edge and nozzle flaps, and angle of attack; wing-canard-strake configurations

2-30

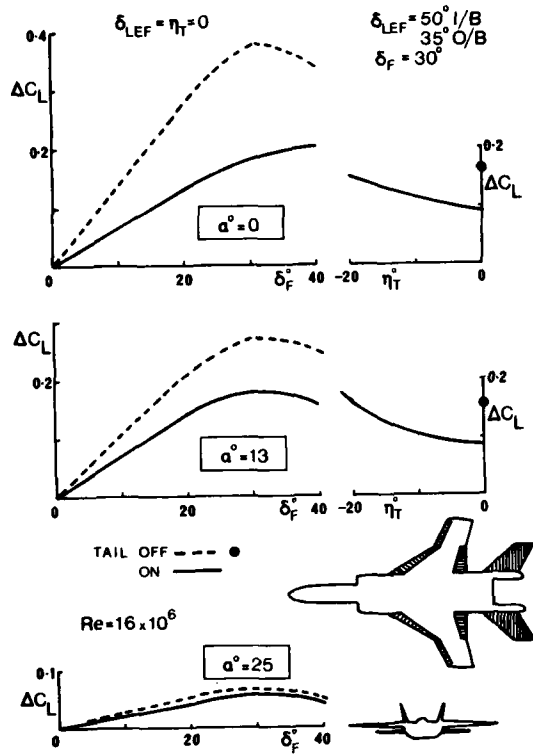


Fig 28 Effect of angle of attack and tail setting on the variation of incremental lift due to flap deflection and high lift system; fighter concept

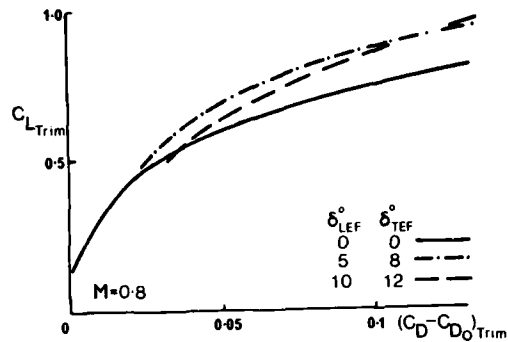


Fig 30 Lift v drag envelope for F-18 flap schedule

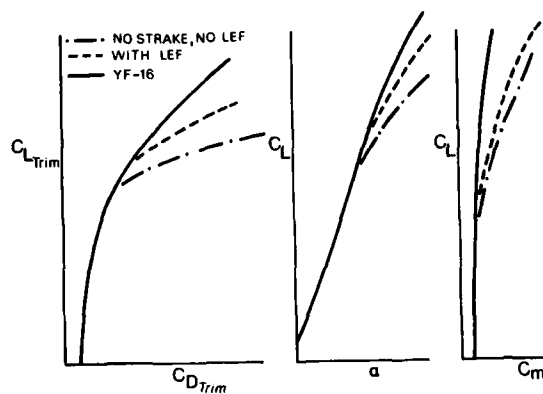


Fig 31 Effects of strake and leading edge flap on trim; YF-16

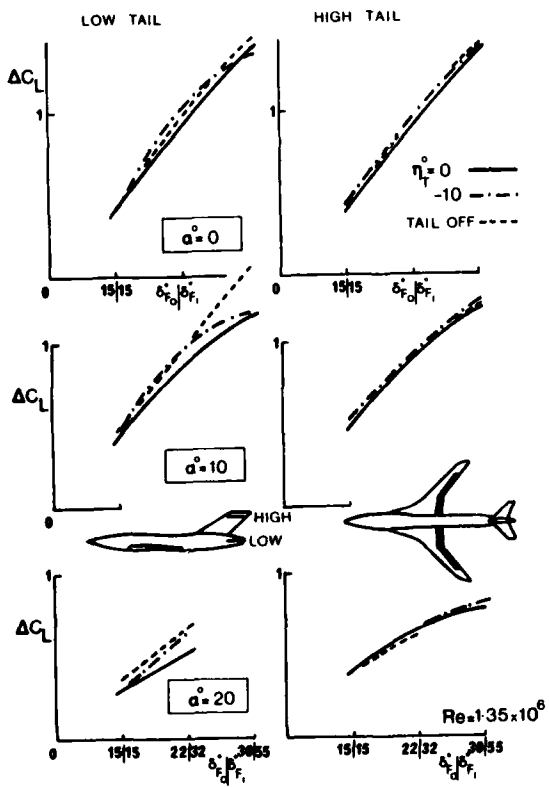


Fig 29 Effect of angle of attack and tail position on incremental lift due to trailing edge flaps; supercritical

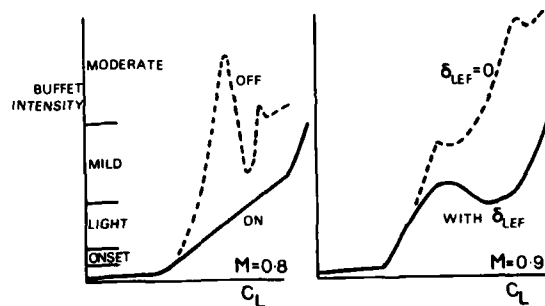


Fig 32 Effects of strake and leading edge flap on buffet; YF-16 (a) effect of strake (b) effect of schedule flap

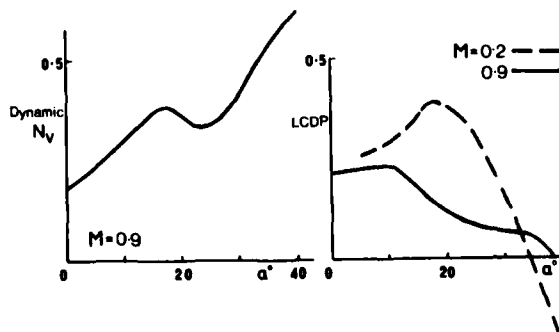


Fig 33 Departure parameters for YF-16

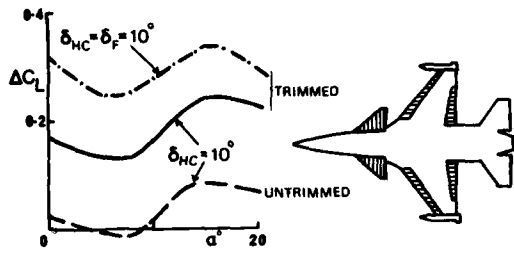


Fig 34 Direct lift due to horizontal canard and trailing edge flap; CCV YF-16 configuration

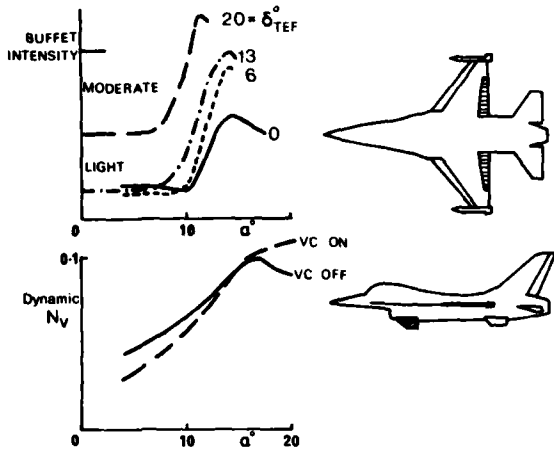


Fig 35 Effects of control systems on handling parameters: CCV YF-16

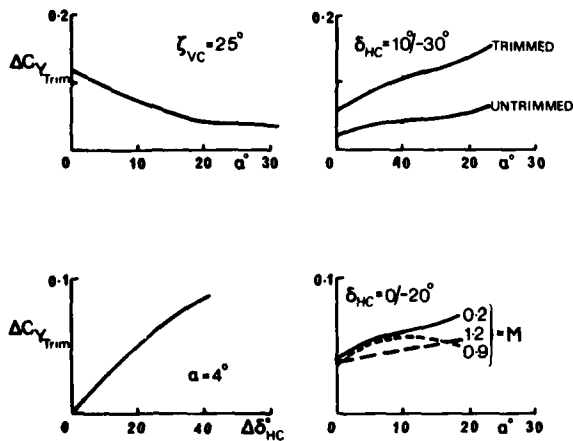


Fig 36 Sideforce due to canards; CCV YF-16
 (a) twin vertical canards
 (b) differential horizontal canards
 (c) variation with deflection of horizontal canards
 (d) variation with Mach number

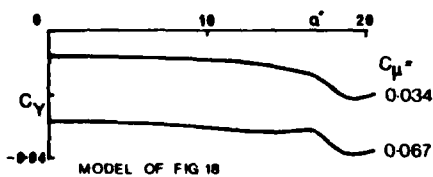


Fig 37 Variation of sideforce due to spanwise blowing with angle of attack; research canard model

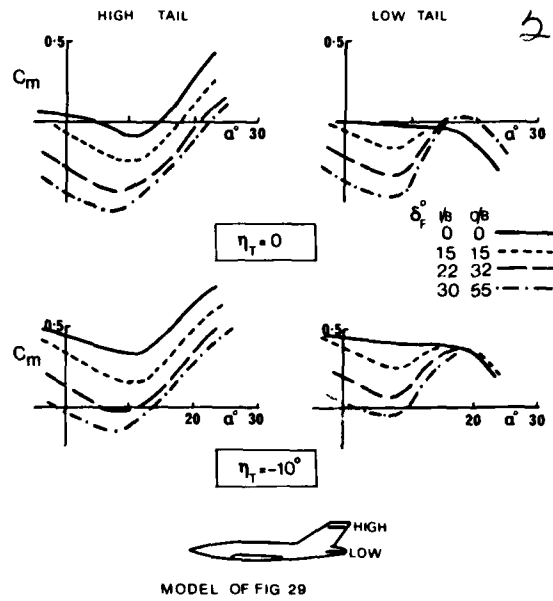


Fig 38 Effect of tailplane position and setting on pitching moment due to trailing edge flap and angle of attack; supercritical wing transport aircraft

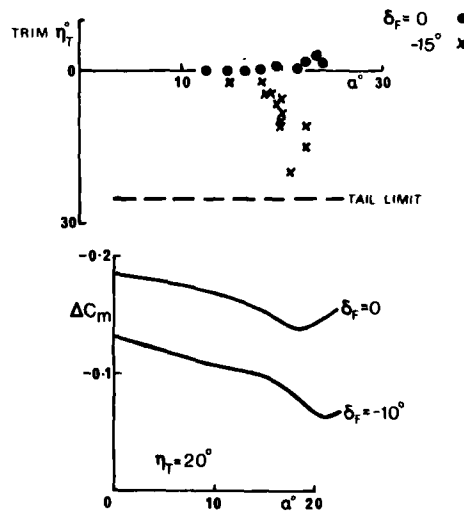


Fig 39 Effect of up-deflection of trailing edge flap on tailplane power; CCV Yf-16
 (a) flight results for tailplane angle to trim
 (b) tunnel results for incremental pitching moment due to tailplane deflection

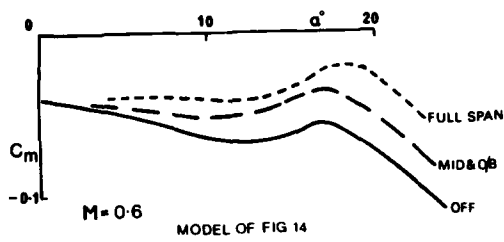


Fig 40 Effect of leading edge slats on pitching moment at angle of attack; F-4

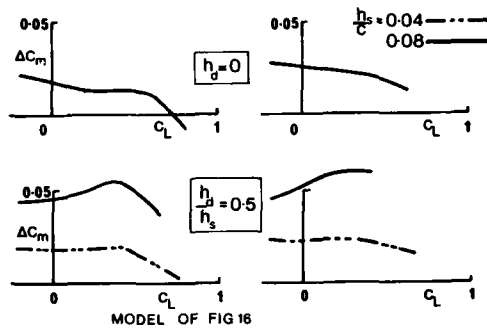


Fig 41 Variation of incremental pitching moment due to spoiler and spoiler-slat-deflector with lift coefficient; research wing
(a) spoiler
(b) spoiler-slat-deflector

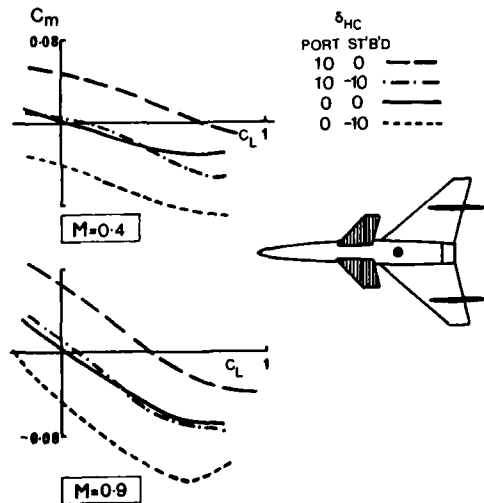


Fig 42 Effect of differential canard deflection on pitching moment due to angle of attack; research canard concept

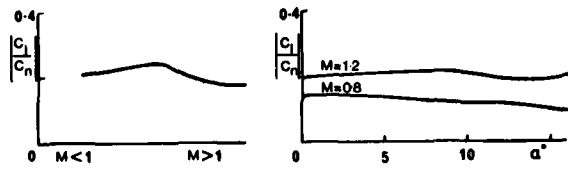


Fig 43 Ratio of rolling moment and yawing moment due to rudder
(a) variation with Mach number, B-1
(b) variation with angle of attack; F-1-11E

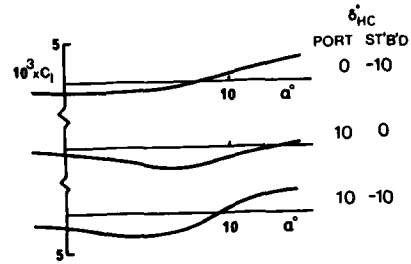


Fig 44 Variation of rolling moment due to differential horizontal canard deflection with angle of attack; research canard concept

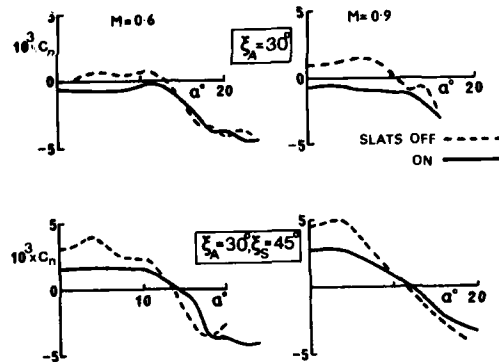


Fig 45 Effects of slats on yawing moment due to aileron and spoiler at angle of attack; F-4
(a) aileron
(b) aileron and spoiler

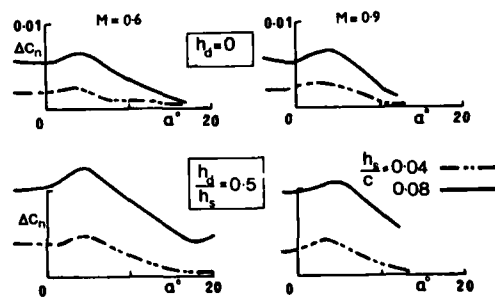


Fig 46 Effect of Mach number on yawing moment due to spoiler and spoiler-slat-deflector at angle of attack
(a) spoiler
(b) spoiler-slat-deflector

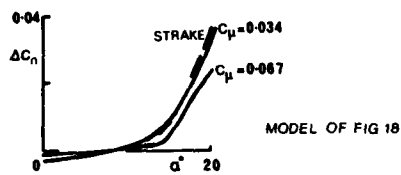


Fig 47 Variation of yawing moment due to differential strake projection or differential spanwise blowing with angle of attack; research canard model

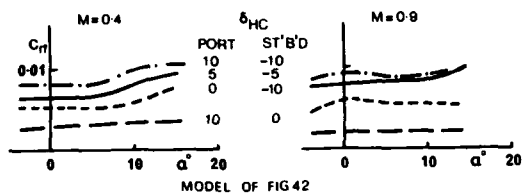


Fig 48 Variation of yawing moment due to differential horizontal canard with angle of attack; research canard concept

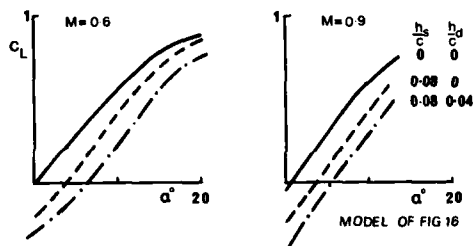


Fig 49 Variation of lift due to spoiler and spoiler-slat-deflector with angle of attack; research wing

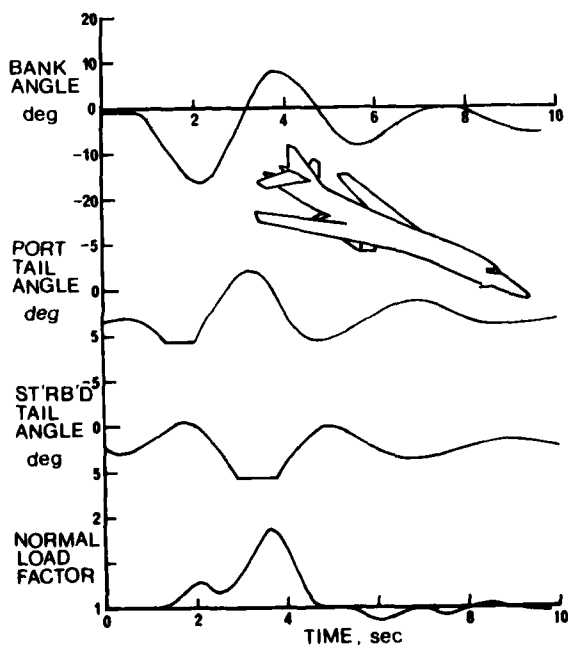


Fig 50 Uncommanded pitch response, during a Dutch-roll motion, following hinge-moment limiting; B-1

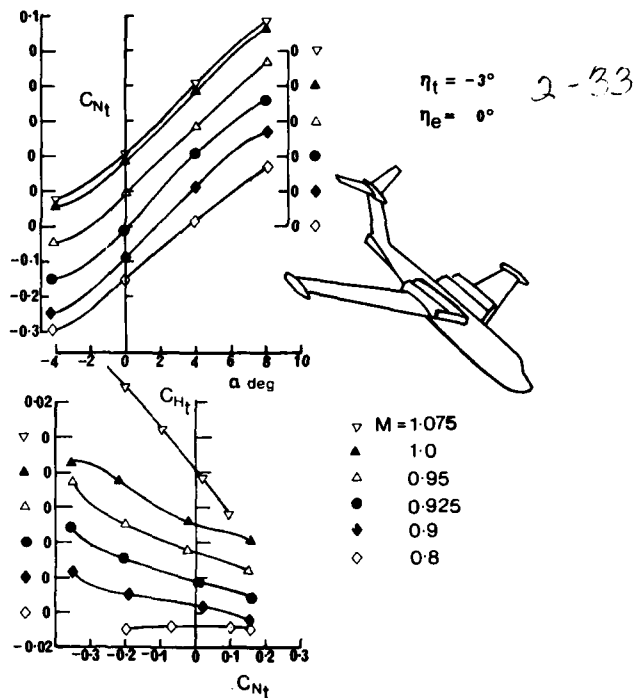


Fig 51 Hinge-moment and normal force coefficient characteristics of an all-moving T-tailplane

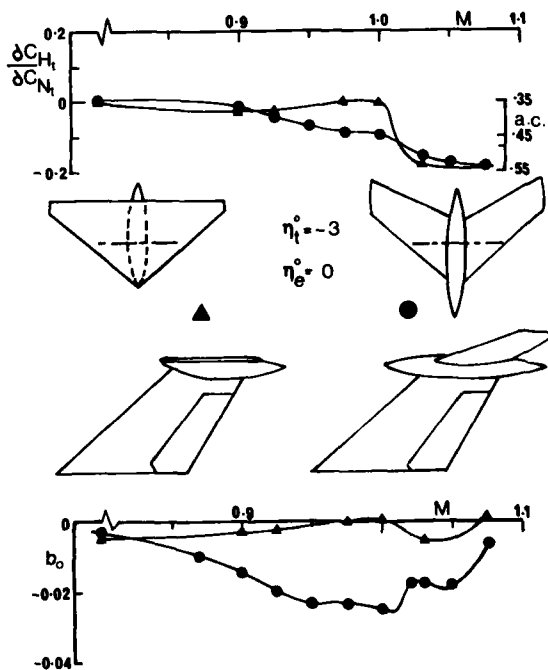


Fig 52 Comparison of hinge-moment characteristics of a sweptback tailplane and a delta tailplane

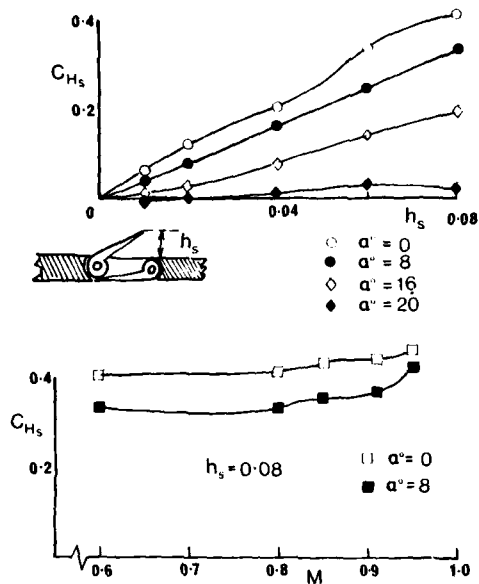


Fig 53 Hinge-moment characteristics of an upper-surface flap spoiler

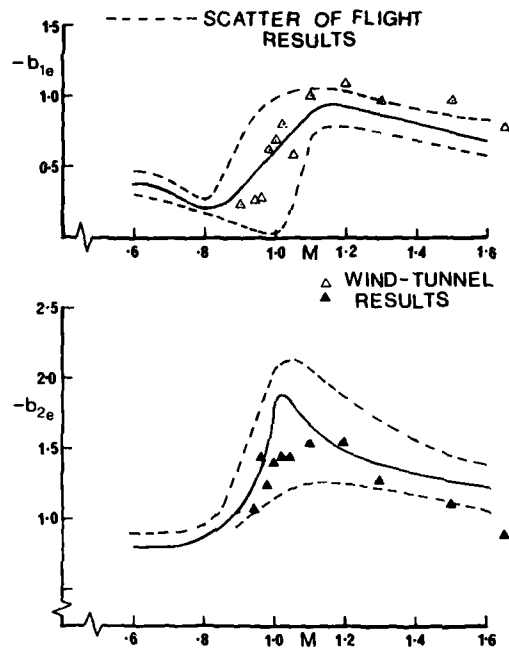


Fig 55 Hinge-moment characteristics of the elevator of the Fairey Delta 2 aircraft (see Fig 57) as measured in flight and in the wind-tunnel

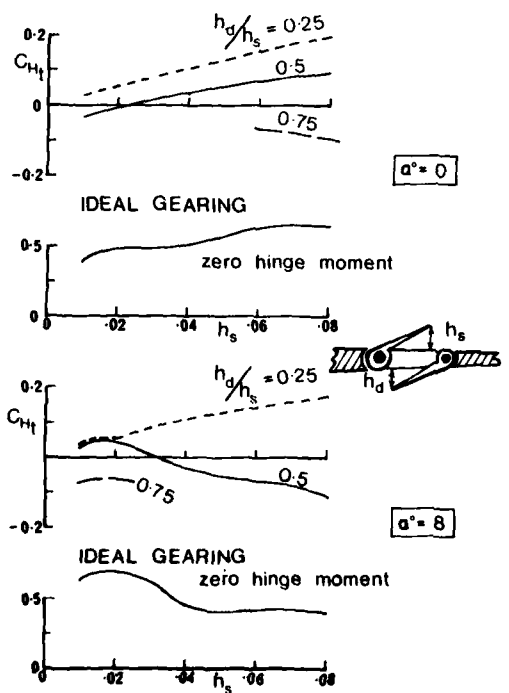


Fig 54 Nett hinge-moment characteristics for geared spoiler and deflector flap arrangements

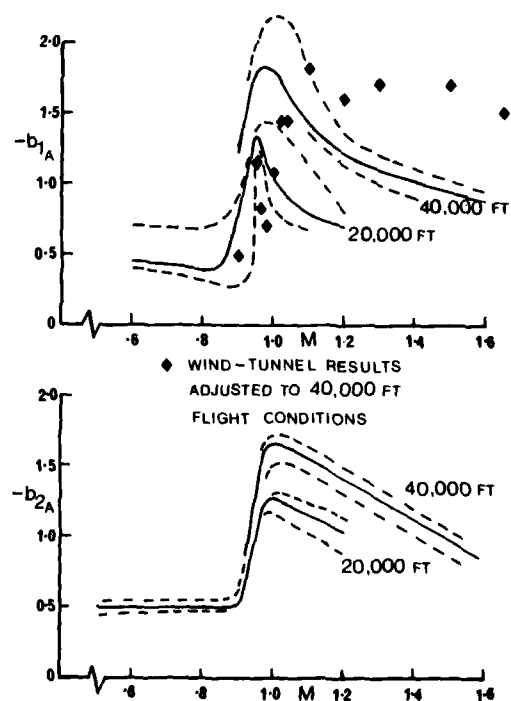


Fig 56 Comparison of flight and wind-tunnel measured hinge-moment characteristics of the ailerons of the Fairey Delta 2 aircraft

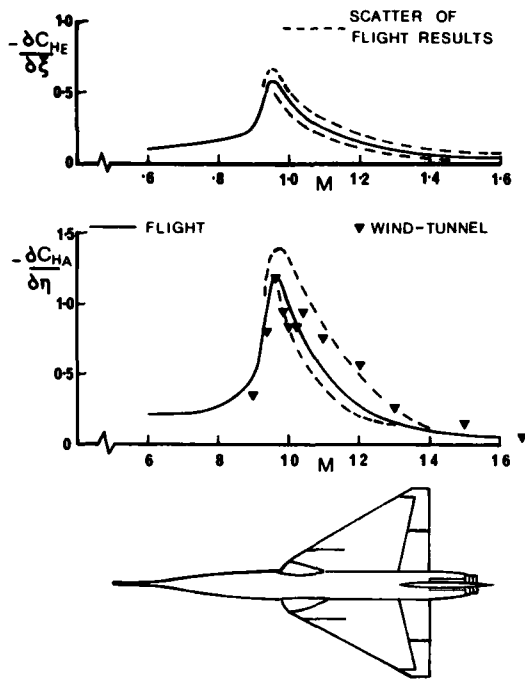


Fig 57 Cross-control hinge-moment characteristics of the elevators and ailerons of the Fairey Delta 2 aircraft

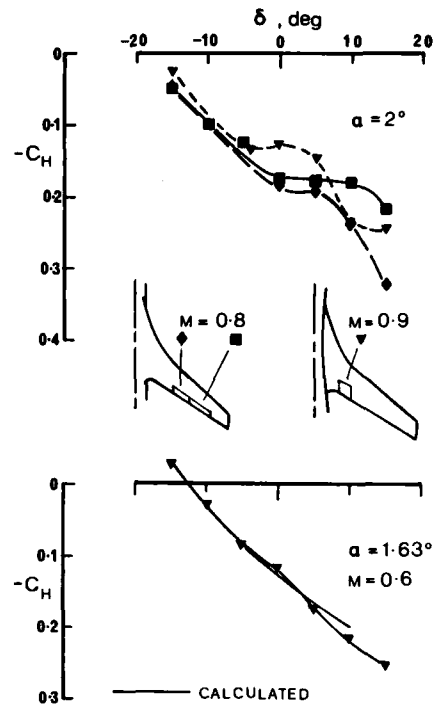


Fig 59 Hinge-moment characteristics of flaps fitted to a high aspect-ratio supercritical wing

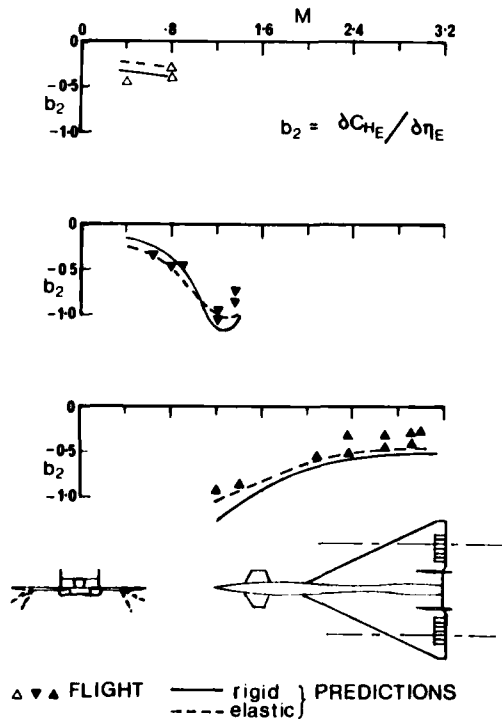


Fig 58 Rate of change of hinge-moment coefficient with elevon deflection, with a comparison of measurements taken in flight with predictions based on wind-tunnel results, with and without aeroelastic corrections; XB-70

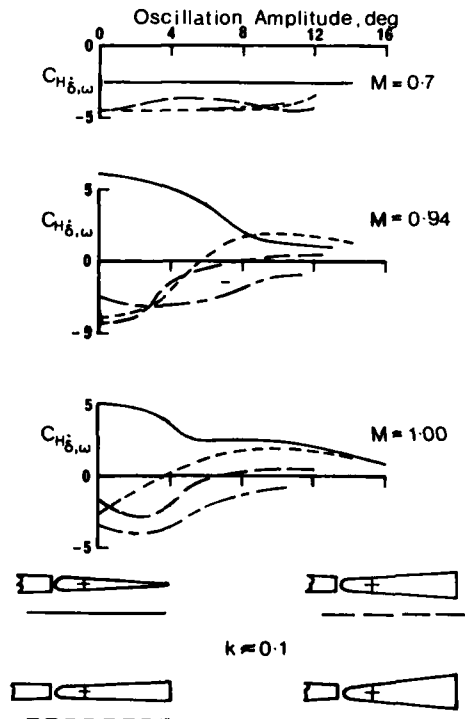


Fig 60 Comparison of the damping derivatives for oscillating control surfaces of wedge-shaped section with those for a control of normal section

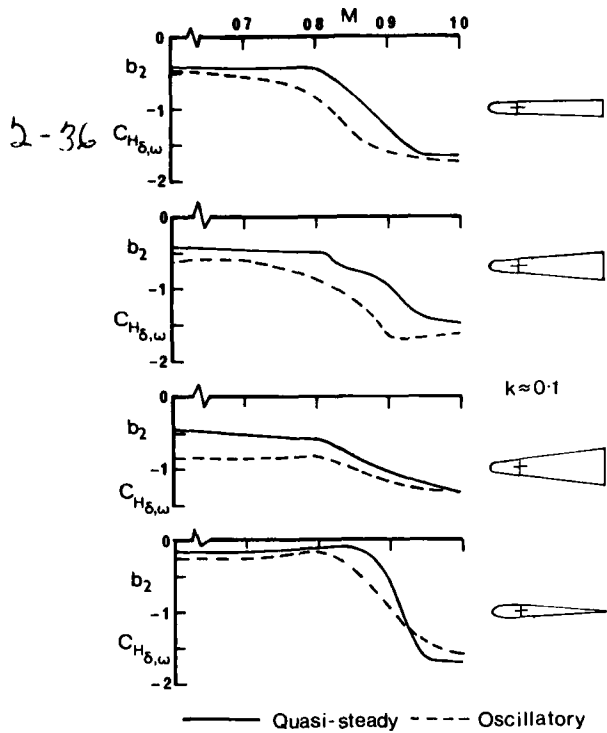


Fig 61 Comparison of the stiffness derivative for oscillating control surfaces of wedge-shaped section with those for a control of normal section

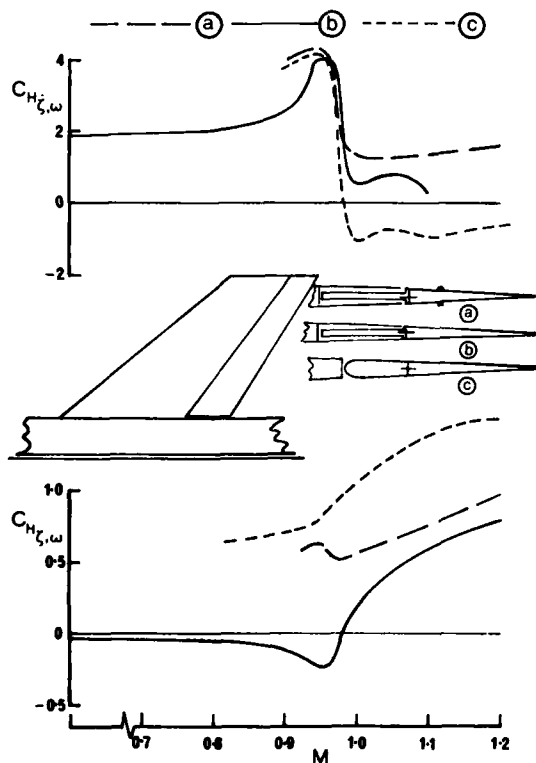


Fig 62 Hinge-moment characteristics of an oscillating rudder control. (Effect of aerodynamic balance and small control surface spoilers)

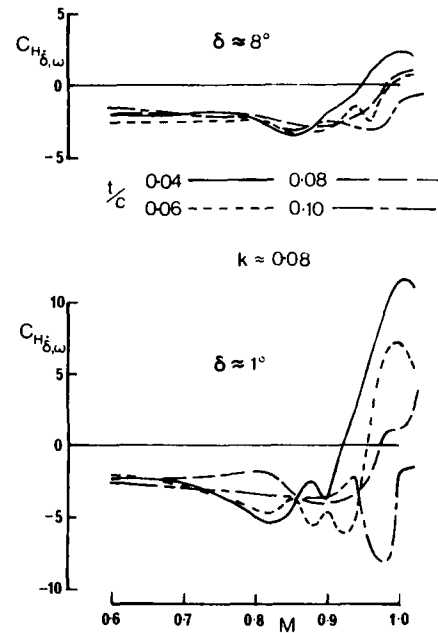


Fig 63 Damping hinge-moment derivatives for flap-type controls on an unswept, rectangular wing (see Fig 65). (Effect of aerofoil thickness-chord ratio and oscillation amplitude)

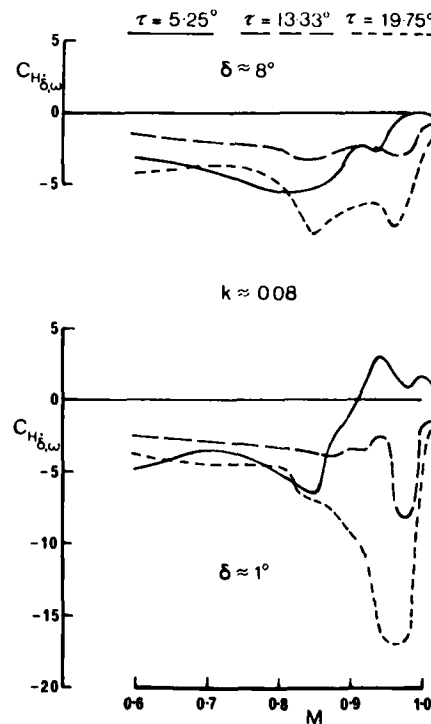
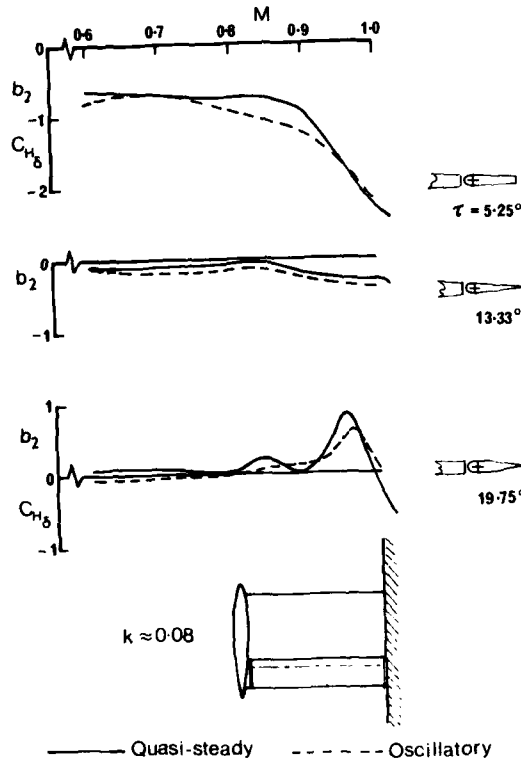


Fig 64 Damping hinge-moment derivatives for flap-type controls on an unswept, rectangular wing (see Fig 65). (Effect of control trailing-edge angle and oscillation amplitude)



2-37

Fig 65 Stiffness hinge-moment derivatives and quasi-steady derivatives for flap-type controls on an unswept, rectangular wing. (Effect of control trailing-edge angle)

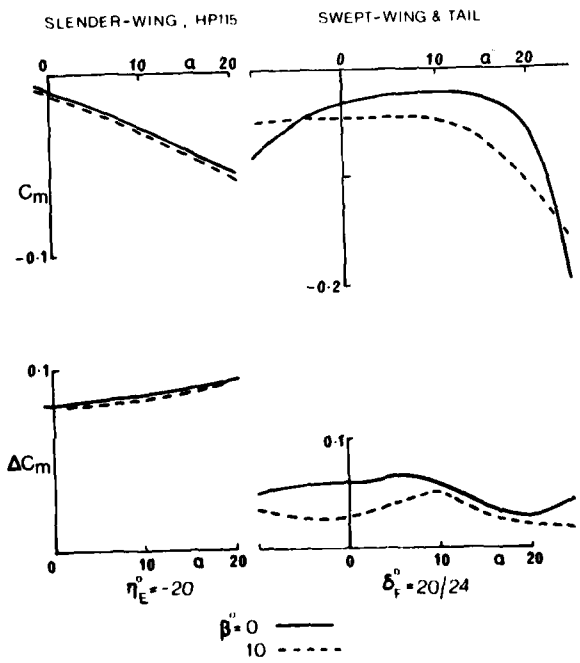


Fig 66 Effect of sideslip on pitching moments
 (a) Pitching moment due to angle of attack, zero control deflections
 (b) Incremental pitching moment due to control deflection, with sideslip

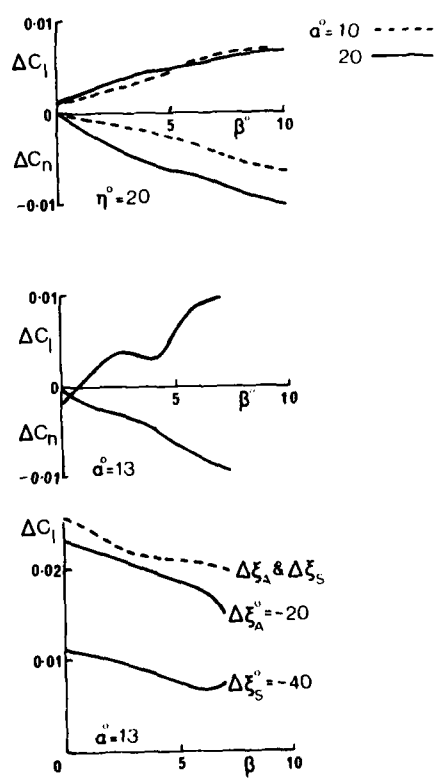


Fig 67 Effect of sideslip on rolling and yawing moments
 (a) Symmetric elevon deflection, HP 115
 (b) Flap deflection, combat configuration (Fig 28)
 (c) Aileron and spoiler deflections, combat configuration (Fig 28)

	ACTUATION FORCE OR MOMENT	CONTROL DERIVATIVES	MAXIMUM POWER
STABILITY AUGMENTATION		▣	
DEPARTURE & SPIN PREVENTION		▣	▣
RELAXED STABILITY			▣
MANOEUVRE ENHANCEMENT		▣	
GUST, LOAD, FLUTTER ALLEVIATION	▣	▣	
MANOEUVRE DEMAND		▣	
DECOUPLED RESPONSE		▣	▣
ADAPTIVE OR INSENSITIVE			▣

Fig 68 Degrees of dependence of various control systems on control characteristics

		RELEVANCE OF DATA TO DESIGN			
		LEVEL	HIGH	MODERATE	LOW
STANDARD OF KNOWLEDGE	GOOD		$C_m(\eta, \alpha) \leftarrow C_L(\eta, \alpha)$ $C_n(\zeta) \leftarrow C_Y(\zeta)$		
	FAIR		$C_l(\xi, \alpha) \leftarrow C_m(\delta, \alpha)$ $C_L(\delta, \alpha) \leftarrow C_n(\xi, \alpha)$ $\leftarrow C_l(\zeta)$	C_H FOR (η, α) (δ, α) $(\xi) \& (\zeta)$	
	POOR		$C_l \& C_n$ FOR $(\delta, \eta \text{ OR } \beta)$ $(\xi, \eta \text{ OR } \delta)$ $(\zeta, \eta \text{ OR } \delta)$	C_D FOR CONTROL DEFLECTIONS	

◀ INFLUENCE OF ACTIVE CONTROL

Fig 69 Status of data on conventional control characteristics

BIBLIOGRAPHY

This Bibliography consists of references selected from the listing obtained from the ESA Information Retrieval system, and so covers the years 1961 to 1978. The main search was based on the keywords "aileron, rudder, tailplane, horizontal tail, elevator, spoiler, taileron", which yielded 806 titles on all aspects. Other searches were made using the combined sets of keywords given below:-

'canard' or 'variable wing', and 'wind tunnel';
'flap' and 'fighter aircraft' (less the subtitle 'aircraft');
'lateral' or 'longitudinal', and 'control' and 'aerodynamic';
'hinge moment'.

(Note: plurals of words were included in the searches when necessary.)

The references are listed here under the following headings:-

SECTION I CONTROL SURFACES

A Pitch motivators

- A.1 Elevator and/or tail Refs 1 to 46
A.2 Canard Refs 47 to 61

B Roll motivators

- B.1 Aileron Refs 62 to 87
B.2 Spoiler Refs 88 to 111

C Yaw motivators

- C.1 Rudder Refs 112 to 120

D Lift motivators

- D.1 Flap Refs 121 to 145
D.2 Blown and jet flap Refs 146 to 164
D.3 Direct lift Refs 165 to 171

E Side force motivators

- E.1 Direct side force Refs 172 to 176

SECTION II JET CONTROLS Refs 177 to 188

SECTION III HINGE MOMENTS Refs 189 to 197.

For each section, the references are further divided into three groups, low speed, transonic (or all speeds), supersonic, and are listed chronologically in each. Cross-references are listed at the end of each group.

I CONTROL SURFACES

A Pitch motivators

A.1 Elevator and/or tail

Low speed

- 1 A.L. Eyrnes, W.E. Hensleigh and L.A. Tolve, Effect of horizontal stabilizer vertical location on the design of large transport aircraft. AIAA 65-331 (1965)
- 2 P.B.E. Engler and G.F. Moss, Low-speed wind-tunnel tests on a $\frac{1}{4}$ th scale model of the Handley Page HP 115. ARC R & M No.3486 (RAE Technical Report 65180) (1965)
- 3 V.E. Lockwood, Low-speed wind-tunnel studies relating to pitch-up on a supersonic transport model with a high-aspect-ratio variable-sweep wing. NASA TN D-3542 (1966)
- 4 E. Erlick and P. Poisson-Quinton, Stability and control analysis of an airplane beyond its maximal lift. AGARD Stability and Control (1966)
- 5 W.B. Kemp, V.E. Lockwood and W.P. Phillips, Ground effects related to landing of airplanes with low-aspect-ratio wings. NASA TN D-3583 (NASA SP124) (1966)
- 6 K. Aoyagi and W.H. Tolhurst, Large-scale wind-tunnel tests of a subsonic transport with aft control at angles of attack above those for wing stall. NASA TN D-3797 (1967)
- 7 D.J. Kettle and D.A. Kirby, Low-speed wind-tunnel tests on the effects of tailplane and nacelle position on the superstall characteristics of transport aircraft. ARC R & M No.3571 (RAE Technical Report 67197) (1967)

- 8 D.A. Lovell, Wall corrections to longitudinal components measured in wind-tunnel models with tails. ARC CP No.1075 (RAE Technical Report 68212) (1968)
- 9 M.M. Winston, Induced interference effects on the aerodynamic characteristics of a 0.16-scale six-jet V/STOL model in transition. NASA TN D-5727 (1970)
- 10 J.C. Morrall and W.G.A. Port, Low-speed flight tests on a tailless delta-wing aircraft (Avro 707B). Part 2 - Longitudinal stability and control. ARC CP No.1105 (RAE Technical Report 67198) (1970)
- 11 D.A. Lovell, A low-speed wind-tunnel investigation of the tailplane effectiveness of a model representing the Airbus type of aircraft. ARC R & M No.3642 (RAE Technical Report 69077) (1970)
- 12 H. Triebstein and J. Becker, Investigation of unsteady interference effects on a harmonically oscillating wing-tailplane model with variable sweep wing, in the low subsonic region. DGLR Paper 71-081 (1971)
- 13 M. Seidel, Studies of the effects of an inclined engine jet on the aerodynamic properties of tail control surfaces. Zeitschrift fuer Flugwissenschaften, Vol 19, pp 13-19 (1971)
- 14 R.E. Goodfellow, An investigation of cross-coupling the elevators and throttle systems for the KC-135 aircraft in the landing configuration. USAF Inst. of Tech. (AD 730153) GGC/EE/71-8 (1971)
- 15 G. Sachs, Improvement of the flight characteristics for the landing approach by the coupling of spoiler and elevator deflection. Zeitschrift fuer Flugwissenschaften, Vol 20 (1972)
- 16 D.J. Giulianetti and R.L. Maki, Low-speed aerodynamic characteristics of a large-scale model with a thin, highly swept, 2.67 aspect ratio wing having a cranked leading edge. NASA TN D-6919 (1972)
- 17 R.J. Margason, R.D. Vogler and M.M. Winston, Wind-tunnel investigation at low speeds of a model of the Kestrel (XV-6A) vectored thrust V/STOL airplane. NASA TN D-6826 (1972)
- 18 D.G. Koenig and M.D. Falarski, Aerodynamic characteristics of a swept augmentor wing. NASA TM X-62252 (1972)
- 19 A.G. Hepworth, The longitudinal stability characteristics of an ogee wing of slenderness ratio equals 0.35. ARC CP No.1227 (RAE Technical Report 71103) (1972)
- 20 H.H.B.M. Thomas and J. Collingbourne, Longitudinal motions of aircraft involving high angles of attack. ARC R & M No.3753 (RAE Technical Report 73011) (1974)
- 21 E. Obert, Low-speed stability and control characteristics of transport aircraft with particular reference to tailplane design. AGARD CP "Take-off and landing" (1975)
- 22 C.D. Catoe, Wind-tunnel tests of a twin-engined, canard configured, mini, remotely-piloted, vehicle. M.Sc. Thesis, USAF Inst. of Tech. (1975)
- 23 D.R. Hoad and G.L. Gentry, Jr, Longitudinal aerodynamic characteristics of a low-wing lift-fan transport including hover characteristics in and out of ground effect. NASA TM X-3420 (1977)
- 24 W. Siegler and B. Wagner, Experimental investigations concerning the stalling characteristics of airplanes with T-tails. ZFW Vol 2, pp 156-165 (1978)
- Transonic
- 25 W.J. Alford, Jr, W.P. Henderson and A.A. Louma, Wind-tunnel studies at subsonic and transonic speeds of a multiple-mission variable wing-sweep airplane configuration. NASA TM X-206 (1959)
- 26 W.B. Olstad, Aerodynamic characteristics in pitch, including effects of horizontal tail negative dihedral angle of a 0.048-scale model of a horizontal-attitude VTOL airplane at transonic speeds. NASA TM X-11 (1960)
- 27 A.A. Louma, Longitudinal characteristics at transonic speeds of two V/STOL airplane configurations with skewed and variable-sweep wing. NASA TM X-527 and TM X-661 (1961)
- 28 O.P. Nicholas, Tests on a Hunter F-2 of two strain gauge methods for measuring tailplane loads in flight, with some loads measured in level flight, pitch-ups, and transonic dives. ARC CP No.754 (RAE Technical Note Aero 2886) (1964)
- 29 J. Barche and G. Krenz, A contribution to the design of horizontal stabilizers and elevators. WGLR Communications on Aerodynamics (1967)
- 30 E.C. Carter, Some measurements of the interference of a sting support on the pressure distribution of a rear fuselage and tailplane at subsonic speeds. Sup. WT Assoc., WT Note 67 (1967)
- 31 C.S. Barnes, R. Rose and A.A. Woodfield, Flight measurements of the lift, longitudinal trim and drag of the Fairey Delta 2 at Mach numbers up to 1.65 and comparisons with wind tunnel results. ARC R & M No.3577 (RAE Technical Report 67036) (1969)
- 32 C.S. Barnes and R. Rose, Some flight and wind-tunnel longitudinal stability measurements on the BAC slender-wing aircraft. ARC CP No.1134 (RAE Technical Report 70054) (1970)

- 33 E.E. Davenport and J.K. Huffman, Experimental and analytical investigation of subsonic longitudinal and lateral aerodynamic characteristics of slender, sharp edge, 74 deg swept wings. NASA TN D-6344 (1971)
- 34 R.B. Eberle, W.C. Fowler and R.T. Stancil, A critical review of canard relative to aft horizontal tail based on low- and high-speed tunnel tests of a fighter/attack configuration. AIAA 71-8 (1971)
- 35 W.J. Pinsker, Some observations on manoeuvre stability and longitudinal control. ARC R & M No.3730 (RAE Technical Report 72068) (1973)
- 36 W.T. Suit and J.L. Williams. Longitudinal aerodynamic parameters of the Kestrel aircraft (XV-6A) extracted from flight data. NASA TN D-7296 (1973)
- 37 H. August, B-1 airplane model support and jet plume effects on aerodynamic characteristics. AIAA Paper 73-153 (1973)
- 38 S.M. Dollyhigh, Subsonic and supersonic longitudinal stability and control characteristics of an aft tail fighter configuration with cambered and uncambered wings and uncambered fuselage. NASA TM X-3078 (1974)
- 39 D.E. Reubush and C.E. Mercer, Effects of nozzle interfairing modifications on longitudinal aerodynamic characteristics of a twin-jet, variable-wing-sweep fighter model. NASA TN D-7817 (1975)
- 40 R.C. Smith, R.T. Jones and J.L. Summers, Transonic lateral and longitudinal control characteristics of an F-8 airplane model equipped with an oblique wing. NASA TM X-73103 (1976)
- 41 S.M. Dollyhigh, Subsonic and supersonic longitudinal stability and control characteristics of an aft-tail fighter configuration with cambered and uncambered wings and cambered fuselage. NASA TN D-8472 (1977)
- 42 B.L. Shrout, Aerodynamic characteristics at Mach numbers from 0.6 to 2.16 of a supersonic cruise fighter configuration with a design Mach number of 1.8. NASA TM X-3559 (1977)

(see also Ref 85)

Supersonic

- 43 G.V. Foster and O.A. Morris, Stability and control characteristics at a Mach number of 1.97 of an airplane configuration having two types of variable-sweep wings. NASA TM X-323 (1960)
- 44 G.V. Foster and M.L. Spearman, Static longitudinal and lateral aerodynamic characteristics at a Mach number of 2.01 of a tailless delta V/STOL configuration having variable-sweep wing panels. NASA TM X-634 (1961)
- 45 F.E. McLean and O.A. Morris, Aerodynamic characteristics in pitch of several M-wing-body combinations at Mach numbers of 2.40, 2.60 and 2.86. NASA TN D-3035 (1965)
- 46 D.E. Fuller, Static stability characteristics at Mach numbers from 1.90 to 4.63 of a 76 deg swept arrow-wing model with variations in horizontal-tail height, wing-height and dihedral. NASA TN D-4076 (1967)

(see also Ref 197)

A.2 Canard

Low speed

- 47 R.D. Vogler, Ground-effects investigation of a STOL air-sea transport model with blowing over the canard and wing flaps. NASA TN D-5988 (1970)
- 48 B.B. Gloss, The effect of canard leading edge sweep and dihedral angle on the longitudinal and lateral aerodynamic characteristics of a close-coupled canard-wing configuration. NASA TN D-7814 (1974)
- 49 W.P. Henderson, The effect of canard and vertical tails on the aerodynamic characteristics of a model with a 59 deg swept-back wing at a Mach number of 0.30. NASA TM X-3088 (1974)
- 50 M.W.M. Jenkins and R.T. Meyer, A large-scale low-speed tunnel test of a canard configuration with spanwise blowing. AIAA 75-994 (1975)
- 51 B.B. Gloss, Effect of wing planform and canard location and geometry on the longitudinal aerodynamic characteristics of a close-coupled canard-wing model at subsonic speeds. NASA TN D-7910 (1975)
- 52 J. Wolkovitch and R.L. Fortenbaugh, Nacelle effects on stability of VSTOL configurations including conventional canard and tandem-wing arrangements. AIAA 78-1504 (1978)

(see also Ref 22)

Transonic

- 53 L.G. Bright and V.L. Peterson, Effects of deflected wing tips on the aerodynamic characteristics of a canard configuration at Mach numbers from 0.7 to 3.5. NASA TM X-392 (1960)

- 2-42
- 54 V.L. Peterson and G.P. Menees, Aerodynamic loads at Mach numbers from 0.70 to 2.22 on an airplane model having a wing and canard of triangular plan form and either single or twin vertical tails. NASA TN D-690 (1961)
- 55 J. Kloos and S.G.L. Elmeland, Static aeroelastic effects on the aerodynamics of the Saab 37 Viggen aircraft, a comparison between calculations, wind-tunnel tests and flight tests. ICAS 74-55 (1974)
- 56 D.H. Bennet, F-4/CCV - flight tests of advanced technology. SAE Paper 740861 (1974)
- 57 B.B. Gloss, Effect of canard location and size on canard-wing interference and aerodynamic centre shift related to manoeuvring aircraft at transonic speeds. NASA TN D-7505 (1974)
- 58 S.C. Stumpf and R.A. Whitmoyer, Horizontal canards for two-axis CCV fighter control. AGARD CP "Impact of ACT on airplane design". (1975)
- 59 R.J. Re and F.J. Capone, Longitudinal aerodynamic characteristics of a fighter model with a close-coupled canard at Mach numbers from 0.40 to 1.20. NASA TP 1206 (1978)

(see also Refs 34, 176, 186, 188, 192)

Supersonic

- 60 L.J. Beecham, D.A. Treadgold and P.E. Watts, Wind-tunnel tests of longitudinal and lateral aerodynamic characteristics of a canard aircraft model. RAE Report Aero 2575 (1962)
- 61 S.M. Dollyhigh, Static longitudinal aerodynamic characteristics of close-coupled wing-canard configurations at Mach numbers from 1.60 to 2.86. NASA TN D-6597 (1971)

B Roll motivators

B.1 Aileron

Low speed

- 62 J.K. Curran, D. Gaukroger and A.T. Marriot, Rolling power tests on an elastic model wing (M-planform) in low speed flow. ARC R & M No.3362 (RAE Technical Note Structures 280) (1962)
- 63 A.D. Hammond and R.J. Margason, Lateral control characteristics of a powered model of a twin-propeller deflected slipstream STOL airplane configuration. NASA TN D-1585 (1964)
- 64 S.F.J. Butler and M.B. Guyett, Low speed wind-tunnel tests on a delta wing aircraft model (SR77), with blowing over the trailing edge flaps and ailerons. ARC CP 710 (RAE Report Aero 2671) (1966)
- 65 H. Friedrich, The problem of roll control requirements for V/STOL transport aircraft in the low speed range. Luftfahrttechnik Raumfahrttechnik, Vol 15, pp 155-159 (1969)
- 66 I. Abel, Evaluation of a technique of determining airplane aileron effectiveness and roll rate by using an aeroelastically scaled model. NASA TN D-5538 (1969)
- 67 H.C. Curtiss, J.J. Traybar and W.F. Putman, The effect of ground proximity on the lateral/directional aerodynamic and control characteristics of a tilt-wing V/STOL aircraft at high lift coefficients. AFFDL-TR-73-151 (1973)
- 68 F. Burdorf, Selected examples of the evaluation of VAK 191B flight tests - roll control characteristic in hovering flight. DLR-Mitt-73-25, (ESRO TT104) (1973)
- 69 J.A. Eney and S. Greenhaigh, Low speed wind-tunnel test of jet flap and floating wingtip ailerons on a fighter wing. NADC-74198-30 (1974)
- 70 H.K. Koerner and R. Loehr, Three-component measurements on a model of a light STOL aircraft with chordwise blowing. DLR-FB-75-74 (ESA TT299) (1975)
- 71 D.R. Ellis and N.W. Tilak, An in-flight investigation of nonlinear roll control. SAE Paper 75028 (1975)
- 72 K. Boettcher, Adaption of the lateral controls for the VFW 614 during the flight tests. DGLR Paper 76-221 (1976)
- 73 W.P. Gilbert, L.T. Nguyen and R.W. Vangunst, Simulator study of the effectiveness of an automatic control system designed to improve the high angle of attack characteristics of a fighter aircraft. NASA TN D-8176 (1976)
- 74 E.J. Hopkins and G.A. Lovette, Aileron and Kruger nose flap effectiveness measured on an oblique wing. NASA TM X-3459 (1977)

(see also Refs 2, 112, 130, 149, 150)

Transonic

- 75 H. Loiseau, Measurement of coefficients of small aspect-ratio ailerons at transonic speeds. ONERA-NT-75 (1964)

- 76 F.W. Dee, Flight measurements at subsonic speeds of the aileron rolling power and lateral stability derivatives $\dot{\delta}_r$ and y_v on a 60 degree delta wing aircraft (Fairey Delta 2). ARC CP 734 (RAE Technical Note Aero 2897) (1964)
- 77 K.J. Turner, A roll-balance free-flight test vehicle for the measurement of aileron rolling power and roll damping at $M = 0.8$ to 2.5 . ARC CP No.679 (1965)
- 78 W.F. Grosser, A transonic wind-tunnel investigation of the rolling effectiveness of a large swept wing transport aircraft with conventional type ailerons and various spoiler configurations. AIAA 65-789 (1965)
- 79 D.L. Millikan, Subsonic wind-tunnel tests of a 0.125 scale model of the OV-10A airplane. CAL-AA-2313 W-1 (1966)
- 80 R.V. Parrish and G.G. Steinmetz, Lateral stability and control derivatives of a jet fighter airplane extracted from flight test data by utilizing maximum likelihood estimation. NASA TN D-6905 (1972)
- 81 D.M. Holford, Aerodynamic data for the BAC 221 up to Mach number of 0.955 as measured in wind-tunnel tests. ARC CP No.1230 (RAE Technical Report 70252) (1972)
- 82 J.L. Williams and W.T. Suit, Extraction for flight data of lateral aerodynamic coefficients for F-8 aircraft with supercritical wing. NASA TN D-7749 (1974)
- 83 T.A. Weisshaar, Lateral equilibrium of asymmetrical swept wings - aileron control vs geometric twist. Journ. of Aircraft, Vol 14, pp 122-127 (1977)
- 84 W.T. Suit, Lateral aerodynamic parameters extracted from flight data for the F-8C airplane in manoeuvring flight. NASA TN D-8276 (1977)
- 85 G.W. Foster, Identification of Hunter Mk 12 longitudinal and lateral aerodynamic stability and control derivatives. RAE Technical Report 77009 (1977)
- 86 N.W. Mathery and D.H. Gatlin, Flight evaluation of the transonic stability and control characteristics of an airplane incorporating a supercritical wing. NASA TP 1167 (1978)
- 87 A. Jean Ross, G.W. Foster and T. Turvey, An investigation of Dutch roll and wing rock oscillations of a Gnat trainer aircraft: flight tests and linear analysis. RAE Technical Report 78032 (1978)

(see also Refs 33, 40, 42, 196)

B.2 Spoiler

Low speed

- 88 G.W. Erasseur, A preliminary investigation to study the effect of flat spoilers on the aerodynamic characteristics of wings at angles of attack from 0 deg to 90 deg. David Taylor Model Basin - Aero 1113 (1966)
- 89 R.D. Murphy and K.R. Reader, Powered model investigation of the effects of gated spoilers on the aerodynamic characteristics of wings at angles of attack from 0 deg to 90 deg. Naval Ship R-D Center - Aero 1132 (1967)
- 90 D.R. Ellis, A.E. Faye and J.W. Olcott, The application of spoilers to a small fixed-wing general aviation aircraft. SAE Paper 710387 (1971)
- 91 H.A. Verstynen, Jr and D. Andrisani, II, Full-scale wind-tunnel investigation of the effects of slot spoilers on the aerodynamic characteristics of a light twin-engined airplane. NASA TN D-7315 (1973)
- 92 J. Roskam, D.L. Kohlman and W.H. Wentz, Spoilers for roll control of light airplanes. AIAA 74-861 (1974)
- 93 D.L. Kohlman and C.H. Brainerd, Evaluation of spoilers for light aircraft flight path control. Journ. of Aircraft, Vol 11, pp 449-456 (1974)
- 94 G.V. Parkinson, G.P. Brown and T. Jandali, The aerodynamics of two-dimensional airfoils with spoilers. AGARD CP V/STOL Aerodynamics (1974)
- 95 J.D. Lang, Experimental results for an airfoil with oscillating spoiler and flap. Symposium Unsteady Aerodynamics. Arizona (1975)
- 96 W.H. Wentz, Jr, H.C. Seetharam and J.T. Calhoun, Wind tunnel and flight development of spoilers for general aviation aircraft. SAE Paper 750523 (1975)
- 97 B.J. Holmes, D.L. Kohlman and H.L. Crane, Preliminary flight-test results of an advanced technology light twin-engined airplane (ATLIT) SAE Paper 760497 (1976)
- 98 D.L. Kohlman, Flight test data for light aircraft spoiler roll control systems. NASA CR 153291 (1977)

- 99 J.W. Paulson, Jr, Wind-tunnel results of the aerodynamic characteristics of a $\frac{1}{4}$ -scale model of a twin-engine short haul transport - in Langley V/STOL tunnel. NASA TM X-74011 (1977)
- 100 D.H. Neuhart and R.B. Oetting, Performance of plain-type spoilers applied to the GA/W/-1 wing. Journal of Aircraft, Vol 14, pp 1019-1020. October 1977
- 101 D.L. Kohlman, Flight evaluation of a spoiler roll control system on a light twin-engined airplane. NASA CR 2935 (1978)

(see also Refs 127, 133, 135, 136, 168)

Transonic

- 102 D.E. Wornom, Transonic wind-tunnel investigations of the effect of control span and large wing-tip nacelles on effectiveness of spoiler-slot-deflector controls on an unswept-wing fighter-type airplane. NASA TM X-280 (1960)
- 103 A.D. Hammond, Aerodynamic characteristics of a spoiler-slot-deflector control on a 45 deg sweptback-wing-fuselage model at high subsonic speeds. NASA TN D-2037 (1963)
- 104 A. Heyser and F. Maurer, Experimental investigations on solid spoilers and jet spoilers at Mach numbers of 0.6 to 2.8. NASA CR 53257 (1964)
- 105 C.S. Barnes. A developed theory of spoilers of aerofoils. ARC CP No.887 (1966)
- 106 M.D. Dobson, An investigation of the pressure distributions on a 45 deg swept half wing, including the effects of upper surface spoilers. ARC CP No.1184 (RAE Technical Report 68118) (1971)
- 107 J.K. Huffman, C.H. Fox, Jr, and S.B. Grafton, Subsonic longitudinal and lateral directional static stability characteristics of a variable sweep fighter configuration employing various control surface deflections at angles of attack of 0 deg to 50 deg and large sideslip angles. NASA TM 74050 (1977)

(see also Ref 78)

Supersonic

- 108 G.V. Foster, Aerodynamic characteristics of variable-wing-sweep configuration with spoiler-slot-deflector control system and swept back outer wing panels. NASA TM X-273 (1960)
- 109 A. Heyser, H.G. Knocke and F. Maurer, Investigation of spoilers at supersonic speeds. ICAS 23 (1962)
- 110 E. Stanewsky, Measurements on slotted supersonic flow. DLR FB 67-08 (1967)
- 111 C. Hayes, Roll-control effectiveness of several spoiler configurations on an airplane model with wing sweep of 55 deg and 75 deg at supersonic Mach numbers. NASA TM X-2165 (1971)

C Yaw motivators

C.1 Rudder

Low speed

- 112 R.J. Pegg, Flight test investigations of ailerons as a source of yaw control on the VZ-2 tilt-wing aircraft. NASA TN D-1375 (1962)
- 113 F.W. Dee, Proving tests of a wing tip parachute installation on a Venom aircraft with some measurements of directional stability and rudder power. ARC CP No.658 (RAE Technical Note Aero 2824) (1963)
- 114 J.C. Morrall, D.H. Perry and W.G.A. Port, Low-speed flight tests on a tailless delta wing aircraft (AVRO 707B) - Part 3 - lateral stability and control. ARC CP No.1106 Part 3 (RAE Aero 2638 Part 3) (1970)
- 115 T.B. Honeycutt, III, Aerodynamic comparison of two double-slotted rudders. M.Sc. Thesis. USAF Inst. of Tech. (1973)
- 116 R.F. Osborn, Jr, Investigation of a double-slotted rudder for application on advanced tactical transport aircraft. AFFDL TR 75-94 (1975)
- 117 C.A. Belsterling, Development of a fluidic rudder. AIAA 76-1990 (1976)

(see also Refs 2, 67)

Transonic

- 118 - , Report on proceedings held by the WGLR committee on aerodynamics, on July 10, 1967 in Darmstadt. DLR-M177-67-24

(see also Refs 55, 79, 81, 82, 84 to 87, 194)

Supersonic

- 119 A. Hammer and R. Jahn, Research on rudders in a supersonic jetstream. WGL Paper 20 (1962)
- 120 A. Hammer and R. Jahn, Investigation of jet rudders. WGLR Yearbook, pp 171-179 (1963)
- D Lift motivators
- D.1 Flap
- Low speed
- 121 W.A. Newsom, Jr, Stability and control characteristics of a four propeller tilt-wing VTOL model with programmed flap. NASA TN D-1389 (1962)
- 122 M.P. Fink, R.G. Mitchell and L.C. White, Aerodynamic data on a large semispan tilting wing with 0.6-diameter chord, Fowler flap, and single propeller rotating up at tip. NASA TN D-2180 (1964)
- 123 V.E. Lockwood, High-lift characteristics of a variable-sweep supersonic transport model with a blended engine-fuselage and engine-mounted horizontal tails. NASA TM X-1199 (1966)
- 124 M.P. Fink, Aerodynamic data on a large semispan tilting wing with 0.5-diameter chord, single-slotted flap, single propeller 0.19 chord below wing. NASA TN D-3884 (1967)
- 125 K.W. Goodson, Effect of ground proximity on the longitudinal, lateral and control aerodynamic characteristics of a tilt-wing, four-propeller V/STOL model. NASA TN D-4237 (1967)
- 126 W.H. Deckert, S.O. Dickinson and V.R. Page, Large-scale wind-tunnel tests of a deflected slipstream STOL model with wings of various aspect ratios. NASA TN D-4448 (1968)
- 127 R.C. Henry and J.W. Stickle, Wind-tunnel study to explore the use of slot spoilers to modulate the flap-induced lift of a wing. NASA TN D-4664 (1968)
- 128 A.M. Cook and D.G. Jones, Large scale wind tunnel investigation to improve the low speed longitudinal stability at high lift of a supersonic transport with variable-sweep wings. NASA TN D-5005 (1969)
- 129 H. Friedrich and H. Wuennenberg, The flight characteristics of a high-lift STOL transport aircraft. Luftfahrttechnik Raumfahrttechnik, Vol 15, pp 150-155 (1969)
- 130 P. Bergmeyer, Aerodynamic development of Fokker F28 wing-flap, lift dumpers and lateral control. De Ingenieur Vol 81, pp 94-100 (1969)
- 131 D. Althaus, Wind tunnel measurements on airfoils with flaps, at medium Reynolds numbers; II. Conference, OSTIV, 12th Congress (1970)
- 132 W.T. Eckert and R.I. Maki, Low-speed wind-tunnel investigation of the longitudinal characteristics of a large-scale variable wing-sweep fighter model in the high-lift configuration. NASA TM X-62244 (1973)
- 133 W.H. Wentz, Jr, Effectiveness of spoilers on the GA(W)-1 airfoil with a high performance Fowler flap. NASA CR 2538 (1975)
- 134 P. Fournier, Low-speed aerodynamic characteristics of a transport model having 42.33° swept low wing with supercritical airfoil, double-slotted flaps and T-tail on low tail. NASA TM X-3276 (1975)
- 135 J.W. Paulson, Jr, Wind-tunnel investigation of a Fowler flap and spoiler for an advanced general aviation wing. NASA TN D-8236 (1976)
- 136 W.H. Wentz, Jr and C.G. Voik, Jr, Reflection-plane tests of spoilers on an advanced technology wing with a large Fowler flap. NASA CR 2696 (1976)
- 137 V.J. Rossow, Lift enhancement by an externally trapped vortex. AIAA 77-672 (1977)
- 138 E.W. Kruppa, A wind-tunnel investigation of the Kasper vortex concept. AIAA 77-310 (1977)
- 139 A.M. Constant, B. Haftmann and D. Welte, Design and wind-tunnel testing of the supercritical wing with manoeuvre flaps for the Alpha Jet experimental aircraft. DGLR Symposium (1978)

(see also Refs 64, 74, 95)

Transonic

- 140 E.J. Ray and J.G. Carmichael, Jr, Subsonic characteristics of a twin-jet swept-wing fighter model with leading-edge Kreuger flaps. NASA TM X-2325 (1971)
- 141 J.E. Forestier, Influence of simple aerodynamic modifications on the performance of an aircraft. AGARD "Lessons with emphasis on Flight Mechanics" (1971)
- 142 W. Staudacher, Improvement of manoeuvrability at high subsonic speeds - application of slotted and unslotted leading-edge and trailing-edge flaps. NASA TT F-15406 (1972)

143 R.C. Monaghan and E.L. Friend, Effects of flaps on buffet characteristics and wing-rock onset of an F-8C airplane at subsonic and transonic speeds. NASA TM X-2873 (1973)

2-46

144 D.R. Stanniland, The effect of deflecting flaps on strike/fighter aircraft wing design. Aero Journal, Vol .8, pp 553-559 (1971)

145 F.W. Boltz and D.F. Pena, Aerodynamic characteristics of an F-8 aircraft configuration with a variable camber wing at Mach numbers from 0.70 to 1.15. NASA TM 78432 (1977)

D.2 Blown and jet flap

Low speed

146 S.F.J. Butler and J. Williams, Aerodynamic aspects of boundary layer control for high lift at low speeds. AGARD 414 (1963)

147 R.C. Innis and H.C. Quigley, Four propeller STOL transport aircraft with boundary layer control on highly deflected flaps. NASA TN D-1647 (1963)

148 K. Aoyagi, D.H. Hickey and J.V. Kirk, Large-scale wind-tunnel investigation of a model with an external jet-augmented flap. NASA TN D-4278 (1967)

149 S.F.J. Butler, Low-speed wind-tunnel tests on a swept-back wing model (Buccaneer Mark 1) with blowing at the wing leading edge and blowing over the flaps and drooped ailerons. ARC R & M No.3655 (RAE Technical Report 67223) (1967)

150 J.A. Lawford, Low-speed wind-tunnel test on an unswept wing-fuselage model of aspect ratio 9.8, with tangential blowing over trailing-edge flaps and ailerons, including the effect of slipstream. ARC CP No.1108 (RAE Technical Report 68111) (1968)

151 L.P. Parlett, H.D. Greer and R.L. Henderson, Wind-tunnel investigation of an external-flow jet-flap transport configuration having full-span triple-slotted flaps. NASA TN D-6391 (1971)

152 C.J. Dixon, Lift and control augmentation by spanwise blowing over trailing-edge flaps and control surfaces. AIAA 72-781 (1972)

153 J.L. Loth, Some aspects of STOL aircraft aerodynamics. SAE Paper 730326 (1973)

154 P.R. Ashill, A theoretical and experimental investigation of the external-flow, jet-augmented flap - jet flap analogy and wind-tunnel tests. ARC CP No.1319 (RAE Technical Report 74089) (1975)

155 K. Aoyagi, M.D. Falarski and D.G. Koenig, Wind-tunnel investigation of a large-scale 25 deg swept-wing jet transport model with an external blowing triple-slotted flap. NASA TM X-62197 (1973)

156 H.G. Owens, R.S. Kaneshiro, D.J. Renselaer and D.W. Schluntz, STOL tactical aircraft investigation: externally blown flap. AFFDL-TR-73-20, Vol 1 (1973)

157 M.H. Roe, Air Force STOL tactical aircraft investigation - evaluation of externally blown flaps. SAE Paper 730914 (1973)

158 E.R. Heald, External blowing flap technology on the USAF/McDonnell Douglas YC15 (ANST) program. SAE Paper 730915 (1973)

159 G.N. Panageas, Fighter technology demonstrator precursor analysis and test. Vol 2: an experimental investigation of the aerodynamic characteristics of a fighter technology demonstrator jet flap development model at low subsonic Mach number. AFFDL-TR-73-112 (1973)

160 D.R. Hoad, Longitudinal aerodynamic characteristics of an externally blown flap powered lift model with several propulsive system simulators. NASA TN D-7670 (1974)

161 W.L. Waites and Y.T. Chin, Small scale wind-tunnel investigation of hybrid high lift systems combining upper surface blowing with the internally blown flap. NASA CR 114758 (1974)

162 J.L. Parker and R.F. Ball, An analysis of the effects of internally blown jet flaps on an advanced fighter aircraft design. AIAA 74-970 (1974)

163 W.L. Cook and D.C. Whittley, Comparison of model and flight test data for an augmentor-wing STOL research aircraft. AGARD "Flight/ground testing facilities correlation" (1976)

see also Refs 47, 69, 70)

Transonic

Yoshihara and D. Zonars, The transonic jet flap - a review of recent results. SAE Paper 751089

M. Barton and J.W. Stickle, Flight tests of a direct lift control system during landing. NASA TN D-4854 (1968)

- 166 G.R. Jansen, Flight evaluation of direct lift control on the DC-8 Super 63. Inst. Soc. of Amer. Symposium (1969)
- 167 W.J.G. Pinsker, The control characteristics of aircraft employing direct-lift control. ARC R & M No.3629 (RAE Technical Report 68140) (1970)
- 168 D. Andrisani, II, G.L. Gentry, Jr and J.W. Stickle, Wind-tunnel study of slot spoilers for direct lift control. NASA TN D-6627 (1972)
- 169 D.L. Kohlman and D.R. Ellis, Direct force control for light airplanes. AIAA 74-862 (1974)
- (see also Refs 15, 23)

Transonic

- 170 W.E. McNeill, R.M. Gerdes, R.C. Innis and J.D. Ratcliff, A flight study of the use of direct-lift-control flaps to improve station keeping during in-flight refuelling. NASA TM X-2936 (1973)
- 171 J. Gera, Wind-tunnel investigation of the aerodynamic characteristics of symmetrically deflected ailerons of the F-8C airplane - conducted in the Langley 8-foot transonic pressure tunnel. NASA TM X-74008 (1977)
- (see also Refs 56, 58)

E Side force motivators

E.1 Direct side force

Low speed

- 172 G.W. Hall, A flight test investigation of direct side force control. AIAA 72-94 (1972)
- 173 C. LaBurthe, J.P. Petit and A. Guillard, Use of direct forces - predictions and flight tests on a light 6-axis variable stability aircraft of Princeton University. AGARD SC Paper 19 (1978)
- (see also Ref 169)

Transonic

- 174 W. Benner and H. Wuennenberg, Problems and implementation possibilities of a direct side force control in the case of fighters. DGLR Paper 74-24 (1974)
- 175 H. Wuennenberg and G. Sachs, Direct side force control - possibilities and problems of an application in the case of fighter aircraft. DGLR Paper 76-239 (1976)
- 176 R.J. Re and F.J. Capone, An investigation of a close-coupled canard as a direct side force generator on a fighter model at Mach numbers from 0.40 to 0.90. NASA TN D-8510 (1977)
- (see also Refs 56, 58)

II JET CONTROLS

Low speed

- 177 D.W. Galey, R.H. Logie and A.J. White, Evaluation of a combination thrust reverser-jet deflector concept. AIAA 64-287 (1964)
- 178 K.P. Spreeman, Free-stream interference effects on effectiveness of control jets near the wing tip of a VTOL aircraft model. NASA TN D-4084 (1967)
- 179 M. Seidel, The influence of an inclined jet on the aerodynamic characteristics of a control surface. DGLR Aero. Interference (1971)
- 180 J.D. Wilson, S. Chandra and J.L. Loth, Thrust augmented wing sections in transition flight. AIAA 75-169 (1975)
- 181 D.J. Renselaer, Low speed aerodynamic characteristics of a vectored thrust V/STOL transport with two lift/cruise fans. NASA CR 152029 (1977)
- 182 L.P. Yip and J.W. Paulson, Jr, Effects of deflected thrust on the longitudinal aerodynamic characteristics of a close-coupled wing-canard configuration - in the Langley V/STOL tunnel. NASA TP 1090 (1977)
- 183 L.O. Leavitt, P.D. Whitten and S.C. Stumpfl, Low speed aerodynamic characteristics of a vectored-engine-over-wing configuration. AIAA 78-1081 (1978)

(see also Refs 9, 13, 17)

Transonic

- 184 F.J. Capone, Supercirculation effects induced by vectoring a partial-span rectangular jet - for fighter aircraft manoeuvrability. AIAA 74-971 (1974)

2-47

- 185 J.A. Cawthon, Design and preliminary evaluation of inlet concepts selected for manoeuvre improvement - of transonic tactical aircraft. AIAA 76-701 (1976)
- 186 J.L. Thomas, J.W. Paulson, Jr and L.P. Yip, Effects of deflected thrust on the stability and performance characteristics of a close-coupled canard fighter configuration. AIAA 77-887 (1977)
- 187 L.D. Leavitt and L.P. Yip, Effects of spanwise nozzle geometry and location on the longitudinal aerodynamic characteristics of a vectored-engine-over-wing configuration at subsonic speeds. NASA TP 1215 (1978)
- 188 R.D. Child and W.P. Henderson, Canard configured aircraft with 2-D nozzle. AIAA 78-1450 (1978)

(see also Refs 104, 120)

III HINGE MOMENTS

Transonic

- 189 T.G. Gainer and W.G. Moseley, Jr, Some effects of control profile and control trailing-edge angle on the oscillating hinge-moment and flutter characteristics of flap-type controls at transonic speeds. NASA TM X-170 (1960)
- 190 D. Isaacs, Analysis of hinge moment data for rectangular and near rectangular trailing-edge controls at supersonic and transonic speeds. ARC CP No.874 (RAE Technical Report 65105) (1966)
- 191 O.P. Nicholas, R. Rose and G. Vorley, Flight measurements of the elevator and aileron hinge-moment derivatives of the Fairey Delta 2 aircraft up to a Mach number of 1.6 and comparison with wind-tunnel results. ARC R & M No.3485 (RAE Technical Report 65143) (1967)
- 192 V.M. De Angelis, E.L. Friend, J.M. Jenkins and R.C. Monaghan, Flight measurements of canard loads, canard buffeting, and elevon and wing tip hinge moments on the XB70 aircraft including comparisons with predictions. NASA TN D-5359 (1969)
- 193 D.R. Gaukroger, D.A. Drane and R. Gray, A technique for measuring oscillatory aerodynamic control surface hinge moments from forced response characteristics. ARC CP No.1253 (RAE Technical Report 71211) (1973)
- 194 J. Krahl, Measurement of hinge moments, rudder and fin loads of a horizontal tail surface, with one- and six-component strain gauge balances - wind tunnel semimodel. DGLR Force measurements on parts of WT models. (1975)
- 195 G.E. Hutton, D.A. Drane and D.R. Gaukroger, Measurements of oscillatory aerodynamic hinge moments from the response of a wind-tunnel model to turbulent flow - comparing steady state response technique results on same model. ARC CP No.1317 (RAE Technical Report 73130) (1975)
- 196 J.N. Ball, Rolling tail design and behaviour as affected by actuator hinge moment limits. AIAA 78-1500 (1978)

Supersonic

- 197 J. Malavergne and L. Tanguy, Hinge moment and efficiency of an elevator in supersonic flight. Ecole Nat. d'Ing. Const. Aero: Aero 2 (1973)

CORRELATION OF F-15 FLIGHT AND WIND TUNNEL TEST CONTROL EFFECTIVENESS

31

J. W. Agnew
Section Chief-Technology-Aerodynamics

and

J. F. Mello
Chief Technology Engineer-Aerodynamics
McDonnell Aircraft Company
McDonnell Douglas Corporation

ABSTRACT

The F-15 aerodynamic configuration and control system development relied on data obtained in an extensive wind tunnel test program. Subsequently, a large body of flight test data was obtained. Control surface effectiveness characteristics have been derived from flight test data and have been compared with the data obtained in the wind tunnel test program. Data correlations are available for the ailerons, rudders, and stabilators. The latter surfaces are deflected symmetrically for longitudinal control and are deflected differentially for roll control. Primary axis effectiveness is addressed for each of these control surfaces. Significant secondary axis contributions (e.g. yawing moments due to aileron deflection) are also addressed. In addition to the conventional control surfaces, the longitudinal control effectiveness of the F-15 movable inlet ramp is discussed.

As a result of the excellent resistance to departure from controlled flight, the spin resistance and spin recovery characteristics of the F-15, it was possible to flight test and to obtain control effectiveness data to 90° angle-of-attack at low speeds and to approximately 40° at transonic speeds. Thus, the correlation of control effectiveness is addressed for a large range of conditions.

NOMENCLATURE

M	Mach number
α , AOA	Angle of attack
δ_H	Collective stabilator deflection, positive leading edge up
δ_I	Inlet ramp deflection, positive leading edge up
δ_R	Rudder deflection, positive trailing edge left
δ_A	Differential aileron deflection, positive for right roll
δ_D	Differential stabilator deflection, positive for right roll
δ_L	Equivalent roll control deflection used to represent combined effectiveness of ailerons and differential stabilator
C_m	Pitching moment coefficient - $M_{c.g.}/qS\bar{c}$
C_n	Yawing moment coefficient - $N_{c.g.}/qSb$
C_l	Rolling moment coefficient - $L_{c.g.}/qSb$
C_Y	Side force coefficient - Y/qS
$\frac{dC_m}{d\delta_H}$	Variation of pitching moment coefficient with stabilator deflection

*The control effectiveness derivatives $C_{m_{\delta_I}}$, $C_{n_{\delta_R}}$, $C_{Y_{\delta_R}}$, $C_{l_{\delta_L}}$, and $C_{n_{\delta_L}}$ are similarly defined.

INTRODUCTION

This paper presents a comparison of the effectiveness of the F-15 primary controls and the longitudinal control effectiveness of the first inlet ramp as measured in wind tunnel tests with the corresponding parameters derived from flight test maneuvers. The primary control surfaces are the twin rudders, ailerons and stabilators illustrated in Figure (1). The stabilators are deflected symmetrically for longitudinal control and are deflected differentially for roll control. As noted in Figure (1), the symmetrical deflection range of the stabilator is from +15° to -27.5° and the differential deflection available is 11° per side or a total of 22°. The ailerons deflect differentially up to +20° per side for a total differential deflection of 40°. Rudder deflection is +30° from the neutral position. All of the aforementioned deflections are zero load limit values. Rudder and aileron deflections are hinge moment limited to lesser values for a significant portion of the flight envelope.

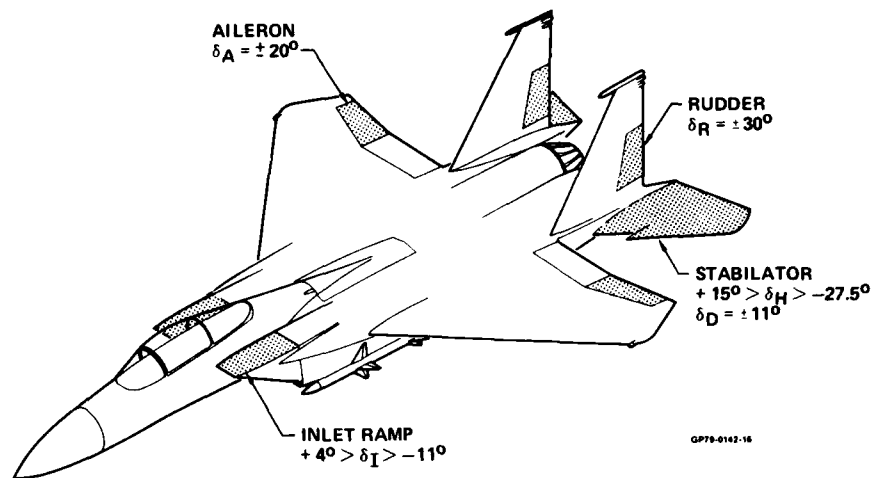


FIGURE 1
THE F-15 EAGLE

The deflection range of the inlet ramp is from $+4^\circ$ (leading-edge up) to -11° . At $\delta_I = 0^\circ$ the upper surface contour at the ramp nacelle intersection is smooth and continuous. The inlet ramp deflection at zero angle of attack is scheduled with Mach number and total temperature to provide maximum excess thrust except where flow quality at the engine is an overriding consideration. The ramp motion, from this initial position, is a direct function of angle-of-attack. At a given flight condition, the motion maintains the inlet ramp orientation relative to free stream until the deflection limits are reached.

The design of these configuration and control system features relied on data obtained in an extensive wind tunnel test program. Static control surface effectiveness data were obtained for a large range of Mach number and angle of attack using 4.7% and 7.5% scale models. Both of these models are sting mounted from the aft end and use internal six-component strain gauge balances for the measurement of forces and moments. Both models feature "flow-through" inlets and ducts and incorporate geometrically scaled aft end distortions for sting entry. This small aft end distortion was found to have no effect on control surface effectiveness or inlet ramp effectiveness in special "sting distortion and interference" tests conducted for that purpose.

The majority of the wind tunnel data presented herein were obtained using the 4.7% scale model in tests conducted at the Arnold Engineering Development Center (AEDC) 16 foot transonic tunnel (16T) and the McDonnell Douglas Corporation (MDC) Polysonic Wind Tunnel (PSWT). The 7.5% model tests were conducted in the AEDC 16T and in the NASA Ames Research Center 12 foot pressure tunnel. The latter facility provided the high angle of attack data at high Reynolds number for stall/spin analyses. It should be noted that the model inlet ducts were blocked at angles-of-attack greater than forty degrees in the Ames tests. This was necessary to avoid problems associated with a tendency for the flow to enter at the exit nozzle and exit at the inlet at high angles of attack.

The static force and moment tests together with forced oscillation tests, free-flight model tests, vertical spin tunnel tests, and helicopter drop model tests, which were all conducted at the NASA Langley Research Center, provided the data required to develop a complete non-linear aerodynamic characteristics model (Aero Model) which was used for control system design, pre-flight trajectory analyses and manned flight simulation activities. The Aero Model was subsequently used as a baseline for a modified maximum likelihood analysis of flight test data in order to derive the stability-and-control characteristics of the airplane. The correlations of control surface effectiveness presented herein are comparisons of the pre-flight Aero Model characteristics with the corresponding values which yield the best match with the dynamic behavior of the aircraft. The pre-flight aerodynamic characteristics are documented in Reference (1) and the characteristics derived from flight test are given in Reference (2). For the sake of simplicity and brevity, the comparisons presented herein are limited to the rigid body characteristics. Therefore, the correlations are applicable to the regions of the flight envelope where aeroelastic effects are negligible. For similar reasons, the correlations of control effectiveness at large sideslip angles are not discussed herein. The F-15 control system is configured to automatically coordinate maneuvers and large sideslips are encountered only when the aircraft is forced into an out-of-control situation (departure) or spin by gross misapplication of the controls.

The control effectiveness parameters discussed herein were determined in a conventional manner in the wind tunnel tests. The models were pitched and yawed through the angle-of-attack range and sideslip angle range of interest with the control surfaces positioned at selected deflections. Deflections were measured with an accuracy of

approximately $\pm 10^\circ$. The nominal increment in primary control surface deflection was 10° except at conditions where linearized derivatives were sought. Deflection increments of as small as 5° could be used where desired.

3-3

The flight values of control effectiveness were derived from analysis of time history data for (a) level flight, (b) longitudinal and lateral stick raps and doublets, (c) steady sideslips, (d) rudder kicks and doublets, (e) wind-up turns, (f) abrupt pullups, (g) rudder rolls, (h) aileron rolls, (i) stalls, (j) forced departures from controlled flight, and (k) quasi-steady spins. Recovery from out-of-control situations and spins also provided data.

It should be noted that the F-15 was required to perform all of the aforementioned maneuvers with the control augmentation system (CAS) on and turned off. The data obtained with the control system feedback loops deactivated (CAS OFF) greatly facilitated the derivation of aerodynamic characteristics from the flight test time histories.

LONGITUDINAL CONTROL EFFECTIVENESS

Figure (2) presents the correlation of longitudinal control effectiveness at low angles of attack. The data are presented for the derivative $C_{m\delta_H}$ as a function of Mach number.

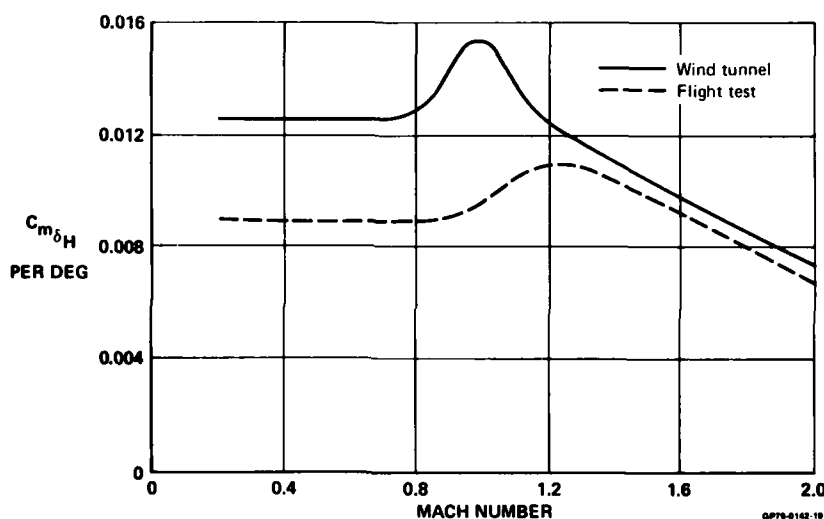


FIGURE 2
LONGITUDINAL CONTROL EFFECTIVENESS
Low Angle-of-Attack

The difference shown at subsonic and transonic speeds may be surprising. The difference is too large to be attributable to data accuracy. As will be evident from the discussion that follows the reduced flight control effectiveness has no significant impact on the system performance. As a matter of fact, only one area has been encountered where the lower stabilator control effectiveness could be discerned from a system performance standpoint. At certain flight conditions, (low bare-airframe damping) the longitudinal damping ratio with the CAS ON was slightly less than predicted. However, the reduction in artificial damping was not sufficient to warrant a control system gain increase. It should also be noted that Flight Loads tests conducted in the low angle of attack range showed that the loss in effectiveness is not associated with a significant decrease in stabilator panel load but is primarily due to a decrease in the interference (carryover) loads induced on the fuselage by the stabilator loads. This phenomenon has not been pursued to the point where a substantiated reason for the difference can be presented. However, it appears that the difference is primarily due to transient aerodynamic phenomena.

In the Mach number range where large differences in control effectiveness are shown in Figure (2), moderate stabilator deflections are required to obtain meaningful flight test data. These deflections produce large pitch accelerations which result in high angle-of-attack rates. Furthermore, it is well known that a small but finite time is required for the steady-state pressure distributions (particularly in the afterbody region) to be established after a control deflection is achieved. Therefore, it is difficult if not impossible for a high agility aircraft to achieve the static aerodynamic load distributions in flight which are representative of the corresponding low angle of attack static wind tunnel test conditions. Thus, it is indicated that the loss in stabilator effectiveness shown in Figure (2) is an "apparent" loss which is, in large

part, due to this aerodynamic "lag". In the Mach number range where the differences in control effectiveness are small, wind-tunnel and flight test data show that the carryover loads are small, therefore the effect of materially reduced carryover loads due to transient flow phenomena would not be expected to affect the correlation of control effectiveness. In addition, the local flows are definitely supersonic and "lags" are significantly reduced.

The current Aero Model uses the reduced stabilator effectiveness shown in Figure (2) in the interest of achieving high fidelity in combat and handling qualities simulations and analyses without introducing the additional complexity of accounting rigorously for the unsteady aerodynamic phenomenon. The stabilator required for trim at low AOA may be in error by a small amount but this is of little consequence, particularly since trimmed drag polars have been determined separately.

Figure (3) presents longitudinal control up to moderate angles of attack at $M = .90$. The data are shown as incremental pitching moment, ΔC_m , versus incremental stabilator, $\Delta \delta_H$, from the stabilator required to trim at the angle of attack noted. These data are typical of the degree of longitudinal control effectiveness correlation achieved at all subsonic speeds up through $M = .90$ at angles of attack to 40° . It is noted how the agreement in stabilator effectiveness is improved near the trim at higher angles of attack. Thus, the reduced control effectiveness (in accordance with the hypothesis discussed above) was not observed at low body rates and did not limit maximum maneuvering capabilities.

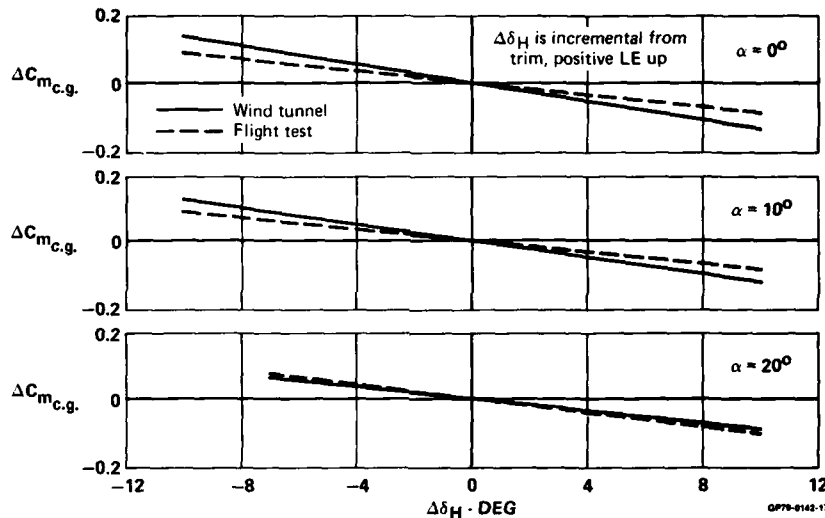


FIGURE 3
LONGITUDINAL CONTROL EFFECTIVENESS
Mach 0.9

Longitudinal control characteristics at moderate angles of attack for $M = 1.2$ are presented in Figure (4). It is evident that the correlation of wind tunnel and flight test data is very good. The degree of correlation shown at $M = 1.2$ is representative of that achieved at all supersonic flight conditions for which data are available.

The low speed high angle of attack longitudinal control effectiveness comparison is presented in Figure (5). Pitching moment coefficient is presented as a function of angle of attack for two stabilator deflections ($\delta_H = 0^\circ$ and -25°). The flight test data exhibits an increased trim angle of attack capability in the 25° to 35° range which is in large part due to reduced stability. Although not shown in the previous figures, this increased trim capability is present through the subsonic speed range. Otherwise, insofar as analyses of stall and spin and recovery characteristics are concerned, the differences shown at the higher angles of attack must be judged small.

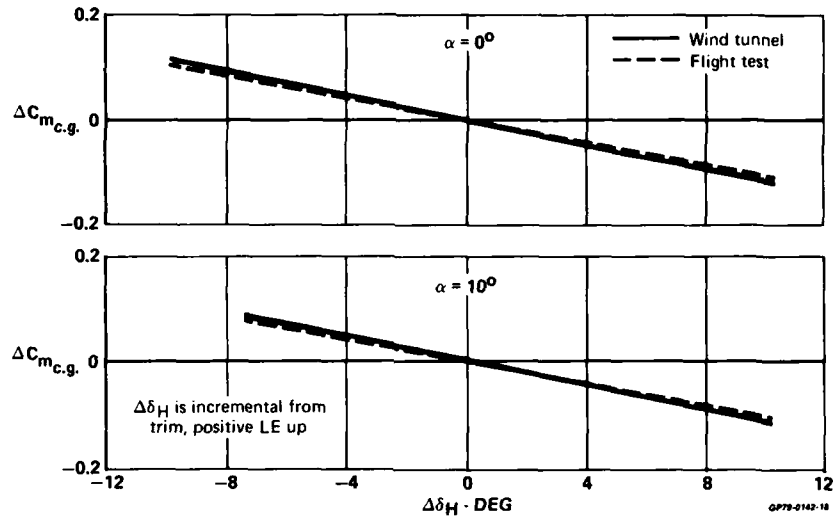


FIGURE 4
LONGITUDINAL CONTROL EFFECTIVENESS
Mach 1.2

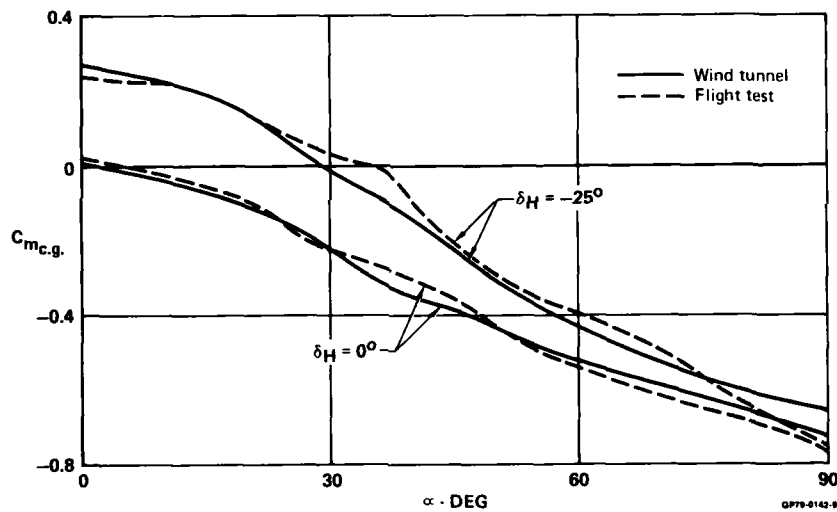


FIGURE 5
LONGITUDINAL CONTROL EFFECTIVENESS
Low Speed

DIRECTIONAL CONTROL EFFECTIVENESS

The directional control effectiveness of the twin rudder configuration obtained in the wind tunnel tests and those derived from the flight test data exhibit excellent correlation. The linearized derivatives shown in Figure (6) as functions of Mach number, and as functions of angle of attack in Figures (7), (8), and (9) illustrate that the degree of agreement was excellent throughout the aircraft flight envelope. The side force and yawing moment derivatives shown in these figures are applicable for up to 10 degrees of sideslip.

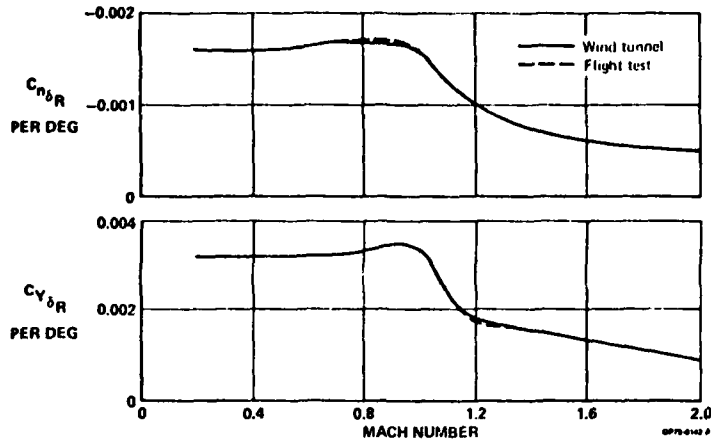


FIGURE 6
 RUDDER EFFECTIVENESS
 Low Angle-of-Attack

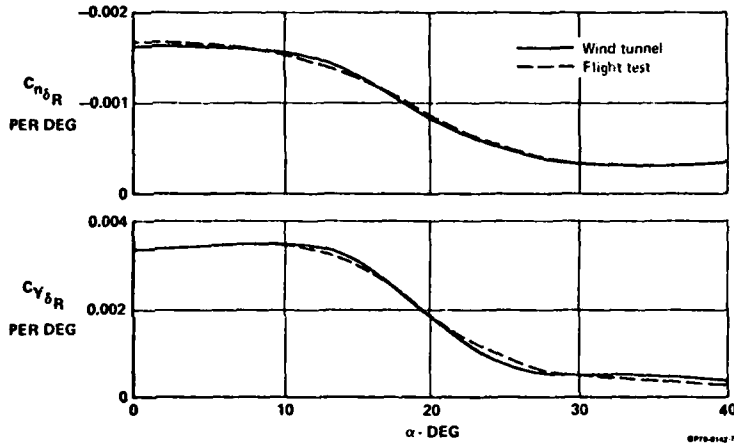


FIGURE 7
 RUDDER EFFECTIVENESS
 Mach 0.9

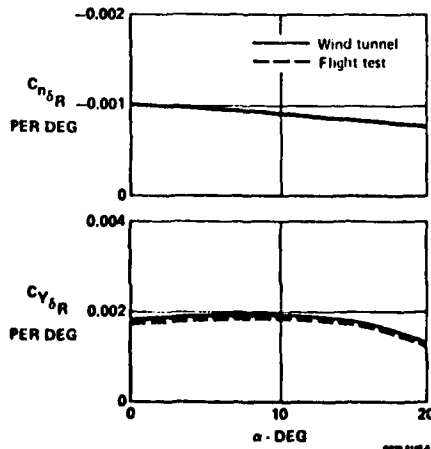


FIGURE 8
 RUDDER EFFECTIVENESS
 Mach 1.2

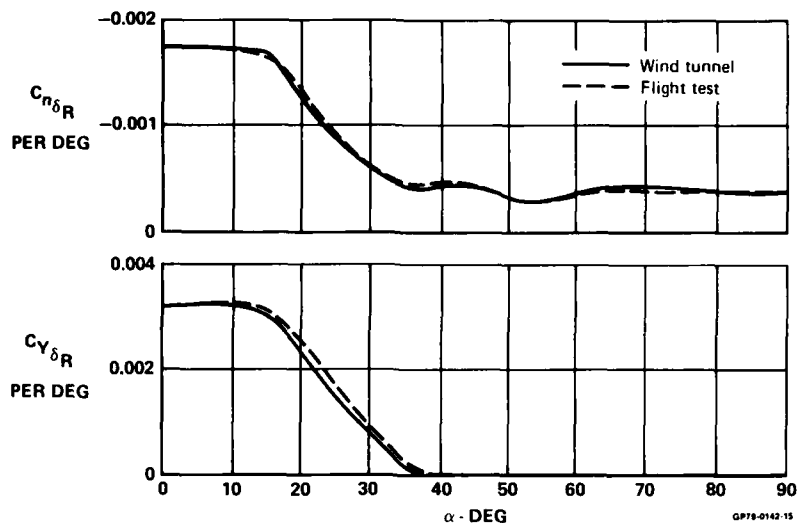


FIGURE 9
RUDDER EFFECTIVENESS
Low Speed

LATERAL CONTROL EFFECTIVENESS

The F-15 uses both ailerons and differential stabilator deflection for roll control. Wind tunnel test data were obtained for these surfaces differentially deflected both separately and in combination. It is of interest to note that for all conditions examined the total rolling moment and yawing moment produced by combined deflection is equal to the sum of the moments produced by separate deflection of the aileron and differential tail. The mechanical control system design is configured to produce differential aileron and differential stabilator deflection in the ratio of 40 to 12. Aileron hinge moment limiting will alter this relation at moderate to high dynamic pressure conditions. The CAS commands only differential stabilator deflection. For the purpose of this presentation, data are presented for the CAS OFF surface deflection ratio and where aileron hinge moment limiting is not a factor. Thus, the deflection ratio of 40 to 12 is assured. The correlations are shown as summed lateral control effectiveness derivatives. This is necessary because the aircraft control system was not modified to allow flight tests to determine the effectiveness of ailerons and differential tails separately. In addition, since differential tail effectiveness is a function of symmetrical stabilator deflection, the control effectiveness data are for differential deflections relative to a symmetrical deflection close to that required for longitudinal trim. At angles of attack in excess of the trim angle-of-attack capability of the aircraft, the lateral control effectiveness data apply for $\delta_H = -25^\circ$.

Figure 10 presents the data correlation in the linear range as a function of Mach number. It is seen that the agreement leaves little to be desired. The small differences in roll control effectiveness at subsonic and transonic speeds do not refute the hypothesis advanced to explain the lower than expected stabilator effectiveness. Reduced afterbody loads due to differential stabilator deflection have negligible effects on roll control because of the small moment arms involved. The data presented in Figure (11) show that the agreement in roll control is not materially changed as the effects of angle-of-attack are examined at $M = .90$. The flight data exhibit a modest increase in roll effectiveness and a reduction in the negative yawing moment derivative at $AOA = 25^\circ$ to 40° . This yawing moment is an "adverse" yawing moment. The differences in moments require less rudder deflection for roll coordination. However, the increment in rudder deflection required for coordination of rolls at 30° angle of attack is only 3° because of the special "roll-control washout" incorporated in the F-15 lateral control system at high angles of attack.

Roll control effectiveness data are presented as functions of angle of attack for $M = 1.2$ in Figure (12). Rolling moment coefficient due to roll control surface deflection derived from flight exhibits a modest increase. The flight test yawing moment derivative is slightly less positive at the higher angles-of-attack. The difference is not large enough to be of concern for the reasons given above.

The low speed high angle-of-attack lateral control derivatives are presented in Figure (13). The agreement at those conditions is considered very good for both the rolling moment derivative and the yawing moment derivative due to roll control deflection. The significant yawing moments and rolling moments available at very high angle-of-attack provide the excellent spin recovery characteristics demonstrated by the F-15.

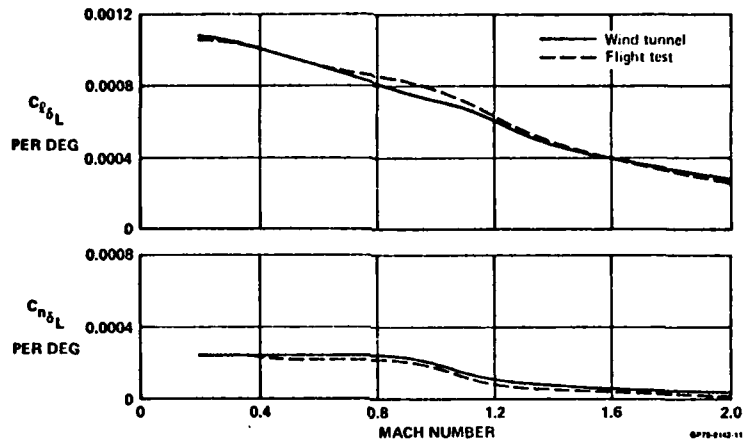


FIGURE 10
ROLL CONTROL EFFECTIVENESS
Low Angle-of-Attack

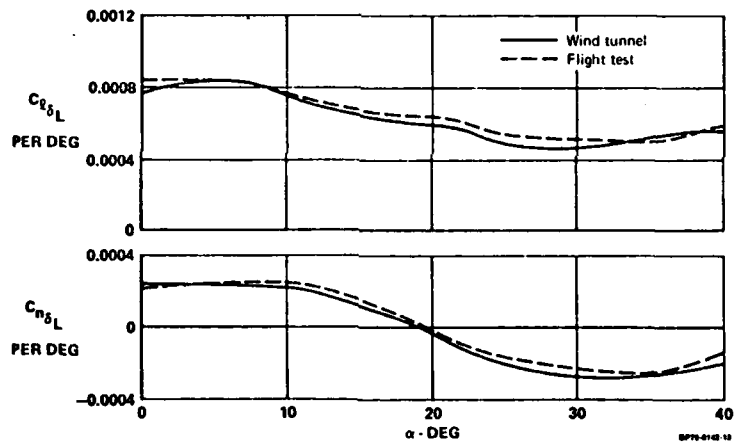


FIGURE 11
ROLL CONTROL EFFECTIVENESS
Mach 0.9

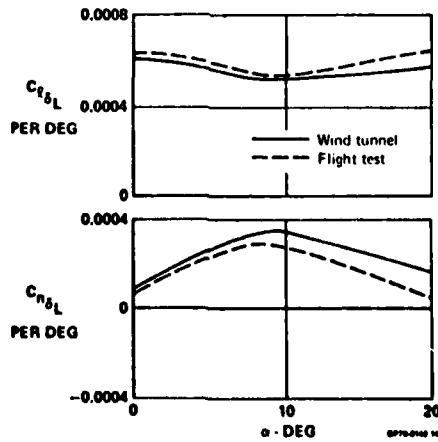


FIGURE 12
ROLL CONTROL EFFECTIVENESS
Mach 1.2

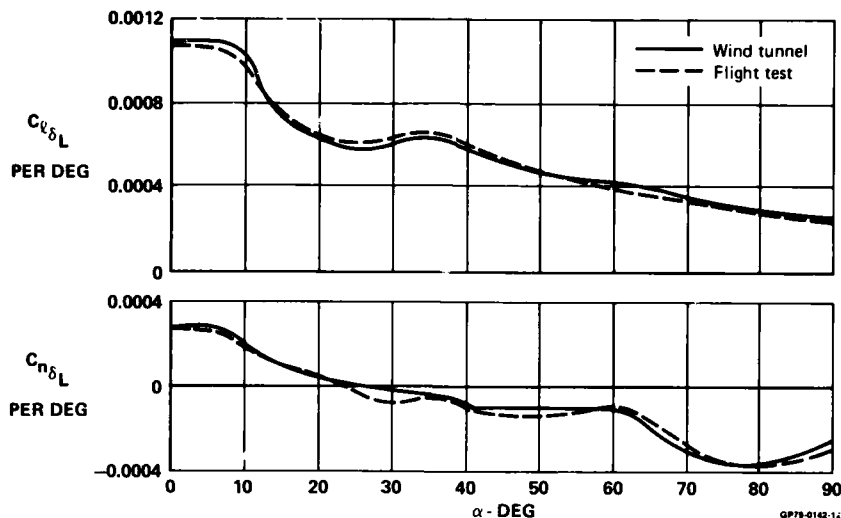


FIGURE 13
ROLL CONTROL EFFECTIVENESS
Low Speed

INLET RAMP EFFECTIVENESS

A unique feature of the F-15 propulsion system is the movable first ramp of the inlet. Some of the details of this feature are indicated in Figure (14). The movable ramp is relatively large and is far enough forward of the center-of-gravity to have a significant effect on longitudinal stability and control characteristics and trim drag. Therefore, definition of inlet ramp schedules required consideration of the impact on these areas as well as considerations of inlet pressure recovery and the flow distortion at the engine face. Optimization of the ramp schedule is discussed in detail in References (3) and (4). Since the optimization depended on the longitudinal control effectiveness of the inlet ramp, it is of interest to address the correlation of wind tunnel test data and flight test data in this paper.

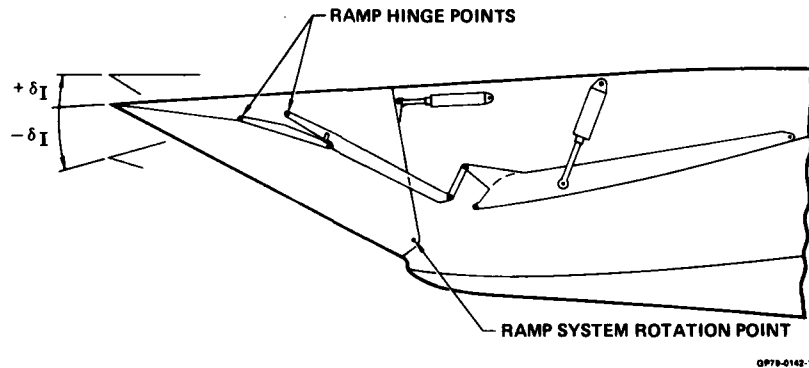


FIGURE 14
INLET CONFIGURATION

The inlet ramp total travel is limited to 15° and varies with angle of attack to maintain a fixed relation relative to the freestream velocity vector. The ramp angle at zero angle-of-attack is scheduled with Mach number and free stream total temperature to maximize excess thrust to the extent allowed by the other aforementioned considerations. For the deflections and angles of attack involved, no nonlinearities have been observed in either ground or flight tests. Thus, the longitudinal control effectiveness is adequately defined by the derivative $C_{m_{\delta I}}$. The correlation of this parameter is presented in Figure (15).

It is seen in Figure (15) that except near $M = 1.0$, the flight test and wind tunnel values are in good agreement. The differences at transonic speeds may be due to the effects of cowl deflection on the wing-body shock locations on the upper surface of the aircraft. These shock locations are difficult to duplicate in model tests at transonic speeds. Similar effects were noted in differences observed in the pitching moment for zero-lift (C_{m_0}) shown in Figure (16). The magnitude of the differences measured in these two parameters required revision of the ramp angle schedule with Mach number. The ramp angle schedules were revised to the extent shown in Figure (17). These revised

3-10 schedules were determined in an additional inlet ramp angle optimization study which used the flight test results and are not simply attempts to compensate for the differences in pitching moment characteristics, (C_{m_0} and $C_{m_{\delta I}}$).

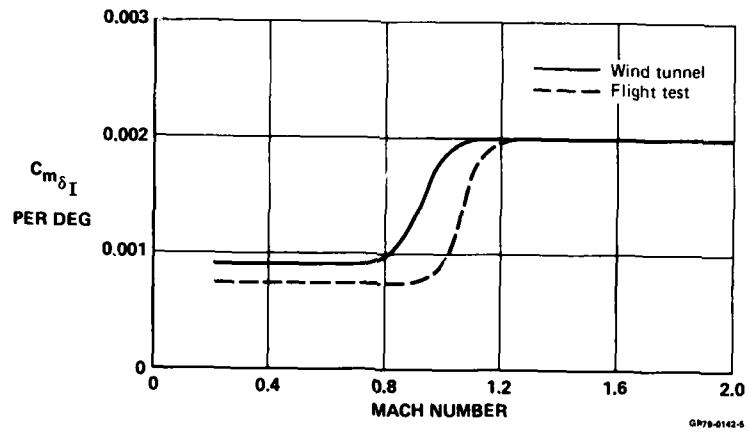


FIGURE 15
LONGITUDINAL CONTROL EFFECTIVENESS OF MOVABLE INLET RAMP

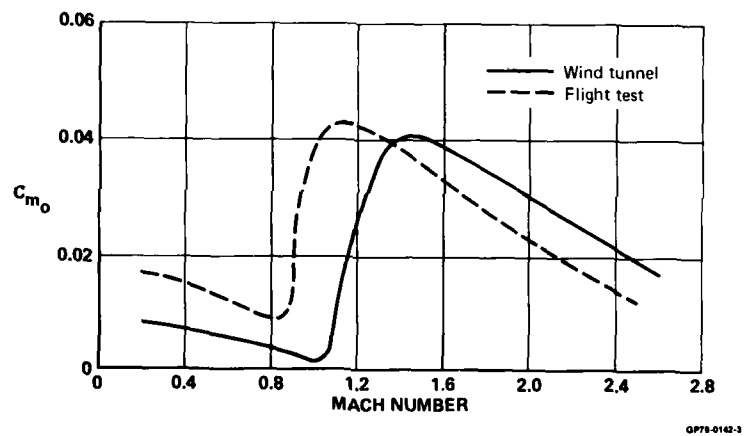


FIGURE 16
F-15 ZERO-LIFT PITCHING MOMENT COMPARISON

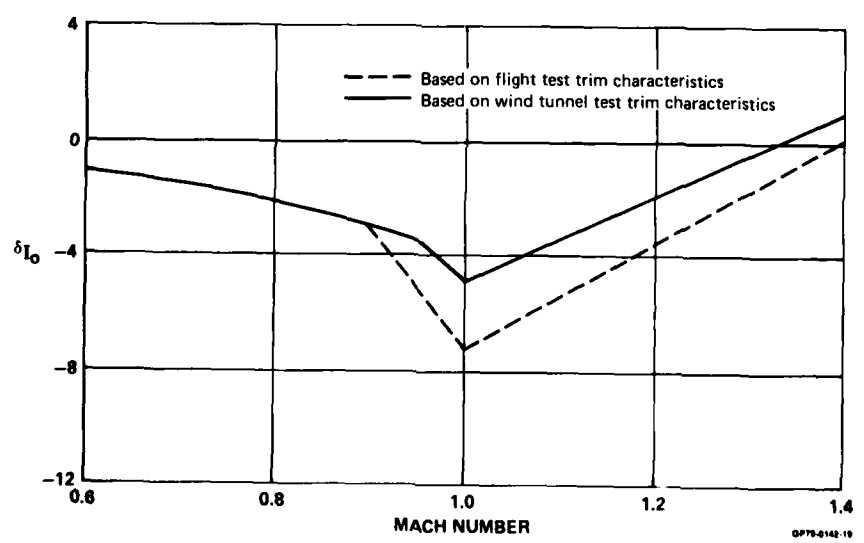


FIGURE 17
INLET RAMP SCHEDULE
 $\alpha = 0^\circ$

CONCLUSIONS

The correlation of control effectiveness determined for the F-15 in wind tunnel tests and flights indicates that wind tunnel tests yield data that are generally satisfactory for analyses, design and maneuver simulations. A major difference in the apparent stabilator control effectiveness was discovered at low angle-of-attack conditions. This difference is believed to be due to dynamic effects encountered in flight test when moderate stabilator deflections produce high angle-of-attack rates. At the pitch rates which are developed for high agility fighter aircraft, transient aerodynamic flow phenomena may be encountered which preclude good correlation with static aerodynamic characteristics measured in wind tunnels at "out-of-trim" conditions. The other area where significant differences were noted pertains to zero-lift pitching moments and inlet ramp effectiveness at transonic speeds. These latter differences are believed to be due to the inability to adequately simulate high Reynold's number flight conditions at transonic speeds in the facilities used in the subject program. The phenomenon is not new and has been attributed to differences in wing and fuselage pressure distributions due to differences in upper surface shock locations. This suggests that configurations employing control surfaces forward of the wing (canards) may experience similar differences. Care should be exercised in providing margins or design adaptability for adjustment of control laws should flight tests uncover such discrepancies.

REFERENCES

1. Abercrombie, J.M. and Havey, J.R., "F-15 Stability Derivatives, Mass and Inertia Characteristics, Part III Flexible Aerodynamic Coefficient and Stability Derivative Data", MDC Report A0502.
2. Agnew, J.W., "F/TF-15 Stability Derivatives Mass and Inertia Characteristics, Flight Test Data Basis, Part II: Aerodynamic Coefficients and Stability and Control Derivatives", MDC Report A4172.
3. Imfeld, William F., "The Development Program for the F-15 Inlet", AIAA 74-1061, presented at AIAA/SAE 10th Propulsion Conference, 21-23 October 1974.
4. Mello, John F., "Testing For Design - F-15 Powerplant Integration", AIAA 75-328, presented at the AIAA Eleventh Annual Meeting, 24-26 February 1975.

AD-A079 292 ADVISORY GROUP FOR AEROSPACE RESEARCH & DEV. NEUILLY-SUR-SEINE FR F/G 1/
AERODYNAMIC CHARACTERISTICS OF CONTROLS CONFERENCE PROCEEDINGS
SEP 79

UNCLASSIFIED

AGARD-CP-262

N/L

2 of 6

780228



117

SOME WIND TUNNEL MEASUREMENTS OF THE EFFECTIVENESS AT LOW SPEEDS OF COMBINED LIFT AND ROLL CONTROLS

by

D S Woodward, Royal Aircraft Establishment, Farnborough, Hants, GU14 6TD, UK

R F A Keating, C S Barnes, Royal Aircraft Establishment, Bedford, MK41 6AE, UK

21-1

SUMMARY

Using a half-model technique, measurements have been made, at low speeds, of the effectiveness of spoilers for direct lift or roll control, with high-lift devices deployed. The wing planform was representative of that of a transport aircraft outboard of the trailing-edge crank. Results are presented which show that appropriate venting beneath the leading edge of hinged-plate spoilers, together with venting through the flap shroud, achieved acceptably linear spoiler characteristics. Similarly, linear characteristics were obtained for a vented spoiler formed by moving the rear of the flap shroud. No reversal of spoiler effectiveness was found at any test condition within the normal operating range of incidence.

In the same way, measurements have also been made of the maximum lift and roll performance of a typical "swing wing" fighter aircraft, for which the design of the leading- and trailing-edge controls has been totally determined by the need to maximise the manoeuvrability at high speed. The maximum lift performance is compared with that obtainable from conventional slats and slotted flaps. Somewhat surprisingly, it is found that adequate rolling moments can be obtained by using full-span plain flaps differentially about a basic drooped position of 30° .

SYMBOLS

A	Aspect ratio
b	Wing span
C_D	Drag coefficient
C_{D0}	Drag coefficient at zero lift
$C_{D_{min}}$	Minimum point on drag polar
C_L	Lift coefficient
\hat{C}_L	Lift coefficient at $C_{D_{min}}$
C_{L0}	Lift coefficient at zero incidence
C_{L_α}	Slope of the tangent to the curve of $\Delta C_L v \alpha$ at $\alpha = \alpha'$ for $\delta = \delta'$, see Fig 19, per degree
$C_{L_{\delta 0}}$	Initial rate of change of ΔC_L with δ at $\alpha = \alpha'$, see Fig 19, per degree
$C_{L_{\delta max}}$	Maximum rate of change of ΔC_L with δ at $\alpha = \alpha'$, see Fig 19, per degree
$C_{L_{\delta tan}}$	Slope of the tangent from the origin to the curve of $\Delta C_L v \delta$ at $\alpha = \alpha'$, per degree, see Fig 19
C_Z	Normal force coefficient
$C_{M_{c/4}}$	Pitching moment coefficient about the $\frac{1}{4}$ -chord point of the mean aerodynamic chord (based on \bar{c})
\bar{c}	Aerodynamic mean chord
\bar{c}	Standard mean chord
c	Local chord
g	Acceleration due to gravity
k	Lift dependent drag factor
l_v	Rolling moment due to sideslip derivative
p	Roll rate (rad/s)
q	Kinetic pressure
S	Wing area
s	Wing semispan

U_0	Free stream velocity in wind tunnel test
V	Forward velocity of aircraft
x	Distance in free stream direction
y	Distance in spanwise direction
α	Incidence, degrees
α'	A particular incidence, see Fig 19
β	Sideslip angle, degrees
ΔC_D	Incremental drag coefficient due to a spoiler
ΔC_L	Incremental lift coefficient due to a spoiler
$\Delta C_{L\delta', \alpha'}$	Lift increment due to a spoiler deflected δ' at $\alpha = \alpha'$, see Fig 19
C_l	Rolling moment coefficient
ΔC_l	Incremental rolling moment coefficient (or root bending moment coefficient) due to a spoiler
ΔC_m	Incremental pitching moment coefficient due to a spoiler (based on \bar{c})
C_n	Yawing moment coefficient
ΔC_z	Incremental normal force coefficient due to a spoiler
ΔL	Incremental lift due to a spoiler
$\Delta \mathcal{L}$	Incremental rolling moment (or root bending moment) due to a spoiler
δ	Spoiler deflection angle, degrees
δ'	A particular spoiler deflection angle, see Fig 19
δ_D	Spoiler dead space, see Fig 19, degrees
ξ	Aileron angle, degrees, defined as $\frac{\text{angle of starboard flap} - \text{angle of port flap}}{2}$
ζ	Rudder angle, degrees

1 INTRODUCTION

This paper describes two separate investigations of controls - in the first part of the paper an investigation of spoiler characteristics in relation to civil aircraft, and in the second part of the paper the characteristics of plain leading- and trailing-edge controls in relation to a swing-wing combat aircraft in the low speed, minimum sweep, configuration. The linking themes lie in the possible use of both types of control as a combined lift and roll control, and in the similar test arrangements used in the two investigations - half-models mounted on an underfloor balance with the floor of the tunnel acting as the reflection plane. However, the motivation for the investigations and the analyses used are different in each case and so the investigations are reported separately.

The attractions of half-models for wind tunnel testing include:

- a. increased Reynolds number
- b. larger scale, making it easier to represent detailed features of full-scale aircraft
- c. lower cost, because it is necessary to manufacture only one set of spoilers, flaps, setting brackets etc
- d. a wind tunnel mounting which is free from the interference of mounting struts, stings, etc.

Furthermore, an indication of the performance of a configuration with asymmetric deflection of either spoilers or trailing edge controls can be obtained by the suitable algebraic addition of two separate tests on the half-model. For instance Fig 1 shows how, if we wish to obtain the rolling and yawing moments for the combat aircraft with, say, five degrees of aileron in combination with ten degrees of flap, these can be estimated from the combination of results on a half model with:

- a. 5° flap and
- b. 15° flap

The same technique can clearly be applied to the estimation of the yawing and rolling moments produced by asymmetric operation of spoilers. But the word "estimated" is used advisedly because the distribution of spanwise loading implied by this combination of half-model results, has a discontinuity at the centre line, as shown by the full line in the diagram at the foot of Fig 1, whereas the actual asymmetric configuration has a spanwise loading like that shown by the dashed line in Fig 1.

Swanson and Toll²⁰ have calculated the necessary corrections for this effect, for wings with ailerons. The correction results in an appreciable reduction in rolling moment, typically by as much as 12%, and an increment in adverse yawing moment. The results for the swing-wing fighter, presented in Section 3, have been corrected in this way. The results of the spoiler investigation in Section 2 have not, however, because the primary interest in that investigation was to identify aspects of spoiler design which led to linear characteristics rather than to examine the control power available.

2 SPOILER CONTROLS ON CIVIL AIRCRAFT

2.1 Introduction

The use of spoilers on the wing upper surface to supplement the control available from the conventional ailerons of transport aircraft at low speeds, is now well established. Their use enables outboard ailerons to be sized for adequate lateral control power at higher speeds, whilst leaving the inboard wing trailing edge free for the installation of high lift devices. For transport aircraft then, spoilers will normally be operated when high lift devices are deployed. Proposals for their incorporation in direct-lift-control (DLC) systems have led to renewed interest in spoiler characteristics but there is a lack of comprehensive published modern data. Many of the earlier spoiler data are summarised in references 1 and 2.

It was considered in the UK during the late 1960's that further information was required to assist in the design of spoiler installations for future swept-wing transport aircraft. Two particular problem areas were identified.

i There are frequent reported occurrences in wind tunnel tests of reversals of spoiler effectiveness (ie a lift increase) at low spoiler deflections. The situations in which such reversals occur are not at all clear, particularly as one assumes some optimisation of high-lift device design for maximum lift has already been achieved. Unpublished British work indicated that reversals in lift of the order of $\Delta C_L = +0.01$ at small spoiler deflections might be expected from the experimental configurations reported here. In the event, no control reversals were found within the usable range of incidence, as will be described later.

ii Non-linear response of lift and rolling moment increments to spoiler deflections are invariably reported. Full-scale data are limited, but Ingle has shown large discrepancies in linearity between flight and wind tunnel results for a simple design of spoiler on the BAC-111 aircraft³.

A theoretical approach to the design problem did not appear worthwhile in view of the complex flows associated with spoilers ahead of high-lift devices. Accordingly an experimental programme was decided upon. Even then the programme had to be carefully aimed because of the wide range of possible variables - spoiler type and size, chordwise position on the wing, spanwise position and extent, the employment of venting through or beneath the spoiler, as well, of course, as the configuration of the basic wing and high lift devices. It was felt that the structural design of the wing tends to define the chordwise position of spoilers and that with the information already available it was not too difficult to decide upon spoiler size. However, it was clear that spoiler configurations which might be aerodynamically acceptable could be completely unacceptable on structural grounds. In parallel with aerodynamic considerations, the structural implications of various spoiler designs and positions were considered and were allowed to influence the proposed programme.

As a result of these considerations it was decided to keep spoiler chord, span, chordwise position and spanwise position constant, and to concentrate on examining the effects of changes in spoiler deflection angle and of variations of gaps and vents which previous experience had shown to be important in relation to control reversal and linearity.

2.2 Experimental Details

2.2.1 Basic Wing

The configuration, Figs 2 to 5 and Table 1, was chosen to be representative of the outboard wing of a possible transport aircraft project. It was of aspect ratio 7 with $30^\circ \frac{1}{2}$ -chord sweep. The high lift devices, which were representative of current practice, consisted of a full span leading-edge slat and a part-span single-slotted tabbed flap extending from the body side to 80% semispan. The following flap settings were tested:

Flap Angle	Tab Angle (Relative to Flap)	Tab Design
10°	0°	Plain hinge
20°	10°	Plain hinge
40°	30°	Slotted

The slat angle of 28° , and the slat and flap gaps were optimised experimentally to achieve a repeatable stalling behaviour with a separation moving forward from the trailing edge of the shroud, rather than a sudden slat stall, so that the effects of spoiler induced separations could be appreciated. The maximum lift achieved was not compromised by this criterion although a higher lift at zero incidence and a better drag polar could have been achieved with a different slat angle. The final settings used are defined in Fig 5 and were:

slat, 2% chord forward of tangential contact with main wing,

flap, zero lap and a gap of $1\frac{1}{2}\%$ chord,

tab, zero lap and a gap of 0.8% chord at 40° flap only.

A tip aileron of 20% semispan was mounted outboard of the flap but tests with this deflected are not reported here.

The model had a wing of 2.13 m semispan mounted in the mid-wing position on a semicircular section half-body. The latter not only made the configuration more representative but also reduced the effects of the tunnel floor boundary layer and of leakage through the 6 mm clearance between body and floor. All model joints were sealed. The model was carried on a mechanical balance measuring normal force, axial force, pitching moment and root bending moment. The balance in turn was mounted underneath the floor turntable, rotation of which allowed the incidence to be varied. The tests were made in the 4 m x 2.7 m (13 ft x 9 ft) low-speed tunnel at RAE Bedford.

2.2.2 The Spoilers

The spoilers were all of constant spanwise extent occupying the region between 40% and 80% semispan. Two basic types were studied.

The first consisted of hinged plate spoilers deflected up from the upper surface of the flap shroud, Fig 5. The basic spoiler of this type, to be referred to as a plain spoiler, was of constant percentage chord, ie 12% of local wing chord. It could be tested with zero gap beneath its upstream edge, in which case its hinge line was at 63% chord, or with a range of constant percentage chord gaps (measured in the plane of the spoiler, Fig 3). In the latter cases it was convenient to maintain the upstream edge of the spoiler at 63% chord at zero deflection so that the hinge line moved progressively upstream as gap increased. The baseline spoiler is shown with a 3% chord gap in Fig 6. Three other more complicated hinged plate spoilers - sawtooth, perforated and castellated - are also shown in Fig 6; these had the same solid area as the baseline spoiler and a maximum chord of 15% local wing chord. They were designed for investigating the effect of alternative means of venting the spoiler itself. Each of the flat plate spoilers could be tested in conjunction with a wide variety of additional vents through the flap shroud. Details of such venting are shown in Figs 7 and 8. It could consist either of a constant percentage chord slot extending over the full span of the spoiler or of a number of discrete holes.

The second type of spoiler is referred to here as a moving shroud spoiler and is illustrated in Fig 7. In this case the rear 12% local wing chord of the flap shroud could be deflected upwards to act on the flow over the upper surface of the shroud. As in the case of the hinged plate spoilers it was possible to operate the moving shroud spoiler with a gap beneath its upstream edge; the hinge line then moves upstream from its basic position at 75% local chord, by an amount equal to the length of the gap. When used with a gap the forward edge of the spoiler was bevelled as shown in Fig 7.

2.3 Test Details and Data Reduction

2.3.1 Tests Made

Great care was taken to eliminate possible sources of misleading data, particularly in relation to the measurement of the small force increments due to small spoiler deflections. To ensure reliable difference data between the datum case with the spoiler undeflected and configurations with the control deflected it was found necessary to do a datum run for each spoiler configuration. Small differences, for instance, between the datum plain shroud and the various shrouds having different amounts of venting, but with the vents sealed, could lead to datum errors greater than the smallest measured lift increment. Similarly, if the shroud vents were not completely sealed in the datum case, or if an ungapped spoiler was not sealed to the wing surface, then significant errors could occur. It is worth noting at this stage that when such precautions were taken no reversals of spoiler lift increments were found in the normal working incidence range ie for all spoiler configurations and deflections the lift increments were always in the expected negative sense.

The bulk of the tests were made at 60 m/s, equivalent to a Reynolds number of 2.5×10^6 based on standard mean chord, and are summarised in Table 2. A limited number of tests was made at lower speed. Transition fixing was achieved by spanwise bands of ballotini approximately 5% chord of each component in width, disposed under the leading edge but avoiding the leading edge radius. Selection of the optimum diameter of ballotini was judged by the achievement of a smooth repeatable lift curve, and the absence of any leading edge bubbles, at a speed of 60 m/s. The datum case (spoiler undeflected) is relatively sensitive to Reynolds number and this is in part attributed to the use of the minimum diameter of ballotini which was effective at 60 m/s.

At 60 m/s the overall repeatability of data obtained from different nominally identical configurations after all precautions had been taken was equivalent to an error in measured lift coefficient of 0.00%. The smallest measured lift increment due to spoiler deflection was of the order of 5 times greater than this.

2.3.2 Data Reduction

The data were reduced to conventional coefficient form, the pitching moment datum, Fig 4, being chosen at 46.9% of mean aerodynamic chord. 4-5

The incremental root bending moment coefficient, ΔC_m , due to spoiler operation (measured about the notional aircraft centreline) is defined as $\Delta \mathcal{M}/4qSs$, where $\Delta \mathcal{M}$ is the measured increment in the moment, S is the area of the half-model and s is its span. The coefficient thus gives the rolling effectiveness of a spoiler on one wing of a complete aircraft as is appropriate for roll control. Since the coefficients of incremental lift, ΔC_L , drag, ΔC_D , and pitching moment, ΔC_m , are more relevant to direct lift control than roll control, they are defined relative to the effectiveness of symmetric operation of spoilers on both wings of a complete aircraft, eg $\Delta C_L = \Delta L/qS$ where ΔL is the measured increment due to a single spoiler.

For this wing, tunnel constraint requires a correction of about 1° of incidence per unit C_L . Since the lift is different at the same nominal incidence on the two separate test runs required to measure spoiler effectiveness, the correction required for tunnel constraint is also different. The corrected results obtained (using the procedure described in ref 4) were interpolated using a Lagrangian formula (non-smoothing) to provide differences between forces at a given corrected incidence. Such derived data are plotted with no data points shown. Conventional corrections were applied for solid and wake blockage.

2.4 Results For The Basic Wing

The characteristics of the basic wing and high-lift system are reasonably typical of those of transport aircraft and are shown in Figs 9 to 11. The lift curves for all flap angles, Fig 9, are seen to be non-linear at low incidence. This is because the relatively high slat angle of 28° , chosen to ensure that the slat did not stall before the main wing, prevents the slat from working efficiently at low incidence. At higher incidence the lift curve is linear until about 5° below the lift break; the progressive reduction in lift curve slope prior to the lift break is due to separated flow regions growing from the rear over both the undeflected aileron and the flap shroud. This is illustrated in the sketch for a flap deflection of 40° at $\alpha = 18^\circ$ included in Fig 9. As a consequence, after the lift break the loss of lift is progressive with no abrupt drop, although there is strong buffeting.

The drag polars are shown in Fig 10 and the pitching moment characteristics in Fig 11.

In all three figures, data are presented for the plain shroud, with no vents, and for a corresponding vented shroud, but with the vents sealed. As noted already in Section 3.2 the small differences in measured forces and moments for these two cases are significant when determining the increments due to spoilers and care must be taken to use the correct datum. As will be shown later, the effect of reducing Reynolds number is greater on the basic wing than on the wing with spoiler deployed so that spoiler incremental performance appears less linear as Reynolds number decreases. Again it is essential to use the correct datum run.

2.5 Spoiler Lift Characteristics

The most demanding situation for spoiler controls, when used either for roll control or for DLC, is on the landing approach. Accordingly the majority of the results presented in this section will be associated with a 40° flap deflection, typical of that used on the approach. Furthermore, the results will all refer to the increments achieved by symmetrical operation of spoilers on both wings. It is worth noting at this stage that, as the model is representative of the outboard wing panels of a transport aircraft, the spoiler span is relatively large in relation to the wing-span; incremental coefficients non-dimensionalised on model wing area will, therefore, also be relatively large.

2.5.1 Hinged Flat Spoilers

Fig 12 shows the lift curves for a plain hinged-plate spoiler with $\approx 1\%$ leading edge gap and with 100% venting through the shroud; the flap deflection is 40° . These results are typical of all measurements throughout the series of tests. There is a progressive reduction in lift curve slope with increasing spoiler deflection. Similarly, the stall becomes progressively less severe with the lift break occurring at a higher incidence. Beyond the lift break the curves tend to the same asymptote as the spoilers become blanked by the separation associated with the stall. Clearly, such characteristics are not suitable for control beyond the stall.

The effects of various parameters are discussed below. It must be stressed that the aim is only to present a selection of reasonably typical data. The main body of data is too large for detailed presentation in a paper of this size.

a. Reynolds Number

A limited investigation of the effect of Reynolds number was made. Fig 13 shows, for speed of 15, 30 and 60 m/s (Reynolds number = $0.6 \rightarrow 2.5 \times 10^6$) the lift coefficient plotted versus spoiler angle at an interpolated constant incidence of 10° for the perforated spoiler with no gap. The effect of Reynolds number is greatest for the basic configuration with spoiler undeflected, and decreases reasonably progressively with increasing spoiler deflection. Data for a plain ungapped spoiler, not shown, suggest that the sensitivity to Reynolds number continues to decrease up to deflection angles of 50° . The data of Fig 13 are replotted in Fig 14 in the form of spoiler lift increments versus spoiler deflection. The apparent sensitivity to Reynolds number is now reversed from that shown in Fig 13, because the datum value for the basic wing is fairly sensitive to Reynolds number, and this value must be subtracted to obtain the increment. The sensitivity of the datum case to Reynolds number demonstrates the difficulty of correlating data obtained at different Reynolds numbers, spoiler deflected, particularly, for instance, between tunnel and flight, and may explain some of the discrepancies shown in ref 3.

The lower figure, Fig 14b, is plotted to an enlarged scale to demonstrate the absence of reversal in spoiler lift increment at low deflection angles anywhere in the Reynolds number range, providing that a datum value appropriate to the correct Reynolds number is subtracted.

b. Spoiler Gap

The effect of opening up a gap beneath a plain spoiler is shown in Fig 15. The flap is deflected 40° and the shroud is unvented. At a constant spoiler deflection, $\delta = 20^\circ$, Fig 15a, it is seen that the relationship between lift increment and incidence below the stall is highly non-linear when there is no gap. Spoiler effectiveness increases markedly with increasing incidence. Opening up a gap of $\frac{3}{8}$ local wing chord (by moving the spoiler hinge line $\frac{3}{8}$ forward) reduces the variation of ΔC_L with incidence and increases the effectiveness significantly at all incidences below the stall. However, it should be borne in mind that, since spoiler chord is kept constant at 12% local wing chord, increasing gap also increases spoiler height. The effect of increasing the gap to 6% chord is not advantageous; in spite of the increased spoiler height above the wing the maximum increment falls and the linearity is not significantly improved. This loss in effectiveness is probably caused because the spoiler is now too remote from the wing either to effectively spoil the flow locally, or to adequately adjust the circulation about the wing.

Above the stall, spoiler effectiveness falls rapidly at all gap settings. Data obtained above the stall are difficult to interpret since the balance readings fluctuate and the Lagrangian interpolation tends to exaggerate any deviations. Certainly the effectiveness falls to a very low mean value (see also Fig 1) but whether it becomes zero or reverses is uncertain.

At a constant incidence, $\alpha = 10^\circ$, Fig 15b, the effect of gap is to reduce the initial 'dead space' in spoiler effectiveness significantly, and to increase the derivative $\frac{d(\Delta C_L)}{d\delta}$ slightly. Again the 6% gap is clearly too large.

c. Venting Through The Shroud

The effect of venting through the shroud behind the plain spoiler with a $\frac{3}{8}$ gap is illustrated in Fig 16 for the configuration with 40° flap deflection. Venting is achieved by constant percentage chord slots extending over the full spoiler span. At a constant spoiler deflection of 20° , with 100% venting (a vent equal in area to that of the spoiler) there is a significant improvement in ΔC_L varying from about -0.05 at $\alpha = 5^\circ$ to about -0.035 at $\alpha = 18^\circ$ relative to the unvented condition, Fig 16a. Results for intermediate vent areas lie progressively between these extremes at low incidence, (note that data for $6\frac{1}{2}\%$ and $12\frac{1}{2}\%$ venting have been omitted for clarity) but at higher incidences 50% and 25% venting yield significantly larger lift increments than 100% venting.

At a constant incidence of 10° , Fig 16b, it is seen that the effect of venting is to improve the linearity of the derivative $\frac{d(\Delta C_L)}{d\delta}$ over the range of spoiler deflection and that the improvement in linearity is reasonably progressive with increasing vent area. The effects of $12\frac{1}{2}\%$ and 25% venting are virtually identical and only fall below those achievable with 100% venting at spoiler deflections well in excess of 20° .

Although spanwise venting behind the spoiler is clearly favourable aerodynamically, such a configuration is not structurally acceptable on a real aircraft. Consequently tests were made with the discrete vents shown in Fig 8 in an attempt to establish configurations which are acceptable both structurally and aerodynamically. The results are summarised in Fig 17 again for a plain spoiler with a $\frac{3}{8}$ gap. The Type B, C and D vents each total $12\frac{1}{2}\%$ of spoiler area but with different disposition of the holes; in general these vents perform less well than the 100% spanwise slot, data for which are presented in Fig 17, for comparison. Of the three types, D, which has the widest distribution of vent area performs best. However, a fourth type of discrete venting, Type A, having 30% vented area spread over 27 discrete holes, Fig 8, is seen to perform as well or better than even the 100% spanwise slot. In particular, the characteristics of the spoiler ahead of the Type D vents is relatively linear at small spoiler angles.

d. Other Hinged-Plate Spoilers

The major part of this section has been concerned with plain spoilers. As shown in Fig 6, perforated, sawtooth, and castellated spoilers having the same solid area as the plain spoiler were also tested. These spoilers were found to offer no aerodynamic advantage, in either linearity or overall effectiveness, over the plain spoiler with a $\frac{3}{8}$ gap at a flap angle of 40° , and no results are therefore presented here (except that results obtained with the perforated spoiler were used earlier to illustrate the effect of Reynolds number). Some limited data are included in later summary figures, Fig 20, 21 and 22, where it is seen that at a flap angle of 20° the performance of these spoilers with more complicated shapes was relatively better than at 40° .

2.3.2 Moving Shroud Spoilers

The characteristics of a 12% chord spoiler are illustrated in Fig 18 for three hinge positions. This type of spoiler forms the trailing edge of the flap shroud when undeflected, Fig 7, and is used, for example, on the A300 Airbus. The performance of the spoiler is seen to be very satisfactory, being almost independent of incidence below the stall and exhibiting no dead space at small deflections. Unlike the hinged plate spoilers, the use of a 6% forward hinge to produce a 6% gap produces a better performance than that with a $\frac{3}{8}$ gap, although the improvement is much less than that achieved by the $\frac{3}{8}$ gap relative to zero gap.

2.5.3 Summary of Lift Increments

So far we have presented typical data chosen to illustrate particular aspects of spoiler lifting effectiveness. A method is now suggested whereby the performance of a spoiler can be described in terms of a limited number of numerical "derivatives" so that a summary of spoiler performance can be easily tabulated. Referring to Fig 19, six parameters are defined:

- 41-7
- $C_{L_{\delta_0}}$ the initial rate of change of ΔC_L with δ at a chosen incidence α' , per degree
 - $C_{L_{\delta_{max}}}$ the maximum rate of change of ΔC_L with δ at $\alpha = \alpha'$, per degree
 - $C_{L_{\delta_{tan}}}$ the slope of the tangent from the origin to the curve of $\Delta C_L \vee \delta$ at $\alpha = \alpha'$, per degree
 - $C_{L_{\alpha}}$ the slope of the tangent to the curve of $\Delta C_L \vee \alpha$ at $\alpha = \alpha'$ for a chosen spoiler deflection δ' , per degree
 - δ_D the "dead space" between the origin and the intersection of the line defining $C_{L_{\delta_{max}}}$ with the δ axis, degrees
 - $\Delta C_{L_{\delta', \alpha'}}$ the lift increment due to a spoiler deflected δ' at $\alpha = \alpha'$.

Expressed in these terms a spoiler with completely linear characteristics would have

$$\delta_D = 0, C_{L_{\delta_{max}}} = C_{L_{\delta_{tan}}}, C_{L_{\alpha}} = 0 \text{ and } \Delta C_{L_{\alpha'}} = \delta' C_{L_{\delta_{tan}}}$$

Assuming that the elimination of dead space and the achievement of reasonable linearity is the aim for a practical spoiler installation, then the extent to which the above values are achieved defines how closely reality has approached the ideal. In fact it is improbable that $C_{L_{\alpha}} = 0$, ie no change of spoiler effectiveness with incidence, is the optimum value since an increase in effectiveness as incidence increases, or speed falls, could be beneficial (providing the increase is steady rather than sudden). The values of the derivatives can be tabulated for as many values of α' and δ' as is thought necessary but for comparative purposes a single value of each is probably sufficient.

Since the work reported here was aimed at achieving acceptable linearity and freedom from dead space within reasonable structural constraints, while keeping constant the major spoiler dimensions (chord and spanwise extent) it is not within the scope of the results to ascribe desirable magnitudes to the three $C_{L_{\delta}}$ derivatives (other than to point out the desirability of their equality). However, the values of the relevant parameters are tabulated in Table 2 where $\alpha' = 10^\circ$ and $\delta' = 20^\circ$, the chosen "mid-range" values which have been used earlier in this paper. These tabulations cover a wider range of configurations and flap angles than the results discussed so far and also include details for all flap angles.

The spoiler data have been further condensed in Fig 20 to illustrate the trend of spoiler effectiveness with increasing gap and shroud venting. The combined parameter $(C_{L_{\delta_{max}}} - C_{L_{\delta_0}}) / C_{L_{\delta_{max}}}$ is plotted versus the dead space δ_D . On this type of presentation, a linear spoiler, which has $C_{L_{\delta_{max}}} = C_{L_{\delta_0}}$ and $\delta_D = 0$, lies at the origin. Hence the proximity to the origin of the point referring $C_{L_{\delta_{max}}}$ to a particular spoiler configuration is a measure of the linearity of that configuration. It is not, of course, a measure of the effectiveness of a particular spoiler.

Fig 20a presents data for a flap angle of 40° and it confirms what was said earlier ie that addition of a gap and of venting through the shroud improve the linearity of plain hinged-plate spoilers significantly, but that gapped moving shroud spoilers appear as the most promising configuration. Fig 20b presents data for a flap angle of 20° , not previously discussed, and it is seen that moving shroud spoilers are again very promising. The more complicated hinged-plate spoilers were not particularly successful at a flap angle of 40° but are more so at 20° flap, and in fact the perforated spoiler with zero gap plots at the origin, as does the rather impractical case of a moving shroud spoiler with a large - 12% of wing chord - gap.

The final two figures in this section, Figs 21 and 22, are included for completeness and show all the data so far discussed collected together in graphical form to give a visual comparison of ΔC_L versus δ at $\alpha = 10^\circ$. Fig 21 refers to the flap angle of 40° and Fig 22 to that of 20° .

2.6 Spoiler Drag Characteristics

The drag due to spoilers is complicated because, at constant incidence, spoiler deflection in general causes an increase in profile drag but a reduction in lift dependent drag because of the loss of lift. Total drag is plotted in Fig 23 against incidence for a plain hinged-plate spoiler with a 3% gap plus 100% shroud venting. The flap angle is 40° . Experimental points are omitted for clarity and the results are typical of those for other spoilers.

The curves cross in a staggered fashion as the drag with spoiler deflected increases at low incidence but decreases at high incidence relative to that with the spoiler undeflected. However, when plotted in polar form against C_L , Fig 24, it is seen that at constant lift there is always an increase in drag. The asymptotic nature of the total drag beyond the stall is equivalent to that noted earlier for lift.

Because of the camber introduced by deflection of the high-lift devices and of the effective spanwise twist introduced by the part-span nature of the flaps, the minimum drag $C_{D_{min}}$ occurs at positive lift rather than at $C_L = 0$. At $C_L = 0$ the individual components of the high lift system are all in general lifting (either in a positive or negative sense) and hence there is still a finite induced drag. Thus even at $C_{D_{min}}$ there are always components of induced drag present. Consequently the plots of C_D versus C_L^2 in

Fig 25, for the same spoiler as above, are not quite linear. In such circumstances ref 6 suggests that the drag can be expressed as

$$C_D = C_{D_{\min}} + K (C_L - \hat{C}_L)^2 / \pi A$$

where A is the aspect ratio. The quantities $C_{D_{\min}}$ and \hat{C}_L are related to the lift due to camber and twist, and the factor K is dependent only on the lift distribution and the aspect ratio.

Using this relation the curves of Fig 25 can be re-plotted in Fig 26. The values of \hat{C}_L were obtained by trial and error since it was not practicable to extrapolate the drag curve back to the hypothetical value of $C_{D_{\min}}$ at $C_L = \hat{C}_L$. The values obtained for \hat{C}_L , $C_{D_{\min}}$ and K are tabulated on the figure where it is seen that:

- i \hat{C}_L decreases with increasing spoiler deflection (ie with decreasing C_L at $\alpha = 0$ as predicted by ref⁵).
- ii $C_{D_{\min}}$ increases with increasing spoiler deflection.
- iii K increases with increasing spoiler deflection because the limited span of the spoiler leads to an increasingly poor spanwise loading distribution as the lift decrement due to the spoiler becomes numerically larger.

$C_{D_{\min}}$ can be considered as a sum of three terms:

- i A basic profile drag, spoiler undeflected, consisting of the sum of the profile drags of the components of the wing and high-lift system.
- ii The profile drag component associated with the width of the separated wake which, following Betz⁶ and Hoerner⁷, is of the order of $\frac{1}{4}$ of the change of lift caused by the wake.
- iii The minimum induced drag⁵ of the configuration.

It is worth noting that the induced drag factor for the basic wing, spoiler undeflected is obtained as 1.29 from the more complete approach shown in Fig 26 whereas absurd values lower than unity can be deduced from the simpler presentation of Fig 25.

2.7 Spoiler Moment Characteristics

Although the title of this report refers to combined lift and roll controls we have chosen to concentrate on the lifting characteristics rather than the rolling characteristics because the latter follow the behaviour of the former so closely. Pitching moment presents a rather more complicated picture about which only limited conclusions can be drawn in the absence of data on the change in downwash at the tail plane caused by spoiler operation. A brief discussion of both moments is appropriate.

2.7.1 Rolling Characteristics

As noted above, plots of incremental rolling moment and lift coefficients are very similar in character. We have chosen, therefore, to present limited data in the form of spanwise centre of pressure (CP) only. Such data, when used in conjunction with the lifting characteristics which have already been presented, can be used to derive rolling moments.

Fig 27a shows the position of the spanwise CP as a function of incidence for the basic wing and for the wing with the plain spoiler with 3% gap and 100% shroud venting. The spoiler deflection is 20° and the flap angle is 40°. The incremental spanwise CP position, or centre of action, associated with the spoiler is included. For the basic wing the spanwise CP is at 44% semispan, almost constant up to the stall. Spoiler deflection moves the CP inboard since the middle of the span is then more lightly loaded. For the case shown, the incremental CP is at about 55% semispan (+ about 2% below the stall); this is slightly inboard of the centre of the spoiler span, at 60% semispan, but is close to the spanwise position of the centre of area of the spoiler. The position of the incremental CP is included in Table 2 and is seen to vary only slightly over the whole range of configurations listed, including three flap angles. A simple approach to obtaining rolling moments from known lift increments would therefore seem to be justified.

2.7.2 Pitching Characteristics

Fig 27b presents pitching moment data expressed in terms of centre of pressure position in a similar manner to that used for illustrating rolling moment characteristics. The wing and spoiler configuration is also the same. Because of the effective camber (and consequent pitching moment at zero lift) associated with the high-lift devices there is now a large chordwise movement, with incidence, of the CP of the basic wing (although the aerodynamic centre of the basic wing is approximately constant at 35% c forward of the reference point (Fig 11) and 2% c forward of the $\frac{1}{4}$ -chord point of the mean aerodynamic chord).

However, below the stall, the incremental CP due to the spoiler moves only slightly with incidence and is at about 20% c aft of the pitching moment reference point. This distance aft of the reference point is equal to about 18% local wing chord ahead of the spoiler leading-edge at the spanwise station of the incremental CP.

The chordwise incremental CP positions for the spoiler configurations tested are listed in Table 2 for $\delta = 20^\circ$ at $\alpha = 10^\circ$; there are seen to be quite large shifts with configuration changes. These shifts are equivalent to distances between 10% and 25% local chord ahead of the spoiler leading edge

at the appropriate spanwise CP positions. The loss of lift due to a spoiler occurs, (i) at the spoiler, (ii) as a lower flap lift and (iii) as lower leading edge (slat) suction, so the CP position would not be easy to predict even if the extent of flow separations was not disturbed.

2.8 Spoilers Used As Controls

Finally we have chosen to give a limited illustration of the practical use of the data obtained in this exercise and for this purpose data relating to the plain spoiler with a 3% gap and with 100% shroud venting have again been used. They are plotted in Fig 28 in incremental form, ΔC_D versus ΔC_L , as a carpet for various incidences and spoiler angles; the figure applies to symmetric operation of spoilers on both wings of a complete aircraft. The flap angle is 40° .

We follow Tomlinson's⁸ suggestion that a normal acceleration authority of, perhaps, $\pm 0.22 g$ is appropriate for ILC on the approach. This value will be used for illustrative purposes in conjunction with data from the present report although, as noted earlier, the spoiler span is relatively large in relation to wing span since the model is representative of only the outboard panels of a transport aircraft wing. When used for ILC, spoilers must be operated about a datum deflection in order to permit positive and negative lifting authority. For convenience we choose this datum to be $\delta = 15^\circ$ for a reason which will shortly become clear.

Interpolating from Fig 12, the maximum C_L is thus about 2.48 and, assuming the normal civil airworthiness margins, $V_{\text{approach}} = 1.3 V_{\text{stall}}$, the approach C_L will be about 1.47 at an incidence of 4.2° . From Fig 28, closing the spoiler at this incidence, point A, will give a maximum lifting authority of ΔC_L equals about +0.33 and hence an approximate normal acceleration authority of $(0.33/1.47 g) = 0.22 g$ ie that employed by Tomlinson*. From Fig 28 the associated drag change is seen to be an increase of about $\Delta C_D = 0.013$. Conversely, opening the spoiler further to give a negative lifting authority of -0.33, point B on Fig 28, again causes a drag increase, in this case $\Delta C_D = 0.029$. The instantaneous longitudinal deceleration due to this drag increment will be about $(0.029/1.47 g) = 0.02 g$ or 0.38 kt/s, a value which would be perceptible to a pilot if this maximum authority deflection were to remain for other than a very few seconds (but would be easily corrected by an autothrottle). These simple calculations suggest that the spoiler configuration considered would be adequate for ILC purposes. Note however that the approach C_L with zero spoiler deflection would be about 1.69 (at $\alpha = 2.9^\circ$) a significant improvement over the value of 1.47 available at $\delta = 15^\circ$.

Considering now the same spoiler used as a roll control on the approach, we can assume that its characteristics are sufficiently linear to operate from zero deflection rather than about a datum deflection displaced from zero as might be needed for a spoiler having poor characteristics. Referring to Fig 12 the approach condition with $\delta = 0$ will now be $C_L = 1.69$ at $\alpha = 2.9^\circ$. Assuming, for example, a spoiler deflection of 15° on the starboard wing, the lift increment at this incidence for a single spoiler is 0.157, point C on Fig 28, giving a rolling moment coefficient of 0.043 on a complete aircraft. (CP spanwise position is taken to be at 0.55% semispan). This would be adequate, for instance, to balance a rolling moment due to sideslip associated with $\beta = 10^\circ$ and $\ell_y = -0.25$. The associated drag change at constant incidence is about $\Delta C_D = -0.0055$, equivalent to a yawing moment coefficient of -0.0015 in the adverse, "out of turn", sense^D (and assuming that the incremental CP position in yaw is the same as that in roll). Note, however, that the ratio of yawing to rolling moment increment is only 0.035 so that the effect of this adverse yaw can be expected to be small.

In the longer term the incidence would be increased to restore the lift loss. If one assumes that the pilot flies the aeroplane to maintain constant speed and rate of descent, ie constant lift, throughout the period when the spoiler is deflected, then with a single spoiler deflected 15° the aircraft achieves $C_L = 1.69$ at about $\alpha = 5.1^\circ$. At that condition the asymmetric drag due to the spoiler is about $\Delta C_D = -0.0075$, from Fig 28, point D, producing an adverse yawing moment of -0.0021. The spoiler lift and roll increments will also have changed slightly.

The above discussion involves simplifications in that the effects of pitching moments due to the spoiler, of changes in downwash at the tail and of the need to include the effect on trim of the tailplane and elevator have been neglected. Nevertheless, it is worthwhile to point out the possible adverse nature of the yawing moments due to spoilers since these controls are often thought of as having proverse yaw characteristics⁹. In fact, Fig 28 shows that the yawing moment characteristics will be adverse over most of the operating range of the spoiler configuration chosen, assuming that the spoiler operates from a deflection of 0° as a roll control. However, it can be seen that if it formed part of a combined ILC/roll control system operating about a datum deflection of, say, 15° with only one spoiler providing roll control, then the drag increments due to deflection would be positive, at least up to $\alpha = 10^\circ$, and favourable yawing moments would result. If two spoilers are used differentially to provide roll control, the drag increments tend to balance and yawing moments would be very small.

In simple terms, the reason for the adverse yaw is that the basic lift, with high-lift devices deflected, is high and hence the reduction in induced drag associated with a given spoiler lift decrement is usually numerically greater than the increase in profile drag. This was not the case with most of the earlier published spoiler investigations which were made in the absence of sophisticated high-lift devices.

*A flight experiment at RAE with ILC on a BAC-111 aircraft has successfully used an authority of 0.15 g for standard 3° approaches; on that aircraft this authority was attained using a datum spoiler deflection of 15° .

Although only one spoiler configuration has been used as an example in this section it is fairly typical and the equivalent plot to Fig 28 for a moving shroud spoiler, for instance, is very similar.

Finally, we should note that the above simple analysis of rolling and yawing moments has been done in the axis system associated with lift and drag ie in aerodynamic stability axes or wind axes (as is invariably the case with other published data). An aircraft such as a transport aircraft, with a roll/yaw inertia ratio not much less than unity, tends to roll about the longitudinal wind axis and this axis system is therefore found from dynamic considerations to be more appropriate. Had the analysis been done in unrepresentative axes aligned with the aircraft body, then the yawing moments would in fact have appeared to be rather strongly proverse.

3 LIFT AND ROLL CONTROLS FOR ADVANCED COMBAT AIRCRAFT

3.1 Introduction

On several existing aeroplanes^{10,11} the manoeuvrability at transonic speeds is enhanced by the use of leading- and trailing-edge flaps to match the chordwise camber of the wing to the demanded "g" and Mach number. On those aeroplanes the flaps used are aerodynamically similar to simple hinged flaps, having sharp changes of curvature around the hinge; more gentle changes in curvature can be achieved by devices such as RAEVAM¹² (Fig 29), which has successfully passed a series of operational checks under simulated loadings¹³, and the so-called "VARICAM" or "contour" flap¹⁴ (Fig 30).

The important feature of both these devices is the flexible skin on the upper surface, the profile of which is controlled by a number of pivoted links. RAEVAM has a hinged lower surface and the necessary increase in length of the upper surface skin as the device deflects comes from the sliding joint at "A" (Fig 29). In contrast, on the contour flap, the upper skin is fixed in length and the lower surface shortens by means of a "folding" process without any sliding contact. (Fig 30)

If the manoeuvre performance demanded from a fighter is such that it can be achieved only by variable camber, then whichever of the above types of manoeuvre device is chosen, there are important ramifications on the low speed performance:

- a. it is clearly impossible to combine the now familiar slats and multi-slotted flaps with the manoeuvre devices, hence the increase in maximum lift necessary to ensure acceptable take-off and landing speeds has to come from deflecting the manoeuvre devices to higher angles. Will the $C_{L_{max}}$ then be adequate?
- b. for a swing-wing fighter, differential tail gives good roll control when the aircraft is in the high sweep, high speed configuration, but in the minimum sweep, low speed configuration, the increases in roll damping and inertia demand additional roll power which is usually obtained from spoilers. However, it may be difficult to combine spoilers with a trailing edge manoeuvre device and one of the alternatives we wish to investigate is to augment the roll control by operating the manoeuvre devices differentially even though they are deflected to high angles. We can clearly expect to obtain less rolling moment for a given differential deflection, and more adverse yawing moment, than from conventional ailerons. Will the roll control be acceptable?

In an attempt to answer these questions a series of tests were undertaken on another half model, slightly smaller than the one used for the spoiler tests, fitted with a RAEVAM leading-edge and a selection of contour and hinged trailing-edge flaps. A slatted leading-edge and a single slotted flap were also available from previous testing and were incorporated into the test programme to provide the important comparisons with conventional high lift devices.

3.2 Experimental Programme

The model, shown in Fig 31, could be tested at $\frac{1}{4}$ -chord sweeps of 20° , 30° and 45° giving the associated values of Aspect Ratio and streamwise thickness/chord ratio shown. In the 20° sweep position the wing planform parameters are very close to those of a typical advanced "swing-wing" fighter in its minimum sweep configuration and hence the major part of the testing was done with the wing in this position. However, in the interests of investigating sweep effects on maximum lift etc, a fairly full coverage was also obtained at the other sweep angles. The results at these other sweeps are presented in this paper but are not analysed in any detail.

The streamwise section of the wing at 30° sweep was derived from a two-dimensional aerofoil by factoring all dimensions normal to the chord line, by $\cos 30^\circ$. Thus the streamwise section at this sweep is identical to that on a parallel chord wing, yawed to 30° , which has the two-dimensional aerofoil section normal to its leading-edge. All the slat and flap angles quoted refer to this two-dimensional aerofoil as do the profiles of the various high lift devices and controls shown in Figs 32 and 33. The different sweep angles were obtained by yawing the wing about a pivot offset spanwise from the body centre line by about 5% semispan.

On the leading edge the model could be fitted with:

- a. an undeflected (or plain) leading-edge L0 (Fig 32a);
- b. a $12\frac{1}{2}\%$ chord slat (L1) at 25° deflection, positioned relative to the wing so as to give the highest value of $C_{L_{max}}$ (Fig 32b);
- c. a RAEVAM leading-edge (L2) at 35° deflection (Fig 32c).

On the trailing edge the model could be fitted with the following full-span controls or high-lift devices:

- a. a simple hinged flap of 25% chord (T0) with the hinge on the lower surface. This flap would be set at angles of 0°, 5°, 10°, 15°, 20°, 30°, and 50°. (Fig 33 a and b);
- b. two simulated contour or "VARICAM" flaps (T1) designed to have the same zero lift angle in potential flow as the hinged flap at 20° and 30° deflection (Fig 33 a and b);
- c. a single slotted flap of 33% chord (T2) with the shroud trailing edge at 30% chord, set at 40° deflection and positioned relative to the wing so as to give the highest $C_{L_{max}}$ (Fig 33c).

Transition was fixed:

- a. on the body about 2/3 of the nose length ahead of the wing, using a wire;
- b. on the lower surface of the wing at 43% chord, using a wire;
- c. on the outer 25% of the semispan of the slat, using ballotini, in order to prevent a "thin aerofoil" stall on the slat.

On the leading-edge behind the slat, the plain leading-edge and the RAEVAM leading-edge, transition of the upper surface boundary layer was allowed to occur naturally; at all lift coefficients of interest this occurred through a shortlaminar separation bubble¹⁵.

The major part of the results for this model were obtained in the 4 m x 2.7 m (13 ft x 9 ft) low speed tunnel at RAE Bedford, at a Mach number of 0.2, using the same balance and test arrangement as for the spoiler tests. Subsequently a few runs at atmospheric pressure and at the same Mach number were made in the new 5m low speed tunnel at Farnborough using a 6-component balance so that the yawing moments due to aileron could be measured, rather than just changes in axial force.

3.3 Presentation and Discussion of Results

3.3.1 Results with Contour Flaps

Fig 34 shows the variation of chordwise pressure distribution across the span for the combination of RAEVAM (L2) with the contour flap (T1) set at 30°. The obvious features of these pressure distributions are:

- a. a high suction peak very close to the leading-edge;
- b. behind this a pressure "plateau" extending to about 20% chord - the point where the flexible skin of the RAEVAM merges into the basic section shape;
- c. this "plateau" is terminated by a steep pressure rise occupying about a further 20% chord;
- d. the pressure coefficient at the trailing-edge is approximately -0.4 indicating separated flow over the trailing edge.

If, instead of the RAEVAM and the contour flap, the wing had been fitted with hinged flaps at the leading- and trailing-edges, then one would have expected to see secondary suction peaks occurring over the "knuckles" of these controls; the larger radii of curvature obtainable from the use of flexible skins has enabled these to be eliminated.

Despite the high suction peaks near the leading edge there would be no advantage in increasing the deflection angle of the RAEVAM (at least at this Reynolds number) because the adverse pressure gradient aft of the plateau ((c) above) is sufficient to cause a local separation of the turbulent boundary layer which subsequently re-attaches about 20% chord further downstream (Fig 35).

Fig 36 compares the performance of the two contour flaps (T1) with that of the hinged flap (T0) when set at the corresponding angles of 20° and 30°. Clearly the differences in lift and pitching moment behaviour are very small, but the contour flaps have considerably less drag than the hinged flaps.

Since the lifting performance of the two types of flap is so similar, it was decided to concentrate the investigation on the more easily varied hinged flaps.

3.3.2 Results with Hinged Flaps

The basic lift, drag, and pitch results for flap angles up to 50° with (a) the RAEVAM leading-edge (L2), and (b) the slatted leading-edge (L1), are shown in Fig 37 for 20° sweep and Fig 38 for 30° sweep; Fig 39 shows similar results for the plain leading-edge (L0) with flap angles up to 10° at sweeps of 20°, 30° and 45°.

Figs 37a and 38a both show that the stalling angle tends to decrease as the flap angle increases. With the slat, the rate of decrease increases with flap angle, but for RAEVAM the reverse applies, so that the stalling angle becomes almost constant at the higher flap angles.

This behaviour shows up very clearly in Figs 40 (a) and (b) where the maximum lift and lift at constant incidence are summarised. Fig 40a shows that the increase of $C_{L_{max}}$ with flap angle is much steeper for RAEVAM than for the slat at both 20° and 30° of sweep, with the result that the difference

between them decreases quite markedly with increasing flap angle. In contrast Fig 40b shows that the lift increment at constant incidence due to deflecting the flap, is almost independent of the leading-edge device.

It is interesting to note that, with the sole exception of the 50° flap at 20° sweep, there is a linear correlation between lift and pitching moment at the stall for all flap angles at each combination of leading-edge and sweep (Figs 37c, 38c, 39c). The mild nose-up pitch changes well below maximum lift shown in Fig 38c at low flap angles are probably associated with the local separation outboard shown in Fig 35.

Since the wing had a full span flap it is effectively untwisted and analytic representation of the drag polars is consequently simpler than in Section 2. The form

$$C_D = C_{D_0} + k \frac{C_L^2}{\pi A}$$

is found to fit the data well over the incidence range above about 3° up to approximately 2° below the stall. Below the lower limit, separations occur on the lower surface of the slat and the RAEVAM, leading to an increase in profile drag; above the upper limit, increasingly severe viscous effects also produce an increasing profile drag. Fig 41a shows the variation of the drag at zero lift, C_{D_0} , from this analysis. As might be expected C_{D_0} rises rapidly with increasing flap angle above about 10° of flap, and at 50° flap is almost five times its value at zero flap angle. The values for the contour flaps are considerably lower than those for the hinged flaps, as would be expected from the results already shown in Fig 36. Fig 41b shows that the lift dependent drag factor, k , decreases slightly as flap angle increases, thereby offsetting to some extent the large increases in C_{D_0} shown in Fig 41a.

3.3.3 Roll Performance

Roll requirements for modern aeroplanes are usually specified in terms of the time taken to roll through certain angles starting from zero roll rate. Clearly these cannot be used to assess the adequacy of rolling moments due to aileron measured on a wind tunnel model without making assumptions about rolling inertias, flying speeds etc. However, in the past, the non-dimensional steady (or asymptotic) roll rate ($Pb/2V$) has been used as a criterion for designing roll controls - Perkins and Hage¹⁶ suggest a minimum acceptable figure of 0.09 for fighter aircraft, and Etkin¹⁷ quotes a corresponding value of 0.07. This criterion is particularly suitable for the assessment being attempted here, since the differential flap or "aileron" angle, ξ , required to generate this rate provides an easily understandable measure of the roll control and can be easily calculated from the steady state roll equation,

$$\frac{\partial C_\ell}{\partial \xi} \xi = - \left(\frac{pb}{2V} \right) \ell_p$$

where C_ℓ = rolling moment p = roll rate (rad/s)
 ξ = aileron angle (degrees) = $\frac{1}{2}$ (starboard flap angle - port flap angle)
 b = wingspan V = forward velocity
 ℓ_p = roll damping = $(\partial C_\ell) / \partial ((pb)/(2V))$

For the analysis presented here, the value of $Pb/2V$ was taken to be 0.09, ℓ_p was estimated for each flap angle from ESDU Data Sheets¹⁸, and the values of rolling moment due to aileron ($\partial C_\ell / \partial \xi$) were obtained by differencing the wind tunnel results (Fig 1), the result being corrected for half-model effects by the method of Swanson and Toll²⁰. The resulting aileron angles, for each flap angle and for both RAEVAM and slatted leading edges, are plotted in Fig 42.

This figure shows that the required aileron angle increases progressively with flap angle, except that the progression is halted, in the case of RAEVAM, and reduced for the slat, between 15° and 20° of flap. The aileron angle also tends to increase with C_L , but below the approach C_L (which is defined in the next section) the increase is fairly small and the roll rate can be obtained with less than 10° of aileron even with 30° of flap. Above the approach C_L the required aileron angle continues to rise and, for 30° flap in conjunction with the slat, almost 25° of aileron is required at maximum lift.

It is useful to generalise these results by expressing them in terms of the aileron angles required at the lowest flap angle. At the approach C_L , increasing the flap angle from 5° to 30° necessitates an increase in aileron angle of about 75% to generate the same roll rate. At maximum lift with the RAEVAM leading edge the increase is about the same, but with the slatted leading-edge the necessary aileron angle is increased by over 100%.

The yawing moment due to aileron is plotted in Fig 43 as a ratio with the corresponding rolling moment. The yawing moment is shown to be consistently adverse, as would be expected, reaching levels around ten times that found for the spoiler for flap angles up to 20°, and 25% more than that with the flap at 30°. However, most of this adverse yaw is lift dependent and does not result from increasing the flap angle. Working along the approach C_L line, it will be seen that the adverse yaw increases by only 30%-35% as the flap angle is increased from 5° to 20°; increasing the flap angle to 30° increases the adverse yawing moment by about another 35%, giving an overall increase of some 65% over the situation with 5° flap. The actual yawing moment corresponding to $C_H/C_L = -0.25$ is approximately 0.013 which could be balanced by a rudder angle of about 15° assuming a reasonable value of $dC_H/d\delta = -0.000/\text{degree}$. On this basis, to balance the maximum adverse yaw shown would require a rudder angle of 25°.

In general terms, it would appear that, although adequate rolling moments can be generated by differential movement of the flaps about a basic position of 30° deflection, the adverse yawing moments thus generated may limit the practical flap deflection to about 20° . In the final analysis, of course, this can only be decided in the context of a particular configuration. 4-13

4.1 Comparison With Other High Lift Systems

The $C_{L_{max}}$ values attained at low speed with the manoeuvre devices deflected to high angles ie by RAEVAM (L2) in conjunction with the hinged flap (T0), are, as might be expected, inferior to those attained on most modern aircraft. If the field performance obtainable under these circumstances is inadequate then, unless boundary layer control is employed, either the leading- or trailing-edge manoeuvre device would have to be replaced by a more powerful alternative. What increases in performance can then be expected in each case?

Unfortunately, simple comparisons of $C_{L_{max}}$ values are not always useful since increases in $C_{L_{max}}$ which arise from extensions to the lift curve at high incidences are, in general, not usable because the maximum incidence of the aircraft on the ground is limited by the tail striking the ground - $\alpha = 17^\circ$ is a reasonable figure to represent this condition. After allowing adequate margins for manoeuvring and gusts, the approach C_L , which was used in the previous section and on which various combinations of high lift devices will be compared, is defined as the smaller of

- a. $70\% C_{L_{max}}$ and
- b. 85% of C_L at $\alpha = 17^\circ$

Fig 44 shows $C_L \sim \alpha$ curves for nine combinations of three leading- and trailing-edge configurations and the table below lists the values of the approach C_L and the incidence at which it is achieved. The various increments are extracted and presented in Tables 3 and 4.

These tables show that, starting from the configuration consisting entirely of manoeuvre devices (L2/T0(50°)), an increment in approach C_L of 0.2 (12%) can be obtained by replacing RAEVAM (L2) by the slat (L1), but replacing the hinged flap (T0) by the slotted flap (T2) produces an increase of 0.79 (47%).

To a large extent this large increment derives from the 23% increase in area that this flap provides, but it is also noticeable in Fig 44 that an increase in stalling angle is obtained over the configuration with the hinged flap. This is due to the relatively high suction at the shroud trailing-edge ($C_p \approx -2$) which is produced by the mutual interference of the flows around the wing and the flap¹⁹.

4 CONCLUSIONS

4.1 Spoiler Controls on Civil Aircraft

No aerodynamic reversal of control effectiveness was found in the normal operating incidence range, but very significant non-linearity of control effectiveness occurred for some spoiler configurations, particularly the plain hinged-plate spoiler.

Overall, the most effective type of spoiler tested was the moving shroud spoiler, with a forward hinge, formed from a portion of the trailing-edge of the flap shroud.

A gap beneath the leading-edge of a spoiler and venting through the flap shroud both improved the linearity of spoiler aerodynamic characteristics.

Although spoilers are traditionally thought of as having proverse yaw characteristics, it is shown that this is not necessarily so, particularly if the control is operated from the closed condition (as for pure roll control) rather than about a finite datum setting (as for direct lift control).

Although the post-stall performance of spoilers was not investigated in detail, evidence suggests that the spoilers tested would not be effective under post-stall conditions.

4.2 Lift and Roll Controls for Advanced Combat Aircraft

The lift increments from contour flaps and hinged flaps were found to be almost identical, provided that both had the same zero lift angle in inviscid flow (although this may not be true for thinner wings) but the contour flap has considerably less drag.

Full span hinged flaps, operated differentially about mean angles of up to 30° , have been shown to be capable of generating sufficient rolling moment to give a steady roll rate of $\dot{\phi}/2V = 0.09$. As the mean flap angle is increased up to 30° , the differential angle between them (the aileron angle) necessary to produce this rate of roll, approximately doubles at a typical approach C_L .

The associated yawing moments increase by about 50% and this may limit the practical flap angle to 20° unless the rudder is powerful or a degraded roll performance can be tolerated on the approach.

The increment in approach C_L obtained by replacing a hinged flap by a single slotted flap has been found to be about four times that obtained by replacing a RAEVAM leading-edge by a slat.

5 ACKNOWLEDGEMENT

The authors would like to express their appreciation to BAe Warton for permission to publish the details of the RAEVAM and contour flap mechanisms and for their interest and assistance in preparing this paper.

REFERENCES

- 1 Langley Research Staff Summary of lateral-control research.
NACA Report 868 (1947)
- 2 J Fischel and M F Ivey Collection of test data for lateral control with full-span flaps.
NACA Technical Note 1404 (1948)
- 3 G Ingle Flight tests on a BAC1-11 200 Series aircraft to determine the suitability of the wing spoilers for use as direct lift control surfaces.
RAE Technical Report 76142 (1976)
- 4 W E A Acum Corrections for symmetrical swept and tapered wings in rectangular wind tunnels.
Aeronautical Research Council, R & M 2777 (1950)
- 5 E C Maskell, D A Kirby and J Y G Evans Aerodynamic research to improve the low-speed performance of transport aircraft for short and medium ranges.
Unpublished RAE Report
- 6 A Betz Theory of lift as a function of boundary layer.
Zeitschrift fur Flugtechnik und Motorluftschiffahrt, p277 (1932)
- 7 S F Hoerner Fluid Dynamic drag, pp13-13
Published by the author (1965)
- 8 B N Tomlinson Direct lift control in a large transport aircraft - a simulator study of proportional DLC.
RAE Technical Report 72154 (1972)
- 9 A W Babister Aircraft Stability and Control, pp394-397,
Pergamon Press (1961)
- 10 N R Anderson Flying the YF-16.
Aerospace, March 1976
- 11 M Hirst
J Marsden
T Hamill F-18 Hornet
Flight, 2 Dec 1978
- 12 G F Moss
A B Haines
R Jordan The Effect of Leading-Edge Geometry on High Speed Stalling.
AGARD Specialist Meeting, Lisbon April 1972
- 13 E J Porter
J Ascroft
H Abraham Functional Tests on a RAEVAM High Lift Device.
Unpublished paper prepared by BAe Warton Division under contract to UK Ministry of Defence
- 14 N Lee
J Hanlon
H Jackson
B Healey Structural and Engineering Research into a range of novel mechanisms for high lift devices appropriate to combat aircraft.
Unpublished paper prepared by BAe Warton Division under contract to UK Ministry of Defence
- 15 B Thwaites (ED) Incompressible Aerodynamics.
Oxford University Press (1960)
- 16 C D Perkins
R E Hage Airplane Performance, Stability and Control.
John Wiley and Sons Inc, (1949)
- 17 B Etkin Dynamics of Flight-Stability and Control.
John Wiley and Sons Inc, (1959)
- 18 Engineering Sciences Data Unit Rolling Moment due to Roll.
ESDU Data Sheet Aircraft 06.01.01
- 19 A M O Smith Aerodynamics of High Lift Aerofoil Systems.
AGARD Conference Proceedings No 102 "Fluid Dynamics of Aircraft Stalling" (1972)
- 20 R S Swanson
T A Toll Jet Boundary Corrections for Reflection - Plane models in Rectangular Wind Tunnels.
NACA TR 770 (1943)

TABLE 1 - DETAILS OF SPOILER RESEARCH MODEL

Quarter-chord sweep	30°
Leading-edge sweep	32.6°
Semi-span	2.134 m
Standard mean chord	0.610 m
Mean aerodynamic chord	0.647 m
Centre-line chord	0.871 m
Tip chord	0.348 m
Taper ratio	0.40
Aspect ratio	7.00
Wing section	NPL "A" 10.5% thick
Flap configuration	Tabbed, Fowler flap, 87% shroud trailing edge
Flap span joints	15, 40, 60, 80, 100% semi-span
Flap chord	40% wing chord (including tab)
Tab chord	15% wing chord
Tab section	Plain hinged from flap section (with a slot when angled 30°)
Flap position	Zero lap 2% gap
Aileron chord	30% wing chord
Aileron span	80-95% semi-span
Slat chord	17% wing chord
Slat span joints	15, 32, 49, 66, 83 and 100% semi-span
Slat section	Arbitrary section
Slat angle	28°
Slat position	2% local chord forward of wing leading-edge (Fig 4)
Computing reference span = semi-span	2.134 m
" " chord = standard	0.61 m
	mean chord
" " area = gross area	1.301 m ²
" " pitching moment axis	0.887 m aft of wing apex
	= 101.8% of root chord
	= 46.9% of mean aerodynamic chord
" " roll or root bending	moment axis is centre-line
Spoiler chord	12% wing chord
Spoiler span	40 - 80% semi-span
Spoiler angles, plain and vented shroud	2½°, 5°, 7½°, 10°, 20°, 30°, 40°
Spoiler angles, moving shroud	2°, 4°, 6°, 8°, 10°, 12°, 14°, 20°, 30°, 40°

TABLE 2 - TEST CONFIGURATIONS AND PERFORMANCE SUMMARY OF TESTS ON SPOILER RESEARCH MODEL

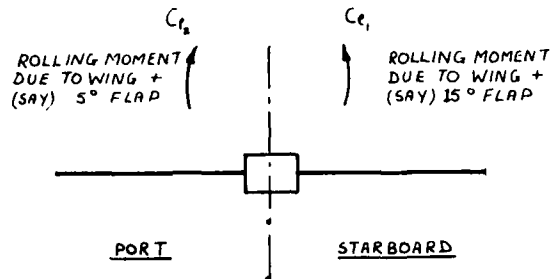
SPOILER CONFIGURATIONS	FLAP	SPOILER	SPOILER GAP % chord	MAXIMUM DEFLECTION degrees	$-C_L \delta_o$ per degree	$-C_L \delta_{MAX}$ per degree	$-C_L \delta_{TAN}$ per degree	δ_D degrees	$\Delta C_L_{20,10}$	$C_L \alpha' = 10$ per degree	$\Delta C_l / \Delta C_z$ $\delta = 20, \mu = 10$	$\Delta C_m / \Delta C_z$ $\delta = 20, \mu = 10$
Plain unvented	40°	Plain	0	40	.0030	.0322	.0202	9	.36	.030	.582	.309
" "	"	"	3	40	.0090	.0356	.0236	6.5	.48	.014	.556	.253
" "	"	"	6	30	.0052	.0314	.0198	4	.38	.013	.588	.329
" "	"	sawtooth	3	30	.0050	.0366	.0216	5.5	.43	.0094	.582	.311
" "	"	Perforated	3	30	.0060	.0274	.0190	5	.38	.012	.588	.344
" "	"	Castellated	3	30	.0050	.0340	.0204	7.5	.41	.011	.586	.330
Vented 100%	40°	Plain	0	40	.0100	.0352	.0234	7.5	.43	.005	.566	.243
" "	"	"	3	40	.0154	.0408	.0274	5.5	.56	.010	.556	.213
" "	"	"	3	30	.0160	.0416	.0282	6.5	.59	.015	.566	.241
" "	"	"	3	30	.0186	.0366	.0276	6	.55	.018	.566	.248
" "	"	"	3	30	.0168	.0432	.0276	7	.56	.013	.554	.244
" "	"	"	3	30	.0120	.0500	.0266	8.5	.54	.011	.558	.259
Vented Type A 30%	40°	Plain	3	40	.0190	.0358	.0282	2.5	.57	.012	.558	.239
" "	"	"	6	30	.0240	.0444	.0366	0.5	.56	.012	.560	.245
" "	"	"	3	30	.0150	.0310	.0234	5	.48	.010	.574	.276
" "	"	"	3	30	.0100	.0286	.0222	3.5	.45	.013	.572	.271
" "	"	"	3	30	.0100	.0348	.0256	4.5	.52	.013	.562	.263
Moving	40°	Trailing Edge	0	30	.0146	.0412	.0330	1.5	.52	.000	.566	.283
" "	"	"	3	30	.0230	.0452	.0378	1.0	.65	.003	.560	.255
" "	"	"	6	20	.0310	.0600	.0476	1.0	.70	.005	.558	.248
" "	"	"	12	10	.0544	.0820	.0674	0.5	-	-	-	-
Plain Unvented	20°	Plain	0	40	.0002	.0220	.0134	8	.22	.010	.568	.260
" "	"	"	1½	40	.0002	.0202	.0142	7	.27	.012	.574	.262
" "	"	"	3	40	.0014	.0198	.0140	5.5	.28	.011	.572	.267
" "	"	"	6	40	.0020	.0170	.0124	3.5	.26	.012	.572	.290
" "	"	"	12	20	.0028	.0162	.0102	3.5	.16	.004	.572	.313
" "	"	Sawtooth	0	30	.0068	.0210	.0162	4	.33	.011	.564	.268
" "	"	"	3	30	.0100	.0176	.0150	2	.30	.007	.568	.287
" "	"	Perforated	0	30	.0140	.0140	.0148	-	.27	.008	.572	.286
" "	"	Castellated	0	30	.0086	.0176	.0148	3	.30	.009	.568	.284
Vented 100%	20°	Plain	0	40	.0040	.0260	.0166	8.5	.30	.005	.552	.181
" "	"	"	3	40	.0076	.0254	.0188	5	.37	.012	.552	.171
Moving	20°	Trailing Edge	0	30	.0118	.0200	.0220	3.5	.28	.001	.580	.253
" "	"	"	3	30	.0130	.0222	.0184	4	.36	.002	.562	.226
" "	"	"	6	30	.0176	.0200	.0192	0.5	.36	.001	.574	.220
" "	"	"	12	10	.0240	.0240	.0240	-	-	-	-	-
Vented 100%	10°	Plain	0	40	.0070	.0164	.0122	6	.23	.008	.552	.129
" "	"	"	3	40	.0110	.0166	.0134	2.5	.27	.013	.558	.140
Moving	10°	Trailing Edge	0	30	.0016	.0144	.09	3	.14	.002	.548	.035

TABLE 3 - INCREMENTS IN $C_{L_{app}}$ DUE TO CHANGING T/E DEVICES

Increment in $C_{L_{app}}$ Due to Replacing	With LO	With L1	With L2	
TO(0°) by TO(50°)	0.44	0.49	0.50	TO - Hinged Flap
TO(0°) by T2(40°)	0.96	1.37	1.29	T2 - 3% Chord Single- Slotted Flap
TO(50°) by T2(40°)	0.52	0.88	0.79	

TABLE 4 - INCREMENTS IN $C_{L_{app}}$ DUE TO CHANGING L/E DEVICES

Increment in $C_{L_{app}}$ Due to Replacing	With TO(0°)	With TO(50°)	With T2(40°)	
L0 by L2	0.11	0.17	0.44	L0 - Plain Leading Edge
L0 by L1	0.32	0.37	0.73	L1 - 12% Chord Slat
L2 by L1	0.21	0.20	0.29	L2 - RAEVAM Leading Edge



$$\xi = \text{AILERON ANGLE} = \frac{\text{ANGLE OF STARBOARD FLAP} - \text{ANGLE OF PORT FLAP}}{2}$$

$$\frac{\partial C_l}{\partial \xi} = \frac{C_{l_2} - C_{l_1}}{5^\circ} \quad \text{AT A BASIC FLAP ANGLE OF } 10^\circ$$

THIS REPRESENTS A ROLLING MOMENT GENERATED BY A SPANWISE LOAD DISTRIBUTION AS DRAWN IN A FULL LINE BELOW. THE TRUE SPANWISE LOAD DISTRIBUTION APPEARS AS A DASHED LINE.



Fig 1 Summary of derivation of rolling and yawing moments due to aileron from half model results

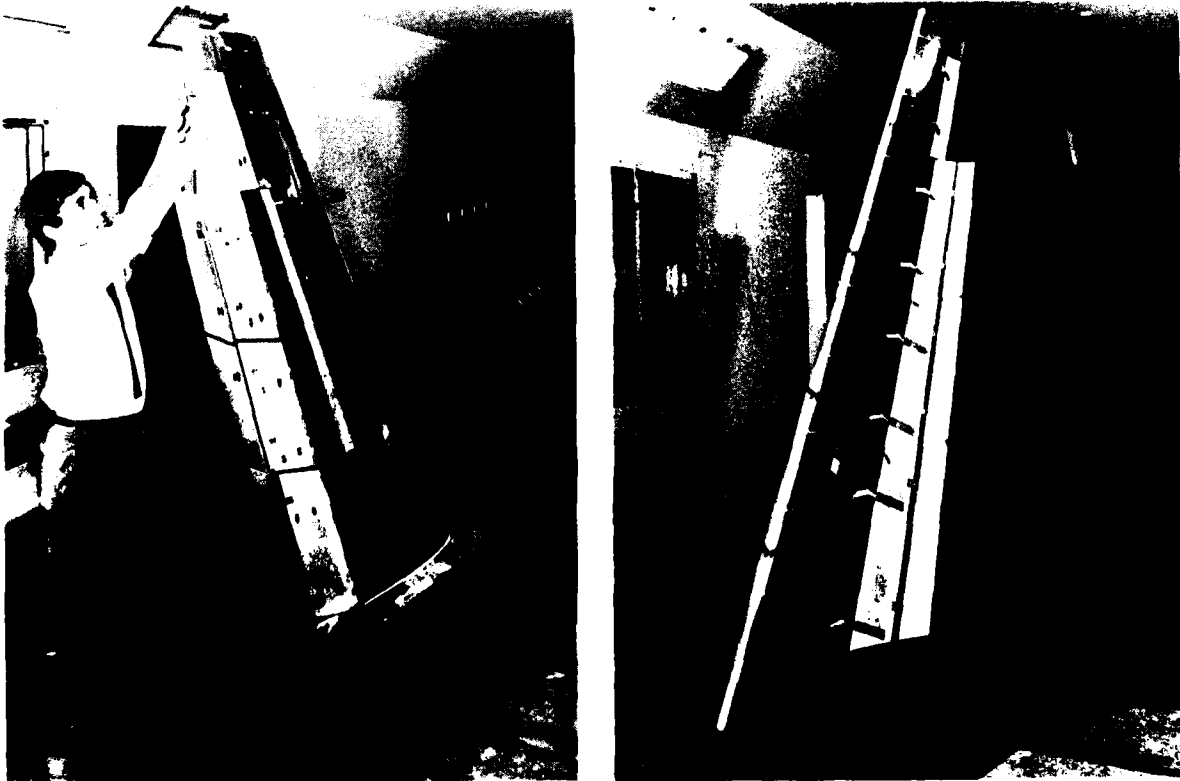


Fig 2 The spoiler research model in the 4m x 2.7m tunnel at RAE Bedford

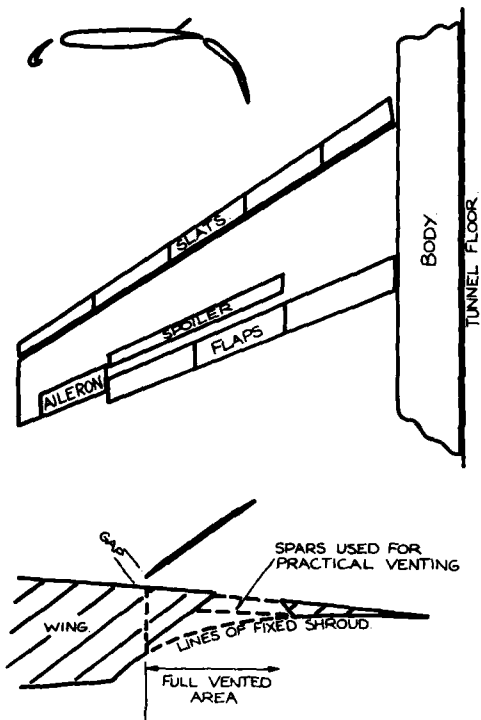


Fig 3 Typical geometry of the spoiler research model

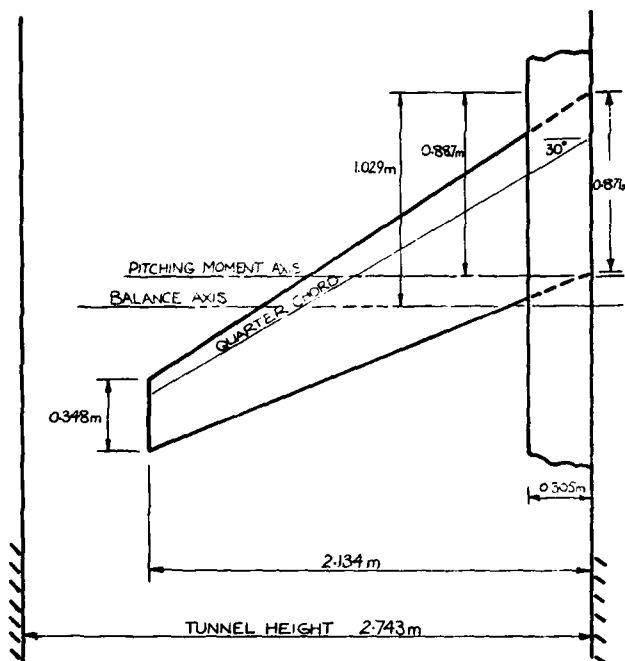


Fig 4 Dimensions of the spoiler research model

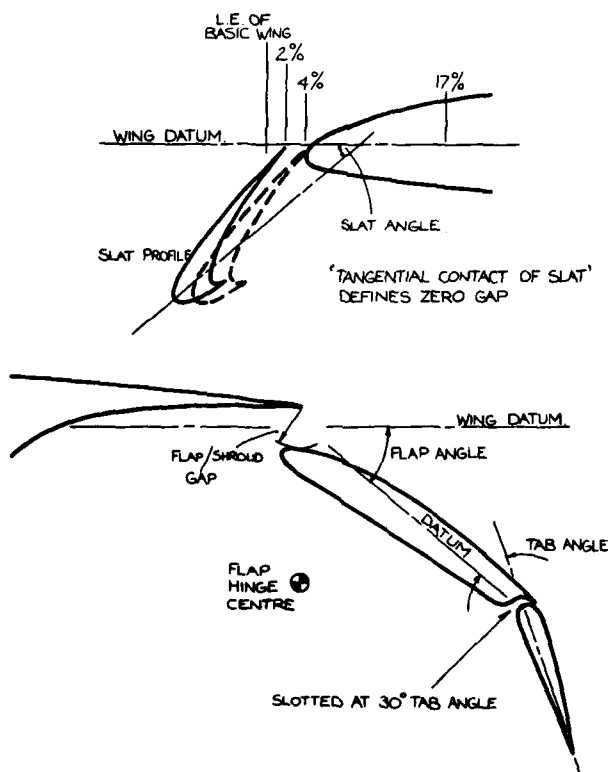


Fig 5 Definition of high-lift geometry on the spoiler research model

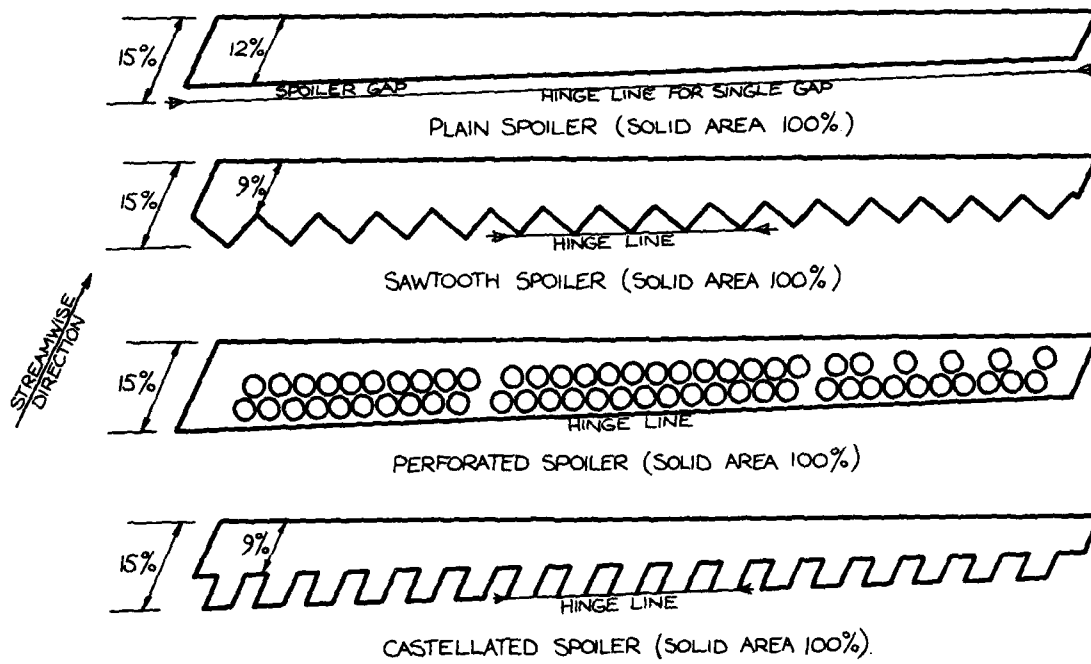


Fig 6 Planforms of hinged-plate spoilers

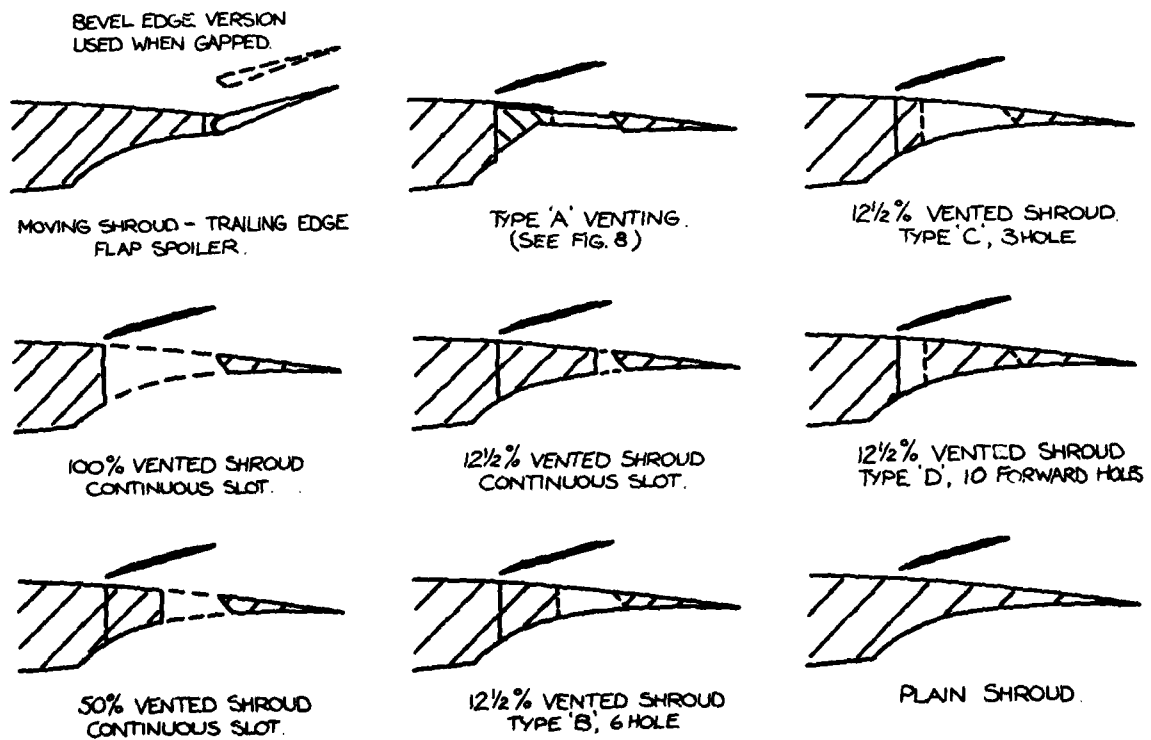


Fig 7 Spoiler and shroud cross-sections

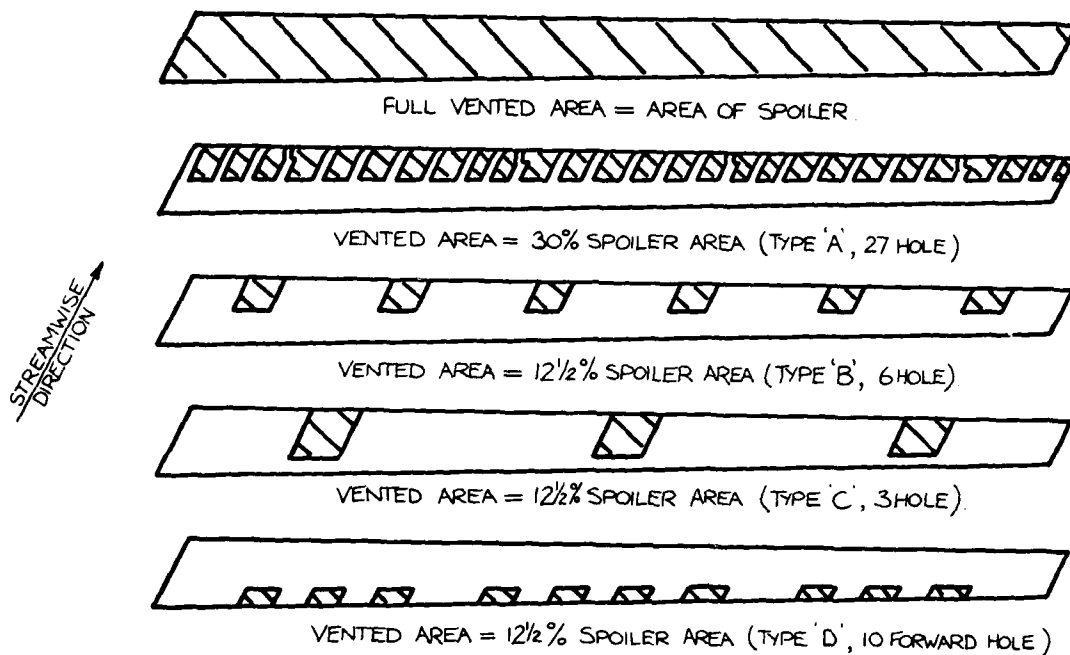


Fig 8 Vented areas in shroud

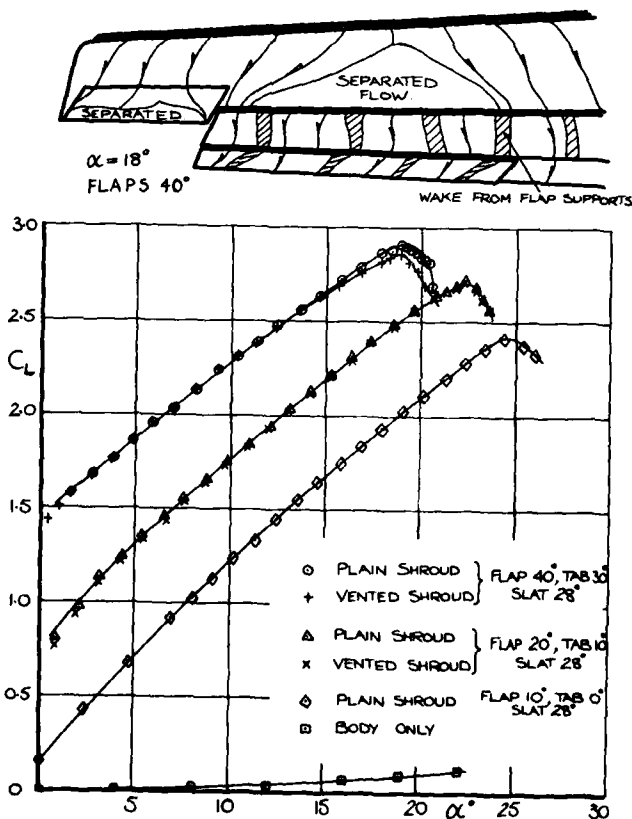


Fig 9 Lift curves for the basic wing

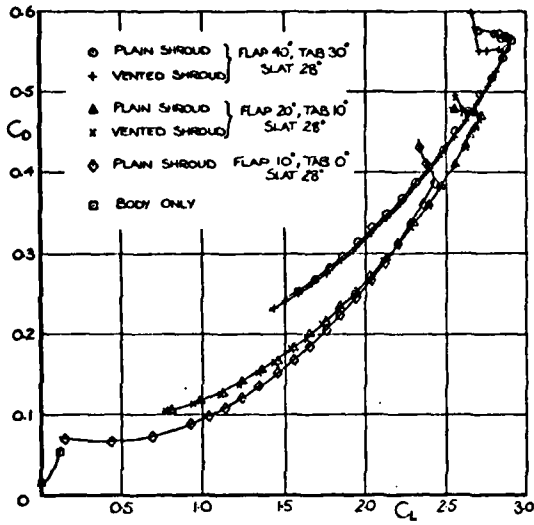


Fig 10 Drag polars for the basic wing

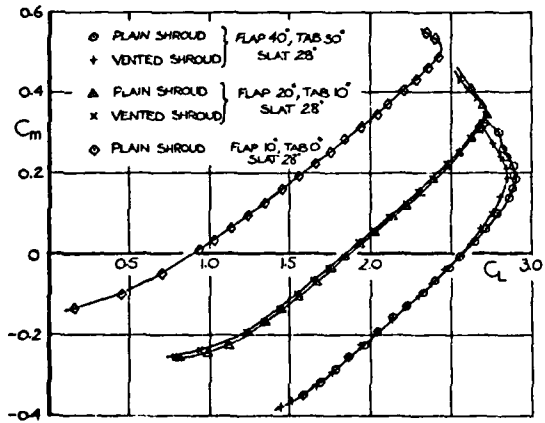


Fig 11 Pitching moment curves for the basic wing

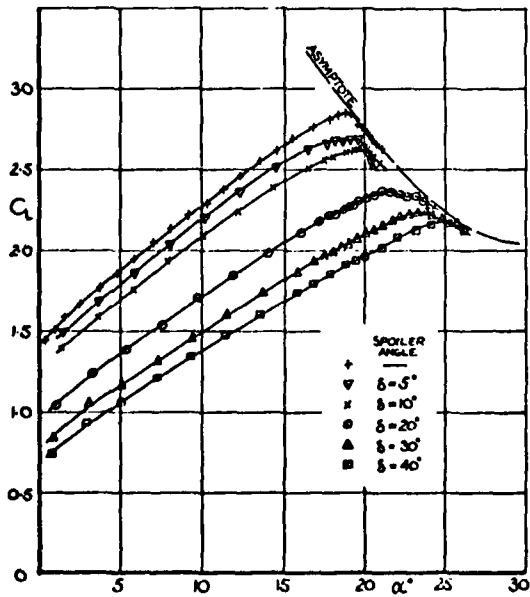


Fig 12 Lift curves: plain spoiler, 3% gap, 100% vented shroud, flap 40°

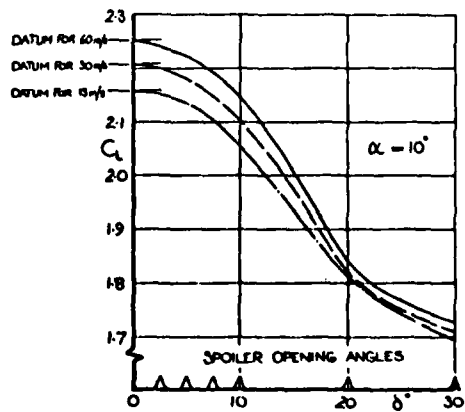
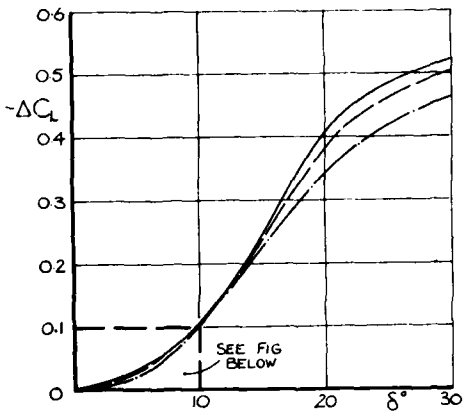
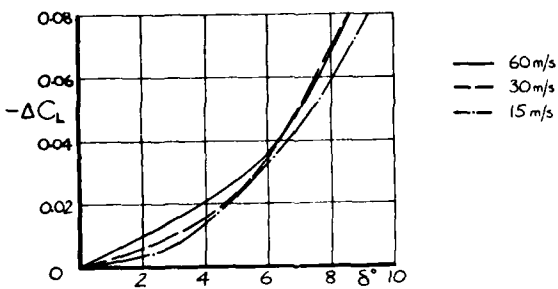


Fig 13 Effect of Reynolds number on total lift: perforated spoiler, flap 40°

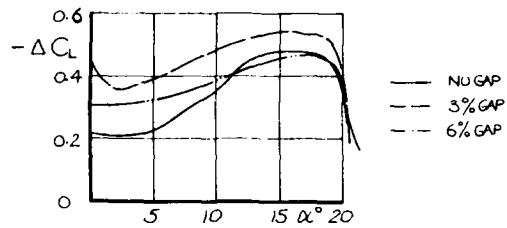


(a) ΔC_L v δ° AT $\alpha = 10^\circ$

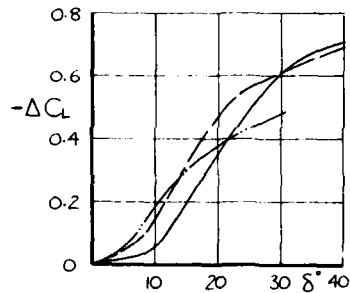


(b) ΔC_L v δ° AT $\alpha = 10^\circ$, ENLARGED SCALE

Fig 14 Effect of Reynolds number on incremental lift: perforated spoiler, flap 40°

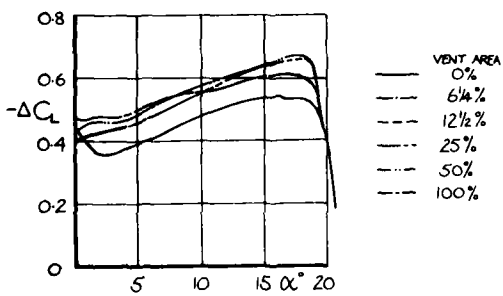


(a) ΔC_L v α AT $\delta = 20^\circ$

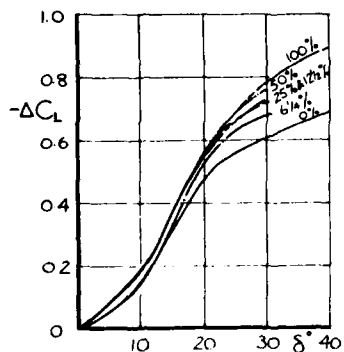


(b) ΔC_L v δ AT $\alpha = 10^\circ$

Fig 15 Effect of gap on incremental lift: plain spoiler, flap 40°

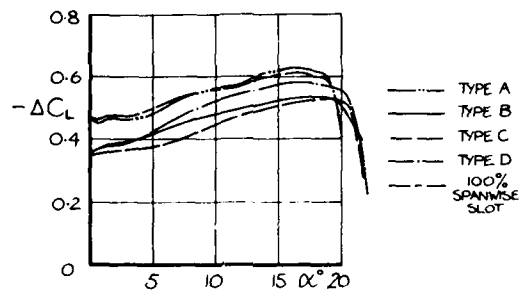


(a) ΔC_L v α AT $\delta = 20^\circ$

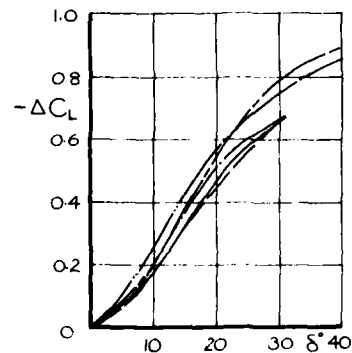


(b) ΔC_L v δ AT $\alpha = 10^\circ$

Fig 16 Effect of venting, through spanwise slots in shroud, on incremental lift: plain spoiler, 3% gap, flap 40°



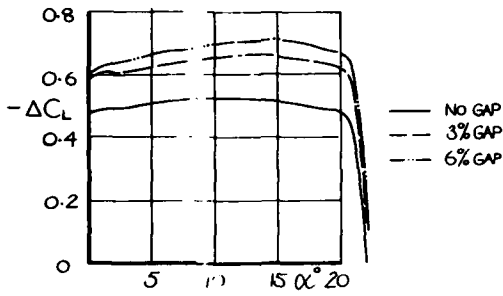
(a) ΔC_L v α AT $\delta = 20^\circ$



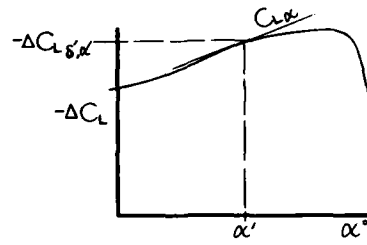
(b) ΔC_L v δ AT $\alpha = 10^\circ$

Fig 17 Effect of venting, through discrete vents in shroud, on incremental lift: plain spoiler, 3% gap, flap 40°

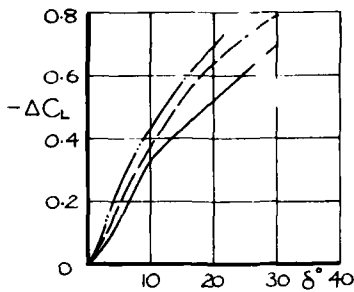
4-24



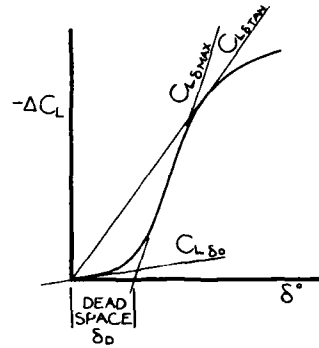
(a) ΔC_L v α AT $\delta = 20^\circ$



(c) EFFECT OF INCIDENCE AT $\delta = \delta'$



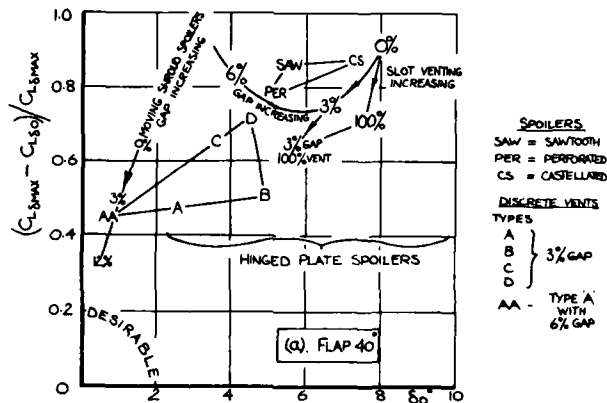
(b) ΔC_L v δ AT $\alpha = 10^\circ$



(b) EFFECT OF SPOILER DEFLECTION AT $\alpha = \alpha'$

Fig 18 Incremental lift due to moving shroud spoilers: flap 40°

Fig 19 Definition of spoiler lift derivatives



SPOILERS
 SAW = SAWTOOTH
 PER = PERFORATED
 CS = CASTELLATED

DISCRETE VENTS
 TYPES
 A } 3% GAP
 B }
 C }
 AA - TYPE A WITH 6% GAP

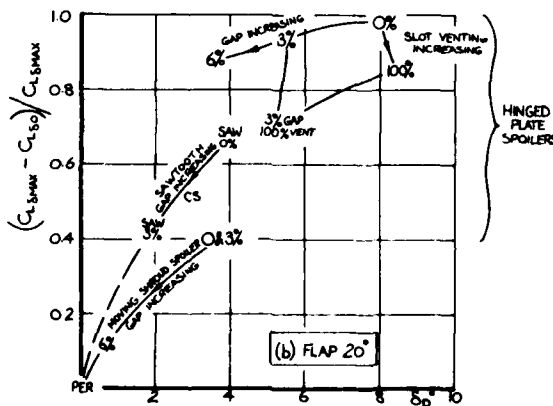


Fig 20 Effect of spoiler configuration on spoiler lift derivatives

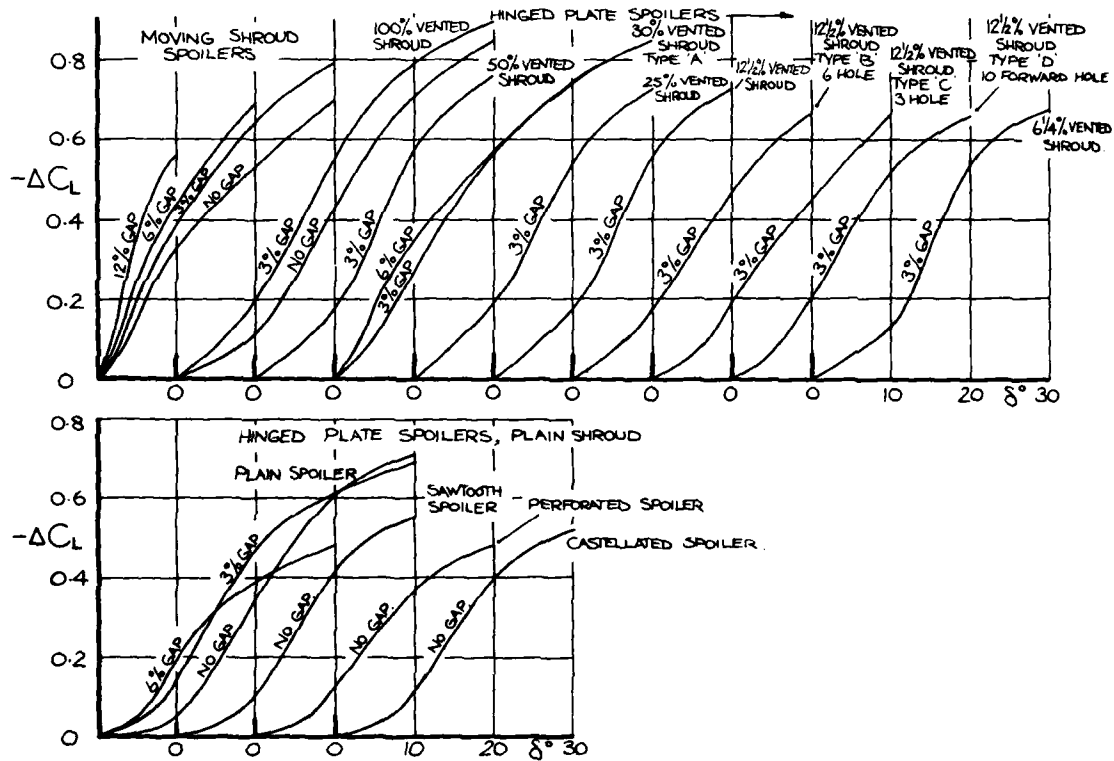


Fig 21 Summary of spoiler lift increments:
 $\alpha = 100$, flap 40°

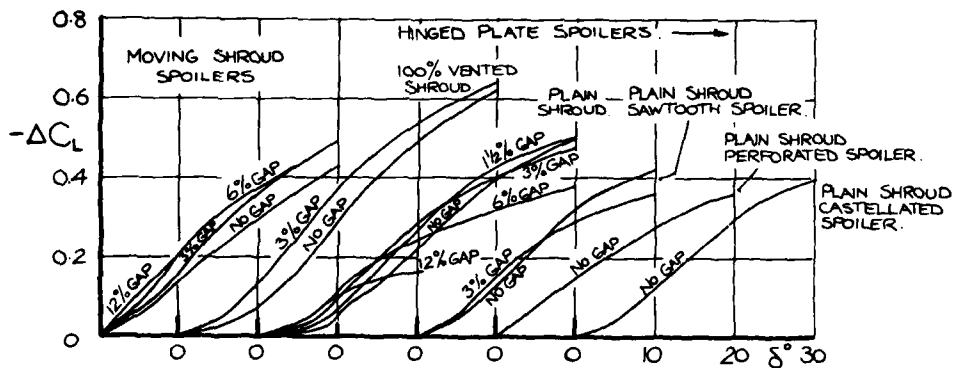


Fig 22 Summary of spoiler lift increments:
 $\alpha = 100$, flap 20°

4-26

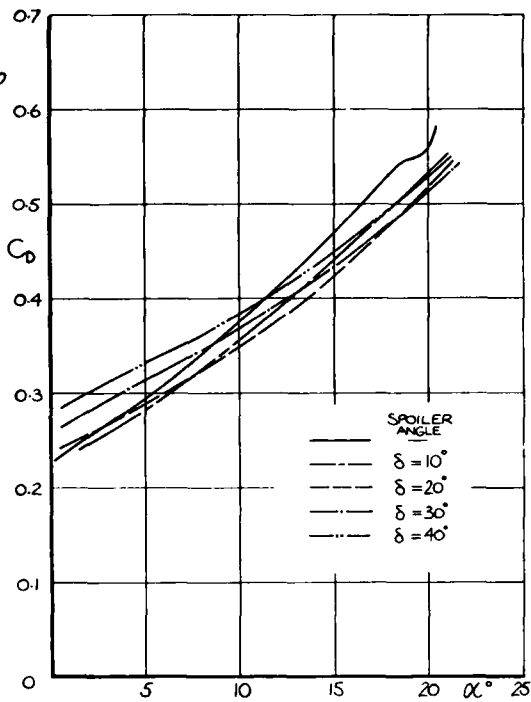


Fig 23 Drag curves versus incidence: plain spoiler, 3% gap, 100% vented shroud, flap 40°

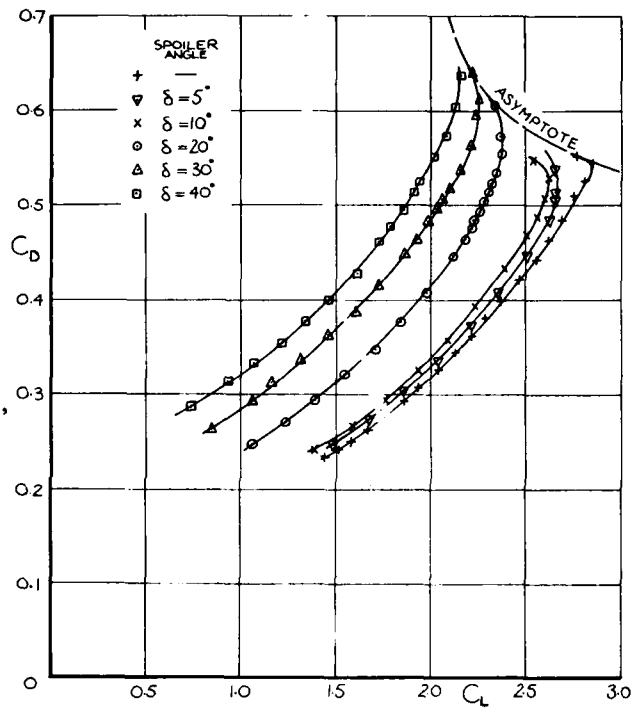


Fig 24 Drag polars: plain spoiler, 3% gap, 100% vented shroud, flap 40°

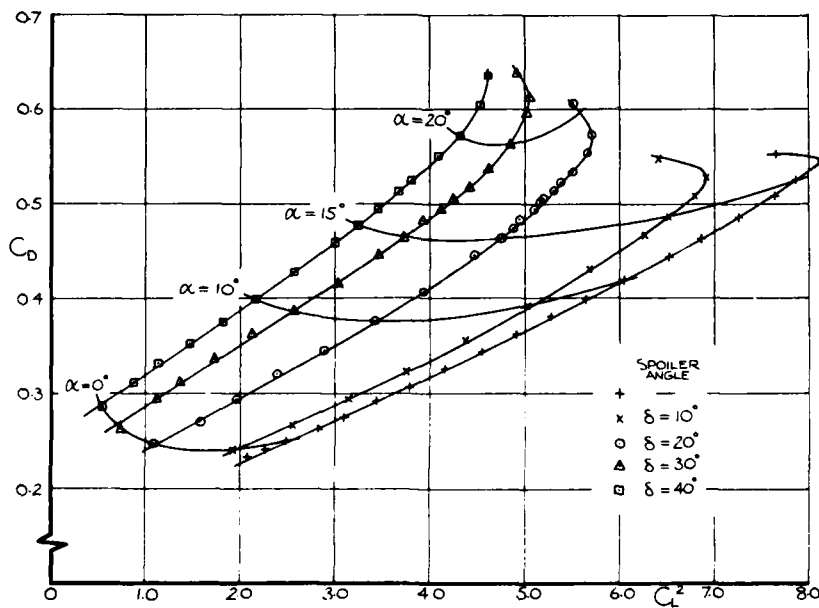


Fig 25 Drag curves versus C_L^2 : plain spoiler,

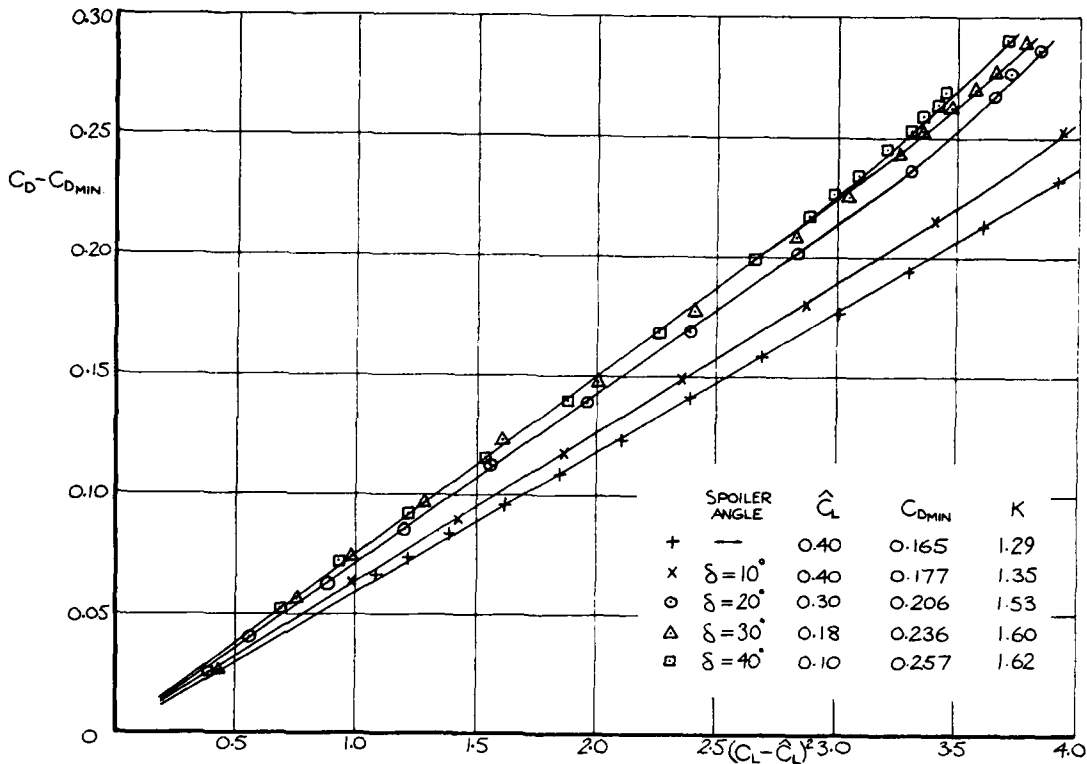


Fig 26 Linearised drag curves versus $(C_L - \hat{C}_L)^2$:
plain spoiler, 3% gap, 100% vented
shroud, flap 40°

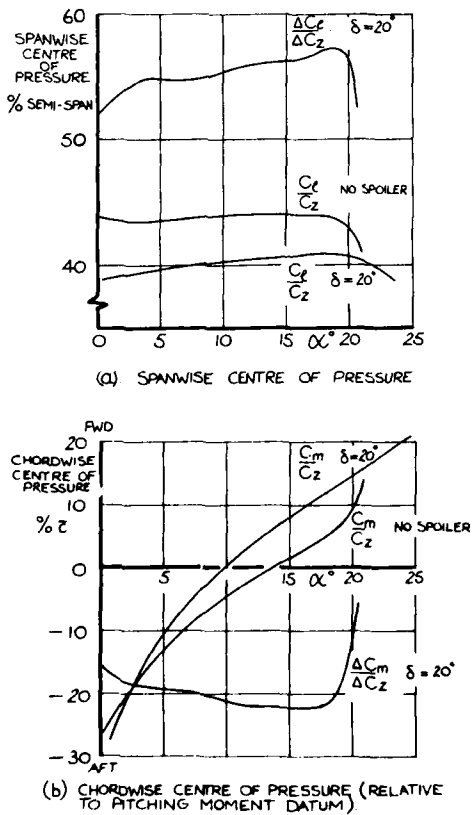


Fig 27 Points of action of forces and incremental forces: plain spoiler, 3% gap, 100% vented shroud, flap 40°

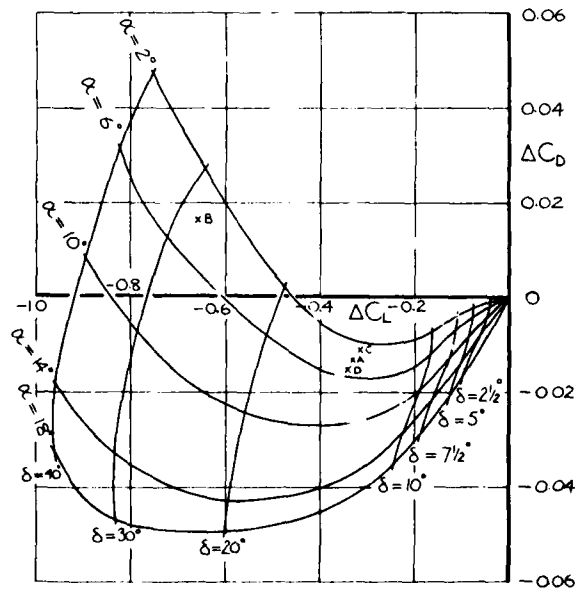


Fig 28 Incremental lift and drag as a function of incidence and spoiler deflection: plain spoiler, 3% gap, 100% vented shroud, flap 40°

4-28

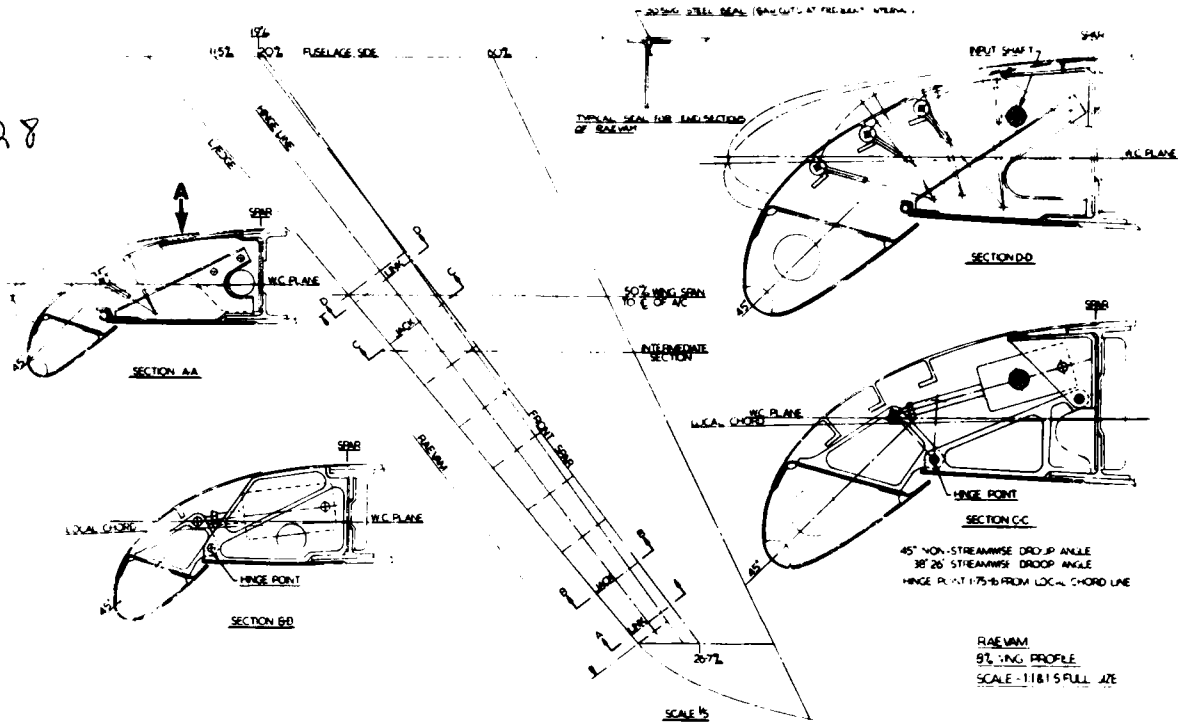


Fig 29 Typical RAEVAM mechanism for a strike fighter wing

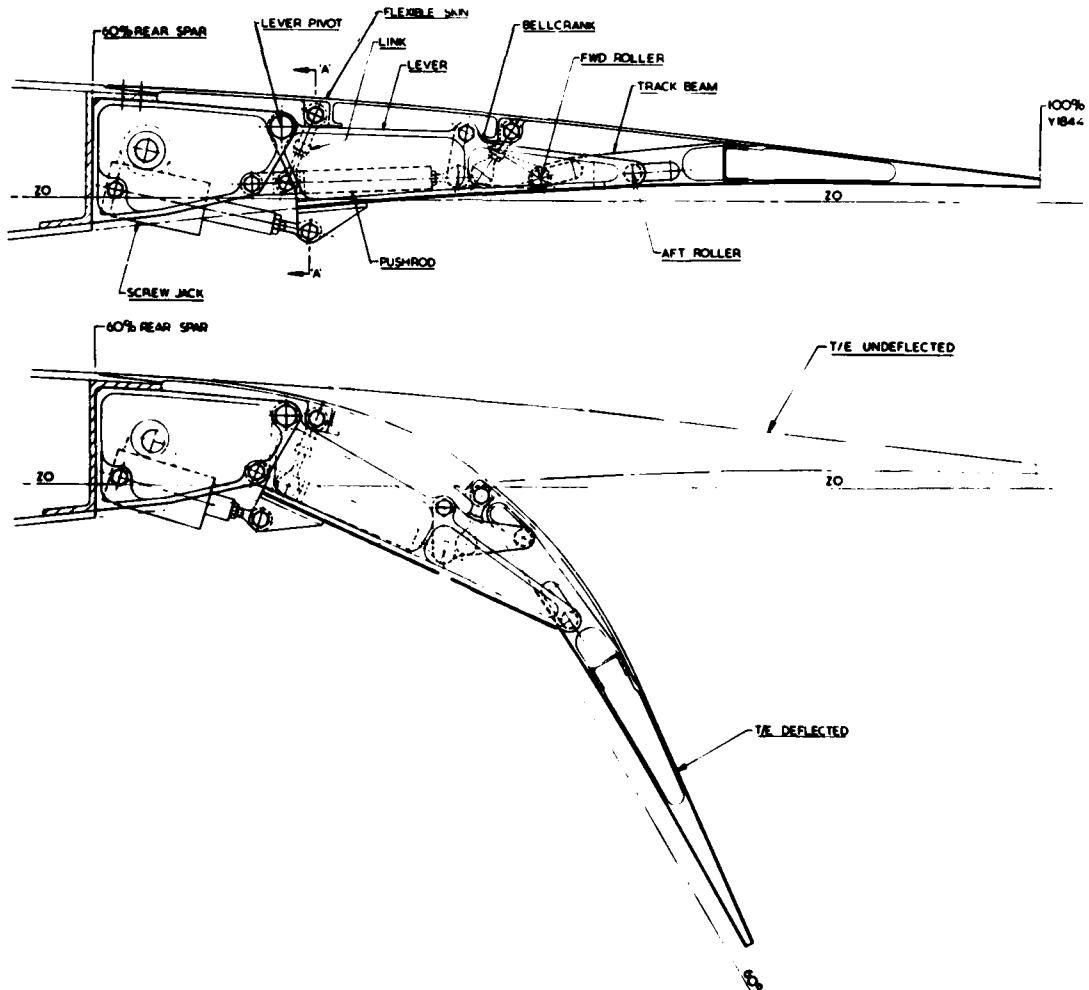
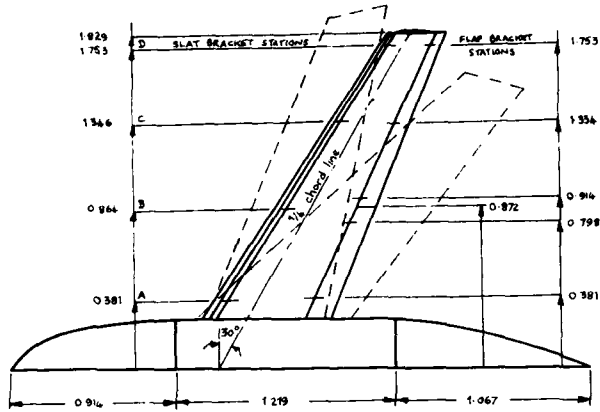


Fig 30 Typical contour flap mechanism



ALL DIMENSIONS IN METERS

PARAMETER	WING & CHORD SWEEP		
	20°	30°	45°
GROSS VALUES :			
WING AREA (m ²)	0.957	0.954	0.959
HALF SPAN (m)	1.957	1.929	1.500
TAPER RATIO	0.4	0.4	0.4
ASPECT RATIO	8.2	7.0	4.69
ROOT CHORD (m)	0.696	0.746	0.899
THICKNESS/CHORD RATIO (streamwise)	10.36%	9.54%	7.79%
PITCHING MOMENT DATUM (m) (8FE of clean leading edge projected to model camber-line)	0.487	0.638	0.874
GROSS AERODYNAMIC MEAN CHORD (m)	1.692	1.819	2.212

4.29

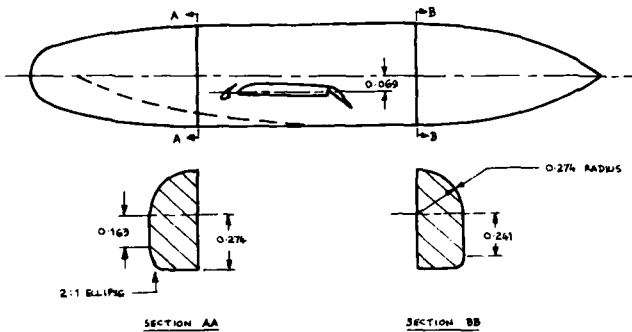


Fig 31 Geometric details of model used for research on swing-wing combat aircraft

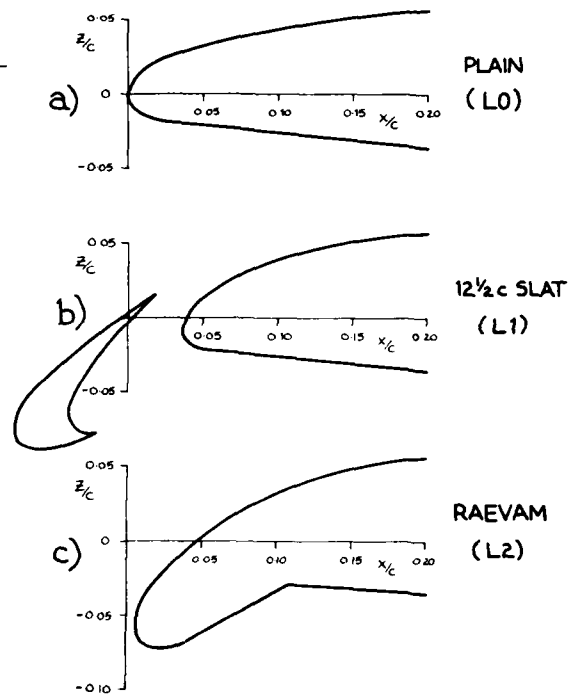


Fig 32 The leading edge devices (two-dimensional sections)

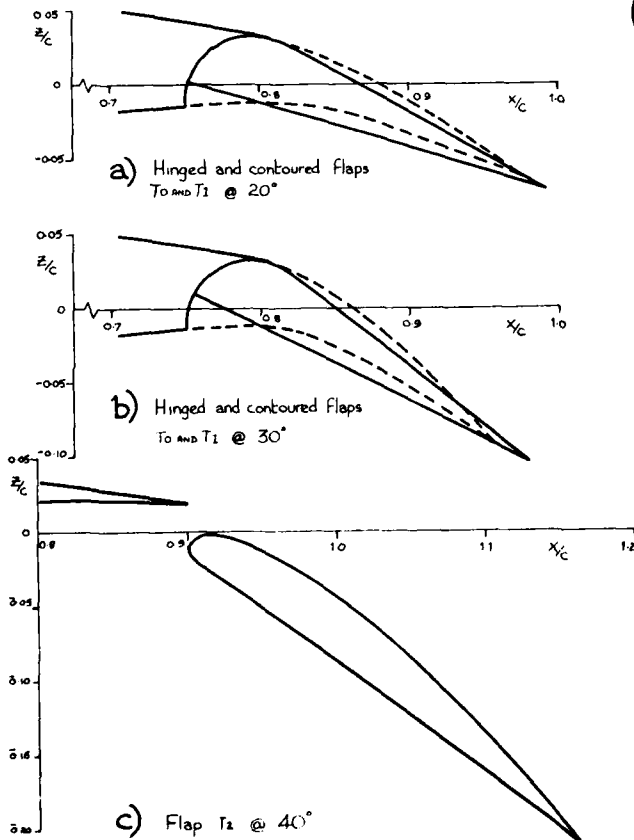


Fig 33 The trailing edge devices (two-dimensional sections)

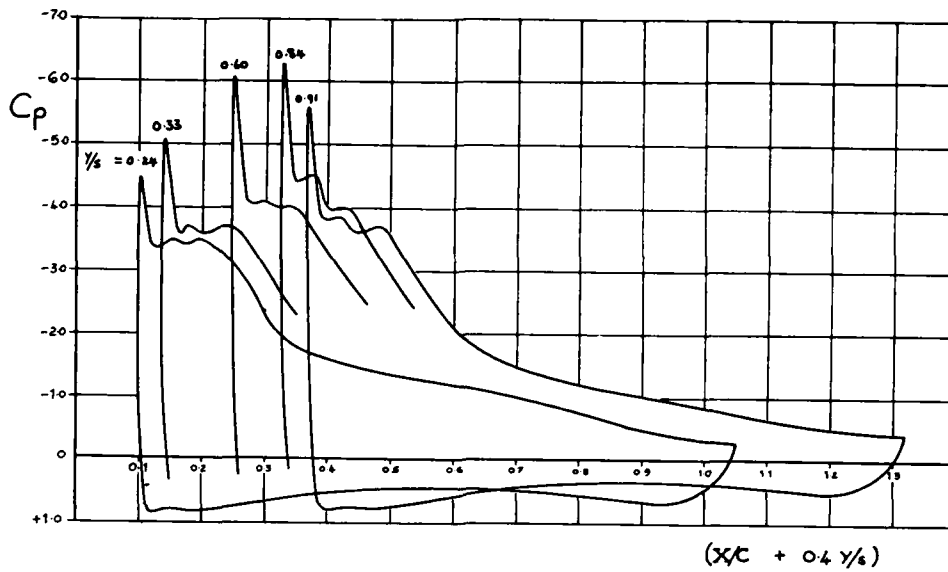


Fig 34 Variation of chordwise pressure distribution across the span for RAEVAM (L2) and contour flap (T1) at 30°

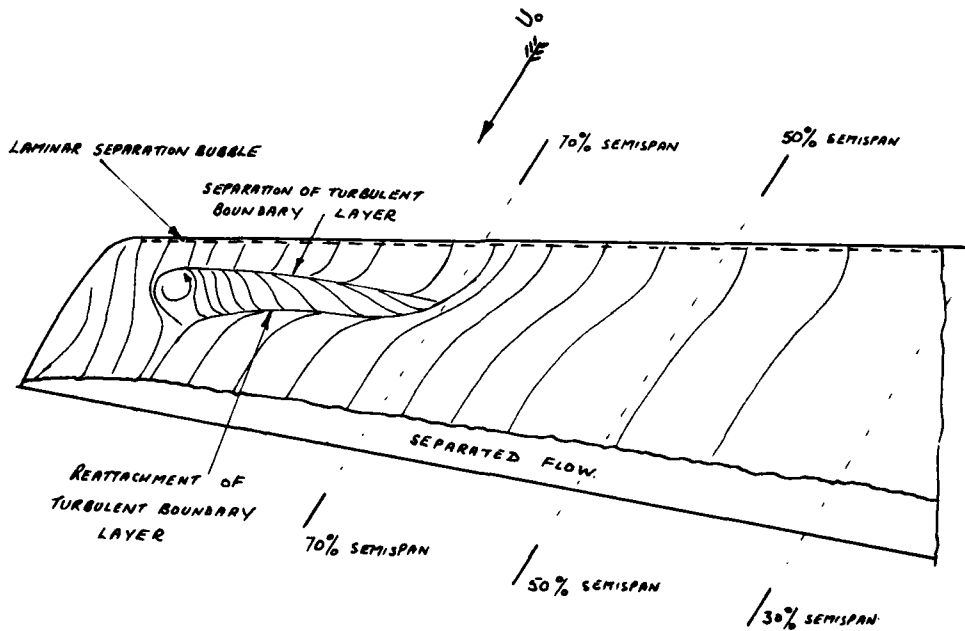


Fig 35 Sketch of surface oil flow pattern with .AEVAM leading edge (L2) and 30° contour flap (T1) near C_{Lmax}

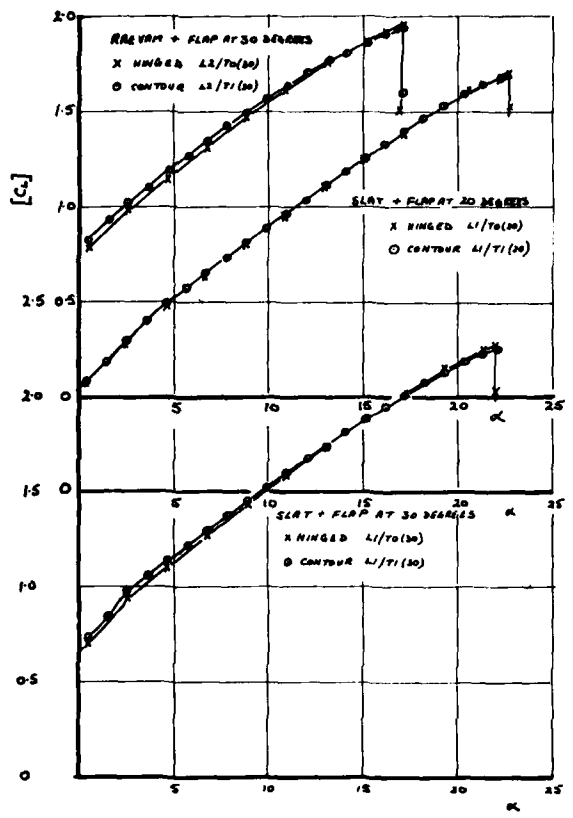


Fig 36a Comparison of hinged and contour flaps

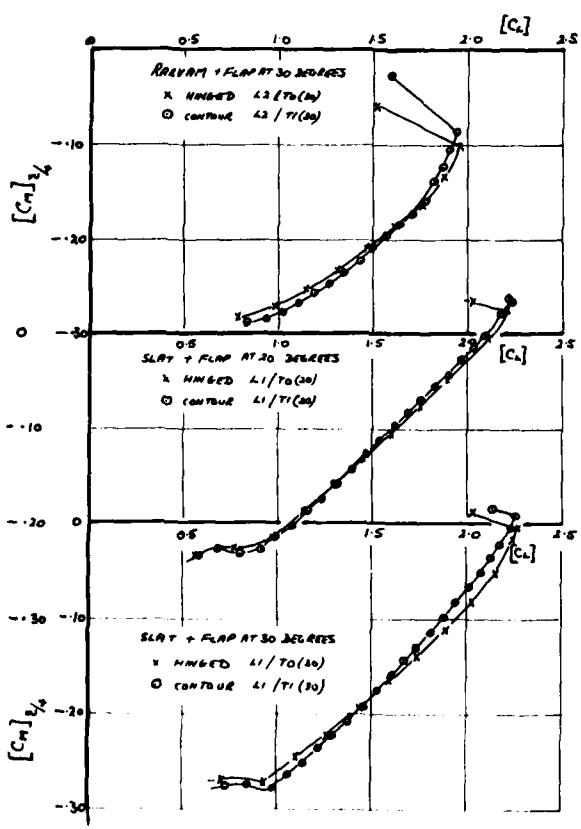


Fig 36c Comparison of hinged and contour flaps

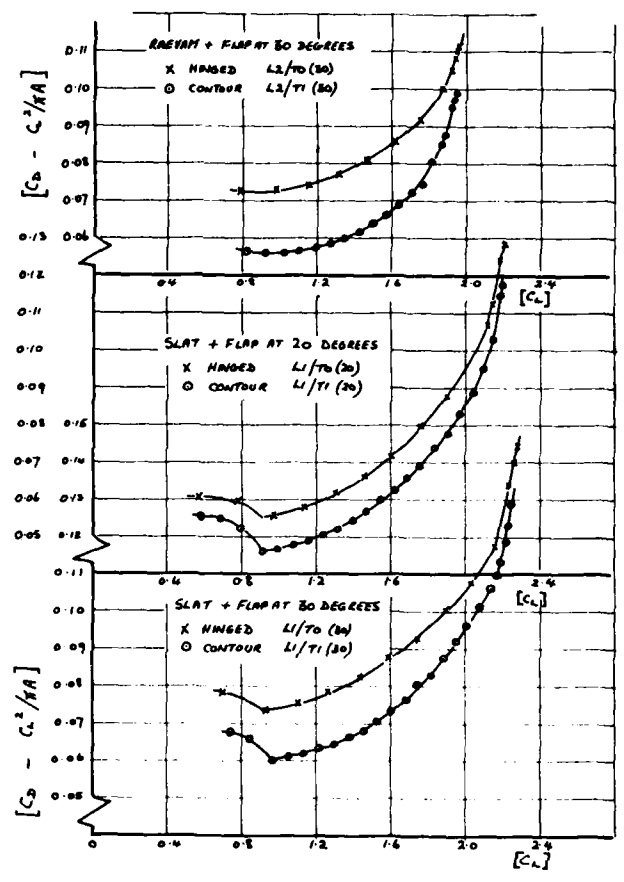


Fig 36b Comparison of hinged and contour flaps

41-32

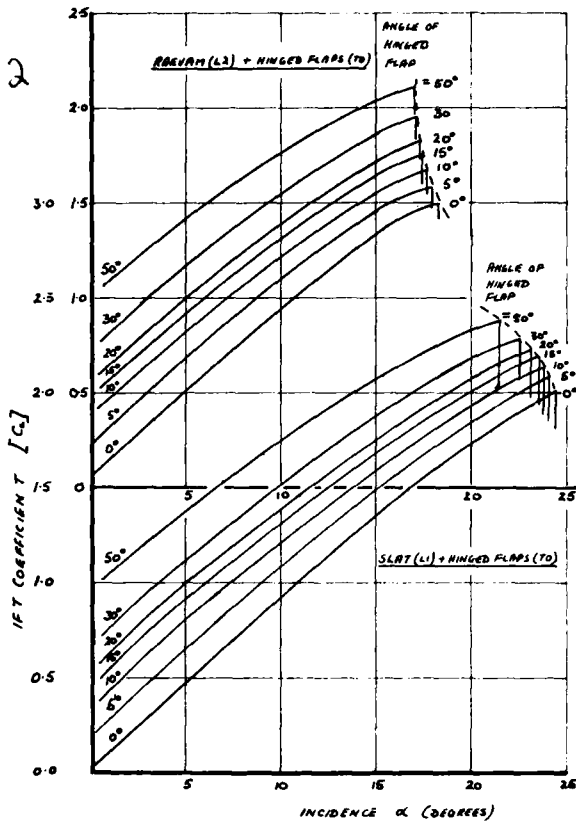


Fig 37a Basic data at 20° sweep

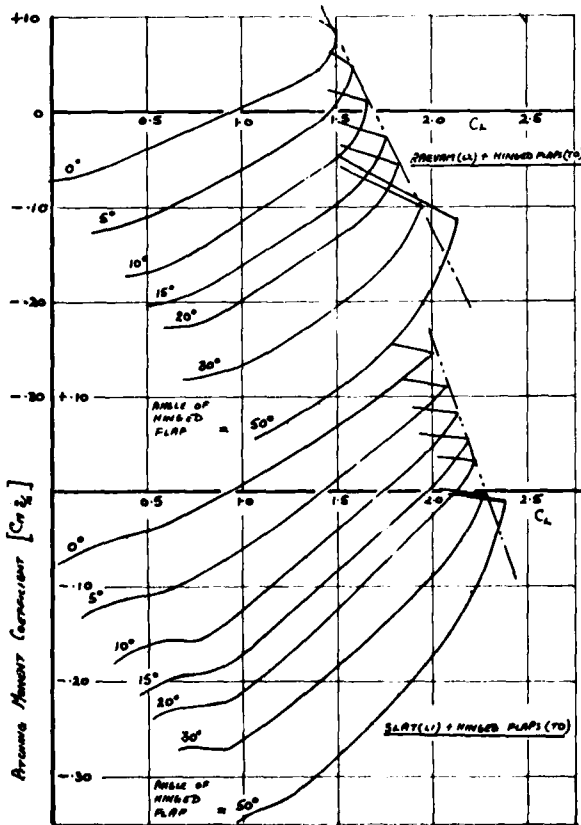


Fig 37c Basic data at 20° sweep

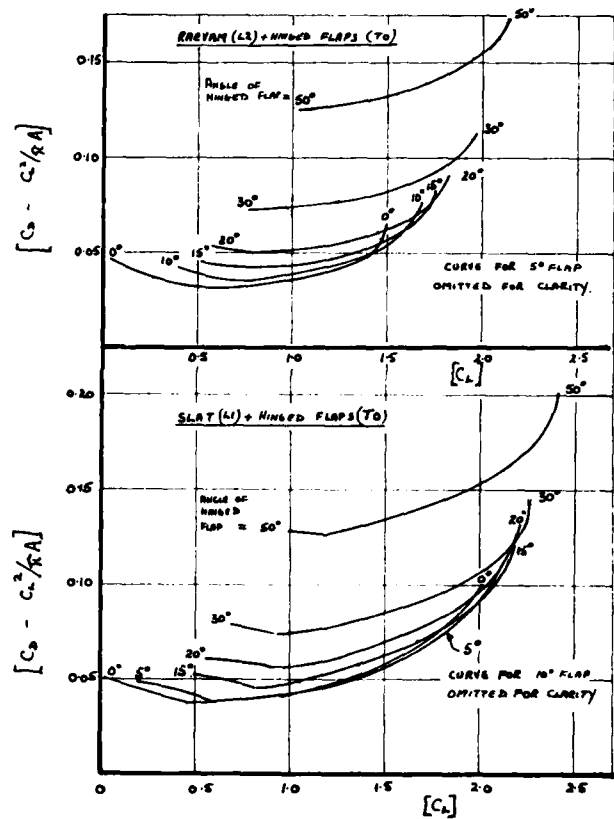


Fig 37b Basic data at 20° sweep

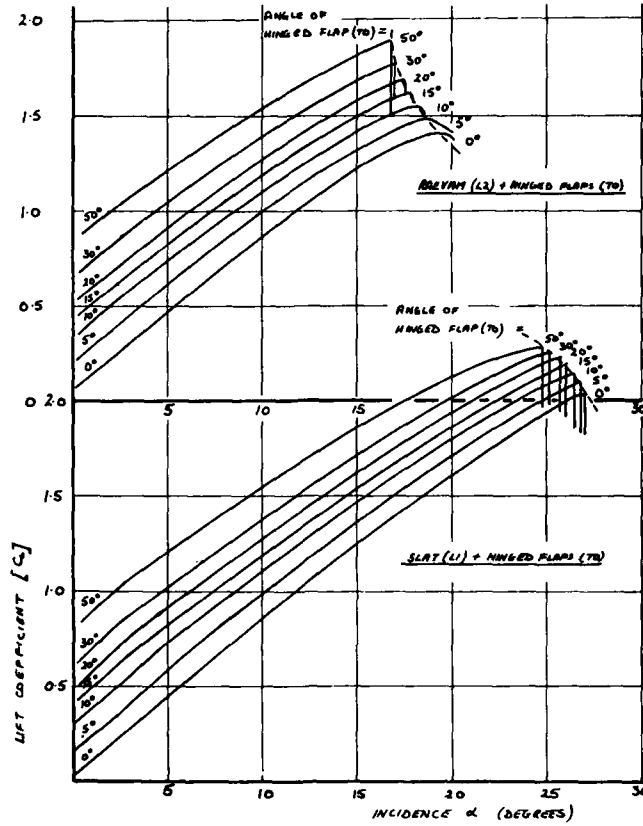


Fig 38a Basic data at 30° sweep

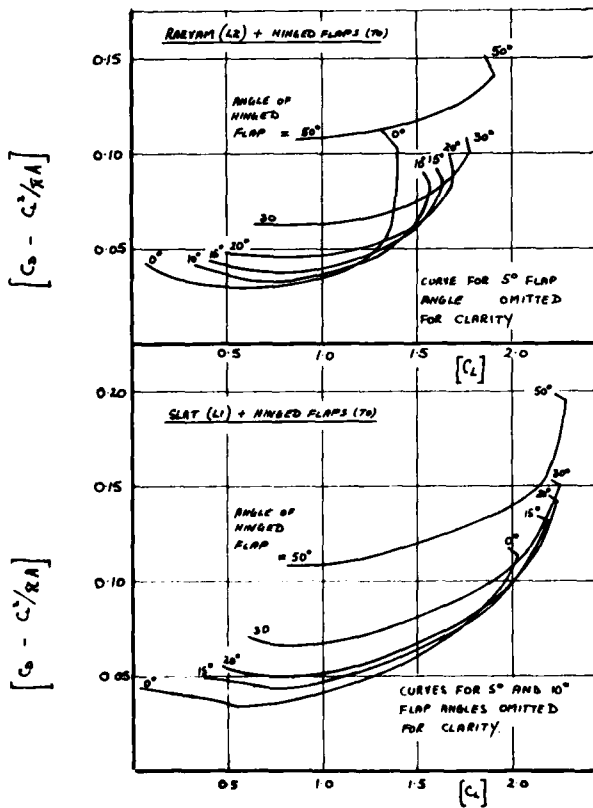


Fig 38b Basic data at 30° sweep

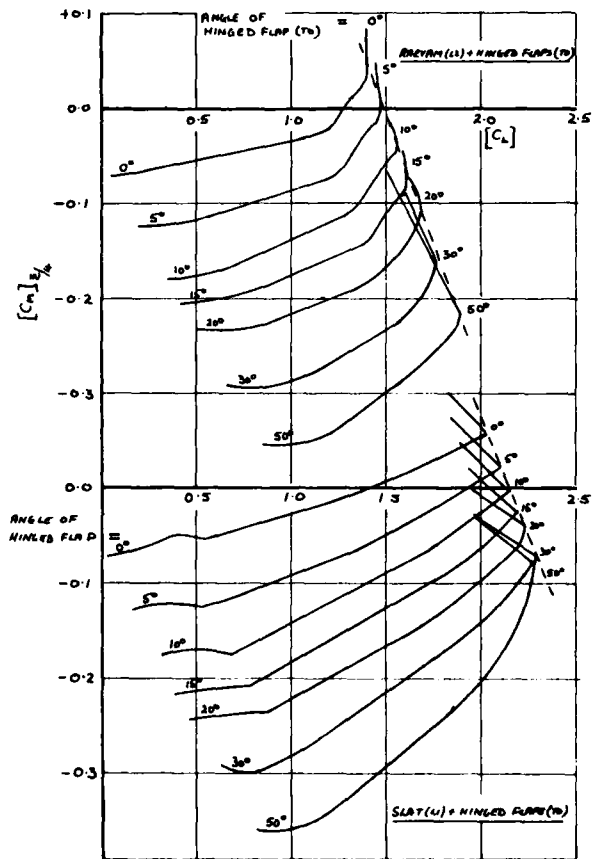


Fig 38c Basic data at 30° sweep

4-34

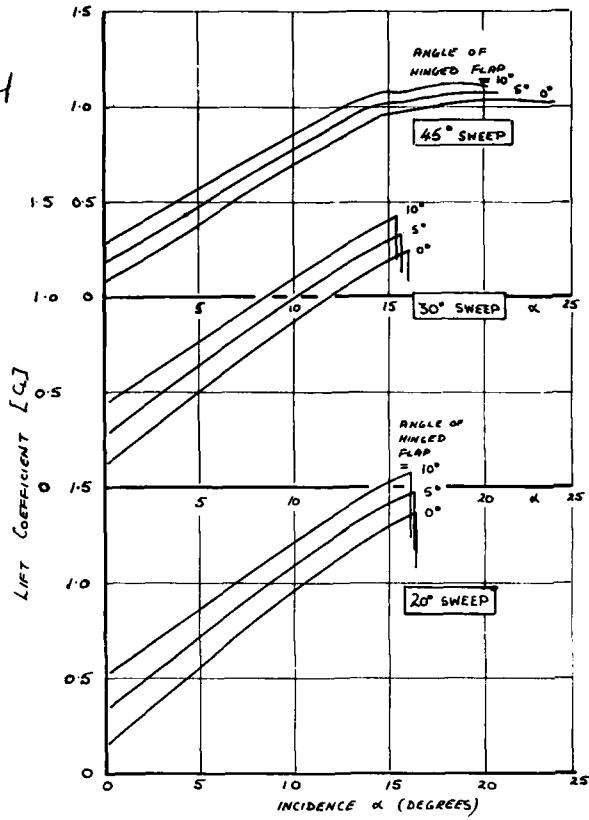


Fig 39a Basic data for plain leading edge (L0)

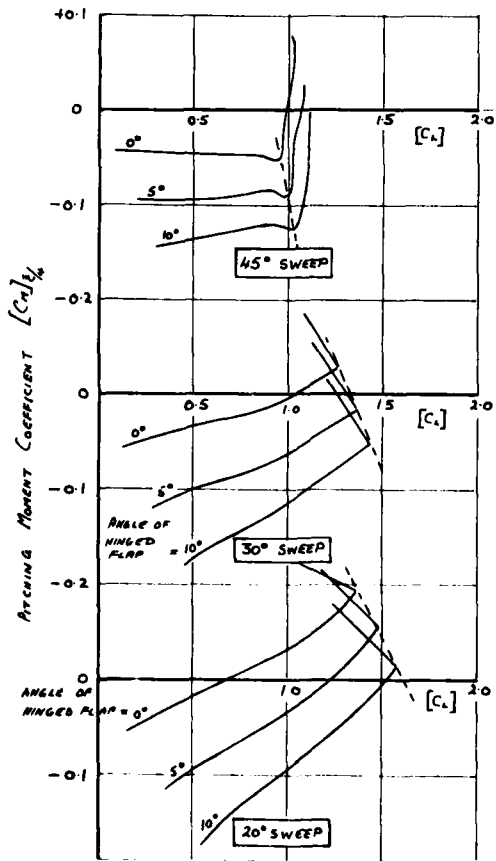


Fig 39c Basic data for plain leading edge (L0)

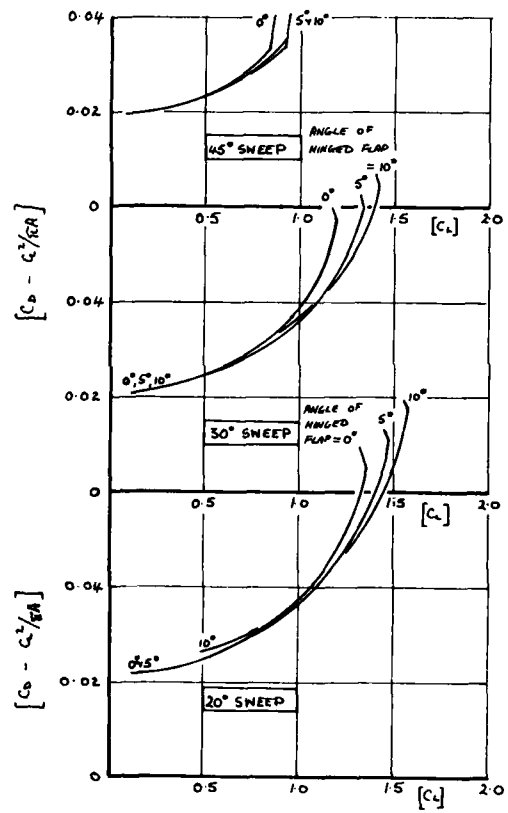


Fig 39b Basic data for plain leading edge (L0)

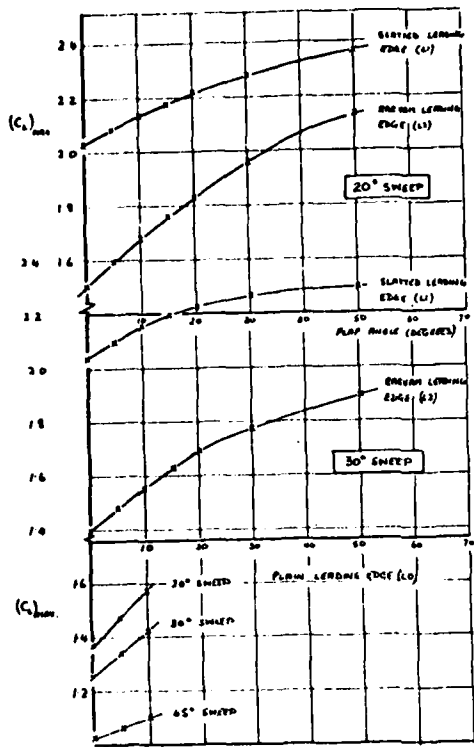


Fig 40a Summary of maximum lift performance

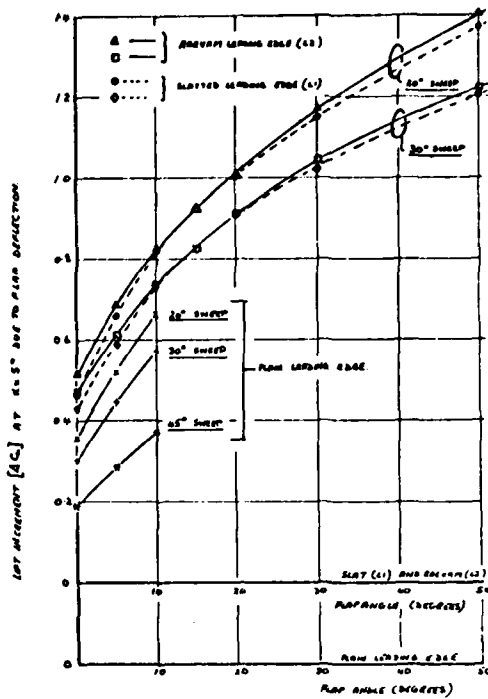


Fig 40b Summary of lift performance at constant incidence

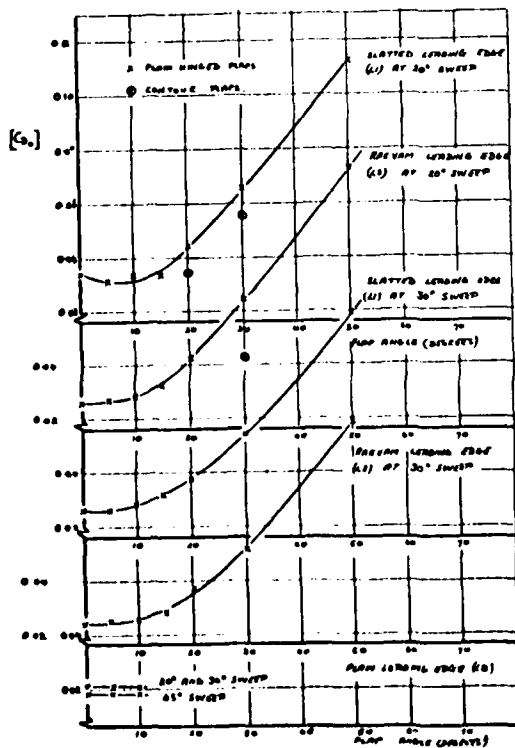


Fig 41a Summary of drag at zero lift

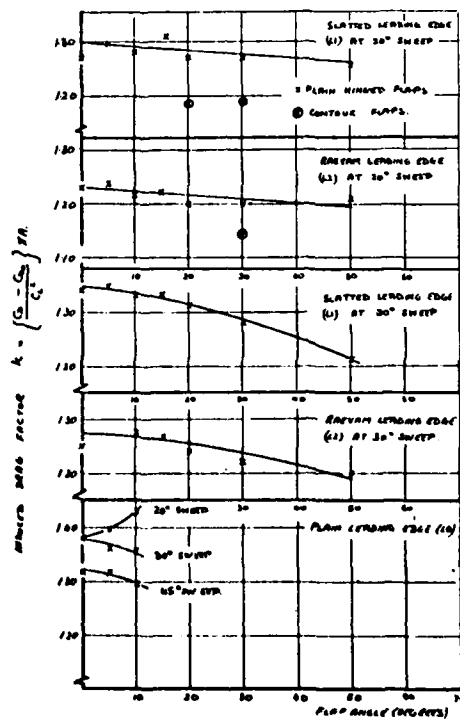


Fig 41b Summary of lift dependent drag characteristics

NOT REPRODUCIBLE

4-36

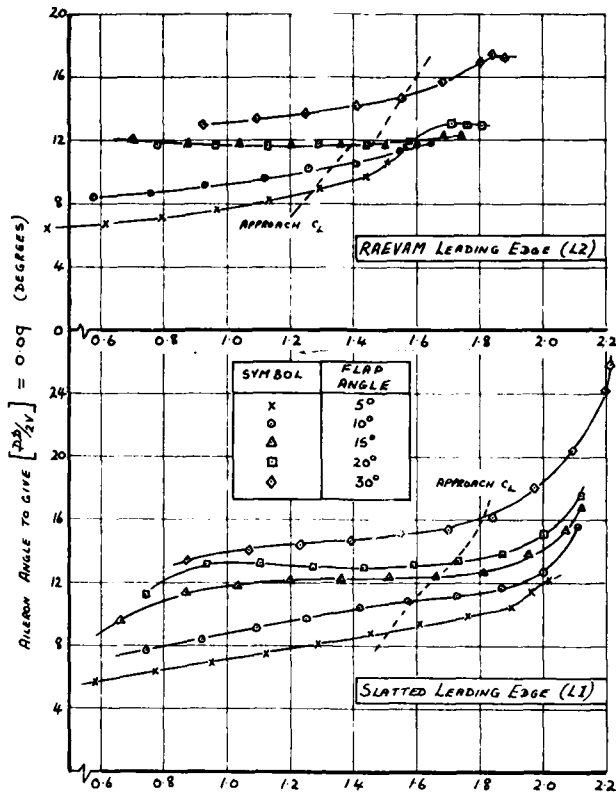


Fig 42 Variation of aileron angle to give $pb/2V = 0.09$ with C_L and flap angle

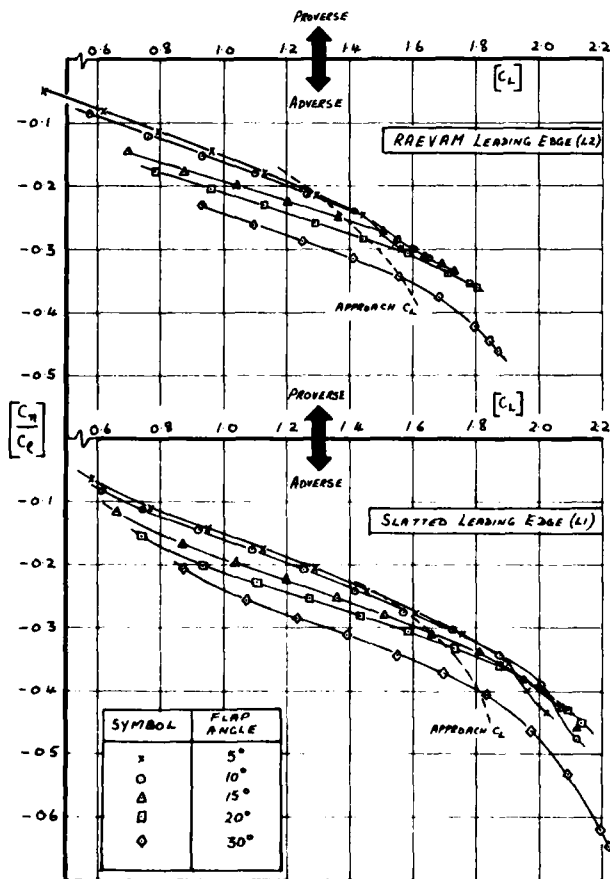
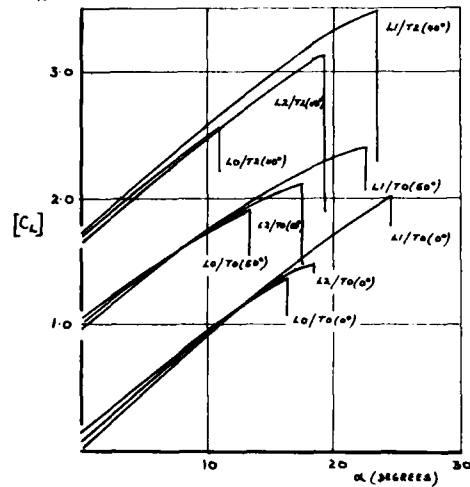


Fig 43 Yawing moment characteristics of hinged flaps used differentially as roll controls

T0 - HINGED FLAP L0 - PLAIN LEADING EDGE L1 - 12% CHORD SLAT
T2 - 33% CHORD SINGLE-SLOTTED FLAP L2 - RAEVAM.



COMBINATION	$C_{L_{max}}$	$C_{L_{REV}}$	OSC_{T0}	OSC_{L1}	$C_{L_{APP}}$	α_{APP}
L0/T0(0°)	1.36	—	1.09	—	1.09	12.0
L0/T0(60°)	1.91	—	1.53	—	1.53	7.0
L0/T2(40°)	2.56	—	2.05	—	2.05	4.0
L1/T0(0°)	2.03	1.66	1.62	1.41	1.41	16.5
L1/T0(60°)	2.37	2.28	1.90	1.94	1.90	12.0
L1/T2(40°)	3.47	3.27	2.77	2.78	2.77	12.5
L2/T0(0°)	1.50	—	1.20	—	1.20	12.0
L2/T0(60°)	2.13	—	1.70	—	1.70	9.0
L2/T2(60°)	3.12	3.11	2.50	2.64	2.50	10.5

Fig 44 Comparison of various high lift systems

FLIGHT CONTROL AND CONFIGURATION DESIGN
CONSIDERATIONS FOR
HIGHLY MANEUVERABLE AIRCRAFT

by

William T. Kehrer
Flight Controls Technology
Chief Engineer

Boeing Aerospace Company
Boeing Military Airplane Development
Seattle, Washington 98124
U.S.A.

SUMMARY

Advanced supersonic cruise tactical aircraft designs are trending towards high wing loading and high wing sweep combined with wing variable geometry to achieve design goals for efficient supersonic cruise and good maneuverability. Active control systems replace inherent aerodynamic stability to provide substantial weight and lift/drag (L/D) improvements and to achieve advanced mission performance capabilities. Working within wing geometry and other design constraints, the controllable limits of instability and the maneuver capabilities of various design approaches are investigated. Preliminary studies conducted to evaluate competitive configuration arrangements indicate that an aft-tail controller concept will be superior to canard and tailless delta configurations. The latter configurations suffer controllability limitations that compromise the ability to achieve design goals for maneuverability and efficient supersonic cruise. Thrust vectoring is explored as a means of improving maneuver load factor capability.

An additional fundamental design requirement for future tactical aircraft is the provision of good roll control for high-angle-of-attack maneuvering. The ability to achieve and sustain high maneuver load factor must be complemented by the ability to reverse heading quickly while at high load factor through rapid bank-to-opposite-bank maneuvers. Effective controls must be developed to achieve this roll control capability.

INTRODUCTION

Development of advanced tactical aircraft capable of superior mission effectiveness and survivability poses formidable design challenges in all areas of technology. Sophisticated defensive systems operating in the 1980/1990 threat environment will be extremely difficult to penetrate without substantial advances in current aircraft technology. Studies indicate that future tactical strike aircraft will require supersonic cruise capability complemented by good maneuverability to ensure penetration and survival of defensive air and ground systems. Active control technology (ACT) can make major contributions to the achievement of tactical aircraft performance goals. Highly reliable digital fly-by-wire control systems will permit relaxed static stability (RSS) and the incorporation of advanced control modes. RSS can allow substantial reductions in weight and drag and improvements in maneuver capability. Special control modes, such as six-degree-of-freedom control and variable-wing-camber control will improve mission performance and survivability. Applying ACT to advanced aircraft designs involves some special aerodynamic control and aircraft stabilization considerations. This paper attempts to identify some of the fundamental stability and control factors associated with design goals that include supersonic cruise capability and good maneuverability.

It is unfortunate that some key design requirements associated with achieving efficient supersonic cruise capability tend to be incompatible with good maneuver capability. Supersonic-cruise designs trend toward high wing sweep and high wing loading in an all-out effort to develop maximum aerodynamic efficiency for supersonic cruise. Without dramatic maneuverability improvements, configurations of this type cannot be expected to maneuver competitively with current supersonic-dash designs, which provide impressive maneuverability through low wing sweep, low wing loading, and some degree of wing variable geometry. Potential developments currently being studied to improve the maneuverability of supersonic-cruise configurations include wing variable geometry, thrust vectoring, lifting canard controllers, six-degree-of-freedom controls, and RSS.

Discussions presented here compare various design approaches for tactical supersonic-cruise aircraft with regard to controllability and stability. The generalized aircraft model assumed in these analyses is a high-thrust-loading, twin-engine configuration incorporating high wing sweep, high wing loading, wing variable camber and twist, and active controls. Various configurations of the generalized model are compared and discussed with regard to control capabilities and design limitations.

CONTROLLABILITY IMPLICATIONS OF RELAXED STATIC LONGITUDINAL STABILITY

5-2

Substantial gains in aircraft performance are obtainable by relaxing requirements for inherent aerodynamic stability to effect substantial weight savings and drag reductions. Fly-by-wire active control systems are then employed to stabilize the airplane. The degree to which longitudinal stability can be relaxed together with available longitudinal control power establish the required longitudinal balance of the airplane. The longitudinal balance, which describes the operational center-of-gravity (cg) range, strongly influences the configuration with regard to such key parameters as wing geometry and placement, empennage size, engine nacelle placement, landing gear location, and stores loading. The optimum longitudinal balance for maximizing trimmed L/D and maneuverability for supersonic cruise aircraft is configuration dependent to some degree, but tends to provide nearly neutral longitudinal stability for supersonic operation. This, however, requires a very unstable aircraft in subsonic regions, because of inherent effects of mach number on the aerodynamic center. The task of the stability and control aerodynamicist is to establish how much longitudinal instability is acceptable, in order to achieve maximum performance gains inherent in RSS.

The longitudinal instability limit establishes the furthest aft cg permissible. It is determined by examining the longitudinal control available to pitch the airplane nose down at high angles of attack. This critical control capability is mandatory to prevent the airplane from attaining a high-attitude, deep-stall condition from which it is not recoverable.

Fighter aircraft are frequently subjected to violent maneuvering that can lead to high-angle-of-attack (α) divergencies about all axes. Typical maneuvers are: rapid pullups or steeply banked, high-load-factor, windup turns; high roll rates inducing inertial coupling with α and sideslip divergence; and steep climbs producing rapid airspeed loss. Alpha limiting incorporated in an active control system can ensure that the aircraft does not exceed its controllimits provided that the alpha-limiting system is supplied with adequate pitch control power to arrest alpha divergencies. The design of the aircraft and its flight control system must consider pertinent stability and control factors and must provide recovery from the dynamic alpha overshoot for all types of maneuvering.

Figures 1 and 2 illustrate high-angle-of-attack longitudinal control and stability considerations that establish the maximum acceptable level of instability. Figure 1 shows pitching moment characteristics of a configuration that has been balanced with excessive instability. This configuration is characterized by pitchup and limited control power. The aft cg limit produces a negative static margin of 9% mean aerodynamic chord (MAC); and full nose-down control is not capable of preventing uncontrolled angle-of-attack departures above an α of about 20 deg. Rebalancing the aircraft to a 4% MAC instability limit, figure 2 provides the margin of nose-down control necessary for the alpha limiting system to prevent high alpha divergencies. The amount of control required for the alpha limiting system is determined through rigorous dynamic analysis of rapid alpha buildups. A value of nose-down pitching moment is selected that provides responsive pitch acceleration, $\ddot{\theta}$, considering and including adverse data uncertainties.

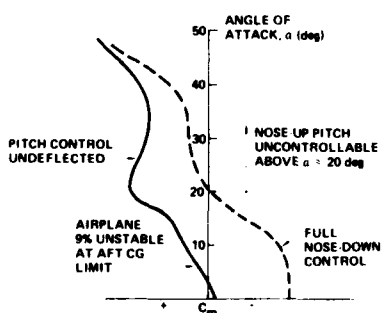


Figure 1. Excessive Instability

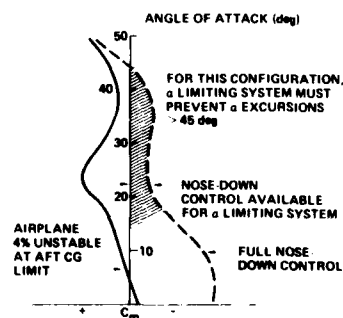


Figure 2. Controllable Instability

CONFIGURATION IMPACT ON DEGREE OF RSS REQUIRED AND ACHIEVABLE

Central considerations in determining the instability limit involve the characteristic shape of the wing-body pitching moment curve, C_m versus α , and the degree of nose-down pitch control that can be generated. Wing planforms with highly swept leading and trailing edges produce strong pitchup at high angles of attack. The pitchup becomes more severe with increasing wing aspect ratio. Thus configurations with highly swept wings cannot be balanced to be as unstable as those with wings of more moderate sweep. Configurations with long, lifting forebodies, or with wing strakes or double delta planforms are much less tolerant of negative static margins. The designer must carefully trade all of these factors to optimize his configuration.

Some generalization can be made about instability tolerance as a function of the pitch control system involved. Aft-tail configurations tend to permit large negative static margins if the tail is located relatively low and is capable of rapid positioning through a large deflection range. Canard configurations are limited in negative

static margin only to the extent that the wing-body aerodynamic center typically must be located behind the aft cg limit, and the canard must be capable of extremely large leading-edge-down deflections to unload itself at high alphas. The tailless configuration, which must rely on wing elevon deflections alone for pitch control, is intolerant of negative stability and typically must be balanced no less than neutrally stable for subsonic operation. 5-3

The following discussions compare aft-tail configurations with canard and tailless concepts with regard to RSS requirements, maneuver capabilities, and special control problems. The baseline supersonic-cruise fighter configuration is a simple slab-surface, aft-tail concept designed for minimum tail size and loads and balanced to ensure lifting tail loads throughout the flight envelope. An identical configuration, employing a canard instead of an aft-tail, is then evaluated. The canard size (exposed surface area) is the same as the baseline aft tail to provide a one-to-one comparison. Finally, a tailless concept is evaluated against aft-tail and canard configurations.

AFT-TAIL RSS CONFIGURATION

Aft-tail aircraft, conventionally designed to provide positive subsonic longitudinal stability margins, will normally trim and control the airplane with down-tail loads during supersonic operation within the cg range dictated by subsonic stability considerations. The down-tail loads will, of course, penalize supersonic trimmed L/D. This problem can be alleviated to a limited degree by designing some positive C_{M_0} into wing and body characteristics. However, it is difficult to achieve without drag penalties positive C_{M_0} values of sufficient magnitude to permit trimming with zero or positive tail loads for other than lg level flight operation. Center-of-gravity adjustment through fuel transfer can be employed for some designs to accommodate the aft aerodynamic center shift that occurs when going from subsonic to supersonic flight. However, this option is not open to designers of tactical aircraft that must traverse the transonic region rapidly in both maneuvering and one g flight. The RSS design approach, if fully exploited, will eliminate the problem of down tail loads supersonically, ensuring up tail loads for trim and maneuver control at all mach numbers and loading conditions. Such an RSS configuration is described in figure 3, which depicts balance and stability characteristics estimated for an aft-tail fighter configuration evolved from design goals combining efficient supersonic cruise and superior maneuverability. This particular configuration has a low-aspect-ratio, highly swept, clipped-tip delta wing and a low slab tail (no elevator) that is approximately 15% of the wing area. The wing-body shape produces substantial pitchup at wing-stall angles of attack, alpha between 15 to 20 deg. Tail input to stability is strong, however, and becomes dramatically stronger at very high angles of attack. The most critical nose-down control requirement exists in the pitchup region, near alpha 18 deg. The instability limit for this configuration is selected at a negative static margin of 13% MAC. This is the furthest aft cg at which full tail deflection leading edge up (25 deg δ_H) will still provide safe nose-down control. For this analysis the $-AC_m$ available was selected to provide a nose-down pitch acceleration, θ , of -5 degree per second², including adverse data uncertainties. If the airplane is balanced to this degree of subsonic instability, it will be stable at all supersonic conditions and will trim with up tail loads (lifting) over the entire cg range at all mach numbers. Moreover, its maneuver load factor capability will in no way be limited by pitch control power.

A major contributing factor to the large negative static margin possible for this configuration is the ability of the tail to continue to produce large normal force with increasing angle of attack. This is typical for low-aspect-ratio tails when they are positioned (low) such that they are not forced to operate in the poor environment of wing-body wake at high alphas. Figure 4 shows the tail normal force (C_N) measured for this configuration developing steadily increasing normal force up to C_N 's approaching 1.8 at aircraft alpha of 70 deg. It is possible that this configuration could support a larger negative static margin than the selected -13% MAC, because the tail C_N is less than maximum at the maximum tail deflection in the critical alpha range. Greater tail deflection should produce some additional nose-down moment. However, the selected tail deflection range of +25 deg (50 deg total) approaches actuation design limits for a control surface. This deflection range accommodates the limiting control requirements at fore and aft cg limits, and with the selected cg range the tail loading appears near optimum for minimum drag over most of the flight envelope.

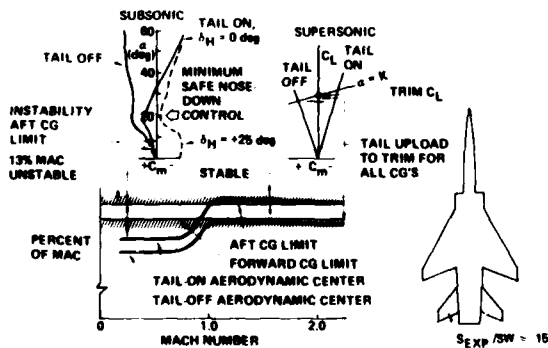


Figure 3. Aft-Tail Instability Limit and Longitudinal Balance

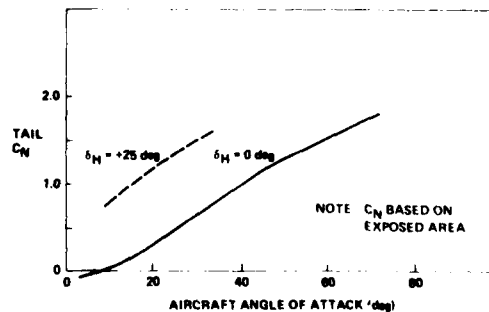


Figure 4. Horizontal Tail Normal Force

CANARD RSS CONFIGURATION

5-4

Preliminary design studies often identify canard configurations as optimum for supersonic cruise strike-fighters. The canard provides the attractive feature of always trimming and controlling the aircraft with uploads that contribute to total aircraft lift. However, this feature is commonly overemphasized in that much canard lift is usually negated by unfavorable interference with the wing throughout the useful alpha range of the aircraft. That is, the canard downwash on the wing unloads the wing, and total aircraft lift is only slightly affected by addition of the canard.

The SAAB AJ-37 Viggen is an excellent example of the successful application of a canard trimmer to improve the overall performance of an elevon-control fighter design. The Viggen uses a close-coupled, highly swept canard located above the wing plane so as to develop favorable interaction between canard and wing vortex systems at very high angles of attack. The canard was incorporated into the Viggen design to increase the trimmed lift capability of the airplane sufficiently to permit short field operation. The lifting canard is effective primarily in generating nose-up pitching moment, permitting down-trimming wing elevon controls to increase wing lift. Compared with a conventional delta-wing design without canard, the Viggen is able to generate approximately 70% greater trimmed C_L in the landing configuration. The Viggen canard is not employed as the primary pitch control. Elevons constitute the pitch controller, and the flapped canard surface is used as a trimming device throughout the flight envelope to optimize trimmed L/D and maneuver capability.

The North American B-70 incorporated a canard trim surface similar to the Viggen application. The B-70 derived increased trimmed lift for low-speed operation through canard-produced nose-up pitch that permitted down-trimming elevon controls. The B-70 also used the canard to optimize trimmed L/D in supersonic operation.

It should be noted that the canard configurations evaluated in this paper are canard-control concepts as opposed to canard-trim designs that employ wing elevons for primary pitch control, as characterized by Viggen and B-70 designs. In this analysis, the canard is evaluated as the aircraft's sole source of pitch control. Wing trailing-edge (and leading-edge) surfaces are reserved for wing variable-camber functions, and thus elevon controls are not available to assist the canard.

The longitudinal instability limit for the canard-controlled aircraft must typically be established by selecting the aft cg limit so that the wing-body configuration (canard off) is sufficiently stable to ensure nose-down pitching moments in the most critical angle-of-attack regions (stall and deep stall). Stall recovery control can then be effected by deflecting the canard leading edge down sufficiently to unload it, thus cancelling its nose-up pitching moment contribution. The degree of aircraft longitudinal instability permissible is determined through design iteration involving determination of wing-body pitching moment characteristics and selection of required canard size and deflection range. Practical limitations on canard deflection range become a key factor in this design iteration. Very large leading-edge-down deflections needed for stall recovery together with leading-edge-up deflections for such maneuvers as takeoff rotation can result in excessive deflection requirements.

Figure 5 illustrates longitudinal balance and control iteration for a typical canard-controlled supersonic fighter. For competitive evaluation, this aircraft employs the same wing planform as the aft-tail configuration previously discussed; the canard exposed area is the same as for the aft tail, 15% of the wing area; and the canard is a simple slab surface without flaps. The canard is located high on the forebody to avoid producing flow distortions at the nacelle inlets and to reduce unfavorable interference with the wing lift. The wing-body pitchup characteristics at subsonic conditions, together with limitations on maximum obtainable canard deflection, dictated selection of an aft cg limit 9% forward of the canard-off aerodynamic center (ac). This balance provided sufficient pitch-down moment to prevent deep stall through an alpha limiting system. Prevention of stall pitchup departure in this case results from unloading the canard by rotating it 40 deg leading-edge down. This control action develops sufficient negative canard C_N to reorient the canard resultant load vector to cancel the nose-up pitching moment produced by the canard. This reverts the pitch

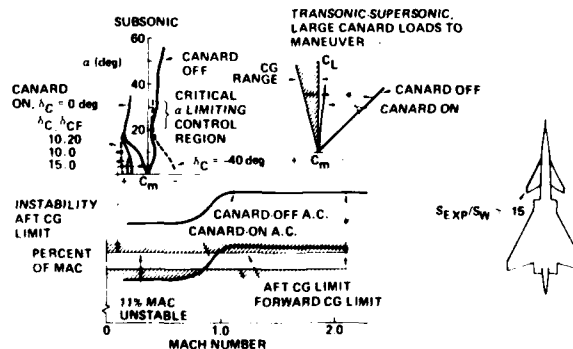


Figure 5. Canard Instability Limit and Longitudinal Balance

balance to the nose-down pitching moment required for stall recovery. The large deflection is made necessary by the large effective angle of attack of the canard resulting from aircraft alpha combined with the wing-body upwash field. For example, at an aircraft alpha of 30 deg, the effective canard alpha at zero deflection is approximately 39 deg for the configuration shown in figure 5. 5-5

The subsonic static stability margin for this configuration is approximately -11 MAC. This is the maximum instability possible while still retaining stall recovery capability. It results simply from the required 9. static margin for the canard-off configuration coupled with the 20. forward ac shift produced by the canard. Figure 5 summarizes the balance and the mach number relationships between the selected aft cg limit and the aerodynamic centers, canard off and canard on.

Comparison of figure 5 with the figure 3 balance picture for the aft tail aircraft shows that the canard is an extremely powerful destabilizing device. In this comparison, the canard at the same exposed area as the tail is approximately four times as powerful as the tail in shifting the aerodynamic center. This is because the canard operates in the upwash flow field of the wing-body, but the tail operates in a flow field comprising strong wing downwash and suppressed dynamic pressure. Further examination of figure 5 shows that even though this configuration is balanced to the maximum acceptable level of subsonic instability, the wing-body ac is still far aft of the center of gravity, resulting in the requirement for large canard uploads to trim and maneuver, particularly at supersonic speeds. For example, a calculation for 1.2 mach at 40,000 ft shows that the canard C_{LMAX} (1.7 based on exposed area) is reached in trimming the airplane at a load factor of 4.3g at the forward cg limit. This limited maneuver capability could be improved by increasing canard size or by improving canard lifting capability with devices like variable camber. Developing positive wing-body C_{M0} would also seem to ease the supersonic maneuver problem, except that $+C_{M0}$ would aggravate the subsonic pitchup control problem and would require increased static margin. A preferable alternative would be to improve the longitudinal balance to reduce canard loads required to trim. This would mean shifting the cg range further aft by devising some means of improving the wing-body stability. As previously discussed, the subsonic static margin for this configuration was established at -11 MAC-the instability limit as determined by stall departure criteria. The effect of reduced subsonic static margin (if attainable) on supersonic maneuver capability is shown in figure 6. For the example shown at 1.2 mach at 40,000 ft, it would be necessary to shift the cg range further aft about 8. MAC to achieve full maneuver capability of the wing. This substantial rebalance could only be achieved by developing major improvements in subsonic stability characteristics. The required improvements could be accomplished by modifying the wing planform or by developing devices to reduce wing-body pitchup.

In addition to the maneuver problem, there is further incentive to improve airplane balance to reduce canard trim loads. This is shown in the figure 7 comparison of canard and aft tail configurations with respect to control surface loads required to trim the airplane in maneuvering flight. Figure 7 compares the maximum canard and aft tail surface loads to trim the maneuvering airplane at 1.2 mach at 40,000 ft. Canard loads are greatest when trimming to the forward cg limit; the aft-tail loads are greatest when trimming to the aft cg limit (figs. 3 and 5). In both cases the control surface loads are positive (lifting). The canard must develop over four times the load that the tail must develop to trim to a given load factor. This comparison is typical of all supersonic operation. An evaluation at subsonic conditions shows comparable trim moment requirements for selected canard and aft-tail balances. However, the canard load to trim is still somewhat larger than for the tail because the canard moment arm (to cg) is substantially less than the tail moment arm.

The previous discussion of canard maneuver control limitations and loading problems is simplified in that it did not consider effects of wing variable camber for maneuvering flight. The negative pitching moment normally associated with cambering the wing to improve maneuver capabilities will require further increases in canard loads to trim the aircraft. The converse of this is true for the aft-tail arrangement; because the wing-body ac is forward of the cg, wing-camber negative C_{M0} will reduce the required tail uploads to trim. Thus inclusion of the wing variable camber effects is expected to further magnify differences between canard and aft-tail maneuver load requirements.

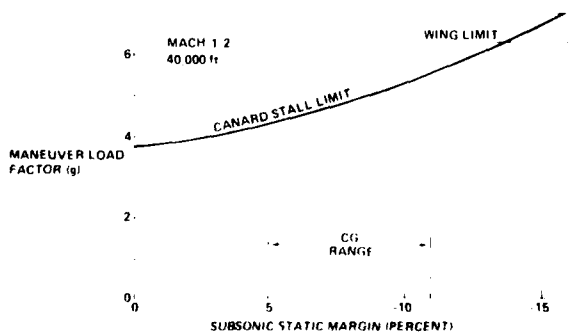


Figure 6. Effect of Longitudinal Balance on Supersonic Maneuver Capability for Canard Control Aircraft

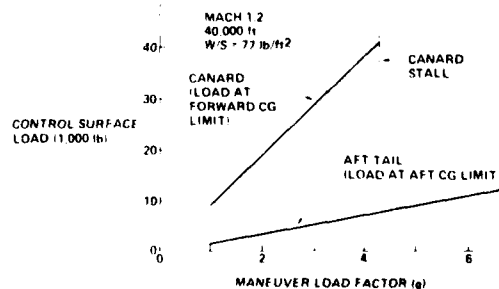


Figure 7. Control Surface Load Required to Maneuver

5-6

Large control surface loads are a critical concern for the designer. Loads for the canard, such as shown in figure 7, pose substantial structural weight penalties and serious design problems in the surface mounting and actuation system. To develop viable canard-controlled aircraft, the designer must develop solutions to these problems.

Canard control limitations are further evident in the C_m versus alpha data for the low-speed regime shown in figure 5. Examination of the canard nose-up ($+\Delta C_M$) control inputs for leading-edge-up canard deflections of 10 and 15 deg and for the canard at 10 deg with an added geared flap assumed at 20 deg down shows pronounced control limitations in the nose-up direction. These limitations result from canard stall problems induced by canard deflection, angle of attack, and body upwash; and aggravated by the canard unporting from the body when deflected. Analysis shows that the selected canard size is not adequate for takeoff rotation. To avoid incorporating wing elevons to assist canard control, increased canard size or a more effective canard high-lift system is required.

Additional design cycling of the canard-controlled aircraft described in figure 5 is required to resolve longitudinal balance and control problems. Configuration modifications that should be evaluated include the following:

- (a) Alter the wing planform or develop devices to improve wing-body stability and to reduce or eliminate the wing-body pitchup. This could allow the cg range to be moved further aft, thus alleviating the canard loading problem. These studies should also examine trades involving the development of wing-body positive C_{M_0} .
- (b) Increase the canard size.
- (c) Incorporate leading- and trailing-edge flaps on the canard to improve its lift capability.
- (d) Abandon wing variable camber to permit use of elevon pitch controls, and re-define the concept to a canard-plus-elevon control system.
- (e) Attempt to augment canard control with thrust vectoring.

Each of the preceding modifications probably constitutes a significant overall design penalty. Further design cycling could develop improvements, but trade studies involving aircraft weight, drag, maneuver performance, and cost factors are expected to show that the canard concept is not competitive with the aft-tail aircraft for the supersonic cruise strike fighter mission.

Discussions so far have dealt only with relatively small, high-load-factor aircraft. Considerable design experience with large supersonic low-load-factor aircraft has brought out additional design considerations for the canard concept. Some of these considerations may become important for supersonic strike configurations that are substantially larger than the fighter concepts. Figures 8 and 9 illustrate the pronounced effects of aeroelasticity on the longitudinal stability and balance of a large supersonic cruise transport configuration incorporating a canard trim and control surface. Figure 8 indicates the nature of aeroelastic effects on longitudinal stability. In maneuvering flight, aerodynamic lifting forces acting on the canard, forebody, and forward inboard wing surface area tend to bend the forebody upwards. Mass effects of the loaded body (structural weight plus payload) produce a downward-bending countertendency. When mass loading is light relative to lift loading, lift effects dominate, resulting in upward bending of the forebody. This is destabilizing because the upward bending induces additional angle of attack and additional lifting force, shifting the effective aerodynamic center forward. When mass loading is heavy relative to lift loads, the mass effects dominate, bending the forebody downward in a stabilizing direction.

Figure 9 shows the magnitude of the aeroelastic lift and mass effects relative to the cg range. This particular example is for maneuvering flight at 1.2 mach.

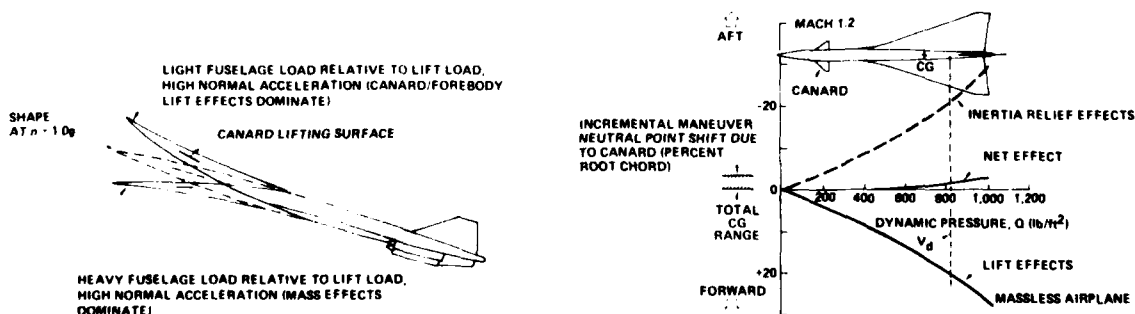


Figure 9. Effect of Aeroelasticity on Canard Contribution

The incremental aeroelastic maneuver neutral-point shifts caused by the canard are plotted against flight dynamic pressure. For reference magnitude, the total center-of-gravity range is displayed. The incremental aeroelastic lift effects are separated from the incremental mass or inertial relief effects to indicate relative magnitudes. The pure aeroelastic lift effect (massless airplane) is shown to be strongly destabilizing. At maximum dive speed, the neutral point is shifted forward 20% reference chord, or almost six times the entire cg range. Counter to this, incremental inertia relief or mass effects are strongly stabilizing, shifting the maneuver point aft 21% CR. The net aeroelastic effects (combining lift and mass effects) are found to be stabilizing. That is, in contrast to the rigid airframe maneuver points, flexible airframe maneuver points are shifted aft because of aeroelastic effects induced by the canard.

5-7

Risks associated with precise longitudinal balance of the flexible canard airplane are clearly evident here. The ability to balance the airplane precisely within the limited cg range is questionable when the canard aeroelastic effects are several times the magnitude of the cg range. Also, variation of the aeroelastic maneuver point shift caused by the canard will be a strong function of gross weight.

Figure 10 shows a directional stability problem encountered with a canard-configured supersonic-transport design. In this case, the canard employed a trailing-edge flap to assist aircraft trim and control. Wind tunnel testing revealed a powerful adverse sidewash induced at the vertical tail by the lifting canard. This is evidenced in figure 10 by the unstable gradient of C_n versus sideslip. Attempts at modifying canard location-fore and aft, high and low-were unsuccessful in correcting this problem; the solution was to alter the vertical tail configuration to an outboard twin tail arrangement.

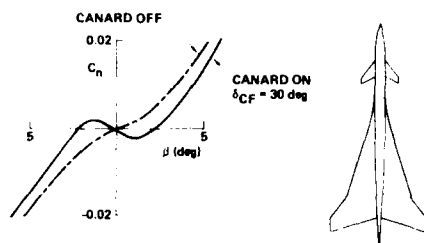


Figure 10. Canard Effect on Subsonic Directional Stability

Preceding discussions have pointed out some problems facing the designer who attempts to configure a canard-controlled aircraft. Successful canard trimmer configurations, e.g., the Viggen, the IAI Kfir, and the B-70, have been designed in the past. However, to date, the canard has been employed mainly as a trim device and not as the only means of pitch control. As an addition to an elevon-controlled, tailless configuration, the canard will provide improved trimmed lift and augment pitch control power. But a number of questions remain about the viability of employing a canard as the sole source of pitch control. Pursuit of this goal appears well-justified considering that the canard provides an attractive means of incorporating pitch control in configurations that integrate thrust-vectoring exhaust nozzles with the wing to augment wing lifting capability. This application provides incentive to continue expanding the research data base for canard controller conceptual development.

TAILLESS RSS CONFIGURATION

The tailless delta wing concept has been an attractive design because of its simplicity, structural efficiency, and light weight. Properly configured, it offers the potential of being the most efficient supersonic cruise configuration attainable. It is not attractive, however, as a highly maneuverable strike-fighter capable of efficient supersonic cruise, unless a breakthrough is developed in the flight control area. The fundamental problem is the severely limited control power inherent in a configuration that employs wing trailing-edge surfaces alone for both pitch and roll control. The tailless aircraft commonly mixes pitch and roll commands with elevon control surfaces so that a lateral command limits available pitch control and vice versa. Control limitations resulting from the shared control functions are further compounded by control surface volume limitations in the configuration geometry: limited pitch-control-moment-arm relative to aircraft cg; control surface area limited by wing span and taper ratio; and available wing trailing edge span sometimes limited by nacelle placement. The aerodynamic effectiveness of elevon controls is also known to deteriorate seriously at high angles of attack where wing flow separation dominates. This characteristic limits the elevons' capability to provide adequate control in the wing stall regions. Additional control deficiencies are experienced as mach number increases and the flow becomes supersonic over the wing surface. This problem is aggravated by structural aeroelastic effects that cause substantial losses in elevon effectiveness at high dynamic pressures (q). The mach and q effects render the elevon a relatively poor control choice for a supersonic aircraft, especially when further compromised by the shared pitch and roll functions.

Figure 11 illustrates control and balance problems inherent in the tailless concept. For comparison, this configuration employs the same wing planform previously used in the aft-tail and canard configurations. However, the design is compromised to the extent that wing variable camber cannot be used to enhance mission capabilities because the wing trailing edge must be devoted entirely to primary flight controls. The low-speed C_m versus alpha graph illustrates the pitchup characteristic of this planform and shows the serious deterioration of elevon effectiveness at high angles of attack. In this case, the combination of pitchup and limited nose-down pitch control power at stall alphas forces a longitudinal balance that permits no less than 6% MAC positive stability at the aft cg limit. The limiting case is for the pilot holding a command of full roll control while simultaneously commanding nose-down pitch in an attempt to prevent stall departure. This combined control command provides 25 deg differential elevon control for roll, permitting only 5 deg pitch control. The pitch-up and inadequate control power compel the provision of a positive stability margin to ensure nose-down pitching moments in high-alpha maneuvers.

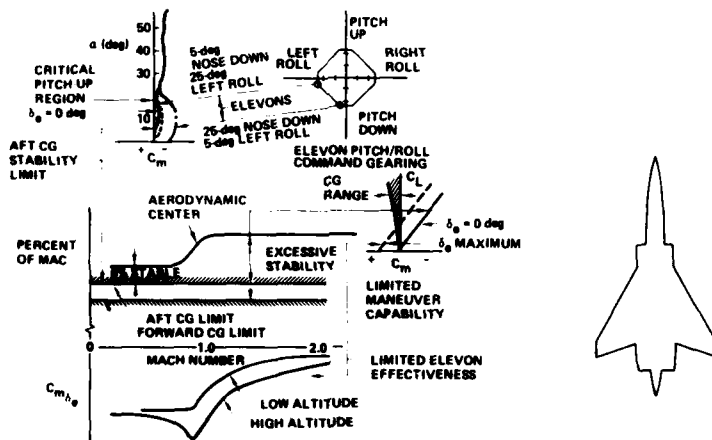


Figure 11. Tailless Aircraft Control and Stability Limitations

Inability to balance the tailless aircraft so that it is unstable subsonically results in excessive longitudinal stability for supersonic operation. Excessive stability results in high trim drag and limited maneuver load factor capability. For example, a calculation at 1.2 mach at 40,000 ft shows that maximum maneuver load factor capability at the forward cg limit is approximately 2g. The maneuver capability deteriorates further at higher mach numbers as elevon effectiveness decreases. This poor maneuver capability results from the combination of excessive stability and relatively ineffective elevons, as shown in figure 11.

The problem of excessive stability at supersonic conditions can be eased by solving the subsonic pitchup problem, thus allowing the aft cg limit to be shifted further aft. Wing planform modification could greatly reduce the pitchup. Also, the present planform could benefit from incorporation of devices to alleviate pitchup. However, reducing the stability margin to improve supersonic maneuver capability may lead to other control problems at supersonic conditions. Highly swept configurations commonly experience severe pitchup problems at both high- and low-speed conditions. An example of this is shown in figure 12, which depicts stability and control characteristics of a highly swept aircraft at 1.8 mach at 60,000 ft. In an attempt to achieve improved supersonic maneuver capability, the aft cg limit was selected to provide a supersonic static margin averaging about 8% MAC (at low alphas). This balance did not provide adequate subsonic margin to prevent pitchup divergence; but it was assumed that means would be developed to cure the subsonic pitchup.

Figure 12 shows that maneuver capability is not limited by control at the forward cg limit. However, the supersonic pitchup results in the aircraft experiencing uncontrolled alpha departures at aft cg's as load factor exceeds 2.4g. Assuming a simultaneous full roll command with full nose-down control command, the limited nose-down control available results in out-of-control pitchup at load factors below 2g. The pitchup characteristics for this configuration are identifiable through wind tunnel test and aeroelastic analyses. The high wing sweep produces the basic rigid wing-body

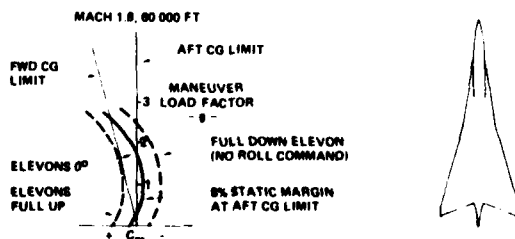


Figure 12. Pitch-Up Control Characteristics for Highly Swept, Tailless Supersonic Aircraft

pitchup, which is aggravated by forebody-strake upward bending produced by the forebody-strake loading. Pitchup will be most severe at light fuel loadings where inertial relief effect is low.

The preceding discussions have pointed out some of the major problems inherent in attempting to design tailless aircraft to fill the supersonic-cruise strike-fighter role: mach aerodynamic center shift, limited control, and pitchup. Aft shift of the aerodynamic center with mach number will inevitably result in excessive stability that will severely penalize maneuver capability over a substantial range of supersonic mach numbers unless the designer can develop and apply countermeasures. Rapidly deployable and retractable stability adjusters such as canards, tails, or folding wingtips may prove effective. The option of center-of-gravity adjustment through fuel transfer may be employed by large transport or bomber configurations to solve the ac shift problem. However, this option is not open to the designer of tactical aircraft that must traverse the transonic region rapidly in both maneuvering and lg flight. The very limited control capabilities of tailless designs must be augmented by additional control devices, and pitchup must be eliminated or greatly reduced through wing-sweep reduction or through application of automatic devices such as variable camber or other variable geometry.

THRUST VECTORING CONTROL FOR TAILLESS AIRCRAFT

Recent research efforts have been directed towards developing nonaxisymmetric engine exhaust nozzles for application to advanced fighter concepts. Two-dimensional nozzles are well-suited to incorporating in-flight thrust vectoring and thrust reversing for enhancement of aircraft maneuver capabilities. In an attempt to improve the tailless fighter concept previously discussed, the application of thrust vectoring pitch control was investigated. This twin-engine aircraft design has high thrust loading (sea level static maximum T/W exceeds 1.0) and benefits from a long moment arm from exhaust nozzles to cg. For this configuration the nozzle moment arm to the aft cg limit is approximately 1.0 MAC. It therefore derives powerful control moments from thrust vectoring. Thrust vectoring was evaluated as a device to prevent the angle-of-attack departure inherent in an unstable configuration; this permitted balancing the aircraft longitudinally unstable. An unstable subsonic balance of -13% MAC at the aft cg limit was selected to provide nearly neutral stability over the operating cg range at supersonic conditions. This degree of relaxed static stability was chosen to obtain minimum cruise trim drag and to ensure that maneuver load factors would not be control limited.

Figure 13 summarizes the results of the evaluation of thrust vectoring as a primary pitch control to prevent alpha departures for the unstable aircraft. The two upper C_m versus alpha sketches in the figure show the establishment of the nose-down pitch control requirements. It is assumed that elevons combining pitch and roll functions are not effective at high alphas. The $-\Delta C_m$ required from thrust vectoring therefore must be sufficient to counter the unstable $C_{m\alpha}$ up to high angles of attack and also must provide responsive nose-down pitch acceleration, $\ddot{\theta}$. This evaluation uses a $\ddot{\theta}$ of -5 degree per second². A further increment of $-\Delta C_m$ is also provided to account for uncertainties involved in predicting full-scale aircraft stability and control characteristics (a common design practice). Thus requirements result for nose-down thrust vectoring at all mach numbers to control instabilities and pitchup. The total ΔC_m required for the angle-of-attack limiting system is plotted versus mach number in the lower graph of figure 13. The same graph compares the alpha-limiting requirement with the pitching moment available from thrust vectoring that employs maximum gross dry thrust for 30 and 90 deg vector angles. Comparison of the required ΔC_m with ΔC_m developed by thrust vectoring shows vectoring to be inadequate even at vector angles up to 90 deg. The greatest control deficiencies occur in the 0.6 to 0.9 mach regions. At the lower thrust vectoring angles considered practical by many of today's designers, vectoring is inadequate for pitch-down control at all but the lowest mach number conditions.

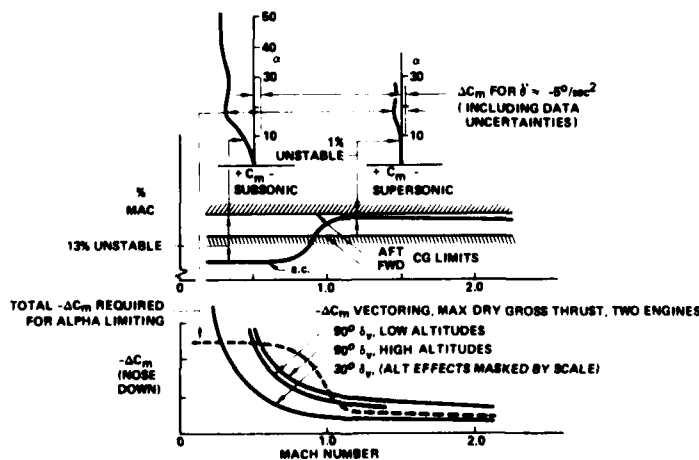


Figure 13. Thrust Vectoring Pitch Control for Alpha Departure Prevention, Unstable Tailless Aircraft

5-10

Thrust vectoring used as a primary pitch control device that is flight safety critical would impose demanding design requirements on the nozzle vectoring control system. Operational reliability must be equivalent to that of primary flight controls. Nozzle actuation systems must provide redundancy and structural integrity comparable to that provided in aerodynamic controls. For flight-safety-critical areas, such as pitch control, it is relatively straightforward for the designer to incorporate aerodynamic control surface redundancy and fail-operable, fail-safe actuation systems that, in total, contribute to very high reliability. The designer of a flight-safety-critical exhaust nozzle control system would appear to have fewer redundancy options and face more severe design problems.

The twin-engine thrust-vectoring design must also consider the failed-engine problem and must control rolling moments produced by asymmetric thrust vectoring.

It is possible that further design cycling of this concept would develop an acceptable degree of pitch-down control, assuming nozzle vectoring capabilities approaching 90 deg. Reducing instability levels through rebalance or placement of the exhaust nozzles further aft might develop acceptable control moments. However, nozzle control design problems remain formidable.

THRUST VECTORING FOR MANEUVER ENHANCEMENT

Considerable attention is currently being directed toward development and application of two-dimensional thrust vectoring engine exhaust nozzles for advanced fighter concepts. Emphasis is on employing the propulsion system for maneuvering lift augmentation. Many different concepts are being evaluated. The most effective provide substantial jet-induced supercirculation lift and direct thrust vectoring in the lift direction.

An ideal concept appears to be a synergetic arrangement involving thrust vectoring and a canard controller. The canard, in trimming out the nose-down pitching moments generated by vectored thrust, adds additional lift to the aircraft. It is perhaps this application that offers the major incentive to develop the canard into a more acceptable pitch controller.

ROLL CONTROL FOR HIGH ANGLE OF ATTACK MANEUVERING

Development of highly maneuverable aircraft tends to concentrate heavily in areas involving high load factor capability for both instantaneous and sustained maneuvering. High maneuver load factor capability, however, does not define a superior maneuvering aircraft unless this capability is complemented by good roll control at maneuvering angles of attack. Good high-alpha roll control is necessary both for precise bank angle control at high load factor and for quick heading reversal through rapid bank-to-opposite-bank maneuvers.

The problem that continues to plague fighter pilots is severe deterioration of lateral control effectiveness at high angles of attack. Typically, the lateral control power fades to zero or reverses in high alpha maneuvers, and the lateral control becomes more effective as a yaw device. The pilot then must use the rudder control to roll the airplane through sideslip and wing dihedral effect. Aircraft that possess these characteristics and that suffer decreasing directional stability at high alphas are prone to departure from controlled flight through excessive manipulation of lateral directional controls. Stall departure and spin entry are an all too common occurrence.

In recent years, designers have developed impressive improvements in high alpha directional stability to inhibit stall departure. However, little progress has been made in developing strong roll control at limit angles of attack. Though detailed examination of this area is beyond the scope of this paper, devices that may significantly improve high-angle-of-attack roll control warrant consideration here.

Figure 14 shows the high-alpha deterioration in lateral control effectiveness typical for low-aspect-ratio, highly swept configurations and indicates the sort of improvement that could reasonably be expected from a variable wing camber system. Such a system could be programmed with angle of attack, mach number, and roll command through an active flight control system to provide substantial rolling moment improvements at high alphas. Also shown in figure 14 is an approximation of rolling

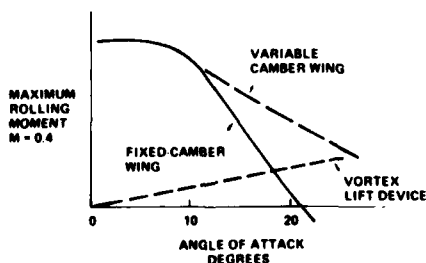


Figure 14. Lateral Control Deterioration With Angle of Attack

moments expected from a vortex lifting device acting on the outboard span of a highly swept delta wing. The vortex-produced rolling moments may become quite significant at alphas above 10 deg and continue to build linearly with alpha increase. Recent NASA Langley research in vortex flow technology is producing an interesting and valuable data base in this area.

5-11

The spoiler-slot-deflector lateral control system is by no means a new device, but it has proven to be an attractive roll control in several supersonic designs. NASA and others have developed an ample data base showing the effectiveness of this type of roll control over wide-ranging conditions of mach number and angle of attack. Figure 15 shows the increased effectiveness provided by a spoiler-slot-deflector system over that offered by plain spoilers; it also shows the advantage of spoiler-slot-deflector systems over conventional ailerons with regard to aeroelastic effectiveness. The spoiler-slot-deflector system characteristically remains effective to very high angles of attack, and its control is much less susceptible to aeroelastic losses than trailing edge controls. Another attractive feature is its ability to link spoiler and deflector so as to greatly reduce control actuation power requirements. The Boeing SST design used both upright and inverted spoiler-slot-deflector panels working symmetrically for left and right wings. This design approach was selected to optimize the yaw and roll interactions of the lateral control system while maintaining good roll control to high angles of attack.

An application of vectored thrust as a roll control device is shown in figure 16. The aircraft model used in this case is the generalized twin-engine model discussed previously in comparing aft tail, canard, and tailless concepts. The maximum rolling moment predicted for the elevon control system is compared with that developed by deflecting engine exhaust nozzles symmetrically ± 30 deg. The comparison at 40,000 ft altitude shows thrust vectoring providing substantial rolling moments and nearly competing with the elevon system at higher mach numbers. A calculation of the roll rate capability at 0.9 mach number shows that the thrust vectoring roll control will develop 70 deg per second roll rate. This capability should remain essentially constant with increasing alpha and should be quite acceptable for maneuvering at angle-of-attack limit. Aircraft designs with further outboard engine nacelle placements will, of course, provide more effective deflected-thrust roll control than the example evaluated here. In any case, thrust vectoring appears to offer significant potential as a high-alpha roll control device.

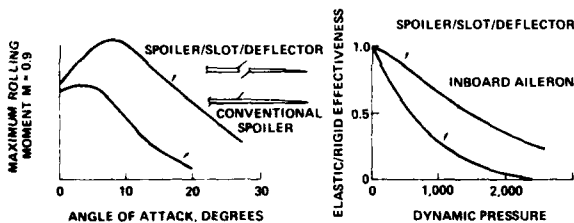


Figure 15. Spoiler Slot/Deflector Lateral Control Effectiveness

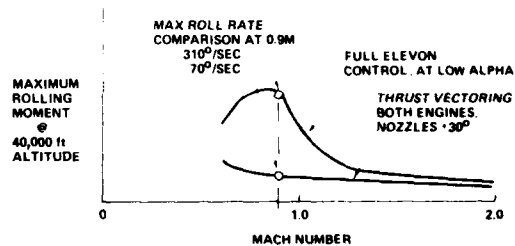


Figure 16. Effectiveness of Thrust Vectoring Roll Control

The preceding devices are cited as examples of approaches that offer potential for dramatic improvements in roll control. Additional research in lateral control technology is required to develop a data base that will supply attractive options for improved roll control systems.

CONCLUSIONS

Development of advanced tactical aircraft that combine efficient supersonic cruise capability with competitive maneuver capability strongly challenges the technology of aircraft stability and control. The use of active control systems to replace traditional inherent aerodynamic stability establishes aircraft control as the chief design consideration. The ability to meet design goals for supersonic cruise trimmed L/D and supersonic maneuver load factor capability characteristically hinges on the ability to achieve high levels of controllable subsonic longitudinal instability. Stability and control evaluations of competitive aircraft design concepts indicate that aft-tail configurations will be superior to canard or tailless configurations in achieving design goals. The latter concepts experience inherent longitudinal balance and control limitations that compromise their ability to compete with the aft-tail design arrangement. Additional research is recommended to overcome these deficiencies.

Another fundamental design consideration is the development of an effective lateral control system that will ensure good roll control for high-angle-of-attack maneuvering. The ability to achieve and sustain high maneuver load factor must be complemented by the ability to make rapid bank angle changes with precision. Devices such as thrust vectoring, vortex lift controls, wing variable camber, and spoiler-slot-deflector systems offer potential of meeting design goals for advanced maneuver capabilities.

A need for continuing research exists in a wide variety of stability and control areas that become involved in design iterations and trade studies. Development of data base and advances in the technology of controlling and stabilizing supersonic aircraft are fundamental to achieving design goals for highly-maneuverable, supersonic-cruise aircraft.

WINDTUNNEL MEASUREMENTS AND ANALYSIS OF SOME
UNUSUAL CONTROL SURFACES ON TWO SWEEP WING
FIGHTER CONFIGURATIONS*)

by

6-1

D. Welte and S. Ehekircher
Dornier GmbH, Postfach 1420
D-7990 Friedrichshafen
Germany

SUMMARY

Force measurements were made in a low-speed and in a high-speed wind tunnel with a 1:20 scale, 35° swept-wing fighter configuration model. Surfaces which are deflected for longitudinal trim are: horizontal tail, leading- and trailing-edge flaps, a strake and a strake leading-edge flap. For lateral control the following surfaces are deflected: ailerons, tiperons, flaperons and a strake leading-edge flap. The main conclusions from this study are: (1) trailing edge flaps are very useful to trim an unstable configuration and have minimum drag, (2) tiperons are very effective means for roll-yaw control up to very high angles of attack, (3) differentially deflected leading edge flaps and a vortex fin, positioned on the wing upper surface, decrease the directional instability at high angles of attack.

In addition low-speed tests were made with a new wing concept for a future fighter configuration, so called supersonic biplane, to investigate the effectiveness of the upper- and lower-wing trailing edge flaps.

As supplement to the wind tunnel measurements some flight mechanical maneuver calculations were made to check the suitability and to compare the effectiveness of the different controls.

NOTATION

b	span
\bar{c}	mean aerodynamic chord
c_D	drag coefficient
c_L	lift coefficient
c_l	rolling moment coefficient (reference length: $b/2$)
c_m	pitching moment coefficient (" " : \bar{c})
c_n	yawing moment coefficient (" " : $b/2$)
c_y	side force coefficient
M	Mach number
n	load factor
P	roll rate
R	Reynolds number
S	wing area
s	half-span
t	time
x,y,z	coordinates
α	angle of attack
β	angle of side slip
η_A	aileron deflection
η_F	trailing-edge flap deflection
η_H	horizontal tail deflection
η_L	strake leading-edge deflection
η_N	leading-edge flap deflection
η_S	strake deflection
η_T	tiperon deflection
θ	bank angle

All aerodynamic coefficients shown are given in the experimental axis system.

*) This work was sponsored by the German Ministry of Defense within the RUFo 4- and ZIL-Program

INDICES

6-2 c.g. center of gravity
g geodetical axis system
port port
stb starbord

ABBREVIATIONS

LEF Leading Edge Flap
SLEF Strake Leading Edge Flap
TEF Trailing Edge Flap

1. INTRODUCTION

When designing a new fighter aircraft, the aerodynamicist concentrates on two main goals:

- Minimization of drag
- Guarantee of good control and stability in all flight maneuvers.

The drag components which are influenced by control surfaces - and here not only the conventional aileron and rudder is meant but also flaps and other deflectable surfaces - are the lift dependant drag and the trim drag.

Normally the lift/drag ratio of the wing is increased by flaps, but to trim the aircraft this gain is reduced by the trim losses. For an unstable configuration, on which the center of gravity lies at a certain point behind the low speed aerodynamic center, the gain in lift/drag ratio by the flaps is reached nearly without trim losses, because the flaps produce the trim moment and the horizontal tail has to be floated by use of the CCV technology. Minimization of trimmed drag by controls on the basis of wind tunnel tests with a fighter configuration is the subject of section 3. The tests itself are described in section 2.

The roll control power in the high angle of attack range should not fall much below the value for attached flow over the wing at low angles of attack. For the conventional aileron and flaperon this is not possible, because these surfaces lie in the separated flow field of the wing. The outer part of the wing seems to be a useful surface to produce a rolling moment, since this surface has a large distance from the center line of the aircraft, it is rotatable up to $\pm 180^\circ$ and it is subject to the full ram pressure of the free stream. Further means to produce a rolling moment and a side force is a strake leading edge flap. With the trailing edge flaps a side force and a tangential force is produced. The effectiveness of these control surfaces is shown in section 4.

In spite of the chance by using the CCV technology to solve stability problems one has to strive for directional stability in the whole angle of attack range. The nature of the flow field above and behind the wing influences the directional stability of the whole aircraft. Having this in mind devices have been investigated which influence the flow field above the wing in the angle of attack range between 20° and 35° . The effectiveness of differentially deflected leading edge flaps and of a vortex fin, positioned on the wing upper surface, on the directional stability is described in section 5.

Out of the search for low drag and high performance a biplane configuration with very thin wings arose. This wing has been tested in the low and high speed wind tunnel. Some results of the calculated and measured forces and the effectiveness of the upper and lower wing trailing edge flaps at low speeds are shown in section 6.

Coming back to the above mentioned statement for good control in all flight maneuvers the different control concepts are compared with the aid of simple roll control calculations in 6 DOF, and by a mathematical pilot model, tactical missions have been simulated. Some results of these investigations are described in section 7.

2. DESCRIPTION OF THE WIND TUNNEL MODEL

The wind tunnel model, shown in Fig. 1, consists of a trapezoidal wing with aspect ratio of 4, taper ratio of 0,3 and a leading edge sweep of 35° , a body of constant cross section with a pointed nose, and horizontal and vertical tailplanes. The leading edge extension at the wing root, called a strake, has a gothic shape and an area of 11 % of the reference wing area.

The following control surfaces on the wing are movable:

- Trailing edge flaps: of 30 % chord divided into 3 spanwise parts between the wing root (5 % to 64 % semispan) and tip. The inner two parts are also used as flaperons.
- Ailerons: of 30 % chord, from 64 % semispan to 100 % semispan, divided at 82 %.

- Tiperon: consists of the outer wing, from 82 % span to the wing tip and can be deflected about a lateral axis through the 50 % chord point from + 15° to - 75°. The trapezoidal tiperon can be replaced by a triangular shape of the same area but larger span.
- Strake: the strake can be deflected by + 4° (nose up) about a lateral axis at the leading edge of the wing root.
- Strake leading edge flap: the curved part of leading edge of the strake can be deflected by ± 20° about an 80° swept axis as shown on Fig. 1.
- Strake vane: this small triangular plane can be adjusted relative to the front part of the strake as shown on Fig. 1. It has an area 20 % of the strake.

6-3

The wind tunnel tests were performed in the 2,6 x 3,6 m² Low Speed Wind Tunnel and in the 1 x 1 m² Transonic Wind Tunnel, both of the DFVLR in Göttingen. The same model was used in both wind tunnels so that the Low Speed Tunnel was large enough for tests at very high angles of attack up to 60°. The Reynolds Number in the Low Speed Tunnel was 0,59 x 10⁶ and in the Transonic Tunnel 1,61 x 10⁶.

3. USE OF CONTROLS TO MINIMIZE THE TRIMMED DRAG

An unstable aircraft can partly be trimmed by trailing edge flaps. The low-speed and high-speed wind tunnel tests have been analysed, assuming that the center of gravity lies at the aerodynamic center of the aircraft without horizontal tail for a low supersonic Mach number. In our case this is $X_{c.g.} = 0,4 \bar{c}$ for $M = 1.1$. Since normally the pitching moment increases with increasing Mach number, see Fig. 2, the trimmed lift increases for a given flap deflection. Since, on the other hand, the lift curve slope increases with increasing Mach number, the flap schedules, i.e. flap deflection over angle of attack, for different Mach numbers are very close together as shown on Fig. 3. The maximum increase of lift and pitching moment by the plain flaps is reached with 24° deflection for $M = 0,2$ to $M = 0,5$ and with 18° for $M = 0,8$. In all tests the optimum deflection of the leading edge flaps have been nearly the same as for the trailing edge flaps.

The large pitch-up moment at high lift comes from the strake when the flow over the outer wing is fully separated.

The drag polars of the low speed tests are analysed in more detail. As shown in Fig. 4 for a lift up to $c_L = 0,8$ the aircraft is trimmed only by flaps for minimum drag, that is the horizontal tail is unloaded. The drag increases nearly linearly with c_L squared which shows a good aerodynamic efficiency of the configuration. If, for higher c_L , the horizontal tail remains unloaded, the drag increases very rapidly and the maximum trimmed lift is below $c_L = 1$. For that, above $c_L = 0,8$, when the flap angle of 24° is reached, the horizontal tail has to help to trim the aircraft.

If one chooses a c.g. position of 30 % \bar{c} the trimmed drag increases in the whole lift range. The reason is that in this case the c.g. lies nearer to the a.c. of the aircraft and the horizontal tail has to compensate the zero lift moment of the flaps.

The maximum pitching moment, which has to be provided by the horizontal tail to trim a c.g. position of 40 % \bar{c} , is large and means a relative large tail plane area which can be up to 30 % of the wing area. The maximum pitch-up moment can be reduced by decreasing the size of the strake. To hold the maximum lift constant it is necessary to increase the flap effectiveness by using for example slotted flaps. The same results can be reached by increasing the wing area. The optimization of all these parameters has to be done by the designer and goes beyond this paper.

For flight at supersonic Mach number one gets the lowest drag if the horizontal tail is nearly unloaded. For our aircraft the a.c. lies at 40 % \bar{c} for $M = 1.1$ and goes forward with increasing Mach number up to $\Delta x = 7 \text{ % } \bar{c}$ for $M = 2.0$. This shift of 7 % \bar{c} could be compensated by the extension of the strake vane. The strake vane has 3,9 % of the wing area and shifts the a.c. forward by 7 to 9 % \bar{c} for subsonic as well as for supersonic flight as shown in Fig. 5.

A further means for reducing the a.c. shift is the incidence of the strake. The tests showed, that a strake with an incidence of 4° relative to the wing has 4 % less a.c. shift from subsonic to supersonic Mach number than a strake which lies in the plane of the wing.

4. LATERAL AND AXIAL CONTROL POWER OF SOME CONTROL SURFACES

4.1 Tiperons

As described in section 3, two planforms of the tiperons, a trapezoidal and a triangular one, have been investigated and compared with a conventional aileron. The span of the trapezoidal tiperon is half that of the aileron, which gives, after a linear potential theory method (vortex lattice), nearly the same effectiveness. The trapezoidal and triangular tiperons are equal in planform area. Both tiperons can be deflected from + 15° to - 75°. From Fig. 6 it is seen that the rolling moments of the tiperons for high angles of attack between 30° ≤ α ≤ 60° are nearly equal. In the low angle of attack range up to $\alpha = 30°$, the triangular tiperon is better, probably because of its larger aspect ratio. The triangular tiperon will be treated further on. Fig. 7 gives a comparison of the maximum rolling moments produced by the conventional aileron, by the two inboard flaps used as flaperon and by the triangular tiperon. For angle of attack greater than 10°, when the flow on the upper surface of the plane, thin wing, is separated, the aileron effectiveness falls down to about half of that of the tiperon. The rolling moment produced by the flaperon is only more

than half of that of the tiperon and falls down to zero for $\alpha > 40^\circ$. The influence of Mach number on the rolling moment up to $M = 1,2$ is shown on Fig. 8. With increasing Mach number the effectiveness of the aileron decreases, while it increases for the tiperon, presumably because of the large leading edge sweep of the triangular tiperon.

The direction of the vector of rotation of the aircraft is decisive whether it turns in the right or wrong way. To show this it is illustrative to work with a c_l - c_n -diagram, in which the vector of rolling and yawing moment for different tiperon deflections at constant angle of attack is plotted. Fig. 9 shows the vector-diagram for $\alpha = 0^\circ, 20^\circ, 40^\circ$ and 60° for the triangular tiperon. From this diagram it can easily be seen whether the yawing moment goes in the right direction for a certain rolling moment.

For better interpretation of the figure the special cases where $c_n = 0$ is analysed. It is found, that the tiperons of both sides have to be deflected so that the angle of attack relative to the free stream direction has the same value but opposite sign. For example at $\alpha = 20^\circ$, $c_n = 0$ for $\eta_{\text{stb}} / \eta_{\text{port}} = + 15^\circ / - 55^\circ$ which gives an angle of attack of $+ 35^\circ / - 35^\circ$. Another example: for $\alpha = 40^\circ$, with $\eta_{\text{stb}} / \eta_{\text{port}} = - 5^\circ / - 75^\circ$ gives an angle of attack of $+ 35^\circ / - 35^\circ$. This means, that the wing doesn't influence the flow field about the tiperons essentially and we can predict the optimum deflection of the tiperons for any angle of attack of the aircraft. For example for $\alpha = 60^\circ$ with a deflection of $\eta_{\text{stb}} / \eta_{\text{port}} = - 35^\circ / - 95^\circ$ the incidence will be $+ 35^\circ / - 35^\circ$ and the yawing moment is predicted to be zero.

The normal force of a flat plate increases with increasing angle of attack up to 30° to 50° and remains constant for higher angles of attack up to 90° . This gives the maximum useful tiperon deflection to produce a rolling moment without a yawing moment for any angle of attack of the aircraft as shown in the table below and it is seen, that for $\alpha > 60^\circ$, the tiperon has to be deflected more than 90° .

α	η for $c_{l\text{max}}$ $c_n = 0$
20°	- 55° to - 70°
40°	- 75° to - 90°
60°	- 95° to - 110°
90°	- 125° to - 140°

The influence of the Mach number on the roll and yaw moment produced by the tiperons is shown in Fig. 10 for $\alpha = 8^\circ$. The effectiveness increases with increasing Mach number and the direction of the turn vector remains constant.

4.2 Strake Leading Edge Flap (SLEF)

The strength of the strake vortex, which is created between an angle of attack of 5° to its total burst at 40° , can be controlled by deflecting a flap at the strake leading edge. On the side of the wing, on which the SLEF is deflected upwards the vortex strength increases. Since the strength of the vortex influences the lift on the wing, this can be used to control lift and rolling moment. The rolling moment due to the deflection of the SLEF is shown in Fig. 11. Both deflections, the 20° nose down and the 20° nose up, give rise to a roll moment of appreciable size for an angle of attack of $20^\circ \leq \alpha \leq 40^\circ$. At the same time a proverse side force is produced, Fig. 12. This side force is highly dependant on the angle of attack. For low angle of attack it is nearly zero and not useful for fuselage aiming. The rolling moment of the SLEF could be useful in addition to the ailerons in the angle of attack range between 20° and 40° .

4.3 Trailing Edge Flaps

The side force produced on the model without vertical fin by the deflection of the two inboard trailing edge flaps has, depending on the angle of attack, a considerable magnitude. For both, positive and negative deflections a yawing moment is produced, Fig. 13. To compensate for the latter a side force on the vertical fin is necessary which goes in the same direction as the basic side force. To compensate the rolling moment ailerons have to be deflected. They don't produce a side force.

The trailing edge flaps are divided into three and the ailerons into two parts in the spanwise direction. Each of them could be deflected by $\pm 40^\circ$. To produce high drag the flaps can be deflected in two different modes as shown in Fig. 14. First, the two inboard flaps are deflected down and the three outboard flaps are deflected up. Second the flap segments are deflected in an alternating manner, beginning with the inboard flap deflected down and ending with the two outboard flaps deflected up. The lift and drag increments are shown on Fig. 14 as a function of α . Both deflection modes produce nearly the same drag, but the lift of the alternating mode remains near zero for increasing angle of attack which is favourable. The pitching moment without horizontal tail is nearly zero for both modes.

5. MEANS TO DECREASE DIRECTIONAL INSTABILITY AT HIGH ANGLE OF ATTACK

Directional- and Roll-Instability have been investigated with a wind tunnel model similar to that described above but with a more realistic fuselage and with double vertical fins.

Directional stability is lost at an angle of attack between 25° and 30° . It is not only the strake vortex which breaks down more rapidly on the upper surface of the windward wing than on the leeward one but it also was observed, that the windward outer wing stalled earlier and more heavily than the leeward one. From these observations two new devices have been investigated.

6-5

5.1 Differential deflection of the leading edge flaps

By deflecting the windward leading edge flap more down than the leeward one, the stalling behaviour and the flow field downstream of both sides of the wing can be made more similar than with symmetrically deflected flaps.

Starting from the 17° flap deflection on both sides as a reference condition, the windward flap was deflected down 29° . A second test series has been done with the windward flap deflected 29° and the leeward one retracted to 0° .

As shown in Fig. 15 at an angle of sideslip of $\beta = +10^\circ$ the yawing moment becomes negative at around $\alpha = 20^\circ$, for the differential deflections earlier than for the symmetrical one. At $\alpha = 30^\circ$ however the adverse yawing moment of the symmetrically deflected flaps is more than twice that of the differentially deflected ones. The rolling moment at $\beta = +10^\circ$ shown in the same figure is always adverse, at high angle of attack between 20° and 30° it decreases rapidly for the symmetrical flaps, but remains roughly constant for the differentially deflected ones. The directional stability at constant angle of attack is shown in Fig. 16. For $\alpha = 20^\circ$ all flap deflections give a proverse yawing moment whereas at $\alpha = 30^\circ$ the adverse yawing moment of the symmetrical flaps is more than twice that of the differentially deflected ones.

Tests without the strake showed similar results. Proverse yawing moment at $\alpha = 20^\circ$ shown on Fig. 17 is not changed by the differential flap deflection, whereas at $\alpha = 30^\circ$ the symmetrically deflected flaps have an adverse yawing moment but it is proverse with the differentially deflected flaps up to $\alpha = 25^\circ$. The rolling moment is similar for both cases.

As a conclusion it is suggested to deflect the leading edge flaps for angle of attack greater than 25° as a function of β differentially on the windward and leeward wing as qualitatively shown in Fig. 18. For an aircraft using the CCV technology in principle this can be realized.

5.2 Vortex fin on the wing upper surface

A vertical fin is attached to the upper surface near the wing root on the leading-edge flap. It has a shape of the half of a delta with the leading edge sweep angle of 50° . This sweep angle results from the assumption, that for $\alpha = 30^\circ$ and flap deflection of 17° the fin leading edge should be swept more than 60° to the free stream. If now, the wing has a sideslip angle, then at the leading edge of the windward fin a vortex is induced which rotates in the same sense as the strake vortex and so the latter is amplified. On the leeward wing the contrary happens, i.e. the vortex of the fin decreases the strength of the strake vortex. As a result it was hoped that the directional instability at $\alpha > 25^\circ$ would be decreased. This is verified by the results of some wind tunnel tests. Fig. 19 shows that the yawing moment at $\alpha = 20^\circ$ is nearly unchanged by the fin, whereas at $\alpha = 30^\circ$ the adverse yawing moment is reduced by 30% at $\beta = 10^\circ$. The rolling moment, shown in the same figure, is nearly unchanged for $\alpha = 20^\circ$ by the fin, whereas at $\alpha = 30^\circ$ for small angles of sideslip it is changed by the vortex fin dramatically by increasing the lift on the windward wing. The fin provides a stable contribution to directional stability and reduces the large change in the rolling moment for angle of attack greater than 15° ; see Fig. 20. In the last experiment the fin and the differential flap deflections have been added together. As shown on Fig. 21, the large adverse yawing moment for $\beta = +10^\circ$ could be reduced nearly to zero for angles of greater than 25° , and as shown in the same figure, the rapid decrease of the rolling moment for $\alpha > 15^\circ$ is changed in a gradually increasing one.

6. SOME RESULTS OF THE BIPLANE CONFIGURATION

The supersonic biplane configuration arises out of a search for lower drag and higher performance. By tying the wing tips of a biplane together, a structural box is obtained which enables the use of thinner air foil sections than on a conventional design. Fig. 22 shows a three view drawing of such an aircraft. The wings of the biplane are staggered so that the trailing edge of the upper wing lies exactly above the leading edge of the lower wing. The conventional wing beside is used as a reference. Fig. 23 shows the discretization of both wings for calculation using the vortex lattice method. In the same figure the calculated and measured lift and drag is shown. The lift curve slope as well as the measured maximum lift is greater for the biplane than for the conventional wing. Allowing for full nose suction the calculated induced drag of the biplane is 12% less than that of the plane wing. The wind tunnel tests also indicate this drag reduction above $c_l = 0,8$.

The theoretical effectiveness of the 25% deep trailing edge flaps on lift and pitching moment was calculated. The flap on the lower wing produces three times Δc_l and Δc_m than the upper wing flap. The flap on the upper wing produces a nose-up moment and for this, both flaps together produce the same lift as the flap on the plane wing, but the zero lift moment is 25% less on the biplane.

The structural analysis of the biplane showed that the additional of a small wing outboard of the tying point decreases the deformation of the biplane structure under high loads. The measured flap effectiveness on the modified model is shown in Fig. 24. The tests give a confirmation of the theory. The upper wing produces a nose-up pitching moment which is one third of that produced by the lower wing flap. For a stable aircraft configuration a flap which produces lift and a nose-up pitching moment at the same time can be used to reduce the trim drag.

As one would expect from the lift curves the deflected flaps improve the lift/drag ratio as shown in the figure.

The flaps were deflected on one side only as a flaperon. Fig. 25 shows measured rolling moments due to flaperons for the biplane and for the plane wing. The deflection of the flaperons have been chosen for the same rolling moment at $\alpha = 0^\circ$. For higher angle of incidence the flaperons of the biplane are much more effective than the ones on the plane wing.

7. COMPARISON OF THE DIFFERENT CONTROL CONCEPTS WITH THE AID OF FLIGHT MECHANICAL MANEUVER CALCULATIONS

With a mathematical model of a future tactical combat aircraft simple roll control calculations in 6 DOF and by an additional mathematical pilot model also tactical mission have been simulated for the three roll control concepts: aileron, flaperons and tiperons. The aim of these investigations was a comparison of the three concepts as a main roll control device in relation to practicability and effectiveness. As the main aerodynamic data of the reference aircraft model were only available up to an angle of attack of about 20° , the most favorable angle of attack region for the tiperons (very high angles up to the post stall region) could not yet be regarded.

As a first example, Fig. 26 shows a 360° roll maneuver in 6 DOF. The maximum deflections used were $\pm 22,5^\circ$ for the ailerons and the tiperons and $\pm 40^\circ$ for the flaperons. The speed was taken equal to Mach 0.6. At the low angles of attack for this flight condition the aileron is the most effective device followed by the tiperon. The side slip excursions which can be used as an index for the perturbation of the maneuver have the largest values for the ailerons and the smallest values for the flaperons.

A comparison of the flight path variations during a roll reversal maneuver is shown in Fig. 27 for two angles of attack. The roll reversal maneuver consists of a quick change from $+90^\circ$ bank angle to -90° followed by a pull-up maneuver. To make use of the full rolling capacity of the tiperons it was assumed here that they have been deflected differentially ($+22,5^\circ/-45^\circ$). Especially for the higher angles of attack the advantages of the tiperons are obvious. This is partly due to the fact, that the aerodynamic effectiveness is higher but also due to the lower unfavorable aerodistorsion effects of the tiperons.

Another interesting result of these investigations was the fact that it is possible to use the flaperons as an emergency roll control device, if the main roll control system fails, which can be seen by these figures.

The same figure shows the different parameters of the dynamic transfer behaviour for the reversal maneuvers. Also by this figure it can be seen obviously that the commanded bank angle is most rapidly obtained by the tiperons.

As a resumé of these flight mechanical investigations it can be said, that for a combat aircraft with its extended flight and maneuvering regime the tiperons offer the best capacity for an effective roll control. Whether this can be realized taking into account other design aspects (i.e. weapon storage) is another point.

CONCLUSIONS

1. The 35° swept wing fighter configuration has the lowest trimmed drag for a c.g. position of $40\% \bar{c}$ (which is the a.c. for a low supersonic Mach number), with an unloaded tailplane up to a lift coefficient of 0.8. Above this lift the tailplane has to support the flaps to trim the aircraft.
2. Tiperons are effective for roll control up to very high angles of attack. Deflections of more than 90° are necessary. The influence of the strake leading edge flap on rolling moment and side force depends very much on the angle of attack and is not attractive. Differentially deflected trailing edge flaps produce very high drag without great influences on the lift and pitching moment.
3. Differential leading edge flap deflection and a vortex fin vertically attached on the upper surface at the root of the leading edge flap, considerably decreases the directional instability of the aircraft in the angle of attack range between 25° and 35° .
4. For a biplane configuration with very thin wings, the lower wing trailing edge flap produces more lift and more rolling moment at high angles of attack than a flap on a plain wing.

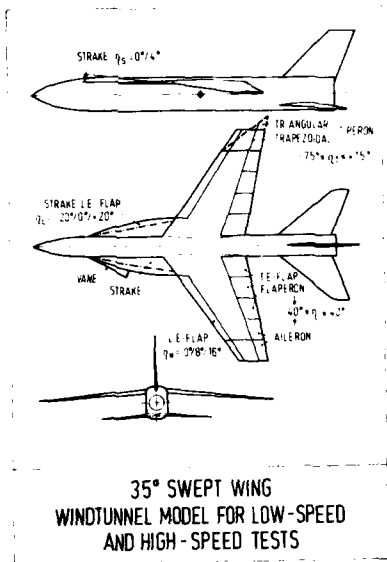
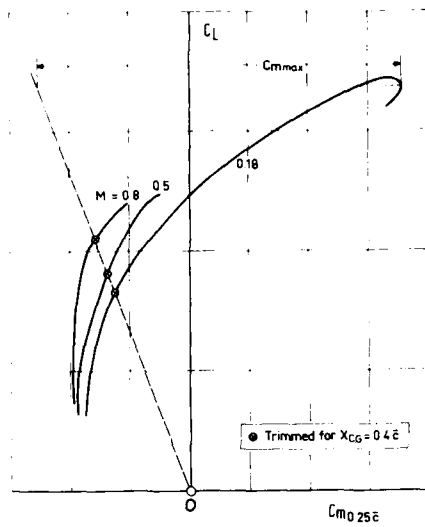


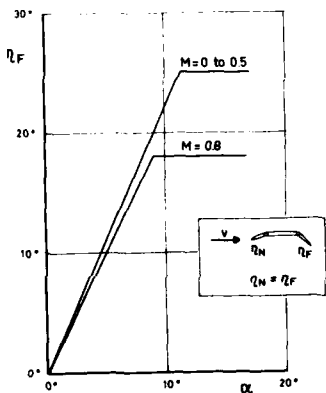
Fig. 1



PITCHING MOMENT WITHOUT TAIL
Flaps 15°, M = 0.18 / 0.5 and 0.8

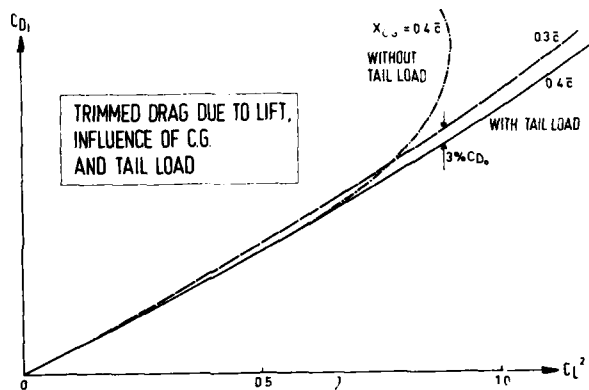
Fig. 2

6-7



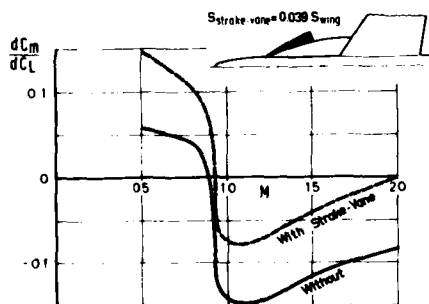
FLAP SCHEDULES

Fig. 3



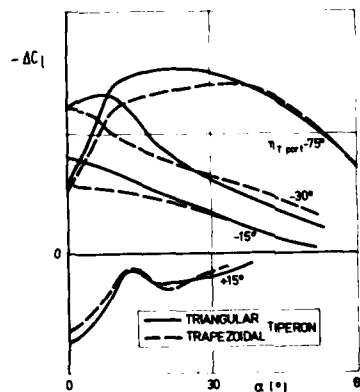
TRIMMED DRAG DUE TO LIFT,
INFLUENCE OF C.G.
AND TAIL LOAD

Fig. 4



Shift of Static Margin by the Strake-Vane

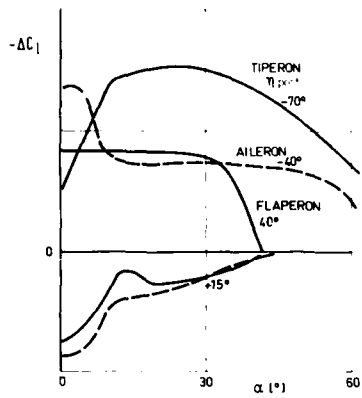
Fig. 5



ROLLING MOMENT DUE TO TIPERON,
INFLUENCE OF PLANFORM

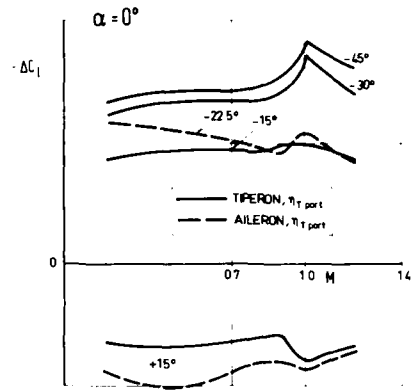
Fig. 6

6-8



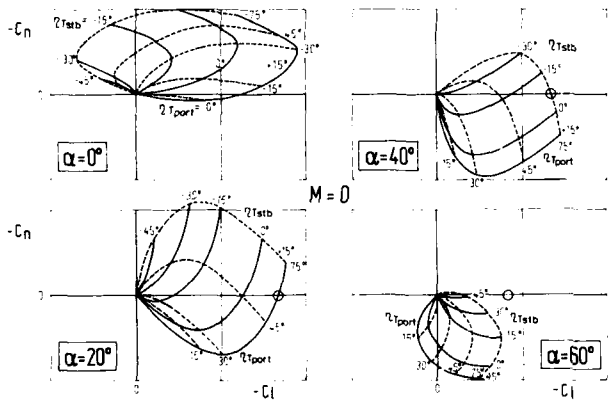
ROLLING MOMENT DUE TO TIPERON AND AILERON

Fig. 7



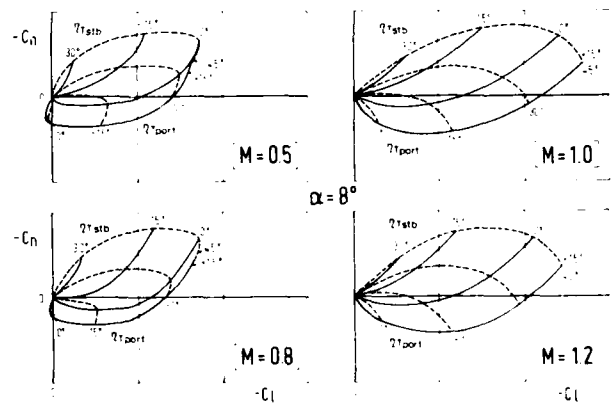
ROLLING MOMENT DUE TO TIPERON AND AILERON, INFLUENCE OF MACH-NUMBER

Fig. 8



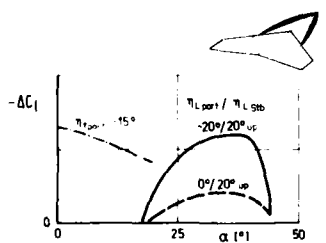
ROLL AND YAW MOMENTS DUE TO TIPERONS, INFLUENCE OF ANGLE OF ATTACK

Fig. 9



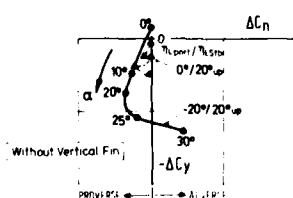
ROLL AND YAW MOMENTS DUE TO TIPERONS, INFLUENCE OF MACH NUMBER

Fig. 10



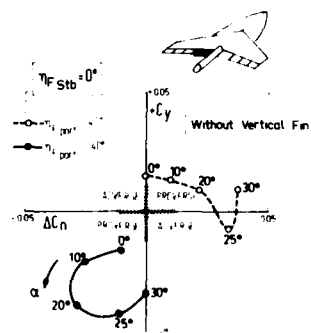
ROLLING MOMENT DUE TO STRAKE LEADING-EDGE FLAP

Fig. 11



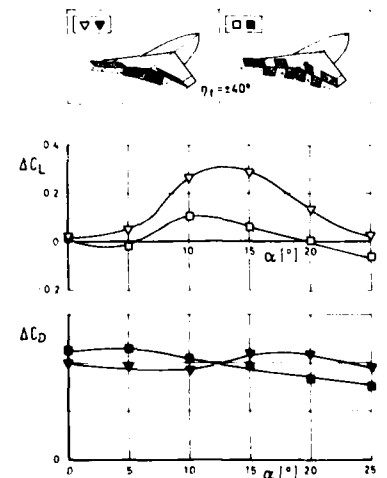
SIDE-FORCE DUE TO STRAKE LEADING-EDGE FLAP

Fig. 12



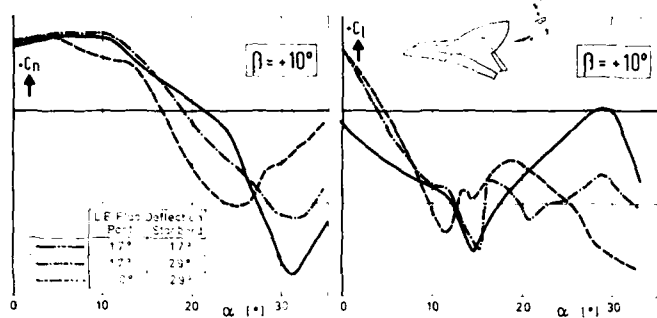
SIDE FORCE DUE TO TRAILING EDGE FLAP

Fig. 13



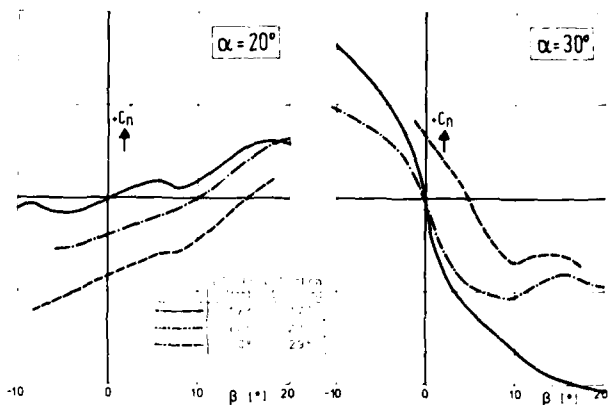
DRAG AND LIFT DUE TO AIRBRAKES REALIZED BY TRAILING EDGE FLAPS

Fig. 14



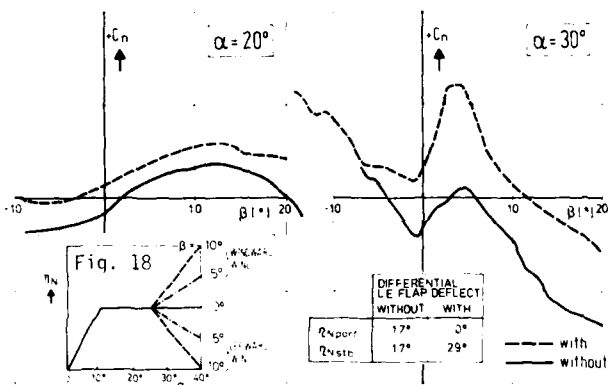
INFLUENCE OF DIFFERENTIAL LE FLAP DEFLECTION ON C_n AND ON C_l

Fig. 15



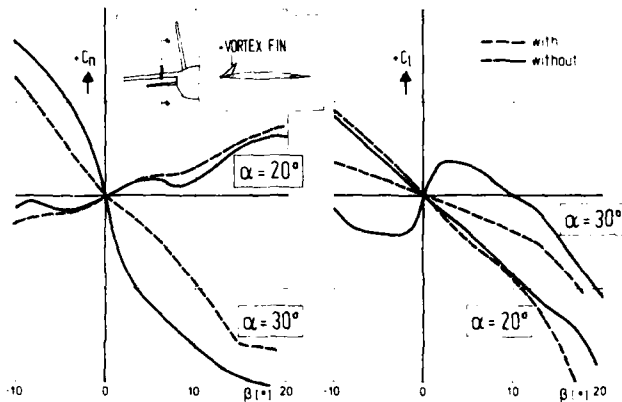
INFLUENCE OF DIFFERENTIAL LE FLAP DEFLECTION ON $C_n(\beta)$

Fig. 16



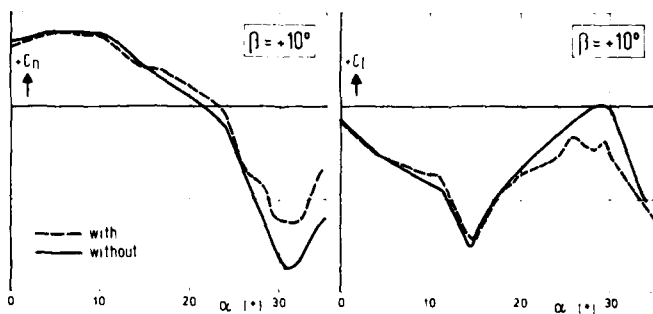
INFLUENCE OF DIFFERENTIAL LE FLAP DEFLECTION ON $C_n(\beta)$, WITHOUT STRAKE

Fig. 17



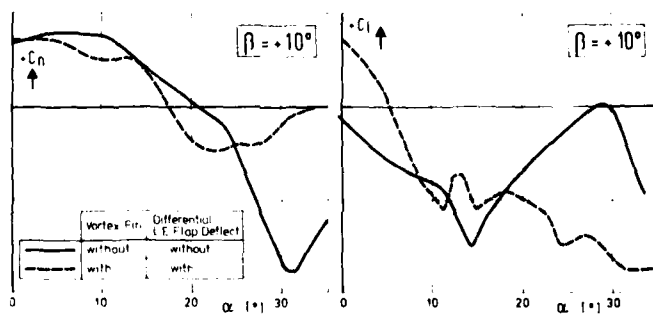
INFLUENCE OF VORTEX FIN ON $C_n(\beta)$ AND ON $C_l(\beta)$

Fig. 19



INFLUENCE OF VORTEX FIN ON C_n AND ON C_l

Fig. 20



INFLUENCE OF VORTEX FIN AND DIFF LE FLAP DEFLECTION ON C_n AND ON C_l

Fig. 21

6-9

6-10

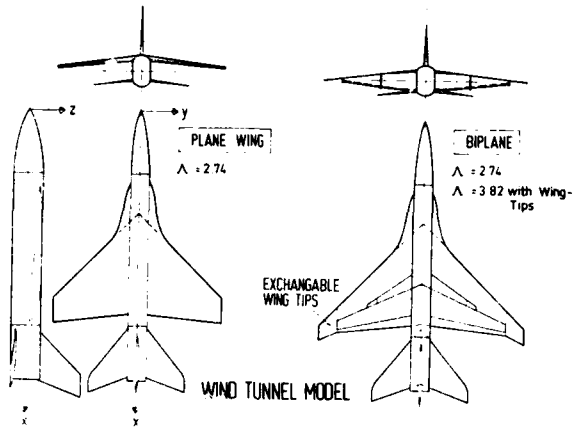
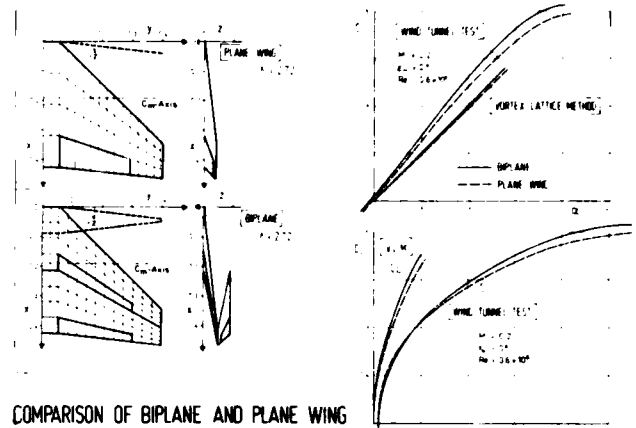
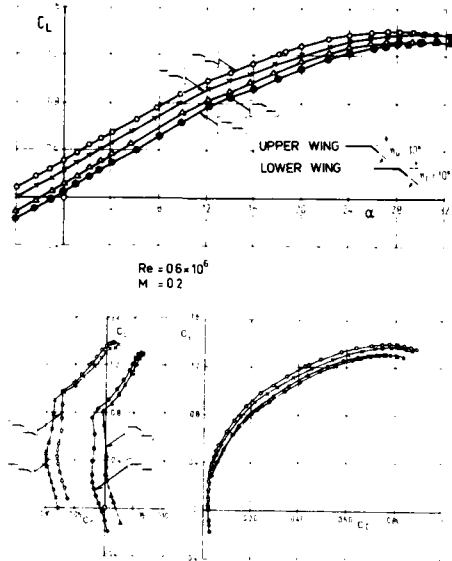


Fig. 22



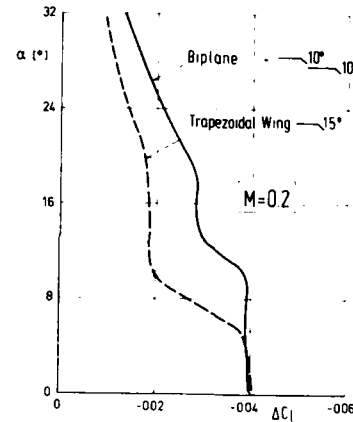
COMPARISON OF BIPLANE AND PLANE WING

Fig. 23



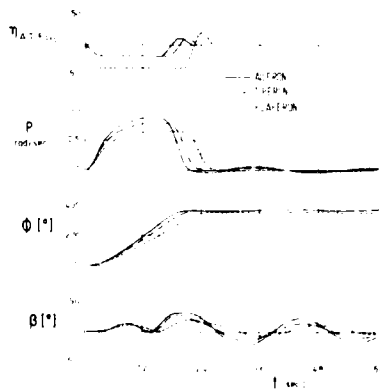
FLAP EFFECTIVENESS ON SUPERSONIC BIPLANE,
WIND TUNNEL TEST

Fig. 24



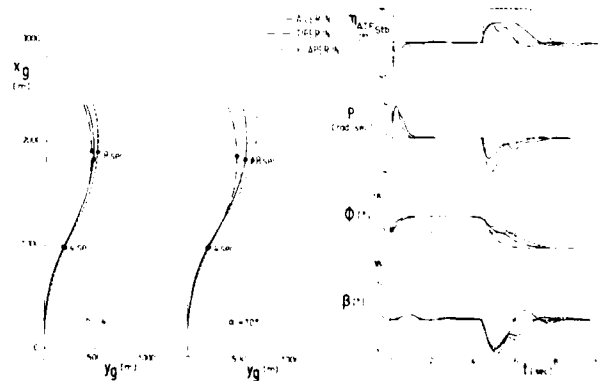
ROLLING MOMENT DUE TO PORT FLAPERON DEFLECTION

Fig. 25



360° ROLL MANEUVER, DIFFERENT
CONTROL DEVICES

Fig. 26



FLIGHT PATH ABOVE GROUND

DYNAMIC TRANSFER BEHAVIOUR

REVERSAL MANEUVER

Fig. 27

ROLL CONTROL BY DIGITALLY CONTROLLED SEGMENT SPOILERS

by

Dipl.-Ing. Klaus Jonas
Dipl.-Ing. Horst Wünnenberg
Dornier GmbH
Postfach 1420
D-7990 Friedrichshafen

Dipl.-Ing. Karl-Heinz Horstmann
Deutsche Forschungs- und Ver-
suchsanstalt für Luft- und Raum-
fahrt e.V. (DFVLR)
Flughafen
D-3300 Braunschweig

SUMMARY

To realize total wing span flaps for improving the maneuvering and landing performances of a combat aircraft, the roll control has to be realized by spoilers. To overcome the nonlinearity and control reversal problems at low deflections the continuously deflected spoiler is replaced by a certain set of digitally controlled single spoilers, which provide only three discrete deflections. It was found by simulator tests that by a proper combination of these segment spoilers it is possible to provide a roll control, which is judged as continuous by the pilot, with a relatively low number of single spoilers. In cooperation between Dornier and the DFVLR different windtunnel programs were performed, to investigate the system-efficiency and aerodynamic effectiveness. Several roll spoiler configurations have been tested in two and three-dimensional configurations with and without landing flaps at different spanwise positions, spoiler deflections and -spans. It will be shown that the effectiveness related to the deflection is linear for flaps-up and highly nonlinear for flaps-down configurations. The spoiler span is of no more influence at a certain value and the optimum spanwise location is about 0.8 of the semispan. Furthermore the effectiveness and the influence on lift and pitching moment for a possible test aircraft are shown. Finally the practical application within an intended flight test program is discussed.

1. INTRODUCTION

Maximum use of all available possibilities to improve take-off-, landing- and maneuvering performance characteristics of fighter aircraft leads consequently to full span flaps, as the lift gain values of the more usual aileron presetting equipment is not very high, fig. 1. Making use of this possibility the roll control has to be realized somehow else. The taileron alone is not very effective at landing configuration where large amounts of roll control power usually are needed. The other possibility by spoilers has not been used very often. Though the roll control by spoilers is very effective especially in the landing flap down configuration, there are usually two main disadvantages:

- a strong nonlinear behaviour
- reversal problems at smaller deflections.

Fig. 2 shows the typical and wellknown behaviour. Due to these facts the design engineer normally hesitates to take spoilers as main roll control devices.

The basic idea of a program, which is sponsored by the ZTL/KEL-program of the German Ministry of Defense, is therefore to overcome these problems by a set of smaller spoilers, which are digitally controlled into three positions, avoiding especially the difficult area between zero and 20 deg. of deflection. In a joint program between Dornier and the DFVLR, Brunswick, the task of Dornier is mainly to find out a proper combination of these segment spoilers in extension and deflection steps for a given test aircraft to provide a roll control by the smallest possible number of single spoilers, which is judged as continuous by the pilot, while the task of the DFVLR is mainly to find out basic aerodynamic data of spoilers, especially with low span.

For these purposes two- and threedimensional windtunnel tests and simulator studies have been performed, the main results of which will be presented in this paper.

2. MINIMUM STEPS FOR CONTINUOUS ROLL CONTROL

To answer this question simulator studies with the aid of the Dornier-Alpha Jet fixed base simulator have been performed. Three testpilots were involved in this program, two of Dornier and one from the GAF-Flight Test Center Manching.

The simulation program included normal Air to Ground Approaches with different speeds, landing approaches and defensive anti-gunnery maneuvers with high roll activity. The results showed that a remarkable low number of individual steps already fulfils the continuity-requirement, if the available stick displacement is divided into three areas, fig. 3. For the larger displacements only three steps are necessary independent from the flight condition. For the smaller displacement there was a difference between high and low speed. For the low speed case area I should have 10 steps whereas for speeds higher than 200 kts 6 steps are sufficient. The time histories of the main data of a simulated high-speed Ground-Attack approach with a complicated anti-gunnery maneuver is shown on fig. 4. The digitalization of the rolling control moment can be seen on the upper trace.

3. SPOILER EFFECTIVENESS

Basic windtunnel research of the spoiler effectiveness depending on spoiler deflection, span and spanwise position was done by the DFVLR.

The windtunnel tests at a Reynolds-number of 1.5×10^6 were realized on a rectangular wing model with a 16 % thick wing equipped with a fowler-flap and two spoiler configurations (fig. 5) for three different test arrangements.

- A Twodimensional tests, airfoil and spoiler covering the whole tunnel-width
- B quasi-twodimensional tests, spoilers of finite span and airfoil covering the whole tunnel-width and
- C threedimensional tests with a half-model of the wing and spoilers of finite span.

Forces and moments as well as pressure distributions have been measured. Some of the main results will be briefly discussed here.

The change in lift coefficient of both spoiler configurations for the twodimensional case A is shown in fig. 6. Obviously it is seen that no control-reversal occurs. For the case of no fowler-flap-deflection the change in lift coefficient is nearly linear with spoiler deflection. For 30° fowler-flap-deflection the gradient of lift coefficient change is increased in the region up to 30° spoiler deflection. Furthermore it comes out that the spoiler configurations II is superior to spoiler I concerning the effectiveness.

Results for spoilers with finite span in the quasi-twodimensional test set up case B, are shown in fig. 7, presenting the change in lift coefficient, depending on spoiler-span for different angles of attack and two spoiler deflections. If the spoiler span is reduced below 0.4 of the actual wing chord a significant reduction of the effectiveness occurs. For the smaller deflections of 20° even a reversal happens at higher angles of attack. The consequence of this result is the fact, that the single segments of the spoiler control should not be reduced below this value without effectiveness losses.

Results for the threedimensional case C are shown in fig. 8 where the influence of spanwise location on spoiler effectiveness is demonstrated. The change in rolling moment coefficient decreases when the location of the spoiler is nearer to the wing tip. At higher angles of attack a maximum in rolling moment coefficient change can be recognized at 0.8 of semispan.

The aims of the windtunnel measurements performed by Dornier with an available Alpha-Jet model equipped with spoilers of type I of fig. 5 were:

- effectiveness of the provided segment spoiler for the Alpha-Jet as a possible test aircraft
- influence of the spanwise position and chordwise extension of the segment spoilers
- influence of the deflection and the angle of attack
- order of magnitude of the coupling yawing and pitching moment effects.

The spoiler arrangement for these tests are shown in fig. 9. This configuration has been chosen based on the DFVLR windtunnel results in order to approach the possible segment spoiler configuration, which would be able to fulfil the required number of the digitalization steps of fig. 3.

Fig. 10 shows the measured effectiveness of rolling moment of the different segment spoilers for flaps-up and flaps-down configuration. The main results of the DFVLR tests for the straight wing have been verified by these tests also for the swept wing. The control reversal for the smaller deflections of the shorter segment spoilers Nr. 1, 2, 3 and 6 are found, too, a result which was already shown by the DFVLR measurements. Consequently the first segment spoiler Nr. 1 will be deflected to 40° as the first step. The most effective spoiler is Nr. 5 which is situated between 50 % and 60 % of the semispan. Though the single effectiveness of the small spoilers near to the wing tip is small, they are nevertheless necessary to realize the required high number of small steps in effectiveness about the neutral stick position.

Fig. 11 shows the influence of the spanwise position on the effectiveness of the spoiler for the swept wing. In comparison to the results for the rectangular wing of fig. 8 the maximum is not as significant at 0.8 of the semispan and more shifted to the inner part of the wing. This is caused by the taper ratio which increases the effectiveness at the inner part and decreases it at the outer part. Due to the sweep-back effect on the other hand, which increases the local lift coefficient at the outer wing again, this is compensated and leads to the flatter curve. An examination of these results shows that the optimum spanwise position for the maximum rolling moment lies between 60 % and 80 % of the semispan, fig. 11.

The chordwise extension evaluation, fig. 12, showed a nearly proportional relation to the chord length which proves the assumption, that the spoiler effectiveness is depending linearly on the projected area vertical to the direction of the airflow.

The effectiveness of the one by one combined segment spoilers, fig. 13, shows that there nearly is the expected and required linearity of the effectiveness for full deflection of the segment spoilers. Fig. 14 gives a comparison of the wellknown theoretical method /3/ for the estimation of the spoiler effectiveness with the windtunnel results. Although the measured effectiveness is lower a nearly linear relation between the rolling moment coefficient and the projected spoiler area multiplied with the spoiler location can be seen.

A very important aspect of the problem using spoilers as roll control devices is illustrated by fig. 15, which shows the influence of the angle of attack on the effectiveness of the combined segment spoilers. Especially at the flaps-down configuration the effectiveness beyond the angle of attack for maximum lift is decreased suddenly and significantly. As shown by the 2-dimensional WT-measurements this break down of the effectiveness in the wing stall angle of attack region is mainly caused by a superimposed rolling moment, which is produced by a spoiler induced unsymmetrical stall of both wing parts. Due to the spoiler deflection this part of the wing stalls some few angles of attack later and the so produced rolling moment is adverse to the primary commanded by the roll control.

The remaining effectiveness can be increased in the landing flaps down configuration by the use of a flap-roof spoiler system (Spoiler type II of the DFVLR-2-dimensional measurements), which was not used for these measurements. The technical realization of this spoiler type seems to be too complicated for the envisaged test aircraft.

Nevertheless the clarification of the high angle of attack problem is one of the purposes of the provided flight test program, which should be realized by a two-seater fighter aircraft, where one cockpit station will remain connected to the usual aileron roll control for safety reasons. There are some existing aircraft which are flying by a pure spoiler-roll control. This fact indicates that there are possibilities to avoid a strong loss in spoiler effectiveness at high angles of attack, perhaps by favourable Reynolds number effects. The aileron roll control is also decreased at high angles of attack, therefore a comparison in flight seems to be of large interest and importance.

4. SECONDARY EFFECTS

4.1 Yawing moment

The proverse yawing moment of a spoiler roll control is one of the significant advantages of this control system. This tendency remains valid up to high angles of attack where the aileron type roll control produces already adverse yaw.

Fig. 16 shows the windtunnel values for two angles of attack and flap settings. If this secondary yawing moment is not compensated by an adequate rudder input, the resulting side slip angle will support the roll control via the rolling moment due to side slip. But even if this yawing moment is compensated by a rudder-input, the rudder rolling moment will support the roll control, too.

4.2 Pitching moment

The shape of the secondary pitching moment which occurs by deflecting the combined segment spoilers is given in fig. 17. As can be seen, there is a significant influence of the flap setting and the reference lift coefficient. Whereas the outer parts of the combined spoiler produce nose-up pitching moments the inner parts are giving nose-down contributions.

This can be explained for the outer spoilers by a combined effect of an increased down-wash, which increases the nose-up moment of the horizontal stabilizer and a negative lift at the spoiler wing position, which is normally and in this case aft of the moment reference point. In the case of the inner spoilers it is just the contrary: the additional negative lift is near or in front of the moment reference point and as the main effect the down-wash at the horizontal stabilizer is reduced, which both leads towards an additional nose-down pitching moment.

It was one of the aims of the simulation campaign to find out the acceptable values of these secondary pitching moments. The results are depending on the flight condition and the fact, whether a pitch damper system was engaged or not. The presented values are within the limits without pitch damper. Only the upper trace for a flap setting of 32° and a lift coefficient of 0.4 are beyond these acceptable values for medium segment spoiler deflections.

But even this doesn't lead to problems, as this case is an unrealistic one from a flight mechanical point of view: the lift coefficient is too low for this flap setting of 32° landing flaps and 20° aileron pre-setting. Furthermore there are some possibilities to overcome these problems by using small pitch compensation spoilers at the inner wing, changing the spoiler configuration in a proper manner or finally using a pitch damping system, which is already available for the provided test aircraft Fiat G-91.

4.3 Lift and Drag

The lift losses at full spoiler deflections are of course remarkable in comparison of the values of an aileron type roll control. Also the additional drag is significantly higher, see Tab. 1:

	ΔC_L	ΔC_D
Aileron	- 0,02	0,006
Spoiler	- 0,26	0,04

Tab. 1 Additional lift and drag at full aileron and spoiler roll control deflection

Though these differences are high, the practical consequences are nearly negligible. Full roll control inputs are used only for very small time intervals, therefore no significant changes in flight path angle will occur due to the lift losses. The effects of the additional drag on fuel consumption or average cruising speed can also be neglected, as can be followed by a statistical flight test evaluation of the average used aileron deflections during some typical Alpha-Jet test flights. The values are 0.12° average of the used aileron deflection during a normal flight with little maneuvering and 0.76° for a test flight where among other points the roll control itself was tested.

5. PRACTICAL APPLICATION

The possibilities and the practicability of digital roll control with the aid of segment spoilers is provided to be demonstrated in flight test by a Fiat G-91 T3, two seater jet aircraft. The arrangement of the set of spoilers for this aircraft is shown in fig. 18.

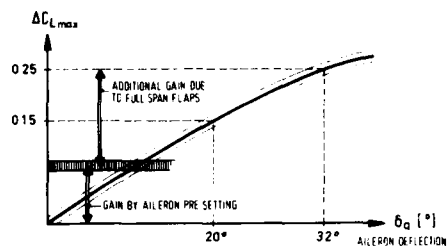
This year high and low speed windtunnel measurements are done at the DFVLR Göttingen with a high speed model loaned from Aeritalia. By these tests especially the secondary effects for the G-91 shall be examined. Furthermore it will be decided from the measured effectiveness whether the spoiler Nr. 6 will be necessary or not.

The single spoilers will be actuated by a digital electro-hydraulic actuator, fig. 19. This device provides two intermediate positions between zero and maximum deflection. One position is realized by the travel of piston 1, the next by the travel of piston 2 and the maximum deflection by the sum of travel of both pistons.

If the design studies, which are performed now, lead to the finding, that a flight test program can be realized with low technical risk and a finite amount of money there is the chance to go into the flight testing in 1982.

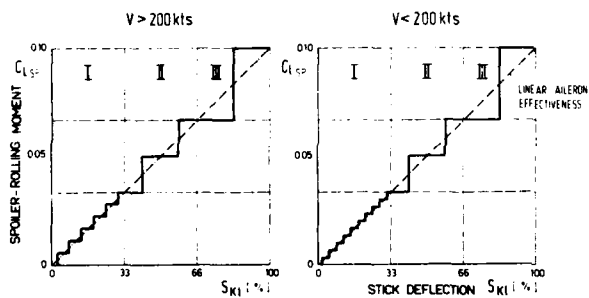
6. REFERENCES

- /1/ H.J. Munser, H.J. Proksch, K. Jonas:
"Rollsteuerung durch Segmentspoiler mit Digitalansteuerung"
ZTL-Bericht Do 77/44 B
- /2/ A.L. Jones, O.P. Lamb, A.E. Crank:
"A Method for Predicting Lift Effectiveness of Spoilers at Subsonic Speeds"
JAS 4/56
- /3/ USAF Stability and Control Datcom
Mc Donnell Douglas Corporation (1969)
- /4/ H. Lück, A. Kühn:
"Rollsteuerung durch Segmentspoiler, Niedergeschwindigkeitsmessungen am Alpha-Jet"
Do-Bericht 78/17 B bzw. DFVLR IB 157-78 C17



LIFT GAIN BY FULL SPAN FLAPS

Fig. 1



ACCEPTED DIGITALISATION OF THE ROLL CONTROL MOMENT

Fig. 3

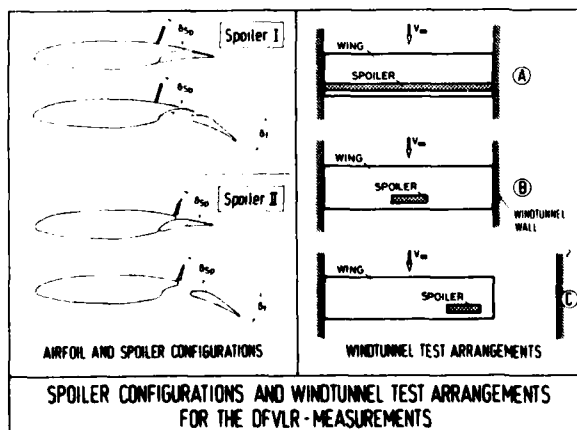
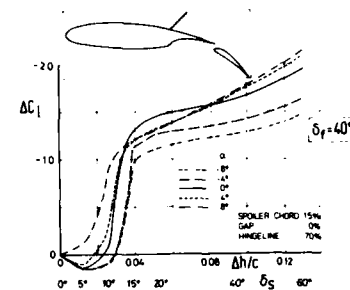
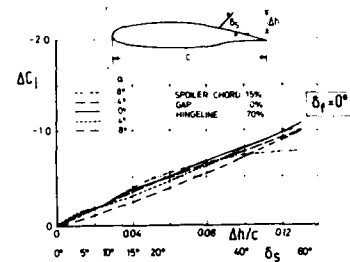
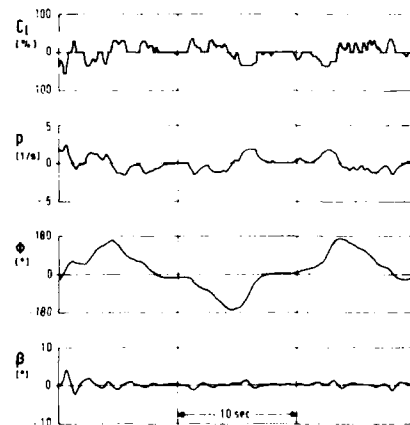


Fig. 5



EFFECTIVENESS OF A GA(W)-PROFIL

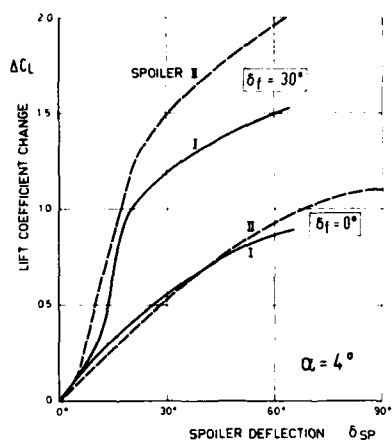
Fig. 2



SIMULATED ROLLING MANEUVERS AT CAS = 470 kts

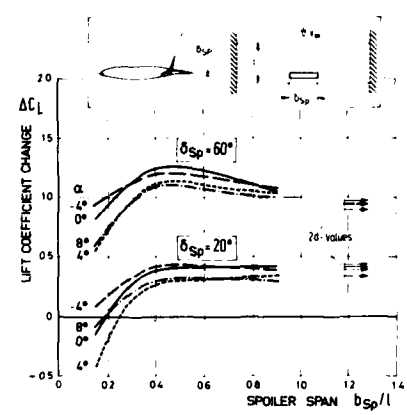
Fig. 4

7-6



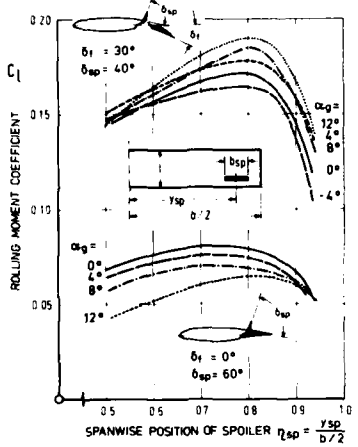
SPOILER EFFECTIVENESS FOR TWO SPOILER CONFIGURATIONS AT $\alpha = 4^\circ$ IN THE TWODIMENSIONAL CASE

Fig. 6



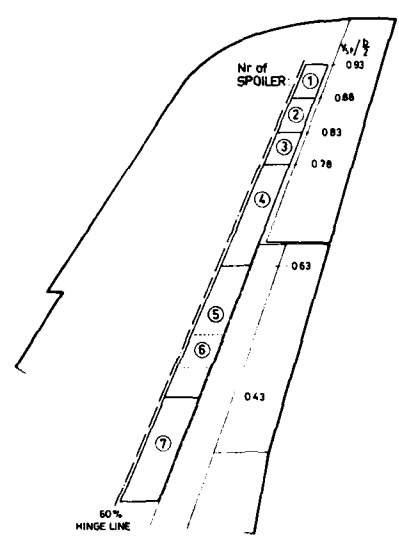
SPOILER EFFECTIVENESS DEPENDING ON SPOILER SPAN FOR TWO SPOILER DEFLECTIONS AND VARIOUS ANGLES OF ATTACK MEASURED IN THE QUASI TWODIMENSIONAL TEST ARRANGEMENT

Fig. 7



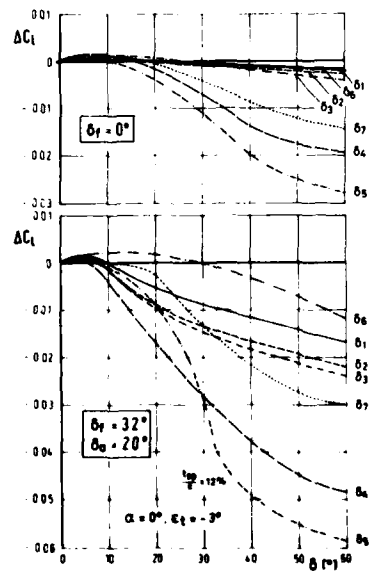
INFLUENCE OF SPANWISE SPOILER POSITION AND FOWLER FLAP DEFLECTION ON ROLLING MOMENT COEFFICIENT FOR A RECTANGULAR WING WITH OO A5 AIRFOIL

Fig. 8



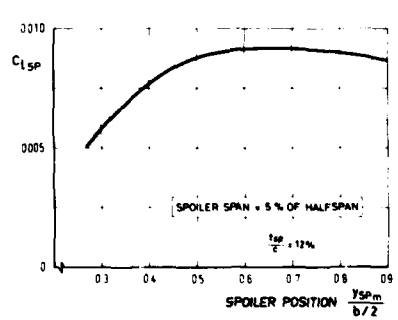
SPOILER ARRANGEMENT FOR WT-MODEL

Fig. 9



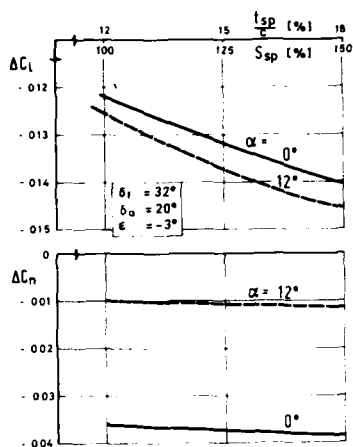
EFFECTIVENESS OF THE SINGLE SEGMENT SPOILERS

Fig. 10



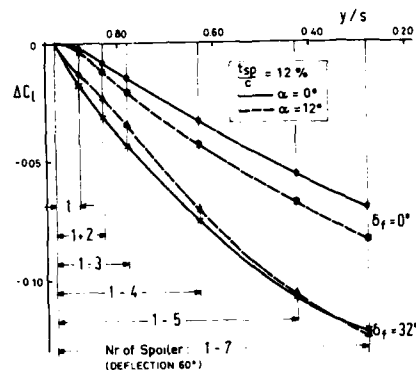
INFLUENCE OF SPANWISE POSITION ON THE SPOILER EFFECTIVENESS

Fig. 11



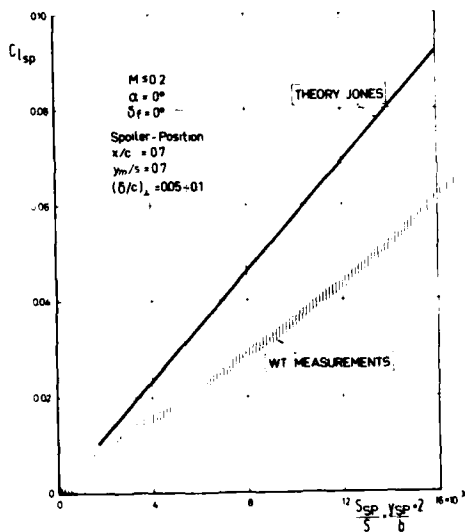
INFLUENCE OF THE CHORDWISE EXTENSION OF THE SPOILERS ON THE EFFECTIVENESS

Fig. 12



EFFECTIVENESS OF THE COMBINED SEGMENT SPOILERS

Fig. 13



SPOILER-EFFECTIVENESS, COMPARISON BETWEEN THEORY AND WT-MEASUREMENTS, $M=0.2$

Fig. 14

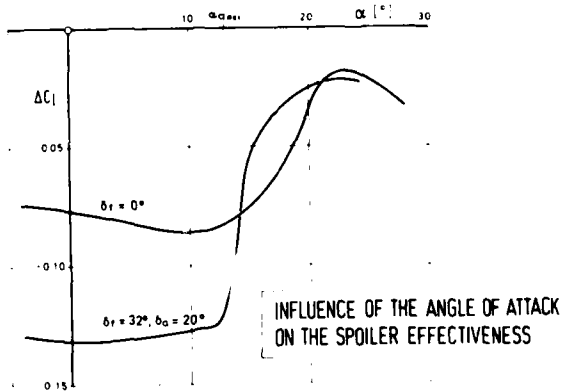
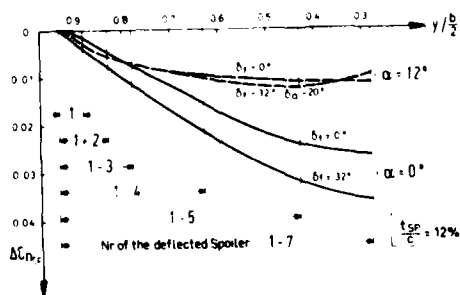


Fig. 15



YAWING MOMENTS FOR COMBINED SEGMENT SPOILER

Fig. 16

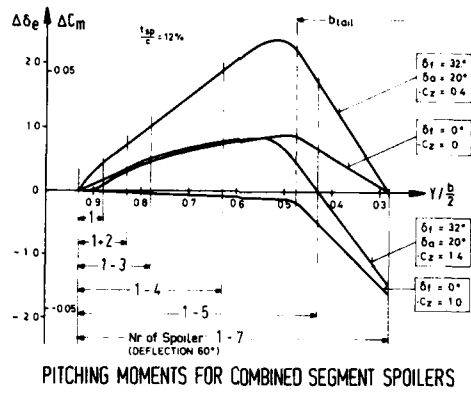
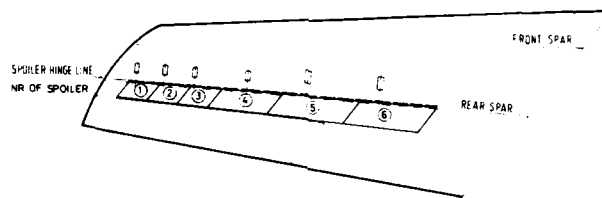
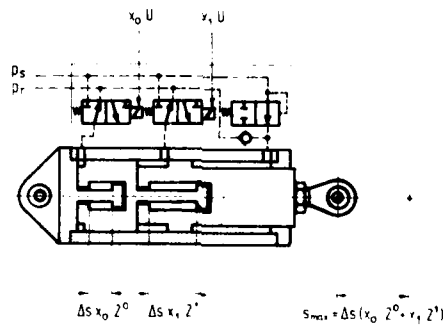


Fig. 17



SPOILER ARRANGEMENT ON PROVIDED FIAT G91-TEST AIRCRAFT

Fig. 18



DIGITAL ELEKTRO-HYDRAULIC ACTUATOR FOR SPOILER CONTROL

Fig. 19

THE YC-14 UPPER SURFACE BLOWN FLAP: A UNIQUE CONTROL SURFACE

By

Alan H. Lee
 Manager, C-14 Flight Control Technology
 Boeing Aerospace Company
 Box 3999
 Seattle, Washington, U.S. A. 98124

SUMMARY

Several versions of powered-lift technology have been applied to STOL aircraft in the past decade. One of these aircraft, the Boeing YC-14, can be controlled during STOL landings using conventional pilot techniques. That capability stems from the use of its upper surface blown (USB) flaps as control surfaces. The USB flaps are used to help control aircraft lift and airspeed. They are positioned automatically by the flight control system to eliminate undesired lift changes caused by thrust changes or external disturbances and to work with the autothrottle to attain and hold a selected airspeed.

USB flaps are ideally suited as control surfaces. Their aerodynamic characteristics are orderly and predictable. Actuator sizes are reasonable since the flaps are relatively small and can be installed so their resultant forces act near the hinge line. Large lift increments can be developed by efficient engine exhaust turning and induced super-circulation. When deflected at large angles, incremental USB flap deflections principally affect drag.

By controlling engine throttles and USB flaps together in a predetermined manner, engine thrust and USB flap position changes can produce forces to accelerate the aircraft tangential or normal to the flight path as desired. The result is a powered-lift, STOL aircraft that can be controlled to precise STOL landings by pilots using the same conventional control techniques they use for other aircraft.

NOTATION

C_D	drag coefficient, D/qS
C_L	lift coefficient, L/qS
C_J	gross thrust coefficient, T_G/qS
D	drag
EBF	externally blown flap
L	lift
NASA	National Aeronautics and Space Administration
q	dynamic pressure
S	wing area
STOL	short takeoff and landing
T_G	gross thrust
USB	upper surface blown
V	velocity, airspeed
\dot{V}_N	acceleration normal to the flight path
\dot{V}_T	acceleration tangential to the flight path
W	weight
α_w	wing angle of attack
γ	flight path angle
Δ	incremental
Δ_{USB}	USB flap angle
θ	pitch attitude

1.0 INTRODUCTION

8-2

The application of powered-lift technology to short takeoff and landing (STOL) aircraft with jet engines has received considerable attention during the 1970's. Methods of producing powered lift included augmentor wing flaps, externally blown flaps, and upper surface blown flaps. Of four representative STOL aircraft, one, the Boeing/USAF YC-14, can be controlled throughout its flight envelope, including STOL landings, using conventional control techniques.

May 1972 saw the first flight of a National Aeronautics and Space Administration (NASA) STOL research aircraft using augmentor wing flaps. It was developed for NASA by Boeing through modification of a Canada DHC-5 Buffalo airplane. The flaps are blown internally by the cold bypass flow from two Rolls Royce Spey engines. The aircraft is being used by NASA in research on STOL operation.

In 1972, the United States Air Force issued a request for proposal for prototypes of advanced medium STOL transport (AMST) aircraft. The winners of the competition were the Boeing YC-14 and the McDonnell Douglas YC-15. The YC-15, using externally blown flap (EBF) technology that had been developed extensively by NASA during previous years, flew first during August 1975. Boeing selected the newer, upper surface blown flap (USB) technology. The additional time required to develop it for aircraft application delayed the YC-14's first flight until August 1976.

One NASA program involves research leading to quiet, jet-powered STOL aircraft. As part of the program, another Canada DHC-5 Buffalo airplane was modified by Boeing to become NASA's Quiet STOL Research Aircraft (QSRA). The QSRA takes advantage of the inherent noise reduction of over-the-wing engine installation and USB flap powered-lift technology. Powered by four engines, it first flew during July 1978.

Each of these aircraft demonstrated the ability to take off and land on very short runways. The two AMST aircraft also demonstrated the ability to cruise at the high airspeeds associated with jet aircraft. The two NASA research aircraft were restricted by their missions to low-speed operation.

Only the YC-14 allows the pilot to use conventional control techniques during STOL landings. With the other aircraft, the pilot must reverse the usual roles of elevator and engine controls and use what is called "backside control." Instead of using the elevator to control glide path and the engines to control airspeed, the pilot uses the throttles to control glide path and the control column to control airspeed. Two factors are responsible for this control technique requirement:

1. By intentional design, thrust changes cause lift changes on powered lift aircraft. Thrust changes can cause more acceleration normal to the flight path than tangential to it.
2. Powered lift STOL aircraft approach at high lift coefficients. The use of the control column to control flight path can cause an instability because of "backside" effects.

With the mission requirements of the AMST aircraft, it was decided at Boeing that the pilot should be able to use the same control technique during all phases of the mission. This was considered especially important during landing. This paper describes experience using the USB flap as a control surface to achieve that objective.

2.0 YC-14 CONFIGURATION

The most notable feature of the YC-14 configuration, shown in figure 1, is the engine location over the wing and close to the fuselage. Engine exhaust from two General Electric CF-6 engines is turned by USB flaps to produce powered lift. The inboard location of the engines minimizes performance losses that result from trim drag when one engine is inoperative. Double-slotted flaps are used between the USB flap and the ailerons. Variable camber Krueger leading edge flaps and leading edge boundary layer control keep flow attached to high angles of attack. The unswept wing was selected to reduce production costs. Advanced technology airfoil sections enable jet airplane cruise speeds and reduce airplane weight. Powerful control surfaces provide desirable response to control commands at the low airspeeds associated with STOL operation.

Flight control surfaces of the YC-14 are shown in figure 2. The surfaces are relatively large and powerful to provide prompt aircraft response to pilot commands. The USB flap, which is used as a full-time control surface during STOL landings, is controlled electrically by the flight control system. Its position can be varied from retracted to 70 degrees down.

3.0 UPPER SURFACE BLOWN FLAP

A profile of the USB flap installation is shown in figure 3. Flow from the fan bypass and the central core is mixed internally and exhausted over the flap. During normal operation, the USB flap surface is sealed to prevent leakage from the upper surface. Low pressure developed by the Coanda effect, the tendency of jet flow grazing a convex surface to remain attached to the surface, turns the engine exhaust flow and produces lift. The exhaust spreads outward as shown in figure 4 and entraps additional air external to the engines. This in turn causes supercirculation on the wing and produces a substantial amount of lift in addition to that gained from turning engine thrust.

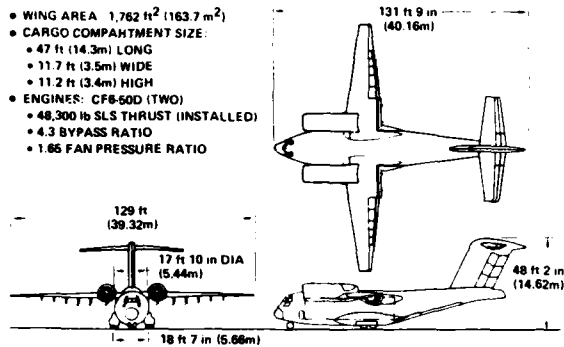


Figure 1. YC-14 Configuration

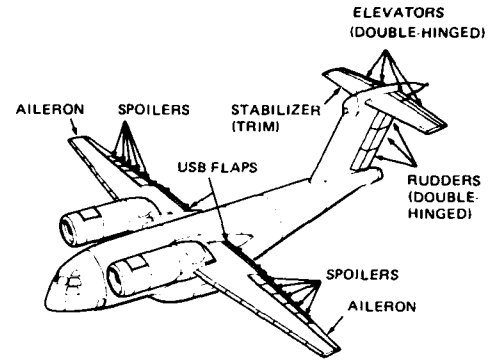


Figure 2. Flight Control Surfaces

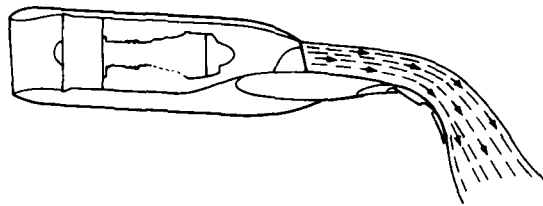


Figure 3. Overwing Engine Installation

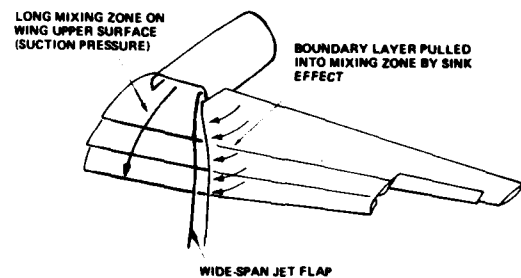


Figure 4. Airflow Over USB Flap

One measure of powered-lift efficiency is its ability to develop lift while minimizing propelling thrust losses. The USB flap has been found to be more efficient than the externally blown flap (EBF) during static tests, as shown in figure 5. Reasons suggested for the USB flap's advantage are less surface wetted by the jet, the absence of slots, and elimination of the underwing reentrant corner, which tends to cause unwanted spanwise flow. Although good flow turning during static conditions is necessary for efficient powered lift, it is not sufficient. Careful attention must be given to the engine exhaust nozzle and flap design to make the exhaust turn through large angles in the presence of slipstream effects. Some important parameters are jet thickness and flap radius. The effects of these parameters on the ability of flow to remain attached to the flap in the presence of external flow with an airspeed similar to that of the YC-14 during landing approach are presented in figure 6. As shown, a large flap radius and a thin jet allow the use of larger flap angles. The section lift coefficients at the largest effective flap angles for specified ratios of flap radius to jet thickness are presented in figure 7. Lift coefficients increase as flap radius is increased and jet thickness is decreased. If flap deflection is limited, lift coefficient increases as the ratio of flap radius to jet thickness decreases until a limiting condition is reached where the flow separates from the flap. More information on this subject is presented in reference 1.

Flow must be turned over the largest practical angle to enable landing approach at steeper than normal flight path angles. Lift must be developed, but thrust force along the drag vector must be minimized. The shape of the nozzle has a substantial influence on the alignment of the resultant force. Figure 8 presents the influence of nozzle aspect ratio on lift and drag forces. Aspect ratio is defined as the effective nozzle area divided by the square of the nozzle centerline height. As shown, increasing aspect ratio enhances powered-lift production with little effect on force in the drag direction.

Similar data, including other parameters, were used during the design of the YC-14 USB flap and engine exhaust nozzle. If low-speed operation were the only consideration, a high-aspect-ratio nozzle could be used to provide a thin jet. However, at cruise speeds, drag caused by the large boattail angle of the nozzle and scrubbing on the wing surface would be unacceptable. A satisfactory compromise was attained by locating a door on the outboard side of the nozzle that opens when wing flaps are extended. This feature helped provide the thin jet desired at low speeds while minimizing the cruise drag penalty. In addition, retractable vortex generators were installed on the USB flaps, as shown in figure 9, to improve flow turning.

Very good STOL performance with one engine inoperative was a Boeing-imposed design requirement for the YC-14. The USB flap was built with two chordwise segments to help attain that requirement. During normal operation, the flap segments touch to make a smooth, sealed contour. When an engine is inoperative, the chordwise segments separate to open a slot and improve performance of the USB flap behind the inoperative engine. The other USB flap continues to function normally.

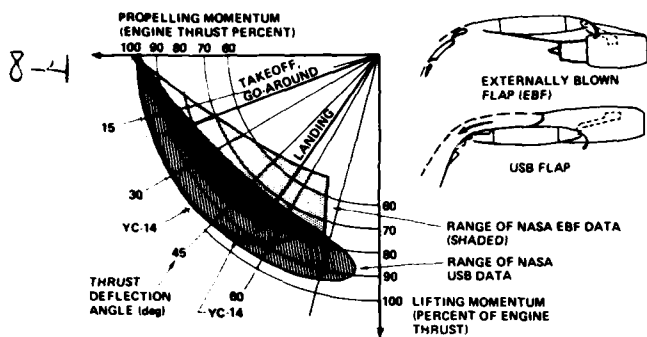


Figure 5. Powered Lift Efficiency

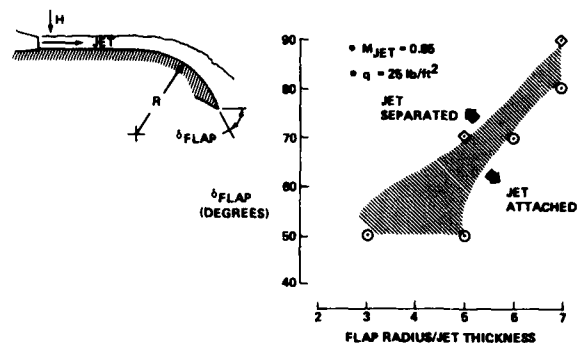


Figure 6. Jet Attachment Limits

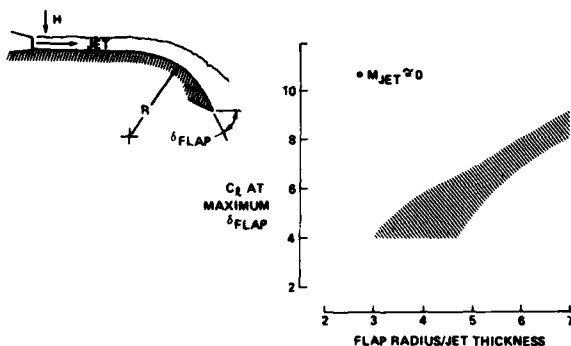


Figure 7. Lift at Limiting Flap Angle

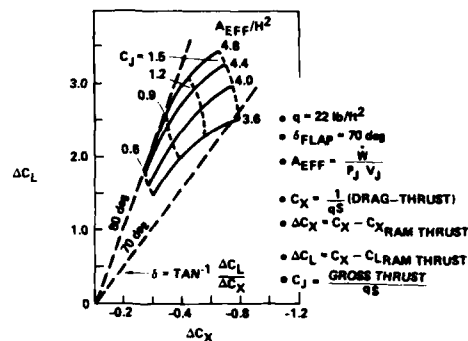


Figure 8. Effect of Nozzle Aspect Ratio on Forces

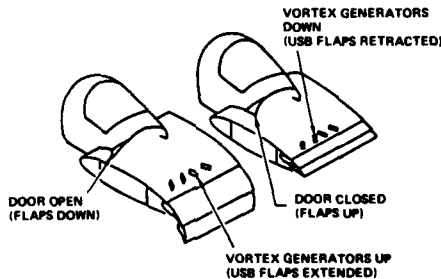


Figure 9. USB Flap Vortex Generators

Its size and the nature of the forces acting on the USB flap enhance its use as a control surface. Each of the two USB flaps on the YC-14 has a span of 17 feet. The line of action of the resultant forces acting on the flap passes close to the flap pivot. As a result, relatively small hydraulic actuators can be used to provide USB flap deflection rates that are compatible with the control surface function.

4.0 CONTROL OF TYPICAL POWERED-LIFT STOL AIRCRAFT

Before describing the use of the USB flap as a control surface on the YC-14, flight path and airspeed control of a typical STOL aircraft are discussed. The YC-14 with its USB flaps maintained at a constant position will be used as the example, although a fixed USB flap position is not typical of YC-14 operation.

4.1 Lift and Drag Characteristics

Since flight path angle and airspeed are the controlled parameters discussed herein, aerodynamic characteristics shown are limited to lift and drag. They are presented in figure 10 for the STOL landing configuration with the USB flaps positioned at 60 degrees. YC-14 capability is slightly better than shown since the flaps can be deflected to 70 degrees. The data were obtained from a wind-tunnel test with thrust on balance. A drawing of a model installed in the tunnel is shown in figure 11. Compressed air is brought into the model through the sting and across the internal balance within the model. It is then ducted to the nacelles and exhausted through a series of choke plates to duplicate engine thrust. Engine exhaust scrubbing drag is included in the data.

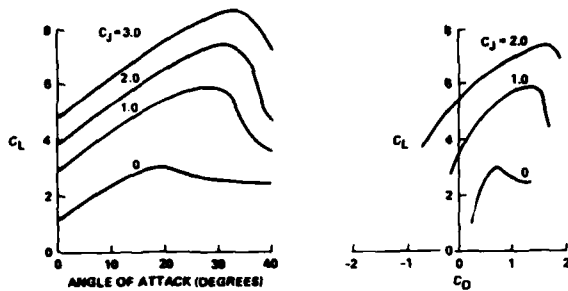


Figure 10. Aerodynamic Characteristics With USB Flap at 60 Degrees

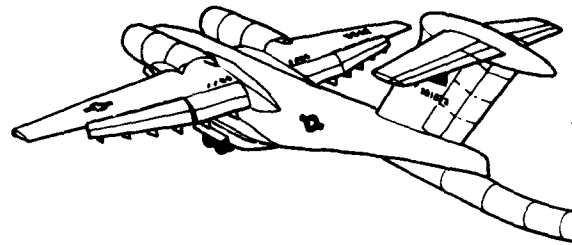


Figure 11. High-Lift Powered Model in Boeing-Vertol 20-by 20-ft V/STOL Wind Tunnel

As shown in figure 10, very high lift coefficients are developed. Lift continues to increase with the gross thrust coefficient, C_J , but its use is limited since the aircraft must be designed to operate safely with one engine inoperative. Much of the lift is induced through supercirculation effects. A cross-plot of incremental lift and drag coefficients with C_J at the YC-14 STOL landing approach angle of attack, 8 degrees, is presented in figure 12.

With the data in figure 10, thrust required for stabilized flight can be determined as a function of airspeed, as shown in figure 13, for the YC-14 during STOL landing approach. As can be seen, increased thrust is required for stabilized flight when airspeed is decreased. This characteristic is sometimes described as operation on the back side of the speed-thrust curve.

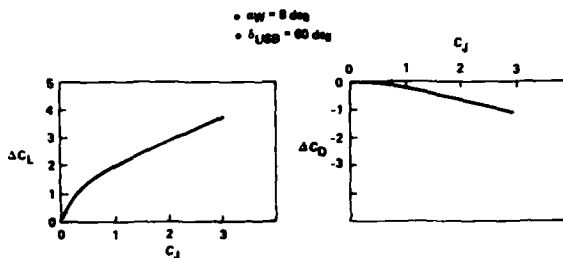


Figure 12. Effect of Thrust on Aerodynamic Characteristics

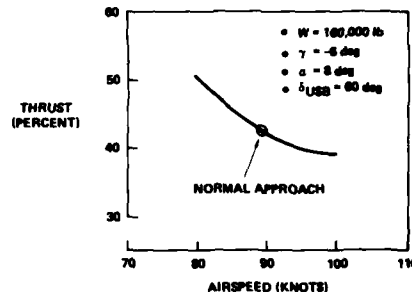


Figure 13. Thrust Required During STOL Landing Approach

4.2 Response to Pilot Commands

Insight to the controllability of typical STOL aircraft can be gained by observing the response of the YC-14 to control commands when its USB flaps are fixed at 60 degrees. Figure 14 shows aircraft response to a control column force. The control and stability augmentation system (CSAS) provides pitch rate response to the column force and holds pitch attitude when the force is released. As shown in figure 14, a flight path angle increase initially accompanies the pitch attitude increase. Airspeed decreases when the flight path angle increases, and, because of the "backside" characteristics of the aircraft, the flight path angle subsequently decreases. The aircraft stabilizes with a pitch attitude increase of 7 degrees, an airspeed loss of 13 knots, and a flight path decrease of 1 degree.

The aircraft's response to a 66% thrust increase with the USB flaps fixed at 60 degrees is presented in figure 15. Airspeed increases slowly from 90 to 92.5 knots. Flight path increases more rapidly from -6.0 to -1.5 degrees. It is apparent that throttle is a much better controller of flight path than of airspeed just as column force was shown to have more effect on airspeed than on flight path angle. If pitch attitude had been held tighter during the thrust increase of figure 15, the effect would have been even more dramatic. The responses in figures 14 and 15 demonstrate clearly why a pilot uses the unconventional backside control technique with typical powered-lift, STOL aircraft.

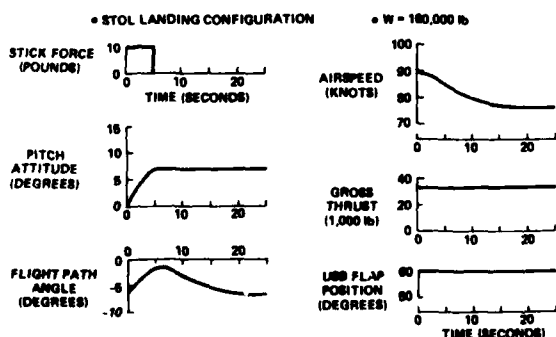


Figure 14. Response to Column Force, $\delta_{USB} = 60$ Degrees

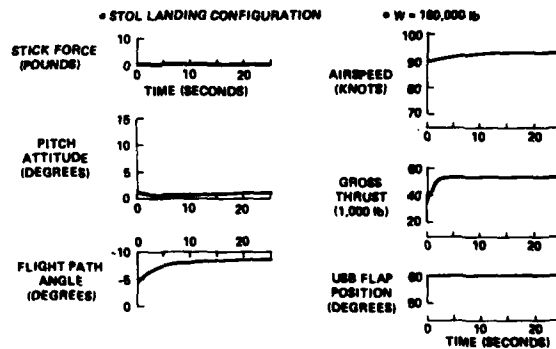


Figure 15. Response to Thrust Increase, $\delta_{USB} = 60$ Degrees

5.0 THE USB FLAP AS A CONTROL SURFACE

8-6

During STOL landings, the YC-14 does not operate like the typical STOL aircraft described in Section 4. With the YC-14, the USB flaps function as full-time control surfaces with their positions commanded automatically by the flight control system.

5.1 Lift and Drag Characteristics

Incremental contributions of USB flap position and thrust to lift and drag are presented in figure 16 for the nominal STOL landing approach angle of attack, 8 degrees. The USB flaps contribute modestly to lift when thrust is zero. At an 8 degree angle of attack and zero thrust, USB flaps deflected 60 degrees add a ΔC_L of 0.4 to the base value of $C_L = 1.75$ with USB flaps retracted. The 60-degree/USB flap deflection adds 0.12 to C_D .

Even with the USB flaps retracted, the application of takeoff rated thrust ($C_J = 1.75$) during STOL landing approach adds an incremental C_L of 1.2. That substantial lift is developed by turning the engine exhaust over the upper surface contour of the wing. With the USB flaps positioned at 60 degrees, takeoff thrust adds a ΔC_L of 2.6. The lift addition is 6.5 times the incremental lift provided by the USB flaps when thrust is zero.

The contribution of thrust force along the flight path is indicated by changes in drag coefficient. The effect of thrust on drag decreases as the USB flaps are deflected. At the trimmed thrust for nominal STOL landing approach, $C_J = 0.68$, powered lift contributes about 2.0 to lift coefficient and very little to drag.

To use the USB flaps as control surfaces, data similar to that shown in figure 16 must be developed for all operational angles of attack. The characteristics remain orderly even up to the angle of attack for minimum airspeed. A small discontinuity in lift and drag, too small to be significant with the scales of figure 16, occurs when vortex generators deploy. As shown in figure 17, vortex generators are retracted at small USB flap angles to maximize thrust force along the flight path. At high USB flap deflections, vortex generator deployment improves flow turning, as evidenced by increased lift and drag. The small discontinuities shown were not objectionable to the pilot.

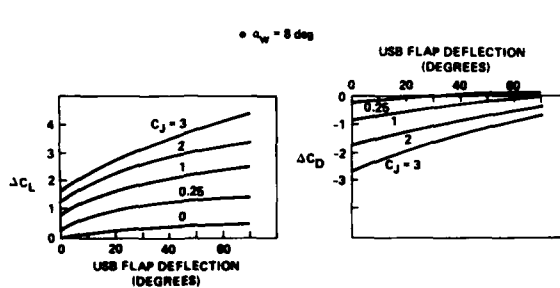


Figure 16. Effect of USB Flap Deflection on Aerodynamic Characteristics

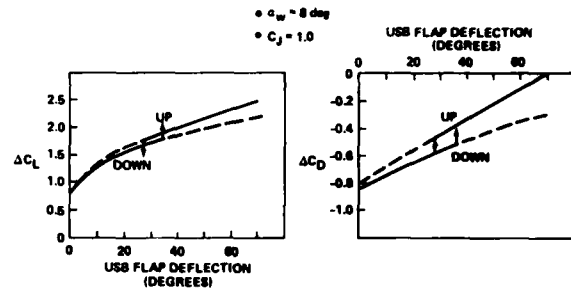


Figure 17. Effect of Vortex Generators on Lift and Drag

5.2 Thrust Force Decoupling

Acceleration is the initial reaction of the aircraft to a thrust change or USB flap position change. The acceleration may be resolved into components tangential and normal to the flight path as presented in figure 18. The flight condition represented is the nominal STOL landing condition of the YC-14. The data in figure 18 assume that the flight control system holds attitude perfectly as thrust or USB flap position varies. Actually, the pitching moment produced does change pitch attitude slightly, as is shown later.

As shown in figure 18, the YC-14 is in equilibrium with the USB flaps at 58 degrees and the engines at 39 percent takeoff rated thrust. If the USB flaps are suddenly retracted to zero degrees with no change in thrust, the aircraft accelerates positively about 5.5 ft/sec² along the flight path and about 12 ft/sec² downward normal to the flight path. The sudden application of full thrust accelerates the aircraft only 3 ft/sec² tangential to the flight path, and 10 ft/sec² normal to it.

Pure accelerations tangential or normal to the flight path can be achieved if thrust and USB flap position are changed together according to the schedules indicated along the figure axes. A pure acceleration of 11.1 ft/sec² along the flight path can be attained by increasing thrust to 100 percent and retracting the USB flaps to 15 degrees. Conversely, a pure acceleration of 7.7 ft/sec² normal to the flight path can be attained by increasing thrust to 75 percent and positioning the USB flap at 70 degrees.

Details of control laws and of thrust and lift decoupling are outside the scope of this paper. However, the parameters and control system gains have been developed for the YC-14 to allow decoupling and have been implemented in the aircraft's triplex digital computers. With this implementation, the pilot is able to direct the aircraft to the desired landing spot by applying force to the control column. Airspeed is held automatically. If the pilot wishes to change airspeed while transitioning to a landing,

he selects the desired airspeed by turning a knob on the control and display panel as described in reference 2. Thus "backside" and thrust and lift coupling effects are eliminated, allowing the pilot to use the same control techniques during STOL landings that he uses during other flight conditions and with other aircraft. 8-7

5.3 Response to Pilot Commands

The result of decoupling thrust and lift on the YC-14 response to a control column force is presented in figure 19. As shown, pitch attitude and flight path angle respond promptly. Airspeed decreases momentarily from 89 to 87 knots and regains its initial value within a few seconds. Thrust increase and USB flaps retract to direct increased force along the flight path. Equilibrium is then attained in the example shown with a flight path angle increase of 6 degrees, a thrust increase of 12,000 pounds and a reduction in USB flap angle of 24 degrees.

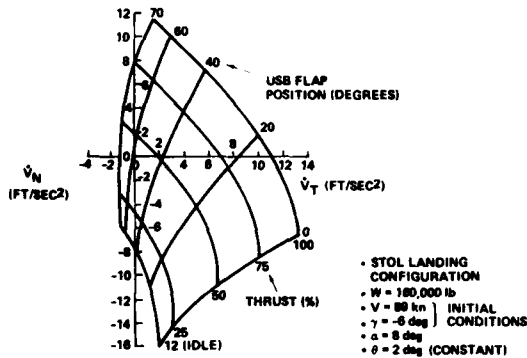


Figure 18. Effect of Thrust and USB Flap Position on Airplane Acceleration

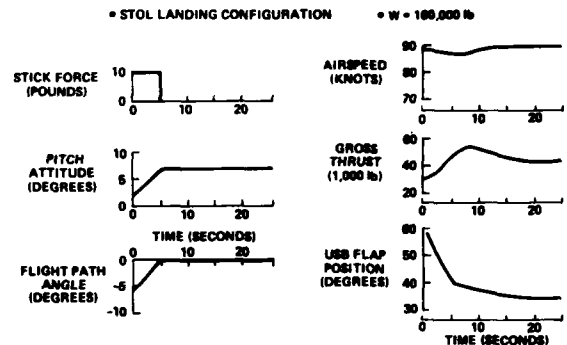


Figure 19. YC-14 Response to Column Force

Aircraft response to a selected 10-knot increase in airspeed is presented in figure 20. As shown, pitch attitude remains constant at 1.5 degrees. The flight path angle, with no pitch commands by the pilot, increases 1.5 degrees and then resumes its initial value. Airspeed increases smoothly from 89 to 99 knots, reaching 90 percent of its change within 10 seconds. Thrust increases initially, accompanied by USB flap partial retraction, to direct more force tangential to the flight path. Equilibrium is reached at the higher airspeed with a 10,000-pound thrust decrease and a 22-degree USB flap angle decrease.

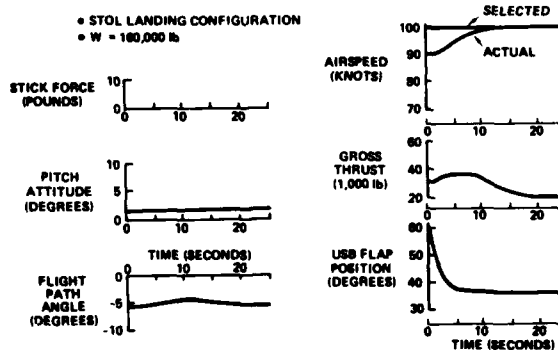


Figure 20. YC-14 Response to Speed Command

6.0 FLIGHT TEST EXPERIENCE

The USB flaps functioned as expected during flight tests. The aircraft responded promptly and smoothly to conventional control commands. The only aerodynamic surprise was the equilibrium position of the USB flap during a STOL landing approach. It was deflected about 10 degrees less than predicted from wind-tunnel data and flight simulator analyses. Prototype program austerity and the absence of any effect on performance or flying qualities did not allow the time to determine the cause. Powered-lift predictions were met or exceeded as verified by minimum airspeed tests.

The ability to control the aircraft using conventional piloting techniques enabled precision STOL landings even by pilots without STOL experience. An example of that precision is presented in table 1, a record of a flight test in which pilots were asked to touch down on a line drawn across the runway. As shown, a pilot without previous STOL landing experience missed the touchdown aim point by an average of only 77 feet in nine landings. His greatest miss was only 125 feet beyond the aim point. A pilot who had made several STOL landings during earlier flights missed the aim point by an average of only 34.5 feet in eight landings. His greatest miss distance was 75 feet.

CONDITION (1 LANDING EACH)	DISPERSION (ft)
22	+25
23	+10
24	+40
25	+80
26	-110
26.1	+88
22.7	-75
27	-45
21.1	+125
28	+80
27.1	-20
27.2	-10
27.3	+80
28.1	-45
18	-10
20	-75
21	+80
17 LANDINGS, 87-ft AVERAGE	

PILOT LEARNING EFFECT			
PREVIOUS EXPERIENCE	NO. OF LANDINGS	AVERAGE DISPERSION (ft)	MAXIMUM DISPERSION (ft)
YES	8	34.5	-75
NO	9	-77.0	+125

Notes:

1. Test Plan 52-1, APL 72-01873, 8 March 1977
2. Touchdown aiming point panels did not contrast well with surroundings
3. Dispersion measured with a tape line

Table 1. Small Touchdown Dispersions During Initial STOL Operation

During a European and United States tour of the YC-14 in conjunction with the Paris Air Show in June 1977, 54 guest pilots flew the aircraft. All pilots adapted readily to the airplane and made STOL takeoffs and landings during their first flight.

The desired good performance with an engine inoperative was achieved. Although powered lift behind the failed engine is reduced substantially and only one USB flap is used in the control mode, the pilots reported the airplane easy to fly using natural control reactions. The aircraft transient following an engine failure is very mild. Additional information is presented in references 2 and 3.

7.0 CONCLUSIONS

Aerodynamic and physical characteristics of USB flaps make them excellent control surfaces. They are used on the YC-14 to decouple thrust and lift by commanding USB flap position automatically by the flight control system. Their aerodynamic contributions are predictable throughout the flight envelope. The application of USB flaps in the control mode produces an aircraft that can be controlled to precision STOL landings by pilots with very little special training.

REFERENCES

1. Davenport, F. J., and Hunt, D. N., The Boeing Company, "Deflection of a Thick Jet by a Convex Surface: A Practical Problem for Powered Lift," AIAA Paper No. 75-167, January 1975.
2. Lee, A. H., The Boeing Company, "YC-14 Flight Control," AIAA Paper 75-1027, August 1975.
3. Lee, A. H., The Boeing Company, "YC-14 Flight Control System Development Experience," Proceedings of the Flight Control Systems Criteria Symposium, 11 to 13 July 1978, Naval Postgraduate School, Monterey, California.

FLAPERON CONTROL - THE VERSATILE SURFACE
FOR FIGHTER AIRCRAFT

JOHN F. MOYNES & WALLACE E. NELSON, JR.
NORTHROP CORPORATION

9-1

SUMMARY

The versatility of a flaperon is presented for roll performance and for several longitudinal active control modes. Particular emphasis is given to the advantages of a segmented flaperon over a full span flaperon for a YF-17-type aircraft.

The areas of ride smoothing, direct lift, pitch pointing, vertical flight path control and flight control system reconfiguration are addressed for the active longitudinal control modes. The effect of flaperon pitching moment on the implementation of these modes is discussed.

SYMBOLS

\bar{A} - root mean square acceleration response, g's/feet per second
ALT - altitude
 $C_{D\delta F}$ - coefficient of drag due to flaperon deflection, per degree
 $C_{L\alpha}$ - lift curve slope, per degree
 $C_{L\delta F}$ - coefficient of lift due to flaperon deflection, per degree
 $C_{L\delta H}$ - coefficient of lift due to horizontal tail deflection, per degree
 C_l - rolling moment coefficient, nondimensional
 $C_{m\alpha}$ - coefficient of pitching moment due to angle of attack
 $C_{m\delta F}$ - coefficient of pitching moment due to flaperon deflection, per degree
 $C_{m\delta H}$ - coefficient of pitching moment due to horizontal tail deflection, per degree
 C_n - yawing moment coefficient, nondimensional
 M_F - Pitching moment due to flaperon deflection, per second²
 M_H - pitching moment due to horizontal tail deflection, per second²
 M_q - pitching moment due to pitch rate, per second
 M_α - pitching moment due to angle of attack, per second²
 N - yawing moment, degrees per second²
 \hat{Q} - arbitrary pitch rate, degrees per second
 $T_{AF}(\Omega)$ - Transmissibility of airframe at pilot station, g-second/feet
 V - total aircraft velocity, feet per second
 Z_F - angle of attack rate of change due to flaperon, per second
 Z_H - angle of attack rate of change due to horizontal tail, per second
 Z_q - angle of attack rate of change due to pitch rate, nondimensional
 Z_α - angle of attack rate of change due to angle of attack, per second
fps - feet per second
 g - acceleration of gravity, $1g = 32.2 \text{ ft/sec}^2$
 n_z - vertical load factor of aircraft center of gravity, $n_z = 1$ for level flight, g's
 n_{zp} - vertical load factor at pilot station, g's
 q - pitch rate, degrees per second
 \dot{q} - pitch acceleration, degrees per second²
 u - aircraft forward velocity with respect to body axis, feet per second
 w - aircraft vertical velocity with respect to body axis, feet per second
 \dot{w} - aircraft vertical acceleration with respect to body axis, feet per second²
 w_{gust} - vertical gust with respect to aircraft's body axis, feet per second
 $\Phi(\Omega)$ - power spectral density of turbulence, (fps)²/hz
 Ω - Frequency, hz
 Ω_c - cutoff frequency, (frequency beyond which aeroelastic responses are no longer significant in turbulence)
 Δ - increment of (used as prefix for aerodynamic terms)
 α - angle of attack, degrees
 $\dot{\alpha}$ - angle of attack rate of change, degrees per second
 δ_F - flaperon deflection, degrees
 δ_H - horizontal tail deflection, degrees
 $r_{inboard}$ - nondimension location of flaperon inboard edge
 σ - root mean square load factor at pilot station, g's
 σ_{nzp} - root mean square load factor at pilot station, g's
 σ_{w-gust} - root mean square turbulence level, feet per second

INTRODUCTION

9-2

With the advent of the control configured vehicle, the early stages of design for modern aircraft become increasingly influenced by the potential capabilities of the flight control system design. Thus, as this article demonstrates, today's control development engineer must be increasingly aware of the aerodynamic characteristics of the aircraft in general, and control surfaces in particular, at an early phase of development. This way, the most benefit can be derived from an integrated flight control system design.

One of the most demanding control surface design tasks is to obtain adequate roll power for tactical aircraft. Many approaches have been taken in this area including the spoiler/aileron approach on the F-4, the elevon design of the Swedish Viggen, the full span flaperon rolling tail of the F-16, and the aileron/rolling tail concept of the YF-17.

At this time, Northrop is performing an extensive investigation of flaperon control in an effort to maximize the flaperon's potential beyond the benefit of increased roll power for a YF-17-type aircraft

This paper represents some of the preliminary results of an investigation that deals with both the longitudinal and lateral/directional aspects of a flaperon system, including the rationale for employing a segmented panel flaperon presented in Figure 1 rather than a single panel flaperon also shown in Figure 1. The use of the segmented flaperon is analogous to the conventional aileron/flap configuration which is now utilized on the YF-17 to provide the functions of roll and lift control. The study presents several active control modes which can be realized with the use of a flaperon and it attempts to give some insight into how the aerodynamic characteristics of the aircraft in general, and flaperon configuration in particular, affect the employment of the flaperon for these modes.

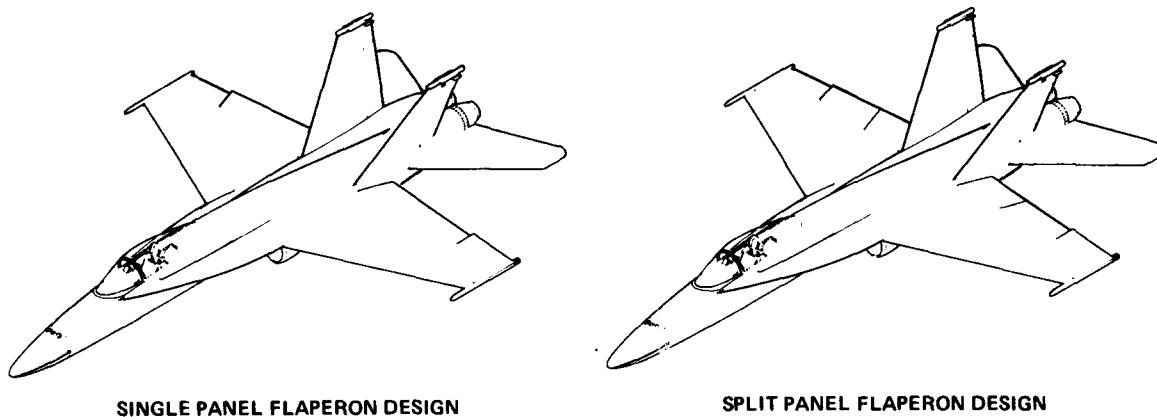


FIGURE 1. FLAPERON CONFIGURATIONS

FOCUS

Analysis for this study focused in the transonic region, typically below an elevation of 15,000 feet. This was considered one of the most critical for the evaluation of flaperon performance and the earliest available flaperon aerodynamic data was for this region. The study addressed the potential application of flaperon control in concert with the horizontal tail for primary and auxiliary modes of control in the lateral/directional and longitudinal axes. The primary modes addressed were roll performance, maneuvering flaps and longitudinal ride smoothing. The auxiliary modes considered were maneuvering enhancement, vertical flight path control, direct lift, longitudinal fuselage pointing and reconfiguration control. Reconfiguration control is the ability to reconfigure the flight control system in order to compensate for some failure which has occurred within the flight control system.

ANALYTICAL TOOLS

The primary tools for analysis consisted of three Continuous System Modeling Program (CSMP) models for time-domain analysis, where each model incorporated a Control Augmentation System (CAS). A Control System Analysis Program (CSAP) was used where applicable for frequency domain analysis of the CSMP models. The three CSMP models represent: a three-degree-of-freedom lateral/directional airframe model, a three-degree-of-freedom longitudinal airframe model and, for preliminary analysis, a two-degree-of-freedom longitudinal model. The two-degree-of-freedom model was used for the study of the auxiliary modes where the auxiliary mode maneuvers rely on decoupling the short period dynamics of the aircraft.

All three CSMP models incorporated rigid body aerodynamics with corrections for aeroelasticity. The aerodynamic coefficient buildup for the three degree of freedom models utilized linear derivatives for only the flaperon data. The two degree of freedom model however, utilized linear derivatives exclusively.

FLAPERON CONTROL - THE LATERAL DIRECTIONAL ASPECTS

ROLL PERFORMANCE

In the initial study for increased roll performance, a single panel, full span flaperon, depicted in Figure 1, was chosen. However, early into the analysis of the full span flaperon it became apparent, as the following discussion indicates, that a segmented type of flaperon, also shown in Figure 1, was the preferable configuration.

As an introduction to the discussion for the preference of flaperon configuration it is pertinent to consider some of the aerodynamic characteristics associated with the empennage of a YF-17-type aircraft. In addition to the leading edge extension, which plays no role in this study, a YF-17-type aircraft is typified by a short coupled horizontal tail and toed in, canted out twin vertical tails, as indicated in Figure 2. Due to the close proximity of the vertical and horizontal tails to the trailing edge of the wing, flaperon deflections can have a significant effect on the downwash acting on the horizontal tail and the sidewash acting on the twin vertical tails. It is these downwash and sidewash effects which determine the most effective flaperon design and in addition contribute to the complexity of the aerodynamics.

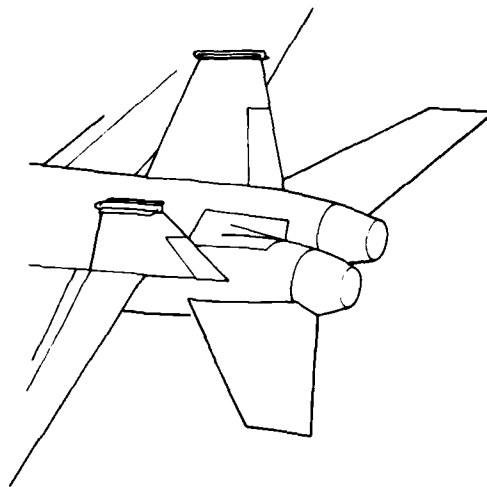
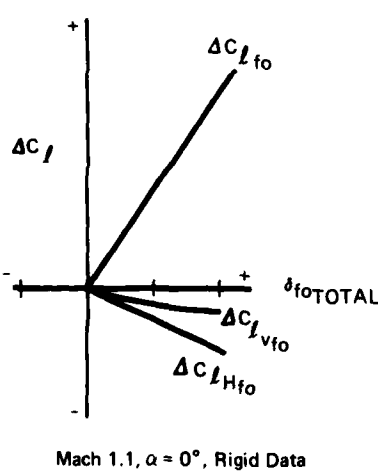


FIGURE 2. YF-17-TYPE EMPENNAGE

SINGLE PIECE FLAPERONS

ROLL POWER

For the large span flaperon, at Mach 1.1, 10,000 feet, a relatively large rolling moment, typified by Figure 3*, is generated for a differential deflection of 20 degrees.



$$\delta_{fo} \text{ TOTAL} = \delta_{fo} \text{ LEFT} - \delta_{fo} \text{ RIGHT}$$

$$\Delta C_{l_{\text{outboard flaperon}}} = \Delta C_{l_{fo}} (\delta_{fo}, \alpha) \cdot K_{e/r}^{fo} + \Delta C_{l_{vfo}} (\delta_{fo}, \alpha) \cdot K_{e/r}^v + \Delta C_{l_{Hfo}} (\delta_{fo}, \alpha) \cdot K_{e/r}^h$$

$\Delta C_{l_{fo}}$ = roll due to outboard flaperon

ΔC_{l_v} = roll due to vertical interference effects

ΔC_{l_H} = roll due to horizontal interference effects

$K_{e/r}^{fo}$ = outboard flaperon flexibility coefficient

$K_{e/r}^v$ = vertical flexibility coefficient

$K_{e/r}^h$ = horizontal flexibility coefficient

FIGURE 3. TYPICAL FLAPERON LATERAL/DIRECTIONAL COEFFICIENT BUILDUP

With the incorporation of aeroelastic effects, this value is changed to a reversed rolling moment due to a large opposing rolling moment generated at the empennage and worsened by the significantly higher elastic to rigid ratios of the empennage surfaces. The major portion of reduced flaperon effectiveness in the high dynamic pressure region can be attributed to the flexibility of the wing itself.

The effect of moving the inboard edge of the flaperon outward yielded a reduction in the interference effects between the flaperon and empennage, but also a reduction in the effectiveness of the flaperon so, as demonstrated in Figure 4, there was no significant improvement in the overall roll effectiveness.

* The coefficient buildup shown in Figure 3 for the outboard flaperons is the same as for the full span flaperons coefficient buildup.

9-4

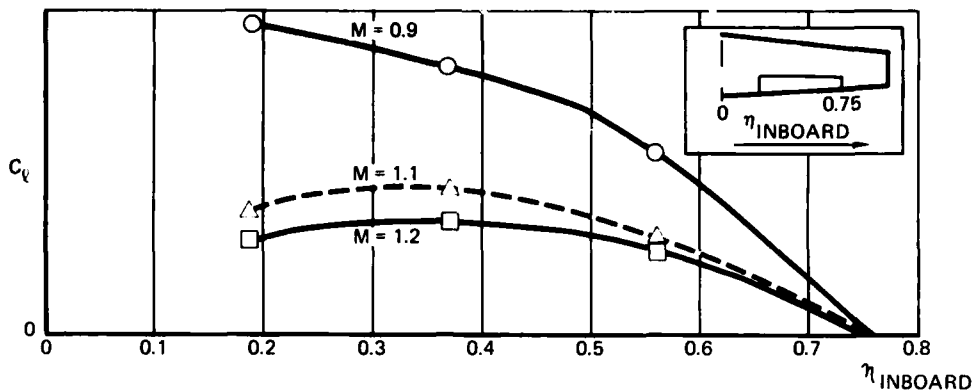


FIGURE 4. RIGID ROLLING MOMENT VERSUS FLAPERON INBOARD EDGE LOCATION

YAW/ROLL EFFECTS

Along with roll power, the minimization/control of induced yawing moments is another type of improved roll performance and turn coordination. The yaw/roll ratios for the analysis at Mach 0.9, 1.1 and 1.2 revealed values greater than unity for both supersonic cases, shown in Figure 5. Test data taken with the vertical tails removed, Figure 6, show that the sidewash effects at the vertical tail are solely responsible for these yawing moments. Depicted in Figure 7, as the right and left hand flaperons are differentially deflected, the circulation about the wing creates a sidewash. This sidewash in turn acts against the twin vertical tails, resulting in a yawing moment. While the movement of inboard edge outboard did improve the C_{n_u}/C_ℓ ratio, Figure 8, it resulted in a decrease in roll power as previously noted.

A conventional aileron system, such as on the YF-17, induces yawing moments which are relatively small and can be controllable with the application of an aileron rudder interconnect. However, as a result of increased aerodynamic interaction on the vertical stabilizer, the yawing moments induced by the full span flaperons are so large that there is insufficient rudder power to compensate or moderate them in the transonic, high dynamic pressure flight region.

Therefore, the single piece flaperons are unacceptable for a YF-17-type aircraft in that they provide:
 1) inadequate rolling moments and 2) induced yawing moments which cannot be cancelled by the available rudder hinge moment capability.

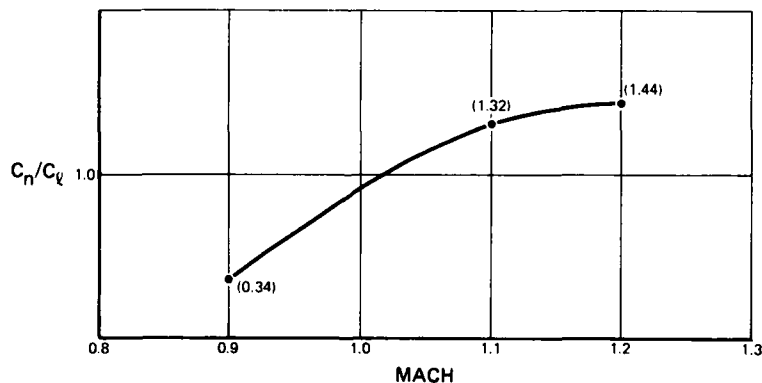


FIGURE 5. YAW/ROLL RATIO FOR FULL SPAN FLAPERONS

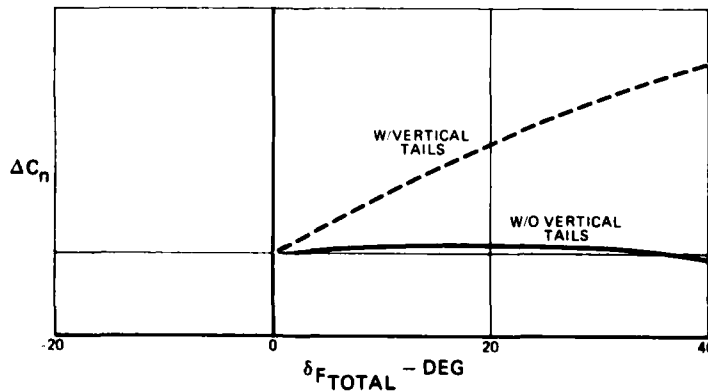


FIGURE 6. EFFECT OF VERTICAL TAILS ON INDUCED YAWING MOMENTS

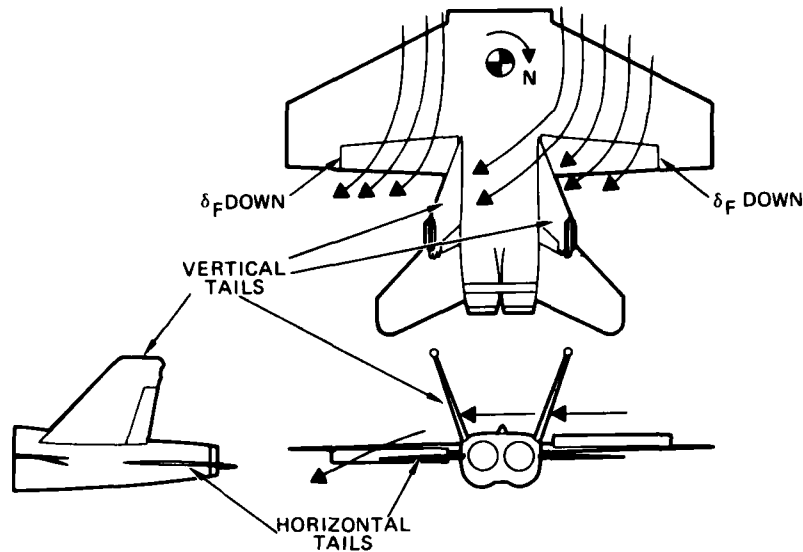


FIGURE 7. EFFECT OF SIDEWASH ON VERTICAL TAILS

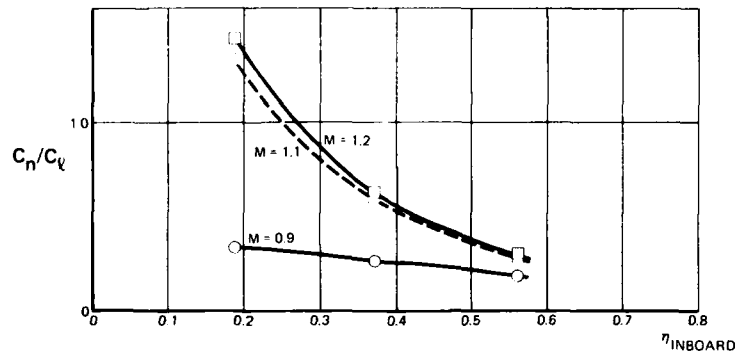


FIGURE 8. YAW/ROLL RATIO VERSUS FLAPERON INBOARD EDGE LOCATION

SEGMENTED FLAPERON

ROLL PERFORMANCE

As a result of testing on the full span flaperons the decision was made to investigate the potential of segmented flaperons. With fly-by-wire technology, the inboard panels of the segmented flaperons can be deflected symmetrically or asymmetrically with the outboard panels, Figure 9, in order to provide the best possible roll performance for a given flight condition. In contrast to the full span flaperons, during a high dynamic pressure, transonic flight condition, the segmented flaperons with the inboard panels oppositely deflected provide the capability for adjusting the level of induced yawing moment while having a favorable rolling moment interference on the empennage. In Figure 10, a comparison of the rigid rolling and yawing moment coefficients and the elastic rolling moments at 10,000 feet clearly present the advantages of the segmented flaperons over the full span flaperon. For the rigid data the rolling moment is up to 50 percent more and the yawing moment is reduced by over 50 percent. For the elastic rolling moment data, not only does the segmented flaperon provide greater roll power, it precludes roll reversal at Mach .95.

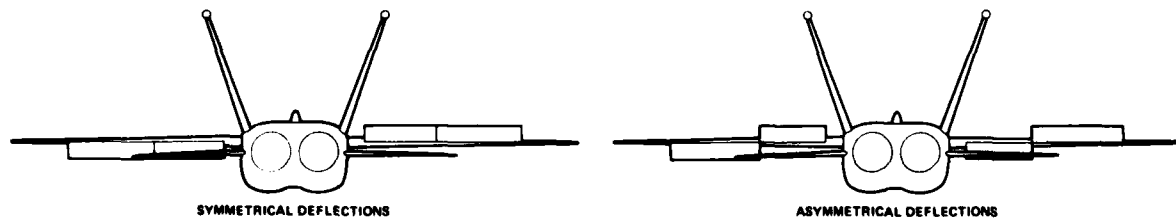


FIGURE 9. SEGMENTED FLAPERON ROLL CONFIGURATIONS

Testing during the study of the full span flaperon revealed that the interference effects between the flaperon and the horizontal tail which resulted in an adverse roll input from the empennage also served to reduce the hinge moment which acted upon the horizontal tail. While the hinge moment relief provided by the full span flaperons

9-6

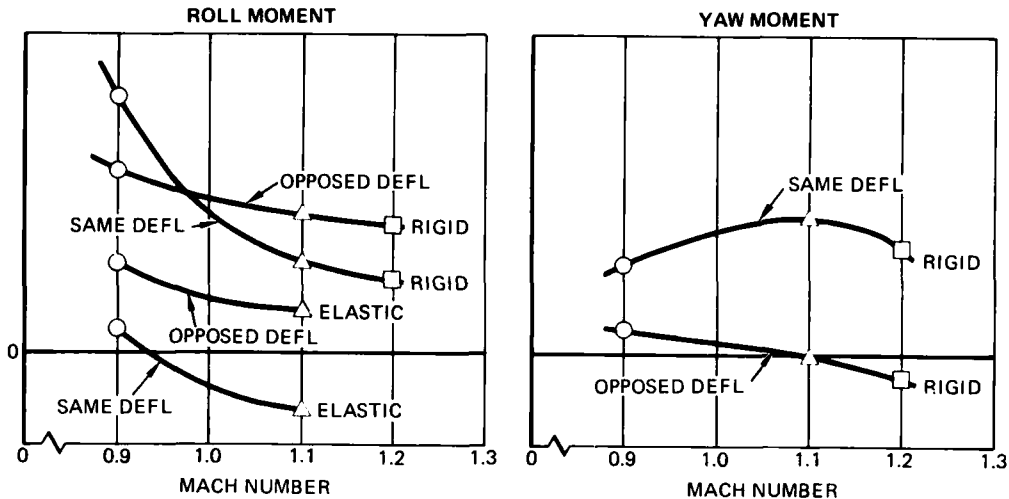


FIGURE 10. SEGMENTED FLAPERON PERFORMANCE ADVANTAGES

could not be effectively utilized, the segmented flaperons can fully exploit this benefit. For a flight condition of Mach 1.1 at 10,000 feet the calculated rolling tail deflection is five degrees without hinge moment relief. With the hinge moment relief from the deflected flaperons, however, the rolling tail can obtain its total differential authority of 20 degrees.

On the basis of the increased roll power and minimization of induced yawing moments, the segmented flaperons are considered to be the baseline configuration for any future YF-17 derivatives utilizing flaperon control.

OTHER CONSIDERATIONS

In addition to the tradeoff for increased flight control system complexity, a disadvantage of the segmented flaperons is the associated increase in the complexity of the aerodynamics. The ability to move the inboard panels symmetrically or asymmetrically with respect to the outboard panels in conjunction with the flaperon interference effects at the empennage makes the flaperon aerodynamics a very complex problem, typified by the rigid data and buildup equations presented in Figure 3 for the outboard flaperons. The reduction of the lateral directional data for a particular angle of attack requires determining the coefficient contribution from the flaperon, the horizontal tail and the vertical tail. A large change in the horizontal tail position will result in a change in the coefficient. Separate elastic to rigid ratios must be applied to each component and the particular coefficient for a panel will vary depending on symmetrical or asymmetrical deflection of the adjoining panel. Thus, we are dealing with a very complex configuration, one that is capable of bringing a grimace to the face of those responsible for test requirements and data reduction.

LONGITUDINAL MODES

For the study of the potential longitudinal modes utilizing active flaperon control there was no distinction made between full span and segmented flaperons. The inboard/outboard panels are treated as one surface with the exception of the maneuvering flaps mode.

The ability to move all four panels symmetrically gives the flaperons a longitudinal control capability comparable with that of the horizontal tail. With the existence of two independent longitudinal control surfaces, it becomes possible to decouple the two airframe state variables, angle of attack and pitch rate that dominate the aircraft's short period frequency characteristics.

The longitudinal modes include both closed loop and open loop modes. The closed loop modes require feeding back one or two airframe variables to achieve the desired aircraft response in addition to or instead of the normal feedback variables of the Control Augmentation System presented in Figure 11. The open loop modes require only interconnected deflections of the flaperon and horizontal tail and rely on the dynamics of the airframe to achieve the desired aircraft response. All of the results presented are for a flight condition of Mach 0.9 at either 500 or 1000 feet. The application of these modes for most other flight conditions can be achieved through gain scheduling as a function of Mach and altitude.

For the preliminary study of the longitudinal flaperon modes, the derivation of values for the longitudinal flaperon derivatives were incomplete. While preliminary analysis indicated the value of $C_{L_{\delta F}}$ was positive and at least 0.010 per degree for Mach 0.9 at Sea Level, and $C_{D_{\delta F}}$ was insignificant, neither the magnitude nor the sign of $C_{m_{\delta F}}$ was certain. While in all likelihood $C_{m_{\delta F}}$ is positive for a short coupled aircraft like the YF-17, until the elastic to rigid increments are determined there is some possibility that the value may be negative. Therefore, the influences of positive, zero and negative values of $C_{m_{\delta F}}$ are indicated in the discussions of the longitudinal modes.

MANEUVERING FLAPS

Before proceeding into new areas for the application of flaperon control, it is important to cover an area which was successfully implemented on the YF-17, maneuvering flaps.

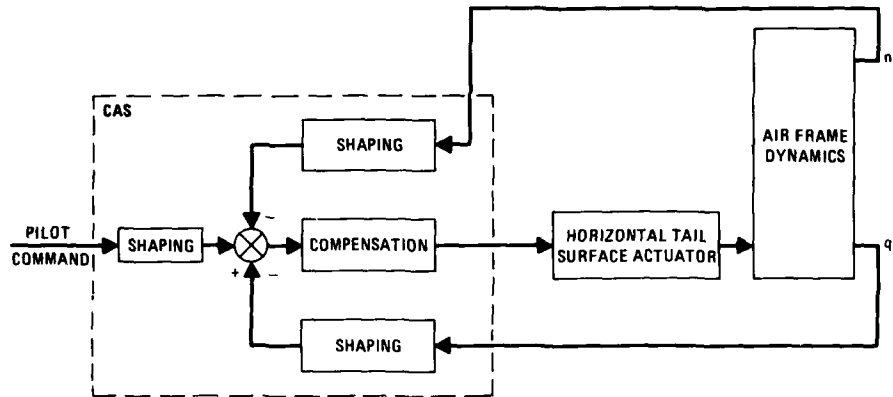


FIGURE 11. BASIC CONTROL AUGMENTATION SYSTEM CONFIGURATION

For the segmented flaperon design, the maneuvering flaps mode utilizes the leading-edge flaps and the inboard flaperons to vary the effective wing camber during maneuvers. The surfaces are positioned in accordance with schedules of angle of attack and Mach number to obtain the optimum lift-drag ratio during maneuvering, as presented in Figure 12. In addition to enhancing flight path control and aircraft agility, the flap system is beneficial in obtaining high resistance to spin, Reference 1.

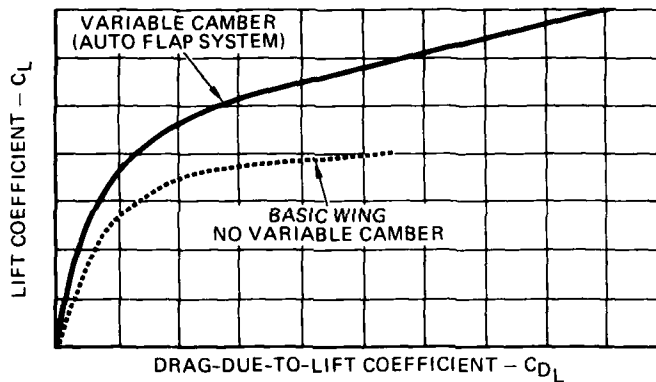


FIGURE 12. EFFECT OF MANEUVERING FLAPS

- LEADING EDGE/TRAILING EDGE FLAP SCHEDULED TO MAXIMIZE LIFT AND MINIMIZE DRAG

RIDE SMOOTHING

In order to increase the survivability of modern fighter aircraft, new emphasis is being given to the capability of low-altitude high-speed penetration. For an aircraft such as the YF-17, the low-wing loading/high-lift curve slope which maximize turn rate capability and maneuverability essential for survival in air combat also tend to deteriorate the ride quality during high-speed penetration, which can lead to reduced mission success in attacking heavily defended ground targets, or in the worst case even mission failure.

For the evaluation of ride quality through turbulence, \bar{A} is used. \bar{A} is the rms load factor at the pilot station (unless otherwise noted) divided by the rms gust level (fps) as defined in Equation 1.

$$\bar{A} = \left[\frac{\int_0^{\Omega_c} |T_{AF}(\Omega)|^2 \Phi(\Omega) d\Omega}{\int_0^{\infty} \Phi(\Omega) d\Omega} \right]^{1/2} = \frac{\sigma_{nz_p}}{\sigma_{w-gust}} \quad (1)$$

The \bar{A} values are determined from the rms load factor and turbulence levels which are computed by sampling n_z and $w-gust$ during time domain simulation of the CSMP models. Each ride quality run is simulated for sixty seconds.

To simulate turbulence the nongaussian Tomlinson turbulence model, Reference 2, was used with an rms gust intensity level of approximately 6.6-feet per second as prescribed by MIL-F-9490D, Reference 3, for a 10^{-2} probability of exceedance at an altitude of 500 feet. This turbulence model is based on the atmospheric turbulence modeling work performed by J. G. Jones, Reference 4. The Tomlinson model was chosen in preference to the Dryden turbulence model because its velocity increment distribution was considered more realistic of atmospheric turbulence. The power spectral density for the Tomlinson turbulence model is comparable to

9-8

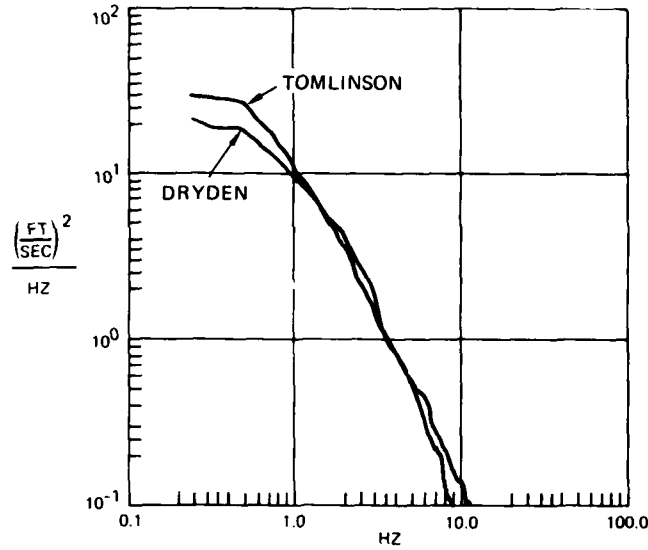


FIGURE 13. POWER SPECTRAL DENSITY FOR DRYDEN AND TOMLINSON TURBULENCE MODELS, MACH= 0.9, 500 FT

Based on the results of Table 1, for the pitch CAS shown in Figure 11 it is evident that the CAS ON condition offers only a slight improvement over the CAS OFF condition. Furthermore, for 30 minutes of exposure neither level is acceptable based on the chart in Figure 14, from which an \bar{A} greater than or equal to 0.048 is intolerable for an rms intensity level of 6.6 fpc.

TABLE 1

	CAS OFF	CAS ON
\bar{A}	0.087	0.081

WINGLOADING - 65 LBS/FT²

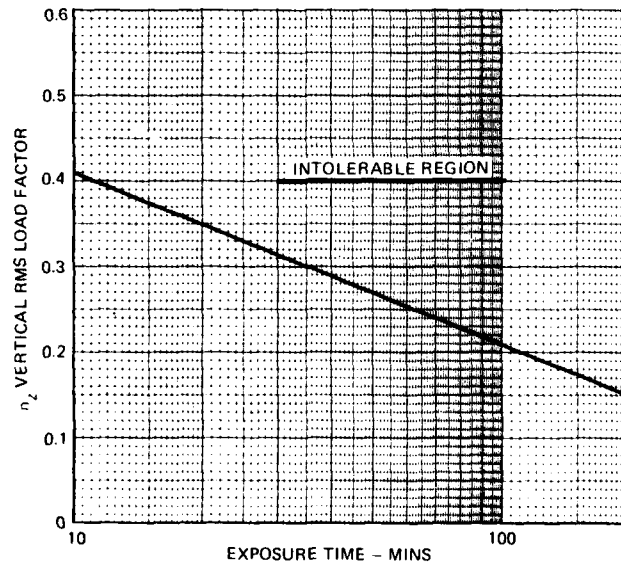


FIGURE 14. RIDE QUALITY CRITERIA, REFERENCE 5

To obtain satisfactory ride qualities during low altitude high speed flight, extensive effort has been expended in the development of a ride improvement mode system, References 6 and 7. The system, presented in Figure 15, tries to maintain a constant value of lift for changes in angle of attack due to turbulence, Figure 16. This is performed by sensing the load factor at the pilot station and using that as a control signal to command the high rate flaperons, so that the flaperons can minimize the turbulence-induced incremental load factor at the pilot station.

Operating in parallel with the ride mode is the CAS which uses a blend of load factor and pitch rate to maintain aircraft stability while trying to minimize uncommanded pitch rate and load factor.

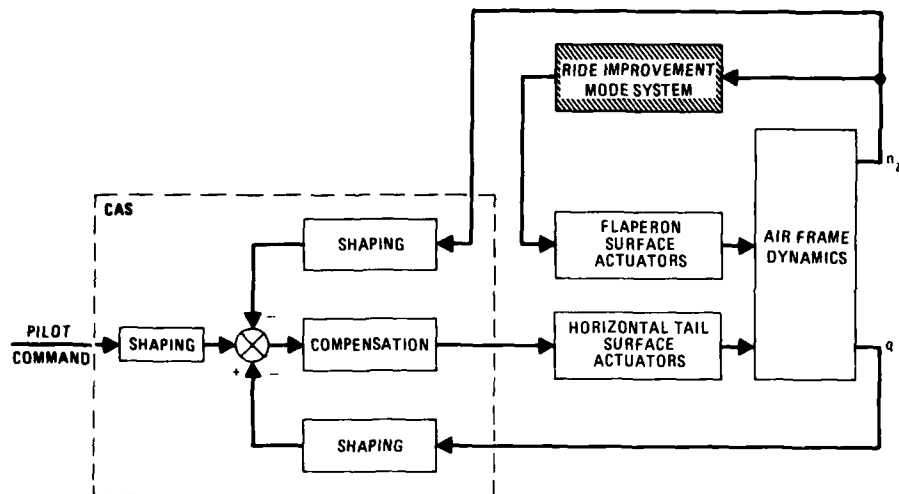


FIGURE 15. CAS/RIDE MODE SYSTEM CONFIGURATION

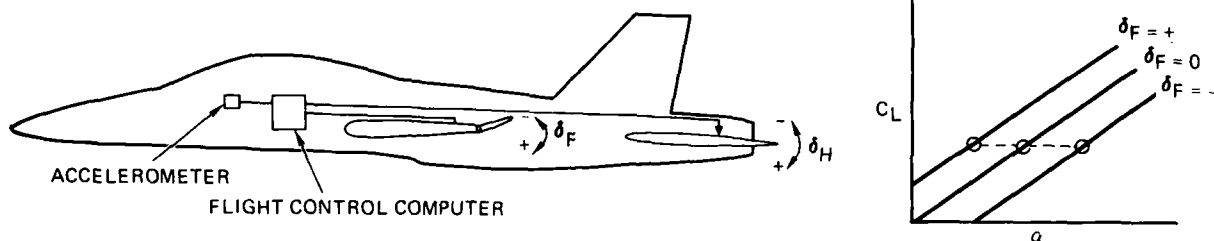


FIGURE 16. RIDE MODE SYSTEM CONCEPT

As demonstrated in Figure 17, when an upgust strikes the aircraft in straight and level flight it causes an increase in the angle of attack at the wing and therefore an increase in lift (for positive $C_{L\alpha}$) and a nose-down pitching moment (for negative $C_{m\alpha}$). The resulting positive load factor causes the flaperons to be deflected in the negative direction to cancel the increase in lift. At the same time, the flaperon deflection causes additional nose-down pitching moment for the positive $C_{m\delta_F}$ values. The total nose-down pitching moment generated by the aerodynamics of the wing and flaperon create a pitch acceleration that when multiplied by the distance of the pilot station from the cg reduces the total positive load factor acting at the pilot station.

The nose down pitching motion also drives the horizontal tail in the up (or negative) direction to cancel the nose-down pitching motion. Because of the positive $C_{L\delta_H}$ values of the horizontal tail this also acts to reduce the positive lift produced by the gust. The effect of zero or negative $C_{m\delta_F}$ values is to lessen the total pitching moment.

A look at the results in Table 2 indicates that the ride mode in operation with the CAS provides a better than 50-percent reduction in rms vertical load factor, placing the aircraft well within the tolerance limits for 30 minutes of exposure. While the positive $C_{m\delta_F}$ value provides the best ride smoothing, all three values provide more than satisfactory performance.

TABLE 2

CAS ON, RIDE MODE ON			
$C_{m\delta_F}$	-0.001	0.0	0.001
\bar{A}	0.035	0.031	0.029

MACH 0.9 AT 500 FT

Most previous work in the areas of ride qualities had implemented a flap tail interconnect that would work the tail to cancel the pitching moments generated by the deflections of the flap. Our previous work in this area indicated that with the pitch CAS system this was neither necessary nor desirable.

However, when it was realized that we could use pitch acceleration to help minimize load factor at the pilot station, the implementation of a feed forward from the flaperon to the horizontal tail was examined. In addition to normal CAS commands, the horizontal tail was commanded to move in phase with the flaperon. The result was to generate an increased pitch acceleration that would offset the load factor at the pilot station resulting from

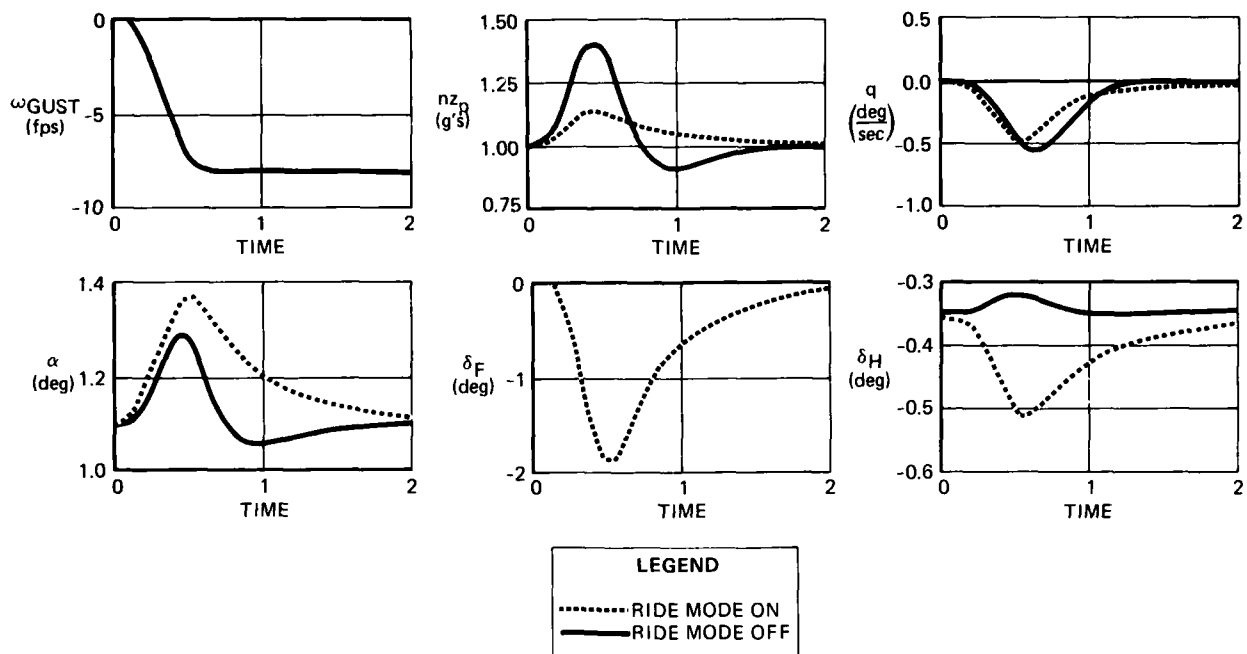


FIGURE 17. RIDE MODE ON VS RIDE MODE OFF FOR A DISCRETE GUST

turbulence. The improvement in load factor reduction as compared to normal ride mode operation is presented in Table 3 and Figure 18. In spite of the improved performance to reduce pilot load factor, the feed forward appears to be unsatisfactory, since the slight improvement in load factor at the pilot station results in a considerable increase in load factor at the cg, Table 4.

TABLE 3

	CAS ON, RIDE MODE ON	
	W/O FEED FORWARD	W/ FEED FORWARD
\bar{A}	0.029	0.023

TABLE 4

	CAS ON, RIDE MODE ON	
	W/O FEED FORWARD	W/ FEED FORWARD
rms n_z	0.20	0.33

MANEUVERING ENHANCEMENT

With the availability of the flaperons to provide additional control over lift and pitch, several CCV modes such as utilized on the YF-16 CCV aircraft, Reference 8, can be investigated. One of these, the maneuvering enhancement mode, is basically a fallout from the ride mode. By creating a control path from the pilot input command to sum with the n_z feedback loop of the ride mode, Figure 19, the pilot can command a flaperon deflection as a function of desired g's. The command to the flaperons then becomes the error signal between the commanded g's and the actual g's.

As presented in Figure 21, the function of the maneuvering enhancement mode is to increase the aircraft's response to pilot commands for vertical load factor, allowing the pilot to increase the initial rate of climb or descent.

For variations in the value of $C_{m\delta_F}$, from 0.001 to -0.001, the effects on the maneuvering enhancement mode response were insignificant. Although for large values on the order of 0.010 there was some reduction in damping of the aircraft response with a corresponding increase in the aircraft's altitude gain, Figure 21.

FLIGHT PATH CONTROL

As a flight path control, the ability to pitch the aircraft with no change in angle of attack. Figure 22, is the response of the aircraft accomplished through the implementation of open loop control. It's potential benefit is improved maneuvering performance.

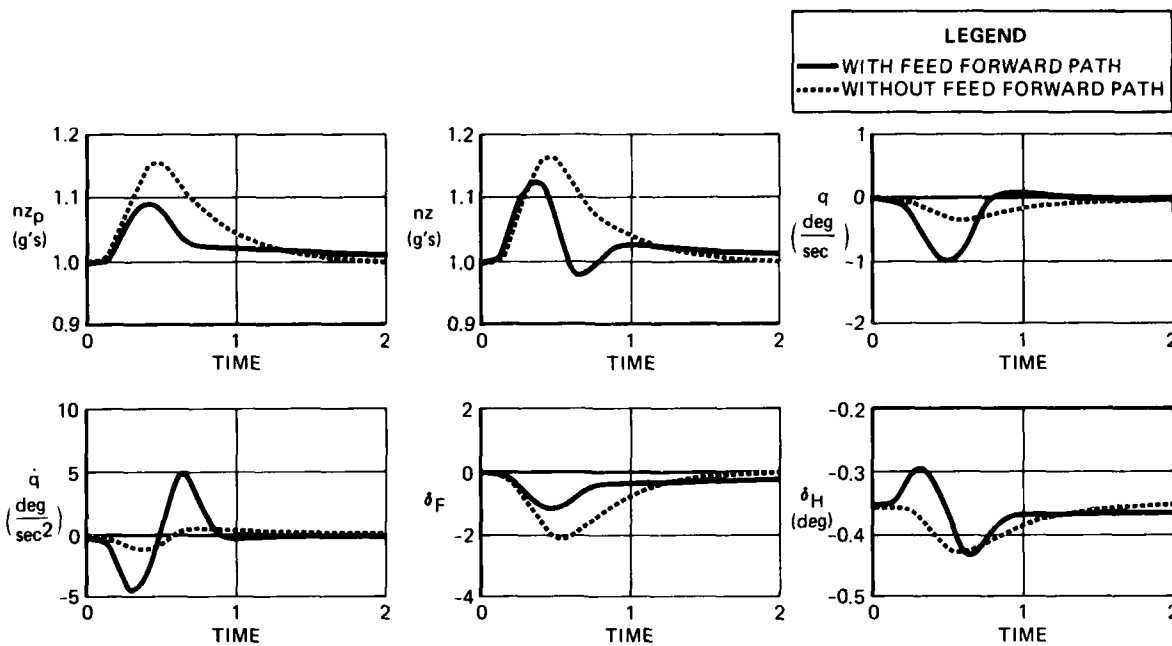


FIGURE 18. RIDE MODE ON WITH AND WITHOUT FEED FORWARD PATH

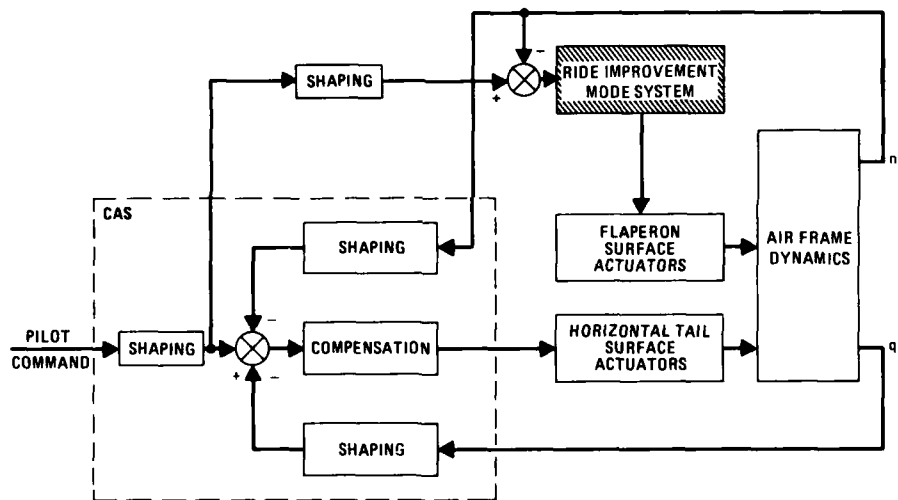


FIGURE 19. MANEUVER ENHANCEMENT BLOCK DIAGRAM

To control the vertical flight path as shown in Figure 23, the coordinated deflections of the horizontal tail and flaperons command the desired pitch rate while maintaining a constant angle of attack by cancelling any changes in lift due to pitch rate.

For linear aerodynamics, the relation of the horizontal tail deflection to flaperon deflection is independent of pitch rate and can be determined by solving the short period equations of motion, Equation 2, for an arbitrary pitch rate, \hat{Q} , where α dot (the angle of attack rate of change) and \dot{q} (the pitch acceleration) are constrained to zero. Note that for small vertical flight path maneuvers the gravity terms have been ignored.

$$\begin{bmatrix} \dot{\alpha} \\ \dot{q} \end{bmatrix} = \begin{bmatrix} Z_{\alpha} & Z_q \\ M_{\alpha} & M_q \end{bmatrix} \begin{bmatrix} \alpha \\ q \end{bmatrix} + \begin{bmatrix} Z_H & Z_F \\ M_H & M_F \end{bmatrix} \begin{bmatrix} \delta_H \\ \delta_F \end{bmatrix} \quad (2)$$

Since alpha trim is equal to zero, with all constraints applied the equations reduce to:

$$\begin{bmatrix} 0 \\ 0 \end{bmatrix} = \begin{bmatrix} Z_q \\ M_q \end{bmatrix} \begin{bmatrix} \hat{Q} \end{bmatrix} + \begin{bmatrix} Z_H & Z_F \\ M_H & M_F \end{bmatrix} \begin{bmatrix} \delta_H \\ \delta_F \end{bmatrix} \quad (3)$$

with the resulting control deflections being represented by Equations 4, 5 and 6.

9-12

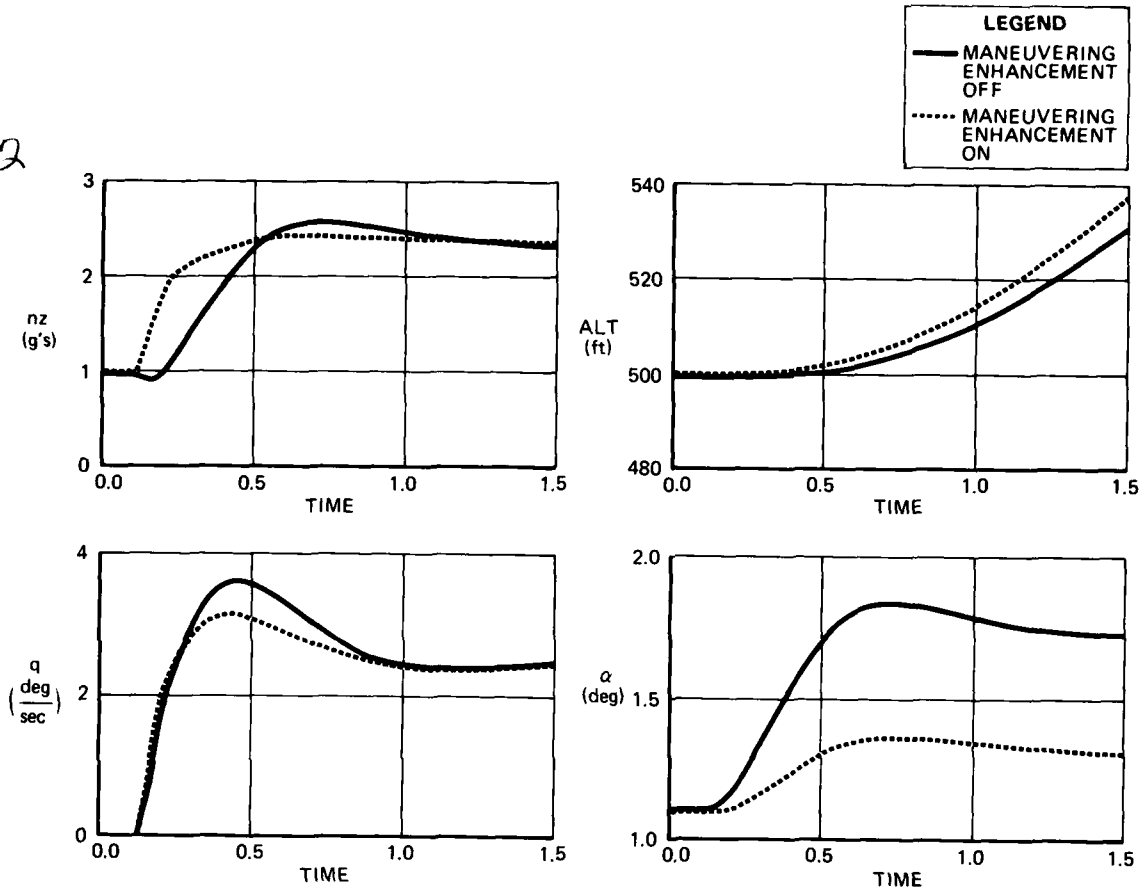


FIGURE 20. EFFECT OF MANEUVERING ENHANCEMENT ON VS OFF

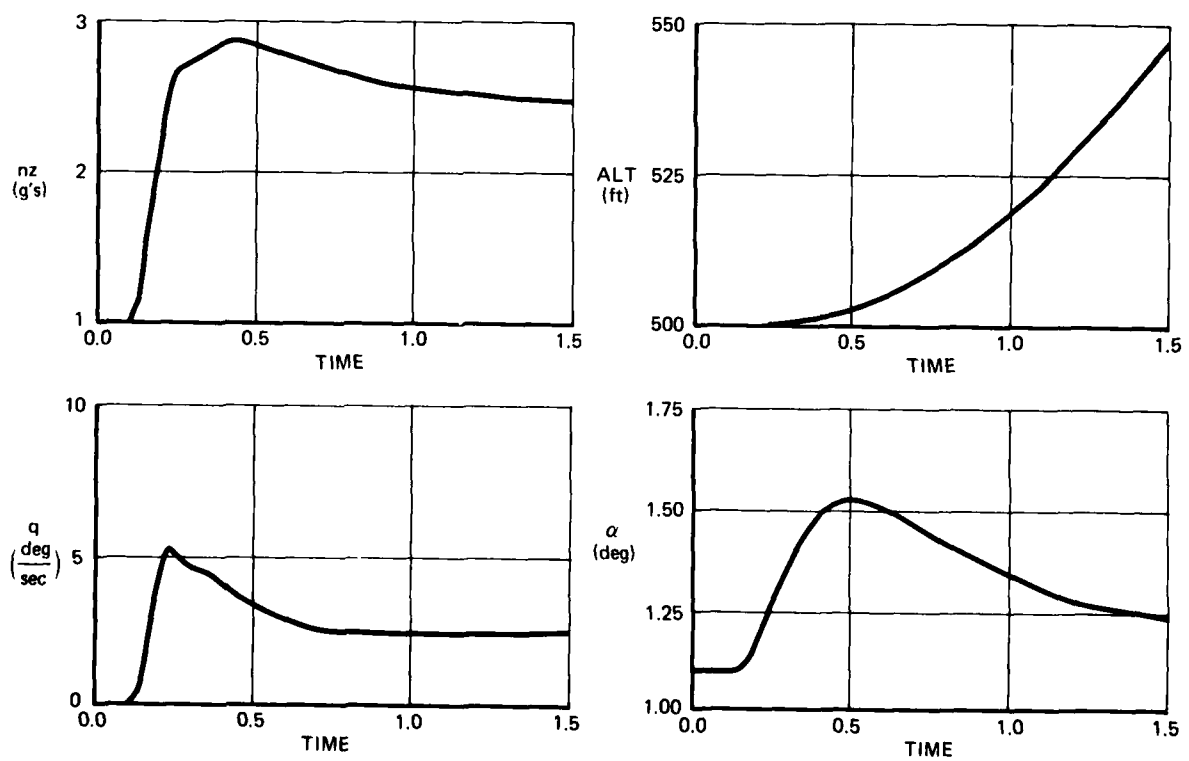


FIGURE 21. EFFECT OF LARGE $C_{M\delta F}$ VALVE ON MANEUVERING ENHANCEMENT

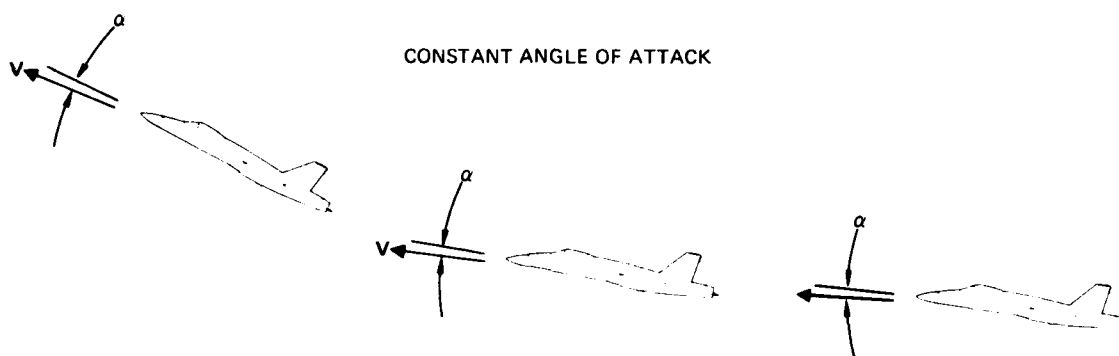


FIGURE 22. VERTICAL FLIGHT PATH CONTROL

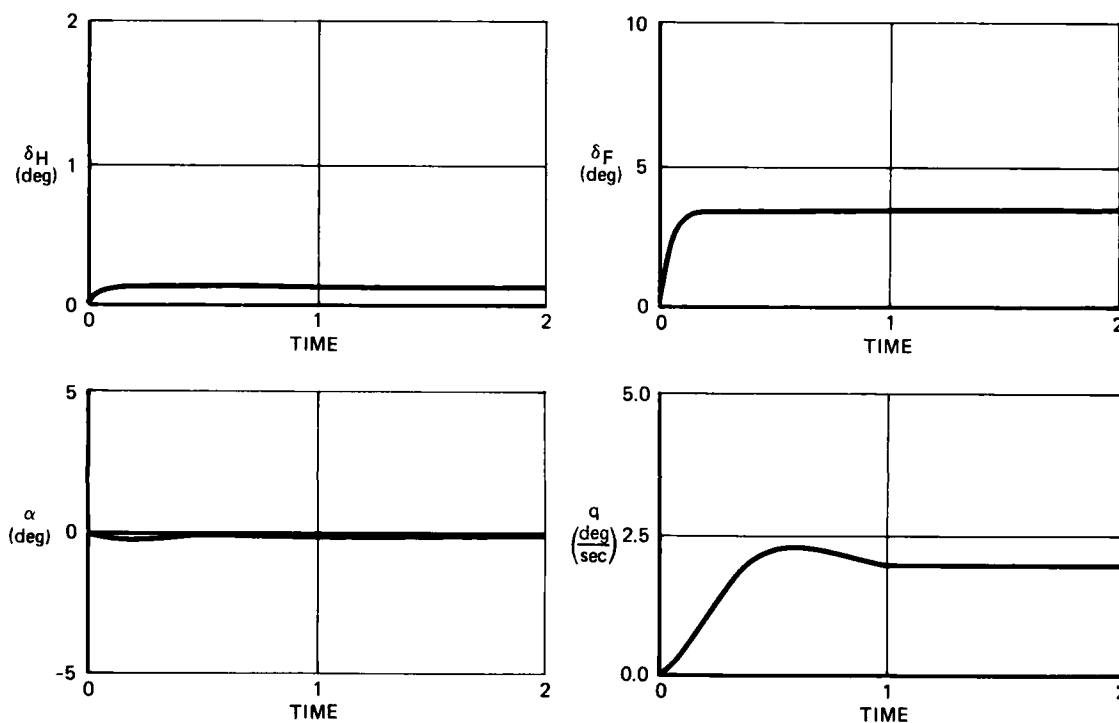


FIGURE 23. VERTICAL FLIGHT PATH CONTROL

$$\delta_F = \frac{(Z_H M_q - Z_q M_H) \hat{Q}}{Z_F M_H - M_F Z_H} \quad (4)$$

$$\delta_H = \frac{(Z_q M_f - Z_F M_q) \hat{Q}}{Z_F M_H - M_F Z_H} \quad (5)$$

$$\frac{\delta_H}{\delta_F} = \frac{Z_q M_f - Z_F M_q}{Z_H M_q - Z_q M_H} \quad (6)$$

Using Cramer's Rule to solve the two steady state equations for the flaperon horizontal tail deflections, Equations 4 and 5, it becomes apparent that the ratio between flaperon deflection and horizontal-tail deflection, Equation 6, for vertical flight path control is independent of \hat{Q} .

Thus, for a step command to the flaperons the horizontal tail follows according to the ratio defined by Equation 6. Any changes made to the value of $C_{m\delta_F}$ will affect the M_F term and in turn affect the interconnect relationship between the flaperons and horizontal tail. However, its effect on the overall aircraft dynamics for this maneuver are negligible for reasonable $C_{m\delta_F}$ values.

DIRECT LIFT

Direct lift on vertical translation, as described in Figure 24, is the act of producing a \dot{w} and thus w without inducing any pitch rate. In this manner the aircraft is capable of an orthogonal translation at constant attitude. This maneuver is accomplished by commanding the flaperons to provide the desired increment of lift to translate the aircraft and controlling the horizontal tail through the appropriate feedback loops to cancel any pitching moments generated predominantly by the flaperons and the aircraft's $M\alpha$ term. For this investigation, a feed forward path from the flaperon command to the horizontal tail combined with a blend of pitch rate and angle of attack feedbacks were used to control the pitch rate to a zero value.

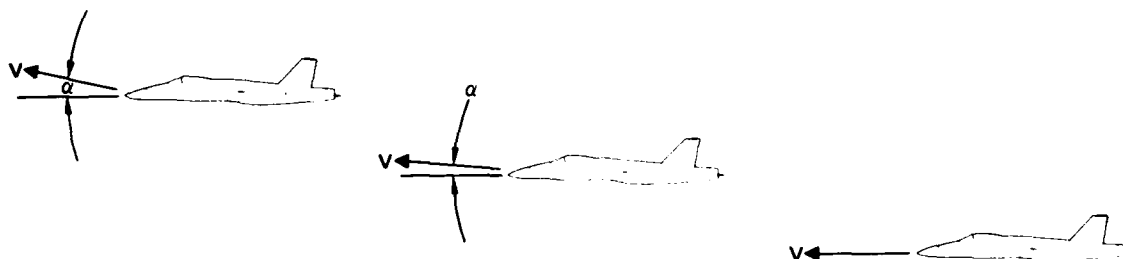


FIGURE 24. DIRECT LIFT CONCEPT

The results for this mode are presented in Figure 25. While variations in the value of $C_{m\delta_f}$ had influence on the interconnect relationship between the flaperons and horizontal tail, they had no effect on the overall aircraft response, Figure 26.

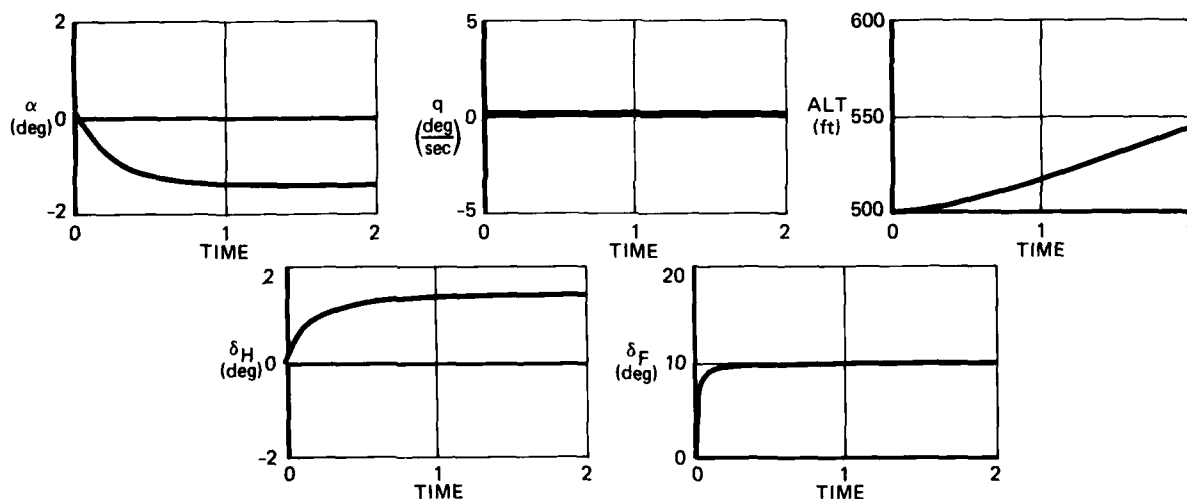


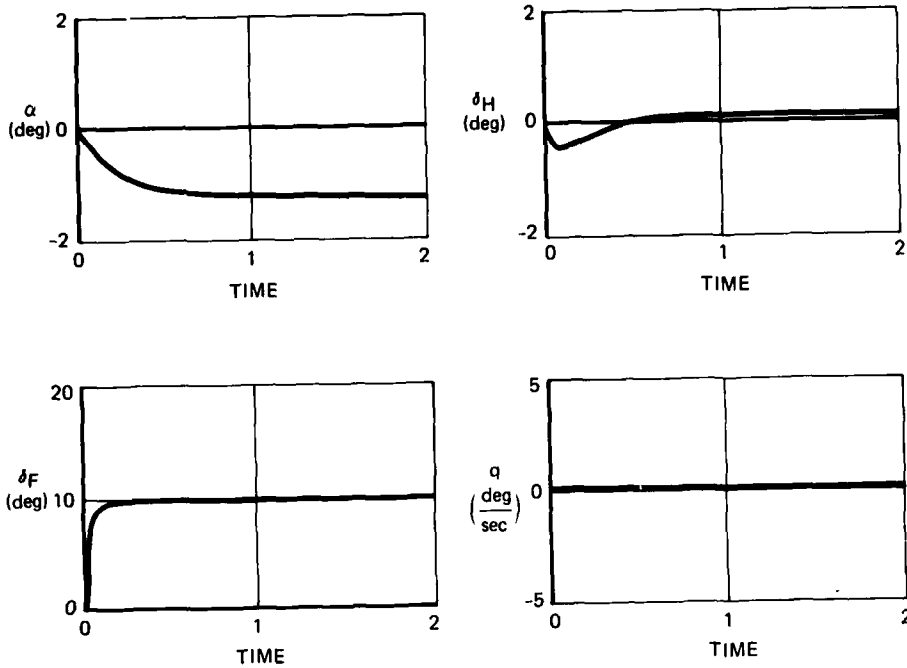
FIGURE 25. DIRECT LIFT TIME HISTORY

LONGITUDINAL FUSELAGE POINTING

For improved performance for the air to ground role, a Longitudinal Fuselage Pointing mode was developed. The purpose of this mode is to allow the pilot to pitch the aircraft to a new angle of attack with no change in altitude or flight path angle, Figure 27. This allows the pilot to improve his air to ground tracking ability and is said to make air to ground tracking runs more comfortable and easier to accomplish, Reference 8.

In the point-up motion presented in Figure 28 the horizontal tail commands a transient pitch rate while the flaperons spoil the lift generated by the increased angle of attack. The result is to create a new equilibrium condition where α and q are zero. Initially, this mode was pursued as an open-loop mode where the position of the flaperon and horizontal tail was simply a function of the desired angle of attack, however, this caused a constant loss in altitude during the maneuver. To zero out this change in altitude, the rate of change in altitude was fed back to the flaperons.

Similar to the previous auxiliary modes, the effect of variations in $C_{m\delta_f}$ was negligible. Again, the only significant effect the value of $C_{m\delta_f}$ has is in the relation between the initial flaperon and horizontal tail deflections.



9-15

FIGURE 26. EFFECT OF $C_{M_{\delta F}}$ ON DIRECT LIFT

PITCH ATTITUDE CONTROL AT CONSTANT FLIGHT PATH ANGLE

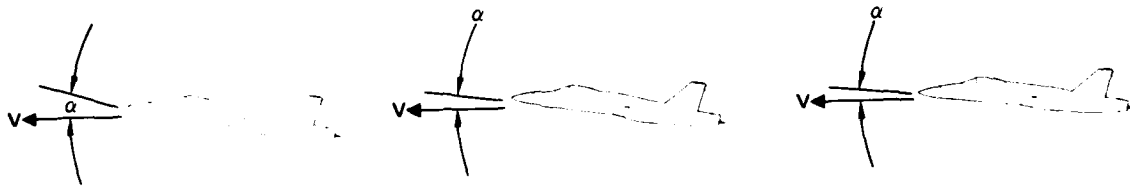


FIGURE 27. LONGITUDINAL FUSELAGE POINTING CONCEPT

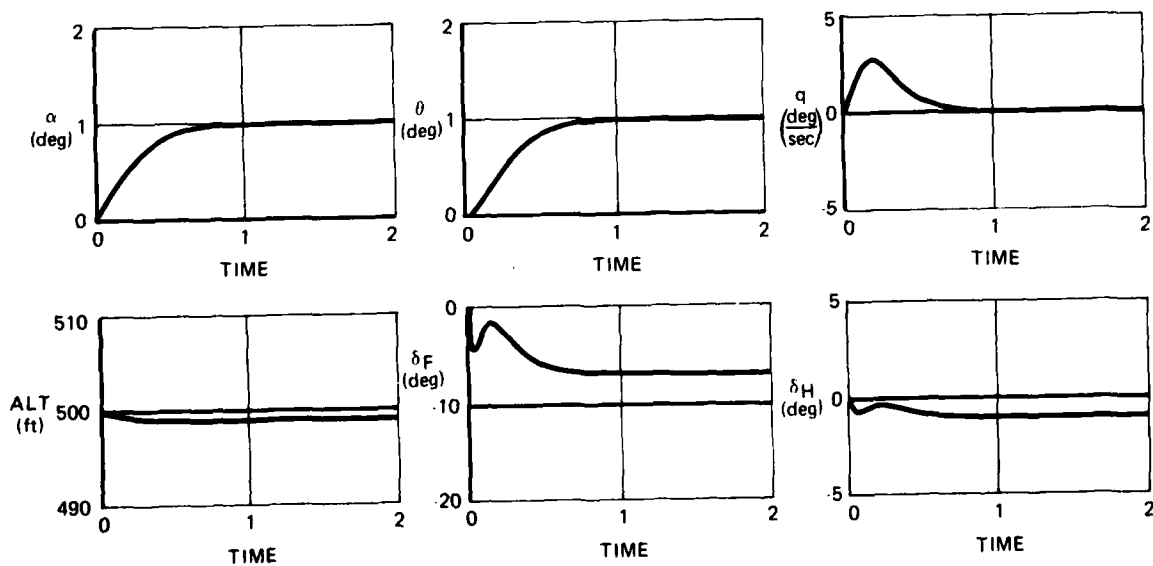


FIGURE 28. LONGITUDINAL FUSELAGE POINTING TIME HISTORY

THE RECONFIGURABLE FLIGHT CONTROL SYSTEM

9-16

Provided an aircraft utilizes a digital flight control system and a flaperon which has a large $C_{m\delta F}$ coefficient, it could be viable to use the flaperons as the primary longitudinal flight control surface in the event that longitudinal control of the horizontal tail is lost. The control of the flaperons for primary longitudinal control of the horizontal tail is lost. The control of the flaperons for primary longitudinal control would occur through the reconfiguration of the flight control laws which normally commanded the horizontal tail, Figure 29.

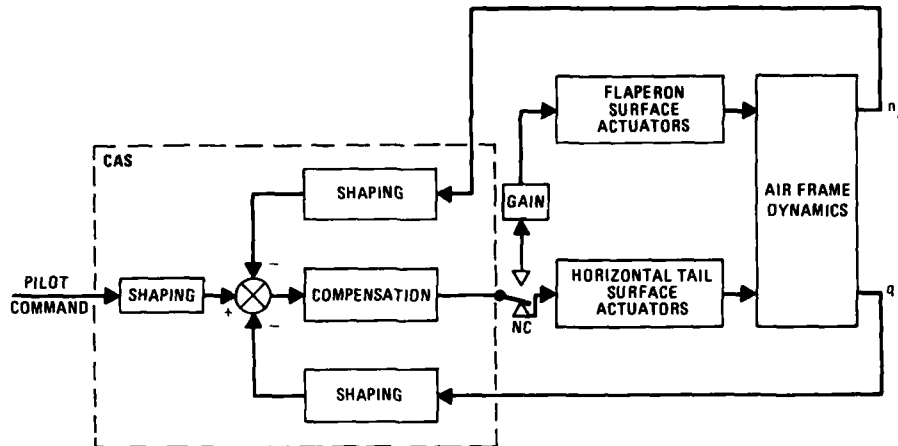


FIGURE 29. RECONFIGURATION CONTROL CONCEPT

With the loss of the horizontal tail, the control law would be reconfigured so instead of commanding a horizontal-tail deflection it would command a flaperon deflection. To provide adequate pitch authority, there would be an increase in gain from the normal horizontal-tail command to the reconfigured flaperon command. This increased gain would be the ratio of $C_{m\delta H}/C_{m\delta F}$.

Based on YF-17 aerodynamics, including the ratio of the YF-17's trailing-edge flap pitching moment versus horizontal tail pitching moment presented in Figure 30, a root loci study was performed. The two CAS ON root locus plots for Mach 0.9 at 500 feet, Figures 31 and 32, compared very favorably and indicated that this area may warrant future study. Although the flaperon may not provide sufficient pitch authority to land the aircraft, it could prove very effective in allowing a pilot to reach a desirable area for ejection for increased survivability.

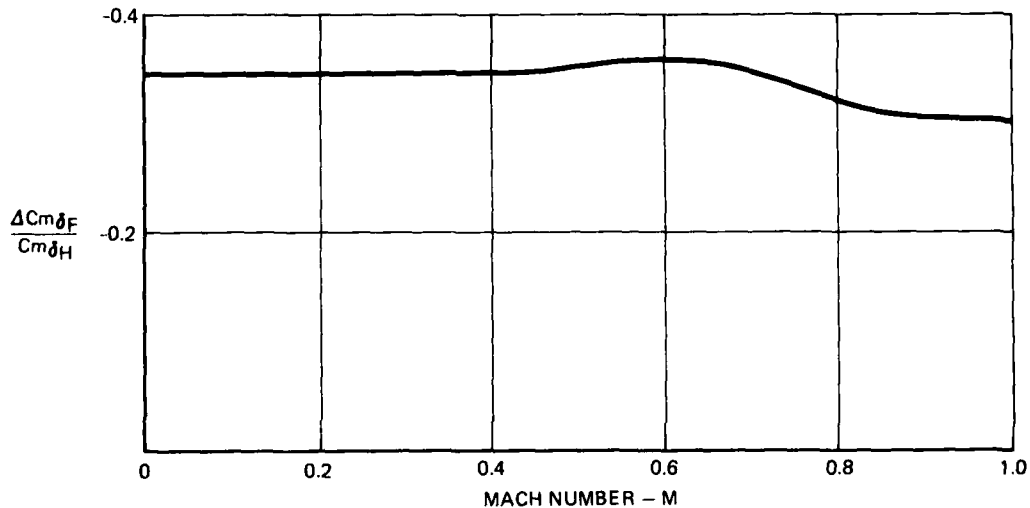


FIGURE 30. YF-17 TRAILING EDGE FLAP/HORIZONTAL TAIL PITCHING MOMENT COMPARISON

AREAS FOR ADDITIONAL STUDY

To exploit the potential for these primary and auxiliary modes to be implemented on an aircraft employing active flaperon control several areas need additional study. While the segmented flaperon roll mode and the ride mode have been integrated into an overall flight control system design, the auxiliary modes require further study on the Northrop Large Amplitude Simulator to determine the extent to which these modes can be effective and if so, how they could best be integrated into the overall flight control system design.

Other areas which were not discussed here but warrant investigation are the active control of the segmented flaperons for empennage load alleviation and the potential for some limited direct side force control.

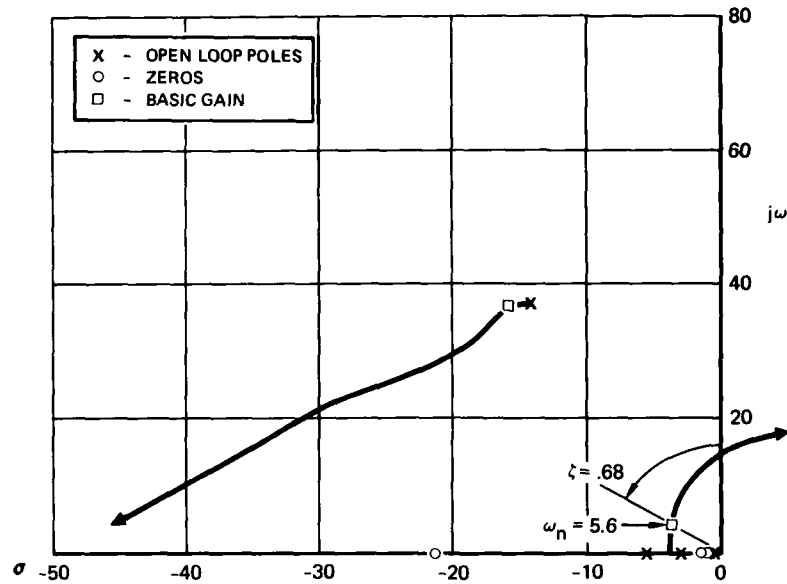


FIGURE 31. ROOT LOCI FOR LONGITUDINAL CAS, n_z LOOP CLOSURE WITH HORIZONTAL TAIL CONTROL

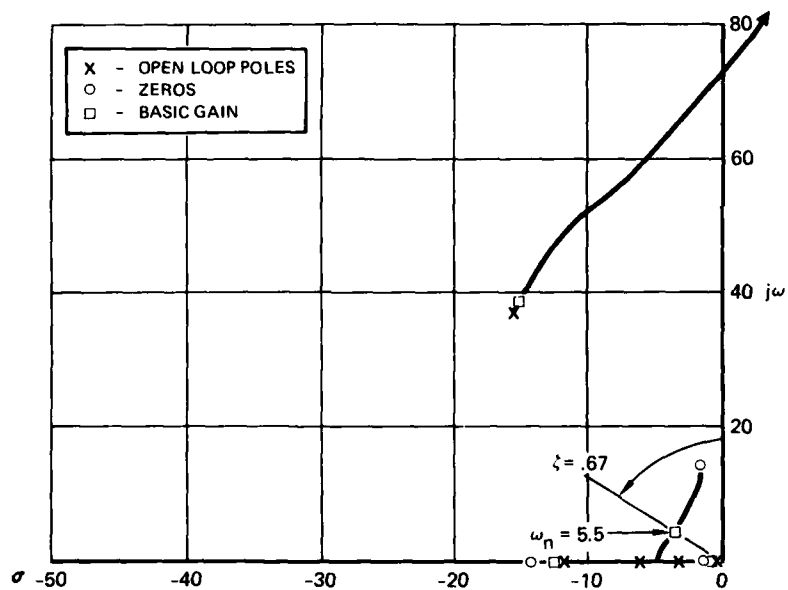


FIGURE 32. ROOT LOCI FOR LONGITUDINAL CAS, n_z LOOP CLOSURE WITH FLAPERON CONTROL

CONCLUSIONS

In terms of the aerodynamic characteristics of a flaperon, for the implementation of active longitudinal control it appears that the ability to predict what the value of an aerodynamic coefficient is, is more important than the actual value of the coefficient.

With the presence of a digital flight control system to allow for complex control law configurations without hardware modifications, it is possible through the choice of a segmented flaperon configuration to increase a YF-17-type aircraft's overall performance and multirole capability. This is accomplished by increasing both lateral/directional and longitudinal performance. Lateral directional improvements include increased roll power and the minimization of induced yawing moments. Longitudinal improvements include improved ride quality, the decoupling of short period dynamics to provide new maneuver capabilities for increased air-to-air, air-to-ground performance; and the potential for flight control system reconfiguration for increased survivability.

REFERENCES

1. Saworotnow, I.; Nelson, W. E. Jr.: Limitations in the Use of Angle of Attack Information in the Flight Control System, 1978 Air Data Conference Proceedings.
2. Tomlinson, B. N.: Developments in the Simulation of Atmospheric Turbulence, AGARD CP198, 1976.
3. Anon.: Flight Control Systems - Design, Installation and Test of Piloted Aircraft, General Specification for MIL-F-9490D (USAF) 6 June 1975.
4. Jones, J. G.: Modeling of Gusts and Wind Shear for Aircraft Assessment and Certification, CAARC Symposium of Operational Problems, 1976.
5. Notess, C. B.: Triangle - Flexible Airplanes - Gusts - Crew, C. A. L. (Cornell) Rep. No. FDM 343, May 1963.
6. Moynes, J. F.; Gallagher, J. T.: Flight Control System Design for Ride Qualities of Highly Maneuverable Flight Aircraft, AGARD CP 240, 1977.
7. Dull, T. C.; Moynes, J. F.; Gallagher, J. T.: Active Control of Ride Quality for Advanced Fighter Aircraft Within Various Turbulence Environments, Control Systems Criteria Symposium Proceedings, 1978.
8. Swortzel, F. R.; McAllister, J. D.: Design Guidance from Fighter CCV Flight Evaluations, AGARD Flight Mechanics Panel Symposium, Sept 1978.

AFFDL EXPERIENCE IN ACTIVE CONTROL TECHNOLOGY

by

Robert P. Johannes

and

Robert A. Whitmoyer

Air Force Flight Dynamics Laboratory (FG)
Wright-Patterson AFB, OH 45433 USA

SUMMARY

This paper traces the evolution of active control technology (ACT) from the viewpoint of the Air Force Flight Dynamics Laboratory (AFFDL). Emphasis is placed on the aerodynamic control forces necessary to fully exploit ACT and in describing AFFDL development programs which merge these two disciplines and transition technology into operational flight equipment. Specific ACT programs described are: (1) the LAMS Program, (2) the CCV B-52 Program, (3) the SFCS F-4 Program, (4) the CCV/PACT F-4 Programs, (5) the Variable Stability NT-33 Program, (6) the CCV YF-16 Program, (7) the A-7D Digital Multimode Program, (8) the IFFC I/FIREFLY III Program, and (9) the AFTI-16 Program. Experiences indicating areas of need for extension of fluid dynamics technology are also discussed.

LIST OF SYMBOLS/ABBREVIATIONS/ACRONYMS

A	aileron
ACT	active control technology
AFAL	Air Force Avionics Laboratory
AFFDL	Air Force Flight Dynamics Laboratory
AFTI	Advanced Fighter Technology Integration
ALDCS	Active Lift Distribution Control System
AS	Augmented Stability
ATLIS	Automatic Tracking Laser Illumination System
BS	body station
\bar{c}	mean aerodynamic chord
C*	longitudinal response parameter (C-star)
CAS	Command Augmentation System
CCV	Control Configured Vehicle
C.G.	center of gravity
CH	horizontal canard
deg, DEG	degrees
DFC	direct force control
DFCS	Digital Flight Control System
DLC	direct lift control
DSFC	direct sideforce control
DN	down
EAS	equivalent airspeed
FBW	fly-by-wire
FMC	Flutter Mode Control
FR	Fatigue Reduction
ft, FT	feet
g	acceleration of gravity

GASDSAS	Gust Alleviation and Structural Dynamic Stability Augmentation System
H	horizontal tail
HC	horizontal canard
IFFC	Integrated Flight and Fire Control
ILAF	Identical Location of Accelerometer and Force
in, IN	inches
KTS	knots
LAMS	Load Alleviation and Mode Stabilization
lbs, LBS	pounds
m	meters
MAC	mean aerodynamic chord
MM	multimode
MLC	Maneuver Load Control
NASA	National Aeronautics and Space Administration
PACT	Precision Aircraft Control Technology
PVI	Pilot/Vehicle Interface
R	rudder
RC	Ride Control
S	stabilator; surface area
SAS	Stability Augmentation System
sec	second
Seg	segment
SFCS	Survivable Flight Control System
SP	spoiler
Sta	station
T.E.	trailing edge
TEF	trailing edge flap
TIFS	Total In-Flight Simulator
TWEAD	Tactical Weapon Delivery
TYP	typical
V	velocity
VC	vertical canard
vs, VS	versus
WBL	wing buttock line
WL	water line
WRP	wing reference plane
α	angle of attack
β	angle of sideslip
δ	deflection angle
Δ	increment or change

1. INTRODUCTION

The continuing advancement of active control technology (ACT) has given the aircraft designer new tools for the optimization of performance and mission effectiveness. Application of advanced flight control techniques during the preliminary design stages, on an equal basis with the traditional disciplines of aerodynamics, structures, and propulsion, can lead to synergistic benefits. The Air Force Flight Dynamics Laboratory (AFFDL) has pioneered in this area, conducting and sponsoring a series of active control technology development programs involving flight test validation. Figure 1 depicts the sequence of the more significant of these AFFDL ACT programs, starting with the LAMS Program in 1966 and progressing through the current AFTI-16 Program. The following paragraphs present individual summaries of the programs, with emphasis on the relationships between ACT and aerodynamic control requirements. 10-3

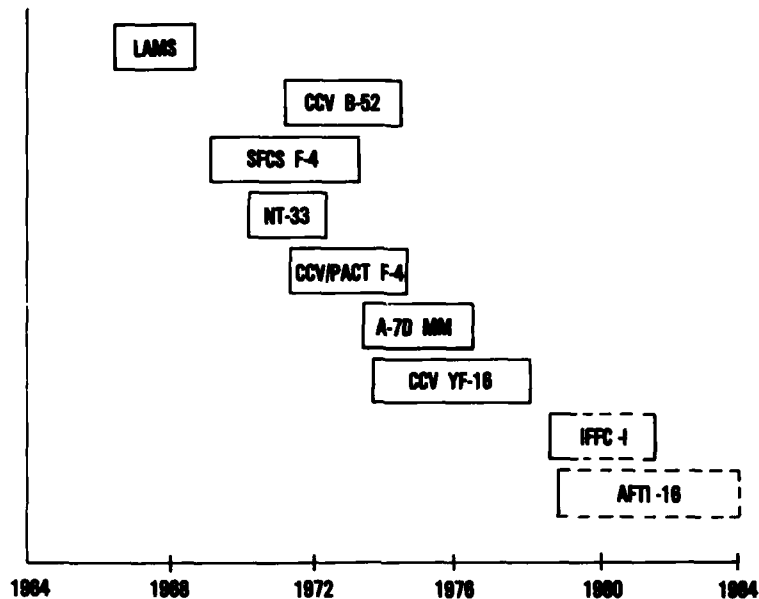


FIG 1: Sequence of AFFDL ACT Development Programs

Aircraft active control technology had its beginnings in autopilots to provide pilot relief functions. Full-time application of feedback controls for vehicle rigid body dynamic compensation followed when it became apparent that basic vehicles lacked adequate handling qualities and dynamic characteristics. An extension beyond rigid body stability augmentation concepts began in the mid 1950's on ballistic missiles to alleviate structural loads while accelerating through high dynamic pressure regions. Similar structural problems began to appear in the early 1960's on structurally light and elastic aircraft configurations. The prominent design factors causing this trend were thin lifting surfaces, long slender fuselages, low mass-fraction structures, high stress design levels, and low load factors. In light of advances in ACT, these facts made it imperative to investigate the potential for simultaneously controlling rigid body and structural motion. This was the dominant motivation for the Load Alleviation and Mode Stabilization (LAMS) Program.

2. THE LAMS PROGRAM (1966-1968)

The Load Alleviation and Mode Stabilization (LAMS) Program was conducted on a B-52 testbed to demonstrate the capabilities of an advanced flight control system to alleviate gust loads and control structural modes on a large flexible aircraft using existing aerodynamic control surfaces as force producers (1, 2). Figure 2 shows that all available control surfaces were used in the LAMS system, and also depicts the gyros which provided structural mode rate signals to the flight control system. The two outboard spoiler panels were operated symmetrically around a 15° biased position, the ailerons were used both symmetrically and asymmetrically, and the elevator and rudder were used in the normal manner.

A 65 degree-of-freedom math model of the LAMS vehicle was developed for design synthesis and evaluation of the flight control system. The model included 30 longitudinal and 35 lateral-directional degrees of freedom (including the Wagner and Küssner lift-growth functions), gust-penetration lags and fourth order actuator and control surface dynamics (3). Initially, quadratic optimization theory was used in the LAMS control law synthesis, to identify the critical modes and the feedbacks to stabilize these modes. However, control laws defined by the optimization theory were not usable, since the computational capability was not available to implement these in a practical system. The optimum control laws were reduced to a successful practical system using classical methods which were later verified on the 65 degree-of-freedom simulation. The complex cause-and effect relationships

10-4

that result from such a large matrix of structural and rigid body modes presented a formidable challenge in control law development. New wide bandwidth electro-hydraulic servo actuators were also required to provide high frequency response capability and acceptance of both mechanical and electrical commands.

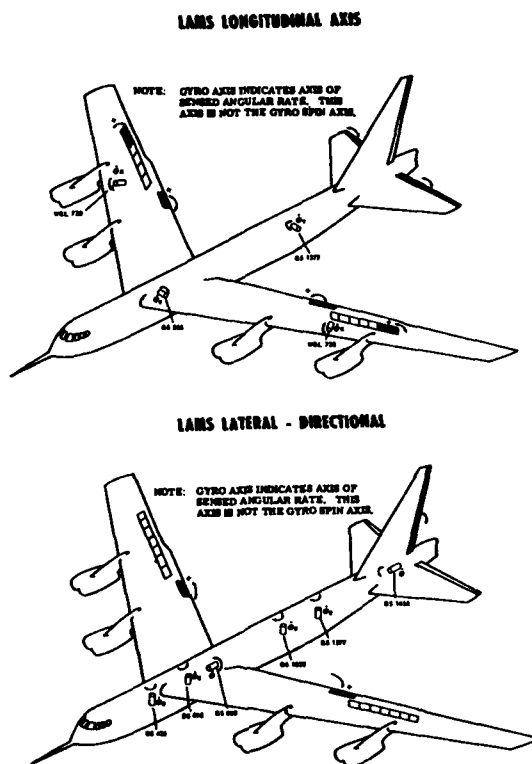


FIG 2: LAMS Control Surfaces and Gyros

The figure of merit for the LAMS system was the percent reduction in fatigue damage due to turbulence. Figure 3 presents the reductions in turbulence-induced fatigue damage rates obtained with the LAMS system. These data are based on test results at three flight conditions and include effects of vertical, lateral, and rolling gusts. For comparison purposes, a conventional baseline SAS (Stability Augmentation System) was implemented to control only rigid body motions. The LAMS system reduced the basic aircraft wing fatigue damage rate by about 50% and also significantly bettered the baseline SAS fatigue rate reductions. LAMS also demonstrated large improvements in fatigue damage rates at the mid-fuselage stations. Even more important than these quantitative results was the demonstration that a control system can be designed to significantly alter the structural response characteristics of an aircraft.

The LAMS Program indicated a limited ability to reduce acceleration at the pilot station using only existing aerodynamic control surfaces. However, because of the structural mode shapes it was evident the force had to be located near the point of desired effect. The need for force producers at the site of desired acceleration reductions was the basis of the Identical Location of Accelerometer and Force (ILAF) concept (4). The ILAF technique was applied to the XB-70 during the Gust Alleviation and Structural Dynamic Stability Augmentation System (GASDSAS) Program, which used small horizontal canard surfaces to obtain significant reductions in pilot-station acceleration (5). In this application, structural vibration caused by actuator motion fed back into the sensor causing a resonance to occur. The resonance was eliminated by proper filtering, but the occurrence indicates the need for careful attention to such things during design.

A direct lift control (DLC) study conducted during the LAMS Program also showed the desirability of uncoupling the rotational and translational degrees of aircraft motion (6). Spoilers and symmetrical ailerons were used with elevators to implement DLC. Flight test results showed that uncoupling pitch and heave through DLC greatly simplified the precise maneuvering required during aerial refueling and instrument approaches. The B-52 LAMS testbed had no means of obtaining direct sideforce control (DSFC).

The potential benefits available from decoupling the flight motions and from having force producers at critical locations led to a decision to reconfigure the LAMS B-52 control surface complement to more fully explore newly emerging ACT concepts. The LAMS biased spoilers were obvious candidates for replacement as ACT control surfaces. First,

their drag would be prohibitive in an operational configuration. Second, during the LAMS flight testing, a wing flutter mode exhibited degraded stability because of initial failure to accurately account for time phasing between the spoiler deflections and the resulting aerodynamic force. This points out the necessity for considering aerodynamic lag effects. Elimination of spoiler segments as ACT surfaces and other aerodynamic changes was a part of the CCV B-52 Program which was the next major AFFDL effort to further exploit the lessons learned from LAMS and related programs.

10-5

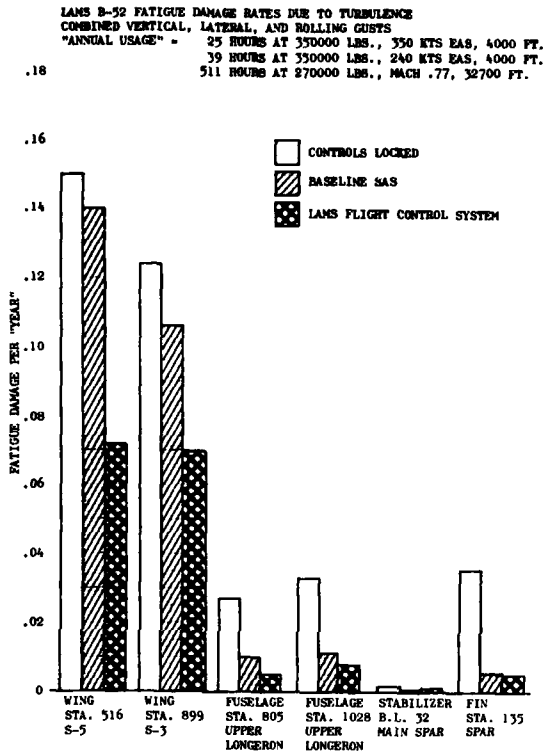


FIG 3: Fatigue Damage Rates

3. THE CCV B-52 PROGRAM (1971-1974)

The term Control Configured Vehicles (CCV) was introduced to describe a design philosophy in which modern control technology is allowed to impact total vehicle design through its inclusion early in the aircraft design cycle. Applying this philosophy allows control concepts to be incorporated which can potentially give performance improvements and weight reductions. Such ACT concepts for large aircraft include Flutter Mode Control (FMC), Maneuver Load Control (MLC), Ride Control (RC), Fatigue Reduction (FR), and Augmented Stability (AS).

A Fly-By-Wire (FBW) control system is fundamental to implementation of the above concepts. As used herein, FBW means an electrical flight control system employing feedback such that the vehicle motion is the controlled parameter. The LAMS aircraft had a full FBW system for the left-hand pilot, while the right-hand co-pilot retained the mechanical system for backup. The CCV B-52 Program took advantage of this FBW capability by using the LAMS aircraft as the CCV bomber testbed (7).

The CCV B-52 flight control surfaces and the concepts they were used to implement are depicted in Figure 4. Several new control surfaces were added to change from the LAMS to the CCV aerodynamic configuration. These include one vertical and two horizontal canards mounted on the forward fuselage at the pilot station, three segments of flaperons on each wing replacing the inboard flaps, and a new aileron located just outboard of the outboard flap on each wing. The new canard surfaces had an area of 10 ft² (0.93 m²) each. Standard flight control surfaces retained were elevator, rudder, five of seven spoiler segments, and the original ailerons. Also shown on Figure 4 are the external fuel tanks which were adversely mass balanced to create a flutter mode within the level flight speed capabilities of the testbed. This was necessary to permit investigation of Flutter Mode Control on the normally flutter-free B-52.

Of the five ACT concepts implemented on the CCV B-52, only Fatigue Reduction was common between the LAMS and CCV Programs. A slightly modified version of the LAMS system was included on the CCV B-52 to demonstrate compatibility of this concept with the other ACT systems. The objective of the Ride Control System was to reduce turbulence-induced

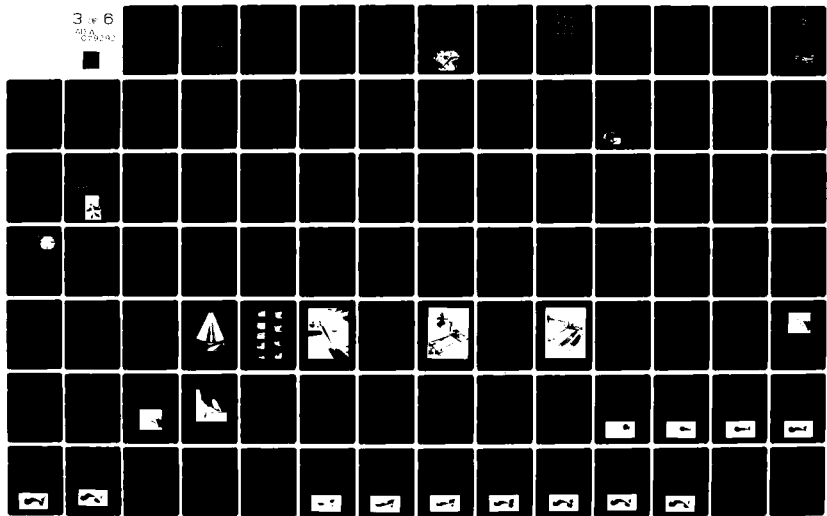
AD-A079 292 ADVISORY GROUP FOR AEROSPACE RESEARCH & DEV. NEUILLY-SUR-SEINE FR F/G 1/:
AERODYNAMIC CHARACTERISTICS OF CONTROLS CONFERENCE PROCEEDINGS
SEP 79

UNCLASSIFIED

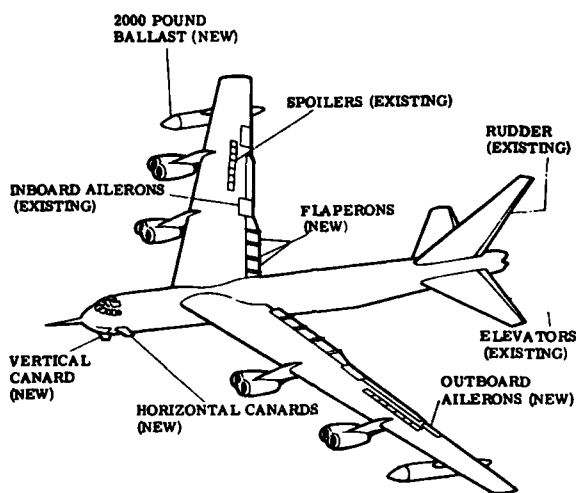
AGARD-CP-262

N/L

3 of 6
09A
050202



accelerations at the pilot's station by 30% without increasing other fuselage accelerations by more than 5%. The goal for Maneuver Load Control was to reduce wing root bending moments by 10% of design limit during a 1g incremental load factor pull up maneuver. The objective of the Augmented Stability system was to provide adequate aircraft flying qualities at centers-of-gravity as far aft as the neutral point. The goals of the Flutter Mode Control System were to increase the flutter placard by at least 30% and flight demonstrate flutter-free operation ten knots (18 km/hr) above the unaugmented flutter speed. Flight test results verified achievement of the CCV B-52 design goals and demonstrated compatibility of the five ACT concepts (8, 9). The flutter suppression testing was the first known instance of a manned aircraft flying beyond its flutter speed, depending on a control system to avoid structural divergence.



SURFACE		SURFACE REQUIRED PER CONCEPT				
		RC	FMC	MLC	AS	FR
EXISTING	ELEVATOR			X	X	X
	RUDDER				X	
NEW	OUTBD. AILERON		X	X		X
	FLAPERON		OUTBD SEG.	X		
	VERTICAL CANARD	X				
	HORIZONTAL CANARD	X				

FIG 4: CCV B-52 Flight Control Surfaces

Large aircraft ACT concepts investigated during AFFDL development programs have found application in operational flight equipment. An Active Lift Distribution Control System (ALDCS) was designed and retrofitted into the C-5A fleet to improve wing fatigue endurance (10). This system applies the MLC and FR concepts to reduce gust and maneuver incremental wing root bending moments by using the ailerons as ACT surfaces. Lockheed Corporation is investigating a MLC system for the L-1011-500 aircraft which uses symmetric active ailerons to reduce wing root bending moments (11). This system would allow 9 feet (2.74m) to be added to the wing span of L-1011-500's without major structural redesign. The L-1011-500 features direct lift control (DLC) for landing approach incorporated through symmetric spoiler deflections.

The B-1 aircraft was designed with a RCS to improve crew acceleration environment during turbulence and terrain following (12). The B-1 RCS employed the ILAF technique through two 5.75 ft² (0.54m²) canard surfaces mounted at a 30° anhedral angle and capable of deflecting 20° at a rate of 200 deg/sec. These unusually high deflection requirements were used to attempt to assure adequate force availability from the relatively small canard surfaces. Originally there was some concern that the unsteady aerodynamics effects at these high rates may be detrimental. However, the effectiveness of the B-1 RCS has been flight demonstrated. Application of ACT during the B-1 preliminary design resulted in an estimated structural weight savings of 9000 pounds (4090 kilograms).

4. THE SFCS F-4 PROGRAM (1969-1973)

During the same time period that the CCV B-52 Program was underway, another very significant and closely related ACT program was being pursued. This was the Survivable Flight Control System (SFCS) Program which addressed the development of fly-by-wire technology using an F-4 aircraft (13). While the LAMS and CCV B-52 Programs addressed ACT concepts applied to large flexible aircraft, the SFCS F-4 effort began a series of AFFDL development programs aimed at the fighter class of aircraft.

The major objective of the SFCS F-4 Program was to establish the practicality of fly-by-wire, which is the key to application of active control concepts in future fighter aircraft. The testbed aircraft retained the F-4 aerodynamic configuration and controlled it by means of a quadruplex analog primary flight control system. In the design of the SFCS, aircraft motion, rather than control surface deflection, is the parameter to be controlled by pilot inputs. This was the first USAF aircraft to fly with a totally FBW system having no mechanical links between stick and surfaces. Sidestick controllers were installed for evaluation in conjunction with the improved handling qualities incorporated through the FBW system. 10-7

The control laws incorporated in the SFCS F-4 aircraft were based on those developed during an earlier AFFDL effort called the TWEAD (Tactical WEAPON Delivery) Program. The TWEAD Program developed and tested a high authority, redundant control augmentation system (CAS) on an F-4C aircraft (14). Particular features implemented on the TWEAD CAS to improve controllability were high-gain feedback control loops which gave the pilot direct control over motion variables, proportional plus integral control which eliminated most of the required trimming, and vernier control which gave the pilot the ability to make small, precise, and rapid changes to his flight path. Because of the success of the TWEAD control laws during flight evaluations, they were selected as the basis for the control law development for the full authority FBW system on the SFCS F-4.

The SFCS was evaluated during a test program consisting of 84 flights. The pilots reported that the response and damping of the aircraft had been significantly improved over the basic F-4. The pitch axis showed better tracking capability as a result of designing the pitch system for compliance with a C^* criteria, as shown in Figure 5. The roll rate command system, for which criteria also were developed, gave much higher responses than typical of an F-4. While the faster roll response was rated desirable for combat applications, it was judged to be too rapid for conventional flight. This result suggested that responses be task-tailored for each mission segment through a multi-mode control system. The FBW technology base developed in the SFCS Program paved the way for further aircraft design improvements through exploitation and application of other advanced concepts such as fighter CCV techniques and multimode controls. It was also becoming obvious that achievement of the full potential of such concepts would require the computational power and flexibility of digital control systems.

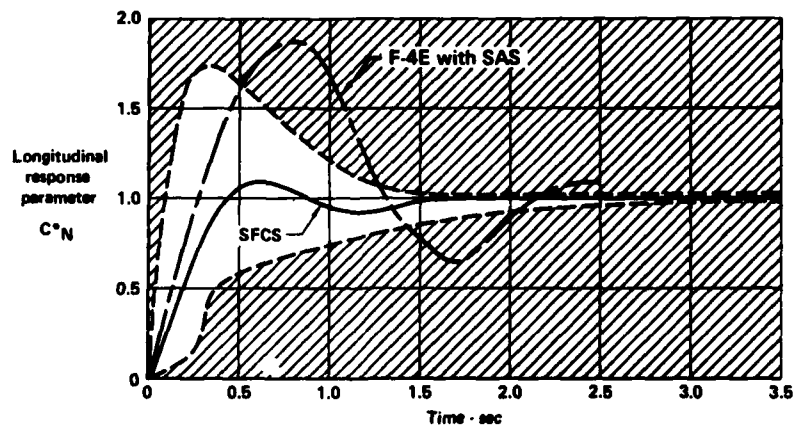


FIG 5: SFCS Flight Test Data - C^* Criteria Compliance

5. PACT/CCV F-4 PROGRAMS (1971-1974)

The next major development effort was the Precision Aircraft Control Technology (PACT) Program (13). This program started out as an AFFDL contracted effort to investigate fighter CCV concepts using the SFCS F-4 as the testbed. After one year, this Fighter CCV Program was redirected to the use of the YF-16 testbed (see Section 7). However, the F-4 investigation was continued by McDonnell Douglas using company resources under the name of the PACT Program.

The PACT Program modified the SFCS F-4 aerodynamic configuration by the addition of two close-coupled horizontal canard surfaces of 20 ft^2 (1.86 m^2) each. Figure 6 shows the aircraft arrangement, including the control surface deflection ranges. The canards moved the aerodynamic neutral point forward and caused the longitudinal axis of the unaugmented aircraft to be unstable subsonically. This permitted the investigation of maneuvering performance improvements achievable through application of the Relaxed Static Stability concept. Static margins as negative as -7.5% of the mean aerodynamic chord were obtained with the horizontal canard configuration. The canards were designed so that their outer panels could be removed, leaving each with an area of 8.5 ft^2 (0.79 m^2). This allowed a two-step build-up to the maximum level of instability.

10-8

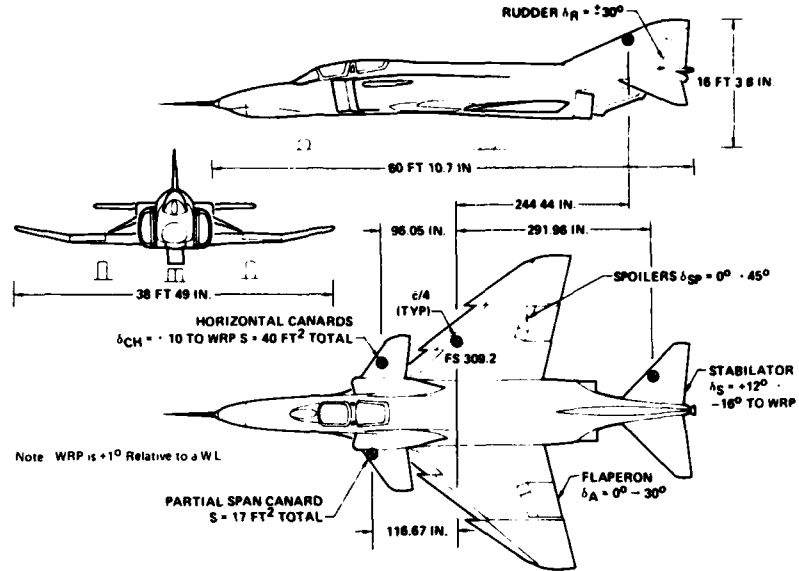


FIG 6: F-4 PACT General Arrangement

The horizontal canards were electronically scheduled as a function of stabilator position to provide a minimum drag combination. Because of the destabilizing effect of the canards, the stabilator travel range was rotated 5° in the aircraft nose down direction. The horizontal stabilator no-load maximum deflection rate of 25 deg/sec was marginal for RSS operation. Only minor changes were needed to the baseline SFCS to enable it to control the unstable PACT airframe and provide good handling qualities.

The PACT flight test program consisted of 30 flights which demonstrated maneuvering performance improvements over the F-4. Fixed leading edge slats were added at the same time as the PACT horizontal canards and these surfaces also contributed to performance. The horizontal canards improved performance through the addition of lifting surface area, through the RSS concept, and through an apparent favorable aerodynamic interaction with the wing. These effects were manifested in increased supersonic control limited load factors, in higher subsonic lift limited load factors, and in lower landing speeds. Buffet levels were also significantly reduced, but most of this improvement came from the slats.

The wind tunnel data base for the PACT effort was established during the earlier CCV F-4 contracted studies. The CCV F-4 Program was to have investigated direct lift and direct sideforce in addition to RSS. Therefore, extensive wind tunnel tests were conducted to size, locate, and document the aerodynamic characteristics of surfaces needed to implement direct force control. A vertical canard was chosen as the primary sideforce generator and horizontal canards were to be used for direct lift implementation (15).

Three different vertical canard planforms were wind tunnel tested on F-4 models to arrive at the most effective surface. The selected vertical canard had an area of 9.4 ft² (0.87m²), a sweep angle of 45° , and a deflection range of $\pm 30^\circ$. The effectiveness of a vertical canard as a sideforce generator is a function of both its sideforce reaction and its yawing moment, which, when trimmed out by the rudder, adds to the sideforce. During the CCV F-4 wind tunnel tests, even the best vertical canard was found to suffer a severe loss in effectiveness as angle of attack increased. This effect is shown in Figure 7, and implies that the vertical canard may be an acceptable sideforce generator for air-to-ground operations, but may be marginal in sideforce for high angle of attack air combat maneuvering.

An alternate method for generating direct sideforce was discovered during CCV F-4 wind tunnel testing. Differentially deflected horizontal canard surfaces were found to provide significant levels of sideforce (16). Figure 8 shows that, unlike vertical canards, horizontal canards produce sideforces that increase in magnitude with angle of attack. The theoretical basis of this phenomenon was not understood at that time. The use of horizontal canards for sideforce generation was explored more fully during the CCV YF-16 Program and will be further discussed in that section.

Use of horizontal canards was found to be an effective way of implementing direct lift control on the F-4 configuration. However, the direct lift capability of close-coupled horizontal canards does not arise from their effectiveness as lift producers. Wind tunnel tests showed that close-coupled horizontal canards are relatively ineffective in producing net lift because the lift generated by the canards is offset by the decrease in wing lift resulting from the downwash induced on the wing by the deflected canards. However, the canards can generate a considerable nose-up pitching moment which may be trimmed by a trailing edge down horizontal stabilator deflection. This positive

stabilator deflection for trim contributes a relatively large amount of incremental lift which, when added to the untrimmed canard increment, gives a significant level of direct lift control. The CCV F-4 would have supplemented the canard/stabilator DLC capability 10-9 with conventional spoiler and flaperon deflections.

Fighter aircraft ACT concepts investigated during the SFCS and PACT/CCV F-4 Programs found application in the F-16 Lightweight Fighter. The F-16 employs a quad-redundant FBW analog flight control system with no mechanical links between cockpit and actuators. It also employs the Relaxed Static Stability concept to achieve improved range and maneuvering performance (17).

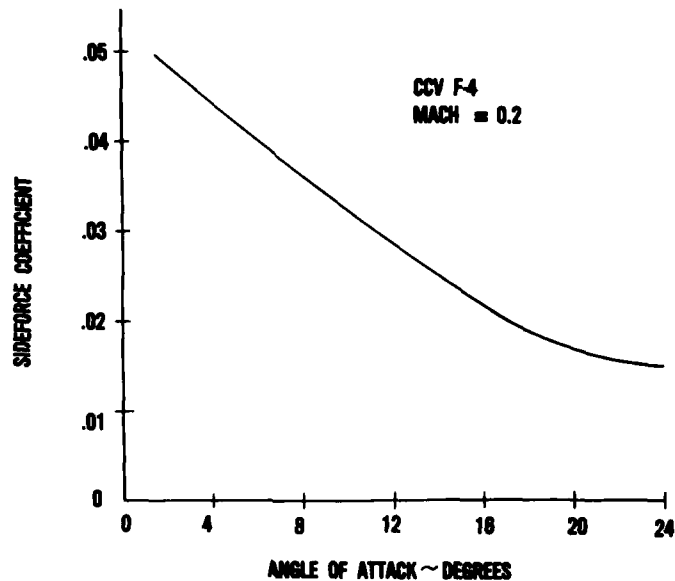


FIG 7: Vertical Canard Sideforce Vs. Angle of Attack

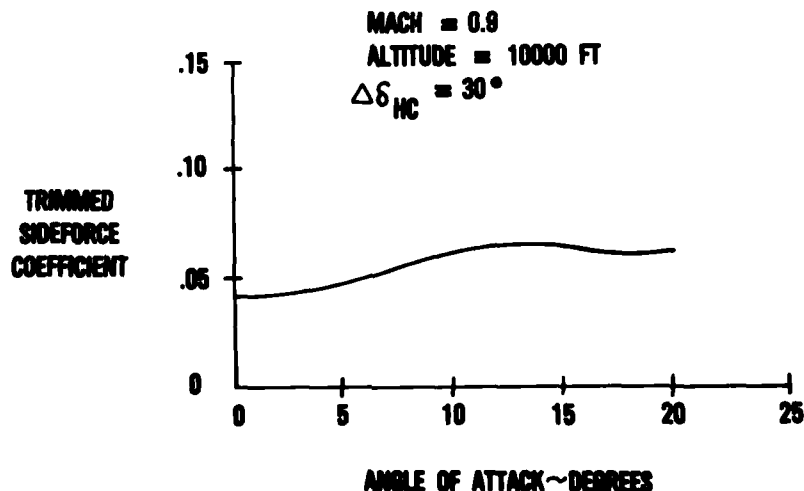


FIG 8: Direct Sideforce From Differentially Deflected Horizontal Canards (CCV F-4)

6. VARIABLE STABILITY NT-33A

Direct force control (DFC) technology has matured much more slowly than other ACT concepts. Though the theory is straightforward, an operationally suitable DFC implementation requires unique approaches to interdisciplinary problems. First, standard aerodynamic configurations normally do not have the means to generate direct sideforce and the normal method of generating direct lift (trailing edge flaps and stabilator) is somewhat inefficient and of low authority. Thus, non-standard aerodynamic configurations and control

10-10

surfaces are indicated. Second, the man machine interface problem is of vital importance when giving the pilot additional degrees of control freedom. The question of how the pilot can best command DFC modes has yet to be resolved. Separate, additional controllers for DFC can increase the workload and cause cross-coupling and other compatibility problems (18). New cockpit displays are also needed to allow the pilot to effectively monitor his use of decoupled control modes. Finally, it has not been conclusively demonstrated to pilots that DFC will allow them to perform combat tasks in a manner superior to conventional maneuvering. Some of the lag in maturing DFC technology can be attributed to the difficulty in adequately representing unconventional aircraft motions in ground-based simulators.

An AFFDL resource used for in-flight investigations of DFC and other ACT concepts is the Variable Stability NT-33A aircraft. As shown in Figure 9, the NT-33A obtained its DSFC by deflecting the rudder to cancel the yawing moment resulting from the asymmetric drag of wing tip tank petals. This scheme was used to evaluate the usefulness of DSFC in simulated dive bombing runs during a 1971 flight test program (19). Three different pilot controllers were investigated for a flat turn mode and for a lateral translation mode. The drag petal/rudder method of generating DSFC was found to be suitable for the high drag configuration normally used in dive bombing. However, the maximum sideforce available on the NT-33A was only 0.17g. Even so, it was concluded that DSFC improved the pilot's ability to acquire and maintain a target and indicated that additional research at higher performance would be worthwhile. A similar concept for generating DSFC employing split ailerons and rudder was included on the Northrop A-9 configuration. However, the full benefits were not realized due to a simple mechanical mechanization, which was in keeping with the design philosophy of the aircraft.

AFFDL in-flight simulators continue to support ACT research and development. The Variable Stability NT-33A was used in handling qualities development support for the F-16 and YF-17 and is involved in flight control development work for the US Navy F-18. Its AFFDL companion aircraft, the Total-In-Flight-Simulator (TIFS) NC-131H, is used for bomber/transport research. The TIFS recently has been used for in-flight investigations of B-1 and Space Shuttle Orbiter handling characteristics and in support of NASA's Supersonic Cruise Aircraft Research Program.

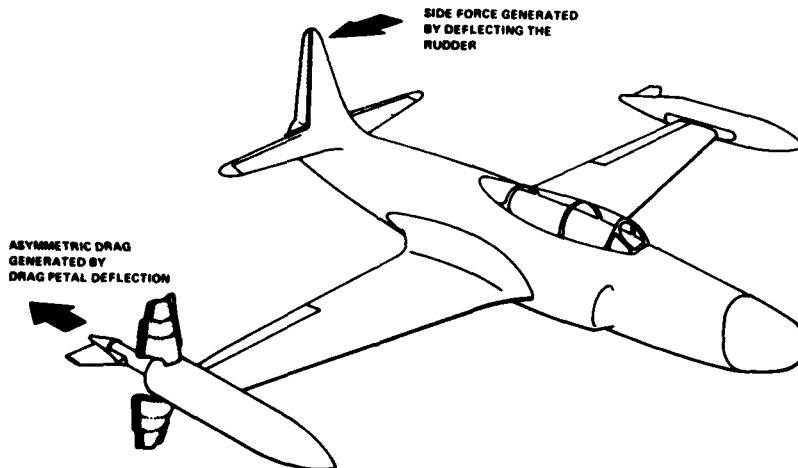


FIG 9: NT-33A Direct Sideforce Technique

7. THE CCV YF-16 PROGRAM (1973-1977)

The Fighter CCV Program started with an F-4 testbed but was redirected after one year to a more modern testbed: the YF-16. This program flight demonstrated seven decoupled control modes attainable through direct lift control and direct sideforce control. The CCV YF-16 achieved higher levels of direct force control than had previously been flight tested, and identified many actual and potential uses of the unique maneuvering capabilities afforded by the ability to independently control the six degrees of aircraft motion. This program also quantified the variation of maneuvering performance with degree of longitudinal aerodynamic stability under an RSS investigation.

The CCV YF-16 Program began with an extensive wind tunnel effort to determine the most desirable method of incorporating direct force capability on the test aircraft. Additional control surfaces tested included vertical canards for DSFC and horizontal canards for both DSFC and DLC. A horizontal canard was attractive because this single surface was found to be capable of providing effective control power in two axes (16). As on the CCV F-4 configuration, differential deflections of horizontal canards on the YF-16 were found to provide high levels of sideforce which increased with angle of attack. Figure 10 compares

the sideforce characteristics of horizontal and twin vertical canards on the CCV YF-16. At low angles of attack, the vertical canards are superior in sideforce generation. However, at angles of attack above about 5° the horizontal canards are more effective. The horizontal canards had the additional advantages of large DLC capability and of providing increased longitudinal control power for RSS investigations. Unfortunately, definition of the complex multi-axis aerodynamic coupling effects caused by horizontal canards would have required increased wind tunnel testing beyond the scope of the program. For example, high angle of attack directional stability was found to be a strong function of canard deflection. Also, incorporating horizontal canards on the YF-16 would have required extensive equipment relocations. For these reasons, it was decided to use the more straightforward vertical canards for DSFC generation and trailing edge flaps for DLC.

10-11

The CCV YF-16 flight test configuration is shown in Figure 11. The selected vertical canards had an area of 8 ft² each (0.74m²) and could be deflected through ±25° at a system rate of 94 deg/sec. Direct sideforce levels up to 0.9g were reached with the vertical canard/rudder combination. Direct lift control was obtained by means of coordinated deflections of the wing trailing edge flaps and the horizontal tail. The flaps could be deflected through ±15° at rates up to 56 deg/sec to obtain DLC levels of up to ±1.2g's.

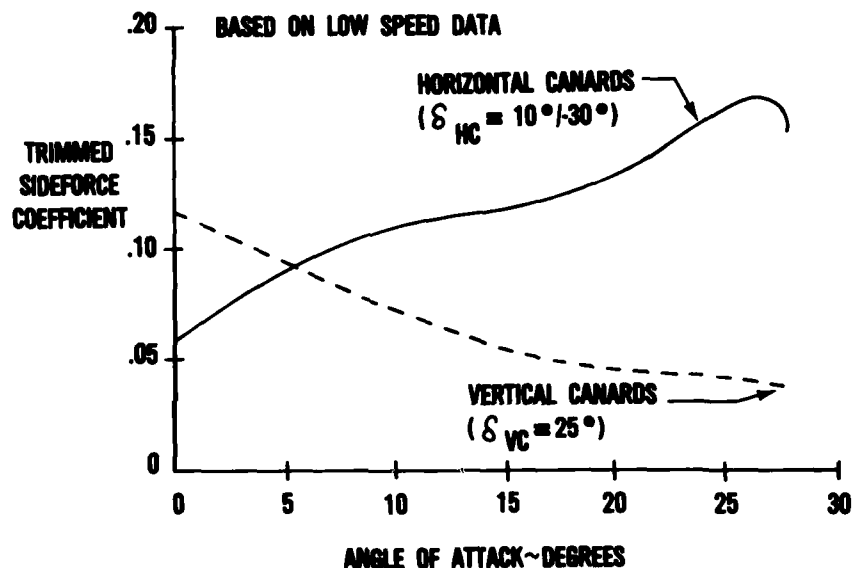


FIG 10: Comparison Between Vertical Canard and Horizontal Canard Sideforces (CCV YF-16)

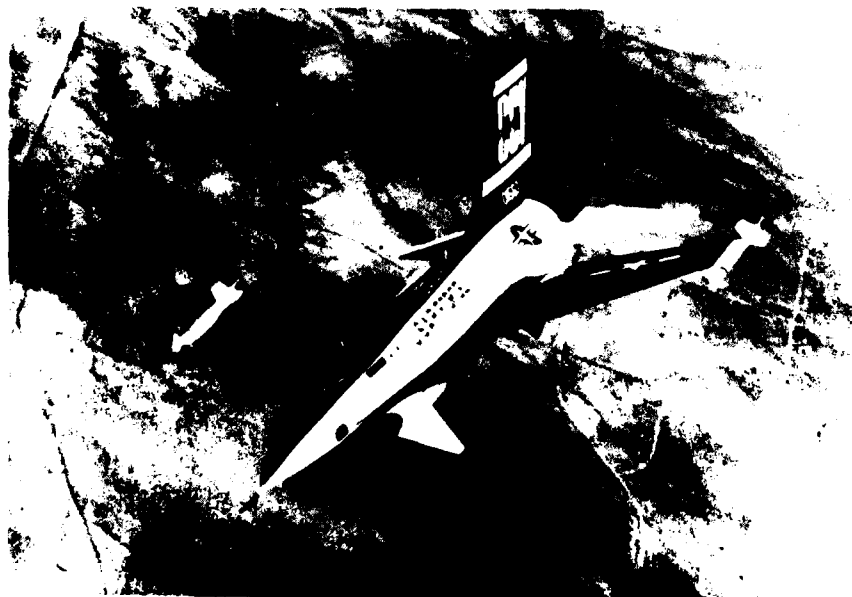


FIG 11: CCV YF-16 Test Aircraft

The manually commanded unconventional control modes that were flight tested on the CCV YF-16 are depicted in Figures 12 and 13. In addition, an automatic DLC mode was incorporated whereby conventional stick inputs resulted in momentary direct lift commands which quickened the initial aircraft response and were then washed out. A flight test program of 87 flights was conducted to evaluate these modes and to investigate the RSS concept (20). During flight testing, pilots identified many beneficial applications for these unconventional aircraft motions. The decoupled pointing modes were rated as having high potential for air-to-air tracking, especially when used in conjunction with an Integrated Flight and Fire Control system. The flat turn and lateral translation modes were found to be well suited for air-to-ground operations and the automatic DLC mode increased precision tracking accuracy. Valuable design guidance was also obtained from CCV YF-16 flight testing in the areas of controllers, response characteristics, evaluation techniques, and aerodynamic characteristics (21).

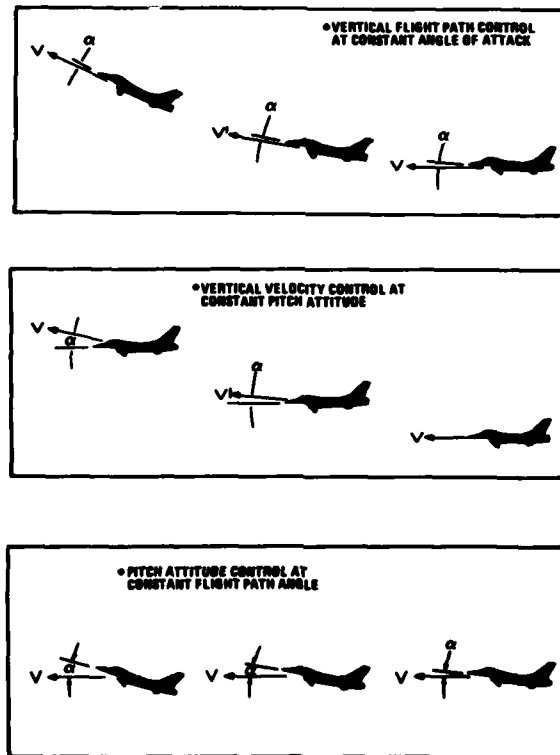


FIG 12: CCV YF-16 Longitudinal Modes

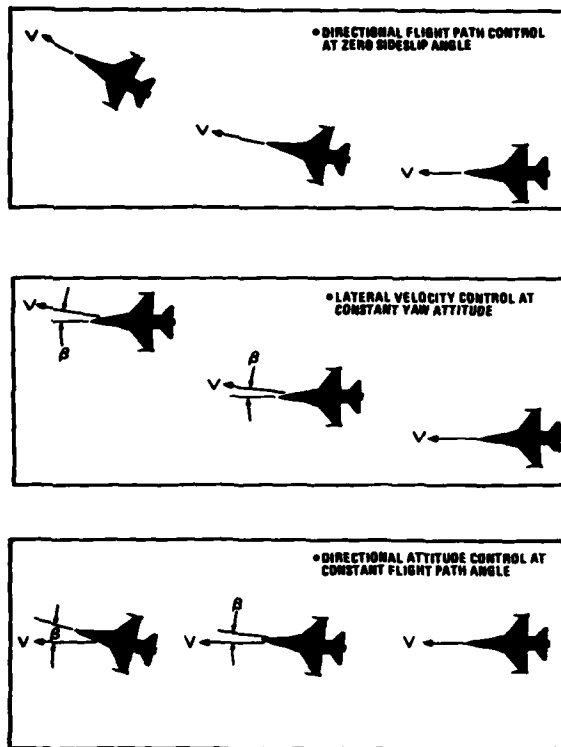


FIG 13: CCV YF-16 Directional Modes

A configuration such as the CCV YF-16 with nine movable surfaces presents a formidable challenge in defining the aerodynamic characteristics to an acceptable level of accuracy. An example where the CCV YF-16 wind tunnel data base was incomplete was in the matrix of flap and horizontal tail deflections needed to define the interaction between these surfaces. Flight test results shown in Figure 14 graphically illustrate the importance of defining significant aerodynamic interactions prior to flight. This plot shows that use of trailing-edge-up flap deflections resulted in sharply increased trim-tail deflections at angles of attack above 18° , whereas only very small trim changes occurred with the flaps undeflected. Such large positive horizontal tail deflection increases were indicative of diminishing aircraft nose-down pitch recovery power. On a statically unstable aircraft such as the CCV YF-16, it is vital that recovery pitching moment be available at all times to prevent locked-in trim points at high angles of attack. The effect shown in Figure 14 resulted in a control system modification preventing DLC application above 18° angle of attack.

Other aerodynamic interaction effects resulted from the use of trailing-edge flaps as DLC surfaces and from the use of vertical canards as DSFC surfaces (22). DLC operation at elevated angles of attack was accompanied by an increase in buffet level, although not severe enough to impair tracking ability. Energy maneuverability losses accompanied maximum DFC inputs, averaging between 70 and 90 fps (21 to 27 m/sec) depending on flight condition and mode. The vertical canard surfaces were found to interact with the ailerons and horizontal tail, reducing the effectiveness of these surfaces slightly. The aerodynamic interferences and nonlinearities noted during the CCV YF-16 program reinforced the importance of a thorough and accurate definition of bare airframe aerodynamics. Although the closed-loop flight control system was generally effective in masking undesirable aerodynamic characteristics, there are definite limits to this capability.

Like most research efforts, the CCV YF-16 Program surfaced as many new questions as it answered and indicated appropriate areas for additional study. Flight testing showed a clear need to specifically tailor the authorities and response characteristics of each control mode to the task being performed. For instance, the CCV YF-16 flat-turn mode was judged too sensitive for air-to-ground tracking, but more authority was desired for maneuvering during air-to-air encounters. The pilots recognized the great potential of the pointing modes, but their inability to satisfactorily control them manually suggested the desirability of automating these functions. Because of funding considerations, the CCV YF-16 Program did not attempt to optimize the controllers; this detracted from the evaluation. Also, the compatibility of unconventional flight modes with advanced fire

control systems was not addressed. Such unanswered questions form the bases of other AFFDL ACT programs.

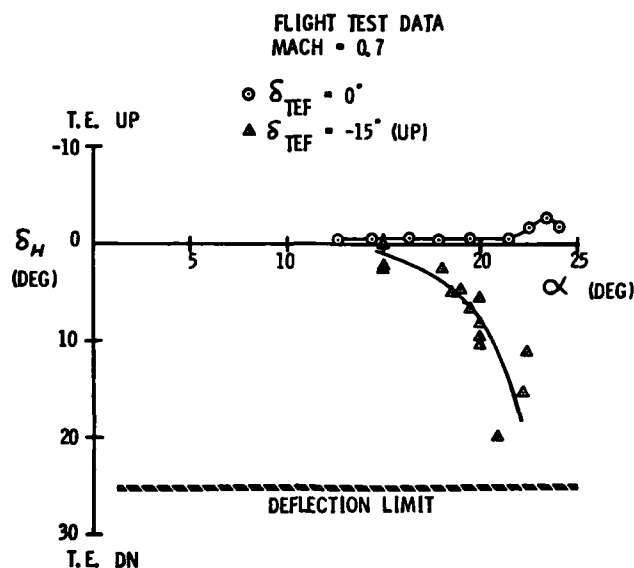


FIG 14: CCV YF-16 Trim Tail Deflection vs Angle of Attack

8. AD-7D DIGITAL MULTIMODE FLIGHT CONTROL SYSTEM PROGRAM (1973-1976)

While the CCV YF-16 Program was investigating decoupled control modes, an A-7D aircraft was exploring the benefits available from conventional task-tailored multimodes incorporated through a digital command augmentation system. The control laws were tailored to increase pilot effectiveness in accomplishing the air-to-air and air-to-ground weapons delivery tasks. A dual redundant digital mechanization was used to duplicate the standard operational A-7D inner loop stability and control augmentation functions and outer loop pilot relief functions, and also to incorporate two new multimode control laws. The first of these new multimodes was termed the Flight Path mode, which was basically a C* controller providing a steady-state stick force per g that increased at low speeds and approached a constant value at high speeds. The Flight Path mode also featured a zero stick breakout force, increased normal acceleration response speed, and a reduction in stick trim forces with changing flight condition. The second new multimode, termed the Precision Attitude mode, was tailored specifically for making the small attitude changes required for precision tracking maneuvers. Both modes featured revised lateral-directional control laws providing stick shaping and gain scheduling for tighter roll control and improved turn coordination and damping based on a sideslip rate feedback signal.

A test program, consisting of 56 flights, was conducted to evaluate the A-7D digital multimode system. In general, the results showed that significant weapon delivery performance improvements were possible, even though only conventional surface motion was commanded (23). The Precision Attitude mode was preferred over the Flight Path mode since the air-to-air tracking and air-to-ground strafing and bombing experiments were primarily oriented toward accurate attitude control. Although the multimodes provided no appreciable improvement in dive bombing accuracy relative to the standard control augmentation system, the pilots preferred the multimodes because of their pseudo-neutral speed stability. There were, however, measurable benefits from the multimodes in tracking and strafing accuracies. The multimodes provided a 38% average reduction in tracking error for air-to-air and air-to-ground tasks with respect to the standard control augmentation system. There was a corresponding 27% improvement in strafing scores.

The results of the A-7D flight test program showed that digital flight control systems can effectively provide task-oriented control laws. The flexibility afforded by alterable core memory of the digital system proved to be a large asset in the optimization of the control laws during development flight testing. The variation in control laws needed to establish a full-up mission-tailored multimode control system, incorporating decoupled maneuverability, requires even more complex inner loop functions to provide the necessary mode switching logic, feedback blending, signal shaping, gain schedules, filters, compensation networks, etc. The simplified lateral-directional axis block diagram of Figure 15 illustrates an example of the level of switching required to alter a basic, normal mode to a specialized air combat mode (24).

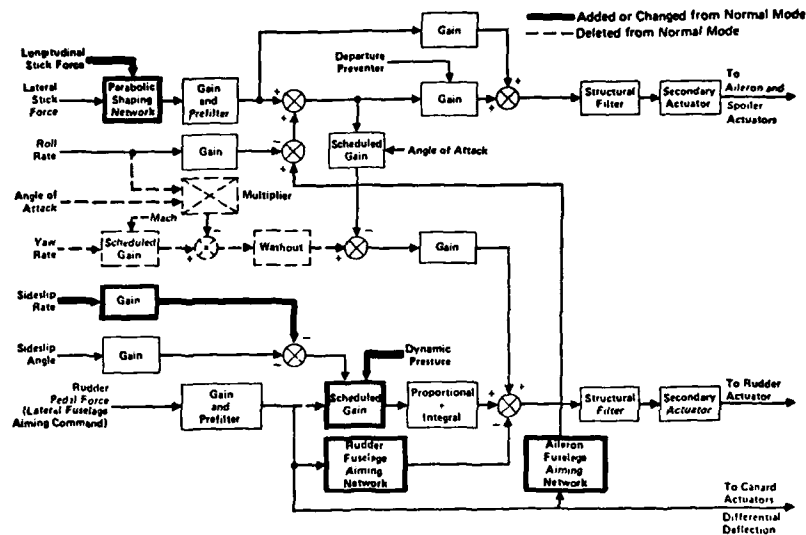


FIG 15: Multimode Lateral-Directional Block Diagram

Digital flight control technology has found application on the F-18, which employs a three-axis quadruplex DFCS with full analog backup and mechanical backup in pitch and yaw.

9. THE IFFC-I/FIREFLY III PROGRAM (1978-1981)

The concept of Integrated Flight and Fire Control (IFFC) provides the opportunity to demonstrate a technology which can potentially improve the combat effectiveness of all tactical aircraft. IFFC design involves the blending of flight control, director fire control, and weapons system technologies together with the pilot's abilities to enhance weapon delivery accuracy and survivability. Accurate delivery of air-to-ground ordnance during evasive maneuvering and pilot-aided air-to-air tracking are the cornerstones of the IFFC concept.

The IFFC-I/FIREFLY III Program is the culmination of a series of joint AFFDL and AFAL (Air Force Avionics Laboratory) programs to mature the interdisciplinary technologies to the extent necessary to effectively blend them into a total weapon system. The program is being conducted under coordinated AFFDL/AFAL contracts and will result in flight validation of the IFFC concept using a production F-15 testbed. In this IFFC-I/FIREFLY III effort, no attempt is being made to completely redesign the flight or fire control system, or to initiate large component development efforts. The IFFC configurations are to be designed to minimize the configuration impact on our latest operational fighters, consistent with achieving the program objectives. Under this philosophy, only conventional flight control maneuvers will be exploited. It is believed that this effort has significant short-term potential, therefore emphasis is placed on living within the physical and functional limitations of the F-15 baseline systems, if feasible.

The F-15 IFFC system will be designed to accommodate varying levels of pilot participation in the control tasks, ranging from full manual control to pilot-aided automatic control. Also, the pilot will be able to designate certain axes for automatic control while retaining manual control of the remaining axes of motion. Emphasis will be placed on assisting the pilot in the terminal phase of attack where precision control is critical, after the pilot has accomplished the necessary air combat maneuvering to acquire the target.

In air-to-air gunnery, delegation of control authority to an automatic system results in the "big pipper" concept. Under this scheme, the pilot's control task is simply to move the target within the confines of a sighting rectangle whose dimensions correspond to the authority limits of the automatic system. The IFFC system will then achieve the firing solution.

In air-to-ground operations, the IFFC system will be designed for ordnance delivery during turning maneuvers, as depicted in Figure 16. The traditional technique of rolling out to a wings level attitude before weapons release is not only unnecessary but also undesirable. Returning the advantages of speed and maneuverability to the attacker has obvious survivability benefits.

10-16

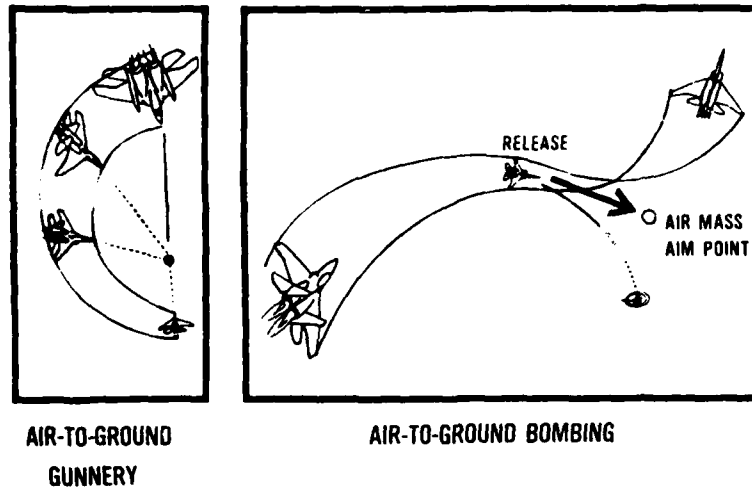


FIG 16: IFFC Turning Attack Maneuvers

The success of the IFFC concept is critically dependent on the ability of the sensors and trackers to provide accurate target state information. The F-15 IFFC configuration will use a Martin-Marietta ATLAS II (Automatic Tracking Laser Illumination System) as the primary sensor/tracker. Air-to-air range information will be obtained from the radar.

The ultimate success of the F-15 IFFC system design will be determined by scoring live gunnery and inert bombing against realistic targets. Simulation results were used to set the IFFC flight test performance goals (25). For air-to-air gunnery, these goals are a 3:1 increase in expected hits, a 2:1 reduction in time to first firing opportunity, a 4:1 increase in number and duration of firing opportunities, and the demonstration of a greatly increased employment envelope in high angle-off and high line-of-sight rate encounters. The goals for air-to-ground gunnery and bombing are a 10:1 increase in survivability against linear predictor anti-aircraft artillery, a 2:1 increase in weapon delivery accuracy of the IFFC system over a similar non-wings-level manual maneuver for the baseline F-15, and retention of present weapon delivery accuracy while releasing in maneuvers. IFFC system performance versus the goals will be determined during a test program of about 200 flights. The progress and results of this program will also directly support the advanced IFFC task of the AFTI-16 program discussed below.

10. THE AFTI-16 PROGRAM (1978-1983)

The AFTI-16 Program will extend and integrate into a single F-16 test aircraft most of the fighter technologies that were investigated individually under the previously described AFFDL ACT programs. The AFTI-16 aircraft will tie together the decoupled control capability provided by direct force control with an integrated flight/fire control system, all implemented through a task-tailored multimode digital flight control system. Pilot/Vehicle Interface (PVI) advancements necessary to permit complete evaluation of the technologies will also be implemented, including a wide field-of-view head-up-display, a helmet-mounted sight, new controllers, and multifunction displays. The approach of integrating several ACT concepts on a modified aircraft was the culmination of several years of studies and proposals.

Initial design studies conducted under the Advanced Fighter Technology Integration (AFTI) effort were directed at identifying the configuration of a small new demonstrator vehicle on which ACT concepts could be validated (26). Figure 17 shows one innovative configuration that evolved from these studies. This design uses just six control surfaces to provide control of all six independent degrees of flight freedom. By contrast, recent operational fighters require coordination of nine to eleven surfaces to provide control in the conventional four degrees of flight freedom. Other configurations proposed during the early AFTI studies featured advanced aerodynamics such as close-coupled horizontal canards and supercirculation through jet flaps. The new demonstrator concept was appealing because it would avoid some of the compromises necessary when integrating technologies on a modified vehicle. However, the costs associated with building a new aircraft for technology demonstration purposes was a drawback. It was decided that ACT concepts could be effectively integrated and demonstrated on a modified existing aircraft, and this is the approach being pursued on the AFTI-16 Program.

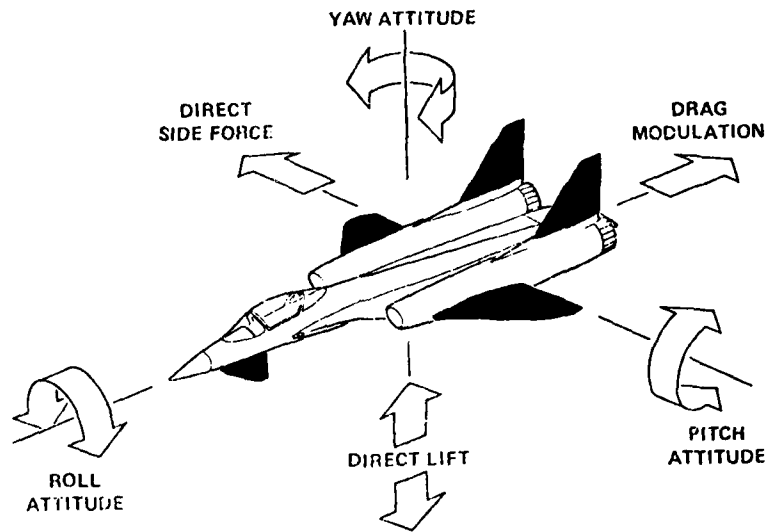


FIG 17: Early AFTI Configuration

The AFTI-16 test aircraft is depicted in Figure 18. It is a modified F-16 Full Scale Development aircraft. An added dorsal fairing is used to accommodate flight test instrumentation. The vertical canards used for direct sideforce control are the same surfaces that were used during the CCV YF-16 Program. The AFTI-16 method of obtaining direct lift control with the trailing-edge flaps and horizontal tail is also the same as on the CCV airplane. Overall, the configurations are similar enough that the CCV YF-16 aerodynamic data base can be used to reduce the risk and cost to the AFTI-16 Program. A major aerodynamic challenge during the AFTI Program will be in clearing the aircraft to drop bombs during non-wings level and unconventional IFFC maneuvering.



FIG 18: AFTI-16 Test Aircraft

The AFTI-16 triplex Digital Flight Control System (DFCS) should be well suited for implementing the higher order control loop functions, logic schemes, and complex interfaces with controls, displays, and other AFTI subsystems. The task oriented multimode control law implementation and selection capability will go beyond concept demonstration

to provide an operationally suitable configuration. Digital technology offers flexibility and growth potential for system changes through software rather than hardware modifications. A good test of the AFTI-16 Digital Flight Control System will be its capability to compensate for the many aerodynamic nonlinearities and interference effects expected as a result of CCV YF-16 findings.

The IFFC task of the AFTI-16 Program will expand the scope of the F-15 IFFC Program by incorporating decoupled maneuvering capability and other advanced features. As mentioned previously, automatic command of aircraft pointing independent of flight path is expected to show big payoffs in IFFC gunnery operations. The advanced IFFC system on the AFTI-16 is expected to produce mission effectiveness improvements even more impressive than those being sought for the conventional IFFC system on the F-15 testbed.

A test program consisting of approximately 250 flights is planned to validate the integrated AFTI-16 technologies. Although the AFTI vehicle will not be able to fully exploit the design versatility available from a new configuration, it should provide a viable and cost effective alternative for providing proven technology for transition to systems application. The AFTI-16 Program will also mature the techniques for merging ACT with novel aerodynamic control concepts.

11. CONCLUSIONS

Over the past decade, the AFFDL has pursued a systematic approach to the advancement of Active Control Technology through a series of flight test development programs. The AFFDL programs were concurrent with other highly significant ACT research efforts accomplished in the United States and throughout the international aerospace community. The overall effect has been to mature aspects of the technology to the point where they have been accepted and incorporated into production weapon systems.

Flight control and aerodynamics are highly interdependent on ACT aircraft which require localized force and moment producers for structural mode control or unconventional maneuverability. One aspect of ACT that has not yet been fully exploited is the application of direct force control for improving mission effectiveness. To take full advantage of decoupled maneuver modes, aerodynamic control surfaces are needed which provide high levels of effectiveness over a wide range of flight conditions, with acceptable drag and buffet penalties, minimum interference and cross-coupling effects, and benign nonlinearities. The advent of ACT design techniques, rather than reducing the importance of bare airframe aerodynamics, has resulted in an increased requirement for a thorough and accurate definition of aerodynamic characteristics.

The AFFDL ACT programs progressed from a test aircraft using existing aerodynamic control surfaces and a single thread analog fly-by-wire system up to an aircraft having new surfaces for unconventional task-tailored multimode control implemented with a full digital flight control system. ACT concepts have been developed for both the bomber and fighter classes of aircraft. Perhaps the most significant finding in all this activity was that the effectiveness of employing all these new flight and control modes cannot be fully assessed by the traditional analysis and performance methods. Hence, intensive research efforts are required to further develop the mathematical analysis and design techniques to fully exploit the capabilities and the tactical utility of the many benefits that are available.

REFERENCES

1. Burris, P. M. (The Boeing Company) and Bender, M. A. (Honeywell, Inc.), Aircraft Load Alleviation and Mode Stabilization (LAMS) Flight Demonstration Test Analysis, AFFDL-TR-68-164, Air Force Flight Dynamics Laboratory, Wright-Patterson AFB, Ohio; December, 1969.
2. Johannes, R. P., Burris, P. M., and Dempster, J. B., "Flight Testing Structural Performance of the LAMS Flight Control System", AIAA Paper 68-244; March, 1968.
3. Ostgaard, M. A., and Swortzel, F. R., "CCVs: Active Control Technology Creating New Military Aircraft Design Potential", Aeronautics and Astronautics; February, 1977.
4. Wykes, J. H. and Knight, R. L., "Progress Report on a Gust Alleviation and Structural Dynamic Stability Augmentation System (GASDSAS) Design Study", AIAA Paper 66-999; November, 1966.
5. Wykes, J. H., Nardi, L. U., and Mori, A. S. (North American Rockwell Corp.), "XB-70 Structural Mode Control System Design and Performance Analyses", NASA CR-1557; July, 1970.
6. Lee, J. A. and Johannes, R. P., "LAMS B-52 Flight Experiments in Direct Lift Control", SAE Paper 690406; April, 1969.
7. Johannes, R. P. and Kass, G. J., "B-52 Control Configured Vehicles Program", 4th AIAA Aircraft Design, Flight Test, and Operations Meeting, Los Angeles, California; August, 1972.
8. Kujawski, B. T., "Control Configured Vehicles B-52 Program Results", AGARD CP-157; October, 1974.
9. The Boeing Company, B-52 CCV Program Summary, AFFDL-TR-74-92, Air Force Flight Dynamics Laboratory, Wright-Patterson AFB, Ohio; March, 1975.
10. Grosser, W. F., Hollenbeck, W. W., and Eckholdt, D. C., "The C-5A Active Lift Distribution Control System", AGARD CP-157; October, 1974.
11. Lenorovitz, J. M., "L-1011 Active Control System Tested", Aviation Week & Space Technology; September 19, 1977.
12. Wykes, J. H., Mori, A. S., and Borland, C. J., "B-1 Structural Mode Control System", AIAA Paper No. 72-772; August, 1972.
13. Krachmalnick, F. M., et al, "Survivable Flight Control System Active Control Development, Flight Test, and Application", AGARD CP-157; October, 1974.
14. Rubertus, D. P., "TWEAD Control Augmentation System", National Aerospace Electronics Conference, Dayton, Ohio; May, 1972.
15. Bennett, D. H. (McDonnell Douglas Company), Program Summary for Control Configured Vehicle Concepts Applied to Fighter Aircraft, AFFDL-TR-74-51, Air Force Flight Dynamics Laboratory, Wright-Patterson AFB, Ohio; May, 1974.
16. Stumpfl, S. C. and Whitmoyer, R. A., "Horizontal Canards for Two-Axis CCV Fighter Control", AGARD CP-157; October, 1974.
17. Watson, J. H., "Fly-by-Wire Flight Control System Design Considerations for the F-16 Fighter Aircraft", AIAA Paper 76-1915; August, 1976.
18. Barfield, A. F., "Flight Experience with Manually Controlled Unconventional Aircraft Motions", 14th Annual Conference on Manual Control, Los Angeles, California; April, 1978.
19. Hall, G. W. (Cornell Aeronautical Lab), A Flight Test Investigation of Direct Side Force Control, AFFDL-TR-71-106, Air Force Flight Dynamics Laboratory, Wright-Patterson AFB, Ohio; September, 1971.
20. McAllister, J. D., et al (General Dynamics Corporation), Fighter CCV Phase IV Report, AFFDL-TR-78-9, Air Force Flight Dynamics Laboratory, Wright-Patterson AFB, Ohio; February, 1978.
21. Swortzel, F. R. and McAllister, J. D., "Design Guidance from Fighter CCV Flight Evaluations", AGARD FMP Symposium on Stability and Control, Ottawa, Canada; September, 1978.
22. Whitmoyer, R. A., "Aerodynamic Interactions on the Fighter CCV Test Aircraft", AGARD CP-235; May, 1978.
23. Yechout, T. R. and Oelschlaeger, D. R., "Flight Evaluation of a Digital Multimode Flight Control System in an A-7D Aircraft", AIAA Paper 76-1913; August, 1976.

24. Ramage, J. K. and Swortzel, F. R., "Design Considerations for Implementing Integrated Mission—Tailored Flight Control Modes", AGARD GCP Symposium on The Impact of Integrated Guidance and Control Technology on Weapons Systems Design, Sandefjord, Norway; May, 1978.

25. Bell, R. A., et al (General Electric Company), Integrated Flight/Fire Control System (FIREFLY II), AFFDL-TR-78-172, Air Force Flight Dynamics Laboratory, Wright-Patterson AFB, Ohio; December, 1978.

26. Preyss, A. E., Williams, W. G., and Cosenza, C. J., "AFTI-Advanced Fighter Technology Integration", AIAA Paper 76-888; September, 1976.

Control Considerations for CCV Fighters
at High Angles of Attack

By

Luat T. Nguyen, William P. Gilbert, and Sue B. Grafton
NASA Langley Research Center
Hampton, Virginia 23665

11-1

SUMMARY

Wind tunnel and piloted simulation studies were conducted to investigate the potential high angle of attack control problems that are introduced by the use of the CCV concept of relaxed static pitch stability (RSS) on fighter aircraft. The configurations investigated were a conventional wing/aft tail design incorporating modest levels of static instability and a close-coupled canard/wing design exhibiting very high levels of instability. The results of the studies indicate that two types of high angle of attack control problems can result from the use of RSS: (1) pitch departures caused by coupling; and (2) deep stall trim. Avoidance of these problems requires that the airplane have sufficient nose-down pitch control at high angles of attack. With regard to this requirement, the effectiveness of several pitch control configurations were investigated including conventional aft-mounted stabilators, wing-mounted elevators, canard-mounted flaps, and all-moveable canards. Varying the incidence of the canards was found to be the most effective scheme; however, very large deflections may be required on highly unstable configurations to prevent pitch departure without sacrificing roll performance and to avoid deep stall trim. For situations where the high angle of attack pitch control requirement is not met, control laws were developed to inhibit the departure and to allow deep stall recovery. However, these schemes involve limiting airplane roll capability and therefore can potentially compromise maneuverability.

INTRODUCTION

Rapid advances in aircraft avionic technology in recent years have made possible the application of control-configured-vehicle (CCV) concepts to fighter aircraft. In particular considerable interest has arisen regarding the principle of relaxed static stability (RSS) in which the airframe is designed to have low or negative inherent static longitudinal stability at subsonic speeds. The potential performance benefits of this concept are well known and fighter designs incorporating very high levels of inherent longitudinal instability are now being considered.

Obviously, in RSS designs the reliance on the control system to provide satisfactory stability and control characteristics is quite high. Fundamentally, the control system must provide artificial stability such that the airframe/control system combination has static stability throughout the flight envelope. The use of RSS, however, can also introduce potential stability and control problems at high angles of attack which impose severe requirements on the design of the control system in order that the desired characteristics of maximum maneuverability and departure/spin resistance can be attained. It should be noted that these problems exist in addition to the more familiar lateral/directional problems that generally occur near maximum lift. This paper will concentrate on some of the inherent high angle of attack problems resulting from the use of RSS, the design requirements on the flight control system for such conditions, and some airframe and control system concepts which can be used to satisfy these requirements. In addition, the limitations of such concepts and the subsequent effects on aircraft maneuverability and departure/spin resistance will also be reviewed. The foregoing points are discussed for two specific airplane configurations, one of which utilizes a conventional aft tail, and the other a canard.

SYMBOLS

a_n	normal acceleration, g units
C_m	pitching moment coefficient
I_x, I_y, I_z	moments of inertia about X, Y, and Z body axes, kg-m ²
M	Mach number
M_{ic}	pitching moment due to inertia coupling ($I_z - I_x$) pr, N-m
p	airplane body axis roll rate, deg/sec or rad/sec
p_s	airplane stability axis roll rate, deg/sec or rad/sec
q	airplane body axis pitch rate, deg/sec or rad/sec
\bar{q}	free-stream dynamic pressure, N/m ²
r	airplane body axis yaw rate, deg/sec or rad/sec

t	time, sec
V	airplane resultant velocity, m/sec
X, Y, Z	airplane body axes
α	angle of attack, deg
β	angle of sideslip, deg
δ_a	aileron deflection, positive for left roll, deg
δ_c	canard deflection, positive for trailing-edge down, deg
δ_{cf}	canard flap deflection, positive for trailing-edge down, deg
δ_e	elevator deflection, positive for trailing-edge down, deg
δ_h	horizontal stabilator deflection, positive for trailing-edge down, deg
δ_r	rudder deflection, positive for left yaw, deg
Θ, ϕ, ψ	Euler angles, deg
Ω	total angular rate, deg/sec

BACKGROUND

The fundamental aerodynamic characteristics of RSS configurations which can result in the high angle of attack control problems discussed herein are illustrated in figure 1 which shows an idealized plot of aerodynamic pitching moment coefficient C_m versus angle of attack which might be expected for a statically unstable configuration. Data are shown for neutral, full nose-up and full nose-down pitch control deflections. The two main potential problem areas are indicated by the shaded regions as an indication of where they are likely to occur. The lower α region below maximum lift represents an area of susceptibility to uncontrollable pitch departures due to lack of sufficient aerodynamic nose-down control moment. As indicated, if the angle of attack exceeds α_{crit} , additional nose-down moment cannot be generated and the airplane will pitch up into an out-of-control situation. Thus, a critical requirement of the control system in this case is to limit the maximum angle of attack to values where control can be maintained. Note, however, that in the α region immediately below α_{crit} there is very little nose-down moment available to prevent α excursions above α_{crit} . For angles of attack higher than α_{crit} , it is seen that the C_m curves change slope due to increasing breakdown of the flow over the entire configuration which causes the aerodynamic center to move aft, resulting in stable deep stall trim points at very high angles of attack. If the airplane enters these deep stall-trim points, recovery may be very difficult since aerodynamic controls for most fighter configurations are generally not very effective at these extreme angles of attack.

With these aerodynamic characteristics in mind, it is appropriate to examine how control saturation and departure may be encountered during maneuvering at high angles of attack. Towards this end, it is useful to review several kinematic and inertia-coupling phenomena which can significantly influence the high angle of attack flight dynamics of RSS configurations. One important effect is the kinematic coupling between angle of attack and sideslip that occurs when an airplane is rolled about its X-axis at high angles of attack as illustrated in figure 2. If the airplane is flying at angle of attack with the wings level [figure 2(a)] and the pilot generates a pure rolling motion about the airplane X axis [figure 2(b)], after 90° of roll all of the initial angle of attack will have been converted into sideslip. Because it is undesirable to generate large amounts of sideslip at high angles of attack from a roll performance and lateral-directional departure susceptibility viewpoint, most current fighters are designed to roll about the velocity vector rather than the body axis. It is obvious that this conical rotational motion (indicated by p_s) eliminates the coupling between α and β . Resolving p_s into the body axis system shows that this motion involves body axis yaw rate as well as roll rate and that these rates are related by the expression

$$r = p \tan \alpha$$

If the above equality is not satisfied during a roll, sideslip will be generated due to kinematic coupling with β varying as: $\dot{\beta} = p \sin \alpha - r \cos \alpha$. Modern fighter control systems generally incorporate roll/yaw control interconnects and stability axis yaw dampers which attempt to make the airplane roll about its velocity vector at high angles of attack.

Turning to the case of rolling with an initial sideslip, it is seen from figure 2(b) that body axis rolling will result in the initial β being converted into α after 90° of roll with $\dot{\alpha}$ varying as

$$\dot{\alpha} = q - p \cos \alpha \tan \beta$$

The second term in the above expression indicates that rolling with adverse sideslip (p and β having the same signs) tends to reduce α whereas rolling with proverse sideslip (p and β having opposite signs) tends to increase α . This latter effect can be important in RSS configurations requiring an angle of attack limit because substantial increases in α can be generated due to kinematic coupling if the airplane is rolled with proverse β (using excessive rudder for example). This increase in α could overpower the available nose down control and result in a pitch departure.

The second form of coupling important to the high angle of attack dynamics of RSS configurations is due to inertial effects. Figure 3(a) illustrates the inertial pitching moment that is produced when a typically fuselage-heavy fighter airplane is rolled about its velocity vector at high angles of attack. The desirability of this type of roll from a kinematic coupling viewpoint was previously discussed; unfortunately, the resulting nose-up pitching moment caused by inertia coupling can be a problem for RSS configurations. As an aid in visualizing this effect, the fuselage-heavy mass distribution of the airplane is represented as a dumbbell with the mass concentrated at the two ends. If the airplane rolls about its velocity vector, the dumbbell will tend to pitch up to align itself perpendicular to the rotation vector p_s . This nose-up pitching moment due to inertial coupling, M_{ic} , can be expressed as:

$$M_{ic} = (I_z - I_x) p r$$

substituting

$$p = p_s \cos \alpha \quad \text{and} \quad r = p_s \sin \alpha$$

$$M_{ic} = (I_z - I_x) p_s^2 \cos \alpha \sin \alpha = 1/2 (I_z - I_x) p_s^2 \sin 2\alpha$$

The above expression shows that the pitch inertia coupling moment resulting from stability axis rolling is always positive (nose up) for positive α , increases with increasing α , and varies as the square of the roll rate. For RSS configurations, this nose-up inertial moment must be opposed by the available nose-down aerodynamic moment. If the control moment is less than the inertia coupling moment, the airplane may pitch up beyond the critical α boundary (illustrated in figure 1) resulting in loss of control.

The inertia coupling yawing moment which results from the combination of roll and pitch rates is illustrated in figure 3(b). The airplane mass distribution is represented by the dumbbell and the airplane is shown rolling to the right and pitching up. As can be seen, the dumbbell will tend to yaw nose-left to align itself perpendicular to the rotation vector Ω . Thus, the airplane would be rolling and yawing in opposite directions. Recalling that to minimize adverse sideslip due to kinematic coupling r must be equal to $p \tan \alpha$, it is seen that this form of coupling can contribute to the build-up of large amounts of adverse β which in turn can result in loss of lateral-directional control at high angles of attack.

In summary, RSS configurations can be susceptible to pitch departures at high angles of attack when there is insufficient nose-down aerodynamic moment to prevent angle of attack from increasing above some critical limit beyond which the airplane cannot be controlled in pitch. Two dynamic phenomena which can generate large angle of attack excursions during high- α maneuvering are kinematic coupling and inertia coupling. Kinematically, substantial increases in angle of attack can be generated by rolling with proverse sideslip; in addition, large α excursions can also occur during push-over recoveries from steep attitude climbs to very low airspeed. Inertially, significant nose-up moments are generated during stability axis rolling at high angles of attack. If these moments are greater than the available nose-down aerodynamic moment, a pitch departure is likely to occur. This problem is further illustrated in figure 4. Shown is the variation of the nose-up inertia coupling moment caused by stability axis rolling with roll rate; as noted earlier the moment varies with p^2 so that very substantial moments can be produced at high roll rates. Also shown are representations of the available nose down control moment for a specified α at two values of dynamic pressure, \bar{q}_1 and \bar{q}_2 ($\bar{q}_1 < \bar{q}_2$). The points of intersection with the coupling moment curve indicate the highest roll rates (p_{s1}^* and p_{s2}^*) at which sufficient control moment exists to counter the nose-up coupling moment. If the roll rate should increase and be sustained above these values, then it is very likely that a pitch departure will occur. Note that $p_{s1}^* < p_{s2}^*$, indicating that the susceptibility to this type of departure becomes more acute as airspeed decreases. Once a departure beyond the critical α limit occurs, the airplane is likely to continue to pitch up to very high angles of attack and potentially restabilize in a deep stall trim point as indicated earlier in figure 1. Furthermore, the results of figure 4 point out a rather unique characteristic of RSS configurations -- that the maximum sustainable roll rates that can be controlled at high angles of attack are a direct function of the effectiveness of the nose-down pitch control.

The remainder of this paper will discuss the problems of pitch departure and deep stall trim as studied during investigations recently conducted at the NASA Langley Research Center of two representative fighter configurations. The studies included low speed wind tunnel tests and real time piloted simulator studies.

The first fighter configuration studied (referred to herein as configuration A) was designed to operate at very moderate inherent levels of pitch instability [static margin (S.M.) = -.04] and incorporated a conventional aft-mounted all-moveable horizontal stabilator for pitch control. The configuration had a moderately-swept wing and a highly-swept wing-body strake to enhance lift and maneuverability at high angles of attack. The second configuration (referred to herein as configuration B) was a close-coupled canard design operated at relatively high levels of pitch instability (S.M. = -.20). Wing trailing-edge elevators, canard-mounted trailing-edge flaps, and an all moveable canard were available for pitch control.

Shown in figure 5 are the neutral-control pitching moment coefficient variations with angle of attack for the two configurations investigated. The data show the modest level of instability exhibited by configuration A in the low to moderate angle of attack range ($\alpha < 20^\circ$) and the very high level of instability for configuration B. The pitchup exhibited by configuration A between 40° and 50° was caused by the highly-swept wing body strake. Above $\alpha = 50^\circ$, the pitching moment broke stable and exhibited a deep stall trim point at about $\alpha = 62^\circ$. The close-coupled canard configuration also had a deep stall trim point, however it occurred at an angle of attack 10° higher than that of configuration A.

The simulator studies were conducted on the Langley differential maneuvering simulator (DMS) facility shown in figure 6 and input data were based on results of wind tunnel force tests in several facilities. The capabilities of the DMS allow thorough evaluation of departure/spin susceptibility characteristics with a pilot in the loop performing maneuvers representative of air combat. A detailed discussion of the techniques used in DMS simulations to assess fighter high- α flight characteristics is given in reference 1.

Results for Configuration A

Pitch Departure

As discussed earlier, the susceptibility of RSS configurations to pitch departures at high angles of attack is a function of the available nose-down moment. Figure 7 shows the increment in pitching moment coefficient produced by full nose-down deflection of the stabilators ($\delta_h = +25^\circ$) for configuration A. The data indicate that a nearly constant level of control effectiveness was maintained up to $\alpha = 25^\circ$. However, above 25° there was a marked loss in nose-down stabilator effectiveness due to stall of these surfaces. These results highlight a basic disadvantage of using aft-mounted pitch controls on RSS configurations in that the critical nose-down control moment required at high angles of attack must be generated by increasing the flow incidence on the surface in attempting to get more lift from the control. Obviously, as α increases the surfaces will stall and nose down control effectiveness is lost at the higher angles of attack where it is most needed.

The control system of configuration A incorporated an angle of attack limiter that attempted to limit the angle of attack to below $\alpha = 25^\circ$. However, if an angle of attack increase above 25° was generated by one or more of the coupling phenomena discussed earlier, figure 7 shows that the amount of nose down control moment available to counteract the nose-up disturbance decreases rapidly so that a departure in pitch would likely ensue. Figure 8 shows an example of such a loss of control situation encountered during the simulation study of configuration A. Shown is an attempted 360° roll using full lateral stick input applied at $\alpha = 25^\circ$ in an accelerated turn. In addition to maximum roll control deflections, maximum coordinating rudder was also obtained to make the airplane roll about the velocity vector. As a result, the body axis roll and yaw rates began to build up rapidly in the direction of the stick input. Initially, α dropped slightly due to kinematic coupling; however as p and r increased the inertia coupling moment caused a significant nose-up pitch rate to build up and α began to increase. At this point, q coupled with p to create a yaw coupling moment which opposed the yaw rate and halted its growth ($t = 14$ sec.); on the other hand, p was still increasing and thus resulted in the kinematic generation of a large amount of adverse β ($t = 15$ sec). By this time, α had increased to above 30° despite the angle of attack limiter system applying full nose down stabilator deflection ($+25^\circ$). The nose-up inertia coupling moment was much greater than the nose-down aerodynamic moment produced by $\delta_h = +25^\circ$; as a result, a pitch departure occurred as the airplane completed about 270° of the roll. During the ensuing loss of control period, α reached a maximum of 68° while β oscillated between $\pm 26^\circ$.

The foregoing results showed that the airplane roll rate capability at high angles of attack was too high to prevent pitch departures with the available pitch control and it was clear that the only means of alleviating the pitch departure problem (other than resizing the control surfaces or further limiting α) was to limit the maximum obtainable roll rates. The degree of limiting required would of course vary with the level of pitch instability. The motions shown in figure 8 were obtained for a nominal c.g. location which resulted in a static margin of $-.04$. The c.g. position was moved fore and aft from this point to determine the effect of pitch stability level on the degree of roll rate limiting required to prevent the inertia coupling pitch departure. The results obtained are summarized in figure 9.

Shown in figure 9 are data for c.g. locations resulting in static margins of $.02$, $-.04$, and $-.10$. As expected, the conventional S.M. = $.02$ configuration did not have an inertia-coupling pitchout problem, and maximum roll rate was limited only by the available roll control. Avoidance of coupled departures for S.M. = $-.04$ required that the roll rate above $\alpha = 20^\circ$ be restricted to values below those which could be produced by the roll control. Comparison to the results obtained for S.M. = $.02$ indicate about a 30% penalty in maximum roll rate was incurred at $\alpha = 25^\circ$ for a static margin of $-.04$. The roll performance penalty rapidly became more severe as the level of instability was increased as indicated by the S.M. = $-.10$ data. At this level of instability, the roll rate had to be restricted above 13° angle of attack such that at $\alpha = 25^\circ$ the maximum allowable roll rate was only about 30% of the value provided by the roll control.

Having documented the susceptibility of configuration A to pitch departures at high angles of attack, an attempt was made to modify the control system to inhibit these departures. The features developed to achieve this goal are summarized conceptually in figure 10. Obviously, an essential element is a roll rate limiter system which inhibits the roll rate from exceeding the critical values indicated in figure 9. Four parameters were used to evaluate what the roll rate limit should be at any instant in time -- dynamic pressure, angle of attack, symmetric stabilator deflection, and roll rate magnitude. Angle of attack was chosen for two reasons: (1) the nose-up inertia coupling moment varies with $\sin 2\alpha$; and (2) the amount of nose-down control moment available to counter the nose-up coupling moment decreases as angle of attack increases. Similar reasoning was used in choosing q . As illustrated in figure 4, the nose-down control moment decreases with q resulting in lower rates of roll that can be sustained before a pitch departure occurs. Symmetric stabilator deflection was chosen because it directly indicates the pitch control remaining to oppose the inertia coupling moment. Finally, roll rate magnitude was used to schedule the total level of limiting imposed. For low roll rates, where coupling is not a factor, no limiting was imposed regardless of the values of the other scheduling parameters. The limiting scheduling was used only when the roll rate magnitude approached significant magnitudes. With this scheme, the initial roll response degradation was minimized and roll performance was compromised only where it was essential to prevent occurrence of the pitch departure.

A second feature was incorporated to minimize the generation of proverse sideslip during rolls at high angles of attack. As discussed earlier, rolling with proverse β will increase angle of attack through kinematic coupling and therefore it is not desirable for RSS configurations for which there is a requirement to maintain the angle of attack below some critical value. Proverse β minimization was accomplished by scheduling the maximum rudder deflection that the pilot could command through his pedals as a function of angle of attack and roll rate magnitude such that at high values of α and $|p|$, no deflection could be commanded. In this situation, the only direct rudder response to pilot inputs came from coordinating rudder commanded by the roll control input and hence no over-coordination of high α rolls was possible.

The final feature incorporated in the control system to inhibit the pitch departure was an inertia-coupling compensator for the pitch axis to assure proper stabilator response during high α rolling maneuvers. The system used angle of attack and roll rate magnitude to drive the pitch control in the nose-down direction to oppose the nose-up coupling moment.

The effectiveness of the above control system design in preventing inertia coupling departures is illustrated in figure 11 which shows a 360° roll using full lateral stick applied at $\alpha = 25^\circ$ in an accelerated turn. As discussed earlier, this maneuver performed with the basic airplane resulted in loss of control (see figure 8). However with the modified control system, the maneuver could be completed. Although the pilot applied and held full roll command, the system began to decrease the roll control deflection as the roll rate approached critical values above which there would not be sufficient nose-down control to oppose the coupling moment. Note that near the completion of the maneuver, only about 25% of maximum roll control deflection was used. Because roll rate was properly limited, the stabilator never reached its maximum deflection and consequently no departure occurred. Angle of attack did not exceed the 25° limit value and the maximum β generated was only 3°.

The question naturally arises as to whether the scheme of limiting roll rate to prevent the pitch departure degrades air combat capability. This issue was investigated during the simulation study by flying the basic and modified airplanes against the same adversary performing recorded maneuvers that were exactly repeatable from run to run. Three separate tracking tasks were used: (1) a steady wind-up turn for assessment of fine tracking ability; (2) a bank-to-bank maneuvering task to assess roll response and controllability; and (3) a complex, vigorous air-combat maneuvering task. Results of this study determined that the roll rate limiting scheme used in the modified airplane flown at the nominal c.g. location resulted in no degradation in air combat effectiveness. On the contrary, the higher level of departure resistance provided by the modifications was found to provide slightly improved tracking while reducing pilot workload and increasing pilot confidence. It should be emphasized, however, that only very moderate reductions in roll rate capability were required at the instability level associated with this c.g. location (see figure 9). Operation at higher levels of instability requiring more drastic roll performance penalties could significantly compromise tactical effectiveness.

Deep Stall

As discussed earlier, the second major high angle of attack control problem introduced by use of the RSS concept is the potential for deep stall trim. Figure 12 summarizes the neutral control pitching moment variation with angle of attack for $-80^\circ \leq \alpha \leq 80^\circ$ for the two configurations studied. As shown previously in figure 5, configuration A exhibited a weak but stable deep stall trim point at $\alpha = 62^\circ$ while configuration B showed a very strong, stable trim at $\alpha = 72^\circ$. Furthermore, examination of the negative α data indicates that stable trim points also existed at $\alpha = -52^\circ$ and $\alpha = -62^\circ$ for configuration A and B respectively. Thus, the deep stall problem existed for inverted as well as erect flight and the severity of the problem increased with increasing levels of static pitch instability.

Because the erect deep stall trim point exhibited by configuration A was comparatively weak, an investigation was conducted during the simulation study to determine if it was possible to fly into a stabilized deep stall. With the basic airplane, two techniques were found for generating a pitch departure which would result in angle-of-attack excursions into the deep stall trim region. The first technique was the coupling departure discussed in the preceding section of this paper. It was found that these departures did not often result in stabilization in the deep stall trim point due to the fact that the motions were violent about all three axes, so that although the trim point was traversed during the out-of-control motions, the angular momentum was enough to overpower the weak static equilibrium. Furthermore, the inertia coupling departures could essentially be eliminated by the control system design discussed earlier. However, a second deep stall entry technique was found which the control system was unable to prevent. The maneuver involved putting the airplane into a steep nose-up attitude, decelerating climb with θ reaching a maximum of about 70° and allowing airspeed to bleed off to about 35 KIAS at the top of the climb. The airplane was then allowed to fall through at essentially 0g. The resulting kinematic generation of a large angle-of-attack excursion could not be effectively opposed by the pitch control due to lack of control effectiveness at the very low levels of dynamic pressure involved. An example of such a maneuver is shown in figure 13.

The data of figure 13 show that, at the top of the maneuver, the airspeed and normal acceleration decreased to $M = 0.1$ and $0.1g$, respectively. As the airplane fell through, the angle of attack increased to 70°, despite the application of full nose-down control. After several cycles of oscillation, the airplane stabilized in a deep stall with $\alpha = 58^\circ$, $\phi = 0$, and $a_n = 1g$. The milder motions (low angular rates) obtained with this technique resulted in many more departures locking into the deep stall trim point.

Once it was determined that the airplane could be flown into the deep stall, techniques were developed for recovery. Several schemes were investigated for obtaining the needed nose-down pitching moment, involving such procedures as using flap reconfiguration and speedbrake extension. These techniques generated only very small nose-down pitching-moment increments at the deep stall angles of attack and therefore were not consistently effective in providing recovery.

Examination of the pitch control effectiveness in the deep stall region prompted an investigation into an additional recovery technique. The data showed that at the deep stall trim point ($\alpha = 60^\circ$), a comparatively large pitching-moment increment ($\Delta C_m = 0.1$) resulted from full nose-down to full nose-up control deflection. Thus, a possibility existed to use this available control moment to initiate and buildup a pitch oscillation by moving the control stick in phase with the airplane motions with the hope that sufficient angular momentum in pitch would be created during a downswing cycle to drive the airplane angle of attack down to the normal α envelope of the airplane.

A recovery attempt using this technique is shown in figure 14. Starting from a stabilized deep stall at $\alpha = 62^\circ$, the pilot applied full aft stick at $t = 71.3$ sec. The resulting nose-up moment caused α to increase to 75° at which point the pilot reversed his controls and applied full forward stick. About 14°/sec nose-down pitch rate resulted and the associated angular momentum was sufficient to cause the

airplane to continue to pitch downward until a recovery was obtained at $t = 78$ sec. It should be noted that in this particular case, the pilot very accurately kept his inputs in phase with the motions and therefore obtained a recovery within one oscillation cycle. However, it was found that in situations where the pilot was somewhat out of phase with the oscillation, recoveries were delayed significantly. Nevertheless this technique was found to be consistently effective in providing recoveries from the erect deep stall trim exhibited by configuration A.

Results for Configuration B

Pitch Departure

The high α pitch control problems discussed for configuration A would be expected to be more severe for configuration B due to the much higher level of pitch instability involved (Figure 5). As discussed earlier, three pitch control devices were wind-tunnel tested on this configuration: wing-mounted elevators, canard-mounted trailing-edge flaps, and a variable-incidence canard. Figure 15 shows the nose-down effectiveness of these controls in terms of the variation of pitching-moment increment with angle of attack. Data for the wing-mounted elevators deflected full nose-down ($+30^\circ$) indicate a steady decline in effectiveness with increasing angle of attack such that the effectiveness is zero at $\alpha = 39^\circ$ and actually reverses at higher α . The canard-mounted flaps deflected to -40° are seen to be less effective than the elevator below 10° angle of attack. Their effectiveness are about equal in the $10^\circ \leq \alpha \leq 25^\circ$ range; however, above $\alpha = 25^\circ$ the data show that the canard flaps maintain their effectiveness to about 10° higher angle of attack than the elevators. Referring back to the neutral control data for configuration B shown in figure 5, it is seen that the moment increments provided by either the elevators or canard flaps are clearly inadequate to allow controlled flight at high angles of attack; no net nose-down aerodynamic moment can be generated by either control for $\alpha > 12^\circ$.

Because the pitch instability of this canard configuration is caused by the lift produced by the canard far forward of the c.g., it is obvious that an effective means of obtaining nose-down moments is to unload the canard itself. The question remains, however, as to how much canard deflection is required to provide sufficient pitch control to allow safe and effective maneuvering at high angles of attack. Data are shown in figure 15 for deflections of -15° and -45° . The $\delta_c = -15^\circ$ data show a near constant effectiveness up to $\alpha = 20^\circ$. There is a steady decline in effectiveness at higher α , particularly above $\alpha = 35^\circ$ such that no nose-down increment is produced for $\alpha > 60^\circ$. The $\delta_c = -45^\circ$ data indicate a very high level of effectiveness up to $\alpha = 35^\circ$ followed by a steady decline with further increases in angle of attack. Note, however, that some nose-down moment increment is produced, even at $\alpha = 80^\circ$. Again, referring back to the neutral control data shown in figure 5, it is seen that -15° of canard deflection allows controlled flight up to at most $\alpha = 20^\circ$ above which no net nose-down static moment can be generated. On the other hand, the data indicate that -45° of canard deflection should be sufficient to allow controlled flight up to very high angles of attack in that net nose-down static moments can be generated with $\delta_c = -45^\circ$ up to $\alpha = 30^\circ$ and higher.

The high angle-of-attack pitch-departure resistance provided by the three pitch control schemes discussed above are summarized in figure 16 in terms of the maximum roll rate that can be sustained before the inertia-coupling pitching moment exceeds the available nose-down aerodynamic moment. The calculations were made based on the assumption of $1g$ level flight. As expected, the data for canard flap and elevator show that use of either of these surfaces alone did not allow any maneuvering at all above about 12° angle of attack. The situation was improved somewhat if -15° of canard deflection was used in that some roll rate capability was available up to $\alpha = 20^\circ$. It should be noted, however, that limiting the airplane to 20° angle of attack was rather restrictive from a performance viewpoint in that maximum lift occurred near $\alpha = 35^\circ$. Only with the very large canard deflection of -45° did the data indicate that the airplane could be maneuvered effectively at angles of attack up to and beyond maximum lift.

Although a detailed simulator study of configuration B was not conducted, it is apparent that the unique canard arrangement offers high potential for pitch departure resistance as a result of high levels of available aerodynamic pitch control if the canard is of the variable incidence type with large travel and high angular rate capability.

Deep Stall

The pitch oscillation deep stall recovery technique discussed for configuration A would not be expected to be as effective for configuration B due to the much stronger deep stall trim point (figure 12) and the fact that it occurred at a higher angle of attack ($\approx 72^\circ$) where aerodynamic control effectiveness would be further degraded.

Thus, the approach followed was to determine if any of the available pitch controls could provide sufficient nose-down moment for recovery. It is clear from the previous discussion of the characteristics of the elevator and canard flap that their usefulness in the deep stall region would be minimal in that their effectiveness degrade to essentially zero in the 35° to 45° angle-of-attack range. Again, unloading the canard was clearly the most effective technique. Figure 17 indicates the magnitude of canard deflection required to recover from both the erect and inverted deep stall trim points. Plotted are the variations of C_m with α for $\pm 30^\circ$ and $\pm 45^\circ$ canard deflections. The data show that $\pm 30^\circ$ of deflection is not sufficient to eliminate either the erect or the inverted trim points. Only with canard deflections of $\pm 45^\circ$ can recovery from the deep stall be achieved. It is interesting to note that in the earlier assessment of departure susceptibility, it was found that canard deflections on the order of 45° were also needed to allow effective high α maneuvering. It should be noted, however, that the requirement for such large canard deflections may present severe implementation problems from an actuation viewpoint in terms of control travel and rates.

SUMMARY

The use of the CCV concept of relaxed static pitch stability on fighter configurations can result in rather demanding stability and control problems at high angles of attack. The two major problems are: (1) pitch departure susceptibility caused by inertia and/or kinematic coupling, and (2) deep stall trim. To address these problems, the pitch control system for such configurations must have sufficient control for: (1) prevention of pitch departures due to coupling to avoid roll performance penalties, and (2) deep stall trim prevention or recovery capability. With regard to these requirements, the effectiveness of aft-mounted controls are limited in that the critical nose-down moment required at high angles of attack must be generated by increasing the angle of attack on the surface in attempting to get more lift from the control. As α increases the surfaces will stall prematurely and nose-down control effectiveness is lost at the higher angles of attack where it is most needed. Similar disadvantages are encountered with trailing-edge surfaces such as canard-mounted flaps or wing-mounted elevators. A variable incidence canard with a large travel range is an effective means of obtaining the needed level of high α pitch control since nose-down moments can be generated by unloading the canard.

11-7

For situations where it is not feasible to obtain sufficient control to prevent pitch departures and deep stall trim under all conditions, the control system can be designed to alleviate these problems. Roll rate limiting control laws are effective in inhibiting departures caused by inertia coupling; however, excessive limiting will degrade maneuverability. Other features that enhance resistance to pitch departure include minimization of proverse β during high α rolls and pitch axis roll-coupling compensation. With regard to the deep stall trim problem, the control system should be designed to allow the pilot to most effectively use the oscillation technique to obtain recovery. The effectiveness of this technique, however, is a direct function of proper input timing by the pilot; furthermore, the technique may not be successful even with optimum pilot inputs for configurations which exhibit strong trim points or which have ineffective pitch control at the deep stall angle of attack.

REFERENCES

1. Gilbert, William P.; and Nguyen, Luat T.: Use of Piloted Simulation for Studies of Fighter Departure/Spin Susceptibility. Presented at AGARD Flight Mechanics Panel Specialists' Meeting on Piloted Aircraft Environment Simulation Techniques, Brussels, Belgium, April 24-27, 1976.

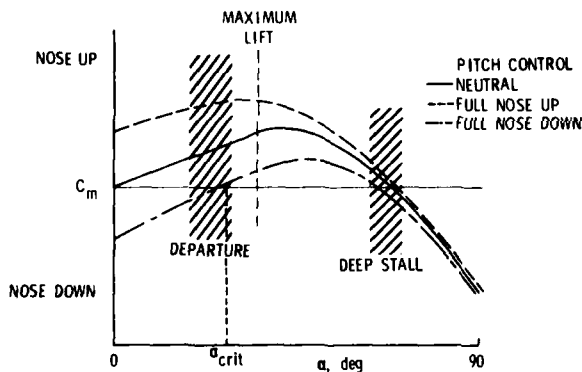
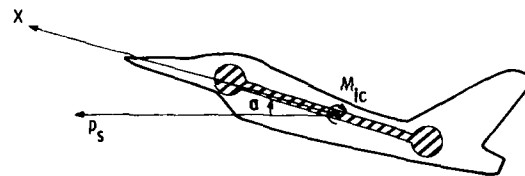


Figure 1.- Pitching moment variation with α for idealized RSS configuration.



(a) pitching moment created by roll and yaw rates.

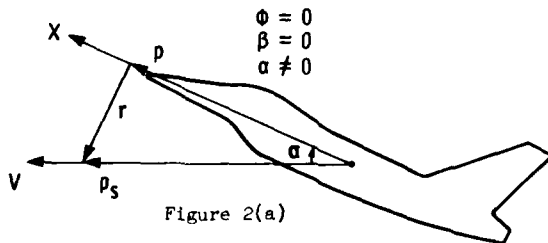


Figure 2(a)

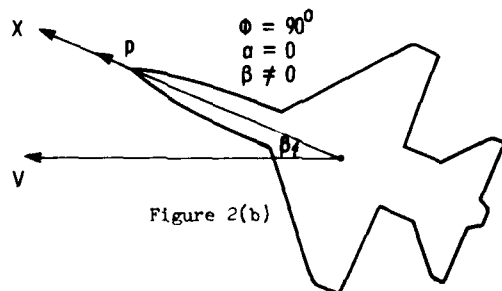
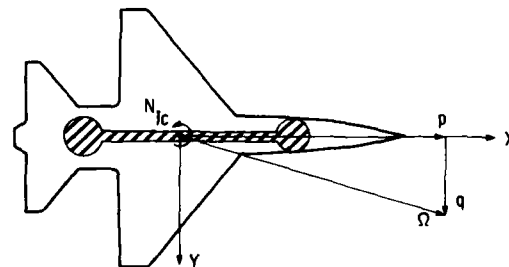


Figure 2(b)

Figure 2.- Illustration of kinematic coupling of angle of attack and sideslip.



(b) yawing moment created by roll and pitch rates.

Figure 3.- Illustration of inertia coupling phenomena.

11-8

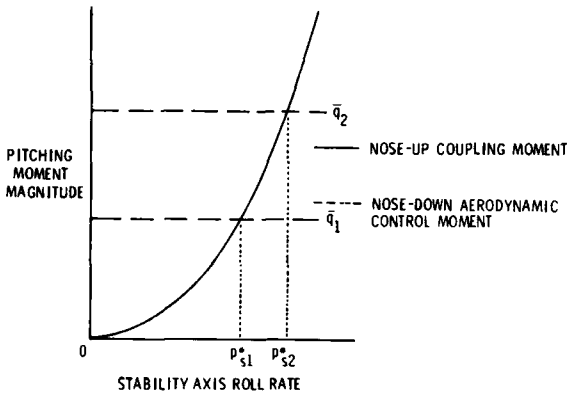


Figure 4.- Comparison of inertia coupling moment for increasing roll rate with available aerodynamic pitch control moment at two values of dynamic pressure.

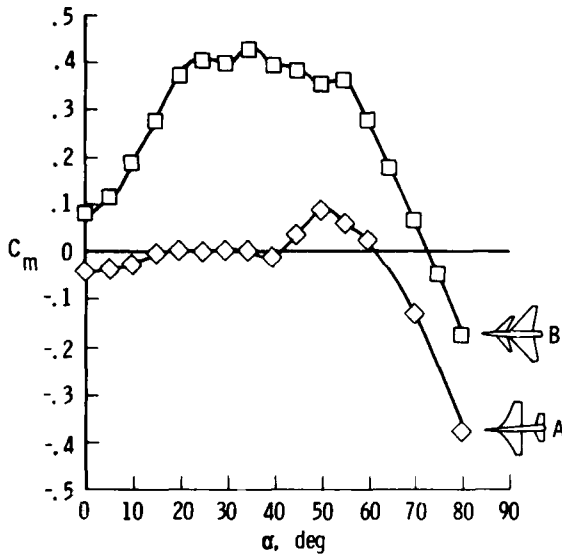


Figure 5.- Variation of neutral control pitching moments with α for the two study configurations.

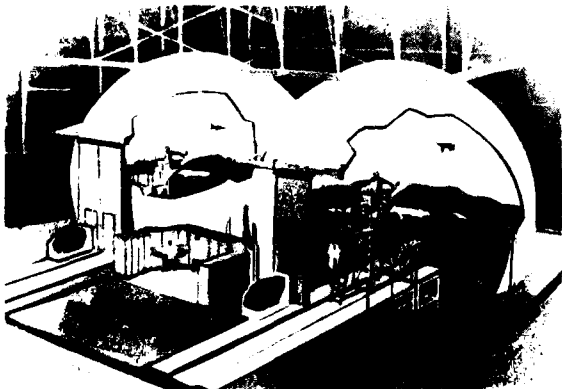


Figure 6.- General arrangement of the Langley differential maneuvering simulator (DMS) facility.

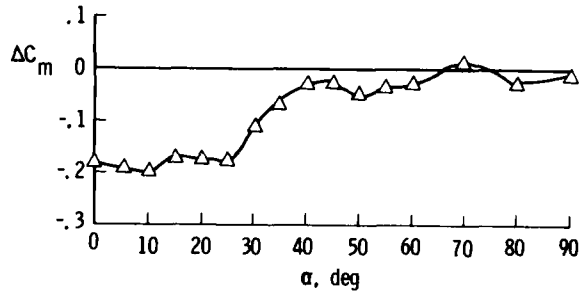


Figure 7.- Incremental pitching moment obtained with full nose-down stabilator deflection on configuration A.

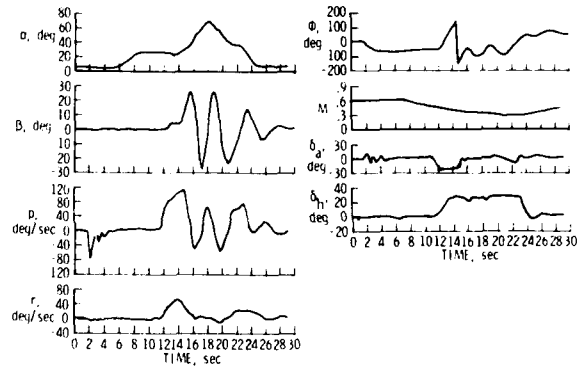


Figure 8.- Pitch departure for configuration A during 360° roll attempt.

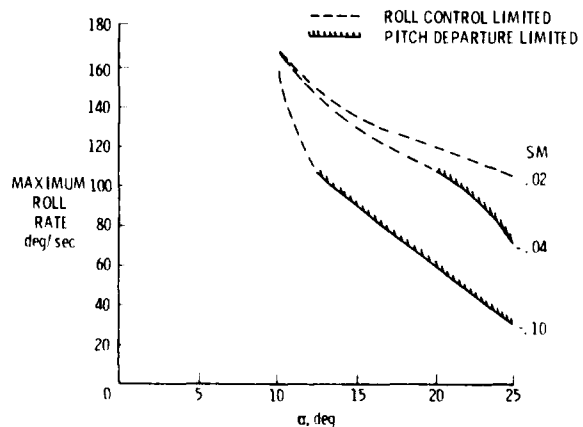


Figure 9.- Variation with α of maximum sustainable roll rates during lg, 360° rolls for various levels of static margin (Configuration A).

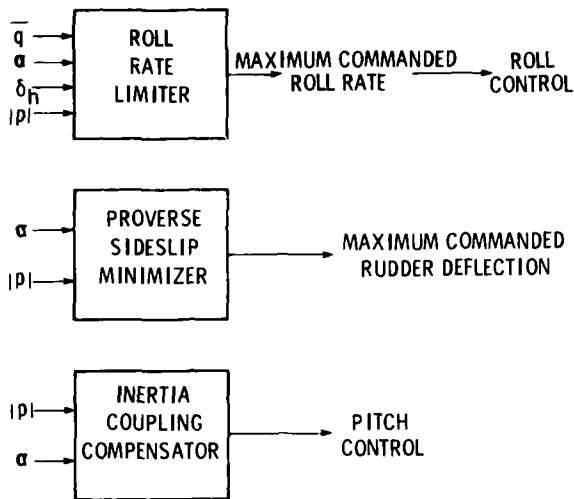


Figure 10.- Conceptual schematic of control system features designed to inhibit high- α pitch departures for configuration A.

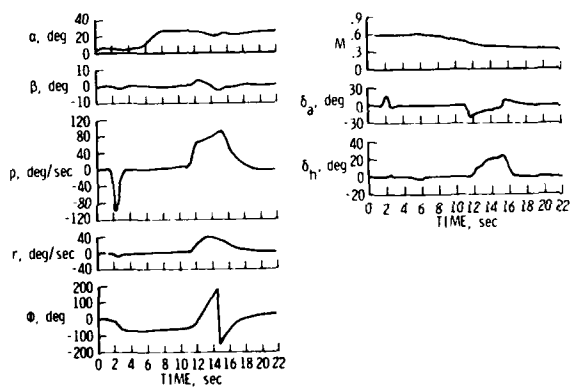


Figure 11.- 360° roll using full lateral stick input applied in an accelerated turn at $\alpha=25^\circ$ (Configuration A, modified control system).

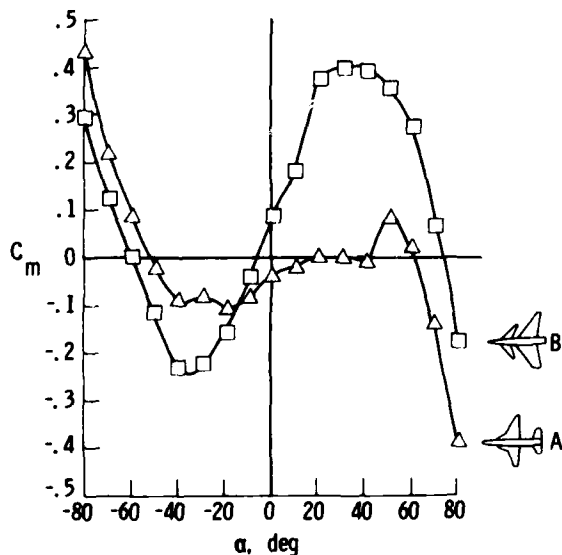


Figure 12.- Variation of neutral control pitching moments with α for the two study configurations.

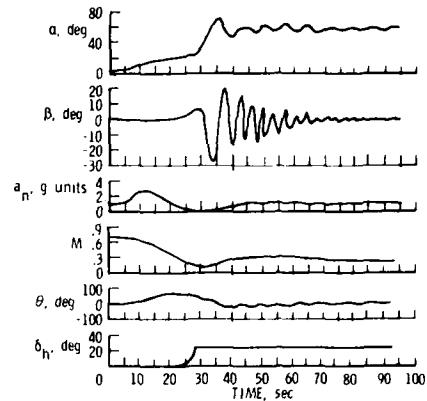


Figure 13.- Time histories of deep stall entry (Configuration A).

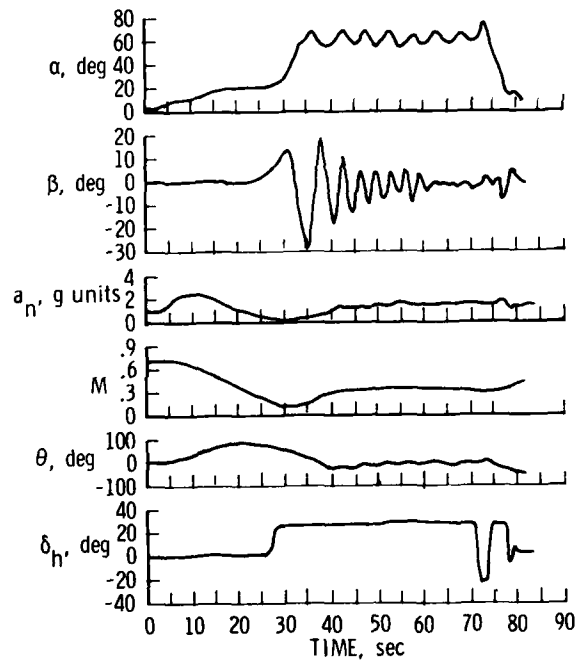


Figure 14.- Time histories of deep stall recovery using pitch oscillation technique (Configuration A).

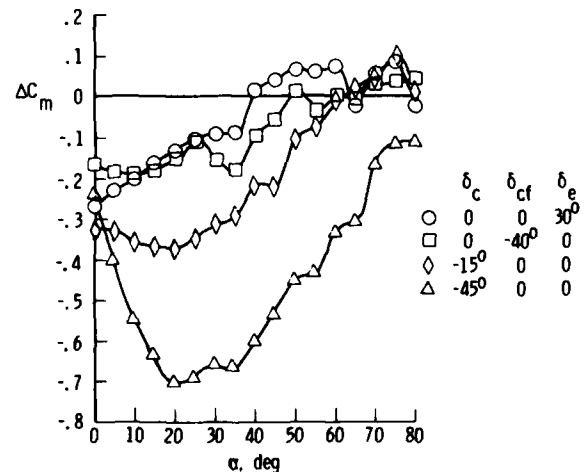


Figure 15.- Incremental nose-down pitching moments obtained with elevator, canard flaps, and total canard deflections (Configuration B).

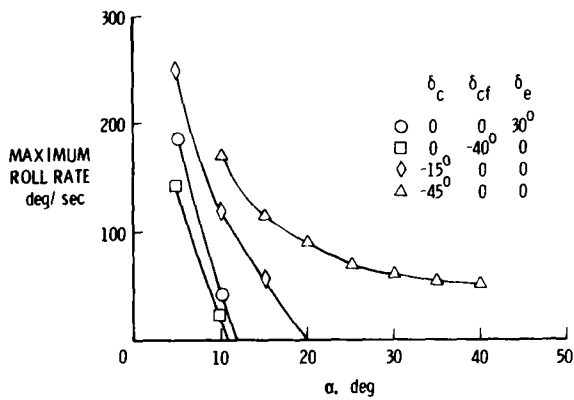


Figure 16.- Variation with α of maximum roll rates that can be sustained during lg rolls for various pitch control schemes (Configuration B).

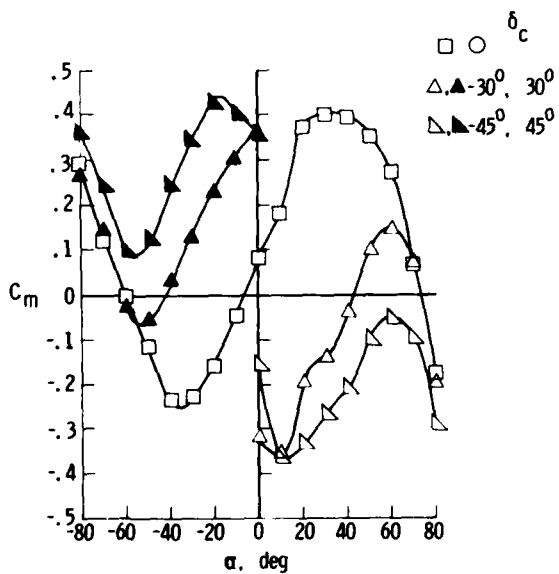


Figure 17.- Variation of pitching moment with α for various total canard deflections (Configuration B).

FIN DESIGN WITH A.C.T. IN THE PRESENCE OF STRAKES*

by D. J. Walker, British Aerospace, Brough

12-1

1. SUMMARY

Aerodynamic behaviour of the fin can limit the high incidence capability of an aircraft, especially so with the development of straked wings capable of producing useful lift at very high incidences. Wind tunnel tests on a combat aircraft model are reported in which the effect of fin size and various types of fin controls were investigated. The results indicate that a rudder (rather than an all moving fin) using A.C.T. is probably the best solution for incidences of up to about 50° . Also the use of such a system would allow a 20% reduction in the size of the basic fin.

2. INTRODUCTION

It is probably true to say that the fin has not received the (research) attention it deserves when one considers the numerous development problems and accidents that have occurred as a result of inadequate initial design. It can be argued that the fin is a relatively easy surface to modify as a result of initial flight trials - this has happened on many occasions - but this can be costly and may involve the loss of an aircraft.

Traditionally fins were designed to give adequate directional stiffness and damping up to, by today's standards, only moderate incidences. The loss of fin effectiveness at supersonic speeds dominated the fin design for that class of aircraft. However, the aspect designing the fin of today's fighter is the ability to provide sufficient stability and control during the high incidence manoeuvres of which the aircraft is potentially capable (see Fig. 1). The trend towards more "g" and more S.E.P. means that these incidences can be generated at high subsonic Mach Nos. What then, could be a more difficult design case - transonic Mach No. and separated flow!

A large body contribution to lift has been a feature of existing aircraft capable of very high incidences and this same body has in some cases allowed a twin fin solution. There is today a trend towards the light-weight fighter relying on its strake and variable camber wing to provide the lift at high incidence (and maybe strong vortices impinging on the fin!). It is this type of aircraft which is considered in this paper - there is no sensible twin fin solution (even if one were desirable) and thus only the single fin has been considered here.

To gain the most out of an engine the aircraft's weight and wetted area must be kept as low as possible - extra fin area and weight is most undesirable. Careful design and active control technology (A.C.T.) are seen as ways of achieving this objective.

This paper presents the results from a series of wind tunnel tests of fin (and rudder) effectiveness on an aircraft with strakes, and indicates the way in which A.C.T. can assist.

3. WIND TUNNEL TESTS

3.1 The Model

B.Ae. Brough has been responsible for the manufacture and testing of a 1/28th scale S.M.A.R.M. (Small Military Aircraft Research Model) - Figs. 2 and 3 refer - primarily to support advanced wing design but also for a variety of stability and control tests.

The tests reported here are for an early standard of wing design but incorporating up to 15° of leading edge flap, and a symmetric (as opposed to cambered) strake. The Reynolds number is 1.3×10^6 based on wing S.M.C., with a Mach No. of 0.85 limited to 0.6 at the higher incidences.

3.2 Longitudinal Results

The lift and pitching moment results shown in Fig. 4 suffice to show the potential beneficial effect of strakes. Although there is a relatively large change in stability with strakes at high incidence, there are no violent discontinuities. Given the tail power, these high incidences should be within the capabilities of an A.C.T. system.

3.3 Dynamic Pressure Study

A rake with a total of 48 holes, each able to provide a measurement of the dynamic pressure in a predominantly fore and aft direction was attached to the rear of the model immediately behind the fin location.

These pressure measurements, originally intended to provide a guide to the dynamic pressure in the region of the fin, also clearly identify the position of the strake vortices. Fig. 5 shows the growth of the strake vortices with incidence and at an incidence of 35° the effect of increasing sideslip is shown, (without the fin) in Fig. 6. Fig. 7 shows the effect of the fin at 15° sideslip for 21° and 35° of incidence. The fin has apparently little effect on the vortex at 35° but at 21° there is a marked change in the vortex pattern.

Correlation with overall forces will be discussed below.

* Prepared for the AGARD Symposium "Aerodynamic Characteristics of Controls", Naples, May, 1979.

3.4 Fixed Fin Results

12-2
Two sizes of fins were tested and the overall forces and moment derivatives due to sideslip are shown in Fig. 8. Note that the larger fin produces, of course, a significantly larger N_v than the smaller fin. At low incidences the 47% increase in fin effectiveness is consistent with a 40% greater area and a larger aspect ratio - and even without A.C.T. is probably too large for this aircraft. However, its benefit emerges at high incidence where the increase in fin effectiveness is 100% greater than for the smaller fin ensuring a positive N_v up to 37° , compared with about 27° for the smaller fin. Similar benefits are shown in Fig. 9 at sideslip angles of about 15° , but as expected N_v is considerably smaller than at low sideslip angles.

The effectiveness of the top of the fin can also be seen by examining the results of the dynamic pressure survey. Fig. 10 shows (though not as positively as expected) that the top of the fin is the last to lose effectiveness.

It should be noted that fin-off, zero sideslip pressure surveys can give a good indication of fin behaviour with incidence.

3.5 Moving Surfaces Results

These cover rudder, all moving fin and differential tailplane. The tests were devised with a view to assessing their relevance to the design philosophy of the fin. The scarcity of published data on such tests has been noted.

Physical restraints on the model permitted only small control angles on the fin and differential tailplane but angles of up to 30° were tested for the rudder.

Figure 11(a) compares their effectiveness at zero sideslip and for small displacements. The results are as may be anticipated with the fin half as powerful again as the rudder until they both lose their effectiveness completely at about 50° of incidence. Also shown is the yawing moment due to differential tailplane. Although primarily considered to be a roll producer at transonic speeds, there is a potentially useful but small source of yawing moment at very high incidence. Body axis results are also shown since these give a better indication of its use as a control device. Fig. 11(b) gives a more detailed look at the behaviour of the rudder over the range of incidence and control angles tested. Note the usefulness of the rudder at CLMAX but following the trend indicated in the previous figure, this is greatly diminished at 52° of incidence.

4. IMPLICATIONS OF ACTIVE CONTROLS

4.1 Conventional Stability Criteria

This report is constrained to consider only a simplistic view of stability since tests have not been carried out to determine damping derivatives. However one apparently suitable criterion that can be applied is to determine when the "dynamic N_v " ($= N_v \cos \alpha - \frac{1}{T_a} L_v \sin \alpha$) tends to become negative, indicating a tendency to departure in yaw.

Fig. 12 compares dynamic N_v for the two fins at both low and high sideslip values. The curve follows the same shape as those for the basic N_v but the difference between the two fins in terms of achievable incidence is more than halved at low sideslip. This is due to the magnitude of L_v being largely determined by the wing at high incidence.

4.2 The Effect of Active Tail Surfaces

An A.C.T. system can fairly easily give additional stability and control provided that:

- (a) Sufficient aerodynamic control power exists
- (b) There is no major discontinuity in the aerodynamics of the control surface

Regarding (a), Fig. 13 shows how much sideslip can be trimmed in wings level flight (maybe this is slightly unrealistic but it is a guide and offers a ready comparison of the control surface powers). It is assumed that the rudder can deflect 30° but the fin to only 15° because of design and structural problems. The rudder can accommodate half as much sideslip again as the fin throughout the incidence range, with both losing their effectiveness at 45° - 50° of incidence.

Although aerodynamic forces always lose their linearity at large incidences or control deflections no unmanageable discontinuities were discovered during these tests. However it is quite conceivable that if smaller sideslip increments had been tested then some discontinuities would emerge. From the flow survey tests reported earlier the sideslip angle at which the strake vortex is likely to unfavourably interfere with the fin has been deduced and superimposed on Fig. 13. There still remains available a generous sideslip range in which to manoeuvre. That this itself varies with incidence - and indeed will vary with Mach. No. - presents no major problem since the A.C.T. system can provide a scheduled boundary beyond which the aircraft will not be expected to fly in a controlled manner.

5. FINAL COMMENTS

The object of these tests was to provide aerodynamic data for the design of the lightest,

smallest and cheapest fin capable of providing sufficient stability and control over the whole flight envelope. (Although take off and landing is another important area - it is the subject of current tests - the incidences reached are not expected to be as high as during combat). The results suggest the following conclusions:

1Q-3

- (a) If directional stability and control is required at and beyond C_{LMAX} the fin has to be sized for this condition.
- (b) A high fin is essential because the root is likely to be in an area of low dynamic pressure.
- (c) To operate at these high incidences A.C.T. can allow a reduction in fin size, typically by 20% (Fig. 14 refers).
- (d) A fixed fin with rudder is considered to be a 'better solution than an all moving fin because it not only offers more aerodynamic control but is simpler and less weighty to engineer.
- (e) Although the strake vortex may produce some undesirable discontinuities in control effectiveness at high incidence and sideslip, there is considered to be adequate sideslip in which to manoeuvre, particularly if assisted by an A.C.T. manoeuvre limiting system.

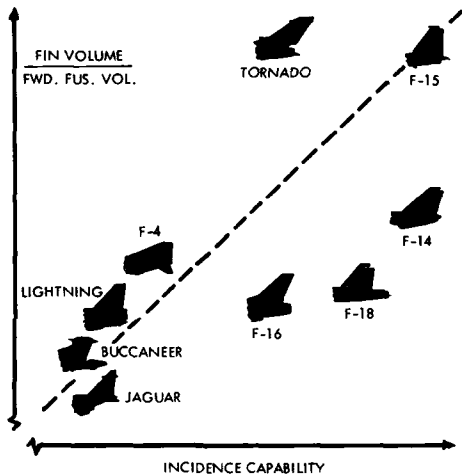


Fig.1. FIN GROWTH WITH INCIDENCE CAPABILITY

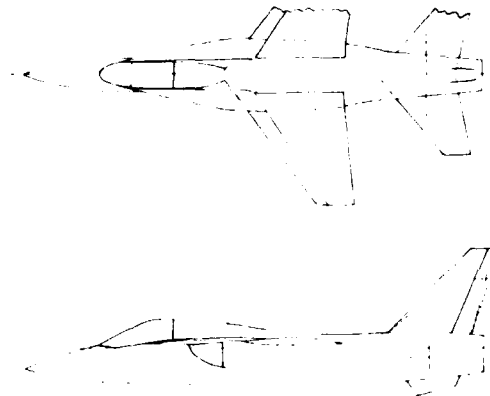


Fig.2. SMARM II WIND TUNNEL MODEL



Fig.3. SMARM II HIGH INCIDENCE TESTING

SOLID LINE - STRAKE + 15° LE FLAP
 DASHED LINE - NO STRAKES OR FLAP

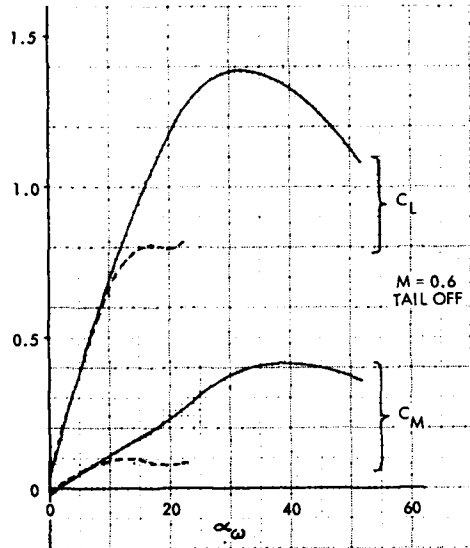


Fig. 4. TYPICAL SMARM C_L/C_M V α CURVES

KEY — POSITION OF PROJECTED STRAKE
 + POSITION OF PROJECTED WING TIP
 TAKING INTO ACCOUNT THE EFFECTS
 OF INCIDENCE AND SIDESLIP, AS SEEN
 AT FIN TIP TRAILING EDGE, LOOKING
 AFT.
 NUMBERS ARE THE DYNAMIC PRESSURE
 COEFFICIENT

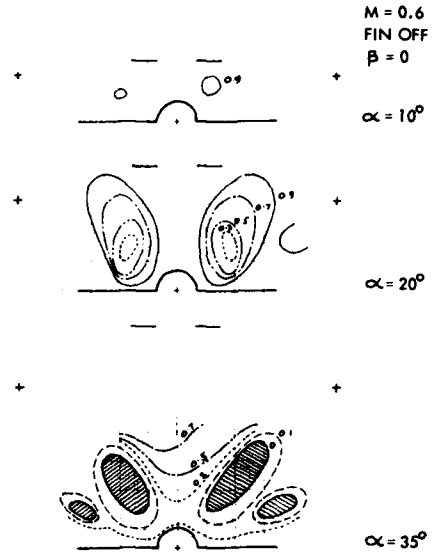


Fig. 5. DYNAMIC PRESSURE SURVEY
 - EFFECT OF INCIDENCE

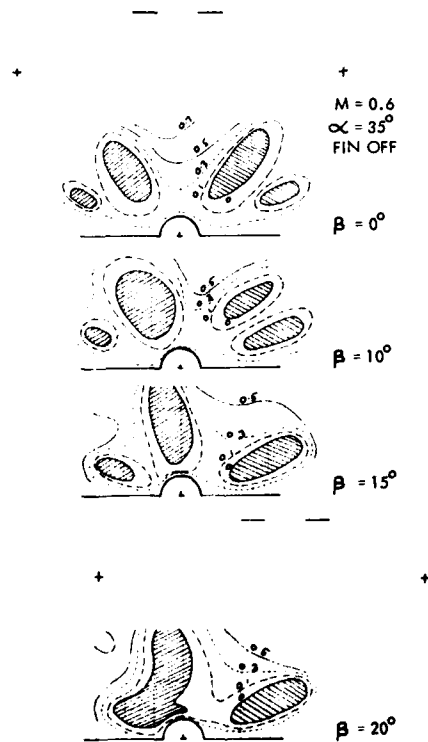


Fig. 6. DYNAMIC PRESSURE SURVEY
 - EFFECT OF SIDESLIP

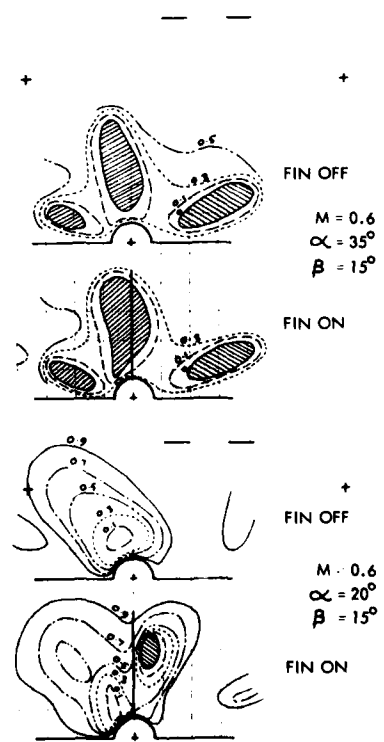


Fig. 7. DYNAMIC PRESSURE SURVEY
 - EFFECT OF FIN

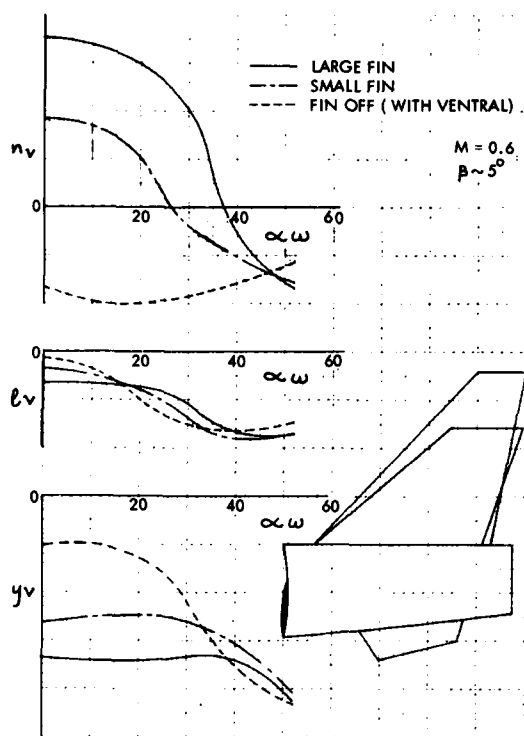


Fig. 8. DIRECTIONAL STABILITY - FIN VARIANTS

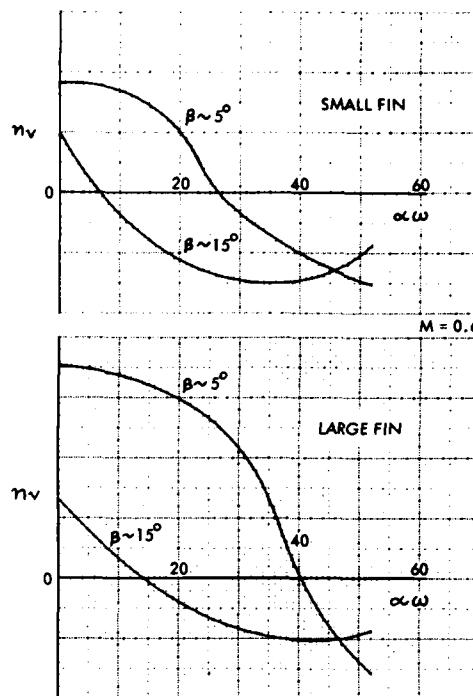


Fig. 9. DIRECTIONAL STABILITY - EFFECT OF SIDESLIP

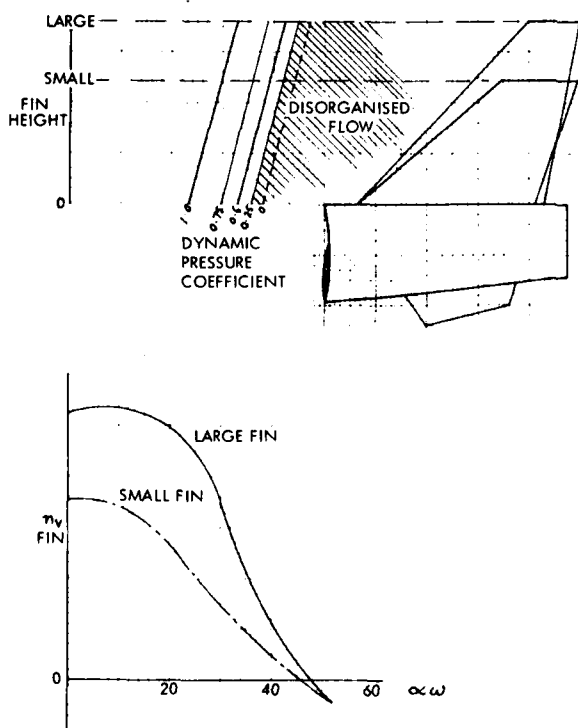


Fig. 10. CORRELATION OF DYNAMIC PRESSURE AT FIN OVERALL FORCES

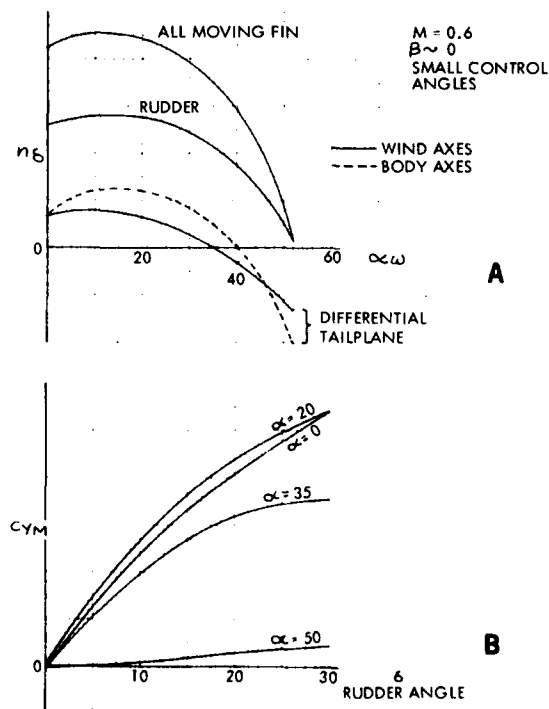


Fig. 11. YAWING EFFECTIVENESS WITH VARIOUS CONTROLS

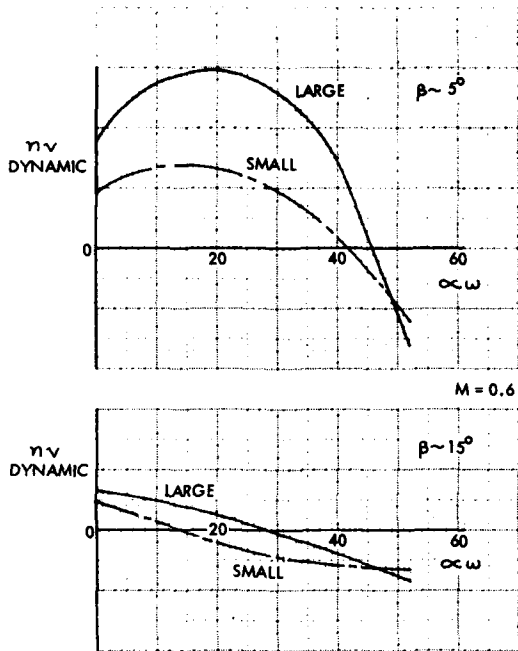


Fig. 12. EFFECT OF FINS AND SIDESLIP ON N_v DYNAMIC

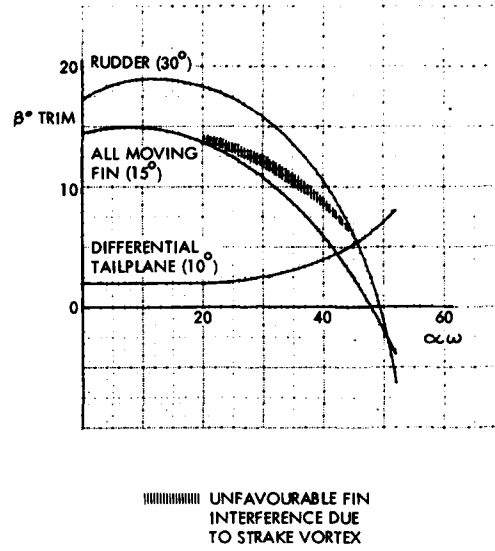
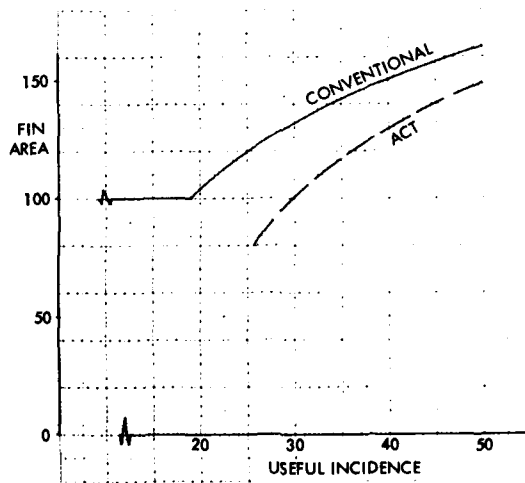


Fig. 13. MAXIMUM TRIMMABLE SIDESLIP



"FIN AREA" assumes height is the major parameter
 "CONVENTIONAL" assumes limited authority autostab, etc.
 "ACT" assumes full authority rudder, etc.
 "USEFUL INCIDENCE" allows moderate manoeuvring in sideslip

Fig. 14. EFFECT OF ACT ON FIN SIZE.

CONTROL INTEGRATION TECHNOLOGY IMPACT

By

Charles A. Scolatti
McDonnell Aircraft Company
P.O. Box 516
St. Louis, MO 63166 USA

13-1

SUMMARY

This paper presents some of the essential elements of an integrated technology development program. The integrated flight and fire control system programs, called IFFC I/FIREFLY III (or IFFC as a shorter acronym), is used as an example. The operational relevance of the example will be discussed briefly. The major problems in air-to-ground attack, and the introduction of maneuvering weapon delivery (with IFFC mechanization required to achieve bombing solutions), are covered. The impact of this IFFC technology, and its extension on other areas of technology, such as aerodynamics, is indicated.

LIST OF SYMBOLS/ABBREVIATIONS/ACRONYMS

AFAL	Air Force Avionics Laboratory
AFFDL	Air Force Flight Dynamics Laboratory
B	Baseline (subscript)
CCV	Control Configured Vehicle
CEP	Circle Error Probable
E	East
FIREFLY III	Fire/Flight Control Phase III
h	Altitude
IFFC	Integrated Flight and Fire Control
IFFC I	Integrated Flight and Fire Control Phase I
LOS	Line of Sight
M	Mode (Bombing) (subscript)
N	North
PACT	Precision Aircraft Control Technology
P_S	Probability of Survival
SFCS	Survivable Flight Control System
WL	Pilot Workload

1. INTRODUCTION

Operational requirements provide the importance and basis necessary to define, develop, and demonstrate fighter or attack aircraft technology concepts. The technological concept to be pursued, on the other hand, must be based on such factors as relative performance improvements, technological timeliness, and feasibility (including affordability). Therefore, whether the technology concept involves a single discipline technology, or a combination of technologies to form a technology set, the reason for its importance and subsequent execution must be fundamentally based on operational need and technological opportunity.

The AGARD paper by Johannes and Whitmoyer (1) provides some specific cases which emphasize the merging of flight control and aerodynamic disciplines and establish the fundamental interdependent relationships. Using the case for integration of flight and fire control (IFFC) systems, for example, the technologies primarily involved are flight control and avionics. The operational need is established on the basis of improving "the combat effectiveness of all tactical aircraft" (1).

2. OPERATIONAL RELEVANCE

The IFFC program is a partial answer to an operational need for tactical air warfare. Major General Maxson (2) presents a mission analysis for air-to-ground attack which provides an excellent beginning point for establishing the operational need for the development of the IFFC program. Mission area analysis and planning formalizes

13-2

with air-to-surface (air-to-ground) attack missions. The tasks in air-to-ground attack missions in Reference 2 were weighted sequentially with respect to each mission segment, beginning with availability of, and ending with the landing of, the attack aircraft.

If the assumption is made that the necessary equipment; personnel; munitions; POL; navigation; command, control, and communications; and take-off and landing requirements are met and performed successfully, then the remaining major combat tasks can be re-grouped and residually weighted as shown in Figure 1. While IFFC has a key role in all three of the remaining major combat tasks, the primary discussion that follows will focus on two of these tasks; namely, survivability (in the target area) and effective ordnance delivery on the target (weapon delivery accuracy).

MAJOR COMBAT TASK	RESIDUAL WEIGHTING
SURVIVABILITY	0.42
TARGET ACQUISITION, CLASSIFICATION, AND IDENTIFICATION	0.23
EFFECTIVE ORDNANCE DELIVERY ON TARGET	0.35
TOTAL	1.00

OP79-0406-7

FIGURE 1
AIR-TO-GROUND ATTACK
MISSION MAJOR COMBAT TASKS

Cost is a prime factor, whether in terms of integrated logistics (acquisition cost, training cost, life cycle cost) or combat cost effectiveness. Conventional ordnance weapon delivery cost factors can be summarized for the air-to-ground attack mission for a medium to high threat environment as shown in Figure 2.

ORDNANCE	LOGISTICS COST	TRAINING COST	COMBAT COST EFFECTIVENESS
UNGUIDED	LOW	LOW	LOW
GUIDED	HIGH	HIGH	HIGH

FIGURE 2
RELATIVE COST FACTOR RELATIONSHIPS OP79-0406-8

Combat cost effectiveness includes such factors as: the ability to deliver ordnance accurately on the target; and survivability, in a medium to high threat environment. In all cases, it is assumed that equal countermeasures are employed. The low combat cost effectiveness of unguided conventional ordnance is primarily associated with lower than acceptable levels of survivability. The main advocacy argument for guided ordnance (3) is weapon delivery accuracy with survivability.

With unguided ordnance, operational tactics are needed to reduce the vulnerability of the attacking aircraft in the target area. Even though attacking aircraft may have an inherently high accuracy for delivering conventional unguided ordnance, tactical procedures are tailored to minimize or prohibit unwarranted time exposure to the ground-to-air threat in the target area. While reduction in exposure time increases the probability of survival, it also decreases the probability of target damage or kill.

The criterion then is to search for a lower cost solution which provides combat cost effectiveness. Air-to-ground attack missions combat cost effectiveness factors of high value include, but are not limited to:

- o Ordnance delivered on targets accurately;
- o Highly survivable weapon delivery modes;
- o Minimum number of aircraft, equipment, and personnel; and
- o Lowest possible cost.

While bullets, bombs, and rockets are included in the general listing of unguided conventional ordnance, for this paper the discussion is limited to bombing missions in a high threat environment. Some of the important criticisms that have been made against the delivery of unguided bombs on targets in a high threat environment 13-3 are as follows:

- o Takes too much time to achieve solutions;
- o Long exposure increases vulnerability to unacceptable levels;
- o The accuracy after a short-time solution is too low; and
- o The missions can only be successfully accomplished by a small fraction of the attacking force because of the high skill levels required in this high workload condition.

The problem then is to identify the cause and effect of each criticism and to derive means for improving or minimizing these critical elements, as appropriate, for effective delivery of bombs. If the means and improvements are successful, the solution raises the combat cost effectiveness of delivering unguided bombs to a level competitive with guided weapons and lower in overall cost since unguided ordnance has lower logistics and training costs.

3. IFFC I/FIREFLY III PROGRAM

The precursor programs noted in Reference 1 (such as the SFCS F-4 program, the CCV/PACT F-4 program, and the A-7D Digital Multimode Program) provide much of the basis for the technological feasibility and opportunity to exploit the IFFC technology. The explicit extension of this IFFC example into the elements of the operational requirements and the case for IFFC on conventional tactical aircraft has surfaced some yet to be resolved problems identified for the field of aerodynamics.

One of the major thrusts of the AFFDL and AFAL IFFC I/FIREFLY III program (1) is to flight demonstrate accurate bombing using maneuvering-aircraft/weapon-delivery profiles for increased survivability. The pilot workload is reduced and accuracy and survivability are improved by using a coupled flight and fire control system. The accuracy is improved by using an electro-optical sensor/tracker from the FIREFLY-III program. The sensor/tracker produces a continuously updated flow of data for the target state and relative position with respect to the attack aircraft. In turn, the inherent capabilities of fighter aircraft to perform high g maneuvers at high speed is exploited to provide improved survivability. Figure 3 briefly summarizes the IFFC system features along with a brief rationale for each key element. The pilot is provided with the means to select the weapon delivery option that best fits the mission requirements, and the bombing pattern needed to inflict greatest damage to the target.

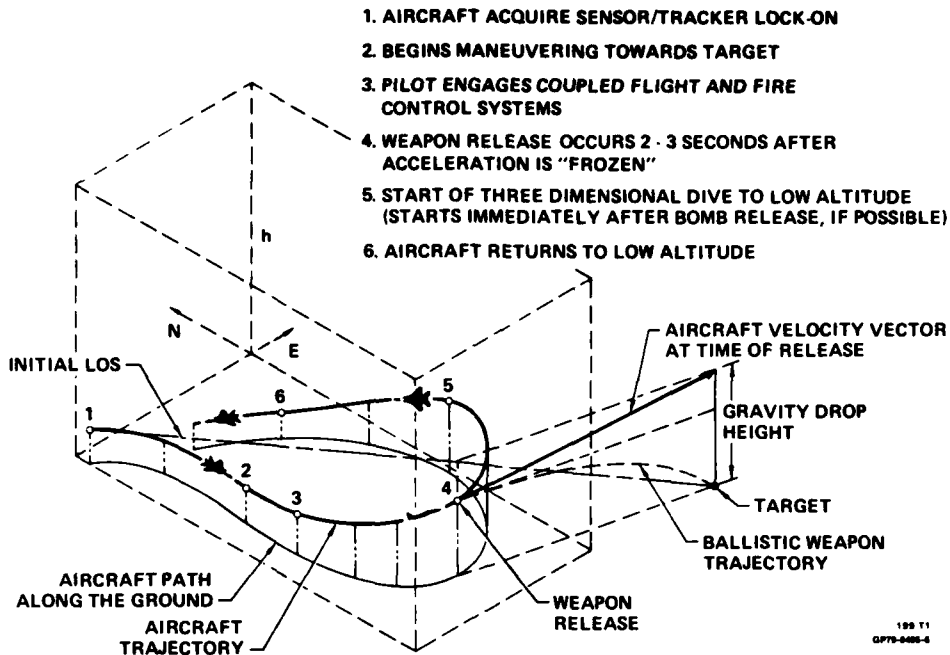
KEY ELEMENTS	ROLE	FUNCTION
SENSOR/TRACKER	DIRECTOR FIRE CONTROL INPUT	CONTINUOUS TARGET STATE ESTIMATION
COUPLED FLIGHT/FIRE CONTROL	BLENDS INPUTS PILOT AND FIRE CONTROL	MANUAL TO FULLY AUTOMATIC OPTIONS
AIRCRAFT AGILITY	HIGH g MANEUVERING WEAPON DELIVERY	SURVIVABILITY
PILOT	SELECTS OPTIONS	WORKLOAD TAILORING

FIGURE 3
IFFC SYSTEM

OP78-0406-0

Figure 4 depicts a typical maneuvering-aircraft/weapon-delivery profile for bombing. The actual profiles can be adjusted throughout giving the pilot the ability to continuously maneuver and to adjust the range of release. Just prior to release (about 2 or 3 seconds) the acceleration is "frozen" to provide for maximum accuracy. The sensor/tracker is continuously updating the fire control computations and eliminating error build-ups. (In addition, after bomb release, the sensor/tracker can be used to monitor the target and record the bomb point of impact for quick-look damage assessment.) Figure 5 depicts and compares the relative performance of five bombing modes in terms of relative accuracy, survivability, and pilot workload. The baseline is used as a point of reference for each mode. The general objectives of improved accuracy, increased survivability, and reduced pilot workload are achievable with a coupled flight and fire control system and maneuvering-aircraft/weapon delivery.

13-4



100 T1
OP79-0005-6

FIGURE 4
MANEUVERING - AIRCRAFT/WEAPON - DELIVERY

PARAMETER	BOMBING MODE (M)				
	BASELINE WINGS LEVEL	BASELINE MANEUVERING-AIRCRAFT/WEAPON DELIVERY	IFFC WINGS LEVEL	IFFC MANEUVERING-AIRCRAFT/WEAPON DELIVERY UNCOUPLED	IFFC MANEUVERING-AIRCRAFT/WEAPON DELIVERY COUPLED
RELATIVE ACCURACY (CEP_M/CEP_B)	-	MUCH GREATER ERROR	BETTER THAN BASELINE	EQUAL OR BETTER THAN BASELINE	BETTER THAN BASELINE
RELATIVE SURVIVABILITY (PS_M/PS_B)	-	MUCH BETTER THAN BASELINE	SLIGHTLY BETTER THAN BASELINE	MUCH BETTER THAN BASELINE	MUCH BETTER THAN BASELINE
RELATIVE PILOT WORKLOAD (WL_M/WL_B)	-	MUCH GREATER WORKLOAD	LESS WORKLOAD THAN BASELINE	EQUAL OR LESS THAN BASELINE	MUCH LESS THAN BASELINE

FIGURE 5
BOMBING MODE COMPARISONS

OP79-0005-10

There are several other related features and benefits that can be derived from the IFFC system using a sensor/tracker and control coupling. These are listed below without comment since their relative importance is yet to be determined:

- o Longer range target acquisition/classification/identification;
- o Longer range weapon release with equivalent baseline accuracy;
- o Target coordinates and rates stored in computer with continuously computed target location prediction;
- o Pilot freed to keep head out of cockpit;

- o Profile changes to match changing situations;
- o Degree of automation selectable;
- o Adaptable to all weather conditions;
- o Bombing patterns can be tailored to the target geometry to maximize target damage; and
- o Target feinting and surprise tactics can be employed.

4. TECHNOLOGY IMPACT

The introduction of maneuvering weapon delivery profiles for bombing, through the implementation described in the IFFC program, has identified areas of aerodynamics data deficiencies. The maneuvering weapon delivery profiles are essentially high g maneuvers with high bank angles, high angles of attack, and possibly high sideslip angles. Aircraft aerodynamic problems are primarily associated with these flight conditions. Normal store clearances are based on wings-level flight attitudes. The local flow conditions are important (5) for positive separation and clearance from the aircraft and for ultimate accuracy of the weapon delivered. The pressure distribution and flow fields need to be accurately known so that weapon delivery computations can be made to compensate for station, position, and release sequences. The local flow fields are also important in determining the attitude of each weapon released. In turn, the aerodynamic characteristics of the ordnance, before and after release, needs to be known to a greater degree of accuracy since the aircraft attitude in some profiles may be such that the weapon may be released upward (bank angles greater than 90°). Interference effects, both with respect to the aircraft on the weapon, and between weapons, also take on a new importance. These are the more easily identifiable problems that need attention.

The aircraft aerodynamics areas take on a new importance from the design point-of-view, when the IFFC technology is incorporated. Some design features which are of immediate importance are gust sensitivity, precise force control, drag build-up rates, buffet, wing rock, and departure control (6, 7). These problems are yet to be quantitized for relative importance.

Also, as the development or feasibility demonstration program progresses, new problems can be expected and anticipated which will require, and in turn justify, developments in other technology fields.

The extension of IFFC, using Advanced Control Concepts such as direct force control, will further compound these investigations. Independent fuselage aiming achieved with direct force control introduces new variations in the aerodynamic data needed to fully understand all of the aspects available for determining the most combat cost effective weapon delivery options.

5. CONCLUSION

Mission-analysis provides a means for assessing the importance of these types of R & D efforts, and in particular, R & D efforts pertinent to tactical mission deficiencies. The opportunity to formulate and execute a technology demonstration concept is dependent upon a well established technology base and a recognized operational need or deficiency. The IFFC system is such a program aimed at achieving a lower cost alternative solution to the problem of combat cost effectiveness of conventional unguided ordnance. The aim is to provide a capability in attack missions which overcomes important tactical deficiencies. Near-term solutions, with high payoffs are desired. The implementation of coupled flight and fire control systems, which is potentially applicable to many tactical aircraft, allows for the introduction and exploitation of maneuvering weapon delivery with accuracy and survivability.

The IFFC system investigation has surfaced new problems in related areas of technology, such as aerodynamics. The extension of IFFC in the future on unconventional force control aircraft further magnifies this interdependent relationship and the need to initiate and solve the problems expected.

Further, when the improvements for IFFC conventional unguided ordnance delivery are established the opportunity will exist to exploit these results to benefit guided ordnance.

REFERENCES

1. Johannes, R. P. and Whitmoyer, R. A., "AFFDL Experience in Active Control Technology" AGARD FDP Symposia on Aerodynamic Characteristics of Controls, Naples, Italy, May 1979.
2. Maxson, W., Major General, USAF, "Mission Area Planning as the Basis for Air Force TACAIR R&D" AIAA Preprint 79-0547, AIAA 15th Annual Meeting and Technical Display, Washington DC, February 1979.
3. McMullen, T. H., Major General, USAF, "TACAIR Outlook", Aeronautics and Astronautics; September 1978.
4. Hughes, J. D., Lieutenant General, USAF, "Tactical Air Warfare of the Future", AIAA Journal of Aircraft, March 1978.
5. Smith, H. and Carlton, D., "Weapon Delivery Impact on Active Control Technology", AGARD-CP-157 Impact of Active Control Technology on Airplane Design, October 1974.
6. Madelung, G. O., "Characteristics of Fighter Aircraft", AIAA Journal of Aircraft, March 1978.
7. Stengel, R. F. and Berry, P. N., "Stability and Control of Maneuvering High Performance Aircraft", AIAA Journal of Aircraft, August 1977.

DIRECT SIDE FORCE AND DRAG CONTROL
WITH THE AID OF PYLON SPLIT FLAPS

by

PETER ESCH
HORST WÖNNENBERG

Dornier GmbH, Friedrichshafen
Germany

SUMMARY

To demonstrate the possibilities of a direct sideforce and drag control for a simple combat aircraft small pylon split flaps will be used at an Alpha Jet aircraft as a test vehicle. The pylon split flaps have been chosen as control force generators to avoid drag and stability penalties in the nonoperating position and to reduce the necessary compensation effort for unwanted cross coupling effects to a minimum, as the control forces are occurring about the center of gravity. Operating the DSFC one flap on each pylon is driven electrohydraulically and generates the required side force. Symmetrical simultaneous use of all pylon split flaps provides a rapid acting drag control.

Two configurations of split flaps have been examined, a long one with small deflections and a short one with large deflections. The short one led to the same effectiveness at reduced values of hinge moments and cross coupling effects. Due to high interference effects it was not possible to get the effects of all flaps by superposition of the single flap results. The angle of attack, the landing flap setting and the lateral projection area of the external stores have a significant influence on the effectiveness whereas the Mach number is less important. The examination of the wind tunnel results led to the necessary control laws for the operation of the flaps and the compensation equipment. The flight test program with an Alpha Jet preproduction aircraft will start at 1980.

1. INTRODUCTION

Combat aircraft of the next generation will be provided with direct force control equipment, if the requirements to be met include a supreme maneuverability. These possibilities known under the terms "direct lift", "direct side force", and "drag control" allow the control of the translatory degrees of freedom of an aircraft.

Beside a general theoretical and experimental investigation for the effectiveness of different technical solutions, a study for the direct side force control performed by Dornier and supported by the Ministry of Defence aimed at finding out those configurations for the Alpha Jet aircraft enabling a realization with fewest possible modifications at the aircraft and without a complex control system.

Three different possible applications resulted from the general investigations for DSFC:

- side-slip-free change of course with constant bank angle (n_y -mode)
- lateral displacement with constant attitude (β -mode)
- deceleration flight (n_x -mode)

An ideal n_y -mode allows a side-slip-free course correction with constant roll and pitch attitude, while, for conventional aircraft, lateral corrections in ground attack approach are performed via roll maneuvers (see fig. 1) by turning the lift vector so that it causes a change of course. This requires a certain time and moreover disturbs the moments equilibrium.

The application of an ideal β -mode on the contrary allows a lateral displacement of the aircraft without a change of course also with constant roll and pitch attitude. The β -mode suggests itself for corrections in ground attack approach with a crosswind component above all however for corrections in formation flight and as an aid for landing approaches with crosswind.

The maneuverability of combat aircraft can also be improved by drag control. The so-called n_x -mode does not suggest itself only for sudden decelerations in air combat but it enables also steeper approaches at a sufficient engine thrust level, a quicker deceleration from cruising to approach speed and a glide-path control.

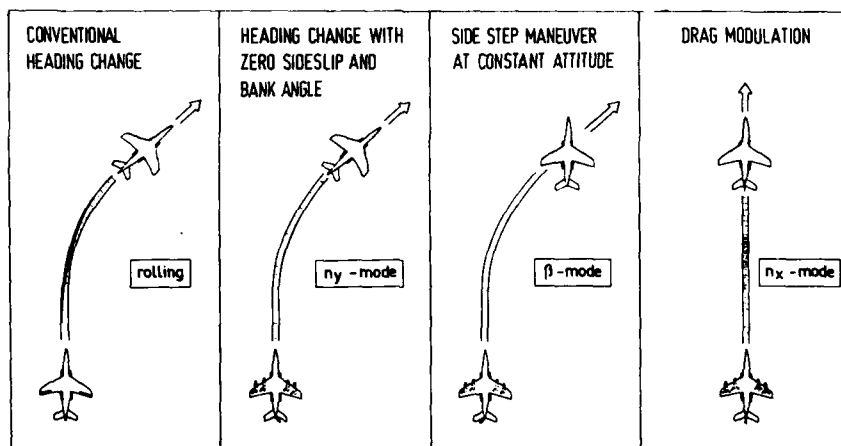


Fig. 1: Operational Possibilities by DSFC-Modes

Different configurations of DSFC control surfaces were analysed in the theoretical and experimental study

- special control surfaces under the wing
- use of the pylons as control surfaces
- attach of split flaps and spoilers at the pylons
- control surfaces at the fuselage nose section

Fig. 2 shows the effectiveness measured in the wind tunnel of the different configurations.

The criterium to achieve an effectiveness as great as possible with small coupling moments and low technical complexity finally led to the decision to pursue the configuration with split flaps at the four external store pylons for later realization at an Alpha Jet test aircraft.

Since the center of pressure of the pylon split flaps is situated near the aircraft center of gravity with respect to the z and x -direction, it could be expected that with DSFC flap deflection no or only inconsiderable coupling moments will occur so that a coupling between DSFC and the conventional control surfaces is not necessary for the compensation of these moments.

Fig. 3 shows the forces and moments acting at the aircraft when applying the β - and n_y -modes.

When the DSFC control surface center of pressure is situated within the aircraft center of gravity, it depends on the sign of the remaining interference yawing moment, whether the rudder must be deflected so that the available C_y will be increased or decreased. Fig. 3 shows that the effectiveness will be increased with positive interference moments.

Already the first wind tunnel tests within the low-speed range which served for the configuration selection showed that a purely theoretical consideration does not suffice to determine with the required accuracy all aerodynamic forces and moments arising by the DSFC flap deflection as the interference effects were considerable and could not be estimated. A support of the theoretical considerations by experiments proved to be of pressing necessity.

The first test series with a 1:5 low-speed wind tunnel model of the Alpha Jet provided with the DSFC control surface configuration represented in fig. 4 and selected from the pretest results served to answer three important questions

- effectiveness of the single control surfaces as a function of the flap deflection
- quantity of the coupling moments arising
- quantity of the hinge moments to be expected

Particularly the question for the quantity of the coupling moments is of high importance for the realization of as simple control laws as possible. It should be aimed by selecting a proper combination of the single split flap deflections so that with greatest possible effectiveness no or only very small proverse yaw or roll coupling moments will occur. Moreover, the secondary effects, such as the lift, drag, and yaw influences should be ascertained.

Fig. 5 shows the 1:5 Alpha Jet model in the wind tunnel. The pylon split flaps extended to the starboard can be clearly recognized, in this picture however only on the aircraft port.

The analysis of the first wind tunnel results led to the conclusion that it must be possible to achieve an almost equal effectiveness using smaller however more extended flaps located more in the back part of the pylon. In this connection, the interference effects would be smaller and the hinge moments required for flap deflection and which would have demanded a high hydraulic driving force would be less considerable.

Using the flap 1 and 2 as example, the fig. 6 and 7 show that the shorter DSFC pylon flaps reduced by abt. 50% with respect to the surface actually produce considerably smaller coupling and hinge moments however with a slight loss of side force effectiveness. Due to the smaller unfavourable coupling moments the total effectiveness was about in the same range as with the longer flaps.

Extensive investigations with the new defined flap configuration cover the following main points:

- optimization of deflection of the single flaps with respect to side force effectiveness
- influence of external stores attached to the pylon
- optimization of combined flap deflections with respect to side force effectiveness and coupling moments
- influence of landing flap deflections and angle of attack
- high-speed tests to determine the compressibility effect
- investigation for the use of DSFC flaps as speed brakes (n_x -mode)

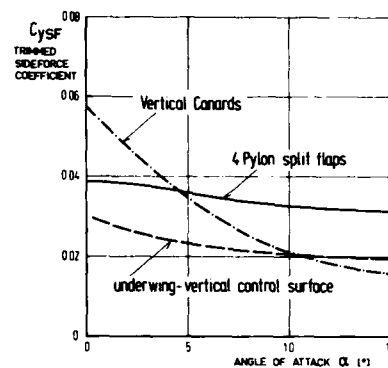


Fig. 2: The Effectiveness of Different Methods to Generate Direct Side Force

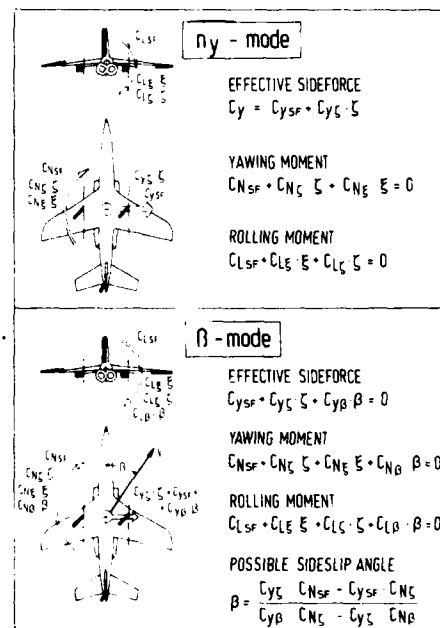


Fig. 3: DSFC - Mathematical Relations

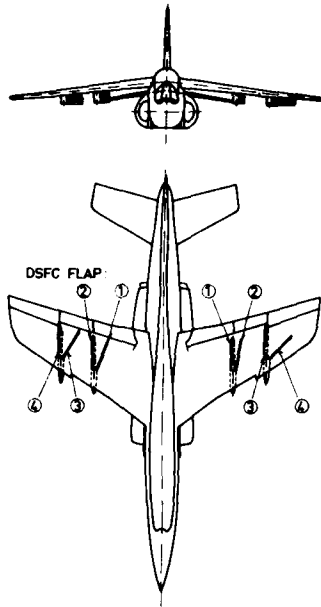


Fig. 4: Pylon Split Flap Arrangement at Alpha Jet

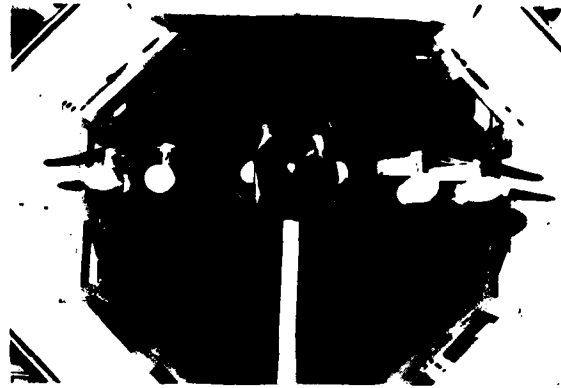


Fig. 5: 1:5 Alpha Jet WT-Model with DSFC Flaps

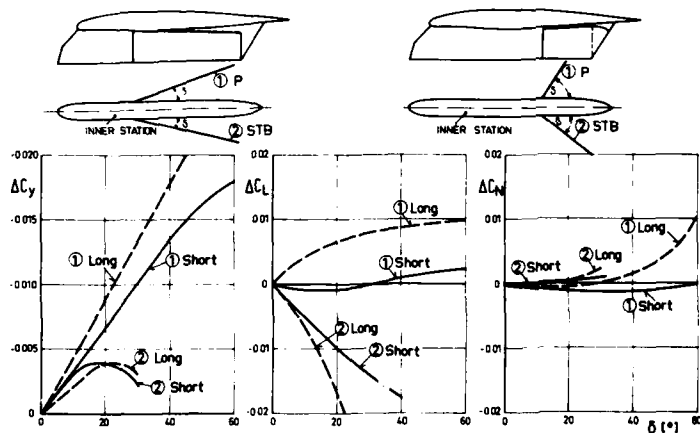


Fig. 6: Effectiveness and Coupling Moments Comparison between Long and Short Flap Configuration

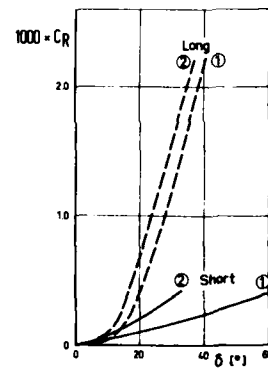


Fig. 7: Comparison between Long and Short Flap Configuration Hinge Moments

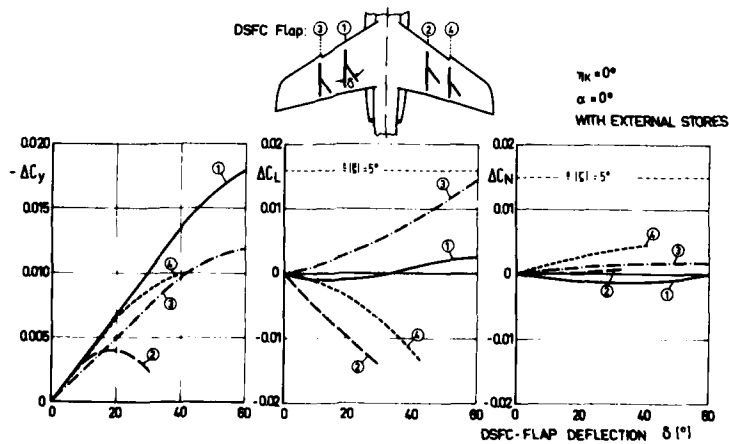


Fig. 8: Effectiveness and Lateral Coupling Effects of the Single Flaps

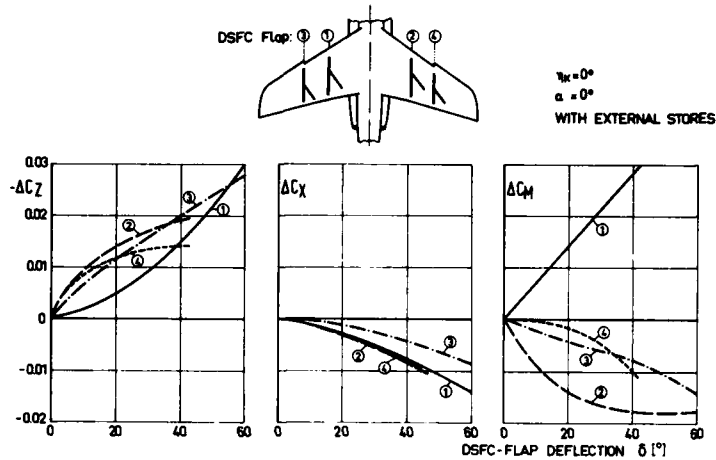


Fig. 9: Longitudinal Coupling Effects of the Single Flaps

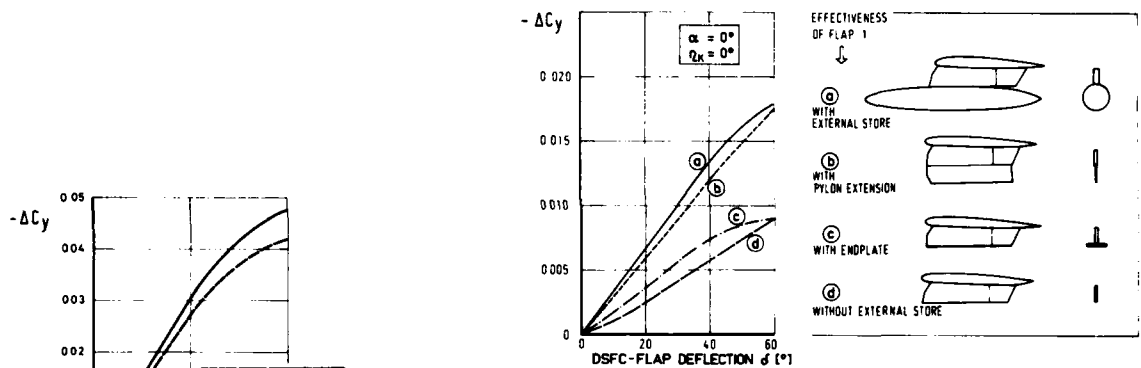


Fig. 10: Effectiveness of Flap 1

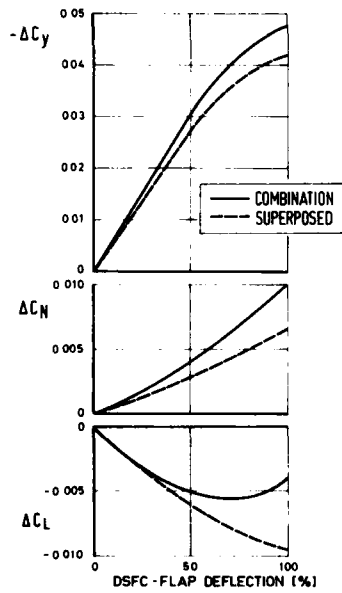


Fig. 11: Difference between Superposed and Measured Flap Combinations (Lateral)

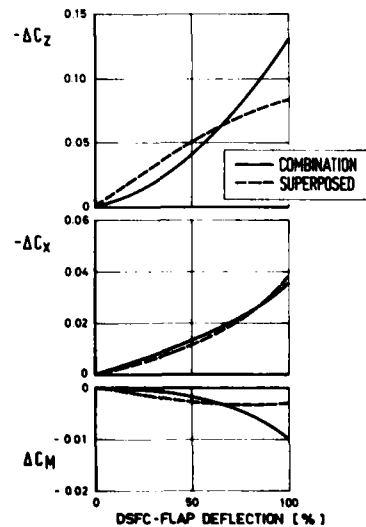


Fig. 12: Difference between Superposed and Measured Flap Combinations (Longitudinal)

2. OPTIMIZATION OF THE SINGLE FLAP DEFLECTIONS

Fig. 8 represents the effectivenesses of the single flaps. Although flap 1 and flap 2 are almost of the same size, the measurements show a surprisingly widely differing side force effectiveness. This phenomenon can only be explained by extremely great interference effects. Detailed aerodynamic investigations proved that due to the interference effects changes arise in the effective direction of air flow of the pylon flap combination. These changes cause for instance in case of flap 1 an increase of the effective angle of attack and thus a greater Δc_y due to the stagnation of air between flap and fuselage, whereas a decrease of the effective angle of attack and thus a considerable less Δc_y occurs at the pylon with extended flap 2 due to the air-flow deflected to the outside.

The lift variations represented in fig. 9 are also to be attributed to a stagnation of air below the wing. While the drag change shows no unusual effects, there is in pitch a considerable change of moments acting nose-up with the deflection of flap 1 and nose-down with the deflection of flap 2 and 4.

This varying effect of flap 1 compared to the three other flaps can be explained by the fact that the air-flow at flap 1 is deflected in direction of the horizontal stabilizer and thus causes an increased effectiveness of the nose-up trimmed horizontal stabilizer. With respect to the other flaps the horizontal stabilizer is not considerably affected so that the additional lift of the split flaps behind the center of gravity produces an expected nose-down moment. The differences in the order of the nose-down pitching moment with flap 2 and 3 can be explained by the fact that the air-flow deflection caused by flap 3 can still cause a certain influence on the horizontal stabilizer.

3. INFLUENCE OF EXTERNAL STORES ATTACHED TO THE PYLON

Measurements without external stores showed a considerable decrease of the split flap effectiveness. As the missing end plate effectiveness of the external stores was to be blamed for this, extensive detailed experimental investigations were performed using end plates of the most different geometry and position. Fig. 10 shows only a few results, namely by the example of flap 1

- pylon with external stores
- pylon without external stores
- pylon with large end plate
- pylon with a pylon extension in z-direction

None of the tested end plate configurations produced the desired result of an increased effectiveness. An extension of the pylon was, however, successful, as a duplication of the surface was achieved by an extension which was provisionally realised by metal sheet. The drastic reduction of the effectiveness of the DSFC flaps in the aircraft configuration without external stores cannot be ascribed to the missing end plate effect of the external store but rather to the reduction of the surface.

4. OPTIMIZATION OF COMBINED FLAP DEFLECTIONS

The already mentioned considerable interference effects which are hardly ascertainable do not allow to draw conclusions from the effectiveness of single flap deflections on the effectiveness of flap combinations; it is true that measurements of single deflections are important for the determination of tendencies, but the real optimization with respect to a maximum side force effectiveness with simultaneous lowest possible coupling moments requires extensive measurements with the most different combined DSFC flap deflections that are feasible.

The fig. 11 and 12 show that a simple addition of the forces and moments ascertained with the single deflection leads to different results as they were measured with combined deflections.

The side force effectiveness with the combined DSFC flap deflection exceeds that resulting from the sum of the single flap effectivenesses. The differences with respect to the aerodynamic forces are particularly serious; but exactly these moments are required for the establishment of control laws, as it depends on them, if a coupling of DSFC flaps with the conventional control surfaces is required for the compensation of the arising coupling moments.

These investigations established control laws which vary according to the configuration and the mode.

Since the feasibility of DSFC equipment shall be submitted to flight tests using the Alpha Jet as test vehicle which has no stability augmentation and since as few modifications as possible are to be carried out at the aircraft itself for time and cost reasons, it is necessary to realize as simple control laws as possible.

Simulation tests established that the pilots desire a control of the DSFC flaps by the rudder pedals.

Fig. 13 demonstrates by an example a control law possible for the η -mode having the considerable advantage that it is not necessary to change the primary control of the pedal rudder assignment of the Alpha Jet. Within a certain pedal and rudder deflection automatically connected with it, the DSFC flaps are extended to the respective angles considered as being optimal; only the rudder reacts on a further extension of the pedal, while the DSFC flaps keep the maximum values.

From the assignment rudder deflection to DSFC flap deflection selected in this control law result the low pitching moments and even low proverse roll coupling moments, which should be controllable by the pilot or a simple automatic compensation equipment with low authority.

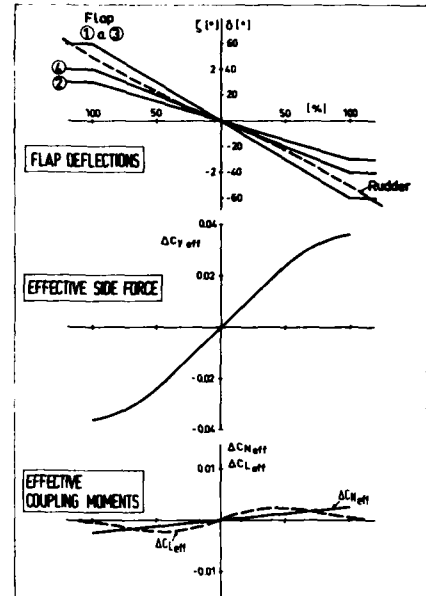


Fig. 13: Possible Control Law

5. INFLUENCE OF LANDING FLAP DEFLECTION AND ANGLE OF ATTACK

Fig. 14 demonstrates by the example of flaps 1 and 2 - flap 1 is extended to the angle of 60° , flap 2 to 40° , angles which are optimal for the application of the η -mode - how the side force effectiveness is changed when the trailing edges of the aircraft are extended. In case of flap 1 small landing flap deflections produce no loss of effectiveness, while high deflections even result in a - though small-opposite side force.

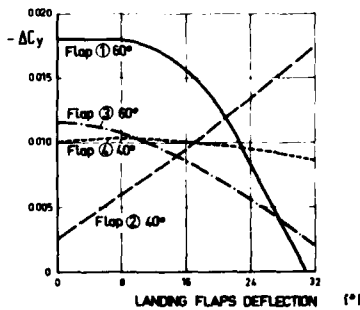


Fig. 14: Influence of Landing Flap Deflection on Effective Side Force

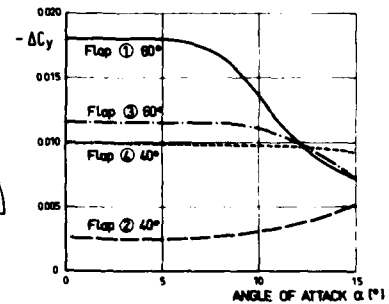
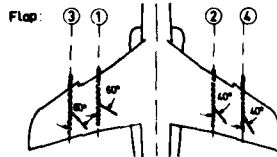


Fig. 15: Influence of Angle of Attack on Effective Side Force

14-8

Flap 2 shows a completely different behaviour. Its effectiveness permanently increases with increasing landing flap deflection in the investigated range. There are also similar phenomena with an increase of the angle of attack (see fig. 15). As from $\alpha = 6^\circ$, a clear reduction of the effectiveness of flap 1 can be recognized, which is extended to 60° also in this example, while flap 2 shows a C_y gain with increasing angle of attack.

For the understanding of this phenomenon it must be looked at the sweep angle of the wing trailing edge towards the aircraft longitudinal axis. By the pylon split flap deflection the airflow is locally accelerated and the reaction force acting on the trailing edge flap or on the trailing edge of the wing with angle of attack causes only due to the geometry a side force reduction in case of flap 1 and 3 and a side force increase in case of flap 2 and 4.

6. INFLUENCE OF COMPRESSIBILITY

Fig. 16 shows the Mach number influence achieved with a 1:10 Alpha Jet model in high-speed tests with maximum deflection of the pylon split flaps. The Mach number effects are surprisingly low, although considerable effects had to be expected due to the relatively great blocking occurring with the flap deflection.

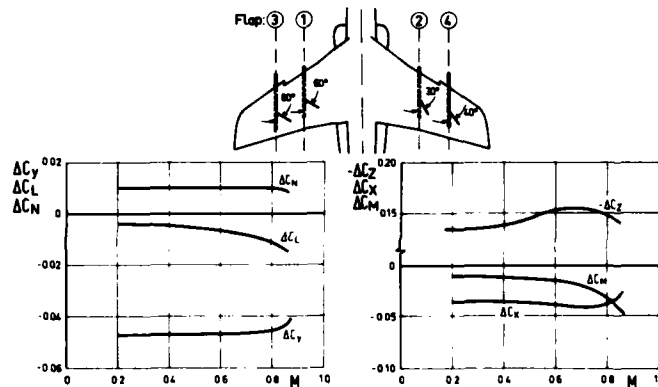


Fig. 16: Influence of Mach Number on Effectiveness and Coupling Effects

7. INVESTIGATION WITH RESPECT TO AN APPLICATION OF THE DSFC FLAPS AS SPEED BRAKES

A considerable increase of the drag coefficient which is practically independent on the Mach number is achieved by a symmetrical deflection of all pylon split flaps. A DSFC flap deflection of 30° already produces the drag increase which is achieved with the speed brakes extending from the fuselage back of the Alpha Jet (fig. 17)

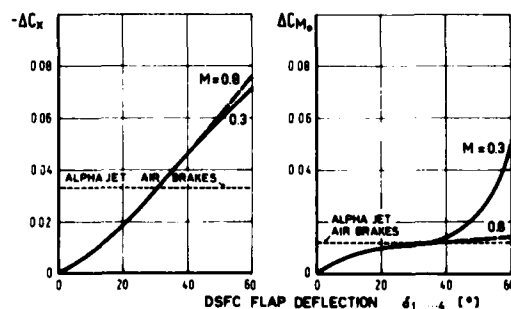


Fig. 17: Effectiveness of Drag Modulation by the Pylon Split Flaps

A maximum deflection of all flaps to 60° leads to a pitch-up moment which must be trimmed by an elevator deflection of abt. 1.5° only at low Mach numbers. In case of greater Mach numbers moment changes are to be expected in the same order of magnitude as they occur with the original speed brakes.

8. ACTUAL STAGE OF THE EXPERIMENTAL PROGRAM

The hardware-phase of the program has already begun. All specifications have been defined and the fabrication of the split flaps and the modification of the pylons have started. The functional tests are provided for the end of this year, whereas the flight test program which will be performed as a joint program of Dornier and the "Luftwaffe" - Flight Test Center at Manching ist planned for 1980.

9. LITERATURE

JENNY, KRACHMALNICK, LA FAVOR: Air Superiority with Control Configured Fighters
J. Aircraft Vol., Nr. 5, May 1972

WARREN G.: A Flight Test Investigation of Direct Side Force Control
The Society of Experimental Test Pilots, Technical Review.

KUBBAT: Investigations on Direct Force Control for CCV Aircraft During Approach and Landing.

MBB-Bericht UFE 1090 (ö)
(AGARD FMP "Take off and Landing")
Edinburgh, May 1974

MILLER: USAF Plans Advanced Fighter Program
Aviation Week + Space Technology, July 16, 1973

YAFFEE: New Controls to Shape Future Aircraft
Aviation Week + Space Technology, October 16, 1972

HALL, WEINGARTEN, LOCKENOUR: An In-Flight Investigation of the Influence of Stability and Control Parameters on Weapons Delivery Accuracy
Aug. 6-8, 1973, AIAA Paper 73-783

BENNER, WONNENBERG: Problematik und Realisierungsmöglichkeiten einer direkten Seitenkraftsteuerung bei Kampfflugzeugen
Vortrag 74-84, 7. Jahrestagung der DGLR in Kiel

BENNER, WONNENBERG: Untersuchungen zur Seitenkraftsteuerung von Kampfflugzeugen
Dornier Report 74/46/B, 1974

WONNENBERG, HERDING, SCHNEIDER, HEDERMANN: Durchführbarkeitsstudie zur Realisierung einer direkten Seitenkraftsteuerung für den Alpha Jet als Versuchsträger
Dornier Report 76/43/B, 1976

D.J.THIGPEN, R.A.WHITEMOYER, P.A.MERKEL: Flight Test Status of the Fighter CCV
AIAA Paper 76-884

F.R.SWORTZEL, J.D.Mc ALLISTER: Design Guidance from Fighter CCV Flight Evaluations
Paper presented at AGARD-FMP Symposium on Stability and Control, Ottawa, Canada, Sept.78

CONTROL OF FOREBODY THREE-DIMENSIONAL FLOW SEPARATIONS

David J. Peake
Senior NRC Research Associate
Ames Research Center, NASA
Moffett Field, California 94035, U.S.A.

15-1

F. Kevin Owen
Owen International, Inc.
Palo Alto, California 94302, U.S.A.

SUMMARY

Some experiments involving the development of the turbulent symmetric and asymmetric vortex flow about the lee side of a 5° semiangle (θ_c) conical forebody at high relative incidence (u/θ_c) are discussed. The cone was immersed in a Mach 0.6 airstream at a Reynolds number of 13.5×10^6 based on the 1.4-m (54-in.) axial length of the cone.

Novel means of controlling the degree of asymmetry using blowing very close to the nose were investigated. Small amounts of air injected normally or tangentially to the cone surface, but on one side of the leeward meridian and beneath the vortex farthest from the wall, were effective in biasing the asymmetry. With this reorientation of the forebody vortices, the amplitude of the side force could be reduced to the point where its direction was reversed. This phenomenon could be obtained either by changing the blowing rate at constant incidence or by changing incidence at constant blowing rate. Normal injection appeared more effective than tangential injection. The contrarotating vortices in the penetrating jet flow were of opposite hand to the rotational directions of the forebody vortices. A distinctively organized and stable flow structure emerged with the jet vortices positioned above the forebody vortices.

SYMBOLS

Note: All force coefficients are referenced to cone base area = 449.6 cm^2 (69.7 in.^2) and free-stream dynamic pressure.

A	cone base area
C_N, C_{NB}	normal-force coefficient from balance
$C_p = \frac{p - p_\infty}{q_\infty}$	local static pressure coefficient
$C_{pp} = \frac{p_p - p_\infty}{q_\infty}$	local pitot pressure coefficient
C_Y, C_{YB}	side-force coefficient from balance
C_{YP}	side-force coefficient from integrated surface pressures at $x/L = 0.87$
$C_\mu = \frac{\dot{m}u_j^*}{q_\infty A}$	jet momentum coefficient
D	base diameter of cone = 23.9 cm (9.4 in.)
L	axial length of cone = 137.2 cm (54.0 in.)
\dot{m}	jet mass flux
M	Mach number
p	local static pressure
p_p	local pitot pressure
q	dynamic pressure
r	cone radius
R_{L_∞}	Reynolds number based on axial length of cone and tunnel free-stream conditions
u	local velocity in direction of tunnel axis
\bar{u}	local velocity, parallel to model axis
u_j^*	sonic jet velocity
v	lateral velocity, normal to tunnel (or model axis)

w	vertical velocity normal to tunnel axis
\bar{w}	vertical velocity normal to model axis
x	distance along tunnel axis
\bar{x}	distance along model axis, origin at pointed apex of cone
y	lateral distance from tunnel (or model axis)
$\bar{y} = \frac{y}{r}$	nondimensional lateral distance
z	vertical distance, normal to tunnel axis
\bar{z}	vertical distance, normal to model axis
$\bar{z} = \frac{z}{r}$	nondimensional vertical distance
α	angle of incidence
θ_c	cone semiangle
ϕ	circumferential angle around cone surface, measured from windward generator, negative on port side and positive on starboard side (pilot's view from base of cone)

Subscripts

∞	free-stream mean flow conditions
s1	primary separation line
s2	secondary separation line

1. INTRODUCTION

1.1 Flow Asymmetry in the Lee-Side Vortex Flow Field at High Angles of Incidence

A present-day missile or military fighter aircraft must perform and be controllable up to high angles of incidence, where complex vortical flow fields exist about the leeward side of the vehicle. These vortices are generated at relatively sharp leading-edge extensions, wing leading-edges, and on the forebody. Once a given ratio of incidence α to seminose angle θ_c (the relative incidence) is exceeded, usually between 1 and 2 for a slender conical or tangent-ogive nose shape attached to a fuselage or cylindrical body, the orientation of the forebody vortices becomes asymmetrical with respect to the meridional plane (Refs. 1-5). (For the cone or tangent-ogive alone, the relative incidence at which the onset of asymmetry occurs is closer to 3.) Substantial side forces and yawing moments then develop to affect the stability of the vehicle. In addition, these forebody vortices, perhaps in conjunction with the vortical flows from the wings, may interfere with downstream control surfaces to provide significant nonlinearities that are unpredictable. Depending on the strengths, locations, and breakdown of these vortices, an aircraft may be departure-prone or departure-resistant to spinning (Ref. 5).

The onset of asymmetry and the initial direction of the side force are responsive to small changes in geometry at the nose, Reynolds number, and Mach number, up to incidences where conditions in the lee-side crossflow become transonic. As speed increases further, the significant side forces disappear (Ref. 2). The asymmetries occur in both laminar and turbulent flows so that transition is presumably not an essential ingredient causing asymmetry. Notwithstanding, the implication from recent tests by Lamont (Ref. 6) with a tangent-ogive cylinder at incidence, at Reynolds numbers encompassing laminar, transitional, and turbulent boundary-layer separation, is that the vortex wake is less structured in the transition domain leading to reduced side and normal forces at a given subsonic Mach number. In the fully laminar or turbulent regions, on the other hand, where the organization of the flow field is well defined, the respective magnitudes of the side force are larger and are closely matched. It is likely that the levels of vorticity and acoustic disturbance in most wind tunnels will also affect the initial occurrence of asymmetries (Ref. 7). A rational explanation for the development of asymmetry in the flow may be related to the stability of the velocity profiles in the vicinity of the saddle singular point that exists in the stream above the body vortices (see Fig. 1). In the example of the flow about a circular cylinder situated perpendicularly to an oncoming stream, Nishioka and Sato (Ref. 8) determined instabilities to amplify initially in the region of the saddle point, to herald the commencement of asymmetric but well-structured wake flow. Thus, for a body of general shape at high incidence, we may conjecture that flow perturbations will impose fluctuations on the saddle point flow that will accentuate the instability mechanism. Evidence points to extremely small surface irregularities in the surface curvature at the nose as governing the initial direction of the asymmetry in the vortex flow field. This is understandable from the fact that a given body at incidence, under identical flow conditions, will provide a repeatable side force direction at a prescribed roll orientation; and near-mirror images of the side-force/incidence performance for roll angles $\pm 90^\circ$, as we show in Fig. 2. Despite this knowledge, production tolerances on a typical fighter aircraft may alter the asymmetric vortex flow development sufficiently to provide unpredictable stability problems (Ref. 5). We do not yet understand the influence of geometrical imperfections on the fluid mechanics, nor how the nominally small disturbances of the fluid flow at these imperfections can amplify so considerably. A small flat, for instance, machined in turn on each side of the nose of a fighter/bomber swing-wing aircraft model was effective in completely switching the sign and amplitude of the yawing moment (Ref. 9).

1.2 Control of Asymmetries in the Forebody Vortex Flow Field

As the development of the asymmetry is particularly sensitive to surface curvature or roughness at the nose, it is conceivable that the degree of asymmetry in the forebody flow field could be controlled by deploying a single small strake or by spinning the nose (Ref. 10). The permanent installation of symmetrical nose strakes at the 90° circumferential angle station (Refs. 3, 11) or in helical form from the leeward meridian to the windward meridian (Ref. 12), have been shown to be effective at suppressing the onset of asymmetry, and roughness has been demonstrated to provide a similar benefit (Ref. 3). Unfortunately, the fixing of "add-on" large excrescences to the airframe is usually detrimental to the cruise-drag performance, and strakes that transform the symmetry of the cross section of the nose are accepted less than enthusiastically by radar designers. 15-3

It would appear that at forebody relative incidences (incidence to seminose angle, α/θ_c), where asymmetry of the vortex wake commences, we are always dealing not only with separation of the primary boundary layers that develop on each side from the windward generator, but with secondary separations of the lee-side boundary layer in addition (see Fig. 1). The onset of asymmetry would seem to be characterized initially by a rapid, local movement circumferentially of one (or both) secondary separation lines followed, as incidence is increased further, by circumferential movement of the primary separation lines (Refs. 1 and 2). The asymmetric skin friction line pattern on the conical surface development shown on Fig. 3 illustrates this latter flow situation, with "wobbly" primary and secondary separation line traces existing all along the cone (Ref. 13). Here, the free-stream Mach number is 2.94 and the relative incidence is 4.5.

The asymmetric vortex wake usually develops from asymmetric separation line positions on the body, but the latter does not appear to be a necessary condition for the former to occur. An appraisal (Ref. 14) of some earlier, low-subsonic speed tests of Shanks (Ref. 15) where forces and moments were measured on very slender, flat-plate, delta wings (sweep angles from 70° to 84°) at incidence, indicates that even though the separation lines were fixed at the sharp leading-edges, asymmetry in the leading-edge vortices, as determined by the onset of significant rolling moment, occurred when the angle of incidence was about 3 to 4 times the wing seminose angle. This incidence for asymmetry is splendidly illustrated, on the vapor screen pictures (Fig. 4), about another very slender delta wing immersed in a Mach 2.8 flow (Ref. 16). Nonetheless, the sharp edges have a beneficial effect in delaying the onset of asymmetry to higher relative incidences than those obtained with smooth pointed forebodies or forebody/cylinder configurations (Refs. 2-4).

Hence, we have the scenarios of (1) leeward asymmetries in primary and secondary separation line positions coupled with asymmetric vortex flow (Fig. 3, for example), or (2) symmetric fixed primary separation line positions (but asymmetries no doubt, in secondary separation position) in Fig. 4, still yielding asymmetric vortex flow at suitably high angles of attack. The reasons for such flow behavior are evidently complex and perplexing. Nevertheless, the amplification of perturbations to produce an instability at the saddle point (Ref. 8) (and to which we alluded previously) would seem to cover the scenarios presented.

Thus, the objective of the present investigation is to understand the fluid mechanics and to assess the efficacy of making small changes to the nose geometry by novel active or passive means to alter asymmetries in the lee-side flow field about a typical conical forebody. This takes the form of symmetrically and asymmetrically disposed blowing from, respectively, an external compressed air source, or from a combined passive suction/blowing scheme from the windward side to the leeward. Some recent results of Sharir, Portnoy, and Rom (Ref. 17), for instance, have demonstrated the potential for control by symmetrical blowing normal to the surface. They offered the surprising result that blowing symmetrically from jets on the windward side of the nose of a missile configuration provided the most effectiveness in diminishing the side force. We conjecture that blowing from the lee side, in the vicinity of the separation lines, should produce an even greater impression on the asymmetric flow development.

It will be noted that in its offering of some comprehension of the fluid mechanics of pneumatically perturbing the asymmetric vortex flow on a typical forebody, this paper is a companion to the paper presented at this meeting by Skow, Moore, and Lorincz (Ref. 18) which discusses the recovery of control and the enhanced stability afforded by nose blowing on a fighter aircraft configuration.

2. MODEL AND EXPERIMENTAL METHOD

A circular cone is the basic nose shape of many flight vehicles. At relative incidences typically less than 3, it provides a useful configuration on which to develop symmetrical three-dimensional separated boundary layers growing, respectively, on the port and starboard sides from the windward meridian to the leeward meridian. Because of the near conicity of the separation lines and vortex development in both subsonic and supersonic turbulent flows (that is, neglecting the effects of transition), the cone also provides a convenient experimental model to explore three-dimensional separations from detailed measurements at only one axial station. In so doing, a quantitative understanding of three-dimensional separation can be obtained that may be applicable to many other complex flow regimes. Above a relative incidence of 3 for the circular cone, however, the lee-side separations become asymmetric in subsonic flow.

Recent measurements have been made of the symmetric and asymmetric flow regimes on a 1.4-m (54-in.) long, 5° semiangle cone, sting-mounted on a roll-gear in the Ames 1.8- by 1.8-m (6- by 6-ft) closed circuit wind tunnel (Fig. 5) at a Mach number of 0.6. Stagnation pressures were subambient, yielding a typical Reynolds number of 13.5×10^6 based on the cone length with nominally zero heat transfer conditions at the cone surface. No artificial tripping of the laminar boundary layer was employed in the nose region. Transition was considered to occur along the initial 20% of the cone length in this wind tunnel at Mach 0.6 where the relatively high acoustic disturbance level equalled 3% of the free-stream dynamic pressure. (Unpublished data by D. Buell and K. Raman, NASA-Ames Research Center.) The cone model was fitted with a slightly blunted tip with a radius of 4% of the base radius.

All detailed measurements on the cone surface ($0^\circ < \phi \leq 180^\circ$) and in the lee-side flow field were made at an axial station 0.87 of the cone length aft of the (pointed) apex. Circumferential mean pressure distributions were obtained with 0.51-mm (0.020-in.) diameter static holes spaced at 2-1/2° intervals for $0 < \phi \leq 90^\circ$ and at 1° intervals for angles $90^\circ < \phi \leq 180^\circ$. These orifices, as well as others along a cone generator and at the 0.85 and 0.95 axial length stations, were connected via "scanivalves" to unbonded

strain-gage pressure transducers. We note that "port" and "starboard" refer to the left-hand and right-hand sides of the cone as a pilot would view them. The positive ϕ direction is on the starboard side.

At a relative incidence of 2.5, where symmetrical separated flow conditions still prevailed, pitot pressures were measured in the lee-side vortex wake with an array of 77 pitot tubes. Supportive three-dimensional laser velocimeter measurements of mean and root-mean-square velocities were obtained at the same relative incidence at the 0.87 axial station. The velocity field in the wake at points in the crossflow plane (perpendicular to the model axis) was measured with a two-color, forward-scatter, frequency-offset laser velocimeter, allowing two velocity components to be obtained simultaneously. A line diagram of the layout of the velocimeter is shown on Fig. 6(a) and a photograph of the sending optics in Fig. 6(b). With this system, the two primary laser lines, namely 4880 and 5145 Å, were separated by means of a prism, P. These primary beams were each split by the Bragg cells B_1 and B_2 to obtain two pairs of divergent, frequency-offset beams. Each pair of beams then passed through a "cube" (C_1 and C_2) that was ground to be slightly "off-square" to rectify the divergence. The four resultant parallel beams proceeded through the sending optics and were focused at the same point within the flow test region. Collecting optics on the far side of the wind-tunnel test section re-focused the scattered light onto a pair of photomultiplier tubes. The signals from those tubes were then processed to obtain two components of velocity of particles passing through the focal volume. Since we were seeking three velocity components, two sets of measurements were taken. In the first set, the laser beams were set normal to the tunnel axis so that the axial (u) and vertical (w) velocity components were found. From these two components the axial and vertical velocities in the crossflow plane perpendicular to the body axis could be resolved (see Fig. 6(c)). For the second set, the transmitting optics were rotated 21° about the z-axis and the measurements repeated. Now, one velocity component measured was again the vertical velocity whereas the second was a combination of the axial velocity (u) and the lateral velocity (v) in wind-tunnel coordinates. Thus, since the axial velocity had already been measured, the lateral velocity could then be calculated. In other words, the lateral velocity in the crossflow plane is obtained, since it is the same in both wind-tunnel and body coordinates.

The Bragg cells, which produce zero-velocity frequency offsets in both color systems, were incorporated to remove directional ambiguity from the measurements. Without this capability, Owen and Johnson (Ref. 19) have cautioned against believing any measurements in flows that are unsteady or possess a high degree of turbulence.

Prior to obtaining the pitot and laser velocimeter measurements at the relative incidence of 2.5, the position of the lee-side vortices adjacent to the cone surface was established under symmetrical and asymmetrical wake conditions utilizing a vapor-screen technique. Water was introduced into the tunnel flow and a thin cross section of the flow, about 2 mm (0.1 in.) thick was illuminated. This was accomplished by passing either the green beam or the blue beam of the laser through a cylindrical lens (Fig. 7). By changing the location of the beam focus, a light sheet of variable divergence angle could be produced to illuminate the crossflow. The lens could be rotated manually about the y-axis and longitudinally and vertically using the velocimeter traverse gear such that any cross-sectional plane in the flow within the field of view circumscribed by the tunnel window could be observed (see Figs. 5 and 7). Photographs of the scattered light were taken with a camera mounted on the sting/strut support, the camera axis being set nominally parallel with the cone surface. Prior to each test run a grid, placed at the axial test station, was photographed; the dimensions of the separated shear layers could then be compared against the grid. This flow visualization experiment was clearly important to determine a suitable mesh area over which to scan the focused laser beams to obtain the flow velocities.

Once the symmetrical separated flow field had been investigated, small amounts of blowing near the nose were introduced in an attempt to control the gross asymmetries in the lee-side flow that develop above a relative incidence of 3. The frustum at the front of the cone model is detachable, as shown in Fig. 8(a). Several new frustra of identical external shape were machined to include blowing holes at various circumferential stations (0° , $\pm 60^\circ$, $\pm 120^\circ$, and $\pm 150^\circ$) and two orifice diameters, 2.4 mm (0.096 in.) and 3.6 mm (0.140 in.) (Fig. 8(b)). The holes were drilled normal to the cone surface at the 12% axial station (from a pointed apex). As well as providing for blowing normal to the surface, sets of right-angle tubes were constructed that could be inserted and glued into one or more of the surface holes to direct the air upstream or downstream along the local cone generator. The air passed to the plenum chamber in the nose frustum via a steel and flexible pipe within the cone model that was supplied with compressed air from an external source. A sensitive throttle valve outside the tunnel permitted control of the blowing pressure up to a maximum of 8 atm in the blowing plenum, corresponding with a maximum rate flow \dot{m} of about 0.023 kg mass/sec (0.0016 slugs/sec). The jet momentum flux was calculated assuming sonic conditions at the jet orifice and a discharge coefficient of 0.8. The thrust coefficient, C_{Tj} , was referenced to the base area of the cone. Note that if the cone length is considered representative of an airplane nose as far back as the cockpit and the airplane is akin to a F-5 fighter, say, an equivalent thrust coefficient based on wing area is 0.05 times C_{Tj} .

Overall force and moment measurements were obtained with an internal strain-gage balance. Mean and root-mean-square forces were measured. (Prior to the test runs, the natural resonances in the cone/sting strut support system were determined by shaking the model in the normal-force and side-force directions.) Initially all blowing ports were blocked with epoxy sealer. Once the no-blowing side-force direction versus incidence performance was ascertained, the appropriate side on which to eject the blowing air was conjectured as that opposite to the direction of the side force. In other words, if the pilot's view were side force to starboard, the starboard vortex would be closer to the surface, and opening a blowing port beneath the port-side vortex would reduce the asymmetry from the jet sink and entrainment effect (see Ref. 18). In a practical aircraft installation, yaw rate as measured on a yaw accelerometer would indicate the appropriate side from which to inject air (or other suitable gas). The degree to which this philosophy was successful and the rationalization for the choice of the circumferential blowing location(s) are presented in the following sections. Typical results are also shown in the form of the effect of incidence on side force development at a constant blowing rate; and the effect of blowing rate on side force at a constant incidence. The effectiveness of symmetrical blowing versus asymmetric blowing is also discussed.

3. RESULTS

3.1 Symmetric Separation of the Lee-Side Cone Flow

The physical characteristics of the symmetric mean flow field about the 5° semiangle cone immersed in a Mach 0.6 stream at a relative incidence of 2.5 were discussed in Ref. 20. Salient features of those results, however, are included to support the present laser velocimeter measurements. Figure 9 displays circumferential pressure distributions at the 0.87 length station for a relative incidence of 2.5. We note good agreement between the two scans of data shown on the respective port and starboard sides. However, between the two sides there is a discrepancy in pressure level which may be attributable to a slightly yawed condition of the model relative to the oncoming free stream.

As the three-dimensional boundary layer develops from the windward attachment line region ($\phi = 0^\circ$) toward the minimum pressure point at $\phi \sim 100^\circ$, the crossflow grows rapidly. Figure 10 is a representative sketch of a typical skin friction line trajectory corresponding with this accelerating flow field. Once past the flank, the boundary layer proceeds around the lee side of the cone and encounters a stiffening adverse pressure gradient (Fig. 9). It thickens rapidly as we see in the laser vapor screen flow visualization photograph on Fig. 11. The angle between the skin friction line and a cone generator gradually reduces to zero (Fig. 10) at which point the skin friction line runs parallel to a generator, the primary separation line, $\phi_{S1} \approx 145^\circ$. The boundary layer detaches from the surface to form a tightly coiled vortex shown in Fig. 11. Contours of constant pitot pressure deficit in the vortical flow field are plotted in Fig. 12. The vortex core location is close to $\phi = 170^\circ$ above the surface, further evidence of which is shown on the pressure distribution of Fig. 9. At this same circumferential angle, we detect a substantial suction peak on either side of the leeward meridian. This roll-up of the primary boundary layer scavenges fluid from the region of the leeward meridian encouraging a new boundary-layer growth outward and beneath the primary vortex structure. This new boundary layer, after initially accelerating, then meets its own adverse pressure gradient and separates at $\phi_{S2} = 160^\circ$ as a small secondary vortex tucked beneath the primary. The secondary vortex is within the small lobular region shown on the pitot contours of Fig. 12.

The rotational sense of the secondary flow (see Fig. 1) could also be seen when viewing the laser vapor screen through the tunnel window, but is not resolvable from the photographs of the flow. The typical converging skin friction line directions close to the primary and secondary separation lines are drawn on Fig. 10. At the locations of the separation lines, the root-mean-square voltages (normalized by the voltage of the onset mean flow) measured by a buried wire in the cone surface as the cone was rolled about its pitch axis indicated substantial amplification of fluctuation levels. (This can be done, as there is virtually no sensitivity of the symmetrical separated flow to roll orientation, in distinct contrast to the asymmetric flow.) Correspondingly, when the root-mean-square pressure fluctuation at the surface was normalized with respect to the value of the local resultant shear stress, large increases in signal level were also obtained at the separation line positions. These and additional details are explained fully in Ref. 20.

Preliminary assessments of the distributions of axial and vertical velocities in the crossflow plane obtained by the laser velocimeter and shown on Figs. 13 and 14 appear to confirm the dispositions of the primary and secondary vortices in relation to the pitot and vapor screen results. Figure 13, for example, at $\bar{z} = 0.3$, shows that the axial velocity grows from a minimum value at the inboard extremity of the primary vortex (nearest to the meridian plane) to a maximum at the outboard extremity. Maximum values of root-mean-square velocity fluctuations occurred in the vicinity of the core positions (see also Ref. 20). The vertical velocities are shown on Fig. 14. The plot on Fig. 15, obtained from Fig. 14, illustrates the vertical velocity in the meridian plane and indicates the position of the saddle singular point that we drew on Fig. 1. Comparing this result at $\bar{z} = 0.43$ with the region of measured pitot contours shown on Fig. 12, we observe this saddle-point location to be above the extremity of the vortex, in accordance with the flow model postulated on Fig. 1. We note further that in the conjectured crossflow projection (not a conical projection) of the streamlines about the cone cross section in Fig. 1, that the sum of the number of half-saddle singular points at the surface, nodes (foci) and saddle point in the stream, satisfy the appropriate topology law (see Refs. 21 and 22). Hence, this flow topology, verified in most respects by the measurements, appears to be a rational model of the flow.

The lateral velocities, to be obtained from the inclined optics measurements, have not yet been reduced from the data. Sample checks, however, indicate peak values to exist above and below the vortex centers, in accordance with intuitive reasoning.

3.2 Asymmetric Separation of the Lee-Side Cone Flow

Figure 16 is a laser vapor-screen crossflow picture of the Mach 0.6 lee-side separated flow about the cone at a relative incidence of 2.9, once asymmetry has commenced. As incidence is raised further, the secondary vortices (see Fig. 1) become agitated, increasing in unsteadiness to the point of imposing motion on the primary vortices and their associated feeding shear layers. At this particular combination of Mach number, Reynolds number, and cone configuration with 4° nose bluntness, the starboard vortex moved away from the cone surface, tending to roll over on top of the port-side vortex. This event is shown on Fig. 17 as an oblique pilot's view from the port side. The vortices appear more diffuse than in the symmetrical separated flow, but there is no evidence of shedding.

Along with this movement in the lee-side flow structure, we would expect the resultant force vector to move toward the side of the cone against which one vortex is closest (the port side in this case). Figure 18 demonstrates that the initial direction of side force is indeed toward the port side (i.e., a negative side-force coefficient, C_{yp}) in the free-stream Mach number range $0.6 < M_\infty < 0.95$ at $R_{L_\infty} = 13.5 \times 10^6$. A switch in side-force direction will occur if the vortices reverse their disposition so that the starboard vortex is now closest to the surface. Figure 18 illustrates that at Mach 0.6 the reversal is imminent at a relative incidence of about 4.4. At all Mach numbers, we should point out that a small positive offset in C_{yp} exists at low incidences systematic with the discrepancy between the port and starboard pressure distributions displayed on Fig. 9.

15-6
As Mach number increases to supersonic, the commencement in divergence of the side force is less precise and is delayed to higher relative incidences. For purposes of comparison, Fig. 19 presents side force versus incidence data taken with the same cone body as used herein but fitted with a sharp apex, in the NAE Ottawa 1.5- by 1.5-m (5- by 5-ft) blowdown wind tunnel at elevated Reynolds numbers, $Re_{\infty} \sim 35 \times 10^6$. In subsonic flow, the onset of asymmetry occurs at a lower relative incidence with the sharp tip than with the blunt tip. The substantial attenuation of side-force amplitude with increase of Mach number, hinted at in Fig. 18, is demonstrated impressively on Fig. 19. At Mach 4.27, there is no side-force development up to relative incidences of at least 5, under which conditions Rainbird (Ref. 23) has demonstrated the existence of strong embedded shock waves in the lee-side crossflow. These shocks certainly appear to encourage a return to flow symmetry close to the body as we may infer from the highest incidence case shown for the delta-wing flow on Fig. 4.

There is evidently a dependency of onset of asymmetry on cone tip condition (and shape) as well as Reynolds number and Mach number, as we present in summary form on Fig. 20. The critical angle of incidence for the onset of side force is here expressed as the incidence where the side force reaches 5% of the normal force. We note that the onset angle of incidence varies between 2.5 and 4.5 times the cone seminoise angle, a range somewhat higher than the nominal value of 2 reported for sharp cones and tangent-ogives by Keener and Chapman (Ref. 3) for Mach numbers less than 0.6. Their onset condition, however, was taken as the incidence where the divergence in side force commenced, and so will always be less than the criterion used above.

3.3 Control by Blowing of the Asymmetry in the Lee-Side Cone Flow

3.3.1 Side Force/Incidence Performance with a Constant Rate of Normal or Tangential Blowing

We speculated in section 2 (and see Ref. 18) that the injection of a small quantity of air from one side beneath the vortex farthest from the surface would tend to reduce the asymmetry in the lee-side vortex pair, the turning and penetrating jet flow providing an entrainment effect on the vortex. In section 3.2, we learned that the secondary vortices became violently unsteady once asymmetry began and incidence continued to increase. Consequently, the first blowing position tried was a single orifice at $\psi = 150^\circ$ and was situated nominally between the locations of the primary and secondary separation lines (see Fig. 10). Before opening a blowing hole, however, the development of the side force with incidence was measured; the test was then repeated with the epoxy sealer removed from the blowing hole, but with no air injection, to determine whether the roughness of the hole itself had an influence. The usual result was that hole roughness introduced on the lee-side of the cone made negligible change to the relative incidence at which significant side force developed.

The effect of blowing normally to the cone surface from a single 2.4-mm (0.096-in.) diameter hole at $\psi = 150^\circ$ is shown as Configuration 3 in Fig. 21. In contrast with the original cone nose labeled Configuration 1, whose initial side-force tendency was illustrated in Fig. 18 to be to port (negative C_{YB}) this replacement nose (Configuration 2) developed side force to the starboard side. Hence the blowing hole was opened at $\psi = -150^\circ$ beneath the high vortex situated on the port side. The introduction of the jet air with $C_{\mu} \sim 0.003$ at relative incidences up to 2.5 exacerbated the no-blow C_{YB} magnitudes by many times C_{μ} . Once a relative incidence of 3 was reached, however, the jet became highly interactive with the lee-side vortices to cause a complete reversal in the trend of side-force development. In Fig. 21, we see that the side-force coefficient reduces rapidly to zero and increases in the opposite direction to that of the no-blowing case. Figure 21 also displays that the root-mean-square amplitude of the side-force fluctuation (obtained from the balance) is attenuated at high incidence once the blowing is activated.

If the one blowing orifice between the primary and secondary separations can exercise such powerful control by fluid amplification, what would be the effect of two jets? A second orifice of the same size of 2.4 mm (0.096 in.) was then opened at $\psi = -120^\circ$. This orifice was situated on the windward side of the primary separation line and is denoted as Configuration 4. In Fig. 21, we demonstrate no additional improvement with two holes blowing over the performance with the single orifice. The significant controlling influence is exerted, evidently, inboard of the primary separation line. Hence the windward position of blowing chosen as optimum by Sharir, Portnoy, and Rom (Ref. 17) on a missile configuration would not necessarily seem to be the most applicable.

A test with a larger blowing orifice was then attempted. Another conical nose frustum was attached to the cone body in which 3.6-mm (0.140-in.) diameter blowing orifices had been machined, Configuration 5. Figure 22 shows that the no-blowing side-force/incidence characteristic for Configuration 5 is once again different than the two previous no-blowing cases (Configurations 1 and 2). The initial direction of the side force is toward the port side but reverses at a relative incidence of 3.6. To control the initial direction of side-force, a blowing orifice was opened at $\psi = 150^\circ$ on the starboard side, Configuration 6. Figure 22 shows that blowing at $C_{\mu} = 0.006$ provided a positive reversal in the initial trend of side-force development, which with increasing incidence, continued to generate ever-increasing positive C_{YB} . Figure 22 also demonstrates the acceptable repeatability obtainable for the given nose over a spread of days between tests.

Next, a passive suction/blowing scheme was tried by opening another 3.6-mm (0.140-in.) diameter hole at $\psi = 0^\circ$ on the windward ray. This is called Configuration 7. With the external supply of compressed air closed off, air from the approaching windward flow could enter the plenum within the frustum and exhaust out of the $\psi = 150^\circ$ hole on the leeward side. The inflow through the $\psi = 0^\circ$ hole was smoothed by means of a countersunk "bell-mouth" entry. Figure 22 shows that no alleviation in side-force divergence occurred when comparing the results with the no-blowing case. A partial explanation for the failure may be attributed to a significant flow loss in the windward hole leaving only a marginal pressure difference to drive any "injected" air through the second orifice on the leeward side.

Does a symmetrical blowing geometry offer an improvement over the asymmetric schemes looked at so far? Retaining the two open orifices at $\psi = 0^\circ, 150^\circ$ as in Configuration 7, the $\psi = -150^\circ$ orifice on the port side was also unplugged (Configuration 8), allowing air to issue symmetrically about the cone. The side-force/incidence performance for this latter blowing arrangement is also displayed in Fig. 22. We detect that

the symmetrical blowing rate of $C_{11} \sim 0.010$ delays the onset of asymmetry up to a relative incidence of at least 3.4, but loses its effectiveness at higher incidences. In terms of degree of side-force control per unit blowing mass or momentum flux, we might infer, from comparing Figs. 21 and 22, that the asymmetric single hole blowing scheme at $\phi = 150^\circ$ is the most effective. 15-7

The windward hole at $\phi = 0^\circ$ was plugged. The result of inserting one right-angle tube in the 3.6 mm (0.140-in.) diameter hole at $\phi = 150^\circ$ with the blowing exit directed along a body generator towards upstream, is shown in Fig. 23. We see that the initial divergence in side force without blowing (Configuration 9) is erased when the injected air issues at $C_{11} \sim 0.005$ (Configuration 10). Blowing in the downstream direction provides a similar, favorable result (Configuration 12 and see Ref. 18).

It is remarkable, perhaps, that the direction of blowing, whether normal, or tangential upstream or tangential downstream, makes negligibly small difference to the degree of control available (compare Figs. 22 and 23). It is as though the asymmetric jet, in terms of its effect on the forebody flow, may be thought of as a "controllable roughness element." Notwithstanding, the role of the jet in the development of the lee-side flow field is evidently more complex and striking than this analogy might allow, as we see on the sequence of laser vapor screen pictures demonstrated in the next section.

3.3.2 Cone Surface Pressures and Laser Vapor Screen Flow Visualization during an Incidence Sweep with a Constant Rate of Normal Blowing, Configuration 6

In Fig. 24, we view selected laser vapor screen pictures and circumferential distributions of surface pressure at the 0.87 axial station for Configuration 6 with a constant blowing rate, $C_{11} \sim 0.006$. These results correspond with the side-force/incidence performance illustrated in Fig. 22, at relative incidences of 0.43, 1.26, 2.08, 2.48, 2.9, and 3.72. The flow visualization pictures are views from the pilot's position, behind the cone base. The bright appearance of the jet/vortex flow, in contrast with the shadowy nature of the vortices with no jet flow shown on Figs. 11 and 16, is thought to be associated with intense scattering of laser light from additional condensation occurring in the jet-vortex flow due to a low stagnation temperature in the jet air.

At low incidences, Figs. 24(a) and (b) illustrate that the under-expanded jet penetrates into the stream from the $\phi = 150^\circ$ orifice, turning rapidly as it plumes outwards. The contra-rotating vortices of the jet flow itself are of opposite sign to those on the cone (with eventual separation) and are contained within the mushroom-shaped top of the vapor cloud. The pressure distributions on the same figures indicate no clearly determinable perturbations resulting from the jet flow. At relative incidences of 2 and above on Figs. 24(c)-(f), the flow visualization shows the jet as a separate snake-like entity existing above the body vortices. The flow visualization records at relative incidences of 2.08 and 2.48, and the pressures in Figs. 24(c) and (d), both correspond with overall side-force magnitudes near zero. Further increase in relative incidence in Figs. 24(e) and (f) shows a striking difference between the size of the port and starboard vortices, with the starboard vortex, as it is closer to the surface, providing noticeable peaks in suction pressure and hence side force to the right. The mushroom cap to the vapor cloud becomes kidney-shaped concomitant with a counterclockwise rotation of the jet vortices as we see in the hypothesized flow structures in Fig. 25. We note that at the highest relative incidence of 3.7 shown in Fig. 24(f), the jet flow has appeared to ally itself with the (weaker) port-side vortex. The equivalent pressure distribution in Fig. 24(f) displays a complete asymmetry at all circumferential locations.

The essential difference between the alternative flow structures shown on Fig. 25 is the saddle-point formation above the body vortices. If any magnification of instabilities in the region of the enclosing saddle point (see Fig. 1) is the governing flow mechanism promoting vortex asymmetry (roughness and waviness at the nose simply providing the initial direction that the side force should take) then Fig. 25(a) allows that the movement of the saddle point of Fig. 1 to a location well away from the body, above the forebody vortices plus jet, should reduce the influence of the saddle point. The sketch in Fig. 25(b), on the other hand, still permits the enclosing saddle point on Fig. 1 to be positioned close to the body surface where its influence on the adjacent flow field would still be dominant. Summing up this conjectural discussion, we might imply that Fig. 25(a) is a more credible flow topology, therefore, than that shown on Fig. 25(b), and can perhaps be better fitted within the vapor screen boundary on Fig. 24(f).

3.3.3 Effect of Changing Blowing Rate on Side-Force Magnitude at Constant Incidence

Figure 26 presents the control of the asymmetric side forces exercised by changing the blowing rate for those configurations (2, 4, 6, and 8) that utilize normal jets. In all cases, a relative incidence of 3 or greater was chosen for the comparison corresponding with the A, B, and C positions on the (no-blowing) side-force/incidence plots of Figs. 21 and 22.

As blowing rate is increased, Configurations 2 and 4 utilizing the 2.4-mm (0.096-in.) asymmetrically disposed blowing orifices do not demonstrate a capacity to reverse the direction of the side force. The maximum change in amplitude is about a 50% reduction. On the other hand, Configuration 6 with the 3.6-mm (0.140-in.) diameter blowing orifice demonstrates powerful control over side-force development. Depending on blowing rate, C_{11} can be set at a positive or negative value, with good repeatability. The usefulness of symmetrical normal blowing with Configuration 8 (at $\phi = \pm 150^\circ$ and 0° , it will be remembered) is also recognizable. It would appear from Fig. 26 that symmetrical blowing is not as powerful as the asymmetric jet, but can nevertheless keep the side force within acceptable limits.

Figures 27(a)-(g) show laser vapor screen flow visualization results and corresponding circumferential wall static pressure distributions for Configuration 6 at a fixed relative incidence of 3.3 and a varying C_{11} . These examples relate to the curve of side force with change of normal blowing rate on Fig. 26 which exhibited the most powerful control and reversal of side-force direction.

The selection of Figs. 27(a)-(c) demonstrates flow features where there is a trickle of blowing air and the stronger port-side vortex generates a negative C_{11} . The jet flow appears "attached" to the weaker starboard vortex. Figure 27(d) displays the flow field, close to zero side force, where the body vortices are virtually symmetrically displaced and the port and starboard pressure distributions show little disagreement.

Increasing C_{μ} above 0.004 in Figs. 27(e)-(g) now drives the side force to an ever-increasing positive value, clearly demonstrated by the lengthening distance displayed between the port-side vortex and the cone surface. Note again that the jet flow becomes inseparable from the weaker vortex.

Clearly the symmetry of the body vortices can be controlled by the jet momentum rate, and this symmetry reflects immediately on to the body pressure field. The asymmetry in the jet flow "suspended above" the body vortices appears to be of lesser importance. Because the rotation of the vortices in the jet flow is of opposite hand to the body vortices, the jet flow cannot engulf them, nor can the jet be entrained into them. The speculative jet sink effect introduced earlier is presumably inadmissible. The jet flow will exist as a discrete entity in analogy, perhaps, with the spiral vortices emanating from foci on the nose region of a blunt body (Refs. 21 and 22). The rotational direction of these nose vortices is replicated in the jet flow. We postulate that these spiral vortices on the blunt body have a stabilizing effect on the lee-side flow field to provide a delayed onset of side force. The characteristic mechanism of the jet flow is to give a new structure or topology to the overall flow field (jet vortices plus body vortices) which at a suitable blowing rate offers a not dissimilar flow to that about the blunt body.

Finally, Fig. 28, for the same chosen incidence as in Fig. 27, compares the effectiveness of blowing tangentially upstream or downstream (Configurations 10 and 12, respectively) with that of normal blowing (Configuration 6). All blowing geometries possess the capability to reverse the direction of the side-force development, but the normal blowing has a wider range of applicable C_{μ} . The effectiveness of the tangential blowing at altering side-force magnitude diminishes at the higher blowing rates. Note, however, that for very small C_{μ} values typically less than 0.0015, the trend of changing side force with C_{μ} is of opposite hand to the trend when $C_{\mu} > 0.0015$.

4. CONCLUSIONS

Based on the pressures, forces, and laser vapor screen measurements about a 5° semiangle cone in a Mach 0.6 flow under turbulent conditions, we may offer the following conclusions on the continuing exploration of the symmetrical separated flow zones at moderate relative incidence ($\alpha/\theta_c \sim 2.5$) and the effectiveness of nose blowing to control asymmetry of the lee-side vortex flow field at high relative incidences ($\alpha/\theta_c \sim 4$):

1. The capability of a new dual-beam laser velocimeter has been exploited to measure the mean velocities in the symmetrically separated flow field and to determine the location of the saddle point above the body vortices in the plane of the leeward meridian. Together with pitot measurements and dimensioning of the boundary of the rolled-up shear layer from the laser flow visualization records, wall pressures, wall shear stresses and directions, plus previously obtained dynamic measurements at the surface (see Ref. 20), a panorama of three-dimensional flow separation is gradually being assembled. The importance of amplification of instabilities at the saddle point, in promoting forebody vortex asymmetry is mooted but has not yet been established; nor whether such amplification by close association with flow near the surface, causes the (eventual massive) unsteadiness of the secondary separations at high relative incidences. Hence, the initial attempt was made to control the asymmetry by injecting air close to one or both of the secondary vortices, and by implication, the region in the vicinity of the saddle point.
2. Blowing on one side of the leeward meridian, from a single circumferential hole situated between the primary and secondary separation lines, but beneath the (weaker) vortex that is farthest from the surface, offers an effective means to reduce to zero (and to subsequently reverse) the direction of the side force.
3. Blowing normal to the surface as a jet spoiler appears to be more effective than either upstream or downstream directed tangential blowing.
4. In contrast to the asymmetric blowing principle, symmetrically disposed blowing nozzles appear less effective at corresponding momentum rates.
5. The blowing rates required are very small, there being a large "fluid amplification" of the jet effect. A typical C_{μ} required for an aircraft could be as low as 0.001 for an equivalent blowing location.
6. The jet does not engulf the forebody vortices in either the normal or tangential blowing arrangements. Its counter-rotating pair of vortices "float above" the forebody vortices forming a well-organized and recognizable topology. This is so for all blowing geometries, but with the tangential blowing, the structure is less well defined.

REFERENCES

1. Rainbird, W. J., Crabbe, R. S., Peake, D. J., and Meyer, R. F., "Some Examples of Separation in Three-Dimensional Flows," *CASI Journal*, Vol. 12, No. 10, December 1966, pp. 409-423.
2. Peake, D. J., Rainbird, W. J., and Atraghji, E. G., "Three-Dimensional Flow Separations on Aircraft and Missiles," *AIAA Journal*, Vol. 10, No. 5, May 1972, pp. 567-580.
3. Keener, E. R. and Chapman, G. T., "Onset of Aerodynamic Side Forces at Zero Sideslip on Symmetric Forebodies at High Angles of Attack," *AIAA Paper 74-770*, August 1974.
4. Keener, E. R., Chapman, G. T., and Kruše, R. L., "Effects of Mach Number and Afterbody Length on Onset of Asymmetric Forces on Bodies at Zero Sideslip and High Angles of Attack," *AIAA Paper 76-66*, January 1976.
5. Titiriga, A., Skow, A. M., and Moore, W. A., "Forebody/Wing Vortex Interactions and their Influence on Departure and Spin Resistance," *AGARD CP-247*, October 1978.

6. Lamont, P. J., "Pressure Distributions on an Ogive-Cylinder at High Angles of Attack with Laminar, Transitional or Turbulent Separation," Working Group Meeting on High Angle of Attack Missile Aerodynamics, AEDC, Tennessee, March 1979.
7. Hunt, B. L. and Dexter, P. C., "Pressures on a Slender Body at High Angle of Attack in a Very Low Turbulence Level Airstream," AGARD CP-247, October 1978.
8. Nishioka, M. and Sato, H., "Mechanism of Determination of the Shedding Frequency of Vortices Behind a Cylinder at Low Reynolds Numbers," Journal Fluid Mechanics, Vol. 89, Part 1, 1978, pp. 49-60.
9. Ericsson, L. E. and Reding, J. P., "Coupling Between Boundary-Layer Transition and Vehicle Motion," Working Group Meeting on High Angle of Attack Missile Aerodynamics, NASA Langley Research Center, March 1978.
10. Neihouse, A. I., Kliner, W. J., and Scher, S. H., "Status of Spin Research for Recent Airplane Designs," NASA TR-R-57, 1960.
11. Jorgensen, L. H., "Prediction of Aerodynamic Characteristics for Slender Bodies Alone and with Lifting Surfaces to High Angles of Attack," AGARD CP-247, 1978.
12. Rao, D. M., "Side-Force Alleviation on Slender, Pointed Forebodies at High Angles of Attack," AIAA Paper 78-1339, August 1978.
13. Bannink, W. J. and Nebbeling, C., "Measurements of the Supersonic Flow Field Past a Slender Cone at High Angles of Attack," AGARD CP-247, October 1978.
14. Keener, E. R. and Chapman, G. T., "Similarity in Vortex Asymmetries over Slender Bodies and Wings," AIAA Journal, Vol. 15, No. 9, September 1977, pp. 1370-1372.
15. Shanks, R. E., "Low-Subsonic Measurements of Static and Dynamic Stability Derivatives of Six Flat-Plate Wings Having Leading-Edge Sweep Angles of 70° to 84°," NASA TN D-1822, 1963.
16. Fellows, K. A. and Carter, E. C., "Results and Analysis of Pressure Measurements on Two Isolated Slender Wings and Slender Wing-Body Combinations at Supersonic Speeds, Vol. 1 - Analysis," ARA Rept. 12, November 1969.
17. Sharir, D., Portnoy, H. and Rom, J., "A Study of the Effects of Jets from a Slender Body of Revolution on the Side Forces Acting on It at Large Angles of Attack in Low Speeds," Technion, Israel Institute of Technology, TAE 337, May 1978.
18. Skow, A. M., Moore, W. A., and Lorincz, D. J., "A Novel Concept to Enhance Departure/Spin Recovery Characteristics of Fighter Aircraft Through Control of the Forebody Vortex Orientation," Paper 24, this meeting.
19. Owen, F. K. and Johnson, D. A., "Wake Vortex Measurements of Bodies at High Angle of Attack," AIAA Paper 78-23, January 1978.
20. Peake, D. J., Owen, F. K., and Higuchi, H., "Symmetrical and Asymmetrical Separations about a Yawed Cone," AGARD CP-247, October 1978.
21. Peake, D. J. and Tobak, M., "Three-Dimensional Separated Flows: Retrospect and Prospect," Paper presented at Project Squid Meeting, Dallas, Texas, January 1979.
22. Peake, D. J. and Tobak, M., "Topology of Two-Dimensional and Three-Dimensional Separated Flows," Paper to be presented at AIAA 12th Fluids and Plasma Dynamics Meeting at Williamsburg, Va., July 1979.
23. Rainbird, W. J., "The External Flow Field About Yawed Circular Cones," AGARD CP-30, May 1968.

ACKNOWLEDGMENTS

The authors express their gratitude to L. H. Öhman of NAE, Ottawa, for kindly making available to NASA the basic 5° cone model and pitot rake. They also acknowledge the substantial efforts of R. Gordon and the Model Shop team at NASA Ames who fabricated the model parts.

Special thanks are also due to: D. Peña of ARO Inc., for his services as project engineer in charge of the tunnel test; to W. J. Rainbird for conveying previously unpublished side-force results obtained on the same model in the NAE Ottawa 1.5- by 1.5-m (5- by 5-ft) blowdown wind tunnel; and to M. Tobak and G. T. Chapman for their enthusiastic support and stimulating discussion.

One of us, F. K. Owen, would also like to acknowledge the support of the Air Force Armament Laboratory, Eglin AFB, Florida, and Ames Research Center, Moffett Field, California, under Contract No. NAS2-9663.

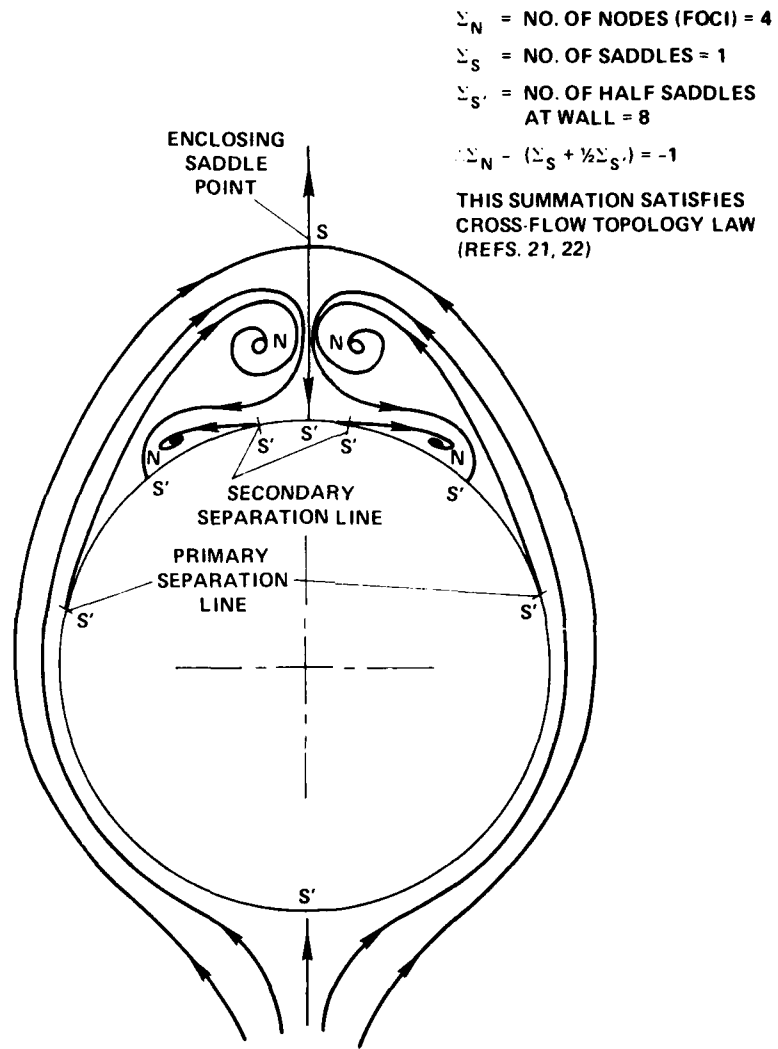


Fig. 1. Cross-flow topology of streamlines about circular cone at incidence with primary and secondary separations.

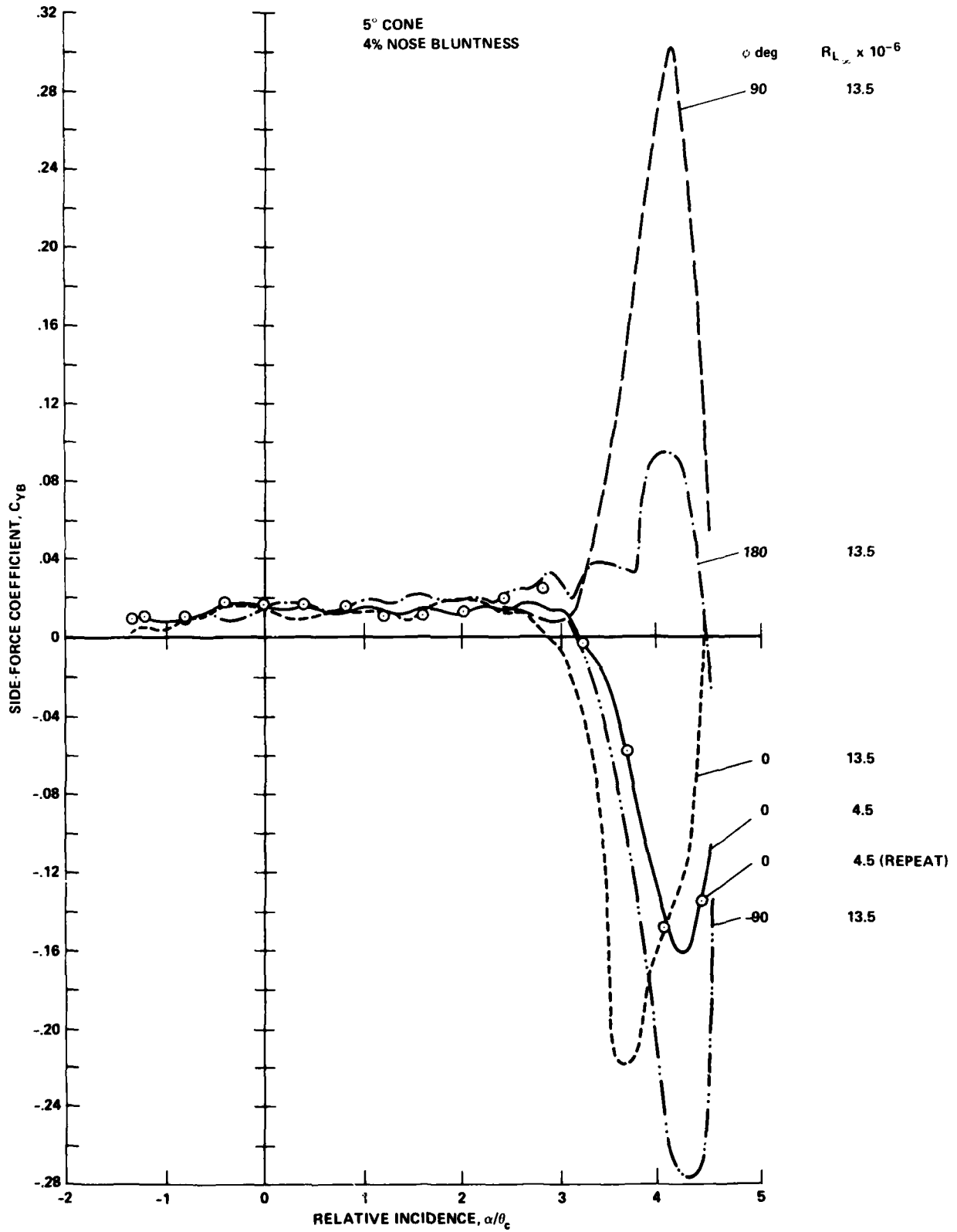
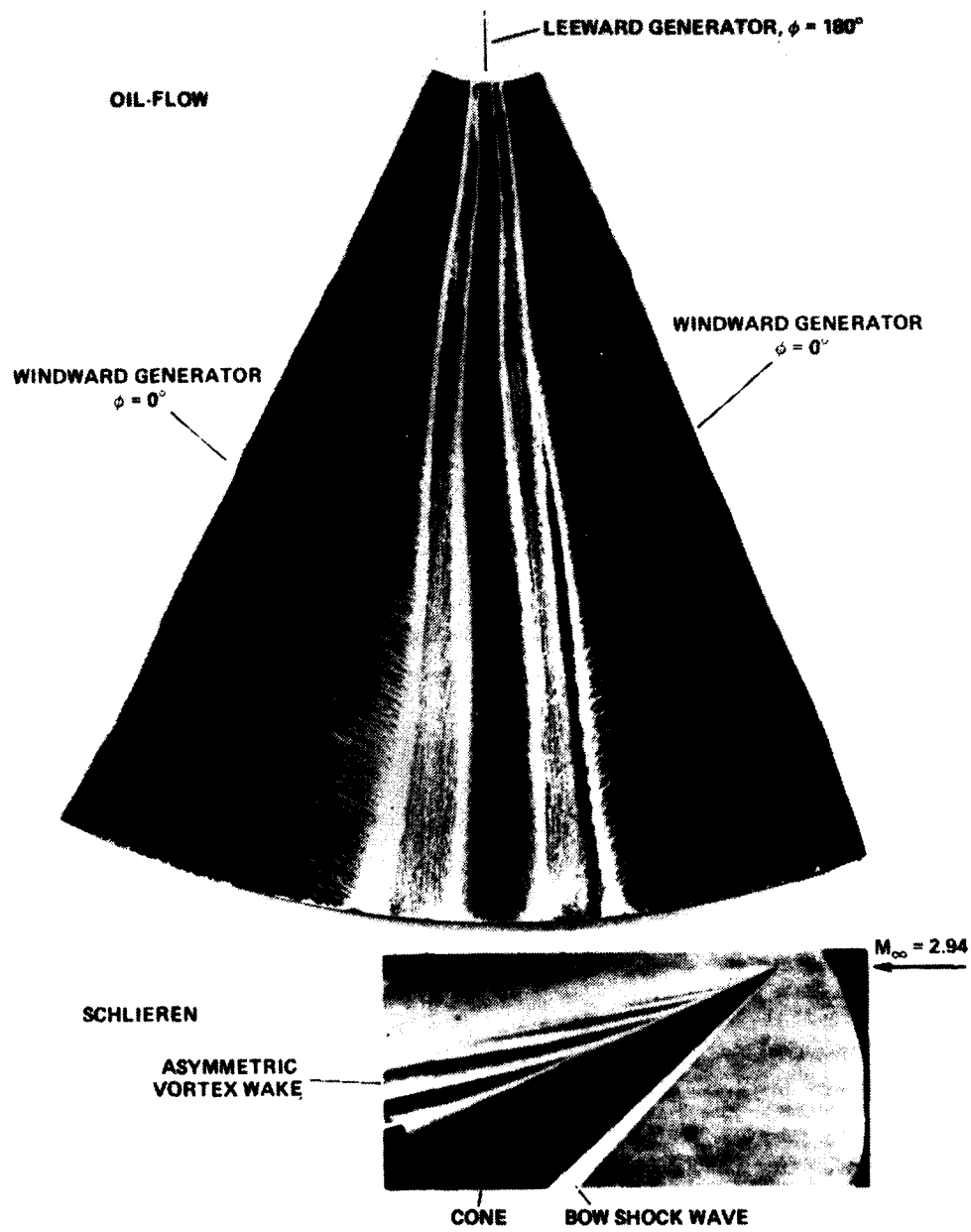


Fig. 2. 5° semiangle cone side-force sensitivity to roll angle and Reynolds number at $M_\infty = 0.6$.



$\alpha = 34^\circ; \bar{\alpha} = 4.53; \text{ASYMMETRY BEGAN AT } \bar{\alpha} \sim 3.7$

Fig. 3. Asymmetric primary and secondary separation lines on $\theta_c = 7.5^\circ$ semiangle cone (Ref. 13).

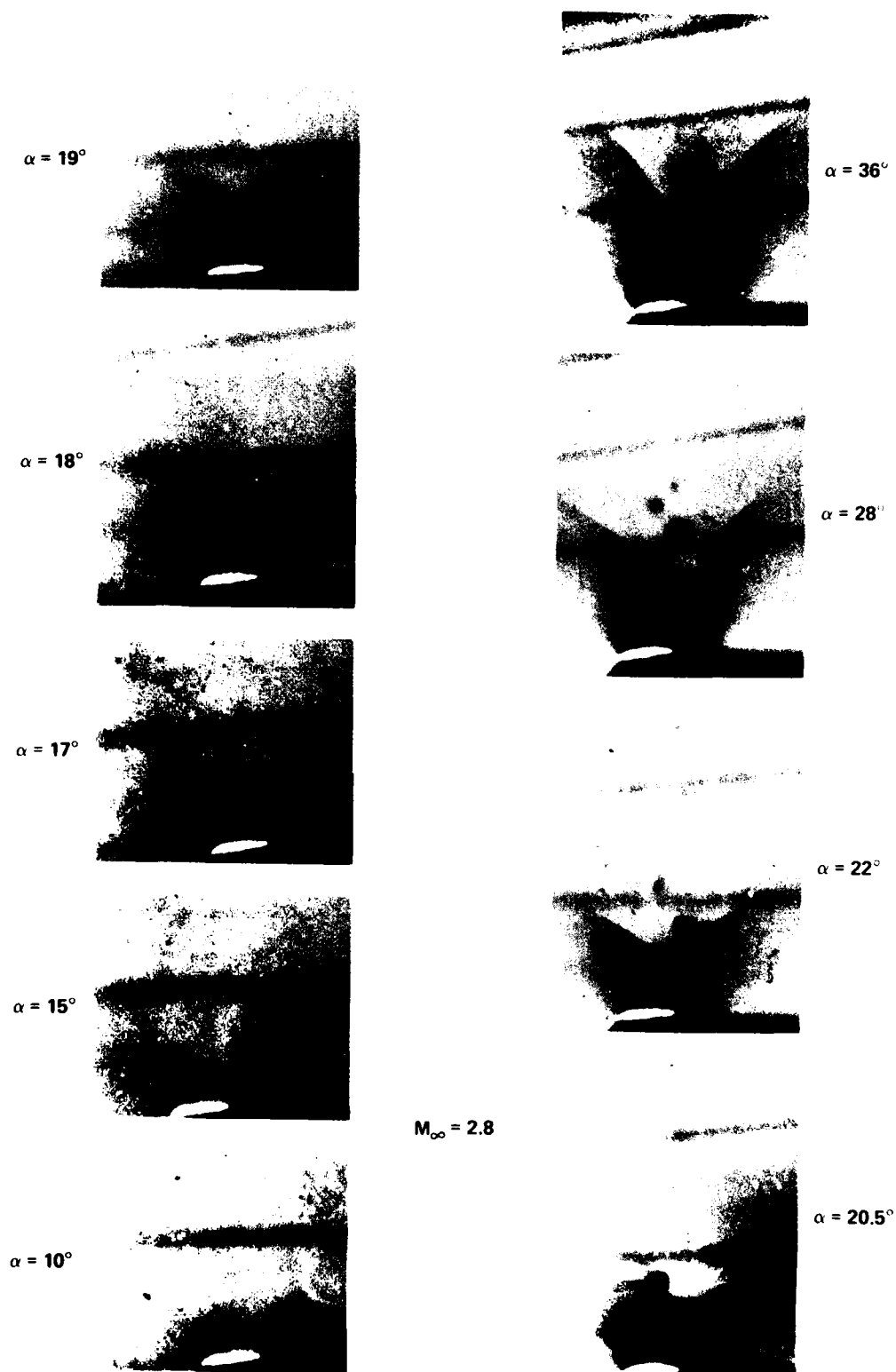


Fig. 4. Asymmetric flow field about 85° swept back delta wing (Ref. 16).

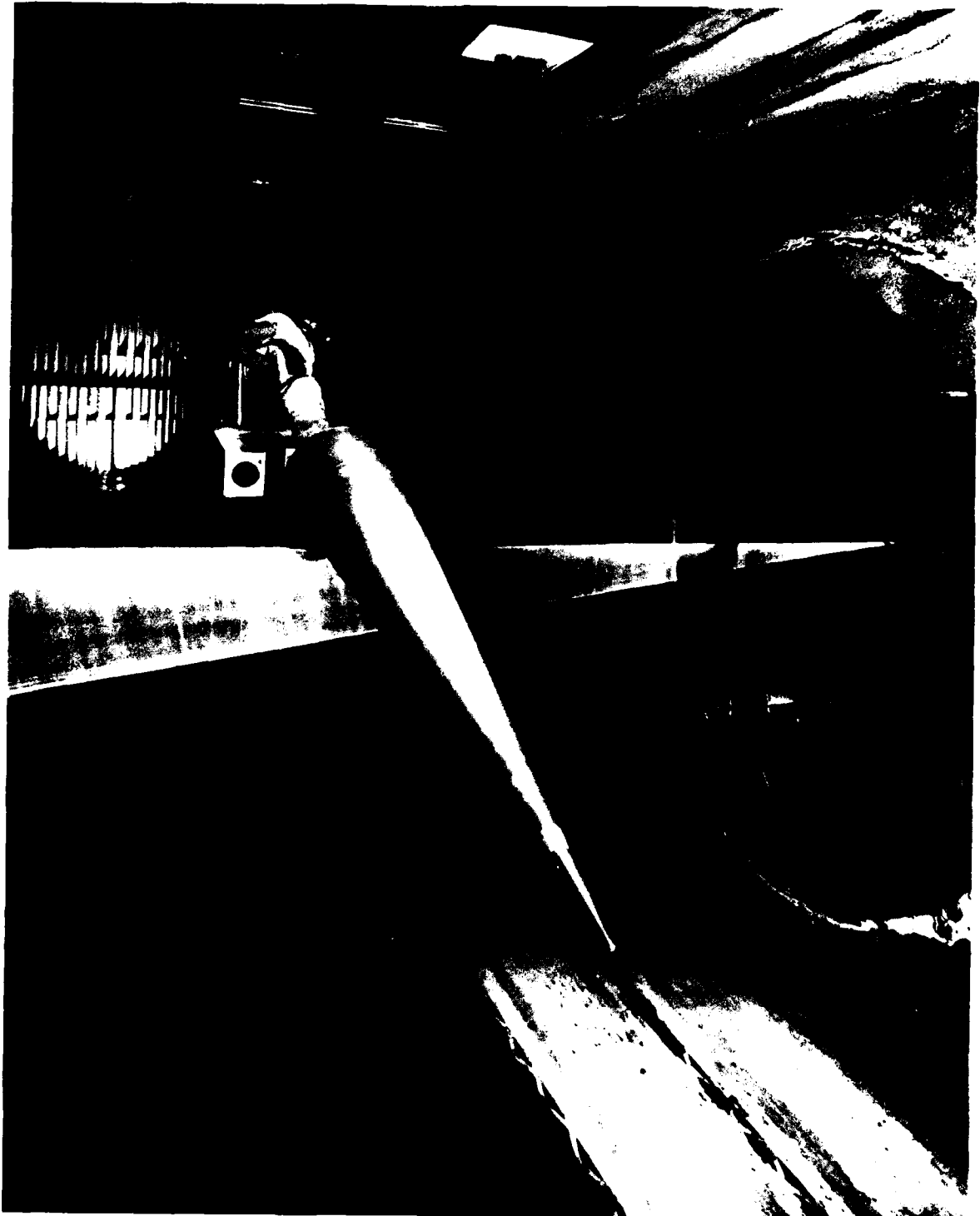
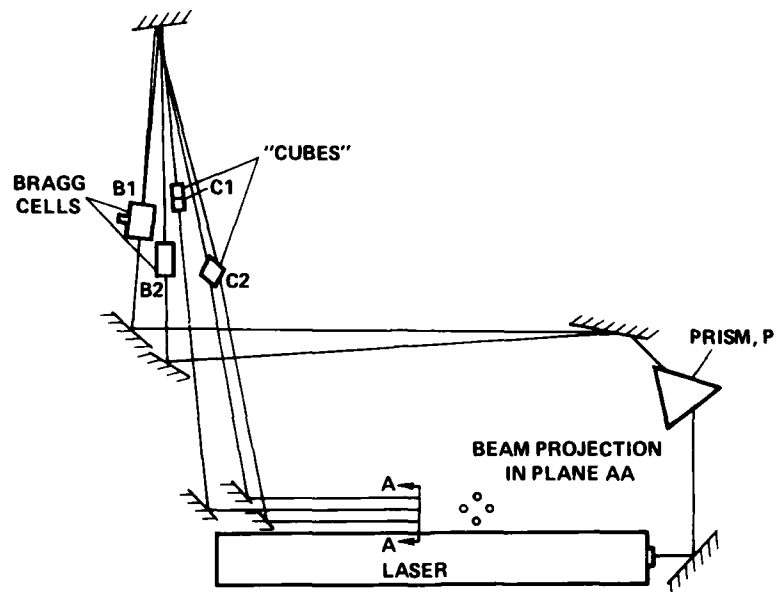
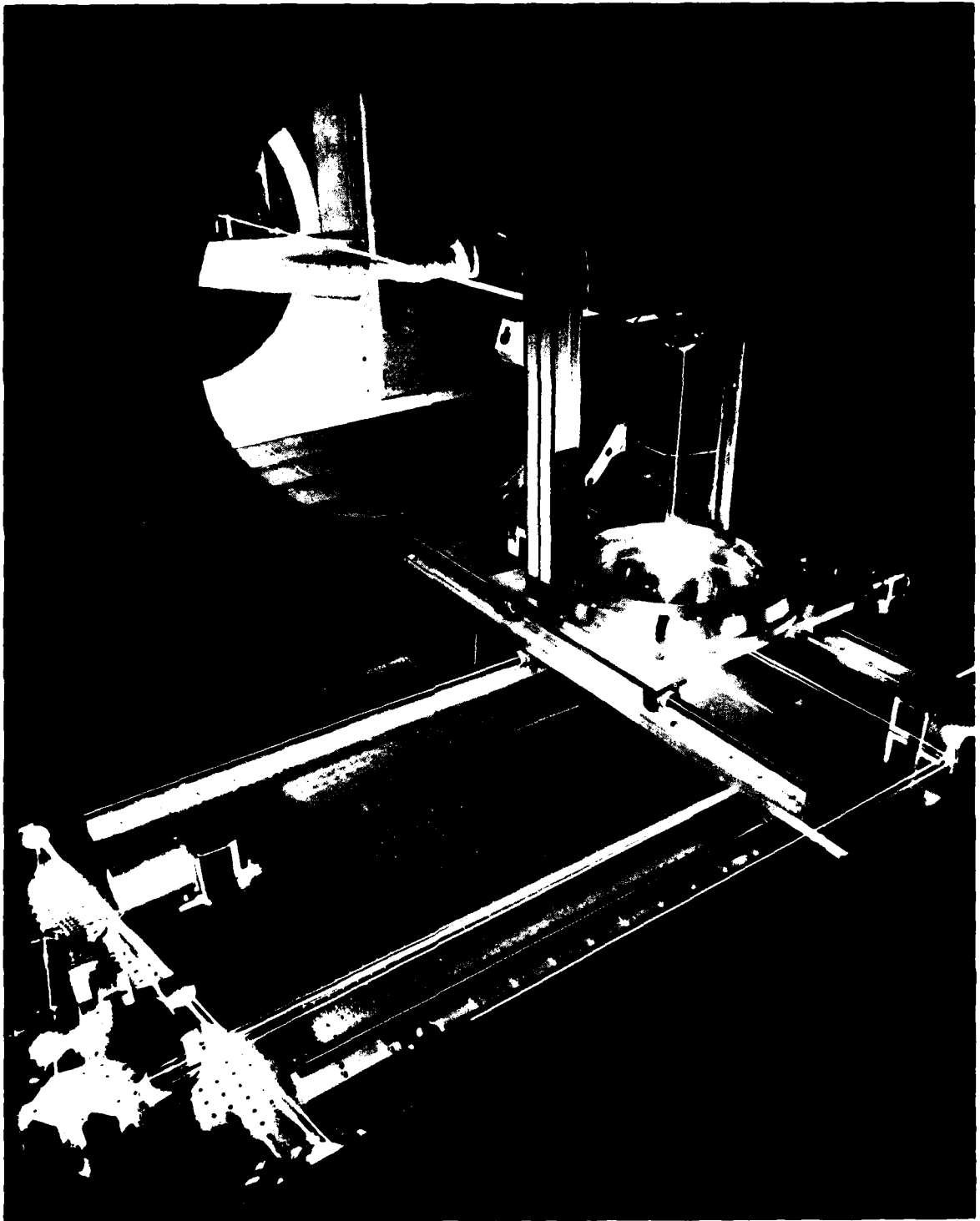


Fig. 5. 5° semiangle cone in Ames 6- by 6-Foot
Wind Tunnel.



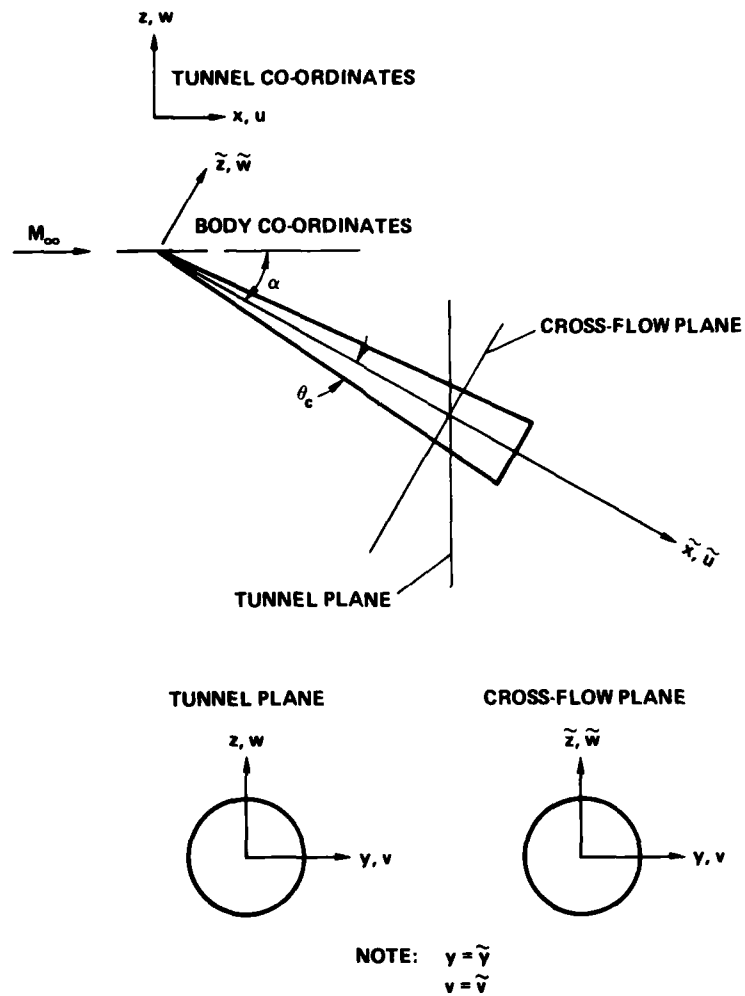
(a) Two-component LDV beam system in Ames
6- by 6-Foot Wind Tunnel.

Fig. 6. Velocity measurements with laser velocimeter.



(b) Sending optics and traverse gear of two-component LDV.

Fig. 6. Continued.



(c) Coordinate system for flow velocities.

Fig. 6. Concluded.

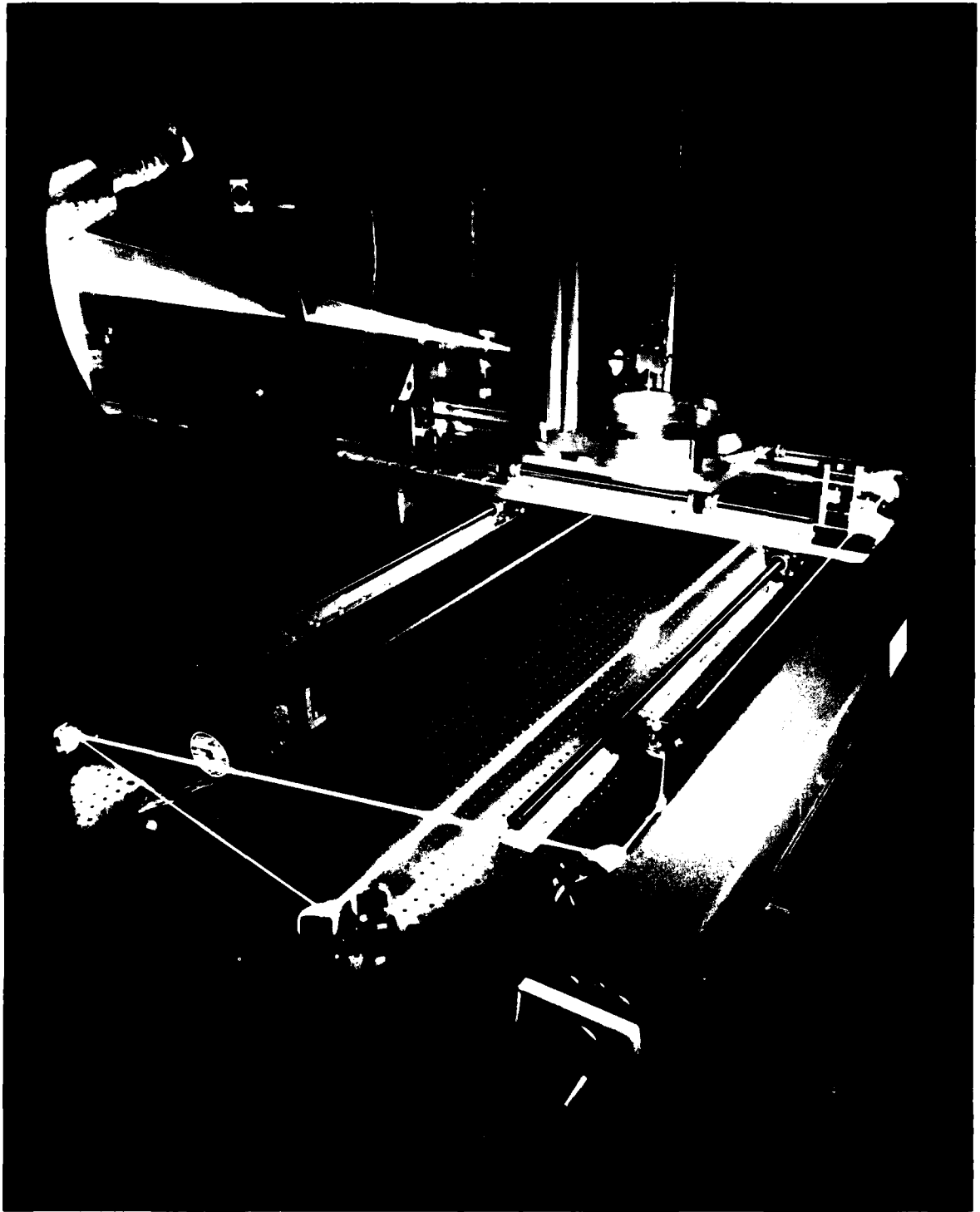
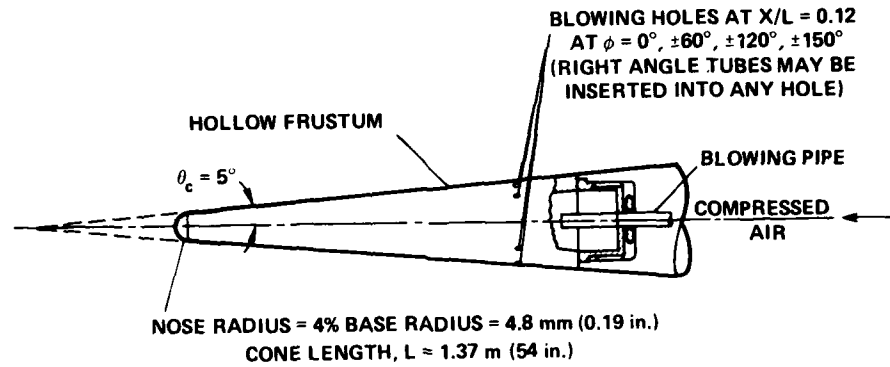


Fig. 7. Spread laser beam for vapor screen.



(a) Blowing plenum in conical frustum.

NO.	ϕ°	JET diam, mm (in.)	NO.	ϕ°	JET diam, mm (in.)	
1		NONE	7	0, 150	3.6 (0.140)	PASSIVE
2	-150	2.4 (0.096)	8	0, +150	3.6 (0.140)	
3	-150	2.4 (0.096)	9	150	3.4 (0.132)	TUBE FACING UPSTREAM NO BLOWING
4	-120, -150	2.4 (0.096)	10	150	3.4 (0.132)	TUBE FACING UPSTREAM BLOWING
5	150	3.6 (0.140)	11	150	3.4 (0.132)	TUBE FACING DOWNSTREAM NO BLOWING
6	150	3.6 (0.140)	12	150	3.4 (0.132)	TUBE FACING DOWNSTREAM BLOWING

(b) Normal and tangential jet positions (pilot's view of body cross sections).

Fig. 8. Blowing design.

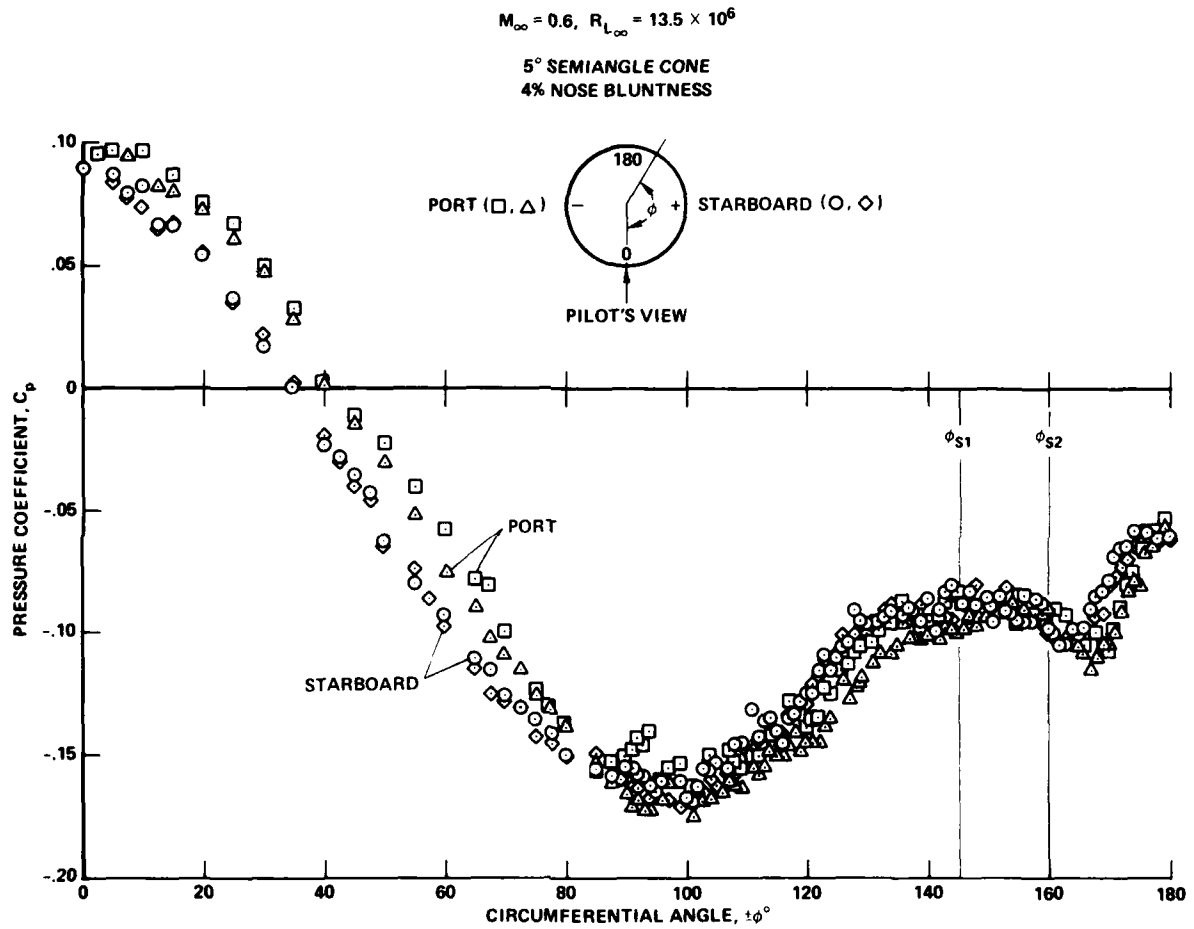


Fig. 9. Surface pressures at $\alpha/\theta_c = 2.5$.

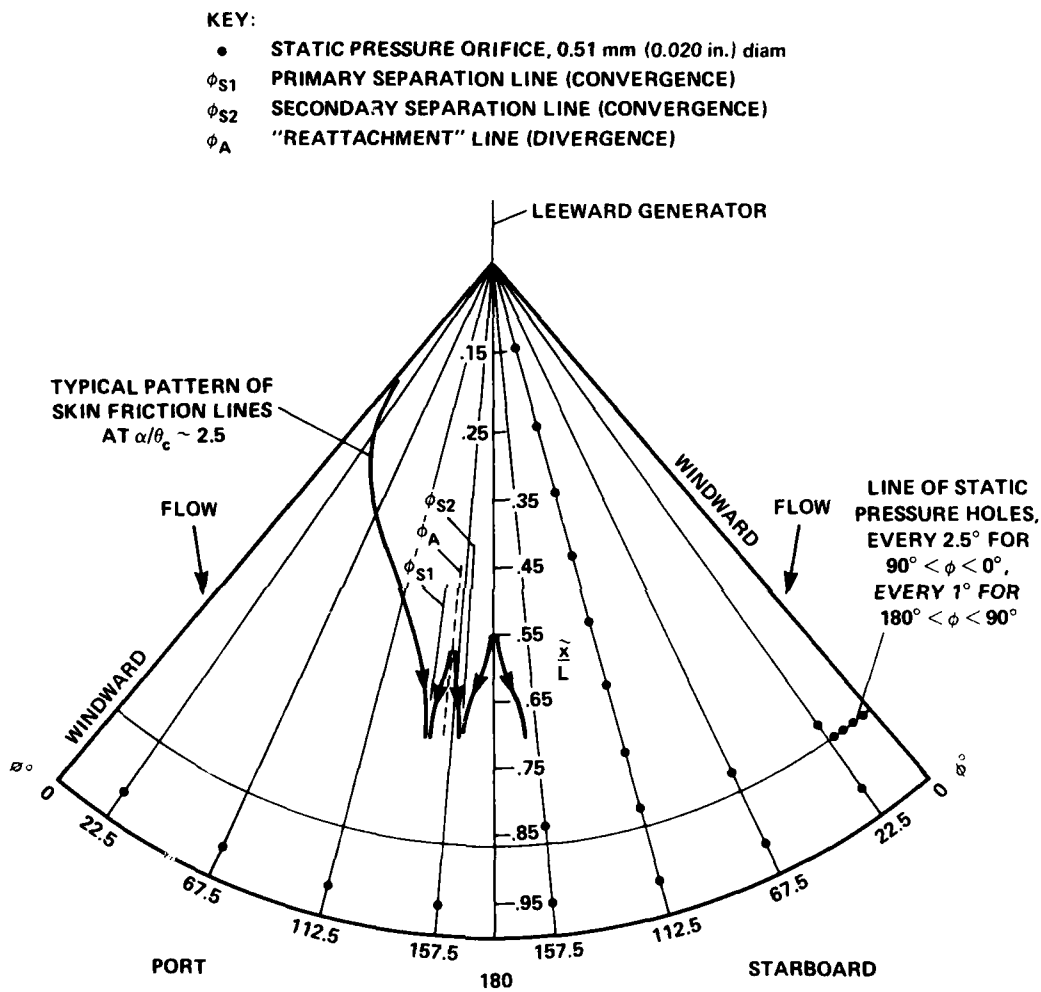


Fig. 10. Unwrapped cone surface.

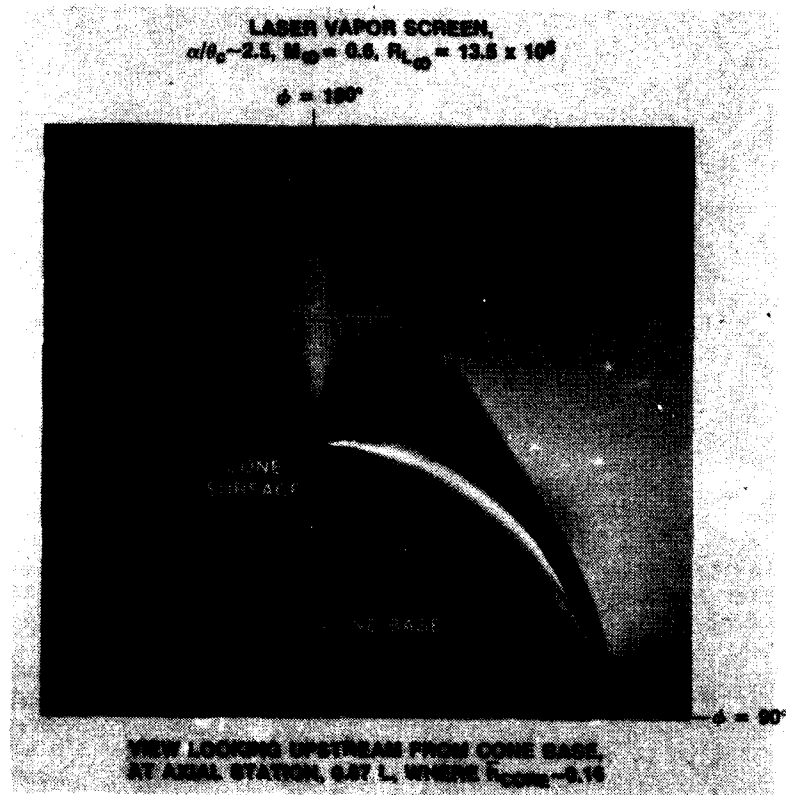


Fig. 11. Laser vapor screen, $\alpha/\theta_c = 2.5$, $M_\infty = 0.6$, $R_{L_\infty} = 13.5 \times 10^6$.

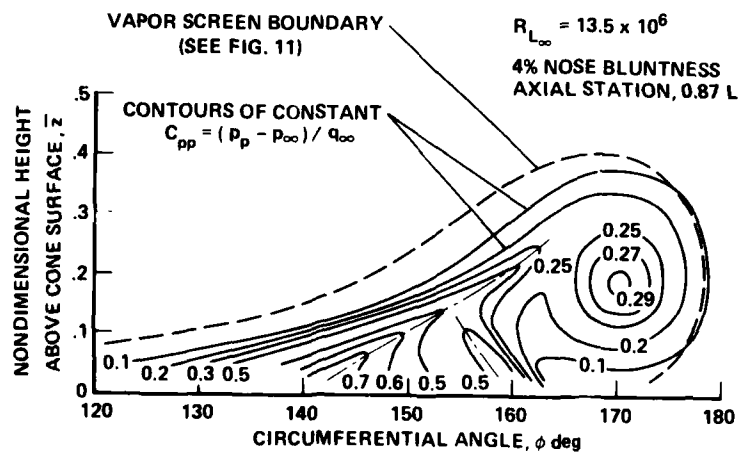


Fig. 12. Pitot pressure deficit, $M_\infty = 0.6$, $\alpha/\theta_c = 2.5$.

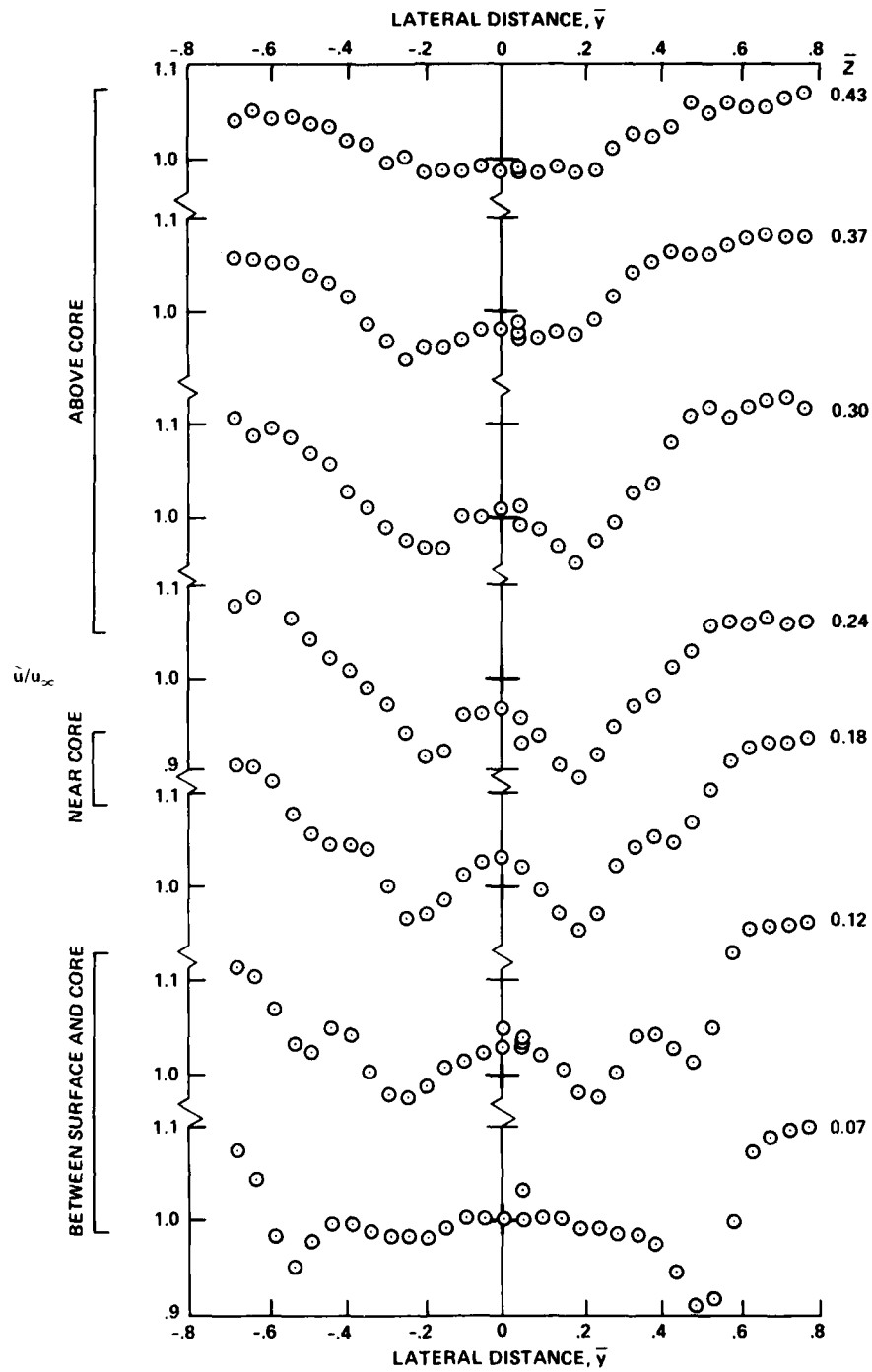


Fig. 13. Mean axial velocities in cross-flow plane at $x/L = 0.87$, $\alpha/\theta_c = 2.5$.

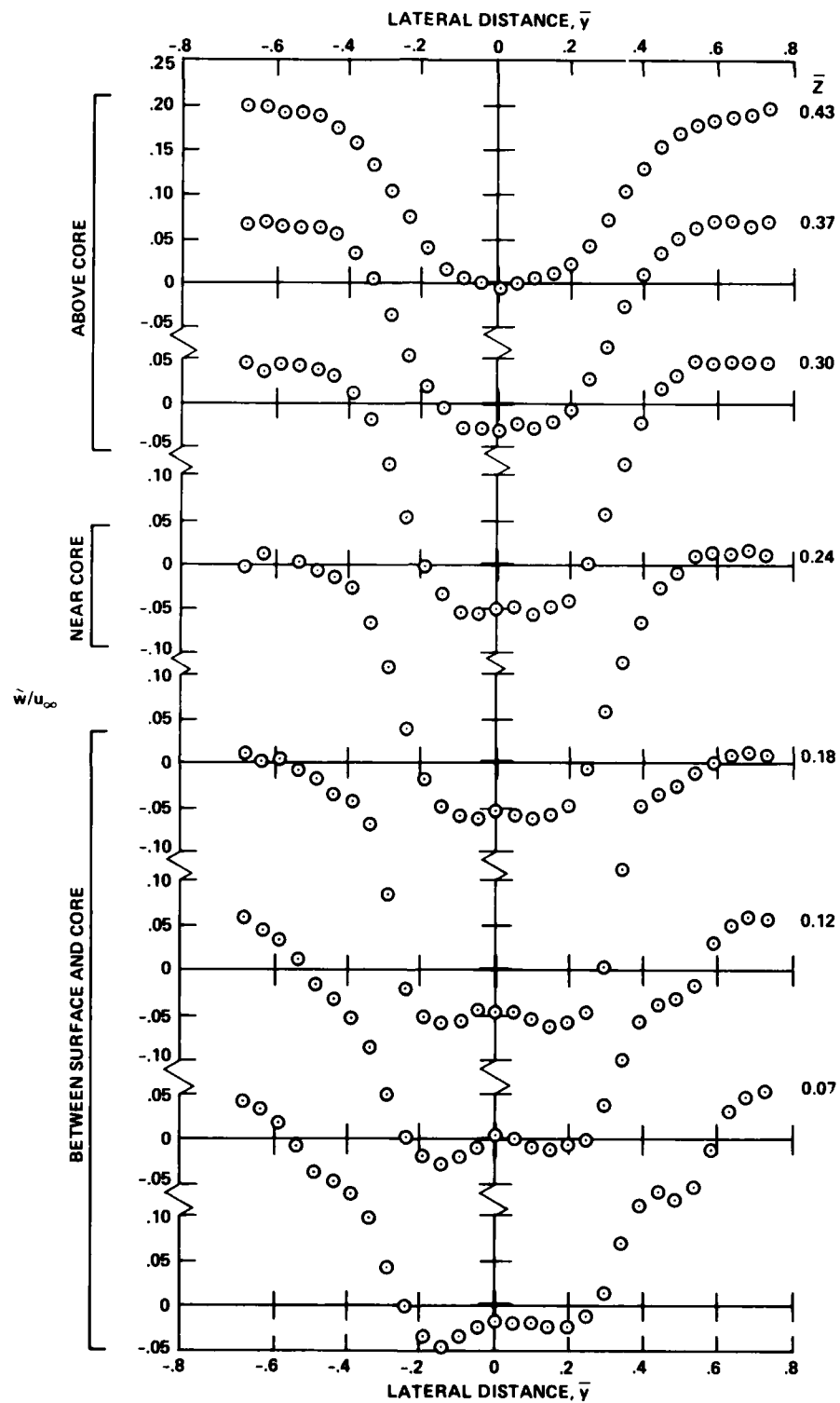


Fig. 14. Mean vertical velocities in cross-flow plane at $x/L = 0.87$, $\alpha/\theta_c = 2.5$.

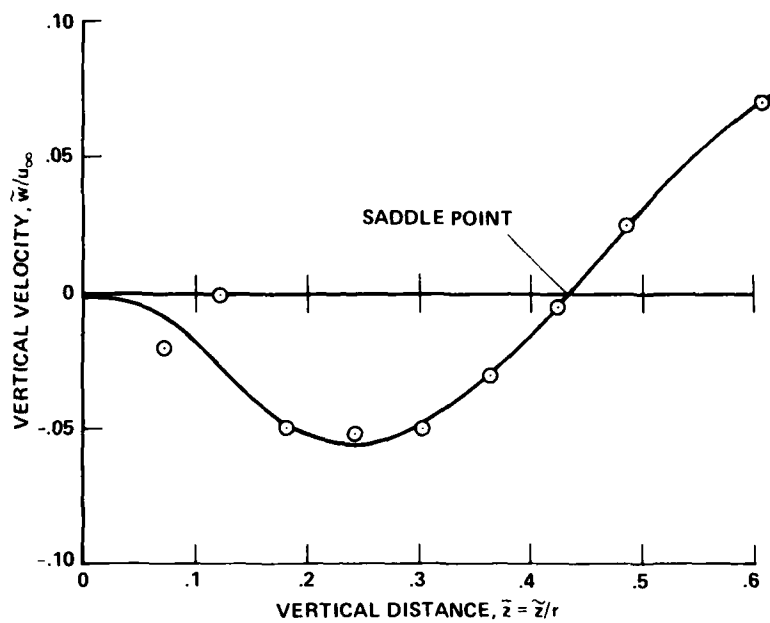


Fig. 15. Vertical velocity in meridian plane,
 $\alpha/\theta_C = 2.5$.

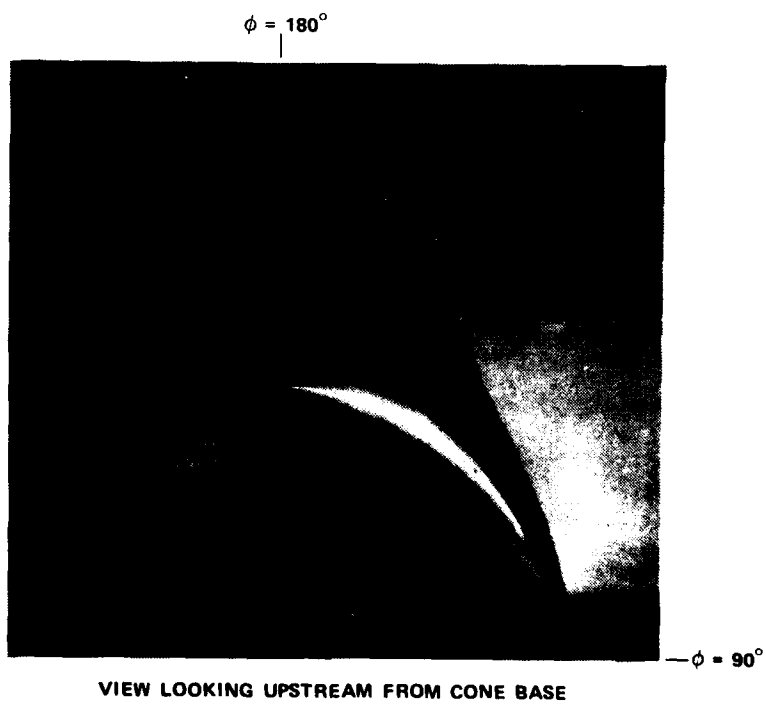
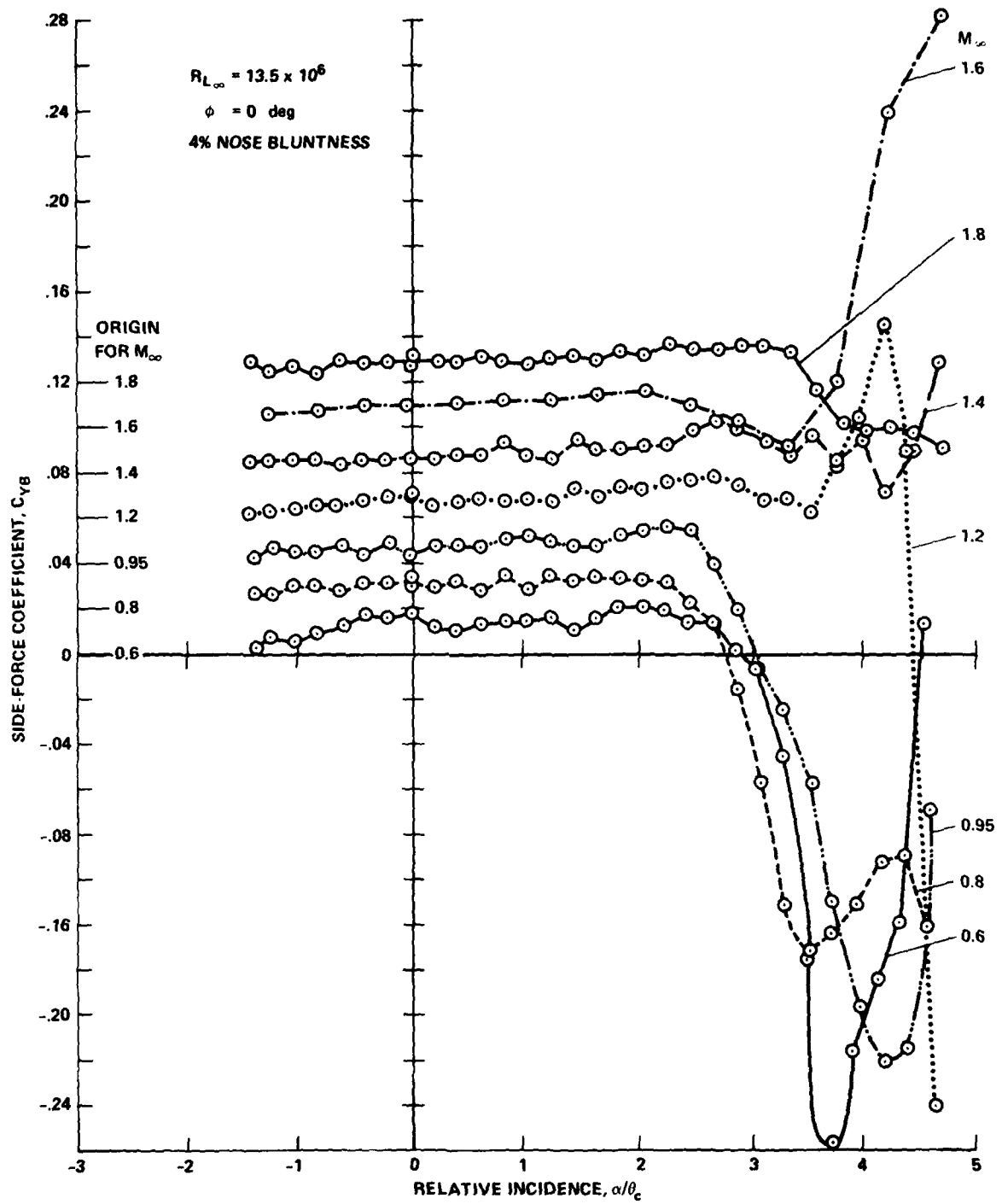


Fig. 16. Laser vapor screen, asymmetry commencing:
 $M_\infty = 0.6$, $\alpha/\theta_C = 2.9$.



Fig. 17. Laser vapor screen of asymmetrical vortices at $\alpha/\theta_c = 3.2$: oblique (pilot) view from port side.


 Fig. 18. Side forces on blunted cone, $0.6 < M_\infty < 1.8$.

15-28

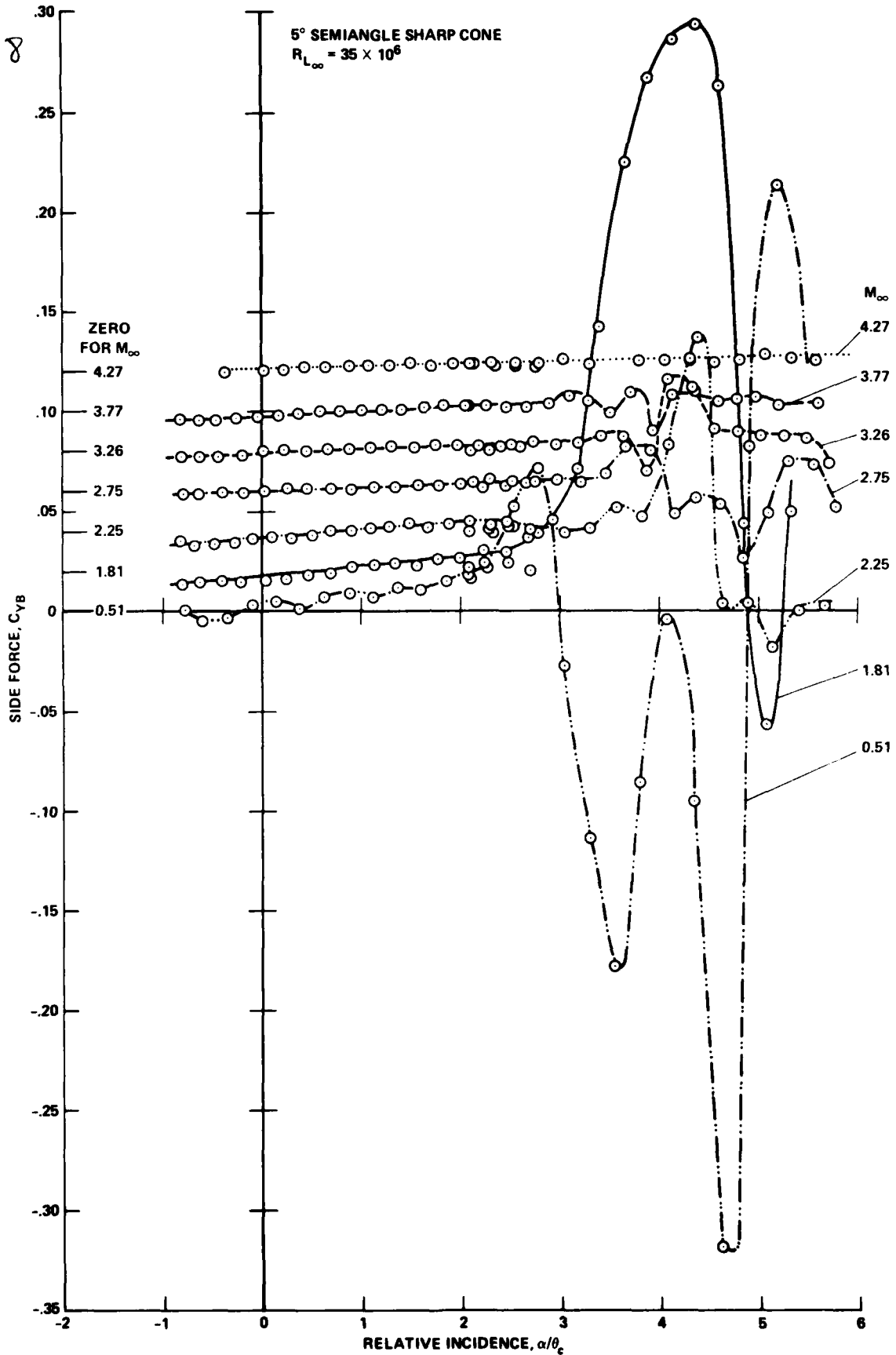


Fig. 19. Side forces on sharp cone, $0.5 < M_\infty < 4.3$, at elevated Reynolds number.

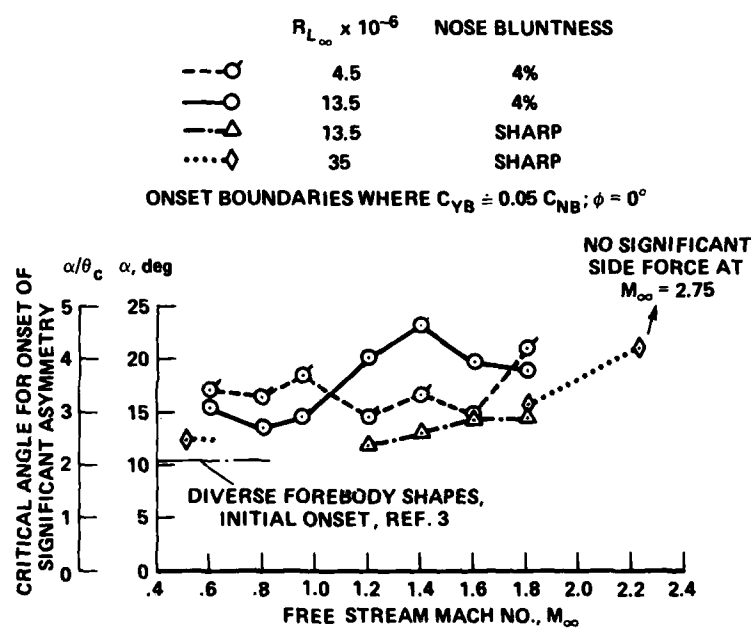


Fig. 20. Onset of significant side-force asymmetry ($C_{YB} = 0.05 C_{NB}$).

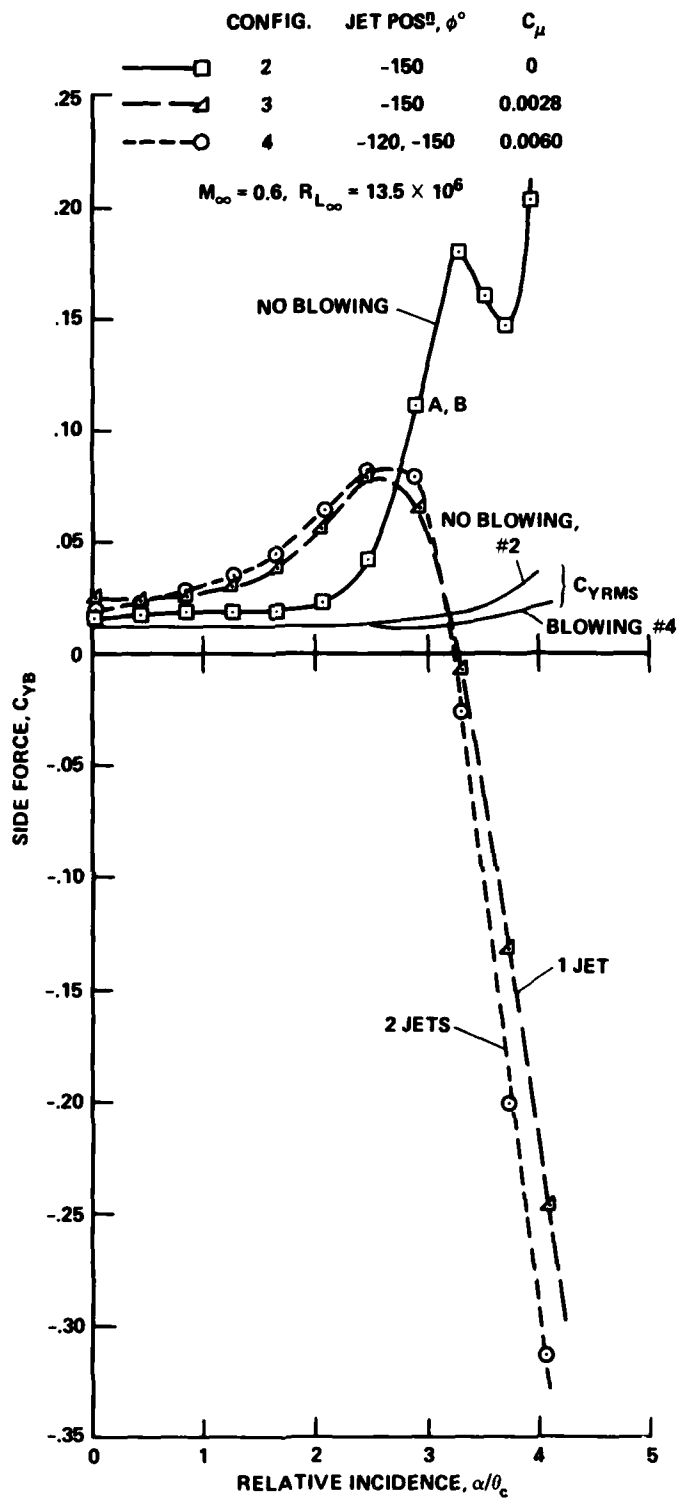


Fig. 21. Incidence/side-force performance with constant normal blowing rate, jet hole diameter = 2.4 mm (0.096 in.).

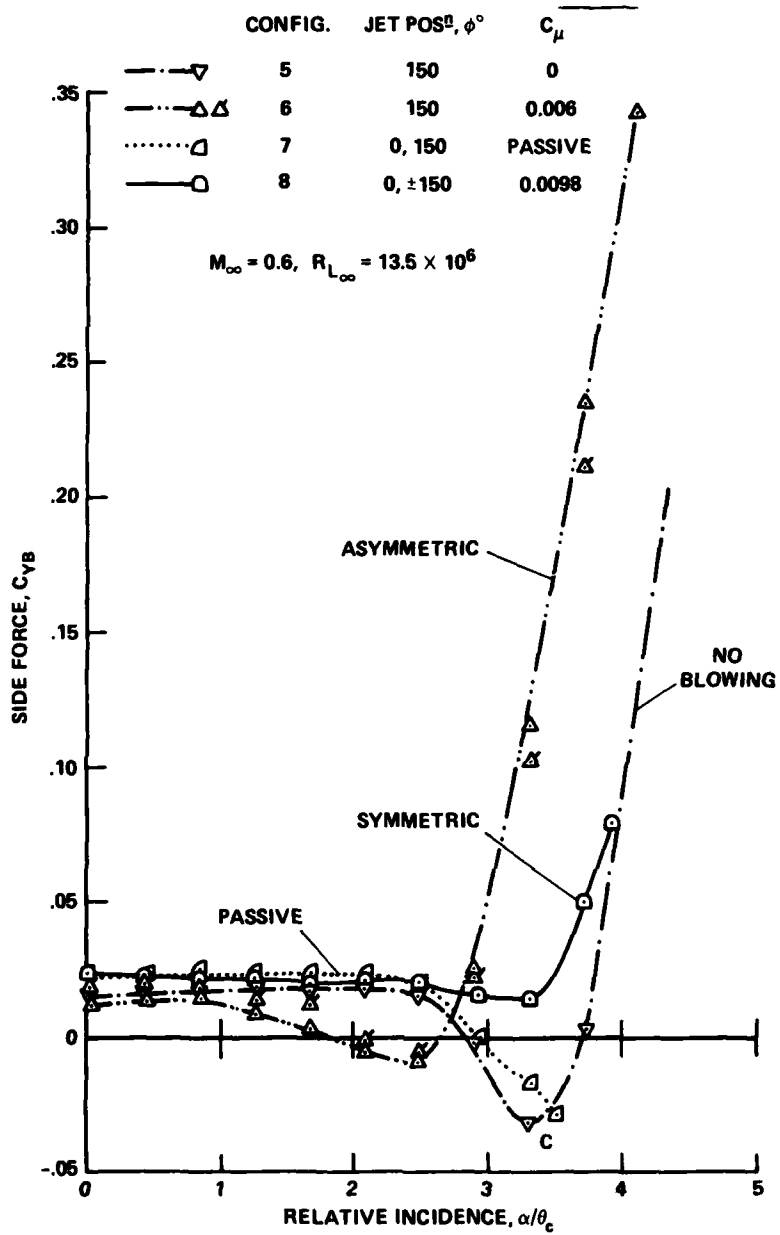



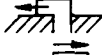

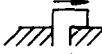

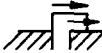


Fig. 22. Incidence/side-force performance with constant normal blowing rate, jet hole diameter = 3.6 mm (0.140 in.).

CONFIG.	JET POS ^N , ϕ°	BLOWING	C_μ	JET diam, mm (in.)
	9		0	3.4 (0.132)
	10		0.0054	3.4 (0.132)
	11		0	3.4 (0.132)
	12		0.0056	3.4 (0.132)

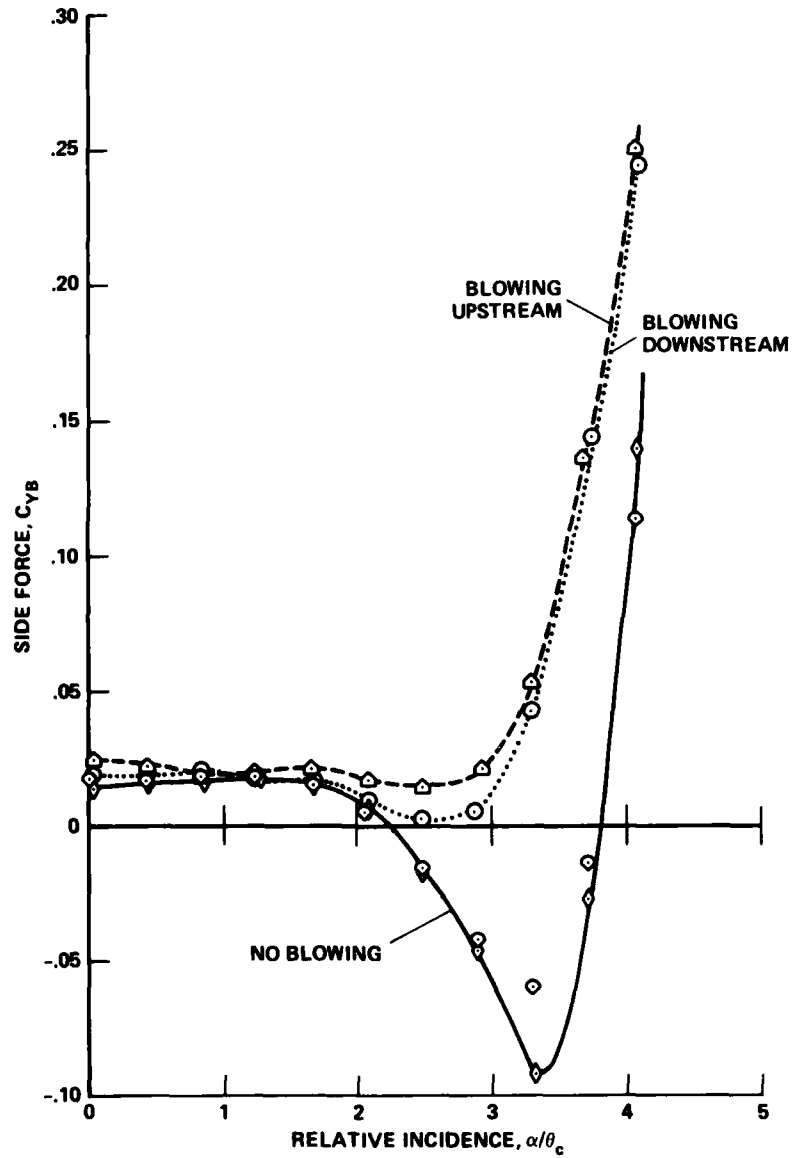
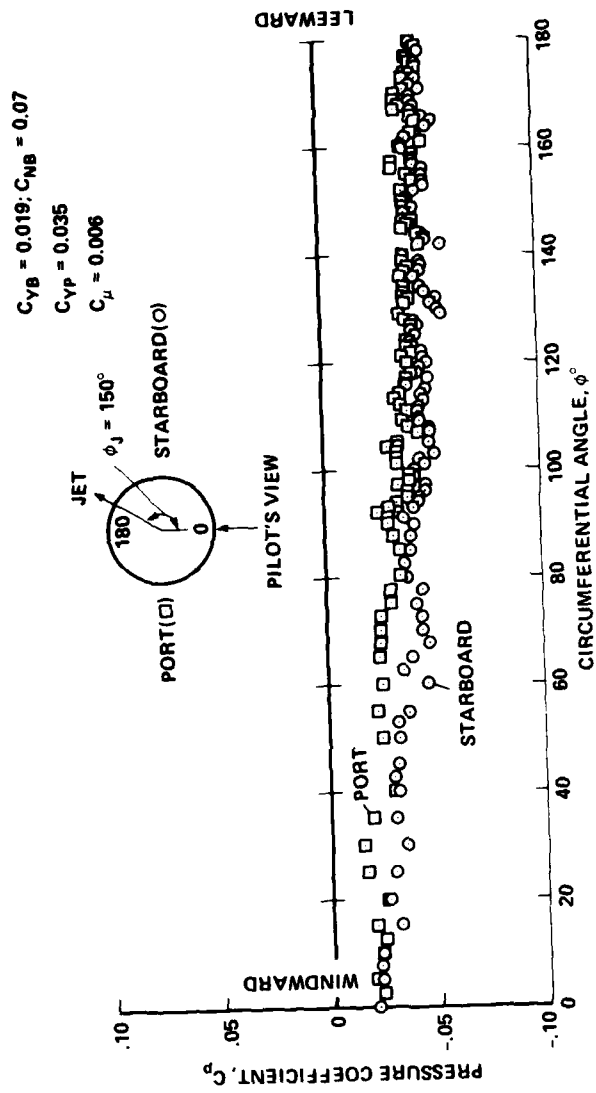


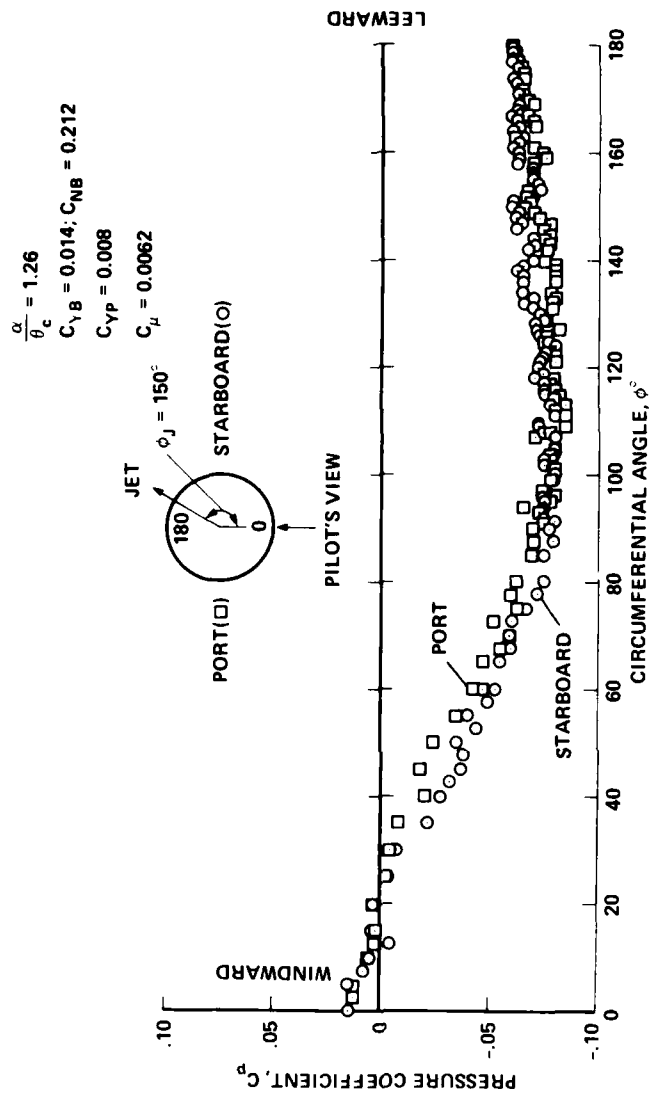
Fig. 23. Incidence/side-force performance with constant tangential blowing rate, jet hole diameter = 3.4 mm (0.132 in.).



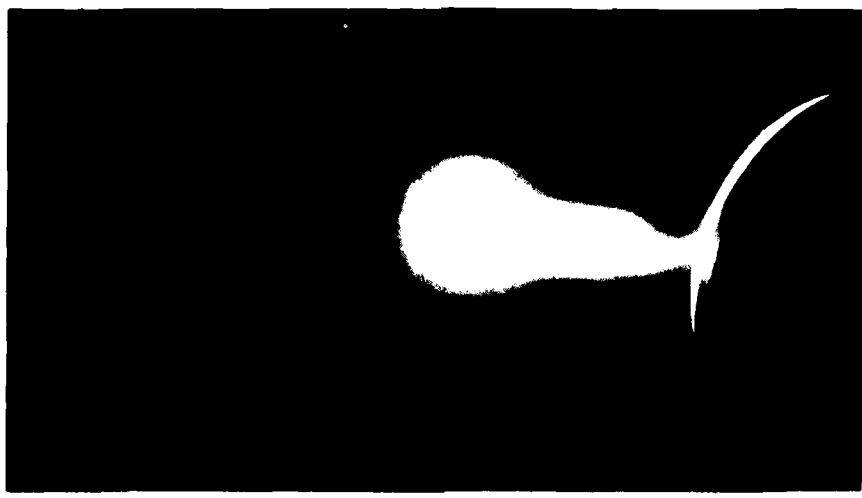
(a) $\alpha/\theta_c = 0.44$.

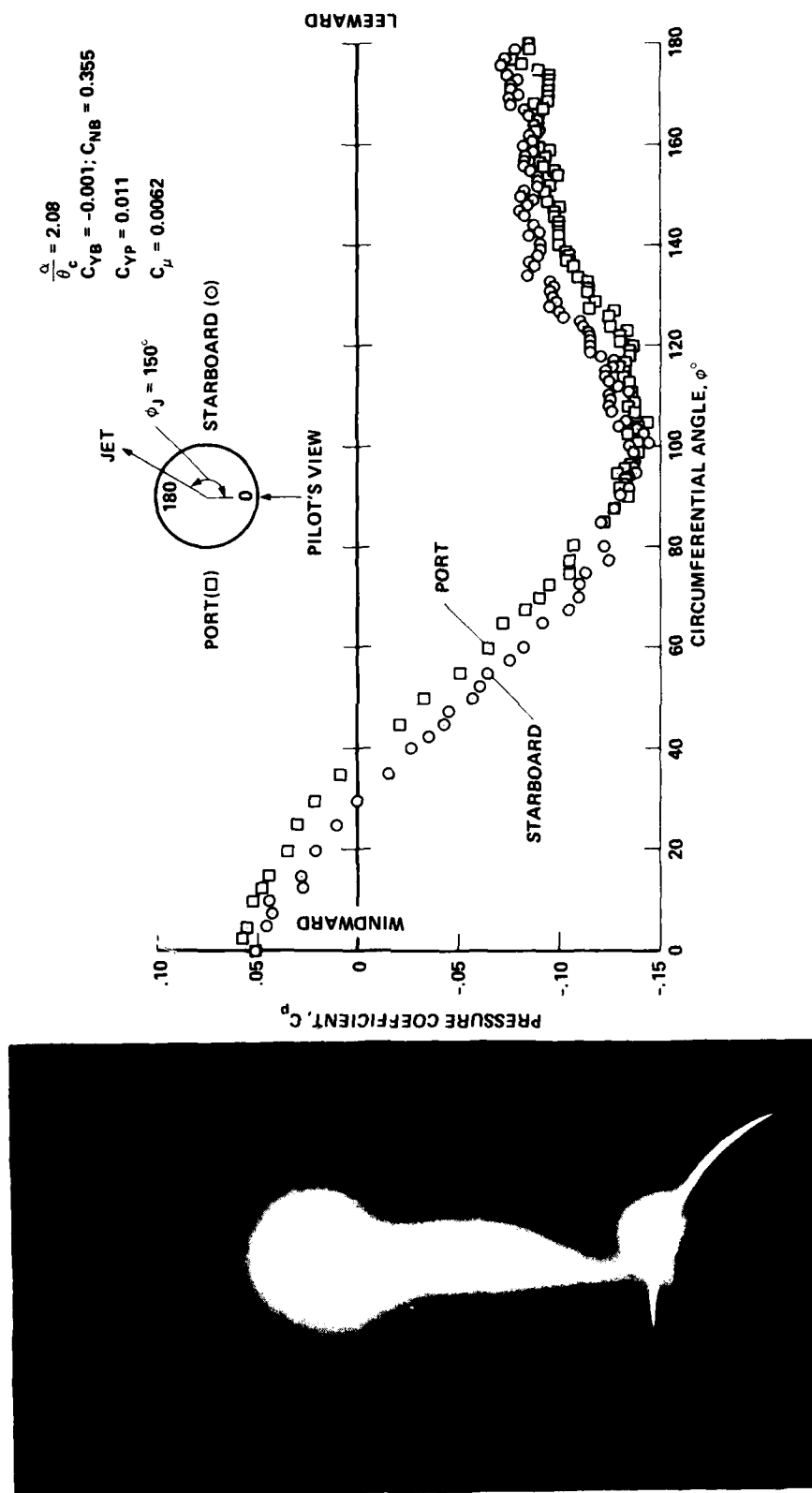
Fig. 24. Effect of changing incidence at constant blowing rate, $C_{\mu} \approx 0.006$: laser vapor screen and circumferential pressures at $x/c = 0.87$ (configuration 6).



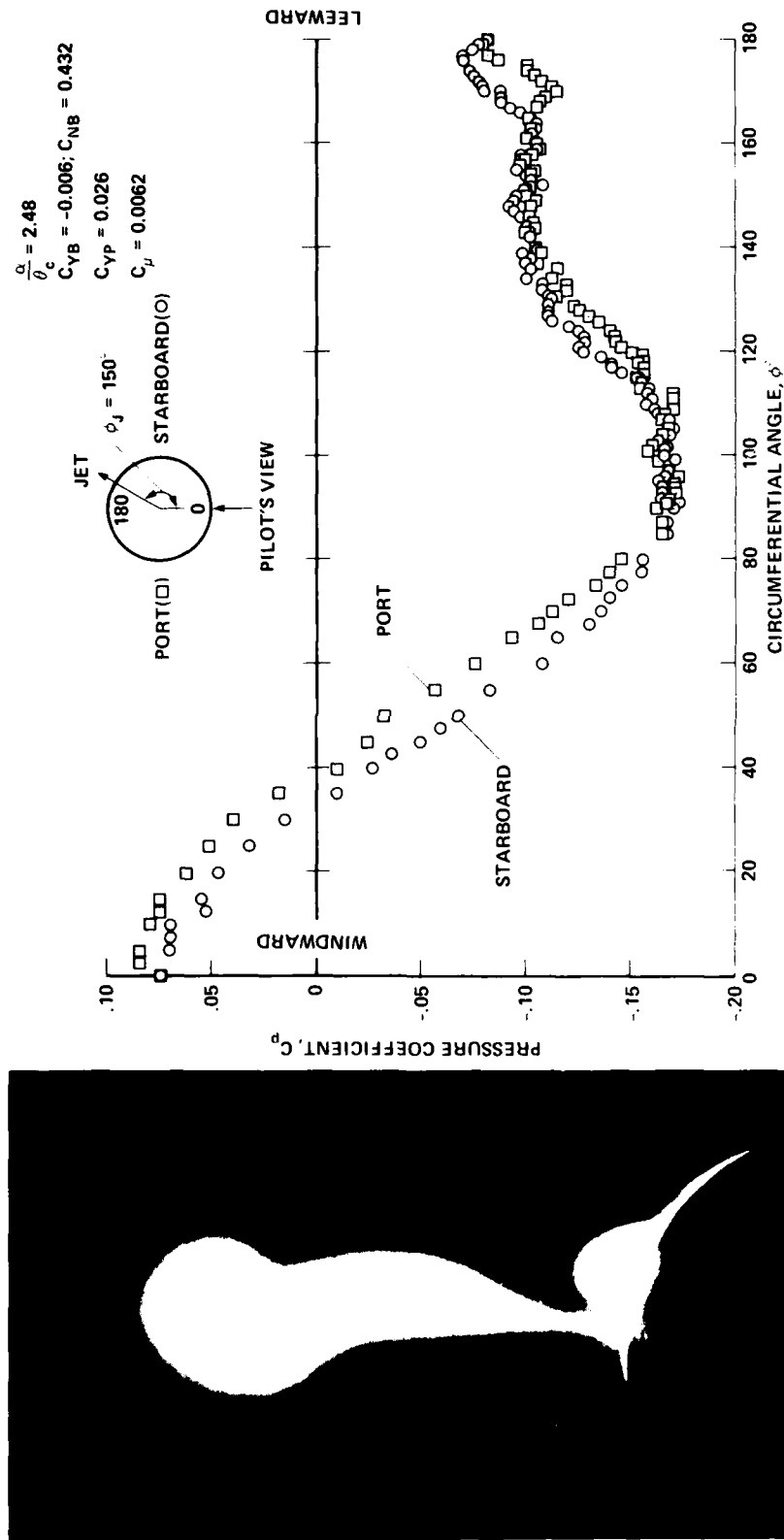


(b) $\alpha/\theta_c = 1.26$.
 Fig. 24. Continued.



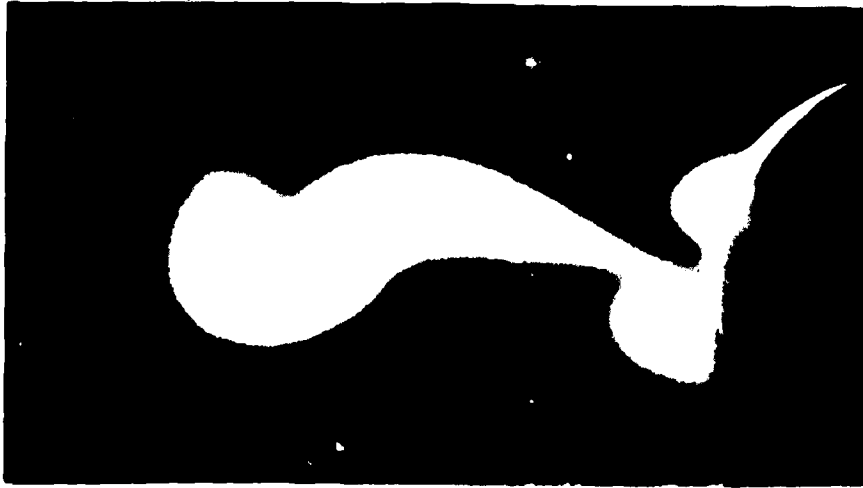
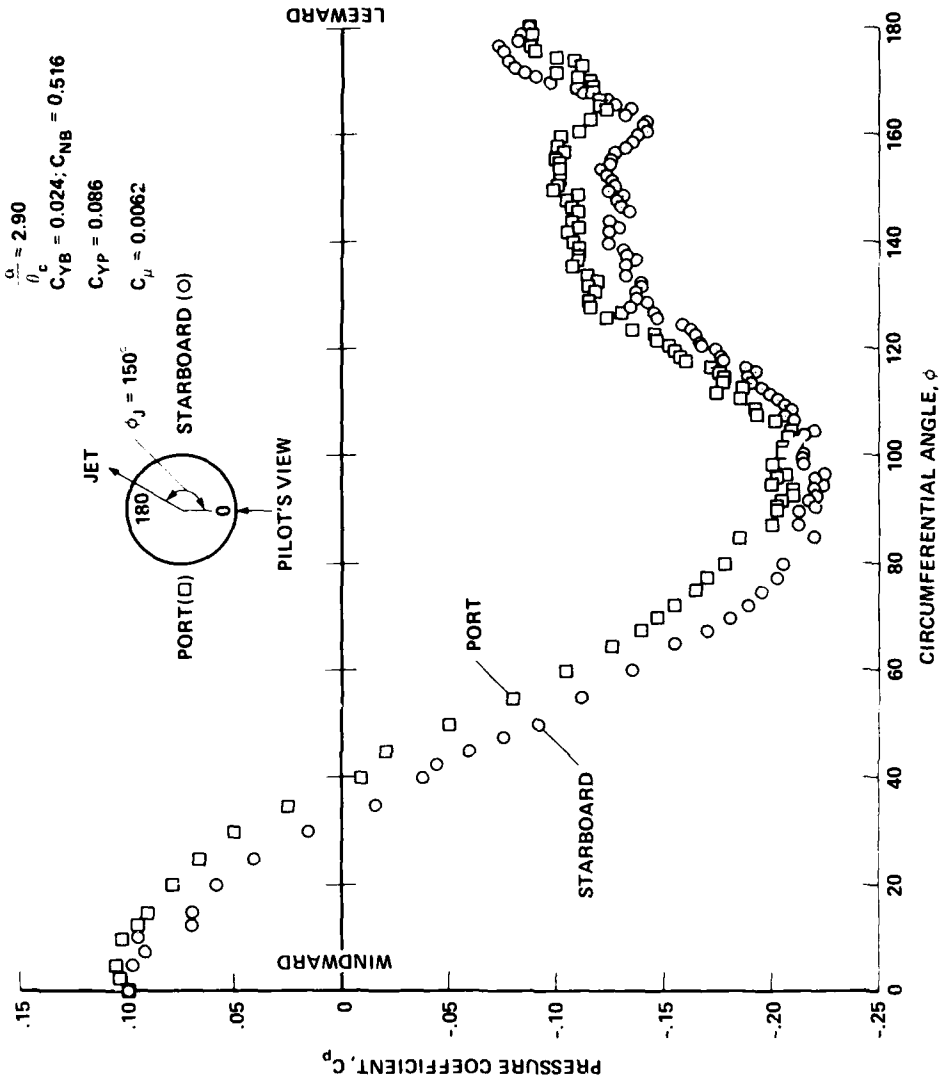


(c) $\alpha/\theta_c = 2.08$.
 Fig. 24. Continued.



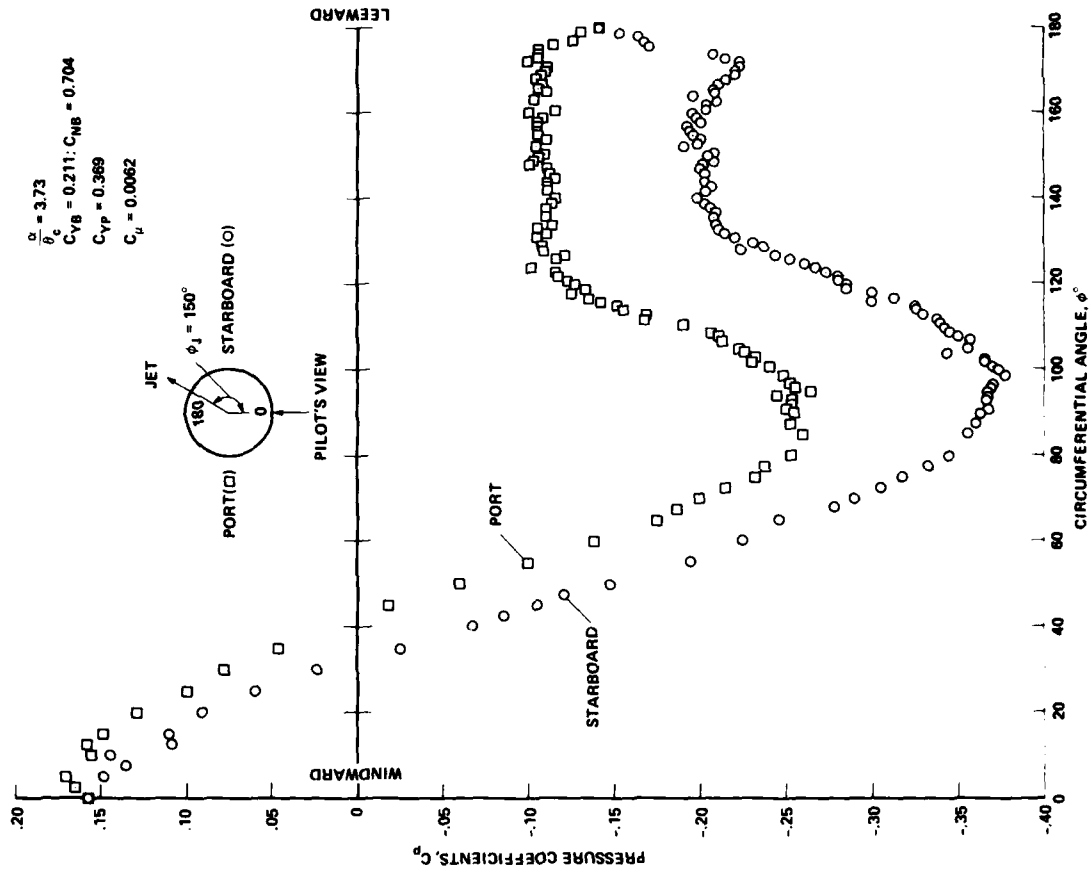
(d) $\alpha/\theta_c = 2.48$.

Fig. 24. Continued.



(e) $\alpha/\theta_c = 2.9$.

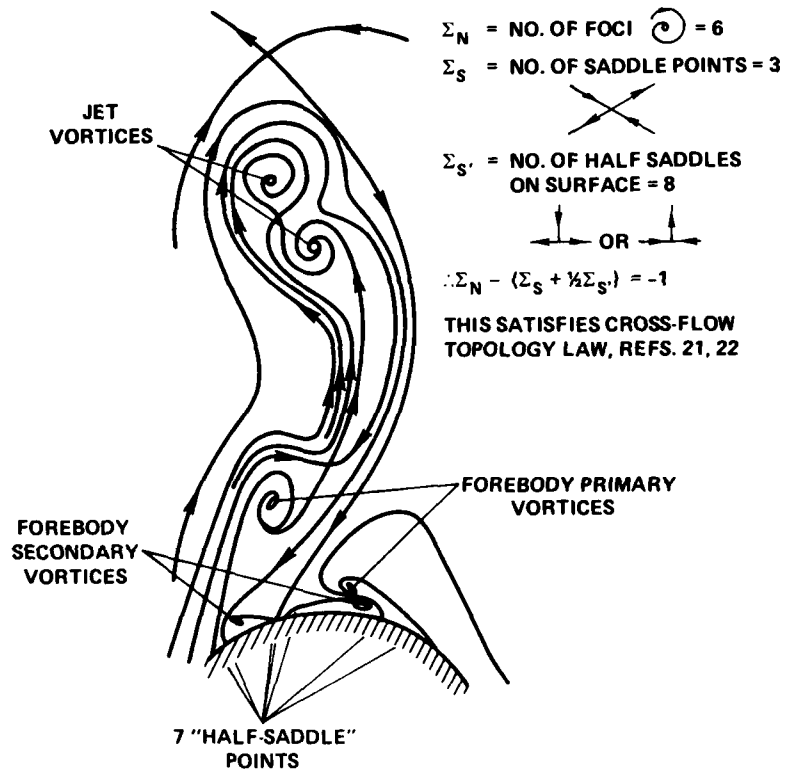
Fig. 24. Continued.



(f) $\alpha/\theta_c = 3.7$.

Fig. 24. Concluded.

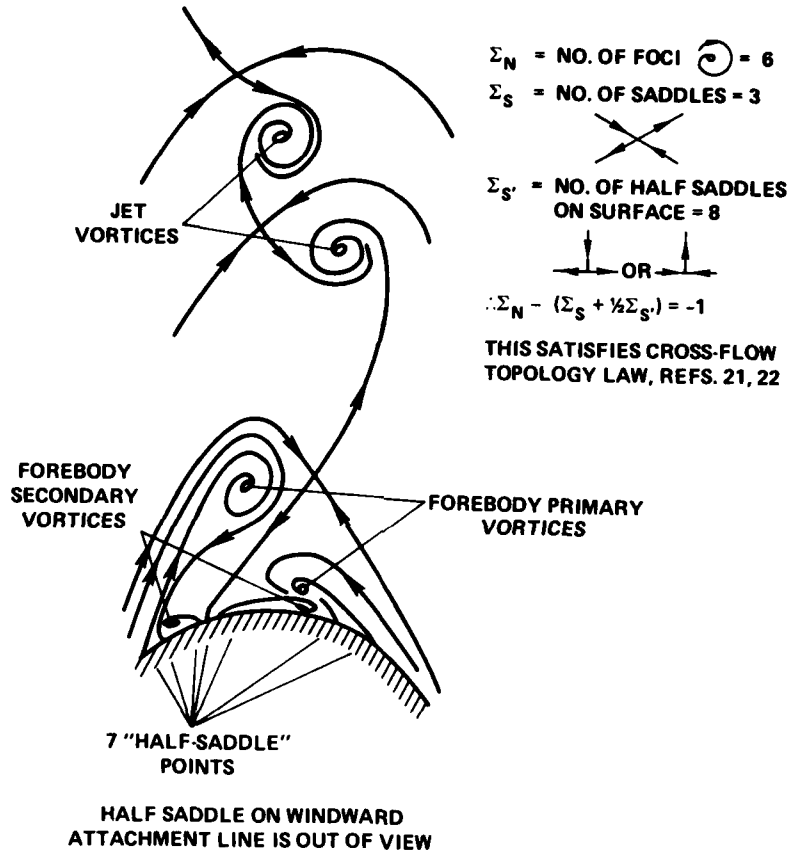




S', HALF-SADDLE ON WINDWARD ATTACHMENT LINE IS OUT OF VIEW

(a) Close-coupled jet vortices and "high" forebody vortices.

Fig. 25. Hypothesized flow structures of jet and forebody vortices.



(b) "Separate" jet and forebody vortices.

Fig. 25. Concluded.

CONFIG. JET POS², ϕ° JET diam, mm (in.)
 2 -150 2.4 (0.096)
 4 -120, -150 2.4 (0.096)
 6 150 3.6 (0.140)
 8 0, ± 150 3.6 (0.140)

$M_\infty = 0.6, R_{L_\infty} = 13.5 \times 10^6$

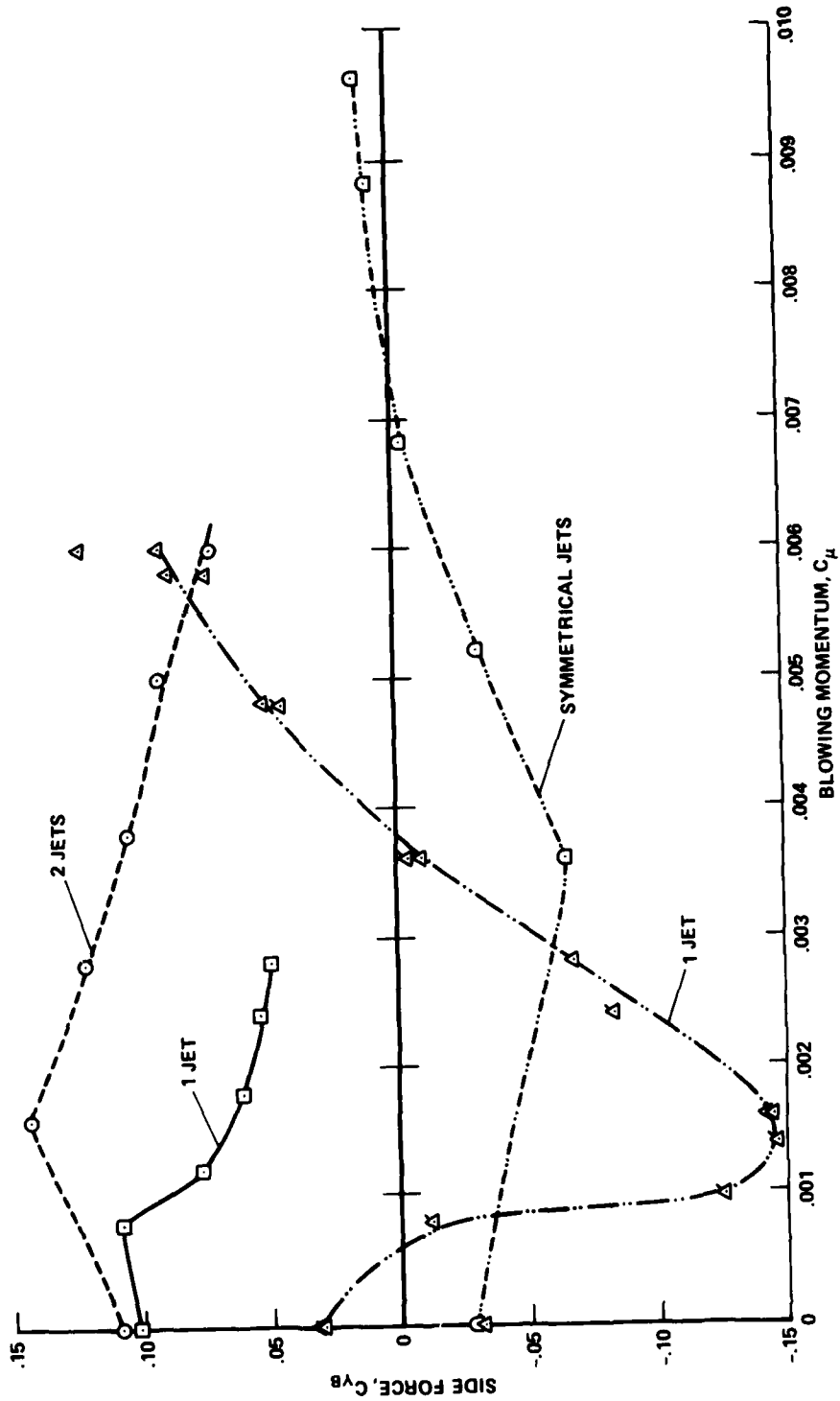
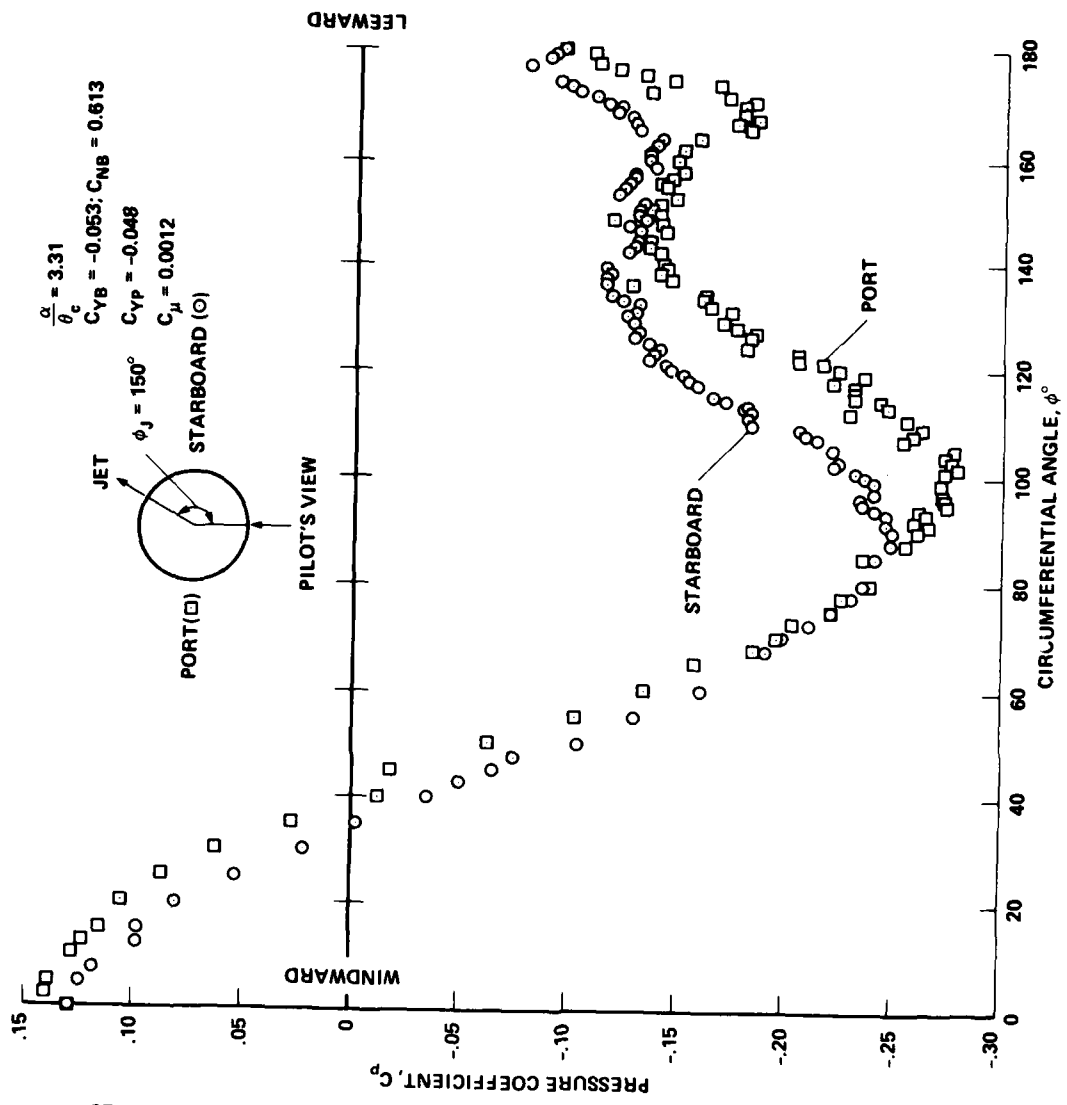
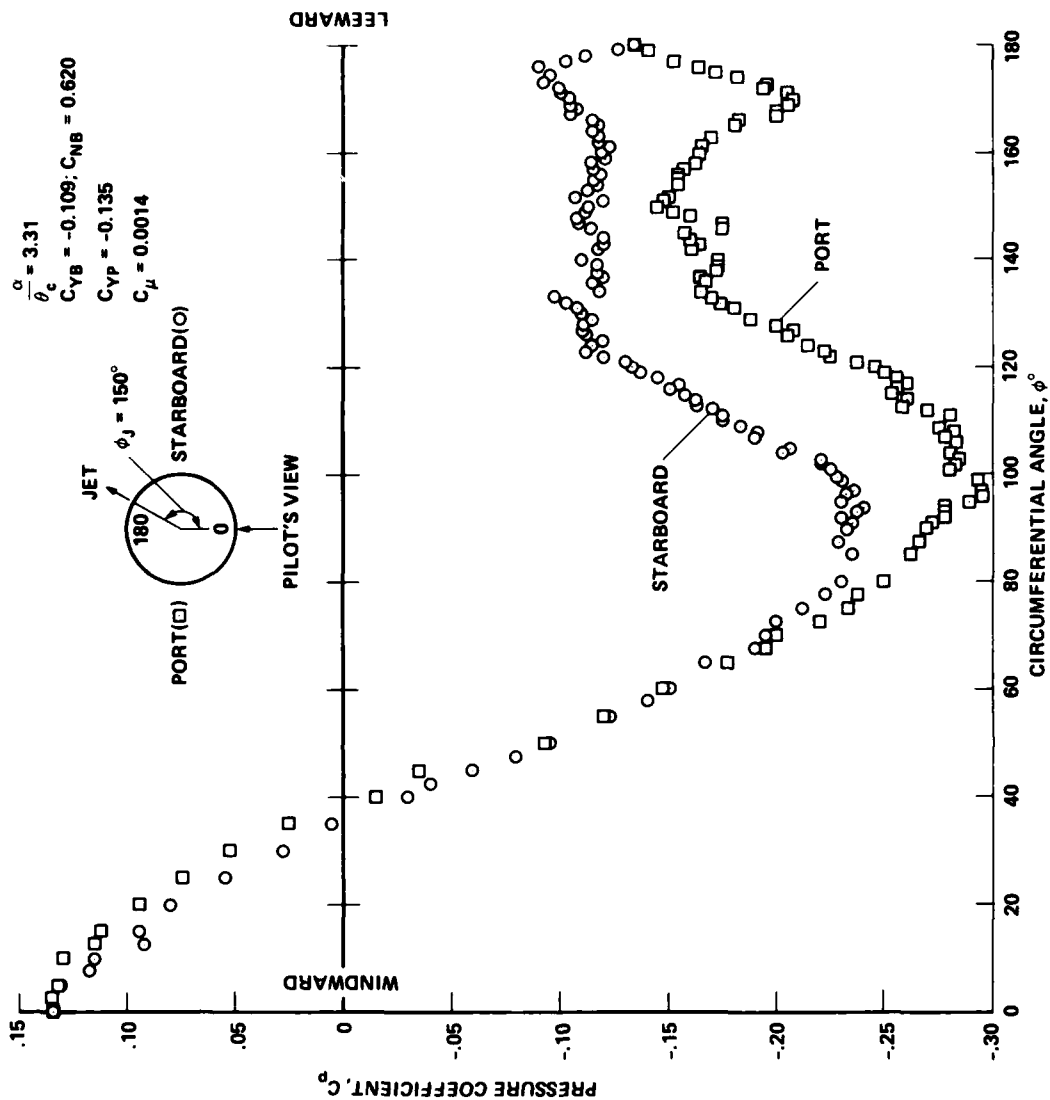


Fig. 26. Effect of normal blowing on side force at constant incidence, $\alpha/\theta_c = 3.2$.



(a) $C_{\mu} = 0.0012$.
 Fig. 27. Changing blowing rate at $\alpha/\theta_c = 3.3$: laser vapor screen and surface pressures at $x/L = 0.87$ (Configuration 6).

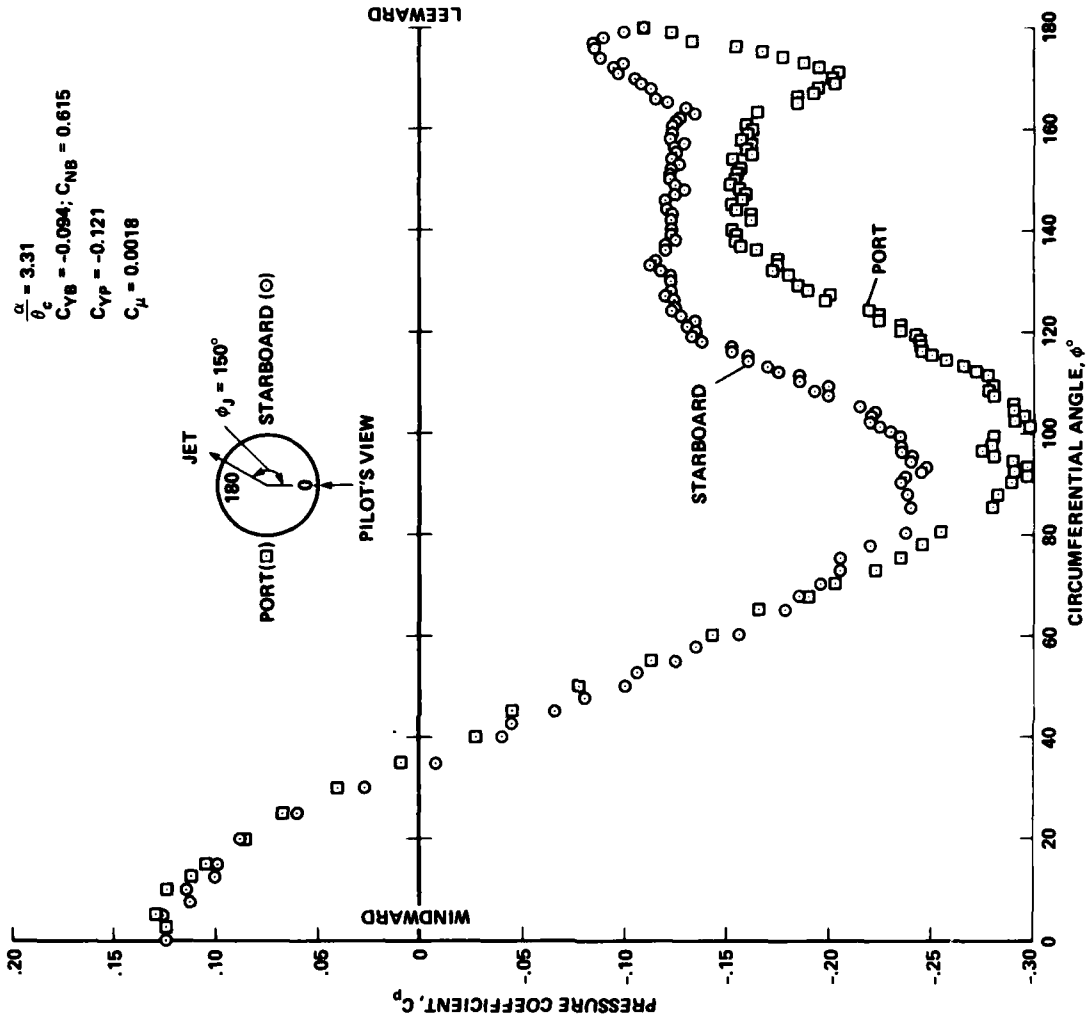




(b) $C_u = 0.0014$.

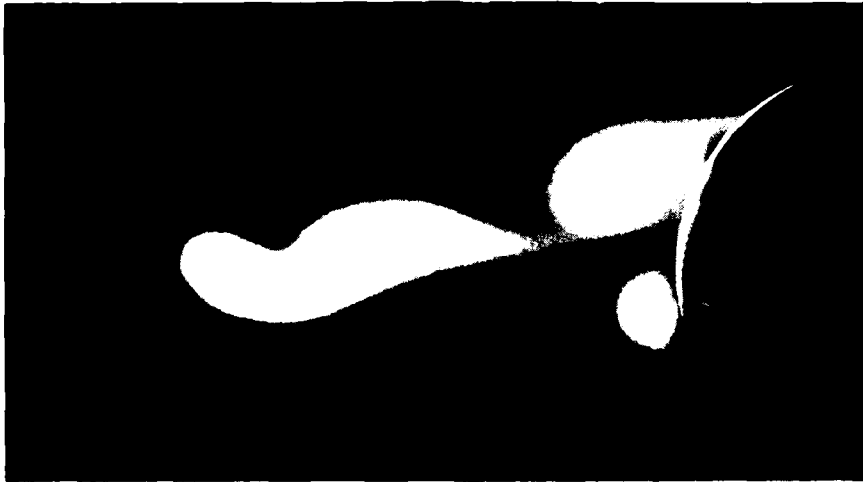
Fig. 27. Continued.

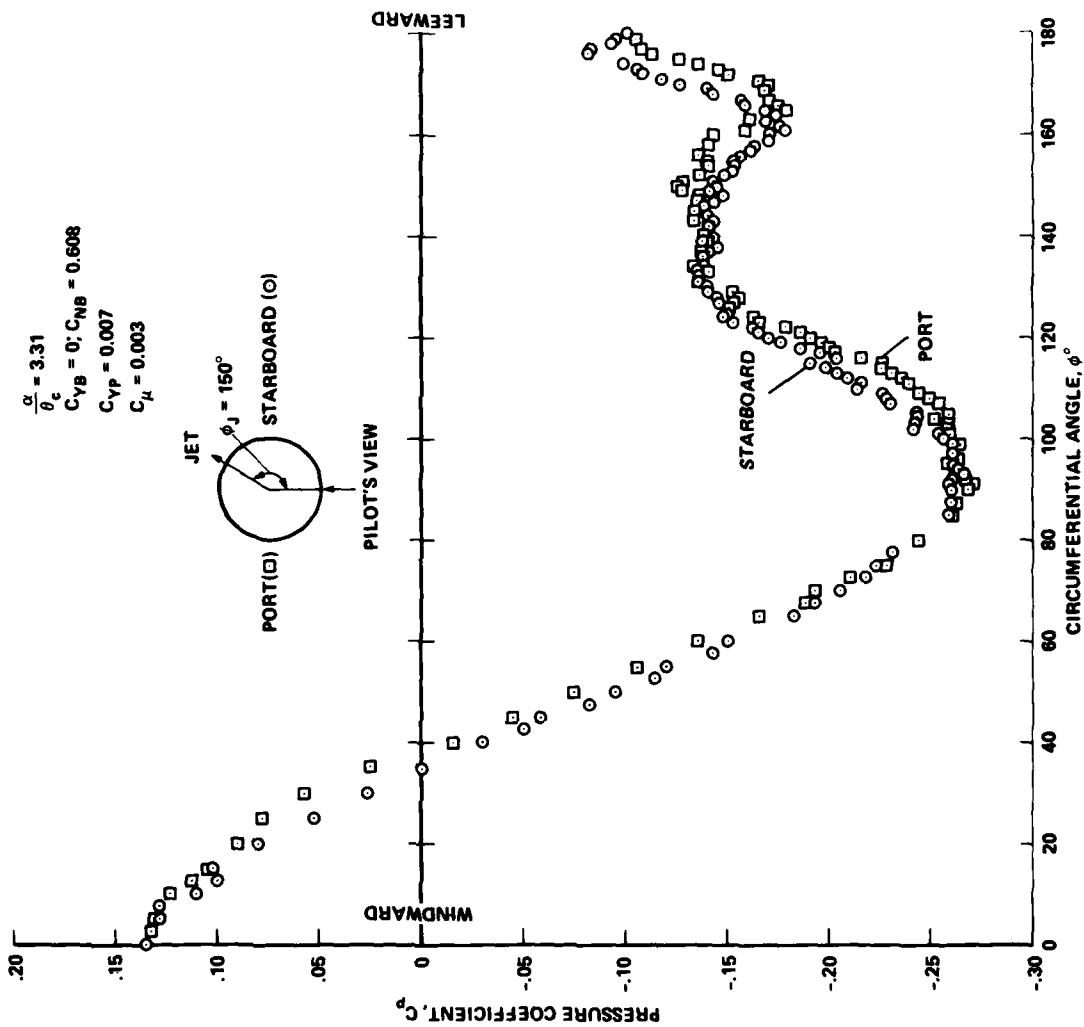




(c) $C_{\mu} = 0.0018$.

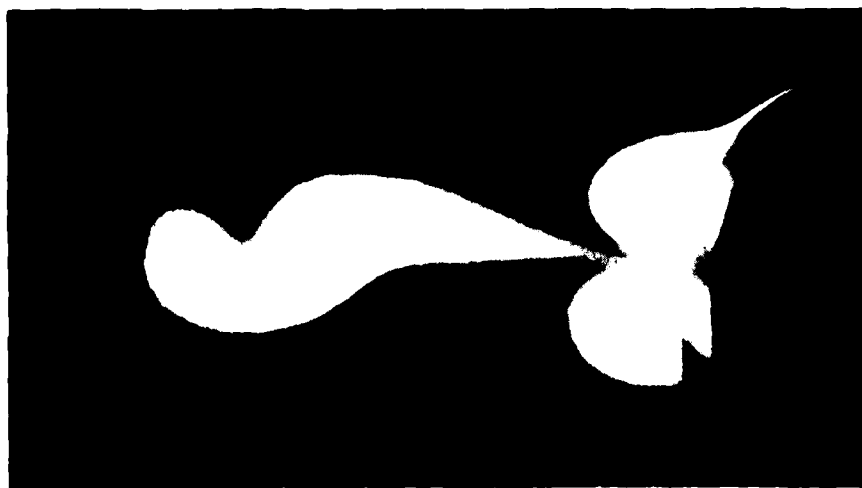
Fig. 27. Continued.

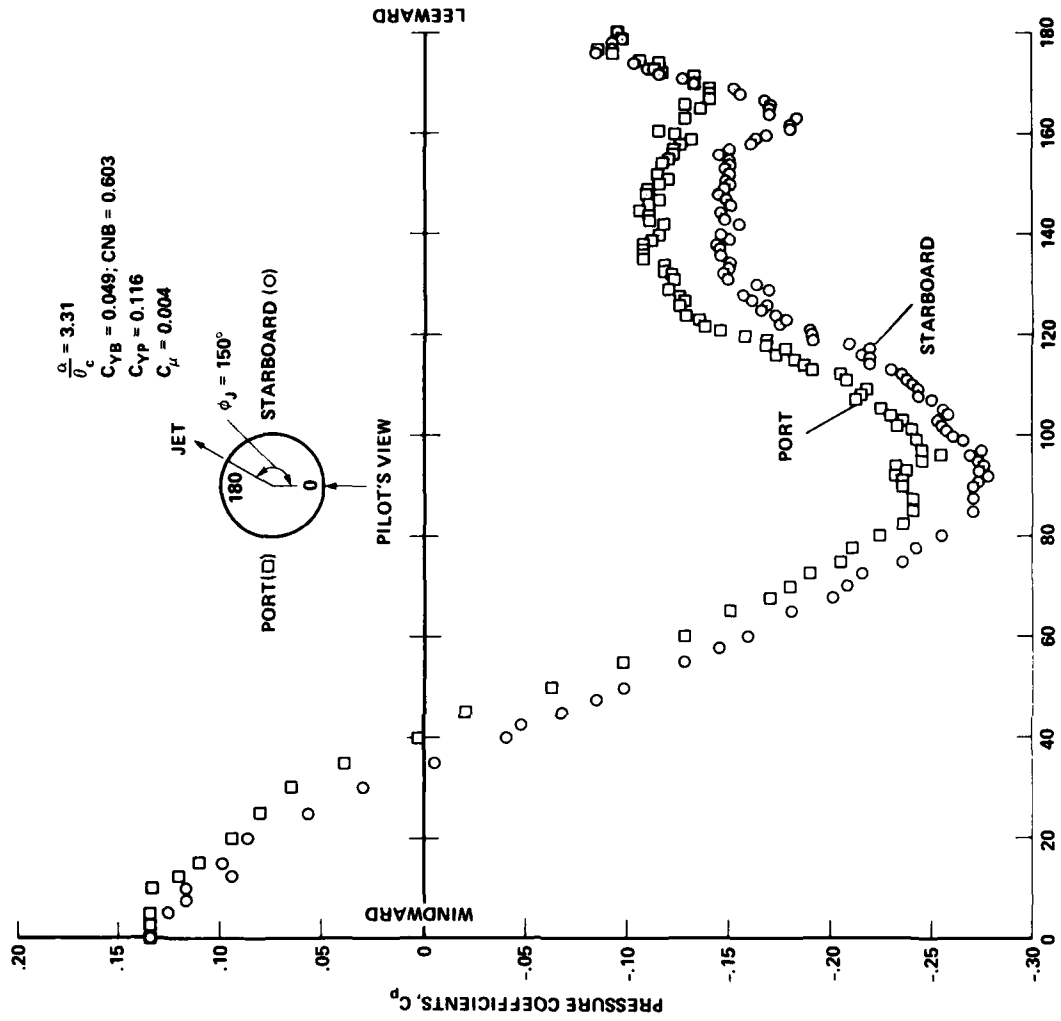




(d) $C_{\mu} = 0.003$.

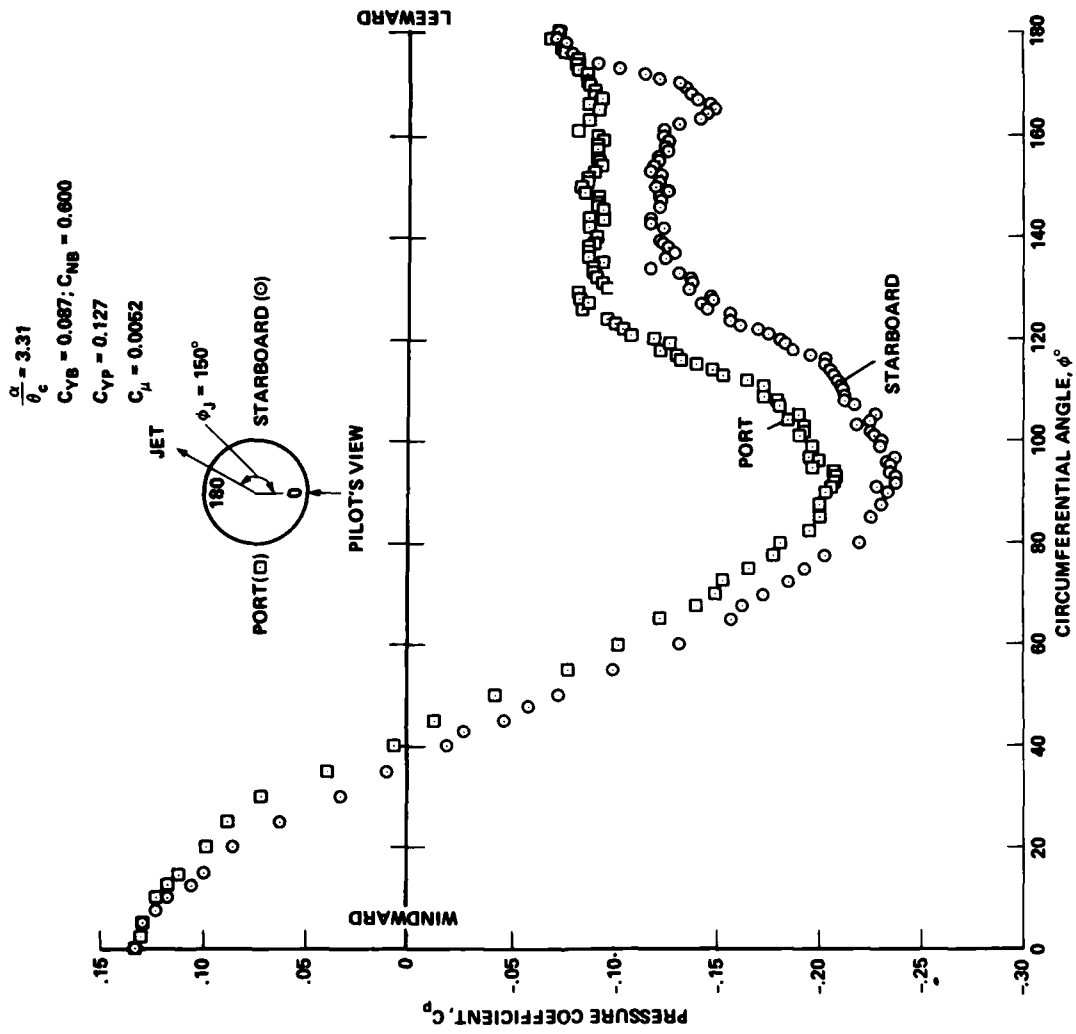
Fig. 27. Continued.





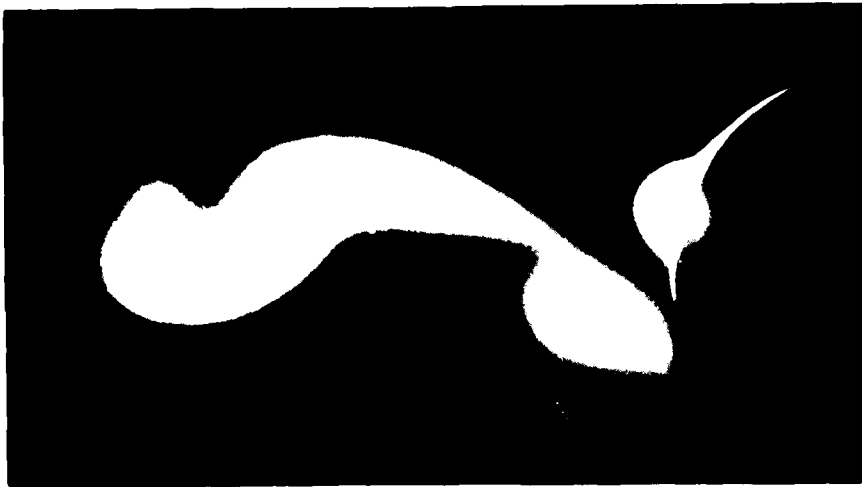
(e) $C_{\mu} = 0.004$.

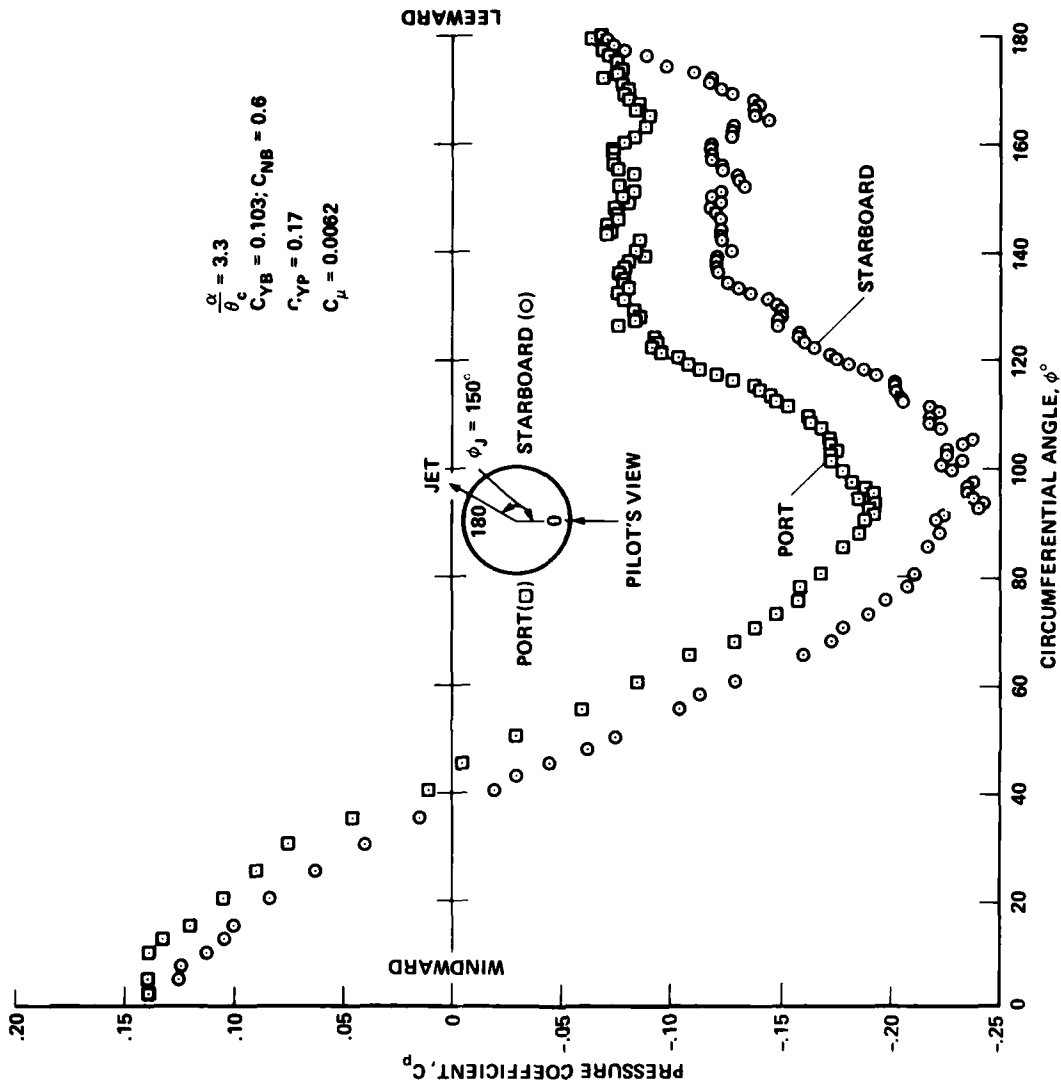
Fig. 27. Continued.



(f) $C_{\mu} = 0.0052$.

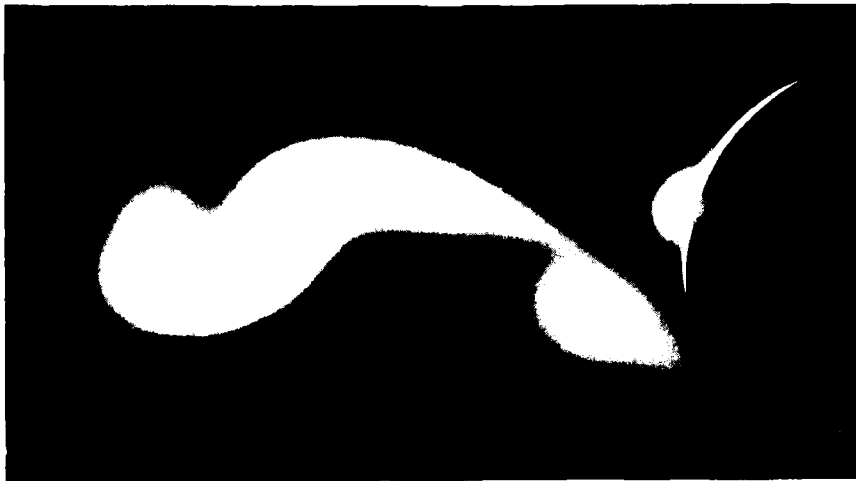
Fig. 27. Continued.





(g) $C_{\mu} = 0.0062$.

Fig. 27. Concluded.



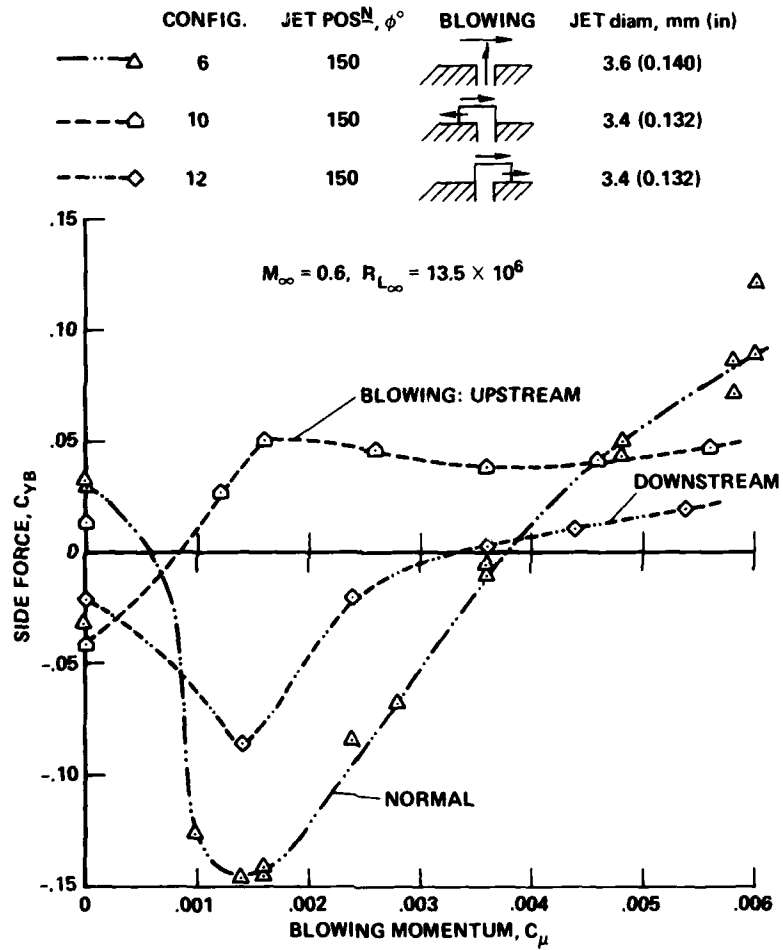


Fig. 28. Reversal of side force: normal and tangential blowing at $\alpha/\theta_c = 3.2$.

IN-FLIGHT MEASURED CHARACTERISTICS
OF COMBINED FLAP-SPOILER DIRECT LIFT CONTROLS

by

O. Rix
D. Hanke

16-1

Institut für Flugmechanik

Deutsche Forschungs- und Versuchsanstalt
für Luft- und Raumfahrt e.V. (DFVLR)
Braunschweig-Flughafen

SUMMARY

The implementation of direct lift control in the aircraft flight control system can improve pilot-vehicle performance and handling qualities for a given requirement. Prerequisite for the control system design is the knowledge of the aerodynamic characteristics of direct lift controls. The influence of direct lift control on longitudinal aircraft dynamics and the requirements for the characteristics of direct lift controls for large transport aircraft in the landing approach phase are discussed. Further, the different characteristics of flaps, spoilers and influence of surface rate on aircraft behaviour are dealt with. A flight test investigation was carried out to determine in-flight flap and spoiler characteristics and, in addition, the characteristics of simultaneously deflected flaps and spoilers as a DLC device. The flight tests are undertaken with the DFVLR HFB 320 In-Flight Simulator. The fly-by-wire control system of this aircraft is ideally suited for electrically applied input signals for system identification. The results show, that flap and spoiler characteristics can be described by linear models, this is valid for flap and spoiler inputs up to + 10 deg and + 30 deg respectively and relatively high surface rates of 10 deg/sec and 62 deg/sec. In addition, combined flap-spoiler deflections show no nonlinear or instationary effects. The aircraft response can be described by simple linear modelling. The spoiler control derivatives are influenced by flap deflection. In this case, the spoiler derivatives valid for combined flap-spoiler deflections are identified.

The in-flight measured flap and spoiler characteristics are compared with windtunnel data showing good correlation with flap data. In contrary discrepancies for spoiler control derivatives are possibly due to different separated flow characteristics between low Re-number windtunnel measurements and higher Re-number full scale flight tests.

LIST OF SYMBOLS

a_x		acceleration along body x-axis
a_z		acceleration along body z-axis
$C_{A(i)}$	$\frac{\partial C_A}{\partial (i)}$	nondimensional lift derivative
$C_{M(i)}$	$\frac{\partial C_M}{\partial (i)}$	nondimensional pitch moment derivative
$C_{W(i)}$	$\frac{\partial C_W}{\partial (i)}$	nondimensional drag derivative
g		acceleration due to gravity
H		altitude
I_y		pitching moment of inertia
$K(i)$		bias of measured signal i
m		aircraft mass
$M(i)$	$\frac{\partial M}{\partial (i)}$	dimensional pitch moment derivative
n		vertical load factor
q		pitch rate

16-2

T_{DLC}		DLC device time constant
U		perturbation velocity along body x-axis
U_0		trim velocity in body x-axis
V		velocity with respect to air
w		perturbation velocity along body z-axis
$X_{(i)}$	$\frac{\partial X}{\partial(i)}$	dimensional X-force derivative
$Z_{(i)}$	$\frac{\partial Z}{\partial(i)}$	dimensional Z-force derivative
α		angle of attack
γ		flight path angle
δ		control deflection
$\dot{\delta}$		deflection rate
δ_e		elevator deflection
δ_F		flap deflection
δ_{sp}		spoiler deflection
θ		pitch attitude
Subscript		
c		command
obs		observation

1. INTRODUCTION

Advancements in fly-by-wire technology have impacted aircraft design by allowing the optimization of both aircraft performance and handling qualities for a given requirement. In particular the application of direct force control results in new and unconventional aircraft control behaviour.

Perequisites for the design of direct force control modes are a proper definition of mission oriented handling qualities including the knowledge of direct force control device dynamic characteristics. Aerodynamic interference problems may arise using simultaneously several direct force control surfaces. For control system design, simple models describing control surface characteristics are desirable. Within the DFVLR research program [1] to investigate the influence of direct lift control on handling qualities using the DFVLR HPB 320 variable stability aircraft separate flight tests were made to identify the flap and spoiler control characteristics using modern parameter identification techniques.

2. INFLUENCE OF DLC ON AIRCRAFT DYNAMICS

Compared with conventional elevator moment control, direct lift control represents a force control where the lift force can be varied directly by flaps or spoilers on the wing. Using an additional direct lift control surface in combination with the elevator, two degrees of freedom of the longitudinal motion, are influenced by two independent control inputs - pitch moments by the elevator and Z-motion by the direct lift device. The direct lift control system can be designed to couple or decouple the two degrees of freedom independent of aircraft inherent pitch/heave motion coupling caused by Z_{α} and M_{α} derivatives.

There are three principle DLC application possibilities to give an aircraft the mission optimized control behaviour shown in figure 2.1 [2].

Firstly a longitudinal control system decoupling pitch and flight path response with

- Decoupled Pitch Control with constant flight path (DPC) and
- Decoupled Flight Path Control with constant pitch attitude (DFPC)

and secondly a longitudinal control system coupling pitch and flight path

- Coupled Flight Path Control (CFPC).

Figure 2.2 illustrates how the lift curve slope can be varied by DLC application due to control input. Further, this figure shows how the lift curve slope should be realized for different control system applications.

The aircraft time response due to step stick input for a DLC system with coupled elevator and flap is shown in figure 2.3.

For elevator control time histories of pitch rate and vertical acceleration response show the known relatively poor vertical acceleration response compared with pitch rate. With increasing DLC effectiveness the response of vertical acceleration is quickend on the other hand the pitch rate response is slowed down.

3. REQUIREMENTS OF DIRECT LIFT CONTROLS

The ideal direct lift device would be a control surface with pure lift force capability producing no change in drag or moment.

In this case the pitch and heave motion of the aircraft could be influenced by a proper combination of the pure lift force device and the pure moment control device (elevator or canards) with low design constraints.

In addition, the lift device should have sufficient control power and sufficient high lift variation rate.

In the past, flaps and spoilers are proposed and used as direct lift device having the following advantages and disadvantages.

1. *Flaps* Advantages: Very effective, therefore low control amplitudes necessary.
Disadvantages: Large adverse pitching moments and positive drag in the case of lift increase.
2. *Spoilers* Advantages: Negative drag in the case of lift increase.
Disadvantages: Not so effective, therefore high control amplitudes necessary.
Large proverse pitching moments.
Buffeting due to large deflections.

A very important parameter is the rate of lift increase which depends on control surface effectiveness and on the maximum surface rates (as follows).

$$\frac{dC_A}{dt} = \frac{\partial C_{A\delta}}{\partial \delta} \cdot \dot{\delta} + C_{A\delta} \cdot \frac{\partial \delta}{\partial t}, \text{ neglecting lift lag effects } \left(\frac{\partial C_A}{\partial t} \approx 0 \right)$$

then
$$\dot{C}_A = C_{A\delta} \cdot \dot{\delta}$$

This means the requirement of DLC had to be the lift change per time and not only the maximum surface rate. Comparing two different DLC devices like flaps and spoilers, with the demand of equal lift change per time then the required spoiler rate is (HFB 320 data):

$$\begin{aligned} \dot{\delta}_{SPREQ.} &= \frac{C_{A\delta F}}{C_{A\delta sp}} \cdot \dot{\delta}_{Fmax} & C_{A\delta F} &= 0.9 \\ & & C_{A\delta sp} &= 0.18 \\ \dot{\delta}_{SPREQ.} &= 50 \text{ deg/sec} & \dot{\delta}_{Fmax} &= 10 \text{ deg/sec} \end{aligned}$$

The surface rates are reciprocal to control effectiveness of both control surfaces.

Now, how great the change in lift per time should be?

16-4

Previous investigations [1] show that too fast lift change results in handling quality problems for flight path tracking in the landing approach. The lift change per time or the vertical acceleration response should be adapted to the short period eigen-motion of the aircraft.

In the case that the angle of attack should be nearly constant during a control input, the first order time constant of the DLC surface transfer function is dependent on the following aircraft derivatives [2]

$$T_{DLC} = \frac{1}{\frac{M_{\delta DLC}}{Z_{\delta DLC}} U_0 - M_q} \text{ sec}$$

A typical value for transport aircraft in landing approach is

$$T_{DLC} \approx 0.4 \text{ sec}$$

Required vertical acceleration variation of $n = + 0.2 \text{ g}$ for the landing approach results in maximum direct lift surface rates from 10 to 20 deg/sec shown as follows

$$\dot{\delta}_{\max} = - \frac{n}{\Delta t} \cdot \frac{g}{Z_{\delta DLC}} = - \frac{0.632 n \cdot g}{T_{DLC} \cdot Z_{\delta DLC}}$$

with values mentioned before and $Z_{\delta DLC} = - 12 \text{ m/sec}^2/\text{rad}$

$$\dot{\delta}_{\max} = \frac{0.632 \cdot 0.2 \cdot 9.81 \cdot 57.3}{0.4 \cdot 12} \approx 15 \frac{\text{deg}}{\text{sec}}$$

4. FLIGHT TEST SITUATION

The main purpose of the in-flight investigation was to refine the mathematical model describing the longitudinal motion of the HFB 320 research aircraft with particular emphasis on the determination of control surface derivatives. The HFB 320 is used as a variable stability aircraft with 5 degrees of freedom simulation capability [3] (figure 4.1). To improve the simulation capability the aircraft was equipped with electrically controlled spoilers with enlarged panels [4]. The arrangement of flap and spoiler surfaces on the aircraft is shown in figure 4.2. The maximum spoiler rate is 62 deg/sec and the maximum flap rate is 10 deg/sec.

The aircraft equipment includes

- primary flight control system, fully fly-by-wire
- electrically controlled flaps and spoilers
- electrically controlled thrust
- on board digital computer
- artificial feel system
- electrically controlled flight instruments
- on board data acquisition system, data recording and telemetry system
- safety equipment.

All these features could be used for parameter identification flight tests. The control surface deflections were commanded by a program running on the on board digital computer.

Thus the control inputs could be reproduced with extreme accuracy in "successive" runs, a most important advantage for parameter identification. All the state variables were digitally recorded on board with 10 Hz sample rate and 18 selected variables were transmitted via telemetry to the ground station to monitor the flight tests.

Two flight missions with 20 separate runs were executed using the following reference flight conditions:

FLIGHT TEST	V [IAS]	H [ft]	γ (deg)	FLAPS (deg)	SPOILERS (deg)
1	145 kts	15000	0	0	0
2	↓	↓	↓	0	45
				30	0
				30	45

As previously mentioned the objective of the tests was to identify the longitudinal control derivatives from flight tests. There are essentially four controls involved namely elevator, spoilers, flaps and spoiler-flap combinations. In the latter case spoilers and flaps are simultaneously deflected. As the flaps are extended the spoilers are retracted and vice versa. By this maximum change in lift is created with minimum change in drag and pitching moments. 16-5

5. PARAMETER IDENTIFICATION METHOD

Numerical values of the aerodynamic characteristics of the controls were obtained by means of a parameter identification method which utilizes measured flight test data together with appropriate mathematical algorithms. An important advantage of using flight test data is that all possible effects of the actual flight environment are included in the measured data. In this program the parameter identification was performed by an output error method, that is, a mathematical method in which we try to fit the output of a mathematical model to the flight motions of the aircraft [5, 6, 7]. The cost function which measures the fit between the motions produced by the mathematical model and the flight is called likelihood-function

$$L = \frac{1}{2} \sum_{k=1}^N [Z(t_k) - Y(t_k)]^T R^{-1} [Z(t_k) - Y(t_k)] + \frac{N}{2} \ln |R|$$

where Z is the system output, Y the model output, N the number of data points and R the covariance matrix of the measurement noise.

This function has to be minimized with respect to R and to x - the vector of unknown parameters. The minimization technique used is a modified Newton-Raphson algorithm which requires only the first derivative of y with respect to x . The result of each iteration is an improvement in x . In general the search can be finished after ten to fifteen iterations. The program used was able to estimate not only coefficients of the linear system but also initial values of the state variables and input and output measurement biases. For these identifications, the following linearized model was used

$$\begin{aligned} \dot{u} &= \frac{X_u}{m} \cdot u + \frac{X_w}{m} \cdot w - g \cos \theta_0 \cdot \theta - V_{z0} \cdot q + \frac{X_{\delta_F}}{m} \cdot \delta_F + \frac{X_{\delta_{SP}}}{m} \cdot \delta_{SP} \\ \dot{w} &= \frac{Z_u}{m} \cdot u + \frac{Z_w}{m} \cdot w - g \sin \theta_0 \cdot \theta + V_{x0} \cdot q + \frac{Z_{\delta_F}}{m} \cdot \delta_F + \frac{Z_{\delta_{SP}}}{m} \cdot \delta_{SP} \\ \dot{\theta} &= q \\ \dot{q} &= \frac{M_u}{I_y} \cdot u + \frac{M_w}{I_y} \cdot w + \frac{M_q}{I_y} \cdot q + \frac{M_{\delta_e}}{I_y} \cdot \delta_e + \frac{M_{\delta_F}}{I_y} \cdot \delta_F + \frac{M_{\delta_{SP}}}{I_y} \cdot \delta_{SP} \end{aligned}$$

with the observation equations

$$\begin{aligned} u_{obs} &= u + K_u \\ w_{obs} &= w + K_w \\ \theta_{obs} &= \theta + K_\theta \\ q_{obs} &= q + K_q \\ a_{x obs} &= \frac{X_u}{m} \cdot u + \frac{X_w}{m} \cdot w + \frac{X_{\delta_F}}{m} \cdot \delta_F + \frac{X_{\delta_{SP}}}{m} \cdot \delta_{SP} + K_{a_x} \\ a_{z obs} &= \frac{Z_u}{m} \cdot u + \frac{Z_w}{m} \cdot w + \frac{Z_{\delta_F}}{m} \cdot \delta_F + \frac{Z_{\delta_{SP}}}{m} \cdot \delta_{SP} + K_{a_z} \end{aligned}$$

$$K_{(i)} = \text{Bias of measured signal } i$$

An important factor for parameter estimation techniques is the proper design of system input signals.

16-6
In selecting the input, it should be appreciated that the eigenmotion of the airplane must be excited since the process of identifying the control derivatives involves identification of the parameters related to the eigenmotion as well. Moreover, a poor identification of the eigenmotion could adversely affect the identification of the control derivatives. This problem does indeed arise in this program where the control derivatives of a spoiler, flap, or spoiler-flap combination should be defined. The following approach was undertaken.

The first step was to identify the eigenmotion parameters by means of the elevator. The inputs selected are shown in figure 5.1. First the short period motion is excited by a so called 3-2-1-1 signal [8] followed by a step elevator input to excite the phugoid motion (Signal 1). Using Signal 2 first the phugoid was excited by a step input followed by the 3-2-1-1 signal to excite the short period motion. Care was taken in Signal 2 to excite the short period motion at such a time when the deviation from reference airspeed caused by the phugoid was minimal.

The eigenmotion investigation was followed by the determination of the spoiler-, flap- and combined flap-spoiler characteristics. Two basic signals are used as shown in figure 5.2. Signal 3 is a combination of two signals with the initial input consisting of an elevator input which excites the phugoid and short period motions. Later in time an input of either the spoiler, flap or flap-spoiler is introduced as required in the analysis. Also, Signal 4 has an input of either spoiler, flap or flap-spoiler as required. This signal should excite the eigenmotion of the airplane and provide sufficient information to identify the control parameters.

6. IN-FLIGHT MEASURED FLAP-SPOILER CHARACTERISTICS

The first step in the identification process was to identify the parameters related to the airplane's eigenmotion. Figures 6.1 and 6.2 compare the results of the identification runs with the flight test data obtained from inputs of Signal 1 and 2, respectively. Note in the figures a clear separation between the short period and phugoid motions. The good curve fits of model responses to in-flight measured time histories over the long time period of 180 seconds indicates that the estimated parameters are representative.

Now that the airplane's eigenmotion can be described by a linear model, one can approach the problem of identifying the additional control derivatives. Identification of the control derivatives, for a particular control surface, is done together with the eigenmotion identification so that one obtains a mathematical model which includes the eigenmotion derivatives and the control derivatives. Since the eigenmotion model was already established from tests with the elevator input, one can check the results of the model with the additional control surface to determine the validity of this result. The parameter identification of the additional controls was done with inputs Signal 3 and Signal 4. From an examination of these results it was clear that the results obtained by using Signal 4 are not valid. In the case of the spoiler, Signal 4 does not introduce sufficiently large changes in the airplane's speed to determine accurately the speed derivatives, but the spoiler control derivatives appear reasonable. In the case of the flaps, the inaccuracy of that section of the model describing the eigenmotion causes inaccuracy in identifying the flap derivatives. The case of the spoiler-flap combination with Signal 4 failed. It became clear that to identify the additional control derivatives one should utilize the elevator plus the additional control surface on interest.

Figure 6.3 presents the results of identifying the spoiler derivatives. In the steady state condition the spoiler is at 45 deg. The fact that when the spoiler is deflected, the time histories are in good agreement (especially in longitudinal and vertical acceleration) suggests that the identification of the spoiler derivatives is very good. The logical explanation is as follows: Excellent agreement of the time histories are obtained when rapid elevator motion is introduced thereby indicating that the mathematical model is correct. Thus when the spoiler is introduced and the time histories continue to be in good agreement, one may conclude that the identification of the spoiler derivatives are accurate.

The numerical results of the spoiler nondimensional derivatives as function of flap deflection compared with windtunnel data are given in figure 6.4.

The windtunnel measurements are carried out with a 1:7.5 scale model in the DFVLR 2.8 m x 3.6 m low speed windtunnel [9] with an effective Reynoldsnumber of $1.64 \cdot 10^6$ compared with $11.14 \cdot 10^6$ in-flight.

Flight test results show higher lift control effectiveness $C_{A\delta}^{SP}$, lower drag control effectiveness $C_{W\delta}^{SP}$ and higher moment control effectiveness $C_{M\delta}^{SP}$ compared with wind-tunnel data. The $C_{W\delta}^{SP}$ general influence of flap deflection on $C_{M\delta}^{SP}$ spoiler control effectiveness obtained from windtunnel measurements agree with in-flight measured data.

The quality of the results obtained from the identification of the flap derivatives (figure 6.5) are similar to the quality of the spoiler results.

The numerical results of flap nondimensional derivatives as a function of spoiler deflection compared with windtunnel data are shown in figure 6.6. For the one reference flight condition investigated with $\delta_{sp} = 0$ deg the lift control effectiveness and the drag control effectiveness of flaps are very close to the windtunnel measured data. A difference occurred for the moment control derivative.

The results show that the control characteristics of the flap and spoiler direct lift devices can be described by a linear model with constant derivatives. This is valid for relatively large deflections up to ± 10 deg flap deflection and up to ± 30 deg spoiler deflection and relatively high surface rate of 10 deg/sec and 62 deg/sec respectively. 16-7

For control system design using a combination of control surfaces like flaps and spoilers simultaneously deflected it is very important to know the significance of aerodynamic interference effects between the control surfaces. Are there nonlinearities, instationary or aerodynamic interference effects in such a way that the resulting control characteristics will be completely changed, or are the effects negligible so that the separated control derivatives can be added in a linear way?

To answer these questions, in addition to separate control surface identification, tests were conducted with spoiler-flap combinations as mentioned earlier. The combinations of amplitude ratios between flap and spoiler used are as follows

	Flap deflection δ_F , deg	
	± 5.0	± 10
Spoiler deflection δ_{sp} , deg	∓ 15	∓ 30

To identify the characteristics obtained from combined flap-spoiler deflections three different approaches are used:

1. The identification is made with one input (flap or spoiler) resulting in equivalent control derivatives.
2. The identification is made with fixed flap and spoiler derivatives obtained from previous 'flap only' and 'spoiler only' identification runs.
3. The identification is made with flap and spoiler inputs resulting in flap and spoiler derivatives valid for combined flap-spoiler deflections.

To avoid computer time consuming identification, the combined flap-spoiler identification was not carried out over the full 180 sec measuring time. The identification 'run' was composed by the elevator input and the flap-spoiler input to identify both the aircraft short period eigenmotion and the control derivatives.*)

The first approach is possible if both surfaces move closely together. A time delay of about 0.2 seconds in the flap actuator system of the HFB 320 results in a nonlinear coupling of both surfaces as shown in figure 6.7. This fact disqualifies the first approach.

For the second approach the flap and spoiler derivatives obtained from the separate control derivative identification runs (figure 6.4 and 6.6) are used. Because of the fact that no in-flight measured flap data for the $\delta_{sp} = 45$ deg reference condition are available, the flap data for the $\delta_{sp} = 0$ deg reference condition are used. These data are reduced by the same amount as $C_{A\alpha}$ and $C_{W\alpha}$ being identified for the $\delta_{sp} = 45$ deg reference condition.

If there are no differences between measured and computed time histories using fixed flap and spoiler derivatives any interference effects can be excluded. But if there are differences, flap-spoiler interference for combined deflection exists.

As illustrated in figure 6.8 the time response due to combined flap-spoiler deflection can be matched with relatively good results. Comparing the vertical and longitudinal acceleration response with flap and spoiler input, it can be seen, that the measured variables follow mainly the flap movement. The error in vertical acceleration response is caused by a too large spoiler effectiveness. Due to this and other flap-spoiler effects, especially the vertical speed and pitch rate response cannot be matched. This indicates that flap-spoiler interference effects exist.

In figure 6.9 the measured data for the same input as shown in figure 6.8 are compared with model response using new flap and spoiler identified derivatives. As shown in this figure an excellent match of all variables is obtained. This means that the flap-spoiler or spoiler-flap interference can be described by changed control effectiveness and, what is very important, the effects can be described in a linear way.

To look for the influence of the amplitudes of control surface deflections (figure 6.10) test runs with higher amplitudes are made resulting in the same matching accuracy obtained before.

*) The authors thank Mr. R. Koehler, DFVLR, Institut für Flugmechanik who helped to produce additional identification results, because Mr. O. Rix retired from the DFVLR.

16-8

Looking at the identified flap and spoiler derivatives valid for combined flap-spoiler deflections as shown in the following table, it can be found that the flap derivatives remain nearly constant for both the low amplitude and for the high amplitude input.

	LOW AMPLITUDE INPUT		HIGH AMPLITUDE INPUT	
	() relative standard deviation, percent		() relative standard deviation, percent	
FLAP DERIVATIVES	$C_{A\delta F}$	0.75 (2.18)	0.77 (1.73)	
	$C_{W\delta F}$	0.127 (2.53)	0.11 (2.01)	
	$C_{M\delta F(19.5)}$	- 0.036 (7.71)	- 0.032 (5.36)	
SPOILER DERIVATIVES	$C_{A\delta sp}$	- 0.13 (4.42)	- 0.15 (2.78)	
	$C_{W\delta sp}$	0.023 (4.29)	0.022 (3.12)	
	$C_{M\delta sp(19.5)}$	- 0.029 (17.33)	- 0.007 (5.04)	

The same tendency is seen for the spoiler derivatives with one exception, the spoiler moment control derivative $C_{M\delta sp}$. There is a large difference between the low and high amplitude case.

Looking at the relative standard deviation of $C_{M\delta sp}$ it can be seen that for the low amplitude input the relative standard deviation is $C_{M\delta sp}$ high (17.33), that means that the spoiler moment influence is low, so that the identification of this value is difficult.

Comparing these data with the windtunnel data shown in figure 6.4 and 6.6 it is seen that the flap control effectiveness $C_{A\delta F}$ and the moment control effectiveness $C_{M\delta F}$ correlate very well with windtunnel data for the 45 deg reference spoiler deflection. A large difference occur for the in-flight measured drag derivative $C_{W\delta F}$ which is much lower compared with windtunnel measured value.

This results show that the aircraft response is mainly influenced by the flaps due to higher control effectiveness compared to the spoiler. So that the flap effectiveness is only slightly influenced by spoiler deflections, this is judicious comparing the flap area behind the spoiler.

The spoiler control effectiveness $C_{A\delta sp}$ is decreased, the drag control coefficient $C_{W\delta sp}$ is increased compared with the 'spoiler only' identified values.

The spoiler moment control derivative is amplitude dependent and is more negative with regard to windtunnel data.

7. CONCLUSIONS

The following conclusion can be drawn from the in-flight measured characteristics of combined flap-spoiler direct lift controls:

1. Parameter identification technique is a valuable tool to identify both aircraft stability parameters and direct lift control parameters.
2. The results show, that the prerequisite for control parameter identification is the identification of aircraft stability parameters using an optimized input to excite the aircraft.
3. In-flight measured data show, that both the flap and spoiler direct lift controls can be identified with sufficient accuracy. The control behaviour can be described by a linear model although relatively high amplitudes and surface rates are used. Possible lift lag effects are so low that they can be neglected.
4. In addition the characteristics produced by combined flap-spoiler inputs can be described by a linear model. The interference effects result mainly in varied spoiler derivatives. Flap derivatives remain nearly unchanged.
5. Comparing in-flight measured flap data with windtunnel data it is shown that lift, drag and moment derivatives correlate well with flight test data for the clean spoiler configuration.
6. Comparing in-flight measured spoiler data with windtunnel data it is shown that large differences occur. Only the general trend due to steady state flap deflection is apparent.

7. The discrepancies obtained from in-flight and windtunnel spoiler measurements show that separated flow measurements in windtunnel cannot be applied to the real aircraft. It is assumed that the spoiler measurements are sensitive to Reynoldnumber variation.

From this the question arises how separated flow effects on aircraft control derivatives can be simulated in windtunnel and how the results have to be scaled for in-flight application?

8. REFERENCES

1. Hanke, D., Lange, H.-H., "In-Flight Handling Qualities Investigation of Various Longitudinal Short Term Dynamics and Direct Lift Control Combinations for Flight Path Tracking Using DFVLR HFB 320 Variable Stability Aircraft", AGARD FMP Symposium on Stability and Control, Ottawa, 25-28 Sept. 1978.
2. Hanke, D., "In-Flight Investigation of Direct Lift Control in Landing Approach", DFVLR IB 154-77/25, 1977.
3. Hanke, D., Lange, H.-H., "Der Fliegende Simulator HFB 320 der DFVLR als Versuchsgerät zur Ermittlung von Flugeigenschaften", Preprint DGLR 77-082, DGLR Symposium Entwicklungssimulation, 5-6 Dec. 1977.
4. Neppert, H., "Abschätzung der Wirksamkeiten vergrößerter Bremsklappen der HFB 320", MBB-Bericht, TN-HE 212-10/75, Sept. 1975.
5. Taylor, L.W., Jr., Iliff, K.W., "A Modified Newton-Raphson Method for Determining Stability Derivatives from Flight Data", Computing Methods in Optimization Problems - 2, Lotfi A. Zadeh, Lucien W. Neustadt, and A. V. Balakrishnan, eds., Academic Press, 1969, pp. 353-364.
6. Plaetschke, E., "Kennwertermittlung mit Maximum-Likelihood-verfahren", DFVLR IB 154-74/20, 1974.
7. Rix, O., Huber, H., Kaletka, J., "Parameter Identification of a Hingeless Rotor Helicopter", 33rd Annual National Forum of the American Helicopter Society, Washington, D.C./USA, 9-11 May 1977, Preprint 77.33-42 (1977).
8. Koehler, R., "Auslegung von Eingangssignalen für die Kennwertermittlung", DFVLR IB 154-77/40, 1977.
9. Amtsberg, J., "Dreikomponentenmessungen an modifizierten Spoilern der HFB 320", DFVLR IB 157-76 C 11, 1976.

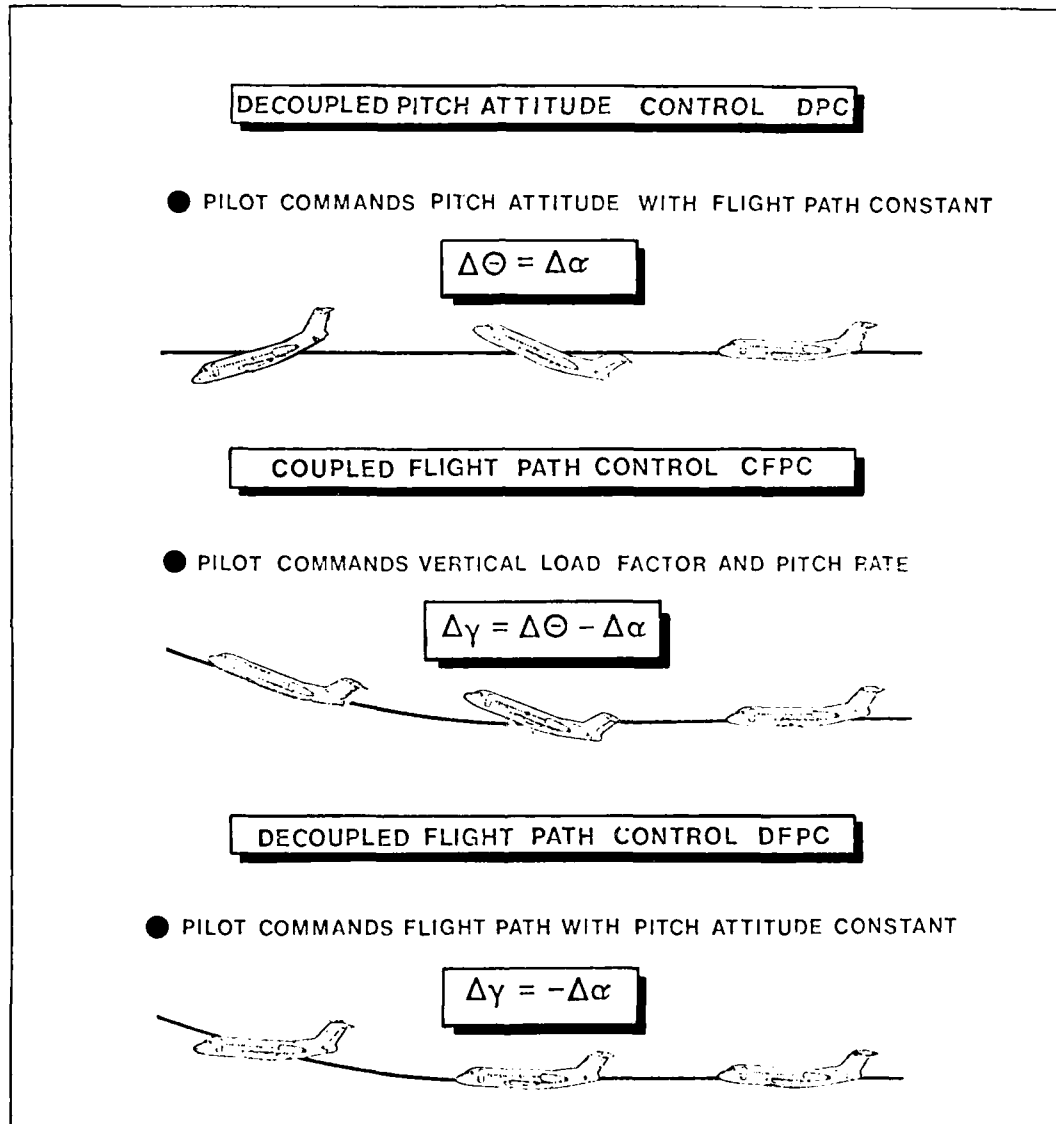


FIG. 2.1

PRINCIPLES OF DLC APPLICATION

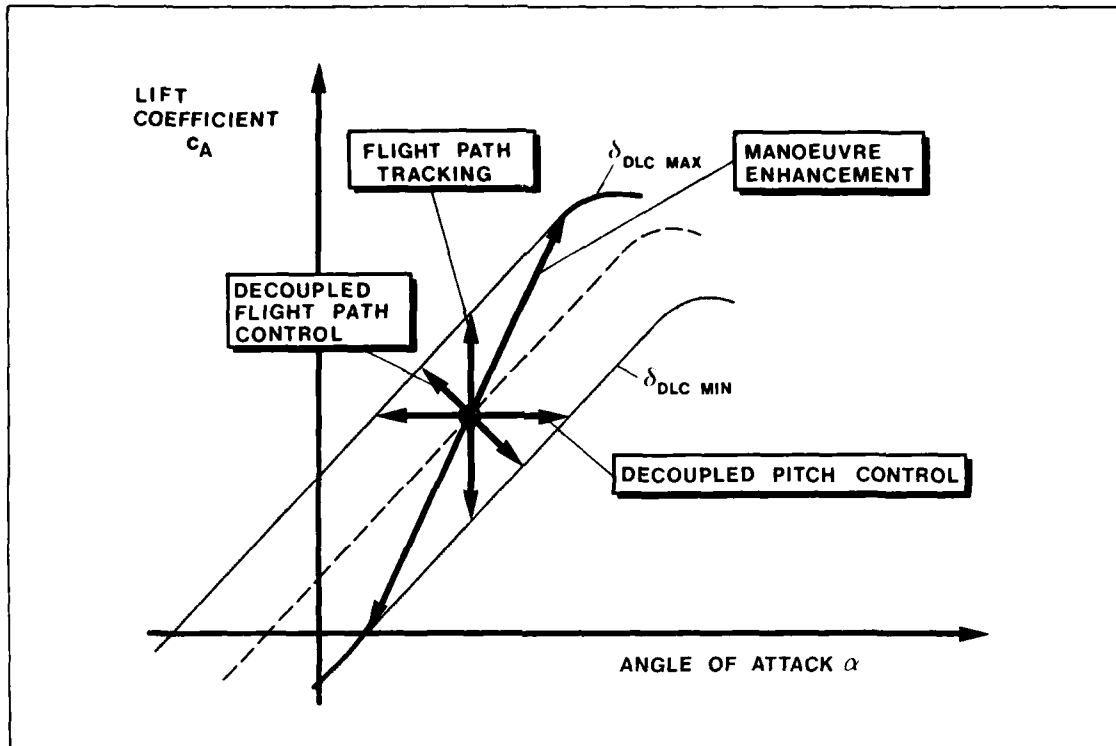


FIG.2.2 EFFECTIVE LIFT CURVE SLOPE VARIED BY DLC APPLICATION

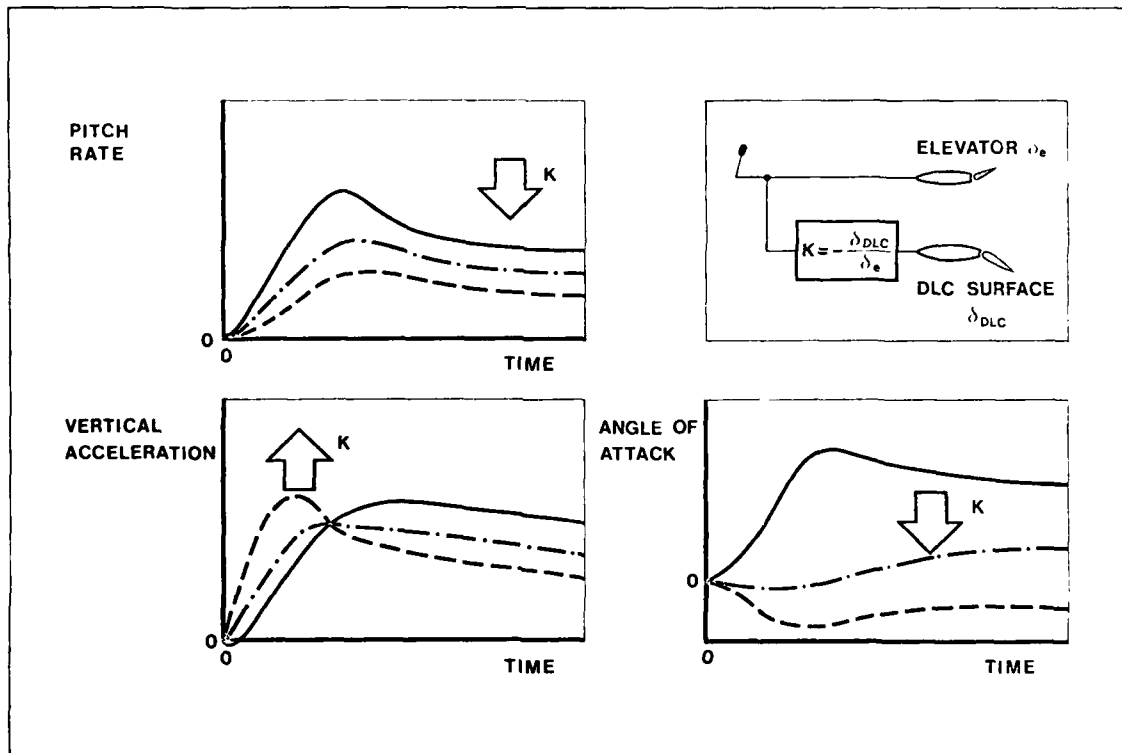


FIG. 2.3 INFLUENCE OF DLC ON AIRCRAFT TIME RESPONSE

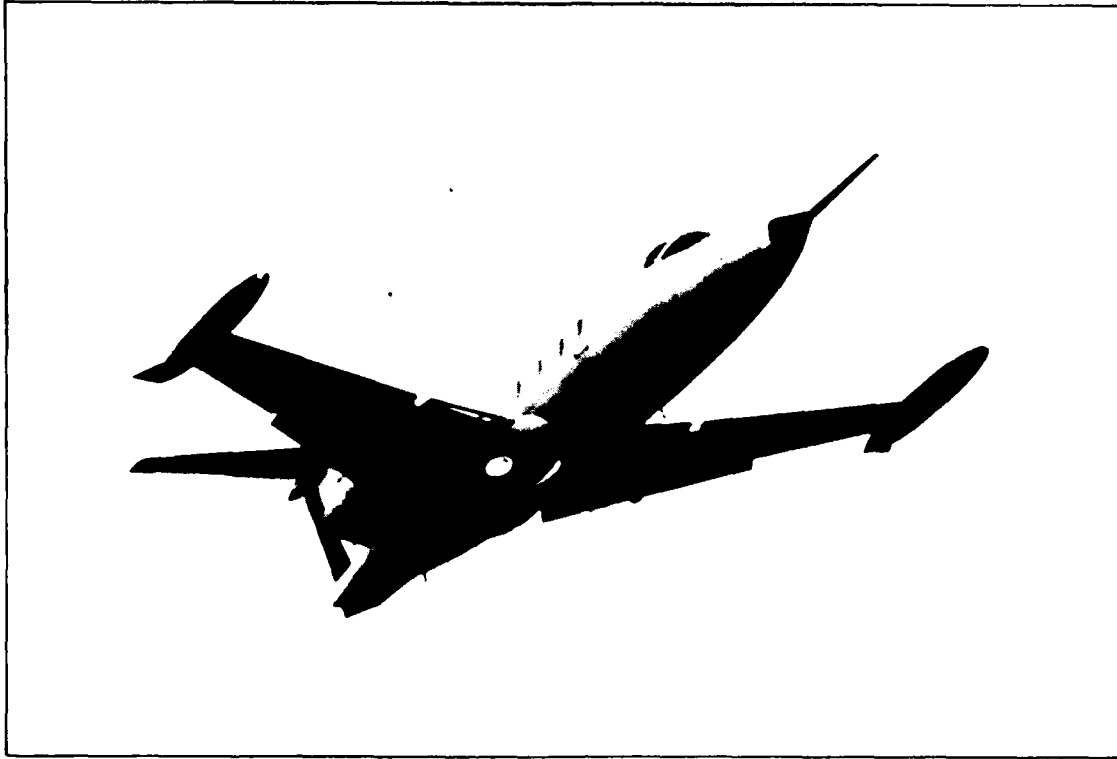


FIG. 4.1 DFVLR-HFB 320 IN-FLIGHT SIMULATOR

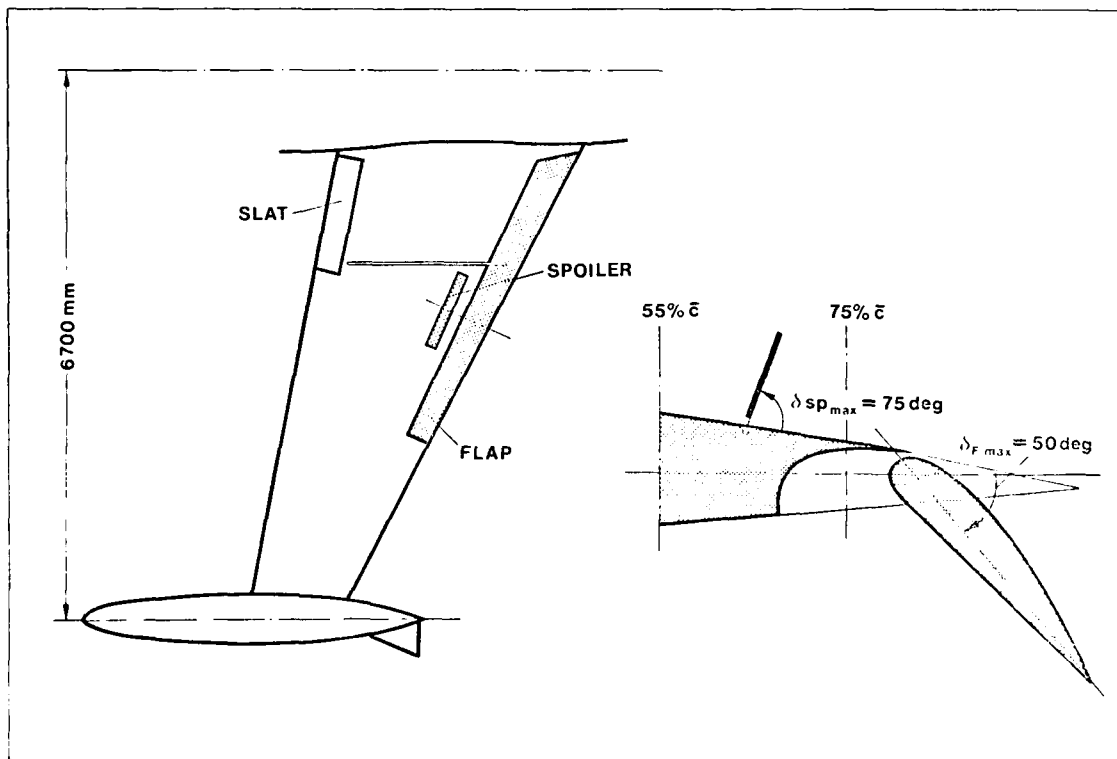
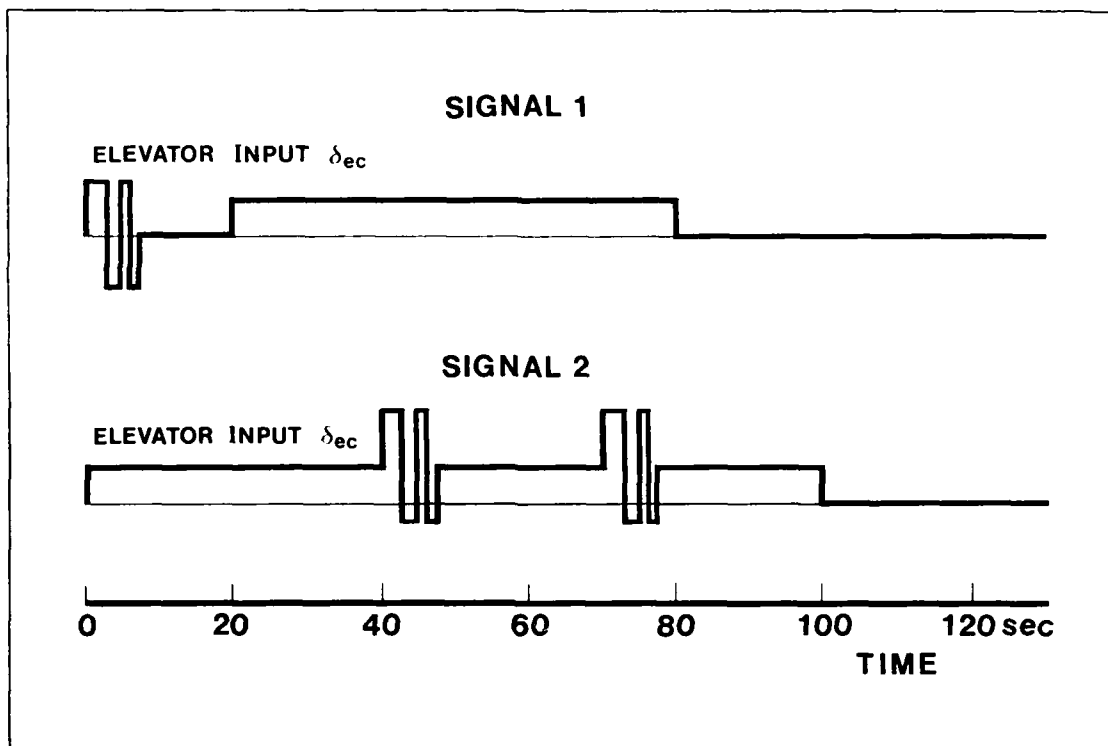
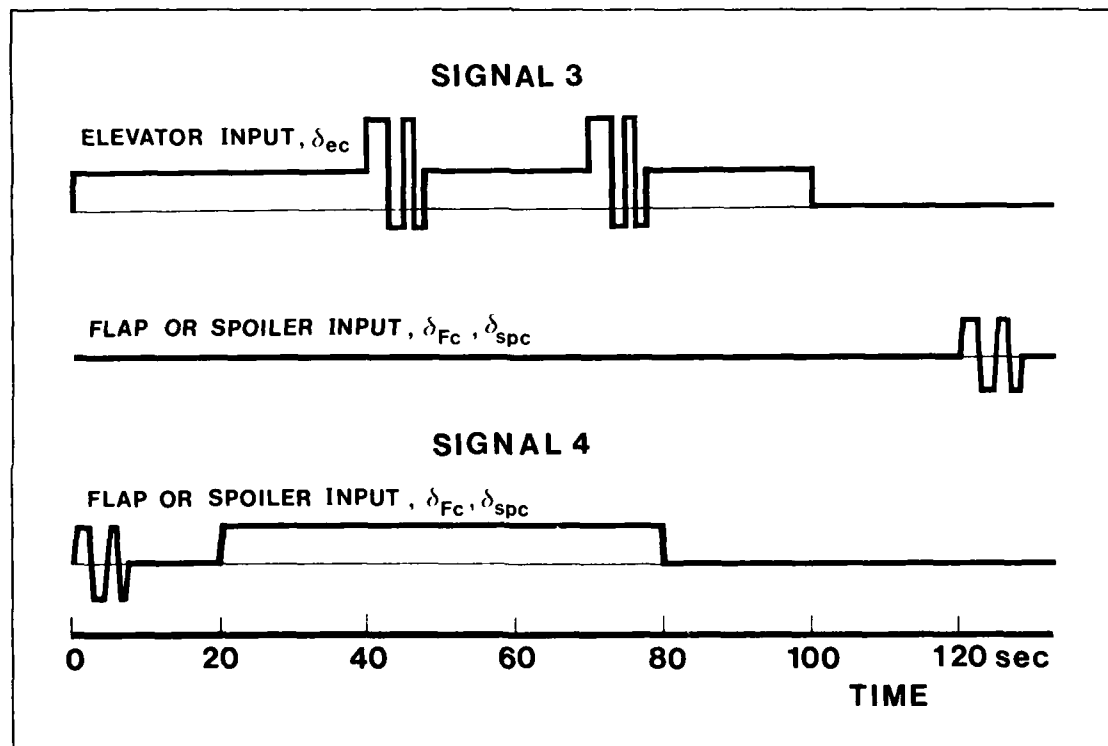


FIG. 4.2 AIRCRAFT FLAP-SPOILER ARRANGEMENT



INPUT SIGNAL USED FOR EIGENMOTION PARAMETER IDENTIFICATION

FIG. 5.1



INPUT SIGNAL USED FOR CONTROL PARAMETER IDENTIFICATION

FIG. 5.2

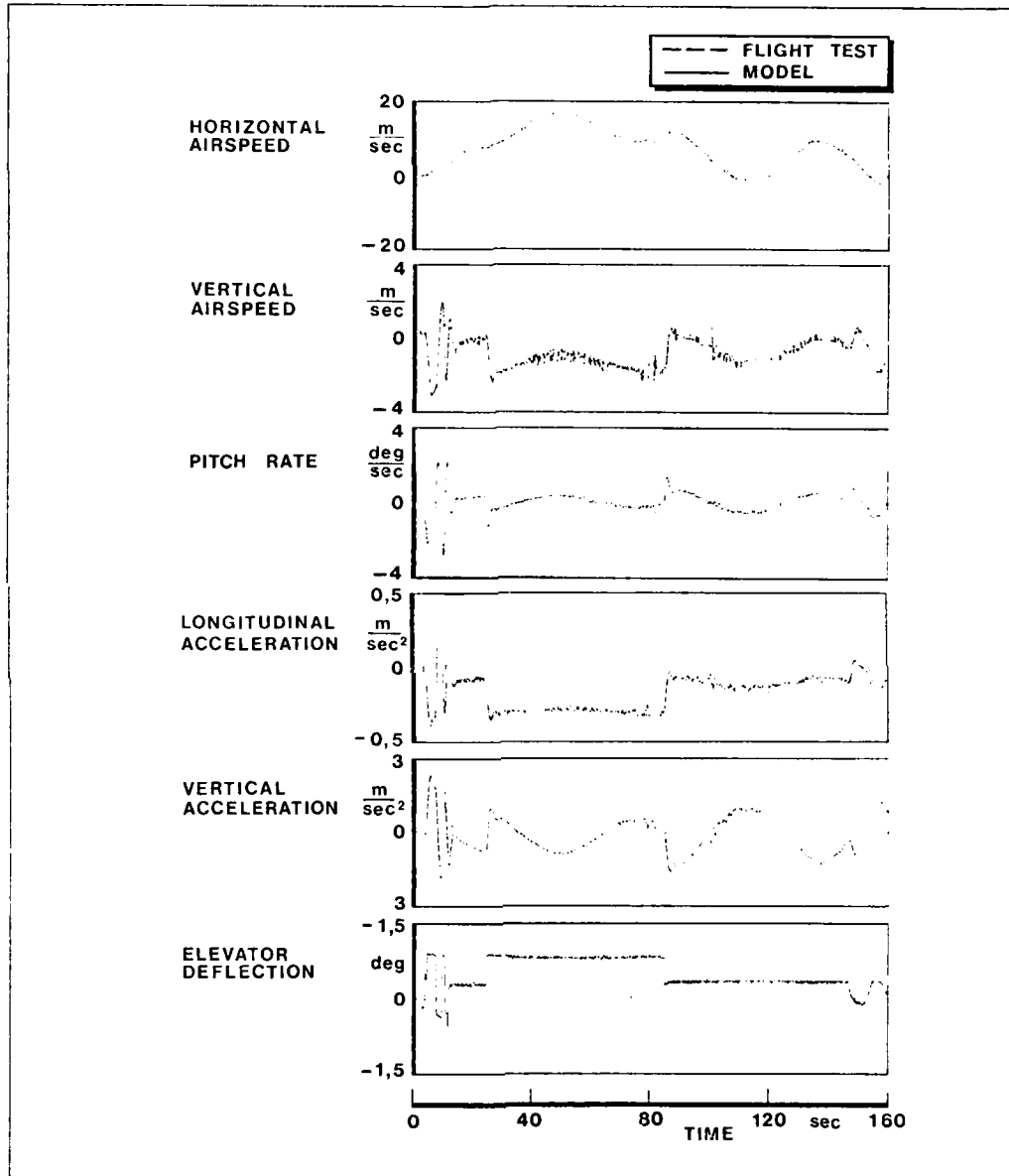


FIG. 6.1 TIME HISTORIES OF EIGENMOTION EVALUATION
(INPUT SIGNAL 1)

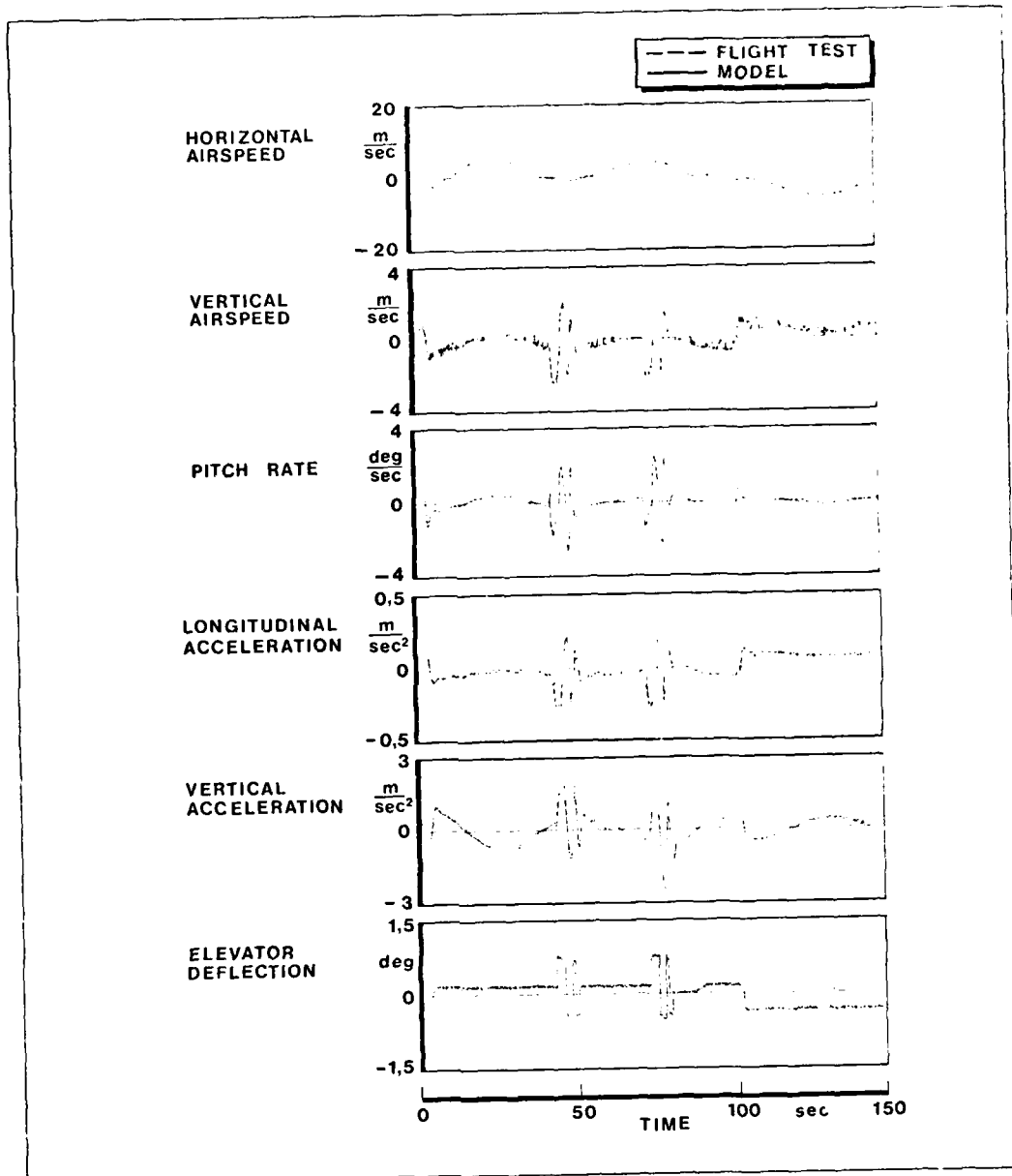


FIG. 6.2 TIME HISTORIES OF EIGENMOTION EVALUATION
(INPUT SIGNAL 2)

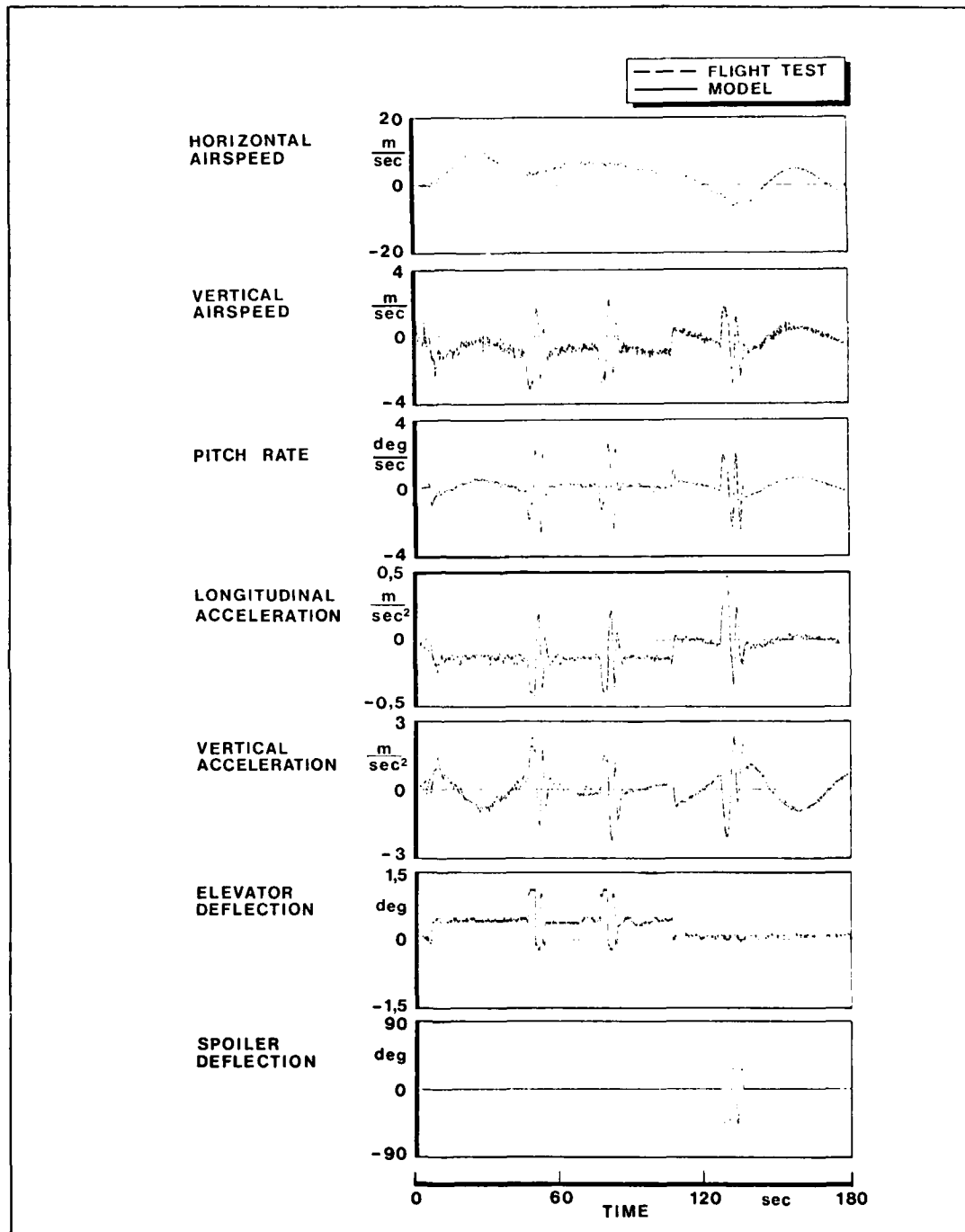


FIG. 6.3 TIME HISTORIES OF SPOILER CHARACTERISTIC EVALUATION

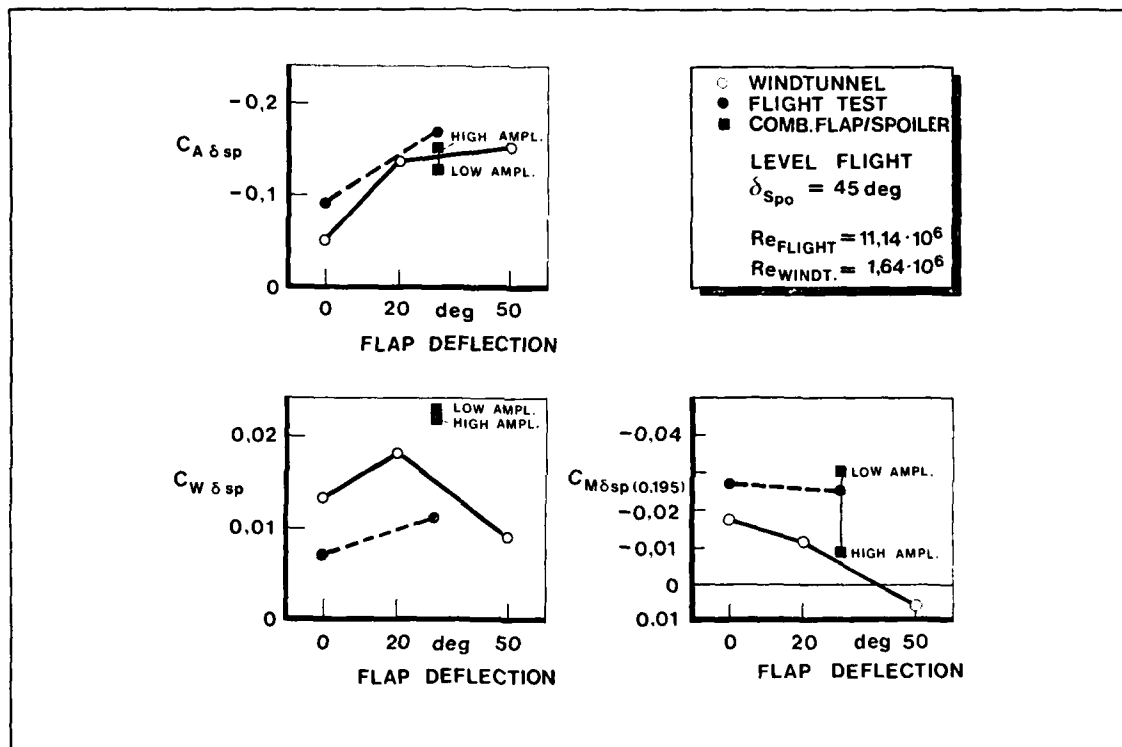


FIG. 6.4 COMPARISON OF IN-FLIGHT AND WINDTUNNEL MEASURED SPOILER CONTROL DERIVATIVES

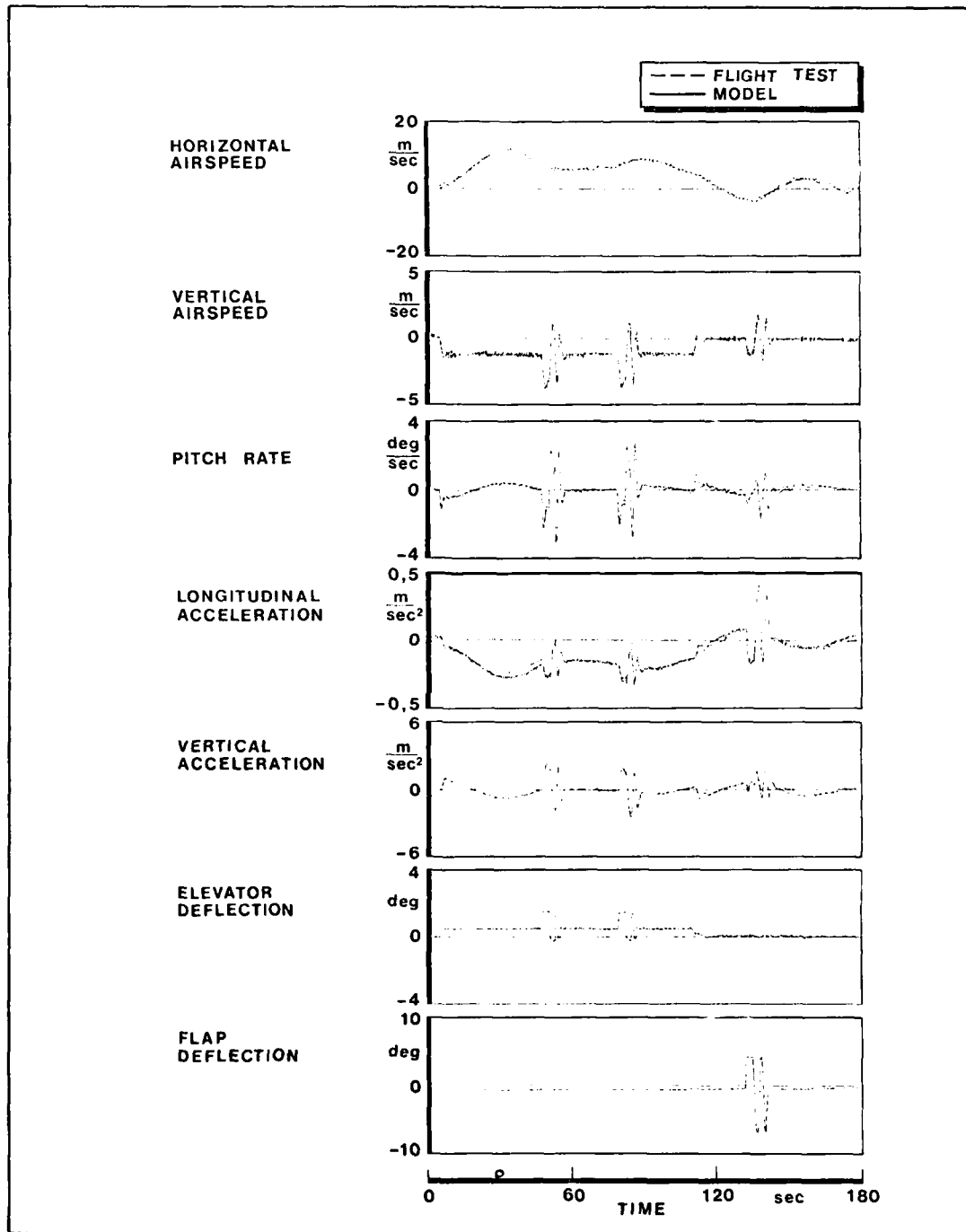
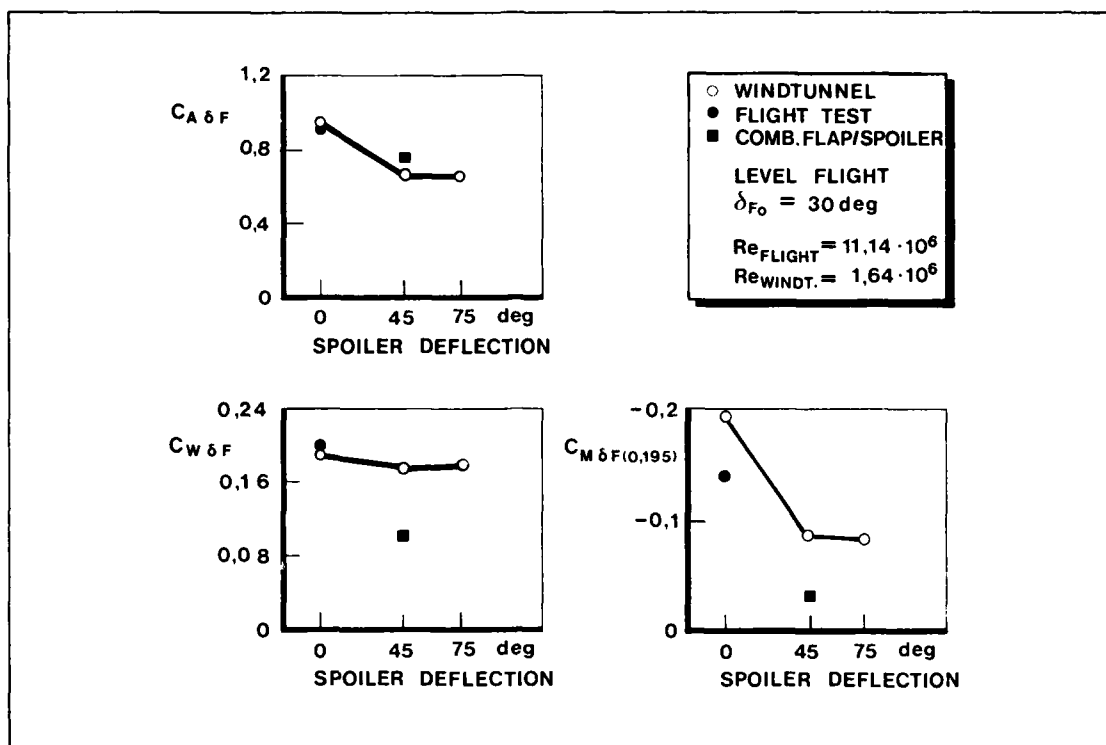


FIG. 6.5 TIME HISTORIES OF FLAP CHARACTERISTIC EVALUATION



COMPARISON OF IN-FLIGHT AND WINDTUNNEL MEASURED
 FIG. 6.6 FLAP CONTROL DERIVATIVES

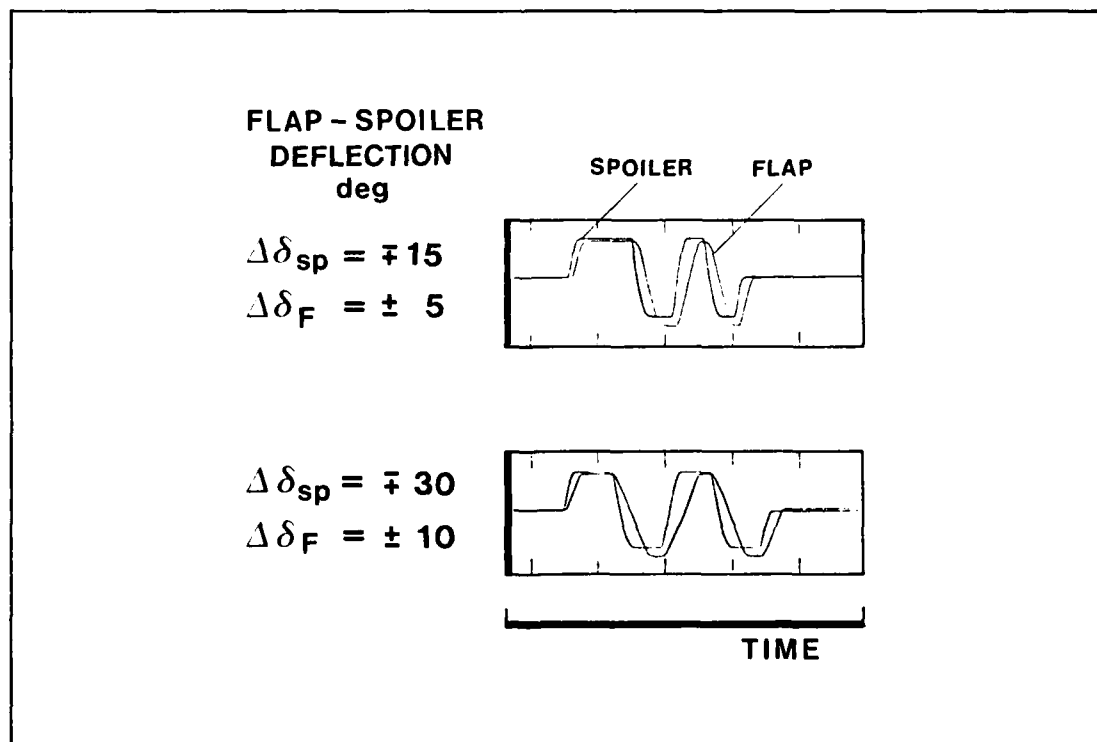


FIG. 6.7 FLAP - SPOILER DEFLECTION COMPARISON

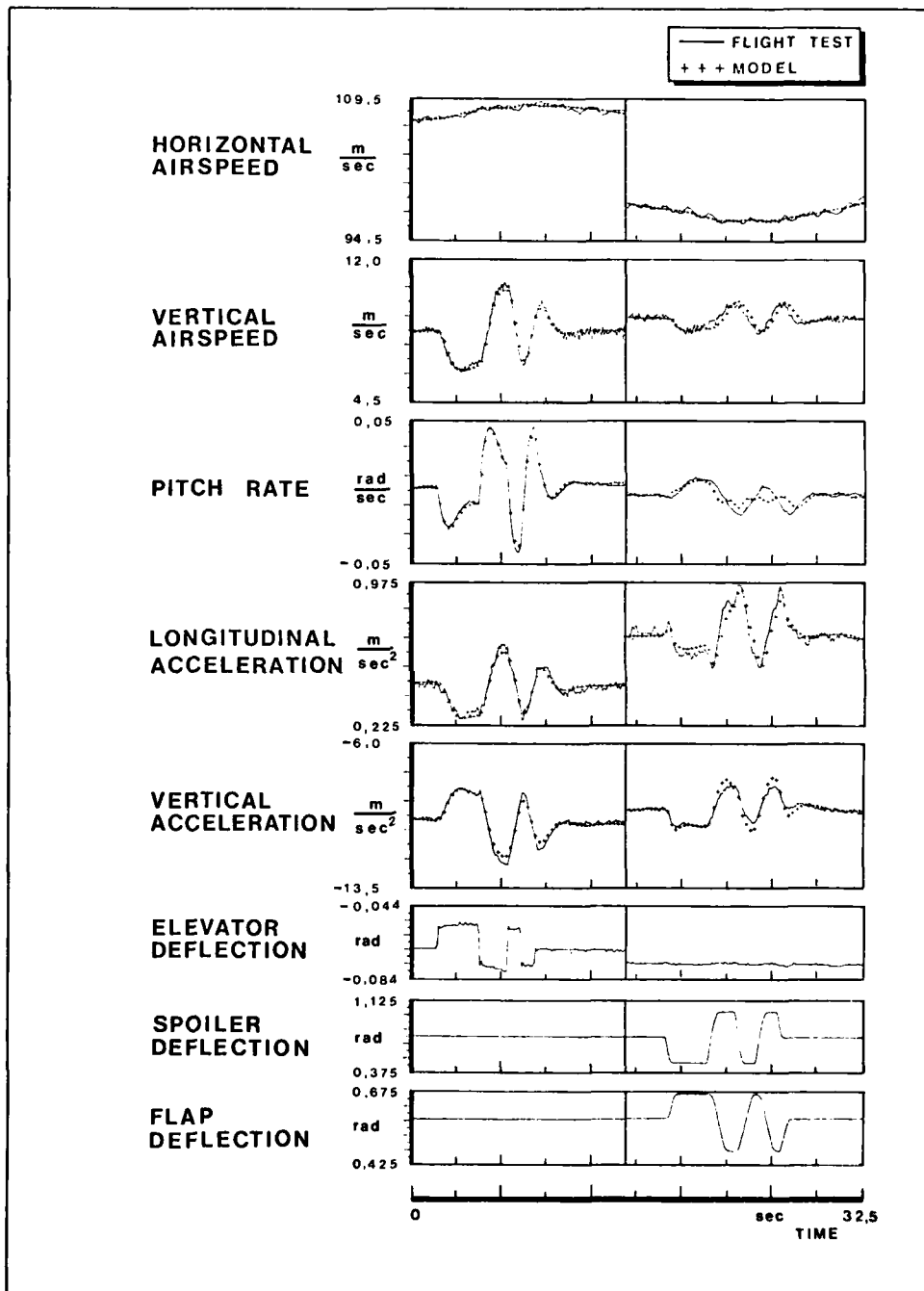


FIG. 6.8 COMBINED FLAP-SPOILER CHARACTERISTIC EVALUATION
 (DERIVATIVES FROM SEPERATE FLAP, SPOILER INPUT)

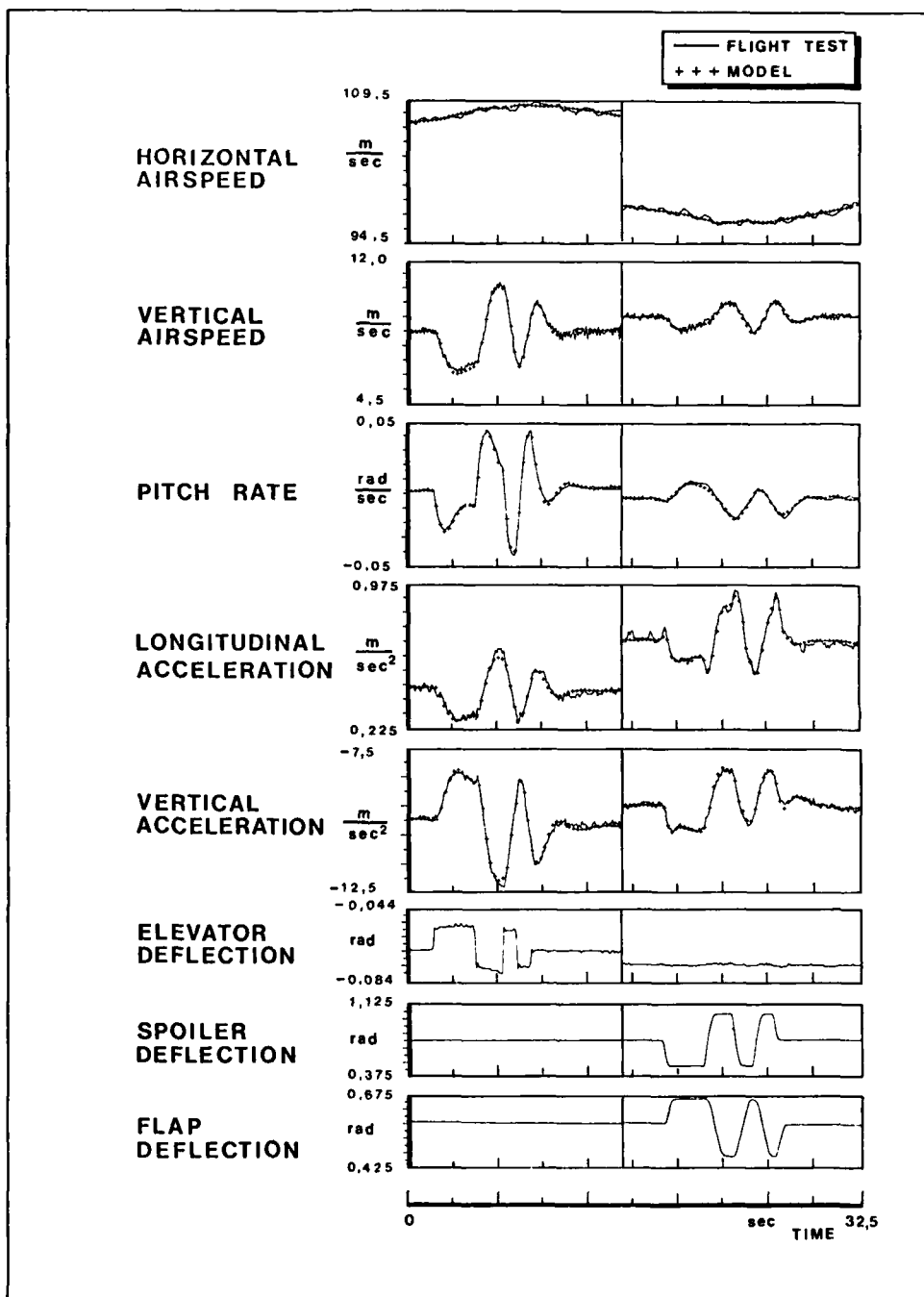


FIG. 6.9 COMBINED FLAP - SPOILER CHARACTERISTIC EVALUATION
(LOW AMPLITUDE INPUT)

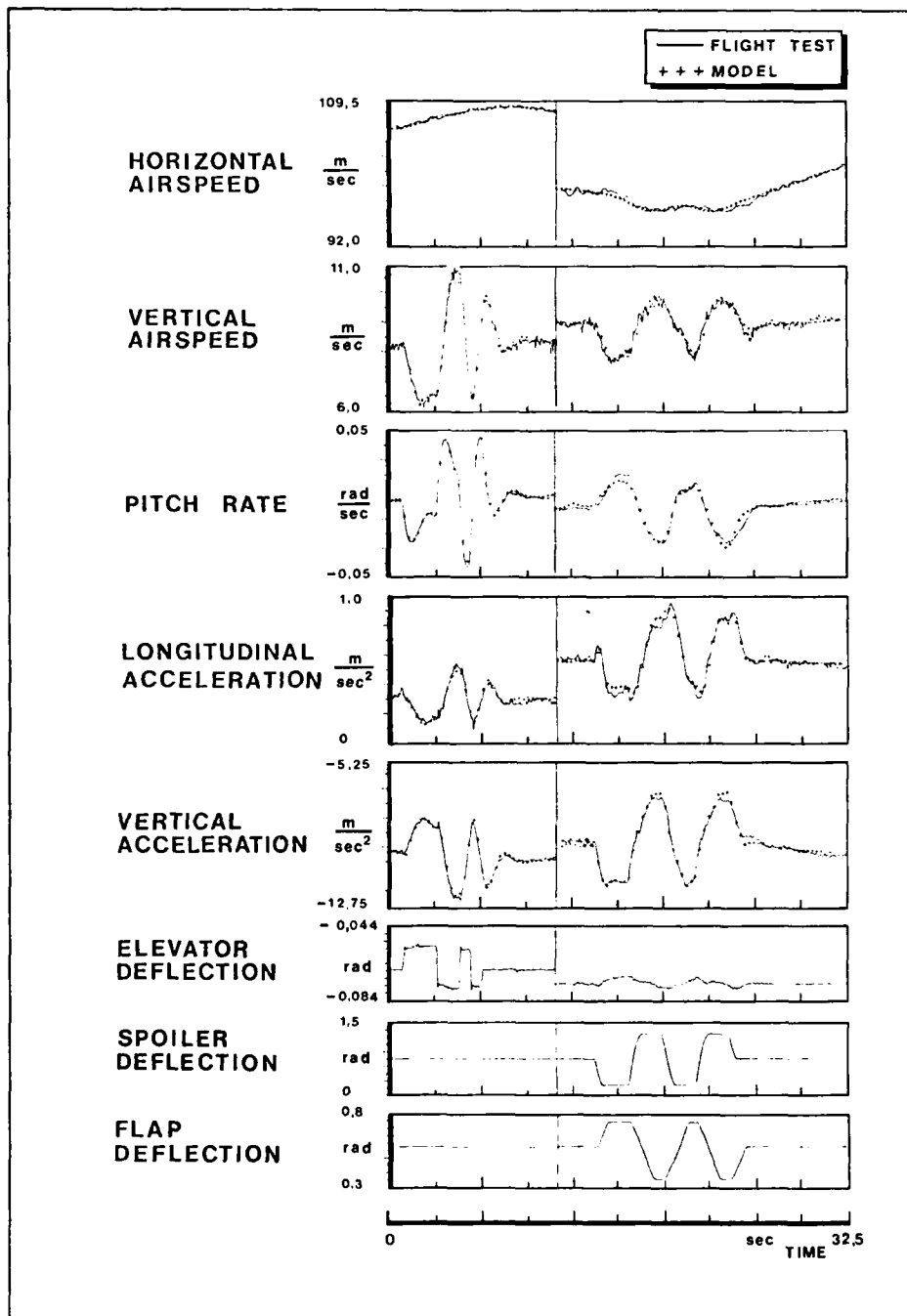


FIG. 6.10 COMBINED FLAP-SPOILER CHARACTERISTIC EVALUATION
 (HIGH AMPLITUDE INPUT)

WINDTUNNEL INVESTIGATION OF CONTROLS FOR DF ON A
FIGHTER-TYPE CONFIGURATION OF HIGHER ANGLES OF ATTACK

Wolfgang Sonnleitner

Messerschmitt-Bölkow-Blohm GmbH
Unternehmensbereich Flugzeuge
Postfach 801160
D-8000 München 80
Germany

SUMMARY

In 1977, a joint investigation (MBB-DFVLR) has been conducted in order to study stability and control characteristics of a fighter-type model at incidences up to 40 degrees.

Primary emphasis of the study was directed towards the stability and control contributions of

- A different control shapes (vertical canards - single, double, vertical tail, winglets)
- B control surfaces in different positions (vertical canard at body nose, at body below wing....)

Isolated and combined effects of devices A, B are demonstrated in the regime of higher angles of attack.

LIST OF ABBREVIATIONS

c_L	Lift coefficient	c_y	Sidelforce coefficient
c_l	Rolling moment coefficient	$c_{y\beta}$	Rate of change of sidelforce with yawing angle
$c_{l\delta_{vc}}$	Rate of change of rolling moment with vertical canard deflection	$c_{y\delta_{vc}}$	Rate of change of sidelforce with vertical canard deflection
$c_{l\delta_a}$	Rate of change of rolling moment with aileron deflection	$c_{y\delta_r}$	Rate of change of sidelforce with rudder deflection
$c_{l\delta_r}$	Rate of change of rolling moment with rudder deflection	α	Angle of incidence
$c_{l\beta}$	Rate of change of rolling moment with yawing angle	β	Angle of yaw
$c_{m,3}$	Pitching moment coefficient referred to .3 MAC	δ_{vc}	Vertical canard deflection angle
c_n	Yawing moment coefficient	$\delta_r = \xi$	Rudder deflection angle
$c_{n\beta}$	Rate of change of yawing moment with angle of yaw	Δ	Increment of coefficient
$c_{n\delta_{vc}}$	Rate of change of yawing moment with vertical canard deflection		
$c_{n\delta_r}$	Rate of change of yawing moment with rudder deflection		

1. INTRODUCTION

A requirement of good supersonic aircraft performance results in wing-designs of high leading edge sweep, low aspect ratio combined with small camber and twist and thin airfoils having nearly sharp leading edges. At increasing angles of incidence ($\alpha > 10^\circ$) the flow field of this type of wings is dominated by concentrated separated vortex systems originating at the inboard leading edge. Due to this vortices lateral stability is lost before reaching maximum lift. So modern fighter aircraft with high thrust to weight ratio is limited not only by available control power, but also by loss of stability.

In [5], [6] significant parameters for directional stability and lateral control departure are

$$c_{n\beta \text{ dyn}} = c_{n\beta} \cdot \cos \alpha - \frac{1}{I_x} \cdot c_{l\beta} \cdot \sin \alpha$$

$$\text{LCDP} = c_{n\beta} - c_{l\beta} \left\{ \frac{c_{n\delta_a} - K_1 c_{n\delta_r} \dots}{c_{l\delta_a} - K_1 c_{l\delta_r}} \right\}$$

with $K_1 = \delta_r / \delta_a$

1.1 Model Geometry

7-2 Seeking a solution for stability and control requirements which arise mainly at lower speeds (depending on wing loading), a wind tunnel study was started, fig. 1, together with the DFVLR Göttingen [1] [2]. The devices and their location have practical configurational constraints like pilot's view, undisturbed intake flow, ground-clearance, minimum wetted surface and so on. However, seeking some insight in aerodynamics, the control surfaces shown in fig. 2, 3, 4, 5 were positioned looking for undisturbed flow and high dynamic pressure at higher incidences, disregarding the above-mentioned constraints. Due to the shortness of time, the results to be presented are confined on the vertical canards and vertical stabilizer modifications shown in fig. 2, 4. More practical configurations like fig. 5 are treated in [4].

1.2 Flow Field

For interpretation of the test results we should have a short look at the aforementioned flow field which is roughly sketched in fig. 6. A survey about these effects and extensive references are given by [3] as a result of several years research on these problems. The essential feature are the stable vortices, which are produced by flow separation at the highly swept wing leading edge and the body nose. At angles of incidence α increasing above 10° the vortices are moving further upward and inboard. At yawing conditions, they are shifted to insymmetrical positions with respect to the vertical stabilizer producing an induced sidewash and downwash. At higher angles of attack, the windward vortex is bursting earlier producing a dynamic pressure reduction at the tail giving destabilizing roll- and yawing moment. It should be mentioned that the flow conditions at the tail are influenced too by the trim position of the horizontal stabilizer, thus by stability margin.

The single vertical canard in the plane of symmetry has nearly no influence on the flow passing the body, whereas the double surfaces change the flow direction along body axis, thus producing a high pressure field in between them.

2. STABILITY AND CONTROL

2.1 Stability and Control of Clean Configuration

Due to the law of momentum conservation, flow field curvature must be found in force and momentum coefficients. In fig. 7 the roll and yawing moments versus α are shown for the clean configuration wing, strake on and off. According to the aforementioned flow field considerations, we find beginning stability problems at the same α when the strake-off wing reaches its maximum lift.

2.2 Tail Modifications

In order to find the decrease of stability independent of dynamic pressure due to separation effects an additional tail surface was placed below the horizontal tail at the body. The results in fig. 8 show for sideforce and yawing moment an analog behaviour to sheared wing theory.

A study concerned with rudder efficiency due to tail size and shape shows in fig. 9 not only the effects of increased size, but also the influence of changes in dynamic pressure due to vortex system inductions. Again rudder efficiency is lost at angles of incidence higher than $\alpha_{c_{lmax}}$ of the low swept outboard wing. This can be understood in the following way. At angles of incidence lower than outboard $\alpha_{c_{lmax}}$ the vortex develops in a low pressure field, which means by Bernoulli's law, higher vortex velocity due to lower vortex core pressure causing higher vortex circulation and induction velocities.

At angles of incidence above $\alpha_{c_{lmax}}$ of outboard wing the vortex is no longer driven by the outboard suction field, but is decelerated until final vortex core bursting by the increasing outboard pressure field. The vortex just transports energy from its generating region by inertial forces to the other regions of flow field. So the tail flow field works in decreasing induced velocities and their corresponding dynamic pressures. This is found in the tail stability and control efficiency curves.

2.3 Vertical Canard Lateral Stability Contributions

In fig. 10 a comparison is shown of single vertical canard surfaces in different positions. It should be noticed, that in all positions the same shape and size was used. The surface above the body nose is seen to diverge without any limit. First the slope in Δc_n up to $\alpha = 10^\circ$ is due to increasing aspect ratio with α , then a reduction is due to the suction field produced by wing and body-nose vortices up to $\alpha = 28^\circ$ and after that, with bursting wing-vortices but full dynamic pressure due to body-nose vortices, further divergence takes place. The side force shows the usual "canard effect", which means that the larger aft surface (vert. tail) compensates the flow field curvature produced by the smaller forward canard. Thus due to the momentum conservation law the side force vanishes until the tail surface is sufficiently swept out of the canard influence.

The surfaces mounted below the body show decreasing sideforce and yawing moment increments with increasing angle of incidence. This shows, analog to sheared wing concept, a decreasing aspect ratio of this vertical canards. Additional to this effect an increasing high pressure field ("stagnation point flow analogy") influence the vertical canard root section.

The surface mounted near an intake position below the wing strake shows in the yawing moment the influence of distance from moment reference point as well as the straightening influence of the wing.

In fig. 11 similar effects for the double surfaces are shown. In contrary to the single surface, the double surface above the body was mounted in the wing-strake apex region. Hence it shows the severe influence of the strake vortices.

In fig. 12 a comparison with the single surface at the same position does not show twice the sideforce and yawing moment as we would expect from the fact that two surfaces were used. But remembering the laws of biplanes it is clear that a relatively close second parallel-surface in the curved flow field of the first one will not develop the same force. Furthermore we note that the first breaks in the curves correspond to $\alpha_{c_{Lmax}}$ of the outboard wing panel.

2.4 Vertical Canard Control Efficiency

In fig. 13 a comparison of single vertical canards in different positions, but with same size and deflection is shown. The results are basically similar to the stability considerations, but are smaller in absolute value. This is due to the fact, that for stability considerations the complete configuration was in a yawing position, whereas here the vertical canard only is deflected.

The comparison of the double control surfaces in fig. 14 again shows similar effects compared with the above mentioned stability considerations. It should be mentioned that for stability, the increments were taken against clean configuration (vertical canards off) whereas for control efficiency increments were taken against symmetric position.

The comparison of double surfaces with single surface in fig. 15 shows a steeper loss of efficiency. The wiggles, shown by all the increment curves, should not be taken too serious because one canard surface was about 5% wing reference area. That means increments are differences of nearly equal numbers with respect to the balance accuracy, thus posing a numerically "ill conditioned" problem.

2.5 Influence of Vertical Canards on Horizontal Stability

At the first glance, the pitching moment curves in fig. 16 are a surprising result. But this strong influence of double vertical canard surfaces on longitudinal stability can be explained with the high pressure field between the nearly parallel canard surfaces mentioned above in the flow field considerations. This is clarified by comparing the increments for single vertical canard surfaces with those of double surfaces as shown in fig. 17 and fig. 18.

3. CONCLUDING REMARKS

- Looking at fig. 19 we find a nearly linear dependence of yawing moment increment up to $\alpha_{c_{Lmax}}$ for nearly all positions.

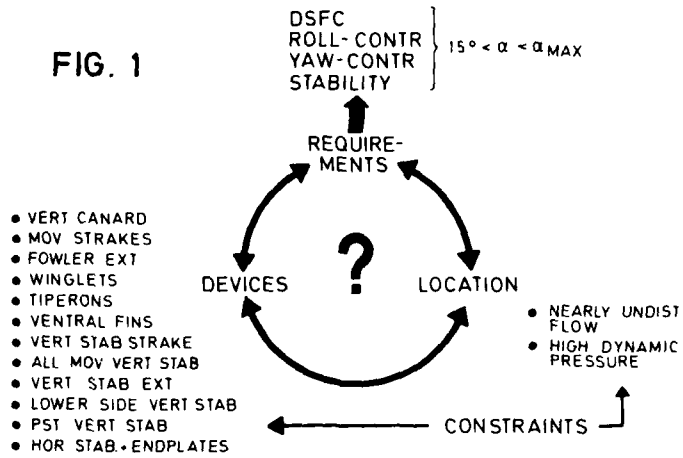
$$\Delta c_n(\alpha) = \Delta c_n(\alpha = 0) \left\{ \frac{\alpha_{c_{Lmax}} - \alpha + \alpha_{IND}}{\alpha_{c_{Lmax}}} \right\}$$

The positional influence is mainly accounted for in the $\Delta c_n(\alpha = 0)$ term. In α_{IND} (induction term) and $\alpha_{c_{Lmax}}$ configurational influences like wing shape, position, flap setting, horizontal canards may be accounted for. A comparison with literature and later experiments on other configurations show that such a relation holds for all vertical canards mounted under the body.

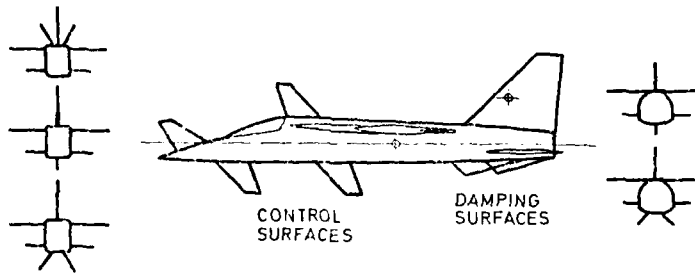
- A similar relation may be constructed for the side force increment dependence, but only up to $\alpha_{c_{Lmax}}$ of the outboard wing. Later on it is nearly constant. This α_{max} of the outboard wing which may be interpreted as an α_{BREAK} for the vortex circulation seems to be an universal feature found for several very different configurations.

17-5

FIG. 1

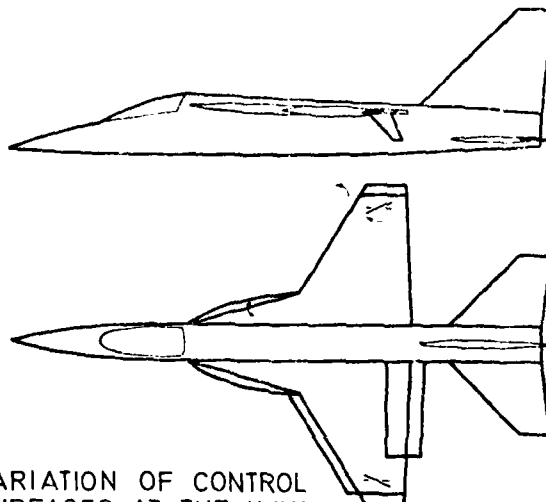


INVESTIGATIONS ON LATERAL STABILITY AND CONTROL AT HIGHER ANGLES OF INCIDENCE



VARIATION OF CONTROL AND DAMPING SURFACES AT THE BODY

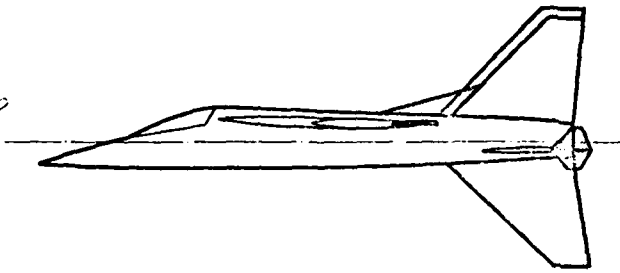
FIG. 2



VARIATION OF CONTROL SURFACES AT THE WING

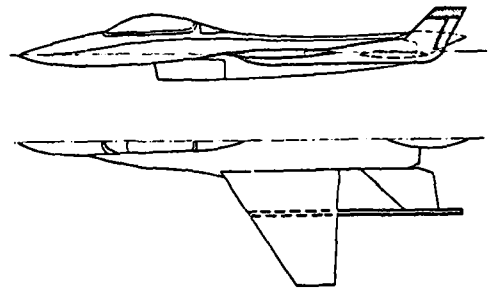
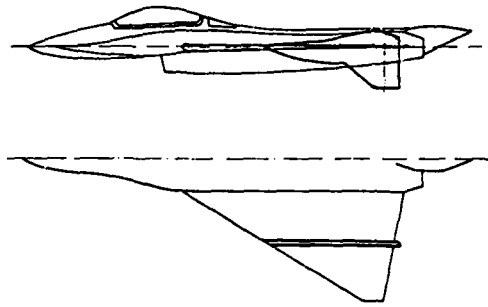
FIG. 3

17-6



TAIL MODIFICATIONS

FIG. 4



POSTSTALL-VERTICAL TAIL

FIG. 5

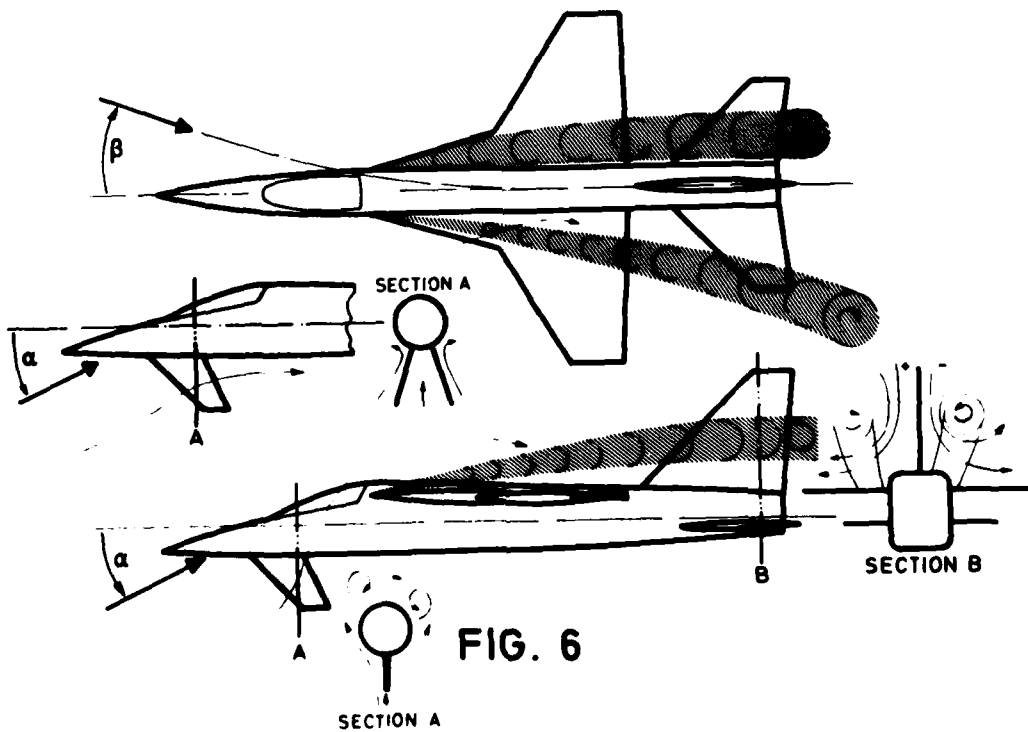
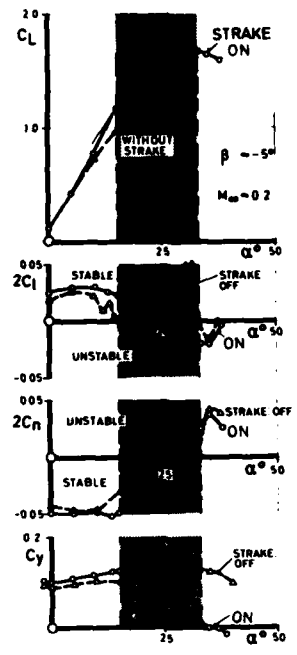


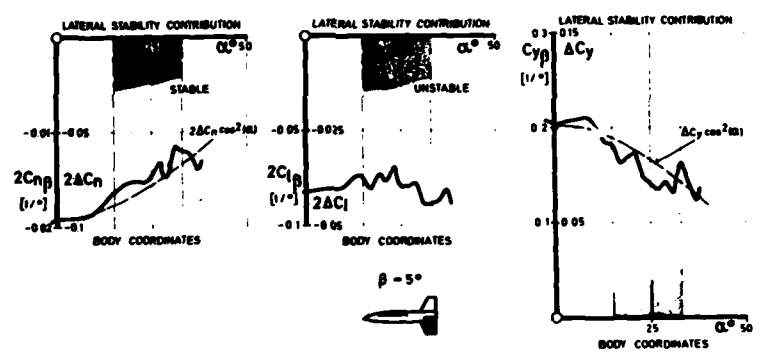
FIG. 6

17-7



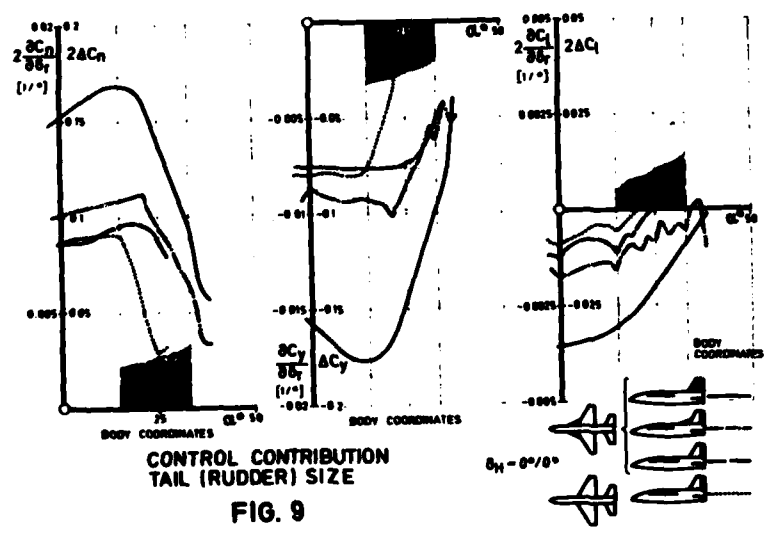
CORRELATION OF LIFT AND DIRECTIONAL STABILITY

FIG. 7



STABILITY CONTRIBUTION TAIL MODIFICATION

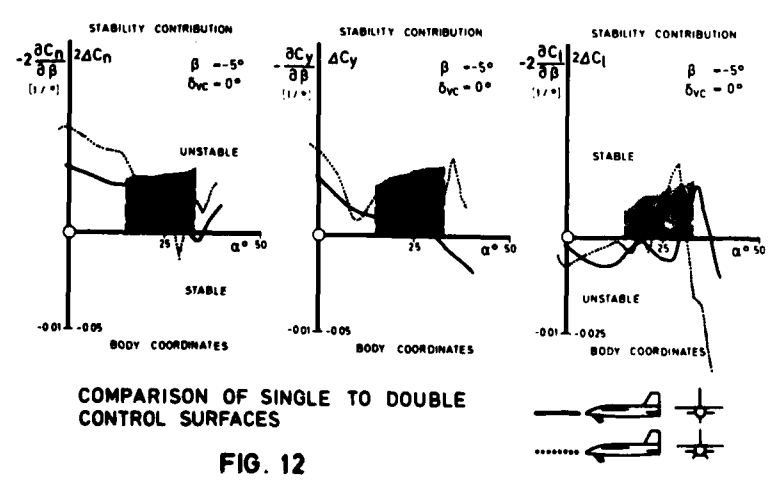
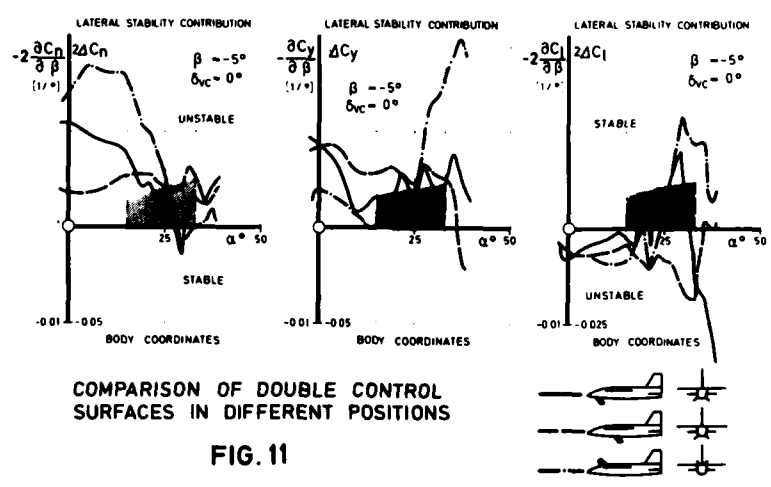
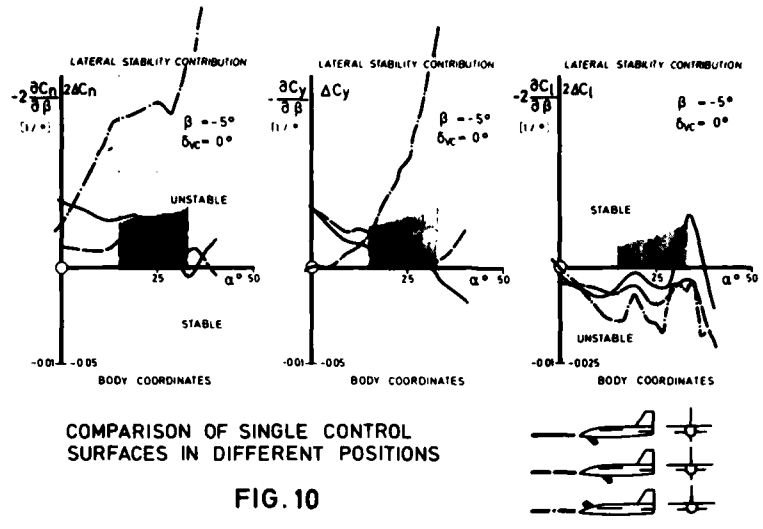
FIG. 8



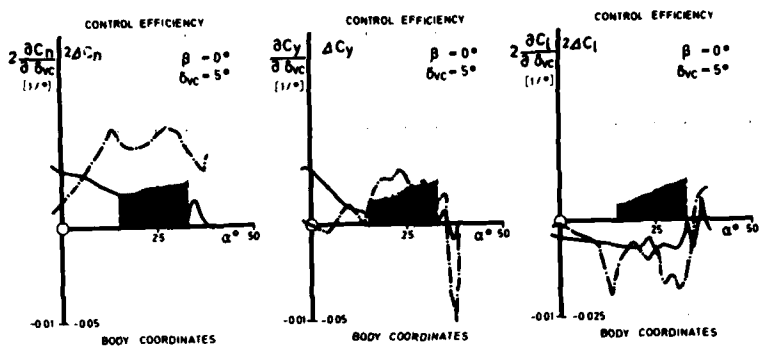
CONTROL CONTRIBUTION TAIL (RUDDER) SIZE

FIG. 9

17-8



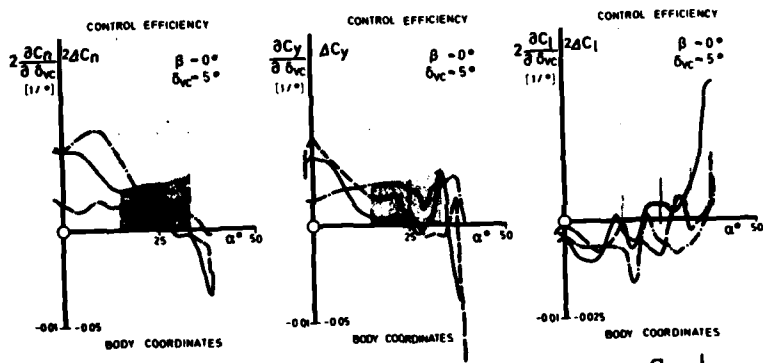
17-9



COMPARISON OF SINGLE CONTROL SURFACES IN DIFFERENT POSITIONS



FIG. 13



COMPARISON OF DOUBLE CONTROL SURFACES IN DIFFERENT POSITIONS

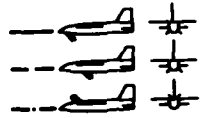
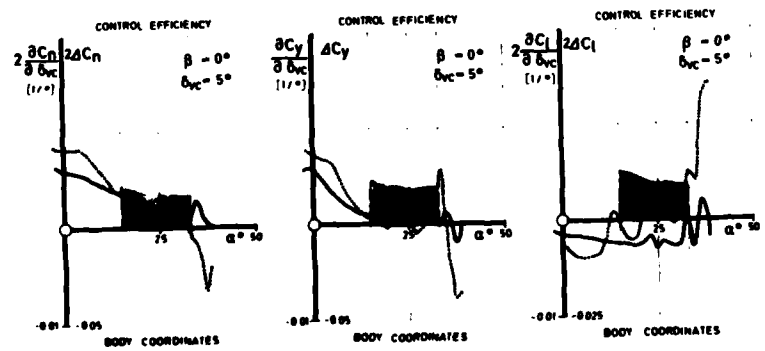


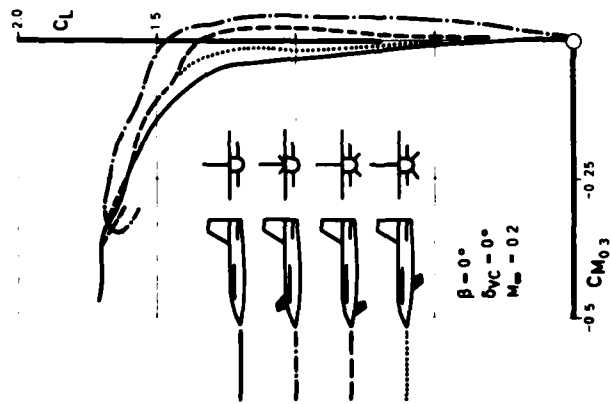
FIG. 14



COMPARISON OF SINGLE TO DOUBLE CONTROL SURFACES

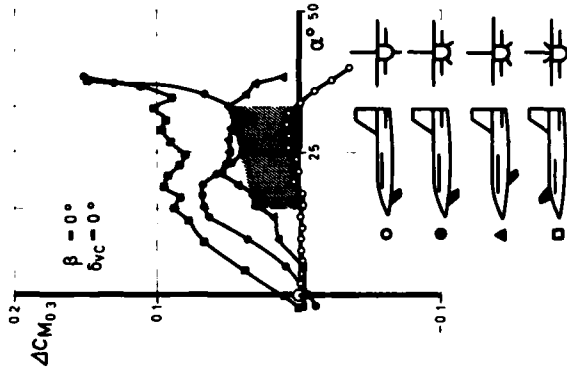


FIG. 15



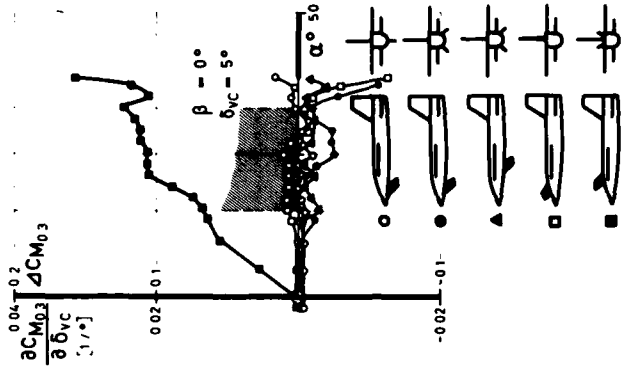
INFLUENCE OF VERTICAL CANARD POSITION ON LONGITUDINAL STABILITY

FIG. 16



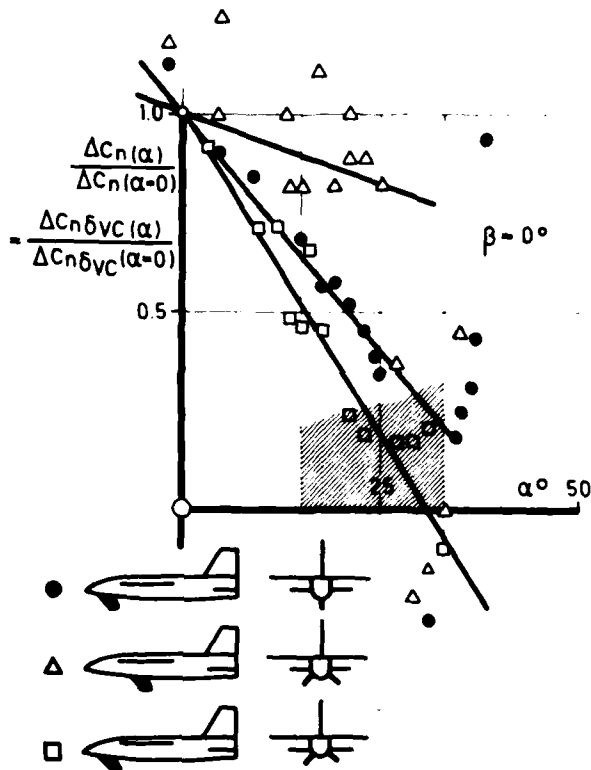
CHANGE OF LONGITUDINAL STABILITY WITH INCIDENCE

FIG. 17



CHANGE OF LONGITUDINAL STABILITY WITH CONTROL DEFLECTION

FIG. 18



$$\Delta C_n(\alpha) = \Delta C_n(\alpha=0) \cdot \frac{\alpha C_{L_{max}} - (\alpha + \alpha_{ind}) \cdot C_{L_{max}}}{\alpha C_{L_{max}}}$$

INFLUENCE OF VERTICAL CANARD POSITION ON α -DEPENDANCE

FIG. 19

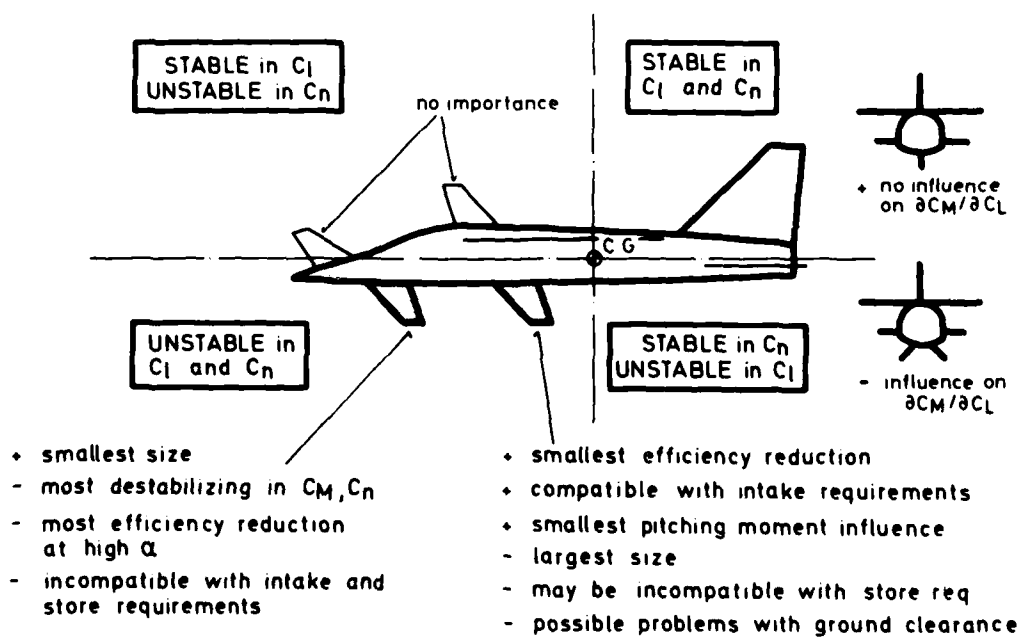


FIG. 20 INVESTIGATION OF STABILITY AND CONTROL OF VERTICAL CANARDS

PROBLEMES D'AERODYNAMIQUE INSTATIONNAIRE POSES PAR
L'UTILISATION DES GOUVERNES DANS LE CONTROLE ACTIF

par Roger DESTUYNDER

Office National d'Etudes et de Recherches Aéropatiales (ONERA)
92320 Châtillon (France)

RESUME

Le développement des techniques de contrôle actif à l'aide de gouvernes, de spoilers ou de surfaces auxiliaires nécessite une connaissance de plus en plus approfondie des forces aérodynamiques instationnaires créées par ces surfaces.

Différents cas se présentent selon les phénomènes que l'on veut contrôler. De plus la nature de l'écoulement subcritique ou supercritique permet soit d'aborder le problème du contrôle par une voie purement théorique ou au contraire nécessite une méthode s'appuyant sur des valeurs théoriques corrigées par des essais. Des surfaces spéciales de contrôle sont aussi considérées qui permettent des simplifications théoriques dans certains cas (Canard-Vane). Les questions de marge de sécurité sont évoquées.

PROBLEMS OF UNSTEADY AERODYNAMICS RAISED
BY THE USE OF CONTROL SURFACES AS ACTIVE CONTROLS

SUMMARY

The development of active control techniques using conventional surfaces, spoilers or auxiliary surfaces requires an ever deeper knowledge of the unsteady aerodynamic forces created by these surfaces. The manoeuvre load control for military aircraft or the lift control for civil aircraft, involve control laws acting in quasi steady conditions. Another field concerning turbulence, gust control and flutter phenomenon calls upon a broader frequency range and the pertaining control problems have to take complex forces into account. Subcritical and supercritical flows are considered. Theoretical and mixed methods based on corrections defined after wind tunnel tests are applied.

INTRODUCTION

Un avion équipé de contrôles actifs est un appareil qui utilise les forces et moments aérodynamiques, créés par ses surfaces de contrôle et mis en mouvement par des vérins hydrauliques. Ces instructions sont fournies par des capteurs à travers une loi de contrôle, dans le but de modifier la distribution des forces aérodynamiques agissant sur la structure.

Trois facteurs interviennent dans tout contrôle actif :

- a) Le choix des surfaces de contrôle (aileron, élévon, canard, spoilers, volet etc...) et les forces aérodynamiques qu'elles peuvent créer.
- b) Le choix du ou des capteurs de détection du mouvement ou des efforts à contrôler (gyroscope, gyromètre, accéléromètre, girouette, strain-gauges etc...).
- c) La détermination de la loi de contrôle que l'on veut faire intervenir.

En parallèle avec ces différents termes deux grandes catégories de contrôle généralisé peuvent être distinguées :

- A - Les contrôles correspondant à des évolutions lentes des paramètres et pouvant être traités à partir de théories aérodynamiques stationnaires ou quasi-stationnaires. Les forces et les moments créés par les surfaces de contrôle sont en phase avec le mouvement de ces surfaces. Tel est le cas des problèmes de stabilité longitudinale négative, de contrôle de portance par réduction des charges etc...
- B - Les contrôles exigeant une connaissance des forces aérodynamiques instationnaires qui interviennent dans les problèmes de turbulence ou de rafales ainsi que dans le contrôle du flottement. Dans ce dernier cas les fréquences à contrôler impliquent non seulement les modes d'ensemble de l'avion, mais encore les modes de déformations de la structure dont la gamme de fréquence utile peut être étendue.

Dans la suite de ce papier nous ne nous intéresserons qu'aux phénomènes instationnaires qui peuvent toutefois dans certains cas être traités avec des forces quasi-stationnaires. Deux classes de problèmes sont à considérer suivant que le régime de l'écoulement sur les profils est du type subcritique ou supercritique. Les différentes théories modernes permettent dans le domaine subcritique de faire des prévisions raisonnables, compte-tenu de l'épaisseur du profil et des effets de couche limite. Dans le domaine supercritique en présence de choc et de décollement il n'existe actuellement que quelques approches qui permettent de donner une solution au problème.

I - SURFACE DE CONTROLE EN ECOULEMENT SUBCRITIQUE

Dans le domaine subcritique, pour des profils minces avec gouverne totale ou partielle et avec ou sans flèche de bord d'attaque on peut estimer que les calculs développés actuellement par les méthodes de doublets ou de l'écoulement inverse donnent une bonne approximation.

Les travaux de Tijdeman au N.L.R. (réf. 1) sur aile bidimensionnelle avec profil NACA 64 A 006, à faible incidence, montrent une bonne concordance entre théorie et essais en ce qui concerne la distribution des coefficients de pression complexe induits par l'oscillation harmonique d'une gouverne de profondeur relative $T = 25\%$.

La comparaison est valable jusqu'à $M = 0,80$ c'est à dire tant que l'écoulement reste subcritique.

Les fréquences réduites considérées, de $\omega_R = 0,25$ à $M = 0,80$, correspondent en ordre de grandeur aux fréquences réduites utilisées pour les premiers modes des avions civils modernes.

D'autre part la continuité entre la distribution quasi-stationnaire et instationnaire est bonne (figure 1, 2 et 3).

Dès que le profil devient localement supercritique la comparaison est mauvaise et se dégrade très vite avec le nombre de Mach. Les perturbations dues à l'oscillation de la gouverne ne remontent pratiquement pas par la couche limite à travers le choc (figure 4).

Dans un travail récent Lambourne (réf. 2) a étudié les termes globaux instationnaires dus à la rotation d'une gouverne partielle sur une aile mince à forte flèche (figure 5, figure 6).

Les comparaisons ont été faites avec la théorie linéarisée de Davies jusqu'à $M = 0,92$.

A - Quelques remarques ressortent de ces comparaisons :

a) Tout d'abord les parties imaginaires des coefficients de portance et de moment sont faibles, les déphasages des coefficients de portance ou de moment induit par rapport au mouvement d'oscillation restent de l'ordre de quelques degrés. Ceci peut être observé dans les résultats de calcul et d'essais de $M = 0,60$ à $M = 0,92$. (La fréquence réduite de $\omega_R = 0,13$ correspond à des fréquences avions de 7 Hz pour une corde moyenne de référence de 2 m à $M = 0,92$, ce qui est conforme aux ordres de grandeur attendus sur avion).

b) La théorie linéarisée prévoit correctement la position du foyer secondaire (c'est à dire le foyer de la partie de la portance en phase avec le mouvement).

Cette remarque est très générale et a été observée dans un grand nombre de cas pour différents types d'aile en flèche, d'ailerons ou de nombre de Mach.

Ceci est sans doute dû au fait que la concentration des termes portant dus au braquage de gouverne est toujours localisée au voisinage de la charnière qui représente la plus grande partie de la contribution à la portance induite (figures 7 et 8).

La discontinuité de pression au niveau de la charnière se produit pratiquement sans déphasage.

c) La théorie surestime, pour des profils minces les termes de portance d'autant plus que le nombre de Mach est plus élevé.

Il en résulte que les lois de contrôle basées sur des forces théoriques induites sur l'aile par la rotation d'une gouverne surestiment de plus en plus avec le nombre de Mach, l'action du contrôle ce qui peut être dangereux. Il en est de même du moment de charnière instationnaire.

Toutefois les valeurs expérimentales montrent que la correction à apporter aux valeurs théoriques se traduit essentiellement par une diminution du gain réel global incorporé dans la boucle de contrôle, ce qui peut être inclus dans les marges de sécurité à donner au gain du contrôle.

Certains auteurs (réf. 1 et 3) ont tenté de réduire ces écarts en incorporant les effets d'épaisseur et de couche limite dans les équations tout en gardant un schéma linéaire.

Les deux effets vont en sens contraire. Si l'on compare avec les résultats du profil mince, l'adjonction de l'épaisseur augmente les pressions en amont de l'axe de rotation de la gouverne tandis que les pressions sur l'aileron lui-même sont très peu modifiées ; l'adjonction de la couche limite à un effet très significatif qui compense et bien au-delà la contribution de l'épaisseur. Enfin si les valeurs expérimentales sont corrigées de l'effet de paroi dû à la soufflerie on peut considérer que les calculs fournissent correctement les champs de pression induits par les gouvernes en écoulement subcritique (figures 9 et 10).

Dans la référence 3 (figure 9) on fait intervenir la vitesse locale u sur le profil, calculée par une méthode de transformation conforme classique. Pour passer aux pressions sur le profil, le champ de pression de la plaque mince est ensuite simplement multiplié par le rapport des carrés des vitesses des deux cas, soit $\left(\frac{u}{V_{\infty}}\right)^2$

La couche limite est schématisée à partir d'une hypothèse sur la forme du profil des vitesses dans cette couche limite. Cette loi est de la forme $\frac{U}{U_0} = \left(\frac{y}{\delta}\right)^n$ avec U_0 vitesse du fluide à une distance δ du profil et V_0 vitesse limite à la distance δ du profil ; n est un coefficient de forme qui a été déterminé de façon semi-empirique et à une valeur égale à $n = 9$.

B - Influence des paramètres d'incidence statique de l'aile ou de la gouverne sur les pressions instationnaires.

Jusqu'à des nombres de Mach $M = 0,80$ et pour des incidences de gouverne jusqu'à 3° , malgré la différence de vitesse locale sur l'intrados et l'extrados il n'y a pas ou peu de répercussion sur les pressions instationnaires à l'intrados ou à l'extrados.

Par contre dès qu'un régime supercritique apparaît sur l'une des surfaces la différence devient très importante et on retrouve deux types de distribution : l'une (côté supercritique qui est liée au nombre de Mach local $M > 1$), l'autre qui se comporte comme un écoulement subsonique. Il est intéressant de noter le peu d'interaction qui existe entre intrados et extrados lorsque l'une des surfaces est supercritique (figure 11).

La même observation avait été faite dans un cas très différent où l'on voulait juger de l'interaction stationnaire et instationnaire entre un réacteur remonté sur un pylône et une aile (réf. 4, figures 12, 13).

A partir d'un certain nombre de Mach la présence du réacteur rend localement l'intrados de l'aile supercritique tandis qu'aucune influence n'est visible à l'extrados. Tout se passe comme si le terme de circulation n'était pas modifié à l'extrados et cela même lorsqu'une grande partie de l'intrados devient supersonique.

II - PROFIL AVEC ECOULEMENT SUPERCRITIQUE

Les différences entre la théorie linéaire et l'expérience deviennent très importantes sur tous les termes (portance ou moment) mais alors que pour des profils minces les valeurs calculées étaient surestimées, ces dernières sont maintenant sous-estimées. En écoulement incompressible bidimensionnel stationnaire, la référence 5 donne un exemple de correction de l'effet d'épaisseur et de la couche limite (figure 14).

Les "corrections" à introduire sont de l'ordre de 50 % sur la portance, la part principale étant due à la correction d'épaisseur du profil. Correction due au très fort gradient de distribution de vitesse sur le profil.

Une approche en bidimensionnel instationnaire transsonique est aussi présentée dans la référence 6.

La comparaison, à $M = 0,854$ et $\omega_R = 0,358$ faite sur le profil NACA 64 A 006, avec la théorie de Magnus-Yoshihara (réf. 7) est excellente aussi bien sur la position du choc que sur les valeurs absolues des coefficients de pression ou sur la phase (figure 15).

Afin de valider les nouvelles théories en écoulement supercritique, différents types d'essai se sont développés.

Les uns portent sur la mesure locale des pressions instationnaires sur aile supercritique en bi ou tridimensionnel, d'autres portent sur la mesure globale des forces aérodynamiques créées par la rotation d'une gouverne.

Enfin une troisième sorte de tests développable en soufflerie et en vol a vu le jour plus récemment :

Il s'agit de déterminer la fonction de transfert complète entre une entrée constituée par exemple par l'excitation en bruit blanc d'une gouverne et la sortie mesurée par un certain nombre d'accéléromètres ou de ponts de jauges incorporés dans la structure.

Nous donnerons un exemple relatif à ce dernier cas pour montrer la complexité du problème. L'essai a été fait en soufflerie à basse vitesse sur une aile droite équipée d'une gouverne (figure 16). La bande de fréquence couverte par le bruit blanc était de 0 à 150 Hz, dans cette bande de fréquence 5 fréquences étaient remarquables. Le niveau du bruit blanc sur la gouverne était suffisamment grand pour que l'on puisse être assuré d'avoir affaire à un système ne comportant qu'une entrée et une sortie. Autrement dit la turbulence de la soufflerie était négligeable dans son action sur l'aile ou la gouverne.

La fonction de transfert $H(i\omega)$ mesurée en boucle ouverte est comparée à la fonction de transfert calculée au même point de l'aile. $H(i\omega)$ est ensuite mis sous forme d'une fraction rationnelle (réf. 8) qui est décomposée en éléments simples, ce qui permet très simplement de séparer les pôles et les résidus des différents modes.

Cette méthode fournit avec précision les valeurs complexes des pôles qui sont en bon accord avec les racines de l'équation générale de l'aérodynamique instationnaire du système :

$$Z(i\omega).q = Q$$

où $Z = -\omega^2 \mu + \varphi + \rho v^2 (A + iB)$ dans la représentation modales.

μ est la matrice diagonale des masses généralisées
 φ est la matrice diagonale des rigidités généralisées
 A et B sont les matrices des coefficients aérodynamiques
 q est la matrice colonne des coordonnées généralisées
 Q représente une excitation sinusoïdale quelconque

Le système est tronqué dans la base des modes propres et est représenté par 5 modes.

On peut noter que dans cette méthode la connaissance des pôles de $H(i\omega)$ suffit pour traduire l'action globale des forces aérodynamiques instationnaires (en supposant connus les modes propres de la structure).

Il n'en est pas de même si l'on veut remonter à chacun des termes de la matrice aérodynamique. Une connaissance complète de la fonction de transfert est nécessaire en autant de points que le nombre de modes dans lequel le système aura été discrétisé, c'est à dire qu'il faudra connaître chacun des résidus complexes de $H(i\omega)$. L'identification qui a été tentée sur la figure 16 a montré des différences de l'ordre de 30 à 40 % sur certains termes aérodynamiques malgré une bonne approximation des pôles. Cette méthode ne peut donc être utilisée qu'avec circonspection.

III - APPLICATIONS

Contrôle par une gouverne d'un cas de flottement transsonique sur une aile de similitude dynamique de l'avion F1 montée à la paroi, équipée de trois charges en dessous et en bout de voilure. On a réalisé un cas de flottement par couplage des modes de flexion et de tangage de l'engin externe (réf. 9, figure 17).

Le point de similitude choisi était de $M = 0,80$ pour une altitude en atmosphère standard de 5000 pieds. Le flottement avait été obtenu en lestant convenablement l'engin d'extrémité. La maquette possédait, outre ses modes de déformations s'échelonnant de 20 à 45 Hz, pour les modes concernés par le flottement, un degré de liberté d'ensemble en roulis à une fréquence de 3,8 Hz.

Deux lois de contrôle ont été superposées sur la même gouverne, l'une en quasi stationnaire maintenant l'aile à calage de roulis constant quel que soit le nombre de Mach ou la pression dynamique en agissant sur le braquage statique de la surface de contrôle ; l'autre, travaillant en instationnaire contrôlait le flottement.

La figure 18 indique la comparaison calcul-essais sans contrôle et donne l'évolution des paramètres de fréquence et d'amortissement des modes critiques en fonction de la pression génératrice de la soufflerie. La prédiction est correcte quant à la pression critique. Le contrôle a été réalisé sous la forme d'une réinjection sur l'aile de forces aérodynamiques de rigidité en phase avec le mouvement de l'aile, ce qui a pour but de faire croiser très rapidement les fréquences des modes critiques.

La figure 19 montre l'action de cette loi de contrôle en calcul et en essais à Mach constant $M = 0,80$.

La même tendance à la suppression du flottement est bien observée sur les courbes théoriques et expérimentales, tendance qui autorise un gain très important sur la pression dynamique critique.

Du point de vue du calcul, les forces aérodynamiques instationnaires engendrées par l'aileron sur l'aile ont été déterminées par une méthode mixte. Les valeurs de force et de moment théorique ont été corrigées à partir de la mesure des champs de pression instationnaire induits par une rotation harmonique de la gouverne. Un exemple de la comparaison calcul (méthode des doublets) essais des pressions induites est donné sur la figure 8.

On retrouve en haut subsonique les résultats énoncés dans la référence 2, à savoir : Surestimation par le calcul, pour un profil mince des coefficients aérodynamiques instationnaires induits par la gouverne, foyer secondaire correctement prévu et très faible valeur, pour une aile à forte flèche, des parties imaginaires.

IV - CONTROLE A PARTIR DE SURFACES SPECIALES

a) Canard ou Vane

Il est possible, à partir de surfaces de contrôle de faible encombrement, (tel un empennage canard ou un volet oscillant extérieur à la voilure) de ramener le problème des forces de contrôle instationnaire à un problème de forces réelles quasi-constantes avec la fréquence réduite.

Cette solution a été développée par Rockwell avec les petits empennages canards du B₁ placés sur le fuselage et calés avec un dièdre de 30° (réf. 10, figure 20), l'application étant faite sur un problème de turbulence

Les dimensions de la surface de contrôle et les fréquences des modes de fuselage à contrôler (flexion longitudinale et latérale du fuselage à 3 et 5 Hz) conduisent à des fréquences réduites très faibles de l'ordre de $\omega_R = 0,07$ à $M = 0,70$, ce qui rend les parties imaginaires des forces nulles, la forte flèche de l'ailette (60°) fait que le foyer évolue peu dans une large gamme de nombre de Mach. De même la force et le moment instationnaire recueillis sur l'axe de rotation du "canard" ne dépendent pratiquement pas de la fréquence dans la gamme considérée (0 à 10 Hz). L'identification des forces créées par la rotation de la palette en vraie grandeur se fait très aisément en soufflerie (avec le même nombre de Reynolds qu'en vol) et permet une bonne prévision de l'amortissement que l'on peut réintroduire dans une structure à partir d'un système I.L.A.F. (Identical Location Accelerometer and Force).

La figure 21 donne un exemple de l'efficacité du système sous la forme du spectre de la densité spectrale, le système de contrôle étant ou non engagé. La même idée de créer un contrôle par introduction d'un amortissement créé par une palette a été appliquée à un phénomène de flottement (réf. 11, figure 22).

Ici encore les faibles fréquences réduites de la palette permettent, tenant compte de la fonction de transfert de l'ensemble servo-valve servo-commande, d'introduire une force d'amortissement pure au point où l'amplitude de la vibration à contrôler est mesurée. Cette méthode très simple et très sûre s'adapte bien aux prévisions de calcul du fait du petit nombre de paramètres à introduire dans la loi de contrôle utilisée, figure 23.

Le problème de l'identification des forces aérodynamiques instationnaires peut être résolu une fois pour toute même en haut subsonique étant donné la faible évolution des coefficients et du foyer avec le nombre de Mach. Le profil de la palette reste pratiquement toujours subcritique.

b) Spoiler

Plusieurs études tant théoriques qu'expérimentales ont commencé à se développer concernant l'utilisation des forces aérodynamiques stationnaires ou instationnaires créées par un spoiler en vue du contrôle actif (réf. 12, 13, 14).

Excepté pour un spoiler de très faible envergure relativement à la corde de l'aile celui-ci est toujours déportant. Mais alors que pour un spoiler dont l'axe de rotation serait sur l'extrados du profil et sans fente, le terme $|\Delta C_z|$ croît avec l'angle de braquage, on observe le phénomène inverse pour un spoiler à fente croissante avec le braquage c'est à dire dont l'axe de rotation est situé, à l'intérieur du profil. Les figures 24 et 25 illustrent ces deux cas.

Les tendances liées à quelques paramètres ont pu être dégagées des premières études connues. Ainsi en instationnaire l'efficacité du module de la portance induite par le spoiler décroît très vite avec la fréquence réduite

$$\omega_R = \frac{\omega l}{2v}$$

D'autre part on constate la très forte influence du braquage d'un volet en arrière du spoiler qui permet de multiplier son efficacité par deux ou trois. Il faut aussi noter le très fort déphasage existant entre le mouvement du spoiler et la phase du module de la réponse en portance.

Très rapidement la force de déportance tend à être en quadrature avec le mouvement du spoiler pour de grandes fréquences réduites, le recul du spoiler le long de la corde accroît son efficacité pour un braquage donné d'un volet placé en arrière. L'effet de fente entre spoiler et aile est très important. Pour de petits angles de braquage statique (8°) la fente reste faible et noyée dans la couche limite, le bord d'attaque du spoiler crêt (comme pour une gouverne) une discontinuité de pression en phase avec le mouvement du spoiler (figure 26). Pour un angle plus grand (17°), donc une fente plus grande (cas d'un axe de rotation dans le profil), la nature de l'écoulement est changée au droit du bord d'attaque du spoiler. Une circulation est introduite entre spoiler et aile et la condition de décollement théorique en arrière du spoiler n'est plus respectée. Le phénomène est très comparable à celui qui existe avec une gouverne pour laquelle on ferait varier la fente avec l'aile. Enfin une dernière propriété remarquable apparaît dans les calculs : l'efficacité maximum de déportance en fonction de l'envergure du spoiler est très vite atteinte dès que cette envergure représente 30 ou 40 % de la profondeur de la corde. Les résultats théoriques de la figure 27 correspondent à un écoulement incompressible.

La figure 28 montre la distribution en envergure des coefficients de pression instationnaire pour quelques pourcentages en corde. On note un effet de plateau au droit du spoiler puis une chute brutale de part et d'autre. En conclusion il semble difficile d'utiliser un ou des spoilers à grand nombre de Mach en instationnaire pour des fréquences élevées (flottement par exemple). La perte d'efficacité avec la fréquence réduite rendrait tout contrôle inopérant. Par contre l'usage en réducteur de charge de portance à l'aide de plusieurs spoilers paraît possible, ce qui permet de réduire le moment fléchissant à l'emplanture de l'aile.

V - PENALITES ET MARGE DE SECURITE A INTRODUIRE DANS L'USAGE DES CONTROLES ACTIFS

Dans le cas où les surfaces telles que ailerons, volets, spoilers etc..., sont utilisées pour des contrôles actifs, les débats qui leur sont affectés réduisent d'autant les marges de manoeuvre du pilote. On peut aussi considérer, pour des commandes hydrauliques, la place qu'occupe une loi de contrôle sur le débit maximum de la servo-valve.

Dans des essais récents en soufflerie on a procédé à la superposition d'une loi de contrôle en pilotage en roulis à une loi de contrôle d'un phénomène de flottement sur le même aileron. 3° étaient consacrés à Mach 0,85 au contrôle du roulis (le critère était de maintenir la demi-maquette à incidence de roulis constamment nulle quelque soit le nombre de Mach et la pression dynamique).

Le contrôle du flottement n'exige un débattement que dans la mesure où il existe dans le fluide des perturbations du type turbulence ou rafales (qui donnent naissance aux conditions initiales du phénomène d'instabilité).

En pointe et en valeur instantanée on a relevé un angle de contrôle de $\pm 2^\circ$. Dans ce cas précis la marge de manoeuvre du pilote en transsonique aurait été très faible.

Il faut noter que ce type de restriction n'existe pas avec des surfaces auxiliaires de contrôle actif du type "vane" ou "canards" construit uniquement pour le contrôle. Un autre paramètre à considérer dans l'utilisation des lois de contrôle consiste dans les marges en gain et en phase qu'il faut attribuer au contrôle pour pouvoir considérer qu'il reste fiable. Ce problème très difficile à définir clairement n'est actuellement explicité, dans les "Milspecs" (spécifications militaires américaines) que de façon arbitraire et sans fondement mathématique.

Un exemple emprunté à la littérature américaine montre l'influence que peuvent avoir les tolérances d'usinage et le vieillissement d'une pièce au cours du temps.

Pour une servo-commande moderne les variations dues à ces paramètres ont été les suivantes :

Variations de 16° sur la phase et de 1,3 db sur l'amplitude de la fonction de transfert de la seule servo-commande dues au vieillissement (à la fréquence de 10 Hz).

Variations de 8° sur la phase et de 0,2 db sur l'amplitude dues aux variations de température que subit un avion au cours d'une mission.

Cet exemple montre la nécessité de couvrir les lois de contrôle par de larges facteurs de sécurité tant sur la phase ou le module du contrôle que sur les amplitudes admissibles intervenant dans les contrôles actifs.

Les "Milspecs" demandent, actuellement, pour les lois de contrôle de flottement des marges de + 6 db sur le gain du contrôle et $+ 60^\circ$ sur la phase pour une loi, qui à Mach constant, augmenterait la vitesse de flottement de 30 %. Il semble qu'une étude très poussée sera nécessaire dans un proche avenir pour valider ou infirmer ces marges.

CONCLUSION

De l'ensemble de l'analyse ci-dessus, quelques points saillants ressortent. Des lois de contrôle instationnaires appliquées à des gouvernes existantes peuvent être établies avec une fiabilité raisonnable en ce qui concerne le domaine subcritique, domaine qui s'étendra d'autant plus loin que l'on aura des profils minces ou des profils pour lesquels les corrections d'épaisseur et de couche limite sont passibles de théories linéaires.

Dans le domaine supercritique malgré des premiers résultats encourageants il est encore nécessaire de faire appel le plus souvent à des valeurs expérimentales obtenues au cours d'essai en soufflerie si l'on veut bâtir des lois de contrôle.

Enfin certaines surfaces de contrôle à usage particulier ("Vane" ou "Canard" pour le contrôle en turbulence des modes souples d'une structure) auront sans doute des débouchés dans un avenir proche étant donné les simplifications théoriques qu'elles apportent.

D'autres systèmes, tels les spoilers, demandent des études plus poussées avant de pouvoir être utilisés de façon industrielle.

Enfin il faut constamment garder présente à l'esprit la notion de marge de sécurité à établir dans les lois de contrôle. Pour certains phénomènes comme le contrôle de la turbulence, la stabilité négative ou le flottement, le problème de la marge sur le gain ou la phase du contrôle revêt une importance considérable. Dans le contrôle du flottement, par exemple, ces marges doivent couvrir les variations produites par les non linéarités ou les déphasages aléatoires si l'on ne veut pas courir le risque d'instabilités.

REFERENCES

- [1] - H. Tijdeman
Investigations of the transonic flow around oscillating Airfoils
Thèse N.L.R. Décembre 1977
- [2] - N.C. Lambourne - K.C. Wight - B.L. Welsh
Measurements of Control-Surface Oscillatory Derivatives on a Sweepback, Tapered Model Wing
in Two Transonic Tunnels
R.M. n° 3806 - 1977
- [3] - J.J. Angélini - P.M. Hutin - S. Chopin
Aérodynamique Instationnaire avec Effet de Couche Limite
R.T. 3149 - Juin 1977
- [4] - R. Destuynder
Mesures de pressions instationnaires sur des configurations d'aile équipées de charges
AGARD - Ankara Septembre 1975
T.P. ONERA n° 1975-102

- [5] - F. Bauer - P. Garabedian - D. Korn - A. Jameson
Supercritical Wing Sections - Economics and Math. Systems
n° 108 Springer Verlag Berlin 1975
- [6] - M. Couston - J.J. Angélini
Solution of Nonsteady Two Dimensional Transonic Small Disturbances Potential Flow Equation
ASME San Francisco 10-15 Décembre 1978
- [7] - R. Magnus
Calculations of Some Unsteady Transonic Flows about Airfoils
AGARD CP 226 - April 1977
- [8] - R. Dat - J.L. Meurzec
Exploitation par lissage mathématique des mesures d'admittance d'un système linéaire
La Recherche Aéronautique n° 1972-4
Traduction RAE n° 1703-1973
- [9] - R. Destuynder
Récents progrès sur les contrôles actifs appliqués aux suppresseurs de flottement
15ème colloque d'aérodynamique appliquée
Marseille 7-9 Novembre 1978
- [10] - J.H. Wykes
B₁ Ride Control System Design Development and Test
VKI Short Course - Active Control Technology - Décembre 4-8 1978
- [11] - R. Destuynder
Essai en soufflerie d'un suppresseur de flottement sur une aile droite
AGARD Bruxelles 13-18 Avril 1975
- [12] - J. Thers
Etude en soufflerie d'une tranche d'aile équipée d'un aérofrein animé d'un mouvement oscillant
R.T. 5108 Juin 1974
- [13] - R. Bernier - G.V. Parkinson
Oscillatory aerodynamics and stability derivatives for Airfoil spoiler motion
AGARD CP 235 - 1978
- [14] - K. Jonas - W. Wünnenberg - K.H. Hirstmann
Roll control by digitally controlled segment spoilers
AGARD FDP Aerodynamics characteristics of Controls - Naples May 1979

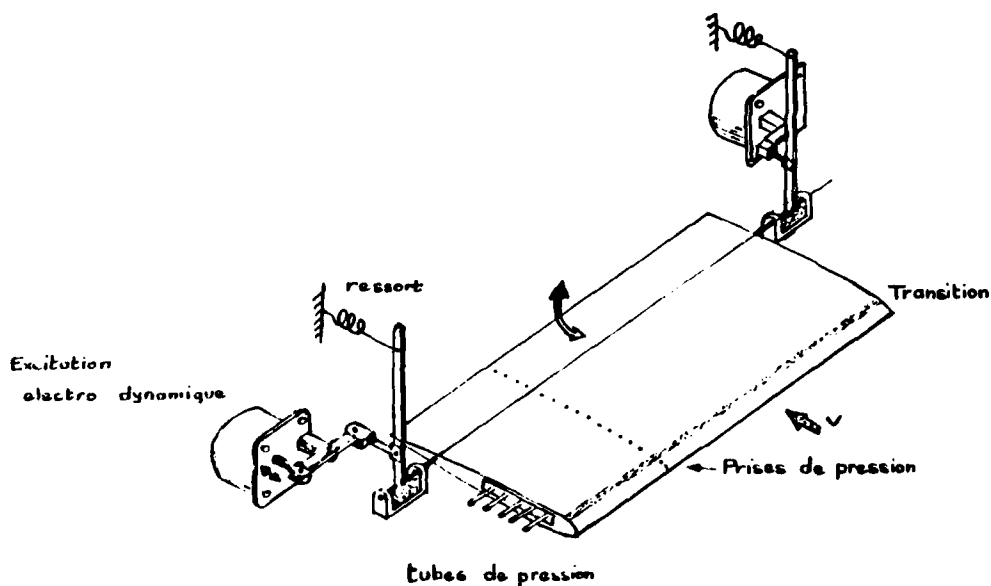


Fig. 1 - Vue schématique du profil bidimensionnel NACA 64A006 en veine. [1]

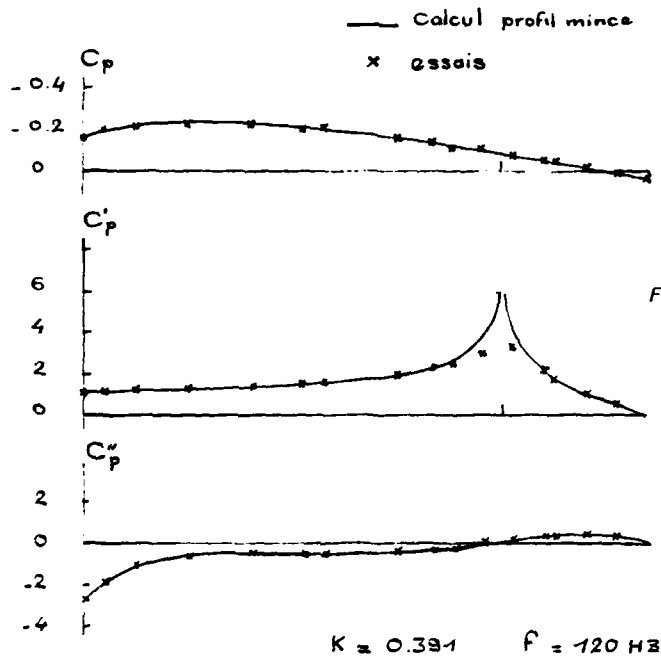
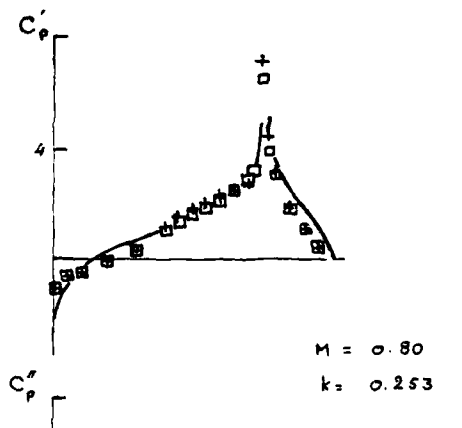


Fig. 2 - Pression stationnaire et instationnaire.
 $M = 0,5$ en régime subcritique [1]

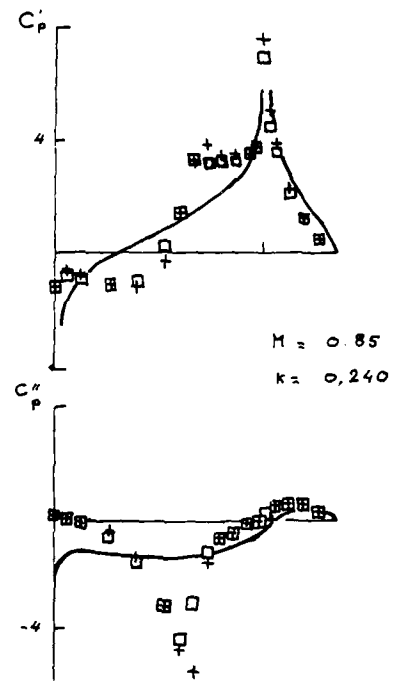


test $\frac{k'd}{k''d} = 1.99 \quad \frac{m'd}{m''d} = 1.48$

theory $\frac{k'd}{k''d} = 2.27 \quad \frac{m'd}{m''d} = 1.09$

NACA 64A006 AIRFOIL
 $\alpha_0 = 0 \quad \xi = 0$
EXP. { + UPPER SURFACE
□ LOWER SURFACE AMPLITUDE 1°
— THIN. AIRFOIL THEORY

Fig. 3 - Aile bidimensionnelle (Tijdeman).



NACA 64A006 AIRFOIL
 $\alpha_0 = 0 \quad \xi = 0$
EXP. { + UPPER SURFACE
□ LOWER SURFACE AMPLITUDE 1°
— THIN. AIRFOIL THEORY

Fig. 4 - Aile bidimensionnelle (Tijdeman).

	Expérience	Théorie	Mach	ωR
$\varphi = \text{arc tg } \frac{h'd}{h''d}$	1,4°	0,4°	0.60	0.20
$\text{arc tg } \frac{h'd}{h''d}$	5,2°	3,3°	0.92	0.13
$\text{arc tg } \frac{m'd}{m''d}$	1°	3,7°	0.60	0.20
$\text{arc tg } \frac{m'd}{m''d}$	2,4°	3,4°	0.92	0.13
$\frac{X}{C} = \frac{m'd}{h'd}$	0,809	0,804	0.60	0.20
	0,901	0,920	0.92	0.13

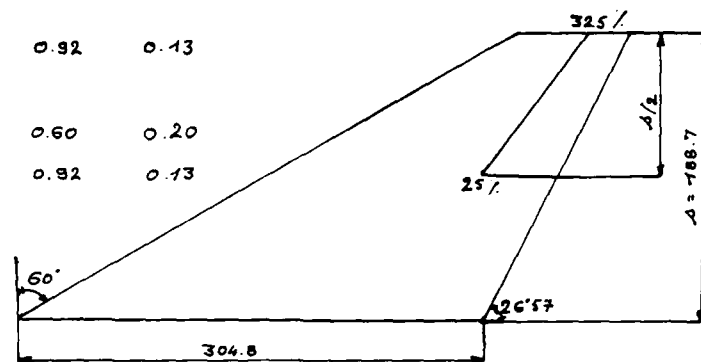


Fig. 5 — Influence des parties imaginaires sur les termes de portance et de moment. [2]

	M = 0.6		M = 0.927	
	EXPERIENCE $\omega_R = 0.205$	THEORIE $\omega_R = 0.207$	EXPERIENCE $\omega_R = 0.135$	THEORIE $\omega_R = 0.140$
$-\bar{Z}_\beta$	0.240 ± 0.003	0.276	0.193 ± 0.003	0.300
$-\bar{Z}_\beta$	-0.013 ± 0.007	0.005	-0.058 ± 0.006	-0.164
$ \bar{Z}_\beta $	0.210 ± 0.003	0.276	0.194 ± 0.003	0.304
ϕ_β (deg)	-1.4 ± 0.8	0.4	-5.2 ± 0.8	-9.3
m_β	0.170 ± 0.003	0.222	0.174 ± 0.003	0.276
m_β	0.007 ± 0.006	0.036	-0.024 ± 0.006	-0.063
$ \bar{m}_\beta $	0.170 ± 0.003	0.222	0.174 ± 0.003	0.276
ϕ_m (deg)	1.0 ± 0.8	3.7	-2.4 ± 0.8	-3.9
$-b_\beta$	0.065 ± 0.001	—	0.061 ± 0.001	—
$-b_\beta$	0.005 ± 0.002	—	-0.010 ± 0.002	—
$ \bar{b}_\beta $	0.065 ± 0.001	—	0.061 ± 0.001	—
ϕ_b (deg)	1.8 ± 0.8	—	-2.8 ± 0.8	—
h_β	0.152 ± 0.004	0.271	0.103 ± 0.002	0.358
h_β	0.126 ± 0.005	0.170	0.200 ± 0.009	0.294
$ \bar{h}_\beta $	0.161 ± 0.004	0.280	0.119 ± 0.002	0.368
ϕ_h (deg)	18.2 ± 0.8	14.1	30.2 ± 0.8	13.4

Fig. 6 — Tableau de comparaison calcul essais des coefficients de portance et de moments dus à une rotation de gouverne. [2]

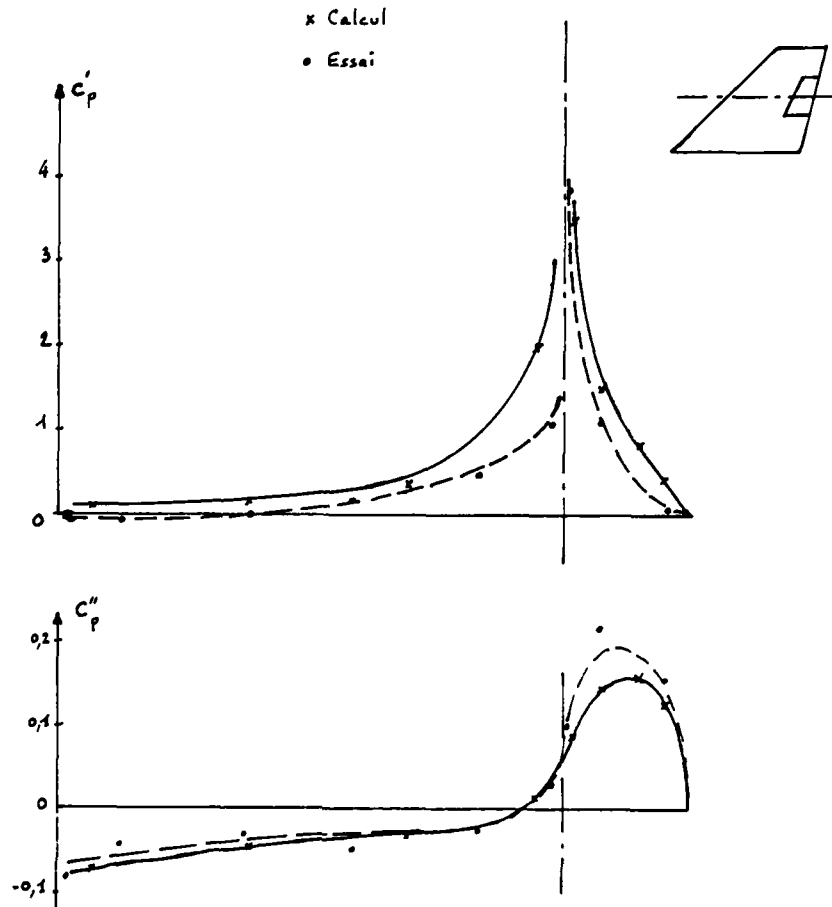


Fig. 7 - Répartition de pression instationnaire. Tranche de gouverne. Aile F1.
 $M = 0,8$ $\omega_R = 0,185$

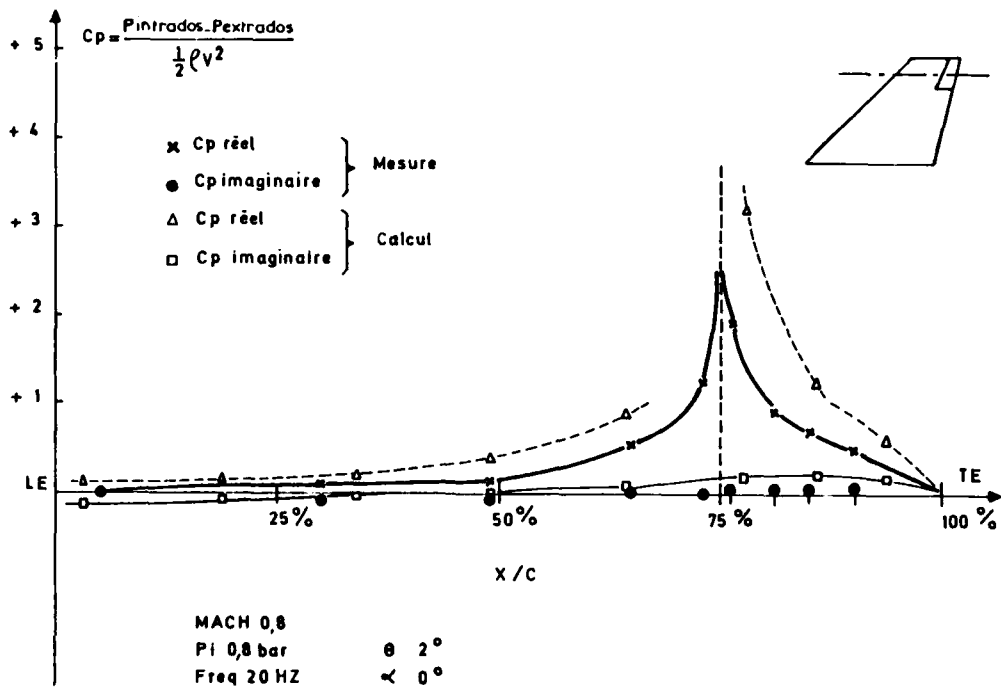


Fig. 8 - Distribution de C_p le long de la corde médiane de l'aileron.

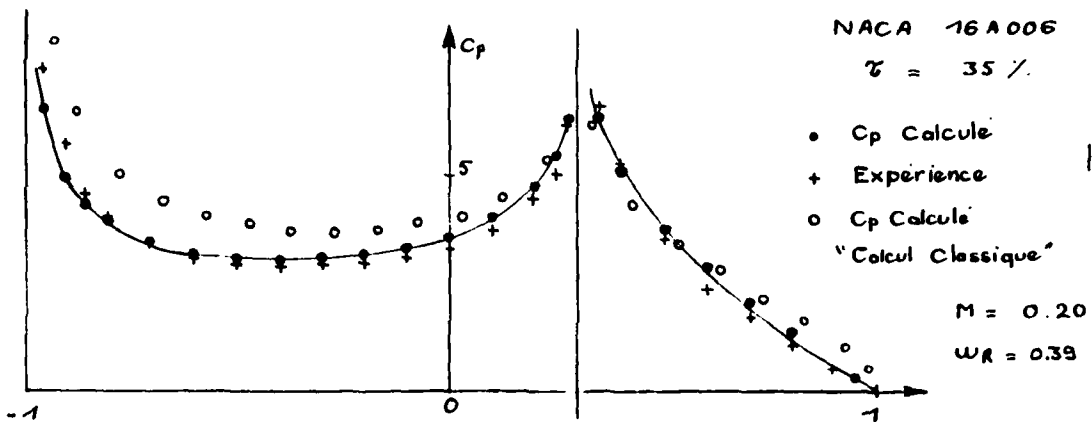


Fig. 9 - Comparaison calcul (couche limite + profil épais) expérience en bidimensionnel. [3]

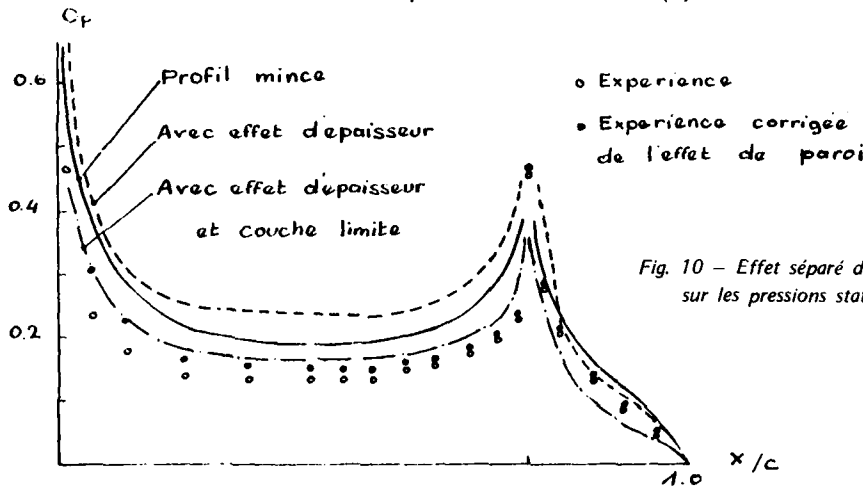


Fig. 10 - Effet séparé de l'épaisseur et de la couche limite sur les pressions stationnaires en subsonique. [1]

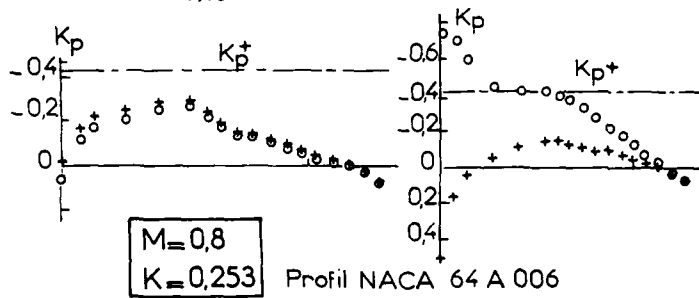
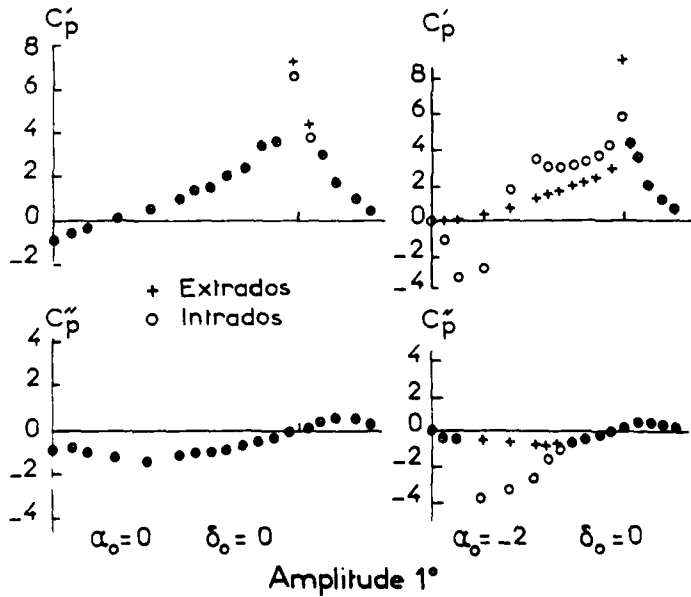


Fig. 11 - Comparaison intrados extrados avec et sans choc. [1]



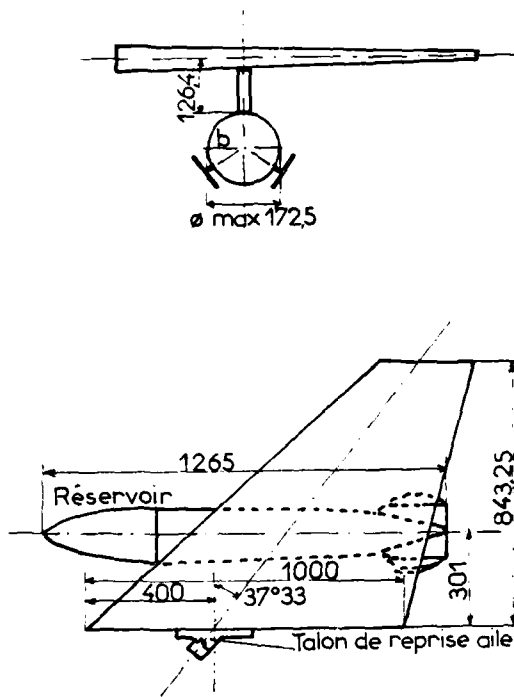
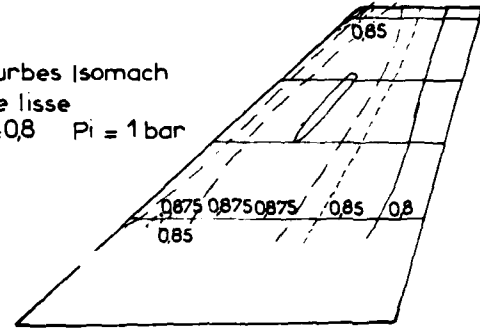


Fig. 12 - Interaction réservoir aile à Mach 0,8. [4]

Courbes Isomach
Aile lisse
 $M=0,8 \quad P_i = 1 \text{ bar}$



Courbes Isomach
Aile + réservoir
 $M=0,8 \quad P_i = 1 \text{ bar}$

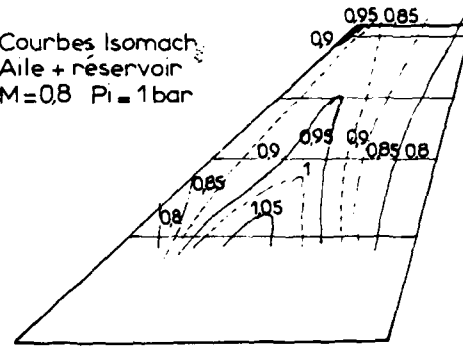


Fig. 13 - Influence du réservoir sur le champ de Mach local $M = 0,8$. [4]

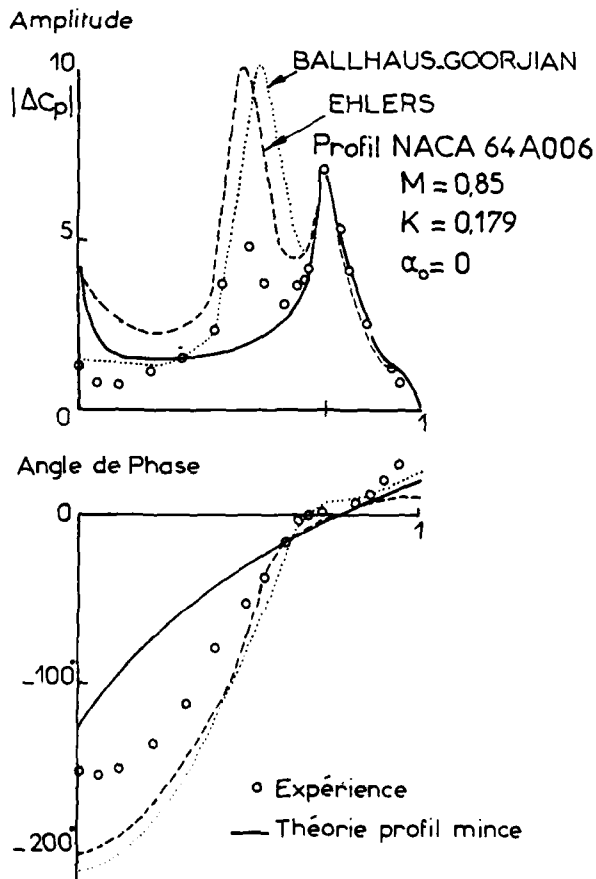


Fig. 14 - Comparaison calculs essais des distributions de pressions instantanées en régime supercritique. [1]

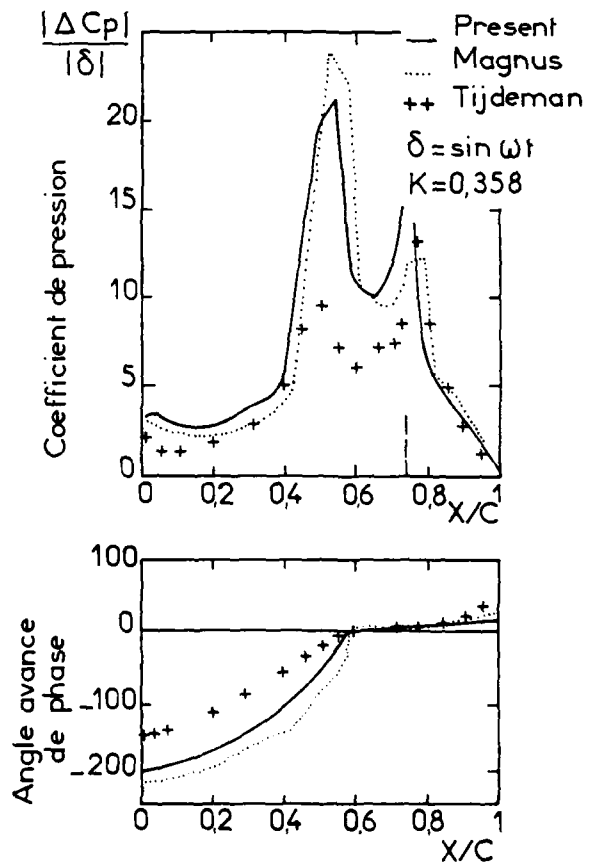
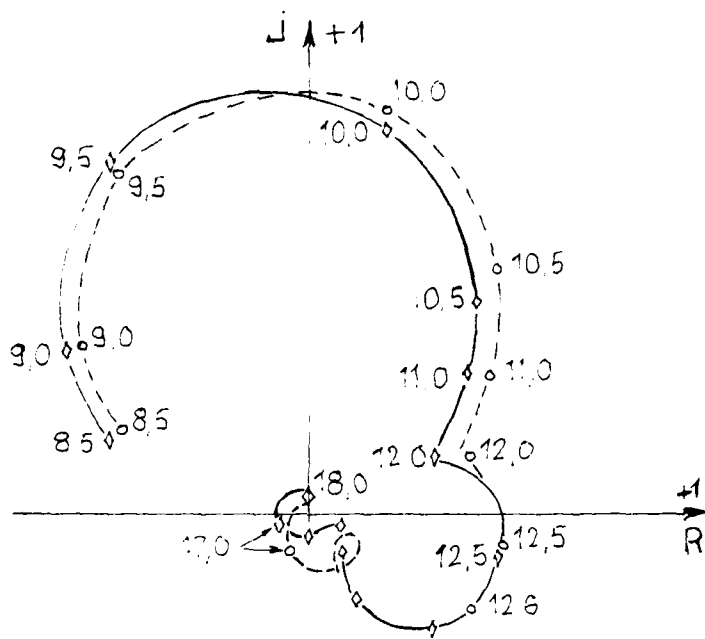


Fig. 15 - Distribution de pression instantanée sur le profil NACA 64A006 à Mach 0,854 en régime supercritique. [6]



Poles	Essais
$\xi = 9.68$	$\alpha = 60^\circ$
12.60	85%
17.90	35%

Calculs	
$\xi = 9.72$	$\alpha = 63^\circ$
12.53	75%
17.24	32%

○ ---- calcul
 ◇ ——— essai

Fig. 16 - Comparaison fonction de transfert calcul - essai $V = 65$ m/s sans loi de contrôle.

Fig. 17 - Maquette avec mouvement d'ensemble en roulis. [8]

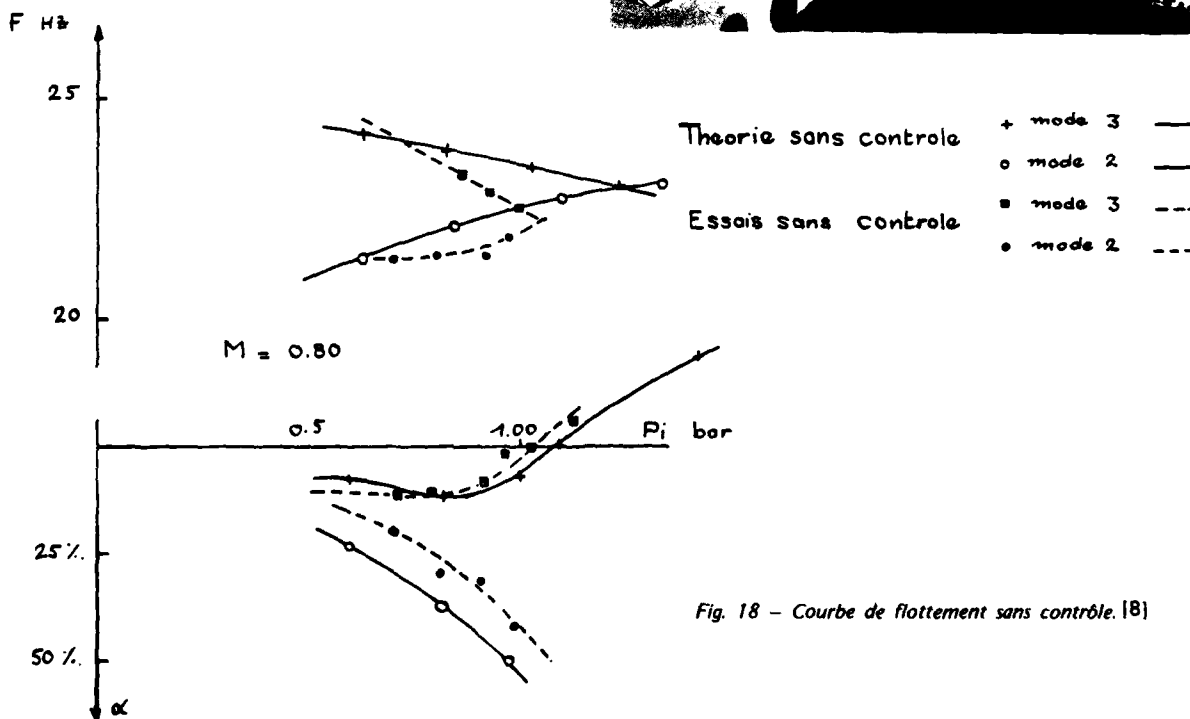


Fig. 18 - Courbe de flottement sans contrôle. [8]

18-14

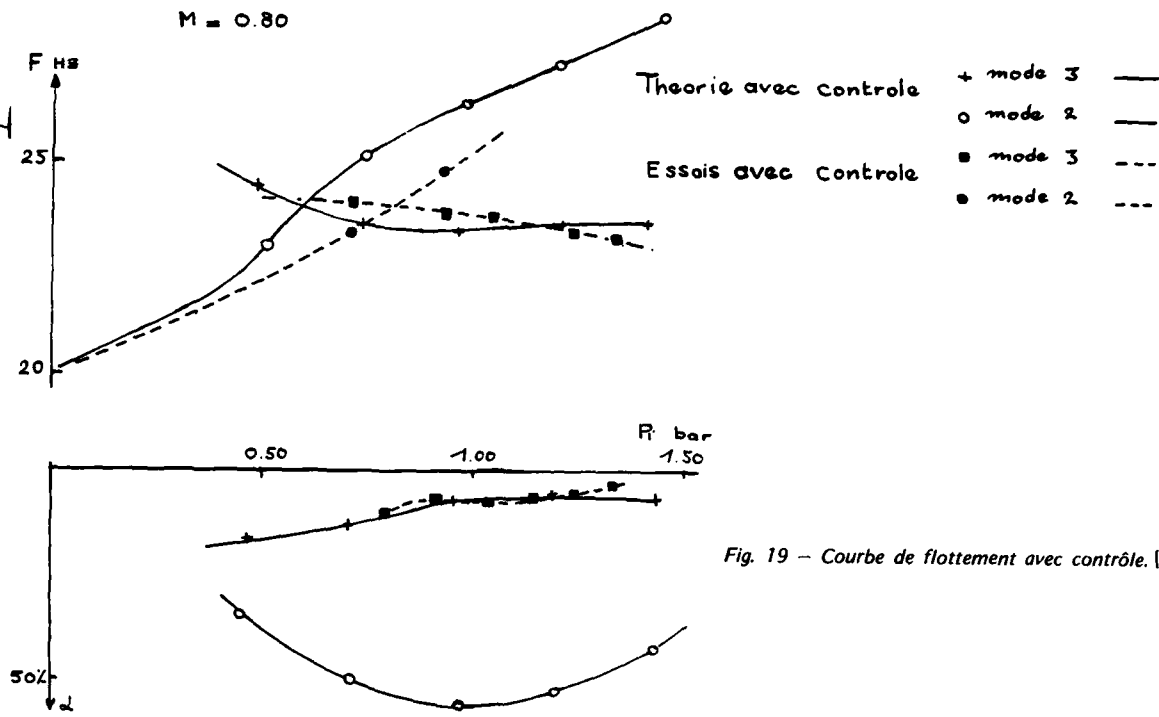


Fig. 19 - Courbe de flottement avec contrôle. [8]

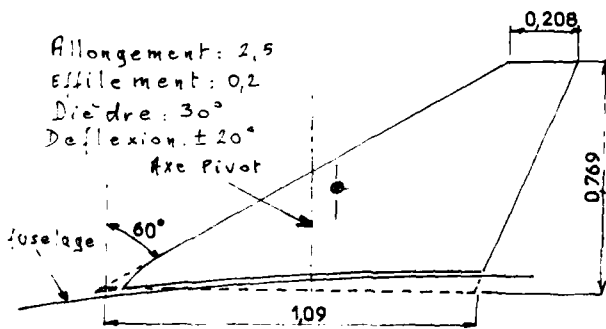
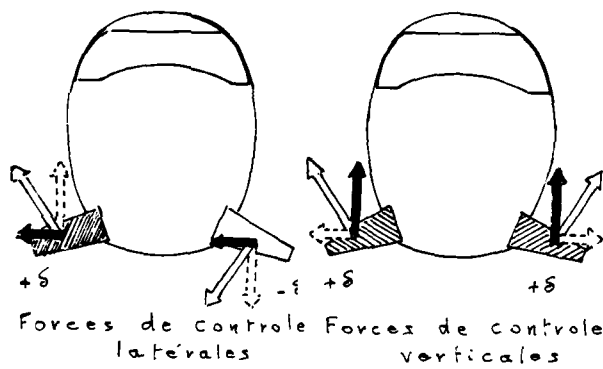


Fig. 20 - Caractéristiques géométriques des surfaces de contrôle des modes de structure. [9]

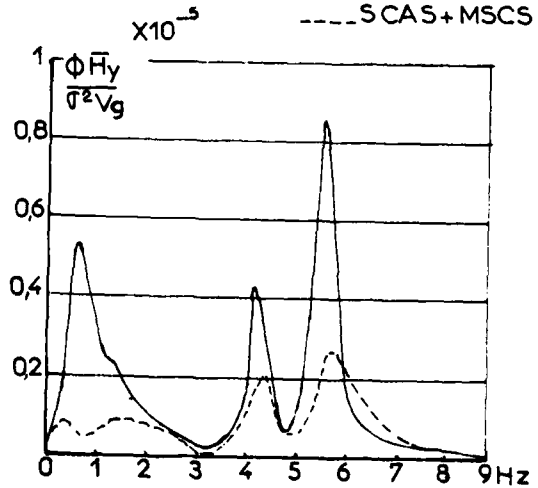
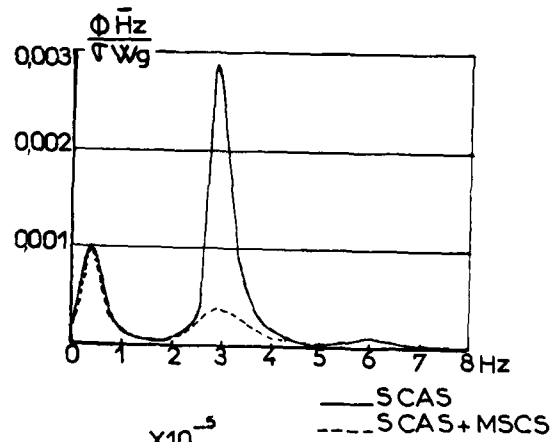


Fig. 21 - Densité spectrale en vertical et en latéral avec et sans mise en action des ailes de contrôle. [9]

Fig. 22 - Maquette de flottement avec palette en bout d'aile. [10]

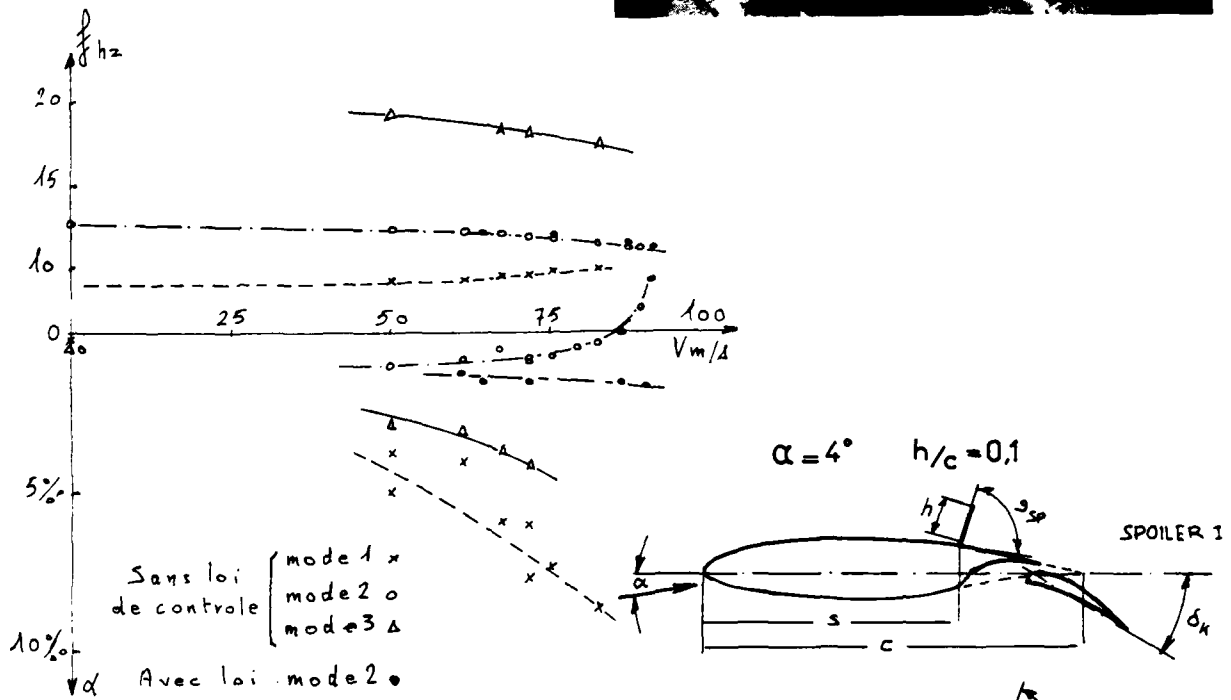
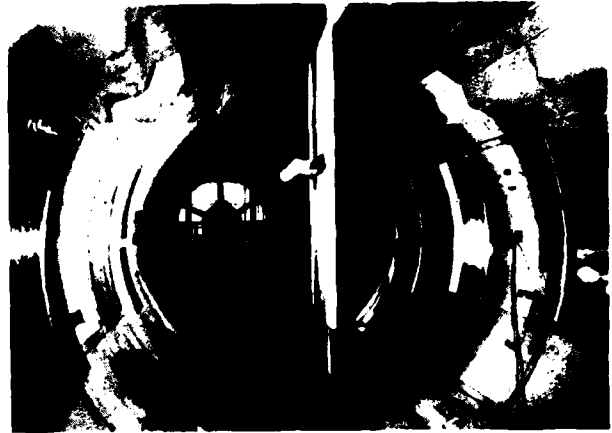


Fig. 23 - Action du supprimeur de flottement par une palette agissant en bout d'aile. [11]

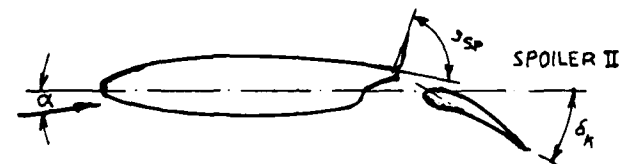
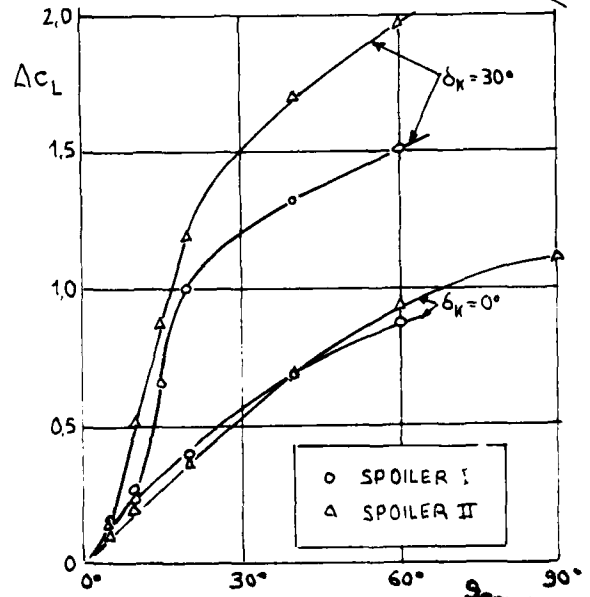


Fig. 24 - Effet de spoiler pour deux configurations selon la corde. $\alpha = 4^\circ$; $h/c = 0,1$ [13]



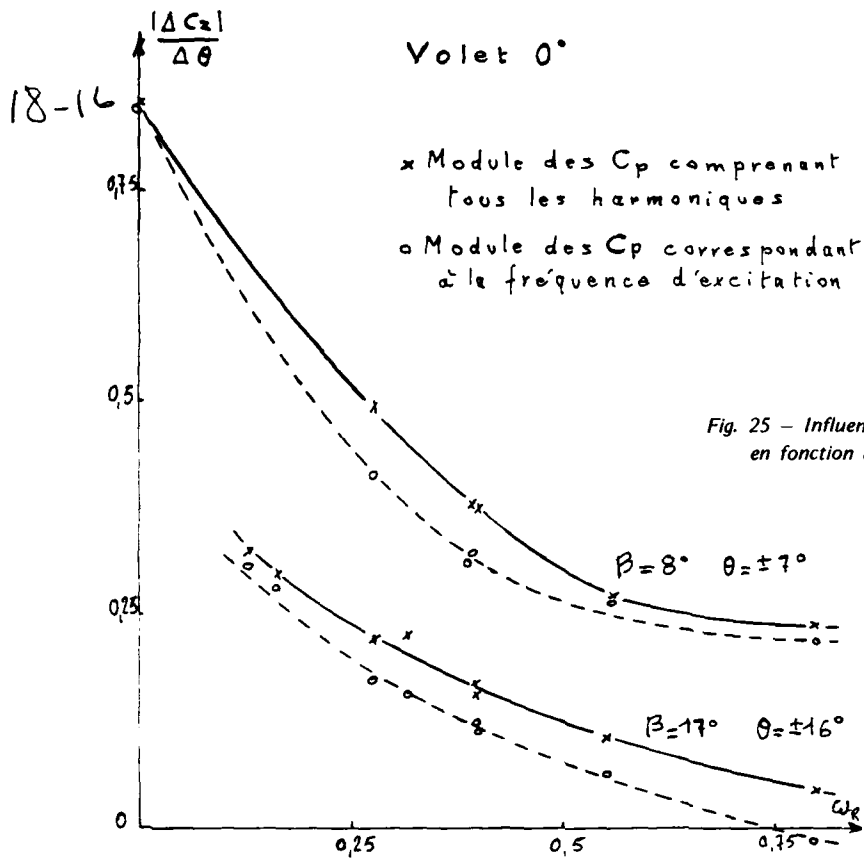


Fig. 25 - Influence de la fente sur la déportance d'un spoiler en fonction de la fréquence réduite. [11]

$M = 0.30$ Volet 10° $\omega_R = 0.285$

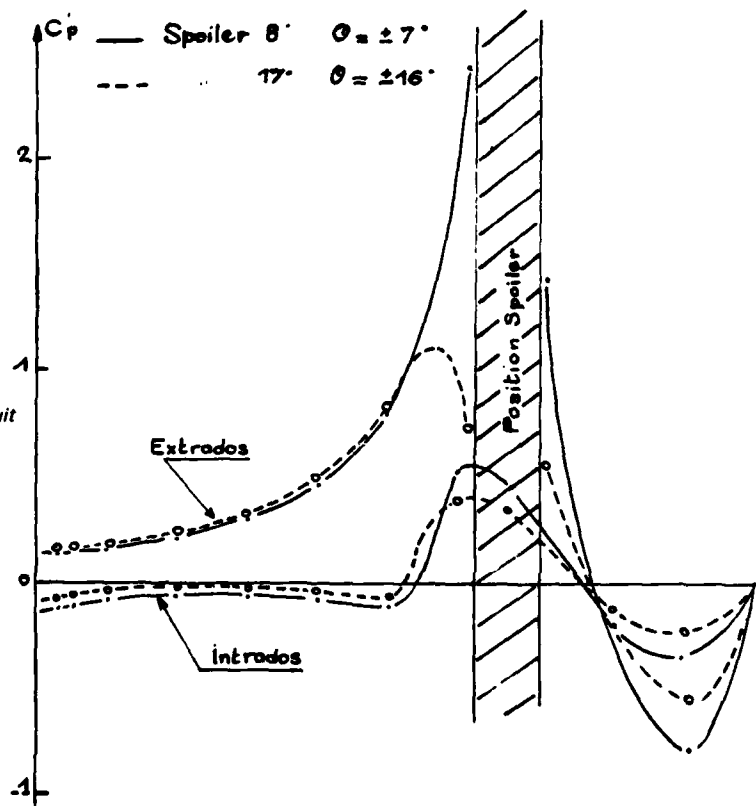
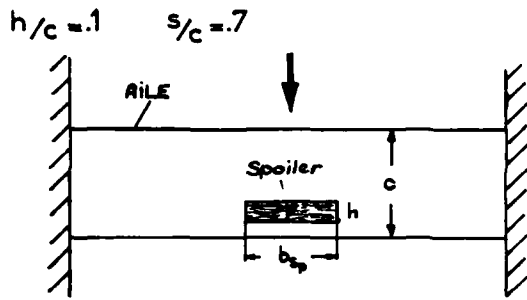


Fig. 26 - Champ de pression instationnaire induit sur l'aile par un spoiler pour différents braquages. [11]



18-17

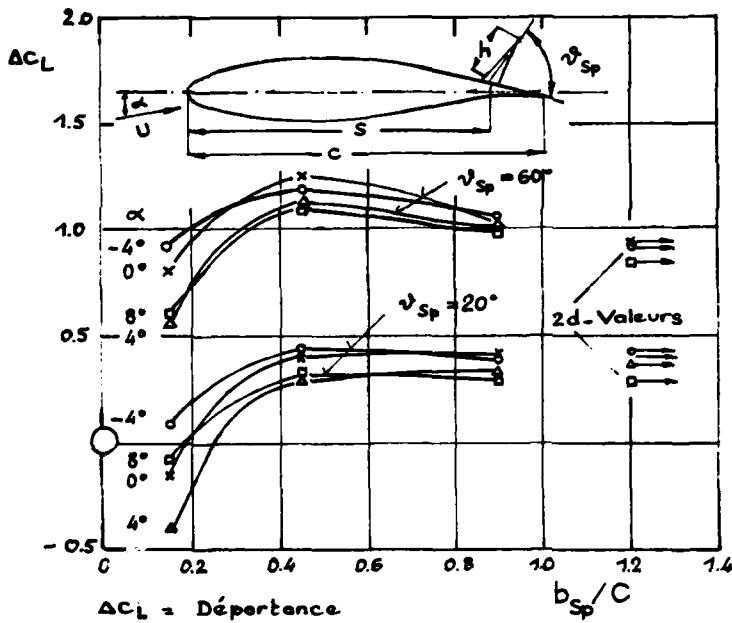


Fig. 27 - Efficacité d'un spoiler en fonction de son envergure. [14]

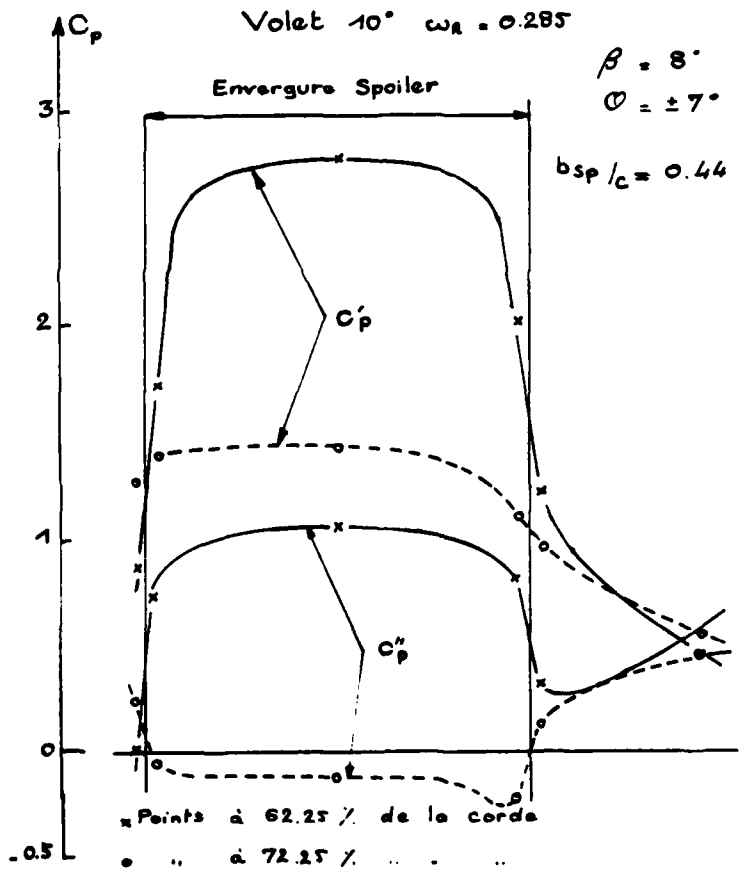


Fig. 28 - Distribution des C_p en fonction de l'envergure. [11]

**EFFETS INSTATIONNAIRES D'UNE GOUVERNE
EN ÉCOULEMENT BIDIMENSIONNEL SUBSONIQUE ET TRANSSONIQUE**

par Richard GRENON, André DESOPPER et Jacques SIDES
Office National d'Etudes et de Recherches Aéronautiques (ONERA)
92320 Châtillon (France)

RESUME -

La conception des avions actuels évolue de plus en plus vers l'emploi des techniques de contrôle actif généralisé (CAG ou CCV) qui requièrent l'utilisation de gouvernes rapides. Dans cette optique, l'ONERA a entrepris une étude expérimentale approfondie des effets instationnaires d'une gouverne oscillante.

On rappelle d'abord les principaux résultats expérimentaux des mesures de pression stationnaire et instationnaire effectuées en écoulement subsonique et transsonique sur un profil supercritique de 16% d'épaisseur relative équipé d'un volet de bord de fuite de 25% de profondeur pouvant être animé d'un mouvement sinusoïdal.

On compare ensuite ces résultats expérimentaux à ceux obtenus à l'aide de diverses méthodes de calcul d'écoulements stationnaires et instationnaires de fluide parfait. On présente également quelques résultats de calculs pour lesquels on a tenté de tenir compte des effets visqueux.

19-1

UNSTEADY EFFECTS OF A CONTROL SURFACE IN TWO-DIMENSIONAL, SUBSONIC AND TRANSONIC FLOW

SUMMARY -

The design of present-day aircraft is more and more governed by the use of Control Configured Vehicle (CCV) techniques which require the utilization of fast moving control surfaces. With this in view, ONERA undertook an in-depth study of the unsteady effects of an oscillating surface.

We first recall the main experimental results of steady and unsteady pressure measurements, carried out in subsonic and transonic flow on a 16% relative thickness supercritical aerofoil, equipped with a trailing edge flap, interesting 25% of the chord, in a sinusoidal motion.

Then we compare these experimental results with those obtained by various methods of steady and unsteady inviscid flow calculations. We also present some calculation results in which viscous effects have been taken into account, for both steady and unsteady flows.

NOTATIONS

a : vitesse du son
 ρ : masse volumique
 V : vitesse de l'écoulement
 M : nombre de Mach
 c : corde
 α : incidence du profil
 δ : braquage du volet, positif vers le bas
 δ_m : braquage moyen du volet
 δ_i : amplitude des oscillations du volet
 t : temps
 ω : fréquence circulaire
 $f = \frac{\omega}{2\pi}$: fréquence des oscillations (Hz)
 $k = \frac{\omega c}{2V_\infty} = \frac{\pi f c}{V_\infty}$: fréquence réduite
 P : pression instantanée
 P_m : pression moyenne
 ΔP : fluctuation de pression

$K_p = \frac{P - P_\infty}{\frac{1}{2} \rho_\infty V_\infty^2}$: coefficient de pression instantanée (ou stationnaire)
 $C_p = \frac{\Delta P}{\frac{1}{2} \rho_\infty V_\infty^2 \delta_i}$: coefficient de pression instationnaire
 K_p^* : valeur de K_p lorsque $M_2 = 1$
 C_z : coefficient de portance stationnaire
 $C_{z\delta}$: coefficient de portance instationnaire
 $C_{m\delta}$: coefficient de moment de tangage instationnaire
 $C_{mc\delta}$: coefficient de moment de charnière instationnaire
 φ : angle de phase
 P_i : pression génératrice
 Re : nombre de Reynolds

INDICES

m : valeurs moyennes (δ, P)
 l : valeurs locales (a, V, M)
 ∞ : valeurs à l'infini amont (a, V, M)
 1 : indice affecté au module et à la phase du 1er harmonique de C_p

19-2

1 - INTRODUCTION -

La conception des avions actuels évolue de plus en plus vers l'emploi des techniques de contrôle automatique généralisé (C.A.G. ou C.C.V en anglais) qui requièrent l'utilisation de gouvernes à court temps de réponse. Dans cette optique, l'ONERA a entrepris une étude expérimentale approfondie des effets instationnaires d'une gouverne oscillante.

Cette communication concerne plus particulièrement les résultats acquis en écoulement bidimensionnel subsonique et transsonique sur un profil équipé d'une gouverne de bord de fuite de 25% de profondeur pouvant être animée d'un mouvement sinusoïdal.

On rappelle d'abord rapidement les principaux résultats expérimentaux des mesures de pression stationnaire et instationnaire effectuées sur ce profil dans la soufflerie S3 de Modane. Ces résultats ont déjà fait l'objet d'une communication à une réunion AGARD en 1977 [1].

Puis, on compare ces résultats expérimentaux à ceux obtenus à l'aide de diverses méthodes de calcul d'écoulements stationnaires et instationnaires de fluide parfait. On présente enfin les résultats des premières tentatives de prise en compte des effets visqueux en écoulement instationnaire.

2 - RAPPEL DES PRINCIPAUX RESULTATS EXPERIMENTAUX -

2.1 - Présentation du matériel d'essai -

Pour cette étude, menée en étroite collaboration par les directions de l'Aérodynamique et de la Résistance des Structures de l'ONERA, le profil retenu est un profil supercritique de 16% d'épaisseur relative développé par la Société Aérospatiale (profil RA 16 SC 1).

La maquette bidimensionnelle a une corde de 180 mm. La gouverne de bord de fuite, de 25 % de profondeur, est actionnée par deux petits vérins hydrauliques rotatifs commandés par des servo-valves synchronisées et pilotées par un générateur de signaux sinusoïdaux. Ce système permet d'obtenir des oscillations de la gouverne de $\pm 1^\circ$ à 100 Hz, l'amplitude pouvant atteindre $\pm 5^\circ$ à 20 Hz [fig.1].

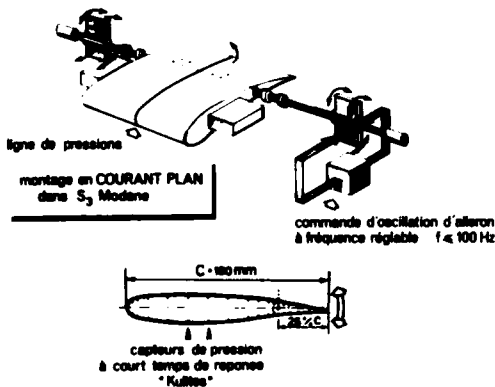


Fig. 1 - Montage d'un aileron oscillant sur profil supercritique épais.

La maquette est équipée de 73 prises de pression statique et de 32 capteurs de

pression instationnaire Kulite à court temps de réponse.

Les essais ont eu lieu dans la soufflerie à rafales S3 de Modane, à des nombres de Mach compris entre 0,3 et 0,8. Le programme d'essai réalisé comprend une partie stationnaire et une partie instationnaire, avec étude de l'influence de nombreux paramètres. Le traitement du signal recueilli par les capteurs Kulite lors des essais dynamiques est précisé figure 2.

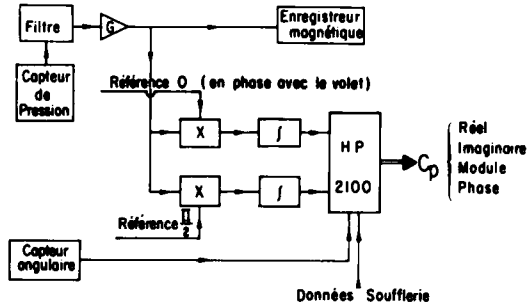


Fig. 2 - Chaîne de mesures instationnaires.

Enfin, un banc de striescopie a permis de filmer le mouvement de l'onde de choc d'extrados dans le domaine transsonique.

2.2 - Caractéristiques stationnaires du profil

A incidence nulle et pour un braquage nul de la gouverne, une zone supersonique apparaît au bord d'attaque extrados vers $M_{\infty} = 0,7$ (fig.3). Lorsque le nombre de Mach croît, cette zone supersonique s'étend rapidement vers l'aval en donnant une répartition de pression en forme de plateau avec un choc assez faible, et l'intrados devient à son tour supersonique.

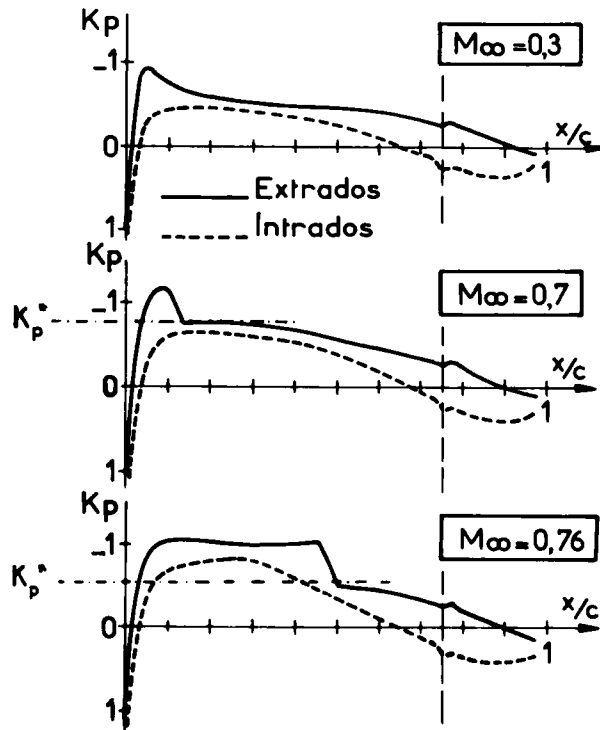


Fig. 3 - Profil SNIAS 16SC1 - $\alpha = 0^\circ$; $\delta \geq 0^\circ$ - Répartitions de pression en écoulement stationnaire.

L'aspect des zones supersoniques est profondément modifié par le braquage de la gouverne (fig. 4), mais le profil étant fortement chargé à l'arrière de par sa conception (fig. 3), la gouverne reste chargée positivement dans la plupart des cas, la charge sur la gouverne ne s'annulant que pour un braquage voisin de $\delta = -10^\circ$.

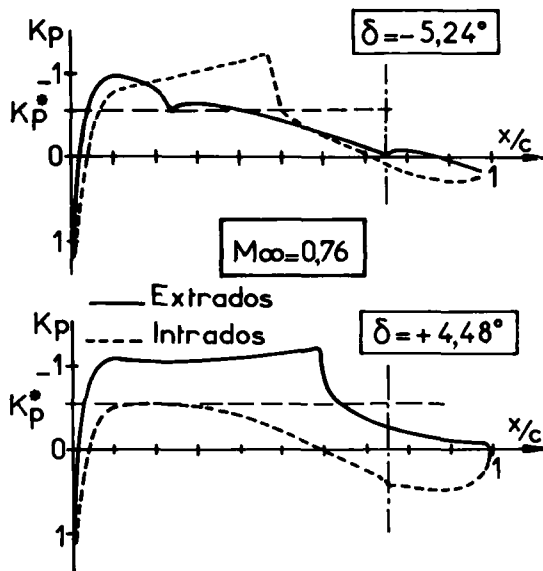


Fig. 4 - Efficacité de la gouverne en écoulement stationnaire. $\alpha = 0^\circ$.

2.3 - Caractéristiques instationnaires du profil -

Les divers coefficients de pression, de portance, de moment de tangage et de moment de charnière instationnaires sont présentés sous forme de module et phase du premier harmonique (terme en ω de la série de Fourier). Ce mode de présentation est justifié par l'expérience, les harmoniques d'ordre supérieur étant négligeables sauf très localement pour les signaux de pression dans les étroites zones balayées par les chocs. Les phases sont déterminées par rapport à la position de la gouverne et les phases de pressions d'extrados sont portées avec un décalage de 180° ; ceci permettrait d'obtenir la même courbe de phase à l'intrados et à l'extrados dans le cas d'un profil symétrique à l'incidence nulle avec une gouverne oscillant autour du braquage nul; ici cela mettra en évidence l'effet de la dissymétrie du profil utilisé.

- Influence du nombre de Mach.

On remarque d'abord l'importance de l'influence du nombre de Mach sur la répartition des coefficients de pression instationnaire pour une même fréquence réduite (fig. 5). En régime subcritique la courbe des modules C_p présente l'allure classique prévue par la théorie de la plaque plane (maxima au bord d'attaque et à la charnière correspondant aux infinis de la théorie), la phase évoluant presque linéairement d'un retard au bord d'attaque à une avance sur le volet.

Lorsque le nombre de Mach croît, il se forme une zone supersonique terminée par un choc plus ou moins intense. Les oscillations

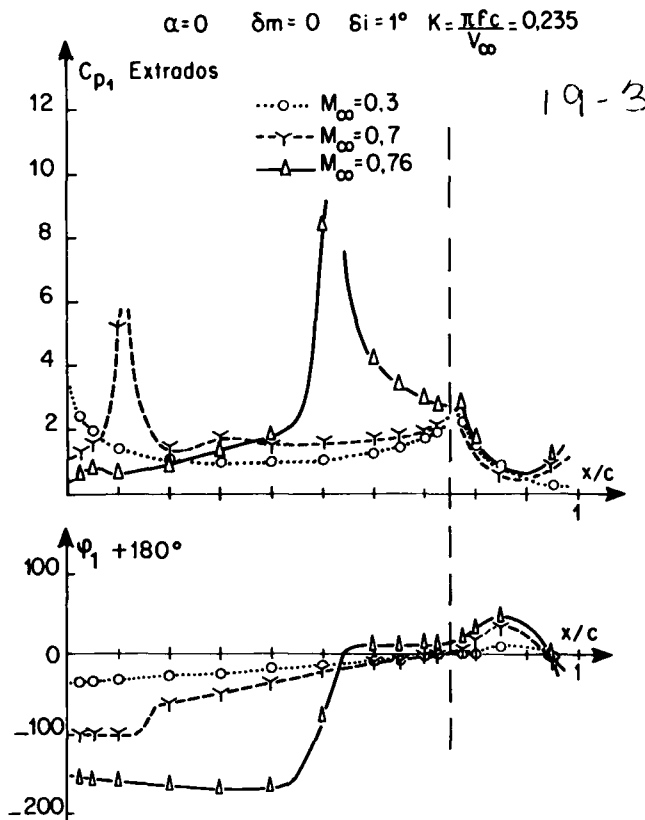


Fig. 5 - Influence du nombre de Mach sur les pressions instationnaires.

de ce choc se traduisent sur la courbe des modules par un pic dont l'intensité dépend de celle du choc. Le niveau des fluctuations de pression en amont du choc, c'est-à-dire dans la zone d'écoulement supersonique, diminue lorsque le nombre de Mach augmente.

Le déphasage croît avec le nombre de Mach au bord d'attaque, mais il garde un niveau pratiquement constant dans la zone supersonique et présente un saut brutal au niveau du choc.

L'allure des répartitions de pression instationnaire est donc très différente selon que l'on se trouve en régime subcritique sans choc ou en régime supercritique avec chocs.

- Influence de la fréquence réduite.

L'influence de la fréquence réduite se traduit d'ailleurs de manière légèrement différente dans les deux cas. En régime subcritique le module des pressions diminue et le retard de phase au bord d'attaque croît lorsque la fréquence réduite augmente, le point à phase nulle se déplaçant vers l'amont (fig. 6). En régime supercritique, si le retard de phase dans la zone supersonique croît avec la fréquence réduite, les modules des pressions instationnaires évoluent par contre en sens contraire de part et d'autre du choc (fig. 7).

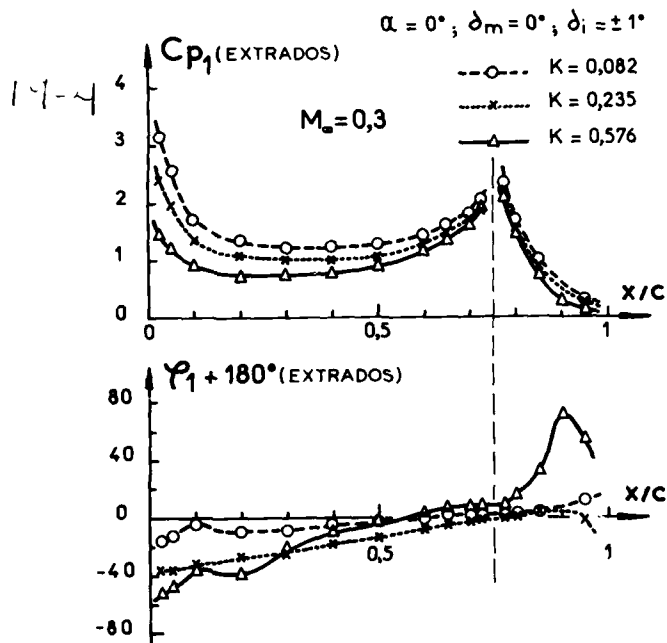


Fig. 6 - Influence de la fréquence réduite sur les pressions instationnaires.

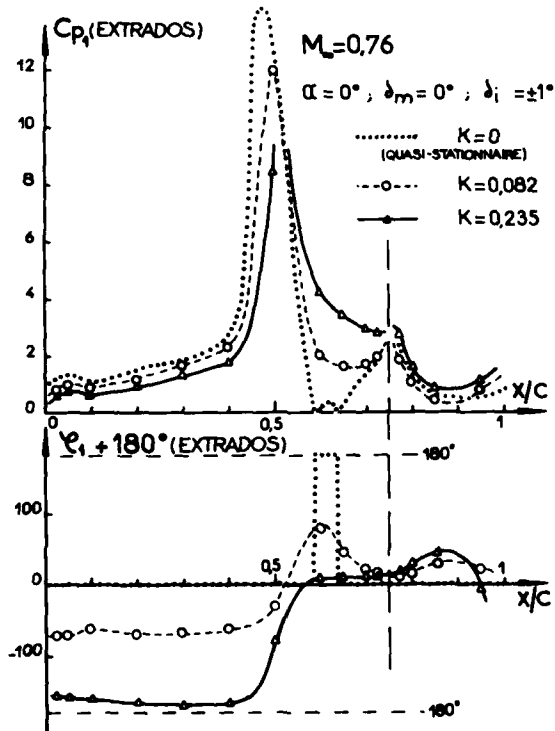


Fig. 7 - Influence de la fréquence réduite sur les pressions instationnaires.

- Interactions stationnaire-instationnaire.

Contrairement à ce que prévoit la théorie linéarisée, il existe une interaction non négligeable des caractéristiques moyennes de l'écoulement sur ses caractéristiques instationnaires. Cette interaction est bien illustrée par l'effet du braquage moyen de la gouverne sur les pressions instationnaires (fig. 8 et 9). Lorsque le braquage moyen de la gouverne augmente, accroissant ainsi la charge moyenne sur l'aile et sur la gouverne, les modules des pressions

instationnaires diminuent, et les phases évoluent légèrement dans le sens d'une avance de phase. Cependant une forte augmentation des pressions instationnaires au bord de fuite apparaît lorsque le volet oscille de plus en plus près du décollement ($\delta_m = 2,5$ dans le cas présent). En régime supercritique (fig.9), on observe en plus une translation du pic de la courbe des modules et du saut de la courbe des phases correspondant au déplacement de la position moyenne du choc.

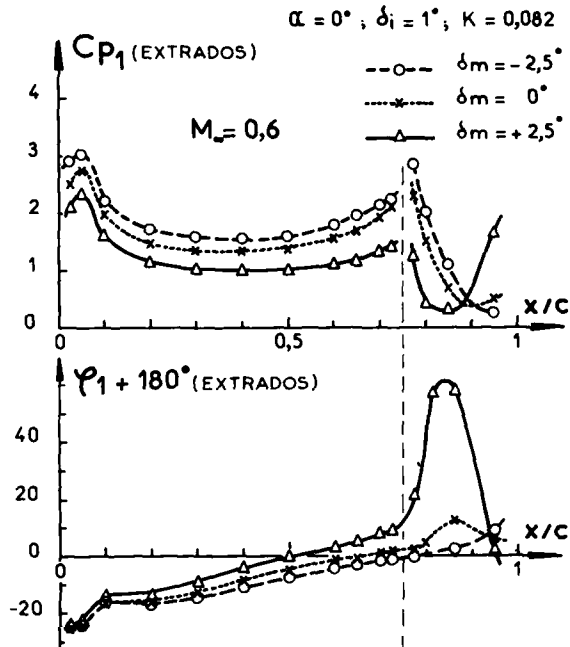


Fig. 8 - Influence du braquage moyen δ_m sur les pressions instationnaires

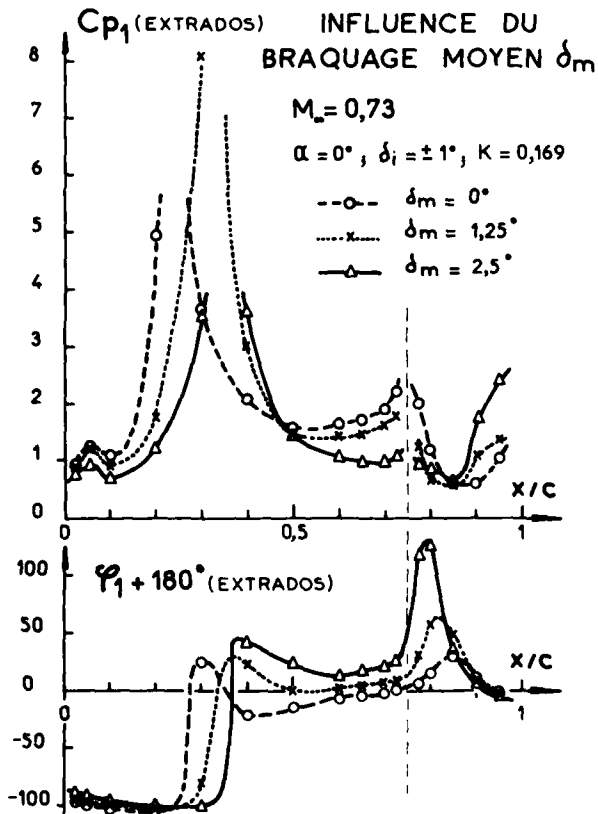


Fig. 9 - Influence du braquage moyen δ_m sur les pressions instationnaires.

3 - COMPARAISONS ENTRE RESULTATS EXPERIMENTAUX ET RESULTATS DE CALCUL -

3.1 - Présentation des méthodes de calcul -

Chacune des méthodes de calcul utilisées sera brièvement présentée. Pour plus de détails, on se reportera aux ouvrages cités en référence.

a) Méthodes basées sur l'hypothèse des écoulements potentiels

- Ecoulements stationnaires :

Les programmes dont on dispose utilisent la méthode de GARABEDIAN et KORN pour prévoir les écoulements stationnaires de fluide parfait en régime supercritique. Les effets visqueux sont pris en compte en faisant un couplage avec un calcul de couche limite, la technique de couplage consistant à calculer l'écoulement de fluide parfait autour du profil engraissé de l'épaisseur de déplacement de la couche limite [2, 3].

- Ecoulements instationnaires de fluide parfait, régime subcritique :

Pour traiter les écoulements instationnaires dans tout le domaine subcritique, on peut utiliser la théorie linéarisée de la plaque plane. Cette méthode, couramment utilisée pour les calculs de structures à l'ONERA, est une méthode de doublets [4] : le profil est assimilé à une ligne sans épaisseur ni cambrure et décomposé en une vingtaine d'éléments comportant chacun un doublet de potentiel d'accélération au 1/4 avant. Les conditions de tangence de l'écoulement sont appliquées au 1/4 arrière de chaque élément. Cette méthode est tout de même d'un emploi limité, car elle ne tient pas compte de l'influence de l'écoulement moyen sur la réponse instationnaire, non négligeable dans les configurations fortement chargées.

Pour représenter l'influence de l'écoulement moyen sur la réponse instationnaire aux basses vitesses, on dispose d'un programme de calcul en écoulement instationnaire incompressible développé par la Société BERTIN [5] et basé sur la méthode de GIESING [6]. Le profil est représenté par des sources et des puits sur son contour et des tourbillons sur la ligne moyenne. Le sillage est constitué de tourbillons libres émis à chaque pas de temps pour conserver la circulation totale de l'écoulement. Cette méthode tient compte de la forme et du mouvement exacts du profil, ainsi que de la déformation du sillage tourbillonnaire.

- Ecoulements instationnaires de fluide parfait, régime supercritique :

Pour traiter les écoulements instationnaires en régime supercritique, on utilise actuellement un programme de calcul résolvant par une méthode de différences finies l'équation du potentiel des vitesses avec l'approximation des petites perturbations pour des écoulements transsoniques bidimensionnels instationnaires. Ce programme initialement développé pour l'étude des écoulements sur pales d'hélicoptère par F.X. CARADONNA [7] a été adapté au cas du volet oscillant par J.J. THIBERT de l'ONERA. Il existe également une autre méthode de petites perturbations transsoniques en cours de développement à la direction de Résistance des Structures de l'ONERA [8] et qui a l'avantage de nécessiter un temps de calcul inférieur à celui du programme CARADONNA.

b) Résolution des équations d'Euler

L'hypothèse des petites perturbations est peu

réaliste sur un profil de 16 % comportant des zones supersoniques parfois étendues pour un nombre de Mach à l'infini amont de l'ordre de 0,73 à 0,75, et il est assez difficile de savoir quels termes peuvent être négligés dans l'équation du potentiel. 19-5

Pour évaluer l'erreur due à l'hypothèse des petites perturbations transsoniques, on se référera à une méthode de calcul d'écoulements instationnaires de fluide parfait résolvant les équations d'Euler [9]. Cette méthode permet de calculer, pour un profil d'épaisseur quelconque, des écoulements supercritiques sans restrictions sur l'intensité et le mouvement des chocs. L'écoulement de fluide parfait autour d'un profil muni d'un volet oscillant est calculé en résolvant les équations d'Euler complètes, sous la forme de lois de conservation intégrales, par la méthode des "volumes finis" généralisée en maillage mobile. La méthode est conservative, en ce sens que dans un bilan numérique de masse, de quantité de mouvement ou d'énergie sur un domaine constitué de cellules, les contributions des flux intérieurs intervenant dans le schéma numérique s'annulent deux à deux. La condition de glissement est imposée sur le volet oscillant dans sa position exacte au cours du temps.

L'inconvénient majeur de cette dernière méthode qui est de type explicite dans sa formulation actuelle est l'importance des temps de calcul requis.

Cette méthode a été testée et mise au point sur un profil NACA 0012 avec gouverne oscillante [9], mais seuls deux calculs en écoulement stationnaire avec le profil RA 16 SC1 ont pu être effectués à temps pour figurer dans cet article. Des calculs en écoulement instationnaire sont en cours.

c) Prise en compte des effets visqueux instationnaires :

Afin de tenir compte des effets visqueux instationnaires, on a effectué le couplage d'une méthode de calcul en fluide parfait avec un programme de calcul de couche limite turbulente instationnaire, à la fois en écoulement incompressible avec le programme BERTIN, et en écoulement transsonique avec le programme CARADONNA.

Tous les résultats présentés ici ont été obtenus avec une méthode intégrale de calcul de couche limite turbulente en écoulement compressible instationnaire développée au CERT [10]. Cette méthode utilise l'équation de Karman (conservation des quantités de mouvement) et l'équation d'entraînement établies en écoulement instationnaire, les relations supplémentaires nécessaires pour résoudre le système d'équations étant les mêmes que celles utilisées en écoulement stationnaire.

Que ce soit en écoulement incompressible ou en écoulement transsonique, la méthode de couplage consiste à faire le calcul de fluide parfait avec une modification des conditions aux limites sur le profil pour tenir compte du développement de la couche limite. Concrètement, cela se traduit par un débit de fluide à travers la pale caractérisé par une vitesse normale v_e dans le programme BERTIN, et par une modification des pentes locales du profil de la quantité $(v/u)_p$ dans le programme CARADONNA. v_e et $(v/u)_p$ sont donnés par la relation :

$$\frac{v_e}{u_e} = \left(\frac{v}{u}\right)_p = \frac{1}{\rho_e u_e} \frac{\partial}{\partial x} (\rho_e u_e \delta_1)$$

où δ_1 est l'épaisseur de déplacement, u_e la vitesse tangentielle de l'écoulement de fluide

19-6

parfait et ρ_e la masse volumique.

Cette relation est identique à celle donnée par J.C. LE BALLEUR pour des écoulements stationnaires [11] : en effet, la relation de couplage à la paroi fait apparaître comme seul terme instationnaire $\frac{1}{\rho_e} \int_0^{\delta} \left[\left(\frac{\partial \rho_e}{\partial t} \right)_x - \left(\frac{\partial \rho_e}{\partial t} \right)_y \right] dy$ qui a été négligé même en compressible.

A chaque pas de temps, on effectue deux ou trois itérations fluide parfait - couche limite, avec éventuellement l'utilisation d'une méthode de relaxation.

Les principaux problèmes rencontrés lors du couplage sont essentiellement liés à l'apparition des décollements au bord de fuite, à la charnière et à la présence de chocs d'intensité non négligeable. Les interactions onde de choc-couche limite et les décollements sont traités de façon simplifiée, et il est bien évident que la technique de couplage n'est utilisable que dans le cas d'interaction onde de choc-couche limite faible et de zones décollées peu étendues.

3.2 - Comparaisons en écoulement stationnaire.

Les figures 10 et 11 correspondent à deux braquages de la gouverne. Pour chaque braquage, on a porté les pressions stationnaires mesurées en veine guidée à $M_\infty = 0,73$ et les calculs effectués en fluide parfait avec la méthode potentielle et avec les équations d'Euler. Ces calculs ont été effectués au nombre de Mach et à

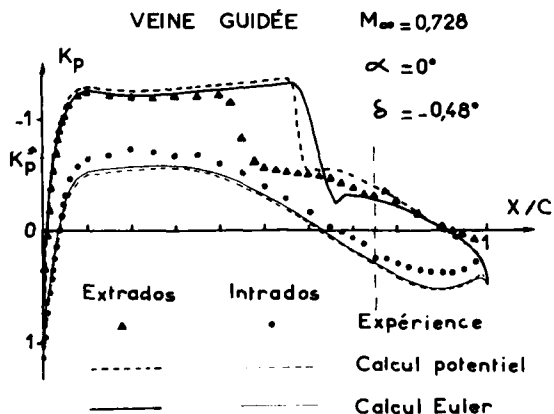


Fig. 10 - Comparaison calcul-expérience en écoulement transsonique stationnaire.

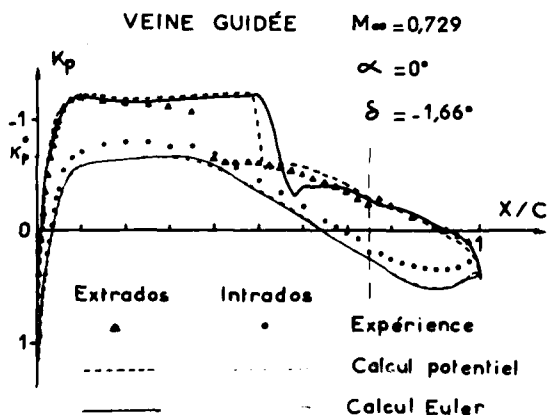


Fig. 11 - Comparaison calcul-expérience en écoulement transsonique stationnaire.

l'incidence corrigés des effets de paroi, ces corrections étant relativement bien connues en veine guidée. Les deux méthodes de calcul donnent des résultats assez semblables, avec un choc beaucoup plus en aval que dans l'expérience à l'extrados. Le choc calculé par les équations d'Euler est toutefois un peu plus en aval que celui calculé par la méthode potentielle.

Des résultats portés sur les figures 10 et 11 on a tiré les valeurs quasi-stationnaires expérimentales et théoriques des coefficients de pression instationnaire : ces valeurs correspondent à une oscillation de la gouverne à fréquence nulle avec une amplitude de $\pm 0,59^\circ$ autour du braquage moyen $\delta_m = -1,07^\circ$ (fig.12). Elles sont obtenues de la façon suivante :

$$C_{Pqs} = \frac{K_p(\delta_1) - K_p(\delta_2)}{(\delta_1 - \delta_2) \text{ rad.}} = \frac{K_p(-0,48^\circ) - K_p(-1,66^\circ)}{1,18 \cdot \pi / 180}$$

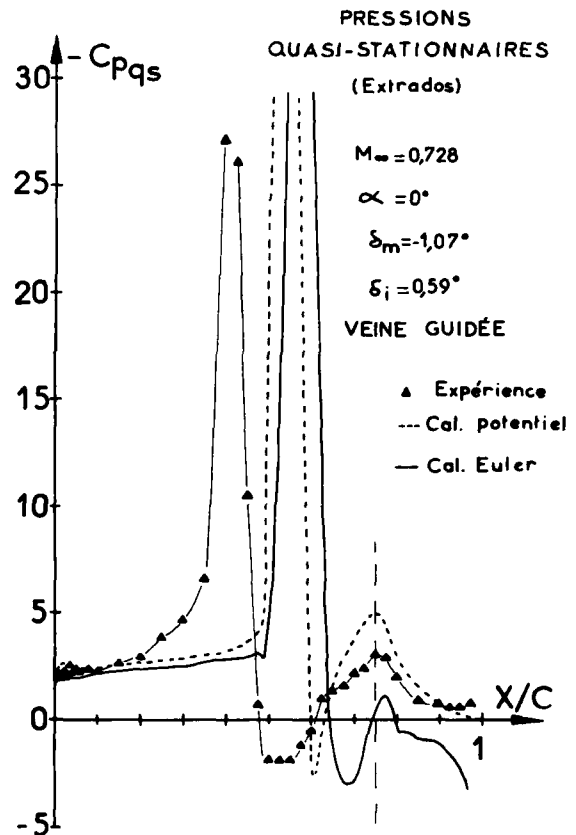


Fig. 12 - Comparaison calcul-expérience sur les valeurs quasi-stationnaires en transsonique.

Le pic dû au déplacement du choc est toujours beaucoup plus en aval dans les théories en fluide parfait que dans l'expérience, celui donné par les équations d'Euler étant légèrement plus en aval que celui donné par la théorie potentielle. Les deux théories donnent des résultats très voisins en amont du choc, par contre elles se différencient nettement en aval du choc et sur le volet.

Sur les figures 13 à 15, qui correspondent à trois braquages de la gouverne, on a porté les pressions stationnaires expérimentales avec celles calculées par la théorie potentielle avec et sans couche limite [2, 3].

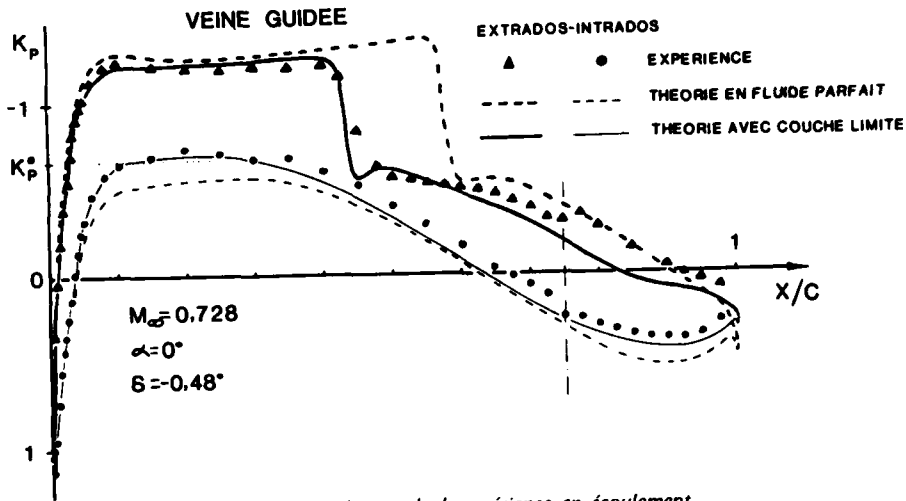


Fig. 13 - Comparaison calcul -expérience en écoulement transsonique stationnaire.

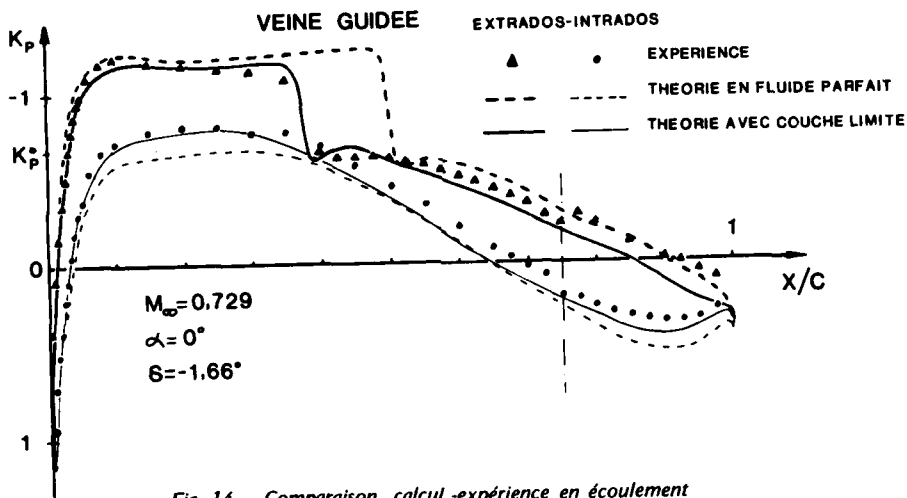


Fig. 14 - Comparaison calcul -expérience en écoulement transsonique stationnaire.

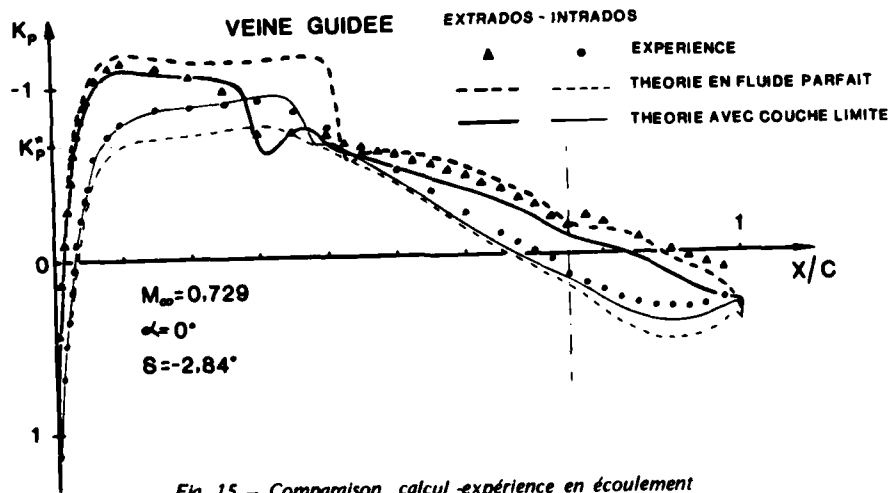


Fig. 15 - Comparaison calcul -expérience en écoulement transsonique stationnaire.

19-8

L'accord entre l'expérience et la théorie avec couche limite est relativement bon, sauf peut être immédiatement en aval du choc, où la théorie indique souvent une réaccélération qu'on ne retrouve pas expérimentalement, et sur l'extrados du volet, où le calcul s'écarte notablement de l'expérience.

Pour expliquer ces écarts, il faut noter que l'interaction onde de choc couche limite est traitée de façon simplifiée dans le calcul, et qu'il existe peut être un effet de soufflage à travers la fente entre l'aile et la gouverne dont le calcul ne peut tenir compte. De plus, dans les trois configurations choisies, le calcul n'a pas toujours très bien convergé et a presque toujours indiqué un décollement sur la gouverne, ce qui limite la validité des résultats.

On a également comparé les valeurs quasi-stationnaires expérimentales avec les valeurs données par la théorie potentielle avec et sans couche limite (fig. 16) dans le même cas que celui de la figure 12.

On note une certaine dispersion des valeurs expérimentales quasi-stationnaires d'intrados, car elles sont obtenues par différences de K_p qui ont des valeurs très voisines.

La figure 16 montre l'intérêt du calcul avec couche limite, en particulier pour positionner correctement le pic dû au déplacement du choc. Mais la partie en aval du choc d'extrados, notamment sur le volet, est encore assez mal prévue par la théorie avec couche limite. Il est donc indispensable d'améliorer le traitement de l'interaction onde de choc-couche limite et des décollements.

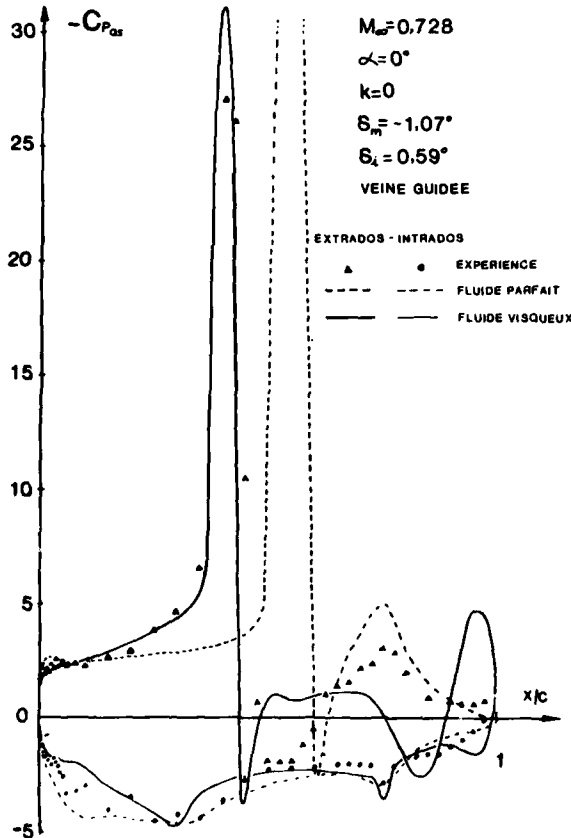


Fig. 16 - Comparaison calcul - expérience sur les valeurs quasi-stationnaires en transsonique.

3.3 - Comparaisons en écoulement instationnaire.

3.3.1 - Domaine subcritique.

Aux faibles nombres de Mach, la théorie linéarisée prévoit assez bien l'évolution en corde des pressions instationnaires (fig.17), mais elle ne différencie pas l'extrados de l'intrados car elle ne tient aucun compte des effets de l'écoulement moyen sur l'écoulement instationnaire, aussi son emploi est-il limité aux configurations faiblement chargées. Dans ce cas, elle bénéficie d'une heureuse compensation entre les effets d'épaisseur et de cambrure d'une part et ceux de la viscosité d'autre part, effets qui jouent déjà en sens contraire en quasi-stationnaire [12].

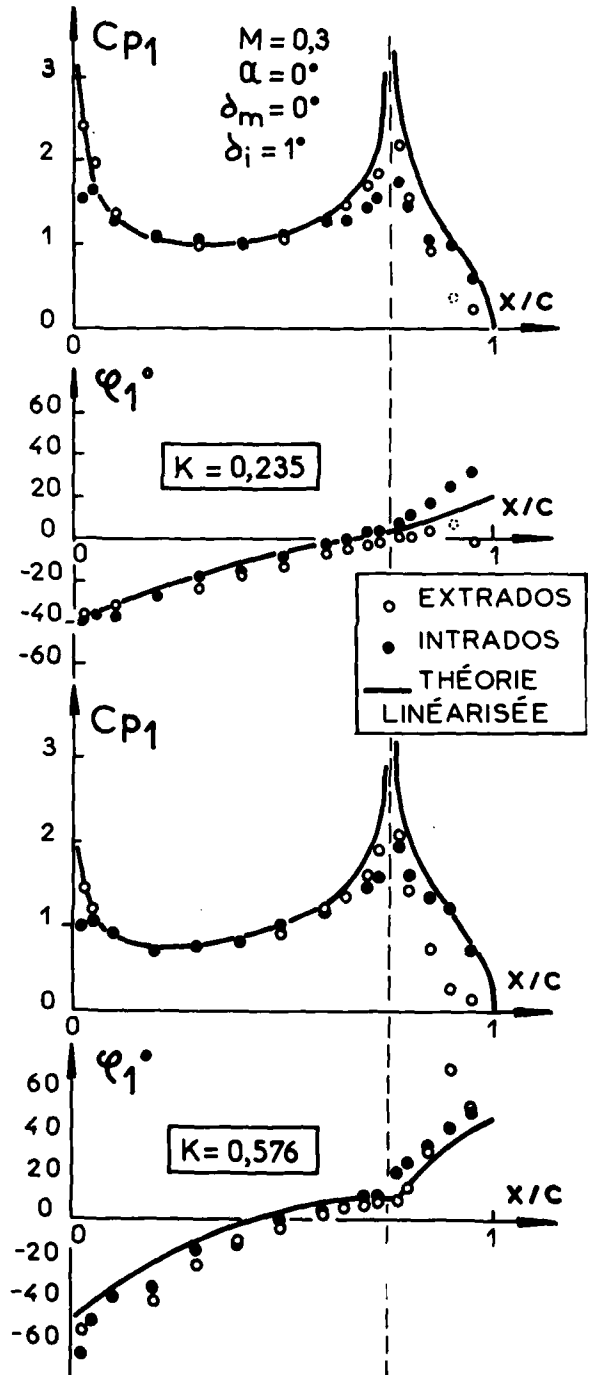


Fig. 17 - Comparaison des pressions instationnaires expérimentales avec la théorie linéarisée subsonique.

On remarquera que cette théorie linéaire donne des pressions instationnaires infinies au bord d'attaque et à la charnière.

Sur la figure 18, l'un des cas expérimentaux présenté avec la théorie linéarisée sur la figure 17 est comparé avec les résultats du programme de calcul en fluide parfait incompressible de la Société BERTIN, avec et sans couplage avec un calcul de couche limite instationnaire turbulente. Le programme de calcul en fluide parfait donne des modules de pression instationnaire plus forts que la théorie linéarisée (voir fig.17), mais il différencie bien l'extrados et l'intrados et donne une meilleure représentation qualitative du phénomène instationnaire notamment au voisinage du bord d'attaque et de la charnière. Le gain apporté par le couplage avec le calcul de couche limite est appréciable : l'écart sur les modules des pressions instationnaire entre le calcul en fluide parfait et l'expérience se trouve réduit de plus de 50 %.

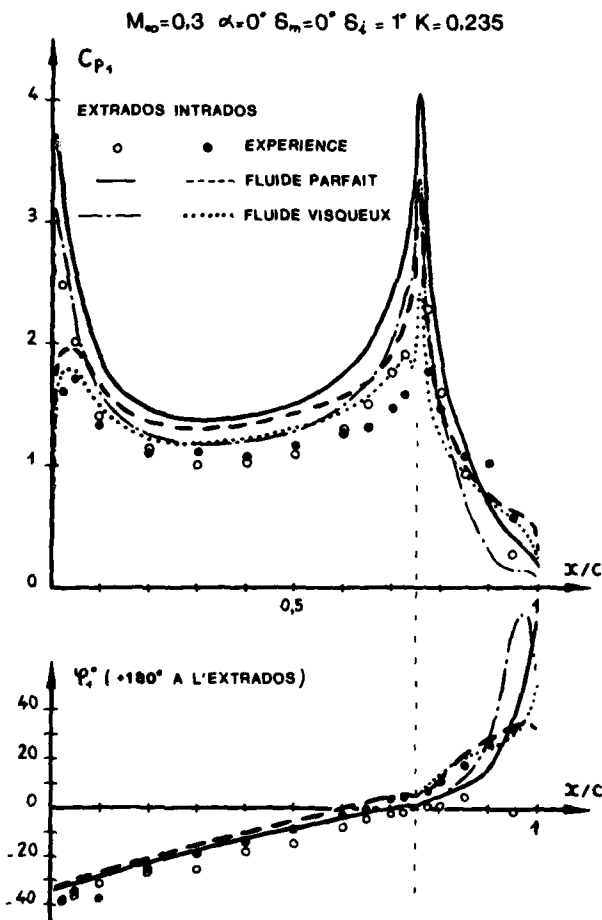


Fig. 18 - Comparaison calcul - expérience : mise en évidence des effets de viscosité en écoulement instationnaire.

Les phases sont pratiquement inchangées par le couplage, sauf au voisinage du bord de fuite.

L'intérêt du couplage apparaît encore davantage sur la figure 19 qui représente un cas de forte interaction visqueuse, avec un braquage moyen du volet de 5° : en effet, lorsque le volet est braqué de 5° en stationnaire, un décollement apparaît au bord de fuite extrados, vers $x/c = 0,95$. Le calcul instationnaire en fluide parfait fournit des résultats très différents de ceux obtenus expérimentalement. Le couplage avec le calcul de couche limite réduit de près de 70% l'écart sur les modules des pressions instationnaires et fait évoluer les phases dans le

sens d'une avance. Le calcul couplé représente assez bien l'évolution des pressions instationnaires le long de la corde jusqu'à $x/c = 0,9$ environ : on observe à l'extrados une très forte avance de phase derrière la charnière et une augmentation des modules des pressions instationnaires vers le bord de fuite. Cependant les dix derniers pour cent de la corde ne sont pas réalistes en raison du traitement simplifié de la zone décollée. Cela entraîne une imprécision des valeurs quantitatives des modules et phases des pressions instationnaires sur l'ensemble du profil. Le programme couplé fonctionne donc ici à la limite de ses possibilités.

$M_\infty=0.3 \quad \alpha=0^\circ \quad \delta_m=5^\circ \quad K=0.167$

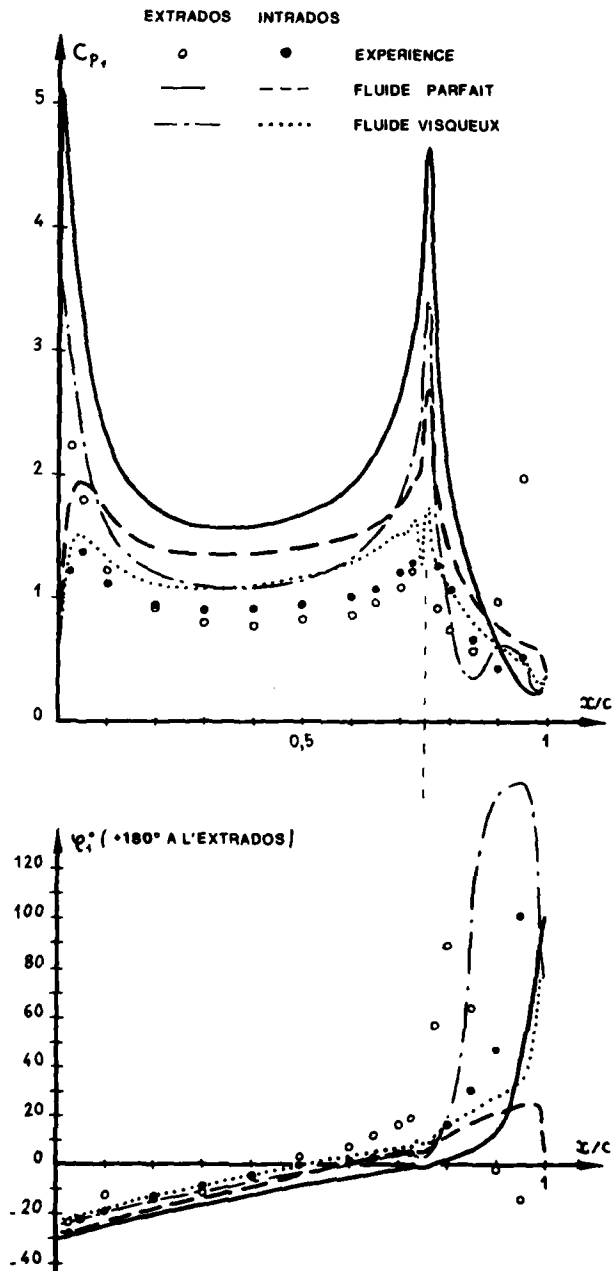


Fig. 19 - Comparaison calcul - expérience : mise en évidence des effets de viscosité en écoulement instationnaire.

Si l'on considère l'intensité des pressions instationnaires entre le bord d'attaque et la charnière par exemple (fig.17 et 18), le calcul non linéaire couplé avec la couche limite peut

19-9

19-10

paraître décevant en regard de la théorie linéarisée qui donne un résultat à peu près équivalent, puisqu'elle bénéficie d'une compensation d'erreur entre les effets d'épaisseur et de cambrure d'une part, les effets visqueux d'autre part.

Cependant, en supprimant les infinis du bord d'attaque et de la charnière, en donnant des résultats bien meilleurs que ceux de la théorie linéarisée sur le volet et en étant très sensible aux paramètres de l'écoulement moyen, le calcul non linéaire couplé donne des résultats beaucoup plus intéressants du point de vue des coefficients globaux. C'est ce que montrent les figures 20 à 22 :

- la figure 20 montre d'abord l'évolution des trois coefficients instationnaires (portance, moment de tangage à 25% et moment de charnière) en fonction de la fréquence réduite à $M_{\infty} = 0,3$ dans des configurations où le braquage moyen de la gouverne est nul. Les résultats expérimentaux sont portés avec ceux de la théorie linéarisée et du programme BERTIN avec et sans couche limite. Le programme couplé donne de meilleurs résultats que la théorie linéarisée, mais il ne donne pas satisfaction pour la phase du moment de charnière. Il faut toutefois remarquer que la

détermination expérimentale du moment de charnière instationnaire manque de précision du fait du nombre limité de capteurs de pression sur le volet (10 en tout), le plus en aval étant situé à $x/c = 0,95$ seulement. D'autre part, il peut exister un soufflage entre l'aile et la gouverne que la théorie ne prend pas en compte.

- L'intérêt d'utiliser le programme couplé apparaît davantage encore sur la figure 21 qui montre l'évolution des trois mêmes coefficients globaux instationnaires en fonction du braquage moyen de la gouverne pour une fréquence réduite donnée à $M_{\infty} = 0,3$. Les coefficients donnés par la théorie linéarisée sont constants, puisque par hypothèse l'écoulement instationnaire ne dépend pas de l'écoulement moyen. Les coefficients donnés par le programme BERTIN en fluide parfait varient très faiblement lorsque le braquage moyen de la gouverne varie de -10° à $+10^{\circ}$. Par contre les coefficients de portance et de moment de tangage instationnaires donnés par le programme couplé sont assez proches des coefficients expérimentaux et évoluent de la même façon avec le braquage moyen : le module décroît de plus en plus vite lorsque la charge moyenne de l'aile augmente et la phase évolue dans le sens d'une avance lorsqu'on approche des configurations où

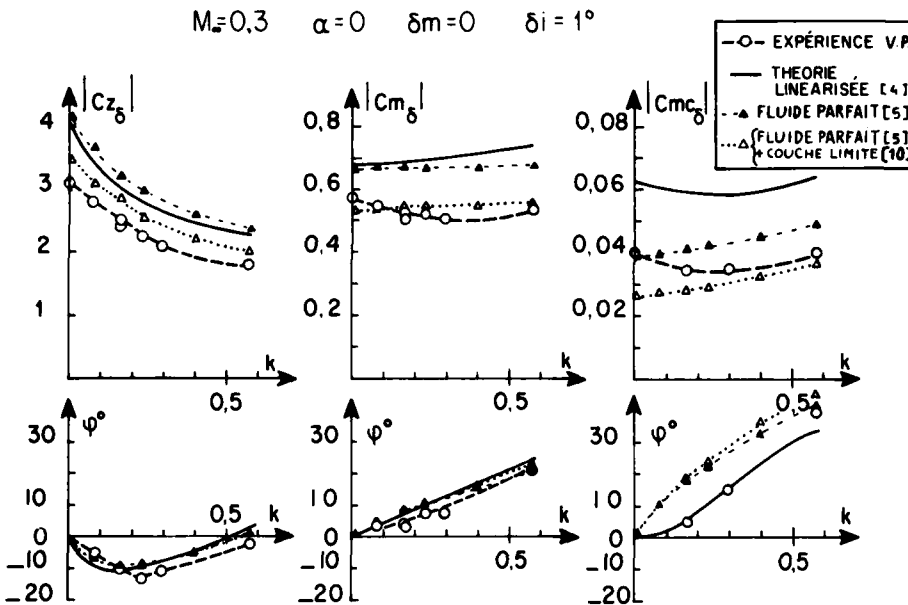


Fig. 20 - Coefficients de portance, de moment de tangage et de moment de charnière instationnaires : influence de la fréquence réduite, comparaison calculs-expériences.

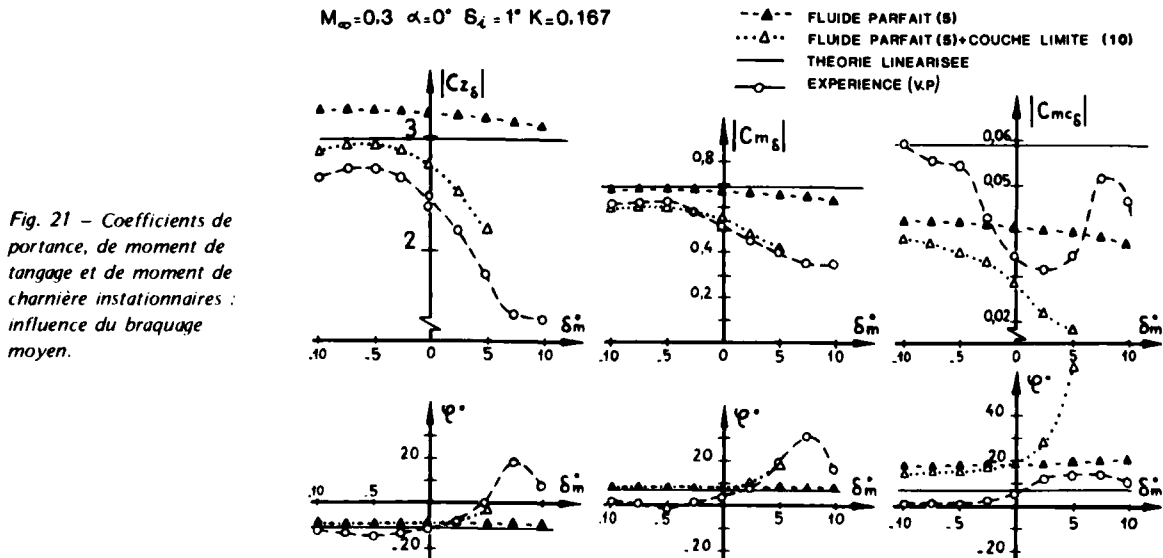


Fig. 21 - Coefficients de portance, de moment de tangage et de moment de charnière instationnaires : influence du braquage moyen.

apparaissent des décollements. On remarquera par ailleurs que le calcul couplé ne donne des phases différentes du calcul en fluide parfait qu'à l'approche des configurations décollées, vers $\delta_m = 5^\circ$. Le calcul couplé n'a pas été poursuivi au-delà de $\delta_m = 5^\circ$ en raison de l'importance des zones décollées. On peut donc conclure que le phénomène de dépendance du braquage moyen qui affecte les performances instationnaires des gouvernes est essentiellement d'origine visqueuse.

$$M_\infty = 0.3 \quad \alpha = 0^\circ \quad \delta_i = 1^\circ \quad K = 0.167$$

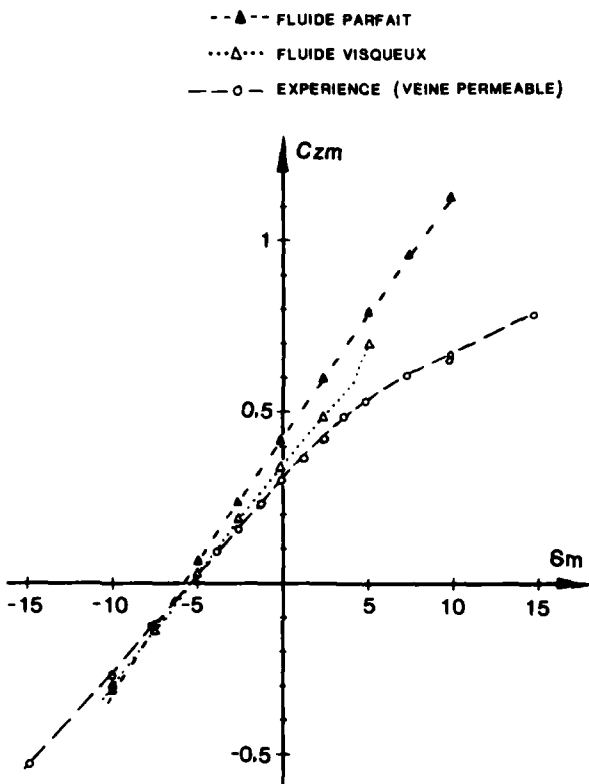


Fig. 22 - Comparaison calcul -expérience sur la valeur moyenne de la portance.

En ce qui concerne le moment de charnière, le calcul couplé montre une évolution en fonction du braquage moyen plus importante que le calcul en fluide parfait, mais les valeurs théoriques s'éloignent de plus en plus des valeurs expérimentales pour les grands braquages, ce qui peut s'expliquer par les raisons déjà citées précédemment.

En dehors de cette imprécision sur le moment de charnière, le programme couplé offre donc de multiples avantages, aussi bien du point de vue de la prévision des coefficients instationnaires que de celle des valeurs moyennes, comme le montre la figure 22 où l'on a tracé les valeurs moyennes du coefficient de portance en fonction du braquage moyen de la gouverne.

Pour tenter d'expliquer les écarts constatés entre les résultats expérimentaux et ceux du programme couplé, il faut rappeler que la couche limite a été supposée entièrement turbulente à partir d'un point situé arbitrairement vers 8% du bord d'attaque. De plus les résultats d'essais n'ont pas été corrigés des effets de paroi.

3.3.2 - Subsonique élevé et domaine super-critique.

La théorie linéarisée étant incapable de prévoir l'existence des chocs, seules les comparaisons avec le programme de petites perturbations transsoniques de CARADONNA seront considérées.

19-11

En régime supercritique, la position des chocs est un point crucial, et elle est fortement influencée par les effets de paroi. C'est pourquoi les calculs ont été effectués à incidence et nombre de Mach corrigés de l'effet de paroi stationnaire, le seul qui puisse être valablement estimé actuellement. En veine guidée, cet effet de paroi est assimilable à une correction de nombre de Mach et a pu être estimé correctement comme on a pu le voir avec les calculs stationnaires (fig. 13 à 16). En veine perméable, l'effet de paroi a été estimé empiriquement et assimilé à une correction d'incidence proportionnelle au coefficient de portance moyen pour un nombre de Mach donné.

En tout état de cause, les variations de portance dues aux petits mouvements de la gouverne (1° d'amplitude) étant relativement faibles, on suppose a priori que les effets de paroi purement instationnaires ont une influence limitée sur les résultats, même pour des fréquences réduites déjà importantes de l'ordre de 0,165 ou 0,235.

$$M_\infty = 0.6 \quad \alpha = 0^\circ \quad K = 0.23 \quad \delta_m = -0.25^\circ \quad \delta_i = 1^\circ$$

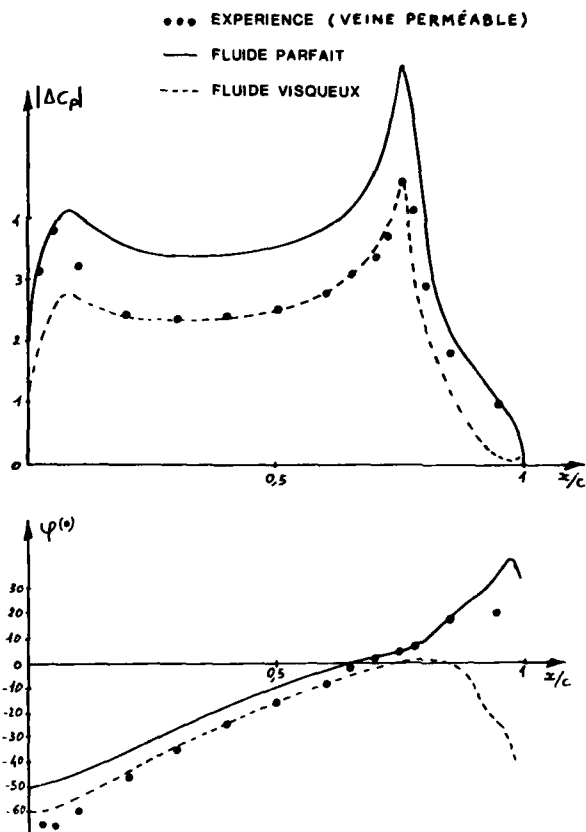


Fig. 23 - Comparaison des pressions instationnaires expérimentales avec la théorie des petites perturbations transsoniques et mise en évidence des effets visqueux.

La figure 23 montre la répartition de portance locale instationnaire $\Delta C_p = C_{p\text{INTA}} - C_{p\text{EXTR}}$ le long de la corde, en module et phase, en veine perméable à $M_\infty = 0,6$, nombre de Mach à partir duquel apparaissent les premiers points soniques au bord d'attaque extrados en écoulement stationnaire. Dans ce cas, la méthode des petites

19-12

perturbations transsoniques couplée avec le calcul de couche limite donne de très bons résultats, le couplage ayant pour effet de diminuer les modules (comme en bas subsonique) mais d'accroître le retard de phase, pour une configuration moyennement chargée (C_z moyen $\approx 0,3$).

Les figures 24 et 25 présentent les évolutions en corde des pressions instationnaires d'extrados à deux autres nombres de Mach pour lesquels on observe un choc, à la même fréquence réduite et dans la même configuration de veine qu'à $M_{\infty} = 0,6$. La figure 26 présente un cas en veine guidée.

Dans l'ensemble, le calcul en fluide parfait par la méthode des petites perturbations transsoniques prévoit assez bien l'allure des phénomènes expérimentaux avec des pics sur la courbe des modules et des sauts de phase plus ou moins accentués liés au déplacement du choc. Ces singularités sont situées plus en aval que dans l'expérience, mais elles se placent beaucoup mieux et l'ordre de grandeur des modules des pressions instationnaires est plus correct lorsque l'on tient compte de la couche limite.

Mais lorsque le choc vient à moins de 30% du bord d'attaque, soit par le calcul en fluide parfait (fig.24), soit du fait de la couche limite (fig.24, 25), il perd son caractère de singularité et donne lieu à un maximum peu important sur les modules. Ceci est peut être attribuable au fait que la méthode de petites perturbations manque de précision au bord d'attaque, surtout pour un profil de 16%.

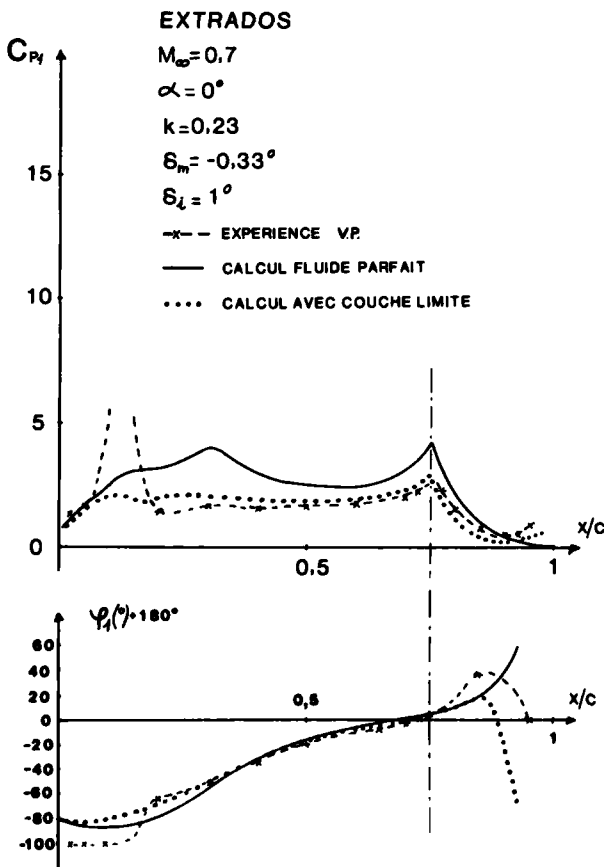


Fig. 24 - Comparaison des pressions instationnaires expérimentales avec la théorie des petites perturbations transsoniques et mise en évidence des effets visqueux.

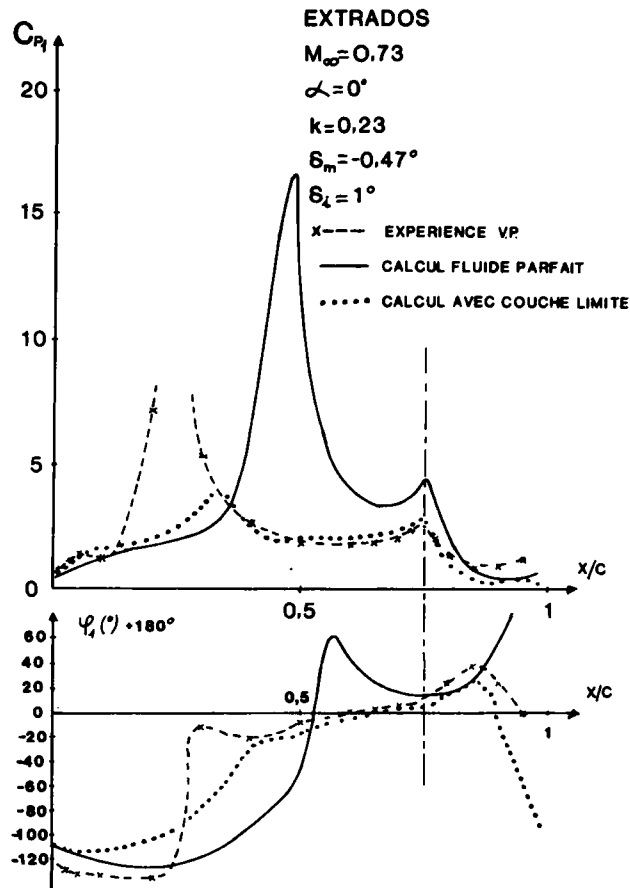


Fig. 25 - Comparaison des pressions instationnaires expérimentales avec la théorie des petites perturbations transsoniques et mise en évidence des effets visqueux.

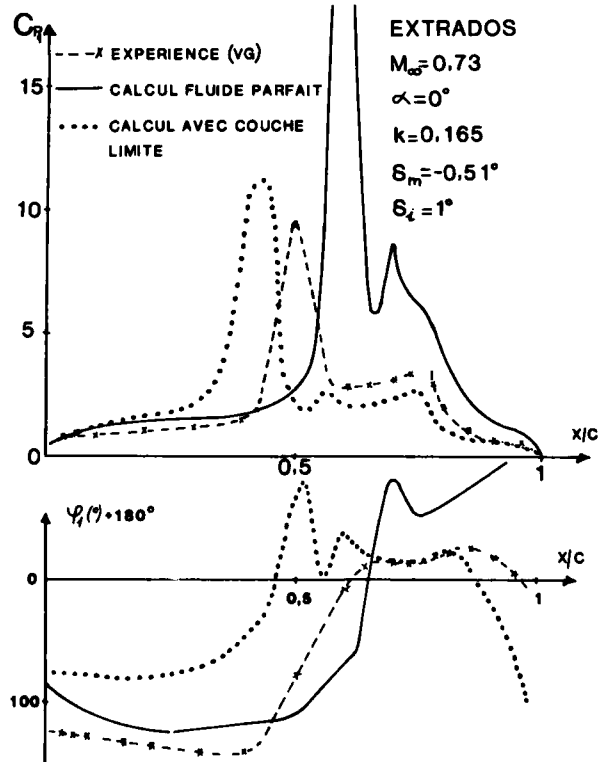


Fig. 26 - Comparaison des pressions instationnaires expérimentales avec la théorie des petites perturbations transsoniques et mise en évidence des effets visqueux.

Pour le cas en veine guidée (fig.26) à un nombre de Mach et une fréquence réduite déjà importants, bien que la correction du nombre de Mach ait été estimée de façon satisfaisante d'après les calculs effectués en écoulement stationnaire (fig.13 à 16), les calculs couplés actuels font un peu trop avancer le choc, l'ordre de grandeur des pressions instationnaires restant correct. En ce qui concerne la phase, le fluide parfait donnant déjà dans ce cas un retard insuffisant du bord d'attaque, la couche limite accentue cet écart en diminuant la taille de la zone supersonique, source de retard. A l'aval du choc, la couche limite agit comme à $M_{\infty} = 0,6$ en apportant un retard de phase assez important.

La figure 27 récapitule pour quelques cas la valeur moyenne, l'amplitude de variation et la phase de la portance expérimentale et théorique avec et sans couche limite.

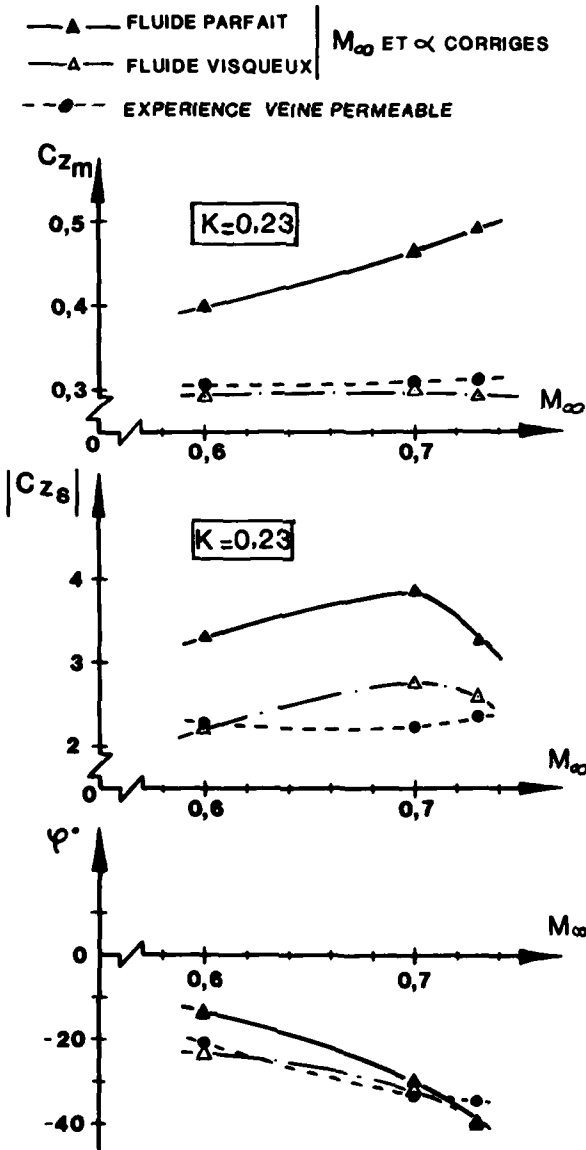


Fig. 27 - Comparaison calculs-expérience sur la valeur moyenne, l'amplitude de variation et la phase de la portance en transsonique : mise en évidence des effets visqueux.

4 - CONCLUSION -

Cette étude montre que dans beaucoup de cas, la réponse aérodynamique instationnaire due à un

mouvement de gouverne dépend fortement des conditions d'écoulement moyen sur l'ensemble profil et gouverne. Il semble que ce phénomène soit dû en grande partie à la viscosité. L'emploi des théories linéarisées pour prévoir les réponses aérodynamiques instationnaires est donc en fait très limité, et il est nécessaire de recourir à des méthodes de fluide parfait non linéaires qui devront être couplées avec un calcul de couche limite.

A cet égard, les résultats des premières tentatives de couplage sont encourageants. Cependant il est nécessaire de pouvoir disposer d'une méthode de fluide parfait aussi précise que possible, sans oublier le compromis entre précision désirée et rapidité du calcul. D'autre part il reste des progrès à faire dans les techniques de couplage, notamment en ce qui concerne le traitement des zones décollées et des interactions onde de choc-couche limite. Il faudra enfin s'efforcer de prendre en compte soit expérimentalement soit par le calcul les effets de paroi instationnaires.

REFERENCES

- [1] R.GRENON, J.THERS -
Etude d'un profil supercritique avec gouverne oscillante en écoulement subsonique et transsonique
AGARD CP 227
- [2] BAVITZ -
An Analysis method for two-dimensional transonic viscous flow.
NASA TN/D 7718
- [3] J.BOUSQUET -
Calculs bidimensionnels transsoniques avec couche limite. 11ème Colloque AAAF 1974
- [4] E. ALBANO, W.P. RODDEN -
A doublet lattice method for calculating lift distributions on oscillating surfaces in subsonic flow.
AIAA Journal vol. 7 n° 2 (1969).
- [5] N.BAUDU, TH. LE -
Etude du comportement aérodynamique d'un profil avec gouverne oscillante.
R.S.F. BERTIN Note 75 CC 06 (1975).
- [6] J.P. GIESING -
Non linear two dimensional Unsteady potential flow with lift.
Journal of Aircraft, vol. 5 n° 2 (1968).
- [7] F.X. CARADONNA (USA AMRDL), J.J.PHILIPPE (ONERA)
The flow over a helicopter blade tip in the transonic regime.
ONERA TP 1976-115.
- [8] M.COUSTON, J.J.ANGELINI -
Solution of Nonsteady Two-dimensional Transonic small disturbances Potential Flow Equation.
ONERA T.P 1978-69 Communication présentée au Symposium sur la Dynamique des Fluides Instationnaires organisé par l'ASME, San-Francisco, 10-15 Décembre 1978.

19-13

- [9] A. LERAT, J. SIDES -
Simulation numérique d'écoulements transsoniques à l'aide des équations d'Euler sous forme intégrale.
ONERA - T.P. 1979-10, Communication présentée à la 21e Conférence Annuelle sur l'Aviation et l'Astronautique, Tel-Aviv et Haïfa (ISRAEL), 28 février - 1er mars 1979.
- [10] J. COUSTEIX, R. HOUEVILLE, A. DESOPPER -
Résultats expérimentaux et méthodes de calcul relatifs aux couches limites turbulentes en écoulement instationnaire.
AGARD CP 227 (1977)
- [11] J.C. LE BALLEUR -
Couplage visqueux - non visqueux : analyse du problème incluant décollements et ondes de choc.
La Recherche Aérospatiale 1977 n° 6
(Novembre - Décembre).
- [12] H. TIJDEMAN, R. DESTUYNDER -
Comments on transonic and Wing Store Unsteady aerodynamics :
High subsonic and transonic effects in Unsteady aerodynamics, by H. TIJDEMAN
AGARD Report 636

AERODYNAMIC CHARACTERISTICS OF MOVING TRAILING-EDGE CONTROLS
AT SUBSONIC AND TRANSONIC SPEEDS

20-1

by

D G Mabey, D M McOwat and B L Welsh

Structures Department, Royal Aircraft Establishment, Bedford, UK

SUMMARY

This paper compares oscillatory pressures calculated and measured at high subsonic speeds for a swept back wing of aspect ratio 6 with a part-span trailing-edge flap. The flap was driven at frequencies of 1 Hz (quasi-steady) and 90 Hz at Mach numbers from 0.40 to 0.95 with both fixed and free transition over a range of Reynolds numbers from 10^6 to 4×10^6 .

The measured oscillatory pressures depend strongly on the boundary-layer displacement thickness at the hinge line. Hence extrapolation from model to full scale requires great care. In subsonic flow, tests with free transition give the thinnest turbulent boundary layer at the hinge line and come nearest to full scale. However, at transonic speeds transition should be fixed at a safe distance upstream of the most forward excursion of the shock wave to obtain results appropriate to higher Reynolds number.

Tests with flap driven simultaneously at two frequencies (90 Hz and 131 Hz) at subsonic and transonic speeds produce the same oscillatory pressures at 131 Hz as when driven independently. Hence the principle of superposition applies, at least for small amplitude motions with attached flows.

NOTATION

C_p / δ	magnitude of vector of oscillatory pressure per radian flap deflection
C_f	local skin friction coefficient
c, \bar{c}, c_o	local, average, and root chords
f	frequency (Hz)
$h_\beta, h_\beta^i; m_\beta, m_\beta^i; z_\beta^i, z_\beta$	respectively hinge moment, pitching moment and lift derivatives in phase and in quadrature with flap displacement (Ref 1)
M	Mach number
P_t	tunnel total pressure
\bar{p}	rms pressure fluctuations
q	kinetic pressure
R	unit Reynolds number
U	stream velocity
x	streamwise distance from local leading-edge
α	angle of incidence
β	flap deflection in streamwise plane (radians, Ref 1)
δ	flap deflection normal to hinge line (radians, unless otherwise stated)
δ_1	boundary layer displacement thickness
n	spanwise distance as a fraction of semi-span
ϕ	phase of pressure oscillation relative to flap motion (deg, positive for pressure leading displacement)
v	frequency parameter = $2\pi f \bar{c} / U$

SUBSCRIPTS

e	local external flow conditions
t	transition position

1 INTRODUCTION

20-2 The effective use of active controls for load alleviation or flutter suppression requires a better knowledge of the dynamic characteristics of aerodynamic controls than is currently available, for even at subsonic speeds wide differences frequently occur between calculations and measurements in wind tunnels. As an example, Fig 1 shows some measurements¹ of the total dynamic lift induced by an oscillating flap on a low aspect ratio wing. The total lift was measured with a dynamic balance fully described in Ref 2. The lift derivative in phase with the motion ($z_{\dot{\theta}}$) is only about 60% of that predicted by the linear theory of Ref 3 over the Mach number range from $M = 0.6$ to 0.9 . The measured lift in quadrature with the motion ($z_{\dot{\theta}}$) does not even have the trend with Mach number predicted by the theory. Fig 2 shows similar evidence for the pitching moment. The position with regard to the flap hinge moment is even more unsatisfactory. Fig 3 shows that the hinge moment in phase with the motion ($-h_{\dot{\theta}}$) decreases with Mach number, whereas the theory predicts an increase. In contrast, the hinge moment in quadrature with the motion ($-h_{\dot{\theta}}$) shows the correct trend against Mach number, but is only about 60% of that predicted. These anomalies on a simple configuration of 5% thickness/chord ratio were tentatively explained in Ref 1 in terms of a semi-empirical correction for aerofoil section and boundary layer effects together with a correction for wall interference. However both corrections were restricted to low frequency and to subcritical flow and would not be applicable to other configurations. Similar anomalies have been cited previously on a number of aerofoils, the measured forces being about 70% of those predicted⁴. For aerofoils the anomalies discussed are often attributed to the omission of wing and boundary layer thickness from the calculations and when these thicknesses are included some improvement is achieved⁴. However no direct experimental evidence for thickness and boundary layer effects has yet been adduced for wings with oscillating controls.

To provide clear evidence of the importance of boundary layer thickness, and to highlight the uncertainties in the linearized theories at transonic speeds and moderately high frequencies, an extensive series of oscillatory pressure measurements has been made, with both fixed and free transition, on a half model of a swept wing of aspect ratio 6 with a trailing-edge flap (Fig 4). This symmetric wing 9% thick (RAE Wing A) was tested mainly at zero incidence. For a wing of this type an understanding of the unsteady flow and how it is affected by Reynolds number is likely to be important in the design of an active control system. This paper provides a preview of some of the more interesting results from the experiments; a full account will be published later⁵.

2 EXPERIMENTAL DETAILS

2.1 Pressure measurements

Fig 4 shows the position of the four spanwise stations used for the pressure measurements, and the flap.

The oscillatory pressures were measured by small transducers (Kulite type XCQL 093-25A) mounted close to the pressure holes to ensure only small changes in the amplitude and phase. With the installation used amplitude errors are estimated to be less than 1.5% and phase errors less than 1.5° , for the highest test frequency (131 Hz). The steady pressures were measured in a separate test in the traditional way by connecting the static pressure holes through long lengths of piping to manometers outside the tunnel. With new amplifiers developed at RAE⁶ the same pressure transducers can now measure both dynamic and static pressure distributions simultaneously.

2.2 Model construction

The method of construction was unusual. The model was made in two halves to allow access to the pressure transducers and to the drive shaft of the flap (Fig 5). These halves were then screwed together and produced a flexible model, which responded significantly to the flow unsteadiness in the tunnel when the flap was undriven. The structural response was a minimum at 90 and 131 Hz and so these frequencies were selected for driving the flap. Nevertheless the flap inertia and the aerodynamic loads developed by the flap forced significant wing deflections, which were determined by internal miniature accelerometers. Typical values of the amplitudes of these deflections are: 2 mm at the wing tip and 0.2° twist. No corrections have yet been made to the measured oscillatory pressures for these wing motions, although in principle this should be possible. When active control systems are used in flight similar dynamic wing deflections may occur because aircraft are relatively flexible - as illustrated by well known static aeroelastic phenomena such as aileron reversal and wing divergence.

2.3 Boundary layer measurements

A novel method was used to estimate the boundary layer displacement thickness, δ_1 , just upstream of the flap hinge line. Instead of making measurements of the boundary layer profile, at several stations on the wing, the local skin friction was inferred from the reading of a single Preston tube of diameter 1 mm just upstream of the flap hinge line and inboard of the flap (Fig 4). The skin friction coefficient, C_f , was computed using the method of reference 7; a probe correction of $0.15 \times$ probe diameter was applied to the distance from the aerofoil surface to the centre of the Preston tube. The boundary layer Reynolds number based on the displacement thickness δ_1 , $R\delta_1$, was inferred from the $C_f - R\delta_1$ relation derived from a viscous three-dimensional flow calculation made by Roberts⁸. This calculation showed (Fig 6) that on the hinge line at $M = 0.40$ there was

a unique relation between C_f and $R_{\delta 1}$, both inboard of the flap (at $\eta = 0.28$) and outboard of the flap (at $\eta = 0.80$). The calculations also showed that C_f at the hinge line only increased a little with the rearward movement of the transition point from $x_t/c = 0.125$ to 0.25 . Hence the same curve could be used to make rough estimates of the boundary-layer thickness at the hinge line for transition-free measurements. Fig 6 shows that the predicted C_f 's are appreciably lower than the corresponding two-dimensional flat plate C_f 's. This is because of the change in boundary-layer profile due to the small adverse pressure gradient towards the rear of the aerofoil. The insert in Fig 6 shows that at a typical station the measured and calculated viscous pressure distributions are in good agreement, despite the unusual method of construction of the model, which involves a discontinuity at the leading-edge and a trailing-edge of small thickness. 20-3

The shape of the pressure distribution remains essentially unchanged in character from $M = 0.40$ to 0.85 so that Fig 6 should be quite adequate to estimate comparative variations in boundary layer thickness at subsonic speeds. The change in the character of the pressure distribution at transonic speeds prevents Fig 6 from being used to estimate the boundary layer thickness at the hinge line at $M = 0.90$ and 0.95 . However, predictions from a viscous transonic flow calculation by Firmin for $M = 0.90$ have recently become available⁹, and these have been used to indicate the probable magnitude of the boundary layer thickness, although the predicted skin friction coefficients are appreciable lower than the measurements (Fig 12).

2.4 Test conditions

The model was mounted on the sidewall of the RAE 3ft x 3ft tunnel and tested over the Mach number range from $M = 0.40$ to 0.95 in the top and bottom slotted section (0.91 m wide x 0.64 m high). Table I lists the Reynolds numbers and boundary layer thicknesses for the oscillatory pressure measurements cited here, and gives typical full scale values.

TABLE I

Standard Test Conditions $p_t = 0.95$ bar			
Mach Number	Reynolds Number	Boundary Layer Thickness	
M	$10^{-6} \times R_{c_0}$	$10^3 \delta_1/c_0$	
		Free	Fixed
0.65	2.8	1.7	2.9
0.80	3.1	2.3	3.7
Predicted values			
0.90	3.3	-	3.9
Typical full scale values			
0.80	120.0	0.7	-

The other tunnel total pressures, p_t , were 0.24, 0.47 and 1.52 bar, giving Reynolds numbers in the range from $R_{c_0} = 10^6$ to 6×10^6 . The roughness band was formed by a thin steel strip 1.6 mm wide glued at $x/c = 0.05$ on both surfaces of the wing. The steel strip was indented by a pyramidically pointed needle to give "coronets" 0.13 mm high 2 mm apart. This roughness was judged to be as effective as a distribution of spheres of 0.13 mm diameter, and could be applied more readily and repeatably.

3 RESULTS

Fig 7 shows that although the wing flow at $\alpha = 0^\circ$ is three-dimensional, the local Mach number contours are swept and straight for two typical free-stream Mach numbers. $M = 0.80$ (subsonic) and $M = 0.90$ (transonic). The flow for $M = 0.80$ is just subcritical, the maximum local Mach number $M_e = 0.96$ occurring near quarterchord, while $M = 0.90$ introduces supersonic flow over half the wing and a peak value of about $M_e = 1.20$ in the region of 35% chord. After consideration of the measured and calculated oscillatory pressure distributions, the role of transition fixing and the influence of the boundary layer is discussed.

3.1 Comparisons with theory

Fig 8 shows a typical comparison of the measured chordwise oscillatory pressure distributions with fixed transition at four spanwise positions for $M = 0.80$ with predictions according to an inviscid linearised theory for three-dimensional flow, developed by Marchbank¹⁰. These measurements are conveniently represented by the magnitude of the vector, C_p/δ , and the phase angle ϕ relative to the movement of the flap.

On the control (at $\eta = 0.45$ and 0.60) the magnitude, C_p/δ , in Fig 8a is large close to the hinge line and agrees well with the linearised theory as far as 75% chord; aft of this the aerofoil thickness and the boundary layer combine to lower the loading. Just inboard of the control at $\eta = 0.35$ the magnitudes are much smaller but still in good

agreement with the predictions. In contrast, just outboard of the control at $\eta = 0.7$, the magnitudes remain fairly high. However the measurements show anomalous variations from 10% to 40% chord which are not in accord with the predictions and which are tentatively attributed to a small laminar separation bubble⁵.

The phase angle of the pressures in Fig 8b shows an interesting variation from section to section. Over the span of the control the measured phase angles lag appreciably behind the predictions, and this must be attributed to the lag effects associated with the higher local velocities caused by the wing thickness. However, just off the control the measured phase angles actually lead the predictions.

More complex and interesting spanwise variations develop at transonic speeds, which are discussed elsewhere⁵. No theoretical calculations of the oscillatory flow are currently available for supercritical flow conditions.

Fig 9 shows another comparison at $M = 0.65$ and $\eta = 0.60$ for two flap amplitudes of 0.5° and 2° at a frequency of 90 Hz. Flap amplitude has only a small influence on C_p/δ and a negligible influence on the phase angle. Upstream of $x/c = 0.6$ the measured C_p/δ is in excellent agreement with the predictions, but there are minor deviations close to the hinge line. The measured phase angles lag about 10° behind those predicted, just as at $M = 0.80$, and may again be attributed to the higher local Mach numbers due to wing thickness.

3.2 Principle of superposition

For active control technology it is important to know the limits of linearity of the pressures induced by control displacement, because these limits determine the region within which the principle of superposition is valid. Fig 10 illustrates some results of a brief preliminary investigation of this question at subsonic and transonic speeds with fixed transition.

With regard to the superposition of different flap frequencies at subsonic speeds, Fig 10a shows the chordwise variation of the oscillatory pressures at $\eta = 0.45$ (Section 2 of Fig 4); the content of oscillatory pressures at 131 Hz is virtually unchanged when a flap oscillation amplitude of 1° at 90 Hz is added to one of amplitude 1° at 131 Hz. Thus the results shown in Figs 9 and 10a and similar tests at $M = 0.80$, confirm that the principle of superposition is valid at subsonic speeds, at least within this restricted range of amplitudes and frequencies.

Fig 10a includes predictions for the higher frequency. The magnitude of the vector is now only in agreement with the predictions upstream of $x/c = 0.4$ (cf $x/c = 0.6$ for the lower frequency in Fig 9), the phase angles measured now lag about 10° to 20° behind those predicted. Thus at the higher frequency the predictions are somewhat less satisfactory, and the phase difference between the measurements and the predictions is roughly proportional to the frequency parameter.

Only a limited test of the principle of superposition was made at transonic speeds. Fig 10b shows the chordwise variation of the oscillatory pressures at $\eta = 0.45$; the frequency content of the oscillatory pressures at 131 Hz is hardly changed when a flap oscillation of amplitude 1° at 90 Hz is added to one of amplitude 1° at 131 Hz, just as at the subsonic speed.

3.3 Transition measurements

The boundary-layer transition position for $\eta = 0.60$ was inferred from the movements of peaks in the surface pressure fluctuations with tunnel total pressure, p_t , when the flap was undriven. On flat plates and cones this method reveals a peak in the broad-band pressure fluctuations of about $p/q = 1.0\%$ in the middle of the transition region¹¹, where rapid local changes in thickness occur within the boundary layer. On a wing the mean pressure gradients at subsonic speeds, and shock waves at transonic speeds, make the interpretation of the surface pressure fluctuation measurements more difficult. This difficulty can be partially overcome by using the local kinetic pressure, q_e , as a reference. Moreover comparison of transition free and transition fixed results generally eliminates any ambiguities. Fig 11 shows some typical transition-free measurements. At $M = 0.80$, Fig 11a shows two well-defined peaks, indicating transition just forward of the hinge line at the lower total pressure $p_t = 0.24$ and 0.47 bar. At the higher pressures, $p_t = 0.95$ and 1.52 bar, the peaks occur at about 40% chord. By comparison with the transition-fixed measurements, we may infer that transition is roughly about 30% chord. In contrast, at transonic speeds Fig 11 shows well-defined high peaks at all pressures. These peaks are caused by the oscillation of the shock terminating the local supersonic region. Initially the peaks and the shock wave/boundary layer interaction move forward as p_t increases because the transition front moves forward as the Reynolds number increases. (In contrast, with transition fixed close to the leading-edge a shock wave would generally move slowly downstream as Reynolds number increases). The large peak pressure fluctuations at the lower pressures ($p_t = 0.24$ to 0.95) indicate laminar shock wave/boundary layer interactions. The smaller peak pressure fluctuation at the higher pressures ($p_t = 1.52$ bar) indicates a turbulent shock wave/boundary layer interaction of more limited extent. Laminar interactions are, of course, much longer than turbulent interactions and therefore are more likely to create large peak pressure fluctuations. A similar change in peak p/q in going from a laminar to a turbulent interaction was also reproduced at lower total pressures transition fixed (omitted here for brevity). Hence at transonic speeds the variation of peak pressure

fluctuations with Reynolds number can be a valuable guide to the state of the boundary layer at the shock even though it cannot give the precise transition position.

20-5

With the roughness band at the standard test pressure ($p_t = 0.95$ bar), transition was always close to the leading-edge so that the boundary layer at the hinge line was excessively thick relative to full-scale values. Hence from the point of view of the trailing-edge flap, the boundary layer at the standard pressure must be described as "overfixed", with all the difficulties that this condition is known to introduce for steady measurements. (See for example the discussion in Refs 12 and 13).

3.4 Skin friction measurements

Fig 12 shows the local skin friction coefficients derived from the Preston tube readings as a function of the Reynolds number based on the root chord. It is convenient to consider first the Mach number range from $M = 0.40$ to 0.90 . Here the skin friction measurements with both free and fixed transition all fall monotonically with Reynolds number. This shows that the boundary layer is always turbulent at the hinge line, even at the lowest Reynolds number. This inference is consistent with the transition measurements. The skin friction is always significantly higher with transition free than with transition fixed, confirming that the transition free boundary layer is appreciably thinner at the hinge line and more representative of full scale flow over the control surfaces.

The transition fixed skin friction measurements at $M = 0.40$ may be compared directly with the estimates given by Roberts⁸. For the higher Reynolds number ($Re_0 > 10^6$) the measured transition fixed skin friction coefficients are about 3% lower than the estimates, consistent with a thicker boundary layer. This is because at these high Reynolds numbers natural transition is close to the roughness band at $x/c = 0.05$ whereas the estimates assume a transition position further downstream at $x/c = 0.125$. In marked contrast, at the lower Reynolds numbers ($Re_0 < 10^6$), the measured skin friction coefficients with fixed transition are appreciably higher than the estimates, consistent with transition moving progressively further downstream of $x/c = 0.125$ as Reynolds number decreases and with the roughness band becoming less effective. A rearward movement of transition at low Reynolds numbers would significantly increase the local skin friction at the measurement station, according to the estimates⁸ included in Fig 12.

The skin friction measurements at $M = 0.95$ are included in Fig 12 to illustrate the dangers inherent in making aerodynamic measurements at transonic speeds with transition free. As the Reynolds number increases, the skin friction first increases and then decreases rapidly as mean position of the shock alters. In marked contrast, with transition fixed the skin friction coefficient decreases monotonically with Reynolds number, just as at the lower Mach numbers. This is consistent with relatively minor movements of the shock wave around $x/c = 0.50$ and with appreciable variations in boundary layer thickness. For this wing, at $M = 0.95$ and zero incidence, it would have clearly been preferable to fix transition with a roughness band at, say, $x/c = 0.3$ rather than at $x/c = 0.05$.

Fig 13 shows the variation of the ratio of the boundary layer displacement thickness at the Preston tube to the root chord, δ_1/c_0 , with Mach number and Reynolds number both with transition free and fixed.

Considering first the measurements at $M = 0.40$, we see that with transition free the boundary layer thickness ratio increases monotonically with Reynolds number while the transition point moves progressively further upstream. In contrast, with transition fixed the boundary layer thickness ratio initially increases rapidly with Reynolds number as the roughness initiates transition and rapidly moves the transition front close to the roughness band¹⁴. Further increase in Reynolds number then slowly decreases the boundary layer thickness ratio. At the standard test pressure, $p_t = 0.95$ bar, the displacement thickness of the boundary layer is 50% thicker with transition fixed than with transition free. The predictions by the three-dimensional viscous flow calculations show that a boundary layer thickness ratio appropriate to a full-scale Reynolds number of 120×10^6 ($\delta_1/c_0 = 0.0007$) could have been achieved with transition free at a greatly reduced Reynolds number of 0.6×10^6 . Although it is not suggested that this method of simulation would be entirely adequate, it should be worth a more detailed investigation in future tests, in view of the strong influence of boundary layer thickness on pressure measurements for oscillating trailing-edge flaps.

The results at higher speeds are similar in character to those at $M = 0.40$, with the boundary layer thickness ratio increasing with Mach number, presumably because of the increasing adverse pressure gradient at the rear of the wing. The important point to notice from Fig 13 is that a marked difference in boundary layer thickness ratio is maintained between transition free and transition fixed measurements at all Reynolds numbers.

3.5 Influence of boundary layer

We now consider the influence of the boundary layer on the oscillatory pressures measured across the chord of a typical spanwise section $\eta = 0.60$ (Section 3 of Fig 4).

In general, with the thin turbulent boundary layer at the hinge line allowed by free transition, the flap lift curve slope is significantly increased relative to the value with the thick turbulent boundary layer formed with fixed transition. Thus at $M = 0.80$ (Fig 14) the increase in flap lift curve slope produces a significant increase in the magnitude of the oscillatory pressures measured over the whole section. A similar increase was expected and observed in the quasi-steady measurements. However in addition with the thinner

boundary layer there is a significant increase (about 6°) in the phase lag of the oscillatory pressures over the forward portion of the section, whereas over the central portion this increase is only about 3° . This change in phase angle was unexpected and is more difficult to explain than the increase in the magnitude of the vector. Moore's review¹⁵ of the limited information available in 1969 on the scale effects on control-surface derivatives suggested that with a thinner boundary layer (obtained either by increasing Reynolds number or by allowing free transition), stiffness derivatives increased but damping derivatives were unaltered. Thus, as in the present measurements, the magnitude of the force vector was increased but there was a decrease in phase lag contrary to the present measurements. Moore concluded that, to obtain results closest to full-scale values, tests with oscillating trailing-edge controls were best made transition free. The change in phase angle is unlikely to be caused by the small differences in the distributions of Mach number in the mean flow between transition fixed and free. In a rough attempt to quantify the effect of these small differences, Tijdeman's two-dimensional acoustic wave formula¹⁶ was used to estimate the equivalent phase lag for a source mounted at the hinge line. The relaxation factor assumed was 0.7, as Tijdeman found appropriate for an oscillating wing, but essentially similar results would have been found with a relaxation factor of 1.0. The dotted curve in Fig 14 shows that the differences between the predicted phase lags with transition fixed and free are negligible. However, the phase lags predicted are much larger than those measured, so that the two-dimensional acoustic theory is plainly inappropriate for this three-dimensional situation, although it suggests that the large change in phase angle may be a dynamic phenomenon within the boundary layer.

Now at any given subsonic Mach number and Reynolds number (ie for a very wide range of transition positions) the same trends occur as those illustrated in Fig 14. Hence the viscous phenomena influencing the changes in both magnitude and phase angle are probably determined by the thickness of the turbulent boundary layer at the hinge line, rather than the influence of the laminar portion of the boundary layer upstream of transition.

Fig 14 also includes the predictions according to linearised theory¹⁰. Generally the magnitude of the vector is well predicted. Although upstream of $x/c = 0.60$ the predictions are in better agreement with the measurements made with transition fixed rather than with transition free, this should be considered fortuitous, because the theory takes no account of wing or boundary layer thickness. Close to the hinge line the predictions are, in fact, in better agreement with the measurements made transition free. It is important to recall that at $x/c = 0.30$ the local Mach number is 0.96, so that such good agreement is really surprising.

As regards phase angles the theory predicts an oscillatory pressure at $x/c = 0.05$ which lags by about 50° . The pressure observed lags by about 60° . Similar discrepancies in phase angle are observed right across the section and must be attributed to the higher local velocities caused by the wing thickness.

When the wing flow is transonic, the pressures produced by oscillation of the flap are dominated by the type of shock wave/boundary layer interaction (Fig 15). Thus at $M = 0.90$, when transition is free, we have seen that the shock wave/boundary layer interaction is laminar and extends over a long portion of the chord (say from $x/c = 0.3$ to 0.6). The interaction causes large oscillatory pressures in this region in addition to the large oscillatory pressures which would be expected in the subsonic portion of the flow field close to the hinge line. In marked contrast, with fixed transition the oscillatory pressures associated with the shock are somewhat smaller and concentrated about the mean shock position at $x/c = 0.3$. Downstream of the turbulent shock wave/boundary layer interaction the oscillatory pressures first fall rapidly and then increase towards the hinge line. The magnitude of this increase is quite small until the hinge line is approached, and its character resembles that observed in the same region at $M = 0.8$ (cf Fig 14). The measurements suggest that the flap lift slope is still appreciably higher with the thin turbulent boundary layer produced by free transition. In addition we notice that there is once again a significant change in phase angle, for upstream of $x/c = 0.5$ the transition free measurements lag behind those with transition fixed by about 10° to 20° . This lag is in the same sense as that observed at subsonic speeds (Fig 14). This again suggests that the lag is not primarily caused by a changed mean flow, but by a dynamic phenomenon associated with the significant change in the boundary layer thickness. The lack of agreement of these measurements made with transition fixed and free suggests that for transonic speeds transition should always be fixed a safe distance upstream of the maximum forward excursion of the oscillatory shock wave, rather than close to the leading-edge, in an attempt to obtain aerodynamic characteristics appropriate to higher Reynolds number. Thus in Section 3.4 above it was suggested that at $M = 0.95$, with the shock at $x/c = 0.5$, transition should have been fixed at $x/c = 0.30$, rather than at $x/c = 0.05$.

Boundary-layer thickness is likely to have a much greater influence on the characteristics of a trailing-edge flap on a thick supercritical wing, particularly when this operates close to separation. Hence, when testing supercritical wings with oscillating trailing-edge flaps, some boundary layer thickness variation should always be included as an aid to the assessment of full scale performance.

4 FUTURE RESEARCH

The results already obtained on this model are judged to be of sufficient interest to justify a further investigation, particularly of the effects of changes in the boundary layer.

One shortcoming of the present tests is that the pressures were not measured close enough to the trailing edge (eg Figs 9 and 14). Hence the aluminium alloy flap has now been replaced with a stiffer flap (Fig 16) made in carbon fibre with 12 instead of 6 pressure orifices. This flap will be driven electromagnetically at higher frequencies and at larger amplitudes. (From about 20° at 25 Hz to 1° at 200 Hz). The flap amplitude will be more precisely determined with a new type of fibre-optic instrument mounted on the drive shaft¹⁷; this instrument has no significant errors up to frequencies as high as 500 Hz.

Although the results for the tests of superposition are, of course, only established for attached flows, they suggest a useful interim practical application of active control technology to reduce the model response to unsteadiness in the tunnel flow. The model is flexible and responds strongly at the fundamental wing bending frequency (about 60 Hz). During the next series of tests the pressures induced by small amplitude flap oscillations at this frequency will be measured, the corresponding phases and amplitudes of all the wing accelerometers will be noted. These "open loop" measurements will then be used to formulate a suitable "closed loop" control law relating one of the accelerometer responses to an appropriate flap movement to reduce the wing responses and thus extend the fatigue life of the model. Ultimately we intend to extend our measurements of flap effectiveness to conditions of fully separated flow when there is significant buffeting.

Development of an effective method of predicting the pressures induced by an oscillating flap at transonic speeds is considered most important if the full benefits are to be derived from ACT. Although the approximate method suggested by Garner¹⁸ works fairly well for a complete three-dimensional wing pitching about a given axis, it has not been applied successfully to a wing with an oscillating trailing-edge flap. There is evidence that Garner's semi-empirical method underestimates the phase lag in the leading-edge region. It is hoped that the method can be developed to cover this important problem. Perhaps some of the much slower numerical methods now being applied to two-dimensional aerofoils could be developed to cover wings, for these theories can now predict the pressures for both oscillating aerofoils and aerofoils with oscillating flaps (see for example the paper by Isogai¹⁹). However the time taken for three-dimensional calculations of this type may be regarded as uneconomic by the aircraft industry.

5 CONCLUDING REMARKS

On this 9% thick symmetric wing the boundary layer has a large effect on the pressures generated by the oscillating trailing-edge flap, even at zero lift. With the thin turbulent boundary layer at the hinge line allowed by natural transition the flap produces appreciably higher forces at subsonic speeds, as was confirmed by the quasi-steady measurements. However, the increase in phase lag with the thinner boundary layer was not expected and has not yet been explained.

It is essential at transonic speeds to ensure a turbulent shock wave/boundary layer interaction, even in the absence of separation. Ideally the turbulent boundary layer should be as thin as possible. This may be achieved either by fixing transition just upstream of the shock, or by increasing the Reynolds number just until a turbulent shock wave/boundary layer interaction is obtained with free transition.

Although the effects of the boundary layer and wing thickness are not included, the predictions from lifting surface theory provide fair overall agreement with the measurements at subsonic speeds particularly at frequency parameters up to about 0.4. The authors hope that the present measurements at transonic speeds, and those yet to be made, will serve as a challenge to theoreticians to develop adequate theories for this difficult speed range.

REFERENCES

- 1 N C Lambourne, K C Wight, B L Welsh. Measurement of control surface oscillatory derivatives on a swept back, tapered model wing in two transonic tunnels. R&M 3806 1976.
- 2 K C Wight, N C Lambourne. A control surface oscillatory derivative rig for use with half models in high speed wind tunnels. ARC CP 1353 1975.
- 3 D F Davies. Calculation of unsteady generalised airforces on a thin wing oscillating harmonically in subsonic flow. R&M 3409 1963.
- 4 H Tijdeman. High subsonic and transonic effects in unsteady aerodynamics. NLR TR 750790 May 1975.
- 5 D McOwat, B L Welsh, B Cripps. Time-dependent pressure measurements on a swept wing with an oscillating flap at subsonic and transonic speeds. RAE TR in preparation.
- 6 B L Welsh, C R Pyne. A method to improve the temperature stability of semi-conductor strain gauge pressure transducers. RAE TR 77-155, October 1977.
- 7 J M Allen. Use of the Baronti-Libby transformation and Preston tube calibrations to determine skin friction from turbulent velocity profiles. NASA TNP 4853 November 1968.
- 8 A Roberts. The spline-Neumann system: comparison of experimental results for W4 with a preliminary boundary layer treatment. BAC Aero Report 34 1977.
- 9 M Firmin. Private Communication, December 1978.
- 10 W R Marchbank. Evaluation of pressure distribution on thin wings with distorted control surfaces oscillating harmonically in linearised compressible subsonic flow. R&M 3783 1978.
- 11 D G Mabey. Boundary layer transition measurements on the AEDC 10° cone in three RAE wind tunnels and their implications. R&M 3821 1978.
- 12 J F Cahill. Simulation of full scale flight aerodynamic tests in existing transonic tunnels. Paper C20, AGARD CP 83-71 April 1971.
- 13 A B Haines. Further evidence and thoughts on scale effects at high subsonic speeds. Paper 43, AGARD CP 174 October 1975.
- 14 E L Van Driest. Boundary layer transition at supersonic speeds. Three-dimensional roughness effects (spheres). Jn Aero Space Sci Vol 29, p 909, August 1962.
- 15 A W Moore. Scale effects on oscillatory control - surface derivatives. ARC CF 1151 1971.
- 16 H Tijdeman. Investigations of the transonic flow around oscillating aerofoils. NLR TR 77090U October 1977.
- 17 B L Welsh. A new angular displacement transducer. RAE TR 79-026.
- 18 H C Garner. A practical framework for the evaluation of oscillatory aerodynamic loading on wings in supercritical flow. Paper 16, AGARD CP 226 April 1977.
- 19 K Isogai. Numerical study of transonic flow over oscillating aerofoils using the full potential equation. NASA TP 1120 April 1978.

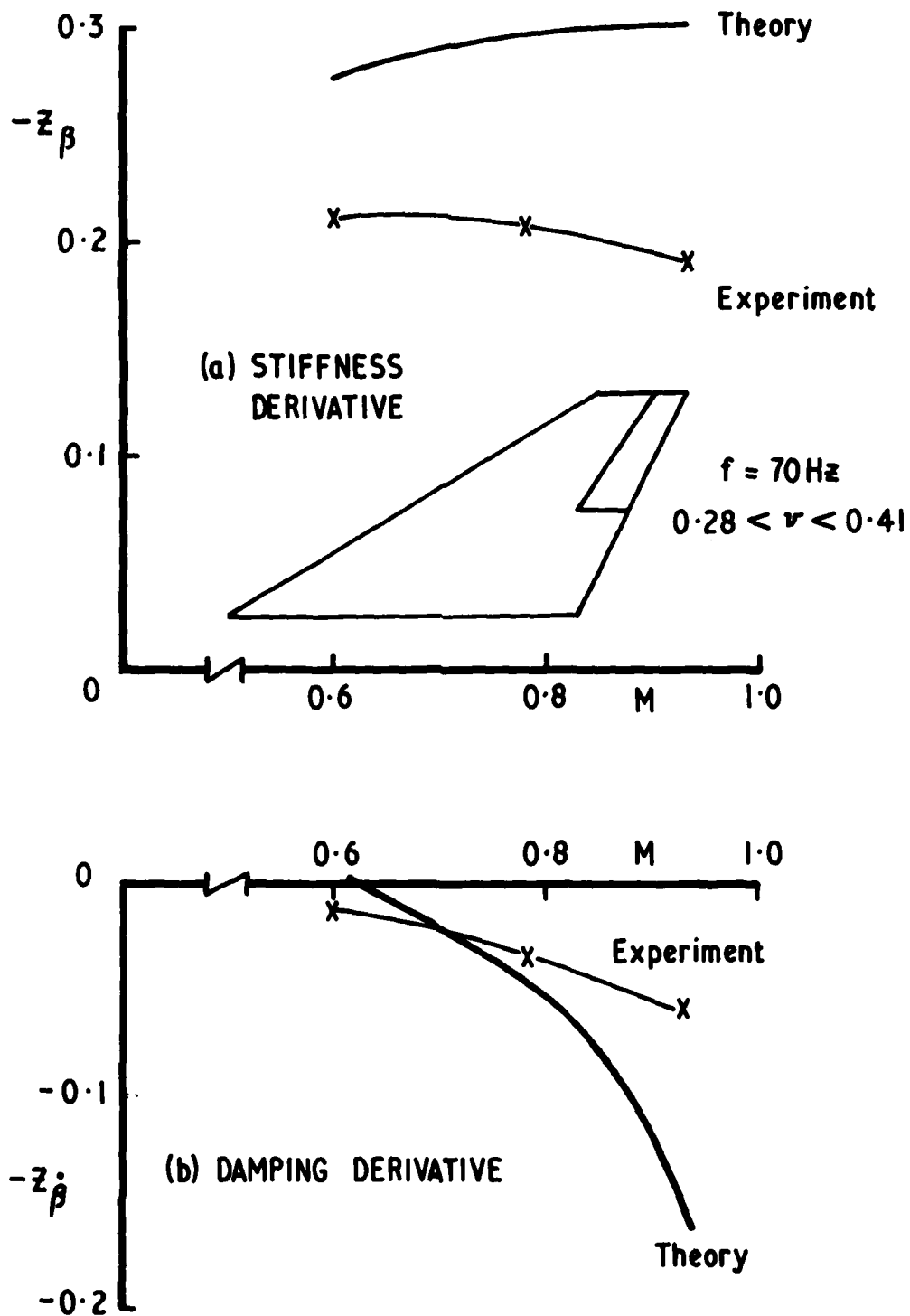


Fig.1 Lift due to oscillating flap ν Mach number

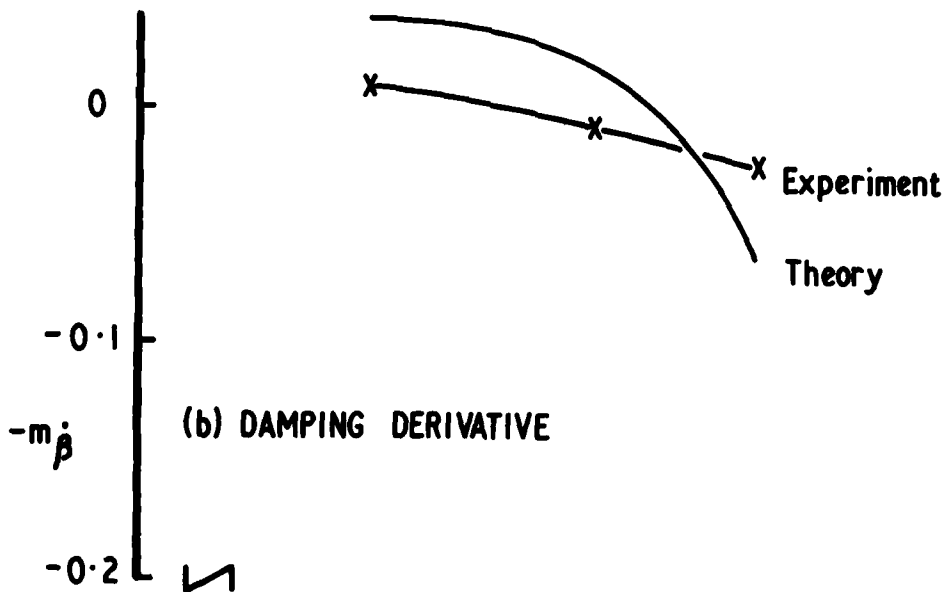
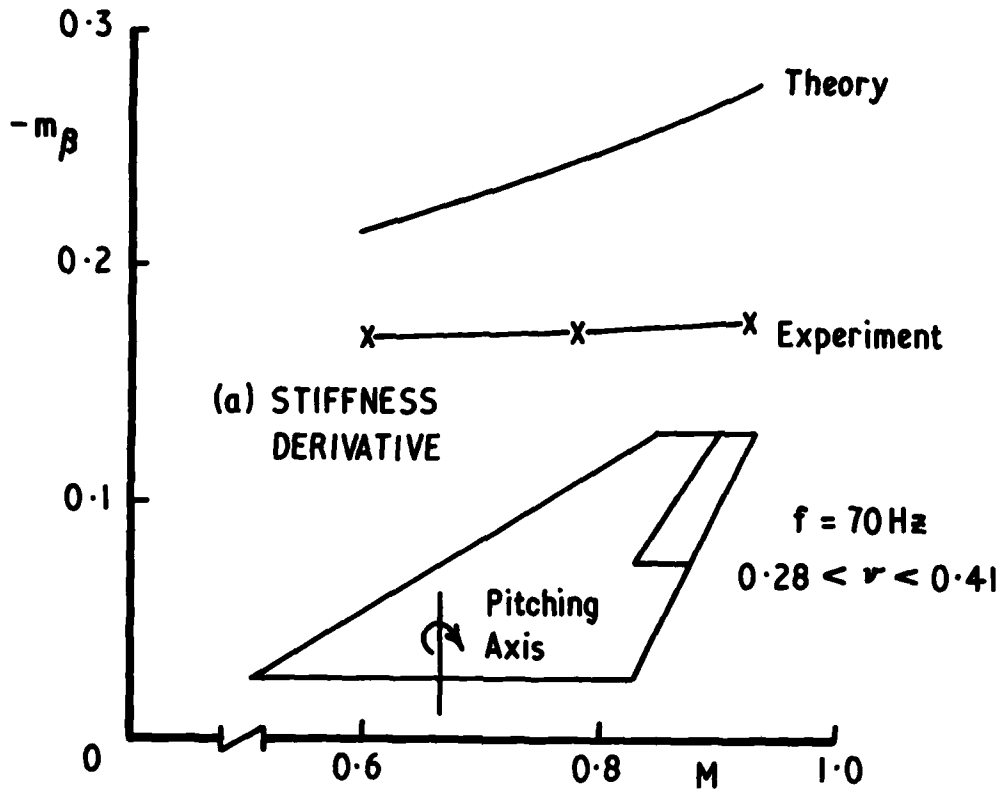


Fig.2 Pitching moment due to oscillating flap v Mach number

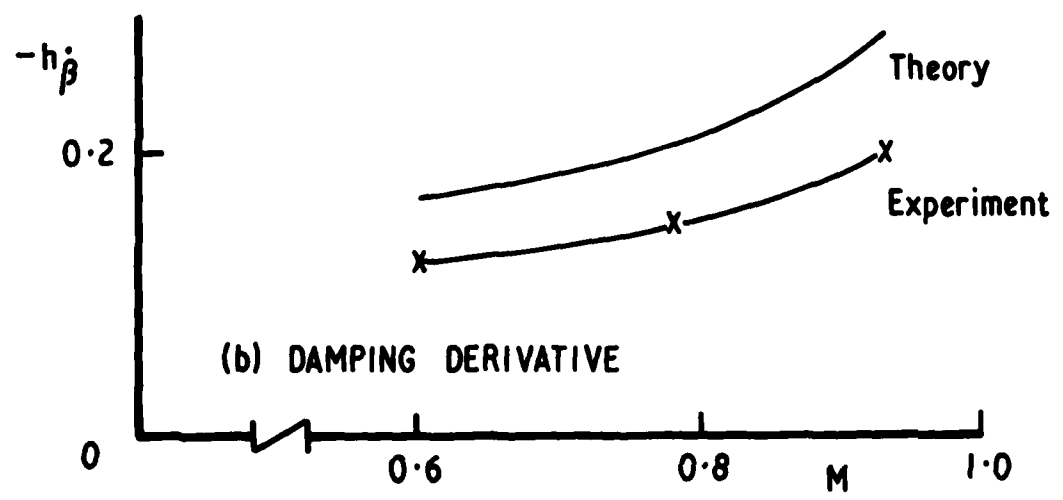
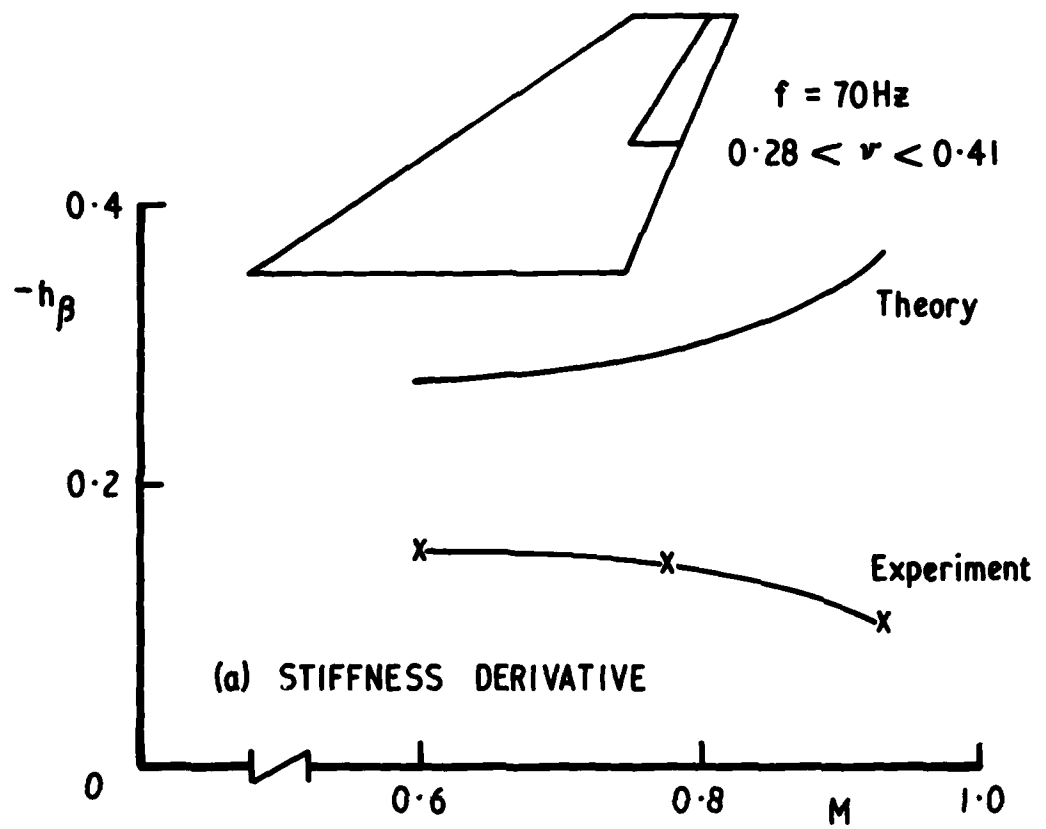


Fig.3 Hinge moment due to oscillating flap v Mach number

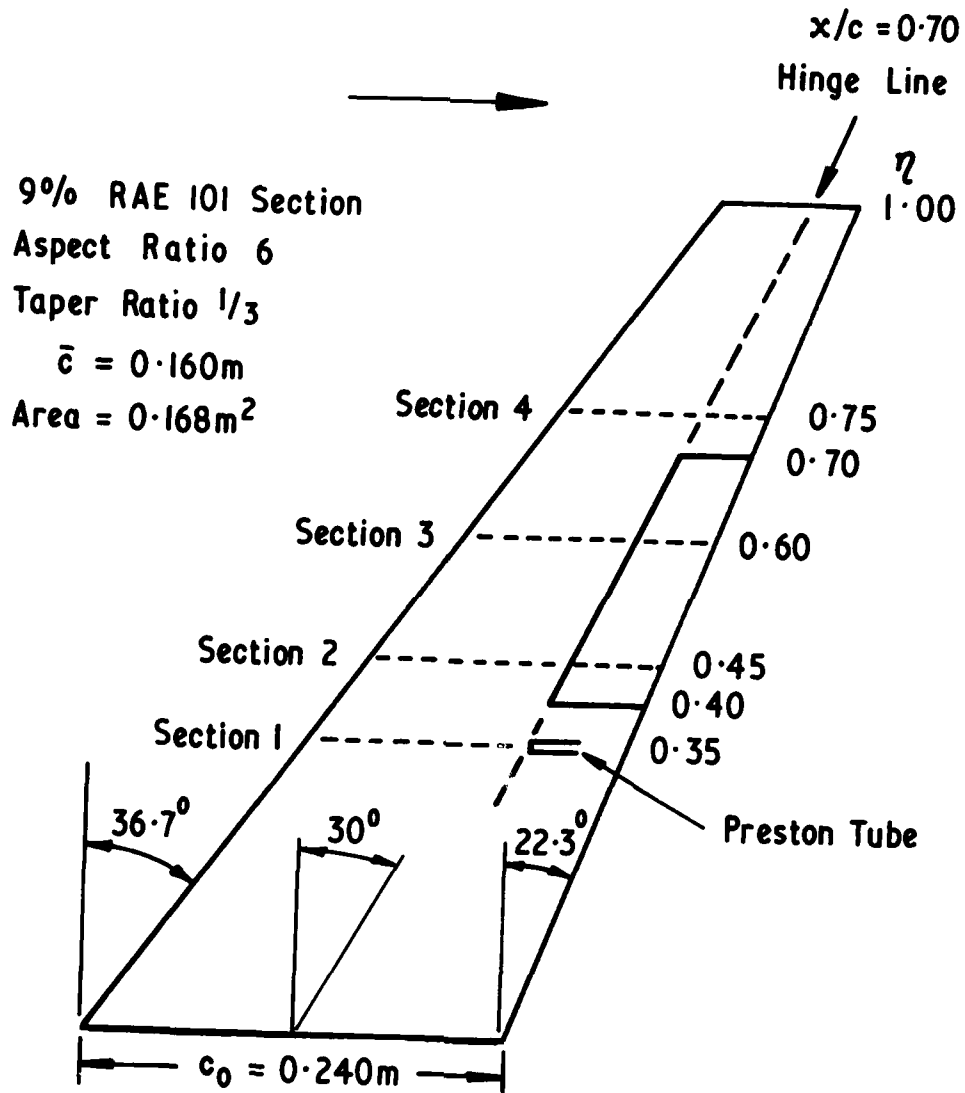


Fig.4 RAE wing A

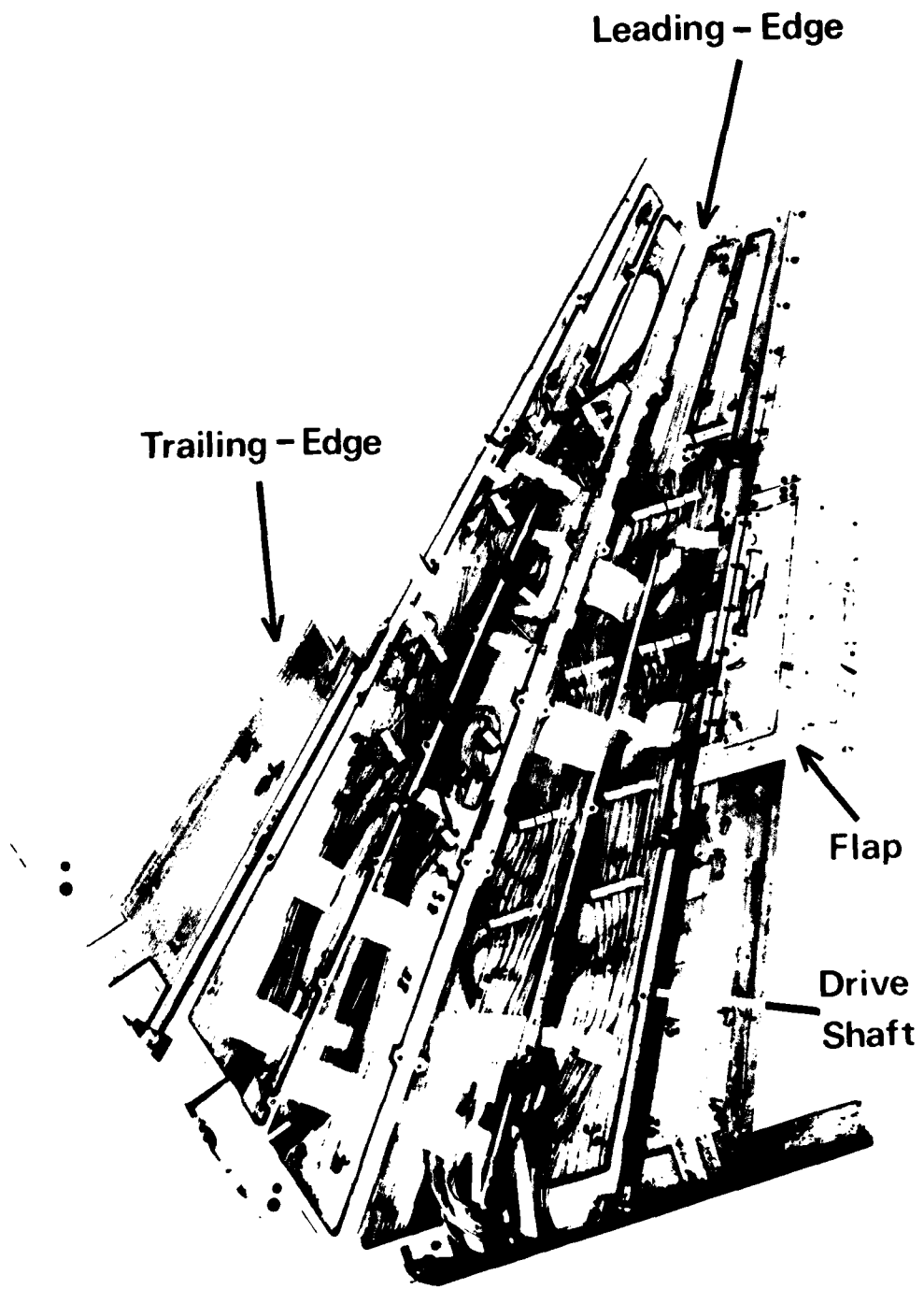


Fig.5 Model assembly

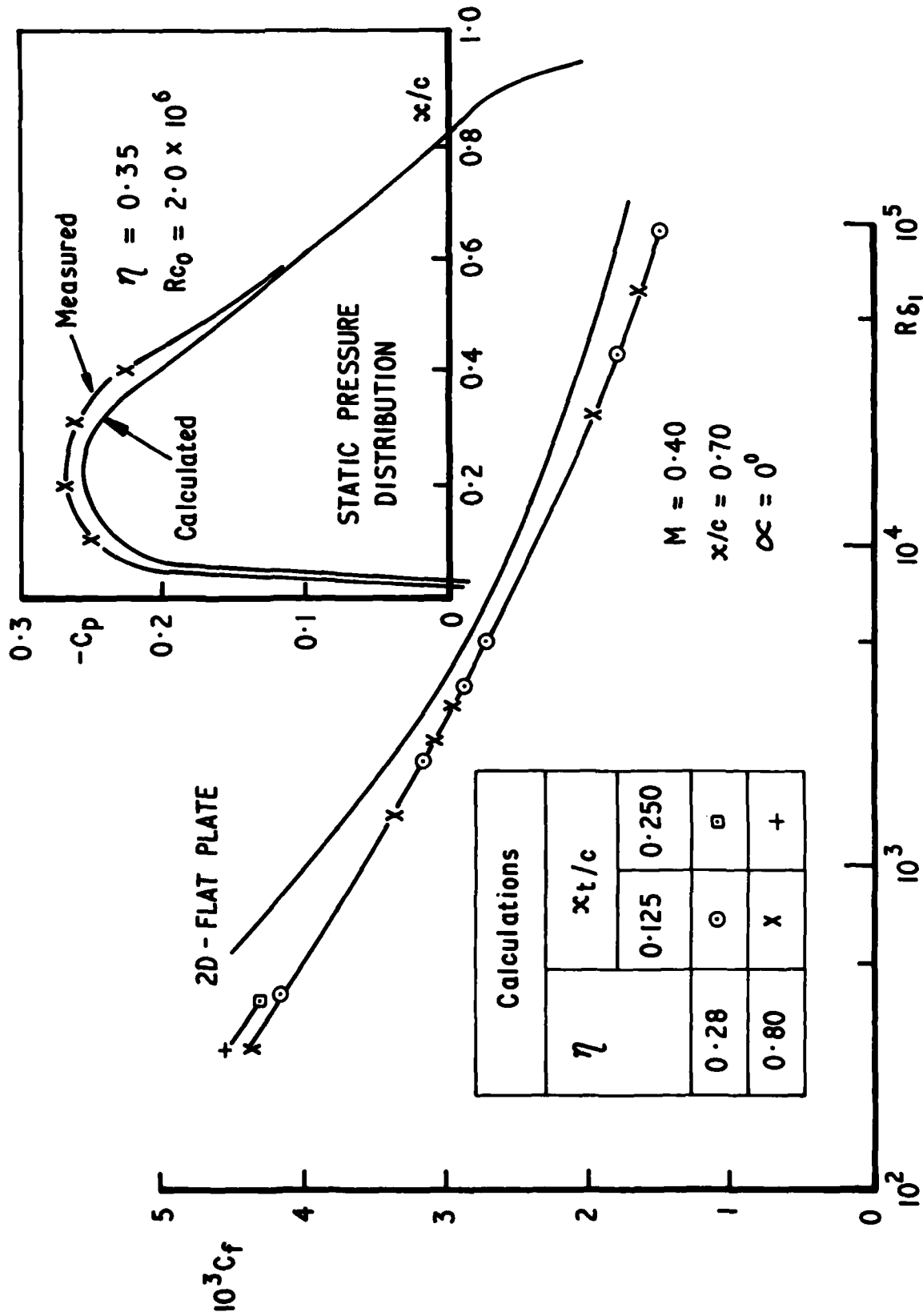
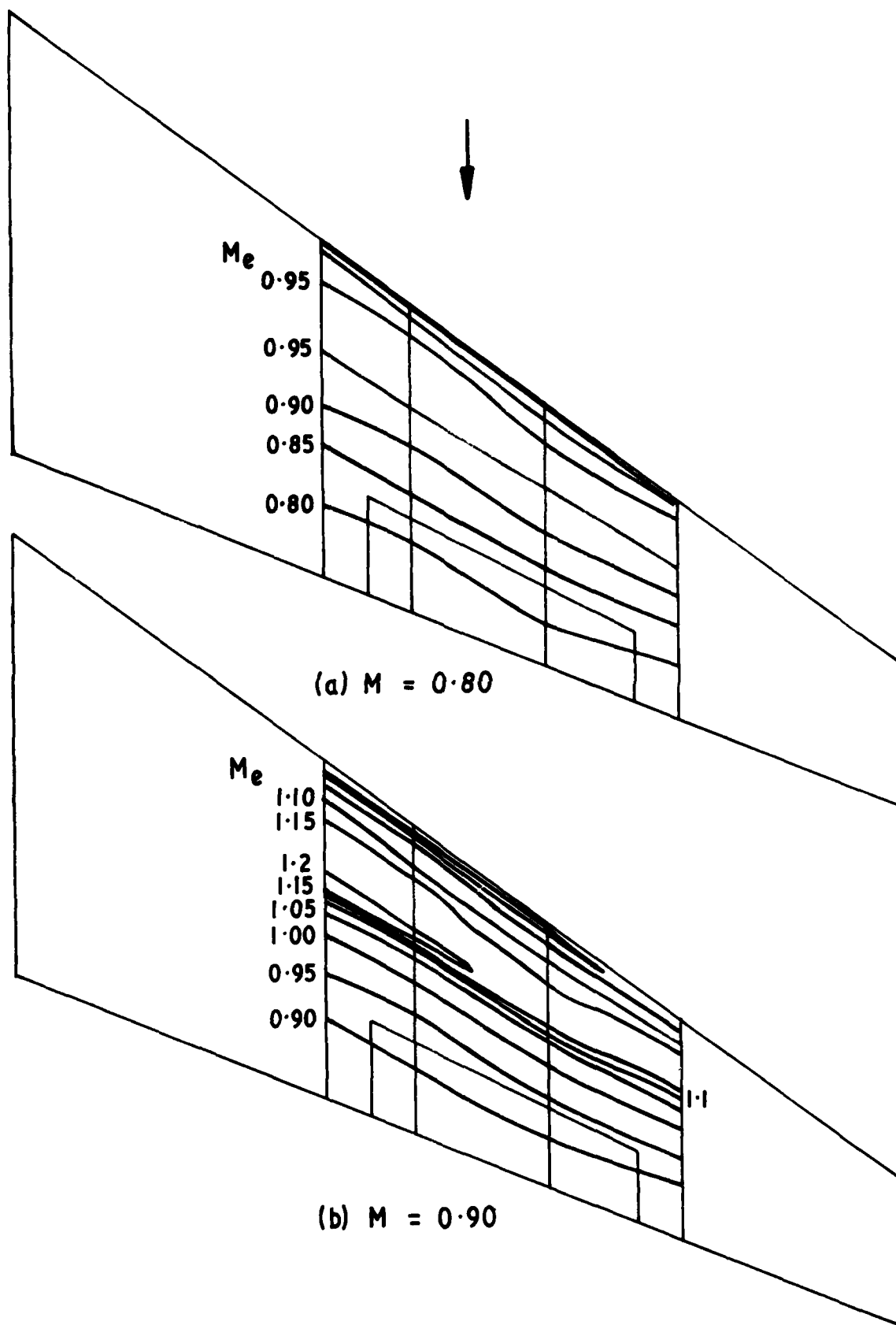
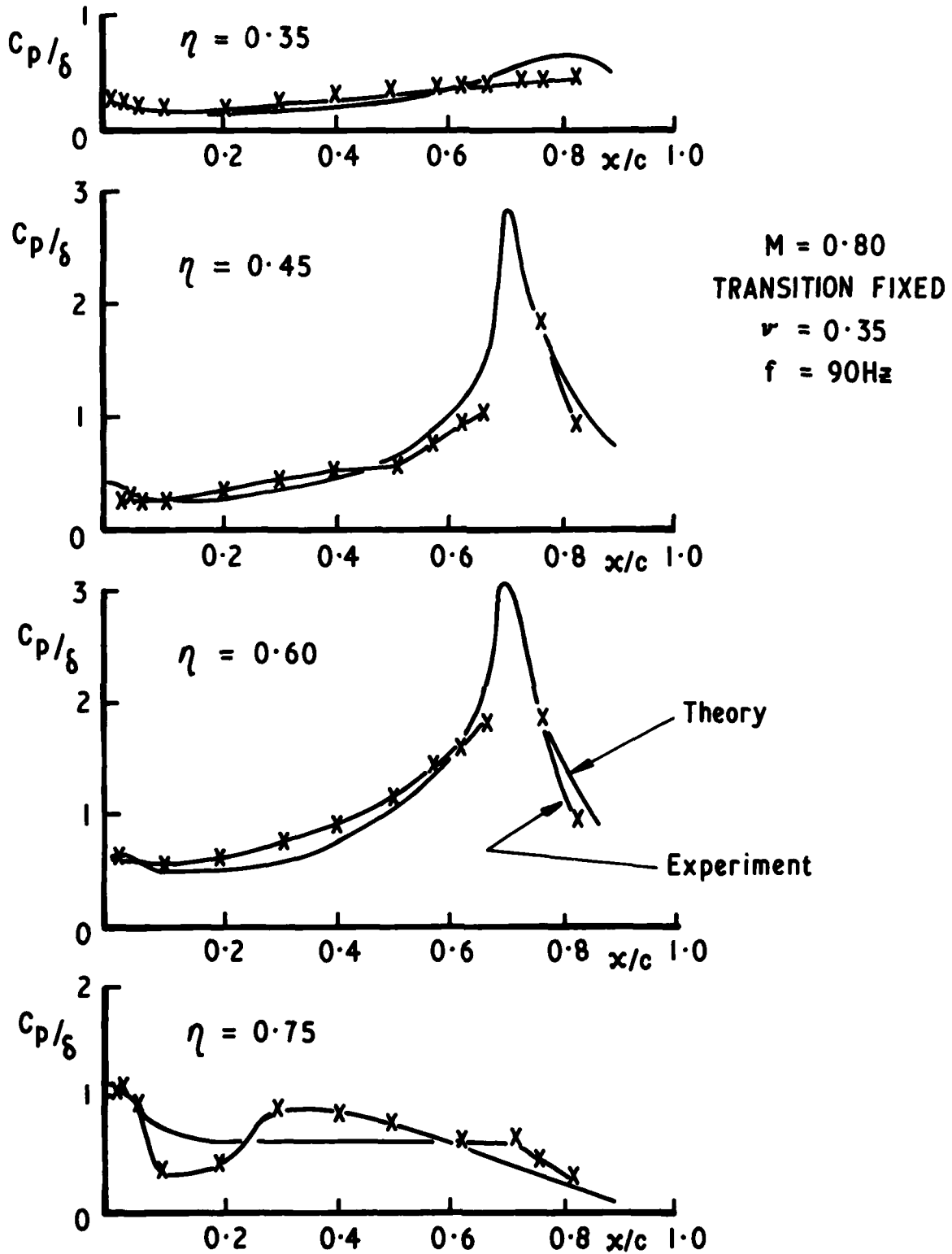


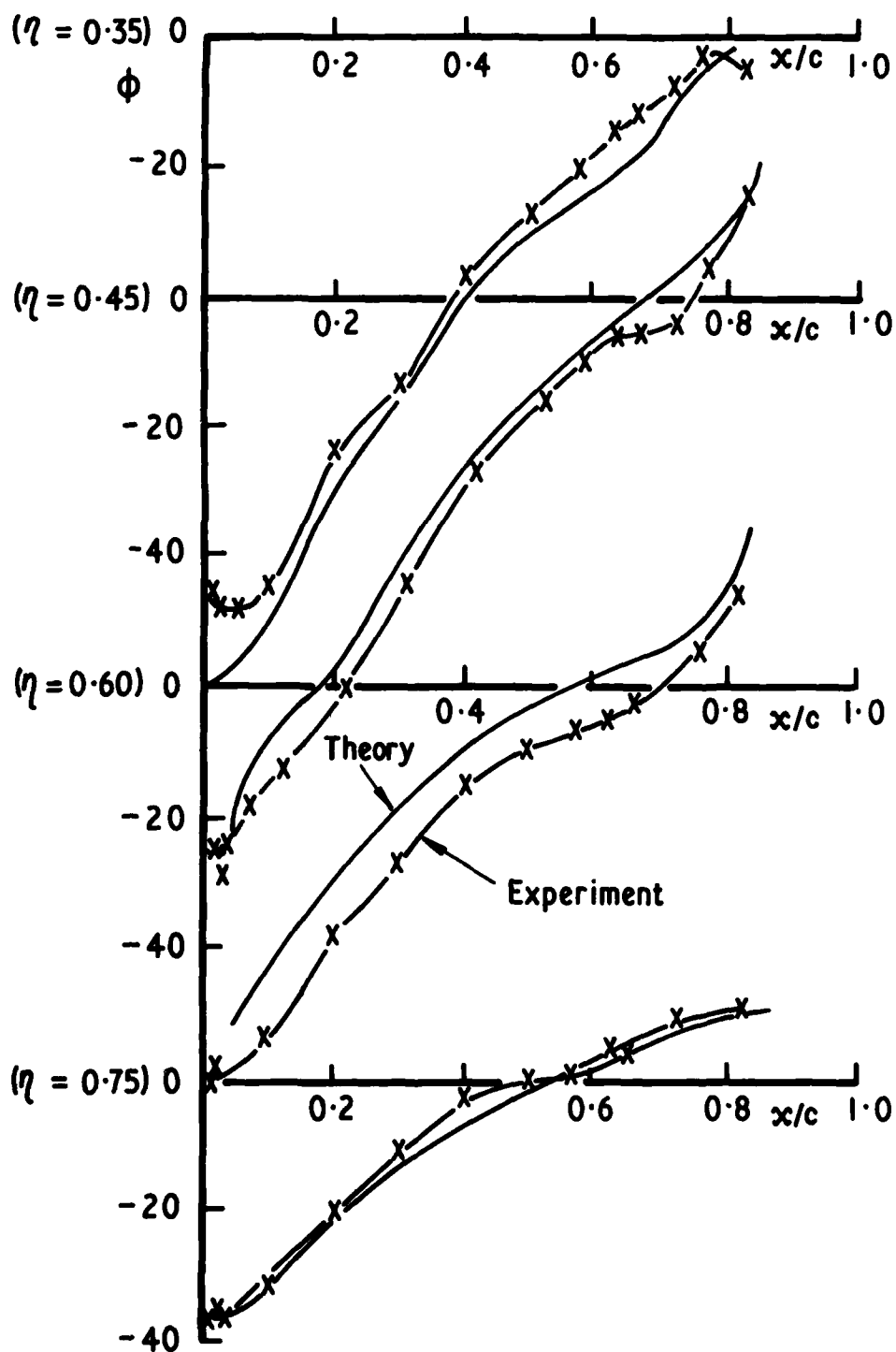
Fig.6 Calculated skin friction coefficient v displacement thickness Reynolds number

Fig.7 Contours of local Mach number ($\alpha = 0^\circ$)



8 (a) MAGNITUDE

Fig.8 Pressure distributions at four spanwise stations



8 (b) PHASE

Fig.8 cncl. Pressure distributions at four spanwise stations

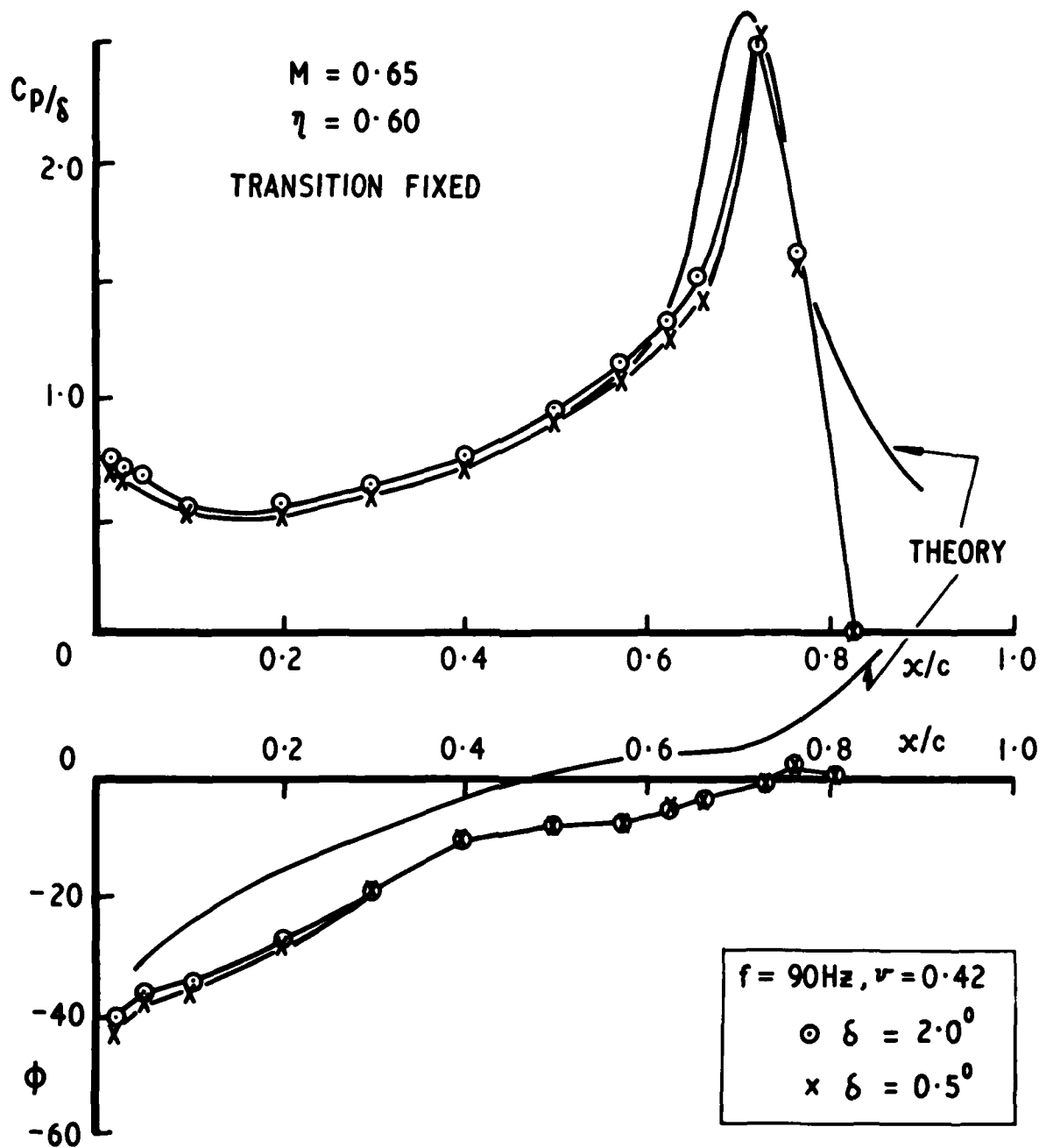


Fig.9 Effect of varying amplitude

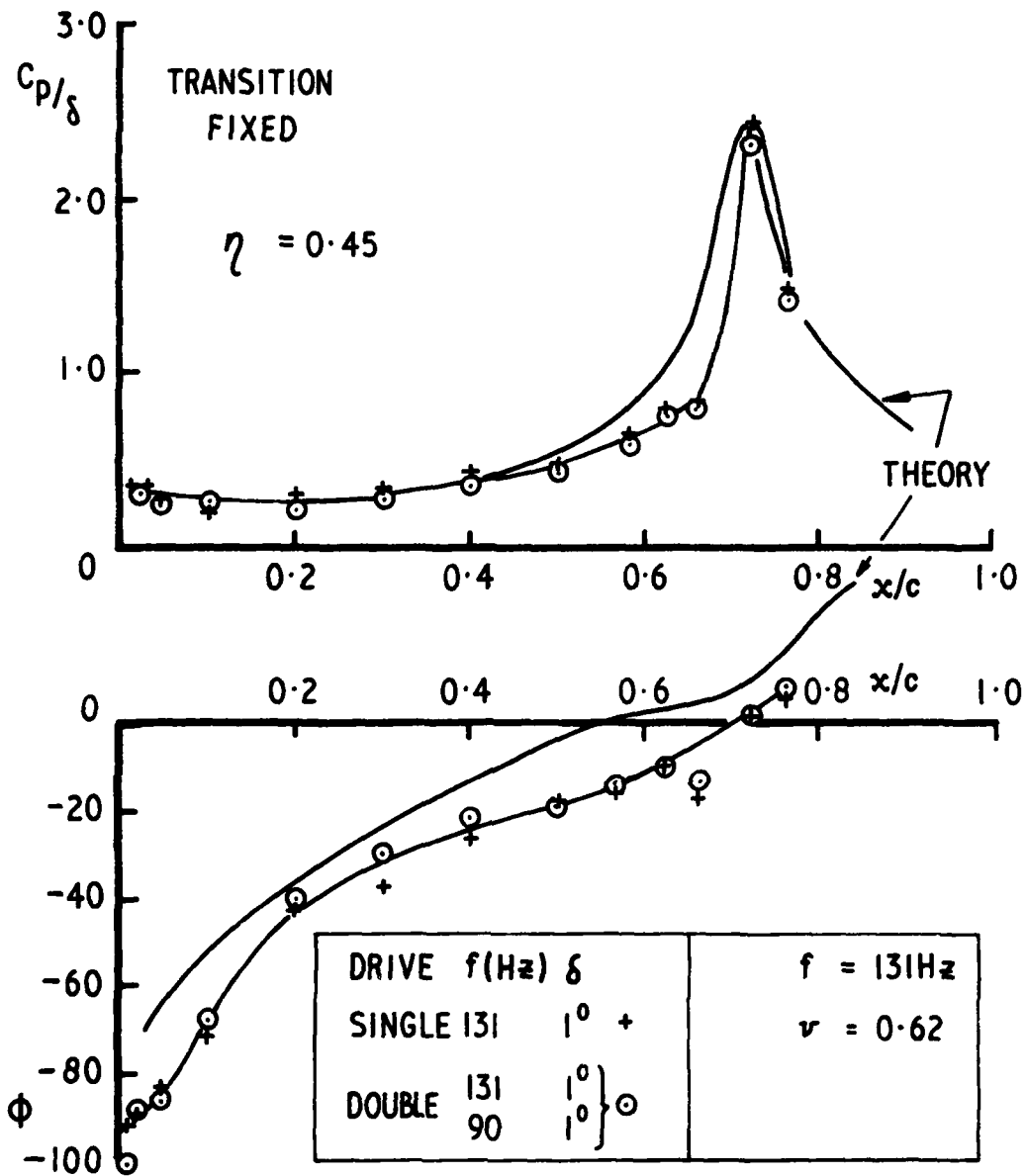
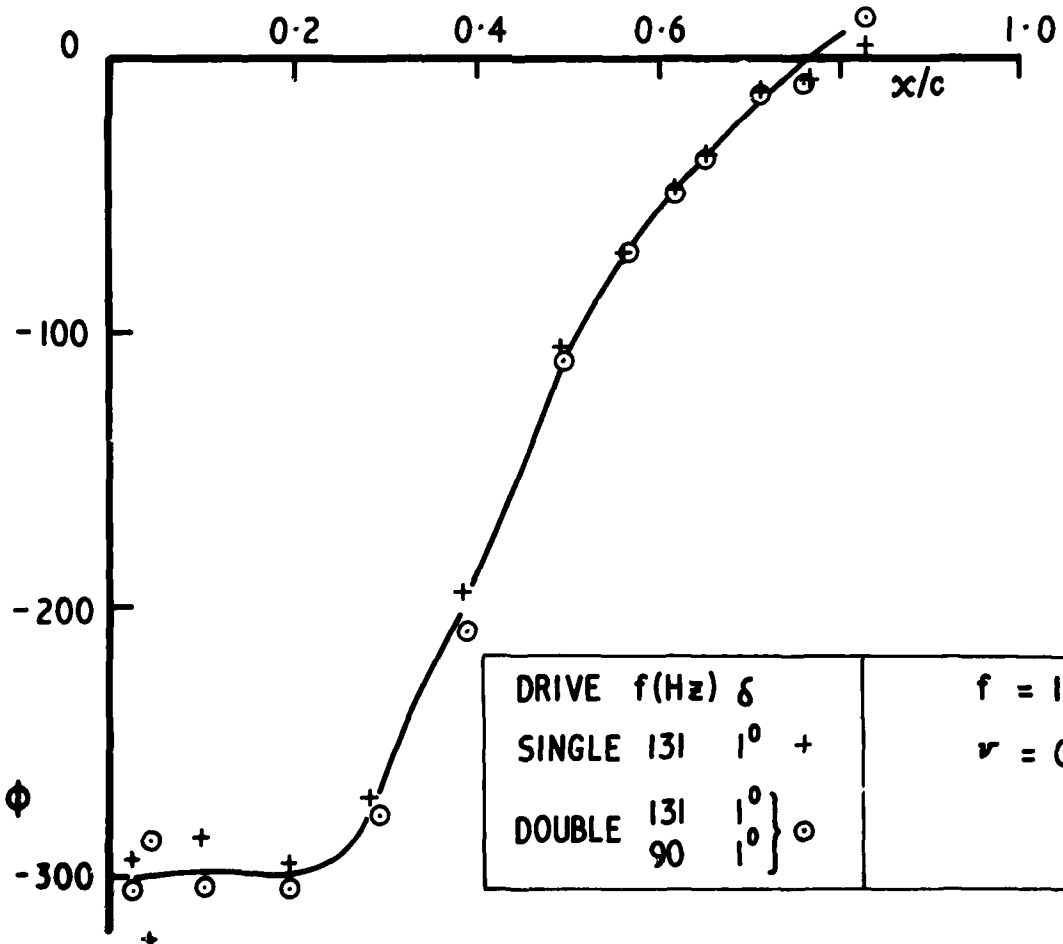
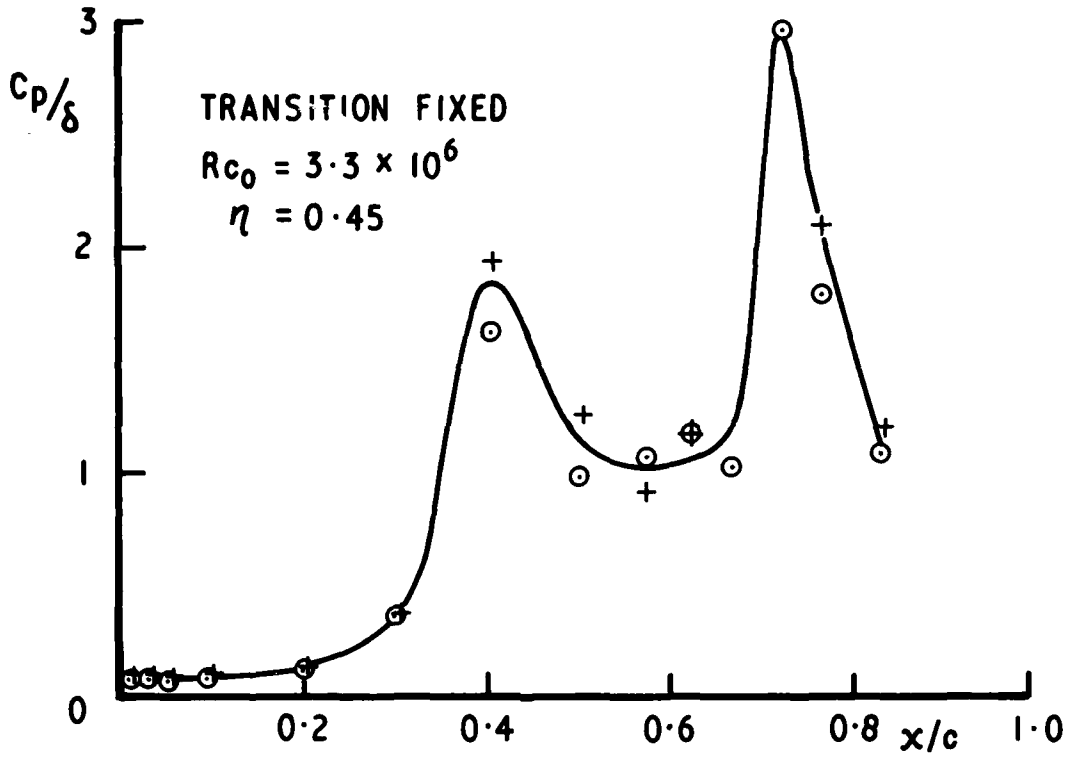
10(a) SUBSONIC $M = 0.65$

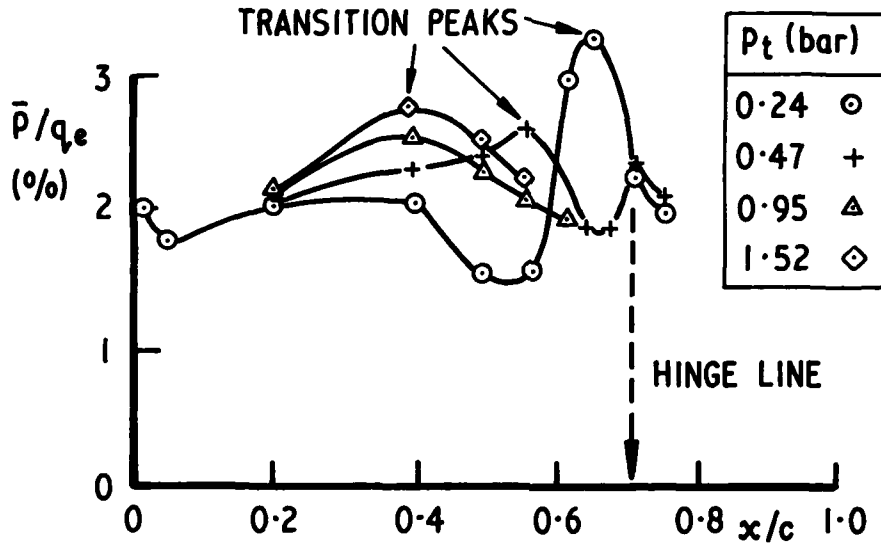
Fig.10 Superposition of two frequencies

20-20



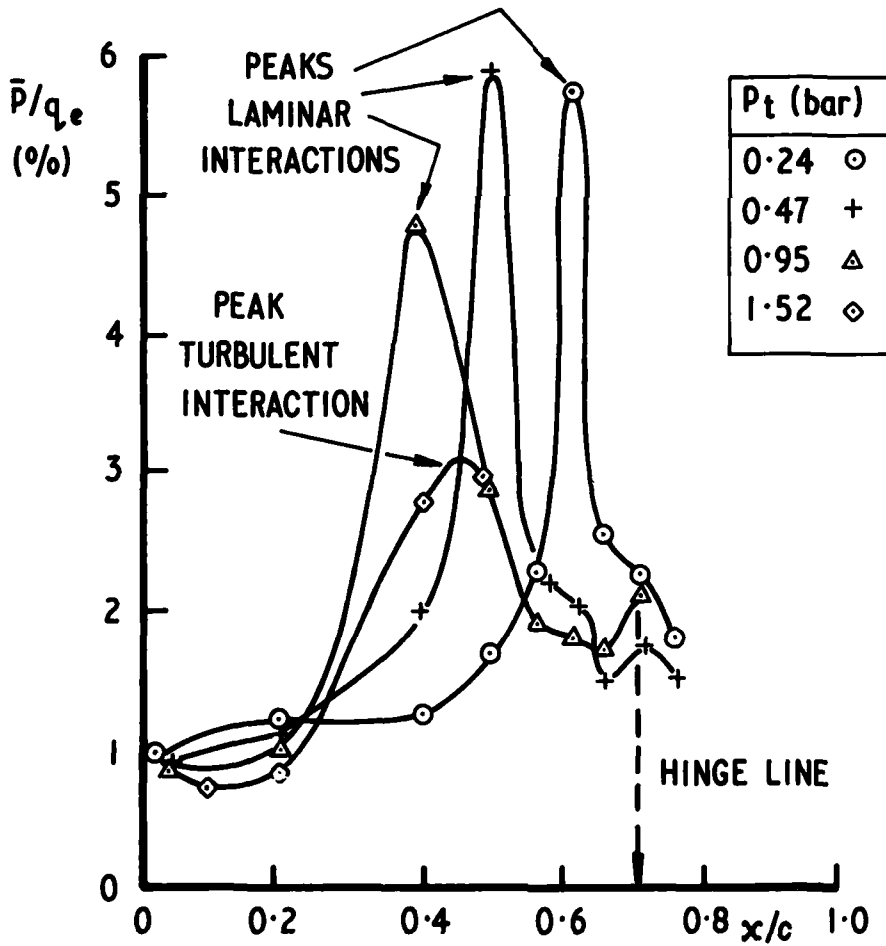
10 (E) TRANSONIC M = 0.90

Fig. 10 encl. Superposition of two frequencies



(a) $M = 0.80$

TRANSITION
FREE



(b) $M = 0.90$

RMS PRESSURE FLUCTUATIONS v CHORDWISE STATION
(FLAP - UNDRIVEN)

Fig.11 Transition determination at $\eta = 0.60$ ($\alpha = 0^\circ$)

20-22

	TRANSITION
$\alpha = 0^\circ$	FREE \circ
$\eta = 0.35$	FIXED \times
$x/c = 0.66$	
$c/c_0 = 0.767$	
$c_0 = 0.24m$	

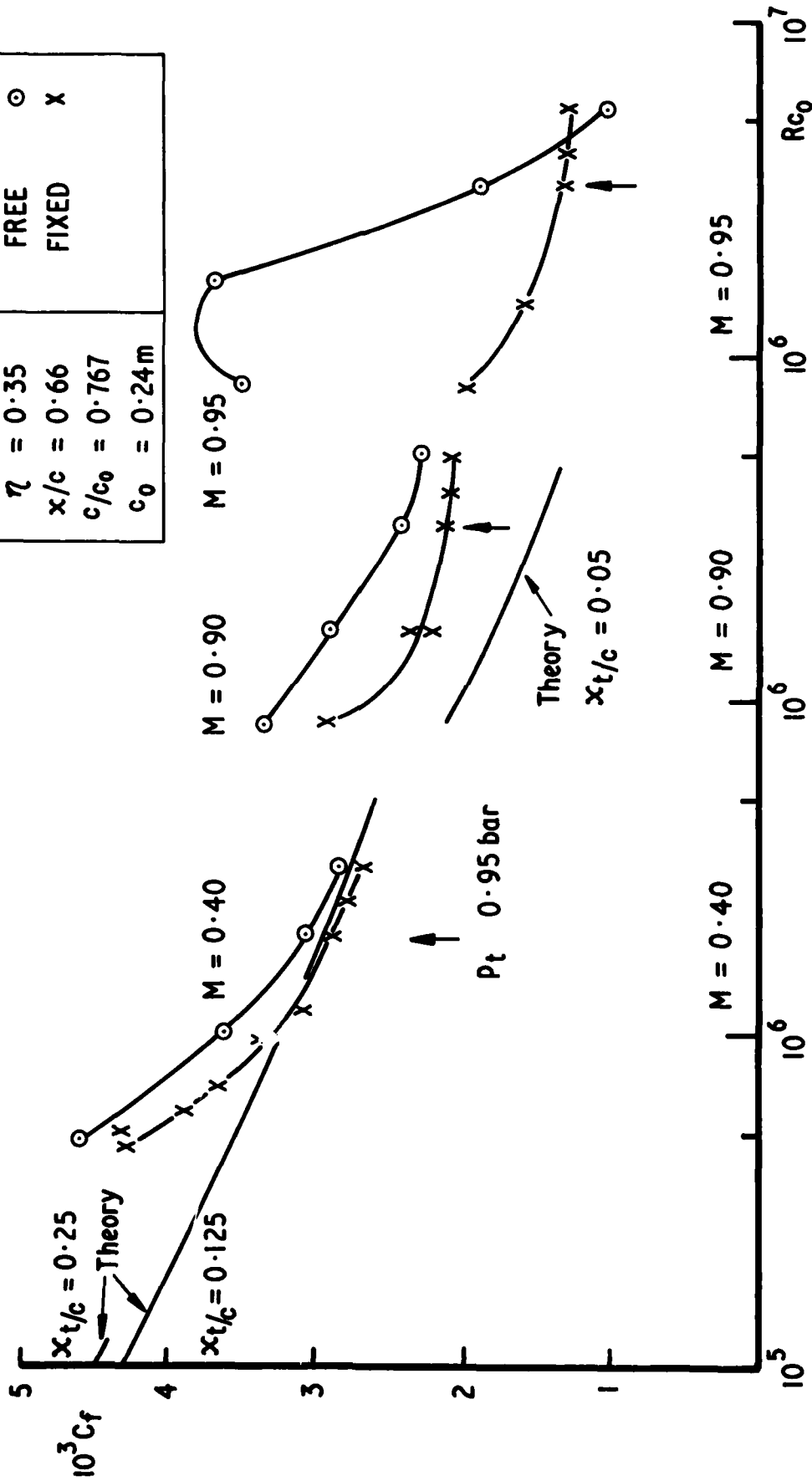


Fig.12 Skin friction coefficients near hinge line

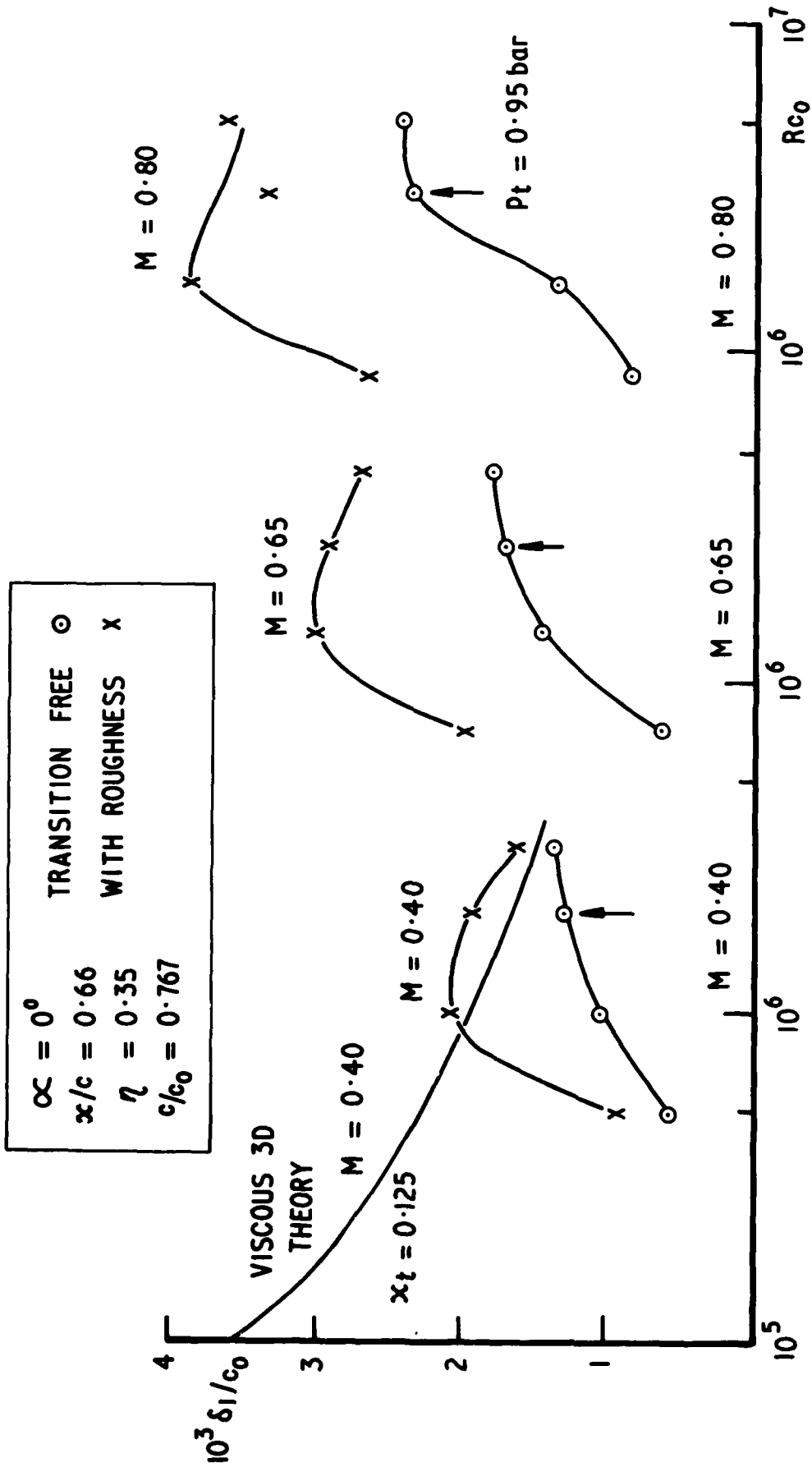


Fig.13 Variation of boundary layer displacement thickness with Mach number and Reynolds number

20-23

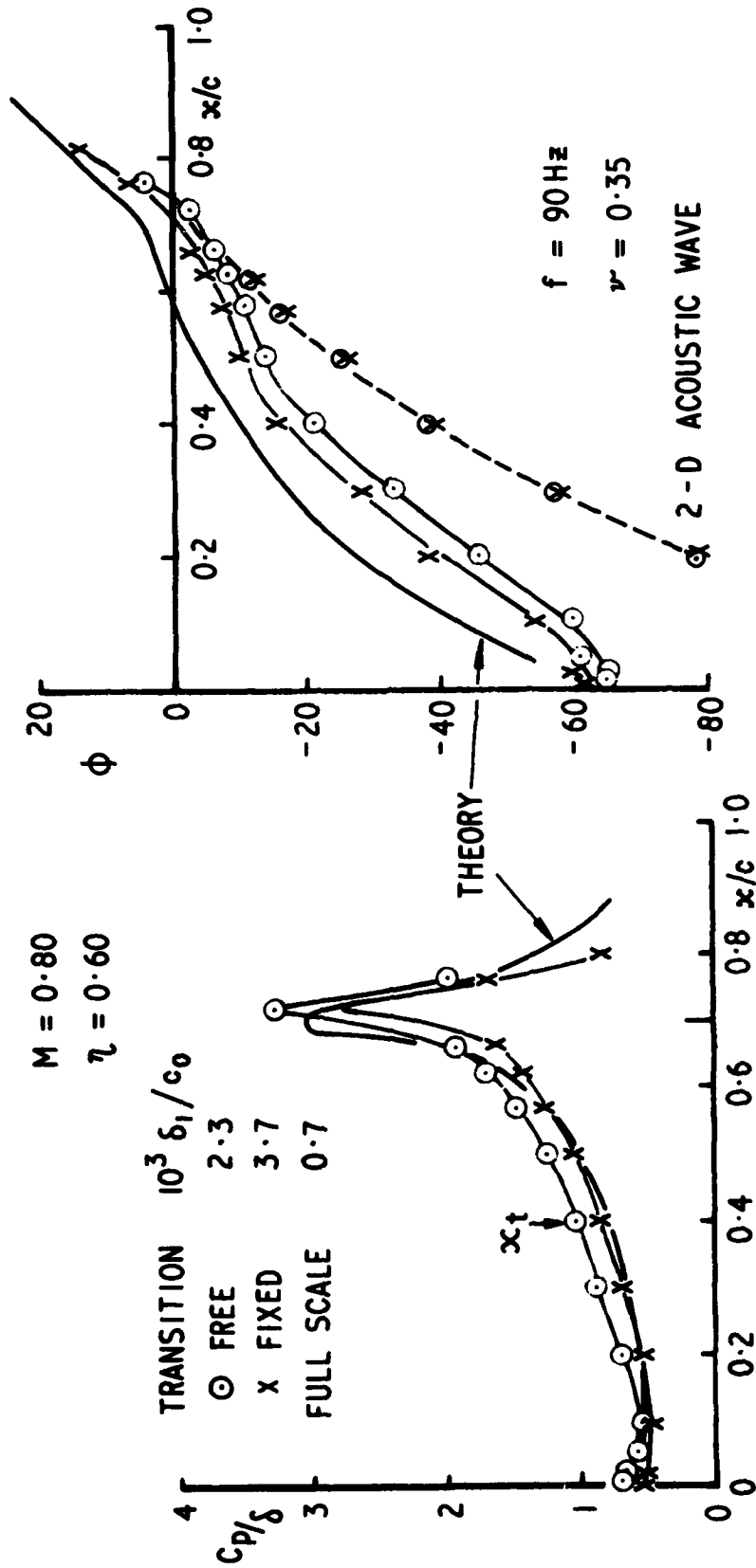


Fig.14 Magnitude and phase of subsonic pressure distribution

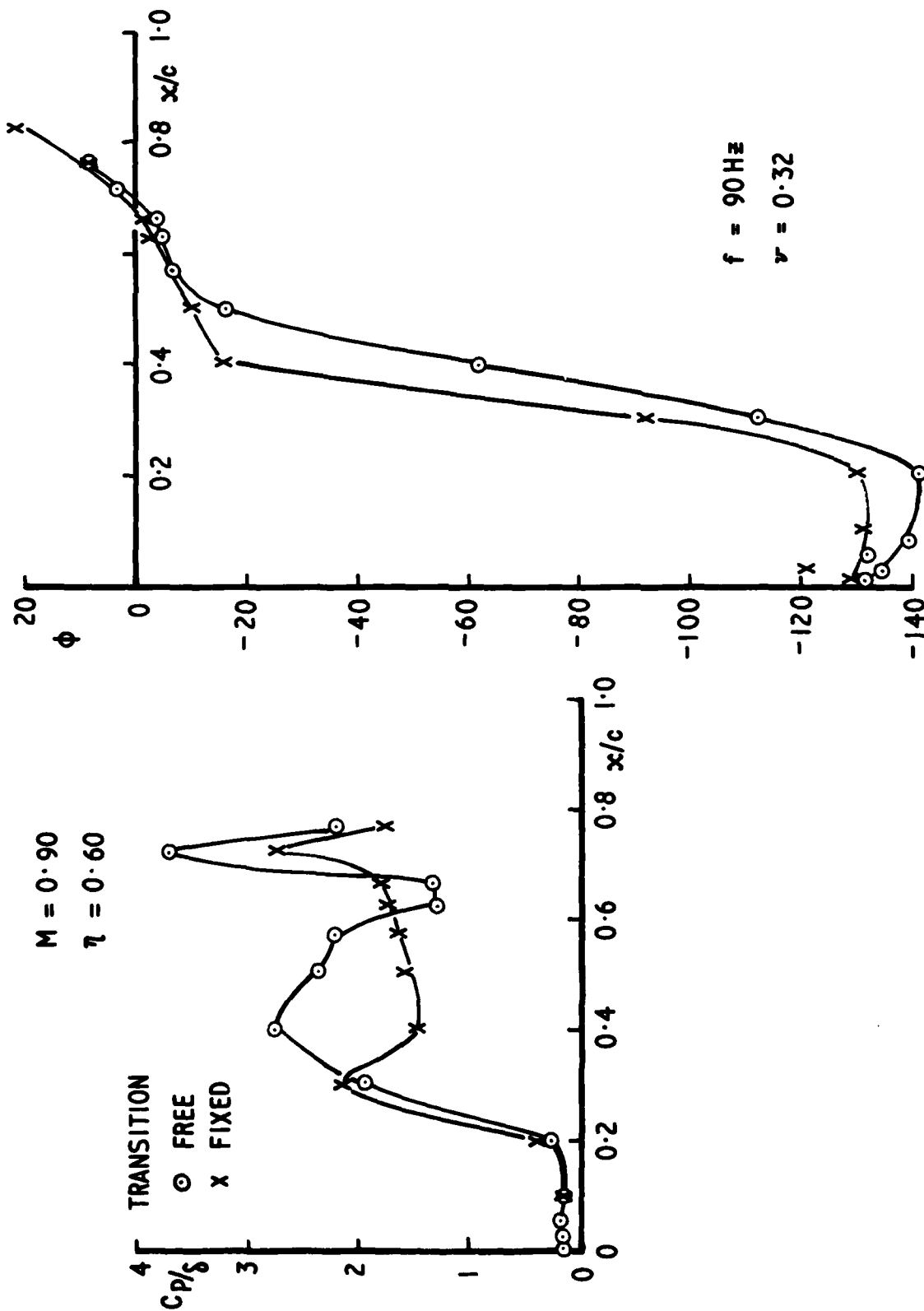


Fig.15 Magnitude and phase of transonic pressure distribution

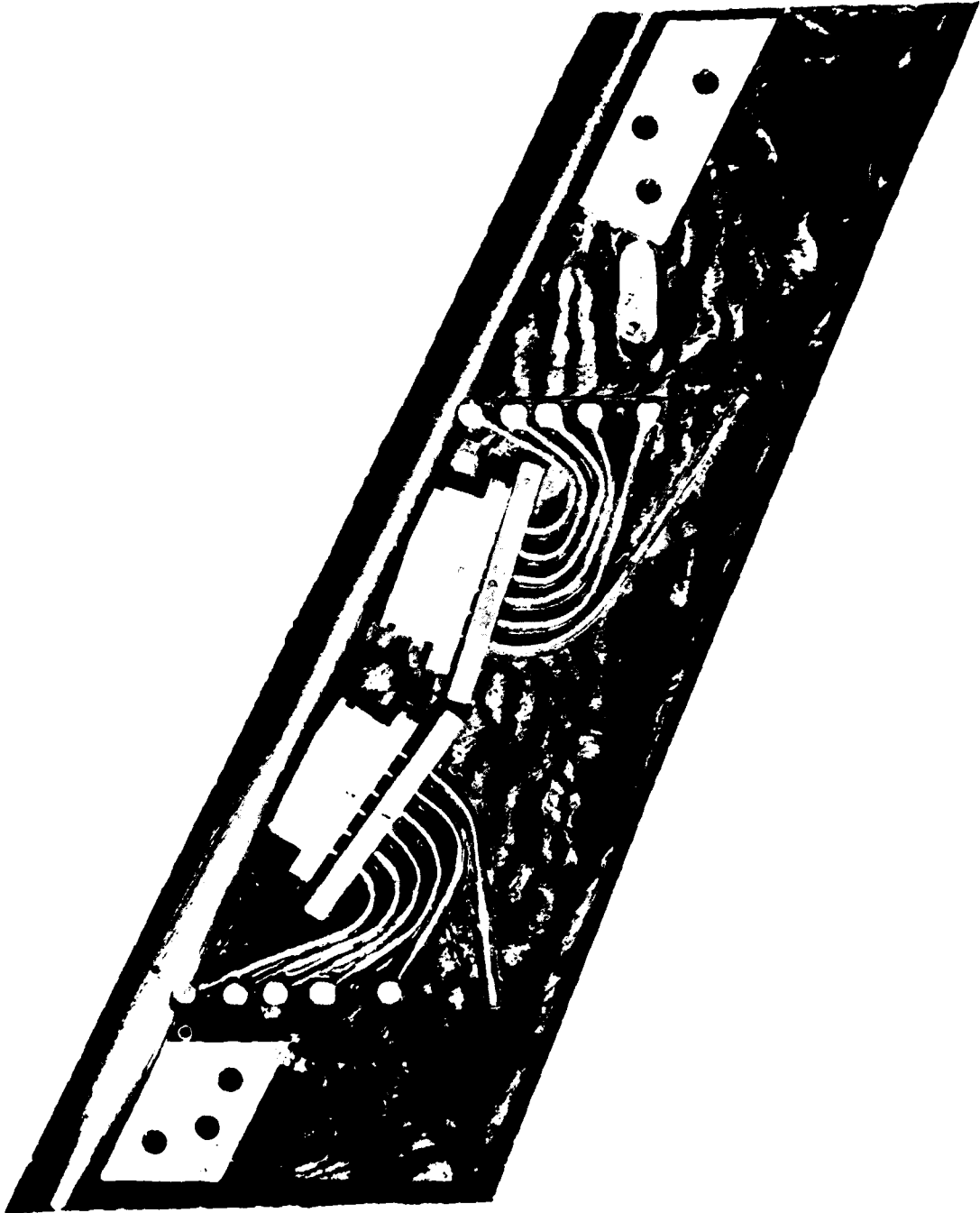


Fig.16 New flap

UNSTEADY AERODYNAMICS OF TWO DIMENSIONAL SPOILERS AT LOW SPEEDS

S.R. Siddalingappa and G.J. Hancock

Department of Aeronautical Engineering
Queen Mary College, University of London
Mile End Road, London, E1 4NS.

SUMMARY

Because of the growing use of spoilers for aircraft control and the possible use of spoilers in ACT applications there is a need to understand more clearly the aerodynamics of spoilers especially the time dependent behaviour of the aerodynamics as spoiler angles are changed.

This paper briefly reviews two complementary aspects of spoiler behaviour.

In the first set of experiments the emphasis has been on the understanding of the local flow about a spoiler. Experiments have been conducted on a two dimensional spoiler on the floor of a small blower tunnel (solid floor, and side walls but open at the top). Steady pressures have been measured along the tunnel floor for various steady spoiler angles and gap sizes between the bottom of the spoiler and the tunnel floor. Transient pressures have been recorded following sudden changes in spoiler angle and for oscillating spoilers. A selection of these results are presented and discussed; for example, for a spoiler with a 20% gap the transient pressures at different locations on the tunnel floor following a sudden change in spoiler angle from 0° to 35° in 0.012 seconds, and the transient pressures at different locations on the tunnel floor while the spoiler undergoes simple harmonic motion.

In the second set of experiments a two dimensional spoiler has been attached to a two dimensional aerofoil. The emphasis now is on the manner in which the spoiler affects the overall pressure distribution on the aerofoil-plus-spoiler combination. Both the aerofoil and the spoiler are pressure plotted. The paper includes a discussion of results of steady pressures, transient pressures following rapid and slower ramp changes in spoiler angle, and transient pressures when the spoiler is moving in simple harmonic motion.

Some conclusions are offered on the aerodynamics of spoilers when used as fast acting controls in ACT applications.

1. INTRODUCTION

The use of spoilers for roll control has a long tradition. During the mid-1930's general guide lines for spoiler design were established based on research at NACA(1). In particular it was found that forward locations of a spoiler on a wing upper surface were unsuitable for roll control because of unacceptable lag effects following roll commands; fortunately spoilers at more aft locations gave more reasonable response characteristics. In more recent times spoilers have become widely used as a roll control on high manoeuvrability combat aircraft because of the reduced efficiency of conventional aileron controls at high speeds.

Looking to the future Active Control Technology might well extend the use of spoilers beyond that of roll control. Gust alleviation systems require primarily rapid lift dumpers, spoilers can be used for this purpose providing that sufficient actuator power and rapid actuator response are available. Improvement of ride quality in turbulence might be possible by using spoilers, but in this case both rapid increase as well as decrease in lift is required. Flutter suppression is also under investigation; the question here is whether or not flutter can be suppressed by the use of spoilers since spoilers might well be present on an aircraft wing for other purposes.

A major effort over the past years by industrial organisations has provided performance data for spoiler design, nevertheless it is probably fair comment that the fundamentals of the aerodynamics of spoilers is little understood. Parkinson and his assistants have made substantial contributions to such understanding of spoiler characteristics in both experimental and theoretical studies (e.g. refs. 2,3) but because of the complexity of the separated flows aft of spoilers and the possible extension of the use of spoilers further effort is required. A programme of research is being undertaken in the Department of Aeronautical Engineering at Queen Mary College with particular emphasis on the unsteady character of spoiler aerodynamics. This paper selects one or two points of interest to emerge so far from that part of the programme which deals with two dimensional spoilers at low speeds.

From a fundamental point of view there are two aspects relating to the non steady spoiler aerodynamics, the first concerns the establishment of the local flow conditions in the neighbourhood of the spoiler while the second concerns the build up (or loss) of the overall loading on an aerofoil or wing. So two investigations have been made, both investigations are primarily qualitative at this stage. One investigation has been made on a two dimensional spoiler on a long flat plate to attempt to understand local conditions. A second investigation has been made on a two dimensional aerofoil on which there is situated a two dimensional spoiler. Pressure measurements have been taken during ramp changes in spoiler angle at rapid and slower rates, tests have also been carried out with the spoiler moving in simple harmonic motion.

2. TWO DIMENSIONAL 'SPOILER' ON A TUNNEL WALL

One reason for investigating a two dimensional spoiler on a long flat plate, namely a tunnel floor, was to develop techniques both for moving a spoiler and for measuring transient pressures. Thus the choice of the tunnel and the choice of the scale of the experiment was to ensure compatibility with, and to build up experience for, the longer term aim of investigating a spoiler on an aerofoil. As pointed out above a 'spoiler' on a tunnel wall is an important fundamental problem in its own right; the present investigation should be regarded only as preliminary, or introductory; some qualitative trends have been observed but quantitative levels should be regarded with caution.

2.1 APPARATUS

The apparatus is shown in Figure 1.

The 'tunnel' which extends from the downstream end of a contraction from a small blower, consists of a floor, which is pressure plotted along the centre line and on which the spoiler is attached. The tunnel has solid side walls but it is open to the atmosphere on the upper side. The working section has dimensions 10 cm x 10 cm. It should be noted that the 'floor' starts just inside the blower exit so the boundary layer remains relatively thin up to the spoiler location.

The spoiler which extends from side wall to side wall has a chord of length 4.5 cm.

The speed of the tunnel flow was about 30 m/s.

The spoiler could be arranged to allow a gap between the bottom of the spoiler (i.e. the hinge line of the spoiler) and the tunnel floor; gaps of 10% and 20% spoiler chord were investigated.

For step changes between one angle and another the spoiler was moved by a spring loaded device; for the harmonic motions the spoiler was moved by a cam arrangement from an electric motor. Attached to the spoiler was a potentiometer which recorded the spoiler motion and also provided a trigger datum for the pressure measurements.

The pressure tubes from the pressure tapings on the floor were connected sequentially to a Statham pressure transducer. To obtain the time pressure record for a particular pressure location the spoiler motion was repeated, the transducer output was stored on a transient recorder and then relayed to an xy plotter. With the trigger datum from the spoiler potentiometer the records for different pressure locations can be compared. The experimental data was repeatable.

The full range of tests covered:

- i) steady spoiler angles 10°, 20°, 35° with 0, 10%, 20% gaps; the maximum angle of all tests was 35° because at higher angles the flow did not reattach onto the floor; it was thought that in this series of tests reattachment should be an essential feature of the flow;
- ii) step changes of spoiler from 0° → 35° and 35° → 0° in 0.0125 seconds (note that the free stream air moves approximately 8 spoiler chords in the time the spoiler moves from one angle to another);
- iii) simple harmonic motion of spoiler with amplitudes 0° ↔ 35°, at frequencies 1 Hz and 5 Hz.

For general information the above ranged tests were repeated for a 'three dimensional spoiler' when the spoiler did not extend from tunnel side wall to side wall.

These tests are obviously not comprehensive and, as found out subsequently, there are some important aspects unresolved.

Because of limitation of space in this written paper, and because of limitation of time in the lecture presentation, it is necessary to be selective in order to give a flavour of the results. A full account will be appearing shortly.

2.2 A STEADY RESULT

Steady pressure on the tunnel floor are shown in Figure 2 for three steady spoiler angles 10°, 20° and 30° when there is a 20% gap underneath the spoiler. The results are plotted not in terms of the conventional c_p because in this experimental arrangement $\frac{1}{2}\rho V^2$ varies with spoiler angle (as can be seen from the curves ahead of the spoiler), but in terms of a k_p which defines the pressure relative to a fixed 'head'. And then k_p is suitable for the subsequent unsteady tests.

The results are of considerable interest because the three spoiler angles demonstrate three distinct curves. Some attempts have been made at flow visualisation to explain the flow characteristics.

Some tentative explanations of these flows are sketched in Figure 3.

For the lowest angle of 10°, as shown in Figure 3(i), the flow underneath the spoiler attaches to the under surface of the spoiler. The flow underneath the spoiler is accelerated but the reattachment process of this flow to the underside of the spoiler imposes a high pressure gradient which is sustained by the spoiler. This explains why there is a peak pressure suction beneath the spoiler followed by a high pressure gradient. The subsequent pressure gradient for the flow underneath the spoiler must then be compatible with the deceleration of the flow from the upper surface of the spoiler after it separates from the spoiler trailing edge. The shear flow from the spoiler trailing edge reattaches to the tunnel floor in about 1 spoiler chord length downstream.

For the middle angle of 20° , as shown in Figure 3(ii), the flow underneath the spoiler does not reattach to the underside of the spoiler but essentially curves upward to oppose and mix with the shear flow from the upper surface of the spoiler aft of the spoiler trailing edge. The 'bubble' on the underside of the spoiler is effectively a constant pressure region, as indicated in the pressure results. The closing of the 'bubble' imposes a downstream pressure gradient and the flow reattaches to the surface.

For the highest angle of 35° , as shown in Figure 3(iii), the flow is similar to that at 20° except that the bubble region is now extended, a consequence of the downstream pressure gradient is the separation of the flow close to the floor, this explains the different form of the behaviour of the pressures aft of the spoiler in Figure 2.

2.3 RAMP CHANGES IN SPOILER ANGLE

Ramp changes in spoiler angle have been investigated. In these tests the angle of the spoiler is held steady at the initial angle, the angle is then increased (or decreased) rapidly and then held steady at the final angle. With the spring loading system used in this experiment repeatable spoiler motions were obtained. In the results shown here the spoiler moves through an angle of $0^\circ \leftrightarrow 35^\circ$ in the order of 0.0125 seconds; thus in the time the spoiler moves through its change of angle the free stream has moved about 7-8 spoiler chord lengths.

The instantaneous pressure distributions are shown in Figure 4 at different times during and following an increase in spoiler angle from $0^\circ \rightarrow 35^\circ$. Because of the flow through the gap these results are difficult to interpret.

At time 0.01 secs, as the spoiler approaches its maximum value, there is a large suction pressure beneath the spoiler, implying that the flow underneath the spoiler is reattaching to the spoiler under-surface. Thus in this transient condition of rapidly increasing spoiler angle the flow underneath the spoiler reattaches up to much higher spoiler angles (i.e. of the order of 30°) than in the spoiler angle in the steady state (i.e. about 10°).

As time increases the flow underneath the spoiler no longer reattaches to the undersurface of the spoiler and this flow then curls upward to mix with the shear layer separating from the spoiler upper surface. In this transient condition there will be a net rotation of the flow, resembling a starting vortex, which will form downstream of the spoiler. This 'vortex' will then convect downstream. This convection can be seen at time 0.03 secs., with the pressure recovery region advancing in front of the pressure suction region. By this time the local flow in the neighbourhood of the spoiler is becoming established. It is only after about 0.06 secs. that the downstream conditions become close to the final steady state values.

The results as a spoiler decreases its angle from 35° to 0° are shown in Figure 5. It is seen that even at this rapid rate the flow virtually follows the spoiler motion in a quasi-static manner, when the spoiler reaches zero then nearly all of the loading has been relieved.

In broad terms, for this two dimensional spoiler arrangement with a 20% gap, the establishment of the flow with the spoiler angle increasing takes about 3 times longer than with the spoiler angle decreasing.

2.4 HARMONIC TESTS

Pressures have also been measured with spoiler oscillating between 0° and 35° at 1 Hz and 5 Hz. It was expected that at 1 Hz the flow should remain quasi-steady. Surprisingly the results for both frequencies are virtually the same, these are shown for different pressure locations in Figure 6.

Underneath the spoiler there is a double frequency effect; although not shown, surprisingly, this effect is more pronounced at the lower 1 Hz input frequency. It is thought that this effect is associated with the movement of the reattachment of the flow underneath the spoiler on and off the lower spoiler surface, inducing additional suction peaks and troughs within one spoiler cycle. Moving downstream this double frequency effect soon decays although one can see some residue just aft of the spoiler. About 1 spoiler chord downstream the response is more or less harmonic; even this apparently innocuous response is deceptive because by reference to the steady results in Figure 2 the quasi steady response should be far more 'spiky' at the crests. The results at 2 spoiler chords downstream are effectively quasi-steady.

3. TWO DIMENSIONAL SPOILER ON A TWO DIMENSIONAL AEROFOIL

3.1 APPARATUS

The aim of this experiment was to investigate the pressure distributions over an aerofoil as induced by spoiler motions; different spoiler locations were to be included on the upper surface, on the lower surface, for both forward and rear locations. This range of options was thought to be desirable to cover possible future applications.

As shown in Figure 7 a special aerofoil of symmetric profile with flat surfaces where the spoilers were to be attached, was designed of chord 47.3 cm. The aerofoil was supported by two end reflecting plates, distance 76.2 cm apart. The end plates were attached to the side walls of the tunnel, the tunnel was open to atmosphere at the top and bottom. A spoiler of 3.8 cm chord could be fitted at locations $16\frac{1}{2}\%$, $22\frac{1}{2}\%$, 50% and $67\frac{1}{2}\%$, although only the two extreme locations were actually tested. The spoiler could have either a zero gap or a $12\frac{1}{2}\%$ gap. The spoiler did not recess into the surface of the aerofoil so a spoiler angle of 0° was somewhat artificial.

There were 56 pressure tapings on the aerofoil and 5 tapings either side of the spoiler. The tunnel speed was 16 m/s for all tests.

The full range of tests covered:

- i) steady pressure measurements for a range of aerofoil incidences with spoiler angles 0° , 45°
- ii) transient pressures for rapid and slower ramp changes in spoiler angle $0^\circ \leftrightarrow 45^\circ$
- iii) transient pressures for oscillatory spoiler motions at 1 Hz, 5 Hz, 18 Hz.

All of these tests were done with aerofoil incidence at 10° , with spoilers sequentially at $16\frac{1}{2}\%$, $67\frac{1}{2}\%$ chord on both upper and lower surfaces.

Again it is necessary to be selective in the results presented here.

3.2 A STEADY RESULT

The steady pressure distribution is shown in Figure 8(i) for the aerofoil and spoiler when the aerofoil is at 10° incidence and the spoiler is on the upper surface at the aft location of $67\frac{1}{2}\%$ chord and when the spoiler angle is zero. There is zero gap between the spoiler and the aerofoil surface. Because the spoiler is not recessed into the aerofoil surface it is seen that there is a disturbance pressure distribution in the neighbourhood of the spoiler. On the lower surface because of the nature of the aerofoil profile there is a slight pressure peak as the aerofoil curvature changes from the flat portion into the curved trailing edge region. There appears to be a small region of separated flow towards the trailing edge on the lower surface.

In Figure 8(ii) the steady pressure distribution is shown of the above arrangement with the spoiler at 45° . On the upper surface there is a pressure recovery ahead of the spoiler, as expected, with a constant pressure region in the separated region aft of the spoiler. On this particular aerofoil profile there is also separation of the flow on the lower surface, with the same pressure in the separated region, as expected from the trailing edge Kutta condition. It is to be noted that there is a significant loss in lift with the deployed spoiler. It is also to be noted that in this case the downward force on the spoiler itself is not an inconsiderable contribution to the loss in overall lift.

3.3 RAMP CHANGES IN SPOILER ANGLE

To investigate a fairly rapid change the spoiler angle was increased from 0° to 45° in 0.032 sec. which is approximately the time taken for the free stream to travel the distance of 1 aerofoil chord. A selection from the set of pressure records is shown in Figure 9.

Underneath the spoiler trailing edge first there is a slight increase in pressure followed by a large transient suction peak, this feature is typical and it is associated with the spoiler 'starting' vortex; the peak suction pressure coefficient, c_p , is of the order of -2.0. The spoiler starting vortex is convected downstream, as seen by the pressure record towards the trailing edge on the aerofoil upper surface. In the process of convection the pressure recovery ahead of the vortex increases while the strength of the spoiler vortex decreases. Exactly why there are subsequent oscillations in pressure are not understood.

It is reassuring to note that the pressures towards the trailing edge on the aerofoil lower surface follow fairly closely the pressures on the upper surface; these two are not identical as expected from the Kutta condition since neither pressure locations are close to the trailing edge but about 2.2 cm from the trailing edge.

In spite of the oscillations in pressure in the trailing edge region the change in pressure at a point on the forward part of the aerofoil upper surface is a fairly smooth progression; this pressure record reflects the overall loss in circulation.

It can be seen that the pressures in the trailing edge region settle down to their final steady values in about 0.16 secs from the start of the spoiler motion, in about 0.13 secs from the end of the spoiler motion. The time of 0.13 secs is equivalent to the time for the free stream to move about 4 aerofoil chord lengths. It is of interest to note that the pressure on the aerofoil upper surface well ahead of the spoiler seems to settle down to its final value before the trailing edge pressures settle down to their final values. It was thought that some of these trends might be due to the fact that the tunnel was open at the top and bottom; the experiments were repeated with solid floor and ceiling but the trends still remained.

Results when the spoiler is decreased from 45° to 0° in the same time, namely 0.032 secs are shown in Figure 10. There are no large pressure fluctuations. The pressures in the trailing edge region settle down to their final steady values somewhat faster than when the spoiler angle is increased, but only about 0.03 secs faster (i.e. equivalent to 1 aerofoil chord length). This settling period is now more uniform over the aerofoil surface, as seen from the forward upper surface location.

It is of interest and reassurance to note that the rate of change of the pressure at the forward location on the upper surface is about the same whether the spoiler angle increases or decreases. This result might be anticipated since the physical process of changing the overall circulation must be similar whether the circulation increases or decreases.

The relative short times for the flows to settle down to their final steady values are worrying. According to linearised aerofoil theory following a sudden change of incidence the overall lift will have reached 85% or more of its final steady value in about 6 chord lengths, this is significantly more than in these experiments. It is thought that these experimental results could reflect the fairly high value

of (chord/tunnel height) ratio, so significant wind tunnel interference effects could affect the rise times.

The response following a rapid ramp change of forward spoiler is of interest. For a spoiler located at 16½% aerofoil chord it is seen clearly in Figure 11 that there are two distinct response features. It is tempting to think that these two different time rates are associated with the change in local flow about the spoiler and the build up of overall circulation. However such an explanation is not satisfactory. A clue to the aerodynamic behaviour can be gleaned from the pressure traces at stations 2 and 3. In this configuration with no gap underneath the spoiler, as the spoiler angle increases a starting vortex is created which then convects downstream; as the vortex convects it loses some of its circulation into the formation of the steady shear layer. This starting and convecting vortex induces a suction pressure underneath it. The progress of the starting vortex can be seen by the suction peak at station 2 to the first suction peak at station 3; it can be seen that the vortex has moved down the aerofoil chord at about ¼ of the free stream velocity, surprisingly slowly. And so this delay in the local effects of the spoiler reaching the trailing edge accounts primarily for the slow change in the overall flow field. The time to settle down to the final steady state is about twice as long as for the aft spoiler location as shown in Figure 9, this result apparently reinforces the point made in the Introduction that forward spoilers had disadvantageous lag effects, although the practical rate of application of spoilers is relatively much slower.

To amplify the last point in practical applications, for example in gust alleviation or flutter suppression, the required rate of change of spoiler in full scale is said to be of the order of 360°/sec. Thus a spoiler motion 0° ↔ 40° in 0.11 sec implies a time in which the air stream travels about 5 aerofoil chord lengths. An analogous ramp time has been applied with the experimental arrangement for the aft spoiler location, the results are shown in Figure 12. It is seen that behind the spoiler in the trailing edge region the response is virtually quasi-static.

3.4 PERIODIC SPOILER MOTIONS

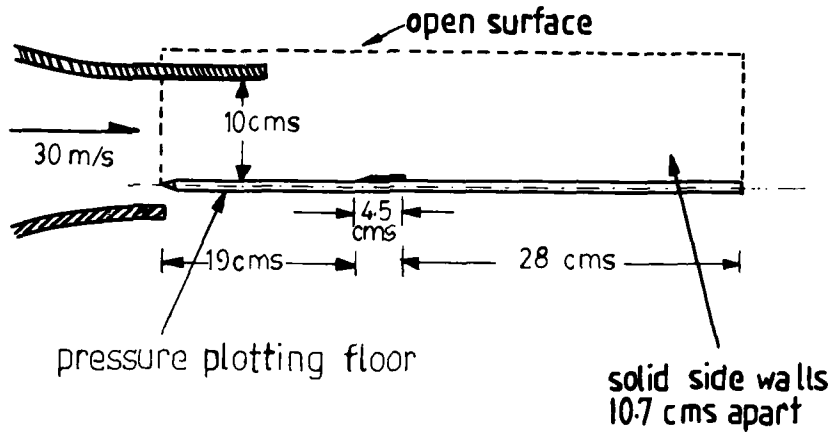
Finally some results are shown in Figure 13 when the spoiler in the aft location is oscillated in periodic additional motion at 5 Hz. It is seen that overall the response follows the spoiler oscillations but there is a shearness about the response; this shearness might be thought to be due to the difference in the build up and shedding of spoiler vorticity but unfortunately this argument would lead to a shearness in the opposite direction.

4. CONCLUDING REMARKS

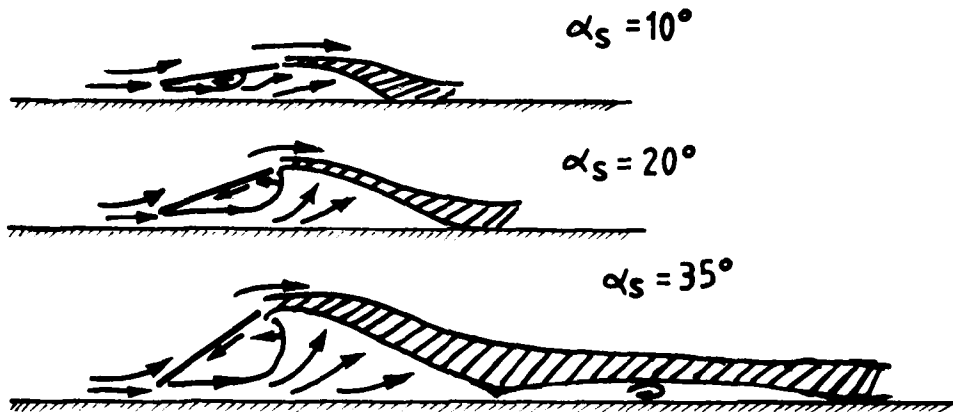
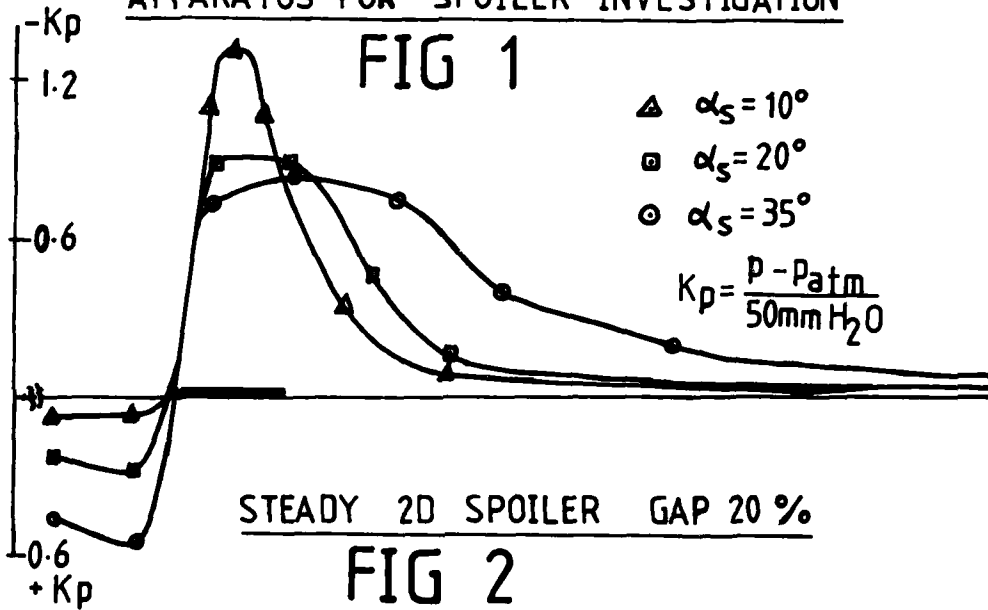
The unsteady results described in this paper are a few selected examples which illustrate some interesting features. The full set of results of this programme will be published in the open literature in the near future.

REFERENCES

1. Langley Research Dept. Summary of Lateral Control Research, NACA/TN/1245, Rept. 868, March 1947.
2. Brown G.P., Parkinson G.V. A Linearised Potential Flow Theory for Airfoils with Spoilers, Jnl. Fluid Mechs. 57, 1973.
3. Parkinson G.V. & Tam Doo P. Prediction of Aerodynamic Effects of Spoilers on Wings, AGARD C.P.204, 1976.



APPARATUS FOR SPOILER INVESTIGATION



THE THREE FLOW REGIMES GAP 20 %

FIG 3

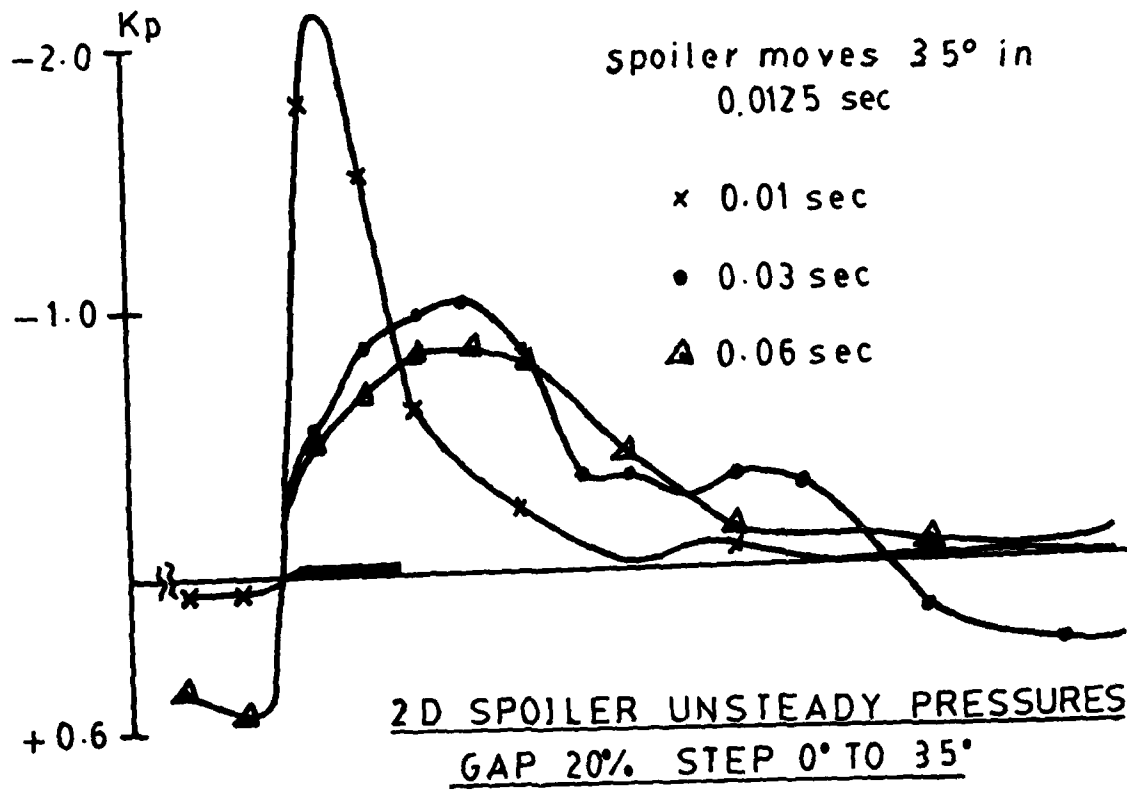


FIG 4

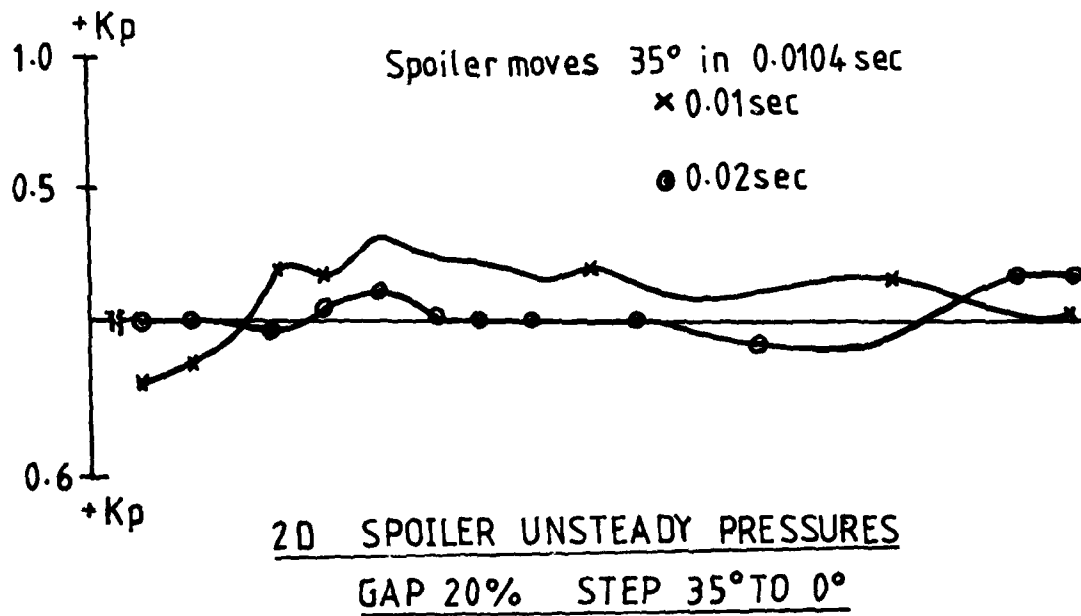


FIG 5

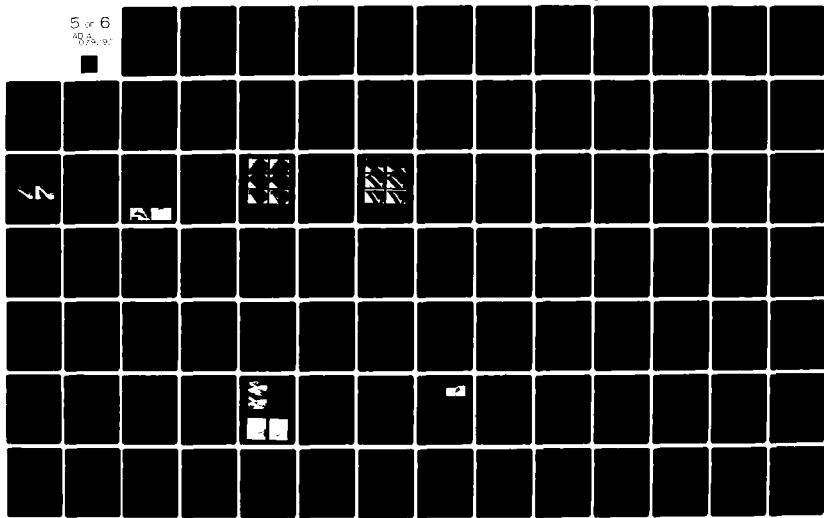
AD-A079 292 ADVISORY GROUP FOR AEROSPACE RESEARCH & DEV. NEUILLY-SUR-SEINE FR F/G 1/
AERODYNAMIC CHARACTERISTICS OF CONTROLS CONFERENCE PROCEEDINGS
SEP 79

UNCLASSIFIED

AGARD-CP-262

N/L

5 of 6
89/9/87



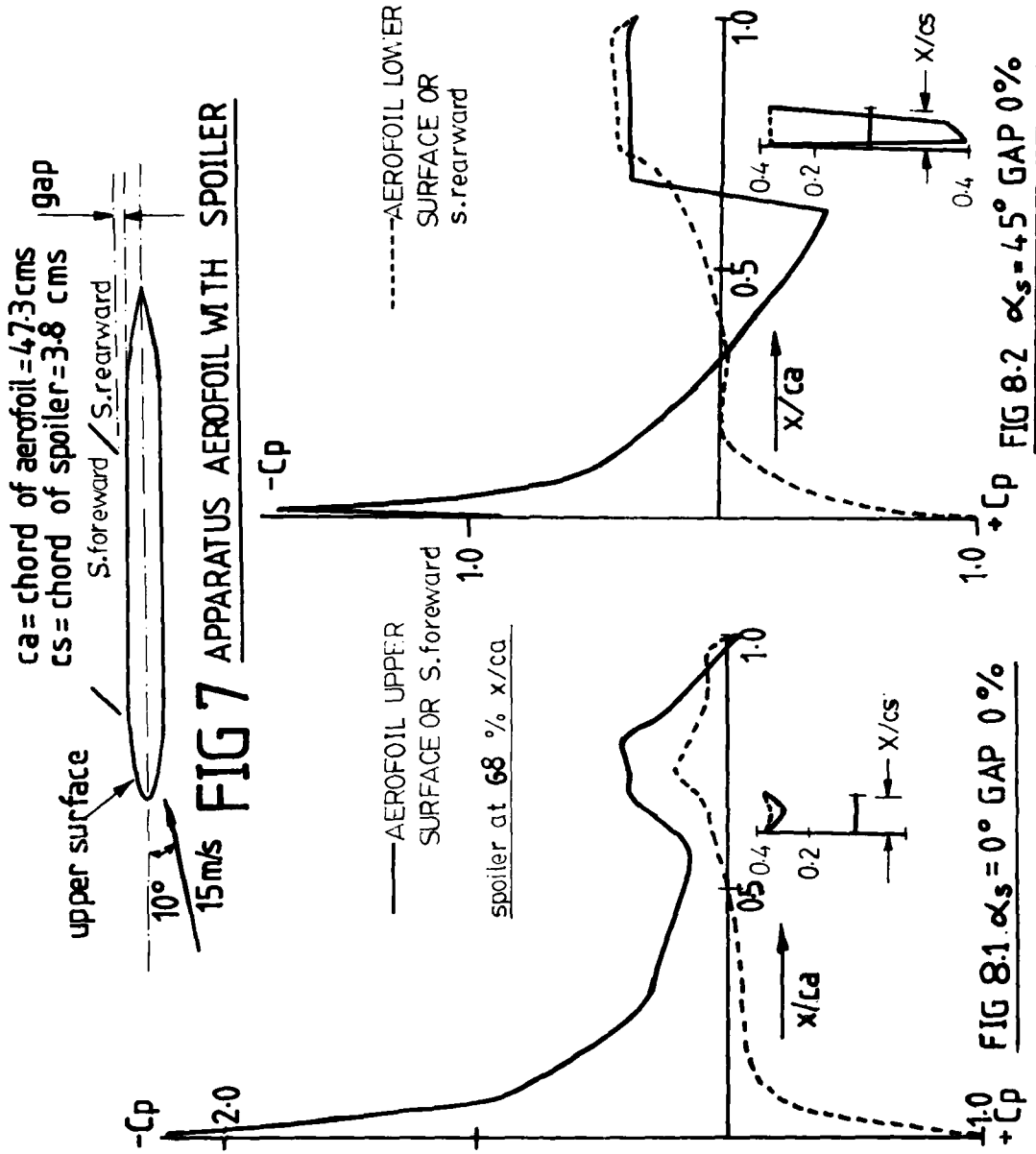
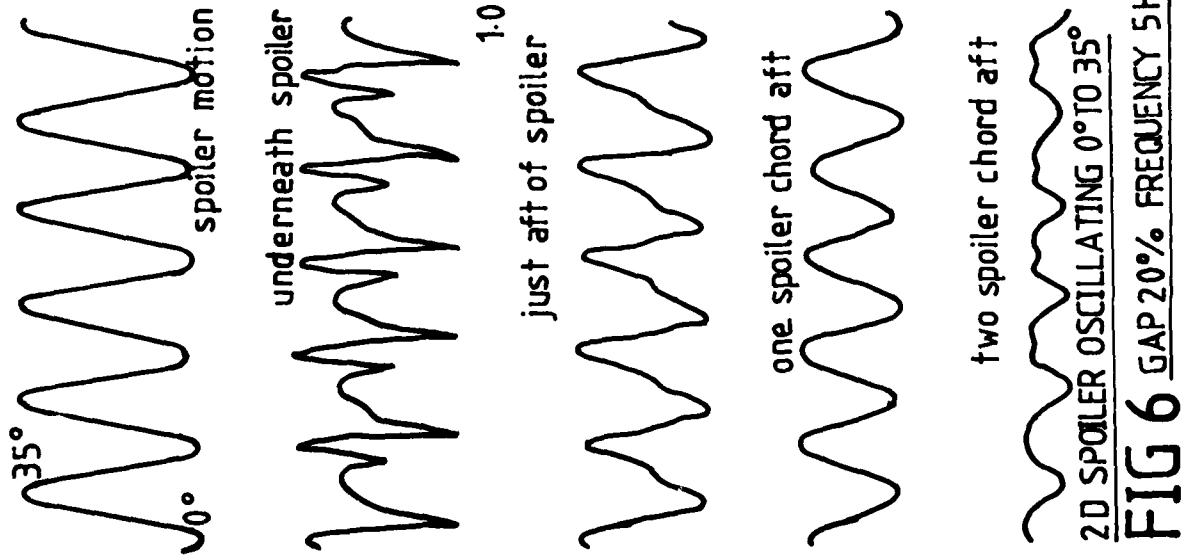
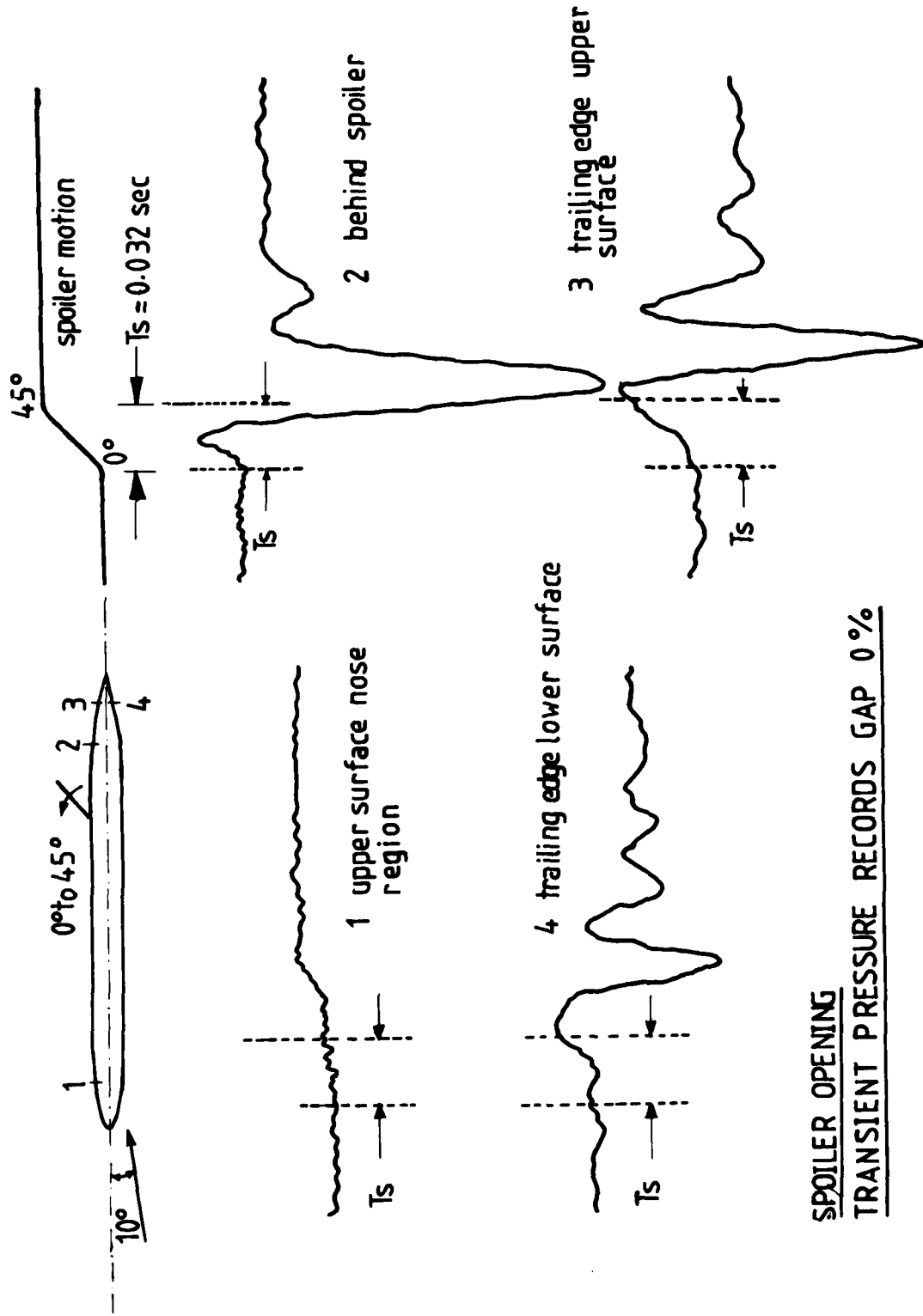
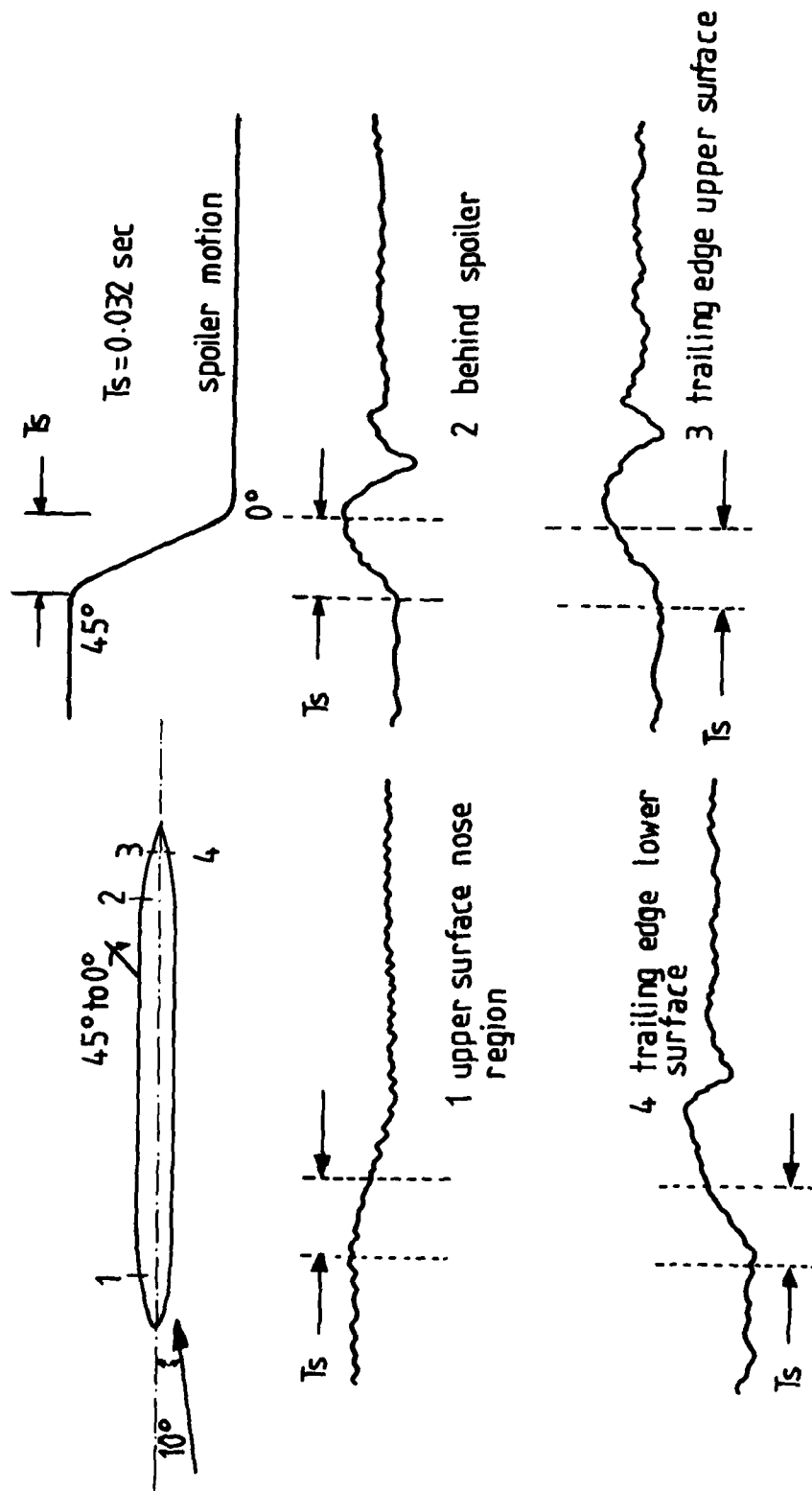


FIG 6 GAP 20% FREQUENCY 5Hz



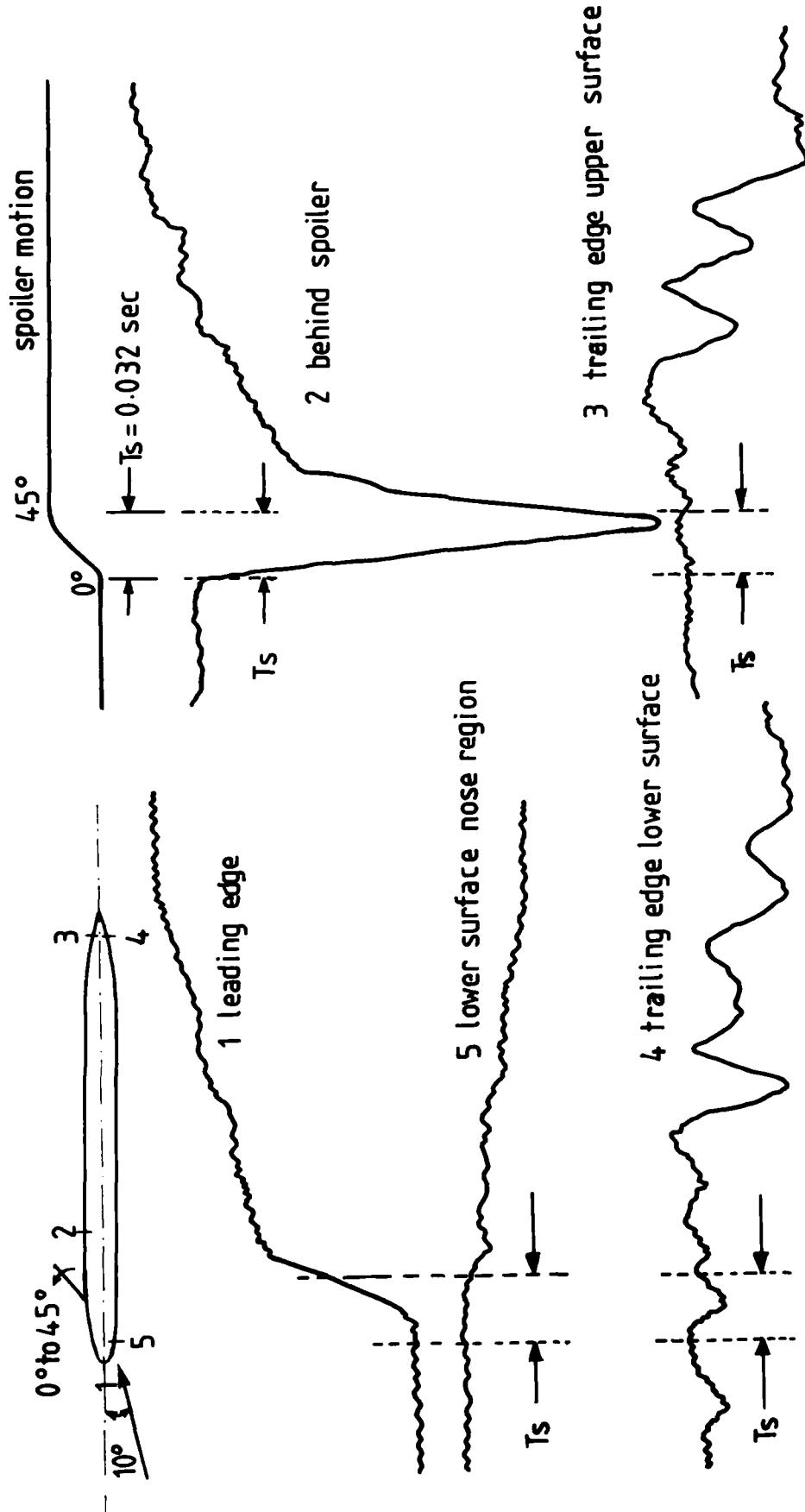
SPOILER OPENING
TRANSIENT PRESSURE RECORDS GAP 0%

FIG 9



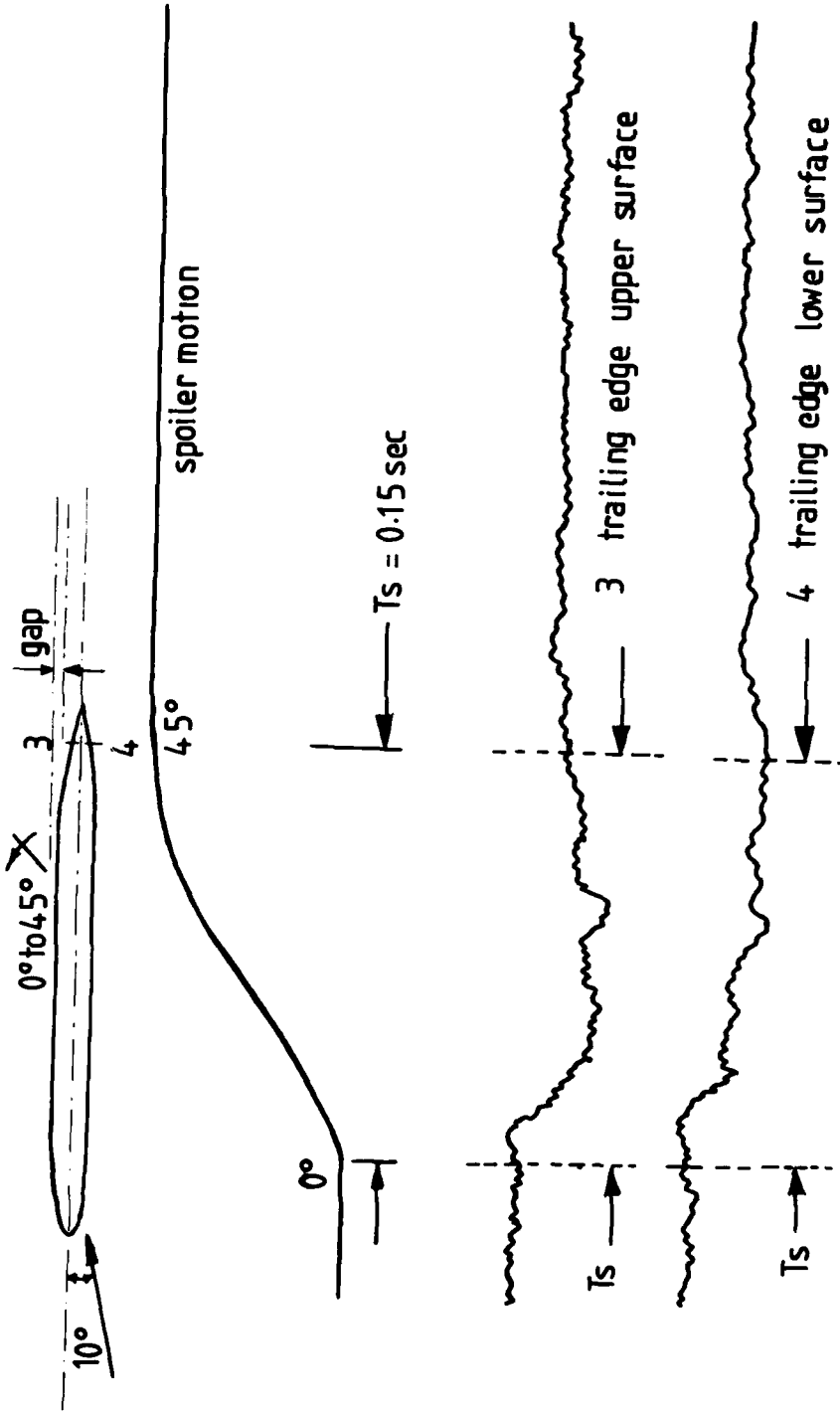
SPOILER CLOSING . TRANSIENT PRESSURE RECORDS . GAP 0 %

FIG 10



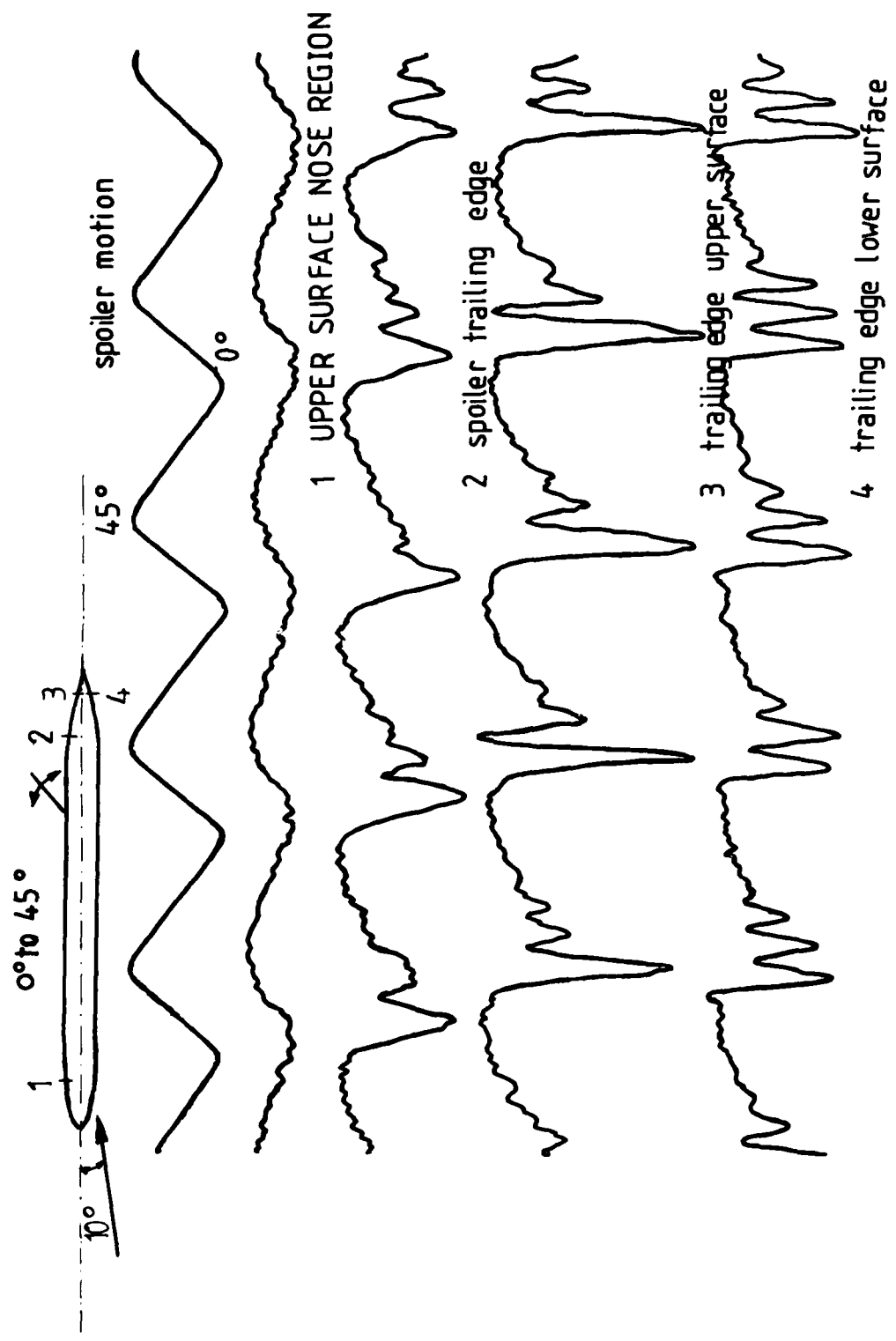
SPOILER OPENING NEAR LEADING EDGE TRANSIENT PRESSURE RECORDS GAP 0%

FIG 11



SPOILER OPENING TRANSIENT PRESSURE RECORDS GAP 12%

FIG 12



SPOILER OSCILLATING 0° TO 45° . GAP 0%. FREQUENCY 5HZ

FIG 13

TRAJECTORY BEHAVIOUR OF A CONTROL CONFIGURED
AIRCRAFT SUBJECTED TO RANDOM DISTURBANCES

by

23-1

- Achille Danesi, Professor, School of Aerospace Engineering, Rome University, Rome, Italy.
- Scott Smolka, Research Assistant, Department of Aerospace and Mechanical Engineering, Boston University, Boston, Massachusetts, U.S.A.
- Francesco Borrini, Aerospace Engineer, School of Aerospace Engineering, Rome University, Rome, Italy.

SUMMARY

This study considers the longitudinal behaviour of a Boeing B.747 aircraft with some of its original aerodynamic effectors operating as active controllers in addition to the conventional elevators. The ailerons are collectively used as outboard active flaps and the inboard section of the high lift triple slotted flaps are employed as inboard active flaps. The flight control system structure is implemented as an optimal model-following system in which the optimal feedback gains are computed to minimize the integral performance index. Errors in dynamical response, in wing root bending moment, and in aerodynamic drag computed as deviations from the same quantities related to a specified model responding satisfactorily to disturbances with zero increments in wing root bending moment and aerodynamic drag in flight maneuver at given load factor, are considered. At the same time the minimum effectors activity is included as a design objective. A lighter wing structure has been realized as the result of wing loads reduction and further weight saving (reduced tail size) has been obtained by taking advantage of the beneficial effect of the active controller activity in reducing the elevator deflections required in the pull-up maneuver. Comparisons are made in the response characteristics of the original aircraft and in the optimal closed loop active configurations subjected to continuous atmospheric turbulence. The results, presented in terms of trajectory standard deviation from the reference, indicate that the various active configurations considered in the study differ appreciably in their trajectory-following precision. A proposal for the matching-trajectory problem in the early stage of the active control design is advanced.

LIST OF SYMBOLS

- a_t = turbulence characteristic constant
- b = wing span
- h = white noise intensity
- q = pitch rate
- \bar{q} = dynamic pressure
- \underline{u} = vector of control variables
- \underline{u}_o = vector of optimal control variables
- \underline{x} = vector of state variables
- y = wing section ordinate
- \underline{y} = vector of errors in dynamical response
- \underline{z} = vector of constraint variables

- A = system state matrix
- A^C = closed loop system state matrix
- A_m = model state matrix
- B = control matrix
- C_l = local wing lift
- D = aerodynamic drag
- \underline{K}_{fb} = vector of optimal feedback gains
- K_s = modified to basic tail size ratio
- M_b = wing bending moment
- Q = state weighting matrix
- R = control weighing matrix
- S_{tb} = basic tail area
- S_{tm} = modified tail area
- T = constraint weighting matrix
- V = airspeed

23-2

- α = angle of attack
- δ_e = elevator deflection
- δ_i = inboard active flaps deflection
- δ_o = outboard active flaps deflection
- η = ratio of wing section ordinate to wing semispan
- ϕ = turbulence spectral density function
- σ_t = turbulence standard deviation
- θ = aptitude angle

INTRODUCTION

The active control technology aim is to increase payload capacity and flight endurance while saving the aircraft basic weight. The solution proposed for this purpose is to reduce the wing root bending moment in flight maneuvers, while simultaneously maintaining the active controllers activity at the allowable minimum for maneuvering requirements. In a longitudinal maneuver control system design, active wing mounted aerodynamic effectors are used as Z-force control (direct lift flaps) in addition to the conventional moment producing devices (elevators). These provide wing lift distribution control and reduce the wing root bending moment in flight maneuvers or may be used for structural mode and gust alleviation control purposes. In this study an active configured Boeing B.747 is considered with the original ailerons collectively used as outboard active flaps, and the internal sections of the high lift triple slotted flaps, displaced to the high lift reference positions, as active inboard flaps. To redistribute the lift in a desirable fashion, negative active controller deflections are required, yielding a beneficial effect of reducing the elevator deflections required in the maneuvers. By decreasing the tail size to the limit at which forces and moments generated by the active controllers may compensate the aerodynamic loss derived from the varying tail size, further weight saving may be obtained in addition to the lighter wing structure expected in reducing the wing root bending moments. This advantage may be obtained at the expense of some reduction in stability static margin, so a less stable and a less well-behaved airframe is generally expected in active control configurations. To avoid stability considerations which may impose strong constraints on the airframe geometry, limiting the advantages that can be obtained with active control design, more inherent static longitudinal stability must be built into the basic airframe. The use of a feedback control system is provided to reach the required stability margin, simultaneously maintaining acceptable dynamic behavior. In this sense, an augmented flight control system must be considered in active control design as a fundamental subsystem in which the feedback gains satisfy the active control requirements.

Linear optimal control theory is applied in order to determine the optimal feedback gains which minimize an integral performance index of errors in dynamical response in the wing root bending moment and aerodynamic drag with respect to a specified model system. This system behaves satisfactorily with zero incremental wing root bending moment and aerodynamic drag in flight maneuver at given load factor. The aerodynamic drag was included in the performance index since more drag is experienced in active configurations, hence the optimization procedure was planned to minimize the incremental aerodynamic drag. This also implies the minimization of the active controller displacements which directly influence trim drag and saturation of controls. In the aerodynamic computations, the procedure adopted consisted of the following steps:

- Determination of the spanwise lift distribution due to angle of attack and combinations of active controller deflections
- Computation of the incremental wing root bending moment associated with angle of attack and active controller deflections
- Formulation of the aerodynamic drag and wing root bending moment constraint equations
- Numerical evaluation of the relaxing effects in the wing root bending moment and pitching capability supplementing the elevator deflection required to perform the maneuver
- Proposal of a more effective control configuration from the active point of view are advanced; in each case the percentage reduction in the incremental wing root bending moment and tail size is considered

The above mentioned computations were carried out with the "Aerodynamic and Structural Section" of the S.O.A.C. (Self Organized Active Control) program introduced in Ref.6 from which Fig.1 is reproduced. This figure depicts the overall computational procedure which yields the optimal regulator solution for typical active control problems formulated as a model following problem. The preliminary data obtained from the aerodynamic and structural section are applied to the Aerodynamic Structural Constraint Function Generating (ASCFG) program which generates the matrices pertaining to the constraint equations. Subsequently, the Active Control Relaxing Function Generating (ACRFG) program computes the relaxing functions relating the constraint and control variables to the active controller deflections, aiding the designer in the development of the most effective control configuration in terms of percentage reduction in the basic structural weight of the vehicle due to wing and tail geometry changes. This intermediate phase is carried out in a trial fashion requiring the iterative use of the above-mentioned programs starting with an active control configuration assumed as a first step approximation. The configuration chosen for the configured Boeing B.747 aircraft was derived following the

above-described trial procedure. This proved that the active flaps sections considered in the study are capable of generating the required additional aerodynamical forces and moments. The chosen configuration was submitted to the optimization procedure in order to design an optimal flight control system implementing the solution yielded by linear control theory. To that purpose the "Optimal Control Section" of the SOAC program was employed, yielding an optimal active controller satisfying the design requirements. In this computational stage the mathematical treatment discussed in Ref. 6 was applied to include the aerodynamical and structural constraints in the system state equation in order to obtain a unique mathematical model for the minimization procedure and also to reduce the linear optimal control problem to a standard optimal regulator problem as stated in Ref. 1. This was performed reformulating the performance index and defining, starting with the general two point boundary problem in which a new Hamiltonian function was introduced, an equivalent system inherently accounting for the model response error and the aerodynamical and structural constraints. Also an equivalent weighting matrix which imposes specified weight to all state and control variables was established. The proposed optimization problem is then solved as a standard regulator problem implying the solution of the steady Riccati equation. These computations are numerically carried out in the GAC (Generalized Active Control) subroutine called by the SOAC program, acting as main program, which provides the input data transfer. An iterative procedure is also provided to restate the state and control weighting matrices to allow a satisfactory system convergence toward the proposed model. The resulting optimal closed loop system behaviour in response to random inputs is obtained using the Generalized Graphical Time Response (GGTRESP) program described in Ref. 9.

BASIC AIRPLANE DESCRIPTION

The Boeing B.747 is a wide body, four engine, turbofan commercial transport aircraft designed for long range operations. The dimensions and areas pertaining to this vehicle are shown in the standard technical manuals. The landing configuration at the maximum landing weight (255,825 Kg.) and 33% M.A.C. center of gravity position with landing gear down, trailing edge high lift and Krueger flaps fully extended, is taken as reference in the active control problem formulation. The flight condition is typical in the approach phase at an airspeed of 117 m/sec. on a sub-horizontal glide slope at about 330 meters from the ground. The aerodynamic coefficients and derivatives relative to the above-considered configuration are summarized in Table I where the angles and angular velocity are given in radians; all symbols shown coincide with those of Ref. 4. The perturbed longitudinal motion of the basic airframe is described by the linear state equation

$$\dot{\underline{x}}(t) = A \underline{x}(t) + B U(t) \quad (1)$$

where the state vector $\underline{x}(t)$ is defined as

$$\underline{x}^T(t) = [\Delta V, \Delta \delta, q, \Delta \theta] \quad (2)$$

The appearing components are the vehicle state variables (air speed, angle of attack, pitch rate and aptitude) from the reference condition due to an incremental aerodynamic control (elevator) deflection represented by the scalar variable $u(t)$ in Eq. (1). The elements of the state and control matrices are derived considering the expressions given in Ref. 4.

THE GEOMETRY OF THE ACTIVE CONTROLLERS

The choice of the controller configurations on the wing was accomplished after several numerical trials. In determining the more effective solution from the active point of view, the first priority was the use of the aerodynamic effectors already present in the basic wing for the required functions. The basic low speed ailerons were employed as outboard active flaps with collective displacement superimposed on the aileron differential motion. This is required for lateral control in which these control surfaces act as direct lift flaps. The original triple slotted high lift inboard flaps arrangement was changed to a simple split structure displaced with respect to high lift flaps positions required in landing configuration. The active controller maximum displacements are considered within the linear portion of the aerodynamic effector characteristics, unchanged by active control deflections. Table II presents the geometric characteristics of the control surfaces employed as active controllers, while the view of the wing active configuration is depicted in Fig. 2. The aerodynamic derivatives for the active control surfaces were obtained applying the methods given in Ref. 8 and the numerical values are also given in Table II.

THE MANEUVER CONSIDERED IN CONSTRAINT FORMULATION

The maneuver taken as reference in the formulation of the constraint equations was a stationary pull-up at the load factor of 2.5 under M.L.S. (microwave landing system, see Ref 10 and 12) up-link command initiated at the category II decision height (18,28 mt.) on a glide slope of 2.8 degree. The aircraft was then submitted to a continuous gusting atmospheric turbulence disturbing the actual trajectory from the desired trajectory given by the El-2 M.L.S. station. The angle of attack, lift coefficient, and elevator deflection values pertinent to the flight conditions just before and during the pull-up maneuver appear in Fig. 8.

THE AERODYNAMICS OF THE WING MODIFIED FOR ACTIVE CONTROL PURPOSES

23-4 In this section the changes in wing root bending moment and aerodynamic drag are developed as a function of the active controller deflections which, together with the elevator deflections, force the aircraft to respond to a 2.5 g command. It is assumed that the wing lift distribution due to the active controller deflections are linear with respect to the angle of attack, and with respect to active controller deflections. (Simply additive with no interference effect between control surfaces.) These hypotheses restrict the validity of the solution to the linear range of the lift slope; i.e., for angle of attack lower than 15 degrees and active controller deflections lower than 5 degrees. The lift distributions due to a unitary increment in the angle of attack and active control deflection as a function of the wing section abscissas, expressed as a percentage of the wing semispan, are given in the figures 3,4 and 5.

THE INCREMENTAL WING ROOT BENDING MOMENT DUE TO ANGLE OF ATTACK AND ACTIVE CONTROLLER DEFLECTIONS.

The incremental wing root bending moment due to a unitary increment in the angle of attack and active controller deflections has been computed applying the following formula:

$$\Delta M_{b_i} = y_b \bar{q} S C_{L_i} \quad (i = \alpha, \delta_i, \delta_o) \quad (3)$$

where y_b is the moment arm or position at which an equivalent force will produce the same wing root bending moment as the actual lift distribution does. This moment arm may be obtained directly from the wing lift distributions derived in the previous section via the ratio

$$y_b = \frac{A_M}{A_L} = \frac{\int_0^1 \eta \Delta C_L(\eta) d\eta}{\int_0^1 \Delta C_L(\eta) d\eta} \quad (4)$$

A_M is the area under the curve representing, for each variable, the product of the incremental lift distribution times the span position. Applying (3) and (4) the following incremental wing root bending moment values were obtained:

$$\begin{aligned} \Delta M_{b_\alpha} &= 16,226,901 \quad \text{Kgm/rad} \\ \Delta M_{b_{\delta_i}} &= 1,703,514 \quad \text{"} \\ \Delta M_{b_{\delta_o}} &= 1,581,501 \quad \text{"} \end{aligned}$$

Since these incremental values are unitary increments in the corresponding state and control variables, they may be interpreted, within the assumed linear hypotheses, as the bending moment derivatives with respect to the same variables and simply indicated by the symbol M_{b_i} ($i = \alpha, \delta_i, \delta_o$). The incremental wing root bending moment in maneuver may be written as

$$M_b = (M_{b_\alpha}) \Delta \alpha + (M_{b_{\delta_i}}) \Delta \delta_i + (M_{b_{\delta_o}}) \Delta \delta_o \quad (5)$$

By means of (5) the effectiveness of the proposed active control configuration in relaxing the wing root bending moment in a maneuver at given load factor may be determined. Considering the new system state variable

$$z_m(t) = \Delta M_b(t) \quad (6)$$

Equation (6) may be written in matrix form as:

$$z_m(t) = M \underline{x}(t) + N \underline{u}(t) \quad (7)$$

where $\underline{x}(t)$ is the state vector (2) and $\underline{u}(t)$ is the control vector given by:

$$\underline{u}^T(t) = | \delta_i(t), \delta_o(t) | \quad (8)$$

the components of which are the active controller deflections. The n-row vector M and the m-row vector N (m is the number of active controllers) have the structures

$$M^T = | 0, (M_{b_\alpha}), 0, 0 | \quad (9)$$

$$N^T = | (M_{b_{\delta_i}}), (M_{b_{\delta_o}}) | \quad (10)$$

Equation (8) will be used as constraint equation in the optimal control problem treated later in this study. The other constraint equation taken into consideration is relative

to the incremental aerodynamic drag in the same flight maneuver considered in the incremental wing root bending moment evaluation. Introducing the state variable

$$z_d(t) = \Delta D(t) \quad (11)$$

where ΔD is the incremental aerodynamic drag in maneuvering due to the angle of attack change and active controller deflections:

$$\Delta D = \bar{q} S (C_{D_\alpha} \Delta\alpha + C_{D_{\delta_i}} \Delta\delta_i + C_{D_{\delta_o}} \Delta\delta_o) \quad (12)$$

In (12) the system drag aerodynamic derivatives due to angle of attack and active controller deflections appear. The constraint equation relative to the incremental aerodynamic drag is then written as

$$z_d = L \underline{x}(t) + H \underline{u}(t) \quad (13)$$

where the n-row L vector and the m-row H vector are defined as

$$L^T = | 0, L_{d_\alpha}, 0, 0 | \quad (14)$$

$$H^T = | 0, H_{d_{\delta_i}}, H_{d_{\delta_o}} | \quad (15)$$

For the case at hand, the L and the H matrices are numerically expressed as

$$L^T = | 0, 437,403, 0, 0 |$$

$$H^T = | 0, 46150, 22350 |$$

PROVISION ABOUT TAIL SIZE RELAXATION

The incremental aerodynamic moment with respect to the aircraft center of gravity required to perform the pull-up maneuver is given by

$$\Delta M_G = \bar{q} S \bar{c} (C_{M_{\delta_e}} \Delta\delta_e + C_{M_{\delta_i}} \Delta\delta_i + C_{M_{\delta_o}} \Delta\delta_o) \quad (16)$$

Considering that the active controllers deflection are supplementing the elevators effect in producing the center of gravity moments, it may be concluded that the elevator deflections are reduced in maneuvering by the active controllers activity. The same incremental baricentric moment may be obtained by decreasing the tail size while maintaining the elevator deflection, resulting in a further structural weight saving. To evaluate this effect, the ratio between the modified tail size (S_{tm}) and the basic value (S_{tb}) was introduced:

$$K_s = \frac{S_{tm}}{S_{tb}} \quad (17)$$

The control derivatives were defined as a function of this ratio.

In Table III these functions are summarized and in Table IV the expressions of the state and control matrix elements as a function of the ratio K_s are given. The characteristic equation root locus with K_s as variable parameter is plotted in Fig. 6, giving the critical K_s value at which the system becomes unstable. Assuming for K_s the limit value of 0.8, the state and control matrices for the stable cases $K_s = 0.9$ and $K_s = 0.8$ were computed as given in Table V. For comparison purposes, the case $K_s = 1.0$ was also included. The relaxed configurations relative to the assumed cases together with the constraint equations (7) and (13) were considered in the optimization problem treated in the following sections.

THE ACTIVE FLIGHT CONTROL SYSTEM OPTIMIZATION PROBLEM

In the active control system problem at hand, a feedback control subsystem is proposed to minimize in flight maneuvers, both the error existing in the dynamical response with respect to a specified model which exhibits zero incremental wing root bending moment, and aerodynamic drag. This condition is considered an ideal objective in the active control solution. To solve such a multivariable optimization problem, linear optimal control theory (Ref. 1) was applied. An integral quadratic performance index was formulated as follows:

$$2 J = \int_0^\infty (\underline{y}^T Q \underline{y} + \underline{z}^T T \underline{z} + \underline{u}^T R \underline{u}) dt \quad (18)$$

where \underline{y} is a vector of the errors in the dynamical response of the system with respect to a response model, \underline{z} is the constraint vector (the elements of which are just the aerodynamic and structural constraints imposed by the active problem) and \underline{u} is the control vector. The weighting matrices Q, T and R express the relative emphasis placed on each argument in the performance index. The procedure adopted to solve the proposed optimization procedure is to provide a unique mathematical model in which the aerodynamical and structural constraints are included in the system state equation and to reduce the

problem formulation to a standard optimal regulator problem.

The mathematical treatment from which the above mentioned procedure was derived is discussed in Ref. 5 and the computer program to solve numerically the optimization problem is presented in Ref. 6. The conclusions drawn from these works, are now briefly summarized. To find the optimal control law $u_0(t)$ for the n-order system (2) for which m active controllers and k constraints are considered, the proposed performance index (18) is manipulated mathematically to appear in the compact form

$$2J = \int_0^{\infty} (\xi(t) S \xi(t)) dt \quad (19)$$

Here $\xi(t)$ is an (n+m) augmented vector given by

$$\xi^T(t) = [x^T(t), u^T(t)] \quad (20)$$

and S is an (n+m) squared matrix:

$$S = \begin{vmatrix} F_1 & & F_2 \\ \hline & & \\ F_2^T & & \bar{R} \end{vmatrix} \quad (21)$$

The matrices F_1 , F_2 and \bar{R} , respectively sized (nxn), (nxm), and (m xm) are defined as

$$F_1 = \bar{Y}^T \bar{Q} Y; \quad F_2 = \bar{Y} \bar{Q} \bar{Z}; \quad \bar{R} = \bar{Z}^T \bar{Q} \bar{Z} + R$$

with the (n+k) xn and (n+k) x m \bar{Y} and \bar{Z} matrices given by

$$\bar{Y} = \begin{vmatrix} \bar{A} \\ \hline \bar{Z}_m \end{vmatrix} \quad \bar{Z} = \begin{vmatrix} B \\ \hline A_d \end{vmatrix} \quad (22)$$

The (nxn) \bar{Q} and \bar{A} matrices are

$$\bar{Q} = \begin{vmatrix} Q & & 0 \\ \hline & & T \\ 0 & & \end{vmatrix} \quad A = A - A_m \quad (23)$$

Observe that the matrix \bar{A} represents the difference in the system and model state. The matrices Z_m and Z_d are, respectively, the state and control components of the constraint vector z :

$$z^T = \begin{vmatrix} z_m^T & z_d^T \end{vmatrix} \quad (24)$$

the components of which are defined in (7) and (13), and consequently:

$$z_m = \begin{vmatrix} M \\ \hline L \end{vmatrix} \quad z_d = \begin{vmatrix} N \\ \hline H \end{vmatrix} \quad (25)$$

This yields the equation

$$z(t) = z_m x(t) + z_d u(t) \quad (26)$$

The solution of the standard optimal regulator problem is equivalent to the one for the actual active control problem and is obtained as the solution of the following state equation:

$$\dot{x}(t) = A_e x(t) + B_e u(t) \quad (27)$$

Here

$$A_e = A - B \bar{R}^{-1} F_2^T \quad B_e = B \quad (28)$$

which inherently accounts for the model response error and for the constraints. An equivalent state weighting matrix S_c imposing specified weights on all state and control variables is used in solving the optimization problem for the equivalent system (27), providing the minimization of the following performance index:

$$2J = \int_0^{\infty} (x^T S_c x + u^T \bar{R} u) dt \quad (29)$$

with

$$S_c = \begin{vmatrix} Q_e & & 0 \\ \hline & & \\ 0 & & \bar{R} \end{vmatrix} \quad Q_e = F_1 - F_2 \bar{R}^{-1} F_2^T \quad (30)$$

The optimal feedback control law resulting from the above summarized system transformation is expressed by

$$K_{fb} = -\bar{R}^{-1} \left[B^T P(t) + F_2^T \right] \quad (31)$$

The n-squared symmetric matrix appearing in (31) is obtained as the solution of the standard Riccati equation:

$$\dot{P}(t) = P(t) A_e + A_e^T P(t) - P(t) B \bar{R}^{-1} B^T P(t) + Q_e \quad (32)$$

Since the active control problem is essentially a stationary one in the sense that the searched solution must provide a feedback controller capable of maintaining the stationary equivalent system within acceptable deviation from the model trajectories using a minimum amount of controls, the Riccati equation may be solved for the steady state value of $P(t)$. Within the conventional definiteness hypotheses on the weighting matrices \bar{R} and Q_e , this solution guarantees optimality for all initial states of the equivalent system; i.e., it yields the minimum integral value of the incremental wing root bending moment and aerodynamic drag, and minimum integral of the transient error with respect to the same incremental quantities proposed for the model. The optimal control law,

$$u_o(t) = K_{fb} x(t) \quad (33)$$

when substituted in the equivalent system (26), gives the optimal closed loop representation

$$\dot{x}(t) = A_e^C x(t) \quad (34)$$

$$A_e^C = A_e - B K_{fb}$$

This was used in the following section to derive the dynamical behaviour of the optimized active control system in closed loop configuration in response to a random disturbance from the reference set point.

THE RESULTS OF THE COMPUTATIONAL PROCEDURE

For the active flight control system design of the Boeing B.747 aircraft only the short period mode in the landing configuration was taken into consideration; consequently the response model was also chosen referring to this mode resulting in a second-order state equation with the state matrix given by

$$A_m = \begin{vmatrix} 0 & 1 \\ -2.083 & -8.86 \end{vmatrix}$$

This was obtained by applying the conventional response criteria. Choosing weighting matrices

$$Q = \begin{vmatrix} 10^{10} & 0 \\ 0 & 1 \end{vmatrix} \quad R = \begin{vmatrix} 1 & 0 & 0 \\ 0 & 1 & 0 \\ 0 & 0 & 1 \end{vmatrix} \quad T = \begin{vmatrix} 10^2 & 0 \\ 0 & 10 \end{vmatrix}$$

the output of the SOAC program yields for the case $K_g = 1.0$ the optimal feedback gain matrix elements presented in Table IV.

THE OPTIMAL FLIGHT CONTROL SYSTEM STRUCTURE

Figure 7 depicts the physical configuration of the optimal flight control system in which the α -sensor is substituted with a dynamical controller which provides the recovery of the angle of attack state variable from the measurable variables (see Ref. II) thereby defining the complete system state. The servos employed to activate the elevators and the active inboard and outboard flaps are fed with signals possessing intensity defined by the optimal control law (33). The limiters included in each active controller channel are provided so that the controller deflections do not exceed the maximum value allowable considered for validity under the hypotheses given in the problem formulation. Since the main objective of this study is the evaluation of the active-modified aircraft behaviour in response to a continuous gusting turbulence, the problem regarding the response to command inputs was discarded in the optimization formulation; consequently the computed controller gains will provide an optimal control only when the aircraft is subjected to disturbances.

THE ACTIVE OPTIMAL CONTROL SYSTEM BEHAVIOUR IN RANDOM ENVIRONMENT

The behaviour of the optimal closed loop active system for the various configurations considered in the preceding sections in response to a continuous atmospheric gusting turbulence was digitally simulated employing the GGTRESP program described in Ref. 9. The homogeneous, isotropic turbulence model employed is given by the following widely accepted form of the one-dimensional spectrum function:

$$\phi(\omega) = \frac{2 \sigma_t^2 a_t}{\pi} \frac{1}{\omega^2 + a_t^2} \quad (35)$$

23.8 where σ_t is the standard deviation of the turbulence having zero mean value. Here, a_t is the characteristic constant associated with the turbulence to be evaluated as the ratio between the aircraft airspeed and the integral scale of turbulence. To simulate the spectral density (35), a continuous white noise was shaped by a low-pass filter described by the state equation

$$\dot{\rho}(t) = -a \rho(t) + h^2 \delta(t) \quad (36)$$

where a is the inverse of the filter time function and h^2 represents the intensity of the white noise $\delta(t)$. Imposing that the output power spectral density of the filter output is equal to the turbulence power spectral density (35), the filter time constant and the white noise intensity may be expressed as a function of the turbulence characteristics constant and standard deviation. Augmenting the optimal closed loop equivalent system (34) with the filter state equation (36) yields the augmented state equation

$$\dot{\underline{z}}(t) = \underline{A}_a \underline{z}(t) + \underline{B}_a \delta(t) \quad (37)$$

where

$$\underline{z}^T(t) = \begin{bmatrix} \underline{x}^T(t) & \rho(t) \end{bmatrix}$$

and

$$\underline{A}_a = \begin{bmatrix} \underline{A} & \underline{0} \\ \underline{0} & -a \end{bmatrix}, \quad \underline{B}_a = \begin{bmatrix} \underline{0} \\ h^2 \end{bmatrix}$$

In the simulation, the white noise was replaced by a time series having a flat spectrum over the filter bandwidth. The filter time constant was chosen to attenuate the smaller turbulence wavelength ($\tau = 0.63$ sec.). Three standard deviation values of the turbulence vertical speed ($\sigma_t = 1.03 - 1.223 - 1.82$ m/sec) were taken into consideration with the white noise intensity defined by

$$h^2 = 4 \sigma_t^2 \cdot a \quad (38)$$

Assuming as initial reference conditions those pertaining to the stationary pull-up maneuver, Eq. (37) was integrated and the vertical speed and angle of attack standard deviations from the reference point were derived for the active configurations considered in the study. In Fig. 9 the computed standard deviations are depicted as functions of the turbulence standard deviation. In Fig. 10 the inboard and outboard active flaps displacements required to minimize the arguments considered in the performance index in gusting environments of different intensity are presented. The wing root bending moment relaxation ratio is defined by

$$K_r = \frac{(\Delta M_b)_{ac} - (\Delta M_b)_b}{(\Delta M_b)_b} \quad (39)$$

This represents the percentage reduction in the incremental wing root bending moment obtained by the active configurations with respect to the bare aircraft in the same pull-up maneuver. The effectiveness in relaxing the airframe structure is described in Fig. 13 in which K_r is displayed as a function of the turbulence standard deviation.

The short period flying qualities of the active configurations are compared with those relative to the bare aircraft in the acceptability diagram of Fig. 14 from Ref. 4.

CONCLUSIONS AND RECOMMENDATIONS

A flight control system was designed for the Boeing B. 747 transport aircraft. The aim was to activate some of its basic aerodynamic effectors for use as direct lift controllers, thereby redistributing the aerodynamic load on the wing with the aim of reducing the wing root bending moment in flight maneuver at the maximum load factor, and consequently to save the basic structural weight. The usefulness of the active controllers as turbulence attenuator devices was also examined via digital flight simulation. In this case the modified aircraft was subjected to a continuous gusting turbulence with varied intensities. The flight control system feedback gains were computed to minimize simultaneously the response error to disturbances, the incremental wing root bending moment, and aerodynamic drag with respect to a satisfactory flying qualities model which responds in the same maneuver with zero increments in wing root bending moment and aerodynamic drag. The study considered the more restrictive case where only the aerodynamic effectors on the wing are employed as active controllers in the maneuver performed with the elevators fixed at the position required for a stationary pull-up at the given load factor. The elevators were included in the active control loop to further improve the results obtained considering only the effectors, particularly with regard to turbulence suppression effectiveness. The total reduction in the wing root bending moment obtained using only the wing effectors as active controllers amounts to approximately 6% with respect to the value computed for the bare aircraft. The modified Boeing B. 747 flying qualities were also improved with an increase in the undamped natural frequency approaching the value provided for the model. The wing active

23-9

controllers activity levels proved to be small, validating the hypotheses about the use of the wing aerodynamic effectors within the linearity limits of their aerodynamic characteristics, ensuring as well that they are practically unaffected in their basic functions as high lift flaps (inboard controllers) and as low speed ailerons (outboard controllers) when moved in a modular way under optimized active control. An attempt was made to use the active controllers effect in supplementing the control moments generated by the elevators in order to obtain a further weight saving by reducing tail size. Considerable worsening in flying qualities with insignificant improvements in the other characteristics discouraged consideration of these results in the design. Important advantages appeared instead by considering the effects of the wing active controllers as turbulence attenuators in that increments in angle of attack and vertical speed generated in digital flight simulation by continuous gusting turbulence, were drastically reduced in the optimized active controlled aircraft with respect to the bare configuration. This advantage, when considered with the others previously discussed, makes the proposed active configuration very attractive from the point of view of transport operations. Since the design started with a fixed wing geometry and control effector configurations, only limited advantages may be expected in application of active control strategy. Many other benefits may be obtained by incorporating these concepts into the preliminary design stage of a new airframe. The use of aerodynamic active controllers as independent devices on the wing and tail surfaces activated by an automatic flight control system optimized with respect to disturbances and command inputs, is proposed. Other aspects of the problem and further research efforts in this area have been considered by the authors and the results shall appear in future papers.

TABLE I

BOEING B.747 STABILITY AND CONTROL DERIVATIVES

$C_{L\alpha}$	=	5.406	$C_{D\alpha}$	=	1.031	$C_{M\alpha}$	=	-1.0370
$C_{L\dot{\alpha}}$	=	6.68	$C_{D\dot{\alpha}}$	=	-	$C_{M\dot{\alpha}}$	=	-2.821
C_{Lq}	=	4.25	C_{Dq}	=	-	C_{Mq}	=	-19.95
$C_{L\delta_e}$	=	0.3037	$C_{D\delta_e}$	=	-	$C_{M\delta_e}$	=	-1.2147

TABLE II

ACTIVE CONTROLLERS GEOMETRICAL AND AERODYNAMICAL CHARACTERISTICS

Active Controller	Wing portion cov. (% b/2)	Area (each side) m ²	M.A.C. (m)	Max. defl. (degree)
Inboard	0.11-0.38	8.56	1.1	5
Outboard	0.44-0.95	4.26	0.62	5
	$C_{L\delta_i}$ = 0.3037		$C_{M\delta_i}$ = -0.0004	
	$C_{L\delta_o}$ = 0.185		$C_{M\delta_o}$ = -0.214	

TABLE III

AERODYNAMIC AND CONTROL DERIVATIVES AS A FUNCTION OF THE RELAXATION RATIO K_S

$C_{L\alpha}$	=	$4.815 + 0.591 K_S$	$C_{M\alpha}$	=	$2.217 - 3.254 K_S$
$C_{L\dot{\alpha}}$	=	$9.11 - 2.43 K_S$	$C_{M\dot{\alpha}}$	=	$6.06 - 8.88 K_S$
C_{Lq}	=	$-2.5 + 6.75 K_S$	C_{Mq}	=	$4.74 - 24.7 K_S$
$C_{L\delta_e}$	=	$0.3037 K_S$	$C_{M\delta_e}$	=	$-1.2147 K_S$
$C_{L\delta_i}$	=	0.304	$C_{M\delta_i}$	=	0.004
$C_{L\delta_o}$	=	0.1848	$C_{M\delta_o}$	=	0.2144

TABLE IV

OPTIMAL FEEDBACK GAIN MATRIX ($K_S = 1.0$)

$$K_{fb} = \begin{vmatrix} -10.32 & -0.5 & 10^{-4} \\ -1.25 & 1.2 & 10^{-5} \end{vmatrix}$$

REFERENCES

1. DANESI, A.: "Linear Optimal Control Theory Applied to the Aerospace Flight Control Systems," Series of written lectures held at the Aerospace Department of Rome University, Rome, Italy, 1978.
2. BRYSON, A. E. AND YU-CHI HO: Applied Optimal Control, Halsted Press Book, 1975.
3. RYNASKY, E. G. et al.: "Flight Control Principles for Control Configured Vehicles"-Technical Report AFFDL-TR-71-1954, Air Force Flight Dynamics Laboratory, USA, 1972.
4. ETKIN, B.: Dynamics of Atmospheric Flight, John Wiley Sons, Inc., 1972.
5. DANESI, A. and SMOLKA, S.: "A Mathematical and Numerical Solution of Optimization Problems in the Active Flight Control System Design," Research Report CT-76.00459.07, Aerospace Department of Rome University, Rome, Italy, 1979.
6. DANESI, A.: "Proposal of a Generalized Computer Program as an Aid in the Design of Active Flight Control Systems," Research Report CT-0055.07, Aerospace Department of Rome University, Rome, Italy, 1979.
7. HIRZINGER, G.: "Impact of Active Control Technology on Airplane Design," AGARD CONFERENCE No. 157.
8. PITTS, W et al.: "Lift and Center Pressure of Wing-Body-Tail Combinations at Subsonic, Transonic and Supersonic Speed," NACA TR 1307-1957.
9. DANESI, A. and SMOLKA, S.: "A Generalized Digital Program for the Dynamical Reponse of Multi-Input-Multi-Output Aerospace Control System," Research Report CT.00459.07-2, Aerospace Department of Rome University, Rome, Italy, 1978.
10. DANESI, A.: "Proposta per l'Accoppiamento Ottimizzato degli Autopiloti ai Sistemi di Radioguida M.L.S.," Research Report CT 76.00459, Aerospace Department of Rome University, Rome, Italy, 1977.
11. DANESI, A.: "Controllo Dinamico delle Variabili non Accessibili alla Misura Direta negli Autopiloti a Controreazioni Multiple," Research Report CT-286-76-4, Aerospace Department of Rome University, Rome, Italy, 1976.
12. DANESI, A.: "Analisi della Problematica di Progetto degli Autopiloti Idonei per l'Atterraggio Automatico Radioguidato," Edito dalla Associazione di Aeronautica ed Astronautica, Roma, Italy, 1978.

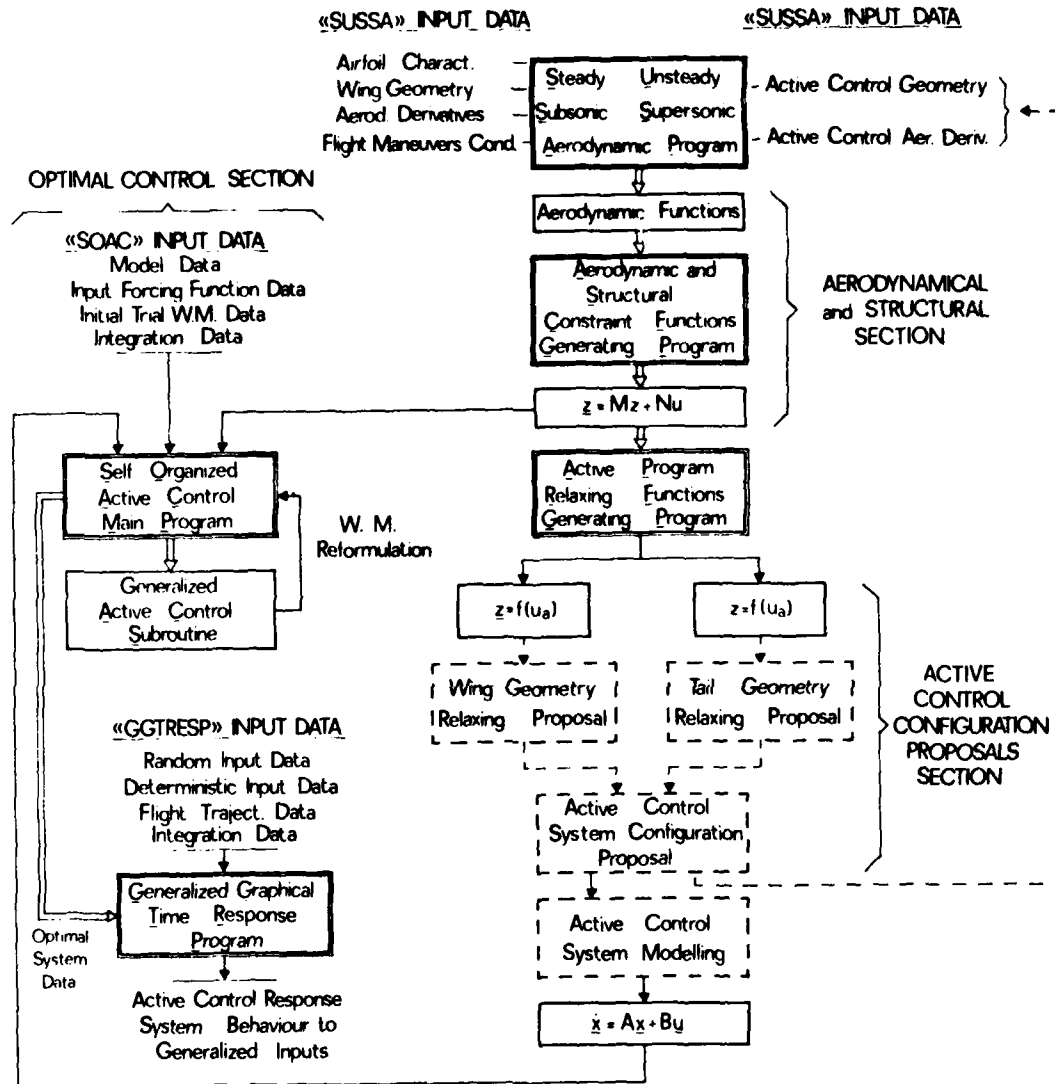


Fig.1 General view of the computational procedure applied to active flight control system design

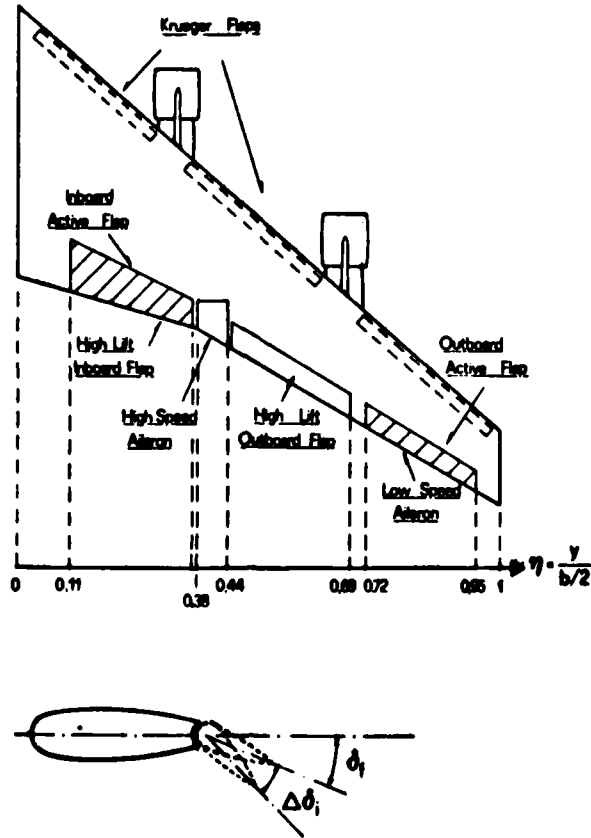


Fig.2 Active controllers configuration

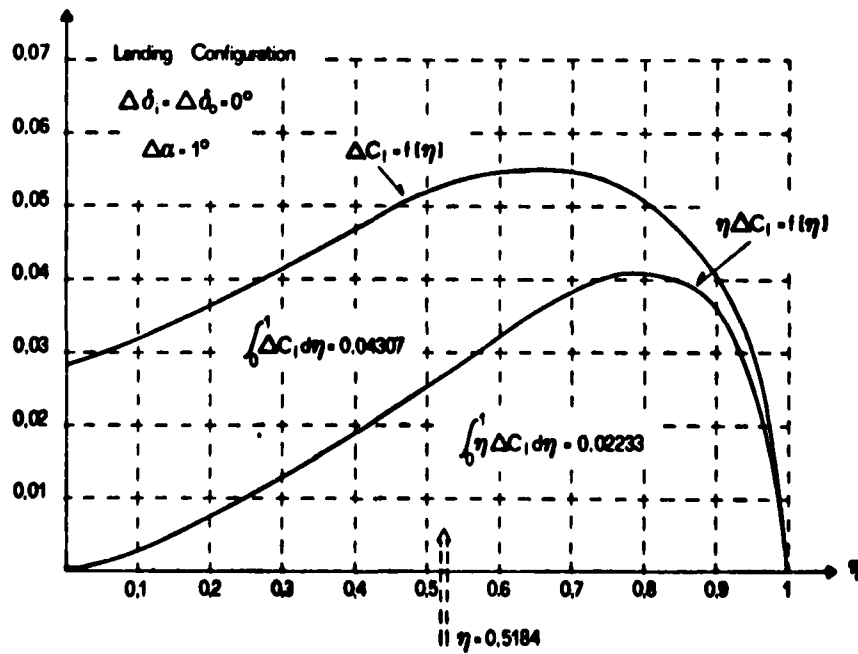


Fig.3 Wing lift and wing root bending moment distribution due to angle of attack

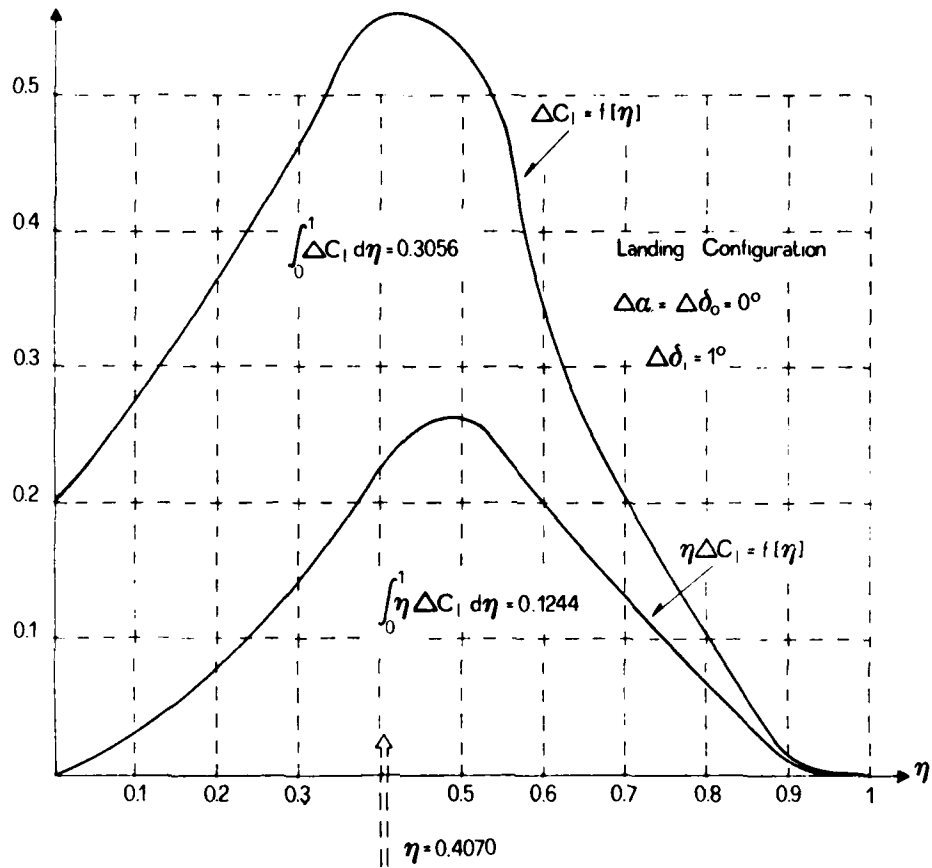


Fig.4 Wing lift and wing root bending moment distribution due to active inboard flap deflection

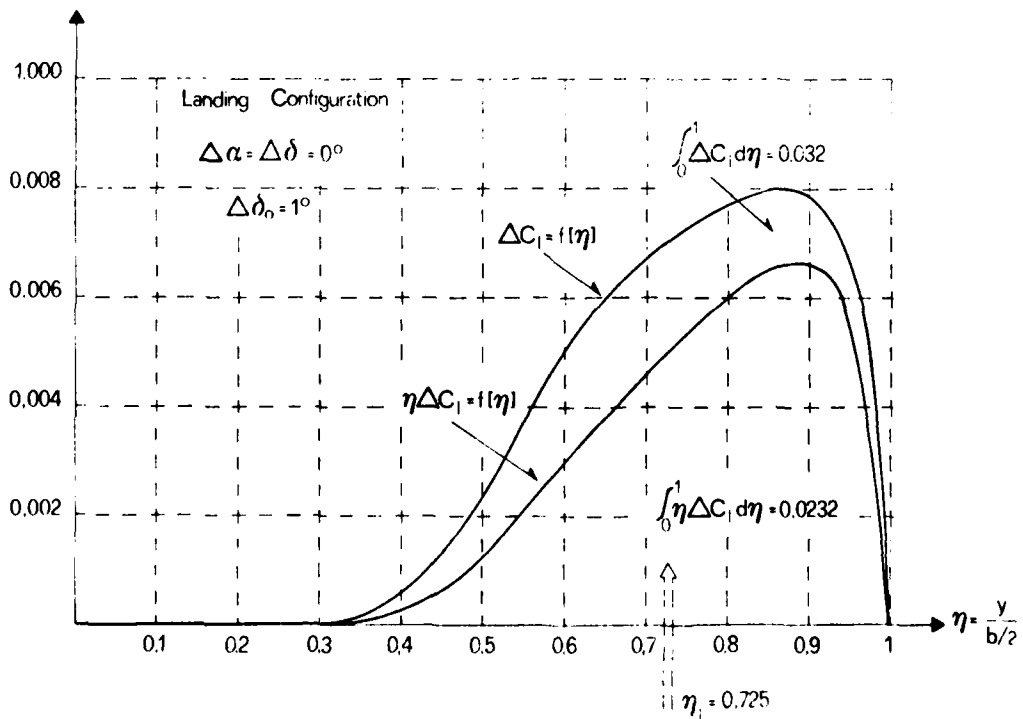


Fig.5 Wing lift distribution and wing root bending moment contribution due to active outboard flap deflection

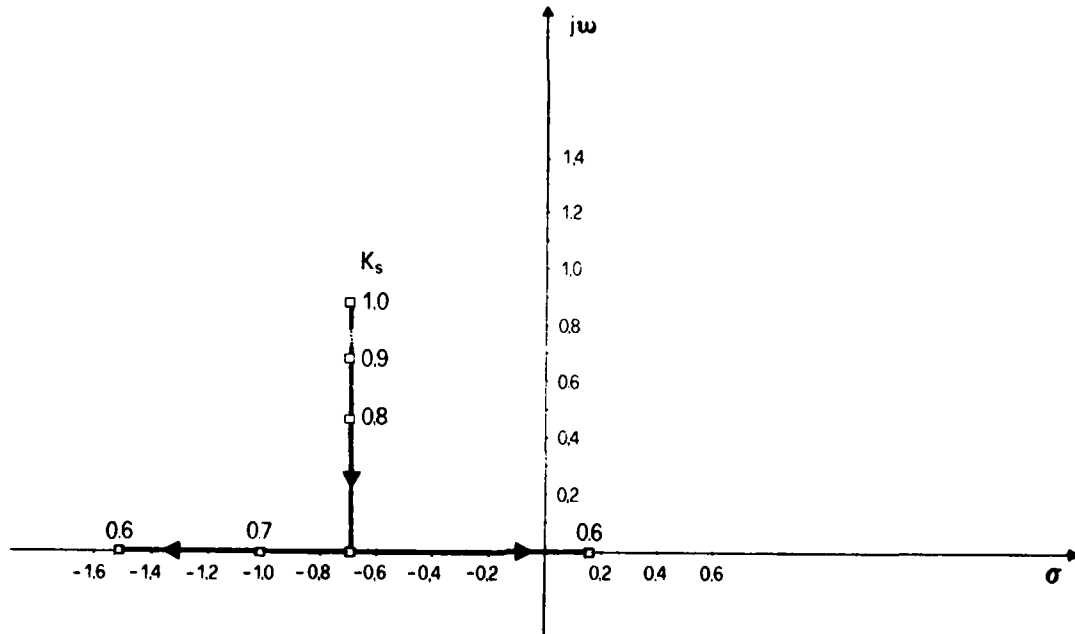


Fig.6 Root locus of Boeing 747 short period poles vs tail area ratio

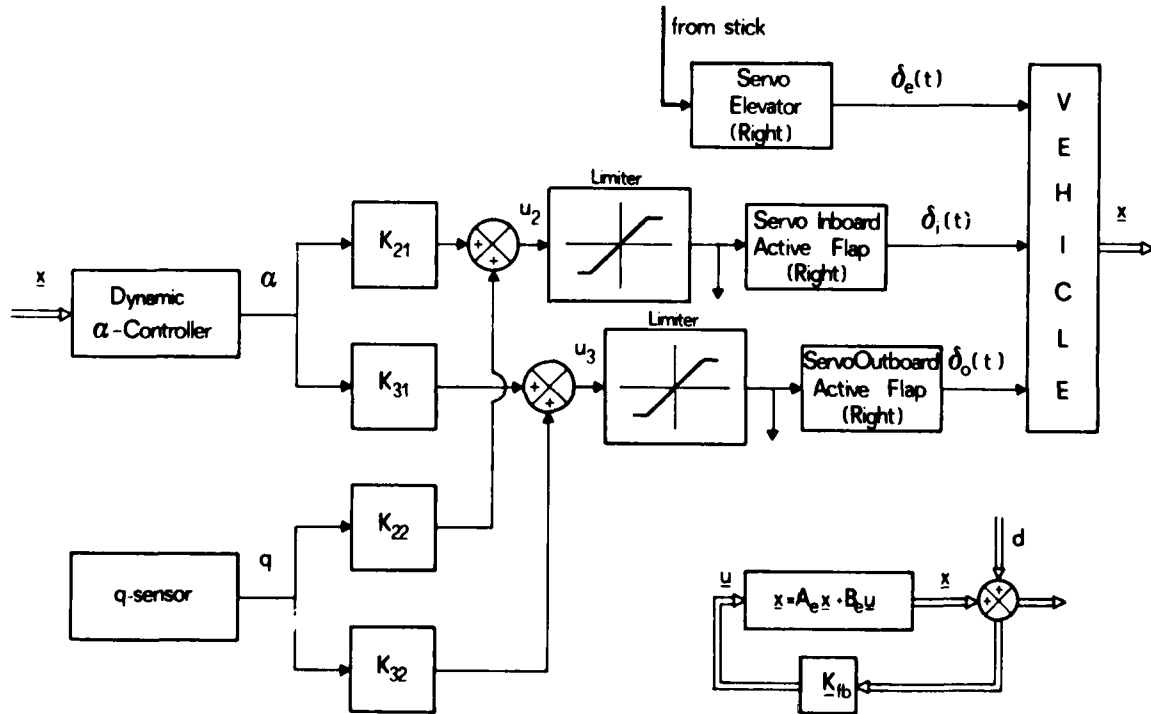


Fig.7 Optimal active flight control system

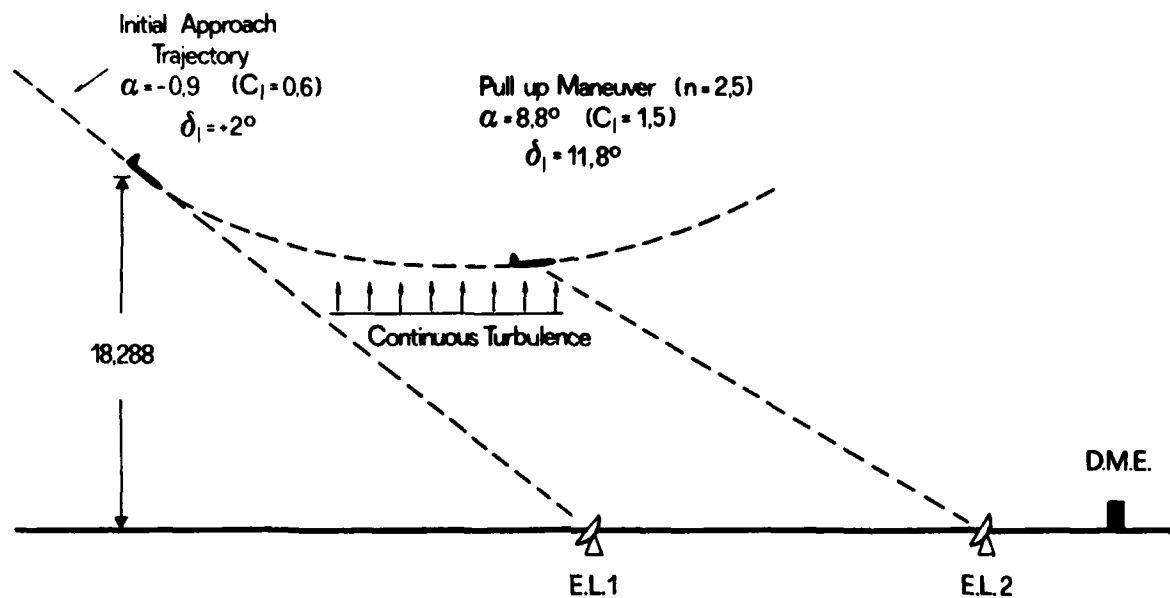


Fig.8 Pull-up maneuver in M.L.S. procedure

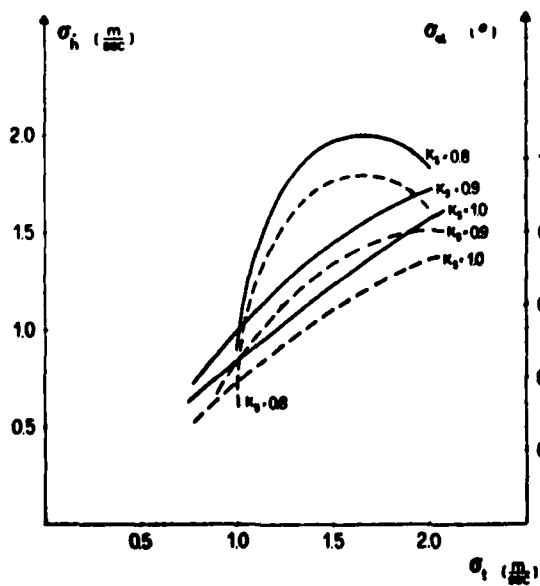


Fig.9 Vertical speed and angle of attack standard deviation due to continuous turbulence

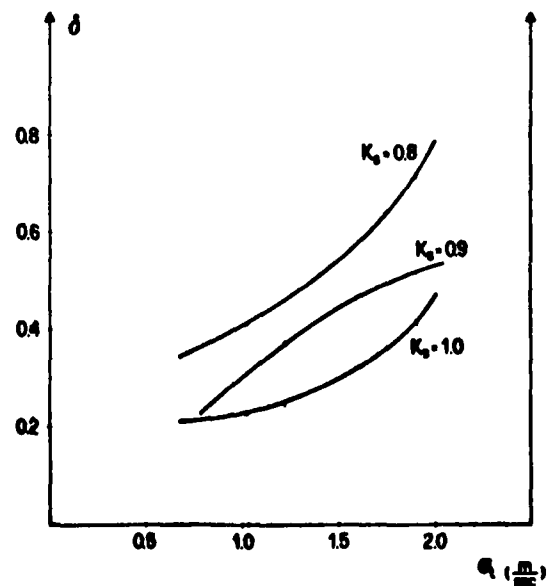


Fig.10 Active inboard and outboard deflections in continuous turbulence

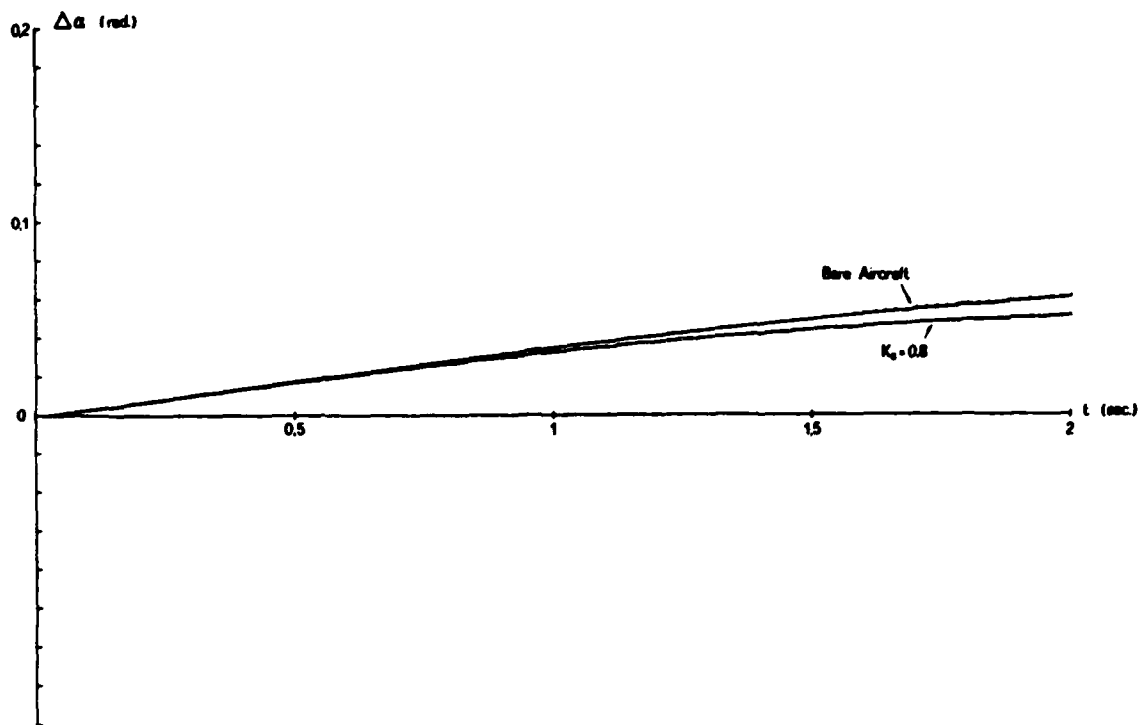


Fig.11 Continuous turbulence effect $\sigma_t = 1,82$ m/s

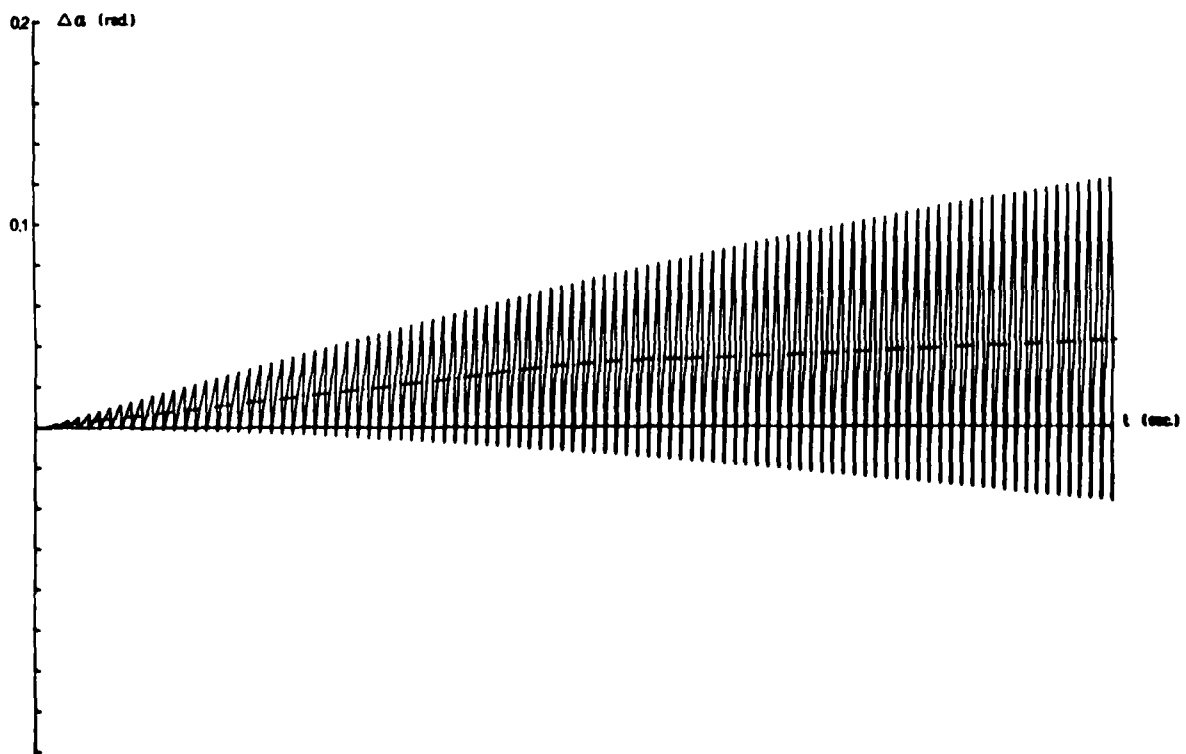


Fig.12 Continuous turbulence effect $\sigma_t = 1.82$ m/s. Enlarged view case $K_s = 0.8$

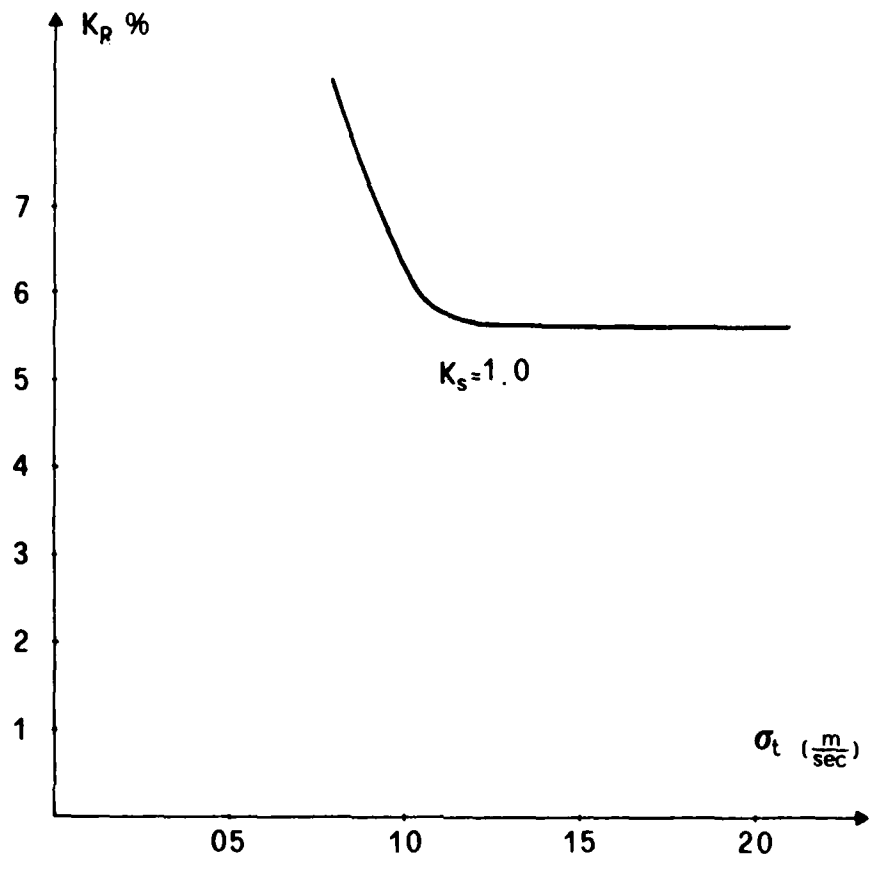


Fig.13 Wing root bending moment relaxation ratio as a function of turbulence standard deviation

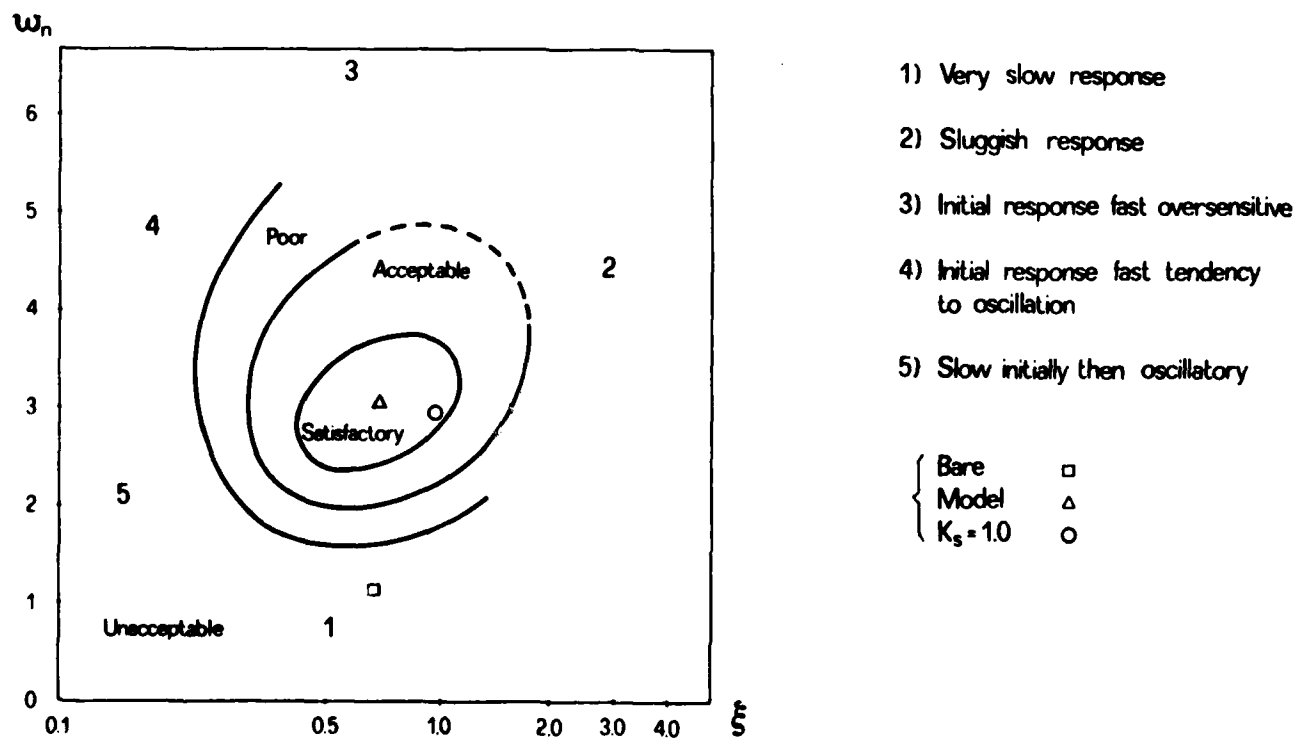


Fig.14 Short period flying qualities comparison

"FOREBODY VORTEX BLOWING — A NOVEL CONTROL CONCEPT TO ENHANCE DEPARTURE/SPIN RECOVERY CHARACTERISTICS OF FIGHTER AND TRAINER AIRCRAFT"

by

Andrew M. Skow*
William A. Moore**
Dale J. Lorincz**

Northrop Corporation, Aircraft Group
3901 W. Broadway, Hawthorne, California

SUMMARY

This paper describes a combined experimental and analytical study which was undertaken to develop active blowing concepts to control the asymmetric orientation of the vortex system emanating from an aircraft forebody at high angles of attack. The overall objective of the study was to utilize the side-force generated by the asymmetric nature of the vortices, in a controlled manner, to enhance the capability of a fighter aircraft to recover from a departure from controlled flight. It is well known that, for slender forebodies, at incidences generally greater than twice the nose semi-apex angle, a vortex system forms in an asymmetric manner and exhibits a bi-stable behavior, preferring to be oriented in one of two mirror-image positions. The choice between these two preferred positions can be influenced strongly by very small geometric imperfections in an otherwise symmetric model or by small asymmetries in the upstream flow such as are caused by flow angularity or turbulent eddies in the free stream. The underlying assumption which precipitated the present work is that the magnitude of the side-force which could be controlled through the use of a very small device is very large due to the fluid amplification afforded by the vortex growth. The results of water tunnel flow visualization studies and a wind tunnel test program are presented which bear out this assumption and show that tangential blowing can effectively alter the forebody vortex system at angles of attack between 25 and 55 degrees and can generate yawing moments comparable to those produced by a conventional rudder at low angles of attack. The results of a six degree-of-freedom digital simulation are presented which show that this concept can substantially enhance departure recovery characteristics and could have potential as a departure inhibitor for some aircraft. The results of a preliminary system design indicate that such a system could be applied to a new or an existing aircraft.

LIST OF SYMBOLS

α	angle of attack (AOA) - (deg)	C_{n_0}	yawing moment coefficient at $\beta = 0$
β	angle of sideslip - (deg)	C_y	side force coefficient
θ_N	nose semi apex angle - (deg)	C_{y_0}	side force coefficient at $\beta = 0$
ϕ	radial position (from windward generator) - (deg)	C_l	rolling moment coefficient
l	length - (in)	C_M	pitching moment coefficient
d	forebody diameter (planform width) - (in)	C_L	lift coefficient
l/d	forebody fineness ratio	C_μ	blowing coefficient $\left(= \frac{\dot{m}V_j}{qA_{ref}} \right)$
X	longitudinal position (from apex) (in)	V_j	jet exit velocity
r_n	nose radius	\dot{m}_j	jet mass flow rate
r_n/d	bluntness	r	yaw rate (body axis) (deg/sec)
δ_H	horizontal tail deflection (deg)	TTR	time to recover
δ_a	aileron deflection (deg)	α_t	threshold AOA
δ_r	rudder deflection (deg)	Re	Reynolds number
C_n	yawing moment coefficient		

1.0 INTRODUCTION

For fighter aircraft which operate in the air combat maneuvering (ACM) arena, flight at high angles of attack (AOA), near the limits of controllability, is an inherent part of both offensive and defensive maneuvering. Reluctance to operate in this regime because of possible departure from controlled flight limits the capability of the man-machine combination to deliver its maximum performance. Figure 1 illustrates a typical ACM gross maneuver envelope for a high performance fighter aircraft. This boundary is an envelope of roll, yaw and pitch excursions resulting from maximum performance air combat maneuvers. Pilot confidence is the key to effectively operating close to control boundaries; and pilot confidence is a function either of the natural resistance of the aircraft system to departure or of the pilot's ability to easily recover from the occasional out-of-control condition associated with high AOA maneuvering. Unfortunately, life is not kind to many pilots on either of these key factors. In the first place, there are many aircraft in the inventories of the free world's air forces that exhibit a high degree of susceptibility to departure and spin entry. Such aircraft have a departure threshold which is generally beyond maximum lift but well within the ACM gross maneuver envelope as shown in Figure 2. Many of these aircraft also have poor departure recovery characteristics, generally requiring the pilot to act quickly and correctly in order to regain control of his aircraft. This brings us to the second unfortunate fact of life. Since most pilots spend relatively little time near control limits in training or in normal operational flying, they are quite unprepared for their first departure. The standard out-of-control reaction often is panic, followed by ejection.

*Manager, Aerodynamics Research

**Research Engineer

24-2

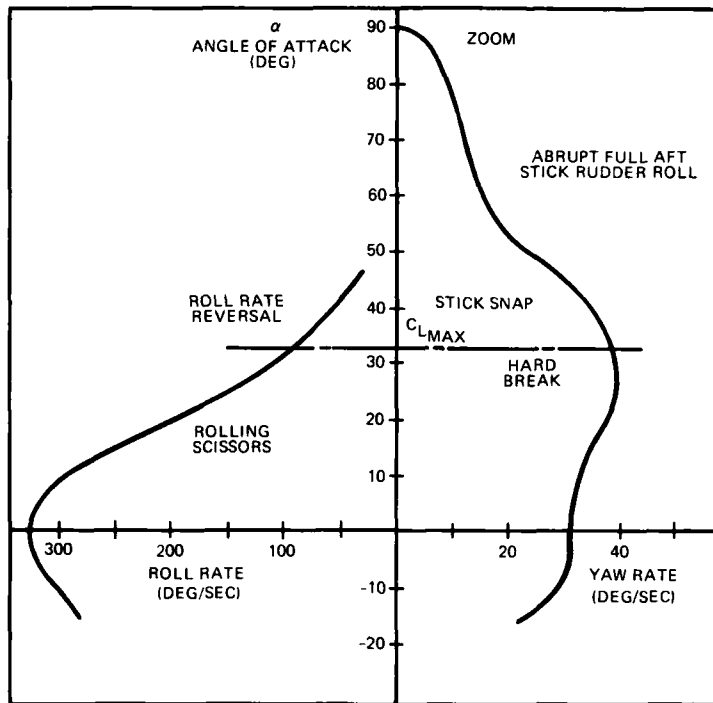


FIGURE 1. TYPICAL HIGH PERFORMANCE FIGHTER ACM GROSS MANEUVER ENVELOPE

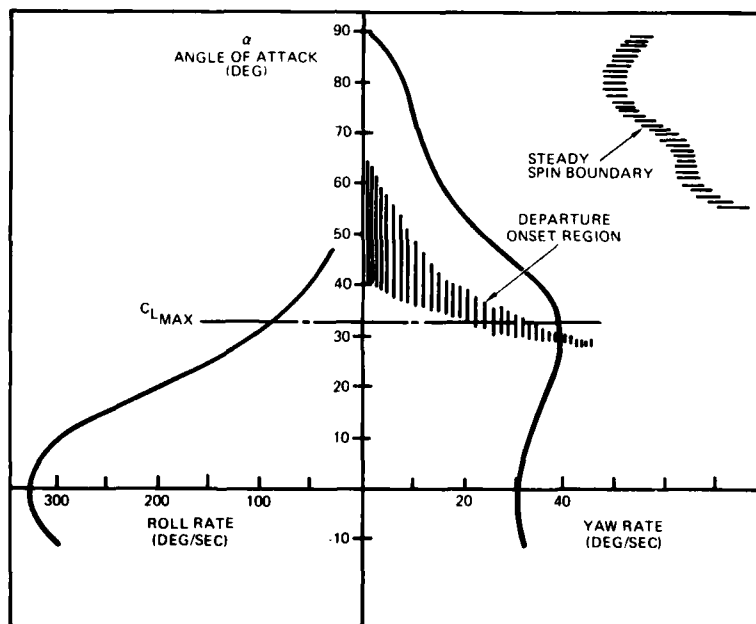


FIGURE 2. TYPICAL DEPARTURE AND SPIN BOUNDARIES

In an attempt to improve this situation, military training commands have instituted programs to better prepare the pilot for the disorientation which he will experience in a departure and to give him a better chance of taking positive recovery action in a timely manner.

Engineers and scientists have tackled the problem also, generally approaching it from three different directions. The first, and most preferred approach is to develop computational or analytical tools and empirical guidelines which can be utilized in the design of new aircraft to ensure that they will have adequate natural resistance to departure so as to make the occurrence of departure only a very remote possibility. Unfortunately, the search for a design with good natural departure resistance is often more of an intuitive endeavor than a scientific one. Also, since aircraft design involves a multitude of compromises, "excess" departure resistance at high AOA sometimes must be sacrificed in order for other design goals to be met. For instance, supersonic wave drag is minimized by a configuration of high fineness ratio, resulting in a long forebody which can have a large adverse effect on high AOA

stability. Radar performance criteria and avionics packaging requirements rather than aerodynamic considerations may determine the cross-sectional and planform shape of this forebody, thereby further degrading high AOA characteristics. These compromises can, however, be made and still lead to a departure resistant configuration as illustrated in Figure 3. Here, the resistance of a configuration to loss of control was greatly enhanced by recontouring the radome cross-sectional shape. Only a small degradation in radar performance resulted from the recontoured "Shark Nose" radome. (See Reference 12)

24-3

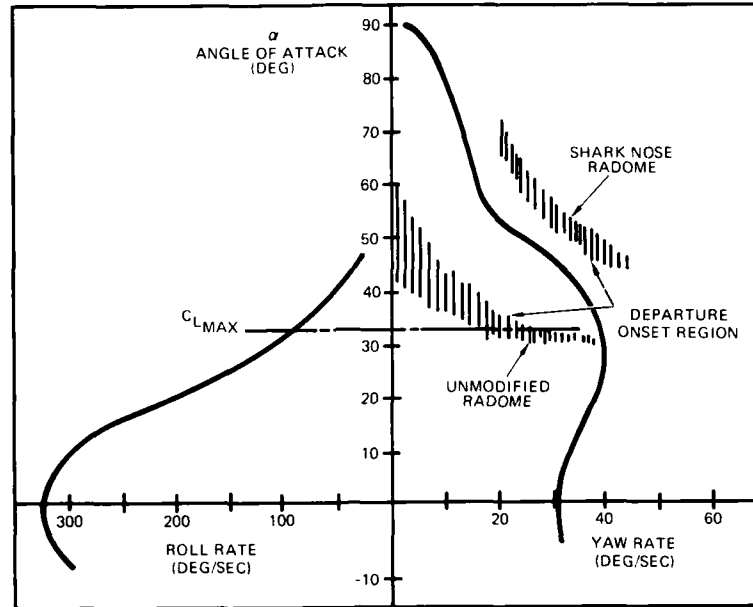


FIGURE 3. EFFECT OF IMPROVED AERODYNAMICS ON DEPARTURE RESISTANCE

If the above preferred approach fails, a second approach which has gained favor in some circles recently, is to prevent the aircraft from operating in an AOA region where departure is possible. This can be done by incorporating into the control system features which take control of the aircraft away from the pilot during maximum performance maneuvering. To ensure success of this approach, angle of attack and sometimes pitch acceleration capability must be limited. In addition, roll capability must sometimes be phased out as AOA is increased to prevent roll-yaw coupling which can cause pitch overshoots which cannot be overcome with the horizontal stabilizer. For some aircraft, a minimum airspeed must be maintained to prevent AOA excursions during low dynamic pressure conditions such as those encountered during a zoom maneuver. Figure 4 illustrates that incorporation of these features into an aircraft configuration can significantly reduce the maneuver performance, even at angles of attack below the AOA limit.

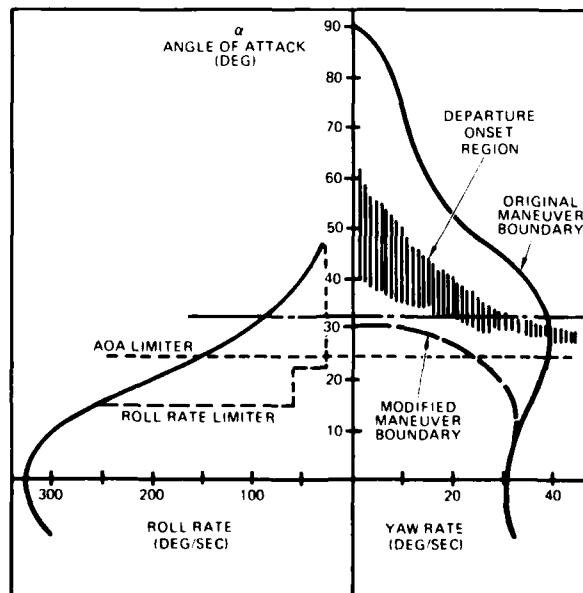


FIGURE 4. EFFECT OF CONTROL LIMITERS ON DEPARTURE RESISTANCE

The third approach which has been taken in the past has been to use motion and attitude sensors in conjunction with the aircraft's control system to "automatically" recover the aircraft from the departure. State-of-the-art sensors can determine whether the aircraft has departed from controlled flight and determine the direction of motion much quicker than an average pilot can. Relatively simple control laws can be programmed into a control system to respond to these sensor inputs and place the control surfaces in positions to optimize recovery chances in a manner that is much more reliable than an average pilot. The only draw back to concepts which have been developed using this approach is that for most aircraft, control effectiveness in the departure AOA region is severely degraded when compared to the effectiveness at lower AOA. This sometimes forces the designer to lower the threshold AOA for the automatic recovery system into a region which could cause it to be activated when it is not needed. However, if more effective control devices could be developed, this general approach could be utilized to design a system which would have the potential to dramatically reduce the loss of life and equipment resulting from out-of-control flight accidents.

This paper describes an analytical and experimental study which was undertaken to develop a novel control concept which is effective in the angle-of-attack region above stall and which could be mechanized in a manner as outlined in the preceding paragraph to enhance the capability of an aircraft to recover from loss of control. The vortex blowing control concepts tested in the present study were designed to alter the asymmetric orientation of the forebody vortex system, taking advantage of the large aerodynamic forces produced by this asymmetry.

This paper will concentrate on the effects which the blowing concepts have on the overall stability and control characteristics of an aircraft at high angles of attack. A companion paper by Peake and Owen (Reference 1) will discuss the results of similar experiments on a cone model and will concentrate on the details of the fluid mechanic phenomena associated with forebody blowing.

2.0 BACKGROUND

2.1 Forebody Flowfields at High Angles of Attack

It is a well known fact that an asymmetric vortex system forms on the leeside of aircraft and missile forebodies at high angles of attack (References 2-6 for example). The degree of asymmetry and the strength of the vortices are dependent on several parameters, the primary ones being angle of attack (AOA), fineness ratio (l/d), nose semi-apex angle (θ_n) and nose bluntness (r_n/d). A typical example of asymmetric vortices is illustrated in Figure 5, where the visualization takes place in a water tunnel.

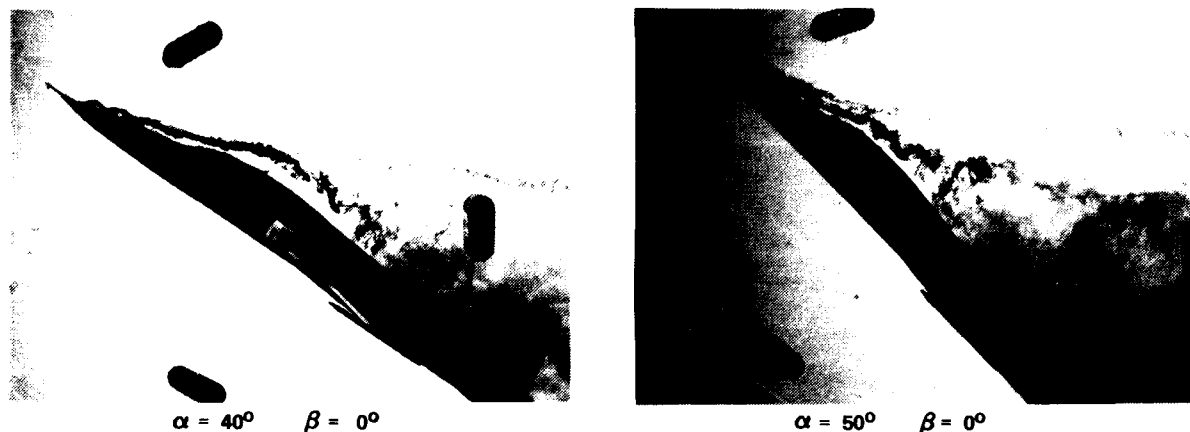


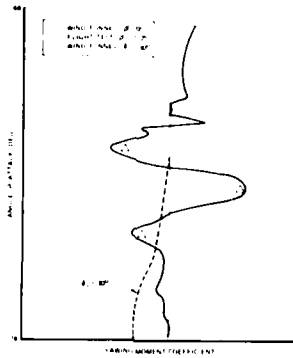
FIGURE 5. WATER TUNNEL VISUALIZATION OF A TYPICAL ASYMMETRIC VORTEX PATTERN AT HIGH AOA

At incidences generally greater than twice the nose semi-apex angle, these asymmetric vortices become strong enough to produce values of side-force and yawing moment large enough to influence the departure resistance of an aircraft (References 7-12). An example of asymmetric yawing moments measured on a typical fighter aircraft is shown in Figure 6, compared with yawing moment produced by full deflection of the rudder. These asymmetric side forces can not only generate a departure from controlled flight but, once the departure has occurred, they can aggravate the tendency of an aircraft to transition to a flat spin mode. In addition, since these vortices have been observed to remain in an asymmetric orientation even under coning conditions (References 13 and 14) they can oppose recovery from a spin.

These vortices have been observed to behave in a bi-stable manner, preferring to orient in one of two, mirror-image states (References 15-17). The choice between the two, mirror-image orientations is thought to be highly influenced by minute geometric imperfections, especially near the apex of the nose.

2.2 The Concept of Asymmetric Vortex Control

In the present study, the overall objective was to harness the power of this vortex system and utilize the side-force generated by its asymmetric nature as a control device. Such a device would have effectiveness in the angle-of-attack region beyond stall and could be used, with the proper system design and following appropriate control laws, to greatly enhance the capability of an aircraft to recover from a departure from controlled flight.



24-5

FIGURE 6. TYPICAL YAWING MOMENT ASYMMETRIES

2.3 Previous Research

The basic concept of controlling the yawing moments generated by long, slender forebodies to aid spin recovery was first proposed by Neilhouse, et. al. (Reference 7) in 1960. Neilhouse, et. al. pursued three means of controlling the yawing moments; strakes or spoiler strips placed along the inboard side of the nose (right side in a right spin), induced circulation about the forebody produced by rotating a conical nose section, and flap-type surfaces placed either on both sides or only on the inboard side of an aircraft nose. Each of these concepts proved effective in promoting rapid recovery from various types of spins on different models. Similar experiments using asymmetric nose strakes were reported by Chambers, et. al. (Reference 18) in 1970 and showed equally promising results on a different aircraft configuration. More recently Fidler (Reference 19) has suggested, that rotating nose cones could be used on missiles to alter the forebody vortex shedding pattern, thereby reducing the time-averaged side-force at high angles of attack. Kruse (Reference 20) conducted experiments on the effect of spinning an axisymmetric body about its longitudinal axis, noting that in addition to reducing the time averaged side-force, the peak-to-peak variation of side force decreases with increased spin rate. Cornish and Jenkins (Reference 21) conducted experiments with symmetrical tangential blowing near the nose of an aircraft but were unsuccessful in affecting the spin recovery characteristics of this particular configuration.

2.4 Present Studies

In a manner similar to some of the previous research just cited, the present work concentrated on the experimental evaluation of concepts to control the forebody side force through asymmetric tangential blowing near the apex of the nose.

Several practical considerations were taken into account early on in order to screen devices which would not find application to a fighter aircraft regardless of their effectiveness. The screening criteria used were:

- The tangential blowing concepts must have sufficient effectiveness so as to not require abnormally large quantities of air or unattainable mass flow rates.
- The blowing nozzles must be located in a region aft of the radar antenna where radar performance would not be adversely affected.

3.0 EXPERIMENTAL APPARATUS AND TEST PROGRAM

3.1 Water Tunnel Tests

Preliminary tests of various forebody Vortex Blowing Control Concepts were conducted in the Northrop 16"x24" Diagnostic Water Tunnel on a 0.025 scale model of an F-5F aircraft. The Northrop Diagnostic Water Tunnel is a single return, low turbulence facility. It is operated at a nominal test section velocity of 0.35 to 0.45 fps which corresponds to a Reynold's number of approximately 3×10^4 per foot. The model used was equipped with two parallel rows of dye injection orifices located on the lower surface of the fuselage forebody. Visualization of the forebody flowfield is achieved when the dye flows out of these orifices and is entrained into the separated shear layer which, in turn, rolls up into well defined vortices.

The water tunnel tests were conducted to screen a large number of blowing schemes by comparing, in a somewhat qualitative manner, the relative capability of each concept to control the forebody vortex orientation. The blowing concepts tested consisted of small nozzles located on the surface of the forebody at various locations. The blowing jet angle relative to the freestream was varied also. Figure 7 shows a sketch of the model and illustrates a sample nozzle location. Water was supplied to the blowing nozzle through a small tube running down the centerline of the model. Accurate mass flow rates were set by using a water flow meter in the supply line, external to the tunnel. Additional water tunnel tests were conducted on two tangent ogive cylinder bodies to determine the effect of vortex blowing control on more generic shapes. The tangent ogive forebodies had fineness ratios of $(l/d) = 3, 5$ and 5.0 . Each was tested with a common $(l/d) = 4.5$ circular-cylinder afterbody. Tangential blowing in a downstream direction was tested for a matrix of positions on the surface of both bodies. Figure 8 illustrates the model geometries tested.

The experiments were performed over an angle of attack range of 0 to 60 degrees. Vortex core vertical and lateral positions were determined at a fixed longitudinal station for the matrix of nozzle geometries at various blowing rates. In this manner, the relative effectiveness of each concept was evaluated and optimum nozzle locations were determined.

24-6

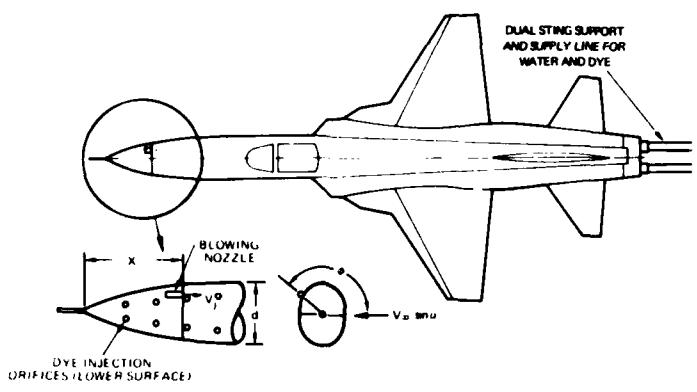


FIGURE 7. F-5F WATER TUNNEL MODEL ARRANGEMENT

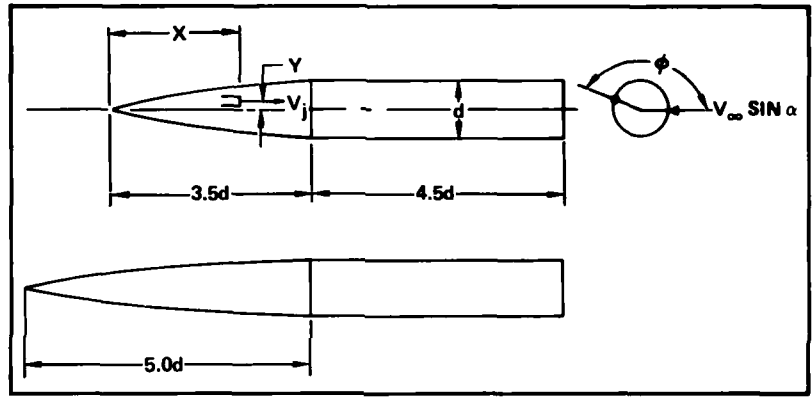


FIGURE 8. TANGENT OGIIVE WATER TUNNEL MODEL ARRANGEMENT

3.2 Wind Tunnel Tests

Based on the results of the water tunnel tests, the most promising nozzle geometries were selected for proof-of-concept testing in the wind tunnel.

Testing was conducted in the Northrop Low Speed Subsonic Wind Tunnel. The tunnel is a horizontal, atmospheric, single return facility capable of test section Reynolds numbers up to 2.4×10^6 per foot and a dynamic pressure of up to 200 psf. The test section is 10 feet wide, 7 feet high, and 20 feet long. The tunnel has a contraction ratio of 12:1 which gives a streamwise turbulence level of less than 0.01% in the test section.

Tests were conducted using a 0.10 scale F-5F model, equipped for asymmetric blowing at two fuselage stations on the upper surface of the forebody. A plenum chamber for the blowing system was contained in the nose of the model. This plenum chamber was pressurized from an external source through an air supply line which routed from a support near the back of the sting, forward along the top of the model until it became buried just aft of the canopy. Care was taken to ensure that the supply line was non-metric. Figure 9 shows the model installation in the tunnel and illustrates the blowing apparatus. Nozzle locations are illustrated in Figure 10.

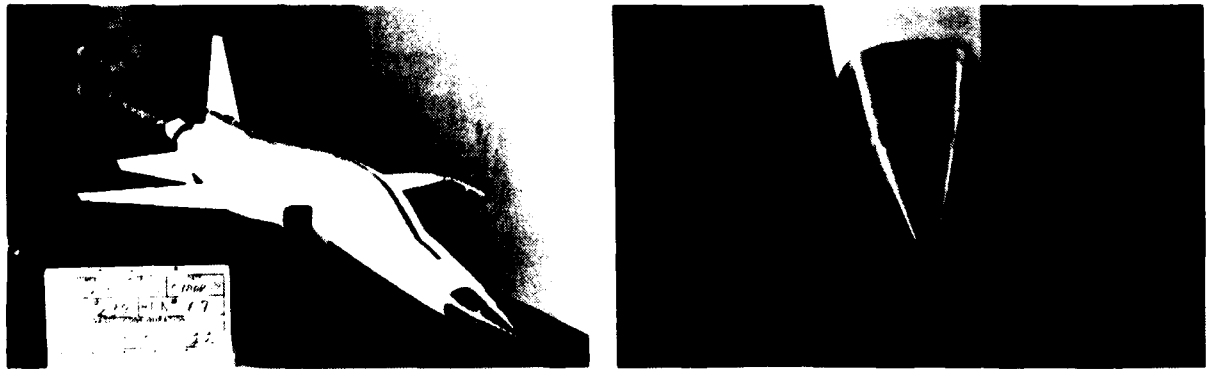


FIGURE 9. F-5F MODEL INSTALLATION
7X10 LOW SPEED WIND TUNNEL

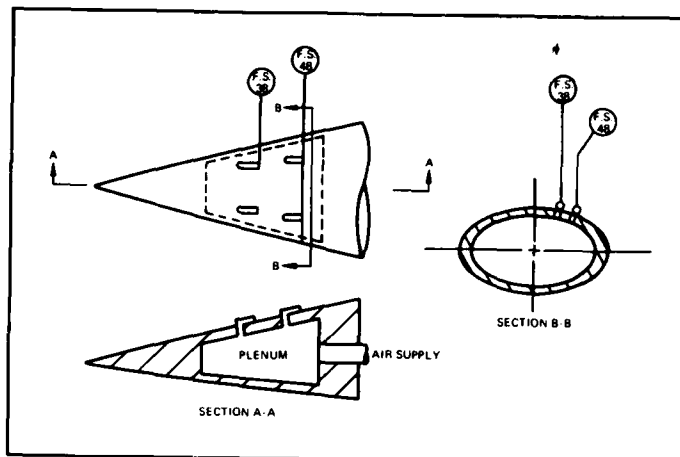


FIGURE 10. BLOWING NOZZLE LOCATIONS

The blowing nozzles were designed to provide choked flow at the nozzle exit plane. A nozzle calibration was performed to determine actual discharge coefficients. Plenum total pressure and temperature and nozzle mass flow rate were measured and used to compute nozzle jet velocity and, hence, blowing momentum coefficient, C_{μ} .

To assure data repeatability and flow conditions representative of full scale, transition grit was applied to the model forebody as shown in Figure 11. The test procedure used was to first determine the characteristics of the model with dummy nozzles installed at the longitudinal position of interest. By noting the direction of the side-force produced, the relative positions of the primary vortices could be inferred; the measured side-force resulting from the vortex nearest to the body. The dummy nozzle on the side of the body which has the higher vortex was then replaced by an open or active nozzle and the effect of blowing mass flow rate was measured over a large angle of attack and sideslip range.

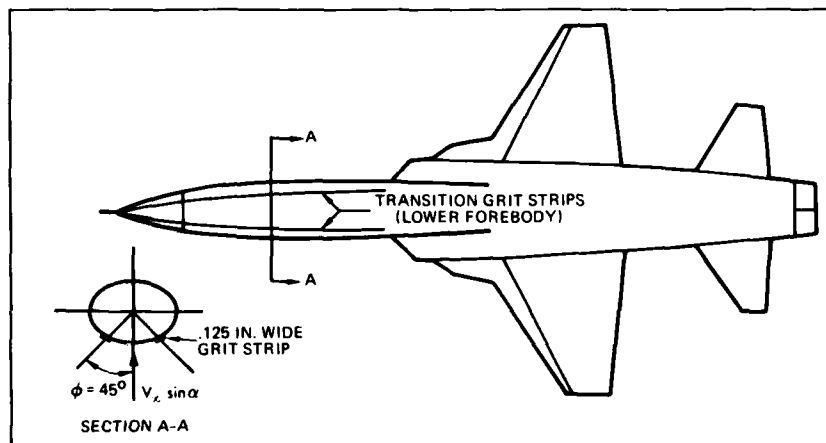


FIGURE 11. TRANSITION GRIT PATTERNS

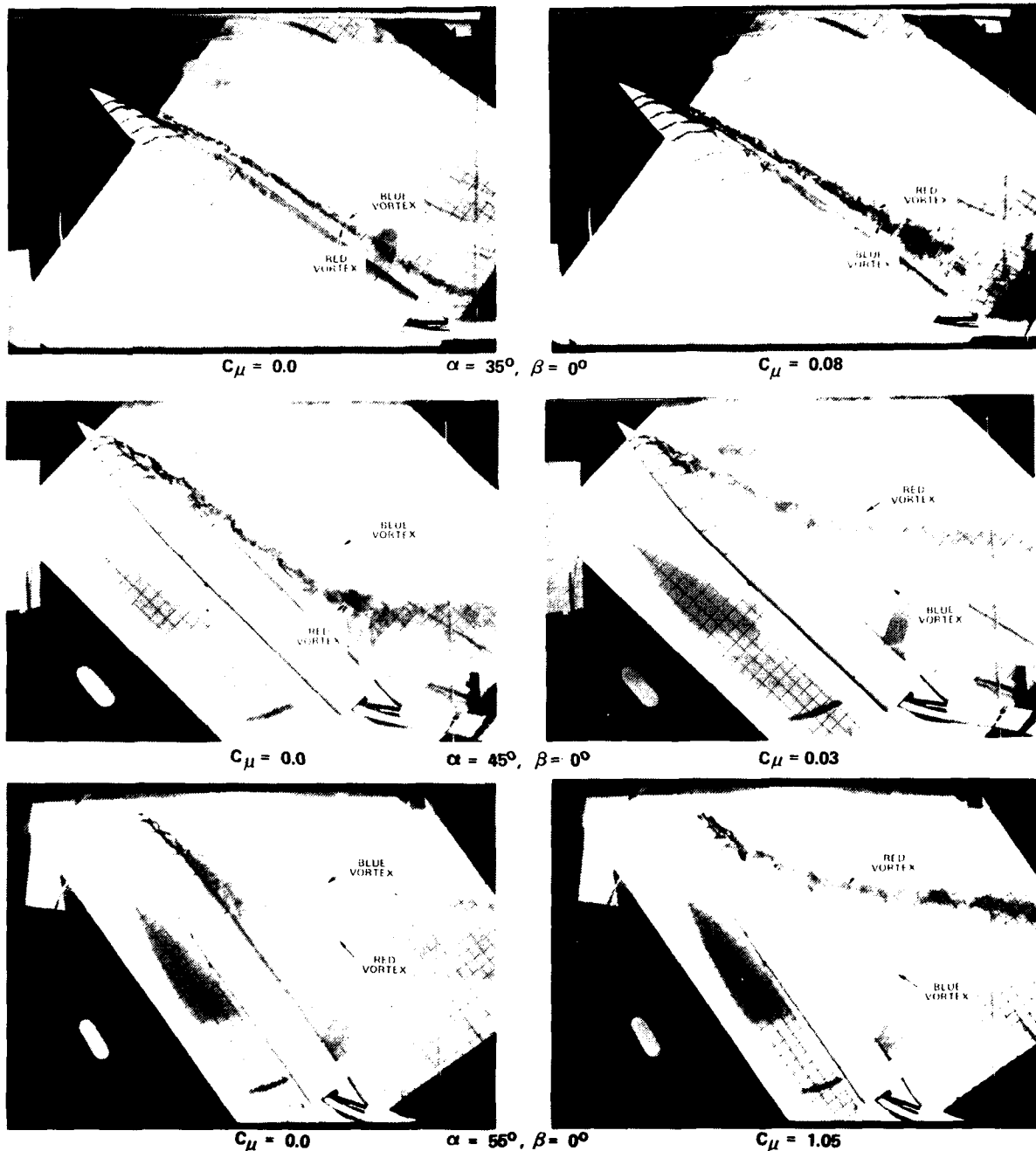
Wind tunnel tests were performed at a dynamic pressure of 50 psf, corresponding to a Reynolds number of 1.308×10^6 per foot. Plenum pressures for the blowing system ranged from 165 psi to 615 psi, yielding blowing momentum coefficients of between $C_{\mu} = 0.008$ and 0.032 , respectively. Data were taken over an angle of attack range of $\alpha = 0^\circ$ to 90° in 2° increments and over a sideslip range of $\beta = \pm 25^\circ$ in 5° increments.

4.0 DISCUSSION OF RESULTS

4.1 Water Tunnel Tests

4.1.1 Asymmetric Tangential Blowing Concepts

Experiments performed in the water tunnel with the 3.5 fineness ratio tangent ogive forebody indicated that, for the range of longitudinal positions tested, (approximately 1.0 to 2.0 body diameters aft of the apex of the nose), the most effective tangential blowing arrangement was found to be with the nozzle directed aft and on the side of the body where the higher vortex was located. This would be on the side opposite to the direction of a departure or spin as the side force is produced by the vortex in the closest proximity to the surface.



Note: C_μ Referenced to Model Base Diameter

FIGURE 12. WATER TUNNEL RESULTS FOR AFT BLOWING ON A 3.5/4.5 TANGENT OGIVE -CYLINDER MODEL - NOZZLES LOCATED AT $x/d = 1.54$

As shown in Figure 12, when a sufficient quantity of mass flow is directed in a concentrated jet beneath the high vortex, the vortex system can be induced to form in its mirror-image state. Blowing coefficients shown are referenced to the model base diameter. The blowing mass flow required to induce a complete reversal of the vortex core positions was found to be a function of the longitudinal position of the nozzle relative to the apex of the nose, the radial position of the nozzle relative to the windward generator and the angle of attack of the model. As seen in Figure 13, significant reductions in required mass flow are noted as the nozzle is moved toward the apex of the nose at a constant Y/D . The approximate location of a typical radar antenna is shown for reference. One can also note that significantly higher values of mass flow are required to produce reversal at higher angles of attack.

Figure 14 illustrates the effect of nozzle radial position on blowing control effectiveness. As the nozzle is displaced angularly away from the leeward generator at a constant longitudinal position, an increase in blowing effectiveness is noted. The optimum radial position appears to correspond to a lateral position slightly outboard of the center of the higher vortex core.

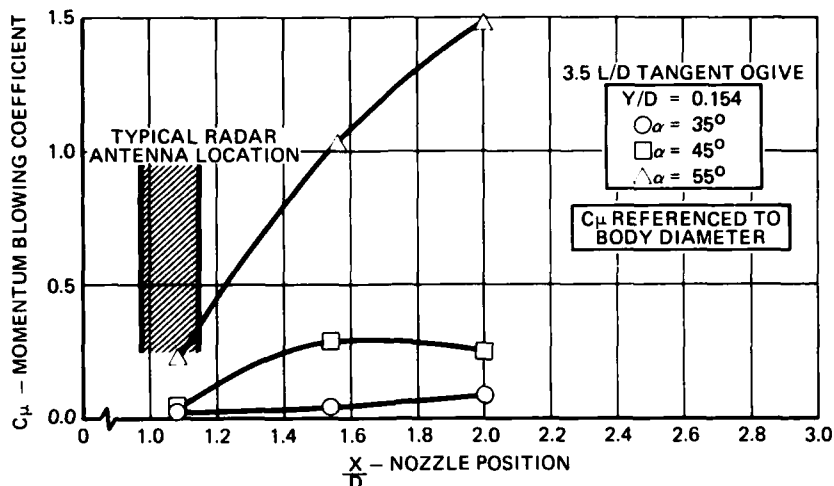


FIGURE 13. TANGENT OGIVE BLOWING REQUIRED TO REVERSE ASYMMETRY AS A FUNCTION OF THE NOZZLE LONGITUDINAL POSITION

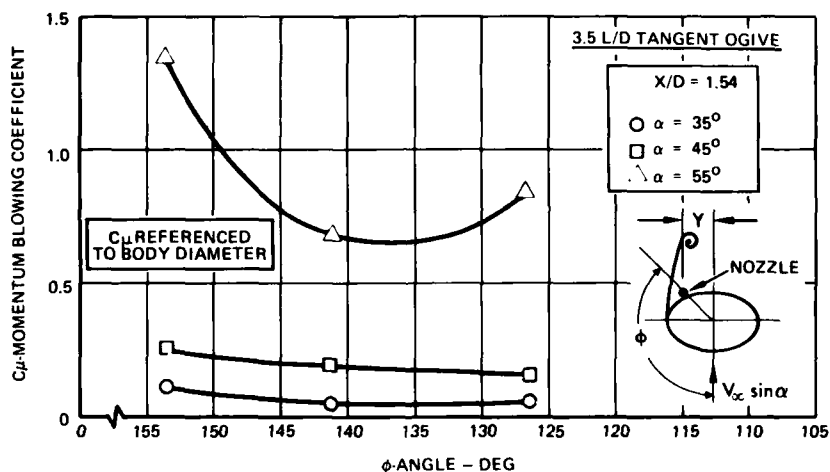


FIGURE 14. TANGENT OGIVE BLOWING REQUIRED TO REVERSE ASYMMETRY AS A FUNCTION OF THE NOZZLE ϕ POSITION

Experiments performed in the water tunnel on the F-5F model using the tangential, aft blowing concept yielded results as shown in Figure 15. These results are consistent with those obtained with the tangent ogive models and illustrate the capability to induce the vortices to switch to the mirror-image state with sufficient quantities of blowing on a realistic fighter aircraft configuration. One important item which can be noted from an inspection of the flow visualization photographs of Figure 15 is the range of angle of attack over which the blowing is most effective. At $\alpha = 35^\circ$ ($\alpha/\theta_n = 2.1$), the vortex patterns have just begun to form in an asymmetric orientation and, hence, the side-force which would be generated is still small and it is easy to control. At $\alpha = 45^\circ$ ($\alpha/\theta_n = 2.9$), the asymmetry is much more pronounced, more difficult to control and the side-force produced would be near maximum. At $\alpha = 55^\circ$ ($\alpha/\theta_n = 3.5$), the asymmetry is still evident, but the vortices have weakened and a turbulent wake is forming. The side-force which would be generated by these vortices is somewhat reduced and the blowing required to reverse the positions of the vortices is quite large. Therefore, from the water tunnel experiments it can be expected that the angle of attack region over which the vortex blowing control would be most effective is $40^\circ < \alpha < 50^\circ$. Blowing momentum coefficients shown in the figure are referenced to the model wing area. Tests were performed on the F-5F model at two longitudinal positions, one just aft of the radar antenna location and one just forward of it. Figure 16 illustrates the increased effectiveness obtained at the forward location relative to the aft location.

4.1.2 Asymmetric Normal Blowing Concepts

Additional water tunnel experiments were performed with the blowing nozzle oriented normal to the surface of the F-5F model and flush with it. The nozzle location was varied, longitudinally from near the apex to approximately 1.5 fuselage diameters aft. In each test, the nozzle was located at the maximum half-breadth ($\phi = 90^\circ$).

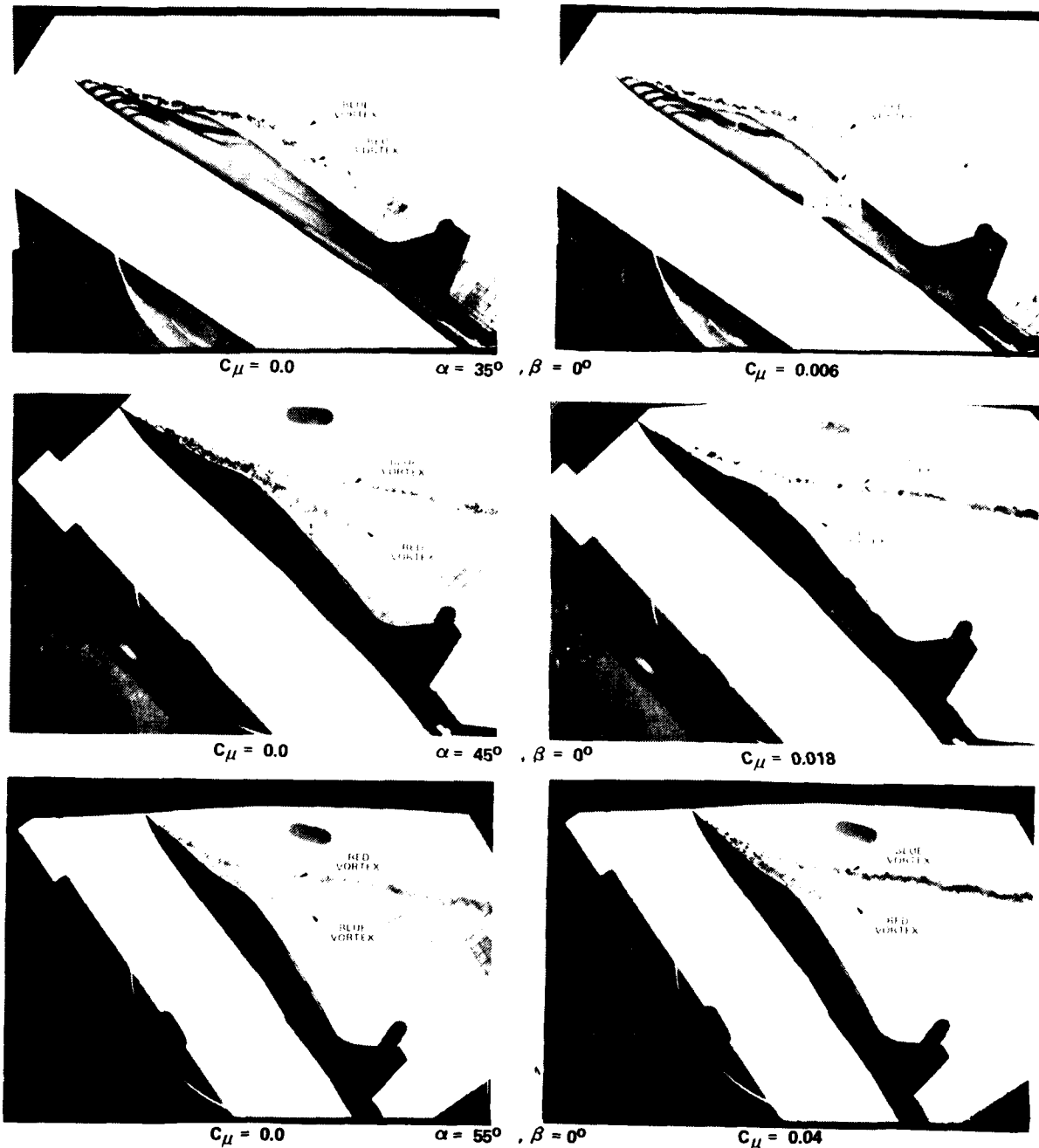


FIGURE 15. WATER TUNNEL RESULTS FOR AFT BLOWING ON THE F-5F MODEL
 $x/d = 0.95$

Blowing in this fashion was found to be effective when the nozzle was located near the apex but efficiency was seen to drop off rapidly as the nozzle location was moved aft. Nozzle positions aft of 1 fuselage diameter were found to be largely ineffective. Inasmuch as the radar antenna is located at $X/d = 1.2$, no further work was performed with this type of blowing. Subsequent to these experiments, Peake (Reference 1) has found, in experiments with a 10° cone model, that blowing normal to the surface is comparable, or perhaps somewhat improved in effectiveness when compared to tangential blowing if the nozzle is located nearer to the leeward generator ($\phi = 135^\circ$).

4.2 Wind Tunnel Tests

From the results of the water tunnel tests previously discussed, the most promising vortex control schemes were chosen for proof-of-concept testing in the low-speed wind tunnel. Two blowing nozzle locations were selected.

4.2.1 Vortex Blowing Control Concepts

Figure 17 presents the measured effect of aft, tangential blowing on yawing moment at $\beta = 0^\circ, \pm 5^\circ$, for the F-5F aircraft. With blowing off, an asymmetry in the yawing moment begins to develop at approximately $\alpha = 32^\circ$ ($\alpha/\theta_n = 2.0$). With the blowing on, even at the lowest jet momentum coefficient tested ($C_{\mu} = .008$), the asymmetry begins to develop slightly earlier, $\alpha = 24^\circ$ ($\alpha/\theta_n = 1.5$) and forms in the opposite sense to the blowing-off case.

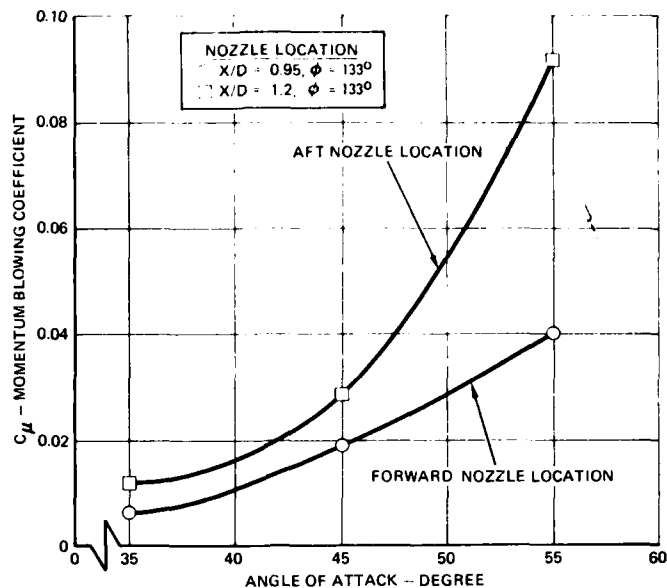


FIGURE 16. EFFECT OF NOZZLE LONGITUDINAL POSITION ON BLOWING CONTROL EFFECTIVENESS - F-5F

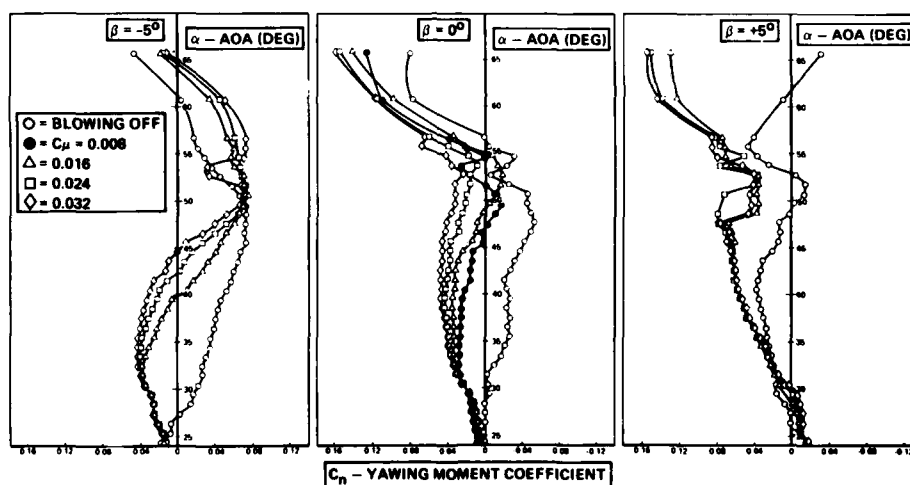


FIGURE 17. EFFECT OF AFT TANGENTIAL BLOWING ON YAWING MOMENT

At angles of attack beyond $\alpha = 24^\circ$, the largest incremental change in yawing moment is obtained at the lowest momentum coefficient tested. The increment then increases approximately linearly as jet momentum coefficient is increased, up to the maximum mass flow rate tested. This is illustrated in Figure 18 at angles of attack of $\alpha = 41^\circ$ and $\alpha = 47^\circ$. Note that quantitative estimates made from water tunnel experiments proved not only to give the correct trends, but also predicted absolute levels with reasonable accuracy.

Figure 19 presents the incremental yawing moment generated by the vortex control as a function of angle of attack. These data are compared with incremental yawing moment produced by full deflection of a conventional rudder. Note that even the lowest jet momentum coefficient tested provides yawing moments in the angle of attack range from $\alpha = 35^\circ$ to $\alpha = 55^\circ$ which are comparable to those produced by the rudder at very low incidences. Also, it is interesting to note that the vortex control effectiveness begins to increase in the same angle of attack region where the rudder effectiveness is declining rapidly. At low angles of attack, directional stability and control are best provided by aerodynamic surfaces located behind the aircraft center of gravity such as a vertical tail and a rudder. These data indicate that at high angles of attack, directional control as well as stability can be best provided by an aerodynamic device located ahead of the center of gravity, near the apex of the nose.

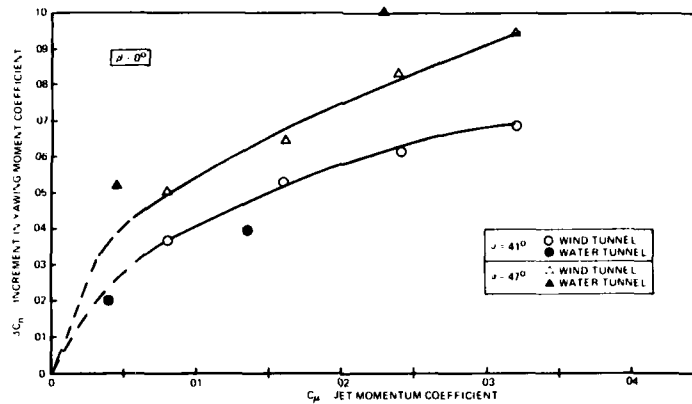


FIGURE 18. BLOWING EFFECTIVENESS

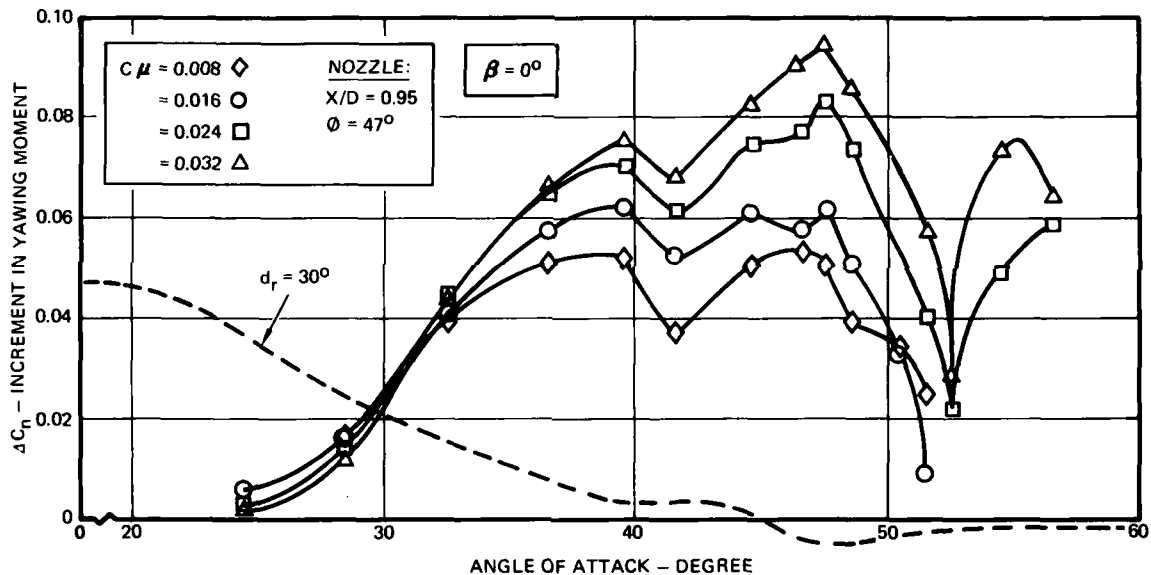
FIGURE 19. DIRECTIONAL CONTROL EFFECTIVENESS COMPARISON
VORTEX BLOWING CONTROL vs RUDDER

Figure 20 illustrates the effectiveness of the Vortex Blowing Control device as a function of sideslip at a constant angle of attack, $\alpha = 47^\circ$.

4.3 Six Degree of Freedom Simulation

The capability of the Vortex Blowing Control concepts to augment the departure and spin recovery capability of a fighter aircraft was evaluated by means of a digital six-degree-of-freedom (6DOF) computer simulation. The baseline aerodynamic model used in this simulation has been validated by comparison of calculated and flight test trajectories of many, coupled, high AOA maneuvers, flown during spin tests of this aircraft. An algorithm was developed to model the incremental forces and moments generated by the blowing devices, as determined from the low-speed wind tunnel experiments.

Maneuvers were simulated by specifying grossly aggravated control inputs which were found, during spin susceptibility testing, to produce departures and spin entries. The departures and spins generated had been found to be difficult to recover from using traditional recovery control inputs both in-flight and in the simulation.

The threshold angle of attack and yaw rate where the Vortex Blowing Control device was activated was varied in the simulation as was the blowing mass flow rate. The optimum yaw rate - angle of attack threshold and the general effect of mass flow were determined in this manner. Figure 21 presents a typical series of time histories at a given mass flow rate where the threshold AOA was varied. Recoveries are seen to be significantly improved when the blowing device is activated early in the departure but severely degraded when the device is activated after the departure has been allowed to progress toward spin entry.

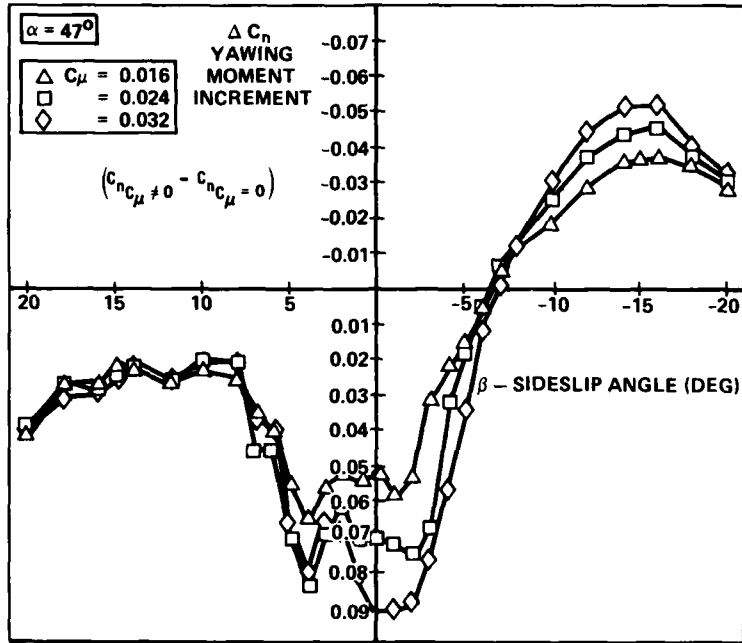


FIGURE 20. VORTEX BLOWING CONTROL EFFECTIVENESS AT NON-ZERO SIDESLIP

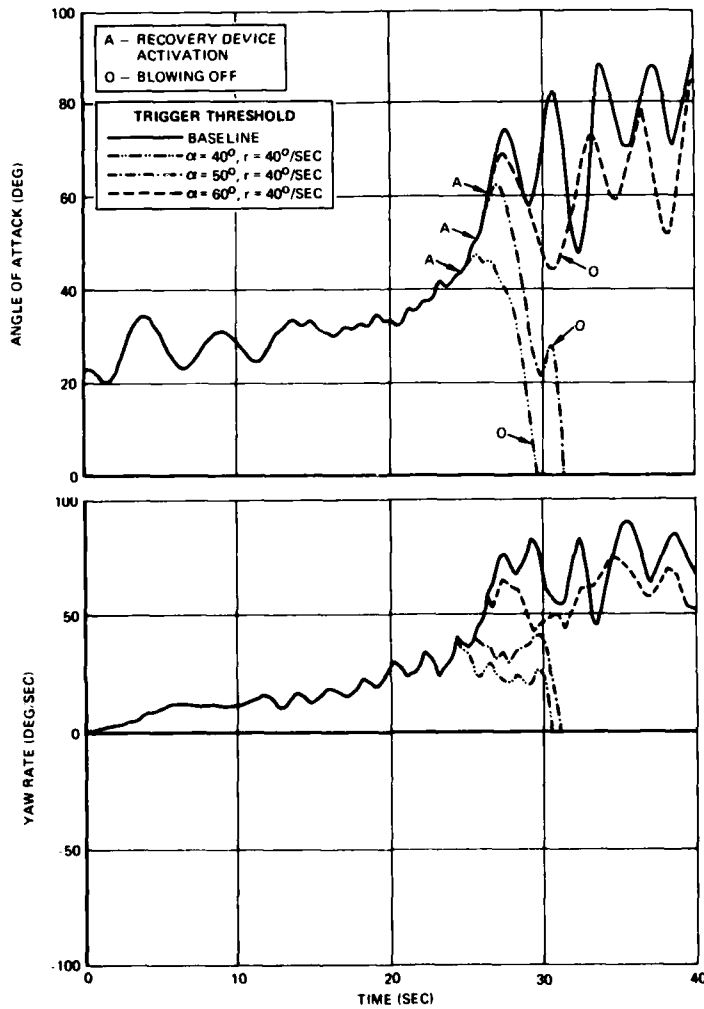


FIGURE 21. TYPICAL 6 DOF TIME HISTORIES OF DEPARTURE RECOVERIES AIDED BY VORTEX BLOWING CONTROL

Figure 22 illustrates the improvement in recovery characteristics for another maneuver. In this case, the trigger threshold is $\alpha = 40^\circ$, $r = 40^\circ/\text{sec}$. A rapid recovery is achieved when the blowing control device is used in conjunction with traditional recovery control inputs. Without the blowing control device, no recovery is achieved.

24-14

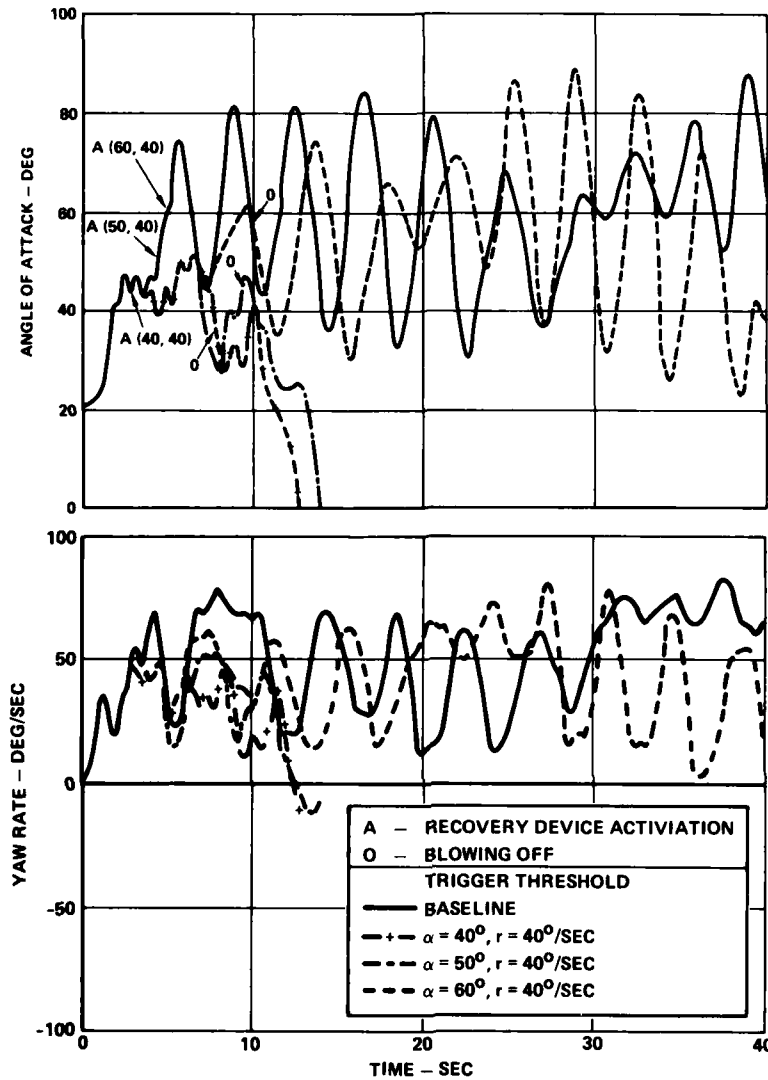


FIGURE 22. 6 DOF TIME HISTORY OF DEPARTURE RECOVERY

Figure 23 presents time-to-recover as a function of threshold angle of attack compiled from a series of simulated maneuvers.

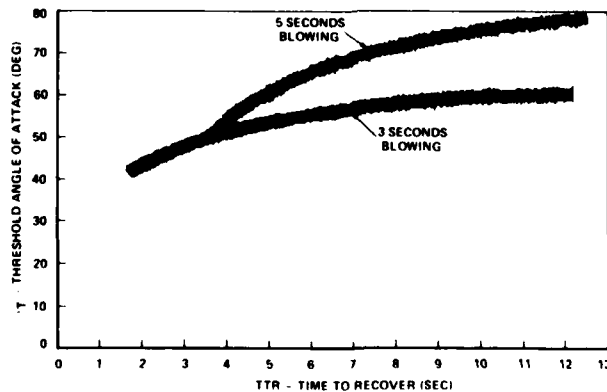


FIGURE 23. VORTEX BLOWING CONTROL - EFFECT OF THRESHOLD ACTIVATION ON DEPARTURE RECOVERY TIME

A blowing threshold angle of attack of $\alpha_T = 40^\circ$ provides excellent recovery augmentation and is well beyond the angle of attack for maximum lift coefficient, thereby not impacting the maneuver capability of the F-5F aircraft. For each simulation, a yaw rate dead-band of $\pm 40^\circ/\text{sec}$ at $\alpha = 40^\circ$ decaying linearly to $\pm 20^\circ/\text{sec}$ at $\alpha = 60^\circ$ was used. In this manner, the blowing device is not activated until the yaw rate exceeds the dead-band limit.

24-16

Figure 24 illustrates the final blowing control device schedule super imposed on the ACM gross maneuver boundary for the F-5F.

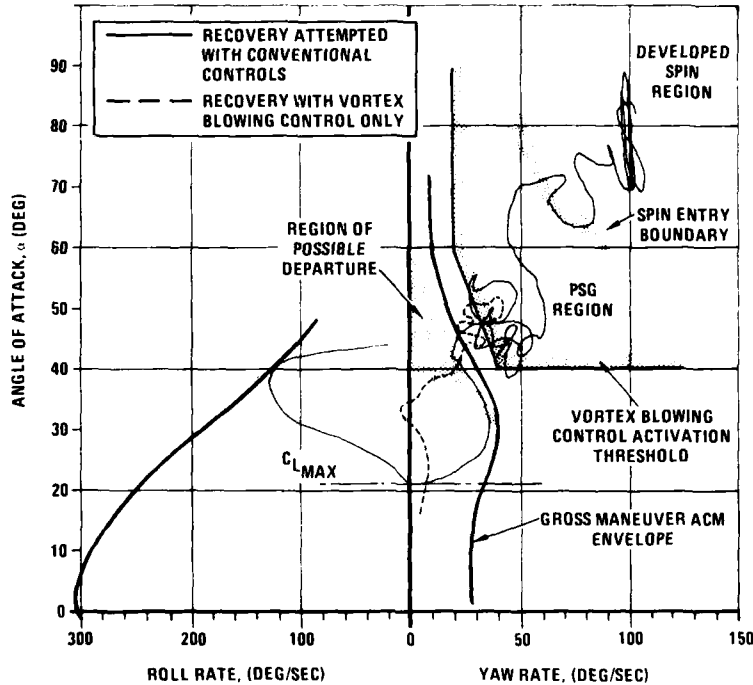


FIGURE 24. FINAL VORTEX BLOWING CONTROL TRIGGER THRESHOLD SCHEDULE

5.0 PRELIMINARY ASSESSMENT OF DESIGN FEASIBILITY

Using the results of the experiments and simulation discussed in the previous paragraphs, some preliminary system design work was done in order to assess the overall feasibility of applying the blowing control concept to fighter or trainer aircraft. Factors considered in the feasibility study included: effectiveness, reliability, complexity, impact on other systems and the retrofitability of the device.

The wind tunnel experiments and 6 DOF simulation showed that an acceptable level of departure recovery enhancement could be achieved at blowing coefficients of $C_{\mu} = 0.015 - 0.025$. The required duration of blowing was found to be between 3 and 5 seconds. In order to maximize the reliability of the system, engine bleed air was not considered as a potential source for the blowing jet, inasmuch as engine flame outs at high angles of attack and yaw rate are to be expected. A solid propellant system was chosen as the most attractive source of blowing. Figure 25 shows a schematic diagram of the proposed blowing system.

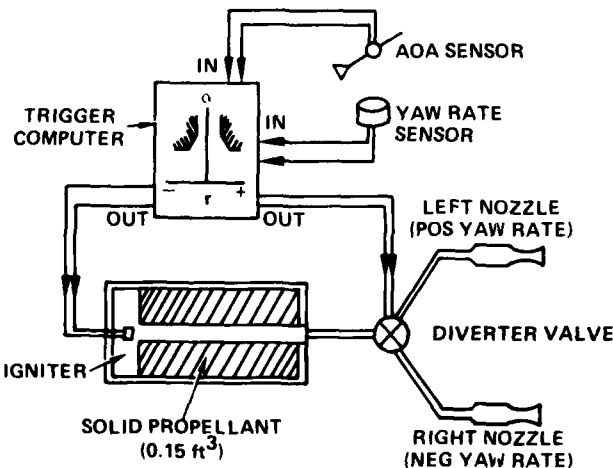


FIGURE 25. SCHEMATIC DIAGRAM OF PROPOSED SOLID PROPELLANT BLOWING SYSTEM

Figure 26 illustrates the region of the flight envelope over which the system is designed to produce the required blowing coefficients.

24-16

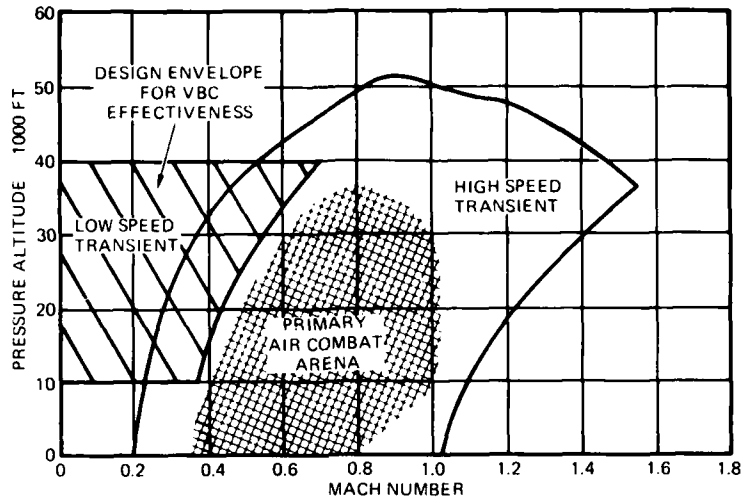


FIGURE 26. REGION OF EFFECTIVENESS OF VORTEX BLOWING CONTROL DEVICE

As illustrated in Figure 26, the system is designed to produce a blowing coefficient of $C_{\mu} = 0.025$ for 10 seconds at an airspeed of 200 KCAS, at altitudes of 10,000 ft to 40,000 ft. An airspeed of 200 KCAS was chosen as representative of the maximum airspeed which could be expected to occur at the trigger threshold of $\alpha = 40^\circ$ during a highly transient maneuver; most maneuvers would result in lower airspeeds at these conditions.

Since the system concept is designed for constant mass flow, airspeeds below 200 KCAS will cause the device to be operated at blowing coefficients higher than 0.025 as shown in Figure 27. The proposed solid propellant blowing system is estimated to require approximately 0.15 ft³ of propellant. The total system weight is estimated to be less than 20 lbs.

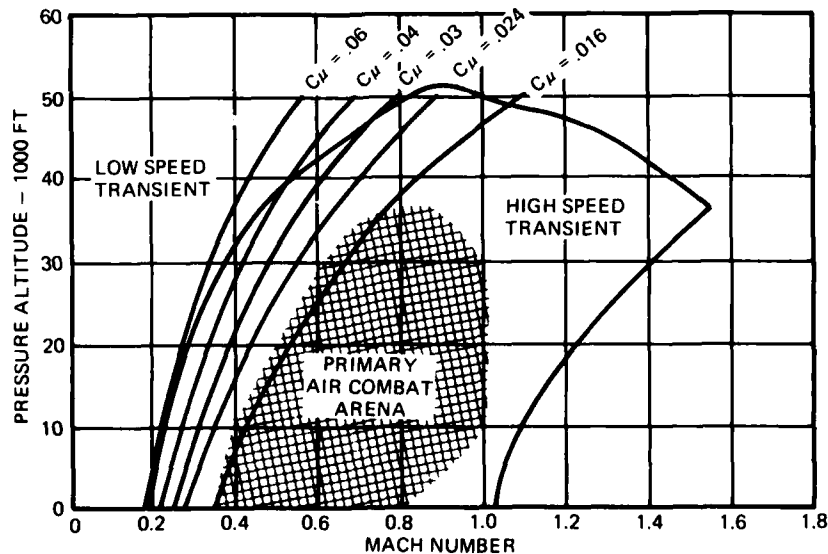


FIGURE 27. BLOWING SYSTEM CAPABILITY

6.0 CONCLUSIONS AND RECOMMENDATIONS

Based on small scale water and wind tunnel experience, it has been shown that asymmetric tangential blowing on the surface of the forebody of an aircraft can be used to control the positional orientation of the leeside vortex system at high angles of attack. Further, it has been shown that the forces and moments produced by these vortices can be used, in a controlled manner, to greatly enhance the predicted departure recovery characteristics of an existing fighter aircraft configuration. Blowing rates required to produce these forces and moments were shown to be quite small, owing to the fluid amplification afforded by the vortex growth. Volume requirements are reasonable and indicate that such a concept could be applied to a new aircraft or retrofitted to an existing aircraft with minimum impact on other aircraft systems.

Further experiments must be conducted on a large scale free-flight model to substantiate the predictions made to date. Further analysis should be done to determine whether this concept could be used not only as a departure recovery enhancement device but also as a departure inhibitor.

7.0 REFERENCES

1. Peake, D.J. and Owen, F. K.: Control of Forebody Three-Dimensional Flow Separation. To be presented at AGARD FDP Symposium, "Aerodynamics of Controls," Naples, Italy, May 1979.
2. Nielsen, J. N.: Non-Linearities in Missile Aerodynamics. AIAA Paper 78-20, Jan. 1978.
3. Allen, H.J. and Perkins, E.W.: Characteristics of Flow Over Inclined Bodies of Revolution. NACA RM A50L07, 1951.
4. Clark, W.H., Peoples, J.R., and Briggs, M. Michael: Occurrence and Inhibition of Large Yawing Moments During High Incidence Flight of Slender Missile Configurations. AIAA Paper 72-968, 1972.
5. Coe, P. L., Jr., Chambers, J.R., and Letko, W.: Asymmetric Lateral-Directional Characteristics of Pointed Bodies of Revolution at High Angles of Attack. NASA TN D-7095, Nov. 1972.
6. Keener, E.R. and Chapman, G. T.: Onset of Aerodynamic Side Forces at Zero Sideslip on Symmetric Forebodies at High Angles of Attack. AIAA Paper 74-770, Aug. 1974.
7. Neilhouse, Anshal I., Klinar, Walter J. and Scher, Stanley H.: Status of Spin Research for Recent Airplane Designs. NASA TR R-57, 1960.
8. Greer, H. Douglass: Summary of Directional Divergence Characteristics of Several High-Performance Aircraft Configurations. NASA TND-6993, 1972.
9. Anderson, C. A.: Stall/Post-Stall Characteristics of the F-111 Aircraft. Paper No. 18, AGARD CP102, Conference on Fluid Dynamics of Aircraft Stalling, Lisbon, Portugal, April, 1972.
10. Skow, A. M. and Titiriga, A., Jr.: A Survey of Analytical and Experimental Techniques to Predict Aircraft Dynamic Characteristics at High Angles of Attack. Paper No. 19, AGARD CP235, Conference on Dynamic Stability Parameters, Athens, Greece, May 1978.
11. Skow, A. M., Titiriga, A., Jr., and Moore, W. A.: Forebody/Wing Vortex Interactions and Their Influence on Departure and Spin Resistance. Paper No. 6, AGARD CP247, Conference on High Angle of Attack Aerodynamics, Sandefjord, Norway, October, 1978.
12. Edwards, O. R.: Northrop F-5F Shark Nose Development. NASA CR-158936, October 1978.
13. Tobak, M., Schiff, L. B., and Peterson, V. L.: Aerodynamics of Bodies of Revolution in Coning Motion. AIAA Journal, Vol. 7, No. 1, Jan. 1969.
14. Schiff, L. B. and Tobak, M.: Results from a New Wind-Tunnel Apparatus for Studying Coning and Spinning Motions of Bodies of Revolution. AIAA Journal, Vol. 8, No. 11, Nov. 1970, pp 1953-1958.
15. Lamont, P.J. and Hunt, B.L.: Pressure and Force Distributions on a Sharp-Nosed Circular Cylinder at Large Angles of Inclination to a Uniform Subsonic Stream. J. Fluid Mech. Vol. 76, part 3, 1976, pp 519-559.
16. Lamont, P.J. and Hunt, B.L.: Prediction of Aerodynamic Out-of-Plane Forces on Ogive-Nosed Circular Cylinders. J. Spacecraft, Vol. 14, No. 1, Jan. 1977, pp 38-44.
17. Hunt, B.L. and Dexter, P.C.: Pressures on a Slender Body at High Angle of Attack in a Very Low Turbulence Level Air Stream. Paper No. 17, AGARD CP247, Conference on High Angle of Attack Aerodynamics, Sandefjord, Norway, October, 1978.
18. Chambers, J.R., Anglin, E. L., and Bowman, J.S., Jr.: Effects of Pointed Nose on Spin Characteristics of a Fighter Airplane Model Including Correlation with Theoretical Calculations. NASA TN D-5921, Sept., 1970.
19. Fidler, J. E., Personal Communication.
20. Kruse, R. L.: Influence of Spin Rate on Side Force of an Axisymmetric Body. AIAA Journal, Vol. 16, No. 4, April 1978, pp 415-416.
21. Cornish, J. J. III and Jenkins, M. W. M.: The Application of Spanwise Blowing to High Angle of Attack Spin Recovery. Paper No. 9, AGARD CP247, Conference on High Angle of Attack Aerodynamics, Sandefjord, Norway, Oct. 1978.

NONLINEAR AERODYNAMICS OF ALL-MOVABLE CONTROLS

26-1

Charles A. Smith and Jack N. Nielsen
 Nielsen Engineering & Research, Inc.
 510 Clyde Avenue, Mountain View, California USA

SUMMARY

A number of nonlinear phenomena appear in the characteristics of aerodynamic controls, and theory is only partially successful in accounting for these effects. Major nonlinear effects originate from fin-body and fin-fin interference, gaps at the fin-body junction, nonuniform body upwash, shock-boundary layer interaction, and control cross-coupling. New experimental data on these effects at high angles of attack have been obtained in recent years. By using existing data these nonlinear effects and their consequences on control effectiveness are described. In particular, both independent control effectiveness (e.g., pitch control) as well as control cross-coupling (e.g., pitch control in the presence of yaw control) are discussed. It is shown that, at sufficiently high angles of attack, the presence of these nonlinearities can completely dominate control effectiveness. The current status of techniques to predict control effects using both analytical and data-correlation techniques is reviewed. Finally, those areas are described where additional theoretical and experimental work is needed.

NOMENCLATURE

a	body radius
AR	wing-alone aspect ratio
C_N	normal-force coefficient in unrolled body coordinates; normal force/ $q_\infty S_{ref}$
C_{N_W}	normal-force coefficient of "wing-alone" formed by joining two opposing fins; normal force/ $q_\infty S_{ref}$
$C_{N_W(B)}$	normal-force coefficient of fin in presence of body
C_1, C_2, C_3, C_4	canard fins, numbered counterclockwise from top at $\phi = 0$
d	body diameter
k_w	fin-body interference factor for control deflection, $\alpha_c \neq 0, \phi \neq 0, \delta \neq 0$
K_w	fin-body interference factor for fin normal force for $\alpha_c \neq 0, \phi = 0, \delta = 0$
K_v	fin-body interference factor for bank, $\alpha_c \neq 0, \phi \neq 0, \delta = 0$
l_F	length of forebody; from nose to first set of lifting surfaces
l_{ref}	reference length
M_c	crossflow Mach number, $M_\infty \sin \alpha_c$
M_∞	free-stream Mach number
q_∞	dynamic pressure of free stream
Re	Reynolds number, based on body diameter
s_m	semispan of fin on body, measured from body axis
S_{ref}	reference area
v_n	component of free-stream velocity normal to surface, $V_\infty \sin \alpha_c$
v_p	component of free-stream velocity parallel to surface, $V_\infty \cos \alpha_c$
V_∞	free-stream velocity
w	upwash velocity in crossflow plane
x, y, z	missile body axes; x measured positive downstream along body rotational axis, y measured positive to right in the plane of C_4 , and z measured upward in the plane of C_1 ; origin is located at nose tip
x_0, y_0, z_0	special set of axes for $\phi = 0$; also called unrolled body coordinates
α_c	included angle of attack; angle between x axis and free-stream velocity

α_{eq}	equivalent angle of attack; that angle of attack of the wing alone for which its normal force is twice that of the fin; the wing alone is formed by joining two opposing fins together
$(\alpha_{eq})_i$	equivalent angle of attack of i^{th} fin, where i can refer to any canard or tail fin
$\alpha_{eq,0}$	equivalent angle of attack of fin with no control deflection
$\alpha_{eq,\delta}$	equivalent angle of attack of fin with control deflection
β	$\sqrt{ M_\infty^2 - 1 }$
δ	control surface deflection angle; at $\phi = 0$, for vertical fins (δ_1, δ_3) δ positive for trailing edges to right when viewed from rear and for horizontal fins (δ_2, δ_4) δ positive for trailing edges down
δ_p	control deflection angle for pitch; horizontal fins (δ_2, δ_4) for $\phi = 0$
δ_y	control deflection angle for yaw; vertical fins (δ_1, δ_3) for $\phi = 0$
$(\Delta\alpha_{eq})_v$	change in α_{eq} due to a collection of external vortices and their images
λ	fin taper ratio
ϕ	body roll angle, angle between z axis and z_0 axis; positive measured clockwise as viewed from rear
ϕ_1	roll angle of fin C_1 , angle between z_0 axis and C_1 ; positive measured clockwise as viewed from rear

1. INTRODUCTION

"A number of nonlinear phenomena appear in the characteristics of aerodynamic controls, and theory is only partially successful in accounting for their effects". This statement was made by one of the authors (JNN) nineteen years ago (Ref. 1). Significantly, it is as true today as it was when first made.

The purpose of this paper is to present some examples of nonlinear phenomena in control aerodynamics and to discuss their implications in terms of the resulting control effectiveness. The term nonlinear phenomena refers to any flow situation that produces, on the geometrical configuration under study, forces and moments which are not linear functions of the flight conditions (e.g., angle of attack). There are many types of examples, both in terms of geometrical configurations and flow conditions, that could be used to describe such nonlinear situations. In order to limit these geometries and flow situations to a number that can be handled in an article this size, only all-movable fins or highly maneuverable, tactical missiles will receive consideration.

Research in the field of missile aerodynamics has been receiving increased interest in the past several years. A primary reason for this interest is the need for high maneuverability in current and future missile system requirements. This necessitates the study of the aerodynamic characteristics of these vehicles at high angles of attack and control deflection. The study of control aerodynamics at these high angles is primarily a study of nonlinear aerodynamics. For an extensive and current review of nonlinear missile aerodynamics the reader is referred to reference 2. One of the first realizations of this recent research is the heretofore significant lack of systematic data on control effectiveness at high angles of attack (Refs. 2 and 3). However, some experimental data have been obtained in recent years from which the nonlinear characteristics of controls at high angles of attack can begin to be examined. It is implications of these data upon which the present article is based.

A typical configuration to be considered is shown in figure 1 at an angle of attack. Also shown is the general vortex flow field produced by such a configuration. The configuration consists of the following components:

- (1) A cylindrical nose section extending back to the first set of lifting surfaces,
- (2) A first set of cruciform lifting surfaces - henceforth referred to as the canard section,
- (3) A cylindrical afterbody section between the two sets of lifting surfaces,
- (4) A second set of cruciform lifting surfaces which will be referred to as the tail section.

Actual configurations can be similar to the one shown or can be geometrically less complex, such as a body-tail design consisting of a long cylindrical section with a single set of cruciform lifting surfaces near the base. Control of the configuration of figure 1 can be accomplished by deflecting either the canard fins or the tail fins. In the examples shown in this article the canard fins are used. 25-3

The vortex system generated by a missile at an angle of attack is of particular interest. The nose section can produce a pair of vortices which can be either symmetric or asymmetric. An asymmetric vortex pair has no mirror symmetry with respect to the plane containing the body axis and the free-stream velocity vector. A symmetric pair of nose vortices is shown in figure 1. The canard fins also produce trailing vortices. Although figure 1 shows only one vortex per fin, results of flow visualization studies (Ref. 4) indicate that the canard trailing vortex sheets often roll up into two distinct vortices per fin. The afterbody, in the presence of the canard vortices and body vortices, can develop asymmetric vortices, especially under conditions of roll or asymmetrical canard fin deflections. Finally, all the vortices can pass over the tail fins inducing nonlinear forces and moments on these fins. The interaction with the control surface of these body and fin vortices is one cause of the nonlinearities to be discussed shortly.

2. RELEVANT PARAMETERS

One method that has been applied in recent years to the prediction of missile aerodynamic characteristics is generally referred to as the data-base technique. This technique is based on a large body of systematic experimental data measured on a general set of geometrical configurations over a wide range of flow conditions (Ref. 5). Methods are then developed for calculating specific missile aerodynamic characteristics using analytical knowledge wherever possible and empirical observations where necessary. This technique has experienced a good degree of success, due in part of course to the large amount of generality in the geometrical configurations chosen to develop the experimental data. Unfortunately, this technique has not yet been applied to the prediction of control characteristics because of the large number of parameters that govern their behavior. These parameters are listed in Table I.

Table I - Parameters Governing Aerodynamic Characteristics of Controls

Control Parameter	Symbol
Geometrical Parameters	
Fin Aspect Ratio	AR
Fin Taper Ratio	λ
Ratio of Body Radius to Fin Semispan	a/s_m
Ratio of Forebody Length to Body Diameter	l_F/d
Flow Parameters	
Angle of Attack	α_C
Mach Number	M_∞
Reynolds Number	Re
Roll Angle	ϕ
Fin Deflection Angle	δ

Although the parameters listed in Table I normally dominate the control aerodynamics, others can affect control behavior to a significant extent. These include the shape of the nose planform, the fin thickness profile, and the body cross-sectional shape. This last item is becoming increasingly important with the new class of tactical missiles that utilize bank-to-turn techniques and have nonaxisymmetric body cross-sections (the majority having elliptical cross-sections) (Ref. 6). Because of this large quantity of parameters affecting the aerodynamic behavior of a control surface, it is not surprising that a systematic control data base, in which the different parameters are varied systematically, is lacking. Such a data base would be of great value.

3. SOURCES OF NONLINEARITY

The sources of nonlinear effects on control behavior are almost as numerous and varied as the parameters. Of these, several have been known for quite some time and exist throughout most of the angle of attack range. These will be described here only in passing. Other sources exist primarily at higher angles of attack and result in large losses of lift effectiveness. Examples of nonlinear effects at high angles of attack will be discussed in some detail.

One of the first recognized sources of nonlinear behavior is due to the presence of a gap at the fin-body juncture. For even the smallest gap, inviscid theory requires that the span loading at the juncture be zero. This is shown qualitatively in figure 2.

25-4 Hence, for even the smallest gap, inviscid theory predicts a significant loss of lift effectiveness. The effect of viscosity usually, but not always, mitigates these losses somewhat for small gaps. However, when the gap width is large substantial losses of normal force will occur.

A second gap effect occurs when the control surface is deflected through a large angle. In this situation the forward part of the control may pass above the body in side view or the aft part may pass below the body. This condition is depicted in figure 3. Positive pressures beneath the control leading edge can produce a download on the body upstream of the hinge line and negative pressures above the control trailing edge can produce an upload downstream of the hinge line. The net result of this effect will be a large couple.

An example of a nonlinear phenomenon due to viscosity is the separation of the flow over the control surface. This results from the interaction of the control boundary layer with the outer flow. As in other examples of flow separation, the location of the point of separation, both with respect to the control geometry and the transition point, significantly influences the type of boundary-layer separation, its reattachment, and its overall effect on the characteristics of the control.

In addition to the sources of nonlinearity already discussed there are two large categories that tend to overlap in certain flow regimes. These categories are interference effects and high angle-of-attack effects. In a sense, all high-angle-of-attack effects can be classified as types of interference, but since many interference effects are present at low or moderate angles of attack the distinction between the two can be important. In the present discussion the cause of the interference effect will be described and then, where applicable, examples of its nonlinear behavior at high angles of attack will be shown.

On a wing-body combination at subsonic and up to moderately supersonic speed, the effect of the body on the wing is to increase the wing lift as long as the angle of attack is small. As an example of this fin-body interference consider the upwash in the crossflow plane normal to the body. As the flow goes around the body it speeds up and produces an effective angle of attack equal to $2\sin \alpha_c$, according to potential flow theory, at the side of the body and as shown in figure 4. Fin panels in this flow field experience an increase in lift over what they would develop if the panels were part of the wing-alone at an angle of attack of α_c . The fin-body interference factor K_w is a measure of this favorable interference.

$$K_w = \frac{\text{Lift of wing panel in presence of body (at } \alpha_c)}{\text{Lift of wing panel as wing alone (at } \alpha_c)} \quad (1)$$

According to potential flow theory, K_w is a function only of a/s_m and varies from 1.0 for no body ($a/s_m = 0$) to 2.0 for a small fin on a large body ($a/s_m = 1$). The quantity $K_w \alpha_c$ is the effective angle of attack of the fin on a linearized basis.

The behavior of K_w at high angles of attack can be quite different from this predicted behavior however. In reference 7, values of K_w were determined from experimental data up to 45° angle of attack for a series of wings and Mach numbers. Some results are shown in figure 5 for a delta fin of aspect ratio 1.0 mounted on a body whose diameter is one-half the total span of the wing-body. As the angle of attack is increased the value of K_w decreases below one, indicating adverse interference of the body on the wing. This adverse interference is substantially worse at high Mach numbers.

At high angles of attack and at supersonic Mach numbers, a curved shock wave can form in front of the body (figure 6) which can cause reduced dynamic pressures where the wing would be and which can also destroy the favorable upwash. The unfavorable effect of the body on the wing is clear in this instance. However, the large reduction in K_w for subcritical crossflow Mach numbers is not understood as yet.

For wing-body-tail configurations, such as the example shown in figure 1, an effect well known to aircraft and missile designers is the classical case of wing-tail interference. At zero roll the tail fins operate in the downwash of the forward fins and suffer a loss of lift and effectiveness as a result. For canard missiles, where additional lift can be generated by the forward fins acting as controls, the effect can be aggravated over the case for fixed forward surfaces owing to the stronger vortex field created by deflection of the forward surfaces. Also the down load on the tail is greatest for a given canard vortex system when the tail span is close to or slightly less than the span of the canard vortex. A formal method for calculating the effects of wing-tail interference on lift and center-of-pressure positions is presented in reference 8 for planar wing-body-tail combinations to angles of attack of about 10° . This method is extended in reference 9 to about 20° angle of attack by considering both the fin vortices shed from the fin leading and side edges using the Polhamus analogy and the nose vortices in the calculation of the tail forces.

Although this discussion has concentrated on fin-generated vorticity, interference effects due to vortex motion over the control surface include vorticity generated by the body as well as the fins. Body vorticity can be generated either at the nose section or afterbody section (see figure 1). When vortices pass over a fin the

effective angle of attack of the fin is changed by flow induced normal to the fins by the external vortices and their images inside the body. In fact, under certain conditions, vortex interference can dominate the fin characteristics. 25-5

Another interference nonlinearity familiar to missile designers is roll reversal. Generally, the use of forward fins for roll control is not very effective. This is because the downwash from these fins induces a force on the tail fins directly behind them. This force in turn induces a rolling moment of opposite sign to the rolling moment produced by the forward control surfaces. In fact it is possible to produce more reverse roll than direct roll under certain circumstances. One method currently under investigation to reduce these induced rolling moments (Ref. 10) uses free-rolling tail fins. This study found that a free-rolling tail configuration provided conventional roll control with no roll reversal. In addition, this configuration reduced the induced roll associated with canard yaw control.

Nonlinearities also occur as a result of control cross-coupling which occurs when the control deflections for one type of control also result in some other type of control being produced. This can best be understood by considering the deflection of one fin. A primary normal force is produced on the deflected fin and secondary normal forces due to panel-panel interference (Ref. 11) are induced on the other three fins which are undeflected. As an example consider a cruciform wing-body combination at a high angle of attack and zero roll angle with the upper and lower fins equally deflected to produce yaw control. The sweepback of the upper fin will be increased by α_c . In addition, at high Mach numbers the fluid density above the body may be less than that below. As a result there will be less normal force on the upper fin. Accordingly, a rolling moment will develop. Thus, cross-coupling between yaw control and roll control occurs. This example is just one of many kinds of cross-coupling that can occur. Based on slender-body theory it is possible to predict a number of different coupling effects for all-movable controls, and to classify them. Such a classification is carried out in reference 1.

The purpose of this discussion on the various sources of nonlinear effects has been to indicate that, at a given set of flight conditions, some or all of these effects can influence the aerodynamic characteristics of the control surface. In the remainder of this paper discussion is limited to the nonlinear effects caused by fin-body and fin-fin interference due to fin deflection. The normal-force coefficient due to fin deflection is measured by the interference factor k_w . One method of describing the interference caused by deflection of an all-movable control is through the relation

$$k_w \equiv \frac{L_{w(B)}}{L_w} ; \alpha_c = 0, \delta \neq 0 \quad (2)$$

where $L_{w(B)}$ is the lift on the two fins in the presence of the body due to fin deflection and L_w is the lift on the wing alone formed by joining the two fin panels together at $\alpha_c = \delta$ (Ref. 1). This term can be evaluated using either slender-body theory (Ref. 1) or linear supersonic theory (Ref. 12). Results from these two methods are shown in figure 7. There is generally small difference between the two predictions, never exceeding about ten percent for values of two or greater. For slender-body theory (SBT) k_w is a function only of a/s_m , the body radius to fin semi-span ratio. It is of interest to note that k_w determined by SBT is not much less than unity for all values of a/s_m . What this means is that, according to SBT, all-movable panels in the presence of a body develop, independent of angle of attack, almost as much lift as the isolated wing formed by joining the two fin panels together. However, as will be shown shortly, there can be significant losses associated with fin deflection at high angles of attack.

Since the SBT value of k_w is independent of angle of attack it does not consider any of the nonlinear characteristics of the fin in the presence of the body or even of the isolated wing that exist at high angles of attack. Therefore, in order to describe more adequately the nonlinear behavior at high angles of attack, a new relation for the control interference factor is introduced. This new relation is based on the equivalent angle of attack concept and is written

$$k_w \equiv \frac{\tan(\alpha_{eq,\delta}) - \tan(\alpha_{eq,0})}{\tan(\alpha_{eq,0} + \delta) - \tan(\alpha_{eq,0})} \quad (3)$$

Before describing these terms a brief description of the equivalent angle of attack concept will be given.

The equivalent angle of attack concept relates the forces experienced by the actual fin in the presence of the body to the lifting surface formed by placing two opposing fins together in the absence of the body (the wing alone). Thus, any nonlinear behavior of the specific fin under investigation acting as part of the wing alone is automatically taken into consideration. The equivalent angle of attack of the fin, α_{eq} , is defined as that angle of attack of the wing alone for which its normal force is twice that of the fin. As originally introduced (Ref. 13) the concept was

25-6 based on linear superposition. As such it was only valid for small to moderate angles of attack (that is, below about 20°). However, more recently (Ref. 7) this concept was extended to the nonlinear range at high angles of attack. The extended definition of the equivalent angle of attack on fin i is given by the relation

$$\tan(\alpha_{eq})_i = \frac{v_{n_i}}{v_{p_i}} \quad (4)$$

In determining α_{eq} of a fin in a cruciform wing-body combination a number of interference effects are considered.

- (1) If the wing-body combination is pitched at zero roll the upflow in the crossflow plane due to α_c is augmented by body-induced upwash. The interference factor describing this effect is K_w .
- (2) If the configuration is yawed at a fixed angle of attack the load will change due to a coupling between the angles of attack and sideslip. The factor for this effect is K_ϕ .
- (3) If vortices are present in the flow field they will induce changes in the normal flow on the fin. The change in equivalent angle of attack due to external vortices is given by the term $(\Delta\alpha_{eq})_v$.
- (4) Finally, when a fin is deflected the increased normal flow is modified by panel-panel interference, lack of a perfect reflection plane on the body, and control gap effects. The factor for this effect is k_w .

Once the results of all these effects on the fin equivalent angle of attack have been determined and combined in a nonlinear fashion, the equivalent angle of attack of the fin is known. Its normal-force coefficient is then found from the experimental wing-alone curve.

Combining the various interference effects (Ref. 7), the equivalent angle of attack is given by the following expression.

$$\alpha_{eq} = \tan^{-1} \left\{ \tan \alpha_c \cos \phi \left[K_w + \frac{4}{AR} K_\phi \sin \alpha_c \sin \phi \right] + \tan (\Delta\alpha_{eq})_v + k_w \left[\tan (\alpha_{eq,o} + \delta) - \tan (\alpha_{eq,o}) \right] \right\} \quad (5)$$

where

$$\tan \alpha_{eq,o} = \tan \alpha_c \cos \phi \left[K_w + \frac{4}{AR} K_\phi \sin \alpha_c \sin \phi \right] \quad (6)$$

This revised relation for k_w therefore compares the lift produced by the deflected fin with that produced by the undeflected fin, using the characteristics of the wing alone as the basis for comparison. If, at given values of α_c and δ , the fin operates at an equivalent angle of $\alpha_{eq,o}$ for no control deflection ($\delta = 0$), it would operate at $(\alpha_{eq,o} + \delta)$ for a control surface deflection angle of δ provided no losses in normal force occurred as compared to the wing alone. The definition of k_w given by eq. (3) yields a value of zero if no normal force results from control deflection and a value of unity for a "perfect" control, one which produces the same increase in normal force it would as part of the wing alone. In actual cases the value of k_w has been found to vary from values of less than zero (indicating an actual loss of lift when the control surface is deflected) to values exceeding one (indicating more lift than the wing alone or favorable wing-body interference).

4. EXAMPLES OF NONLINEAR EFFECTS AT HIGH ANGLES OF ATTACK

The nonlinearities in k_w are difficult to predict analytically. Furthermore, the amount of data available on k_w at high angles of attack and control deflection is not extensive. The data that does exist however can be used to illustrate the nonlinearities present at high angles of attack. Among the systematic data available are the pitch-control data of reference 14 at $M_\infty = 3.36$ and the control data on pitch, yaw, and pitch-yaw cross-coupling at $M_\infty = 0.8$ and 1.3 in reference 15. In this section values of k_w determined from these data are examined.

4.1 Pitch Effectiveness at High Mach Numbers

The study reported in reference 14 tested a semispan model of a wing-body combination mounted on a splitter plate at $M_\infty = 3.36$. Values of k_w resulting from these tests are presented in figure 8 for a delta wing of aspect ratio 1.0 and two values of the body radius to fin semispan ratio - 0.2 and 0.4. Data for angles of attack to 25° and control deflection from -15° to +40° are shown. The experimental values of k_w , calculated using eq. (3), varies from about 0.7 to almost 1.1. The

wing-body combination with the larger value of a/s_m (meaning the configuration with the shorter relative span) has, in general, lower values of k_w . Notice also that there are no significant effects of the value of the control deflection angle on k_w . Slender-body theory, applied to the classical definition of k_w given by eq. (2), predicts a somewhat higher value for most angles of attack and control deflection. However, the slender-body theory value does appear to give a reasonable approximation for k_w at this Mach number even at large angles of attack and control deflection.

There are no data for the variation of k_w with roll angle at high angles of attack and high supersonic Mach numbers. However, it seems likely that, for yaw control, the value of k_w may well be less for the leeward fin ($\phi_1 = 0^\circ$) than the value for the windward fin ($\phi_1 = 180^\circ$). In that case an induced rolling moment will develop as a result of yaw deflection at $\phi = 0^\circ$. This is an effect which must be included in any predictive method when sufficient data or theory to evaluate this effect are available.

4.2 Control Effectiveness at Transonic Mach Numbers

Systematic control data were taken as part of the wind-tunnel tests of the Army generalized missile in the 11-Foot Transonic Wind Tunnel (Ref. 15) and the 6- by 6-Foot Supersonic Wind Tunnel (Ref. 16) of the NASA/Ames Research Center. The configuration, shown in figures 9 and 10, was tested at angles of attack up to 50° with pitch control, yaw control, and combined pitch-yaw control. These data, taken at $M_\infty = 0.8$ and 1.3, included measurements to show how k_w for pitch control varies with α_c at $\phi = 0^\circ$, and how k_w varies with roll angle for a fixed α_c of 15° . For this investigation the canard fins only were deflected. These fins have an aspect ratio of 3.5², a taper ratio of 0.06, and the body radius to fin semispan ratio is 0.4.

Examining first the effects of the control deflection angle on k_w for pitch control, figure 11 shows results for $\delta = 5^\circ, 10^\circ$, and 15° . For $M_\infty = 0.8$ the value of k_w predicted by slender-body theory, which henceforth will be referred to as $(k_w)_{SBT}$, is a fair approximation of the data up to about $\alpha_c = 20^\circ$, but thereafter the experimental values of k_w fall to zero at $\alpha_c = 50^\circ$. This indicates that deflection of these fins for the purpose of pitch control at $\alpha_c = 50^\circ$ produces no increase in normal force. While there is some scatter with δ , a mean curve can be used to represent the nonlinear behavior fairly well. In general, the results for $\delta = 15^\circ$ show the smallest values of k_w .

The behavior of the results for k_w at $M_\infty = 1.3$, figure 11(b), shows a markedly different variation with α_c than the results at $M_\infty = 0.8$. First, as the angle of attack increases from zero, k_w immediately decreases from $(k_w)_{SBT}$. Even more noticeable is the peak in the results near $\alpha_c = 40^\circ$. It is instructive to examine the variation with angle of attack of the actual fin normal-force coefficient for the three conditions used to determine k_w (the wing alone, wing in the presence of the body without control deflection, and wing in the presence of body with control deflection). These three conditions are shown in figure 12 for the corresponding set of flow conditions in figure 11 (i.e., $M_\infty = 1.3$, $\phi = 0^\circ$, pitch control, $\delta_p = 15^\circ$). For all three conditions fin normal-force coefficient increases smoothly with angle of attack. However, there are slight differences with angle of attack in the increase in lift produced by the control deflection. Hence, it is apparent that the nonlinear definition of k_w given by eq. (3) is a sensitive indicator of control effectiveness. Again there is some scatter due to the value of the control deflection angle but a mean curve does give a fair approximation of the behavior of k_w except in the vicinity of $\alpha_c = 40^\circ$. Finally, the values of k_w at the highest angles are not nearly as low as at $M_\infty = 0.8$ where they approach zero.

Before proceeding with further discussion some indication of the precision in the experimental values of k_w can be obtained since measurements were made with fins C1 and C3 deflected and fins C2 and C4 undeflected for body roll angles (ϕ) of $0^\circ, 10^\circ, 20^\circ, 30^\circ$, and 45° . Measurements were then repeated with fins C2 and C4 deflected and fins C1 and C3 undeflected. By assuming symmetry about a vertical plane containing the body longitudinal axis the data can be interpreted as if fins C1 (the top fin at $\phi = 0^\circ$) and C3 only were deflected and the body rolled from $\phi = 0^\circ$ to $\phi = 180^\circ$. That is, examining k_w for deflection of fin C4 at $\phi = 0^\circ$ (pitch control of the horizontal fins) is equivalent to examining k_w for deflection of fin C1 at $\phi = 90^\circ$. In the following the equivalent roll angle of fin C1 will be used (ϕ_1). The actual body roll angle and fin used to produce k_w are given in Table 2 on the following page. For a body roll angle of 45° fins C3 and C4 are symmetric about the vertical plane of symmetry (as well as fins C1 and C2). Therefore they should produce closely the same results for k_w . Figure 13 compares results for these two conditions of mirror symmetry. At $\phi_1 = 45^\circ$ figure 13(a) shows results for fins C3 and C4 which are generally within ± 0.05 in k_w from the mean line. For $\phi_1 = -45^\circ$ fins C1 and C2 show about the same precision in figure 13(b). However, now the value of k_w approaches zero at $\alpha_c = 50^\circ$. Thus there is an effect of ϕ_1 on k_w . This effect will be examined in more detail shortly.

Table 2.- Equivalent Angle of Fin C1

Fin	ϕ ($^{\circ}$)	ϕ_1 ($^{\circ}$)
C1	0	0
C1	10	10
C1	20	20
C1	30	30
C1	45	45
C2	30	60
C2	20	70
C2	10	80
C4	0	90
C4	10	100
C4	20	110
C4	30	120
C3	45	135
C3	30	150
C3	20	160
C3	10	170
C3	0	180

25-8

First, the control effectiveness for yaw control is presented in figure 14. In these and subsequent figures the experimental values of k_w are included only for angles of attack above 20° . Examining first the results for $M_{\infty} = 0.8$, shown in figure 14(a), it can be seen that not only is there a difference in control effectiveness in the angle of attack range from 20° to 30° , but the value of k_w for the leeward fin indicates that this fin is more effective in providing control than it would be as part of the wing alone. The effectiveness of both fins decrease with increasing angle of attack, that of the leeward fin decreasing much faster, so that at the highest angle of attack investigated they both produce about the same effectiveness. Results for $M_{\infty} = 1.3$, given in figure 14(b), show smaller differences at $\alpha_c = 20^{\circ}$ than do the results at $M_{\infty} = 0.8$. Again, k_w for both fins decreases with increasing angle of attack and above $\alpha_c = 35^{\circ}$ both fins produce essentially the same effectiveness.

The reason for the high effectiveness of the leeward fin at $M_{\infty} = 0.8$ and $\alpha_c = 20^{\circ}$ can be seen by examining the fin normal-force coefficient as function of angle of attack as the wing alone, the leeward undeflected fin and the leeward deflected fin. These are shown in figure 15. As the undeflected fin, represented by the square symbols, very little lift is produced as expected since the fin is aligned parallel to the free stream for this case. When the fin is deflected it produces slightly more lift than the wing alone. Since the wing alone experiences a partial stall in this region ($\alpha_c = 20^{\circ}$) a little increase in normal force yields a much larger increase in the equivalent angle of attack. Hence, the relative effectiveness is very high for α_c from 20° to 25° . Notice however, that after a slight increase initially in $C_{Nw(B)}$ for the deflected fin there is a steady decrease until at $\alpha_c = 50^{\circ}$ the fin produces only half as much lift as at $\alpha_c = 20^{\circ}$.

The variation of k_w with ϕ_1 demonstrates a number of nonlinearities. Figure 16(a) shows the variation of k_w with ϕ_1 at $\alpha_c = 20^{\circ}, 30^{\circ}, 40^{\circ}$, and 50° for the canard fin of figure 9 at $M_{\infty} = 1.3$ and a control deflection angle of 15° . For roll angles in the range 0° to 90° (i.e., the fin in the upper right hand quadrant) there is a systematic decrease in k_w with increasing angle of attack. In the absence of vortex effects a decrease might be expected because of increased sweep with increasing α_c and possibly decreased dynamic pressure. No particular effect of the body vortices is obvious. However, some surprising nonlinear effects are clearly present for ϕ_1 greater than 90° .

For $\alpha_c = 20^{\circ}$, k_w essentially increases as ϕ_1 increases from 90° . This increase might be expected because of reduced sweep of the fin leading edge accompanying pitch of the wing-body combination and possible increased dynamic pressure on the impact surface. However, some phenomenon is causing k_w to go through a maximum around $\phi_1 = 100^{\circ}$ for $\alpha_c = 30^{\circ}$ and 40° . The exact reason for this behavior is not known at this time.

Consider now the behavior of k_w with changes in ϕ_1 and α_c for $M_{\infty} = 0.8$ as exhibited in figure 16(b). For $\phi_1 < 135^{\circ}$ there is a general monotonic decrease in k_w with increasing angle of attack. For $\phi_1 > 135^{\circ}$ there is a tendency for k_w to peak at values greater than unity for values of ϕ_1 near 160° . This behavior does not result in a significant increase in control normal force since the control fin is operating in the stalled region of the wing-alone normal-force curve in this case (recall figure 15).

In addition to testing the missile configuration of figure 9 at independent pitch and yaw control, it was also tested at combined pitch and yaw with all four fins deflected $+15^{\circ}$. In the succeeding set of figures the effects on k_w for combined pitch/yaw control are compared to the appropriate results for single (either pitch or yaw) control.

The effect on k_w for yaw control in the presence of pitch control of the upper or leeward fin is presented in figure 17. At $M_{\infty} = 0.8$ there is no longer the

large value of k_w near $\alpha_c = 20^\circ$ for combined yaw/pitch control as there was for single yaw control. However, this does not imply any substantial loss in control normal force because, as mentioned previously, the wing-alone normal-force curve possess a stalled region near $\alpha_c = 20^\circ$ for $M_\infty = 0.8$ and this is where the fin is operating. For example, the fin normal-force coefficient for yaw control at $\alpha_c = 20^\circ$ is 0.340 while for combined yaw and pitch control it is 0.321. As the angle of attack is increased, the values of k_w for combined yaw and pitch control remain less than that for plain yaw control except at the highest angle of attack tested where the two values are equal. This indicates that for yaw control applied to the leeward fin at $M_\infty = 0.8$ there is an additional nonlinearity caused by deflecting the two adjacent fins for pitch control. The same behavior is not present at $M_\infty = 1.3$ however. As shown in figure 17(b), combined yaw/pitch control results in lower values of k_w only up to α_c of about 35 or 40 degrees. Above this both cases have the same control effectiveness.

The windward fin, figure 18, shows very little difference between combined yaw/pitch control and simple yaw control. Only near $\alpha_c = 20^\circ$ for $M_\infty = 1.3$ does combined control result in lower values of k_w .

Effects of pitch control in the presence of yaw control are exhibited in figure 19. At $M_\infty = 0.8$ pitch control is slightly more effective in the presence of yaw control than without, except near $\alpha_c = 50^\circ$ where negative values of k_w indicate an actual loss of lift with control deflection. An interesting effect is seen in figure 19(b) for the results at $M_\infty = 1.3$. Simple pitch control experiences a local minimum for α_c between 25 and 30 degrees and a local maximum near $\alpha_c = 35^\circ$. These two peaks are eliminated when yaw control is also present. However, above $\alpha_c = 35^\circ$ the values of k_w are significantly less for combined pitch/yaw control.

The variation of k_w with ϕ_1 in the presence of combined pitch/yaw control is presented in figures 20 and 21 where results are compared with the corresponding results in figure 16 for single control. Examining results at $M_\infty = 0.8$ first, it can be seen that the greatest differences between single and combined control occurs at the lowest angle ($\alpha_c = 20^\circ$). Except for the range $45^\circ < \phi_1 < 90^\circ$ the lift effectiveness is greater in the presence of combined pitch/yaw control. At $\alpha_c = 30^\circ$ [fig. 20(b)] the two sets of results are very similar except for low values of ϕ_1 where single control is somewhat more effective. In particular, both sets of results exhibit a peak near $\phi_1 = 150^\circ$. This peak in the lower quadrant is present also at angles of attack of 40° and 50° . In addition, at both $\alpha_c = 40^\circ$ and $\alpha_c = 50^\circ$ combined control and single control yield identical values of k_w over at least a portion of the lower quadrant (i.e., the quadrant $90^\circ < \phi_1 < 180^\circ$). This implies that in this region nonlinearities due to angle of attack dominate any additional nonlinearities due to combined pitch/yaw control. Such is obviously not the case at $\alpha_c = 20^\circ$ as shown in figure 20(a) where nonlinearities due to combined control are significant for all values of ϕ_1 . For fins in the upper quadrant at α_c of 40° and 50° combined control results in an actual loss of lift. Implications of this feature are rather obvious.

Results at the higher Mach number, figure 21, exhibit much fewer differences between single and combined control. For each angle of attack both sets of results have the same trend and in many cases the results are virtually identical. There is a slight loss of lift however at the highest angle of attack, figure 21(d).

5. PREDICTION METHODS AT HIGH ANGLES OF ATTACK

Considering the number of nonlinearities which exist for cruciform wing-body-tail combinations at high angles of attack, a purely theoretical approach to the prediction of the aerodynamic characteristics of such configurations is extremely difficult. Hence, at the present time reliance must be made on rational combinations of analytical and empirical results--so called "engineering" prediction methods. While a number of these engineering prediction methods exist for wing-body or body-tail configurations in the unrolled condition, very few methods are available for wing-body-tail combinations under conditions of both roll and control deflection. For no roll, the wing-tail interference problem for a cruciform configuration is the same as that for a planar configuration, and a number of methods applicable to this case are discussed in reference 2. However, as has been shown, the inclusion of roll introduces complex nonlinearities, particularly at high angles of attack.

The method of reference 13 presents a contribution to this field which is valid to approximately 20° angle of attack. It makes use of the equivalent angle of attack concept and treats pitch and yaw control but not roll control. The work reported in references 3 and 7 is an attempt to expand the method of reference 13 up to angles of attack of about 45° and to include effects of roll control. This preliminary method, which utilizes an incomplete data base augmented by engineering approximations, is applicable over the Mach number range 0.8 to 3.0 and for angles of attack from 0° to 45° .

6. CONCLUDING REMARKS

Cruciform fins used as all-movable controls have long been known to exhibit nonlinear aerodynamic characteristics for large angles of attack and control deflections. Up to the present it has been necessary to rely upon experimental data for such properties for use in guidance and control systems. A systematic set of data in this area would do much to further our understanding of these nonlinearities. Such a systematic data base is lacking. As a first step, a data base might be assembled for control pitch effectiveness as influenced by fin aspect ratio, fin taper ratio, Mach number, and body radius-fin semispan ratio. Control cross-coupling could then be addressed. By a combination of systematic data and computational fluid mechanics, major progress could be made in understanding control nonlinearities.

7. REFERENCES

1. Nielsen, J. N.: Missile Aerodynamics, McGraw-Hill Co., New York, 1960.
2. Nielsen, J. N.: Nonlinearities in Missile Aerodynamics, AIAA Paper 78-0020, 16th Aerospace Sciences Meeting, Huntsville, AL, Jan. 1978.
3. Smith, C. A., Nielsen, J. N. and Hemsch, M. J.: Prediction of Aerodynamic Characteristics of Cruciform Missiles to High Angles of Attack. AIAA Paper 79-0024, 17th Aerospace Sciences Meeting, New Orleans, LA, Jan. 1979.
4. Hemsch, M. J.: Reduced Vapor-Screen Data from Canard Missile Tests in Ames 6- by 6-Foot Supersonic Wind Tunnel. NEAR TR 81, 1975.
5. Fidler, J. E. and Bateman, M. C.: Aerodynamic Methods for High Incidence Missile Design. AIAA J. Spacecraft and Rockets, Vol. 12, No. 3, 1975, pp. 162-168.
6. Sawyer, W. C., Jackson, C. M., Jr., and Blair, A. B., Jr.: Aerodynamic Technologies for the Next Generation of Missiles. Paper presented at the AIAA/ADPA Tactical Missile Conference, Gaithersburg, MD, Apr. 27-28, 1977.
7. Nielsen, J. N., Hemsch, M. J. and Smith, C. A.: A Preliminary Method for Calculating the Aerodynamic Characteristics of Cruciform Missiles to High Angles of Attack Including Effects of Roll Angle and Control Deflections. Office of Naval Research Rept. ONR-CR215-226-4F, 1977.
8. Pitts, W. C., Nielsen, J. N. and Kaattari, G. E.: Lift and Center of Pressure of Wing-Body-Tail Combinations at Subsonic, Transonic, and Supersonic Speeds. NACA Report 1307, 1957.
9. Mendenhall, M. R. and Nielsen, J. N.: Effect of Symmetrical Vortex Shedding on the Longitudinal Aerodynamic Characteristics of Wing-Body-Tail Combinations. NASA CR-2473, 1975.
10. Blair, A. B., Jr.: Wind-Tunnel Investigation at Supersonic Speeds of a Canard-Controlled Missile with Fixed and Free-Rolling Tail Fins. NASA TP 1316, 1978.
11. Nielsen, J. N., Spangler, S. B., and Hemsch, M. J.: A Study of Induced Rolling Moments for Cruciform-Winged Missiles. NEAR TR 61, 1973.
12. Nielsen, J. N. and Pitts, W. C.: Wing-Body Interference at Supersonic Speeds with an Application to Combinations with Rectangular Wings. NACA TN 2677, 1952.
13. Hemsch, M. J., Smith, C. A., Nielsen, J. N., and Perkins, S. C., Jr.: Calculation of Component Forces and Moments of Arbitrarily Banked Cruciform Missiles with Control Deflections. Office of Naval Research, Report ONR-CR215-226-3, 1976.
14. Hill, W. A., Jr. and Kaattari, G. E.: Force and Pressure-Distribution Investigation to High Angles of Attack on All-Movable Triangular and Rectangular Wings in Combination with a Body at Supersonic Speeds. NACA RM A56C12, July 1956.
15. Schwind, R. G.: High Angle Canard Missile Test in the Ames 11-Foot Transonic Wind Tunnel. NASA CR 2993, 1978.
16. Hemsch, M. J. and Nielsen, J. N.: Test Report for Canard Missile Tests in Ames 6- by 6-Foot Supersonic Wind Tunnel. NEAR TR 72, 1974.

8. ACKNOWLEDGEMENTS

The work described in this article was primarily sponsored by the Office of Naval Research under Contract N00014-74-C-0050 with additional support provided by the Air Force Flight Dynamics Laboratory. Mr. David Siegel was the Navy Scientific Officer for the Office of Naval Research and Mr. Calvin L. Dyer was the advisor for the Air Force Flight Dynamics Laboratory.

The wind tunnel tests reported in references 15 and 16 were sponsored by the Naval Weapons Center and NASA/Ames Research Center. Dr. Gary T. Chapman and Mr. Gerald N. Malcolm were the NASA advisors. The test model was made available through the courtesy of the Army Missile R & D Command.

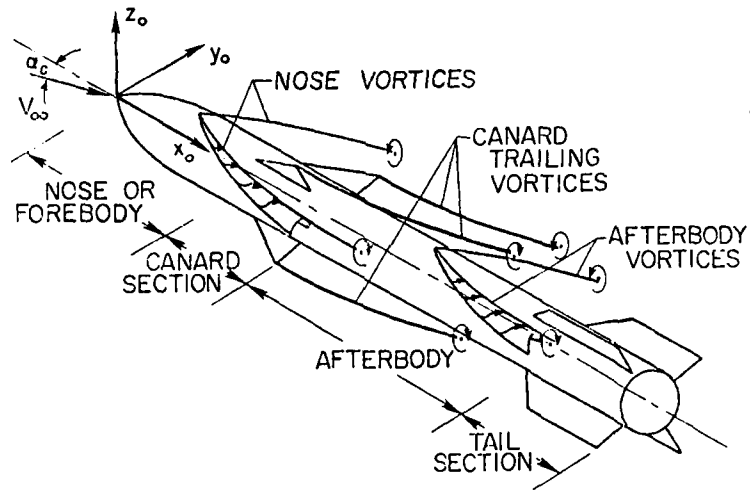


Figure 1.- Banked canard-cruciform missile at angle of attack showing typical vortex flow field.

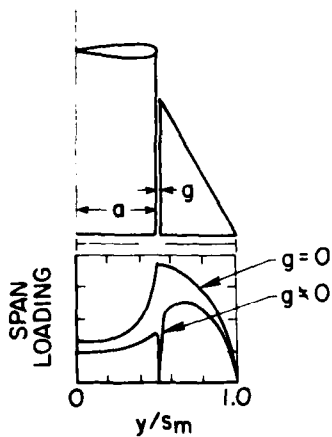


Figure 2.- Effect of gap on span loading of wing-body combination; inviscid theory

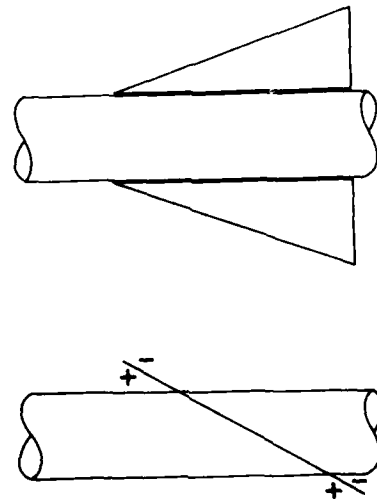


Figure 3.- Gap associated with large deflection of control surface.

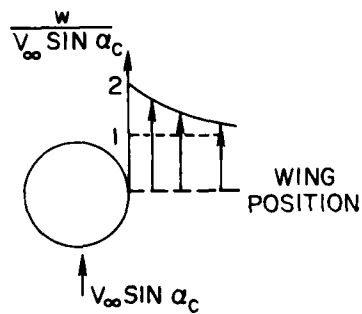


Figure 4.- Upwash in crossflow plane around body of revolution; potential flow theory

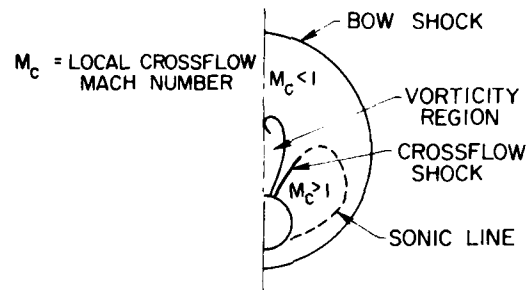


Figure 6.- Inviscid flow in crossflow plane of body of revolution with supersonic Mach number.

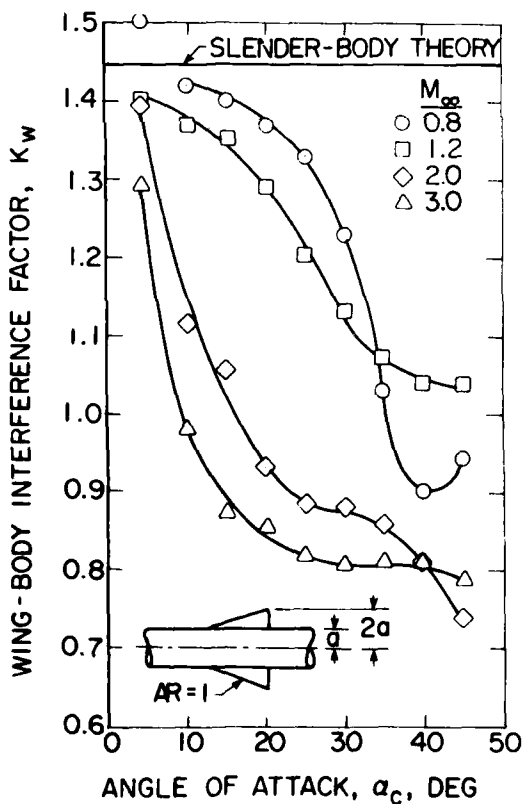


Figure 5.- Effect of angle of attack and free-stream Mach number on interference of body on wing

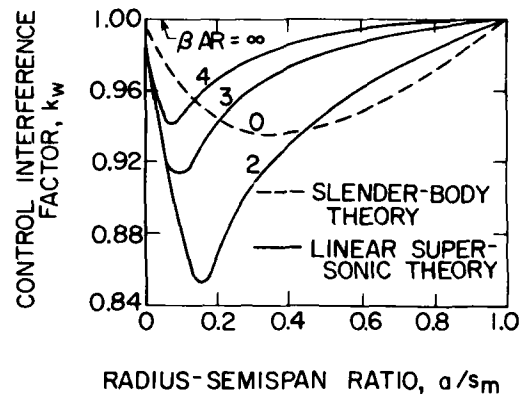


Figure 7.- Theoretical values of control interference factor, k_w , for rectangular wing-body combination.

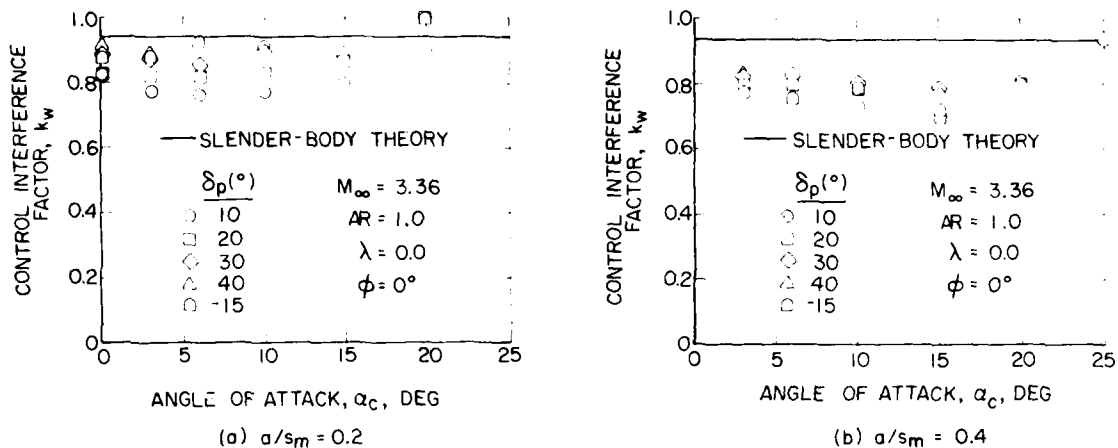


Figure 8.- Effect of angles of attack and control deflection on control interference factor, k_w , for pitch control.

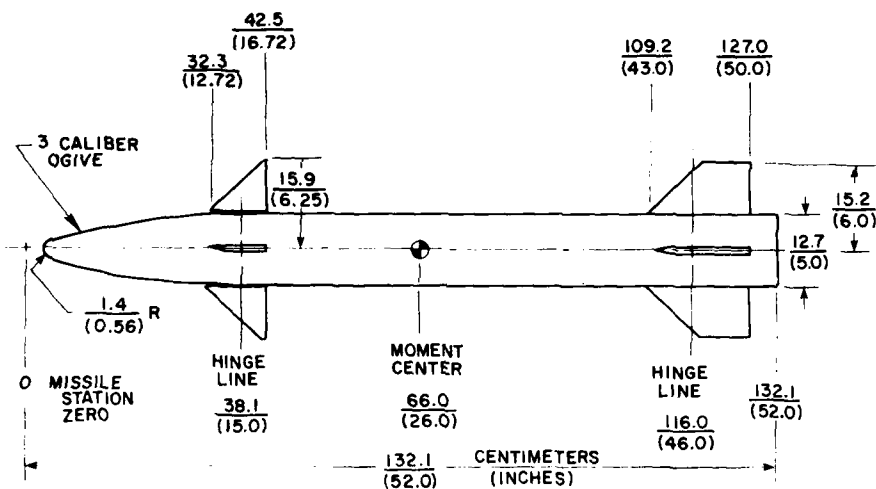


Figure 9.- Body-canard-tail test configuration, Army generalized missile.

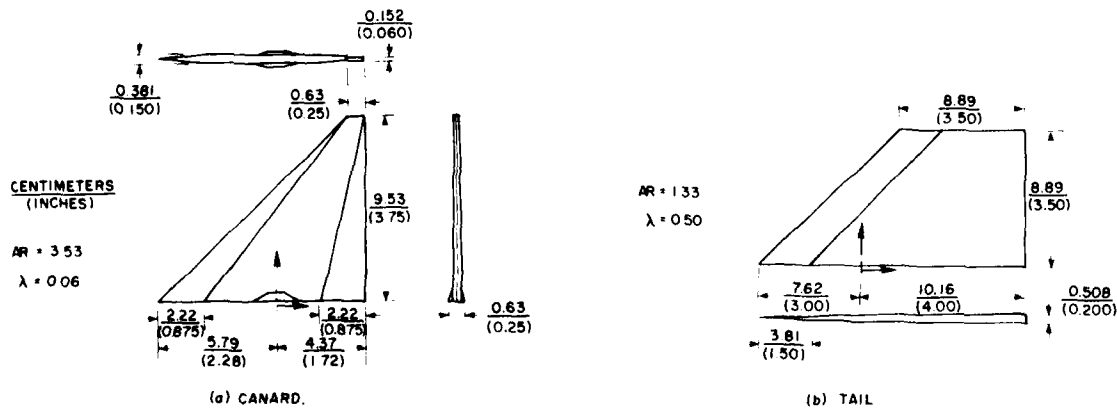


Figure 10.- Canard and tail fins.

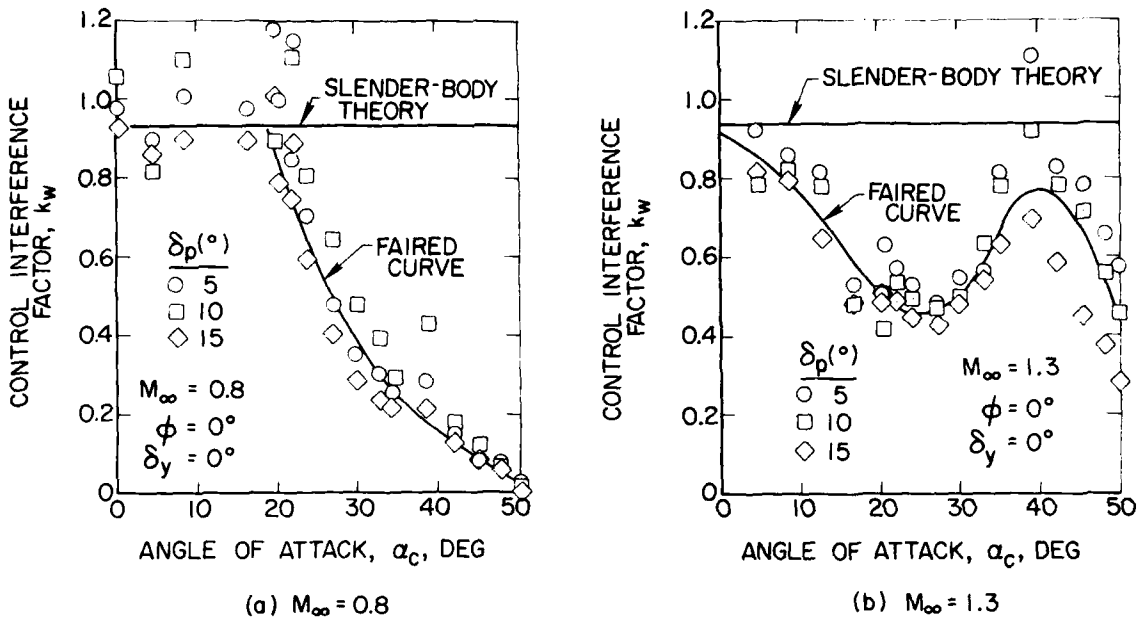


Figure 11.- Effect of angles of attack and control deflection on pitch control effectiveness.

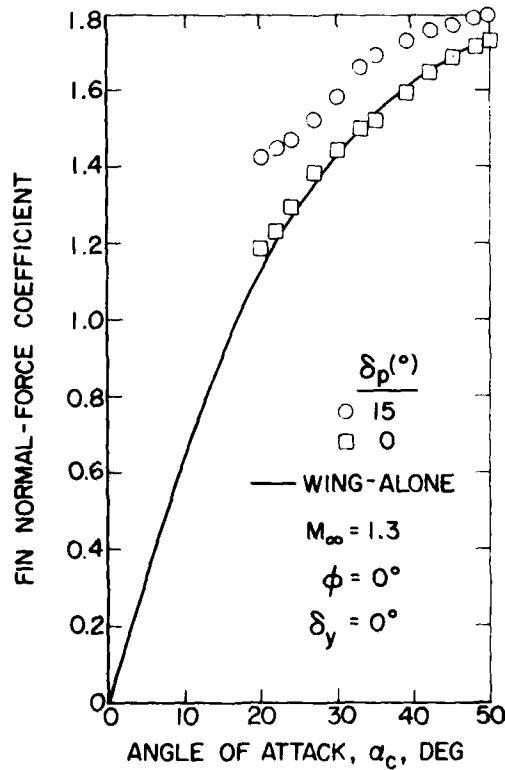


Figure 12.- Effect of angles of attack and control deflection on normal-force coefficient.

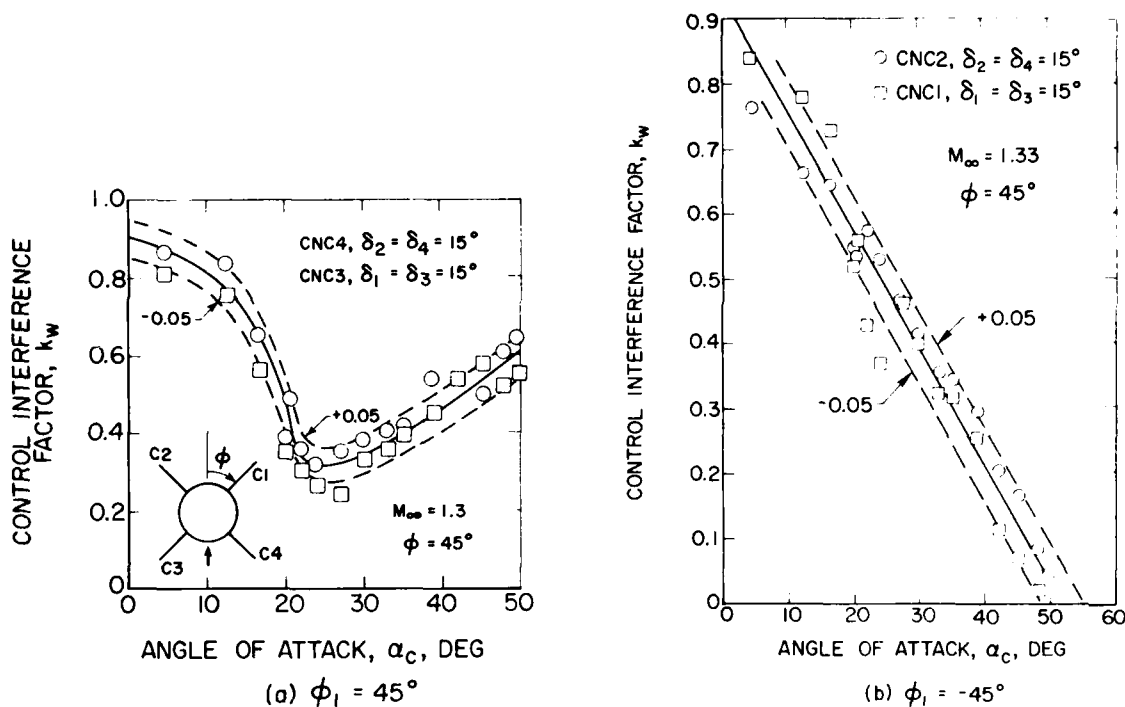


Figure 13.- Effect of assuming symmetry on control interference factor, k_w .

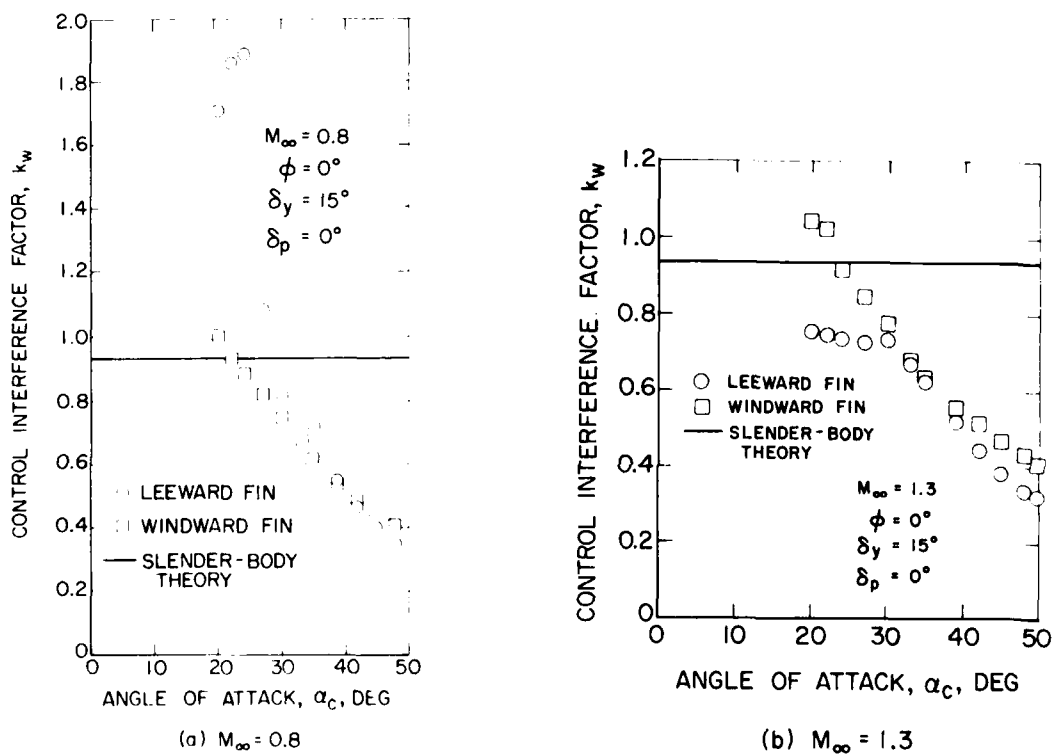


Figure 14.- Effect of angle of attack on yaw control effectiveness.

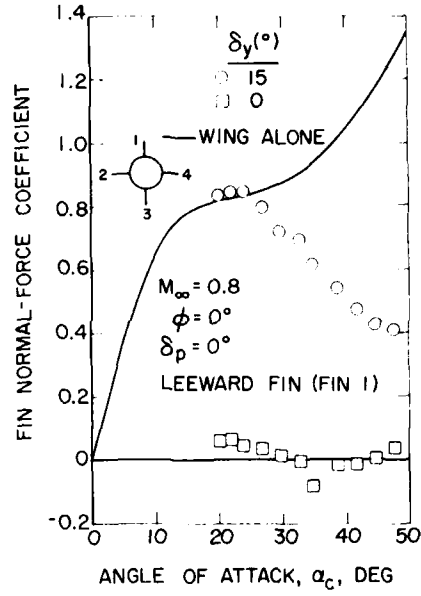
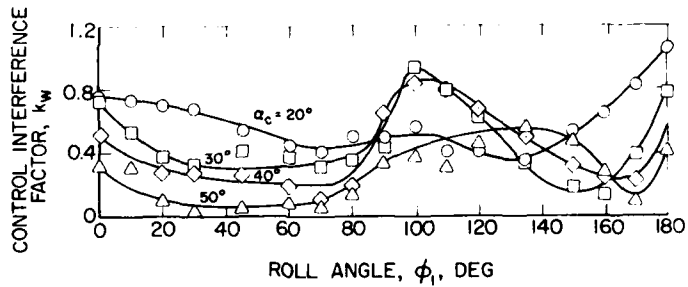
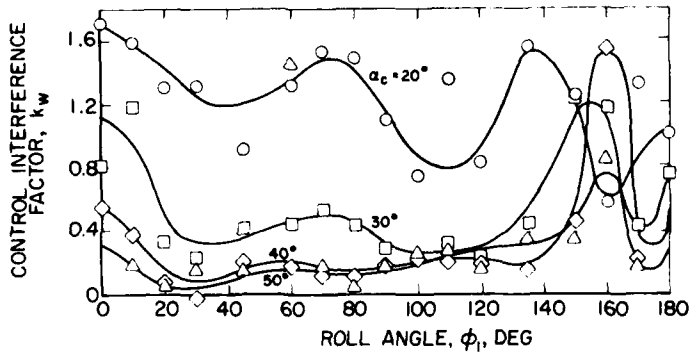


Figure 15.- Effect of angles of attack and control deflection on fin normal-force coefficient.



(a) $M_\infty = 1.3$



(b) $M_\infty = 0.8$

Figure 16.- Effect of angle of attack and roll angle on control interference factor, k_w .

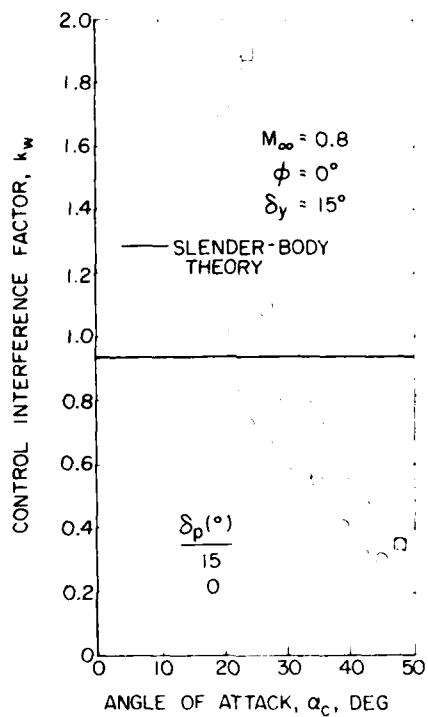
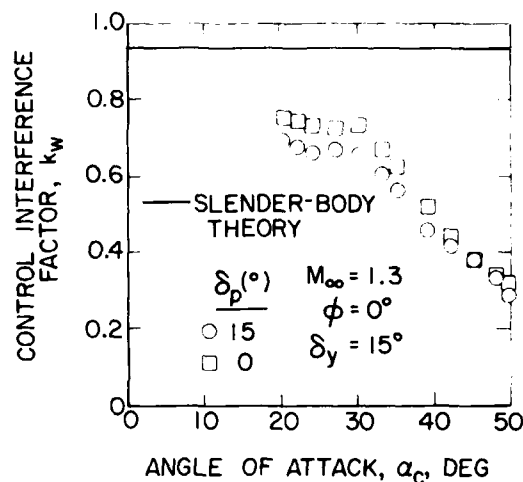
(a) $M_\infty = 0.8$ (b) $M_\infty = 1.3$

Figure 17.- Effect of angle of attack on yaw control effectiveness in presence of pitch control (leeward fin).

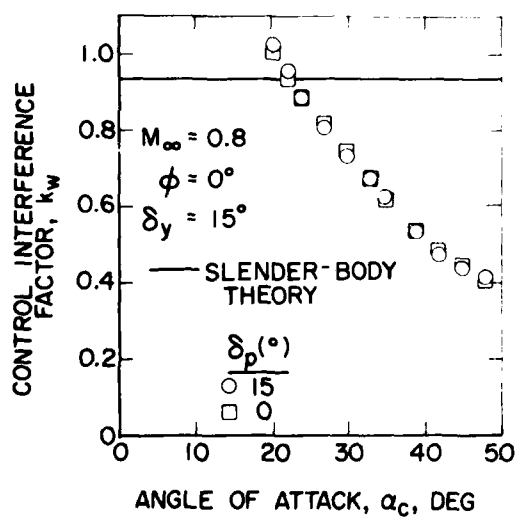
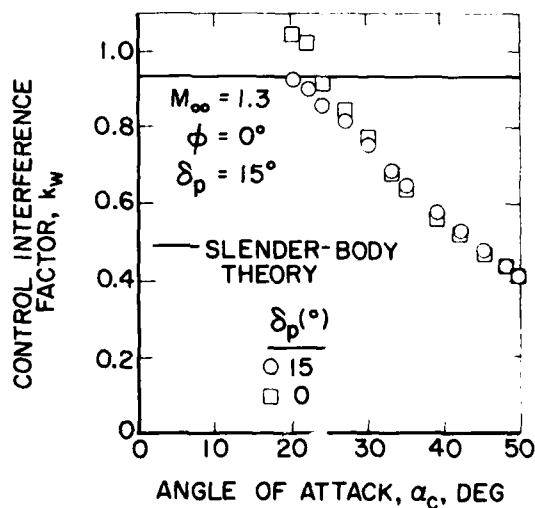
(a) $M_\infty = 0.8$ (b) $M_\infty = 1.3$

Figure 18.- Effect of angle of attack on yaw control effectiveness in presence of pitch control (windward fin).

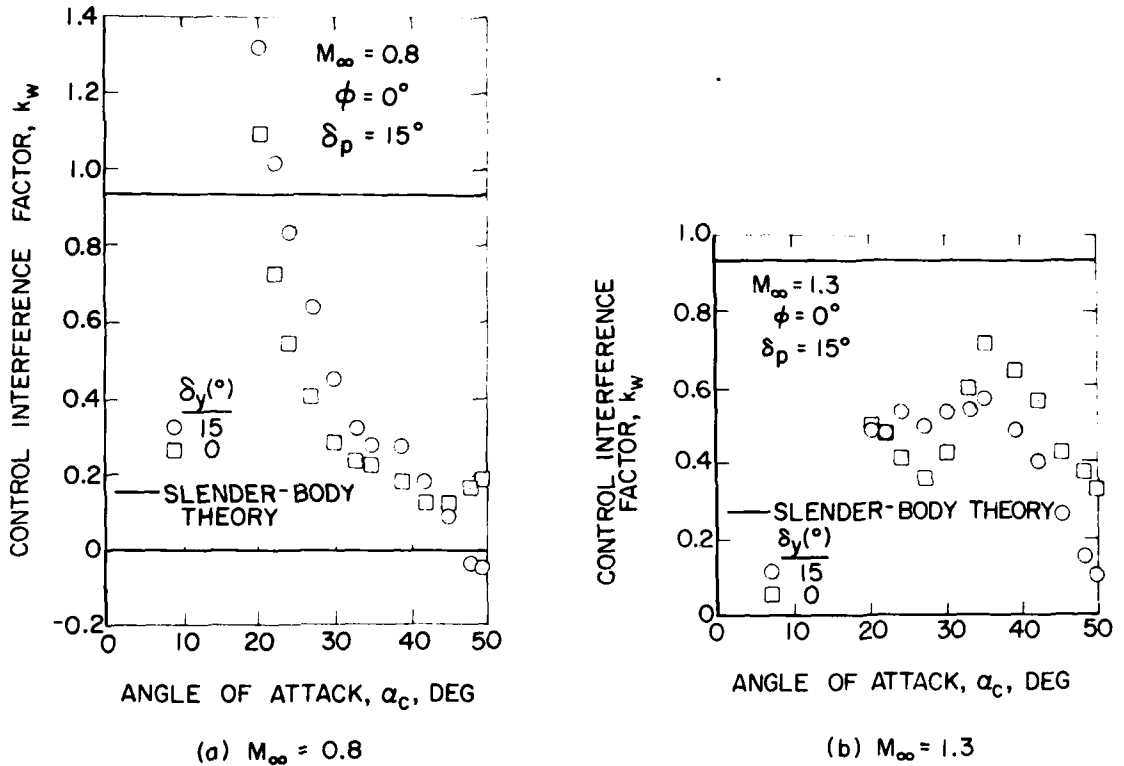


Figure 19.- Effect of angle of attack on pitch control effectiveness in presence of yaw control.

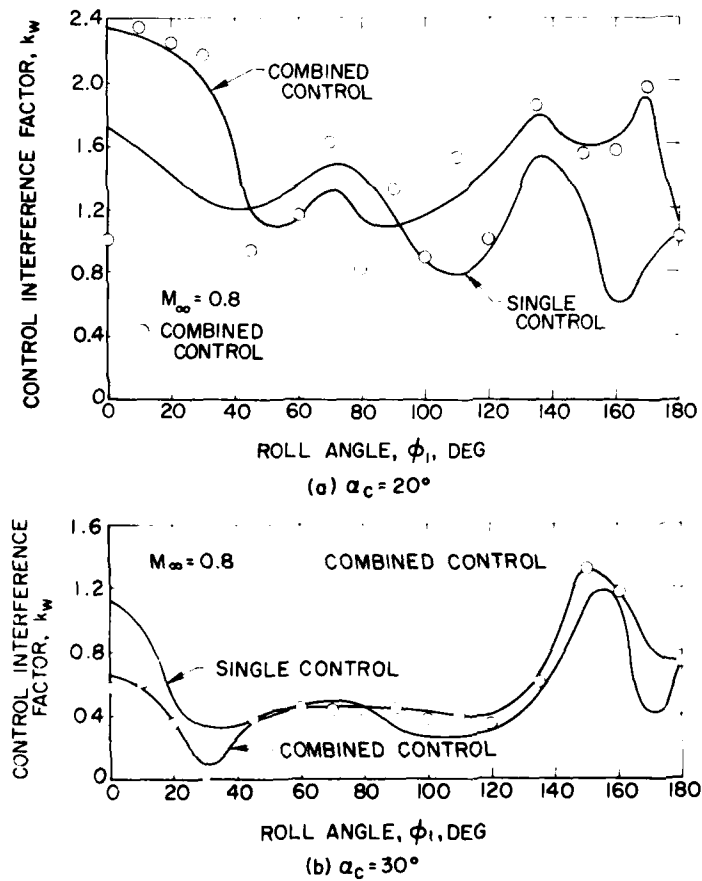


Figure 20.- Effect of roll angle on control interference factor, k_w , for combined pitch/yaw control.

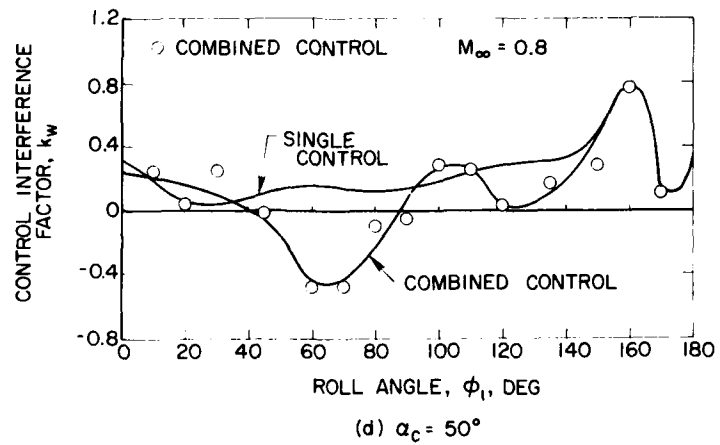
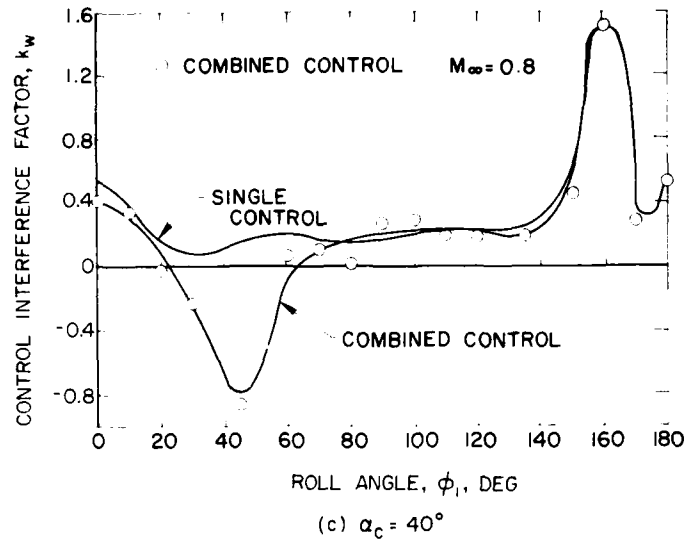


Figure 20.- Effect of roll angle on control interference factor, k_w , for combined pitch/yaw control (concluded).

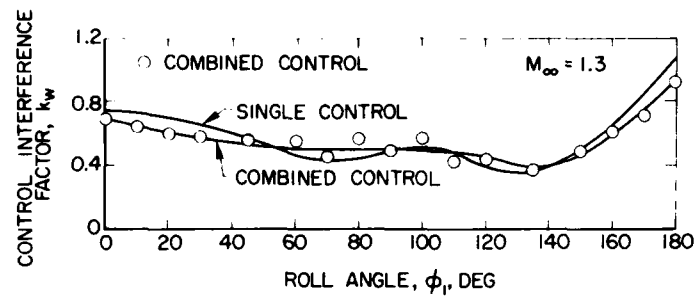
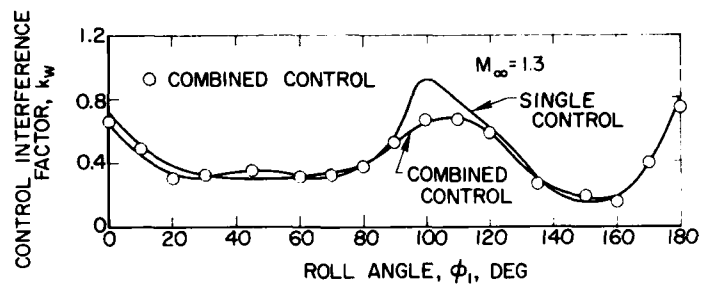
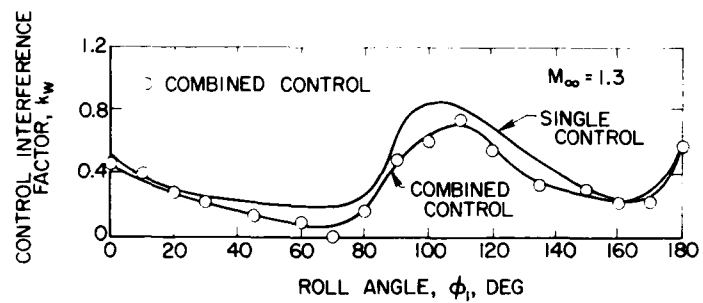
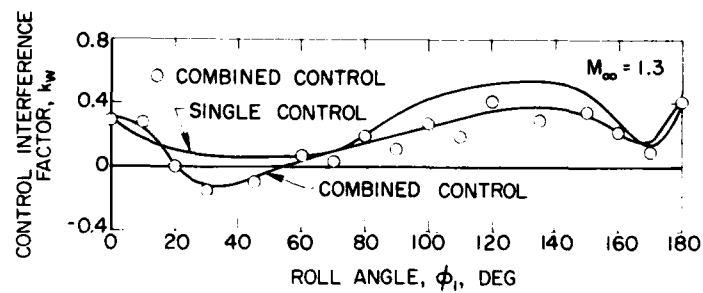
(a) $\alpha_c = 20^\circ$ (b) $\alpha_c = 30^\circ$ (c) $\alpha_c = 40^\circ$ (d) $\alpha_c = 50^\circ$

Figure 21.- Effect of roll angle on control interference factor, k_w , for combined pitch/yaw control.

ON THE EFFECT OF WING WAKE ON TAIL CHARACTERISTICS

by

K. Gersten, D. Glück

Ruhr-Universität Bochum, Germany

SUMMARY

26-1

It is not sufficient to take the local dynamic pressures into account in the calculation of control surface forces located in non-uniform flow fields because of the effects due to the velocity distribution within the wake.

A nonlinear theory has been developed to calculate lift and moment forces for airfoils in a two-dimensional flow field. The oncoming velocity distribution is approximated by a series of step functions which results in a flow field composed of a number of potential-flow fields. The potential flow fields are matched properly at several dividing streamlines where the total pressure changes discontinuously. The solution of the problem is determined by using vortex distributions on both the contour of the airfoil and the dividing streamlines. A special approach makes it possible to calculate the flow field when one of the dividing streamlines merges with the profile.

The comparison between theoretical and experimental results for the aerodynamic characteristics of a tail unit placed in the wake of a wing exhibits considerably improved agreement when the velocity gradient in the wake is taken into account in the analysis.

1. INTRODUCTION

Control surfaces and, in particular, tail units are frequently situated in non-uniform flow fields. The non-uniformities can be caused by the wake of the wing or other parts of the airplane, as well as by engine exhaust jets. These non-uniformities may have a considerable influence on the trim and the stability of the airplane. One particular case is 'super stall' which occurs on airplanes with T-tail units at high angles of attack. At a certain angle of attack the tail enters the wake of the wing. The nose-down contribution of the tail to the total moment is reduced resulting in strong destabilisation of the airplane and finally, at certain angles of attack, in positive pitching moments.

However, further increase of the angle of attack leads to stabilisation because the tail is no longer in the wake and the pitching moment becomes negative again. In this way stable trim is achieved at high angles of attack. The efficiency of the control surfaces is very small because of the wake. Therefore the return from super stall seems to be impossible.

The proper determination of the efficiency of the control surfaces in super stall is possible only when the influence of the wake on tail characteristics is considered. In practice the forces on the control surfaces located in a nonuniform flow field are determined by methods which are analogous to these used for uniform flows but taking into account the particular local dynamic pressure. If, for example, the tail is located within the wing wake, the lift of the tail that enhances the pitching moment is reduced as a result of the local dynamic pressure.

However, taking the different local dynamic pressures into account is not sufficient to determine the forces on the control surfaces. There is an additional effect due to the velocity distribution within the wake or, more generally, in any flow in which the oncoming velocity distribution has velocity gradients. This effect is the main topic of the present study. The effect becomes particularly important for super stall, since the wing drag leads to a distortion of the flow field in the wake which is very pronounced at high angles of attack. The tail unit characteristics are strongly influenced by this effect.

In the following, airfoils in a non-uniform flow field are investigated theoretically as well as experimentally. The final goal is to develop a reliable prediction method for the tail characteristics at high angles of attack (super stall). The comparison with experimental results for wing-tail combinations of W. Siegler and B. Wagner [1] shall demonstrate the applicability of the present method for calculating the tail characteristics of airplanes.

2. FLUID DYNAMIC PROBLEM

The oncoming flow to the tail consists of the wakes from wing, fuselage, engine nacelles and engine exhaust jets. The comparison with experimental results from W. Siegler and B. Wagner [1] and A. Siverstein and S. Katzoff [2] shows that this complicated wake can be simulated by a simple model. The velocity profile for the case when the tail is located within the wing wake is shown in Fig 1. The velocity distribution in the wake depends on the geometry of the airplane, the angle of attack, the Reynolds number and, therefore, on the wing drag. The calculation of the wake for these parameters is shown in the Appendix.

A two-dimensional incompressible steady inviscid flow is assumed. The problem thereby reduces to the calculation of the flow field around the profile of an airfoil in a non-uniform (and therefore rotational) stream. From the calculation of the derivatives for the pitching moment and the lift, the flow around a three-dimensional wing with any aspect ratio can be determined by using well-known methods.

3. THEORY

The continuous velocity distribution of the oncoming flow is approximated by a series of step functions (see Fig 2). Due to this approximation the flow field consists of a number of potential flow fields which must be properly connected at several dividing streamlines, where the total pressure changes discontinuously by a certain given value. The dividing streamlines which are schematically shown in Fig 2, are a priori unknown.

The solution of this problem, which is nonlinear due to the boundary conditions, is found by using vortex distributions on the contour of the airfoil and on the dividing streamlines as well.

The following unknown functions are to be calculated:

1. The vortex distribution on the profile contour.
2. The vortex distribution on the dividing streamlines.
3. The locations of the dividing streamlines.

The boundary conditions for this problem are:

1. The tangency condition at the profile contour.
2. The tangency condition at the dividing streamlines
3. The pressure condition at the dividing streamlines, i.e. equal static pressure on either side of a dividing streamline.

The boundary condition on the contour can be expressed by requiring that the velocity inside the contour must vanish. This formulation is equivalent to the classic condition which requires that the contour be a streamline. The formulation of this condition results in an integral equation of the second kind for the vorticity γ_k on the contour:

$$\gamma_k(\phi) - \frac{1}{2\pi} \int_0^{2\pi} K(\phi, \psi) \cdot \gamma_k(\psi) \cdot \left(\frac{ds}{d\psi}\right) d\psi = R(\psi) \quad (1)$$

The kernel $K(\phi, \psi)$ is a function of the profile geometry only:

$$K(\phi, \psi) = \frac{\dot{x}(\phi) \cdot (y(\phi) - y(\psi)) - \dot{y}(\phi) \cdot (x(\phi) - x(\psi))}{(x(\phi) - x(\psi))^2 + (y(\phi) - y(\psi))^2} \quad (2)$$

For $\phi = \psi$:

$$K(\phi, \psi) = \frac{1}{2} \frac{\ddot{x}(\phi) \cdot \dot{y}(\phi) - \dot{x}(\phi) \cdot \ddot{y}(\phi)}{\dot{x}(\phi)^2 + \dot{y}(\phi)^2} \quad (3)$$

$R(\phi)$ describes the induced velocity on the contour:

$$R(\phi) = \frac{\dot{x}(\phi)}{s(\phi)} \cdot (U_\infty + \sum u_i(\phi)) + \frac{\dot{y}(\phi)}{s(\phi)} \cdot \sum v_i(\phi) \quad (4)$$

u_i and v_i are the components of the induced velocity vector at one dividing streamline. These velocities can be calculated using Biot-Savart's law by integrating over the entire dividing streamlines:

$$u_i(\phi) = \frac{1}{2\pi} \int_{-\infty}^{+\infty} \frac{y(\phi) - y_i}{(x(\phi) - x_i)^2 + (y(\phi) - y_i)^2} \gamma_i \cdot ds_i \quad (5)$$

$$v_i(\phi) = \frac{1}{2\pi} \int_{-\infty}^{+\infty} \frac{x(\phi) - x_i}{(x(\phi) - x_i)^2 + (y(\phi) - y_i)^2} \gamma_i \cdot ds_i \quad (6)$$

The vortex distribution $\gamma_i(s_i)$ and the location $x(s_i)$, $y(s_i)$ of the dividing streamline is unknown and must be calculated by using the other two boundary conditions.

The boundary condition for the pressure at the dividing streamline has the form:

$$w_{mi} \cdot \gamma_i = \text{const.} \quad (7)$$

where w_{mi} is the argument of the induced velocity vector at one of the dividing streamlines. w_{mi} can be calculated from the vortex distributions both on the dividing streamlines and the contour. The components are u_{mi} and v_{mi} .

The tangency condition at the dividing streamlines has the form:

$$\frac{dy_i}{dx} = \frac{u_{mi}}{v_{mi}} \quad (8)$$

Equations (7) and (8) are integral equations. Equation (8) is nonlinear. This complicated system of nonlinear, elliptic integral equations has been solved numerically by an iteration scheme for a given airfoil profile and velocity distribution in the oncoming flow.

There is a particular problem in this procedure which requires special attention. That is the case when a dividing streamline hits the airfoil. Due to the condition that the pressure is continuous, although the total pressure is discontinuous across the dividing streamlines, there can be no ordinary stagnation point at the airfoil. It turns out that the dividing streamline touches the airfoil by approaching it tangentially. That means there will be a semi-stagnation point. In other words, on one side (lower total pressure) there will be a stagnation point, whereas on the other side (higher total pressure) there is continuous velocity without a stagnation point. A similar situation occurs at the trailing edge.

Surprisingly, this peculiar phenomenon does not complicate the numerical problem. In fact it turns out that this behavior is advantageous. The numerical results show that the effect due to the velocity gradient in the oncoming flow, which in our model is simulated by several steps, has its maximum when the dividing streamline hits the body. A very simple example is shown in Fig 3. A symmetrical airfoil at zero angle of attack is located in a flow field with a single step in the velocity distribution of the oncoming flow. It can easily be seen that there is a maximum lift effect when the dividing streamline hits the airfoil. This is not the case when the chord has the same height as the step far upstream. There is always a shift toward higher velocities. Also the lift is always orientated to the area of higher energy. This figure shows very clearly that the particular case when the dividing streamline impinges on the body, plays a keyrole for the calculation of the so-called gradient effects. Linear theories have been used to calculate this kind of flow problem. For example, Ruden [4] investigated the particular case shown in Fig 3. However, Ruden [4] was unable to calculate the special case when the dividing streamline hits the body. Only the nonlinear theory developed here would give the maximum value as shown in Fig 3.

4. EXPERIMENTAL INVESTIGATIONS

Airfoils in two-dimensional flows with non-uniform velocity distributions have been measured in the wind tunnel of the Institute of Thermo- and Fluid Dynamics of the Ruhr-University. The non-uniform velocity distribution in the oncoming flow was artificially produced by using an appropriate honeycomb screen. The location of the airfoil with respect to the maximum gradient of the velocity distribution could be varied. Pressure distributions and, hence, lift and pitching moment coefficients were determined. As an example, Fig 4 shows the variation of the lift coefficient with the position of the airfoil with respect to the "step" for various angles of attack. The lift coefficient has its maximum when the airfoil is located at the point of steepest velocity gradient. The experimental pressure distribution could also be compared with theoretical results. In Fig 5, an example is shown for the symmetrical airfoil NACA 64 A 010. At zero angle of attack, the experimental pressure distribution is compared with two theoretical curves. Curve 1 is a nonlinear theory, whereas curve 2 is the result of a linear theory after Weissinger [5,6]. This particular result corresponds to the situation when the lift coefficient achieves its maximum. The nonlinear theory shows very good results, whereas the linear theory shows large deviations from the pressure distribution. The latter may result from pure deflection of the flow field near the trailing edge of the airfoil. A nonlinear model obviously gives a very good description of the details of the flow field near the leading edge by this semi-stagnation-point flow approximation.

5. APPLICATION TO THE WING WAKE EFFECTS ON TAIL CHARACTERISTICS

The experimental results for a wing tail unit determined by W. Siegler [1] are shown in Fig 6. The pitching moment is plotted against the angle of attack. However, since nonlinear effects are dealt with here, only the difference between the pitching moment and the linear part of the pitching moment is shown. Therefore, the measurements give the deviation of the pitching moment curve from the linear theory. Two additional curves are shown in the figure. One is the theoretical curve calculated with the condition that the wake effect is taken into account only by using the local dynamic pressures. Curve 3 then gives the corresponding theoretical curve, but including the gradient effects. It is obvious that the gradient effect is very important and taking it into account gives much better agreement for the moment characteristics of a tail unit situated in the wing wake.

6. CONCLUSIONS

26-4

- a) A theory was developed to calculate the lift and moment forces for airfoils in a non-uniform flow field.
- b) An experimental investigation was carried out to measure pressure distributions and lift and pitching moment coefficients on airfoils in two-dimensional flows with non-uniform velocity distributions.
- c) Non-uniform velocity distributions in the oncoming flow have a maximum effect on the airfoil forces when the airfoil is located in the area of the steepest velocity gradient. The lift is always directed to the area of higher total energy.
- d) The point of maximum effect can be calculated a priori by the present theory without calculating neighbouring situations. The reason is the theory in this case leads to a special situation with very particular flow field properties which are known a priori. The case of maximum effect can not be treated with linear theories.
- e) The theory can also be applied to situations where the control surface is not within the wake, but in the neighbourhood of a wake or a jet; for example, an engine exhaust jet. This method can also be applied for double- and multi-slotted flaps, where the wakes of the different parts of the flap have to be taken into account. This general problem can be reduced to the problem of the flow past airfoils with nonhomogeneous oncoming flow velocities as considered in the present work.

7. REFERENCES

1. Siegler, W. and Wagner, B.: "Experimentelle Untersuchungen zum Überziehverhalten von Flugzeugen mit T-Leitwerk", ZFW 2 Heft 3, 156-165 (1978).
2. Silverstein, A., Katzoff, S. and Bullivant, W.K.: "Downwash and Wake behind plain and flapped Airfoils", NACA TR 651, 1939.
3. Silverstein, A. and Katzoff, S.: "Design Charts for Predicting Downwash Angles and Wake Characteristics behind plain and flapped Wings", NACA TR. 648, 1939.
4. Ruden, P.: "Theorie des Tragflügelprofils in der Nachbarschaft sprunghafter Gesamtdruckänderungen (Strahl- und Windschatten mit Rechteckprofil)", Jahrbuch 1939 der Deutschen Luftfahrtforschung, I 98 - I 113.
5. Weissinger, J.: "Linearisierte Profiltheorie bei ungleichförmiger Anströmung. Teil I: Unendlich dünne Profile (Wirbel und Wirbelbelegungen)". Acta Mechanica 10, 207-228 (1970)
6. Weissinger, J.: "Linearisierte Profiltheorie bei ungleichförmiger Anströmung. Teil II: Schlanke Profile ", Acta Mechanica 13, 133-134 (1972)
7. Gersten, K.: "Über die Berechnung des induzierten Geschwindigkeitsfeldes von Tragflügeln", Jb. 1957 WGL, S. 172-190 (1958) .
8. Schlichting, H. and Truckenbrodt, E.: "Aerodynamik des Flugzeuges. Band II", 2. Aufl., Springer Verlag, Berlin, 1969.
9. Truckenbrodt, E.: "Ein einfaches Verfahren zur Berechnung des Abwindes von Tragflächen", Ing.-Arch. 18 (1950), 233-238

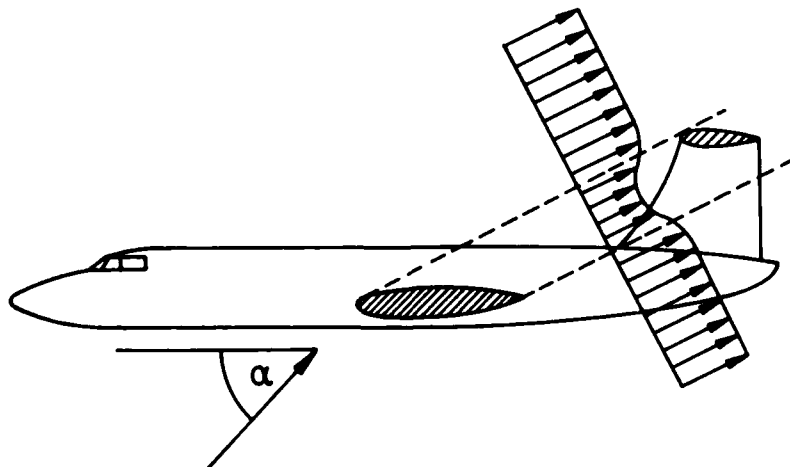


Figure 1: Wake of the Wing at High Angles of Attack

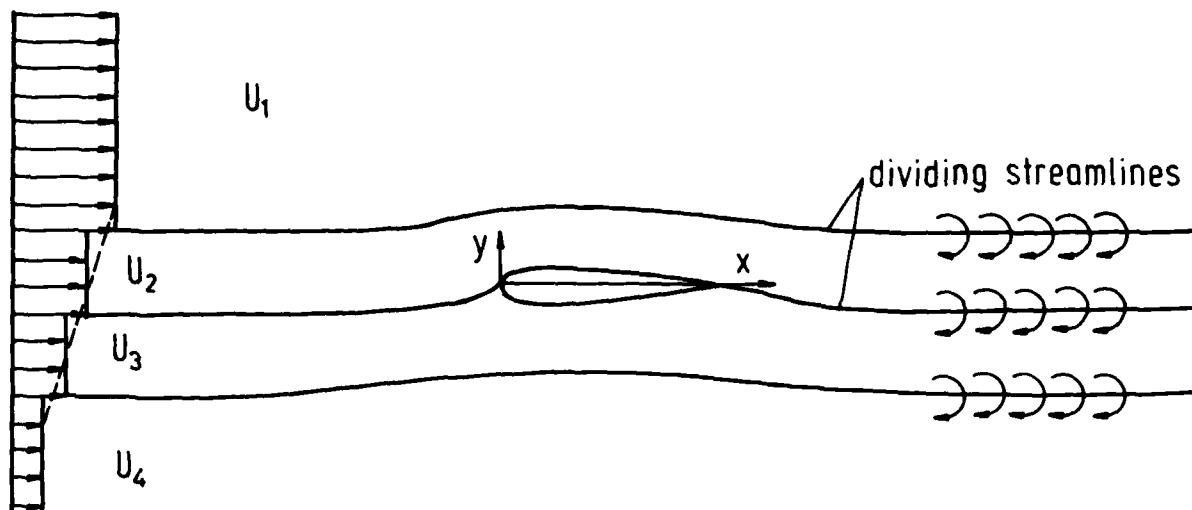


Figure 2: Airfoil in Shear Layer

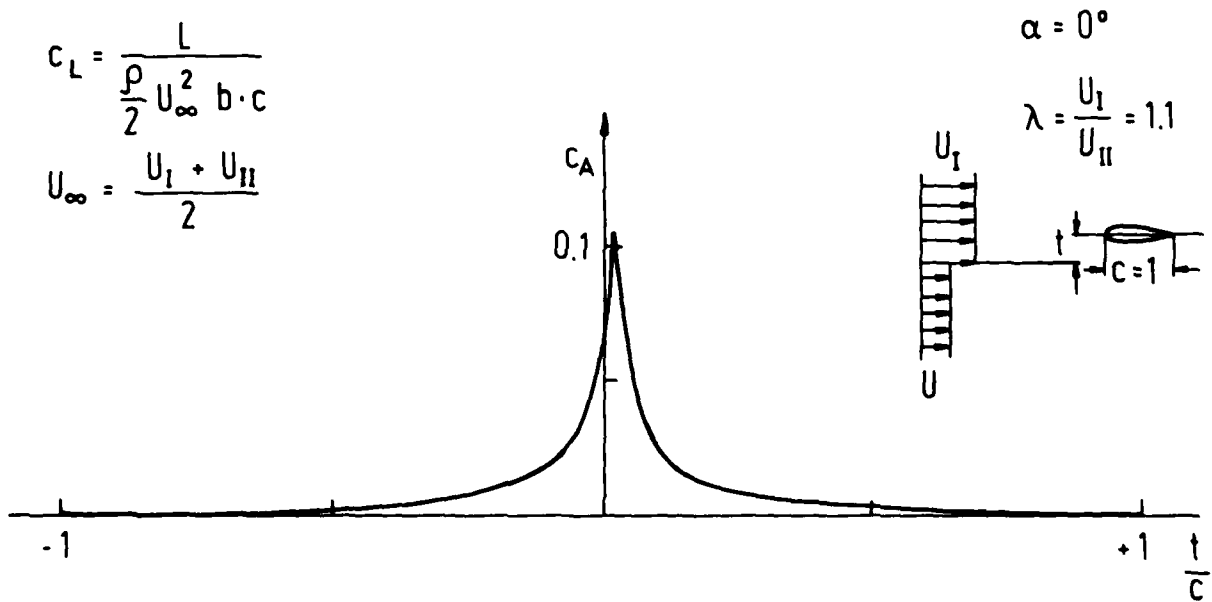
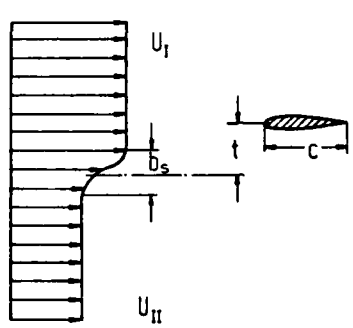
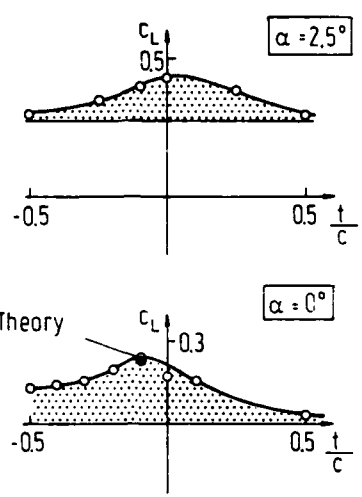


Figure 3: Symmetrical Airfoil NACA 64 A010 at Zero Angle of Attack in the Flow Field with a Single Step

26-6



$$c_L = \frac{A}{\frac{\rho}{2} bc U^2}$$

$$\lambda = \frac{U_I}{U_{II}} = 1.6$$

$$\frac{b_s}{c} = 0.5$$

Figure 4: Lift Coefficient for Different Positions of the Airfoil NACA 64A010 in the Shear Layer and at Different Angles of Attack
 U = Local Velocity

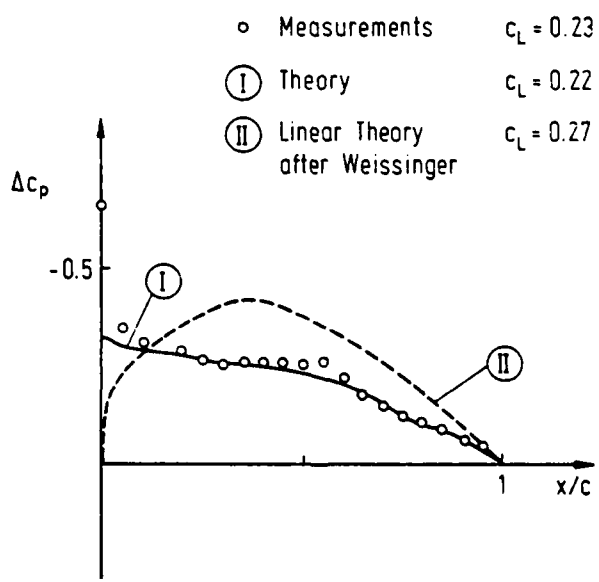


Figure 5: Comparison of Theoretical and Experimental Results for the Symmetrical Airfoil NACA 64 A010 at Zero Angle of Attack

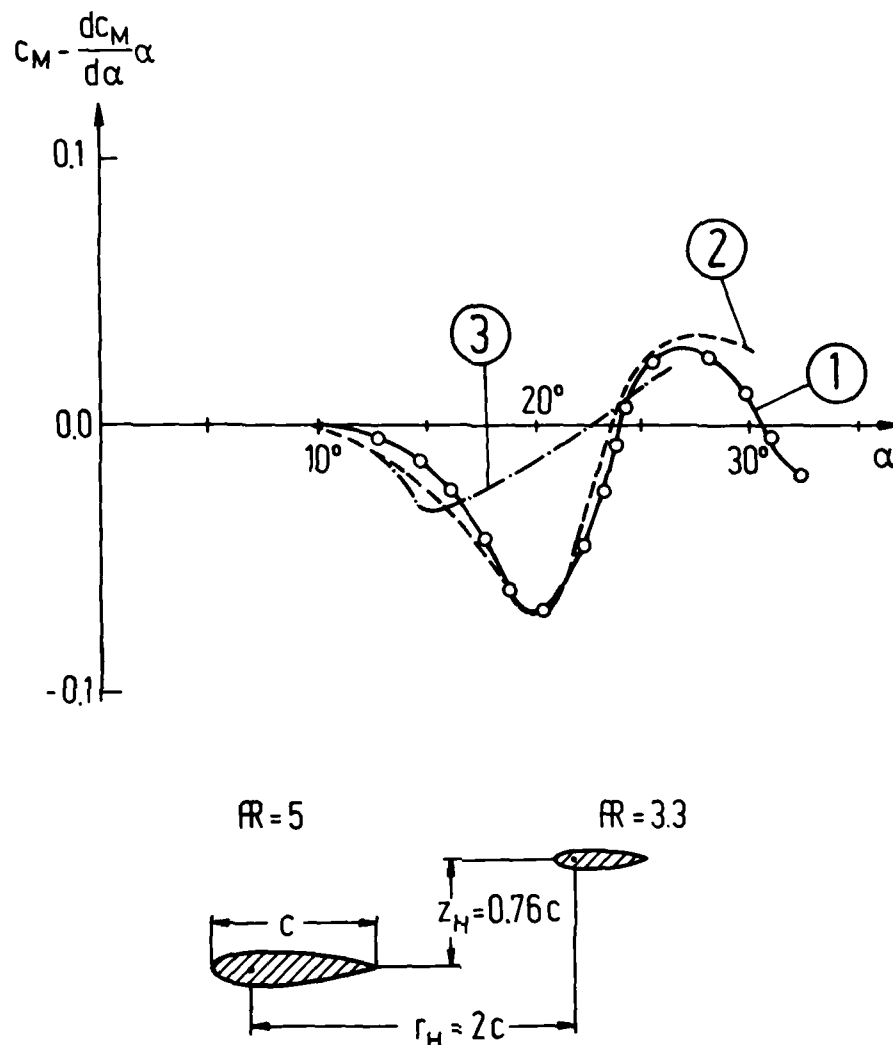


Figure 6: The Effect of Wing Wake on Tail Characteristics

- ① Measurements
- ② Theory with gradient effect
- ③ Theory without gradient effect

APPENDIX A

Calculation of the wing wake.

For a given geometry of the wing it is possible to calculate the vortex -distribution γ in the spanwise direction by one of the well-known theories, e.g. the 'extended lifting-line theory'. From this the down-wash can be determined. For distances between the tail and the wing which are greater than $2 \cdot y/c$ the downwash in the vortex sheet can be calculated from the nonlinear theory of K. Gersten [7].

$$\alpha_w = \left(1 + \frac{\xi}{|\xi|}\right) \cdot \sum_{n=1}^m a_n \gamma_n + \frac{c_L}{4\pi R} \cdot \frac{\xi}{|\xi|^3} \quad (A1)$$

The coordinate $\xi = \frac{x}{s}$ originates at the wing-nose. The coefficients a_n are tabulated in [7]. In the vicinity of the vortex sheet, the downwash can be calculated by:

$$\left(\frac{\partial \alpha_w}{\partial \zeta}\right) = \left(1 + \frac{\xi - \bar{\xi}}{|\xi - \bar{\xi}|}\right) \sum_{n=1}^m \left(\frac{\partial a_n}{\partial \zeta}\right) \gamma_n \quad (A2)$$

ζ is the dimensionless coordinate normal to the vortex sheet and $\bar{\xi}$ the dimensionless distance of the nose to the aerodynamic center. The coefficients $\left(\frac{\partial a_n}{\partial \zeta}\right)$ are tabulated in [7]. If the distance from the tail to the wing is less than $2 \cdot y/c$, the downwash should be calculated by the complete equations presented in [7].

As a first approximation the drawdown of the trailing vortex sheet can be assumed to be proportional to the distance from the trailing edge; see Schlichting and Truckenbrodt [7].

$$\zeta_1(\xi) = (\alpha + \alpha_w(\xi)) \cdot (\xi - \xi_{TE}) \quad (A3)$$

The exact calculation is described by Truckenbrodt [9].

Silverstein and Katzoff [2,3] present empirical equations for calculating the wing wake: The maximum loss of dynamic pressure in the wake occurs at the wake center and its value q_m is given by the formula:

$$\frac{q_m}{q_\infty} = \frac{2.42 \cdot c_d^{0.5}}{\frac{x}{c} + 0.3} \quad (A4)$$

with c_d as the section profile-drag coefficient.

The distribution of the dynamic pressure within the wake is given by the equation:

$$\frac{q}{q_m} = \cos^2 \left(\frac{\pi}{2} \cdot \frac{y}{b} \right) \quad (A5)$$

The half width b of the wake is given by:

$$\frac{b}{c} = 0.68 \cdot c_d^{0.5} \left(\frac{x}{c} + 0.15 \right)^{0.5} \quad (A6)$$

In the present theory it is assumed for the development of the wake behind the wing that the center line, originating from the middle of the wing, moves parallel to the trailing vortex sheet. Consequently the oncoming flow for the tail results from both the wake and the downwash induced by the wing.

INTERACTION AÉRODYNAMIQUE ENTRE UN CANARD PROCHE ET UNE VOILURE

par Yves BROCARD et Volker SCHMITT

27-1

Office National d'Etudes et de Recherches Aérospatiales (ONERA)
92320 Châtillon (France)

RESUME

Des essais relatifs à une configuration canard proche-voilure ont été effectués en subsonique dans la soufflerie pressurisée F1 qui a été récemment mise en service au centre du Fauga-Mauzac de l'ONERA. Le montage en demi-maquette à la paroi utilise comme voilure l'aile rectangulaire AFV-D à génération cylindrique qui est placée à 60° de flèche. La section parallèle à l'emplanture présente une épaisseur relative de 5 % et un grand rayon de bord d'attaque. Les plans canard sont semblables à l'aile principale en forme et en profil.

Des résultats expérimentaux sont présentés sous forme d'efforts globaux et de répartitions de pression sur l'aile principale. L'effet d'un braquage du canard et l'influence du nombre de Reynolds ont été étudiés. Des visualisations de l'écoulement pariétal en soufflerie et du champ d'écoulement en tunnel hydrodynamique sur une maquette plus petite sont utilisées pour aider à la compréhension des mécanismes de l'interaction.

Des comparaisons entre les résultats expérimentaux et des approches théoriques sont relatées. Elles montrent un accord raisonnable bien que la structure fine de l'écoulement tourbillonnaire sur ce type d'aile ne soit pas, au stade actuel, correctement prédite.

AERODYNAMIC INTERACTION ON A CLOSE-COUPLED CANARD-WING CONFIGURATION

SUMMARY

Halfmodel tests were performed on a close-coupled canard-wing configuration in the low speed, pressurized wind tunnel F1 at the new ONERA-Center Le Fauga-Mauzac. The main lifting surface is the rectangular cylindrical, wall mounted, half wing AFV-D in a 60° back sweep configuration. The chordwise wing section has a 5 % thickness ratio and a large leading-edge radius. The canard surfaces are similar in shape and section to the main wing.

Experimental results are presented in terms of longitudinal aerodynamic characteristics and pressure distribution on the main wing. The effect of canard deflexion and of Reynolds number variation were investigated.

Surface oil flow pattern on the wind tunnel model and water tunnel visualization on a smaller model are used to improve the understanding of the interaction mechanism.

Comparisons between the experimental results and theoretical predictions are presented. They show a reasonable agreement although the vortex behaviour of this type of wing is not yet fully predicted.

1 - INTRODUCTION -

27-2

Dans le cadre des études sur le comportement des ailes en flèche aux grandes incidences, l'ONERA a entrepris des travaux sur l'interaction aérodynamique entre un canard proche et une aile en flèche. Il apparaît en effet que, avec le développement des techniques de C.A.G (Contrôle actif généralisé ou CCV) et de commandes électriques, les empennages de type canard proche peuvent avantageusement être utilisés comme dispositif de contrôle [1].

Le bénéfice apporté en plaçant l'empennage horizontal en amont de la voilure est connu depuis longtemps : la force aérodynamique nécessaire pour équilibrer le moment de tangage est alors réduite et permet de réduire les efforts sur la voilure à l'inverse de ce qui se produit avec l'empennage arrière.

La formule du canard a suscité parallèlement un autre intérêt depuis que fut mis en évidence, dans les années 60, en particulier par H. Behrbohm [2], l'effet favorable sur la portance de l'interaction tourbillonnaire d'un canard très proche de la voilure : la portance de l'ensemble canard-voilure peut être plus grande que la somme des portances du canard et de la voilure essayés indépendamment; le décrochage se produit à des incidences et pour des niveaux de portance plus élevés.

En dépit d'un nombre important d'études menées ces dernières années dans divers laboratoires et dont l'orientation vers les applications pratiques est incontestable, beaucoup de questions restent posées quant au mécanisme de l'interaction canard-voilure. L'étude présente a pour objet d'améliorer cette situation. Menée aux basses vitesses, elle a pour support principal le montage à la paroi d'une aile rectangulaire à flèche élevée et à bord d'attaque relativement épais [3]. Cette dernière caractéristique conditionnant une apparition assez tardive de l'écoulement tourbillonnaire n'est pas exempte d'intérêt du point de vue des applications en raison des répercussions sur la finesse.

2 - CONDITIONS EXPERIMENTALES -

2.1 - Configurations canard-voilure -

Le montage d'essai utilise une maquette de l'aile rectangulaire AFV-D déjà décrite ("M" [3]) présentant comme le montre la figure 1 une flèche $\varphi = 60^\circ$. Cette aile non vrillée étant équipée du profil symétrique ONERA-D ($e/c = 0,105$) dans des plans normaux au bord d'attaque, l'épaisseur relative d'une section parallèle à l'emplanture est alors $a/l = 0,052$.

Les plans canard ont le même profil et la même forme en plan rectangulaire que la voilure principale, le rapport des cordes normales au bord d'attaque étant $c_c/c = 0,4$. En vue d'une étude paramétrique relative à l'influence de la géométrie des plans canard, plusieurs angles de flèche ($\varphi = 40^\circ$ et 60°) et plusieurs envergures b_c/b comprises entre 0,25 et 0,78 ont été réalisés, ceci conduisant à des rapports de surfaces S_c/S compris entre 0,085 et 0,235.

En ce qui concerne l'étude paramétrique de l'influence de la position du canard, elle a porté sur la variation des positions longitudinale x_c/l et transversale z_c/l des plans canard ainsi que sur leur braquage δ_c comme l'indique la figure 1.

L'ensemble des données géométriques relatives à l'aile et aux plans canard est résumé dans le

tableau 1. Les positions relatives des plans canard par rapport à la voilure sont consignées au tableau 2.

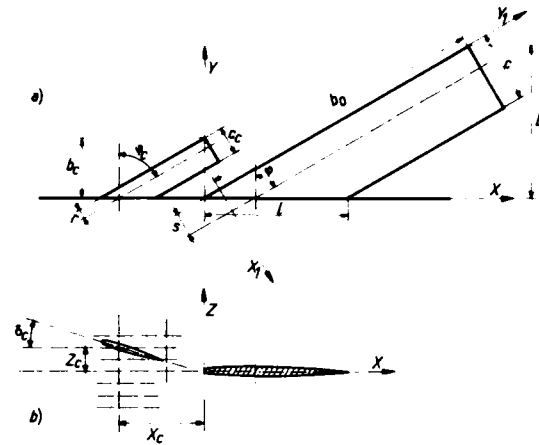


Fig. 1 - Caractéristiques géométriques du montage d'essai. a) vue en plan ; b) section à l'emplanture.

Tableau I

Caractéristiques géométriques du montage d'essai

a) aile ($l = 0,400$ m et $s = 0,075$ m - fig. 1)

b) plans canard ($r = 0,03$ m - fig. 1)

a	φ (°)	λ	b (m)	c (m)	S (m ²)
AFV-D	60	2,69	0,430	0,20	0,1373

b	Conf	φ_c	λ	b_c/b	c_c/c	S_c/S
	C1	40°	6,94	0,778	0,40	0,235
	C2		5,68	0,623		0,184
	C3		3,79	0,390		0,108
	C4	60°	3,20	0,500		0,210
	C5		2,69	0,400		0,160
	C6		1,98	0,250		0,085

Tableau II

Positions des plans canard

Conf	x_c/l	z_c/l	δ_c
P01	-0,60	0,24	120°
P02		0,16	
P03		0,08	
P04		0	
P05		-0,08	
P06		-0,16	
P07		-0,24	
P11	-0,25	0,24	
P12		0,16	
P13		0,08	

27-4

calcul théorique avec et sans prise en compte du supplément de portance dû au tourbillon obtenu par la méthode de R.J. Margason et J.E Lamar [8]. La portance potentielle est calculée au moyen d'une méthode de singularités tandis que la portance tourbillonnaire est évaluée par l'analogie à la succion de E.C.Polhamus [9]. Cette méthode très simple d'emploi, est couramment utilisée pour évaluer les performances globales d'ailes à forte flèche avec formation de tourbillon de bord d'attaque [10], [11]. Elle permet aussi l'évaluation des performances de configurations avec canard proche. Les limitations du programme de calcul utilisé viennent de l'assimilation des surfaces portantes à des plaques planes sans épaisseur et donc à bord d'attaque aigu et des conditions imposées pour le recollement sur l'aile de la nappe tourbillonnaire issue du bord d'attaque. L'analogie à la succion n'a en effet plus de fondement, si cette dernière condition n'est pas satisfaite.

Pour notre cas, l'aile essayée ayant un bord d'attaque épais, la première condition n'est pas respectée. La succion n'est pas entièrement transformée en portance tourbillonnaire ce qui explique que la courbe théorique est distincte du résultat expérimental tout en lui restant assez proche et ce jusque vers une incidence de 20°.

Bien que l'analogie à la succion ne soit pas entièrement applicable à ce type de profil il est possible en fait de reconstituer à partir des valeurs mesurées la succion théorique calculée par la méthode potentielle [7]. La valeur expérimentale de la succion effective est obtenue par

$$C_{s_{exp}} = - \frac{(C_A - C_{A_0} \cos \alpha)}{\cos \phi}$$

C_A étant la force tangentielle et C_{A_0} sa valeur à incidence nulle dont la soustraction permet de tenir compte de la traînée de frottement.

Si la succion était intégralement transformée en portance ce terme devrait être nul comme cela se produit lorsque le bord d'attaque est aigu.

En ajoutant la valeur de la succion non transformée en portance à la valeur de la portance tourbillonnaire normale au plan de l'aile on reconstitue la succion théorique totale.

La portance tourbillonnaire est évaluée en effectuant la différence entre la portance normale expérimentale et la portance potentielle théorique comme dans [7] : $C_{N_t} = C_{N_{exp}} - C_{N_{pot}}$.

Le résultat de cette addition algébrique est comparé à la succion théorique sur la figure 4. L'accord est excellent jusqu'à l'incidence de 20° où les courbes s'écartent sans doute par suite du non recollement de la nappe tourbillonnaire. L'apparition à $\alpha = 5^\circ$ du tourbillon est très nettement marquée sur la courbe de portance tourbillonnaire C_{N_t} .

On peut remarquer enfin que le comportement tourbillonnaire de cette aile présente un aspect intéressant pour certaines applications dû à l'apparition tardive du décollement de bord d'attaque. En effet si le tourbillon apporte un gain de portance aux grandes incidences augmentant ainsi les qualités de manoeuvrabilité des avions équipés de voilures à forte flèche, il augmente aussi considérablement la traînée par rapport à celle de l'écoulement potentiel. La finesse C_z/C_x diminue beaucoup quand l'écoulement devient tourbillonnaire. L'apparition retardée du tourbillon permet donc de conserver une finesse maximale aux faibles incidences du vol de croisière tout en gardant aux grandes incidences un supplément de portance appréciable.

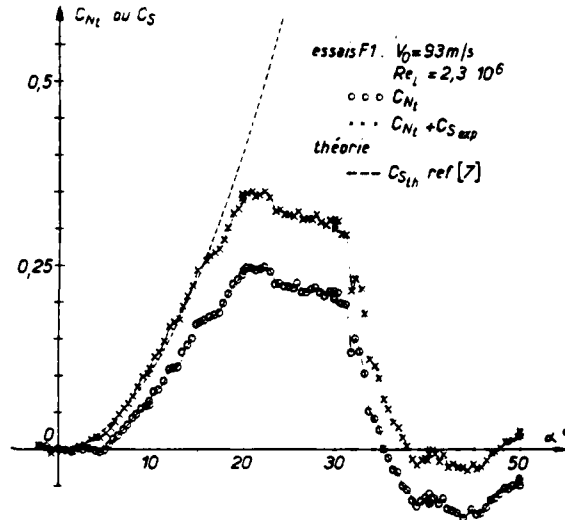


Fig. 4 - Force normale tourbillonnaire et succion de l'aile seule.

3.2 - Interaction due au canard proche -

Sur la figure 5 a été portée la courbe de portance de l'aile en présence du canard C5 dans la position P03. Ce résultat est typique de ceux obtenus pour les différentes configurations et permet de dégager les effets principaux de l'interaction.

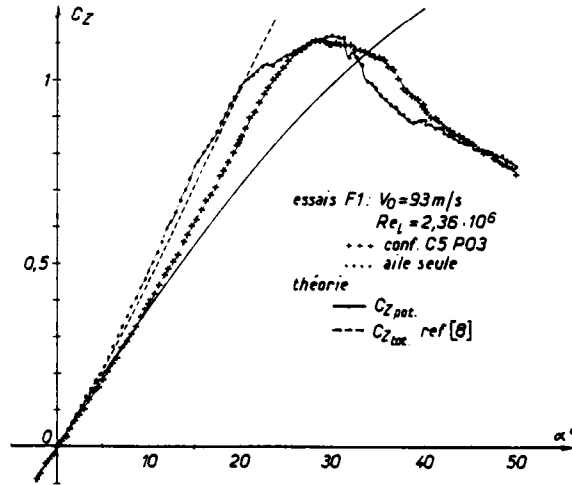


Fig. 5 - Portance de l'aile en configuration canard.

Aux faibles incidences, la déflexion de l'écoulement créée par le canard diminue sensiblement la pente de la courbe $C_z(\alpha)$. Celle-ci reste quasi-linéaire jusqu'à l'incidence de 5°. Le calcul en écoulement potentiel prévoit bien cette diminution de la portance.

L'incidence d'apparition de l'écoulement décollé tourbillonnaire n'est pratiquement pas influencée par la présence du canard. La portance de l'aile reste toujours inférieure à celle de l'aile seule mais on observe que la dégradation de la portance tourbillonnaire qui se produisait dès $\alpha = 20^\circ$ pour l'aile seule ne se fait sentir ici que vers $\alpha = 29^\circ$ (figure 6). La théorie prévoit assez bien la diminution de la succion et par conséquent la diminution de l'apport du tourbillon à la portance. Le décrochage a lieu dans les

deux cas pour des incidences (29 et 30°) et des valeurs de la portance (1.10 et 1.12) très voisines. On a observé des configurations pour lesquelles le décrochage se produit pour des valeurs du Cz plus grandes que pour l'aile seule ce qui est un résultat assez classique ([10], [12]).

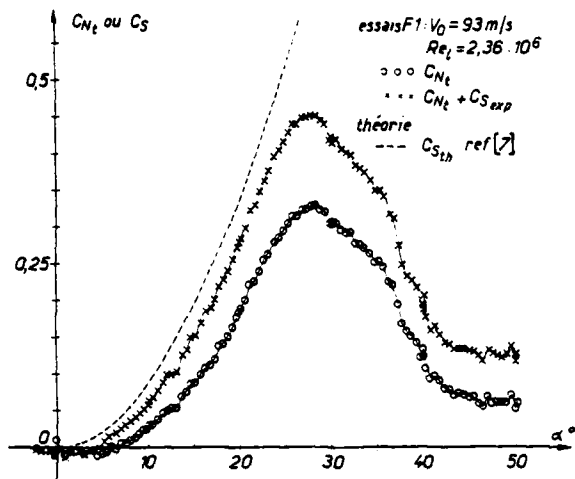


Fig. 6 - Force normale tourbillonnaire et suction en configuration canard CSPO3.

La comparaison des mesures de pression sur la voilure pour des incidences de 19° et 28° confirme ces résultats (figures 7 et 8).

A ces incidences le tourbillon de bord d'attaque est parfaitement développé ; sa présence est dénotée par la forme en cloche, caractéristique de ce type d'écoulement, le lieu de dépression maximale étant au droit du noyau.

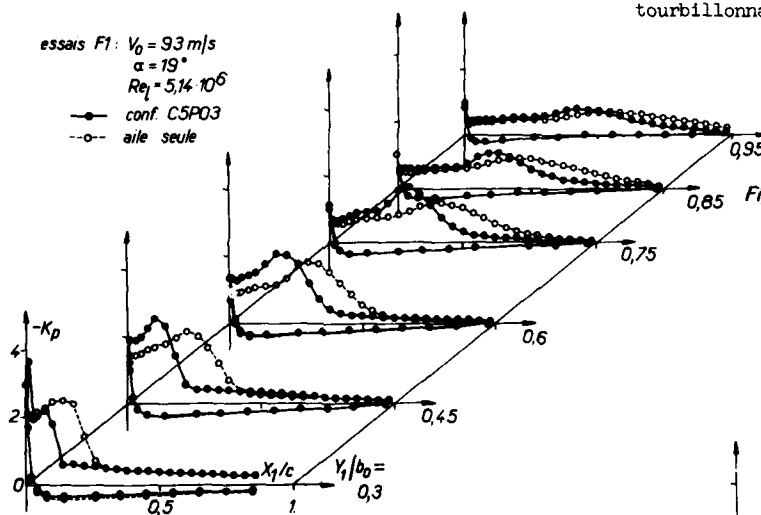


Fig. 8 - Répartitions de pression avec et sans canard.

D'une manière générale, on observe que la trace du noyau du tourbillon est plus proche du bord d'attaque en présence du canard, les pics de K_p sont plus élevés mais intéressent une zone moins étendue suivant la corde, le tourbillon se maintient plus longtemps en envergure ce qui est particulièrement sensible à 28° d'incidence dans les sections 5 et 6.

Ces observations montrent que le tourbillon qui se développe au bord d'attaque de l'aile est plus proche de la surface de l'aile. Sa désorganisation et sa séparation du plan de l'aile se produisent donc moins rapidement.

Des visualisations des lignes de courant pariétales mettent bien en évidence ces résultats. Les clichés dans le cas de l'aile seule et de l'aile avec le canard C4 dans la position P 12 à une incidence de 28° sont présentés, figure 9.

La trace du noyau tourbillonnaire peut être assimilée à la ligne des points d'inflexion des lignes de courant pariétales. La zone balayée par le tourbillon est nettement visible ainsi que l'angle γ entre les lignes de courant et la trace du noyau dont la valeur plus élevée indique bien le rapprochement du noyau à la surface.

Ces clichés donnent aussi des renseignements sur l'écoulement autour du canard. Celui-ci étant placé dans un courant défléchi vers le haut par le bord d'attaque de l'aile se trouve ainsi dans un champ où l'incidence est localement plus grande. Le tourbillon du canard est par conséquent à un stade de développement plus avancé que ne l'est celui de l'aile seule. La trace du noyau est plus reculée, la zone balayée très large. Par contre l'angle γ est assez grand montrant que le tourbillon reste très proche de la surface. Ceci peut s'expliquer par la déflexion, à l'extrados de l'aile principale, de l'écoulement qui tend à suivre le plan de l'aile en entraînant le sillage tourbillonnaire du canard.

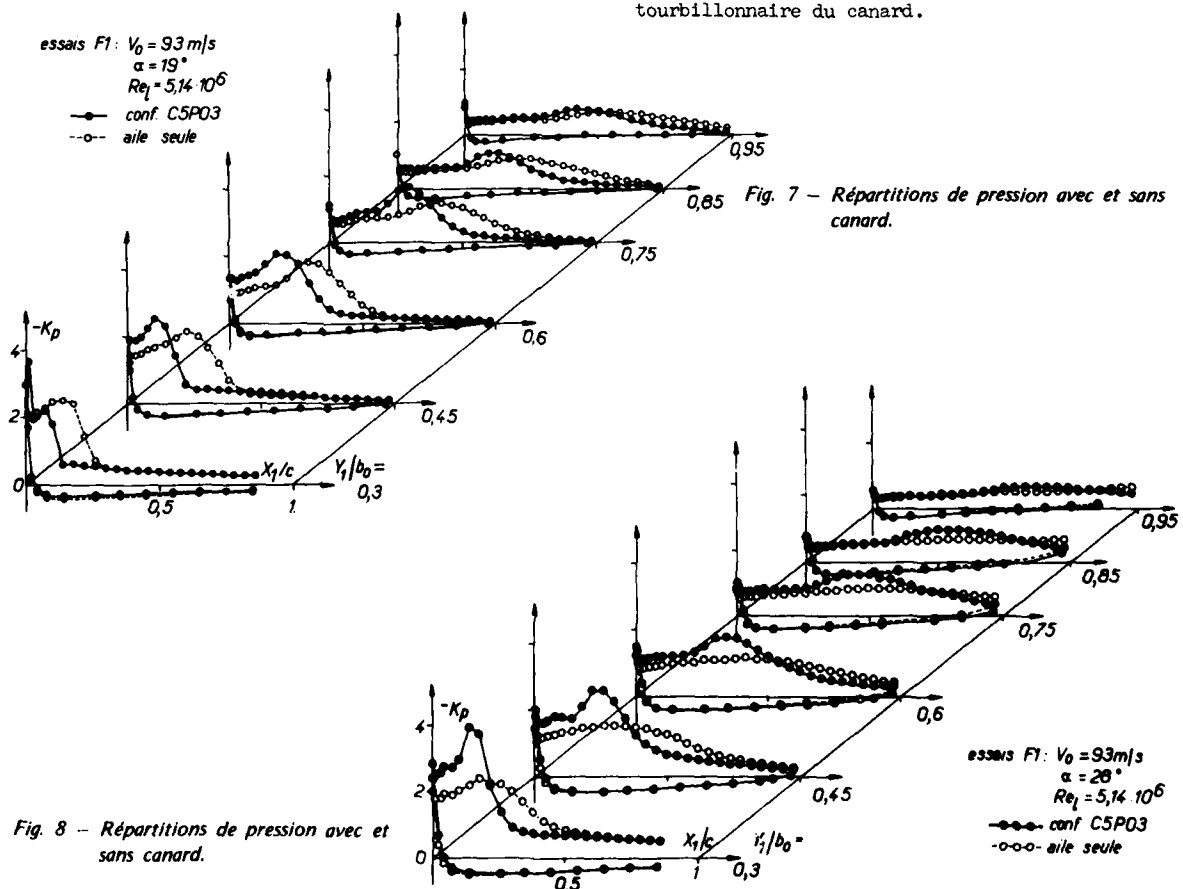


Fig. 7 - Répartitions de pression avec et sans canard.

27-6

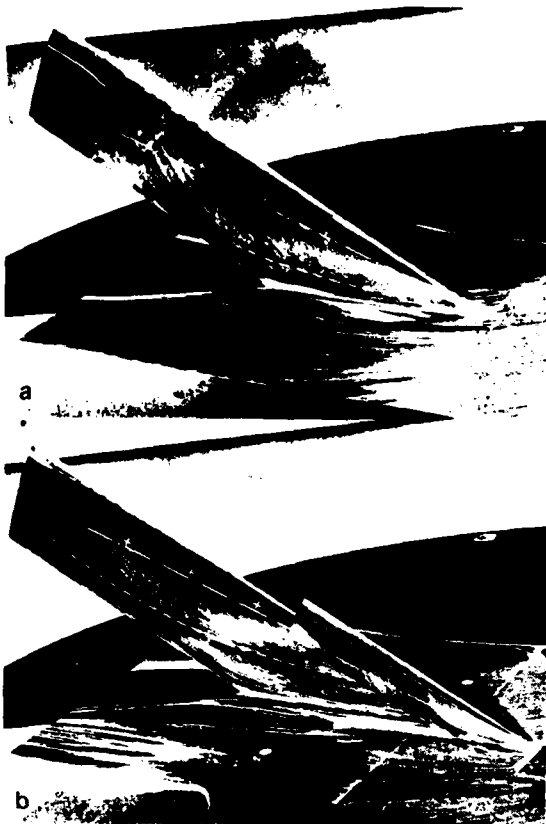


Fig. 9 - Visualisations de l'écoulement pariétal.
a) aile seule,
b) en configuration canard C4P12.



a



b

Fig. 10 - Visualisations au tunnel hydrodynamique.
a) aile seule,
b) en configuration canard C5P12.

Notons encore que si le canard est géométriquement semblable à l'aile, le nombre de Reynolds rapporté à l'une de ses dimensions caractéristiques est 2,5 fois plus petit que pour l'aile. On verra que l'influence importante du Reynolds doit être prise en compte lors de l'analyse de l'écoulement sur le canard.

Enfin des visualisations spatiales au moyen d'émissions colorées sur une plus petite maquette installée dans le tunnel hydrodynamique de l'ONERA (figure 10) corroborent ces observations. Le canard C5 est placé ici dans la position P 12, l'incidence est de 24°.

Le déplacement de l'axe tourbillonnaire sur la voilure est bien celui que l'on attendait. Une information supplémentaire est donnée par la visualisation du point d'éclatement du noyau que la présence du canard tend à retarder. L'éclatement du tourbillon du canard se produit seulement à son bord de fuite.

3.3 - Influence du braquage du canard -

La position en envergure et en hauteur du sillage issu du canard par rapport à l'aile et son intensité tourbillonnaire ont une grande importance sur les caractéristiques du tourbillon propre à l'aile principale.

Des essais ont été effectués pour différentes positions, envergures et flèches du canard. Ils sont actuellement en cours d'exploitation mais on peut dire d'ores et déjà que des effets importants sont constatés sur la position et l'intensité du pic de dépression sur l'aile.

Cependant, si le gain en portance tourbillonnaire dû à l'interaction du canard est parfois important, il n'arrive généralement pas à compenser la perte de portance potentielle observée sur l'aile.

Un autre moyen de modifier les caractéristiques du sillage du canard consiste à braquer le canard par rapport à l'aile, comme s'il s'agissait d'un moyen de contrôle.

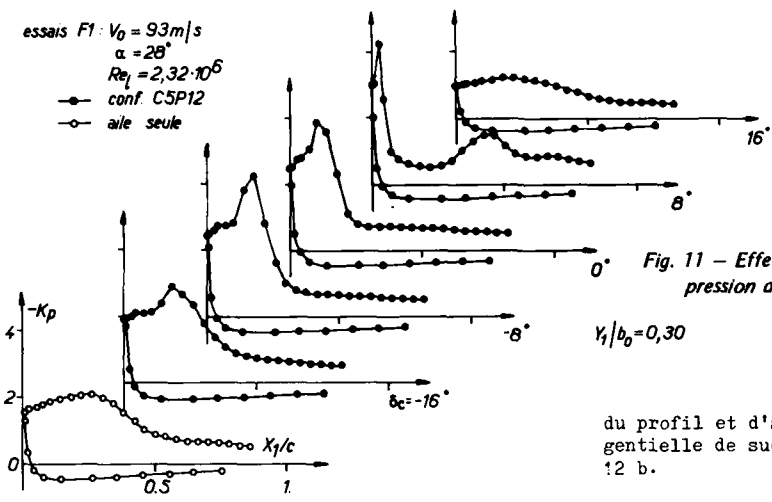


Fig. 11 - Effet du braquage du canard sur la répartition de pression dans la première section de l'aile.

$X_1/b_0 = 0,30$

A titre d'exemple est présentée sur la figure 11 la répartition de pression dans la première section de l'aile, à 28° d'incidence, pour différents braquages du canard de -16° à $+16^\circ$. Le cas de l'aile seule est présenté comme référence. Il correspond sensiblement au cas d'un canard flottant se plaçant dans le lit du vent, c'est-à-dire avec un braquage fortement négatif.

Lorsque, à partir de là, on augmente la valeur du braquage, le tourbillon issu du bord d'attaque du canard s'intensifie et au passage sur l'aile, se rapproche de la surface. On observe alors un rapprochement de la trace du tourbillon de l'aile vers le bord d'attaque et une augmentation de l'intensité du pic de dépression.

Pour un braquage de $+8^\circ$, un autre phénomène se produit, principalement dû à la géométrie de la configuration. En effet, le canard C5 à 60° de flèche, dans la position P12, est très proche de l'aile et pour un braquage de l'ordre de 8° son extrémité vient pratiquement en contact avec le bord d'attaque de l'aile en amont de la première section. Le tourbillon de l'aile ne prend alors naissance qu'au-delà de l'extrémité du canard. La seconde dépression observée vers $x/c = 0,45$ semble être la trace du passage du tourbillon de bord de fuite du canard qui est contrarotatif par rapport au tourbillon de bord d'attaque.

Pour des valeurs du braquage plus élevées, la zone de dépression peu intense et assez étalée est en fait la trace du tourbillon d'apex du canard que les décollements de bord d'attaque de l'aile viennent alimenter.

La force normale locale, obtenue par intégration de la répartition de pression dans la première section (fig. 12a) rend compte des effets du déplacement du tourbillon. On observe en partant de $\delta_c = -20^\circ$ une augmentation de la force normale jusqu'à un maximum pour $\delta_c = -8^\circ$. En effet, si l'intensité du pic de dépression augmente la surface de l'aile intéressée par cette dépression diminue et ces effets se compensent. On assiste ensuite à une diminution de la force normale. Ces tendances sont semblables pour toutes les sections, ce qui fait que l'évolution de la force normale totale a la même allure (fig. 12a). On peut remarquer aussi sur ces courbes l'effet sur l'aile, vers $\delta_c = +4^\circ$ et $+8^\circ$, du tourbillon issu du bord de fuite du canard.

Le rapprochement de la trace du tourbillon vers le bord d'attaque a pour effet aussi de concentrer la zone de dépression en amont du maître-couple

du profil et d'augmenter d'autant la force tangentielle de succion comme le montre la figure 12 b.

On observe donc que des possibilités considérables existent quant au contrôle de l'écoulement sur l'aile par braquage du canard mais que les écoulements rencontrés sont complexes et demandent à être étudiés avec soin.

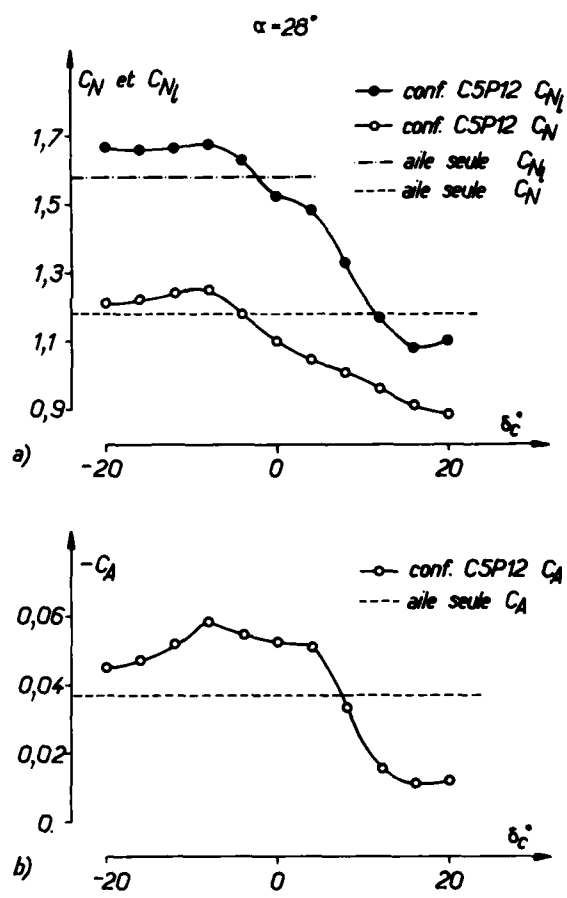


Fig. 12 - Effet du braquage du canard sur :
 a) les forces normales globale et locale,
 b) la force tangentielle globale.

3.4 - Influence du nombre de Reynolds -

L'importance des effets du nombre de Reynolds sur l'écoulement autour d'une telle aile a déjà été analysée [5]. Rappelons que les effets les plus marquants sont l'augmentation de l'incidence d'apparition du régime tourbillonnaire et le déplacement en envergure, le long du bord d'attaque

27-7

27-8

de l'origine du tourbillon lorsque le Reynolds augmente. Ces phénomènes, observés tout d'abord sur l'aile seule, existent aussi pour les configurations avec canards.

Des essais ont donc été faits à trois nombres de Reynolds $Re_1 = 2,4 \cdot 10^6$, $5,1 \cdot 10^6$ et $6,7 \cdot 10^6$ en faisant varier la vitesse et la pression génératrice. Pour les essais aux deux nombres de Reynolds les plus élevés, les mesures des efforts globaux étaient limitées à une incidence de $\alpha = 20^\circ$. Les différences entre les comportements aux deux plus grands nombres de Reynolds sont insignifiantes par rapport aux effets du passage du nombre de Reynolds le plus bas au nombre de Reynolds intermédiaire ($2,3$ à $5,1 \cdot 10^6$).

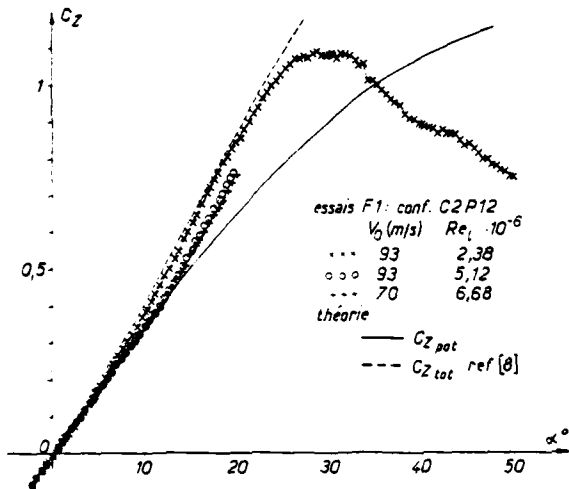


Fig.13 - Influence du nombre de Reynolds sur la portance en configuration canard.

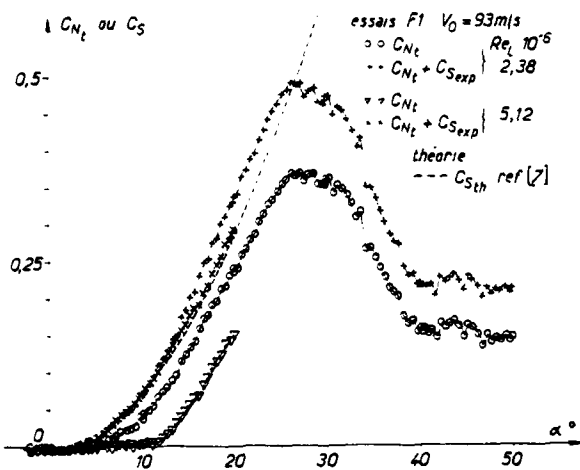
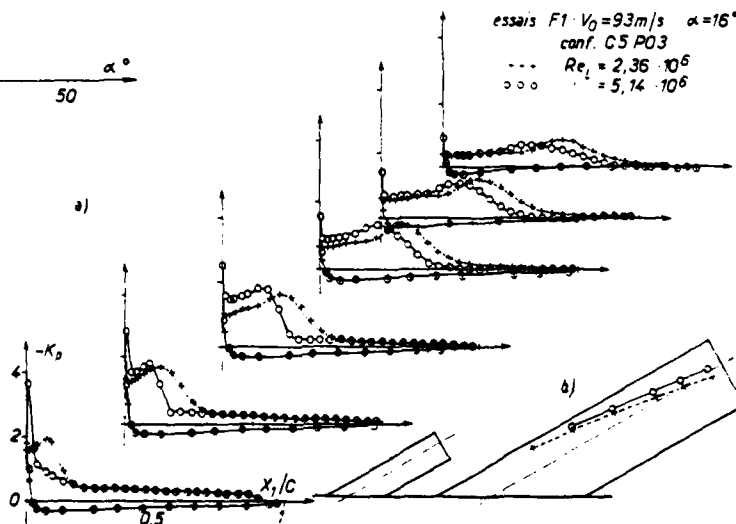


Fig.14 - Influence du nombre de Reynolds sur la force normale tourbillonnaire et la succion en configuration canard C2P12.

Fig. 15 - Influence du nombre de Reynolds en configuration canard.

a) sur les répartitions de pression,
 b) sur la position de l'axe tourbillonnaire projeté dans le plan de l'aile.



L'augmentation de l'incidence d'apparition du tourbillon est très visible sur les courbes de portance (figure 13) : si le tourbillon existe dès $\alpha = 5^\circ$ à $Re_1 = 2,4 \cdot 10^6$ il faut attendre $\alpha = 12^\circ$ aux nombres de Reynolds élevés pour voir les courbes de portance expérimentales se détacher de la courbe Cz potentiel. Dans ces conditions le tourbillon n'intéresse que l'extrémité de l'aile. La répercussion au niveau de la portance tourbillonnaire est mise en évidence figure 14.

Lorsque l'incidence augmente, le lieu de naissance remonte vers l'apex pour s'y fixer à partir de 19° . Les répartitions de pression à 16° pour deux nombres de Reynolds présentées figure 15 montrent bien que le point de naissance, en amont de la première section de mesure au faible nombre de Reynolds, est situé entre les sections 1 et 2 au fort nombre de Reynolds.

Comme il a été indiqué au sujet de l'aile seule, la naissance tardive du tourbillon présente l'intérêt d'augmenter la finesse à faible incidence. Ce retard peut être modifié soit en changeant le rayon de bord d'attaque, soit en faisant varier le nombre de Reynolds. La figure 16 montre bien cet effet et le gain de finesse important pour un Cz donné lorsque le nombre de Reynolds augmente.

On a porté sur cette figure les courbes $Cz = f(Cz/Cx)$ théoriques obtenues par la méthode de calcul déjà citée. La traînée de frottement a été prise en compte en ajoutant à la traînée théorique en fluide parfait la traînée expérimentale à portance nulle. La finesse expérimentale suit la courbe théorique potentielle aux faibles incidences puis s'en détache, lorsque le tourbillon apparaît, pour aller rejoindre la courbe théorique avec tourbillon. Ce détachement est très brusque à faible nombre de Reynolds car le tourbillon, lorsqu'il apparaît, naît directement à l'apex et intéresse alors toute l'aile tandis que, à fort nombre de Reynolds il naît tout d'abord en extrémité d'aile puis remonte vers l'apex lorsque l'incidence augmente. Dans ce cas, dans toute une plage d'incidence, le tourbillon n'intéresse qu'une faible partie de la surface de l'aile, l'écoulement dans la zone située entre l'emplanture et l'origine du tourbillon étant non décollé. La courbe expérimentale à fort nombre de Reynolds se détache ainsi plus progressivement de la courbe théorique potentielle.

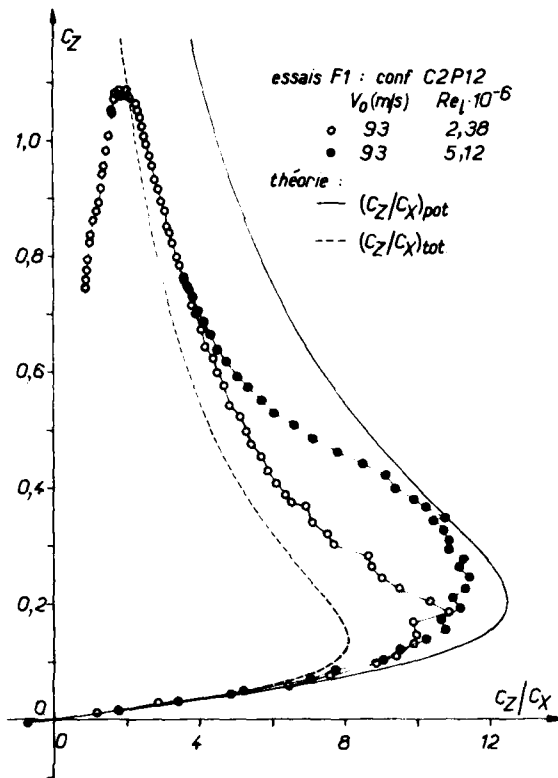


Fig. 16 - Influence du nombre de Reynolds sur la finesse en configuration canard.

4 - APPROCHE THEORIQUE -

Il a été montré dans ce qui précède qu'une méthode de singularités associée à l'analogie à la succion de E.C. Polhamus permet la prévision des performances globales des configurations canard-proche aile même en présence des écoulements tourbillonnaires. En revanche, elle est inadaptée à une description fine de l'écoulement. En vue de cet objectif, l'application d'une méthode originale, actuellement en cours de développement à l'ONERA par C. Rehbach [13] [14] au cas d'une configuration avec canard a donc été tentée. L'originalité de cette méthode instationnaire réside dans une discrétisation ponctuelle des nappes tourbillonnaires. Ainsi, des particules fluides chargées d'un vecteur tourbillon peuvent être émises au bord d'attaque, au bord latéral et au bord de fuite. Elles sont suivies dans leur mouvement après un démarrage brusque de l'écoulement par résolution dans les variables de Lagrange d'un système intégral-différentiel constitué par l'identité de Green et l'équation de Helmholtz. Cette méthode présente l'avantage de ne pas nécessiter de solution initiale et évite donc de préjuger de la forme et de la position des nappes. Par contre, le calcul d'un écoulement stationnaire requiert un nombre assez grand de pas de calcul avant que la solution converge vers un état stationnaire. La méthode est limitée actuellement aux cas d'écoulements incompressibles non visqueux. Les surfaces portantes sont assimilées à des surfaces de discontinuité de vitesse sans épaisseur.

Son application a donné des résultats encourageants dans le cas de l'aile seule avec décollements au bord d'attaque [3]. L'enroulement de la nappe est satisfaisant et se compare bien aux visualisations au tunnel hydrodynamique (fig. 17). Le calcul en présence d'un canard n'est pas actuellement possible avec émissions de particules au bord d'attaque. Par contre, le calcul

avec émissions seulement au bord de fuite et au bord latéral donne des résultats prometteurs. A titre d'exemple, est présenté figure 18 l'aspect des nappes après trente pas en temps pour une incidence $\alpha = 12^\circ$. On observe en particulier

27-9

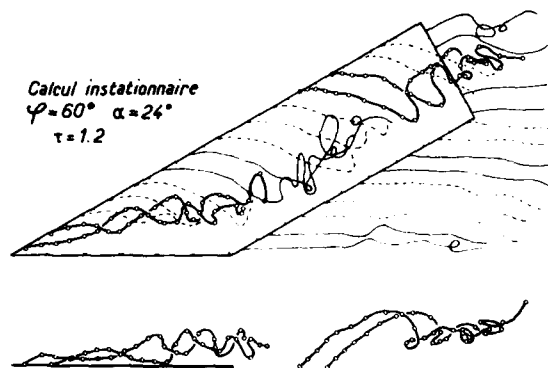
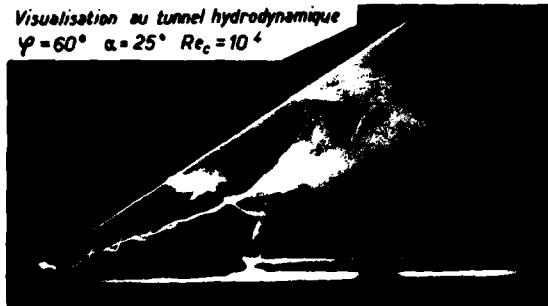


Fig. 17 - Lignes d'émission.

Écoulement décollé au bord d'attaque.

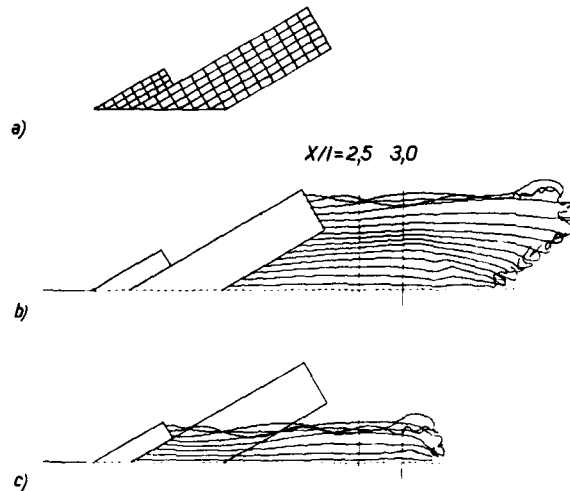


Fig. 18 - Lignes d'émission après trente pas en temps.

Écoulement non décollé au bord d'attaque ($\alpha = 12^\circ$)

- a) maillage du canard et de la voilure
- b) aspect de la nappe issue de l'aile
- c) aspect de la nappe issue du canard.

Des coupes dans deux plans transversaux situés à $X/l = 2,5$ et $3,0$ montrent la position relative des deux nappes (fig. 19). La nappe issue de l'aile à incidence égale pour un calcul en configuration aile seule est représentée en pointillé. La déflexion de l'écoulement sur l'aile provoquée par le canard apparaît nettement. Elle se traduit par la diminution de pente à l'origine constatée sur les courbes de portance. On peut noter aussi

27-10

que cette déflexion n'affecte que la partie interne de la nappe qui est située directement en dessous de la nappe issue du canard.

Calcul avec canard

- nappe issue du canard
- nappe issue de l'aile

Calcul aile seule

- nappe issue de l'aile

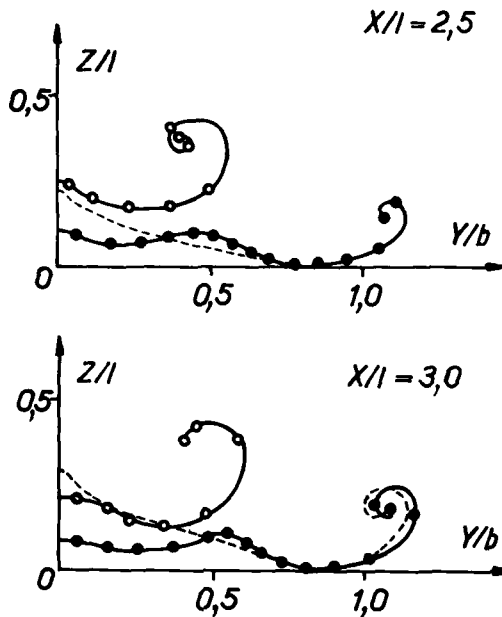
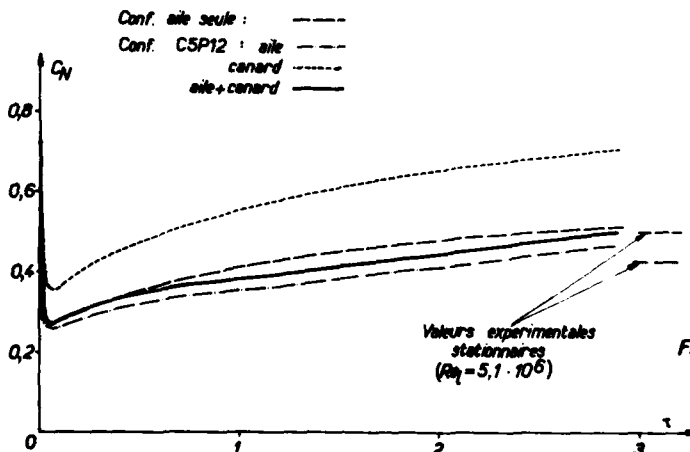


Fig. 19 - Influence du canard sur la nappe issue de l'aile ($\alpha = 12^\circ$).

L'évolution de la force normale résultant de ce calcul, en fonction du temps adimensionné τ (pour $\tau = 1$ une particule se déplaçant avec la vitesse de référence V_0 parcourt une corde de référence l), montre bien une tendance à la convergence vers un état stationnaire (fig. 20).

Dans le cas de l'aile seule le résultat tend bien vers la valeur expérimentale à $\alpha = 12^\circ$ et à fort nombre de Reynolds où l'écoulement n'est pas encore décollé au bord d'attaque. L'accord est légèrement moins bon pour la configuration avec canard.



5 - CONCLUSION -

Les essais en soufflerie sur une configuration d'aile en flèche ont montré des effets importants, tant sur les efforts globaux que sur les répartitions de pression, dus à la présence d'un plan canard proche.

La perte de portance potentielle par rapport au cas de l'aile seule provoquée par la déflexion de l'écoulement par le canard peut être évaluée par une méthode de singularités.

La portance tourbillonnaire que l'analogie à la succion permet d'évaluer évolue également plus lentement mais l'on observe, en configuration canard, un net retard à la désorganisation du tourbillon de l'aile.

Les répartitions de pression mesurées sur l'aile ainsi que les visualisations pariétales montrent que la présence du canard retarde, à incidence donnée, le développement du tourbillon. Son noyau se trouve rapproché du bord d'attaque et du plan de l'aile.

La variation du braquage du canard a montré l'importance des caractéristiques du sillage issu du canard sur le comportement de l'aile principale, et les possibilités offertes par les canards proches comme moyen de contrôle de l'écoulement sur l'aile.

Comme pour l'aile seule, l'influence du nombre de Reynolds étudiée dans le domaine $2,4 \cdot 10^6$ à $6,7 \cdot 10^6$ est importante quant à l'incidence d'apparition de l'écoulement tourbillonnaire. Ainsi, à grand nombre de Reynolds une notable plage d'incidence est couverte sans décollements au bord d'attaque, ce qui conduit à des valeurs élevées de la finesse.

La recherche d'une méthode numérique donnant une description fine des écoulements a conduit à adapter une méthode instationnaire originale qui a donné des résultats prometteurs.

REFERENCES

- [1] POISSON-QUINTON P., WANNER J.C.
Evolution de la conception des avions grâce aux commandes automatiques généralisées. L'Aéronautique et l'Astronautique n° 71 - 1978-4.
- [2] BEHRBOHM H.
Basic low speed aerodynamics on the short coupled canard configuration at small aspect ratio. SAAB - Technical Note n° 60 (7/1965)

Fig. 20 - Evolution en fonction du temps de la force normale théorique. ($\alpha = 12^\circ$).

- [3] MANIE F., REHBACH C., SCHMITT V.
Etude d'une aile à flèche variable en écoulement subsonique ou transsonique.
11ème Congrès ICAS - Lisbonne Septembre 78
(ONERA TP 1978-106)
- [4] PIERRE M.
Soufflerie subsonique pressurisée F1 du centre du Fauga-Mauzac de l'ONERA
11ème Congrès ICAS-Lisbonne Septembre 78.
(ONERA TP. 1978-51)
- [5] MIRANDE J., SCHMITT V., WERLE H.
Système tourbillonnaire présent à l'extrados d'une aile en flèche à grande incidence.
AGARD CP 247 - Paper n°12
- [6] WERLE H.
Le tunnel hydrodynamique au service de la recherche aérospatiale.
ONERA Publication n° 156 (1974).
- [7] HENDERSON W.P.
Effects of wing leading-edge radius and Reynolds number on longitudinal aerodynamic characteristics of highly swept wing-body configurations at subsonic speeds.
NASA TN D 8361 - December 1976.
- [8] MARGASON R.J., LAMAR J.E.
Vortex lattice FORTRAN program for estimating subsonic aerodynamic characteristics of complex planforms.
NASA TN D 6142 - 1971
- [9] POLHAMUS E.C.
A concept of the vortex lift of sharp-edge delta wings based on a leading edge suction analogy.
NASA TN D 3767 - 1966
- [10] HALE R.W. - ORDWAY D.E.
Prediction of aerodynamic loads on close coupled canard configurations - Theory and experiment
AGARD CP 204 - Paper n° 8
- [11] WENTZ W.H. Jr. KOHLMAN D.L.
Vortex breakdown on slender sharp-edged wings.
AIAA Paper N° 69-778
- [12] WHITE R.P. Jr. ZALAY A.D.
High lift generation by the use of vortices
NASA/SRL Report 74-12 (July 1975).
- [13] REHBACH C.
Numerical calculation of three dimensional unsteady flows with vortex sheets
AIAA Paper n° 78-111
- [14] REHBACH C.
Calcul instationnaire de nappes tourbillonnaires émises par des surfaces portantes fortement inclinées.
AGARD CP 247 - Paper n° 14

On the Effects of Gaps on Control Surface Characteristics

by

C. Michael and G.J. Hancock

Department of Aeronautical Engineering,
Queen Mary College, University of London
Mile End Road, London, E1 4NS.

SUMMARY

An experimental investigation has been undertaken at low speeds on a two dimensional 'aerofoil', comprising an elliptic nose, parallel section of 5% t/c ratio, and a 20% trailing edge control surface. The control surface has a semi-circular nose, a parallel section and then a straight taper to the trailing edge. The overall chord of the model is 2m; the height of the wind tunnel is 1m. A large chord model was chosen to give a sufficiently large boundary layer thickness in the neighbourhood of the leading edge of the control surface compared with a typical gap width. It is appreciated that wall interference effects are large, so results should not be interpreted in practical terms, but it is hoped that the main features of gap interference effects are simulated.

Three different geometries of the rear of the main aerofoil have been investigated. Gaps are created by moving the control surface aft of the main aerofoil. Zero gap is when the control surface is in contact with the rear of the main aerofoil so that there is no flow from the lower to the upper surface. The gaps are in 1 mm increments up to a maximum of 10 mm (i.e. 0.5% of chord). Extensive pressure plotting has been carried out for the above range of gaps and control surface angular deflections up to 8°. A range of measurements of mean boundary layer profiles in the neighbourhood of the gap have also been obtained.

The variations of the overall C_L with control angle and gap size, for the three geometries are shown. Qualitative explanations for the trends of these results will be given by reference to measured pressure distributions and by reference to the boundary layer measurements.

1. INTRODUCTION

It is thought that small gaps between an aerofoil, or wing, and its control surfaces, can induce significant effects on aerodynamic characteristics. For practical purposes these effects are incorporated in empirical formulae derived from parametric tests over the past years and which are quoted in ESDU and DATCOM data sheets.

The realisation of the potential of Active Control Technology depends on the effectiveness of the control surfaces, so there is a renewed need to assess and understand the effects of gaps. Such understanding can then hopefully be incorporated into the contemporary advanced numerical methods currently applied to predict aerofoil and wing characteristics.

To illustrate the current situation the following data are taken from ref. 1, which refers to comparisons between various theories and experimental results for a two dimensional NPL 1541 aerofoil with a 20% chord trailing edge control surface. The theories are thin aerofoil linearised theory, an inviscid solution from a standard A.M.O. Smith theory with singularity distributions on the aerofoil profile, and an iterative solution from a combination of the A.M.O. Smith method with an integral equation method for a turbulent boundary layer. The experimental results come from reference 2. The comparisons in Table 1 are for the lift coefficient C_L , the moment coefficient about the $\frac{1}{4}$ chord point $C_{M_{\frac{1}{4}}}$, and the hinge moment coefficient C_H when the aerofoil incidence is zero and the control surface angle 4°.

	Linearised Theory	Thick Aerofoil Inviscid Theory (A.M.O. Smith)	Thick Aerofoil Viscous Theory	Experiment
C_L	0.242	0.275	0.254	0.174
$C_{M_{\frac{1}{4}}}$	-0.044	-0.050	-0.046	-0.034
C_H	-0.0025	-0.0020	-0.0018	-0.0015

TABLE 1

The viscous theory for a conventional aerofoil at low speed usually compares most favourably with experimental results. The cause of large differences between the theories and the experimental results must be due to a major reason. It could be that the boundary layer theories are inadequate for boundary layers which go around the corners at a control hinge, alternatively gaps effects could be the reason. These are the questions investigated here.

2. APPARATUS

28-2
Since the main emphasis of this investigation was on flows through gaps it was thought to be essential that realistic boundary layer features were incorporated. Thus a two dimensional aerofoil, effectively a long thick flat plate of thickness 0.1m and 2 m chord was chosen, with a 20% trailing edge control surface, as shown in Figure 1. The nose of the aerofoil was elliptic. The control surface had a semi-circular nose, a parallel section, continuing the straight line profile of the main aerofoil and a straight bevelled trailing edge region; the trailing edge angle was 14° .

The hinge line of the control surface could be moved aft up to 10 mm and the control surface angles could go up to 8° . The incidence of the main aerofoil was fixed.

Three gap geometries were investigated, again as shown in Figure 1. The first had an internal cavity, the second idealised a contoured geometry and the third was a simple straight rectangular cut off. The blocks for these three geometries were interchangeable and fixed at the rear of the aerofoil section.

The model was fully pressure plotted over the aerofoil and control surface, the semi-circular nose of the control surface was pressure plotted together with the internal surfaces of the various gap geometries.

Considerable care was taken with the model to ensure that it was a two dimensional model especially along the gap from side wall to side wall, and to ensure that it was symmetrical. This last feature was important because boundary layer characteristics in the neighbourhood of the gap were also to be measured but the traversing gear could only be used on the upper surface of the model so traverses had to be taken with the control at positive and negative angles. The boundary layer characteristics were confined to measurements of the mean boundary layer velocity profiles and these measurements were made with a small yawmeter tube developed at Queen Mary College for such measurements.

The tunnel height was 0.75 m so the results are dominated by wind tunnel interference effects.

With the tunnel operating at 23 m/s, the Reynolds number based on the chord was 3.5×10^6 ; the turbulent boundary layer thickness just ahead of the nose of the control surface was about 20 mm.

3. EXPERIMENTAL RESULTS AND DISCUSSION

3.1 LIFT CHARACTERISTICS

From the full set of pressure measurements the overall coefficients of C_L , C_M , and C_H have been evaluated. In this paper only the results for C_L are presented, where C_L is plotted against η , the control surface angular deflection.

Figure 2(i) shows the effect of control surface angle and aft movement of the control surface hinge location (i.e. a measure of the gap) for the contoured gap geometry. It is seen that small gaps 2-5 mm, equal to 0.1-0.25% chord, and much smaller than the boundary layer thickness in the neighbourhood of the gaps, can lead to significant losses in overall C_L in this arrangement. Larger variations appear with gaps between 0-5 mm than in variations between 5mm-10mm.

Figure 2(ii) shows the effects of gap width on C_L for the internal cavity gap geometry. Again there is a similar loss of lift with increasing gap width as shown in Figure 2(i).

Figure 2(iii) shows the effect of gap width on C_L with the rectangular gap geometry. In this case not only is there a loss in C_L with increasing gap width but at the higher values of gap width at low control surface angles there is a reversal of lift which is especially pronounced with the 10 mm gap width.

Comparing Figures 2(i), (ii), (iii), it is seen that for all gap geometries the non-linear effects in C_L appear at the lower angles of control surface deflection. However $\partial C_L / \partial \eta$ is about the same for all gap geometries, and gap widths, apart from the 10 mm gap width in Figure 2(iii), for angles above 4° to 5° .

It is also seen that for the zero gap width the variation of C_L against η is about the same magnitude for all three gap geometries.

It would appear that for small gap widths, i.e. less than 2 mm, there is a smaller loss of lift with the contoured gap geometry than with the other two geometries.

3.2 PRESSURE DISTRIBUTIONS

A selection from the full set of results of the pressure distribution are given here to illustrate how the losses in C_L , described above, manifest themselves in terms of pressure distributions.

Figure 3(i) shows the pressure distributions for the contoured gap geometry with 0 mm and 7 mm gap widths with the control surface angle equal to 6° . According to Figure 2(i), under these conditions there is a loss of lift of about 50%. In crude terms this loss of lift is made up from a reduction of the suction on the upper surface of the main aerofoil by 20% and an increase in the suction on the lower surface by a corresponding 20%. The pressure distributions over the control surface are mostly the same at 2 mm and 7 mm gap width apart from the increased suction on the lower surface around the nose, this effect is associated presumably with the increased mass flow through the gap. It is of interest to note that the flow does not separate at the 'corner' on the control surface at the change of surface inclination, in fact, because of the thinner boundary layer on the lower surface the suction is greater around the corner on the lower surface of the control surface than around the corner on the upper surface. It can be deduced from the constant pressure region near the trailing edge that the flow separates on

the upper surface just ahead of the trailing edge and there is a smaller region of separated flow on the lower surface.

Figure 3(ii) shows very similar trends for the geometry with internal cavity.

28-3

In Figure 3(iii) for the rectangular geometry there is only a small resultant lift because the upper and lower surface suction over the main aerofoil surface tend to cancel out. As might be expected, when the gap width exists there are large suction pressures induced by the flow through the gap, resulting in higher suction pressures over the nose of the control surface.

3.3 BOUNDARY LAYER MEASUREMENTS

Shown in Figure 4 are a set of boundary layer velocity profiles for the contoured gap on the upper and lower surfaces in the neighbourhood of the gap, station $0.79 x/c$ is on the flat surface of the main aerofoil just ahead of the gap and station $0.81 x/c$ is on the control surface nose where the semi circular shape joins the aft flat surface.

From the profiles on the upper surface as seen in Figure 4(i) it would appear that the flow through the gap is of low energy, and thus it tends to reduce the magnitudes of the velocities close to the surface; the subsequent significant increase in boundary layer thickness appears to be independent of gap width.

From the profiles on the lower surface, as shown in Figure 4(ii) it is seen that in the case of the gap there is an increase in velocity close to the surface of the control since the lower parts of the boundary layer have been transferred via the flow through the gap to the upper surface.

Integration of the velocity profiles shown in Figure 4 leads to the displacement thickness distributions around the gap region as shown in Figure 5. It is of interest to note that the increase in displacement thickness on the upper surface is larger than the decrease in displacement thickness on the lower surface, superficially this is a surprising result since it might be argued that all that is involved is a mass transfer from the lower surface boundary layer to the upper surface boundary layer but as discussed later the situation is somewhat more complex.

4. THEORETICAL CONSIDERATIONS

At Queen Mary College a number of standard programmes have been developed for calculating the characteristics of aerofoils at low speeds.

A form of the A.M.O. Smith method has been developed to calculate the inviscid flow about a given profile shape. The profile is divided into straight line elements; on each element is placed a uniform source distribution and a uniform vorticity distribution; the strength of the source distribution varies from element to element while the strength of the vorticity is the same for all elements. The boundary condition of adjacent flow is satisfied at the mid point of each element and the Kutta condition is taken to be equal pressure at the mid points of the two elements either side of the trailing edge.

A boundary layer has also been developed, which is an integral form of the lag entrainment method for non equilibrium boundary layers, it is a method which can deal with pressure gradients.

A combined iterative method has then been developed whereby a new profile is obtained by adding the displacement thickness to the aerofoil profile and then solving the inviscid flow about the modified profile. Satisfactory results have been obtained by keeping the singularities on the aerofoil profile and satisfying the boundary conditions on the displaced surface; a simple source distribution was also assumed to represent the wake. A typical result is shown in Figure 6.

The inviscid A.M.O. Smith solution has been extended to an aerofoil in a confined channel with solid upper and lower walls. A transformation method has been used. A typical result is shown in Figure 7.

These various theoretical methods have been applied to the models used in this investigation with zero gap. The experimental results are those for the gap geometry with the internal cavity but zero gap, it was thought that this experimental arrangement would give the most appropriate set of experimental results for these comparative studies. As shown in Figure 8(i) for the case of zero control surface angle the theoretical results are reasonable. As shown in Figure 8(ii) there is a large difference between the inviscid theory and the theory including boundary layer effects. The agreement of the theoretical results including boundary layer effects with the experimental values is reassuring, exactly why there is good agreement on the upper surface but not such good agreement on the lower surface is not known.

Now for the effects of a gap.

Consider first a gap assuming inviscid flow. It might be thought that the A.M.O. Smith method could be applied directly to this problem, but this approach is not a practical proposition for small gaps. An alternative approach is to recognise that the flow through the gap can be represented by a source ejecting a mass flow out of the upper surface at the upper surface gap location and by a sink injecting the same mass flow into the lower surface at the lower surface gap location. The resulting flow is sketched in Figure 9. There is then the question of the strength of the source (or sink). On the upper surface the suction pressures around the region of the control nose are fairly uniform and the static pressure of the emerging flow through the gap must have this same static pressure, and assuming inviscid flow, then the velocity of the jet must be on a par with the outer stream velocity in that region. What happens at the gap entrance on the lower surface is most complicated; there are large

rates of change of static pressure across the lower gap entrance since there is low pressure at the rear of the main aerofoil and a stagnation point on the under surface of the nose of the control. Nevertheless the mass flow in the gap must be preserved and because conditions on the upper surface across the gap are reasonably uniform then the mass flow through the gap is most directly calculated from these upper surface conditions.

A calculation based on this approach is shown in Figure 10 for an aerofoil in an unbounded stream. It is assumed in this calculation that the mass flux strength of the source is $(2qt)$ where q is the stream velocity of the outer inviscid flow on the upper surface over the gap, the factor of 2 is included to represent the correct (qt) outflow, the other (qt) represents flow internal to the aerofoil profile.

To include the boundary layer effects, then across the gap on the upper surface the conventional boundary layer theory gives the increase in effective profile across the gap as

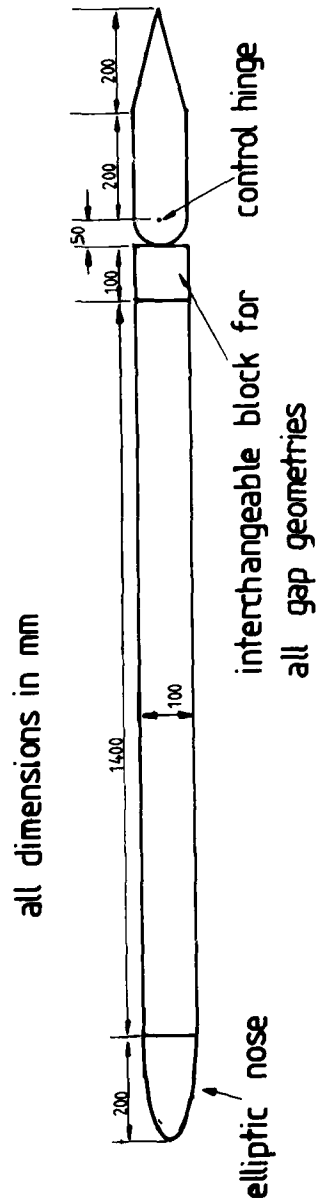
$$\Delta(\zeta_2 - \zeta_1) = (U_2 \delta_2^* - U_1 \delta_1^* - (U_2 - U_1) \delta_2 + m) / (U_1 + U_2) / 2$$

where 1 refers to a station just ahead of the gap, and 2 refers to a station downstream of the gap, and m is the mass flow through the gap. The equation is the same on the lower surface across the gap except that the sign of m is reversed.

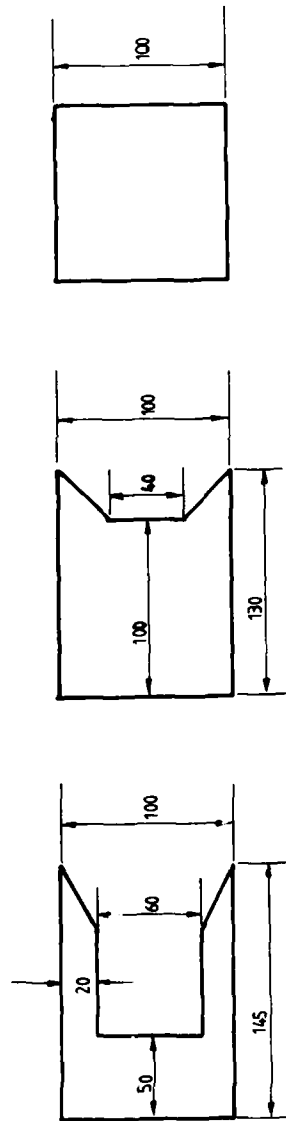
The application of the above formula to the contoured gap geometry (i.e. the middle one in Figure 1) for a control angle deflection of 4° , taking measured values of δ_2^* , δ_1^* , assuming $U_1 = U_2$ with values again taken from measurements, assuming a mass flow through the gap equal to the free stream velocity multiplied by the gap thickness, gives a reduction in C_L of approximately 30%, compared with an experimental reduction closer to 50% (see Figure 2(i)). Although this crude calculation suggests a possible mechanism for reducing C_L much more analysis and understanding is required before the effects of gaps can be predicted.

REFERENCE

1. Basu B.C. An aerofoil with Control Surface in Incompressible Viscous Flow, Aero. Journal, Vol. 81, Dec. 1977.

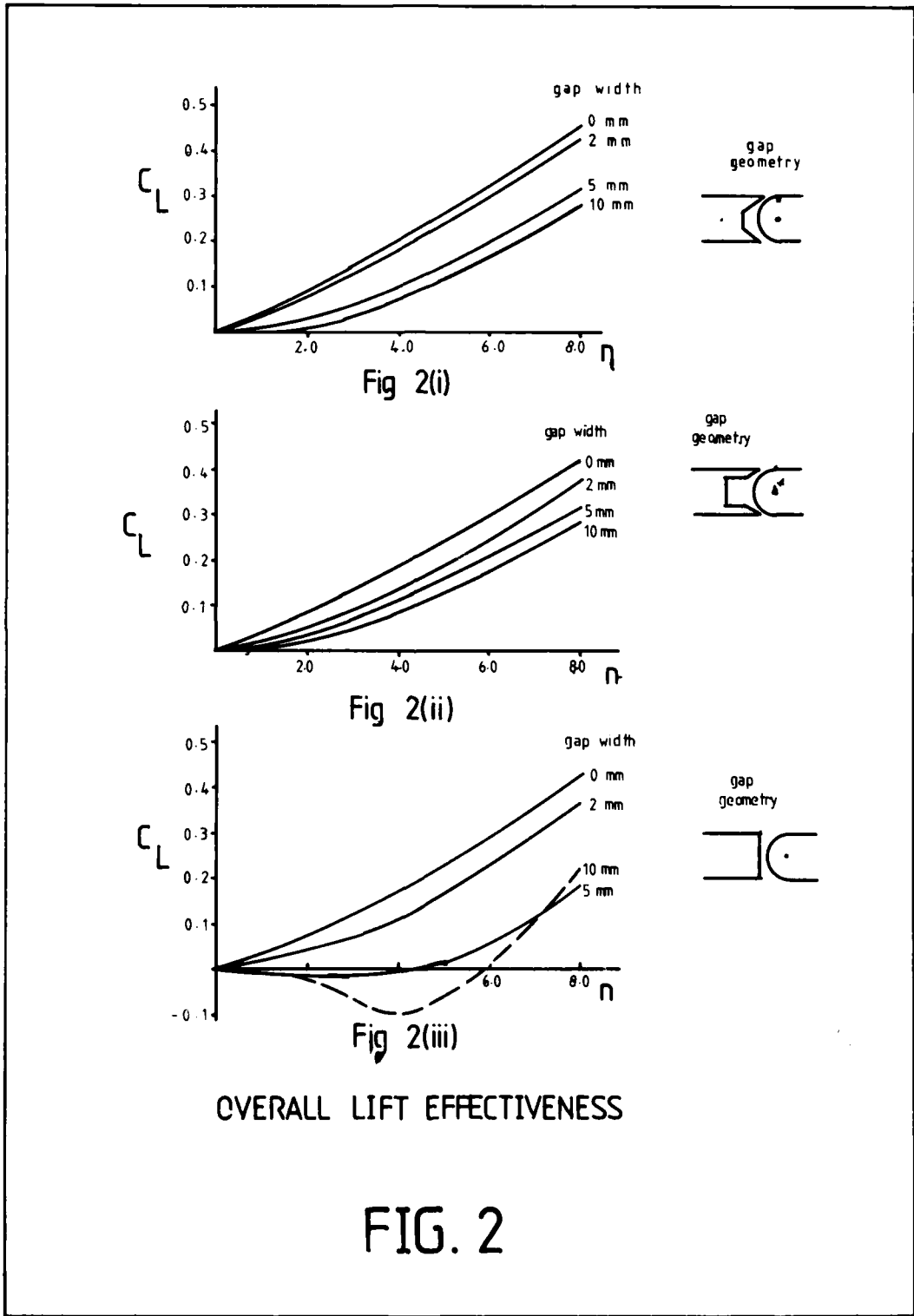


AEROFoil MODEL



GAP GEOMETRIES

FIG. 1



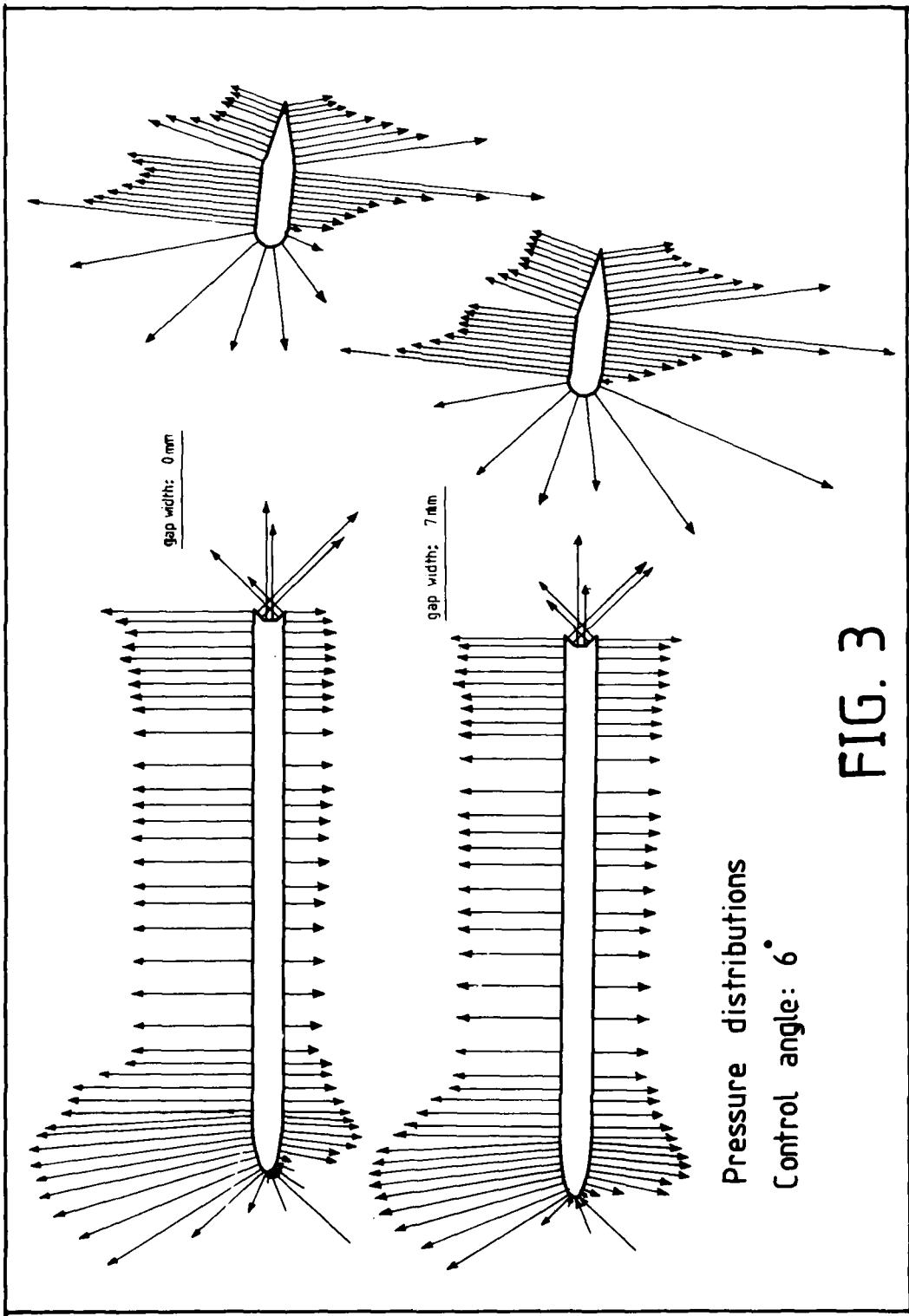


FIG. 3

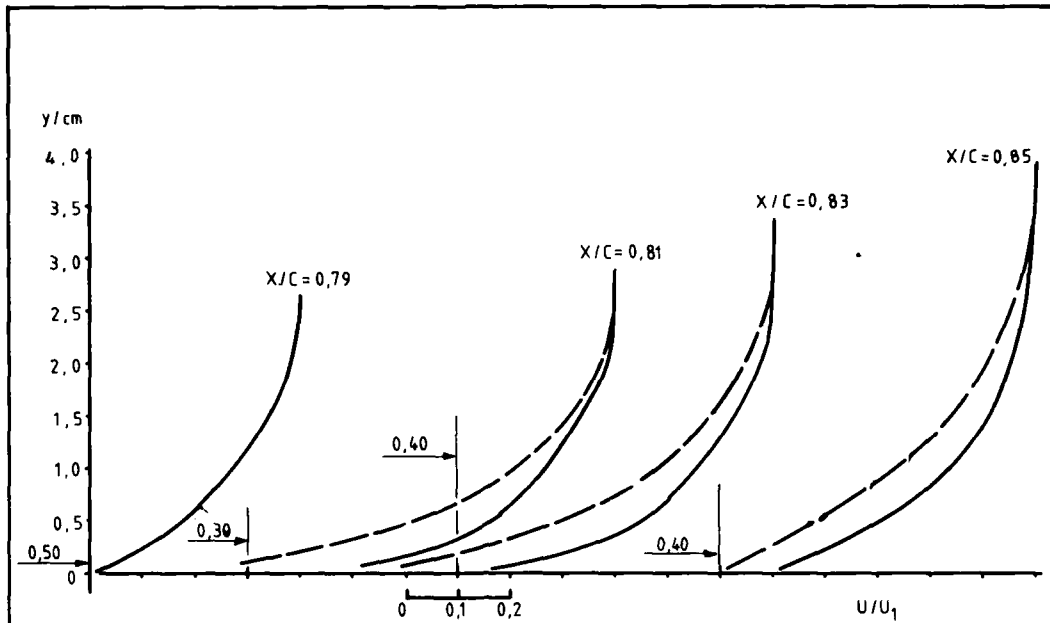


Fig. 4(i): Upper Surface

— gap width: 0 mm
 - - - gap width: 7 mm

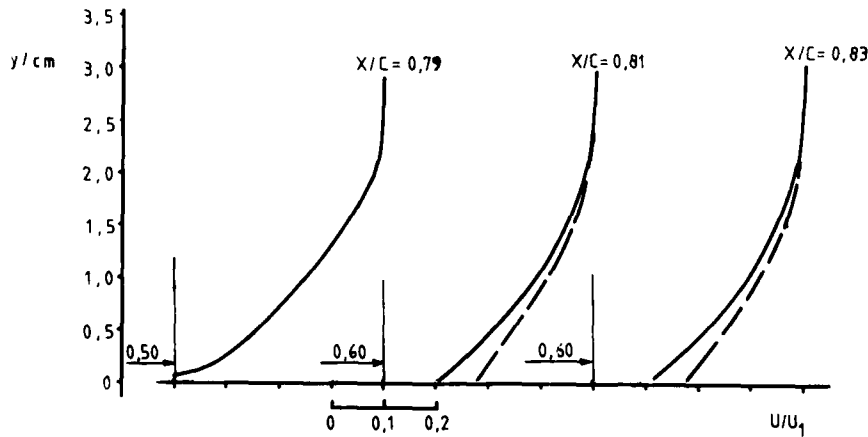
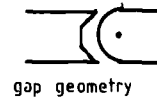


Fig. 4(ii): Lower Surface

BOUNDARY LAYER PROFILES

FIG. 4

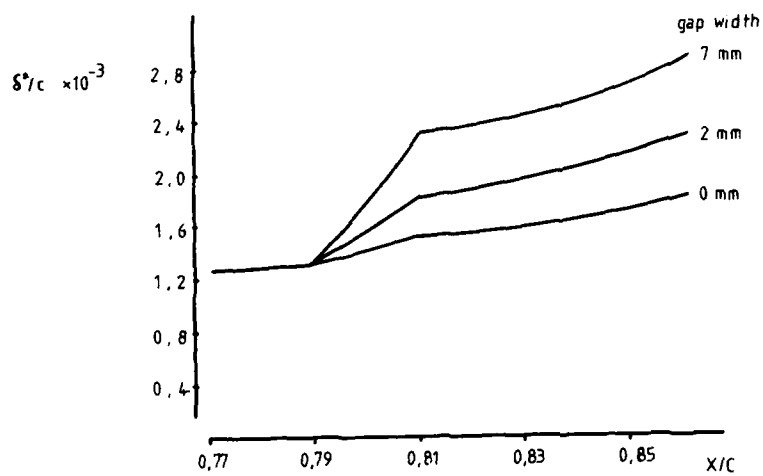


Fig. 5(i): Upper Surface

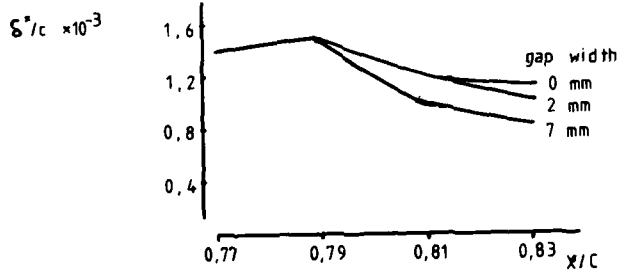
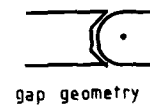
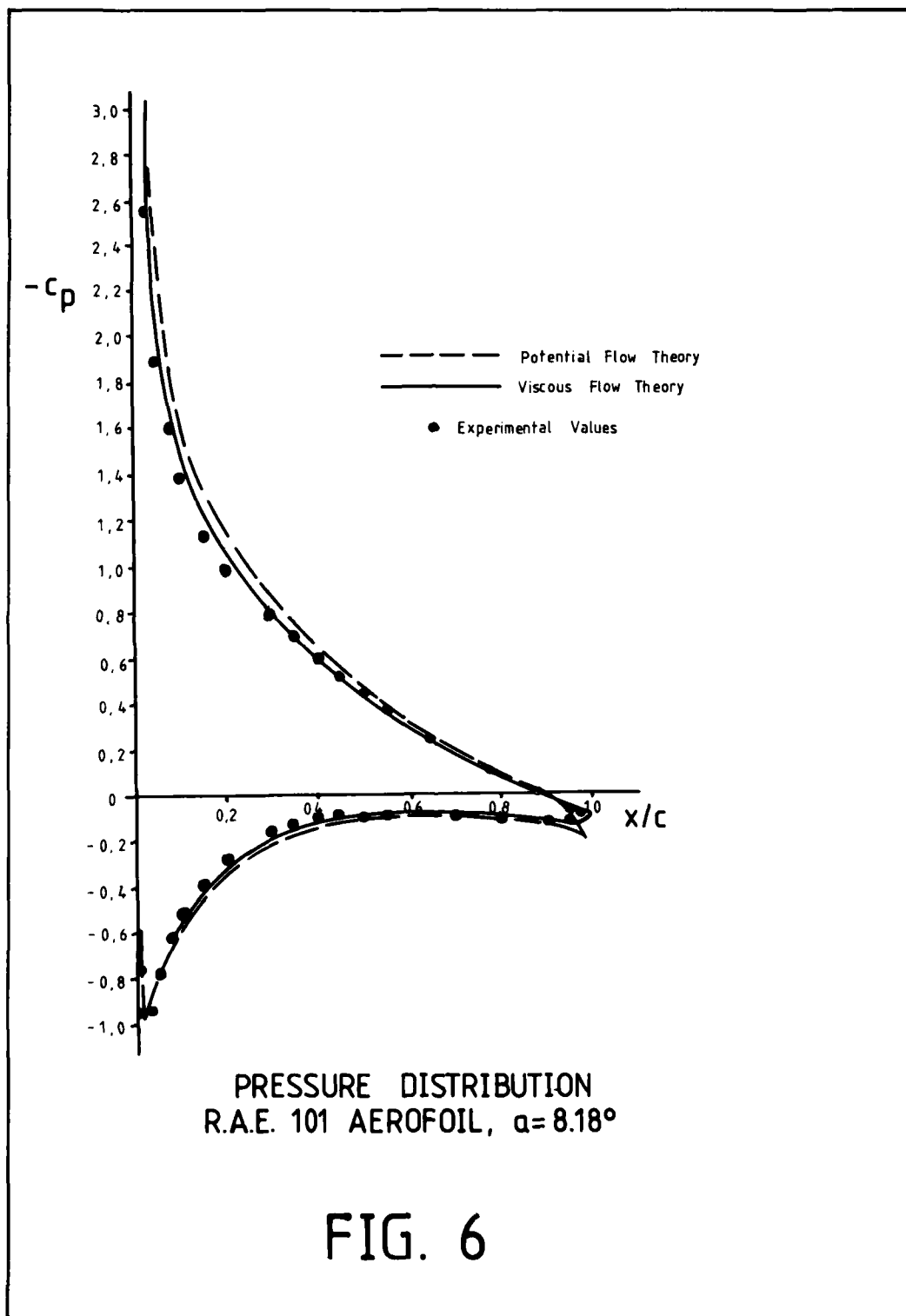
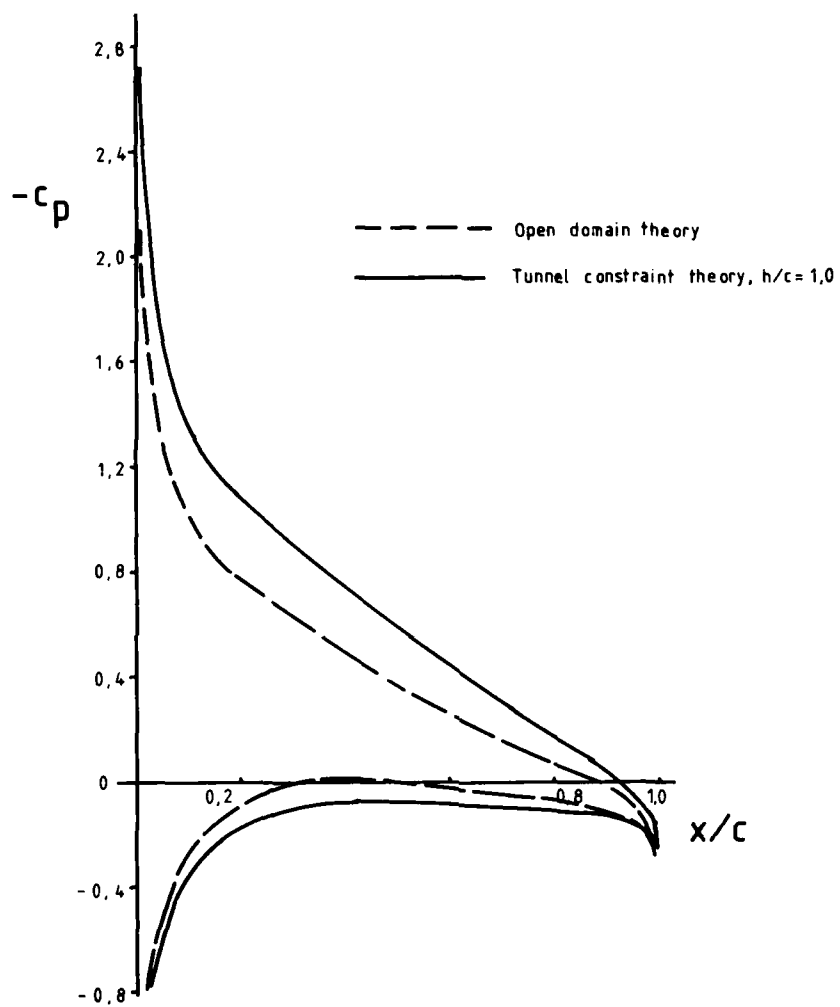


Fig. 5(ii): Lower Surface

DISPLACEMENT THICKNESS ABOUT THE GAP

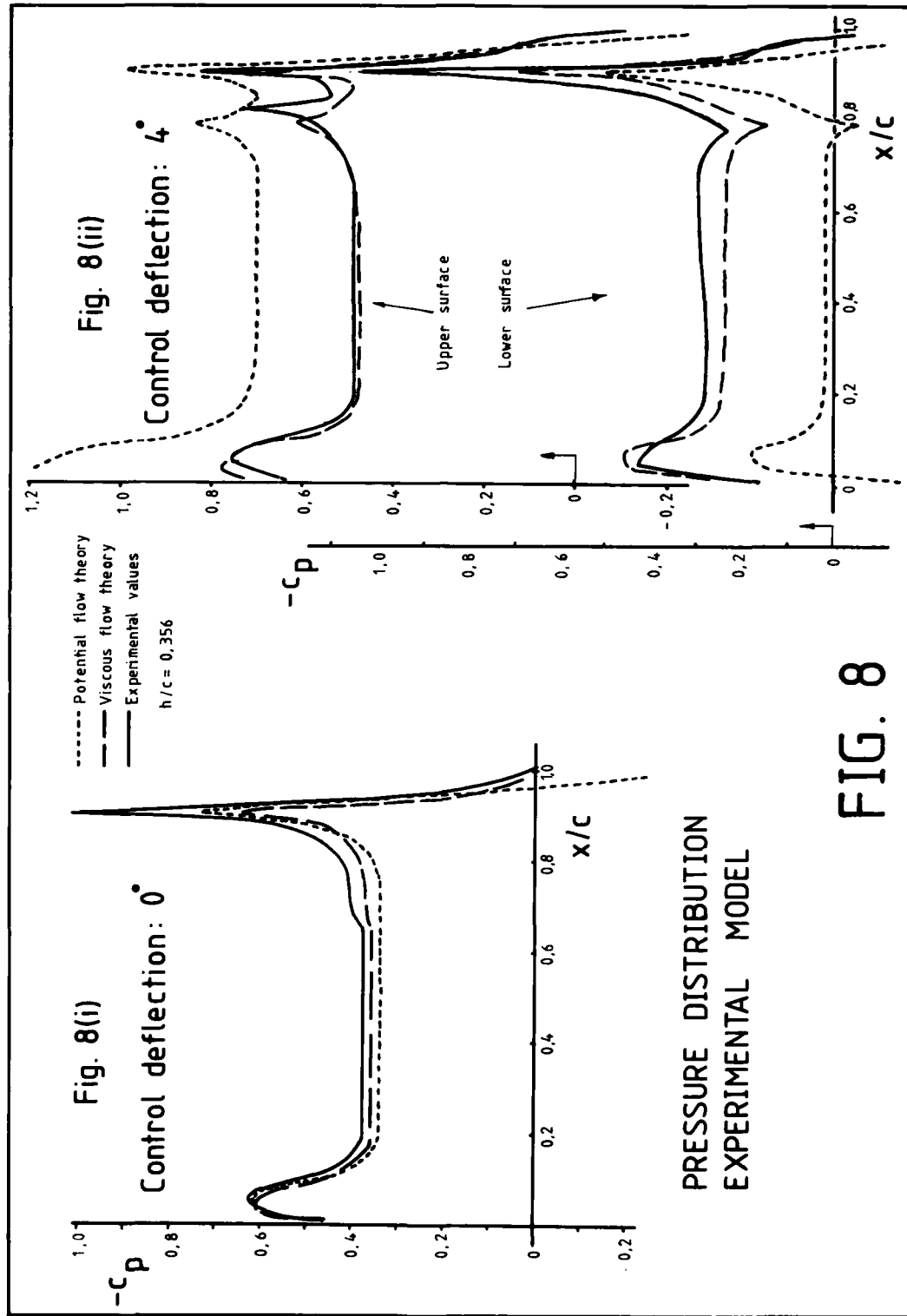
FIG. 5

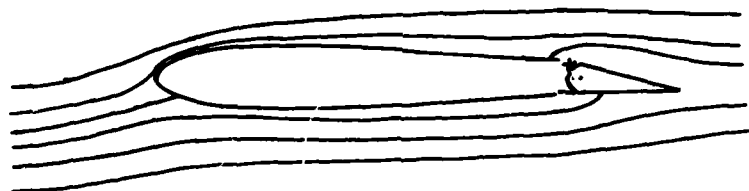




PRESSURE DISTRIBUTIONS
POTENTIAL FLOW
R.A.E. 101 AEROFOIL, $\alpha=5,0^\circ$

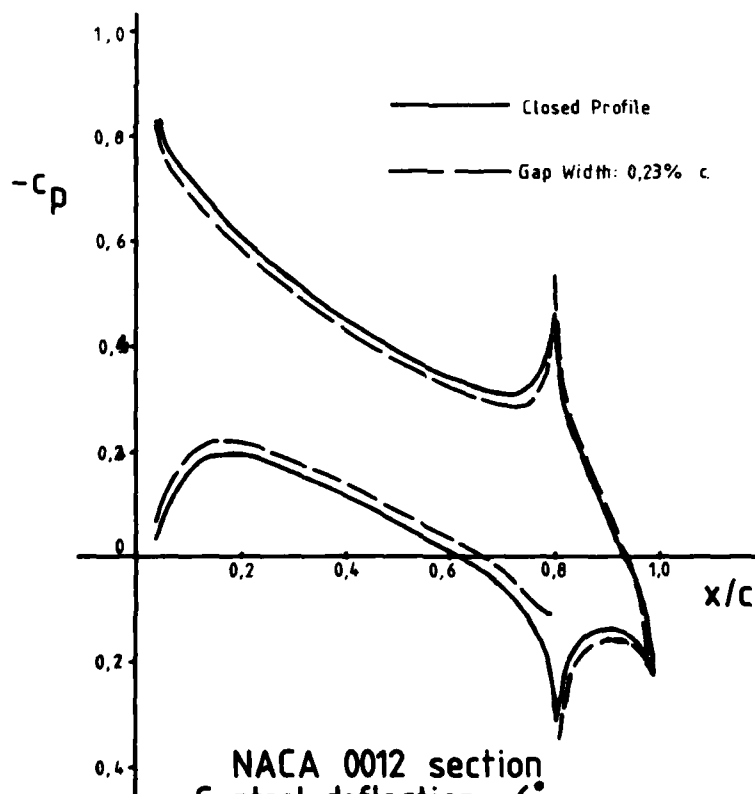
FIG. 7





Inviscid Flow Model of Gap Effect

FIG. 9



NACA 0012 section
Control deflection: 6°
Pressure distribution-Inviscid flow

FIG. 10

Etude aérodynamique des gouvernes de Missile

par J. PERINELLE et L. MIFSUD
MATRA Service Aérodynamique BP 1. 78140 Vélizy (France)

Résumé

Nous rappelons rapidement les principales caractéristiques de base concernant les surfaces à faible allongement dont sont composées généralement les gouvernes de missile.

Après un bref exposé sur les différentes configurations aérodynamiques et leurs implications sur les caractéristiques des gouvernes, nous examinerons plus en détail l'aérodynamique des gouvernes de missile Canard.

C'est pour cette configuration, en effet, que les caractéristiques de la gouverne conditionnent le plus les performances du missile. Il est donc nécessaire d'en repousser au maximum les possibilités.

Les deux directions principales qu'il est nécessaire de travailler particulièrement sont la portance maximum aux grands angles d'attaque et le moment de charnière.

La portance maximum d'une surface fonction de l'allongement, on peut l'améliorer en choisissant sa forme judicieusement ou par l'adjonction de surfaces additionnelles.

L'optimisation du moment de charnière se fait dans la plupart des cas en fonction du nombre de Mach, car cet effet est plus important que ceux de l'incidence et du braquage. C'est un coefficient aérodynamique très sensible au contexte aérodynamique, difficile à calculer, et dont l'optimisation ne peut se faire qu'expérimentalement.

Les progrès réalisés sur l'aérodynamique des gouvernes en incidence et sur la minimisation du moment de charnière, ont permis la mise au point de missiles très performants.

Summary

A quick reminder is given of the main basic characteristics of low aspect ratio surfaces (which is usually the case for missiles control surfaces).

After a review of the different aerodynamic configurations and their implications on performances, we shall discuss the aerodynamics of Canard missiles control surfaces.

In this latter configuration, the characteristics of control surfaces are very effective for the missile performances. It is then necessary to expand their possibilities to a maximum.

The two main features which should be studied are

- (a) Maximum lift at high angles of attack
- (b) Hinge - moment

The maximum lift of a surface is a function of its aspect ratio - it can therefore be improved with a well - chosen shape or with the adjunction of other surfaces.

The hinge - moment optimization is made mainly in relation with the Mach number, for this parameter has more influence than the angle of attack or the deflexion. This aerodynamic coefficient, very sensitive to the aerodynamic field, is difficult to compute. Its optimization can therefore only be experimental.

Progresses in control surfaces aerodynamics in incidence as well as in the minimization of the hinge moment has led to the design of very efficient missiles.

Notations

C_z	Coefficient de portance	α_∞	Angle d'incidence par rapport à l'écoulement à l'infini amont
C_{zm}	Coefficient portance maximum d'une surface	α_1	Angle d'incidence à l'aval d'une surface portante
$C_{z\beta}$	Coefficient de portance dû au braquage	α_l	Angle d'incidence maximum de la portance pseudo linéaire
$C_{z\infty}$	Coefficient de portance dû à l'incidence infinie	α_s	Angle d'incidence de saturation de la surface
C_m	Coefficient de moment de tangage du missile	α_m	Angle d'incidence maximum utile de la surface
$C_{m\beta}$	Coefficient de moment de tangage dû au braquage de la gouverne	β	Angle de braquage de la gouverne
$C_{m\infty}$	Coefficient de moment de tangage du missile dû à l'incidence infinie	ϵ	Angle de déflexion de l'écoulement derrière une surface portante
K_p	Coefficient de pression	ϵ^*	Coefficient de déflexion tenant compte de l'importance respective des surfaces
l_m	Corde moyenne de la surface		
Mch	Moment de charnière de la gouverne		
M	Nombre de Mach		
X_{cp}	Distance du centre de poussée de la surface à un point de référence.		

indices

a Aile
g Gouverne

* moyen

1 - INTRODUCTION.

Il s'offre souvent plusieurs possibilités pour aborder un même problème et chacun le résoud compte tenu de son expérience et de ses possibilités technologiques. Il en est ainsi pour l'étude d'un missile dont l'aérodynamique dépend en grande partie des options fondamentales prises initialement sur l'architecture, les aménagements, le propulseur, la forme d'énergie utilisée pour les servo-moteurs, le type de pilotage : gouvernes aérodynamiques, gouvernes de jet, tuyère orientable, spoiler, etc.....

Les options choisies par la Société MATRA ont toujours conduit à mettre l'accent sur la configuration aérodynamique et plus particulièrement sur celle des gouvernes.

Les gouvernes que nous étudierons dans les pages suivantes sont des surfaces indépendantes, braquables dans leur totalité. Bien que nous ayons étudié des gouvernes de type différent comme par exemple des volets placés au bord de fuite des ailes, nous n'en ferons pas mention, car leur adaptation aux missiles n'a pas présenté de difficultés particulières.

Si les difficultés d'étude de gouvernes aérodynamiques sont d'ordre différent selon que le missile possède une configuration classique ou Canard, c'est pour cette dernière que les problèmes sont les plus ardues. Ceci nous a obligés à étudier particulièrement la portance maximum, ainsi que les moments de charnière des gouvernes.

2 - RAPPEL DE QUELQUES NOTIONS DE BASE.

L'étude des gouvernes nécessite le rappel de quelques notions générales qu'il est nécessaire de garder à l'esprit. Ces considérations s'appliquent aux surfaces de faibles allongements et d'épaisseurs relatives minces qui équipent généralement les missiles tactiques.

2.1. - Déflexion de l'écoulement par une surface (planche 1).

Selon la théorie de la déflexion, une surface portante modifie la direction de la vitesse de l'écoulement. L'angle d'incidence est donc différent en amont et en aval de la surface.

Cette déflexion créant la traînée induite, est une fonction décroissante de l'allongement de la surface portante considérée ; elle est donc particulièrement importante pour les petits allongements qui nous intéressent.

La valeur de cette déflexion varie en fonction du nombre de Mach pour être maximum à $M = 1$ puis redécroître ensuite.

Si nous plaçons une autre surface derrière la première, elle sera soumise à un angle d'attaque inférieur à celui de la première. Nous pouvons la mettre sous la forme

$$\alpha_1 = \alpha_{\infty} - \varepsilon \quad \text{et en linéarisant.}$$

$$\alpha_1 = \alpha_{\infty} (1 - \varepsilon / \alpha_{\infty})$$

Bien, entendu l'effet de la déflexion dépend de l'importance relative des deux surfaces considérées.

2.2. - Portance et centre de poussée d'une surface de faible allongement en fonction de l'incidence (planche 2).

La courbe typique de la portance d'une surface de faible allongement en fonction de l'incidence dans le système Lilienthal se compose de trois parties.

Elle commence à croître, plus ou moins linéairement, selon l'allongement, puis se produit une période de transition au-delà de laquelle la portance reste pratiquement constante jusqu'à des incidences élevées. La transition est généralement courte et l'on peut, en prolongeant les deux sections, déterminer une incidence que nous appellerons incidence maximum, qui est une caractéristique de la surface considérée ; elle se comporte comme une fonction inversement proportionnelle à l'allongement.

Sur la planche 3 ont été tracées les répartitions de pression obtenues sur une corde d'une aile possédant un allongement de 1,7, juste avant et après la saturation. L'intégrale des pressions reste pratiquement la même.

Dans la partie linéaire de la courbe de portance, la répartition de pression l croît régulièrement et le centre de poussée reste constant, puis pendant la phase de transition et la saturation, le centre de poussée recule constamment en tendant vers le centre de gravité de la surface (planche 4).

En fonction du nombre de Mach l'évolution des centres de poussée est légèrement différente suivant la forme de la gouverne. Ils se situent autour de 25 % de la corde moyenne en subsonique, puis reculent constamment vers le centre de gravité en supersonique (planche 5).

3 - GOUVERNES DE MISSILE EN CONFIGURATION CLASSIQUE.

La configuration aérodynamique dite classique est celle où les surfaces portantes principales sont devant les gouvernes.

La portance du missile est alors assurée par l'ensemble corps + ailes, tandis que les gouvernes assurent la stabilité et la manoeuvrabilité (planche 6).

Le missile étant supposé stable, l'équilibre des moments au centre de gravité exige que le braquage des gouvernes soit dans le sens inverse de l'incidence.

L'incidence locale sur la gouverne peut être mise sous la forme $\alpha_g = \alpha_\infty (1 - \epsilon_0 / \alpha_\infty) - K \delta$

K est un facteur de correction qui permet de comparer l'effet d'incidence qui inclut l'influence du corps à l'effet de braquage (qui ne comprend pas cette influence).

L'effet d'incidence étant réduit par la déflexion due à l'aile et, en sens contraire à l'effet du braquage, l'incidence locale sur les gouvernes reste faible et les caractéristiques de saturation de ces surfaces ne sont généralement pas critiques pour les incidences usuelles.

Un autre effet de cette disposition est que la portance due au braquage délest la portance du missile au détriment du facteur de charge.

La tendance actuelle à faire supporter de très fortes incidences aux missiles, soit au départ lors d'un tir en air-air, soit en évolution propre, demande de nouvelles performances aux gouvernes de missile classique. D'autre part, si le missile est piloté en roulis à l'aide des gouvernes de tangage et de lacet, un braquage différentiel se superpose au braquage moyen dans le plan considéré. Ceci conduit à délester une des deux gouvernes et à charger l'autre ; dans ces conditions les caractéristiques des gouvernes en portance maximum et en moment de charnière retrouvent beaucoup d'importance.

4 - GOUVERNES DE MISSILE EN CONFIGURATION CANARD.

Dans cette configuration, les ailes, c'est-à-dire les surfaces principales, sont reportées à l'arrière du corps. Les surfaces avant permettent de régler la stabilité du missile à une valeur raisonnable et, en se braquant, de contrôler son incidence. Contrairement à celles de la formule classique, les gouvernes du "Canard" assurent un pourcentage important de la portance du missile (planche 7).

Pour un missile stable, l'équilibre des moments au centre de gravité montre que l'effet de braquage s'ajoute à l'effet d'incidence.

L'incidence locale moyenne sur la gouverne peut s'écrire :

$$\alpha_g = \alpha_\infty + K \delta$$

La signification du K est la même que précédemment.

Ceci montre que la saturation de gouverne peut être atteinte rapidement et que celle-ci limite directement les performances du missile.

Si l'on prend un $\delta/\alpha = 1$ et un $K = 0,6$ avec un α_g maximum de 17° , on voit que l'incidence du missile est limitée à 10° . Cette limitation est évidemment variable en fonction du nombre de Mach ; c'est en subsonique élevé et en transsonique que la limitation est la plus sévère. Sur la planche 8 est tracé le moment du missile en fonction de l'incidence pour différents braquages et à un nombre de Mach donné.

On voit que quand la gouverne a atteint sa saturation, l'incidence du missile n'évolue pratiquement plus, quel que soit le braquage.

Afin de pouvoir continuer à utiliser la configuration Canard par des missiles modernes et performants, il a été nécessaire d'améliorer largement les caractéristiques de ceux-ci, en particulier l'efficacité des gouvernes. La gouverne étant toujours très chargée, il s'en suit des moments de charnière très élevés.

Or, dès le début des études de missiles, une des options prise par la Société MATRA a été d'activer les gouvernes par des servo-moteurs électriques. Dans ce cas, le niveau des moments de charnière est primordial pour le pilotage, et nous avons dû, très tôt, nous pencher sur cette question.

5 - EFFICACITE DES GOUVERNES.

L'augmentation de l'efficacité des gouvernes ne doit pas se faire au détriment d'une autre caractéristique primordiale de celle-ci telle que le moment de charnière. C'est pourquoi il est difficile d'agir sur l'allongement de la surface qui, pourtant, pourrait augmenter l'incidence maximum admissible. Mais, en diminuant l'envergure au profit de la corde, on augmente l'écart des centres de poussée en fonction du nombre de Mach et, par conséquent, on dégrade le moment de charnière. Cet artifice a été, néanmoins, employé avec succès pour des missiles évoluant dans un domaine réduit de vitesses. Pour la grande majorité des missiles tactiques qui doivent rester efficaces, aussi bien en subsonique qu'en supersonique, il ne peut en être question. (Pl. 9 - 10)

En observant la formule donnant l'incidence locale de la gouverne, on voit que si l'on ne peut agir sur l'effet de braquage, il doit être possible de diminuer l'effet de l'incidence. Supposons que l'on dispose une surface fixée devant la gouverne. En l'absence de braquage, la gouverne se trouve soumise à la déflexion de la surface qui la précède ; son incidence est donc inférieure à celle qui lui était appliquée précédemment. Le braquage se superpose donc à une incidence plus faible, et l'on peut écrire :

$\alpha_g = \alpha_\infty (1 - \epsilon / \alpha_\infty) + K \delta$ Ce qui est gagné sur l'incidence pourra se reporter sur le braquage. Si l'on prend les mêmes valeurs que précédemment $\delta/\alpha = 1,3$ $\alpha_{gmax} = 17^\circ$ $K = 0,6$ avec un ϵ/α_0 de 0,6.

L'incidence d'équilibre maximum deviendra $\alpha_{eqmax} = 14,4^\circ$

Ce qui montre par rapport à l'exemple numérique du paragraphe 4 tout le gain amené par ce dispositif.

Il est bien évident que l'application de celui-ci, outre une optimisation de l'ensemble empenage fixe - gouverne, a nécessité une refonte complète de la configuration du missile car l'adjonction de la surface fixe en amont de gouvernes déstabilise le missile et doit être compensée par une augmentation de la surface arrière.

6 - MOMENT DE CHARNIERE.

Si l'efficacité des gouvernes était suffisante pour la première génération de missiles canard, il a déjà fallu pour celle-ci essayer de minimiser le moment de charnière.

Celui-ci est le produit de la portance de la gouverne par la distance du centre de poussée à son axe. On ne peut évidemment agir sur la portance de la gouverne puisqu'elle conditionne les caractéristiques du missile. Il reste donc à agir sur le centre de poussée.

Celui-ci est fonction de l'incidence, du braquage et du nombre de Mach, tout au moins quand la portance varie encore linéairement avec l'incidence. Les influences de l'incidence et du braquage sont négligeables devant celle du nombre de Mach, sauf dans certains cas particuliers dans lesquels le missile vole à un nombre de Mach presque constant. C'est sur la variation du centre de poussée, en fonction du nombre de Mach qu'il va falloir agir. Si le missile doit être piloté aussi bien en subsonique qu'en supersonique, il convient de rapprocher les centres de poussée entre eux. Nous avons vu précédemment que les centres de poussée reculaient constamment en fonction du nombre de Mach. Une idée émise par le Dr. ANTON, alors responsable de l'aérodynamique à la Société MATRA, a été de limiter le recul du centre de poussée en supersonique en accolant deux surfaces de caractéristiques de portance opposées pour former une seule gouverne. En effet, si une surface d'allongement de 1 à 2 a un gradient de portance autour de l'incidence nulle, décroissant en supersonique, celui d'une surface de très faible allongement 0,2 - 0,3, croît constamment. Les deux surfaces combinées donnent la gouverne composite de la planche 11. Sa portance est légèrement inférieure en subsonique et en transsonique à celle d'une gouverne simple de surface équivalente mais lui est sensiblement égale en supersonique et devient légèrement supérieure pour les nombres de Mach élevés.

Les centres de poussée de la gouverne simple et de la gouverne composite (planche 12) sont pratiquement confondus en subsonique. En transsonique, celui de la gouverne composite s'écarte plus de l'axe que celui de la gouverne simple, mais, ensuite, il s'en rapproche d'une façon continue, tandis que l'autre s'en éloigne.

C'est cette forme de courbe qui est bénéfique puisque le bras de levier de la force diminue lorsque augmente la pression dynamique.

Les calculs de moment de charnière effectués à l'aide des données précédentes, pour une altitude constante, mettent en évidence le gain apporté par cette solution. (pl. 13)

Ce calcul a été donné comme exemple, mais une optimisation de la gouverne en fonction des caractéristiques demandées, est possible en agissant sur l'importance relative des différentes parties de la gouverne composite, ainsi que sur la forme de la partie II (planche 12).

La méthode de calcul employée pour déterminer les caractéristiques de portance et de centre de poussée de la gouverne composite a consisté à considérer les deux surfaces comme indépendantes, mais la deuxième soumise à la déflexion de la première, la première étant la partie I de très faible allongement.

Le gradient de portance à l'incidence nulle de la gouverne peut s'écrire :

$$\left(\frac{dC_z}{d\alpha} \right)_g = \left(\frac{dC_z}{d\alpha} \right)_I + \left(\frac{dC_z}{d\alpha} \right)_{II} (1 - k \varepsilon / \alpha_I)$$

Le foyer correspondant s'écrit alors :

$$X_{fg} = \frac{\left(\frac{dC_z}{d\alpha} \right)_{II} \cdot X_{fII} + \left(\frac{dC_z}{d\alpha} \right)_{I} \cdot X_{fI}}{\left(\frac{dC_z}{d\alpha} \right)_g}$$

k étant un paramètre qui dépend de la géométrie des deux surfaces.

Les résultats d'essais en soufflerie ont confirmé le bien fondé du raisonnement ayant conduit à l'établissement de cette gouverne composite et validé suffisamment la méthode de calcul employée, pour permettre d'effectuer une première approche d'optimisation. La mise au point définitive de la gouverne se faisant ensuite en soufflerie.

Sur la planche 14 est donnée la comparaison de la position des centres de poussée calculée et expérimentale obtenue pour une gouverne de ce type. Le calcul est favorable en transsonique, mais le niveau de pression dynamique ne rend pas cette zone critique, par contre, pour les fortes pressions dynamiques, les résultats expérimentaux sont meilleurs que les prévisions.

Les premiers tirs de missiles expérimentaux munis de ce type de gouvernes datent de 1954. Elles sont encore en ce moment utilisées sur des missiles modernes. Cette technique, qui consiste à corriger l'évolution des caractéristiques d'une gouverne dont la surface et la forme ont été déterminées pour répondre aux conditions de stabilité et de manoeuvrabilité du missile par l'adjonction d'une petite surface auxiliaire, a été largement utilisée depuis, aussi bien sur nos missiles canard que sur nos missiles classiques.

Lorsque la gouverne est soumise à la déflexion et au sillage d'une aile ou d'un empennage fixe, les méthodes de calculs ne sont plus assez précises pour appréhender le problème du moment de charnière et l'optimisation ne peut plus se faire qu'expérimentalement.

7 - CONCLUSION.

Nous avons dû, dès le début de la mise au point de missiles par la Société MATRA, nous intéresser de très près aux caractéristiques des gouvernes. Les premières configurations étant canard, il est apparu rapidement qu'il était nécessaire, pour avoir la maniabilité escomptée, de réduire au maximum le moment de charnière. Plus tard cette nécessité s'est aussi fait sentir pour les missiles classiques eux-mêmes.

La solution adoptée a été la mise au point de gouvernes composites pour lesquelles les caractéristiques de la surface principale étaient corrigées à l'aide d'une surface auxiliaire dont la position ou les caractéristiques propres étaient choisies pour donner un effet dans le sens désiré.

Cette technique a également été employée, mais en considérant deux surfaces séparées, pour obtenir de meilleures performances en manoeuvrabilité du missile en configuration canard. Nous avons été amenés à décharger la gouverne en la soumettant à la déflexion d'une surface fixe ; cette diminution de l'effet d'incidence a eu pour corollaire l'augmentation de celui du braquage et, par conséquent, l'amélioration des incidences d'équilibre du missile.

Ces diverses améliorations, apportées aux caractéristiques des gouvernes, ont grandement contribué à la mise au point de configurations aérodynamiques de missiles modernes très performants.

AD-A079 292 ADVISORY GROUP FOR AEROSPACE RESEARCH & DEV. NEUILLY-SUR-SEINE FR F/G 1/
AERODYNAMIC CHARACTERISTICS OF CONTROLS CONFERENCE PROCEEDINGS
SEP 79

UNCLASSIFIED

AGARD-CP-262

N/L

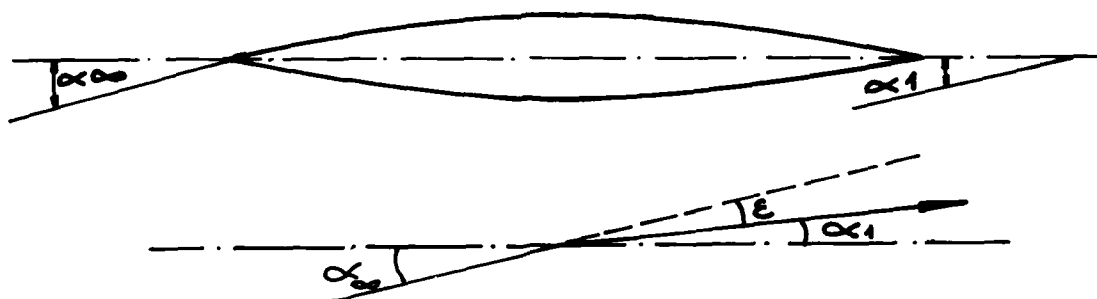
6 x 6

AGARD

CP-262



END
DATE
FILMED
12-81
DTIC

EFFET DE DEFLEXION

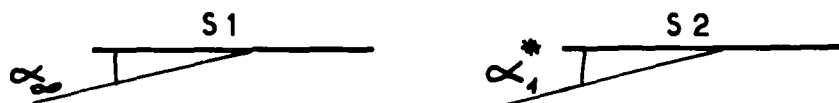
α_{∞} : ANGLE DE LA DIRECTION DE L'ÉCOULEMENT
A L'INFINI AMONT AVEC LA SURFACE
CONSIDEREE

α_1 : ANGLE DE LA DIRECTION DE L'ÉCOULEMENT
A L'AVAL DE LA SURFACE AVEC CELLE CI

ϵ : ANGLE DE DEFLEXION

$$\alpha_1 = \alpha_{\infty} - \epsilon = \alpha_{\infty} \left(1 - \frac{\epsilon}{\alpha_{\infty}}\right)$$

$$\epsilon = f(M, \lambda_1)$$

INCIDENCE SUR UNE SURFACE DEFLECHIE

$$\alpha_1^* = \alpha_{\infty} \left(1 - \frac{\epsilon^*}{\alpha_{\infty}}\right) \quad \epsilon^* = g(M, \lambda_1, A_1, A_2, E_1, E_2)$$

A_1, A_2 : AIRES DES SURFACES PORTANTES

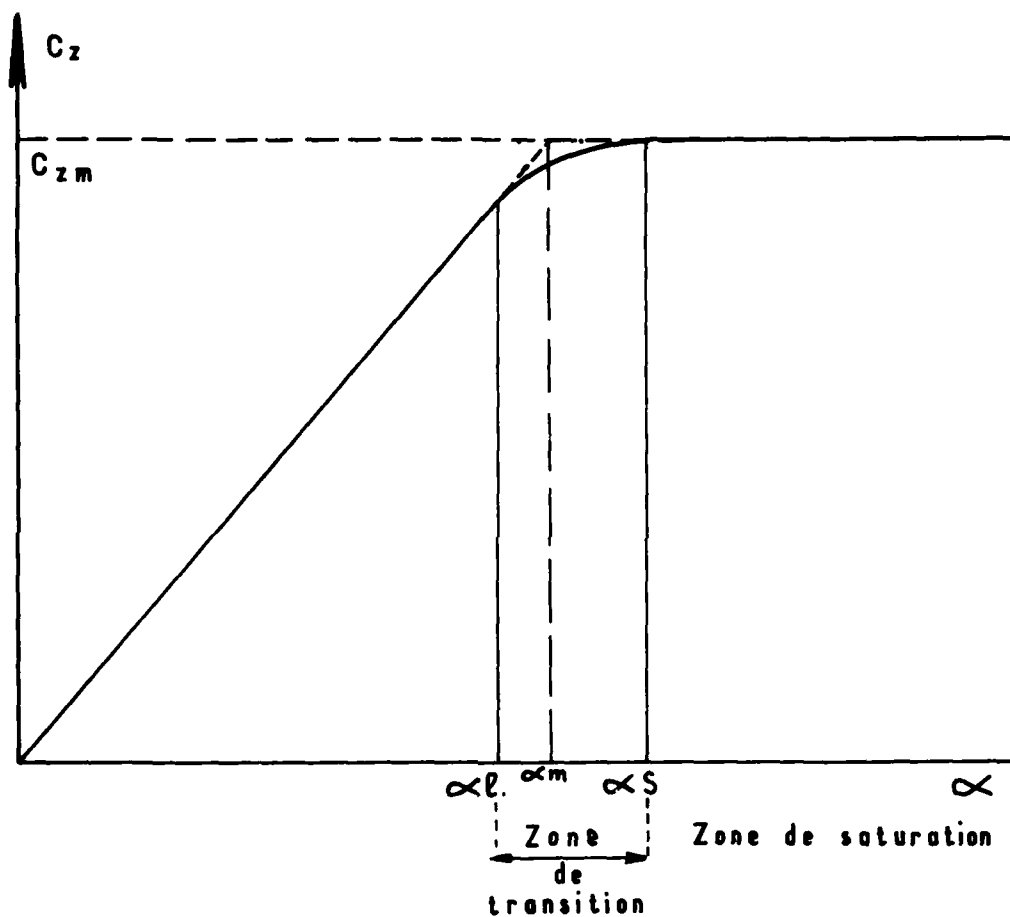
E_1, E_2 : ENVERGURE DES SURFACES PORTANTES

λ : ALLONGEMENT DE LA SURFACE $\lambda = E^2/A$

M : NOMBRE DE MACH

PLANCHE : 2

PORTANCE SCHEMATIQUE D'UNE SURFACE DE FAIBLE
ALLONGEMENT



C_{zm} : COEFFICIENT DE PORTANCE MAXIMUM DE LA SURFACE

α_m : INCIDENCE MAXIMUM UTILE DE LA SURFACE

$$C_{zm} = f(\lambda, M)$$

REPARTITION DE PRESSION SUR UNE CORDE
AVANT ET PENDANT LA SATURATION —

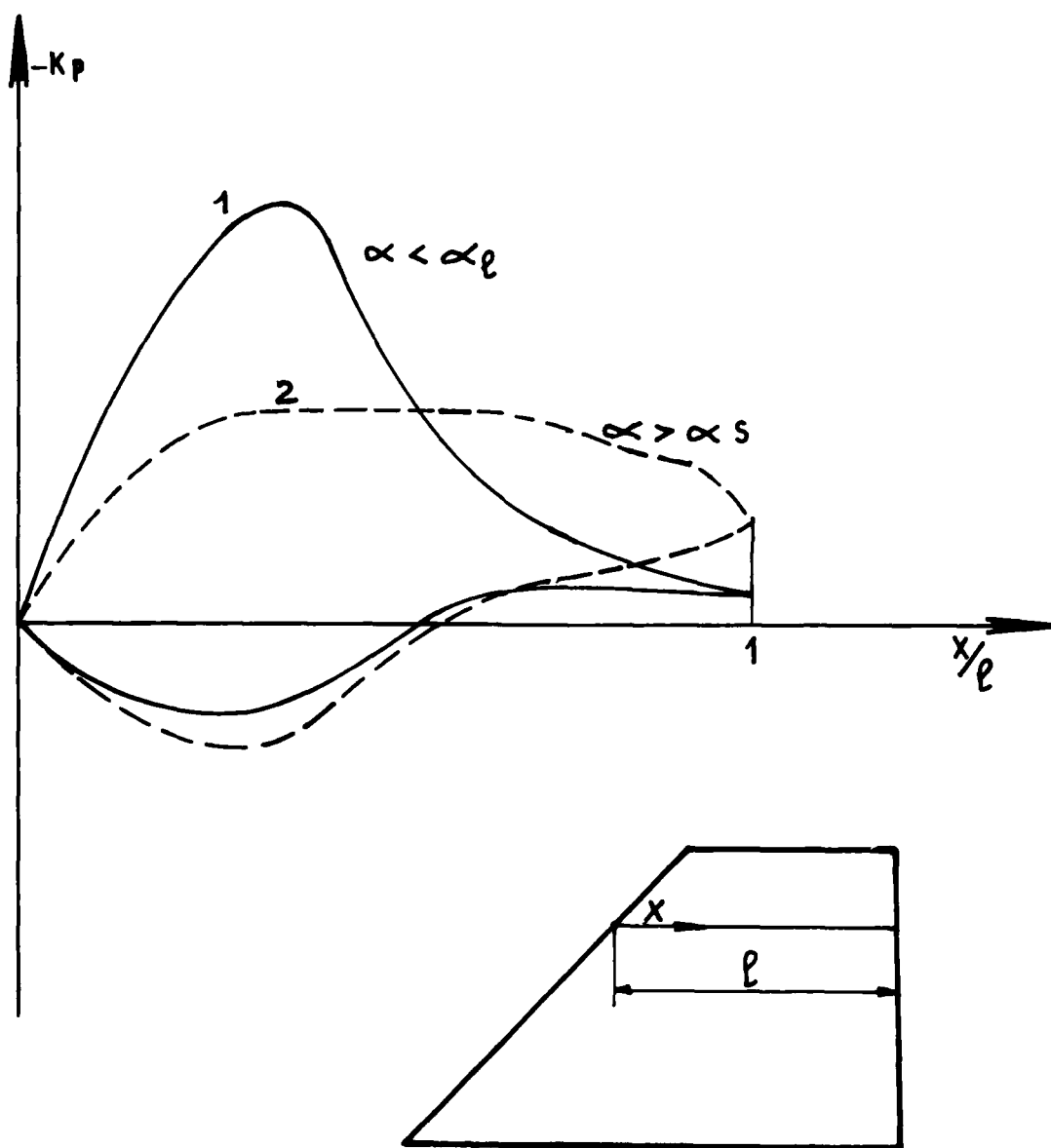
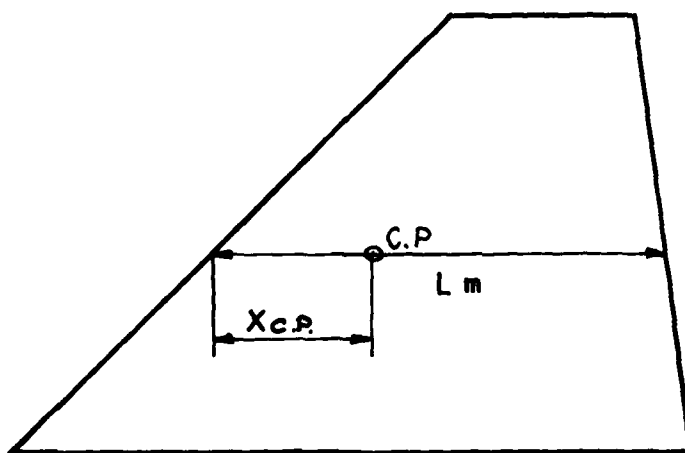
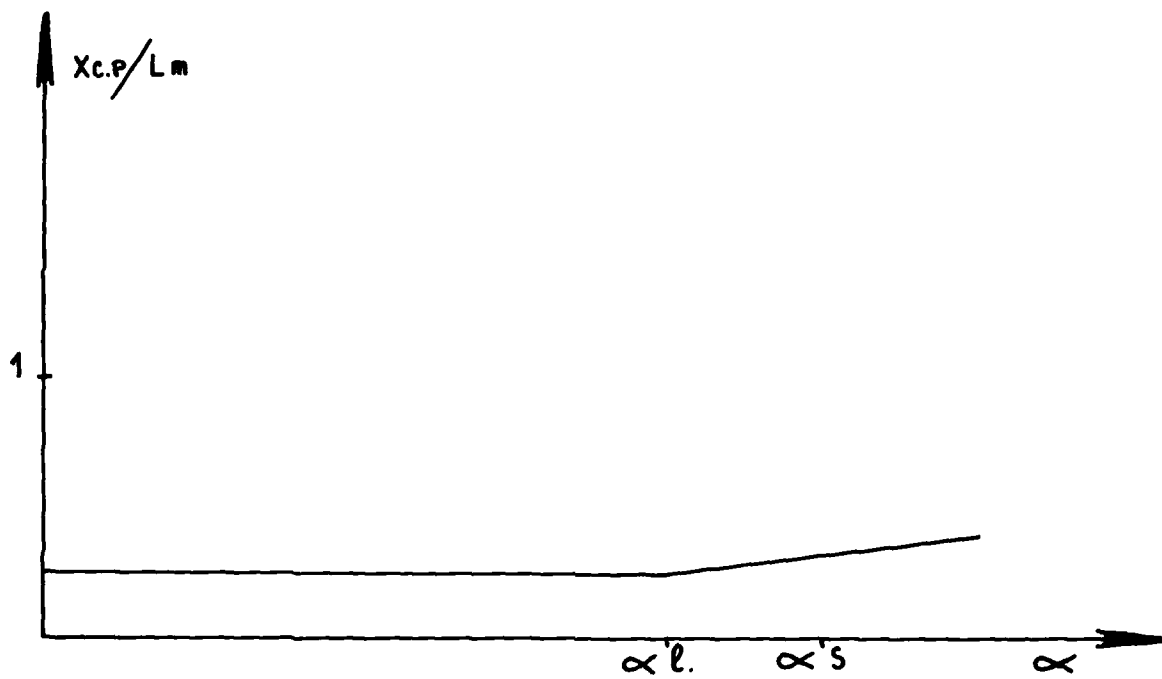
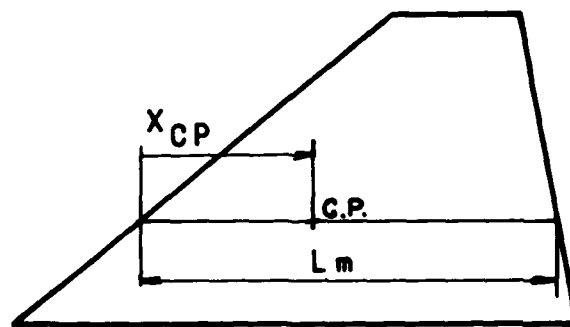
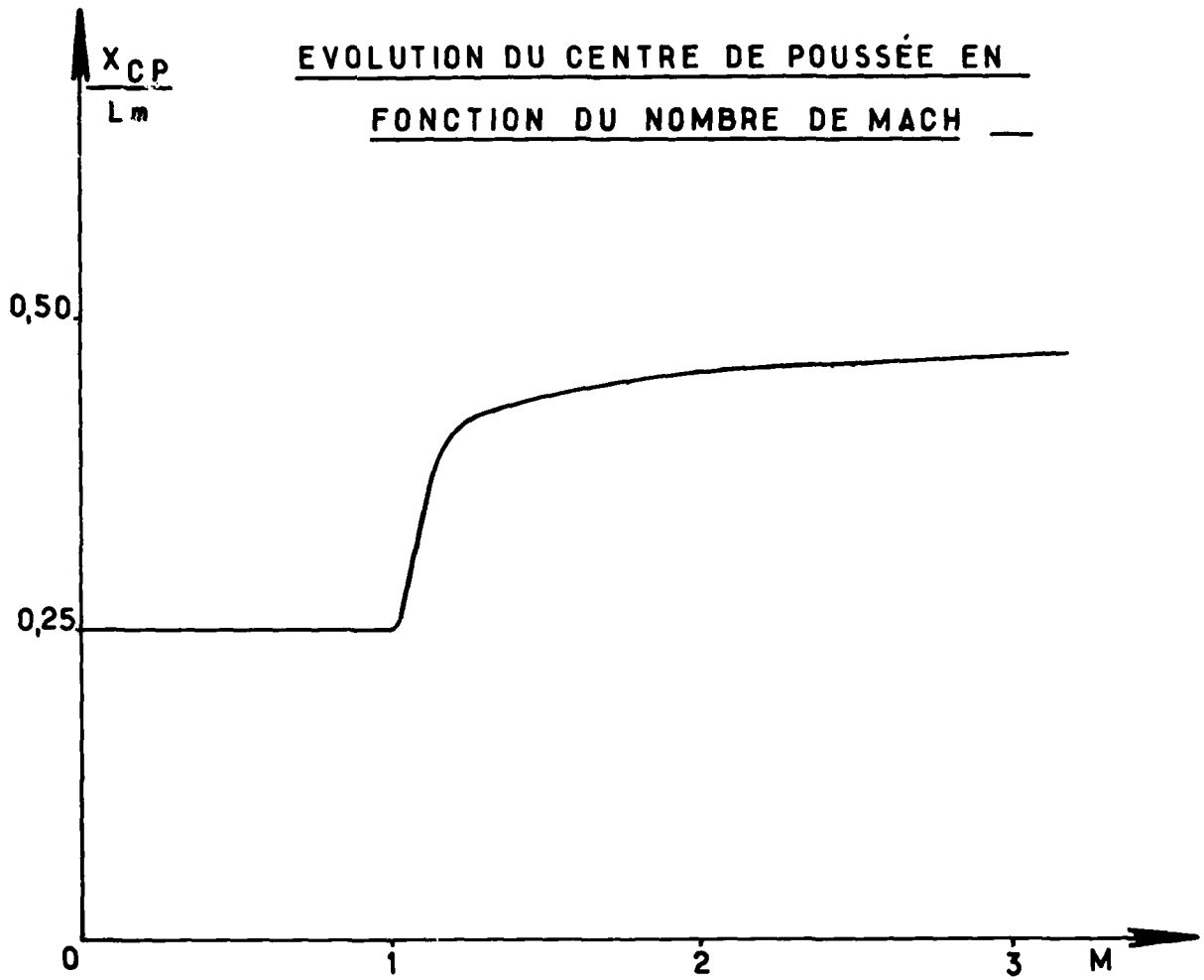
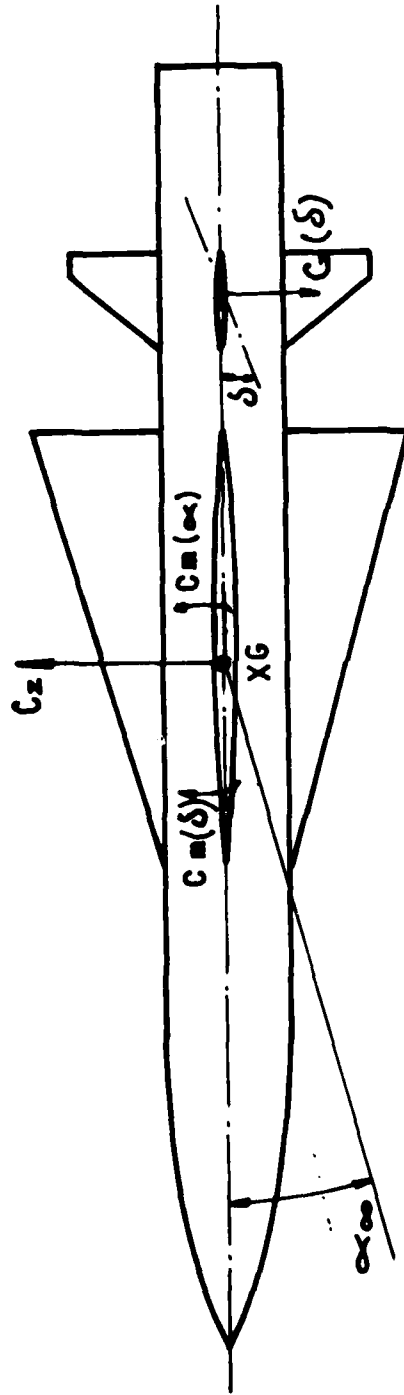


PLANCHE : 4

EVOLUTION DU CENTRE DE POUSSEE AVEC
L'INCIDENCE —



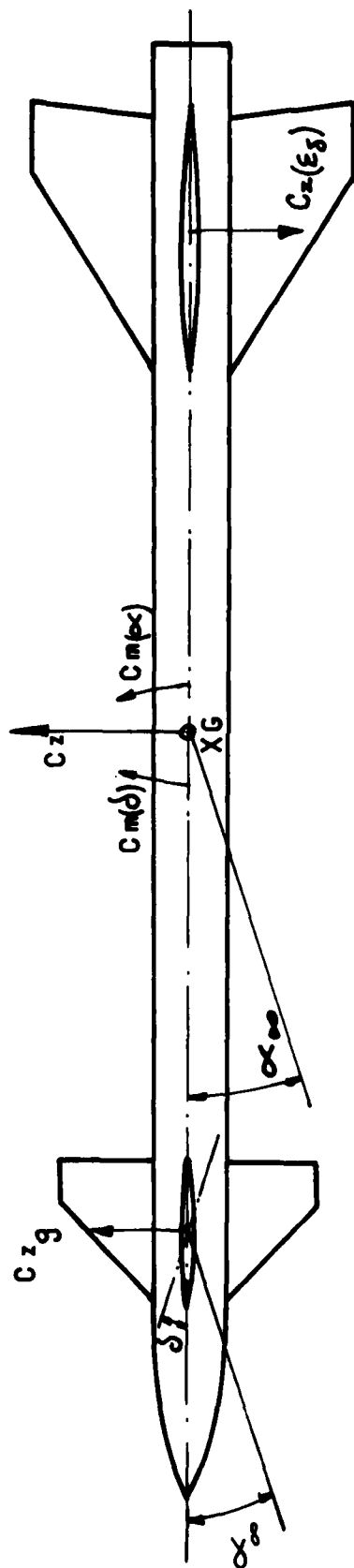
CONFIGURATION 'CLASSIQUE'



$$\alpha_g = \alpha_\infty (1 - \epsilon_g / \alpha_\infty) - K \delta$$

α_g : INCIDENCE LOCALE MOYENNE SUR LA GOVERNE

PLANCHE : 7

CONFIGURATION "CANARD"

$$\alpha_8 = \alpha_{\infty} + K_1 \delta$$

MOMENT D'UN MISSILE A CONFIGURATION

29-13

CANARD —

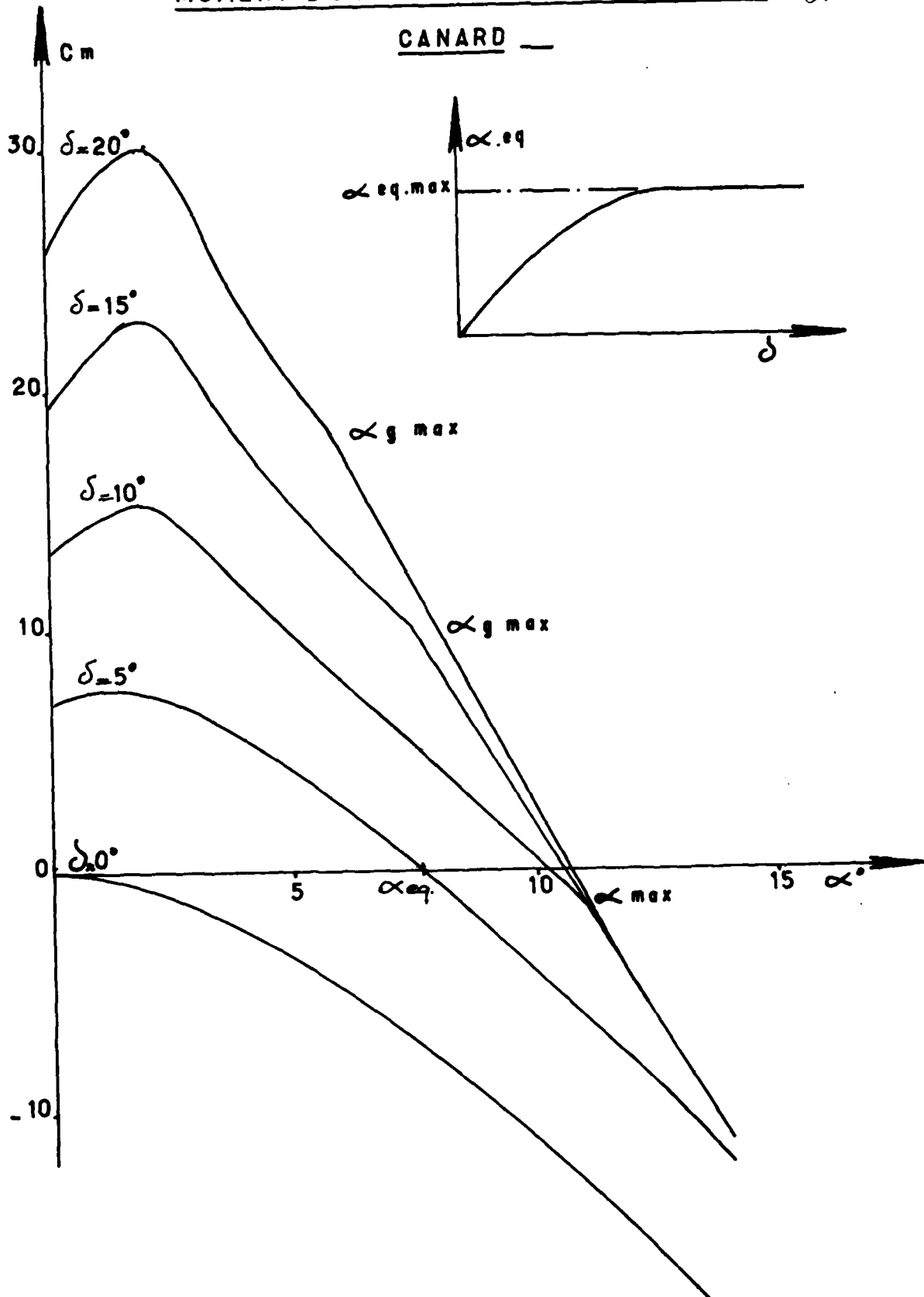
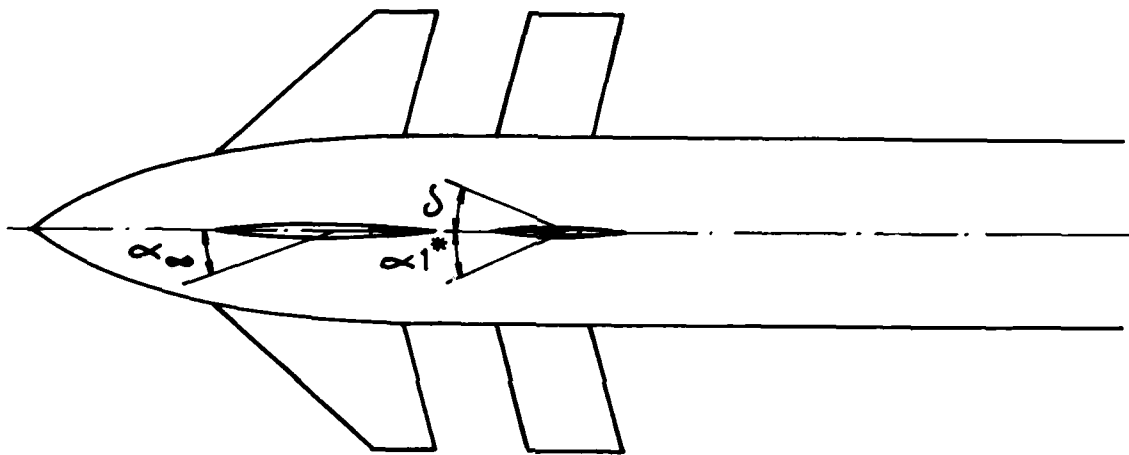


PLANCHE: 9

CONFIGURATION A DOUBLE EMPENNAGE

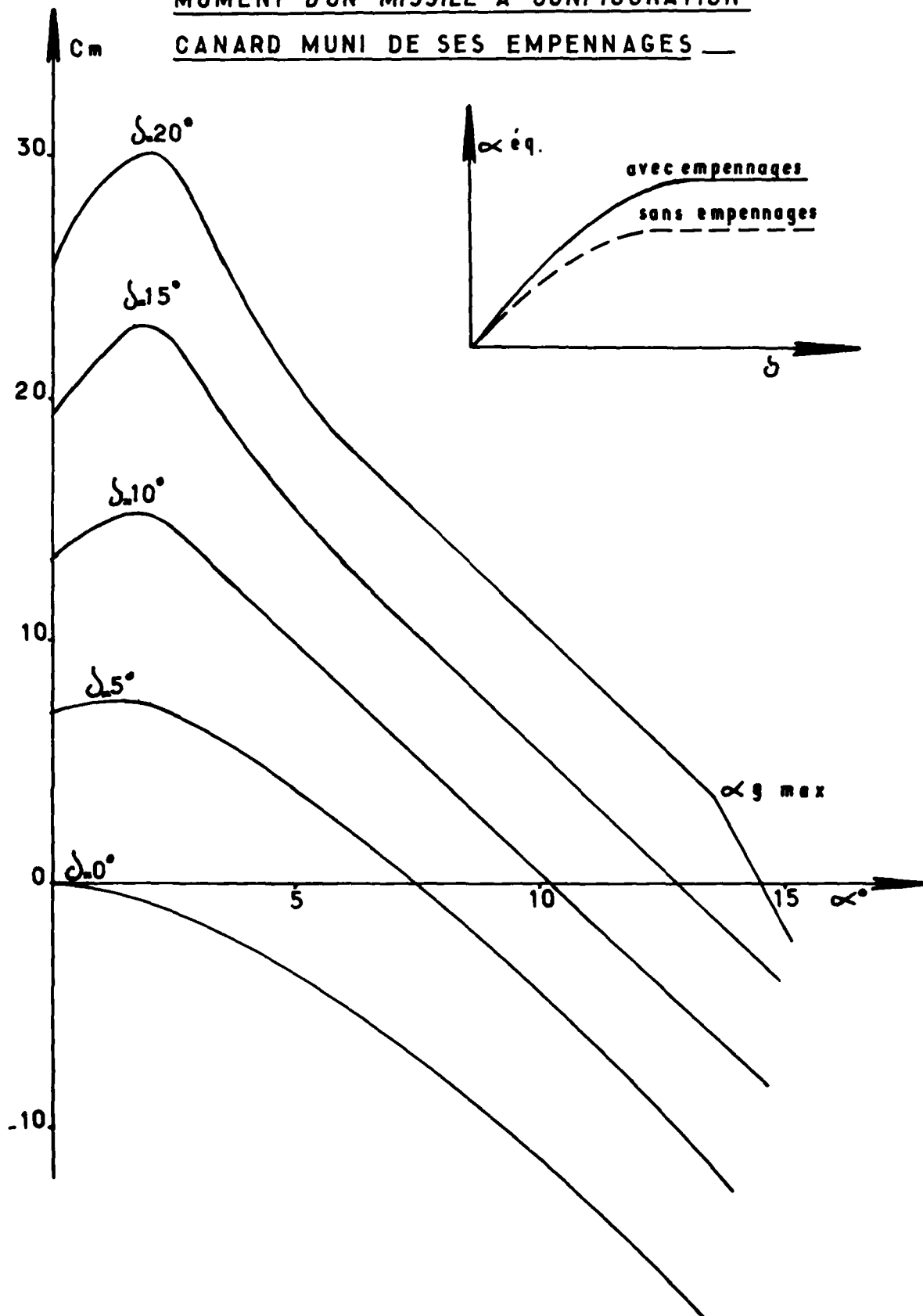
$$\alpha_1^* = \alpha_\infty \left(1 - \frac{\varepsilon^*}{\alpha_\infty} \right)$$

$$\alpha_g = \alpha_1^* + K \cdot \delta$$

$$\alpha_g = \alpha_\infty \left(1 - \frac{\varepsilon^*}{\alpha_\infty} \right) + K \cdot \delta$$

PLANCHE : 10

MOMENT D'UN MISSILE A CONFIGURATION
CANARD MUNI DE SES EMPENNAGES —



GRADIENTS DE PORTANCE

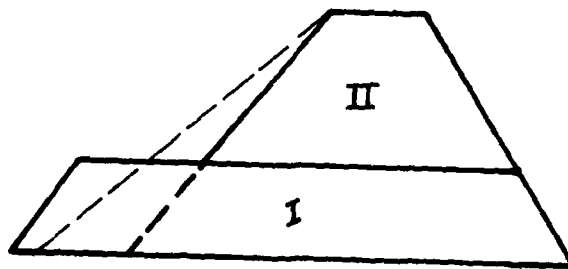
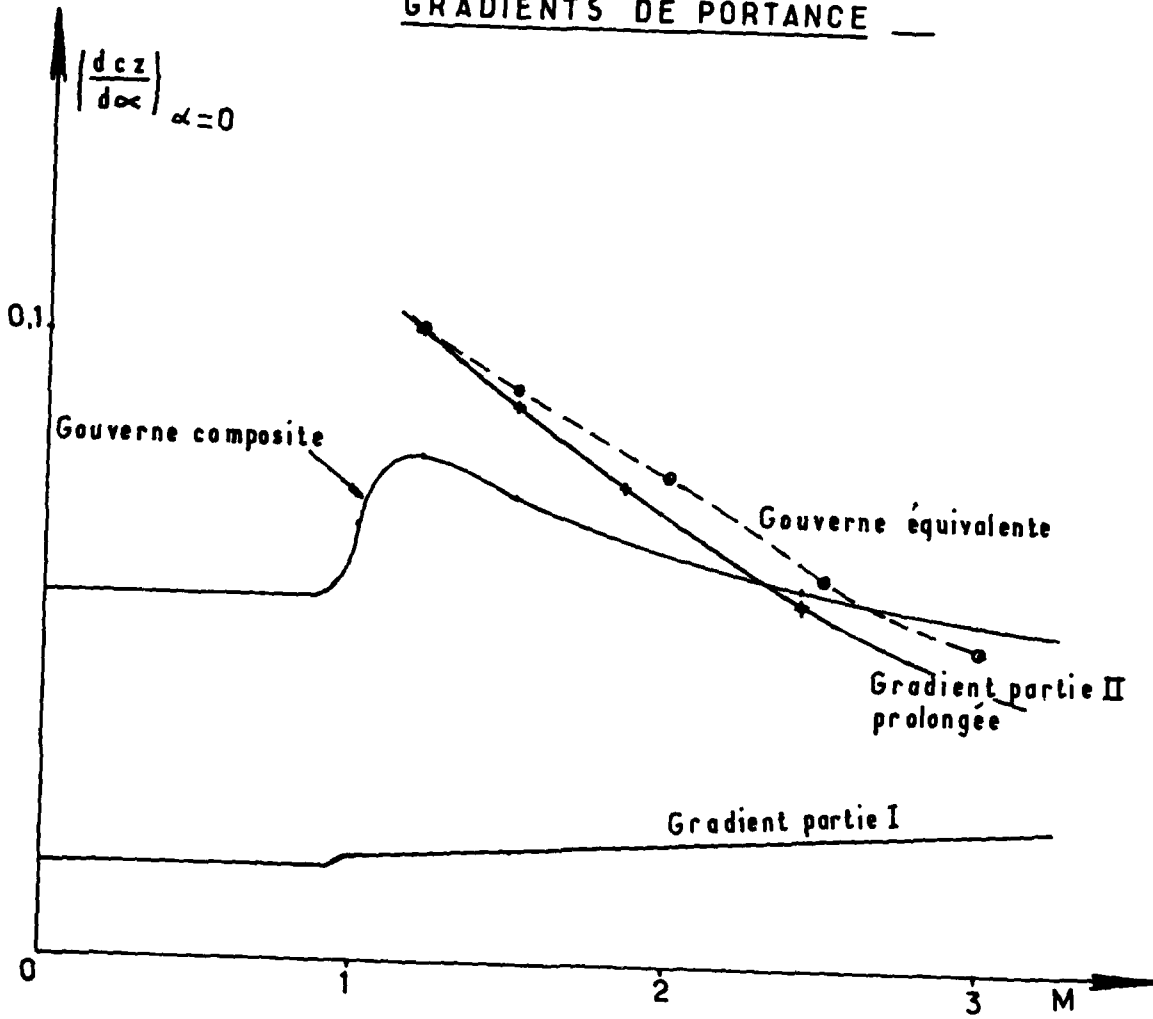
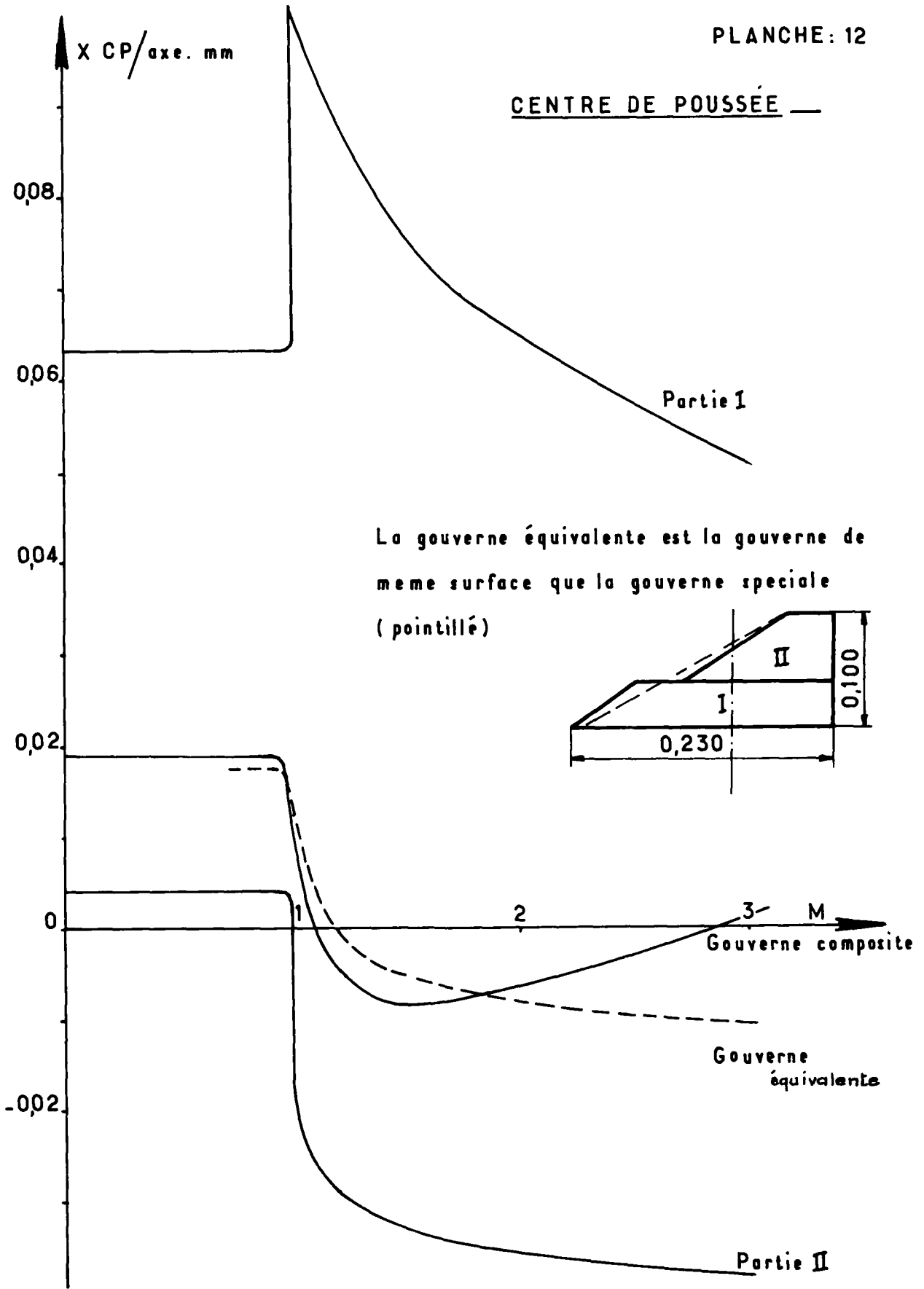
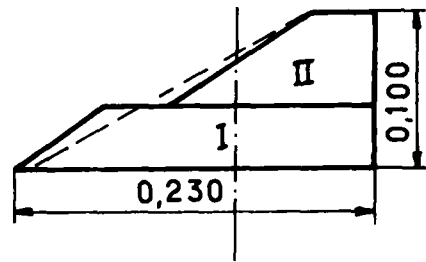


PLANCHE: 12

CENTRE DE POUSSÉE —



La gouverne équivalente est la gouverne de
meme surface que la gouverne speciale
(pointillé)



Gouverne composite

Gouverne
équivalente

Partie II

MOMENT DE CHARNIERE DE LA GOVERNE
PAR DEGRÉ D'INCIDENCE GOVERNE —

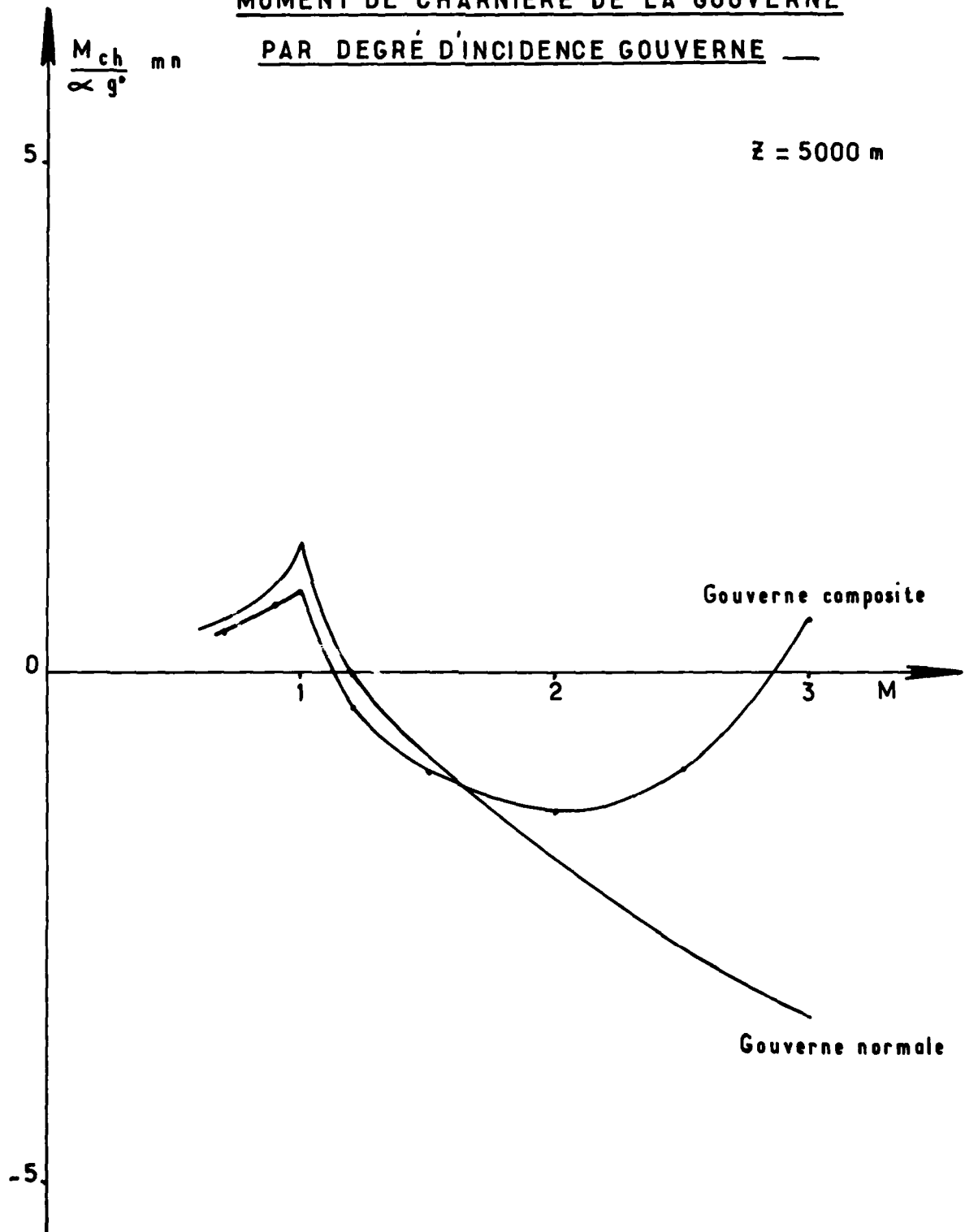
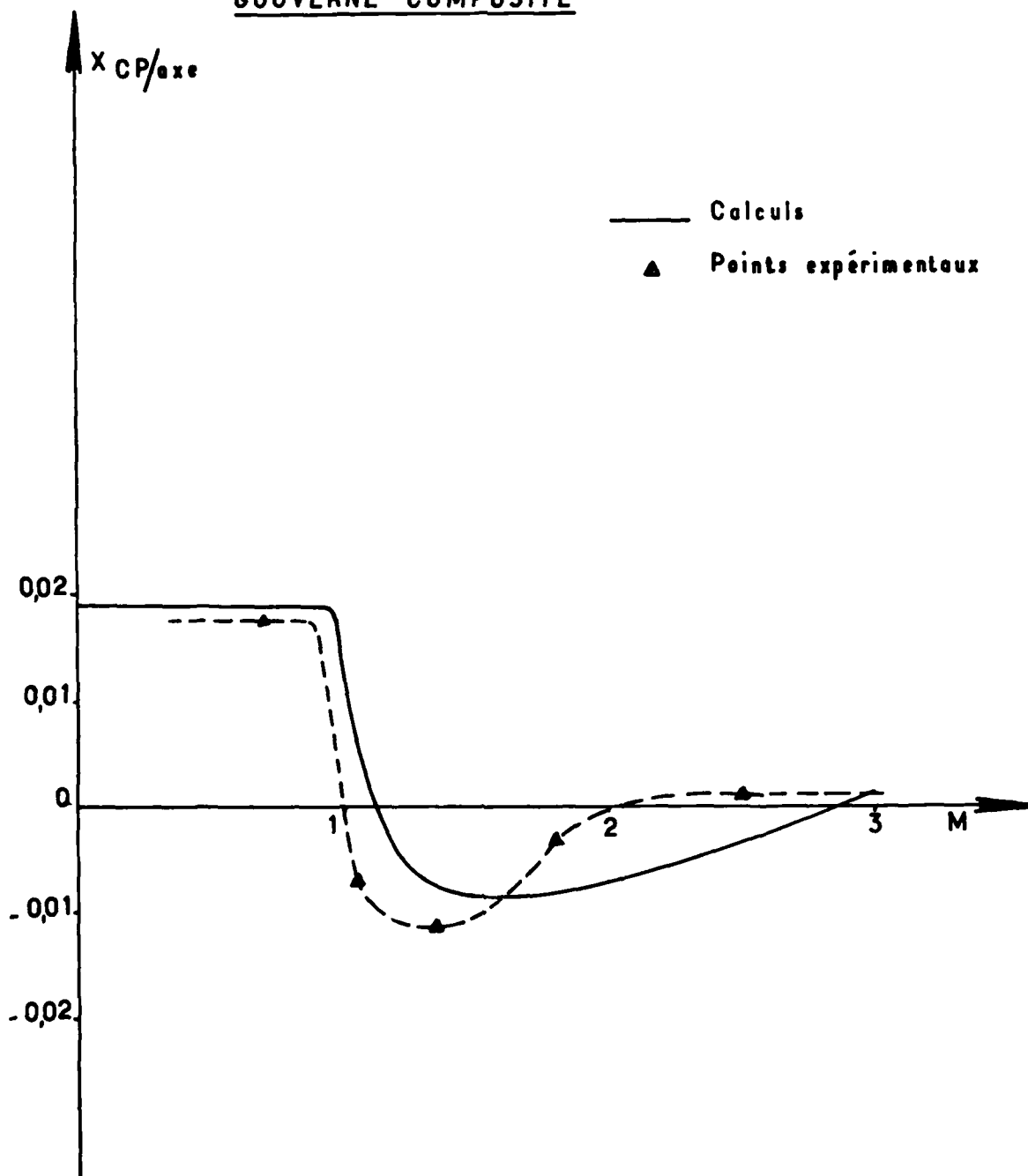


PLANCHE : 14

COMPARAISON DES CENTRES DE POUSSÉE
CALCULÉS ET EXPERIMENTAUX D'UNE
GOVERNE COMPOSITE



SOME INVESTIGATIONS CONCERNING THE EFFECTS OF GAPS
AND VORTEX GENERATORS ON ELEVATOR EFFICIENCY AND
OF LANDING FLAP SWEEP ON AERODYNAMIC CHARACTERISTICS

30-1

by

Herbert Neppert
and
Richard Sanderson

Aerodynamics Department
Messerschmitt-Bölkow-Blohm GmbH
Commercial Aircraft Division Hamburg
2103 Hamburg 95, West Germany

SUMMARY

This paper presents results from both small and full-scale wind tunnel models tested during the development programmes of the Hamburger Flugzeugbau HFB 320 Hansa Jet and the Airbus Industrie A300. The following problem areas are considered:

- Effect of gaps and vortex generators on elevator effectiveness and drag. A tailplane which had been designed to give satisfactory longitudinal stability can still have controllability short-falls in elevator power for rotation or demonstration of V_S . In order to increase the elevator effectiveness, slots or vortex generators upstream of the elevator hinge line can be introduced, this however also increases the cruise drag.
- Effect of single rudder deflection on the effectiveness of a split rudder. The installation of a yaw damper leads, in general, to incorporation of a split rudder to cater for the failure case when one rudder is blocked.
- Finally, wind tunnel results and proposals for improving the aerodynamic characteristics by means of a reduction in the sweep on the landing flap hinge line are described.

SYMBOLS AND NOTATION

A. Geometric

$S; S_t; S_F$ Wing; tailplane; fin reference area
 $b; b_t; b_F$ Wing; tailplane; fin span
 $c; c_t; c_F$ local wing; tailplane; fin chord
 $\bar{c}; \bar{c}_t; \bar{c}_F$ Wing; tailplane; fin reference chord $(= \frac{1}{S; S_t; S_F} \int (c; c_t; c_F)^2 \cdot dy)$
 S_e elevator area
 c_e local elevator chord
 \bar{c}_e elevator reference chord $(= \frac{1}{S_e} \int c_e^2 \cdot dy)$
 A aspect ratio $(= \frac{b^2}{S}; \frac{b_t^2}{S_t}; \frac{b_F^2}{S_F})$
 λ taper ratio
 Λ_{25} 25 % sweep
 Γ dihedral
 δ_t flap angle
 i_t tailplane setting angle - see sketch

δ_e elevator angle - see sketch
 δ_r rudder angle, see fig. 7

B. Aerodynamic

$C_{L_t}; C_{D_t}$	lift; drag coefficient of tailplane ($= L_t; D_t / q_\infty \cdot S_t$)	
$C_{L_{max}}$	wing maximum lift coefficient ($= L_{max} / q_\infty \cdot S$)	
C_{Y_F}	fin sideforce coefficient, see fig. 7 ($= Y_F / q_\infty \cdot S_F$)	
C_{m_t}	tailplane pitching moment referenced to 25% \bar{c}_t ($= M_{y_t} / q_\infty \cdot S_t \cdot \bar{c}_t$)	} see sketch
C_{N_e}	elevator normal force coefficient ($= N_e / q_\infty \cdot S_t$)	
C_h	elevator hinge moment ($= H / q_\infty \cdot S_e \cdot \bar{c}_e$)	
V_T	flow velocity, at tailplane	
α_T	wind direction at tailplane measured from fuselage datum	
α_t	incidence of tailplane to local wind direction ($= i_t + \alpha_T$)	
$C_{p_{1,2}}$	pressure coefficient, see fig. 6 ($= \frac{P_{1,2} - P_\infty}{q_\infty}$)	
V_∞	free stream velocity	
α_∞	incidence	
q_∞	free stream dynamic pressure	
β_∞	angle of yaw, see fig. 12	
R	Reynolds number based on $\bar{c}; \bar{c}_t; \bar{c}_F$	
M	Mach number	
$C_{n\beta}$	yaw moment due to sideslip ($\partial C_n / \partial \beta$)	} $C_n; C_l = \frac{M_z; M_x}{S q_\infty b / 2}$ (referenced to 25% \bar{c} projected on to the root chord)
$C_{l\beta}$	roll moment due to sideslip ($\partial C_l / \partial \beta$)	

1. EFFECT OF GAPS AND VORTEX GENERATORS ON ELEVATOR EFFICIENCY

1.1 Introduction

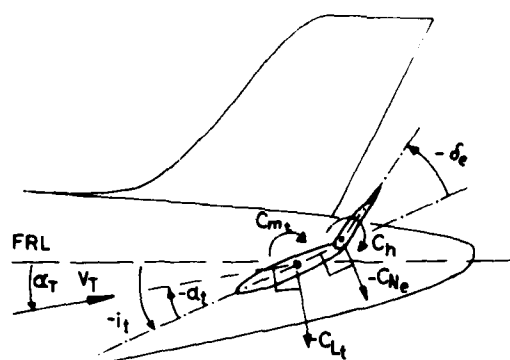
A tailplane which is designed to give the required longitudinal stability can still have problems in delivering the necessary elevator power for rotation or for demonstration of V_g particularly at forward c.g. This latter is particularly critical when stall-fixing devices such as slat closing-plates are present which may provide a very effective pitch-down at the stall.

Particularly in the case of sealed control noses which have a low parasitic drag in cruise the elevator power may not be sufficient to rotate or the stick forces can be too large due to the early separation of the flow from the relatively sharp kink at the nose of the deflected elevator. Early separation of the deflected elevator may also occur when it lies in the low energy wake of a wide rear-body.

1.2 Geometry

Table 1 and fig. 1 show a summary of geometrical data and Reynolds numbers for the test configurations. The effects of vortex generators situated on the lower surface and of laminar separation effects at two Reynolds numbers were investigated on an isolated Tailplane I which had a symmetrical elevator nose and sealed gap aerodynamic balance.

The effect of elevator gap, vortex generators and laminar separation at one Reynolds number have been investigated on Tailplane II which was mounted on a rear-fuselage model. The distribution of the VG's was based on [1]. Due to the loads on the rear-



Definition of angles, forces and moments at the tail (rear fuselage model)

fuselage, the forces and moments on Tail II (fig. 2) are not directly comparable with those from Tail I (fig. 5).

It can be seen from the sketch which shows the definition of angles, forces and moments at the tail that α_T is the local flow angle at the tailplane referred to fuselage datum which is in itself dependent on the wing flow field. The flow angle for the isolated tailplane I is defined by α_t , fig. 5 and 6.

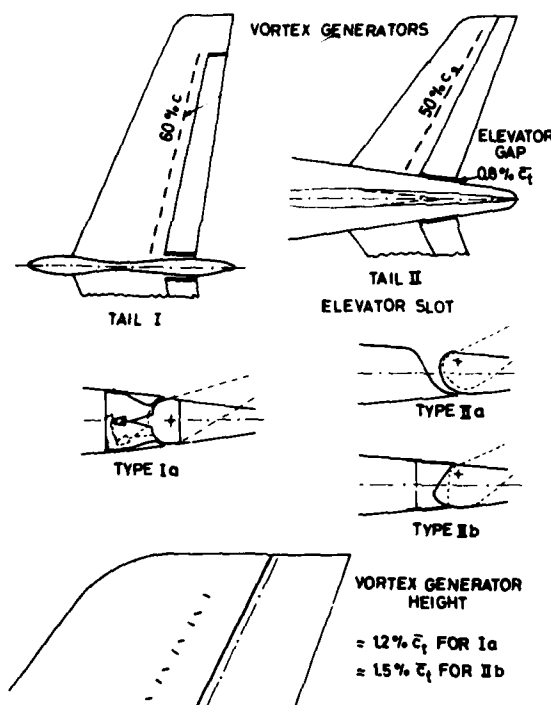


FIG 1. Geometry of tailplane and elevator nose and arrangements of vortex generators

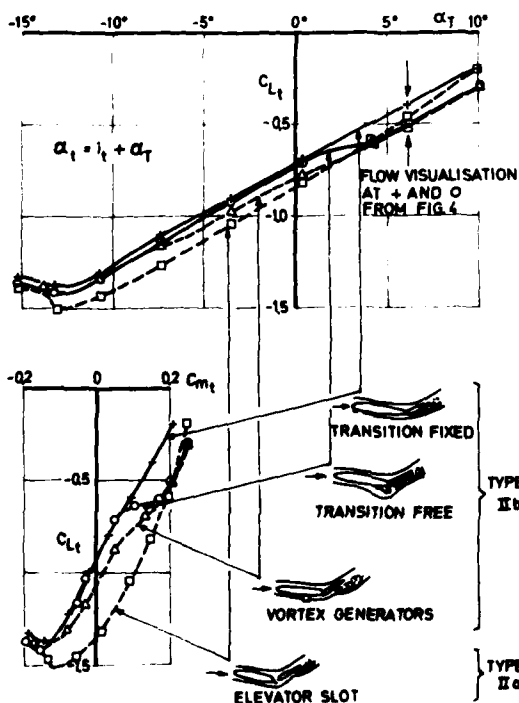
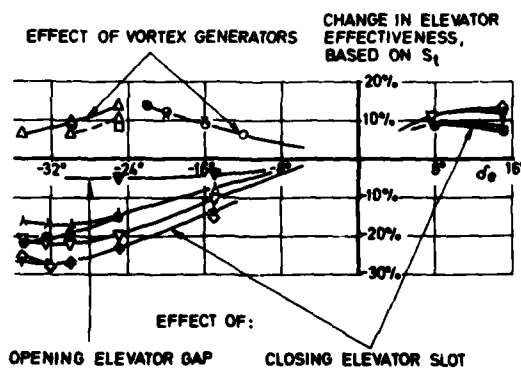


FIG 2. Effect of various flow-control devices on lift and pitching moment, based on S_t with turbulence screen, $d_e = -25^\circ$, $i_t = -2.5^\circ$



SYMBOL	TAIL CONFIGURATION	α_t	i_t	TURB. SCREEN	$R \cdot 10^{-6}$
Δ	DIFFERENCE BETWEEN IIb and IIa	0°	-25°	with	1.3
∇		-25°	-25°		
\circ		-10°	-25°		
\oplus		-25°	-12.5°		
\ominus		-10°	-12.5°		
∇	TYPE IIa	0°	-30°	with	1.3
Δ	TYPE IIb	0°	-25°	without	1.3
\circ		0°	-25°	with	
\square	TYPE Ia	-10°	-25°	without	4.5
\times		0°	-		

FIG 3. Effect of gaps, slots and vortex generators from Fig. 1 on elevator effectiveness

TYPE	TAIL			WING
	I	II	III	IV
Configuration	Tailplane alone	Rear fuselage model with tail		Wing alone
Profile	NACA 64A-010	NACA 64A-010 modified nose	NACA 64A-011	NACA 65A-1.5 13 NACA 63A-1.8 11
A	5.56	4.13	1.52	6.00
λ	0.43	0.44	0.40	0.33
Λ_{25}	20°	33°	40°	-15°
Γ	3°	6°	---	8° (6° at IV c)
Control, rudder or flap types	Ia without slot Fig. 1	IIa with slot IIb without slot Fig. 1	III Fig. 7	IVa one piece double slotted IVb two piece single slotted IVc one piece double slotted
Hinge axis	70 % c_t	70 % c_t	70 % c_F	Fig. 9 and 10
R based on \bar{c} , \bar{c}_t , \bar{c}_F	1.0 · 10 ⁶ HST (M ≈ 0.4) F+W-Emmen 4.5 · 10 ⁶ LST (M ≈ 0.2) F+W-Emmen	1.3 · 10 ⁶ LST (M ≈ 0.2) DFVLR-Braunschweig and Köln		1.5 · 10 ⁶ LST (M ≈ 0.2) INTA-Torrejon
Ref.	[3, 4, 5, 6]	[11]		[12]

Table 1. Summary of geometry and Reynolds number

1.3 Discussion of elevator effectiveness

Fig. 2 shows the lift and pitching moments for the tailplane II (with rear fuselage) at a fixed setting of $i_t = -2.5^\circ$ and $\delta_\theta = -25^\circ$. The Reynolds number of 1.3×10^6 is effectively increased through the use of a turbulence grid having a turbulence factor of 1.65. The effect of fixing the transition on the lower surface of the nose is clearly seen. Thus, with free transition there is a sharp increase in the effectiveness due to laminar separation at positive incidence; fixing the transition eliminates this separation. This effect termed 'control bubble effect' will be described later. Since the character of the boundary layer at model and full-scale are often very different due to surface roughness and Reynolds number, it is very easy to misinterpret elevator effectiveness as measured in the wind tunnel.

The introduction of vortex generators on the lower surface at 1/2-chord brings about an increase in effectiveness which gradually reduces with decreasing incidence. Finally, an elevator slot increases the effectiveness up to maximum lift.

Fig. 3 shows the percentage change in elevator effectiveness due to vortex generators, gaps and slots (defined in fig. 1) as a function of elevator angle. In this presentation, except for interference, the rear-fuselage component is eliminated.

The vortex generators increase the effectiveness on the full-scale model by up to 14 %, this being reduced somewhat in the tests at smaller Reynolds no. The gap between elevator and fuselage reduces the effectiveness by about 5 %. Some of the results at small Reynolds no. can, however, only be qualitatively considered; in particular vortex generator effects are very dependent on Reynolds no.

Closing the elevator slot results in losses of between 17 % and 27 % in effectiveness depending on the incidence and elevator angle. At positive elevator angles the effectiveness is increased by 7 % to 13 % because the large gap on the upper surface is eliminated. These values are summarised in Table 2 for small angles of incidence, α_t , referred to the tailplane area S_t . For the linear range up to $\delta_e \approx -15^\circ$:

$$\begin{aligned} \frac{\partial C_{L_t}}{\partial \delta_e} &= 1.65 \text{ for config. Ia} \\ &= 1.75 \text{ for config. IIa} \\ &= 1.60 \text{ for config. IIb} \end{aligned}$$

The effect on drag has been determined as an average value from various tests for a tailplane lift coefficient of around $C_{L_t} \approx -0.1$ (typical trimmed value). Thus for closing the elevator slot $\Delta C_D \approx -9 \times 10^{-4}$ and for opening the elevator-fuselage gap $\Delta C_D \approx 3 \times 10^{-4}$. Vortex generators increase the drag by $\Delta C_D \approx 10 \times 10^{-4}$.

Effects of closing elevator slot, opening elevator gap and vortex generators, based on S_t					
Effect from	Elevator effectiveness at δ_e				Drag ΔC_{D_t} at δ_e 0°
	-30°	-22°	-15°	15°	
Elevator slot IIb-IIa	-17 %	-12 %	- 8 %	12 %	-0,0009
Elevator gap IIa	- 5 %	- 5 %	- 4 %	---	0,0003
Vortex generators Ia, IIb	10 %	14 %	8 %	---	0,0010

Table 2. Change in effectiveness and drag of tailplanes
at small tail incidence α_t (Fig. 1 and 3)

1.4 Description of 'control bubble effect'

In fig. 4 oil flow pictures are shown for $\alpha_T \approx 6^\circ$ ($\approx \alpha_t \approx 3.5^\circ$) and $\delta_e = -25^\circ$. Referring back to fig. 2, these are values which lie in the region of the 'control bubble effect' (see difference between transition free and fixed). With free transition and positive incidence, a laminar boundary layer develops on the lower surface with an area of unregular separation. This region extends from forward of the kink of the deflected elevator and partially up to the kink and causes a reduction in pressure due to the effective increase in local camber. Thus an effective increase in elevator effectiveness is obtained. This can be seen as a sudden increase in (negative) lift in $C_{L_t} = f(\alpha_T)$ and a sudden nose-up jump in the moment curve, $C_{m_t} = f(C_{L_t})$ equivalent to $\Delta\delta_e \approx -4^\circ$, (see again fig. 2).

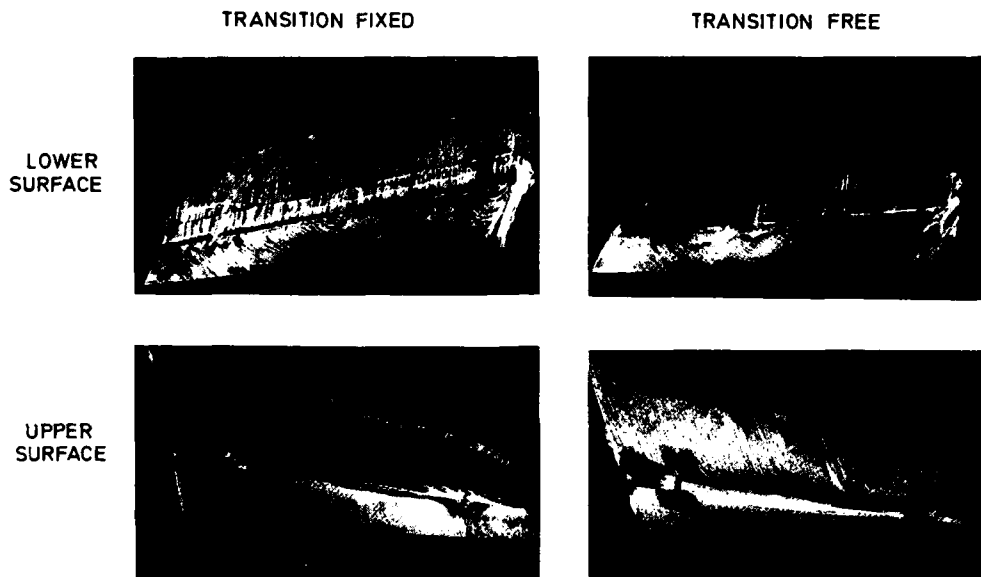


FIG 4. Flow visualisation from DFVLR-Braunschweig for Type II b, with turbulence screen (fixed transition: 0.3mm grit size, from 5% to 10% c_t on the upper and lower surface)

The lower surface first becomes fully turbulent at negative incidences and over the whole incidence range with fixed transition.

Figs. 5 and 6 show test results with the 'control bubble effect' at $\delta_e = -16^\circ$ [4, 5, 6]. The largest effects are in the range $\delta_e \approx -10^\circ$ to -35° with a maximum at about $\delta_e \approx -25^\circ$. The region of 'control bubble effect' is shaded. It is clear that only a modification to the lower surface has any effect and this expresses itself in the tailplane coefficients (C_{L_t} , C_{m_t} , etc.) as well as in the elevator coefficients (C_{N_e} , C_h). The reduction in drag probably comes mainly from the larger regime of laminar flow.

Thus summarising, two explanations can be ascribed to the data presented in fig. 2:

- The 'control bubble effect' is caused by a laminar separation which in turn creates a local increase in camber and thus reduced pressures on the lower surface. This is confirmed by the elevator forces and moments and the pressures, fig. 6
- The introduction of vortex generators or an elevator slot causes an increase in effectiveness which is coincidentally similar to that due to the bubble. In this

case however it is due to a reduction of the separation on the lower surface of the elevator and, for the slot, persists up to C_{Lmax} .

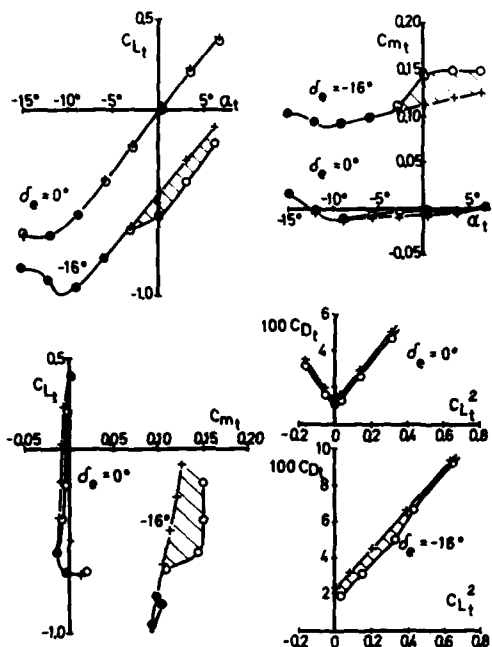


FIG 5. Control bubble effect on Type Ia (HST)
 o transition free
 + transition fixed at 5% c on lower surface

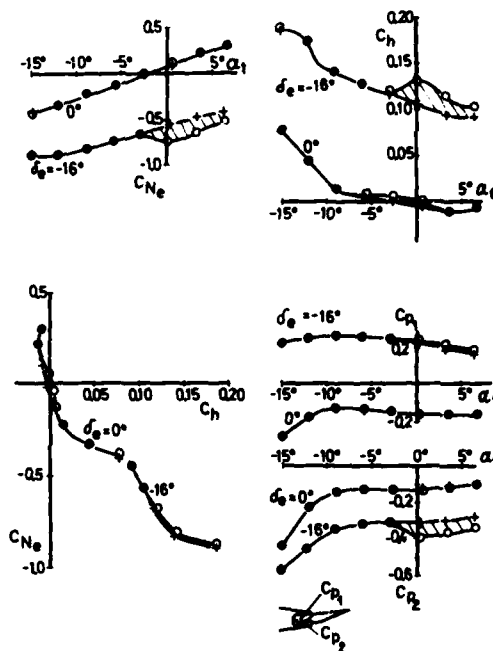


FIG 6. Control bubble effect on Type Ia (HST)
 o transition free
 + transition fixed at 5% c on lower surface

Table 3 summarises the 'control bubble effect' [2-11] and is valid for tailplanes, fins and ailerons under similar conditions. It can be seen that this effect occurs

Ref.	Profile	Hinge axis	$R \cdot 10^{-6}$	Geometric parameter	Control bubble effect
[9]	RAF30 symmetr.	80 % c	0.4 6.7	Maximum thickness relatively forward ↓	without ↓
[7]	Clark Y	80 % c	0.6		possible
[8, 10]	NACA 23012	80 % c	8.4		
[8]	G8409 symmetr.	50 % c	---		
[2]	NACA 65.3-618	80 % c	6.0	Maximum thickness relatively aft ↓	with ↓
	66(215)-216	80 % c 90 % c	6.0		
[4, 5, 6]	NACA 64A-010	70 % c	1.0		
[11]	NACA 64A-010	70 % c	1.3		
[3]	NACA 64A-010	70 % c	4.5	nose roughness	without

Table 3. Summary of control bubble effect

mainly on profiles with relatively aft location of maximum thickness (laminar profiles) at small positive incidence and negative control deflection. Only in the case where the leading edge is roughened or has a protuberance does this effect not occur.

Since it occurs in the wind tunnel at full-scale Reynolds no. of small aircraft and of larger aircraft in the take-off and landing configuration at speeds around the stall, it would seem only to be dependant on a long region of laminar flow which is in itself dependant on the profile and incidence (pressure gradient) and the surface roughness.

2. EFFECT OF SINGLE RUDDER DEFLECTION ON THE EFFECTIVENESS OF A SPLIT-RUDDER

2.1 Introduction

Insufficient directional stability can be cured by increasing the fin area or the fin arm. An alternative is to install a yaw damper which, however, in general, leads to the incorporation of a split-rudder to cater for the failure case. In order to obtain similar effectiveness for both rudder halves it was necessary in this case to locate the split at about 33 % of the fin span. However for other reasons the split had to be located at 38 % thus giving the lower rudder somewhat more effectiveness.

2.2 Geometry

Table 1 and fig. 7 show the geometrical data and Reynolds no. Fin III was mounted on a rear-fuselage model. The rudder nose was semi-circular and without balance. The effect of either a blocked upper or lower rudder with $\delta_{r1,2} = 0^\circ$ and 10° in the presence of a moveable rudder half has been investigated.

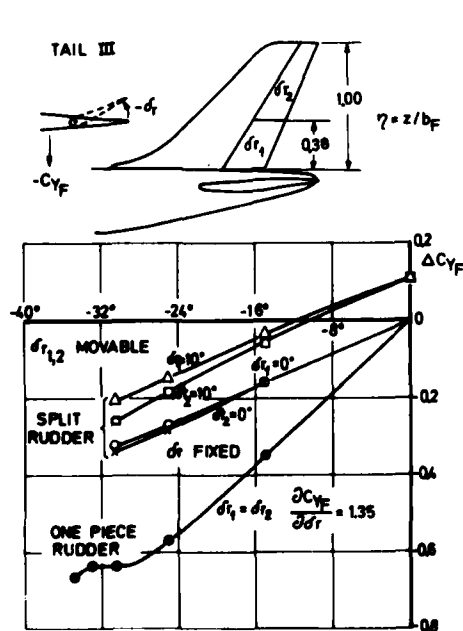


FIG 7. Comparison of split and one piece rudder effectiveness, based on S_F
 $i_t = -3^\circ, \alpha_{max} = \beta_{max} = \delta_\theta = 0^\circ$

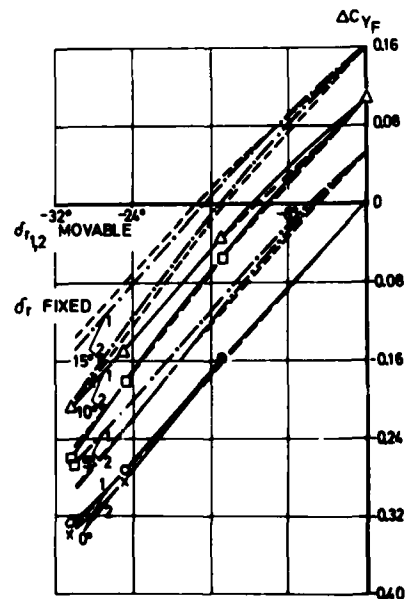


FIG 8. Split rudder effectiveness synthesis
 $i_t = -3^\circ, \alpha_{max} = \beta_{max} = \delta_\theta = 0^\circ$
 — tests results type III
 - - - inter- and extrapolations from $\delta_{r1,2} = 0^\circ$ and 10° (fixed)
 - · - · - approximation for ΔC_{Y_F} from equation in 2.3

2.3 Discussion of rudder effectiveness

Fig. 7 shows the effectiveness of the split-rudder in comparison to the original one-piece rudder. The lower rudder has a somewhat larger effectiveness - partly due to the split at 38 % but also possibly due to the end plate effect of the fuselage and tailplane. Through interpolation and extrapolation of the test results the curves in fig. 8 have been obtained for $\delta_{r1,2} = 5^\circ$ and 15° (fixed). An approximation has been developed for any required combination of fixed and movable rudder. Thus for the ranges of $\delta_{1,2} = 0^\circ$ to -15° (movable) and $\delta_{r1,2} = -15^\circ$ to -30° (movable) linear approximations have been derived. The error due to this approximation is very small up to $\delta_{r1,2} \approx -10^\circ$ (fixed). The following table shows the results:

30-9

	$\delta_{r1,2}$ (movable)	0° to -15°	-15° to -30°
ΔC_{YF} based on S_F	δ_{r2} (fixed)	$0.630\delta_{r1} + 0.613\delta_{r2}$	$0.630\delta_{r1} + (0.547\delta_{r1} + 0.756)\delta_{r2}$
	δ_{r1} (fixed)	$0.630\delta_{r2} + (0.613 - 0.482\delta_{r2})\delta_{r1}$	$0.630\delta_{r2} + 0.739\delta_{r1}$

3. EFFECT OF LANDING FLAP SWEEP ON AERODYNAMIC CHARACTERISTICS

3.1 Introduction

The lateral characteristics of swept wings whose flaps have swept hinge lines can be relatively strongly affected by flap extension. For instance, the rolling moment due to yaw of swept forward wing can be changed from stable to instable; in comparison that of a swept back wing can be made too stable with consequent dutch roll tendencies. Should a stability augmentation system not be desirable, a wing dihedral must be chosen which gives a satisfactory compromise in lateral characteristics between the flaps retracted and flaps extended case. As a further possibility the reduction of the sweep of the flap hinge line during the extension process has been investigated [12] in order to reduce the change in lateral characteristics.

3.2 Geometry

Table 1 and fig. 9 show the geometry of the isolated swept forward wing and flaps IVa and IVb as investigated in the wind tunnel. For this wing the dihedral was 8° , for the wing with flaps IVc, fig. 10, 6° . The expected aerodynamic characteristics of flap IVc which had a hinge line sweep of -16° are interpolated from flap IVa with -24° and IVb with -9° . Various advantages and disadvantages of forward sweep are summarised in [3].

3.3 Discussion of flap characteristics

Fig. 11 shows the measured $C_{L_{max}}$ and the lateral derivatives at the various flap settings for flaps IVa and b. The dashed line shows the expected values for flap IVc.

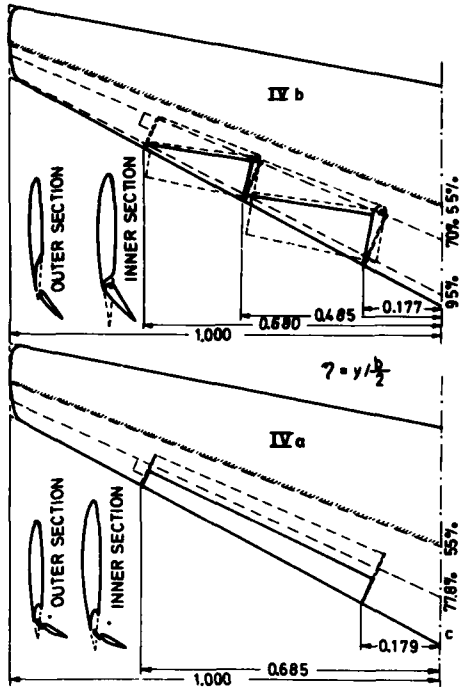


FIG 9. Windtunnel model geometries of trailing-edge flaps IVa and IVb

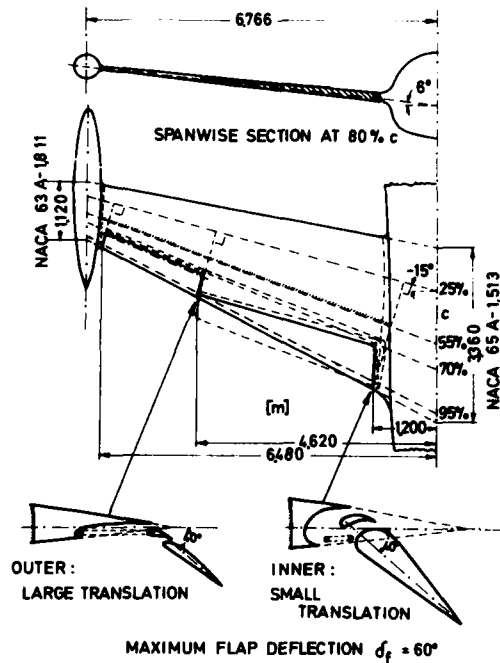


FIG 10. Planned trailing-edge flap geometry IVc (not windtunnel tested)

Extension of the double slotted flaps IVa to the landing setting produce a

$\Delta C_{L_{max}}$ of 0.8 (table 4). In comparison flaps IVb produce a $\Delta C_{L_{max}}$ of only 0.4, this loss being due to the division of the flaps into two segments and also due to them being single-slotted. For the single segment double slotted flaps IVc no loss is expected in comparison to flaps IVa.

The lateral derivatives are dramatically influenced by the sweep of the flap hinge line. Thus $C_{n\beta}$ and $C_{l\beta}$ which, with swept forward wings, tend to unstable values as a result of conventional flap extension (IVa) remain almost constant with extension of flaps IVb. The values are given for $\alpha_{\infty} = 4^\circ$, however similar tendencies are obtained from $\alpha_{\infty} = 0^\circ$ up to $\alpha C_{L_{max}}$. The large change in lateral derivatives for conventional flaps can be so explained that, with forward sweep the flaps on the wing yawed into-wind have a larger effective angle of sweep and are thus less effective as the flaps on the out-of-wind wing. With swept back wings the opposite is the case. Fig. 12 shows the lay-out of the flaps required to give the smallest change in the lateral derivatives for swept forward and swept back wings.

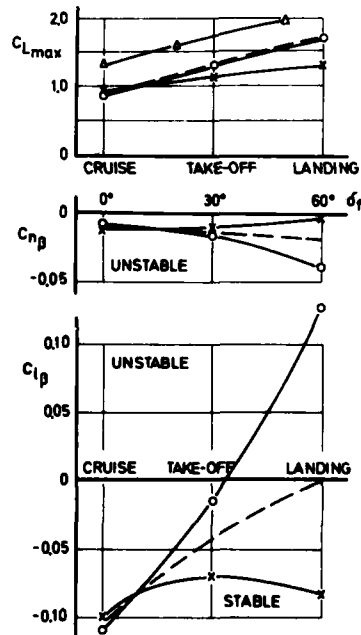


FIG 11. Effect on $C_{L_{max}}$, $C_{n\beta}$ and $C_{l\beta}$ due to translation of hinge axis from wing alone at $\alpha_{\infty} = 4^\circ$
 —○— one piece double slotted flap IVa
 —●— two piece simple slotted flap IVb
 - - - one piece double slotted flap IVc (expected values)
 —△— flight tests at $R \approx 7 \cdot 10^6$ with flap IVa

Effects on coefficients due to movement of the t.e. flap from cruise to landing position			
Fig. 11			
	Measured values		Expected values
Wing	IV a	IV b	IV c
Config.	One piece double slotted	Two piece single slotted	One piece double slotted
Sweep of hinge axis	-24°	-9°	-16°
$\Delta C_{L_{max}}$	0.8	0.4	0.8
$\Delta C_{n\beta}$	-0.03	+0.01	-0.01
$\Delta C_{l\beta}$	+0.24	+0.03	+0.11

Table 4. Measured and expected aerodynamic effects due to movement of trailing edge flaps from $\delta_f = 0^\circ \rightarrow 60^\circ$ for the example wing shown in Fig. 9 and 10

4. CONCLUSIONS

Incompressible effects of vortex generators, elevator slots and boundary layer on tailplanes and elevator effectiveness are described. At negative elevator angles vortex generators increase the elevator effectiveness by about 14 %; on the other hand closing the elevator slot reduces the effectiveness by 17 % to 27 % depending on the incidence. The changes in drag for a typical trimmed tailplane setting in cruise are around $\Delta C_D = \pm 10 \times 10^{-4}$ for the respective case (based on S_t).

The remaining effectiveness of a split rudder with either fixed lower or upper rudder is given. The change in $C_{n\beta}$ and $C_{l\beta}$ due to flap extension on swept wings can be greatly reduced by varying the sweep of the flap hinge line during extension. Thus the lateral derivatives can be improved compared to aircraft with conventional flaps.

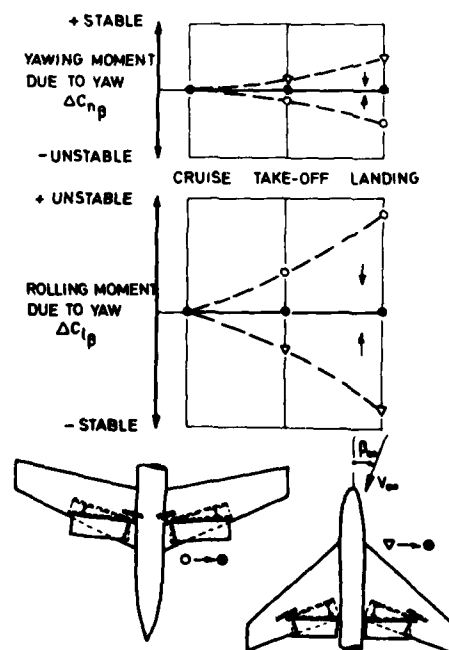


FIG 12. Effect of hinge axis sweep reduction \downarrow on lateral stability
 ---○--- sweep forward } conventional flaps
 ---△--- sweep back } without translation
 —●— reduction of hinge axis sweep

REFERENCES

- [1] Pearcy, H.H. Shock-induced separation and its prevention by design and boundary layer control.
In: Boundary Layer and Flow Control, edited by G.V. Lachmann, Vol 2, Pergamon Press, Oxford, London, New York, Paris (1961), pp. 1277 - 1312.
- [2] Abbott, I.H.
Doenhoff, A.E.
Stivers, L.S. Summary of airfoil data.
NACA Rep. No. 824, In: Annual Report 1945 of the NACA, pp. 460, 495, 499.
- [3] Kamber, H.
Fritschi, H. HFB-320, Höhenleitwerk-Halbmodell M 1:1 im großen Windkanal. Bericht FO913/I, II, III des Eidgenössischen Flugzeugwerkes Emmen (1968).
- [4] Kamber, H.
Niederer, P. HFB-320, Höhenrudermessungen im Transsonik-Kanal Bericht 698/I, II, III des Eidgenössischen Flugzeugwerkes Emmen (1963), S 30-51 in Band I und Beilage 6-12 in Band III.
- [5] Ehrmann, M.
Withop, P. Messungen im Transsonik-Kanal Emmen/Schweiz an einem Höhenleitwerkshalbmodell der HFB-320. HFB-Bericht TB Ae 63/10 (1963), pp. 18, 19 und 35 - 37.
- [6] Roederer, M. Mitt. DA TE 23-M-8/75 (1975)
- [7] Hoerner, S.F. Fluid-Dynamic Lift. Hoerner Fluid Dynamics, P.O. Box 342, Brick Town, N.J. 08723 (1975), pp. 5-4, 8-3.
- [8] Schlichting, H.
Truckenbrodt, E. Aerodynamik des Flugzeuges. Zweiter Band, 2. Auflage. Springer-Verlag Berlin, Heidelberg, New York (1969), pp. 438, 465.
- [9] Jacobs, E.N.
Pinkerton, R.M. Pressure distribution over a symmetrical airfoil section with trailing edge flaps. NACA Rep. No. 360 (1930).
- [10] Abbott, I.H.
Greenberg, H. Testing in the variable-density wind tunnel of the NACA 23012 airfoil with plain and split flaps.
NACA Rep. No. 661 (1939)
- [11] Neppert, H. A300-B10. Windkanalversuche am Leitwerksmodell 5 (rear fuselage model). MBB-Report UH-20-78 (1978)
- [12] Neppert, H. Vergleich zwischen Doppelspaltklappen und einer neuartigen Klappe. HFB-Report TB Ae 65/1 (1965)
- [13] Neppert, H. Spin investigation of the HANSA JET. Stall/Spin Problems of Military Aircraft. AGARD-CP-199 (1975), pp. 15B-1-7.

ROUND TABLE DISCUSSION

Chairman: Professor Young - UK: Ladies and Gentlemen, as you will see at this table are sitting various people who have very kindly given invited talks surveying different aspects of the subject. I am going to call on each in turn to offer their views as to what has emerged as a result of the Symposium of importance in their particular area of interest and what they see as the major problems in those areas to which they would like to draw attention and to which we should direct future research. Now let me just remind you who they are.

At my extreme right is Dr Jean Ross of the RAE, Farnborough, and she will survey what we have covered by way of experimental data. On her left, is Dr Körner of the DFVLR, Germany, and he will deal with the theoretical aspects of the subject. Then we have Dr Kehrer of Boeing, USA, who will look at the subject of novel controls for highly manoeuvrable aircraft. On my left, is Dr Johannes of the Wright-Patterson Air Force Base, USA who will survey what has been said about controls for ACT; and next to him Dr Scolatti of McDonnell Aircraft Company who will, I hope, deal with the subject of direct force controls. Last but not least is Philippe Poisson-Quinton of ONERA, France, who is going to offer some general comments on what we have covered. He claims that he is only a flight mechanics specialist, he is of course a senior member of the Flight Mechanics Panel. However, he is actually a very versatile aerodynamicist and can talk on most aspects of aerodynamics with great expertise; but for this morning he is going to look at what we have covered in a general way, particularly from the point of view of flight mechanics. Now, I am going to ask each one in turn to speak for perhaps five minutes and then we will call on you the participants to offer any comments or questions that you would like to raise. Please feel free to join in the discussion. The only inhibition on you is the fact that this discussion is being recorded so will you please, if you have anything to say, and I hope you will have a great deal to say, give your name and affiliation before you start. Without more ado I ask Dr Ross to speak first. Dr Ross:

Dr Ross - UK: I must begin by explaining that although I am attempting to review some of the experimental data that we have been learning about during the symposium, I am actually a user of such data, rather than a producer of it. Most of my work is involved with devising mathematical models of the aerodynamics to be used in flight dynamics problems, specifying the form of the mathematical model and numerical values to be used. I do have some experience in obtaining data from flight tests, and comparing them with results from wind-tunnels, but I cannot really comment on any of the experimental wind-tunnel techniques that have been described. Last Monday I tried to summarize the work areas that we thought needed attention. Looking through the conference papers I find that they have contributed some experimental information to most of the points we made, although there is still much more to be done. So I thought I would use the same headings for a few comments.

First, for correlation of the experimental data. We have had numerous examples of how difficult this will be. There have been contradictory findings, as far as I can judge, on the oscillatory characteristics of control surfaces and spoilers. There has been some attempt at correlating data on relatively simple cruciform control surfaces, and this has yielded some rather scattered results. We had flight and tunnel comparisons, some of which are so excellent, on the F 15 in particular, that we begin to wonder why they are so good, and some on other aircraft, for example the flap spoiler, where the discrepancies give us food for thought too. We certainly added to the data base of experimental results and also certainly on an ad hoc basis and so, as I say, the correlation is going to be very difficult.

Secondly, we had some papers describing flow fields and their associated interference effects and perhaps all I can say on these is that the nonlinearities and the unexpected results which have been demonstrated emphasize the need for more work. We did learn of some of the large interference effects for segmented flaps, for example, which will be important for active control technology applications.

Thirdly, we also asked for more data on novel controls and most of the remarks on these I will leave to Mr Scolatti. One point that I have found disappointing, is that we have not learned very much about ways of increasing effectiveness. We have all been aiming at achieving reasonable levels of control power, especially at high angle of attack, but we have examples of where we fall short of requirements. The paper describing the YC 14 blown surface flaps was really the only one which achieved anything in this direction. We had not mentioned dynamic effects as needing more experimental work, partly because I was unsure about the importance in regard to active control technology (although I hasten to add, except for systems delaying the onset of flutter or for load alleviation systems). In discussions I had detected uncertainty amongst others as well, about the frequency ranges that might be required and experimenters need to cover: perhaps this is a point for discussion and there might be some members of the audience with experience in this. Lastly, I have been encouraged to find that we have had some papers which take a whole problem from the wind-tunnel results, through simulation, and eventually to a flight test programme, testing one of the active control systems. Most of these have been on one particular system and so the problem of integrating them all remains, but I think the results that we have seen support the statement that Mr Thomas and I made at the beginning, that experimental data on control characteristics have increasing importance in this active control technology era. Thank you.

Professor Young - UK: Thank you Dr Ross. Well with those opening remarks, we can now look to the audience to offer any comments or questions but perhaps, before we do that, I should like to ask Mr Thomas if he has anything he would like to add to what Dr Ross has just said.

Mr Thomas - UK: Well, Dr Ross knows what she is and M. Poisson-Quinton knows what he is, I am afraid I don't know whether I am aerodynamicist or a flight dynamicist. Anyhow, be that as it may, I sit, I think, somewhat uneasily between the two fields so I would like to take up some points which will wander about, Mr Chairman, from the aerodynamics to the dynamics. I like to take up first the point that there has been an emphasis in this conference on what conventional

control can do in an ACT context. To direct the aerodynamic and the fluid dynamic research in the right direction we need to clarify the matter of whether there must be an emphasis on (1) increased effectiveness and (2) novel forms of control. Now and again in the course of the presentations, we were given the impression that there were deficiencies in certain areas, as regards the effectiveness. Something interesting has emerged on segmented control surfaces both spoiler and flap type and the question here I think is: have we achieved the most efficient means of distributing control action? Has giving a smooth surface to the control, any place in this connection.

More basically, in some of the investigations of the more novel controls, there seems to be a tendency to fall into one or two categories: one that aimed at understanding in a very basic and detailed way the flow, the other, the more ad hoc direct acquisition of data. What we need is a happy marriage of these two attitudes to get the best out of our work, especially as with present-day aircraft layouts the aerodynamic characteristics are so configuration dependent.

Another question not adequately addressed, is how strongly we feel about making available the capability of side-ways translation and rotation and if so the aerodynamic power requirements for these. There were a number of papers on canard layouts, and there was a suggestion that there may be no place for the canard in future designs. Perhaps this is so as a trimming and manoeuvring control in its present form, but this is surely only a way of saying to the aerodynamicists go back and have another think. In concentrating on the most difficult of our theoretical problems, we are all guilty of being somewhat complacent about the agreement of theory and experiment in those areas where the flow is more amenable to analysis. Professor Hancock's comments are timely and I would reinforce them. We must be careful of ignoring or dismissing discrepancies between windtunnel results and derivative obtained from flight data. Here, I found Mr Agnew's problem of the CM Delta E disturbing. Finally I was encouraged to hear Dr Johannes express the opinion that we still needed to know the aerodynamics to a high accuracy even if the design success depends somewhat less on the particular value. Thank you.

Professor Young – UK: Thank you. Well now has anyone got any particular comments or questions on the points that have been mentioned by Dr Ross and Mr Thomas. They touched on a number of quite important points and I am sure that there must be some strong feelings about them. If I may just remind you of one that Dr Ross raised; the uncertainty there is about the importance of dynamic effects and the frequency range to concentrate on. Would anyone like to comment on that?

Mr Back – UK: I think one of the messages which has come through to me is the uncertainty which we have on the dynamic effects of spoilers and if, in the future, we are looking for large amounts of load alleviation on the wing, maybe the only control we have available is the spoiler; and, in this respect, if we are not going to get adequate dynamic response from the spoiler we may have to re-think the total gain which is going to be available. This is one of the areas where, particularly in the civil market, one is looking for significant improvements in the future, and an adequate experimental background of dynamic response may not only be necessary from the tunnel, but also from adequate full scale investigations.

Professor Young – UK: Thank you Mr Back. Mr Thomas:

Mr Thomas – UK: On this question of the dynamic effects, if by that we mean unsteady effects, I think one thing is certain, that is, we need these to be included for flutter suppression; we may have to include them for load alleviation on the wing; we may also need them for ride control and things like that. Since we have at least one candidate for which we are pretty certain we need them, we have got to get them.

M. Destuynder – France: Je voudrais dire quelques mots en ce qui concerne les bandes de fréquence. Dans la plupart des exposés qui ont été faits on a parlé d'effets instationnaires mais qui restent du quasi stationnaire en ce sens que les forces induites sur l'aile par des spoilers ou par des gouvernes sont en phase avec les mouvements de ces gouvernes. Dans les problèmes de flottement ou l'on atteint des bandes de fréquences infiniment plus élevées, la notion de forces instationnaires prend tout son sens dans le fait qu'il faut introduire des phases, et le problème est très grave parce que si dans des contrôles de portance ou dans des contrôles, même de rafales, l'efficacité du contrôle, même si elle n'est pas absolue, apporte toujours quelque chose; dans les problèmes de flottement intervient une autre idée, c'est la notion de marge. Si le contrôle est inefficace, on perd l'avion cela veut dire que si la prévision est mauvaise on peut aller à une catastrophe. et dans ce sens les fréquences élevées sont infiniment plus difficiles à traiter, que ce soit en théorie ou en expérience, que les basses fréquences, que celles du contrôle de portance ou du contrôle de rafale, parce qu'elles font intervenir en plus des connaissances théoriques complexes sur les forces, des notions de transfert, (par exemple d'une servo commande qui pilotera le spoiler ou qui pilotera l'aileron). En plus elles ne peuvent agir que dans des bandes relativement étroites parce qu'il est impensable de faire un contrôle, par exemple de flottement, sur tous les modes de structures. C'est un non sens; on arrivera nécessairement à une instabilité de serait-ce que par le fait que la fonction de transfert d'une servo commande balayera tout le plan de fréquences et tout le plan des phases. C'est pour cela que je voudrais insister sur le découplage qui existe, à mon avis, entre les contrôles purement instationnaires, qui eux font appel à des notions de phases sur les forces, par rapport aux idées du contrôles stationnaires ou quasi stationnaire qui ont été développés jusqu'à présent. La notion de marge de sécurité qui n'intervient pratiquement pas dans les contrôles stationnaires ou quasi stationnaires est un élément nouveau qu'il faut faire rentrer en ligne de compte dans les phénomènes instationnaires à fréquences élevées, comme le contrôle du flottement.

I would like to say a few words on frequency bands. The authors of most of the papers presented at this meeting

have considered non-stationary effects which, however, remain quasi-stationary effects, because the forces generated on the wing by spoilers or control surfaces are in phase with the motions of these control surfaces. In flutter problems, where much higher frequency bands are reached, the notation of non-stationary forces becomes quite significant, as phases have to be introduced. The problem is very serious, because, while the efficiency of the control, even if not perfect, plays a part in lift, or even gust control, an additional notion has to be taken into account in flutter problems: the margin notion. If the control is inefficient, the aircraft is lost: that is to say, poor predictions may result in a disaster. Therefore, high frequencies are much more difficult to handle either theoretically or experimentally, than low frequencies as in lift or gust control because they imply, in addition, complex theoretical knowledge of forces and transfer (for instance, servo-control for the spoiler or the aileron). In addition, they can only operate within relatively narrow bands, as flutter control on all the structure modes, for instance, is out of the question. This is meaningless. We shall necessarily be led to unsteadiness, be it only due to the fact that the transfer function of a servo-control will sweep the whole frequency range and the whole phase range. For this reason, I would like to emphasize the de-coupling which exists, I think, between purely non-stationary controls, where force phases are taken into consideration, and stationary or quasi-stationary controls such as they have been developed so far. The safety margin notion, which does not have to be taken into account in stationary or quasi-stationary controls, is a new element which has to be borne in mind in high frequency non-stationary phenomena, such as flutter control.

Professor Young - UK: Thank you Mr Destuynder. Very interesting comment. Does anyone else wish to comment?
Dr Orlik Rückemann.

Dr Orlik-Rückemann - Canada: I would like to address the question of what kinds of control derivatives are needed for an efficient design of an active control system, how much of the information needed do we already have, and where should we go from here. From the information presented at this symposium it appears that the most needed control derivatives are the lift and hinge moment derivatives of oscillating controls; this includes the static as well as to some extent also the dynamic derivatives, that is derivatives with respect to the deflection of a control surface and to the rate of change of this deflection, respectively. Several speakers presented data on these derivatives, but in many cases rather large discrepancies were reported between the analytically predicted and the measured values. In an effort to clarify the reasons for these discrepancies, the in-phase and the out-of-phase pressure distributions on oscillating control surfaces (and spoilers) were measured, such as reported by Grenon for two-dimensional cases and by Destuynder and Mabey for three-dimensional ones. Experimental techniques for measuring the unsteady pressures on oscillating surfaces seem to be well in hand in several countries, such as in France, the UK and the Netherlands; however, the techniques to measure the control derivatives, especially the dynamic ones, are not so widely available and at the present time seem to be limited mainly to the UK. The existing analytical techniques appear fairly adequate for 2D subcritical cases, especially if corrections for thickness and boundary layer effects are included, even if we still do not know what agreement would be obtained in these conditions with regard to the total forces or total hinge moments. I suspect that some discrepancies would still remain. However, the overall situation in these cases is not too bad and any further improvements in our techniques would probably bring greatly diminishing returns.

The situation is much less satisfactory in three-dimensional cases and for supercritical flows: the data presented at the symposium showed that rather large discrepancies still exist even in pressure distributions and phase angles. Also indicated was the large effect that transition location may have on this type of data. Further work in these areas is certainly needed. In general, however, I wonder how far we should go in trying to improve our analytical or experimental methods before we ask ourselves the question of what level of agreement or accuracy we would be prepared to consider sufficient and acceptable. May be it could be useful at this time to conduct some kind of a sensitivity study of the type we discussed a year ago at the Symposium on Dynamic Stability Parameters in Athens, where the relative importance of various stability derivatives was assessed. So far I have not heard of any such attempts made in connection with control derivatives. Perhaps those of us who are involved in designing active control systems could conduct such a study without too much difficulty?

Professor Young - UK: Well perhaps we should move on to our next speaker and no doubt some of the important points that have been raised will come up again in the course of our discussions. I will now ask Dr Körner to offer his comments on the theoretical aspects of the subject that have emerged from our discussions.

Dr Körner - FRG: Only a few papers within this meeting have been concerned with theoretical work. This is specially valid for the development of new algorithms but it is also valid for the use of these methods for the design of control devices. Some more papers have been given where theoretical methods have been checked with the experimental results.

Now, as to new methods, I would draw your attention to the paper of Grenon, Desopper and Sides who have shown remarkable results achieved with the finite volume technique based on the Euler equations. They also showed theoretical results which incorporated unsteady boundary layer calculations evaluated with integral methods following the lines of Michel and I think these results given here for subsonic flow look quite promising. Nevertheless the question of the Kutta condition in these cases is still open. I would like to draw your attention to another paper, the paper by Gersten and Gluck, which showed the influence of shear flow on the characteristics of a wing. I think this pilot work is quite important since it gives us some impression how to incorporate this phenomenon into more complicated methods to calculate complex configurations. I hope that also current gap investigations will bring us similar framework which can be incorporated in more complicated methods.

Several authors have compared experimental investigations with theoretical results, but here the experimental part, I think, was more important than the theoretical part. Some very interesting results were given in Mabey's paper whose special merit lies in providing high quality data and who also shows the deficiencies still existing in linear subsonic theory especially the discrepancies in phase shift. This leads to a somewhat general comment as to the value of experimental results for theoretical methods. The first point is that we need experimental data for the clarification of the physics, learning where vortices exist, where a vortex bursts, what the phenomenology of shock-boundary-layer interaction is, etc. This clarification is necessary to establish appropriate models for theoretical methods. Secondly there is need for experimental data as pressure plots and forces for comparison with theory. Such experiments must give high quality data. A critical point here are the wind tunnel corrections especially at transonic speed.

When I come to summarize what is my impression I would again like to say what I said in my presentation at the beginning of this meeting on Monday. In my view for subsonic and supersonic flow powerful prediction methods on the basis of linear theory exist. Although there are still shortcomings due to a viscous-inviscid interaction, these methods are appropriate in the technical sense for estimation of lift-dependent data. As to the drag-dependent data, theories are still insufficient. In the transonic region, methods have been developed which have still large deficiencies and the question, what will be the most powerful methods for the future is still open. The strong viscous-inviscid interaction complicates the problem extremely. As to the leading edge vortex flow appropriate methods exist which give information for lift dependent data. For separate flow without primary structures the development of methods for the solution of Navier-Stokes equations for simple configurations is under way. Some special hybrid methods have their merits.

Now, what are the requirements for the future: As to theoretical methods it seems not appropriate to give a detailed catalogue of necessities since theories have not been discussed at this meeting in detail, but I would like to point out one thing, which seems most important to me. There is much need to have detailed theoretical and experimental investigations in problems where viscous-inviscid interaction occurs, especially investigations of separated flows, may be with primary structures, may be without primary structures. I think that these informations must be the basis to come forward in the evaluation of separated flow, the key-problem for us aerodynamicists for the future. The theoretical solutions given by Deiwert, Steger and Lomax and others show that there is a real way but we must not forget that it is necessary also to look after the physics, what we are doing there and how to model it in the right way. Therefore when I come back to Braunschweig on Monday, I will be in the Braunschweig low-speed wind tunnel for several days to look after the flow of some very strange wings. Thank you.

Professor Young – UK: Well Dr Körner raised a number of points of considerable interest. Has anyone got anything they would like to offer by way of comment or question? Seems not for the moment. In that case we will pass on to Mr Kehrer.

Mr Kehrer – USA: This has been a very interesting and rewarding symposium. My overall impression of the papers presented at the symposium, and I think that it is typical of most technical symposiums, is that for the most part the papers seem to generate more questions than answers. I think the papers that presented neatly packaged, conclusive, experimental or theoretical results were the exception rather than the rule. I am not intending, of course, to be critical, that is typical and I think is a very healthy situation. Whenever you delve into any specific area of technology you tend to open doors that lead into all sorts of avenues.

In our work at Boeing, in the military airplane organization, we are looking at some very unusual advanced aircraft. In these cases we tend to wave the magic wand called "active control" and say that this is the way we are going to solve all our problems. We are attempting for example to design aircraft that have no empennage surfaces at all, that is, no vertical and no horizontal surfaces to help stabilize the aircraft. So we are examining all sorts of strange controls to use to stabilize these vehicles. The problem that we see most of all is, and this has been commented on rather extensively here in the symposium, is the discouraging lack of good correlation between theory and experimental data. This is particularly true in the areas that are involved in designing an active control vehicle. When controllability becomes the design criterion rather than inherent aerodynamic stability, you inevitably get into the very non-linear corners of the flight envelope: high angle of attack conditions, subsonic and supersonic, and worst of all, transonic, where theory breaks down pretty badly. Lacking good theoretical methods, there is a compelling need for building a better experimental data base. This is what we tend to rely on predominantly in the aeroplane business. Boeing, for example, relies heavily on windtunnel testing when designing a new aeroplane. We in the business of looking at advanced active-controls aircraft are tending to scrounge wherever we can for experimental data base because we find problems with our analytical approaches. I would urge that all of the agencies involved in producing experimental data perhaps realign their research activities a little more into the areas of aircraft control and stability. In recent years experimental data development has placed heavy emphasis on what I call "L/D aerodynamics", at the expense of stability and control aerodynamics. The converse should be the case. In actuality and aerodynamicists job is relatively simple in that he works generally in the low alpha regions where things are nice and linear and theoretical methods work well. It is rare when we in the stability and control business see linear characteristics. I would strongly urge research agencies to re-orient their research to build a better data base in the stability and control areas. However, at the same time I think that we should be working harder to try to develop improved theoretical methods. Here again I would agree with all the previous remarks regarding the extreme importance of developing good theoretical methods and correlating these with experimental data base. We need this in order to generate confidence in our own technology, and in order to convince management that they should adopt the approach that we are recommending for a particular design.

There is another area in which I see a lack of direction these days. I think we should look here to the military research agencies for direction as to what should be the mission requirements for some of these future military products. In my paper, for example, I deliberately looked at the very demanding requirements of trying to develop good maneuver capability in an aeroplane that had been intentionally point-designed, for efficient supersonic cruise. However, with the development of missile performance and electronic guidance systems there may not be the need for the next generation of supersonic tactical aircraft to possess such good maneuver capability. It would seem appropriate to turn to the military for guidance as to what should be the specific mission requirements for the next generation of military aircraft of this type. For example, a relaxation of the maneuverability requirements could save a substantial amount of engineering development cost and could result in improved aircraft performance. Studies to determine mission requirements, or to evaluate the cost of maneuverability and the impact on the aircraft configuration would be well worth while.

In closing my comments I would like to say once again that I have enjoyed very much this interesting symposium and I hope to see more like it. Thank you.

Professor Young – UK: Thank you very much Mr Kehrler. Mr Kehrler stressed two interesting points I thought: one was the need for more attention than in the past to be given to control and stability problems, and the other point was the need to be a little clearer about mission requirements. One suspects of course, that if you ask an Air Force what it needs, it would say what can you give me, and then one would proceed in a circle. Well has anyone got any comments to make on those points? Perhaps Dr Johannes may have comments on some of the points which have been raised as well as his own area of interest.

Mr Johannes – USA: Thank you. I too would like to express my appreciation for having been invited to come to this particular meeting. I think that the one thing I got out of it, more than anything else, was an appreciation of the need for interdisciplinary communications. I think it's becoming increasingly more important, for in my case, the control engineer to understand the language and the problems of, in this specific case, the fluid dynamicist. I think if you attached any credibility to my thesis that the Control Configured Vehicles concept is design process of the future, then it very dramatically points out the need for this interdisciplinary knowledge and awareness.

I think it goes even a bit further than technologists understanding each other, also. At least in our business, that is, the pursuit of which have been termed CCV or active control technology and trying to get maximum benefits, it is extremely important to understand what the end result is supposed to be. By that I mean the desired end results of the vehicle, the airplane, the weapon system. This I think addresses what Bill Kehrler was saying. I don't think it is fair to expect the military, the strategists and tacticians, to be able to really tell you what they want in the technical sense. I think it behooves us to understand what their problem is and to offer them suggestions and demonstrate capabilities to address some of those problems. That is basically all I wanted to say about that particular point.

I think perhaps a means by which you folks could avail yourself of some additional insight, is to go to some of the other AGARD Panel meetings such as the Guidance and Control Panel or the Flight Mechanics Panel. I think attendance and observation of the problems being discussed will give you a facility with the language. I have recently become aware that those of us in the control discipline do not communicate our product very well. We have a certain language that is not well perceived by other people. We talk about high gain, low pass filters and those sort of things. I used the term in my presentation, "two fail operate", and afterwards someone asked me about it. They had misunderstood what I meant. I think that this may be more of a problem in the control discipline than in other major disciplines.

Let me implore you to help us out in that area. I think that control does indeed have a lot to contribute to the future of aeronautical vehicles.

The second point that I wanted to address was the need for you to use your innovation and imagination in coming up with additional ways of doing the things that the control engineer says he would like to do. There were certainly some examples of that contained in the papers that were presented during the proceedings. Specifically two come to mind: the use of fluid injection to switch vortices from side to side; and the use of flaps on pylons for side force control. I think that the methods that have been employed in the past were employed because they were the only ones that we knew about. If you can come up with additional, or new, means of getting the job that needs to be done accomplished, then together we can achieve a more efficient solution. The final point that I wanted to cover is the continued need for the development of analytical and predictive capabilities. This point has already been made by nearly everyone at the table. It's the surprise, it's the thing that you did not expect to happen, that's going to give you trouble. The comment made over here about the potential severity of an unknown in case of active flutter suppression is certainly valid. I think the point that the gentleman made over here about the need to know how accurate we have to be in these predictive techniques is another thing that can be addressed by mutual understanding of the technologies. If the fluid dynamicist knows what the control engineer is trying to do, he can then, perhaps, judge what degree of accuracy in the predictive techniques is required. With that I will close and merely add that I found this experience extremely rewarding. I had no idea of the complexity of the problems, of the high degree of complexity of the problems that the fluid dynamicists were addressing.

Professor Young – UK: Thank you very much Mr Johannes. Again, does anyone wish to add anything to what Mr Johannes has said?

Mr Walker (British Aerospace) – UK: I can make a comment that might help to bridge the gap between the control specialists and the aerodynamic specialists. I believe that we are now entering a second phase of active control technology.

During the first, we would dream up ideas for benefitting the design of aircraft. The second phase, which we are now entering, is really putting these ideas into practice. Here we come up against the problem of implementation, particularly in the writing of soft ware. These problems, I think, are going to mean either some of the original ideas are unacceptable or we will need a very precise definition of the aerodynamics, particularly in the non-linear regions. A further possibility on the systems side is perhaps to develop systems which are self-adaptive, but we come up against the problem of how far should the theoretical aerodynamicists go. In Mr Mabey's paper, which I was discussing with him some minutes ago, he was stating that 10° phase lag was not acceptable for adaptive flutter and I was very doubtful whether, if that was the case, we can ever achieve accuracies of 10° in theoretical models and (in practice) between different types of stores configuration and different types of distortion. Those are my main comments.

Professor Young – UK: Thank you very much Mr Walker. Are there any other comments?

Mr Moss – UK: I would just like to emphasize those remarks made at the table just now about the need for inter-disciplinary communication. I feel very strongly about this because in any system usually a balance has to be found between the degree of engineering simplicity and the amount of aerodynamic benefit. Very often the aerodynamicist does not really grasp this. For instance we've heard this week about the need for a progressive improvement in control aerodynamics, leading us for example from flaps with simple hinges to flaps with slots, flaps with 'contoured' hinges and even flaps with full variable-camber mechanisms. The aerodynamicist naturally tries to get elegant aerodynamic solutions in the laboratory, for instance to the problem of controlling a flap at the back of an aerofoil. However, I think we have to be careful to get across to the other aspects of this type of line of development. We have to think of the balance that occurs with respect to other disciplines. If I can quote you an example that I think was mentioned on Monday: we heard from one speaker about the general improvements in airframe fatigue life from the use of active controls. But of course the more you make your controls work for you in this special way, the more you may run into the extra problem of fatigue of the controls themselves, and you really need to establish a very close working relationship with the engineer who has to make these controls stronger because of this. Every novel system we can think of has its risks; in fact, almost by definition a novel system is likely to be a high-risk system, but obviously in the future we must face up to this situation to make any progress. To reduce these risks we must first of all consider the fundamental aerodynamic flows that are associated with our new device and we must obtain a good understanding of these in order to have the necessary confidence to proceed.

I think for me Andy Skow's paper yesterday was one of the high points of this conference. He was telling us about a new type of aerodynamic control on aircraft for spin prevention and recovery, and I think this is a very new and a very exciting prospect. However, this uses flow mechanisms that very few of us, if anybody, can understand properly: we can't model these flows mathematically very well and we can't even do reliable windtunnel predictions because of the gross scale-effects that accompany such flows. The biggest problem that Andy Skow might have, in fact, could be to persuade his management that, weight for weight, this is a better way to go than, say, putting in a tail parachute, and it could be *that* type of decision that makes the new device a reality or not. Thus the aerodynamicist has a very important responsibility to communicate with his opposite numbers in other disciplines to make advances in technology.

Professor Young – UK: Thank you Mr Moss. Any other comments? If not I will pass on to Dr Scolatti.

Dr Scolatti – USA: The first thing I would like to do is to thank Professor Young and Dr Yoshihara for having invited me to attend this important conference. I also would like to extend my personal thanks to the members of the Italian Air Force Academy for the use of these fine facilities and also to the AGARD staff for their help and kind assistance.

Since I have not attended an AGARD meeting in over seven years, I anticipate that my comments on this panel might reflect a different view, in perspective of time, in comparison with those of the panel members and presenters that are more current in AGARD activities. Several papers presented new data on investigations which were of high quality, thought-provoking and in concert with the latest state-of-the-art in their respective technologies. My comments today, as I remarked earlier to M. Poisson-Quinton, are but a reflection of the discussions and exchanges of thoughts with others here, both on this panel and those in the audience. While the results of investigations presented here were of current origin, there were some recommendations which have not significantly changed with the passing of time.

For example, a particular note was made during the discussion periods, that greater accuracies and understandings were needed in experimental data to improve the quality of the prediction methods, especially in the transonic flow regime. In 1954, I was involved with the design of transonic wind tunnels. The problem at that time was to conduct transonic testing, free of transonic flow interactions. To do this required wind tunnel wall modifications, and the questions of that day were: "Where do we put the slots or holes and how much pressure relief would be required to properly cancel the reflected waves?" and "How can we determine the accuracy of measurements and improve the quality of the prediction techniques?" Dr Yoshihara and his colleague, Dr Guderly, at the time were investigating the theoretical aspects of transonic aerodynamics. That was twenty-five years ago, and the comments and discussions on this subject made here this week indicate that these problems, though somewhat modified, are still with us, and an additional complication has been brought about by the inclusion of active control technology.

Another area of long time concern; namely, aircraft stall and post-stall departure and spinning, was also discussed here. Novel solutions to the post-stall problems, their formulation, and investigation have been, and will be in the future, worthy of support. However, we must exercise caution in advocating beyond the intent of the presenters, the extension of any single potential solution for one aircraft configuration to another configuration; and indeed, for even dissimilar modes of departure on the applicable aircraft configuration. Upright, inverted, and high acceleration departures often

exhibit entirely different spin characteristics on a single configuration. Therefore, while novel spin control devices may be a solution for one particular, well-defined, departure problem, I would not endorse a suggestion or recommendation for removing the spin chute from spin test aircraft equipped with this novel device, let alone a recommendation that it be more universally applied as a departure control device, as has been suggested.

My major point, however, has to do with what I consider the need for developing a better interdisciplinary understanding between the aerodynamicist and the other technologies. Active control and active control modes, as outlined by Bob Johannes, are being introduced and investigated because they offer a means of achieving needed mission performance for the benefit of the system operator. Simply stated, this means that through the use of active control, the operator can perform required tasks with less effort, lower cost, greater survivability and with more precision. Johannes's reference to vertical and horizontal translation, wings-level turns, independent fuselage aiming, propulsion vectoring, and tailored lift to drag are examples of completed feasibility studies which are now within the domain of application for potential system performance improvements. Specific mission segments, such as low-altitude, high-speed terrain following and avoidance, can be accomplished more easily, safely, and effectively with the use of active control. On the other hand, the entire mission performance of aircraft can be improved if it is designed from the beginning with an understanding of the inter-relationship between aerodynamics and active control.

The extension of active control into internal aerodynamics, as has been done in external aerodynamics, needs to be more completely understood if aircraft of the future are to have the levels of effectiveness and efficiency required. In Jim Agnew's paper, one case which illustrated the importance of internal aerodynamics and control was addressed. He showed how benefits can be derived from understanding and employing a tailoring of the inlet and its control system to achieve high levels of performance.

Lastly, as the flight control technologist has done, so must the aerodynamicist do; namely, extend his interdisciplinary understanding to include the fast developing technologies in avionics. As suggested by Mr Walker, avionics technology, especially digital avionics technology and its associated software, must be included in future interdisciplinary exchanges of data and ideas. Groups, like this in AGARD, can play a major role for transitioning ideas and technology from one field to another and finally into operations.

Thank you.

Professor Young – UK: Thank you Dr Scolatti. Any comment on the points that have been raised so far?

Mr Thomas – UK: As a voice that has been crying in the wilderness for a long time, I would like to reinforce the remarks of the last three speakers about this matter of communication between the people on the flight mechanics side and the aerodynamicists. I think that I would take a slightly optimistic viewpoint at the present stage of the aircraft development because with ACT we are getting the flight dynamics and control systems more closely tied up with the actual performance and the various parties will be forced to talk to one another whether they like it or not.

Professor Young – UK: Anyone else like to add anything to that optimistic remark? If not I come to Philippe Poisson-Quinton and ask him to offer his general comments on the symposium at large and any points that he thinks are particularly significant from the flight mechanics point of view.

M. Poisson-Quinton – France: Je pense que c'est très intéressant d'avoir parlé de la communication entre les différentes disciplines et je crois qu'il y a eu pas mal de progrès. Je suis assez optimiste aussi, parce que depuis que nous regardons les problèmes de contrôle actif, disons depuis à peu près cinq ans, nous avons eu un certain nombre de meetings de l'AGARD au Panel de Mécanique du Vol mais aussi au Panel des Structures, au Panel de Guidage et Contrôle, et au Panel d'Avionique, et cela a été l'occasion, je pense, de réunir des gens de différentes disciplines. Pour la première fois, justement, les gens se sont rencontrés autour des sujets parce qu'ils y étaient obligés; maintenant, il n'est plus question d'être seulement aérodynamicien si vous ne savez pas qu'une structure est flexible, et maintenant il faut que l'aérodynamicien apprenne aussi ce que c'est qu'un contrôle. C'est absolument indispensable, sans cela il est complètement perdu, et la réciproque est vraie: il faut maintenant que les électroniciens pensent aussi un petit peu aux structures et à l'aérodynamique. Donc, je crois qu'il va falloir faire une éducation un peu nouvelle des ingénieurs de l'aéronautique, et cela commence actuellement, d'ailleurs, dans les écoles d'ingénieurs; on commence maintenant à cerner assez bien cette nécessité d'être pluridisciplinaire. Dans tout ce qu'on avait étudié depuis quelques années, il n'y a pas de doute que l'on a négligé beaucoup l'aérodynamique, parce que les contrôles actifs étaient très difficiles, du point de vue justement de l'électronique; c'était quelque chose de tout à fait nouveau, cette intégration du computer dans l'avion, et la plupart des travaux ont été faits d'abord sur le contrôle, et l'on a négligé certainement les études aérodynamiques, et maintenant on se réveille avec des problèmes parce que les gouvernes que l'on avait prévues sont insuffisantes; il y a manifestement un manque de contrôle, de puissance de contrôle, sur les avions que l'on a dessinés ces dernières années, et je pense qu'il va falloir faire maintenant un très gros effort sur les études aérodynamiques. Malheureusement c'est très difficile dans un meeting comme celui d'aujourd'hui d'avoir des résultats généraux sur les gouvernes aérodynamiques parce qu'elles dépendent beaucoup de la configuration de l'avion, de la configuration de votre projet, et c'est pourquoi actuellement, à la naissance d'un projet, il est nécessaire de faire une très grande quantité d'essais en soufflerie pour définir les efficacités des différentes gouvernes dans toute l'enveloppe de vol, et c'est un énorme travail quand on veut inclure là dedans les effets de l'incidence, du dérapage, du nombre de Mach etc. Donc cela conduit à des programmes très coûteux de soufflerie et je voudrais dire un mot là-dessus parce que c'est quelque chose, je pense, qui est très très important pour un Panel comme le Panel de la Dynamique des Fluides, il y a une nécessité absolue d'améliorer nos techniques de mesure en

soufflerie, d'améliorer les conditions d'essais pour réduire le temps d'essai, c'est à dire de réduire le prix de ces essais et c'est une partie très importante maintenant dans un projet, le prix, d'ailleurs nous avons le même problème aussi avec les computers: les prix également des calculs théoriques est très élevé mais dans le domaine de la soufflerie il est possible maintenant d'avoir un meilleur équipement des maquettes et, en particulier, il devient très intéressant de motoriser ces maquettes, c'est à dire d'avoir des gouvernes réglables pendant un essai et l'étape suivante, finalement, c'est d'utiliser là encore peut-être des méthodes, des technologies, des contrôles actifs c'est à dire de mettre un petit computer dans la boucle pour contrôler en permanence, par exemple pour l'équilibrage de votre projet, et il est possible de faire des polaires équilibrées en permanence, et à ce moment là vous gagnez énormément de temps sur le temps d'essais puisque vous êtes en permanence en équilibre sur les trois axes, et ce pilotage automatique d'une maquette en soufflerie est, je crois, très intéressant, et actuellement il y a un grand travail qui est fait dans plusieurs laboratoires sur ces nouvelles techniques qui emploient justement les nouvelles technologies de contrôle actif; et puis il faudra probablement avoir des montages tout à fait spéciaux dans les souffleries pour traiter les problèmes d'avions ayant un contrôle actif allant jusqu'à la représentation des rafales etc. pour pouvoir traiter complètement un problème en laboratoire avant d'aller en vol, et je pense que c'est très utile parce que envoyer directement en vol un projet extrêmement complexe en plus, c'est quelque chose de très dangereux évidemment. Je voudrais, le temps presse, je voudrais seulement faire une deuxième remarque: j'ai été un peu déçu du manque, peut-être, de papiers sur les problèmes de l'importance de la motorisation, de la propulsion dans le futur contrôle d'un avion, c'est ce que l'on appelle "engine airframe integration" cela veut dire que l'on essaye maintenant d'utiliser l'énorme quantité de mouvement que nous avons sur un avion pour essayer d'améliorer le pilotage, et cela je pense que c'est quelque chose qui est encore tout à fait dans l'enfance mais qui, dans les prochaines années, va se développer beaucoup. En particulier, vous le savez, on l'a évoqué pendant cette conférence, il y a la possibilité de développer des forces très importantes en orientant le jet de propulsion et il y a une autre façon d'utiliser cette quantité de mouvement, c'est de s'en servir pour des jets de contrôle, soit sous forme de contrôle de couche limite (BLC) pour améliorer l'efficacité des gouvernes et les rendre linéaires, ce qui est très agréable, et la deuxième possibilité c'est d'utiliser par exemple le "spanwise blowing", enfin le soufflage transversal, qui permet de former un régime tourbillonnaire beaucoup plus puissant et d'avoir un contrôle extrêmement intéressant de l'avion dans des régimes de décrochage de l'avion; et cela aussi je pense qu'il y a beaucoup d'avenir dans ces nouvelles technologies et beaucoup de recherches sont encore nécessaire dans ce domaine. J'aimerais avoir l'avis des spécialistes de l'Air Force là-dessus.

I believe inter-disciplinary exchanges are extremely interesting and I am glad this subject has been discussed. Considerable progress has been made in this area and mainly thanks to AGARD since we started considering active controls applications approximately five years ago; a number of AGARD meetings have taken place, not only under the sponsorship of the Flight Mechanics Panel, but also under that of the Structures and Materials Panel, the Guidance and Control Panel and the Avionics Panel. Thus, opportunities have been provided for convening experts in various disciplines. For the first time, precisely, people have met to discuss certain subjects, because they were compelled to. To succeed in a project, is not sufficient to be an aerodynamicist, if you do not know how flexible is your structure, or what electronic systems are available to control the aircraft; the same remark applies to experts in electronics who must be aware of structures and aerodynamics design. Therefore, I believe that aeronautical engineers will require a new type of training. This is already the case, incidentally, in most of Engineering Schools. The necessity of being versatile becomes evident. In all that has been studied about C.C.V. for several years, aerodynamics has been undoubtedly neglected to a great extent, because active control constituted a very difficult subject, precisely from the system standpoint: the integration of the computer into the aircraft design was something quite new. The greatest part of the work performed in this field was first concerned with automatic control, and aerodynamic studies were left aside. Now, problems are being experienced because the control surfaces which had been planned initially are sometimes insufficient. Therefore, I think that considerable efforts have to be made in the field of aerodynamics studies. Unfortunately at a meeting like this, it is difficult to have general results on aerodynamic, control surfaces, since they depend to a great extent on the configuration of your project. This is why it is now necessary, at the initial stage of a project, to carry out preliminary calculations and then a large number of wind-tunnel tests in order to determine the performance of the various control surfaces over the whole flight envelope. This implies a considerable amount of work, if one wants to include the effects of incidence and sideslip, of the Mach number, etc. This had led to very costly wind-tunnel test programmes. In this respect, I would like to make a few remarks, because, for a Panel like the Fluid Dynamics Panel, it is absolutely necessary to improve wind-tunnel measurement techniques, as well as test conditions, in order to reduce test time, therefore test costs. Cost has become a very important facet in a project: the same applies to computers. The cost of theoretical computation is becoming very high. However, as regards wind-tunnels, it is now possible to have improved model instrumentation; it is becoming very interesting, in particular, to fit these models with actuators in order to have control surfaces which can be adjusted in the course of a test. The following step consists in using active controls, that is to say, in incorporating a small computer in the loop for permanent monitoring purposes. This provides the means of achieving constantly trimmed polars and enables you to save considerable test time, since you are in constant equilibrium along the three axes. This automatic control of a wind-tunnel model is, in my opinion, very interesting. A great deal of work is being performed on these new techniques in several laboratories, where the new active control technologies are being applied. In addition, very special mountings will have to be used in wind-tunnels to simulate an aircraft equipped with active controls, including gust generation, etc., so that a problem may be covered completely in a laboratory prior to flight tests. I believe this is very useful, especially as subjecting an extremely complex project directly to flight tests in a very hazardous adventure. As time presses, I shall make only one second remark: I have been slightly disappointed by the lack of papers on the importance of some propulsion integration in the future control of an aircraft. This is what we call "engine airframe integration". It means that, now, we must try to use the huge momentum available from the jet engine to improve control. This technique, which is still in its infancy, will develop considerably in the next few years. In

particular, as mentioned during this meeting it is possible to develop very high forces by orientating the propulsion jet. Another way of taking advantage of this momentum consists in using it for control, either in the form of boundary layer control to improve the efficiency of control surfaces and make them linear, which is very attractive, or in the form of spanwise blowing, which makes it possible to create much more powerful vortex conditions and achieve a very interesting control of the aircraft, even after stall conditions. I believe these new technologies are very promising, and considerable research is still necessary in this field. I would appreciate hearing the opinion of the US Air Force specialists on this subject. RTD-9

Professor Young – UK: Thank you Philippe. Does any one wish to take up any of the points raised by M. Poisson-Quinton? He drew attention to the fact that there was very little, if anything, said during the course of this meeting about the use of the propulsion devices that we have on aircraft to augment in one way or another, our controls. That was largely due to the fact that we had no one come forward with any papers on the subject. If anyone has any comments on that point we could gladly spend a minute or two on it.

Mr Johanness – USA: At the Air Force Flight Dynamics Laboratory, we are pursuing what we call Integrated Flight and Propulsion Control. We have over the years been trying to integrate various technologies. We have worked on control and structures, control and aerodynamics, and control and avionics. Certainly propulsion is another major discipline that, when properly integrated, can improve the overall mission capability of the aircraft. There is a great deal of interest in that area, and perhaps the next time we have a meeting there will be some papers.

Professor Young – UK: Thank you. Well this brings to an end the presentation from the members of the Round Table. I think we have covered during these presentations most of the major points which have been raised but there may be other points that someone wishes to bring up.

Mr Mabey – UK: One thing that has worried me during this conference is that we have only heard the word "buffeting" once or twice. On the occasions when we did hear it, I did not like what I heard. I heard echoes of the ghost of "kinkology", stalking through the corridors of power*.

Taking the low speed range first: so many people spend so many hours in low speed wind tunnels testing very elaborate models and measuring $C_{L C Max}$ to incredible accuracy, without having any unsteady wing root gages which are very cheap, very simple to apply, or wing tip accelerometers which are also easy to apply. Even if they restricted their attention to buffet onset, the information that they could gather would be invaluable and save them hours of time, for example, in choosing the best conditions for flow visualization.

Moving up to transonic speeds a shortcoming of our own experiments is that we have not so far looked into the regions of separated flows. Moreover we can already infer that the aerodynamic characteristics of all forms of controls are going to be radically different once the flows are separated.

One final point: I have been surprised that the words "static and dynamic aeroelastic distortion" have not occurred more often during this conference. Monsieur Poisson-Quinton used them just then and I was pleased to hear it. The sort of models that we at the RAE have to use for our tests are very flexible and that sort of aeroplanes that fly around in the sky are very flexible. I think that many discrepancies between theory and experiment can be attributed to aeroelastic distortion.

Professor Young – UK: Are there any other comments?

Mr Thomas – UK: I would like to back up a bit. It was on M. Poisson-Quinton's remarks about the use of jet engine and airframe integration. Perhaps, Monday is too long ago for him to remember, but there were examples given in the paper by Dr Ross and myself which really demonstrate the force of his arguments.

Professor Young – UK: Any other comments?

Mr Bore – UK: It is perhaps uncharacteristic for me to have remained silent so long in this conference, but I think some comment is needed in response to Poisson-Quinton's remarks about propulsion vectoring.

It is true that we can vector the thrust and get some remarkable manoeuvres. These manoeuvres have been demonstrated both on simulators and in flight, and it has been stated that this produces a new dimension in manoeuvrability. There is no doubt at all that vectoring the thrust is an extremely effective way of outflying the opposition which cannot do this. So one can take that as demonstrated.

Of course there are many interactions between the effluxes and control and not all are completely understood, but we can deal with them in practice. Vectoring the thrust introduces not only a new dimension to manoeuvrability but also a new element to the matrix of interactions that one must understand as well. Although thrust vectoring in forward flight is an established practical reality, there is still scope for further improvements for some time to come.

* The improvements in wing buffeting caused by the postponement of alleviation of flow separations can sometimes be associated with changes in the mean forces and pressures on the wing, particularly for low angles of sweep-back when buffeting is generally heavy. For moderate or highly swept wings this is a much more difficult process. The term "kinkology" has been applied to these methods of determining improvements in buffet.

Professor Young – UK: Thank you Mr Bore. Any other comment? We are getting close to the time when we must stop. We can have one more. Dr Green.

Dr Green – UK: Since the subject of propulsion integration has achieved so much interest could I just put in a commercial. Make a note in your diaries, Spring 1981, in Toulouse, this Panel will be running a meeting on "Engine Airframe Integration".

Professor Young – UK: Thank you. I think it is now time for me to draw this meeting to a close. Before doing so I must first thank our speakers of the Round Table this morning for kindly helping to round off this meeting. I must also thank, of course, everybody who presented papers during the course of the meeting and contributed to the discussions. Some of the discussions could have gone on for a long time but unfortunately there was not the time available but one hopes that such discussions can always be continued elsewhere. As far as this morning's discussions go I will not attempt to summarize the points which have been raised. I think they brought out the most important features of the Symposium and what needs to be done in the future. I am sure everyone will go away stimulated with ideas in the back of their mind for future work as a result of these discussions. I would certainly endorse the final point made about the need for interdisciplinary understanding. By that, I do not mean one needs to be an expert in ten fields but one needs to understand the language and the ideas of people in fields other than one's own. This was also brought home to me by a conversation with one of our translators, who was having difficulty following the rather special jargon we tend to use and the vast number of new hybrid words we are developing like tiperons, wingerons etc. etc. Having referred to the translators may I say how grateful we all are to them for the excellent work they have done throughout these discussions. They have acted as a very effective brake on the speed with which we would otherwise talk and have therefore helped our lecturers to be more easily understood. Lastly I must certainly give my thanks to the Italian Air Force for the magnificent way which they have organized this meeting but I believe our Chairman Mr Lloyd Jones will want to say something about that himself so I'll ask Mr Lloyd Jones preceded first by Col. Vagnarelli to say a few words.

Col. Vagnarelli – Italy: Ladies and Gentlemen, on behalf of the Italian Air Force the Academy and the Italian AGARD Organization, thank you for your attendance and interest. We have been very happy to be your host. Thank you very much.

Mr Jones – USA: I would like to add thanks to a few other people. It takes a large number of people to make a symposium such as this a success. First, I would like to recognise Prof. Young and his Programme Committee for the excellent programme that they put together for us and to endorse his thanks to the Round Table participants who did such an excellent job of ferreting out the basic message from this meeting. I would also like to thank the Authors and the Speakers for their presentations – and all attendees for their active participation, which really makes conferences such as this a useful activity.

I hope you have benefited from these presentations and from the opportunity to discuss privately with others engaged in similar work and who are faced with problems similar to your own. I know you must have enjoyed your visit to this beautiful city and to the neighbouring cities and Islands and so, as I, you will look back on this conference with pleasure. There are a few others who need to be recognised – the AGARD staff from the Paris Office, Mr Rollins and Mlle Rivault and Sgt Calafiore who have been responsible for all of the planning for this meeting and from SHAPE Sgt Treff. I also want to thank Ten. Col. Vagnarelli, the Italian AGARD Staff and his secretary Signora Servi, and from the Academy Staff Col. Foresti and people from the Academy who have worked with them to help us so effectively; and finally to our host the National Delegate from Italy to AGARD, General Fabi and to the Commander of the Academy, General Nenchia and his Deputy Commander, Col. Graciano. Their hospitality, as you are aware, has been most gracious. Let me make one speech for a future FDP programme – our next Symposium will be September 24 through 26 in The Hague on the subject "Turbulent Boundary Layers – Experiments, Theory and Modelling". As you recognize this is a fundamental area that needs to be understood to improve our computational fluid dynamics capability to be more useful to the design engineers. May I at this time wish you all a pleasant and safe journey home and with that I will declare the Symposium adjourned.